Acoustic, Flow Related, and Performance Related Experimental Results for Generation 1.5 High Speed Civil Transport (HSCT) 2-Dimensional Exhaust Nozzles

M. Salikuddin, S. Wisler, and R. Majjigi
General Electric Aircraft Engines, Cincinnati, Ohio

The NASA STI Program Office . . . in Profile

Since its founding, NASA has been dedicated to the advancement of aeronautics and space science. The NASA Scientific and Technical Information (STI) Program Office plays a key part in helping NASA maintain this important role.

The NASA STI Program Office is operated by Langley Research Center, the Lead Center for NASA's scientific and technical information. The NASA STI Program Office provides access to the NASA STI Database, the largest collection of aeronautical and space science STI in the world. The Program Office is also NASA's institutional mechanism for disseminating the results of its research and development activities. These results are published by NASA in the NASA STI Report Series, which includes the following report types:

- TECHNICAL PUBLICATION. Reports of completed research or a major significant phase of research that present the results of NASA programs and include extensive data or theoretical analysis. Includes compilations of significant scientific and technical data and information deemed to be of continuing reference value. NASA's counterpart of peer-reviewed formal professional papers but has less stringent limitations on manuscript length and extent of graphic presentations.

- TECHNICAL MEMORANDUM. Scientific and technical findings that are preliminary or of specialized interest, e.g., quick release reports, working papers, and bibliographies that contain minimal annotation. Does not contain extensive analysis.

- CONTRACTOR REPORT. Scientific and technical findings by NASA-sponsored contractors and grantees.

- CONFERENCE PUBLICATION. Collected papers from scientific and technical conferences, symposia, seminars, or other meetings sponsored or cosponsored by NASA.

- SPECIAL PUBLICATION. Scientific, technical, or historical information from NASA programs, projects, and missions, often concerned with subjects having substantial public interest.

- TECHNICAL TRANSLATION. English-language translations of foreign scientific and technical material pertinent to NASA's mission.

Specialized services that complement the STI Program Office's diverse offerings include creating custom thesauri, building customized databases, organizing and publishing research results . . . even providing videos.

For more information about the NASA STI Program Office, see the following:

- Access the NASA STI Program Home Page at *http://www.sti.nasa.gov*

- E-mail your question via the Internet to help@sti.nasa.gov

- Fax your question to the NASA Access Help Desk at 301–621–0134

- Telephone the NASA Access Help Desk at 301–621–0390

- Write to:
  NASA Access Help Desk
  NASA Center for AeroSpace Information
  7121 Standard Drive
  Hanover, MD 21076

NASA/CR—2004-213117

Acoustic, Flow Related, and Performance Related Experimental Results for Generation 1.5 High Speed Civil Transport (HSCT) 2-Dimensional Exhaust Nozzles

M. Salikuddin, S. Wisler, and R. Majjigi
General Electric Aircraft Engines, Cincinnati, Ohio

National Aeronautics and
Space Administration

Glenn Research Center

July 2004

Acknowledgments

The authors are thankful to J. Brausch for his contribution in designing and acquiring the acoustic hardware and helping the installation of the hardware in GEAE's Cell 41 for testing. The authors are also thankful to J. Hencheck, S. Thomson, and J. Braddy for running the test facility, Dr. C.E. Whitfield for helping in data analysis, and K. Early for covering the tests when needed.

Document History

This research was originally published internally as HSR046 in December 1996.

Available from

NASA Center for Aerospace Information
7121 Standard Drive
Hanover, MD 21076

National Technical Information Service
5285 Port Royal Road
Springfield, VA 22100

Available electronically at http://gltrs.grc.nasa.gov

SUMMARY

The principle objectives of the current program were to experimentally investigate the repeatability of acoustic and aerodynamic characteristics of 2D-CD mixer-ejector nozzles and the effects on the acoustic and aerodynamic characteristics of 2D mixer-ejectors due to (1) the configurational variations, which include mixers with aligned CD chutes, aligned convergent chutes, and staggered CD chutes and aerodynamic cycle variables, (2) treatment variations by using different treatment materials, treating the ejector with varying area, location, and treatment thickness for a mixer-ejector configuration, and (3) secondary inlet shape (i.e., a more realistic inlet) and the blockage across the inlet (a possible fin-like structure needed for installation purpose) by modifying one of the inlet of a mixer-ejector configuration. The objectives also included the measurement dynamic pressures internal to the ejector for a few selected configuration to examine the internal noise characteristics.

Acoustic testing in General Electric's Jet Noise Test Facility, Cell 41, was conducted for five basic mixer configurations, namely, two aligned CD chute mixers of SAR (Suppressor Area Ratio) 2.8 and 3.3, an aligned convergent chute mixer with SAR=2.8, and two staggered CD chute mixers with SAR=2.8. With the variation of treatment type, treatment area, treatment thickness, ejector length, modifications at the secondary inlet, and the above listed five mixer geometry, 25 different configurations, were tested.

Tests were conducted for two aligned CD-chute mixers of SAR 3.3 and 2.8 with long fully treated ejector to establish the repeatability of measurement by comparing the current results with previously obtained data. In general, the repeatability of test results for both the mixer-ejector configurations is very good. Small differences observed in the data shown here could be due to uncertainty of exact duplication of ejector treatment, flight Mach number, and aerothermodynamic conditions. The azimuthal variation of acoustic field for the aligned CD-chute mixers with long ejector is significant and is much higher at lower jet velocities. A variation of about 4 to 6 EPNdB is observed at jet velocities between 1147 ft/sec and 1600 ft/sec. Even at higher jet velocities the azimuthal variation of noise levels is of significance.

Significant noise reduction is observed due to flight simulation for the aligned CD-chute mixers with long ejector. Significant SPL reduction due to flight simulation is observed at higher polar angles for the entire frequency range. Major noise reduction took place

between flight Mach numbers of 0 and 0.24. The static pressure increases with increasing flight Mach number, both on the ramp and chute surfaces due to freejet fan pressure rise, indicating lesser loading for the chutes. The pumping increases with increasing flight Mach number, since the total pressure at the inlet goes up. The transition from subsonic to supersonic mode seems to be slightly delayed with respect to NPR due to flight simulation.

A nickel based brick-like foam metal was used as the bulk absorber, instead of astroquartz, for an aligned CD-chute mixers of SAR 2.8 with long ejector to determine its effectiveness in noise suppression. The foam metal seems to be performing as well as and, in most cases, slightly better than astroquartz treatment. This is a very encouraging result, since maintaining proper astroquartz treatment is more laborious and time consuming. Since the foam metal is solid in structure and did not show any deterioration during testing, this treatment was used in all the subsequent treated configurations, instead of astroquartz.

Acoustically the staggered 10 and 9 full CD-chute mixer performs best compared to other configurations at velocities above 1600 ft/sec. At lower velocities the aligned convergent chute mixer performs much superior to other mixer designs acoustically. The effect of mixer geometry on ramp static pressure distributions is insignificant. The static pressure distributions on the chute surface is more or less the same for the three CD chute mixers. However, it is significantly different for convergent chute mixer, especially at lower NPRs. The static pressure levels for convergent chute are much lower compared to those for CD chute configurations. The static pressure distributions between the mixer configurations clearly indicate that the mode switch is delayed for convergent chute mixer and is relatively early for 9 and 2 half staggered chute configuration.

Tests were conducted for 10 and 9 full CD-chute staggered mixer with fully treated long ejector and with short hardwalled ejector to study the acoustic, flow related, and performance related characteristics at fixed jet velocities by varying the nozzle pressure ratio and total temperature. The EPNL increases with increasing jet velocity. With respect to aerothermodynamic conditions the EPNL increases with increasing NPR and with decreasing nozzle total temperature. The trend is reversed at lower jet velocities, especially, with flight simulation. Based on the fixed EPNL contours, the EPNL increases with increasing NPR and nozzle total temperature. However, it is interesting to note that the fixed EPNL can be achieved by lowering the NPR and nozzle total

temperature together at a lower NPR conditions. With respect to increasing NPR and with decreasing total temperature the pumping decreases.

Based on the dynamic pressure measurements made inside the ejector treatment attenuates internal noise and is more effective at lower NPR (or jet velocity). Treatment closer to the mixer exit is also effective in flap dynamic pressure attenuation, but relatively less compared to a similar treatment area closer to ejector exit, especially for very high NPR. Ejector treatment is important, especially on entire surface, when the externally generated noise component is lower or of the same magnitude compared to the internal noise component.

For the treatment study, the acoustically performing best mixer-ejector configuration (i.e., the 10 and 9 full staggered CD-chute mixer with long ejector) was used to identify any additional acoustic benefit. The mixer-ejector configurations used under current programs generate dominant jet mixing noise compared to internally generated noise in the farfield, especially at higher jet velocity conditions. Thus, the influence of various parameters altered in ejector treatment on the farfield noise is small at higher velocities. However, significant impact is noticed on farfield noise due to treatment variation at lower jet velocities. It is believed that the influence of all these treatment parameters on internally generated noise is similar, even though, not experienced in the farfield for higher jet velocity conditions. If the jet-mixing noise is reduced by better mixer design or suitably applying other innovative means the impact of internal noise will be realized even at higher jet velocity conditions and the treatment study would be beneficial.

The fully treated ejector performs the best. However, 7/9 treatment is close to the full treatment configuration, especially at higher velocities. The 0.5"-thick treatment is better in suppressing acoustic energy. Treatment location closer to ejector exit suppresses more acoustic energy. Fully treated ejector is acoustically better that the flaps only treated configuration. Silicon carbide bulk material seems to have more potential in suppressing internal noise.

Based on the tests conducted to evaluate the impact of secondary inlet geometry the influence of scab-on inlet as a high gradient inlet ramp and the fin as a blockage to the secondary flow is relatively small on farfield acoustic characteristics as well as on the flow and performance related parameters.

CONTENTS

1.0 INTRODUCTION

Environmental acceptability and economic viability are crucial issues in the development of the next generation HSCT (High Speed Civil Transport). An exhaust system design that meets FAR 36 Stage 3 takeoff acoustic requirements and provides high levels of cruise and transonic performance and adequate takeoff performance at an acceptable weight to the success of the program.

To date, test work under NASA/GE Contract NAS3-25415 "Low Noise Exhaust Nozzle Technology Development" has identified a viable candidate 2D mixer ejector nozzle system with high levels of acoustic suppression. The acoustic suppression has been obtained with a primary (mixer) nozzle with aligned (top-to-bottom) mixing chutes. Aerodynamic mixing tests (@ total temperature of primary nozzle of about 860°R) of both aligned and non-aligned (staggered) chutes have indicated, through laser velocimetry plume mapping, that staggered chutes improve the mixing process within the ejector.

It is worthwhile to investigate the acoustic suppression benefits of the staggered chute mixers. In addition, the acoustic characteristics of mixers with convergent chutes, which potentially have improved thrust coefficient and are relatively less complicated to design and fabricate, need to be evaluated. Also, the issues of treatment, with respect to its type, area, thickness, and location, and the ejector inlet geometry with a support fin which may be needed for structural support of the nozzle installation, need to be assessed for future mixer-ejector designs. The Large Engine Technology (LET) program under NAS3-26617 provides an opportunity to investigate all these issues.

The objectives of the current program under two LET Task orders (i.e., 11 and 23) were to experimentally investigate the effects on the acoustic and aerodynamic characteristics of 2D mixer-ejectors due to (1) the configurational variations, which include mixers with aligned CD chutes, aligned convergent chutes, and staggered CD chutes and aerodynamic cycle variables, (2) treatment variations by using different treatment materials, treating the ejector with varying area, location, and treatment thickness for a mixer-ejector configuration, and (3) secondary inlet shape and the blockage across the inlet (a possible fin-like structure needed for installation purpose). In addition, internal dynamic pressures for a few selected configurations were measured to examine the internal noise characteristics. All the experiments were conducted in GEAE's Cell 41 Acoustic Test Facility.

While, the convergent chute mixer study and the treatment study were conducted under LET Task Order #23 subtask C, the tests for staggered chute mixers, internal dynamic pressure measurement, and the influence of modified inlet with and without blockage across it were performed under LET Task Order #11. The test procedure, data acquisition, and data analysis for both the task orders are the same. In addition, significant amount of the hardware is common to both the tasks. Finally, the results from both the tasks are examined simultaneously to evaluate the comparative acoustic and aerodynamic related characteristics of various mixer-ejector configurations. Therefore, a single final report for both the tasks is prepared, which is more effective and useful to reflect the objectives and avoids duplication of common descriptions. This approach to the final report was agreed by the NASA Task Manager for both LET Task Orders 11 and 23 (Mr. Doug Harrington).

## 2.0 TEST FACILITY DESCRIPTION AND DATA ACQUISITION PROCEDURES

All the tests for the 2D mixer-ejector acoustic models were conducted in the General Electric Anechoic Free-Jet Facility, known as Cell 41, located in Evendale, Ohio. Brief description of the facility and data acquisition procedures are included in this section.

2.1 ANECHOIC FREE-JET JET NOISE FACILITY

The GEAE anechoic free-jet jet noise facility, shown in Figure 2-1, is a cylindrical chamber 43' (13.1 meters) in diameter and 72' (21.95 meters) tall. The inner surfaces of the chamber are lined with anechoic wedges made of fiberglass wool to render the facility anechoic above 220 Hz. The facility can accommodate model configurations up to 5.3" (13.5 cm) and 5.5" (14.0 cm) equivalent flow diameter in the inner and outer flow streams, respectively. The corresponding throat areas for these streams are 22 and 24 square inches. The streams of heated air for the dual flow arrangement, produced by two separate natural gas burners, flow through silencers and plenum chambers before entering the test nozzle. The operating domain of the facility in terms of total temperature, pressure ratio, mass flow rate, and jet velocity is indicated in Figure 2-2 for single- and dual-flow operation and for static and simulated flight operation. Each stream can be heated to a maximum of $1960^{\circ}R$ with nozzle pressure ratios as high as 5.5, resulting in a maximum jet velocity of 3000 feet/second.

The tertiary air stream system, which is used to simulate external flow, consists of a 250,000 scfm (at 50" of water column static pressure) fan and a 3,500 horsepower electric motor. The transition duct work and silencer route the air from the fan discharge through the 48" (1.2 meter) diameter free-jet exhaust. The silencer reduces the fan noise by 30 dB to 50 dB. Tertiary flow at its maximum permits simulation up to a Mach number of about 0.4. Mach number variation is achieved by adjusting the fan inlet vanes. The combined model and free-jet airflow is exhausted through a "T" stack silencer directly over the models in the ceiling of the chamber. The "T" stack is acoustically treated to prevent high levels of noise to the surrounding community.

The facility is equipped with two systems of microphone arrays to measure the acoustic characteristics of the test models in the farfield, a fixed array of microphones and an array on a traversing tower. The fixed array has 17 microphones mounted from the false floor,

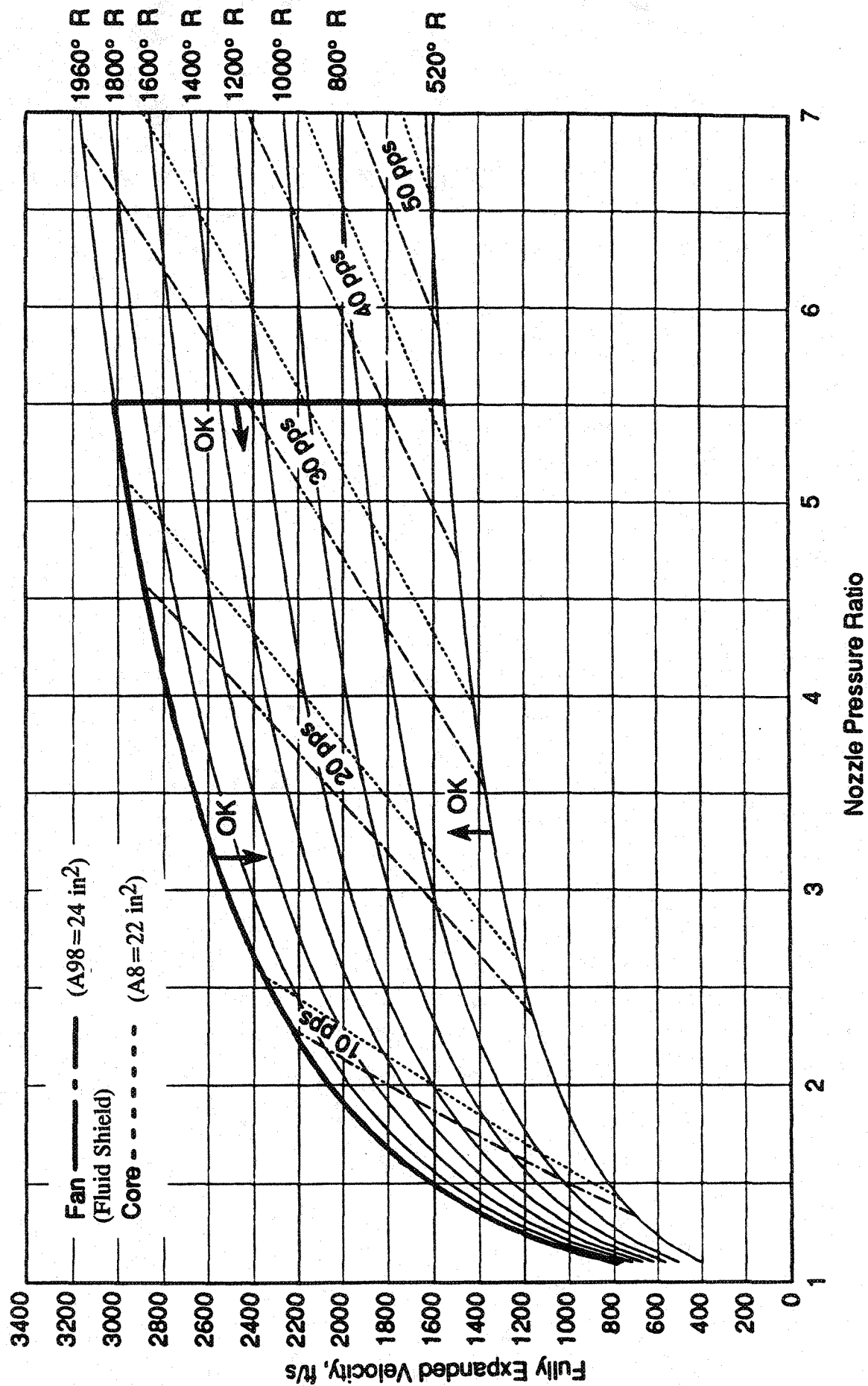Figure 2-1. Side view of Cell 41 Anechoic Free Jet Facility in the azimuthal plane of $\phi = 45°$.
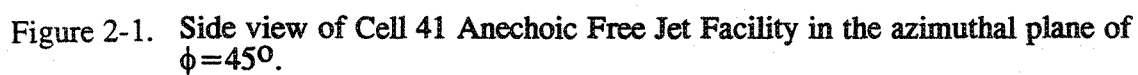
Figure 2-2. Operating domain of the Cell 41 Anechoic Free Jet Facility.

the wall, and the ceiling of the test cell, which provides measurements at a minimum distance of 26.75' (8.15 meter) from the nozzle reference location covering the polar angle (θ) range from 50° to 155°. The traversing tower contains 13 microphones, mounted at polar angles θ ranging from 45° to 155°, and provides measurements at a distance of 22' (6.7 meter) from the nozzle reference location. The traversing tower can be positioned at any azimuthal angle ϕ between $+55^O$ to -55° with respect to the fixed microphone array (or $\phi = -10^O$ to 100°) as shown in Figure 2-3.

The facility is also equipped with a laser velocimeter (LV) system and a shadowgraph system for jet flowfield measurement and flow visualization, respectively. LV and shadowgraph tests were not conducted in Cell 41 for the current program and, therefore, these systems are not described in this section.

2.2   DATA ACQUISITION SYSTEMS

Cell 41 is supported by well-calibrated acoustic and aerodynamic data acquisition systems. Acoustic data measured by both the microphone arrays is analyzed by an on-line system, which computes 1/3-octave band data for model scale at a 40' arc corrected to standard day conditions (i.e., 59^OF and 70 % humidity) and narrowband data as measured. In addition, this data is recorded on magnetic tapes for post processing if desired. All static and total pressures including model surface pressures are measured using an aerodynamic data acquisition system consisting of multiport scanivalve contained pressure transducers, signal conditioner, and analog/digital converters. The pressure signals are supplied to a Micro VAX computer system where it can be analyzed or down-loaded to GE's mainframe or workstation computer systems. Concurrently, a front-end computer with touch-screen application is used for signal and facility control and for real time data monitoring. Temperature data (thermocouple signals) are fed directly to the front-end computer. Online 1/3-octave data are further analyzed for scaling, flight transformation, and extrapolation to any sideline or arc location.
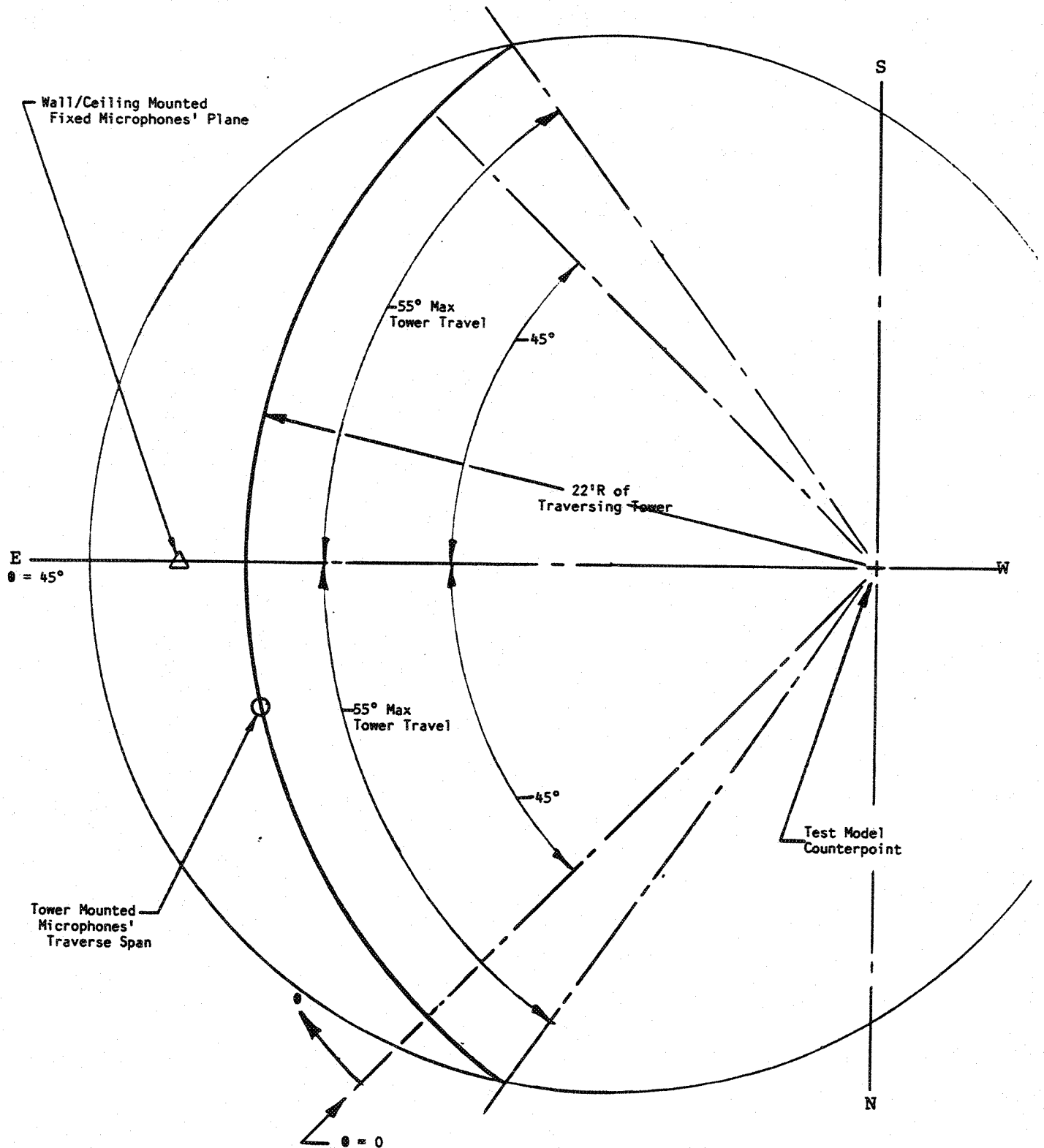
Figure 2-3.   Plan view of Cell 41 Anechoic Freejet Facility showing tower microphone
              traverse capability.

8

3.0 CONFIGURATION DESCRIPTION AND SCOPE OF TESTING

3.1 MODEL GEOMETRY

The basic 2D nozzle system with aligned CD chutes evolved around the GE21/F14 study L1M (VCE) cycle associated with a Mach 2.4 cruise aircraft with a nominal 700 pps size engine. At the 50,000 lb net takeoff thrust (power code 68, altitude=689', M_F=0.32) the exhaust nozzle design point corresponds to NPR=4.0, T8=2040°R, W_p=708.6 pps, and A8=1086 in^2. Figure 3-1 shows a side and a top views of the 2DCD mixer-ejector nozzle model (NRA) attached to the transition section in Cell 41. A close up view of the 2D model is shown in Figure 3-2. The basic 2D mixer-ejector nozzle model system used in the current program was designed and fabricated under Contract NAS3-25415. The various configurations tested under Contract NAS3-25415 used either the SAR 2.8 or 3.3 mixer rack assembly. The ejector has two lengths (16.055" and 11.5" model scale, or about 120" and 80" full scale, respectively) and three mixing area ratio (MAR) hangers resulting in MAR values of 0.95, 1.2, and 1.4. For the current tests a MAR of 0.95 was used for all configurations.

Mixers with Aligned CD Chutes: . Both the CD chute aligned mixers (SAR=2.8 and 3.3), designed and procured under Contract NAS3-25415, were tested under the present test series to verify the repeatability of acoustic results. These mixers have 20 aligned CD chutes, split into upper and lower 10-chute racks, aligned top-to-bottom with a 0.4" center gap. The chute CD cross section was designed assuming chute exit plane local static pressure of 11.0 psia. At takeoff NPR of 4.0 the P_{t8}=58.8 psia. NPR based on local static pressure is therefore becomes 5.34. With γ=1.33 at facility maximum T8=1960°R, A_{exit}/A8 (i.e., CER) becomes 1.43. Based on the model throat area, A8 of 19.14 and 22.16 square inches for the mixers of SAR=3.3 and 2.8, respectively, the mixer exit area (A_{exit}) becomes 27.27 and 31.69 square inches, respectively. Based on the throat area of 19.14 and 22.16 square inches, the equivalent mixer diameters $D8_{eq}$ are 4.94" and 5.31", respectively. Figure 3-3 through 3-5 show the detailed geometry of the SAR 2.8 and 3.3 chutes.

Mixers with Aligned Convergent Chutes: In addition, a SAR=2.8, 20 convergent chutes, aligned top-to-bottom mixer with A8=22.16 in^2, interchangeable with the existing hardware has been designed, fabricated and tested under the current program (Contract NAS3-26617, Task Order #23) to identify noise characteristics of a convergent chute
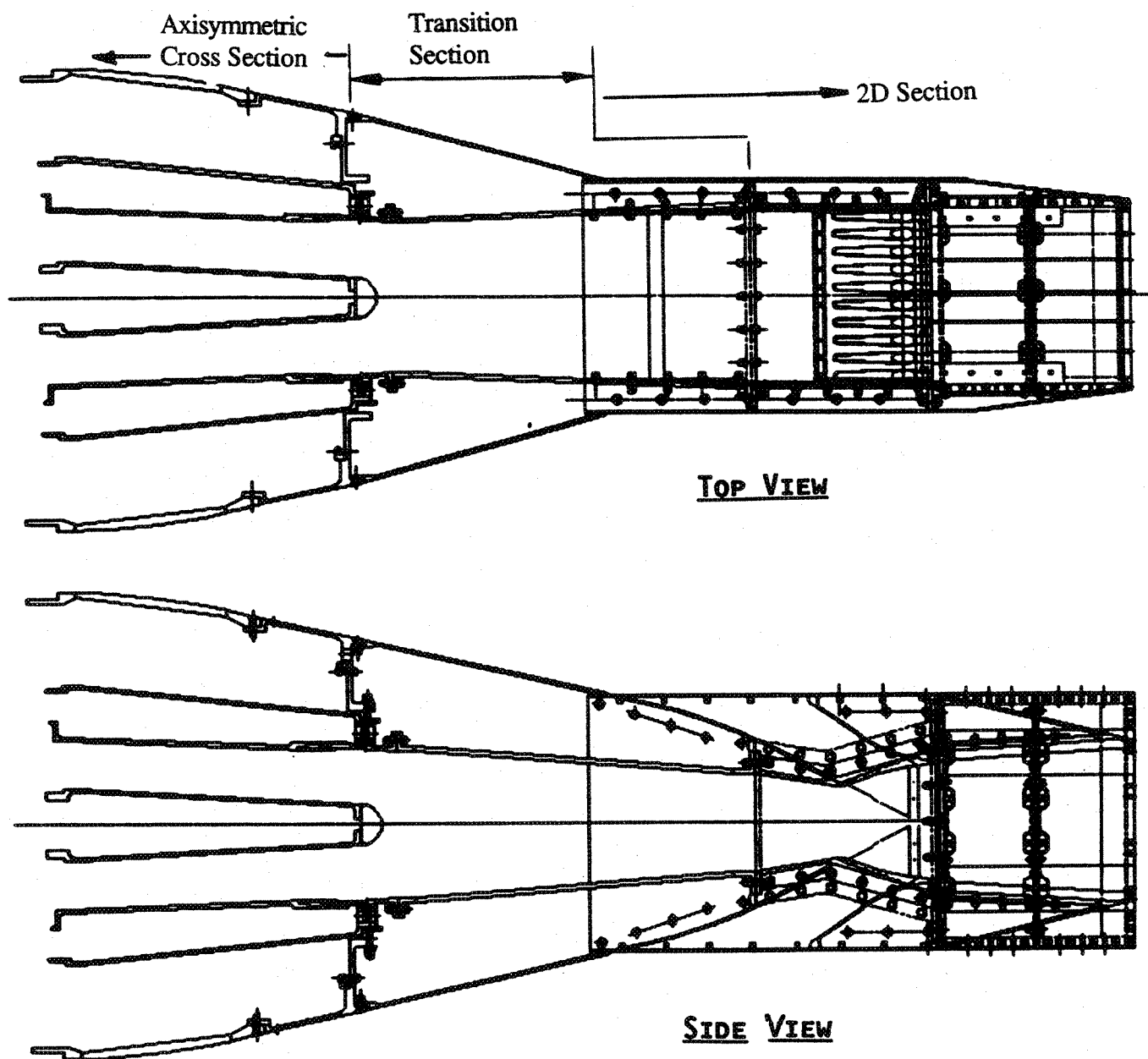
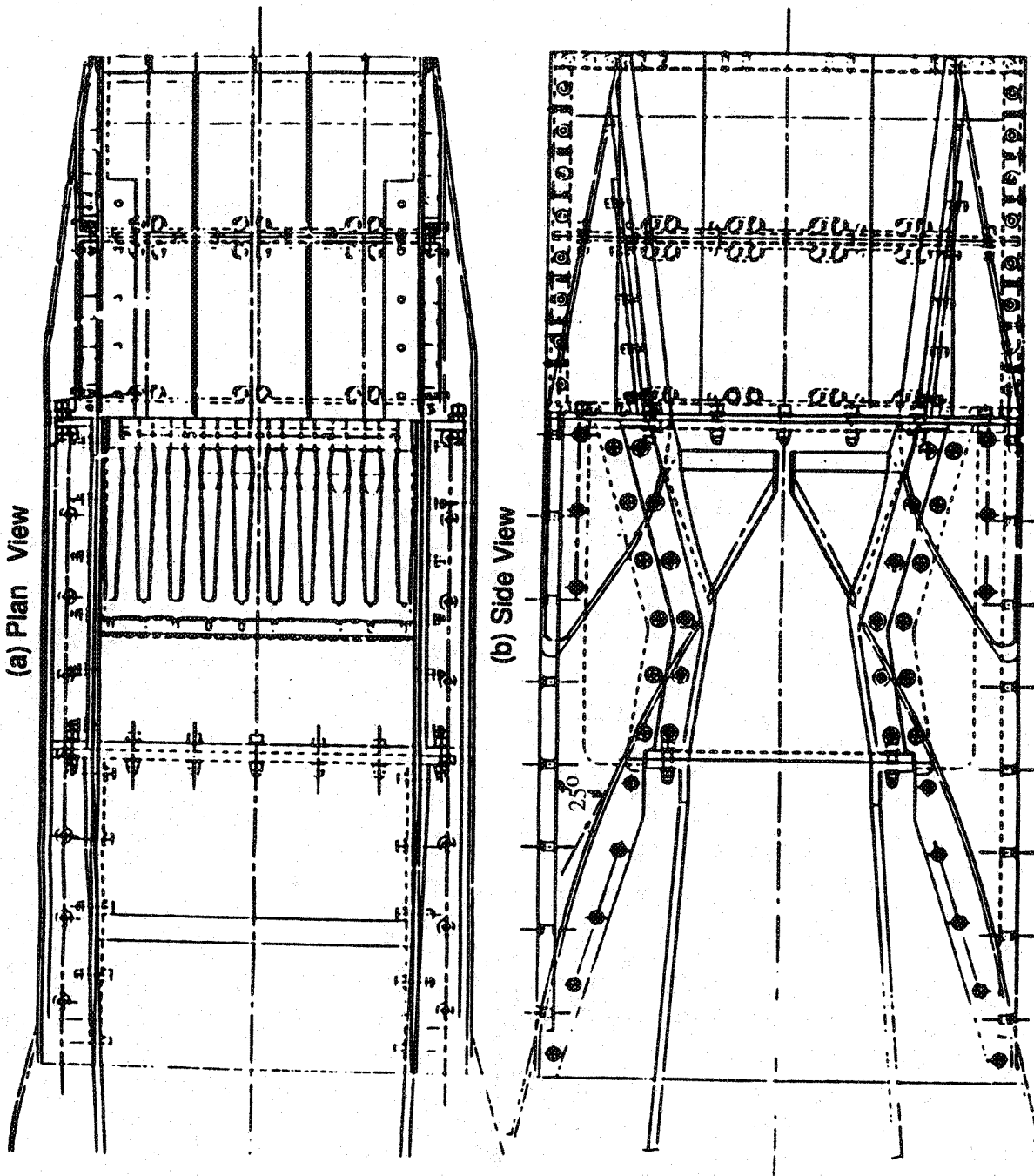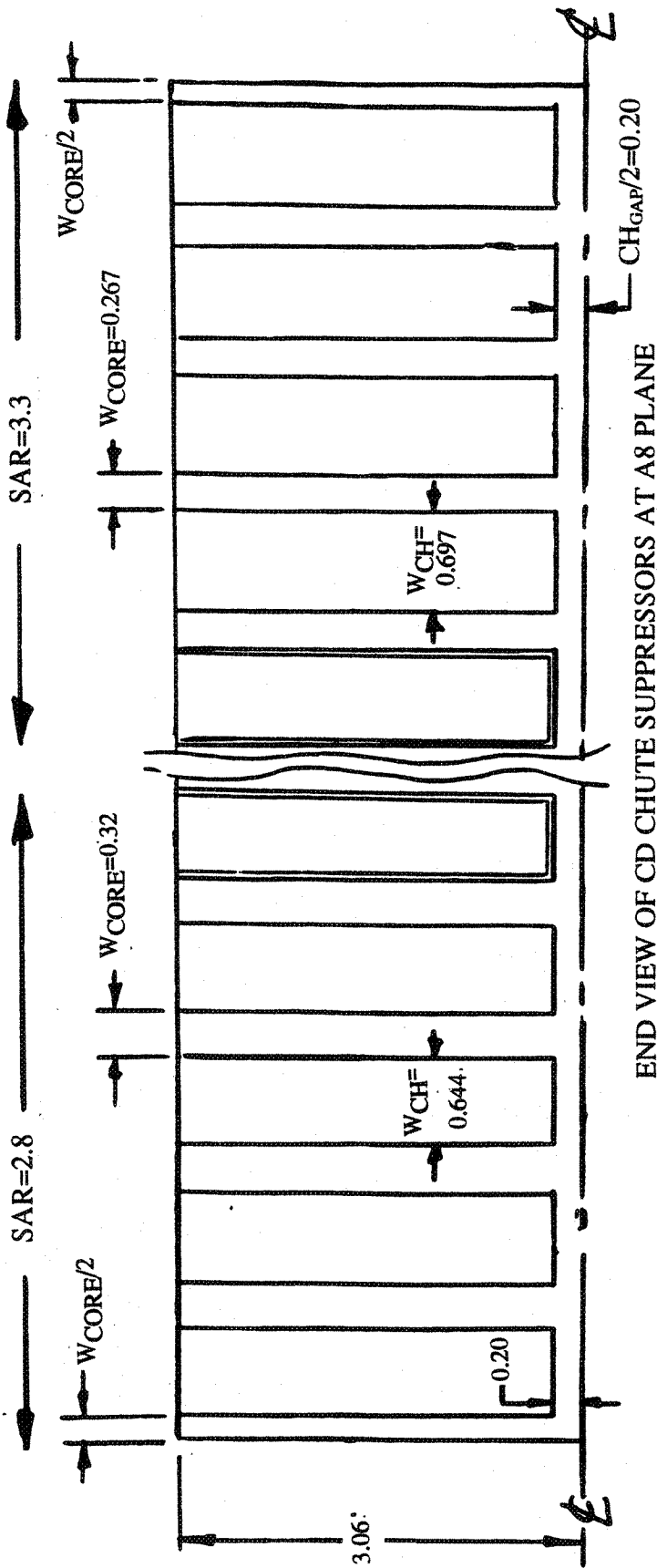Figure 3-1. 2D acoustic model system adapted to GEAE Cell 41.

(a) Plan View

(b) Side View

25°

Figure 3-2. Layout of 2D suppressor-ejector nozzle with CD chutes and 80" full scale ejector; SAR=2.8.

END VIEW OF CD CHUTE SUPPRESSORS AT A8 PLANE

1. SAR = Suppressor Area Ratio = $A_{MIX}/A8$
2. LSF = Linear Scale Factor based on a full scale area of 1086 IN^2
3. A8 = Primary stream throat area
4. $D8_{eq}$ = Equivalent diameter for A8
5. A_{SEC} = Total ambient (secondary) flow area
6. $A_{MIX} = A8 + A_{SEC}$
7. W_{CORE} = Width of core element at throat plane
8. W_{CH} = Chute width at throat plane
9. CH_{GAP} = Chute tip-to-tip gap

1	2	3	4	5	6	7	8	9
SAR	LSF	A8, IN^2	$D8_{eq}$, IN	A_{SEC}, IN^2	A_{MIX}, IN^2	W_{CORE}, IN	W_{CH}, IN	CH_{GAP}, IN
2.84	1/7	22.16	5.31	40.67	62.83	0.320	0.644	0.40
3.3	1/7.53	19.14	4.94	44.01	63.15	0.267	0.697	0.40

Figure 3-3. Key geometric and scale factor parameters for CD-chute mixers (all dimensions are in inches).
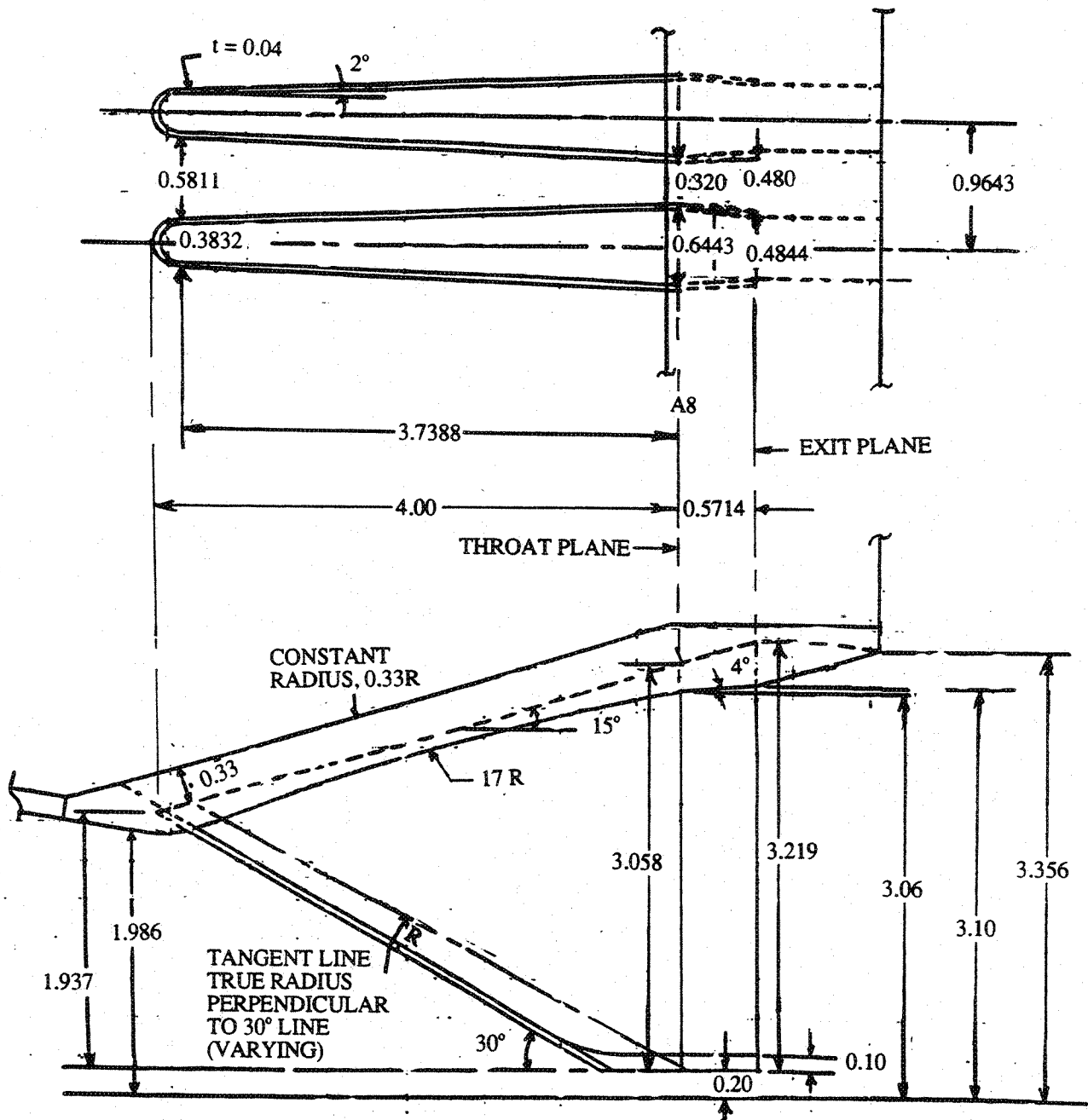
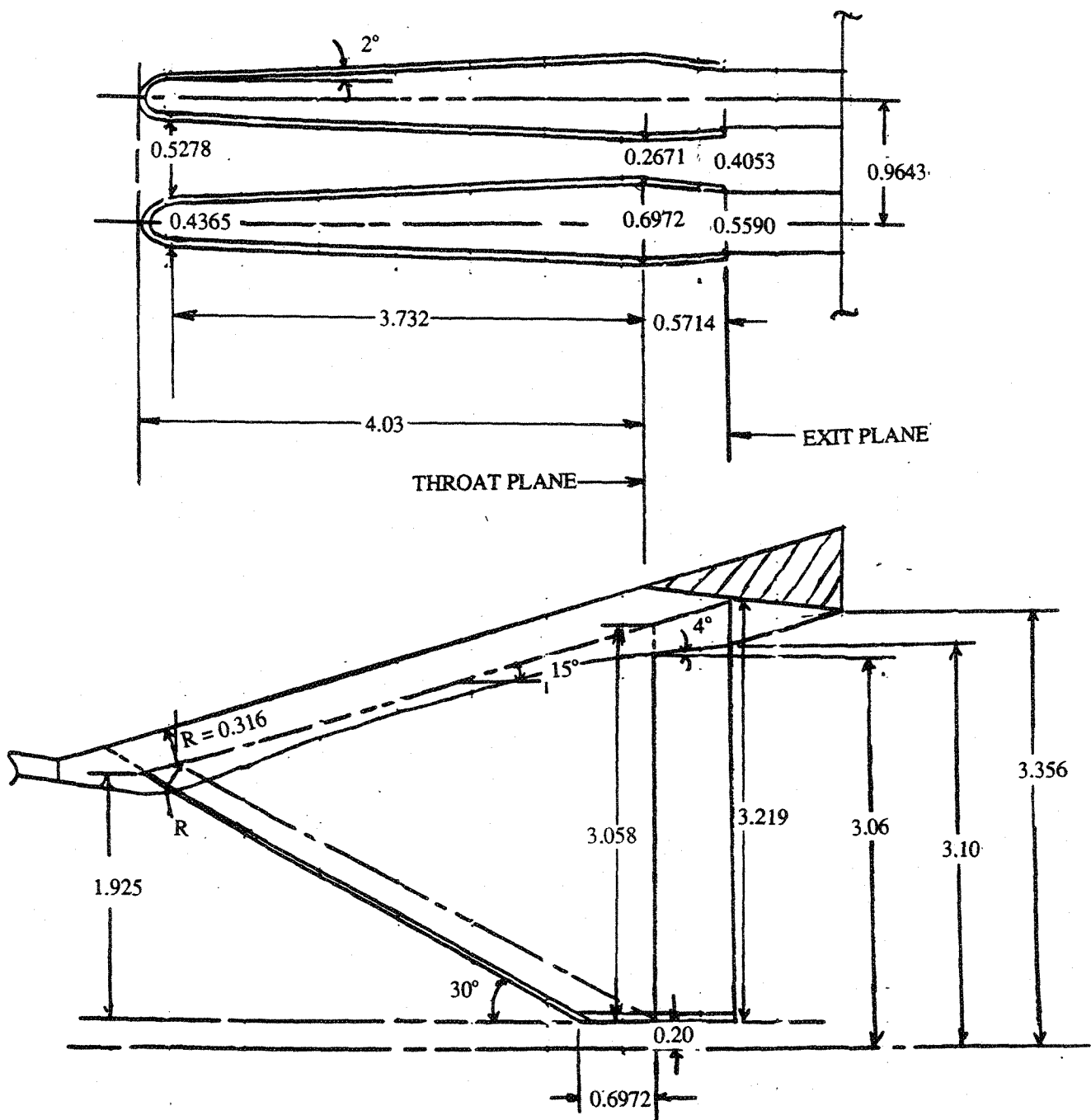Figure 3-4.   Details of SAR=2.8 CD-chute design (all dimensions are in inches).

Figure 3-5. Details of SAR=3.3 CD-chute design (all dimensions are in inches).

design. Figure 3-6 shows an isometric view of the convergent chute rack. The various geometric parameters for the convergent chute design, are shown in Figure 3-7. Note that the chute exit plane (also the throat plane) for the convergent chute terminates at the throat plane of the SAR 2.8 CD chute rack (see Figures 3-6 & 3-7).

Mixers with Staggered CD Chutes: Two staggered CD chute mixers with SAR of 2.8 were designed and fabricated, and tested under the current program Contract NAS3-26617, Task Order 11 and are interchangeable with the hardware of NAS3-25415. Both the staggered chute nozzle configurations used a new lower rack with the existing SAR 2.8 10 CD chute upper rack. One of the staggered lower chute rack configuration has 9 full cold chutes and two half cold chutes, as shown in Figure 3-8. The 9 full chutes are offset laterally by one-half chute-to-chute period, so that the center of the primary stream on the upper rack is aligned with the center of the secondary stream on the lower rack. A half cold chute is placed on each end of the lower rack. This geometry provides uniform stagger of the cold to hot flow elements while matching the hot and cold flow areas. The second staggered lower chute rack configuration has 9 full cold chutes, as shown in Figure 3-9. When coupled with the upper 10 full CD chute rack, the 9 chute rack provides non-uniform chute stagger, the degree of offset increasing to either side of the nozzle minor axis. As with the aligned CD chute racks, the CD flowpaths for the staggered chute lower racks were designed with a CER of 1.43. The core flow area A8 for these two mixers is also 22.16 in^2. All the staggered chute configurations were tested with the existing ejector system.

Ejector Geometry : The ejector system, acquired under Contract NAS3-25415, used for the current program, has two ejector lengths (L_{EJ}), three position MAR capability, and acoustic treatment area variation. The ejector treatment area is varied by treating the entire ejector system, or the flaps alone, or the side walls alone, or select portion of the ejector surfaces. Bulk absorber treatment material and its density is varied within each tray as the trays are removable and repackable.

The treatment trays are divided into compartments to prevent degradation and/or compaction of treatment throughout the tray and allow for uniform packing, especially for softer materials, like astroquartz.. The treatment trays are designed to be packed with bulk material with a rigid back plate and a perforated facesheet with 37% porosity. The facesheet is made out of Hastalloy with 0.045" hole diameters on a straight line pattern, 0.067" spacing on centers. For hardwalled configurations, sheet metal, 0.026"-0.034"
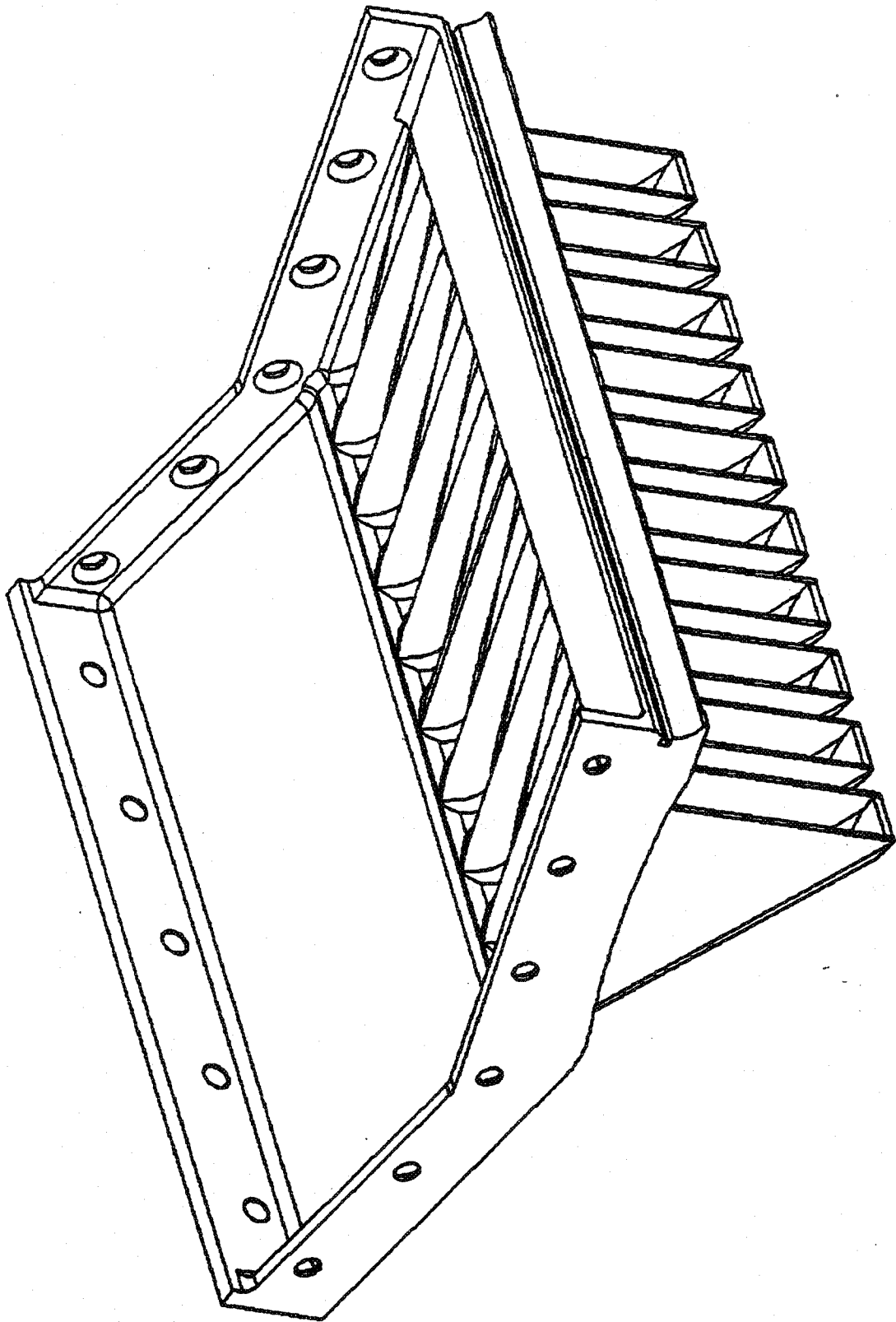
Figure 3-6. Isometric view of the convergent chute 2D mixer model.
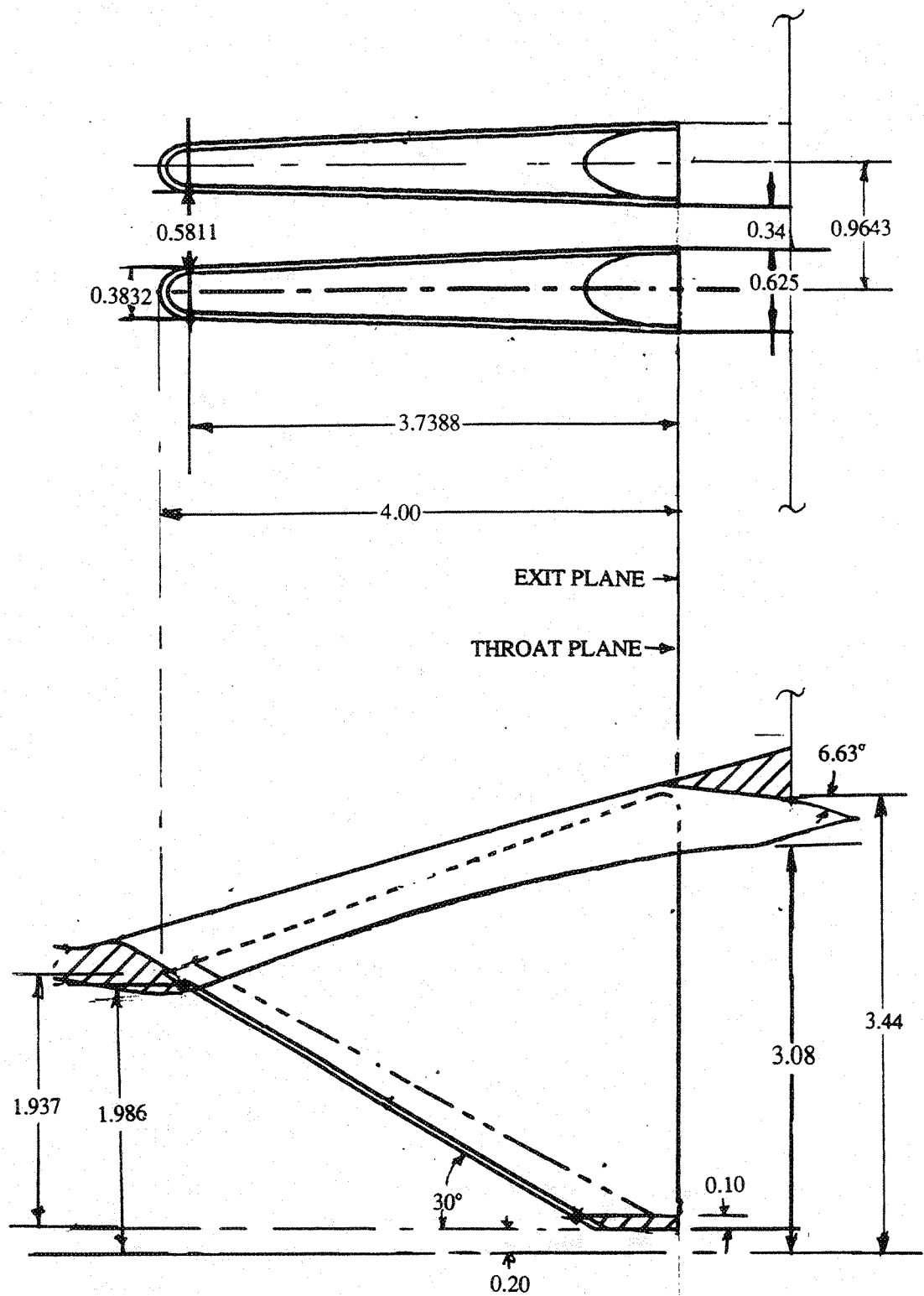
Figure 3-7.   Details of SAR=2.8 convergent-chute design (all dimensions are in inches).
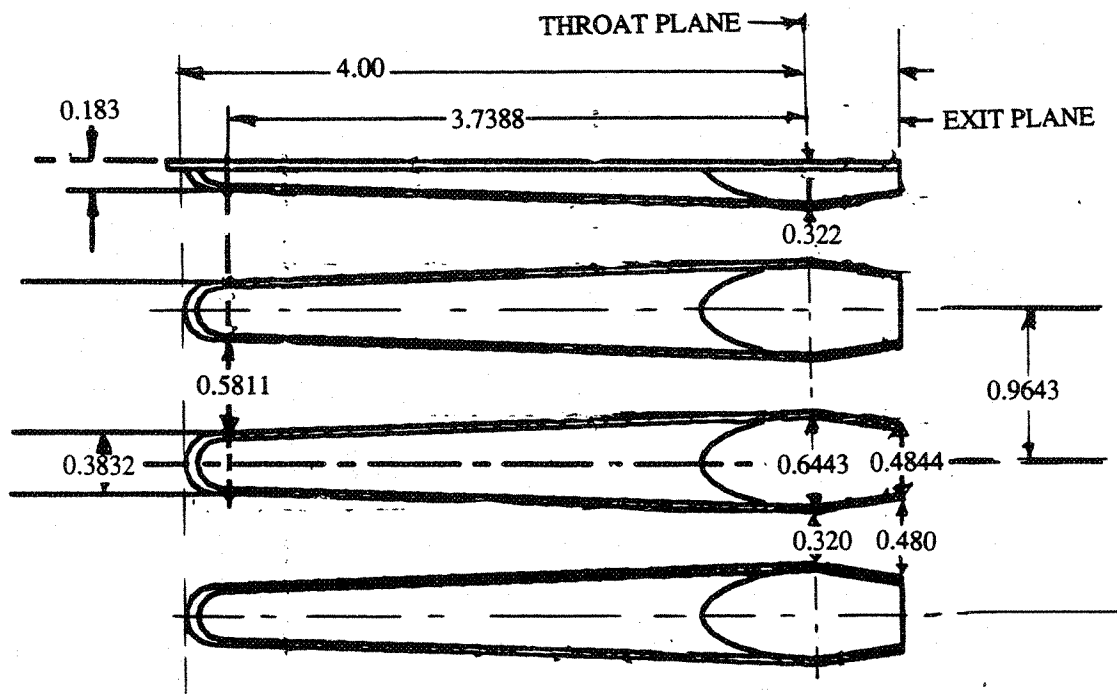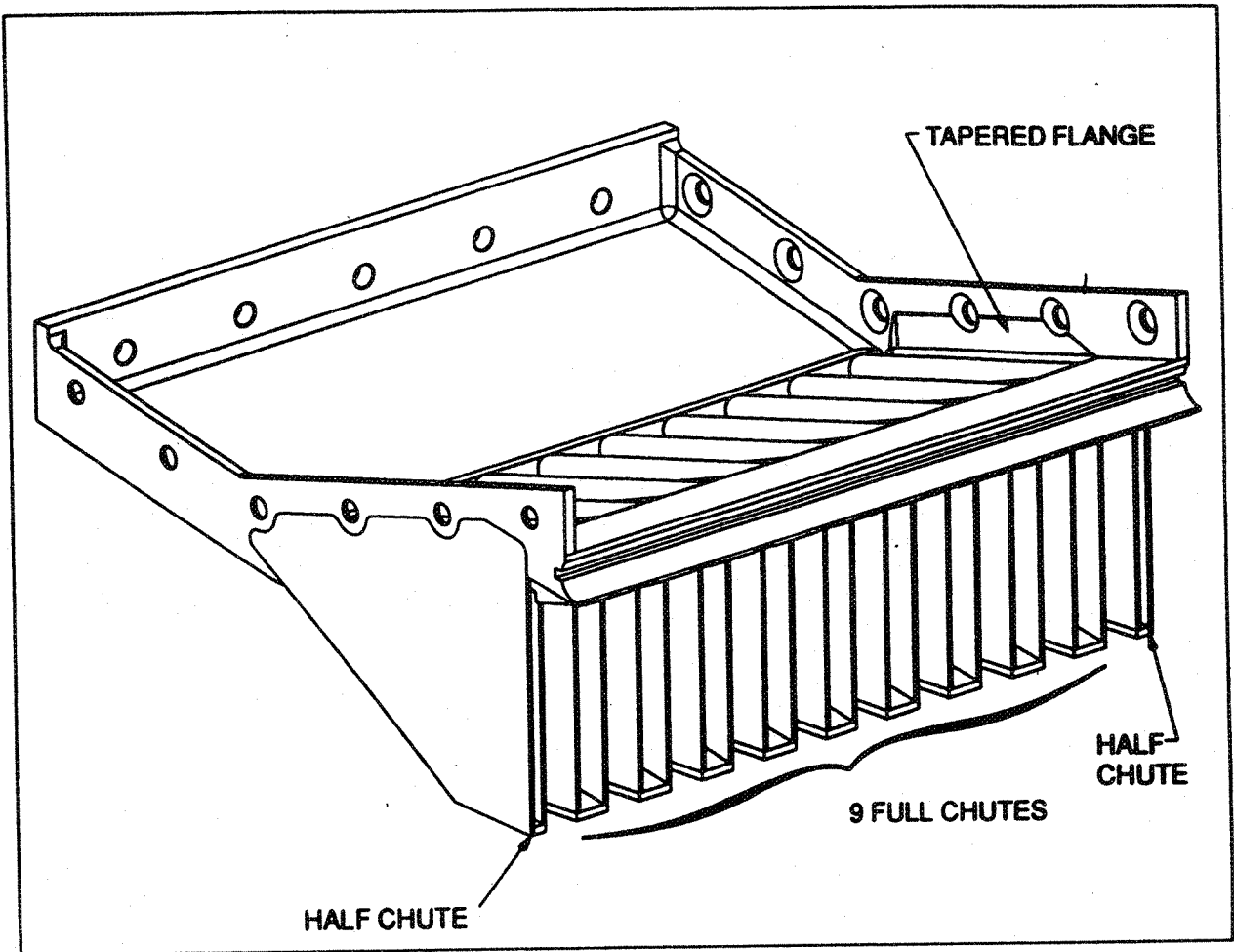
Figure 3-8. Isometric view and the details of SAR=2.8 nine and two halves CD-chute rack design for staggered mixer assembly (all dimensions are in inches).
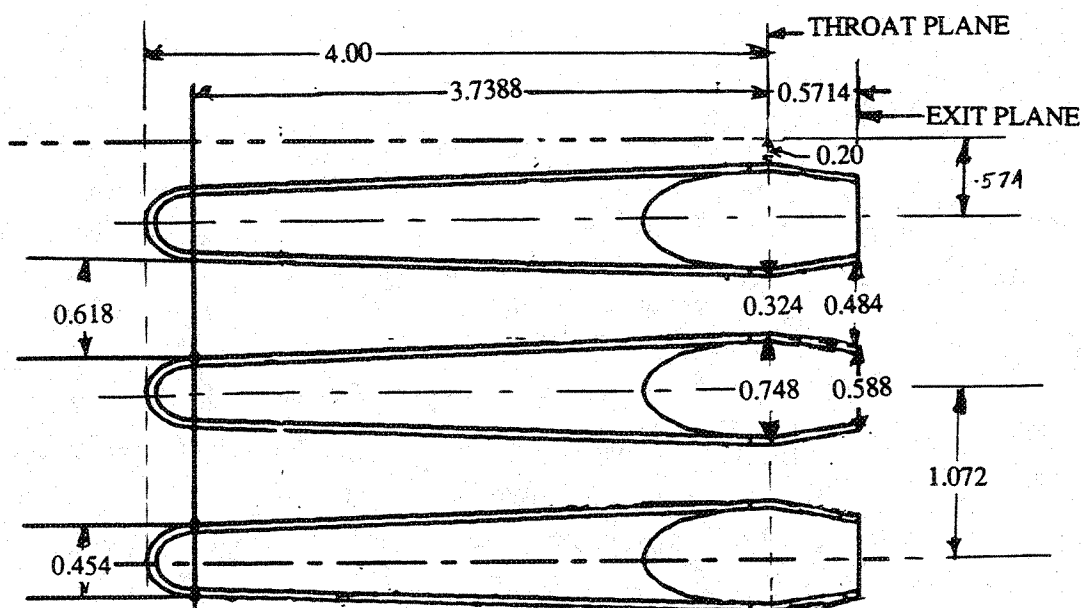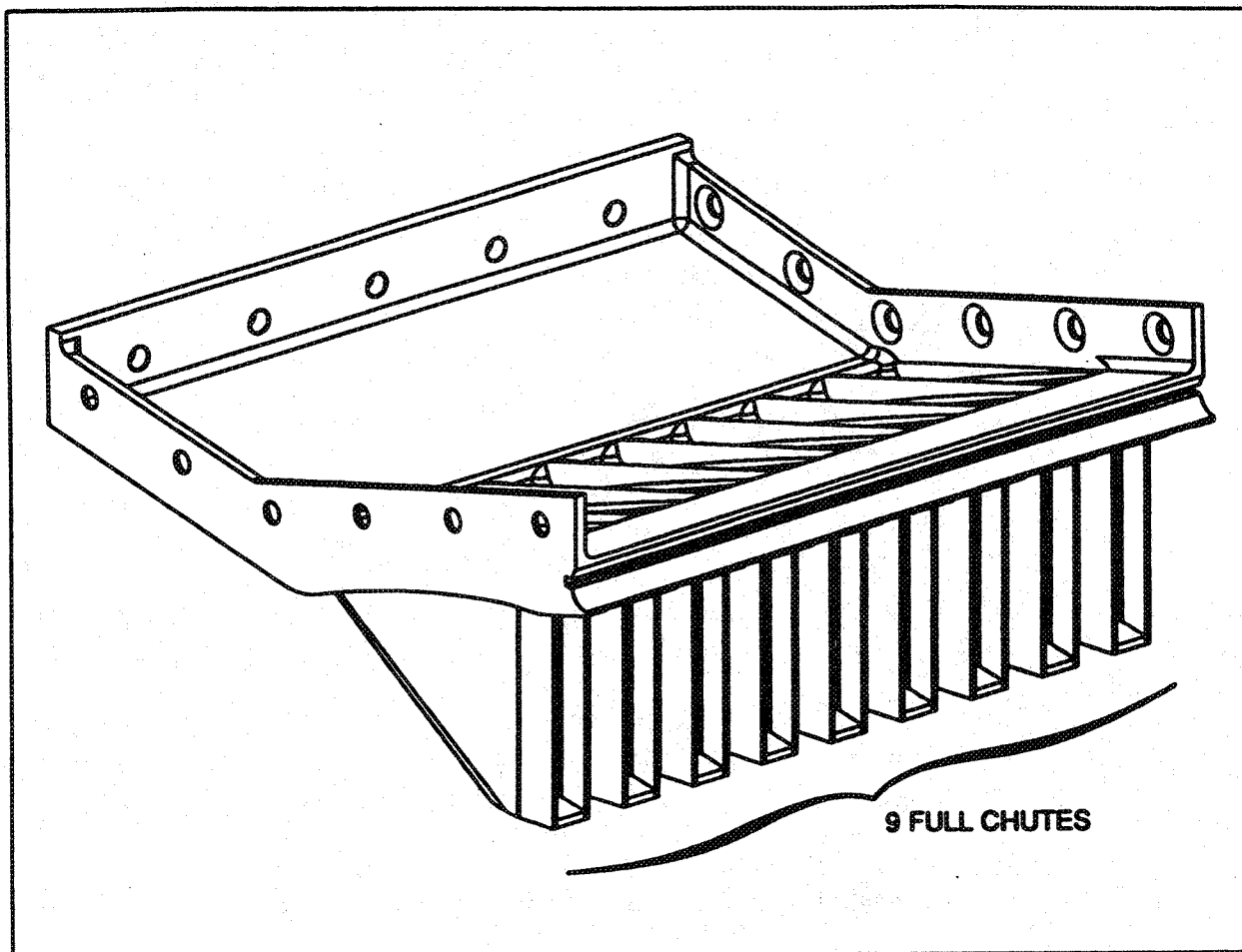
Figure 3-9. Isometric view and the details of SAR=2.8 nine CD-chute rack design for staggered mixer assembly (all dimensions are in inches).

thick, trimmed to fit the tray compartment dimensions, are inserted between perforated facesheet and bulk absorber

Bulk Absorbers: Several bulk absorbers are used to pack the treatment trays under this program. Astroquartz of style 550 mat, 0.0002" maximum fiber diameter, 0.02" thick sheets are compressed inside the treatment tray compartments to a desired density of about 1 lb/ft^3. Retimet metal foam grade 8ONC2, 0.08" thick, 95% porous, 0.03" pore size, is placed over the astroquartz (behind the perforated facesheet) to protect the astroquartz from degradation due to flow turbulence. This treatment was used only for the aligned mixer configurations for verifying repeatability.

A nickel based foam metal, 0.5" thick, is used in most of the configurations. In addition, a silicon carbide (SiC) foam with 100 ppi is also used in one configuration. SiC foam was jointly selected by the EPM and acoustic teams after a series of screening tests for impedance, density, structural strength, sonic environment, etc. Foam metal and SiC foam are cut to fit snugly into the treatment trays and are held in place by the perforated facesheet on the top.

Fin Across the Secondary Flow Inlet : According to conceptual installation studies by Boeing a fin structure across the ejector inlet of the mixer-ejector may be required to support the mixer-ejector nozzles, particularly in the out-board locations due to reduced thickness of wing spar. To get a preliminary assessment of the effect of the fin on the farfield noise and the flow entrainment a 1/7th scale model fin (based on the conceptual design of fin by Boeing) was designed to fit the existing 2D mixer-ejector nozzle hardware, fabricated and tested in Cell 41. Figure 3-10 is a photographic view of the fin attached to the 2D mixer-ejector model in Cell 41 anechoic chamber.

Modified Scab-on Inlet : The basic inlet configuration of the 2D model scale mixer nozzle has a very gentle curvature and is not practical. The inlet for secondary flow has a relatively shallow angle of about 25⁰, shown in Figure 3-2. A more realistic inlet, based on the current 2D fixed chute nozzle preliminary design, has a much smaller inlet length resulting in an ejector inlet angle of about 35⁰, which is relatively steeper compared to Gen 1 design. Aerodynamically, such a steep inlet might cause flow separation and could influence the noise and the performance of the nozzle. Before finalizing the Gen 2 design it is essential to assess the impact of the new inlet design on acoustics and ejector flowfields.
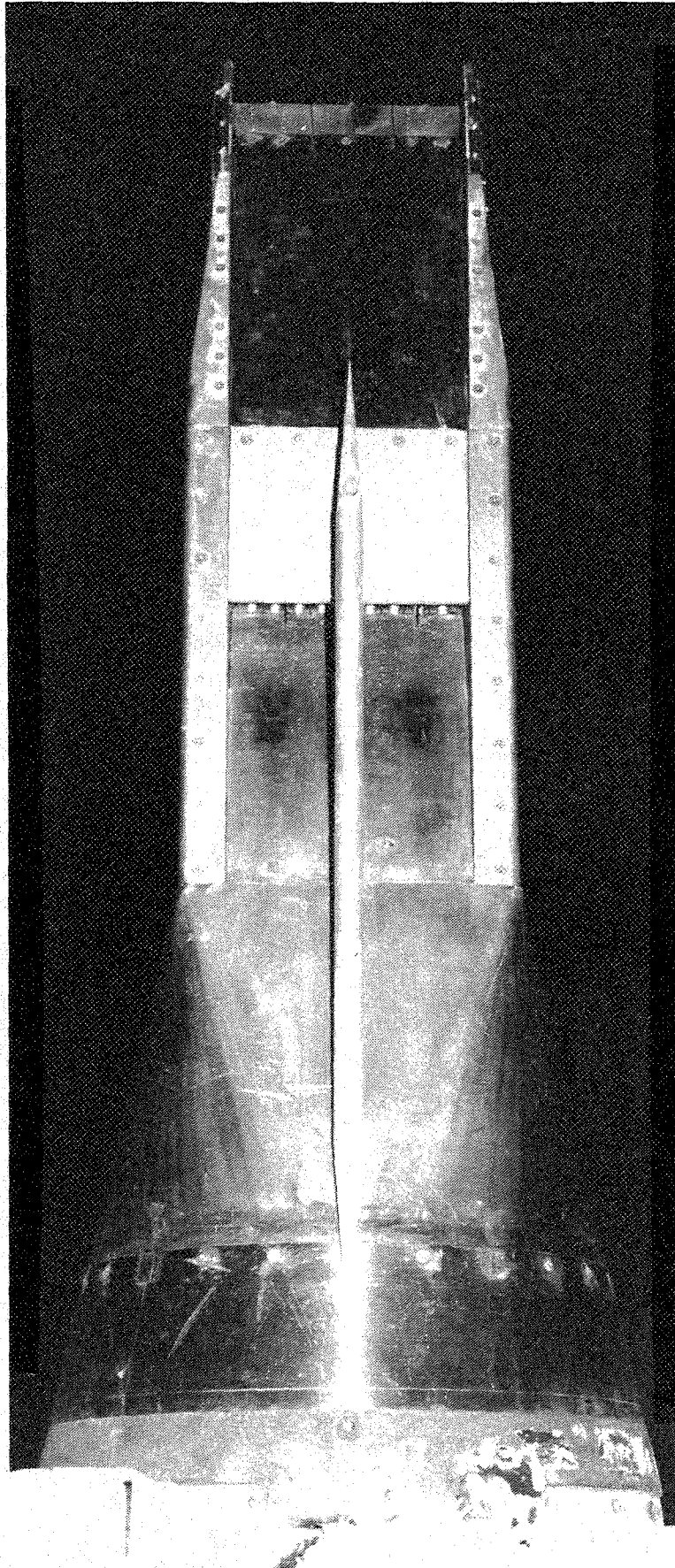
Figure 3-10. Top view of the fin mounted across the 2D mixer-ejector nozzle inlet.

To facilitate this objective a scab-on inlet adapter with 35º inclination was designed and fabricated, which was installed on the existing inlet of Gen 1 scale model nozzle configuration and tested. Figure 3-11 shows the side view of the modified inlet compared to the existing original inlet ramp.

3.2 ACOUSTIC TEST MATRIX

The acoustic test matrix is constructed around the GE21/F14 study L1M cycle (VCE) for the M2.4 HSCT. This is representative engine cycle for dry power (i.e., power code 50). The set of test conditions used for the current test program is shown in Table 3-1 and Figure 3-12. The test points are defined in terms of NPR, T8, and the corresponding ideal jet velocity V_j. Points 1, 68, and 2 through 7 are on the L1M cycle line. The points are nominally selected at even increment of NPR, except for point 68 and 5. The point 68 gives an intermediate ideal jet velocity of 1400 ft/sec at the lower limit of L1M cycle. Point 5 yields a V_j of 2384 ft/sec, which is a typical takeoff velocity with partial PLR. Point 7 is the maximum dry condition for the L1M cycle. Point 8 is on a projected L1M cycle line to obtain acoustic data at maximum jet velocity of possible interest, to evaluate nozzle suppression characteristics along a continuously uniform NPR/T8 line. Point 9 is on the F404-400 cycle line and has the same NPR (i.e., 3.4) of L1M cycle point 5. The T8 for point 9 is slightly higher than that of point 5. This point is chosen to match with the F404-400 cycle for future cycle trade studies.

A mode switch study was performed to quantify its effect on acoustic characteristics of the nozzle. Between the two consecutive L1M points, where a mode switch occurs, several tests were conducted with 0.1 NPR increment to assess the transition NPR. Several tests were conducted by decreasing the NPR in step of 0.1 starting from condition of supersonic mode, until the ejector transitions back to the subsonic mode. This would provide hysteresis influences on acoustics and flowfield.

Several tests for a few selected configurations were conducted to study the effect of temperature (i.e., jet density) on noise and to assess internal and external noise components radiated from the nozzle. For this study, several aerothermodynamic conditions were employed at a fixed jet velocity V_j. In addition, tests were conducted at
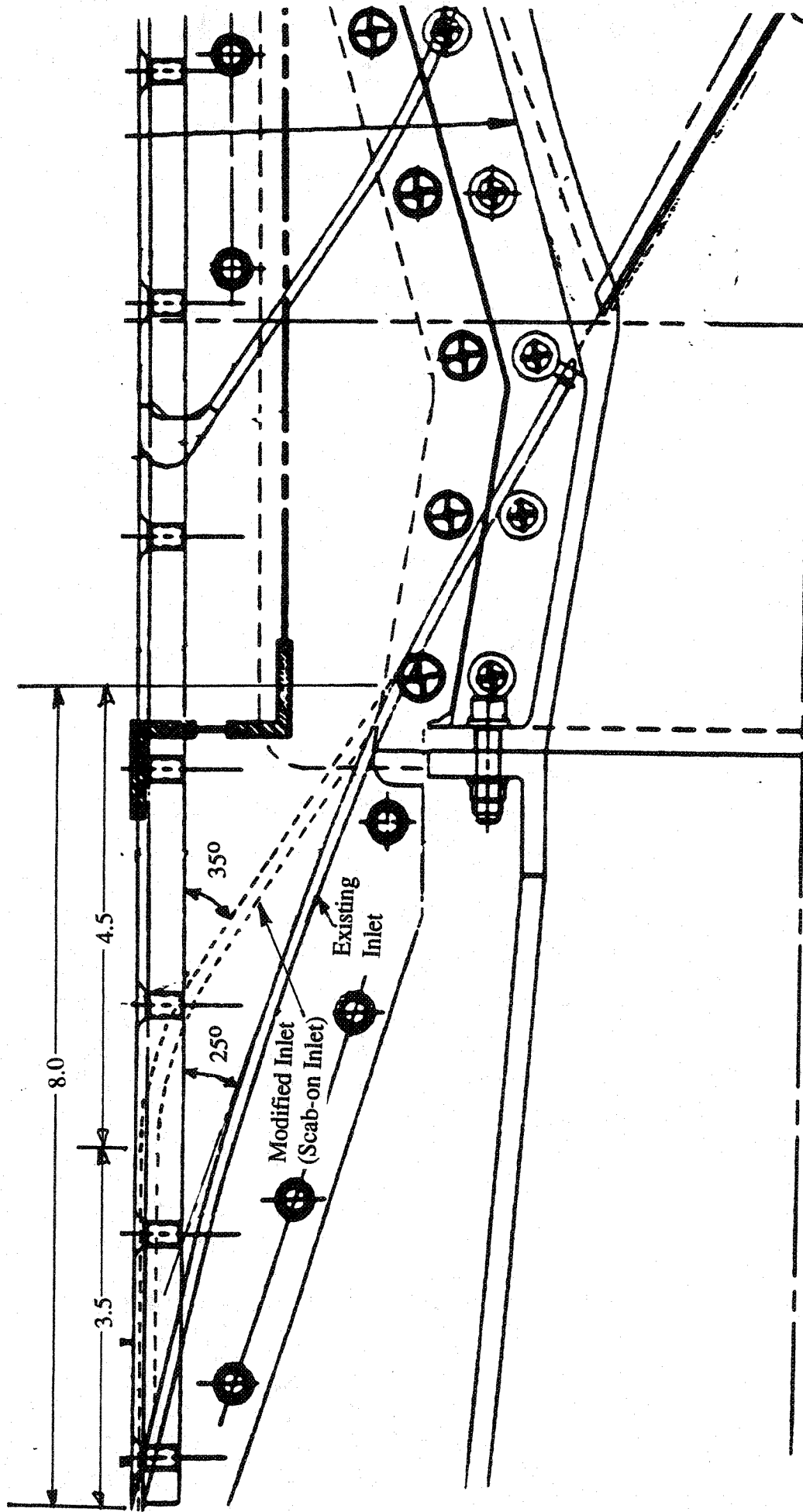
Figure 3-11. A modified inlet (or scab-on inlet) simulating the Gen 2 design used on the existing 2D model scale mixer-ejector nozzle (dimensions are in inches).

Table 3-1. Test point definition for L1M & F404-400 cycles

Test Point	NPR	T8 °R	V_j ft/sec.
1	1.5	1000	1147
68	1.75	1102	1400
2	2.0	1175	1595
3	2.5	1325	1919
4	3.0	1485	2200
5	3.4	1590	2384
6	4.0	1750	2637
7	4.5	1860	1812
8	5.0	1960	2968
9	3.4	1645	2426

Table 3-2. Test point definition for temperature and density study

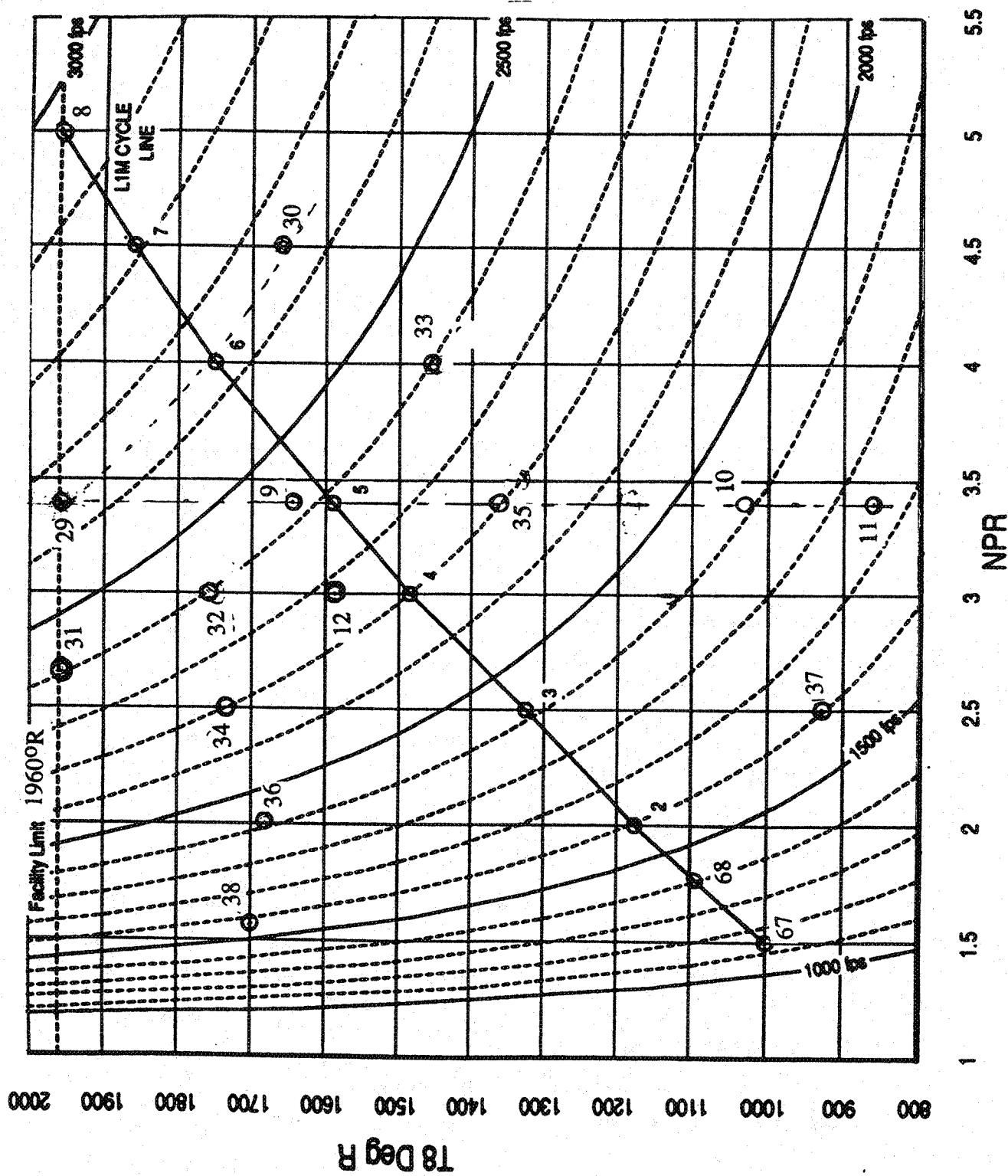| Test Point	NPR	T8 °R	V_j ft/sec	NOMINAL V_j ft/sec.
67	1.5	1486	1400	1400
68	1.75	1102	1400	
38	1.6	1666	1590	1590
69	1.75	1418	1590	
2	2.0	1175	1595	
70	2.25	1016	1590	
37	2.5	913	1590	
36	2.0	1693	1920	1920
3	2.5	1325	1919	
10	3.4	1038	1920	
71	2.3	1881	2200	2200
34	2.5	1732	2200	
4	3.0	1485	2200	
35	3.4	1359	2200	
31	2.75	1863	2384	2384
32	3.0	1738	2384	
5	3.4	1590	2384	
33	4.0	1438	2384	

Figure 3-12. Aerothermodynamic conditions for acoustic tests for 2D mixer-ejector nozzles in terms of nozzle pressure ratio (NPR) and total temperature (T8) with constant ideal jet velocity lines.

fixed NPR by varying T8 and vice versa. The test points for this study are defined in Table 3-2 and in Figure 3-12.

For a few selected configurations internal dynamic pressure was measured using a fiber optic probe. For these tests the total temperature of the primary stream was set at 1360°R due to the temperature limitation of the probe. The NPR for these tests were varied from 1.4 to 4.8 at a step of 0.2.

3.3   ACOUSTIC TEST CONFIGURATIONS

Acoustic testing in Cell 41 was conducted for five basic mixer configurations, namely, two aligned CD chute mixers of SAR 2.8 and 3.3, an aligned convergent chute mixer with SAR= 2.8, and two staggered CD chute mixers with SAR=2.8. With the variation of treatment type, treatment area, treatment thickness, ejector length, modifications at the secondary inlet, and the above listed five mixer geometry, 25 different configurations, as listed in Table 3-3, were tested. All the model configurations were oriented in Cell 41 (see Figure 3-13), such that the acoustic data could be acquired for both community and sideline locations. The community location with respect to minor axis (i.e., $\phi=0°$) is not attainable due to microphone tower positioning limitation. However, the tower could be positioned at $\phi=4°$ instead of $\phi=0°$. Thus, the acoustic data measured at $\phi=4°$ is used for community location with respect to minor axis. For some configurations measurements were made at all these four azimuthal locations and for most cases the community and sideline data were acquired, only, with respect to the major axis (this refers to ejector inlets in top-bottom orientation on the aircraft).

Configurations 1 and 2: Configurations 1 and 2 are the aligned CD chute mixers of SAR 3.3 and 2.8, respectively, with long fully treated (with astroquartz) ejector. Acoustic data was acquired along L1M cycle line for static and simulated flight conditions of Mach 0.12, 0.24, and 0.32 at community and sideline points with respect to both major and minor axis of the ejector. These data were obtained to verify the repeatability of the acoustic results obtained earlier (under Contract NAS3-25415). In addition, the data will also support HEAT (High-lift Engine Aeroacoustic Test) nozzle testing in the NASA Ames Research Center 40'x 80' acoustic wind tunnel. A mode-switch study was also conducted for these configurations.

Table 3-3. Matrix for 2D mixer-ejector nozzle tests in cell 41 (Contd.)

CONFIG NO #	CONFIGURATION DEFINITION				TEST CONDITION	REMARKS
	CHUTE TYPE	SAR	FULL SCALE FLAP LENGTH	TREATMENT TYPE		
1	CD ALIGNED	3.3	120"	ASTROQUARTZ	L1M CYCLE, M_F=0,.12,.24,.32	SIDELINE & COMMUNITY WRT MAJOR & MINOR AXES, MODE SWITCH STUDY
2	CD ALIGNED	2.8	120"	ASTROQUARTZ	L1M CYCLE, M_F=0,.12,.24,.32	SIDELINE & COMMUNITY WRT MAJOR & MINOR AXES, MODE SWITCH STUDY
21	CD ALIGNED	2.8	120"	FOAM METAL	L1M CYCLE, M_F=0,.12,.24,.32	SIDELINE & COMMUNITY WRT MAJOR & MINOR AXES, MODE SWITCH STUDY
3	CONVERGENT ALIGNED	2.8	120"	FOAM METAL	L1M CYCLE, M_F=0 & 0.32	SIDELINE & COMMUNITY WRT MAJOR AXIS ONLY, MODE SWITCH STUDY
4	CONVERGENT ALIGNED	2.8	120"	HARD WALL	L1M CYCLE, M_F=0 & 0.32	SIDELINE & COMMUNITY WRT MAJOR AXIS ONLY, MODE SWITCH STUDY
5	CONVERGENT ALIGNED	2.8	80"	FOAM METAL	L1M CYCLE, M_F=0 & 0.32	SIDELINE & COMMUNITY WRT MAJOR AXIS ONLY, MODE SWITCH STUDY
6	CONVERGENT ALIGNED	2.8	80"	HARD WALL	L1M CYCLE, M_F=0 & 0.32	SIDELINE & COMMUNITY WRT MAJOR AXIS ONLY, MODE SWITCH STUDY
7	9 & 2-Half CD STAGGERED	2.8	120"	FOAM METAL	L1M CYCLE, M_F=0 & 0.32	SIDELINE & COMMUNITY WRT MAJOR AXIS ONLY, MODE SWITCH STUDY
8	9 & 2-Half CD STAGGERED	2.8	120"	HARD WALL	L1M CYCLE, M_F=0 & 0.32	SIDELINE & COMMUNITY WRT MAJOR AXIS ONLY, MODE SWITCH STUDY
9	9 & 2-Half CD STAGGERED	2.8	80"	FOAM METAL	L1M CYCLE, M_F=0 & 0.32	SIDELINE & COMMUNITY WRT MAJOR AXIS ONLY, MODE SWITCH STUDY
10	9 & 2-Half CD STAGGERED	2.8	80"	HARD WALL	L1M CYCLE, M_F=0 & 0.32	SIDELINE & COMMUNITY WRT MAJOR AXIS ONLY, MODE SWITCH STUDY
11	9 CD STAGGERED	2.8	120"	FOAM METAL	L1M CYCLE, M_F=0,.24,.32,.36 TEMP EFFECT	SIDELINE & COMMUNITY WRT MAJOR AXIS ONLY, MODE SWITCH STUDY, INTERNAL DYNAMIC PRESSURE MEASUREMENT
12	9 CD STAGGERED	2.8	120"	HARD WALL	L1M CYCLE, M_F=0 & 0.32	SIDELINE & COMMUNITY WRT MAJOR AXIS ONLY, MODE SWITCH STUDY, INTERNAL DYNAMIC PRESSURE MEASUREMENT
13	9 CD STAGGERED	2.8	80"	FOAM METAL	L1M CYCLE, M_F=0 & 0.32	SIDELINE & COMMUNITY WRT MAJOR AXIS ONLY, MODE SWITCH STUDY
14	9 CD STAGGERED	2.8	80"	HARD WALL	L1M CYCLE, M_F=0,.24,.32,.36 TEMP EFFECT	SIDELINE & COMMUNITY WRT MAJOR AXIS ONLY, MODE SWITCH STUDY

Table 3-3. Matrix for 2D mixer-ejector nozzle tests in cell 41 (Concluded)

| CONFIG NO #	CONFIGURATION DEFINITION				TEST CONDITION	REMARKS
	CHUTE TYPE	SAR	FULL SCALE FLAP LENGTH	TREATMENT TYPE		
16	9 CD STAGGERED	2.8	120"	FOAM METAL 4/9-EJECTOR AREA FROM EXIT	L1M CYCLE, M_F=0 & 0.32	SIDELINE & COMMUNITY WRT MAJOR AXIS ONLY, TREATMENT STUDY
17	9 CD STAGGERED	2.8	120"	FOAM METAL 4/9-EJECTOR AREA CLOSER TO MIXER EXIT	L1M CYCLE, M_F=0 & 0.32	SIDELINE & COMMUNITY WRT MAJOR AXIS ONLY, TREATMENT STUDY
18	9 CD STAGGERED	2.8	120"	0.3"-THICK FOAM METAL 7/9-EJECTOR AREA	L1M CYCLE, M_F=0 & 0.32	SIDELINE & COMMUNITY WRT MAJOR AXIS ONLY, TREATMENT STUDY
19	9 CD STAGGERED	2.8	120"	FOAM METAL FLAPS ONLY	L1M CYCLE, M_F=0 & 0.32	SIDELINE & COMMUNITY WRT MAJOR AXIS ONLY, TREATMENT STUDY
20	9 CD STAGGERED	2.8	120"	0.2"-THICK FOAM METAL 7/9-EJECTOR AREA	L1M CYCLE, M_F=0 & 0.32	SIDELINE & COMMUNITY WRT MAJOR AXIS ONLY, TREATMENT STUDY
22	9 CD STAGGERED	2.8	120"	SILICON CARBIDE FOAM	L1M CYCLE, M_F=0 & 0.32	SIDELINE & COMMUNITY WRT MAJOR AXIS ONLY, TREATMENT STUDY
23	9 CD STAGGERED	2.8	120"	FOAM METAL BOAT TAIL LIMITED CONFIG. (≈7/9 EJECTOR AREA)	L1M CYCLE, M_F=0 & 0.32	SIDELINE & COMMUNITY WRT MAJOR AXIS ONLY, TREATMENT STUDY
24	9 CD STAGGERED WITH MODIFIED INLET	2.8	120"	FOAM METAL (≈7/9 EJECTOR AREA)	L1M CYCLE, M_F=0 & 0.32	SIDELINE & COMMUNITY WRT MAJOR AXIS ONLY, MODE SWITCH STUDY
25	9 CD STAGGERED WITH FIN ACROSS INLET	2.8	120"	FOAM METAL (≈7/9 EJECTOR AREA)	L1M CYCLE, M_F=0 & 0.32	SIDELINE & COMMUNITY WRT MAJOR AXIS ONLY, MODE SWITCH STUDY
26	9 CD STAGGERED WITH MODIFIED INLET & FIN ACROSS IT	2.8	120"	FOAM METAL (≈7/9 EJECTOR AREA)	L1M CYCLE, M_F=0 & 0.32	SIDELINE & COMMUNITY WRT MAJOR AXIS ONLY, MODE SWITCH STUDY
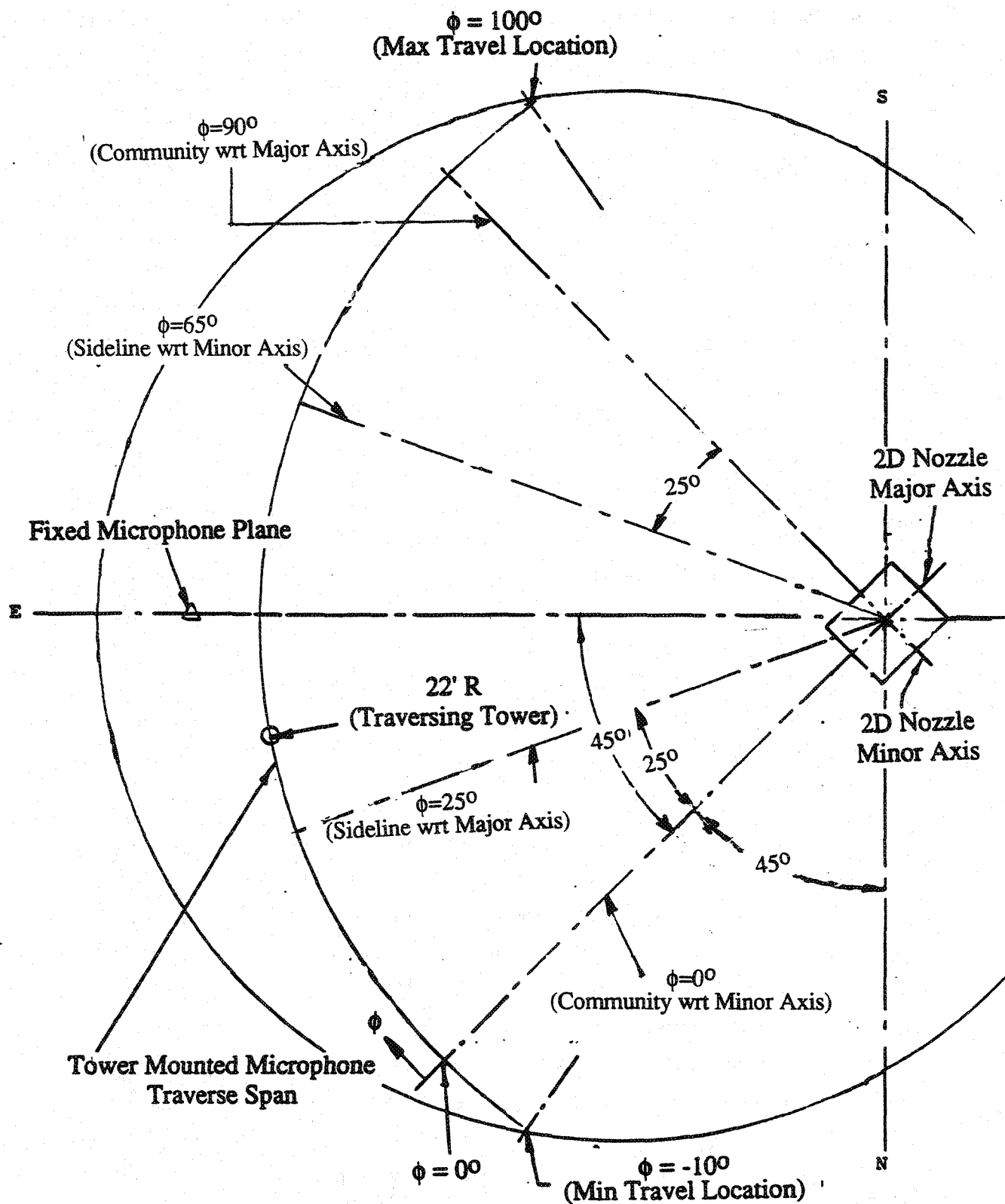
Figure 3-13. Plan view of Cell 41 Anechoic Freejet Facility showing 2D nozzle orientation for acoustic measurements at community (i.e., $\phi = 90°$ and $\phi = 0°$) and sideline (i.e., $\phi = 25°$ and $\phi = 65°$) planes with respect to both major and minor axes.

Configuration 21: Until this test series, the treatment used in the ejector was Astroquartz, which is a soft cotton-like material and consists of quartz fibers. During the testing this material usually gets deteriorated and also gets packed unevenly in the treatment trays. Therefore, frequently, the treatment trays are repacked, which involves more effort and could change acoustic properties of the treatment between and during tests. To avoid these issues a nickel based foam metal, which is a rigid porous foam, was used as the ejector treatment for the aligned chute mixer with SAR=2.8. The results are compared with those for configuration 2 to establish the effectiveness of the foam metal treatment. Based on the excellent agreement of the acoustic results between these two configurations, foam metal was used for most of the configurations.

Configurations 3 - 6: Aligned convergent chute mixer was used for configurations 3 through 6. Long ejector of 16.055" (120" full scale) was used for configurations 3 and 4, while short ejector of 11.5" (80" full scale) was used for configurations 5 and 6. Configurations 3 and 5 were fully treated with foam metal bulk absorber, while configurations 4 and 6 employed hard wall ejectors. Acoustic and model surface static pressure data was acquired along the L1M cycle line at community and sideline points with respect to major axis for static and Mach 0.32 simulated flight conditions. Mode switch study was also conducted for these configurations by measuring the acoustic data at the sideline point with respect to major axis at static and Mach 0.32 conditions.

Configurations 7 - 14: Staggered CD chute mixer with 9 full and 2 half chute lower rack and 10 chute upper rack was used for configurations 7 through 10. Staggered CD chute mixer with 9 full chute lower rack and 10 chute upper rack was used for configurations 11 through 14. Long ejector of 16.055" (120" full scale) was used for configurations 7, 8, 11, and 12, while short ejector of 11.5" (80" full scale) was used for configurations 9, 10, 13, and 14. Configurations 7,9, 11, and 13 were fully treated with foam metal bulk absorber, while configurations 8, 10, 12, and 14 used hard wall ejectors. Acoustic and model surface static pressure data was acquired for configurations 7, 8, 9, 10, 12, and 13 along the L1M cycle line at community and sideline points with respect to major axis for static and Mach 0.32 simulated flight conditions. Mode switch study was also conducted for these configurations by measuring the acoustic data at the sideline point with respect to major axis at static and Mach 0.32 conditions.

In addition, the configurations 11 and 14 were used to study the effect of jet density. Acoustic and model static pressure data was acquired for these configurations along the L1M cycle line at community and sideline points and at aerothermodynamic points defined in Table 3-2 at sideline point only with respect to major axis for static and Mach 0.24, 0.32, and 0.36 simulated flight conditions. Mode switch study was also conducted for these configurations by measuring the acoustic data at the sideline point with respect to major axis at static and Mach 0.24, 0.32, and 0.36 conditions.

Internal dynamic pressures were measured for configurations 11 and 12 by using fiber optic probe at two flap locations, one closer to mixer exit and the other closer to ejector exit, at a fixed primary stream total temperature of 1360°R at several NPR from 1.4 to 4.8 at a step of 0.2 at static condition. Farfield acoustic data and the model surface static pressures were also measured at community and sideline points with respect to major axis simultaneously. These results document changes in internal dynamic environment as well as interpret farfield changes in internal noise characteristics due to ejector length and treatment.

Configurations 16 - 20, 22, and 23: Configurations 16-20, 22, and 23 employed staggered CD chute mixer which has a lower rack with 9 full width cold chutes and an upper rack with 10 full cold chutes. Long ejector of 16.055" (120" full scale) was employed for these configurations for treatment study. Foam metal treatment was used for all configurations except configuration 22. Configurations 23 and 16 had treatment over 7/9th and 4/9th of the total area, respectively, and the results of these tests are compared with those for configuration 11, which was fully treated with foam metal, and also with configuration 12, whose walls were untreated. This comparison would thus assess influence of treatment area on acoustic suppression. Configurations 18 and 20 employed treatment thicknesses of 0.3" and 0.2", respectively, over 7/9th of total area and these results are compared with those for configuration 23 (with 0.5"-thick treatment) to assess the effect of treatment thickness. The effect of treatment location on the acoustic suppression is examined using configuration 17 by treating 4/9th of ejector area starting from the mixer exit plane and compared with the results of configuration 16, for which the same amount of treatment was applied toward the ejector exit. Finally for configuration 22 the long ejector was fully treated with another type of treatment, Silicon carbide (SiC) foam, to examine its effectiveness compared to the nickel based foam metal, used for configuration 11. SiC foam was one of the bulk material that was jointly screened with

EPM team for desirable acoustic and material properties in terms of impedance, density, mechanical strength, sonic fatigue, etc.

Acoustic and model surface static pressure data was acquired for all the configurations along the L1M cycle line. Mode switch study was also conducted for these configurations by measuring the acoustic data at the sideline point with respect to major axis at static and Mach 0.32 conditions.

Configurations 24 - 26: Staggered CD chute mixer with 9 full cold chute lower rack and 10 full cold chute upper rack was used for configurations 24 through 26. Long ejector of 16.055" (120" full scale) with treatment over 7/9th of the total area was used for these configurations. The effect of secondary inlet ramp shape on acoustic and aerodynamic parameters (i.e., pumping, flap static pressures, etc.) were studied by using the modified inlet ramp in configuration 24 and comparing the results with those of configuration 11. A structural fin was installed across the secondary inlet for configurations 25 and 26 with baseline and modified inlet ramps, respectively, and tested to examine its effect on acoustic and aerodynamic parameters. Acoustic and model surface static pressure data was acquired for all these configurations along the L1M cycle line. Mode switch study was also conducted for these configurations by measuring the acoustic data at the sideline point with respect to major axis at static and Mach 0.32 conditions.

3.4 ACOUSTIC DATA NOMENCLATURE AND NORMALIZATION

The farfield acoustic data measured by an array of microphones at an azimuthal location ϕ are analyzed to generate various acoustic parameters as per the flow chart of Figure 3-14. These parameters include Sound Pressure Level (SPL), Sound Power Level (PWL) based on azimuthal uniformity, Overall Sound Pressure level (OASPL), Perceived Noise Level (PNL), Tone corrected Perceived Noise Level (PNLT), and Effective Tone corrected Perceived Noise Level (EPNL). EPNL for static condition is computed using the PNLT values assuming a flight velocity of 360 ft/sec (i.e., M_F=0.32) and is termed as Pseudo EPNL.

Often the noise level parameters are normalized with respect to a reference thrust F_{ref} or with respect to the reference thrust F_{ref} and jet density. These normalization arose out of

```
┌─────────────────────────────────────────────────────────────────┐
│                          Input Data                               │
│       Model Scale Standard Day Data at 40 ft (12.19 m) Arc        │
└─────────────────────────────────────────────────────────────────┘
                               │
                               ▼
┌─────────────────────────────────────────────────────────────────┐
│                      Background Correction                        │
│   Subtract Background Noise Due to Tertiary Flow at each Velocity  │
└─────────────────────────────────────────────────────────────────┘
                               │
                               ▼
            ┌─────────────────────────────────────┐
            │         Flight Transformation        │
            └─────────────────────────────────────┘
                               │
                               ▼
┌─────────────────────────────────────────────────────────────────┐
│                       Convert to Lossless                         │
│      Add Atmospheric Attenuation Δ(f) = α(f)(R)                    │
│                 Where R = Actual Distance, ft.                     │
│  α = Atmospheric Attenuation at Δ(f) for As Measured Day          │
└─────────────────────────────────────────────────────────────────┘
                               │
                               ▼
┌─────────────────────────────────────────────────────────────────┐
│        Extrapolate to 40 ft (i.e., 12.19 m) Arc - Standard Day    │
│     Subtract 20 Log₁₀[40ft (or 12.19 m)/R (Actual Distance)]      │
│  Subtract Atmospheric Attenuation for 40 ft (or 12.19 m) Arc - Standard Day │
│            Δ(f) = α(Standard Day) (f) 40 ft(or 12.19 m)           │
└─────────────────────────────────────────────────────────────────┘
                               │
                               ▼
┌─────────────────────────────────────────────────────────────────┐
│                   Determine Scaled Frequency                      │
│          f(Scaled) = (f(Model Scale))/(Diameter Ratio)            │
│  Diameter Ratio = (Diameter Full Scale)/(Diameter Model Scale)    │
└─────────────────────────────────────────────────────────────────┘
                               │
                               ▼
            ┌─────────────────────────────────────┐
            │            Scale SPL Levels          │
            │     dB = 20 Log₁₀(Diameter Ratio)    │
            └─────────────────────────────────────┘
                               │
                               ▼
┌─────────────────────────────────────────────────────────────────┐
│                   Extrapolate to Arc or Sideline                  │
│            SPL = 20 Log₁₀[R/40 ft (or 12.19 m)]                   │
│  Add Atmospheric Attenuation(Standard Day) = α(Standard Day) (R)  │
└─────────────────────────────────────────────────────────────────┘
                               │
                               ▼
┌─────────────────────────────────────────────────────────────────┐
│                    Output Files (Print & ARD)                     │
│      Untransformed Model Data Corrected for Background Noise       │
│                    Flight Transformed Model Data                   │
│ Flight Transformed Scaled and Extrapolated Data at Desired Arcs and Sidelines │
└─────────────────────────────────────────────────────────────────┘
                               │
                               ▼
┌─────────────────────────────────────────────────────────────────┐
│                          Output Data                              │
│                   Sound Pressure Levels (SPL)                     │
│               Over All Sound Pressure Levels (OASPL)              │
│                  Perceived Noise Levels (PNL)                     │
│                   Sound Power Levels (PWL)                        │
│           Tone Corrected Perceived Noise Levels (PNLT)            │
│      Effective Tone Corrected Perceived Noise Levels (EPNL)       │
└─────────────────────────────────────────────────────────────────┘
```

Figure 3-14. Acoustic data processing flowchart.

establishing velocity dependence of jet noise, using classical Lighthill's scaling laws and the normalization factors are defined as follows:

NF_{th} = Normalization factor with respect to thrust = $-10 \, Log \, ((FG)_i/F_{ref})$, dB

NF = Total normalization factor with respect to thrust and density

$$= -10 \, Log \, ((FG)_i/F_{ref}) \, (\rho/\rho_o)^{\omega-1}, \, dB$$

where,

F_{ref} = Reference Gross Thrust, 60000 lbs

ρ = Jet density based on isentropic expansion of primary stream

ρ_o = Ambient Density of Air

$(FG)_i$ = ideal gross thrust in lbs

ω = Density exponent, 2 for high velocities

Note that the value of F_{ref} = 60,000 lbs is chosen for these studies, which is a typical value for the full scale engine thrust at takeoff for an HSCT.

4.0 ACOUSTIC AND AERODYNAMIC DATA ANALYSIS FOR DIFFERENT MULTI-CHUTE MIXER CONFIGURATIONS

The current test program covers five basic mixer configurations, namely, two aligned CD chute mixers of SAR 2.8 and 3.3, an aligned convergent chute mixer with SAR= 2.8, and two staggered CD chute mixers with SAR=2.8. The aligned CD chute mixers were tested with fully treated long (i.e., 16.055") ejector. Astroquartz was used as the bulk treatment for the SAR 3.3 mixer. However, the aligned CD chute mixer with SAR=2.8 was tested with astroquartz as well as with a nickel based foam metal as ejector treatments.

Each of the convergent chute and staggered CD chute mixers was tested with two different ejector lengths, 16.055" and 11.5". Each of these ejectors was tested with and without acoustic treatment. For treated configurations, the entire ejector, flaps and side walls, were treated with the nickel based foam material with a 37% open perforated facesheet. Acoustic and performance related results for each mixer configuration are presented in this section indicating the influence of treatment, ejector length, and flight simulation on these characteristics for the fixed mixer geometry. In addition, the influence of the mixer geometry on acoustic and performance related parameters is also included in this section.

4.1 ALIGNED CD-CHUTE MIXER CONFIGURATIONS:

The CD chute mixers with SAR=3.3 and 2.8, used for the present configuration, has 20 aligned CD chutes and has throat areas of 19.14 and 22.16 square inches (A8), respectively. The side view of the aligned CD chute mixer-ejector is shown in Figure 4.1-1. The isometric view of the 20 CD chute aligned mixer configuration for SAR=2.8 is shown in Figure 4.1-2.

Instrumentation : Each mixer nozzle has 21 static pressure taps (Ps) and 4 skin thermocouples. The flap and the secondary inlet contain 51 static pressure taps, 24 total pressure taps, and 12 skin thermocouples. Flap static pressure taps are used to identify the flow characteristics in the ejector. The secondary inlet total pressure taps are used to evaluate the secondary flow rate.

The various components of the mixer-ejector nozzle, namely, the ramp, the inlet flow guide, the chute, and the flap surfaces, are instrumented with static pressure taps. The
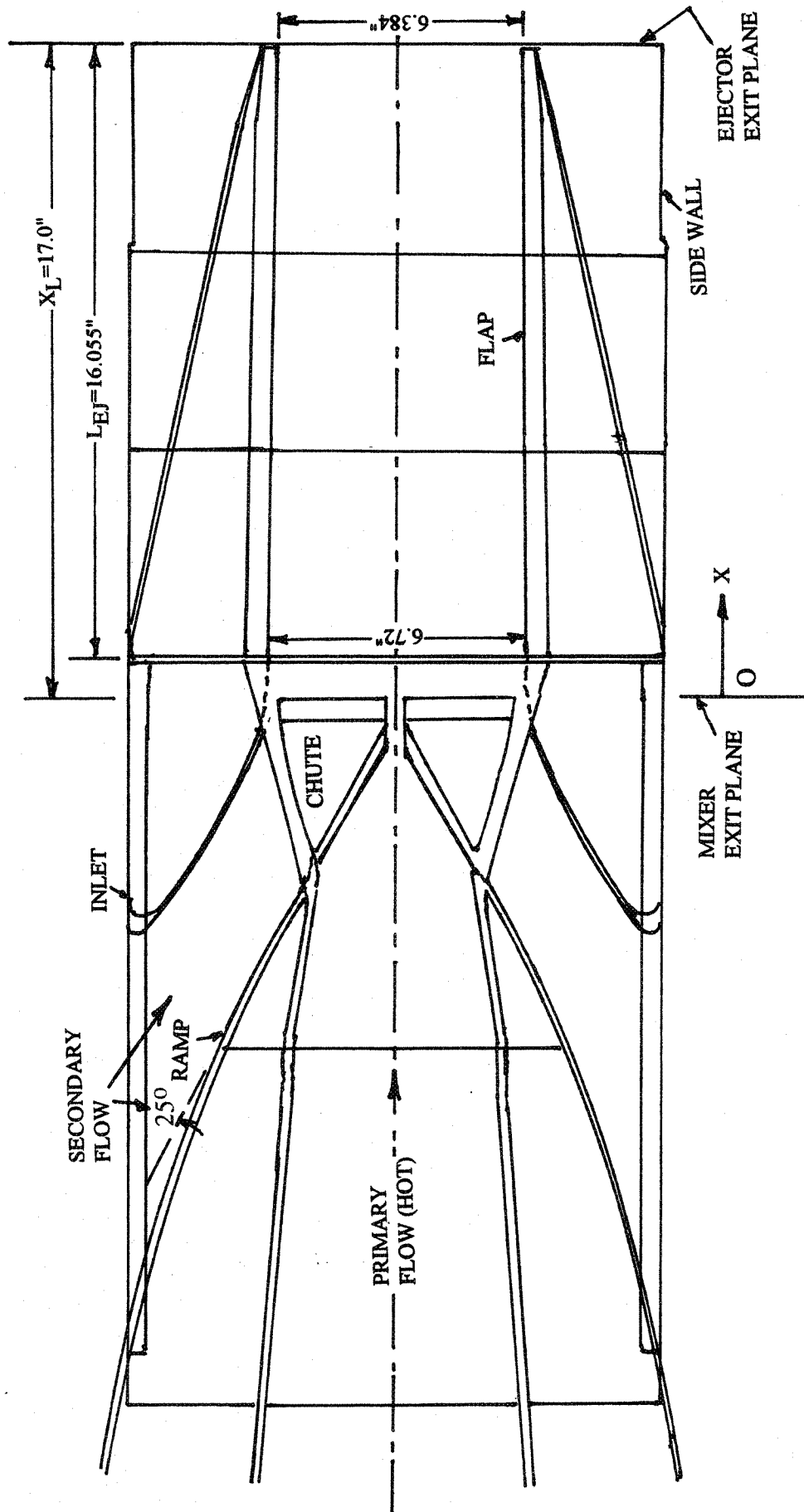
Figure 4.1-1. Side view of a 2D CD-chute mixer-ejector nozzle assembly with 16.055" (120" full scale) ejector; MAR=0.95.
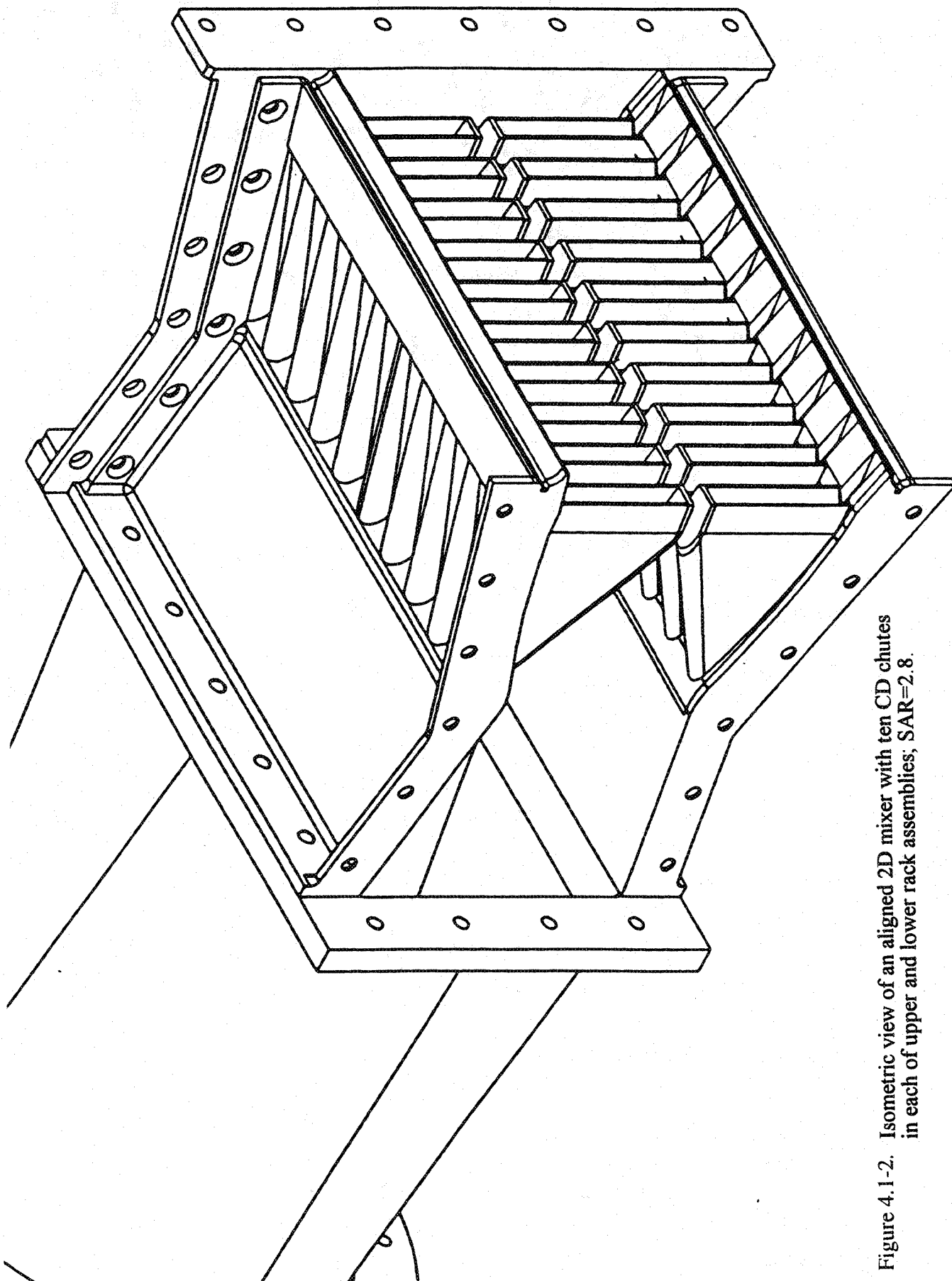
Figure 4.1-2. Isometric view of an aligned 2D mixer with ten CD chutes in each of upper and lower rack assemblies; SAR=2.8.

secondary flow path is instrumented with static pressure taps and total pressure rakes to evaluate the secondary mass flow rate. The model instrument locations are shown in Figures 4.1-3 through 4.1-8. The axial coordinates, X are tabulated with respect to the mixer exit plane.

Figures 4.1-3 and 4.1-4 show the side views and Figures 4.1-5 and 4.1-6 show the plan views (upper and lower racks, respectively) of the model with SAR=2.8 indicating the locations of the static pressure taps on the ramp, inlet flow guide, and the chute surfaces, and the total pressure rakes in the secondary flow path. The instrumentation layout for mixer of SAR 3.3 is similar to that of mixer with SAR=2.8, except the numbering for a few taps are different. Static pressure taps PS1 through PS8 are on the ramp (i.e., the forward inlet ramp) used to assess potential flow separation on the ramp if any. Static pressure taps PS9 through PS16 (PS30 through 37 for SAR=3.3) are spaced on centers of 8 equal projected chute exit area, and are located in the cold flow side of the chutes (see Figure 4.1-4). An integrated force coefficient, called chute loading coefficient, is computed using the static pressure distributions on the chute secondary flow side, using the following expression;

$$\text{Chute Loading Coefficient } (\%) = \Sigma[((P_{sc})_i - P_{amb})\ A_i]\ 100/(FG)_i$$

Where,

$(P_{sc})_i$ = static pressure measured by the ith tap

A_i = elemental projected area in axial direction for the static pressure $(P_{sc})_i$ in in^2

$(FG)_i$ = ideal gross thrust in lbs

This coefficient is not the same as ΔC_{fg} due to chute base drag. Accurate chute base drag calculation needs an integration of axial component of static pressure distribution over the entire chute surface. Hence, this calculation of chute loading coefficient is a qualitative indicator of chute base drag.

Static pressure taps PS17 and PS18 (PS38 and PS39 for SAR=3.3) are placed at axial midspan from the chute leading edge to exit, to gauge static pressure variation with axial location within the cold flow chute, so as to assess whether use of PS9 through PS16 (PS30 through PS37 for SAR=3.3) would yield an accurate estimation of base drag. Static pressure taps PS19 through PS21 (PS40 through PS42 for SAR=3.3) are placed at the
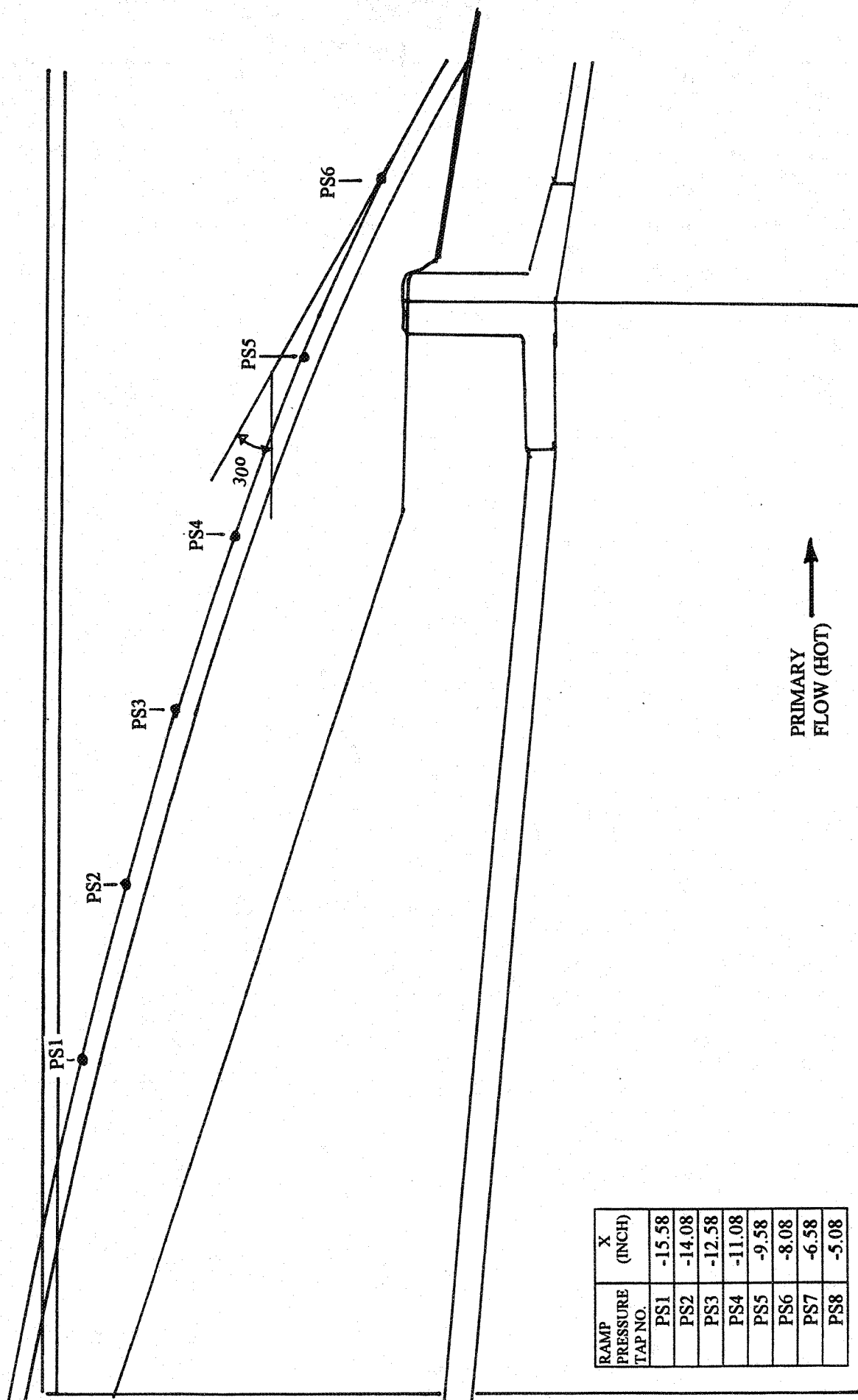
Figure 4.1-3. Side view of the ramp portion of a 2D mixer-ejector nozzle showing the static pressure tap locations.

PRIMARY
FLOW (HOT)

RAMP PRESSURE TAP NO.	X (INCH)
PS1	-15.58
PS2	-14.08
PS3	-12.58
PS4	-11.08
PS5	-9.58
PS6	-8.08
PS7	-6.58
PS8	-5.08

COLD FLOW CHUTE LE PRESSURE TAP NO.	X (INCH)
PS9	-4.63
PS10	-4.19
PS11	-3.78
PS12	-3.32
PS13	-2.88
PS14	-2.42
PS15	-2.0
PS16	-1.56

OTHER CHUTE PRESSURE TAP NO.	X (INCH)
PS17	-2.32
PS18	-1.22
PS19	0.0
PS20	0.0
PS21	0.0
PS22	-0.58
PS23	-0.41
PS24	-0.24
PS25	-0.07

RAMP PRESSURE TAP NO.	X (INCH)
PS1	-15.58
PS2	-14.08
PS3	-12.58
PS4	-11.08
PS5	-9.58
PS6	-8.08
PS7	-6.58
PS8	-5.08

INLET PRESSURE TAP NO.	X (INCH)
PS51	-5.98
PS52	-6.135
PS53	-5.98
PS54	-5.58
PS55	-5.08
PS56	-4.08
PS57	-3.08
PS58	-2.08
PS59	-1.05

Figure 4.1-4. Side view of the inlet and the 10 CD-chute mixer rack for 2D mixer-ejector nozzles showing the static pressure tap locations on the ramp, inlet flow guide, and chute surfaces and total pressure element locations in the secondary flow passage, SAR = 2.8.
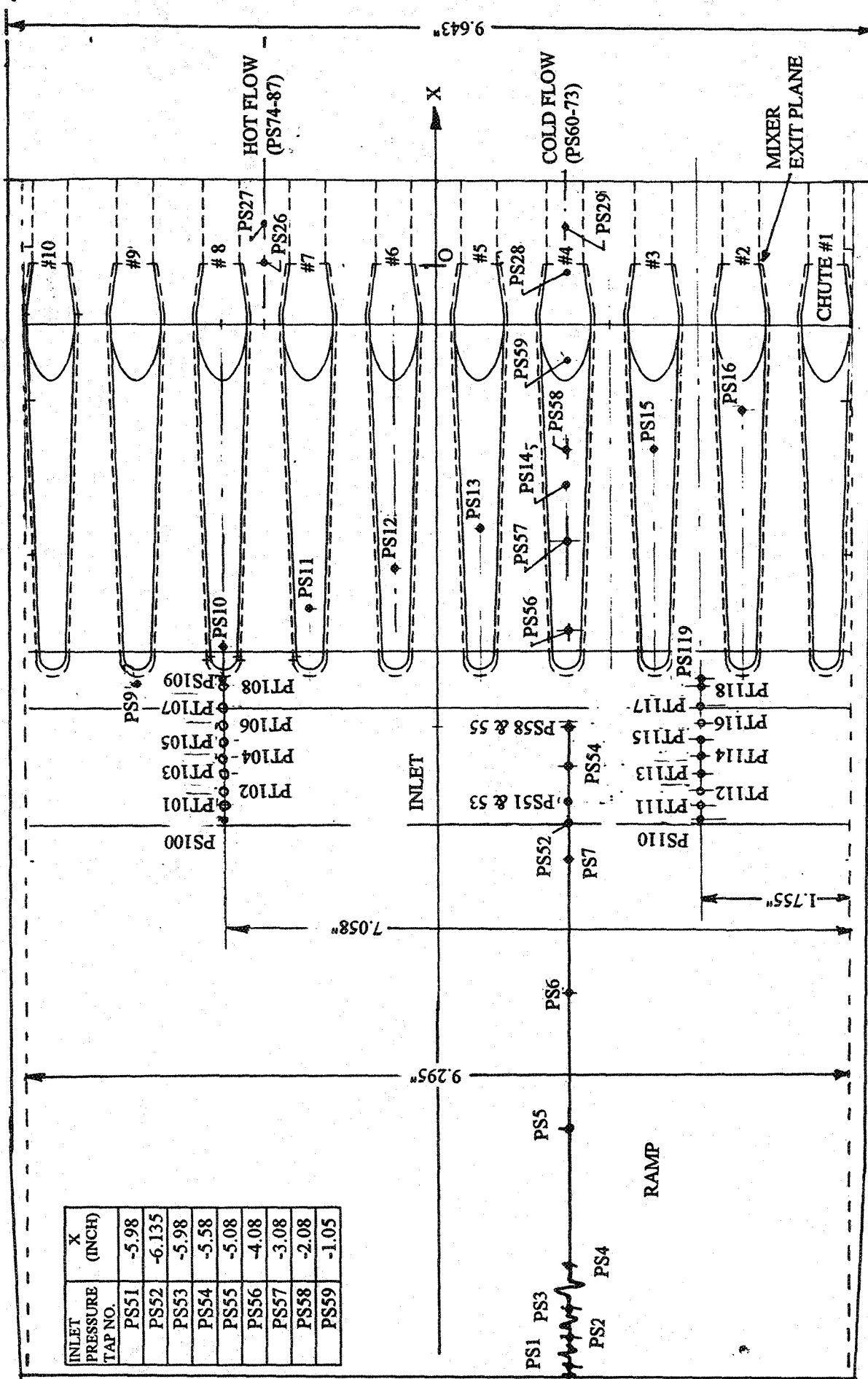
Figure 4.1-5. Plan view of the inlet and the upper chute rack with 10 CD chutes for 2D mixer-ejector nozzles showing the static pressure tap locations on the ramp, inlet flow guide, and chute surfaces and total pressure element locations in the secondary flow passage, SAR = 2.8.

INLET PRESSURE TAP NO.	X (INCH)
PS51	-5.98
PS52	-6.135
PS53	-5.98
PS54	-5.58
PS55	-5.08
PS56	-4.08
PS57	-3.08
PS58	-2.08
PS59	-1.05
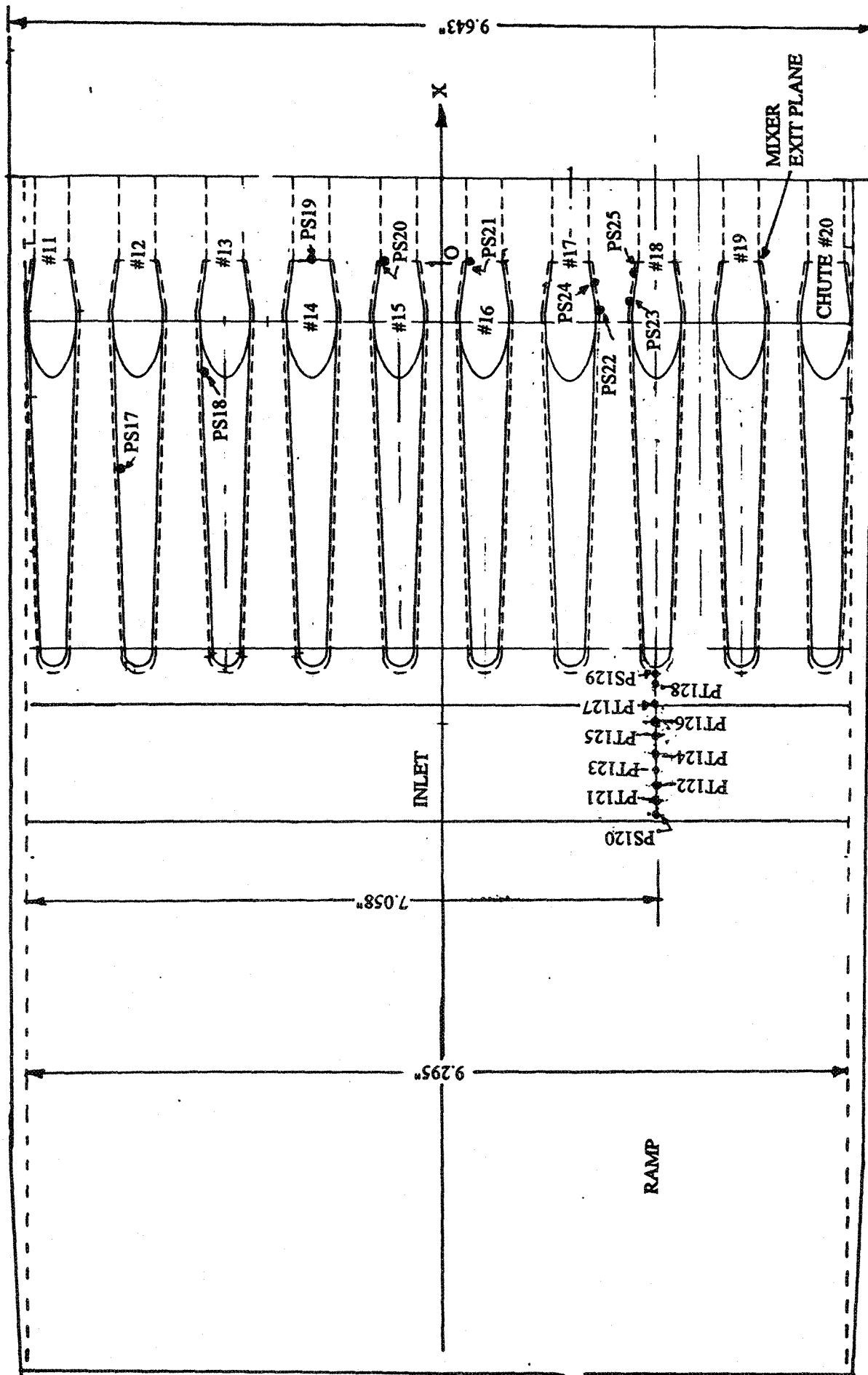
Figure 4.1-6. Plan view of the inlet and the lower chute rack with 10 CD chutes for 2D mixer-ejector nozzles showing the static pressure tap locations on the ramp, inlet flow guide, and chute surfaces and total pressure element locations in the secondary flow passage, SAR = 2.8.
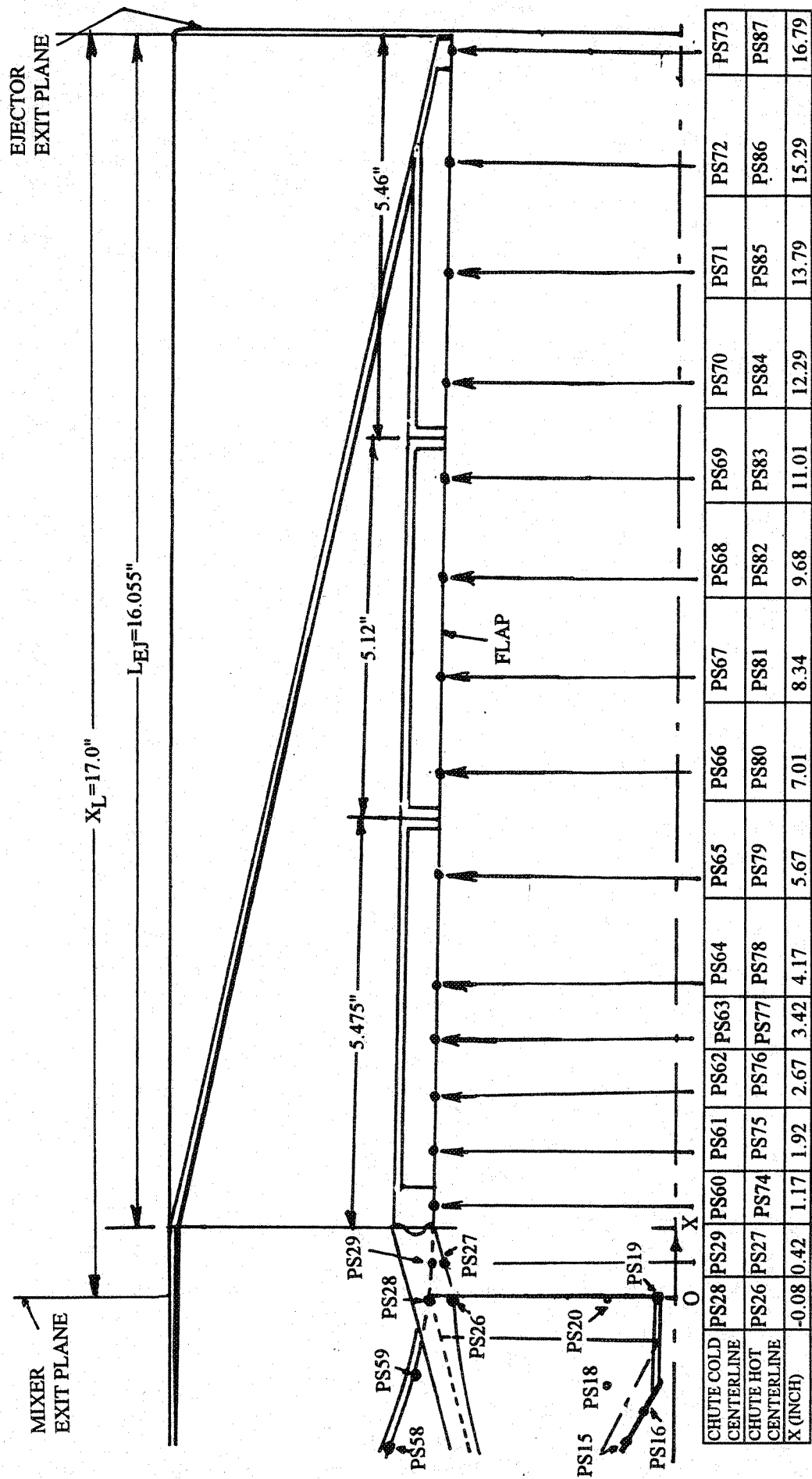
Figure 4.1-7. Side view of the ejector of a CD-chute mixer-ejector nozzle showing the static pressure tap locations, SAR = 2.8, MAR = 0.95.

CHUTE COLD CENTERLINE	PS28	PS29	PS60	PS61	PS62	PS63	PS64	PS65	PS66	PS67	PS68	PS69	PS70	PS71	PS72	PS73
CHUTE HOT CENTERLINE	PS26	PS27	PS74	PS75	PS76	PS77	PS78	PS79	PS80	PS81	PS82	PS83	PS84	PS85	PS86	PS87
X (INCH)	-0.08	0.42	1.17	1.92	2.67	3.42	4.17	5.67	7.01	8.34	9.68	11.01	12.29	13.79	15.29	16.79

FLAP PRESSURE TAP NO.		X (INCH)
CHUTE COLD CENTERLINE	CHUTE HOT CENTERLINE	
PS28	PS26	-0.08
PS29	PS27	0.42
PS60	PS74	1.17
PS61	PS75	1.92
PS62	PS76	2.67
PS63	PS77	3.42
PS64	PS78	4.17
PS65	PS79	5.67
PS66	PS80	7.01
PS67	PS81	8.34
PS68	PS82	9.68
PS69	PS83	11.01
PS70	PS84	12.29
PS71	PS85	13.79
PS72	PS86	15.29
PS73	PS87	16.79

Figure 4.1-8. Plan view of the ejector of a 10 CD-chute mixer rack for 2D mixer-ejector nozzles showing the static pressure tap locations, SAR= 2.8.

exit of cold flow chute at three vertical locations to measure variation in local static pressure. Static pressure taps PS22 through PS25 (PS43 through PS46 for SAR=3.3) are placed within a hot core flow segment from the throat plane to the exit plane, at mid-span height, to assess shock free operation of the CD flowpath at the aerodynamic design point and to aid in adjusting the nozzle pressure ratio to attain shock-free operation if it does not occur at design point.

Static pressure taps PS26 and PS27 (PS47 and PS48 for SAR=3.3) are placed within a hot core flow segment along the "finger", located at and just aft of the chute exit plane, to understand primary flow expansion along the "finger".

Static pressure taps PS51 through PS59 (same for both the mixers) on the aft flow guide (i.e., the inlet) and PS28 and PS29 (PS49 and PS50 for SAR=3.3) on the chute rack in the center of cold flow chute are placed to establish the stagnation point of the flow around the blunt leading edge of the inlet flow guide, to determine whether the inlet is full flowing in the region of the total pressure rakes, and to measure the static pressure distribution over the full axial extent of the inlet for assessing the inlet flow quality.

Twenty-four total pressure elements and 6 static pressure taps comprising three total pressure rake systems within the inlet (two rakes on the upper inlet and one on the lower inlet) are used for secondary mass flow estimation. Total pressure elements PT101 through PT108 and static pressure taps PS100 and PS109 are in one upper inlet rake along the chute cold flow centerline. The second upper inlet rake comprises of total pressure elements PT111 through PT118 and static pressure taps PS110 and PS119 and is placed along chute hot flow centerline (see Figure 4.1-5). The third rake, formed by total pressure elements PT121 through PT128 and static pressure taps PS120 and PS129, is placed in the lower inlet along the chute cold flow centerline (see Figure 4.1-6). For each rakes the total pressure elements are located on centers of 8 equal areas perpendicular to the secondary throat to measure the ambient air entrainment. The total and static pressure elements are numbered the same for both the mixers. The secondary mass flow rate W_S is evaluated using the average contributions of the three total pressure rakes with a double weighting for the rake along the chute hot flow centerline. The pumping is expressed as the ratio of secondary to primary mass flow rates, W_S/W_P, where W_P is the primary stream mass flow rate, evaluated using nozzle pressure ratio, total temperature, rake measurements at the primary stream charging station, and throat area. The corrected pumping is expressed as follows;

$$\text{Corrected Pumping} = W_S/W_P \sqrt{\frac{T_{tS}}{T8}}$$

where, T_{tS} and T8 are the secondary and primary stream total temperatures, respectively. Using the primary and secondary stream mass flow rates, total temperatures, total pressures, and assuming complete mixing at the ejector exit plane a mixed velocity (V_{mix}) is also computed on the basis of 1D ejector model.

A line of 14 static pressure taps, PS60 through PS73, are placed on the flap in line with the centerline of a cold flow chute. Similarly, another 14 static pressure taps, PS74 through PS87, are placed on the flap in line with the centerline of a hot flow chute (see Figures 4.1-7 and 4.1-8). The static pressure nomenclature remains the same for both the mixers. These static pressure taps are used to assess the ejector flow characteristics. The axial static pressure distribution on the flap surface would indicate the mode of flow (i.e., subsonic or supersonic modes) and the presence or absence of shocks in the ejector. Integrated static pressures and integrated moment of the static pressures with respect to flap leading edge would yield various flow and performance related ejector characteristics. The normalized force and moment of the force are expressed as follows;

$$\text{Normalized Force} = \frac{1}{L_{EJ}} \sum_{i=1}^{N} \left(1 - \frac{(P_{Sa})_i}{P_{amb}}\right) \Delta x_i$$

$$\text{Normalized Moment of the Force} = \frac{1}{(L_{EJ})^2} \sum_{i}^{N} \left(1 - \frac{(P_{Sa})_i}{P_{amb}}\right) x_i \Delta x_i$$

where;

L_{EJ} = length of the flap

N = number of pressure taps on the flap

$\left(\dfrac{(P_{Sa})_i}{P_{amb}}\right)$ = ratio of average flap pressure (i.e., average of hot [i.e., $(P_S)_h$] and cold [i.e., $(P_S)_c$] flow chute centerlines) at ith tap and ambient pressure

x_i = axial coordinate of ith pressure with respect to flap leading edge

Δx_i = $(x_{i+1} - x_{i-1})/2$

Tests for both the mixer configurations (i.e., #1, #2, and #21) were conducted along the L1M cycle line for static and simulated flight conditions of Mach 0.12, 0.24, and 0.32.

Acoustic data was acquired for both the major and minor axis community points (i.e., at ϕ = 90° and 4°), and their respective sideline angles ((i.e., at ϕ = 25° and 65°) using the traversing microphone array (see Figure 4.1-9). In addition, acoustic data was also acquired at ϕ = 45° using the fixed microphone array. The actual azimuthal location for the community point with respect to minor axis is ϕ = 0°. However, due to the facility limitation the acoustic data for this location was acquired at ϕ = 4°. Static and total pressures were measured for the mixer, secondary inlet, and flap pressure taps.

4.1.1 Comparison with Old Data:

Aligned CD chute mixers were tested earlier (under Contract NAS3-25415) with and without long treated ejectors. The flaps and sidewalls for these configurations were fully treated with astroquartz of 1 lb/ft^3 with a 37% porous facesheet. Acoustic data was measured at the community and the sideline points with respect to the ejector major axis at static and with flight simulation of Mach 0.32. The acoustic results from these tests are compared with the similar results obtained from the current repeat tests of the same configurations.

Results for the Mixer with SAR=3.3

Figure 4.1-10 shows the comparison of EPNL, peak PNLT, and PNLT at various polar angles (θ) as functions of jet velocity (V_j) at a sideline distance of 1629' with respect to major axis at static condition and with a simulated flight Mach number of 0.32. Agreement between old and current EPNL values is excellent for static condition. With flight simulation the EPNL agreement is also excellent, except for the lowest and highest jet velocities of 1147 and 2812 ft/sec. Small differences of PNLT values are observed between old and current results.

At several jet velocities the PNLT directivities are compared between old NRA and current results in Figure 4.1-11. Except for lower jet velocities of 1147 and 1595 ft/sec the agreement between old and current results is very good at static condition. With flight simulation the PNLT comparisons show the similar trend as observed for static condition, except for 2812 ft/sec, where the old NRA data show lower PNLT levels. Spectral comparisons at various polar angles (θ) for different jet velocities are shown in Figures 4.1-12 through 4.1-15. Reasonable agreement is observed between old and current data.
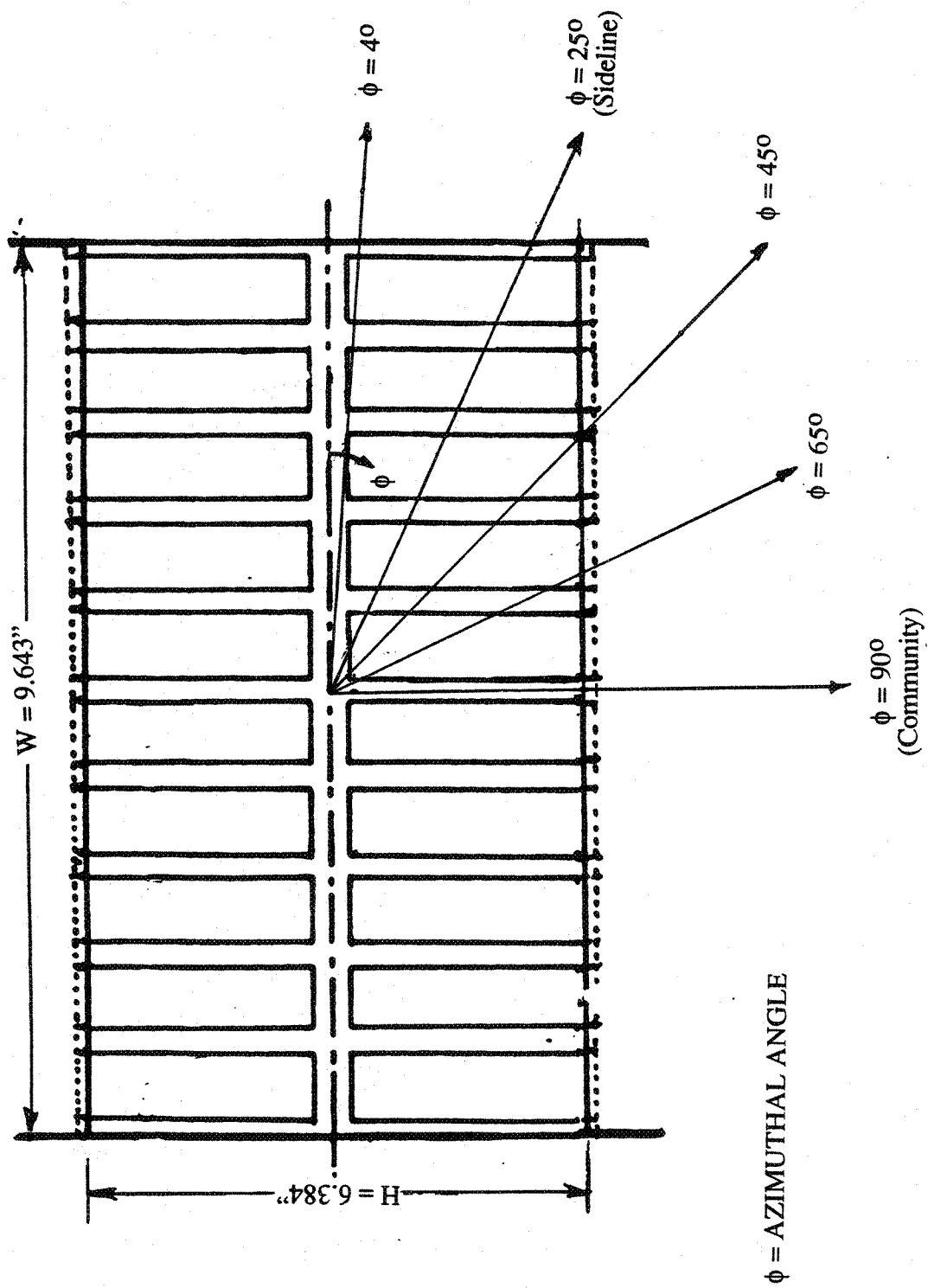
Figure 4.1-9. Azimuthal measurement locations indicated on the end view of an aligned CD-chute mixer-ejector; MAR=0.95.
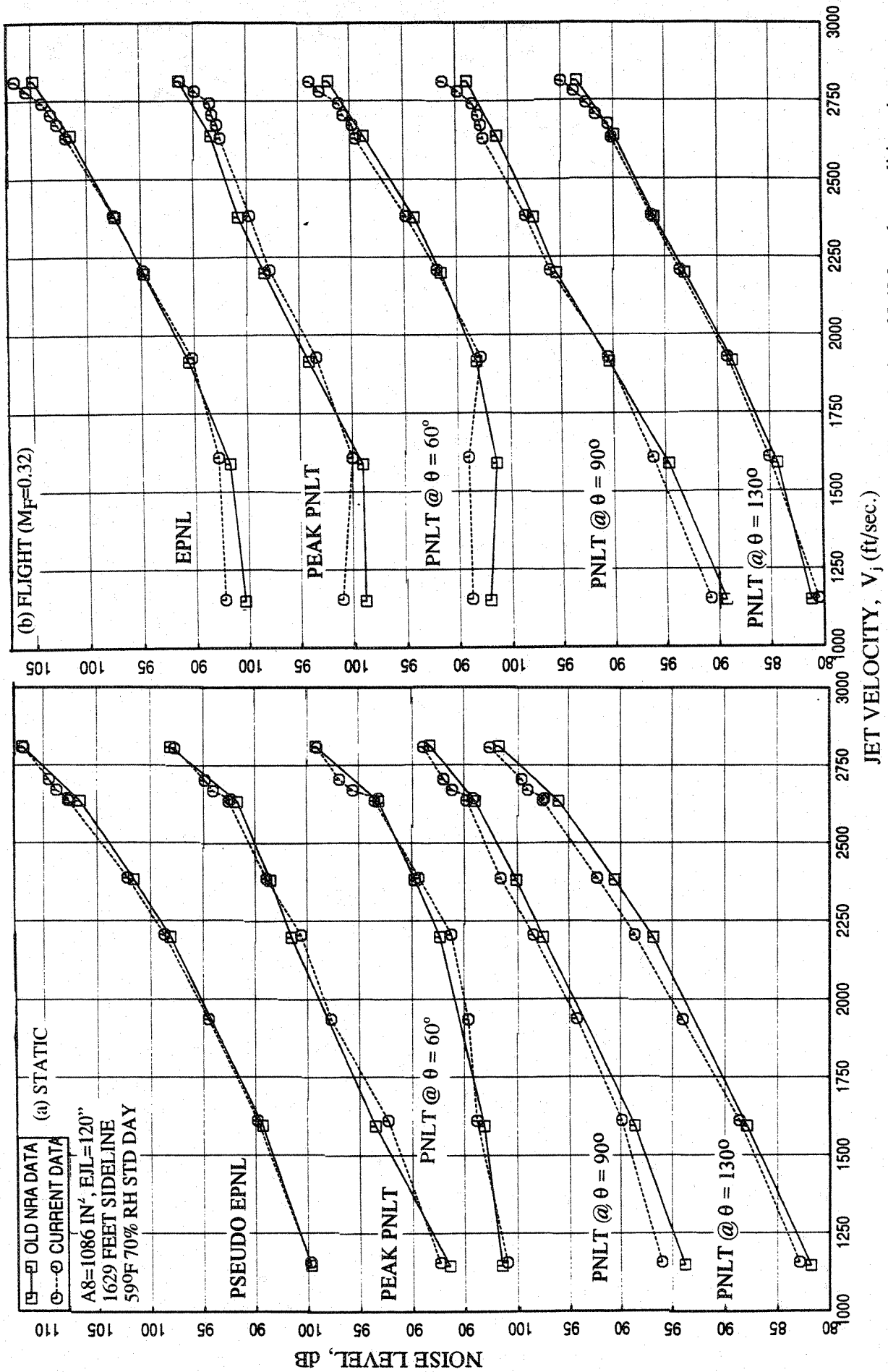
Figure 4.1-10. Comparison of EPNL, peak PNLT, and PNLT at various polar angles (θ) as function of jet velocity of L1M cycle conditions between old NRA and the current data for an aligned CD-chute mixer with fully treated long ejector; SAR = 3.3, MAR = 0.95, φ = 25°.
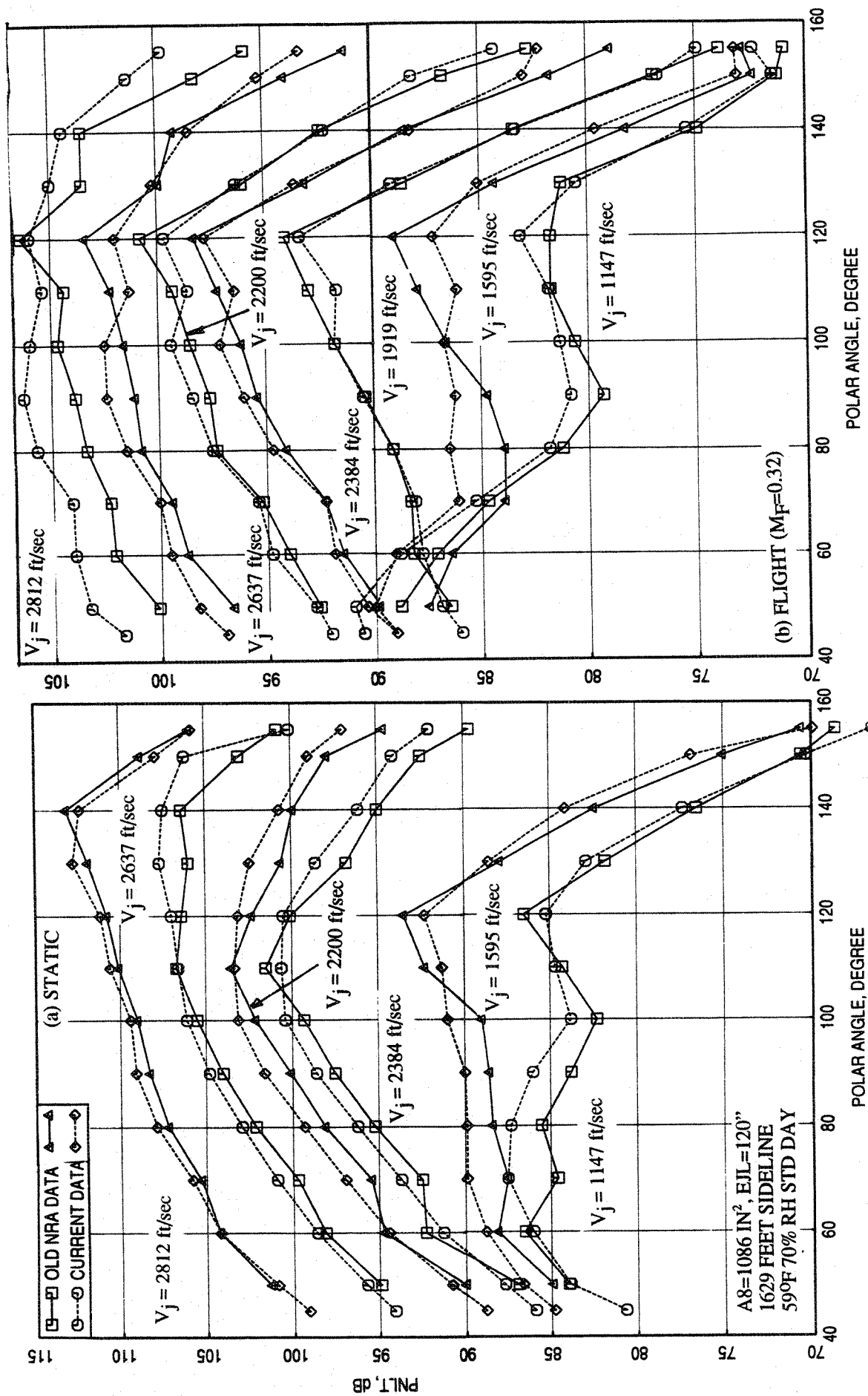
Figure 4.1-11. Comparison of PNLT directivities at different L1M cycle conditions between old NRA and the current data for an aligned CD-chute mixer with fully treated long ejector; SAR = 3.3, MAR = 0.95, $\phi = 25°$.
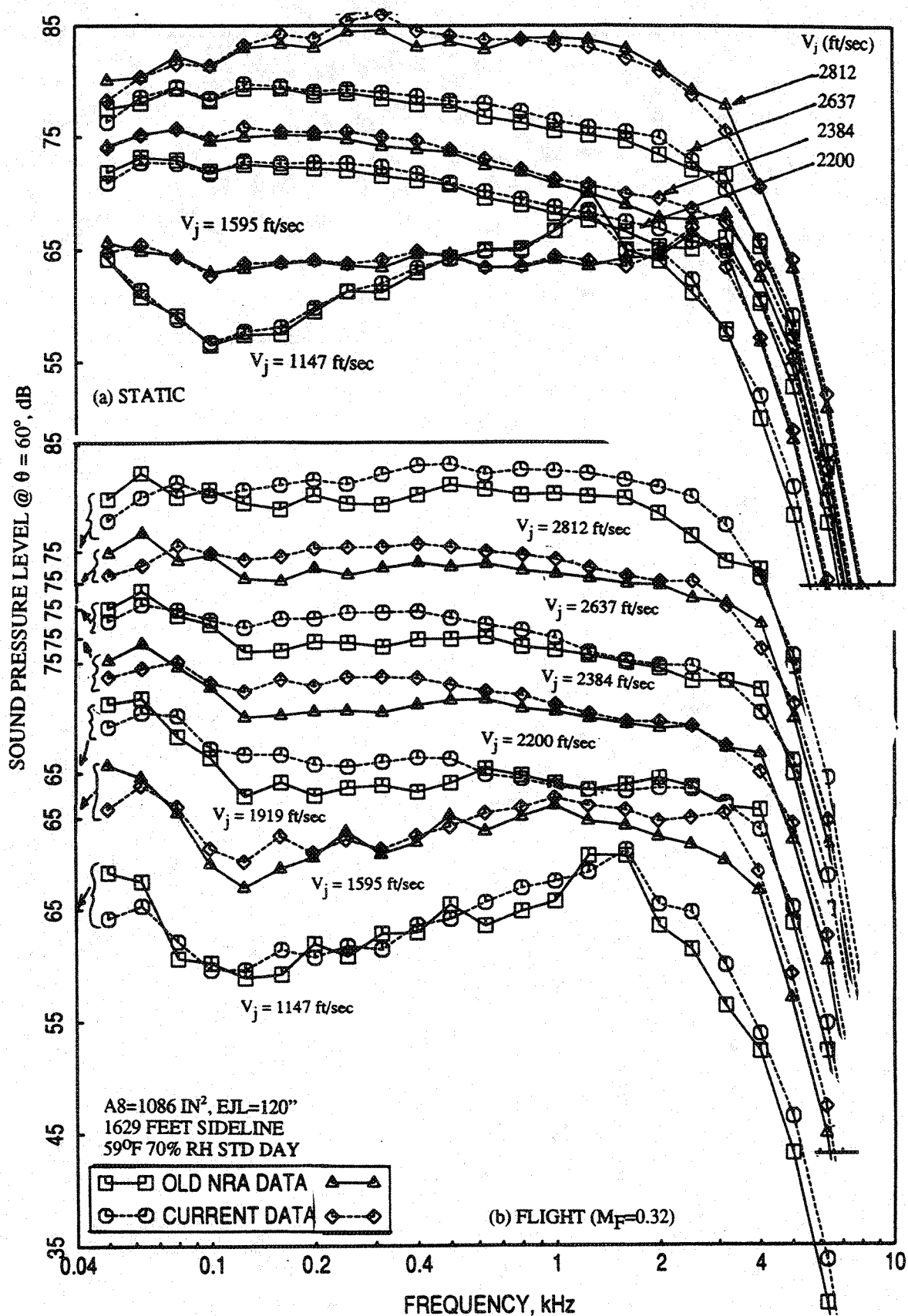
Figure 4.1-12. Comparison of SPL spectra at polar angle θ = 60° at different L1M cycle
conditions between old NRA and the current data for an aligned CD-chute
mixer with fully treated long ejector; SAR = 3.3, MAR = 0.95, φ = 25°.
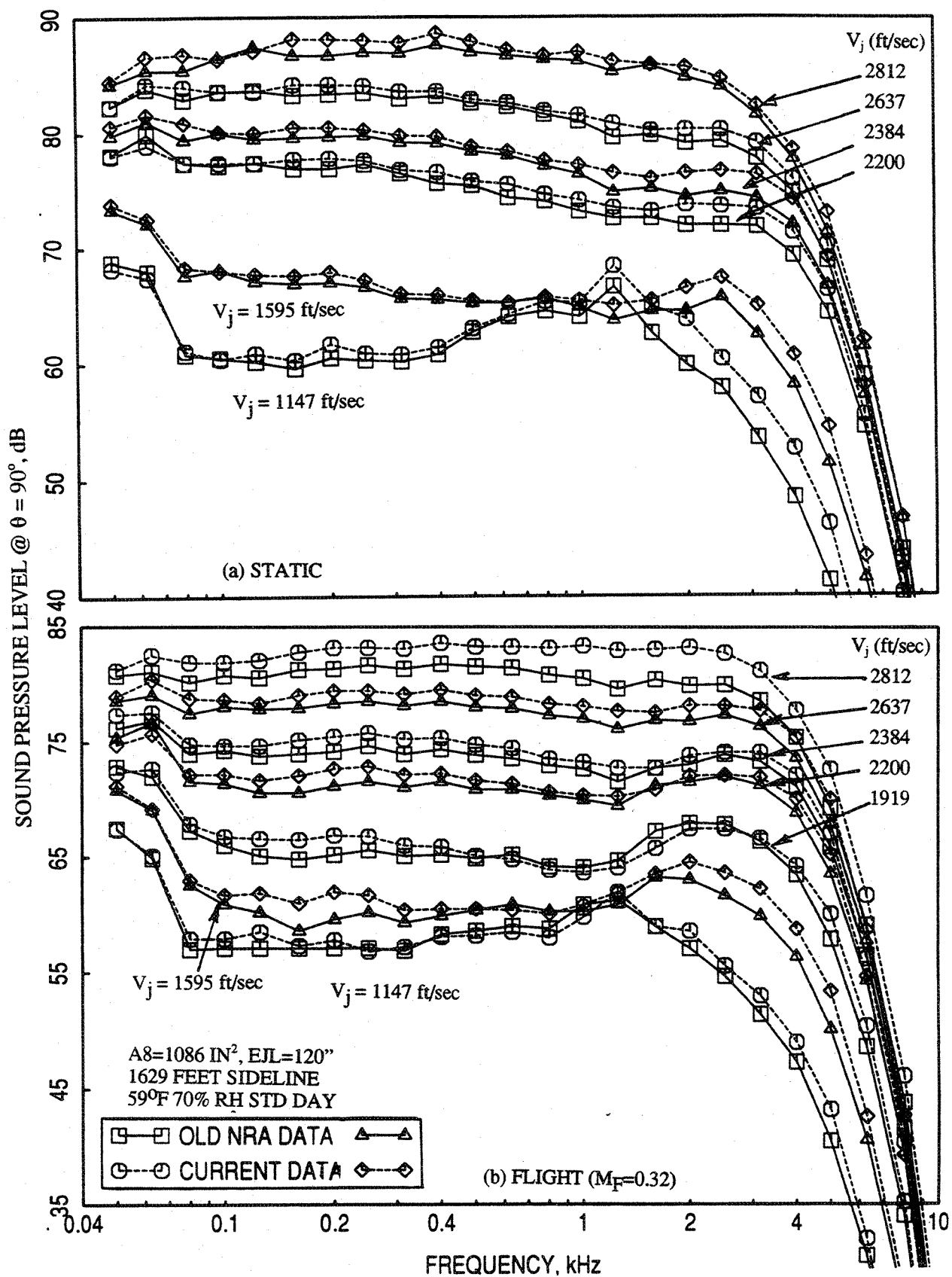
Figure 4.1-13. Comparison of SPL spectra at polar angle θ = 90° at different L1M cycle
conditions between old NRA and the current data for an aligned CD-chute
mixer with fully treated long ejector; SAR = 3.3, MAR = 0.95, φ = 25°.
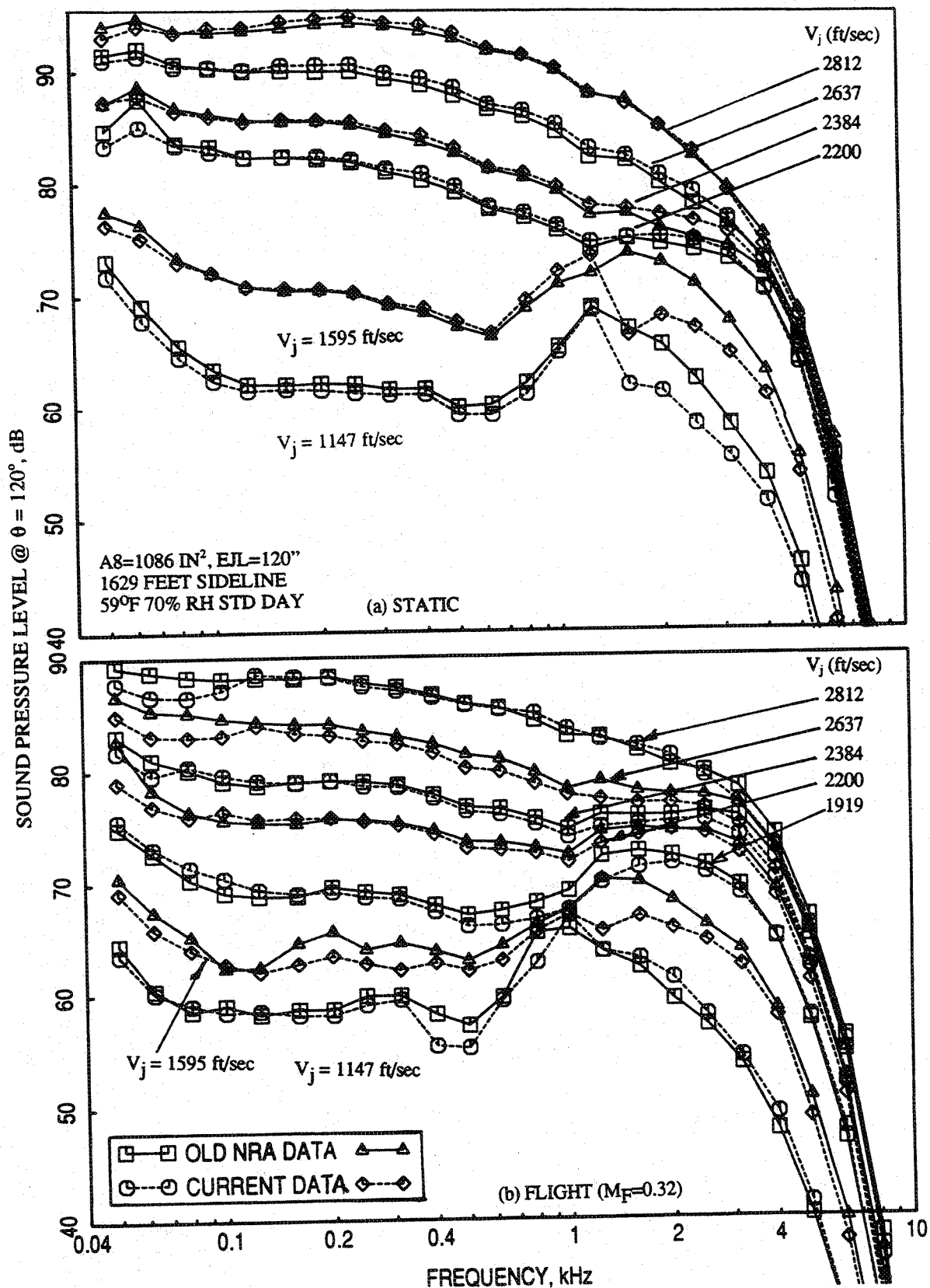
Figure 4.1-14. Comparison of SPL spectra at polar angle θ = 120° at different L1M cycle
conditions between old NRA and the current data for an aligned CD-chute
mixer with fully treated long ejector; SAR = 3.3, MAR = 0.95, φ = 25°.
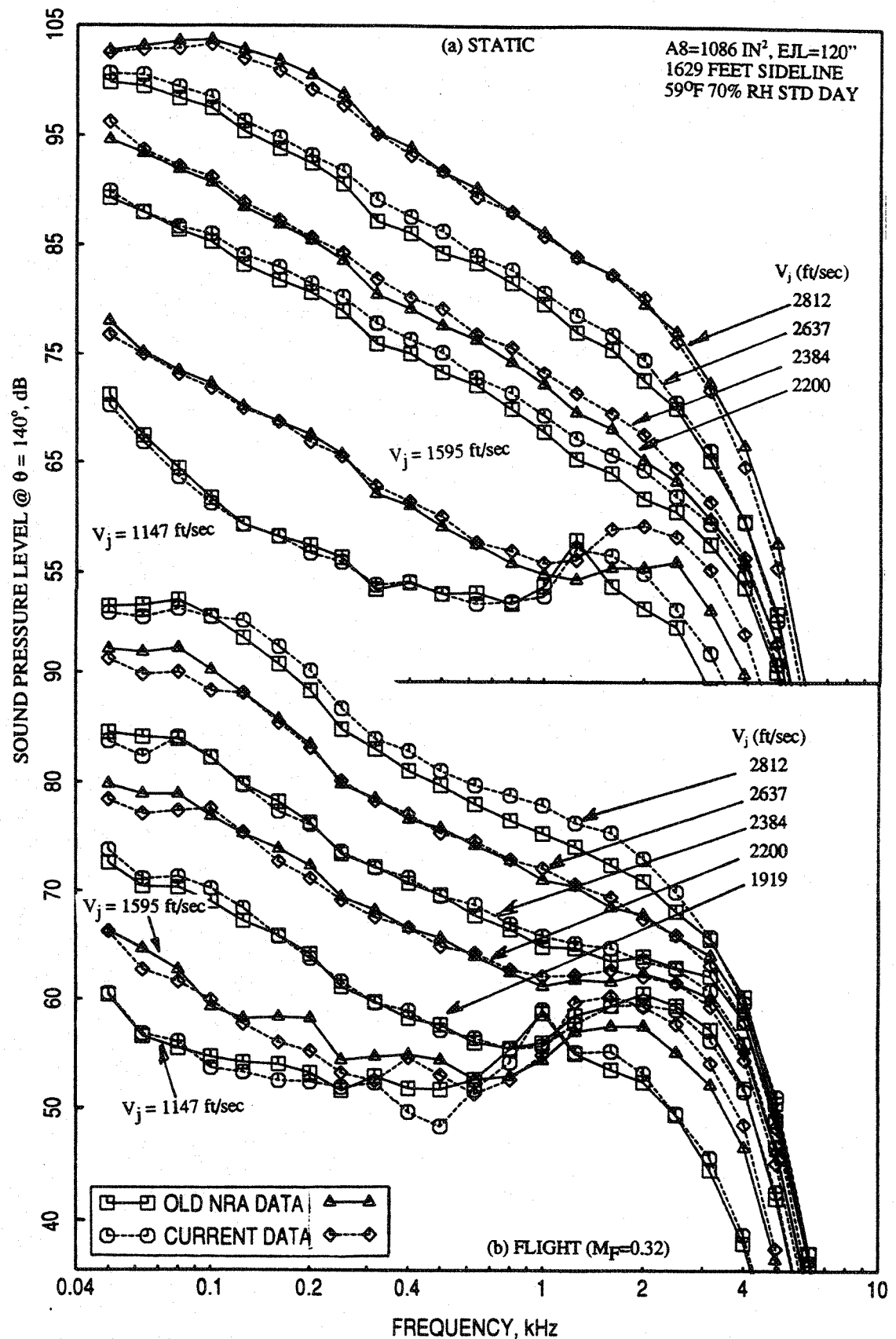
Figure 4.1-15. Comparison of SPL spectra at polar angle θ = 140° at different L1M cycle conditions between old NRA and the current data for an aligned CD-chute mixer with fully treated long ejector; SAR = 3.3, MAR = 0.95, φ = 25°.

Figure 4.1-16 shows the comparison of EPNL, peak PNLT, and PNLT at various polar angles (θ) as functions of jet velocity (V_j) at a sideline distance of 1629' with respect to major axis at static condition and with a simulated flight Mach number of 0.32 between present data and the results obtained under NRA program. Statically, the agreement between old and current EPNL values is excellent up to about 2400 ft/sec. For higher velocity conditions, the present levels are slightly higher compared to the NRA results Small differences of PNLT values are observed between old and current results at higher velocities at static condition. With flight simulation, except for the lowest jet velocity of 1147 ft/sec the agreement between old and current EPNL values is excellent. Small differences of PNLT values are observed between old and current results, mostly at lower velocities with flight simulation.

At six different jet velocities the PNLT directivities are compared between old NRA and current results in Figure 4.1-17. Statically the agreement between old and current results is very good for all cases, except for velocities 1147 and 2812 ft/sec, for which small differences are observed between old and current data at some polar angles. With flight simulation the agreement between old and current results is also very good for lower jet velocities. At higher jet velocity conditions the old NRA PNLT levels are relatively lower compared to the current data. Spectral comparisons at various polar angles (θ) for the six jet velocities are shown in Figures 4.1-18 through 4.1-20. Reasonable agreement is observed between old and current data.

In general, the repeatability of test results for both the mixer-ejector configurations is very good. Small differences observed in the data shown here could be due to uncertainty of exact duplication of ejector treatment, flight Mach number and aerothermodynamic conditions. It should be noted that the NRA tests were conducted at a flight Mach number higher than 0.32 (at about 0.36) due to an erroneous pressure measurement, whereas, the flight transformation to these data was applied for 0.32 Mach. This could introduce a small amount of disagreement between the current and old data, especially lowering the noise levels for old NRA tests.
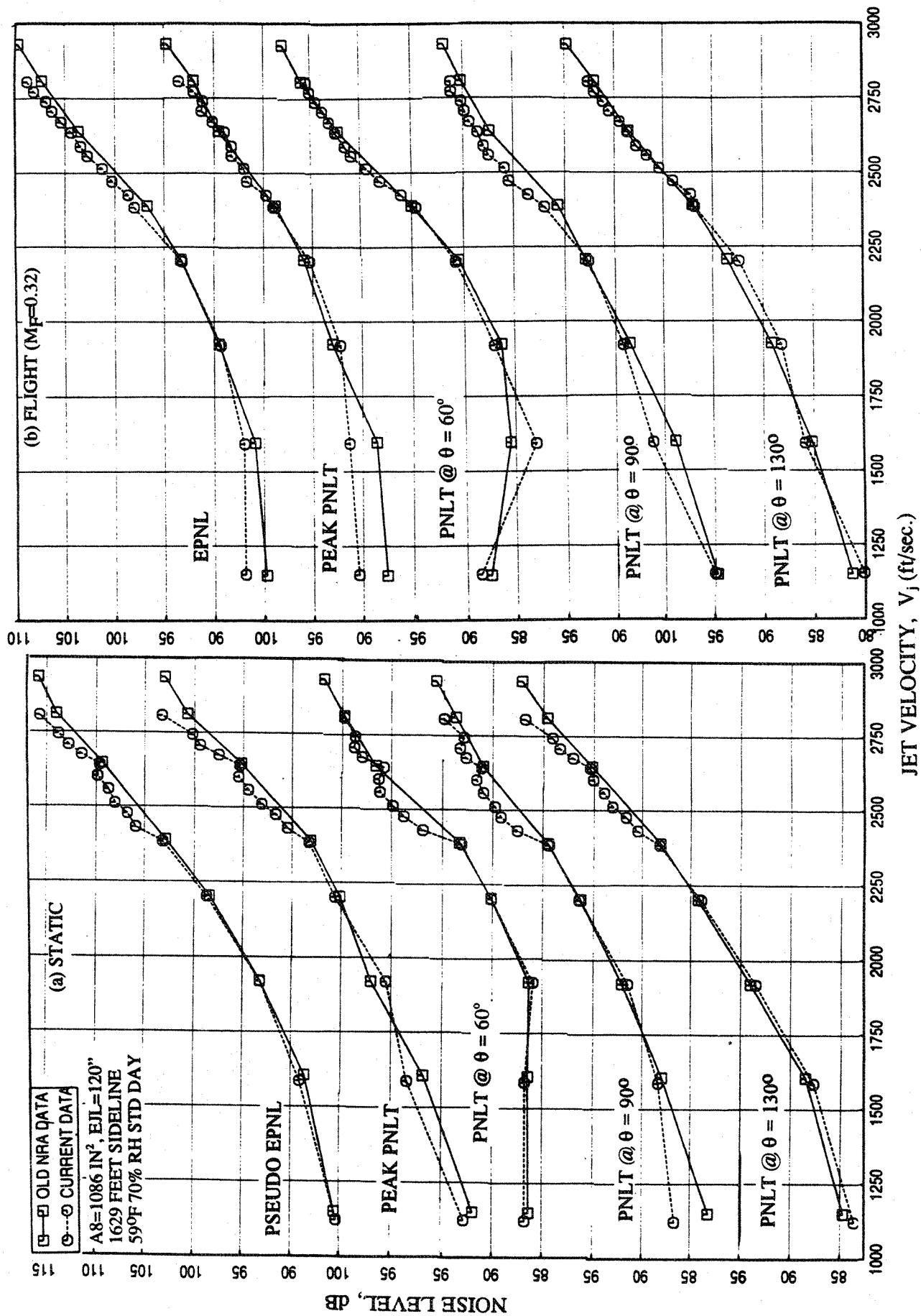
Figure 4.1-16. Comparison of EPNL, peak PNLT, and PNLT at various polar angles (θ) as function of jet velocity of L1M cycle conditions between old NRA and the current data for an aligned CD-chute mixer with fully treated long ejector; SAR = 2.8, MAR = 0.95, ϕ = 25°.
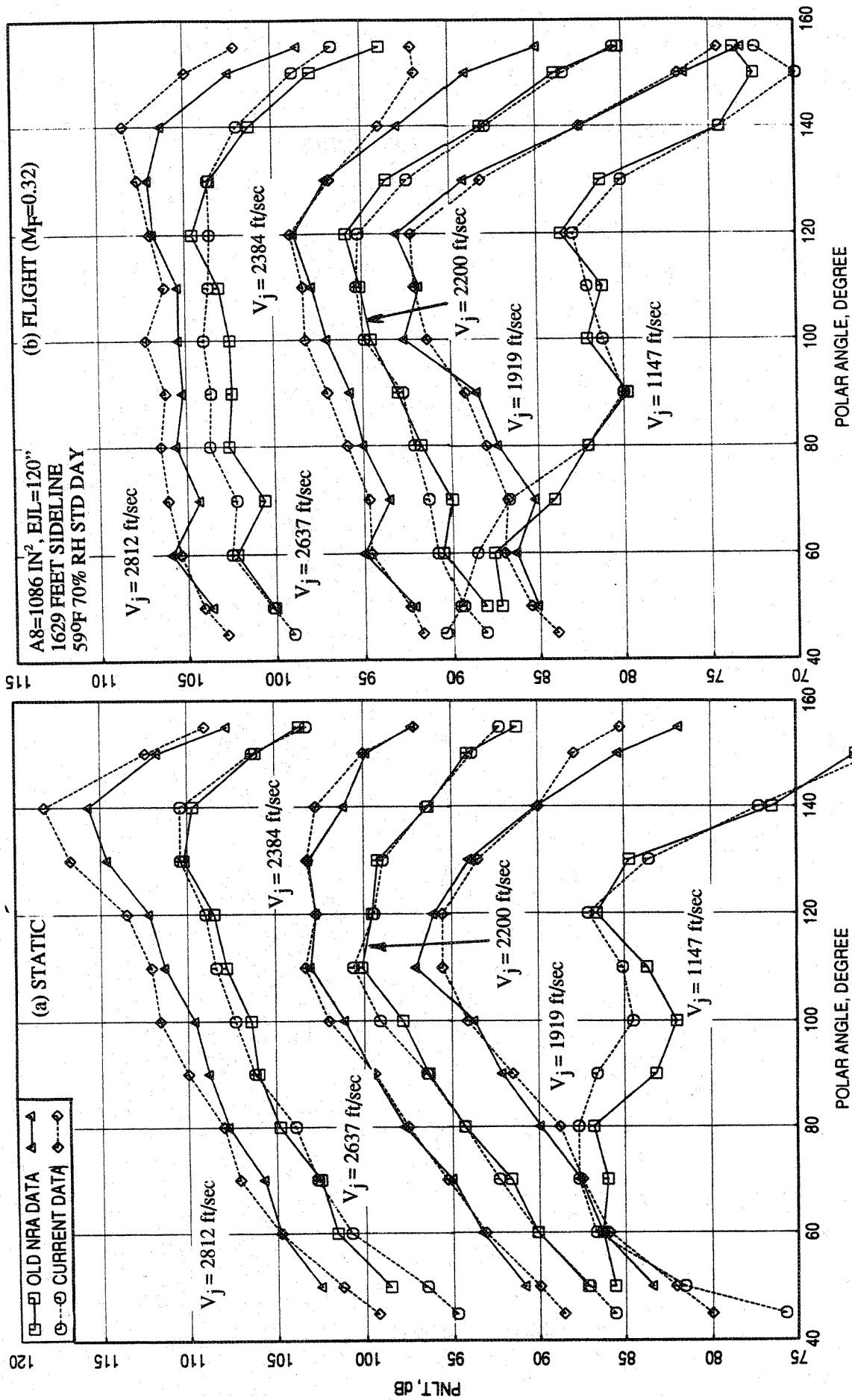
Figure 4.1-17. Comparison of PNLT directivities at different L1M cycle conditions between old NRA and the current data for an aligned CD-chute mixer with fully treated long ejector; SAR = 2.8, MAR = 0.95, $\phi = 25°$.
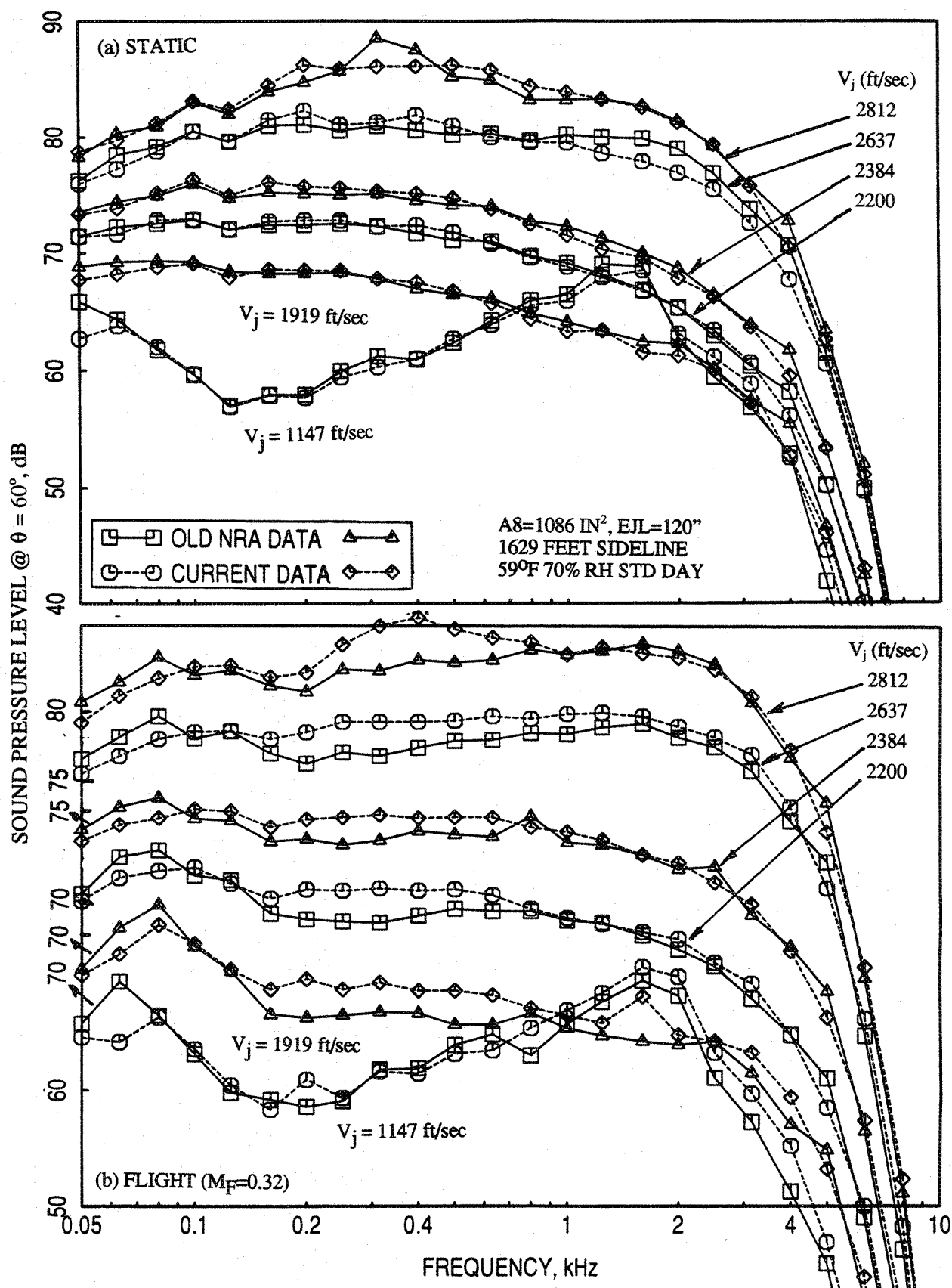
Figure 4.1-18. Comparison of SPL spectra at polar angle θ = 60° at different L1M cycle conditions between old NRA and the current data for an aligned CD-chute mixer with fully treated long ejector; SAR = 2.8, MAR = 0.95, φ = 25°.
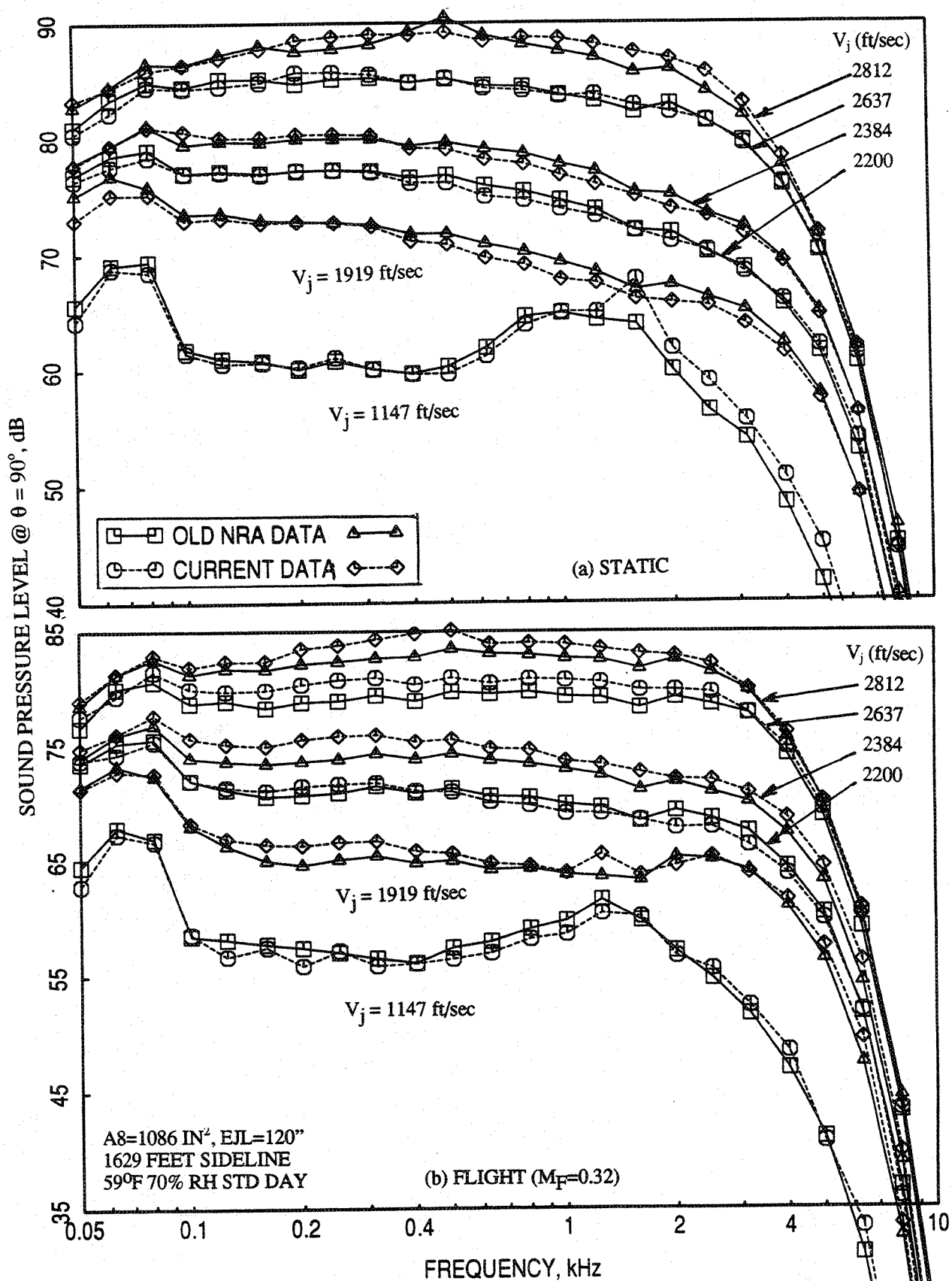
Figure 4.1-19. Comparison of SPL spectra at polar angle θ = 90° at different L1M cycle
conditions between old NRA and the current data for an aligned CD-chute
mixer with fully treated long ejector; SAR = 2.8, MAR = 0.95, φ = 25°.
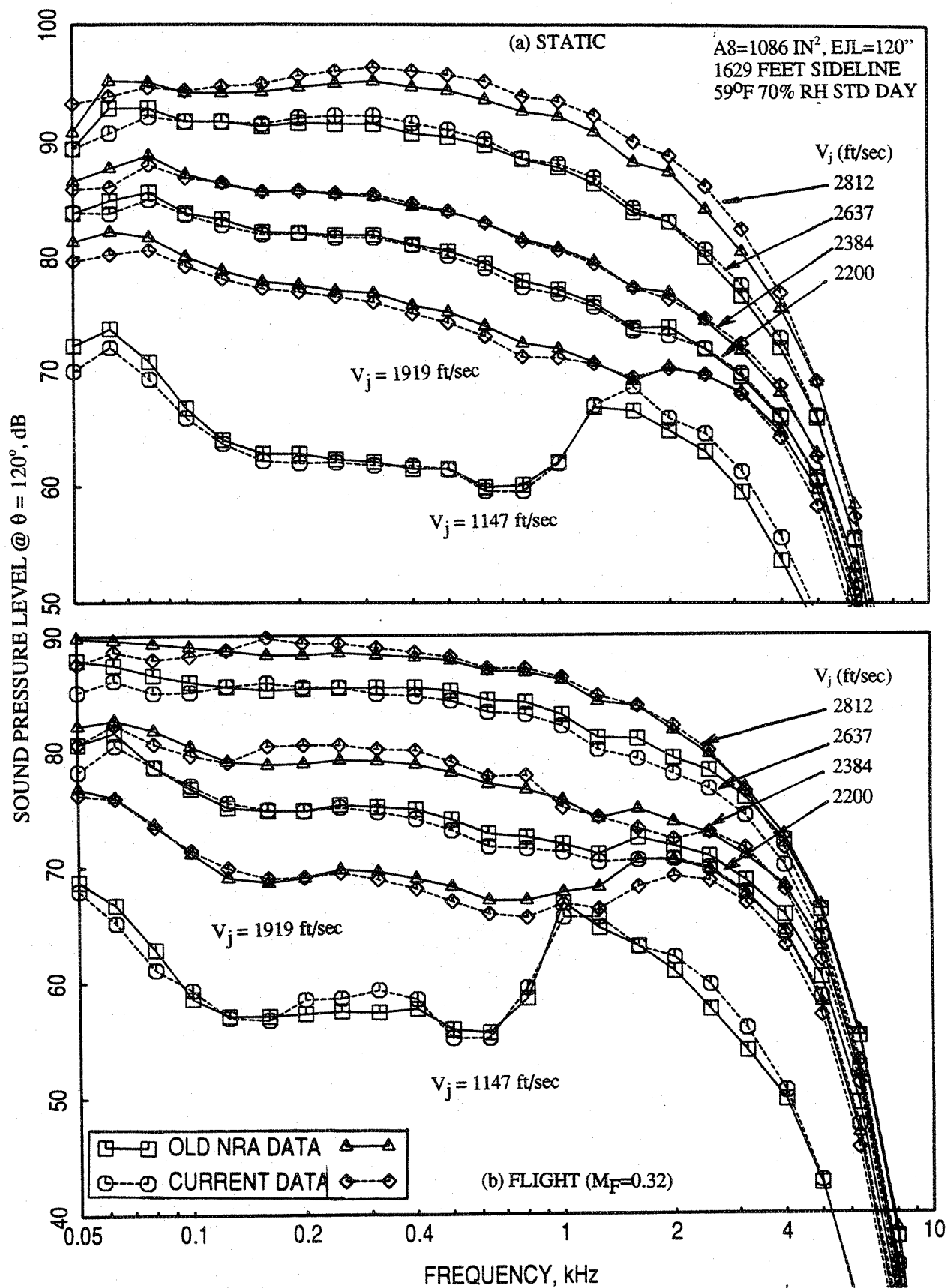
Figure 4.1-20. Comparison of SPL spectra at polar angle θ = 120° at different L1M cycle conditions between old NRA and the current data for an aligned CD-chute mixer with fully treated long ejector; SAR = 2.8, MAR = 0.95, φ = 25°.

4.1.2 Effect of Treatment Type:

Tests for configuration #21, SAR 2.8 mixer with long ejector, fully treated with nickel based foam metal, were conducted along the L1M cycle line for static and simulated flight conditions of Mach 0.12, 0.24, and 0.32. Acoustic data was acquired for both the major and minor axis community points, and their respective sideline angles. Static and total pressures were measured for the mixer, secondary inlet, and flap pressure taps. Typical results presented in this section are the comparisons of acoustic data between the same mixer-ejector with astroquartz acoustic treatment (i.e., from configuration #2) and the nickel based foam metal treatment (i.e., from configuration #21) at sideline (i.e., $\phi = 25°$) and community (i.e., $\phi = 90°$) locations with respect to the ejector major axis with flight simulation ($M_F = 0.32$).

Figure 4.1-21 shows the comparison of EPNL, peak PNLT, and PNLT at various polar angles (θ) as functions of jet velocity (V_j) at a sideline distance of 1629' with respect to major axis with a simulated flight Mach number of 0.32 between ejectors with astroquartz and foam metal treatments. The agreement between EPNL from both treatments is excellent for entire velocity range at $\phi = 25°$ and for higher velocity conditions at $\phi = 90°$. Small differences of PNLT values are observed between these configurations of different treatments, especially at lower velocities. However, the levels with foam metal treatment seem to be slightly better in most cases.

PNLT directivities at six different jet velocities are compared between astroquartz and foam metal treated configurations in Figure 4.1-22. The agreement between both sets of results is very good, except at lowest and highest velocity conditions. Again, the foam metal treated configuration resulted in lower noise levels at most angles for each velocity condition. Spectral comparisons at various polar angles (θ) for the six jet velocities are shown in Figures 4.1-23 through 4.1-26. Both the sets of results are very close to each other with slight improvement in the noise levels due to foam metal treatment.

In general, the foam metal seems to be performing as well as and, in most cases, slightly better than the astroquartz treatment. This is a very encouraging result, since maintaining proper astroquartz treatment is more laborious and time consuming. Since the foam metal
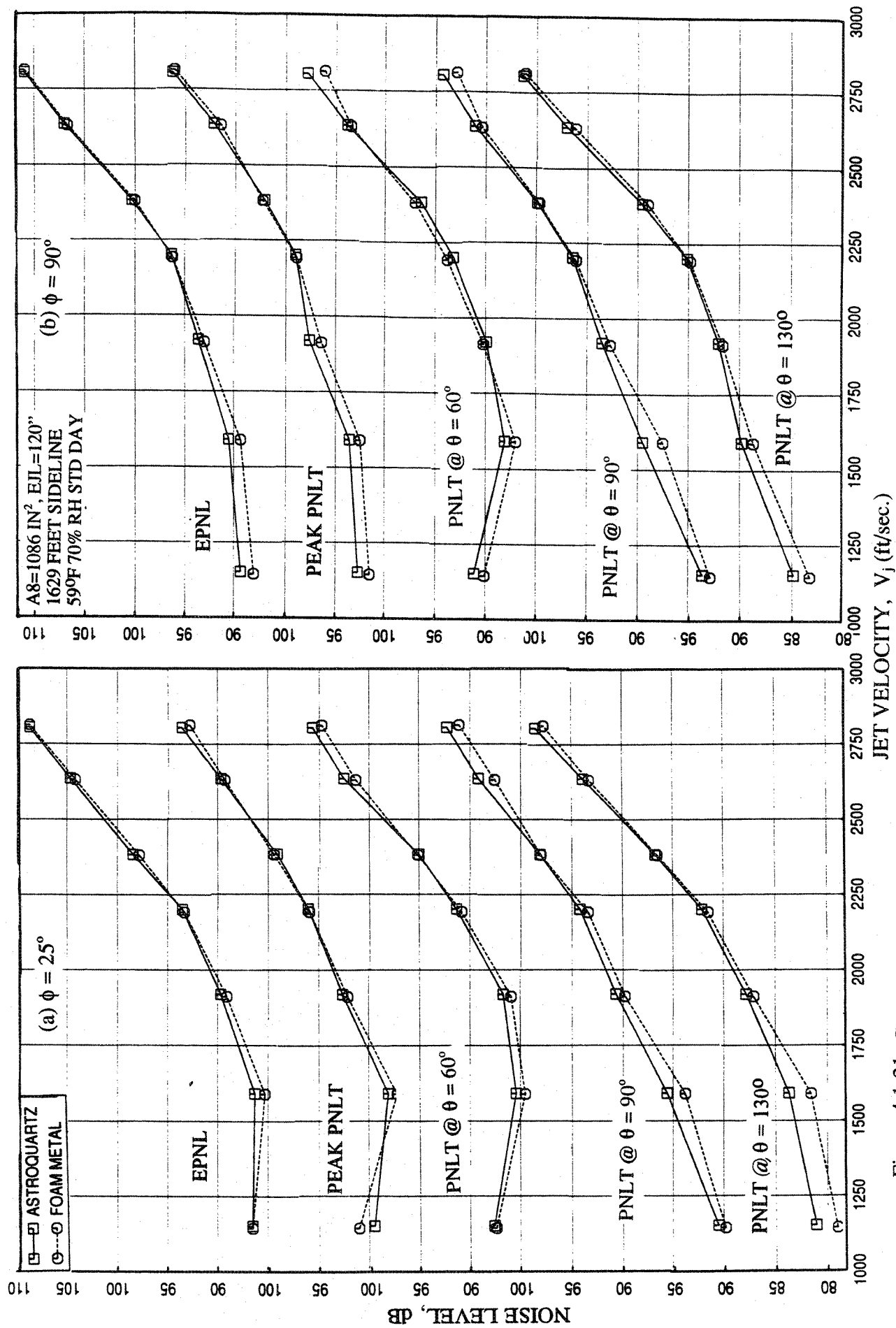
Figure 4.1-21. Comparison of EPNL, peak PNLT, and PNLT at various polar angles (θ) as function of jet velocity of L1M cycle conditions between astroquartz and a foam metal treated long ejector for an aligned CD-chute mixer with flight simulation ($M_F = 0.32$); SAR = 2.8, MAR = 0.95.
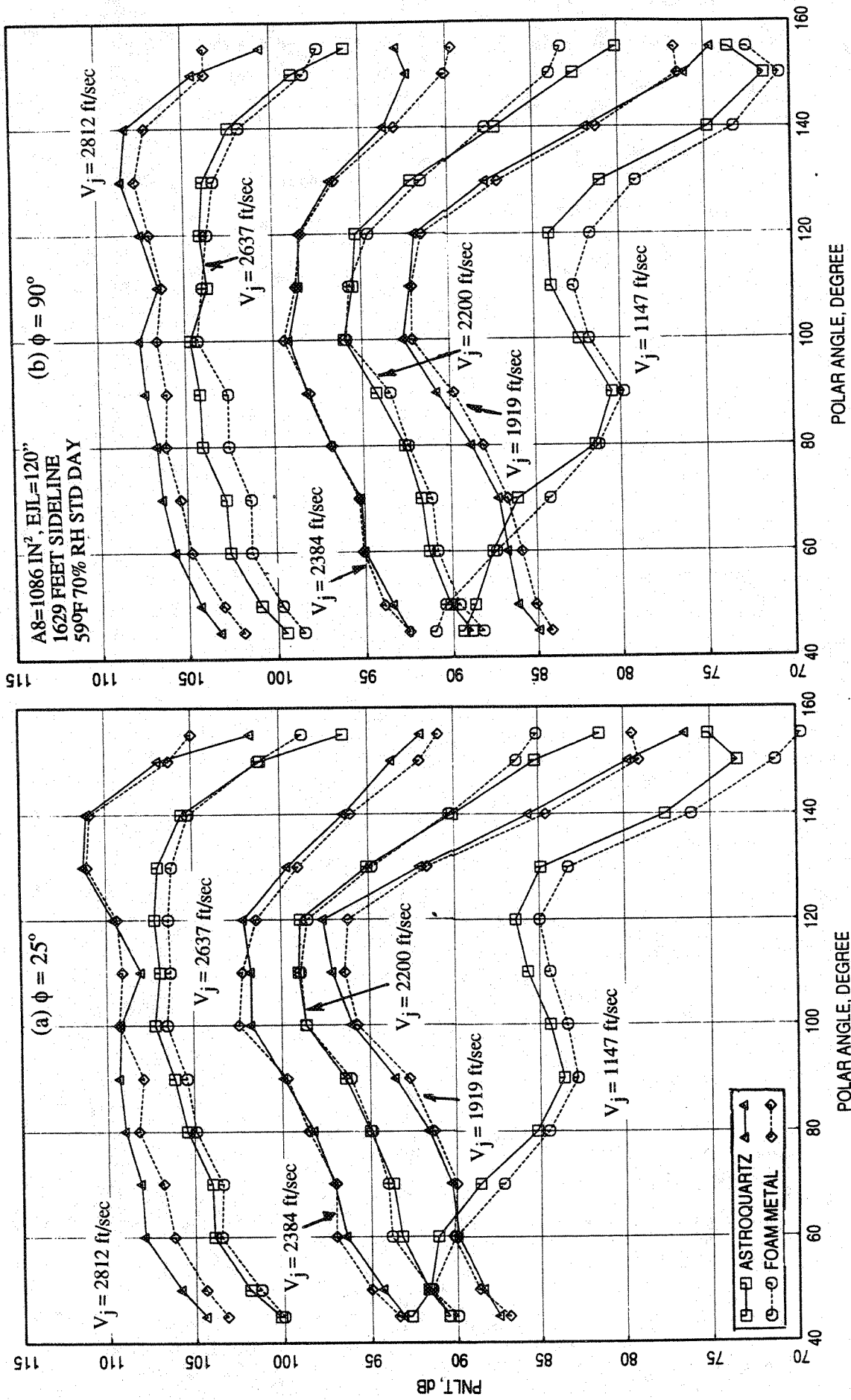
Figure 4.1-22. Comparison of PNLT directivities at different L1M cycle conditions between astroquartz and a foam metal treated long ejector for an aligned CD-chute mixer with flight simulation ($M_F = 0.32$); SAR = 2.8, MAR = 0.95.
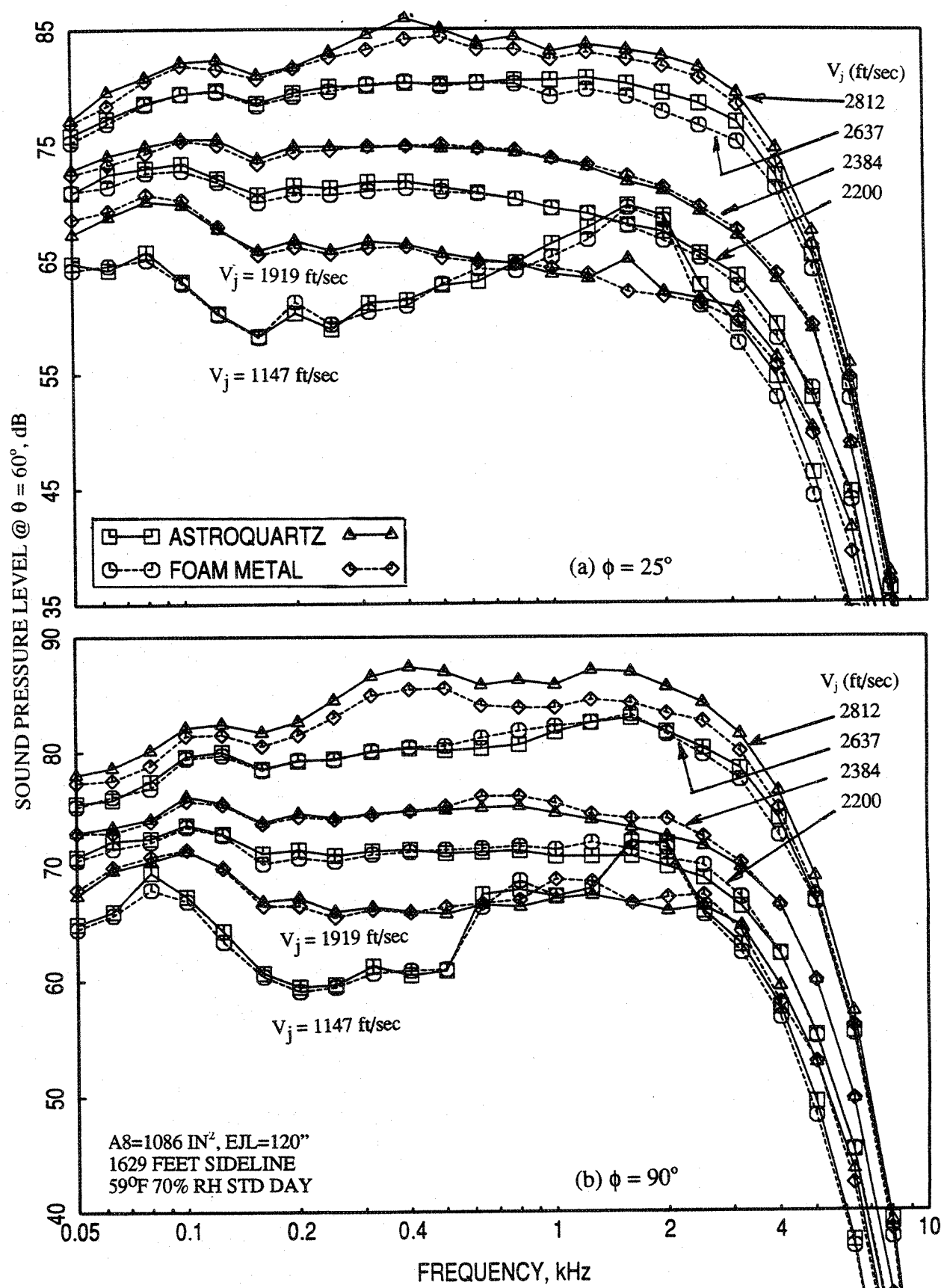
Figure 4.1-23. Comparison of SPL spectra at polar angle θ = 60° at different L1M cycle conditions between astroquartz and a foam metal treated long ejector for an aligned CD-chute mixer with flight simulation (M_F = 0.32); SAR = 2.8, MAR = 0.95.
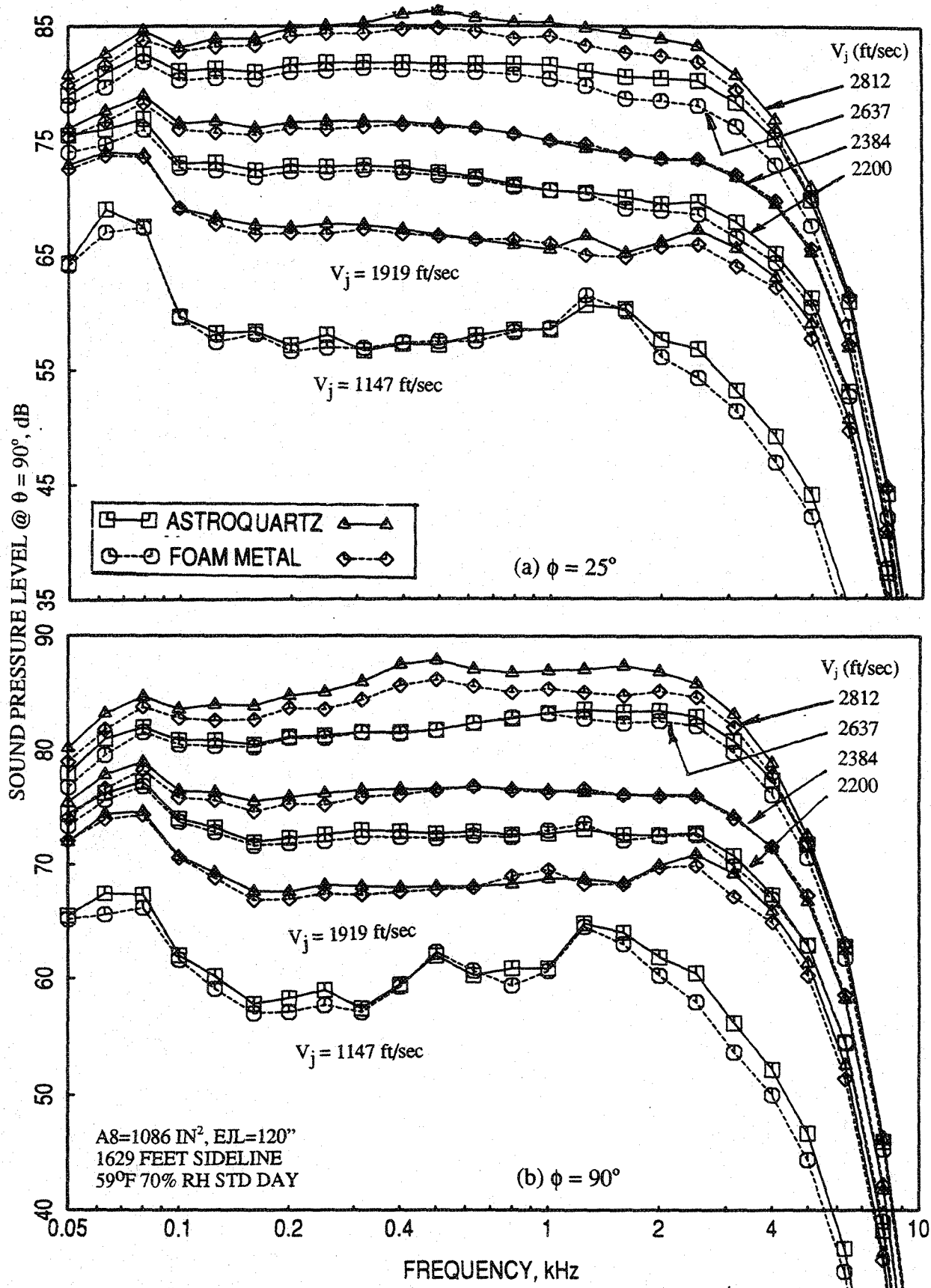
Figure 4.1-24. Comparison of SPL spectra at polar angle θ = 90° at different L1M cycle conditions between astroquartz and a foam metal treated long ejector for an aligned CD-chute mixer with flight simulation (M_F = 0.32); SAR = 2.8, MAR = 0.95.
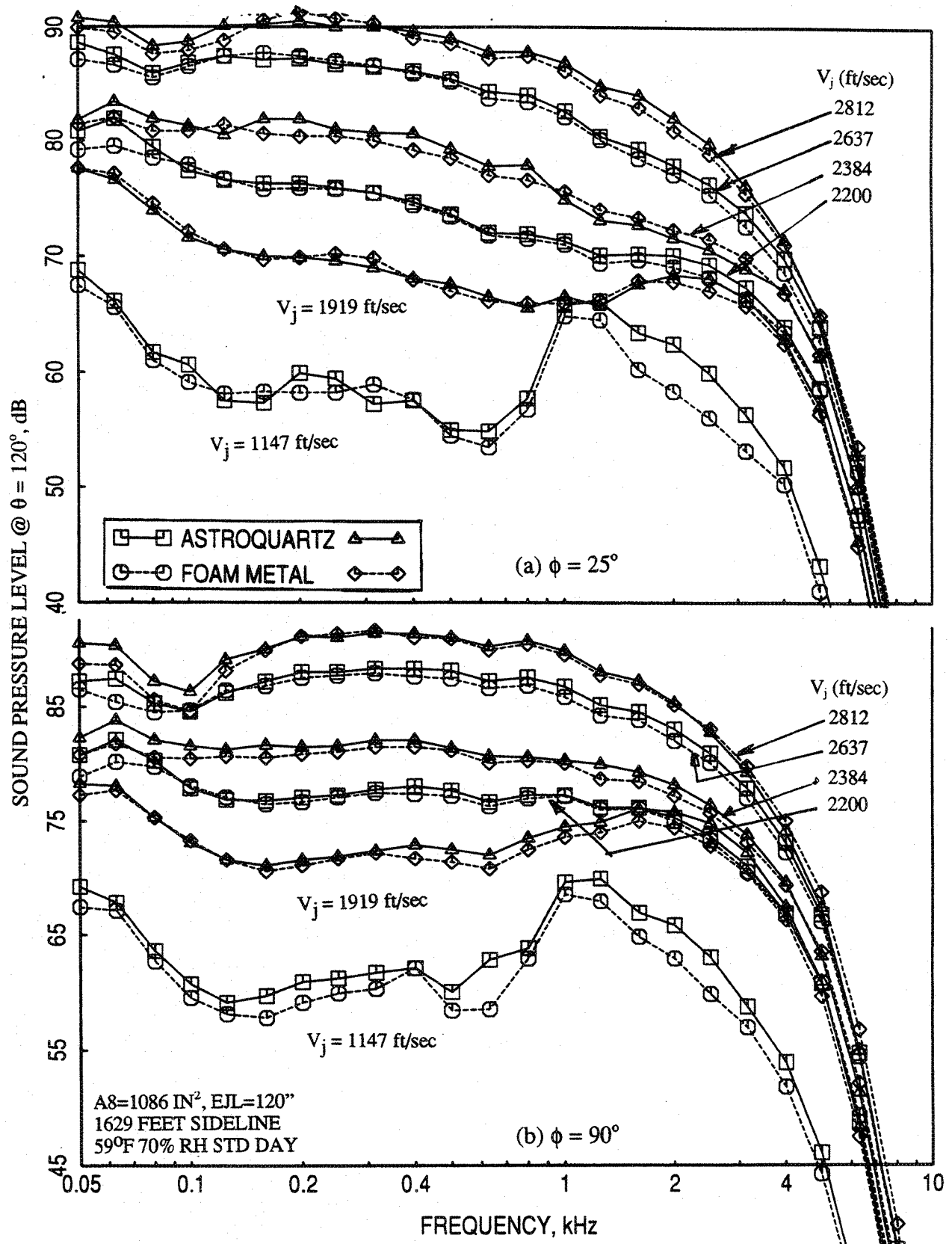
Figure 4.1-25. Comparison of SPL spectra at polar angle θ = 120° at different L1M cycle conditions between astroquartz and a foam metal treated long ejector for an aligned CD-chute mixer with flight simulation (M_F = 0.32); SAR = 2.8, MAR = 0.95.
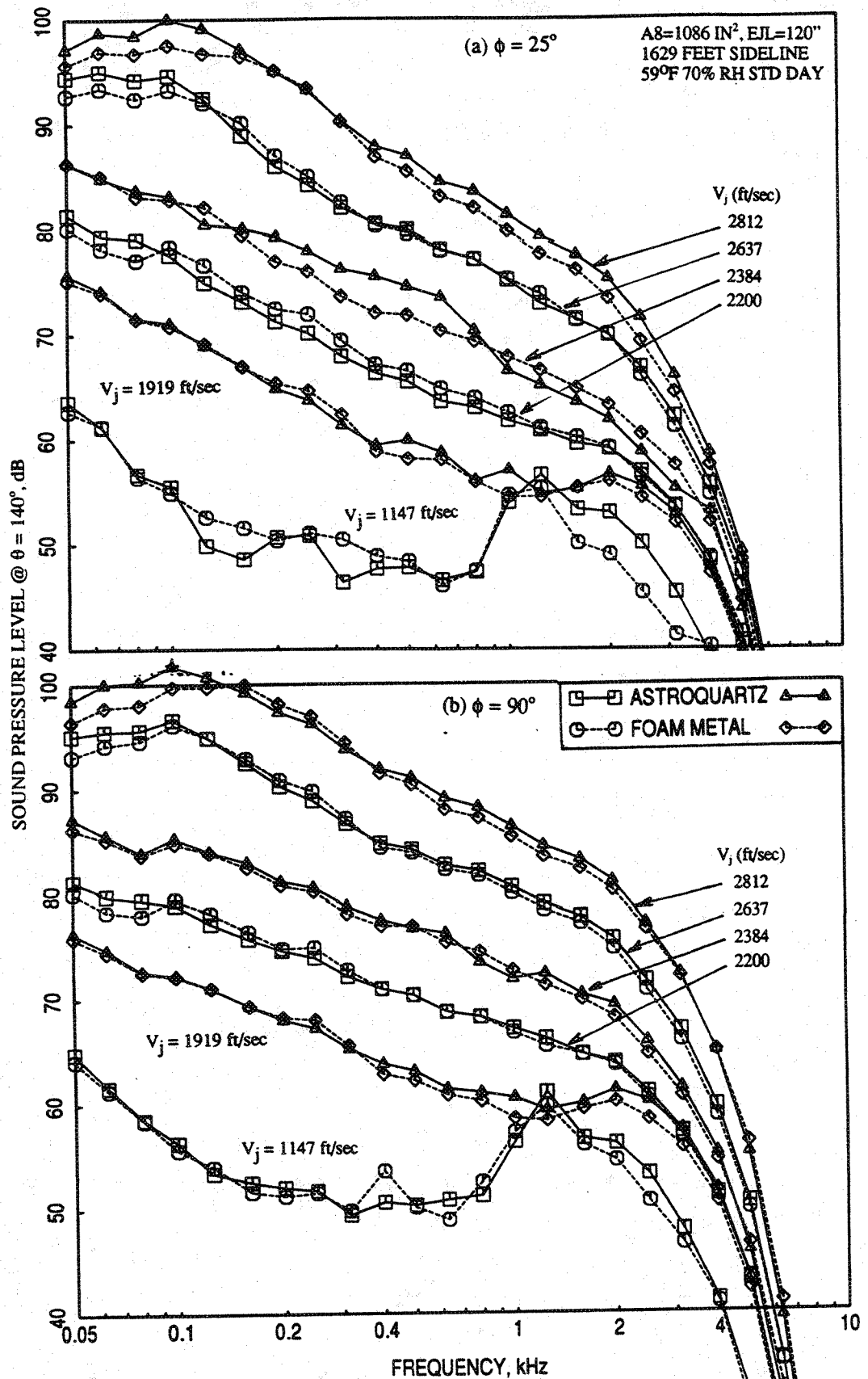
Figure 4.1-26. Comparison of SPL spectra at polar angle θ = 140° at different L1M cycle conditions between astroquartz and a foam metal treated long ejector for an aligned CD-chute mixer with flight simulation ($M_F = 0.32$); SAR = 2.8, MAR = 0.95.

is solid in structure and did not show any deterioration during testing, this treatment was used in all the subsequent treated configurations, instead of astroquartz.

4.1.3 Azimuthal Variation:

The azimuthal variation of acoustic characteristics of the aligned CD chute mixer-ejector configurations of SAR 3.3 and 2.8 with astroquartz and nickel based foam metal treatments, respectively (i.e., configurations #1 and #21), are obtained from the measurements made at five azimuthal locations.

Results for the Mixer with SAR=3.3:

Figure 4.1-27 shows the azimuthal variation of EPNL and PNLT at various polar angles (θ) as functions of jet velocity (V_j) at a sideline distance of 1629' for static and with flight simulation conditions. Significant azimuthal variation is observed in these figures. In general, the azimuthal variation is more at lower jet velocities. The variation diminishes with increasing jet velocity. With respect to EPNL the levels are higher at both the community points and between the community points the levels at $\phi = 90^o$ are higher compared to $\phi = 4^o$. The levels are lowest at the sideline with respect to major axis (i.e., $\phi = 25^o$). In the forward arc for lower polar angles PNLT levels are lowest at $\phi = 4^o$. For higher polar angles the PNLT variations with respect to azimuthal angle are similar to EPNL. The azimuthal variation of EPNL and peak PNLT is further studied by plotting these noise levels with respect to azimuthal angle for different L1M cycle conditions in Figures 4.1-28 and 4.1-29. Again, a minimum EPNL is observed at $\phi = 25^o$ for most cases.

At four different jet velocities the azimuthal variation of PNLT directivities are shown in Figure 4.1-30. The azimuthal variation is higher at lower velocities and is observed for all polar angles. For velocities above 2000 ft./sec, the azimuthal variation of PNLT is much less and is even smaller in the forward arc. Spectral comparisons at various polar angles (θ) for each of the four jet velocities are shown in Figures 4.1-31 through 4.1-34. Azimuthal variation of SPL is more dominant for lower jet velocities and at higher frequencies. For higher jet velocities, the azimuthal variation of SPL is small and is insignificant at lower frequencies.
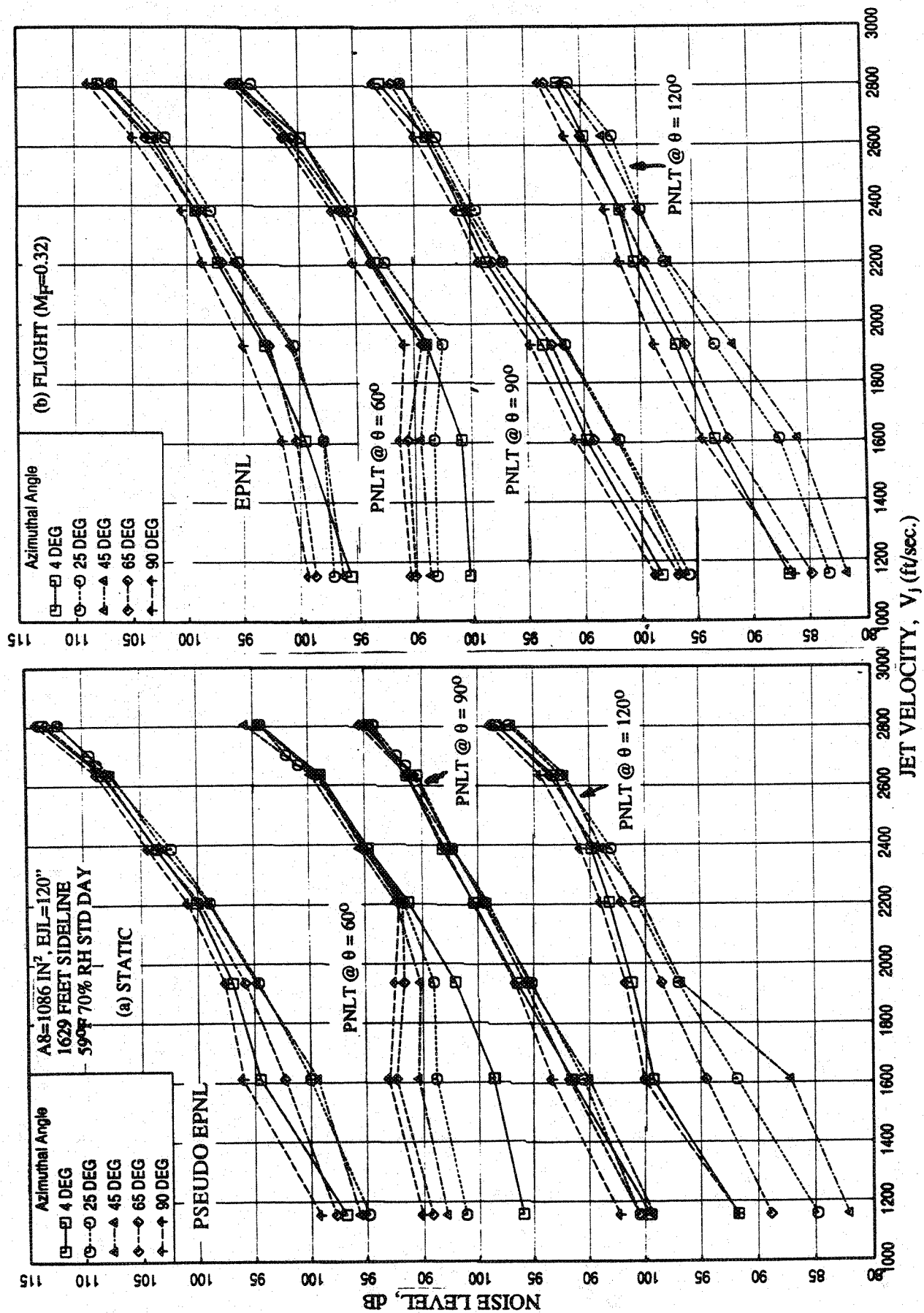
Figure 4.1-27. Azimuthal variation of EPNL and PNLT at various polar angles (θ) as function of jet velocity of L1M cycle conditions for an aligned CD-chute mixer with treated long ejector; SAR=3.3, MAR=0.95.
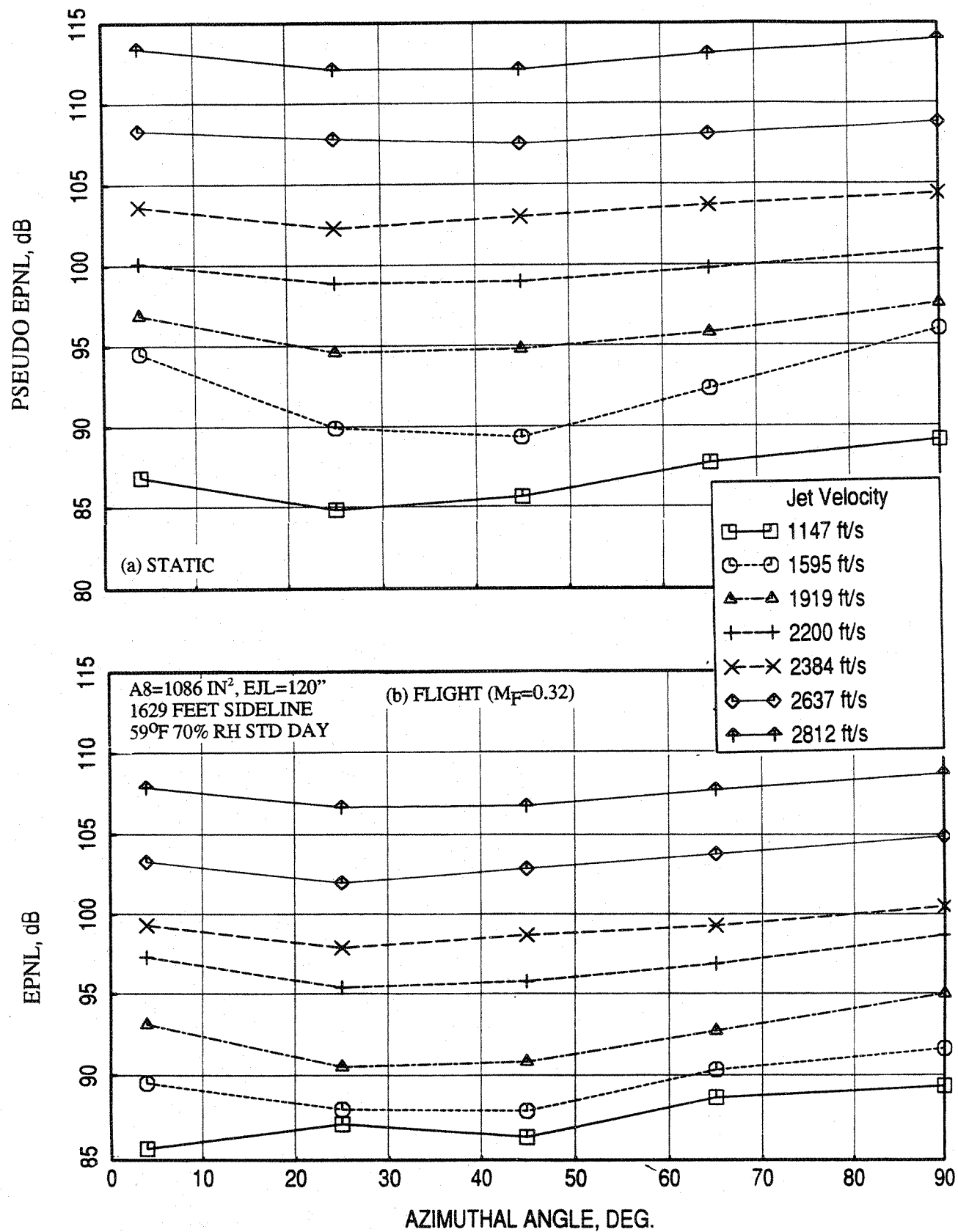
Figure 4.1-28. Variation of EPNL with respect to azimuthal angle (ϕ) at different L1M cycle conditions for an aligned CD-chute mixer with treated long ejector; SAR=3.3, MAR=0.95.
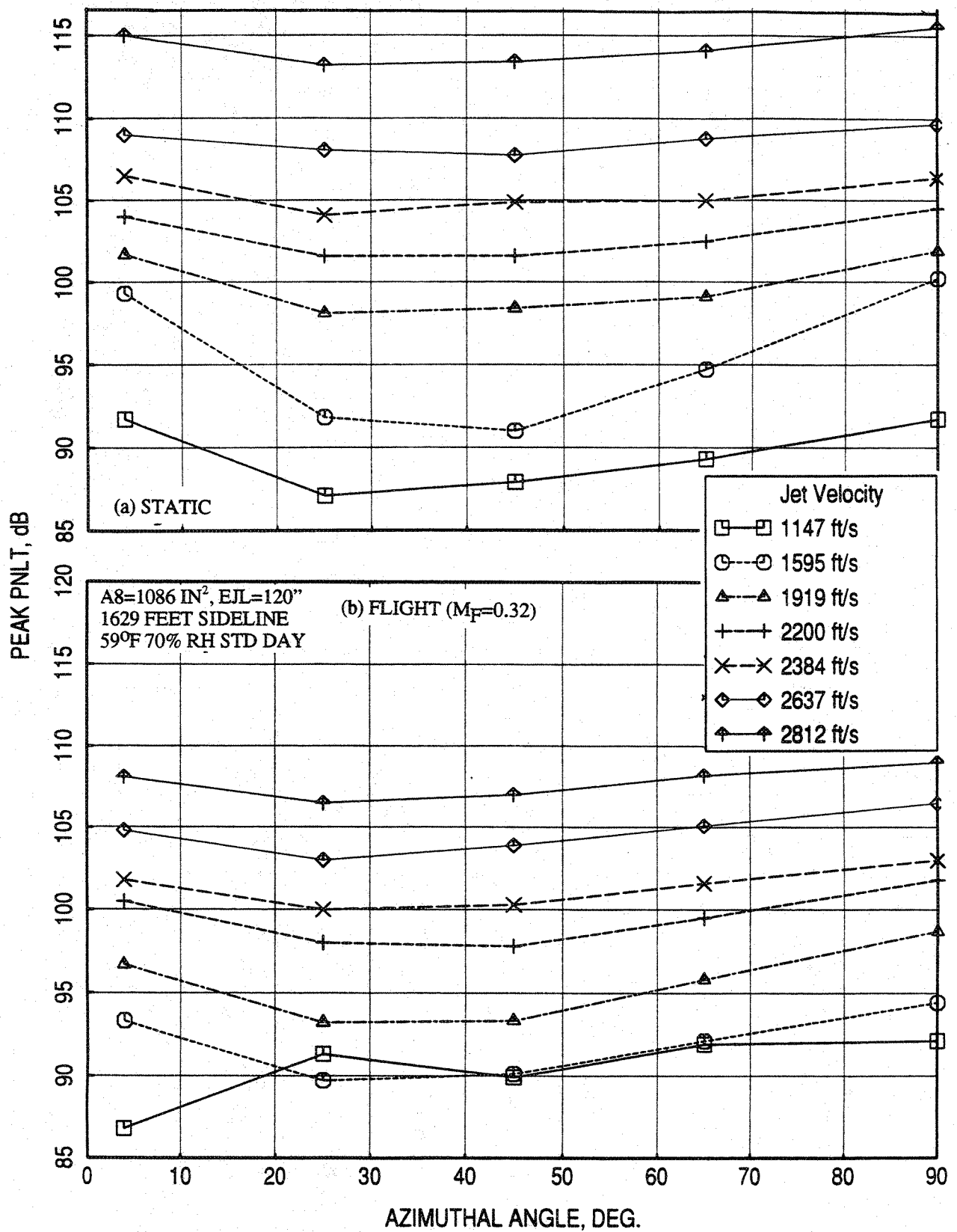
Figure 4.1-29. Variation of peak PNLT with respect to azimuthal angle (ϕ) at different L1M cycle conditions for an aligned CD-chute mixer with treated long ejector; SAR=3.3, MAR=0.95.
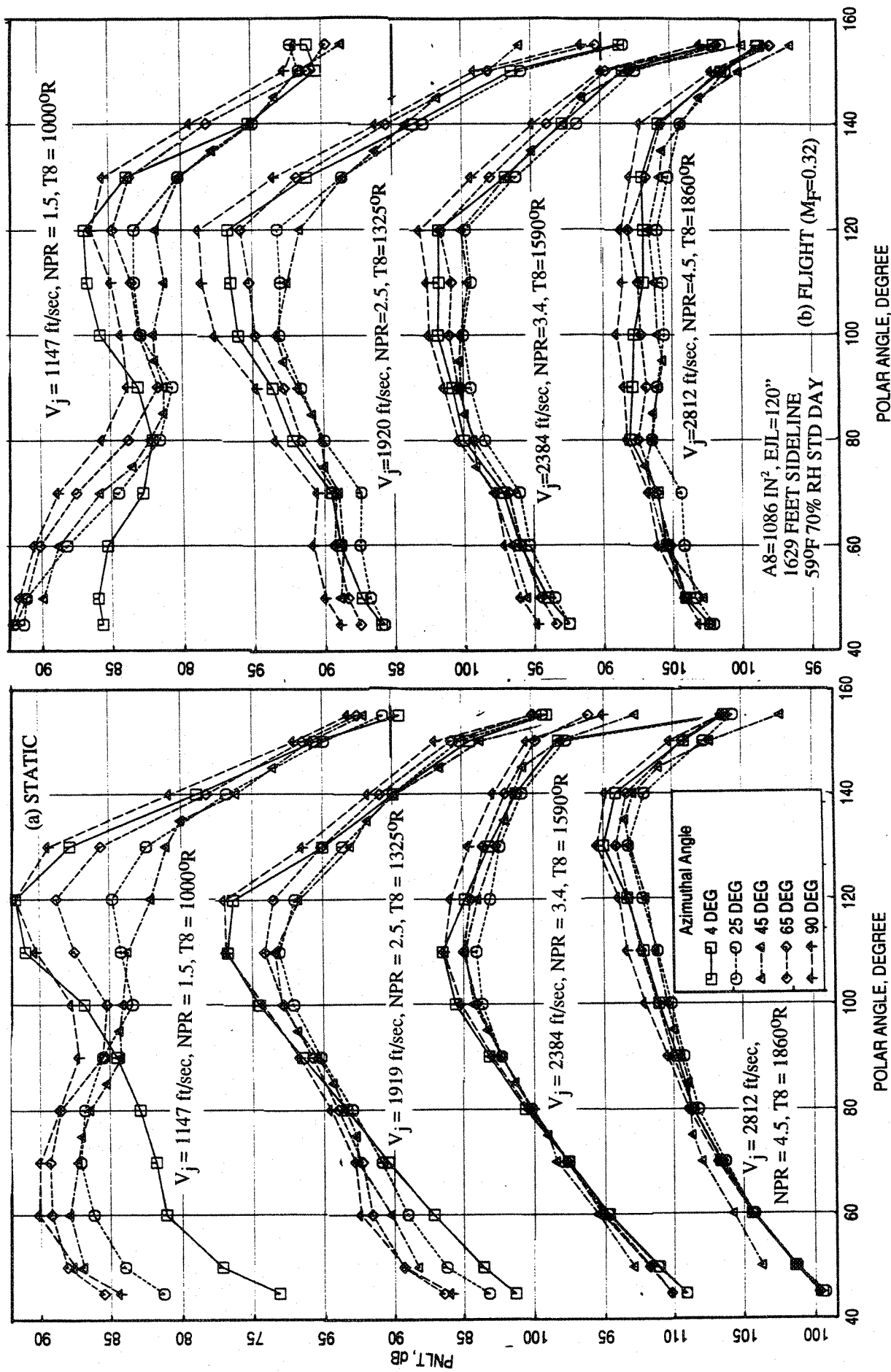
Figure 4.1-30. Azimuthal variation of PNLT directivities for different jet velocities (V_j) of L1M cycle conditions for an aligned CD-chute mixer with treated long ejector; SAR=3.3, MAR=0.95.
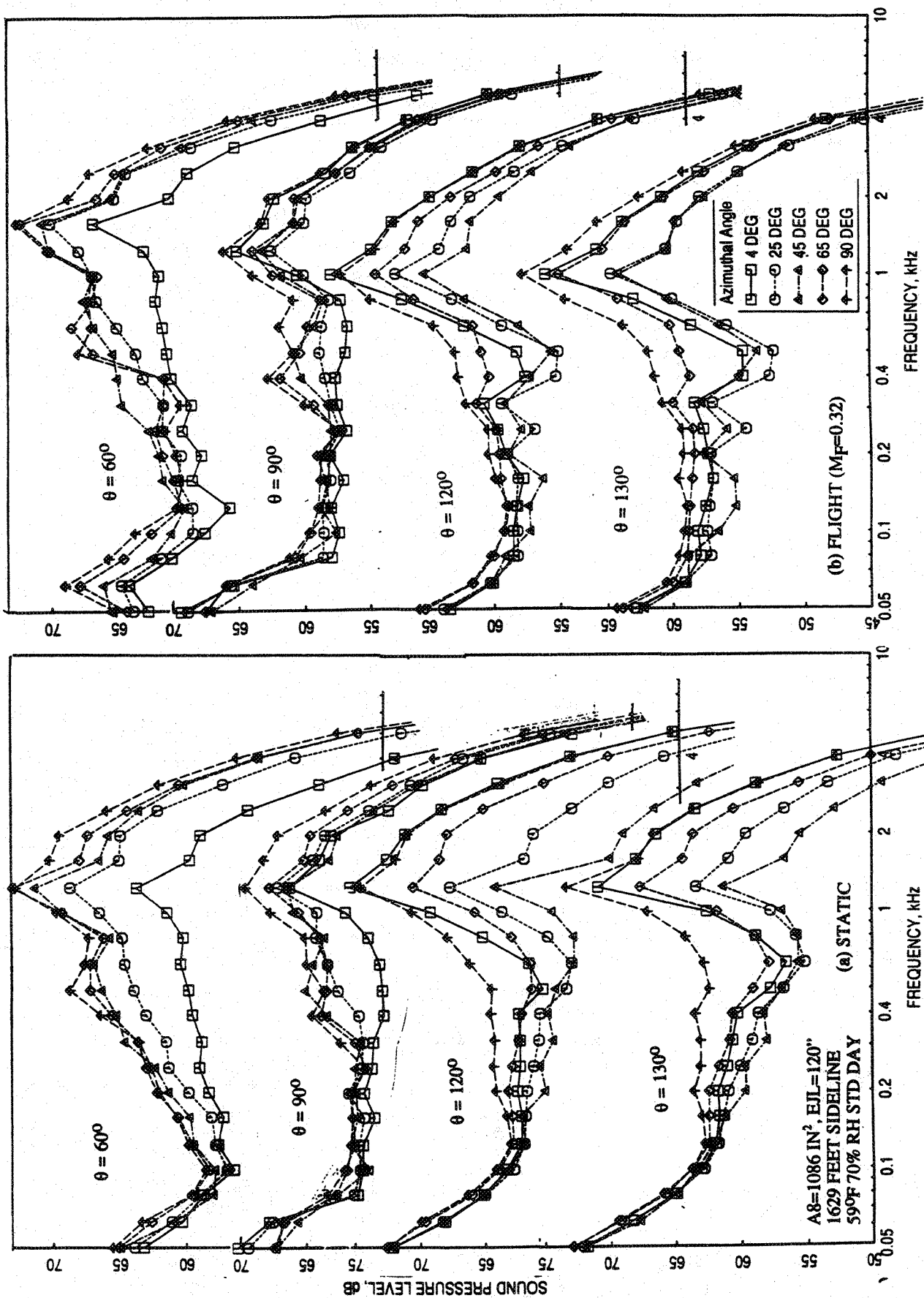
Figure 4.1-31. Azimuthal variation of SPL spectra at various polar angles (θ) for an aligned CD-chute mixer with treated long ejector; SAR=3.3; MAR=0.95, V_j = 1147 ft/sec, NPR = 1.5, T8 = 1000°R.
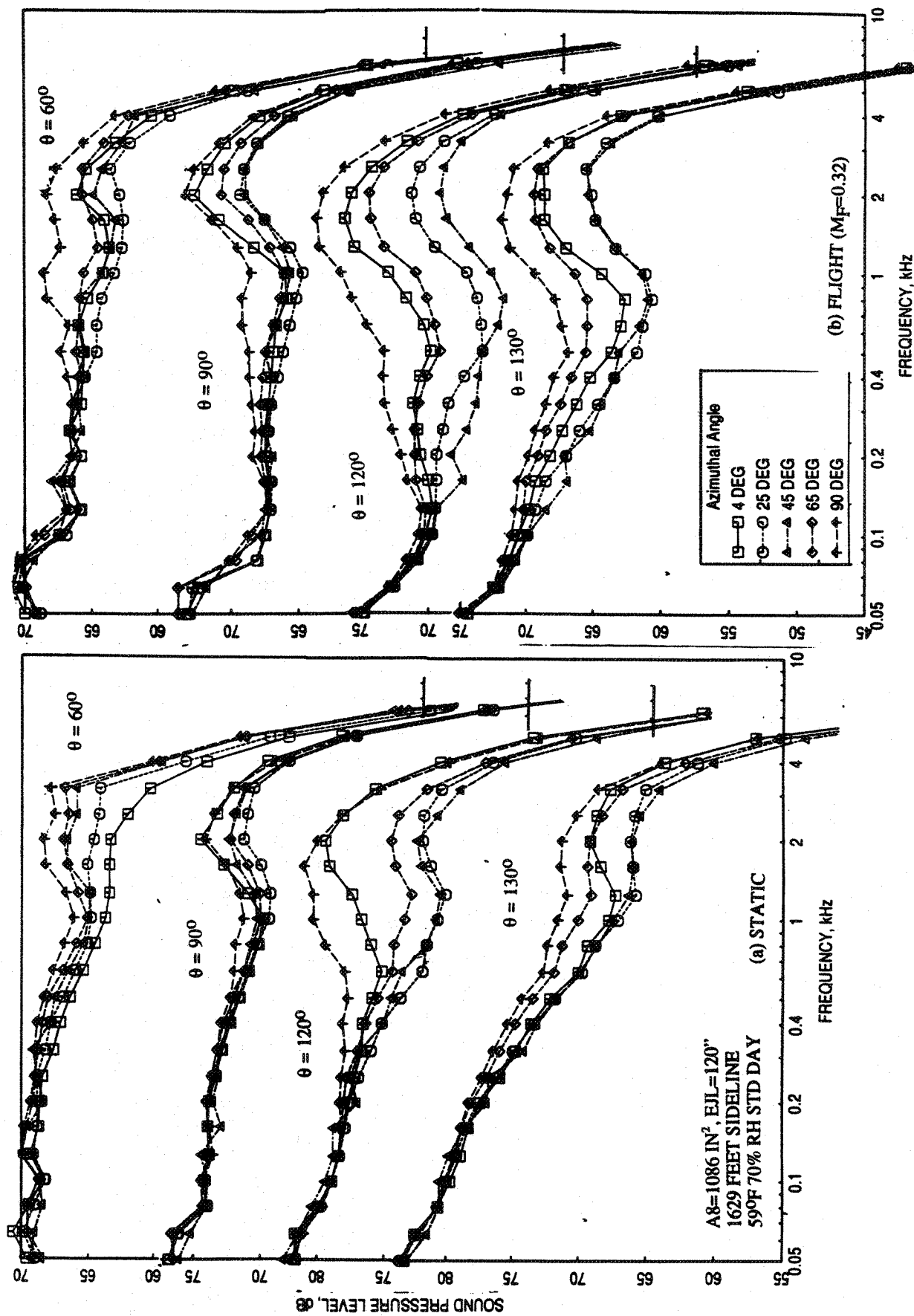
Figure 4.1-32. Azimuthal variation of SPL spectra at various polar angles (θ) for an aligned CD-chute mixer with treated long ejector; SAR=3.3, MAR=0.95, V_j = 1919 ft/sec, NPR = 2.5, T8 = 1325°R.
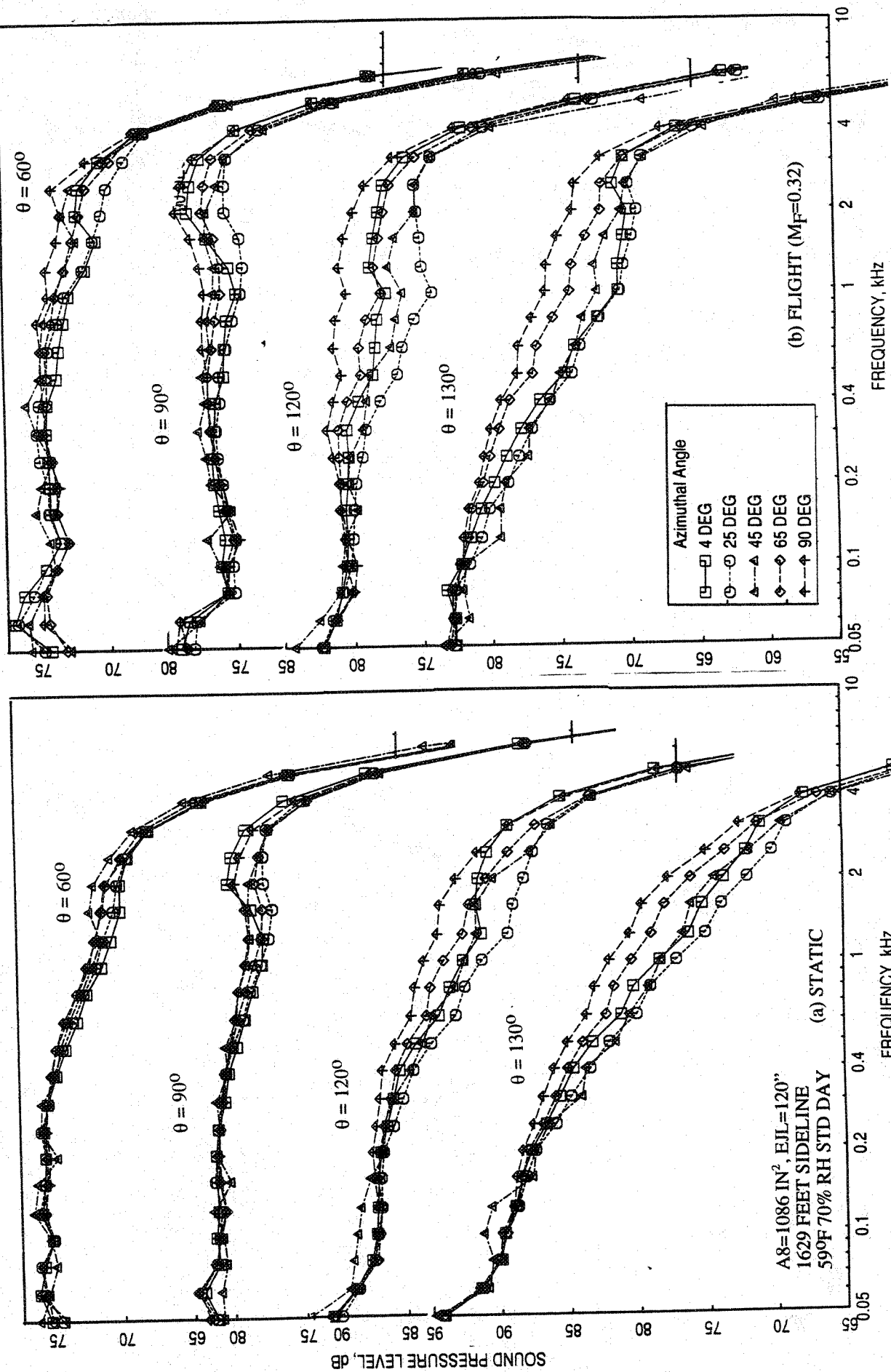
Figure 4.1-33. Azimuthal variation of SPL spectra at various polar angles (θ) for an aligned CD-chute mixer with treated long ejector; SAR=3.3, MAR=0.95, V_j = 2384 ft/sec, NPR = 3.4, T8 = 1590°R.
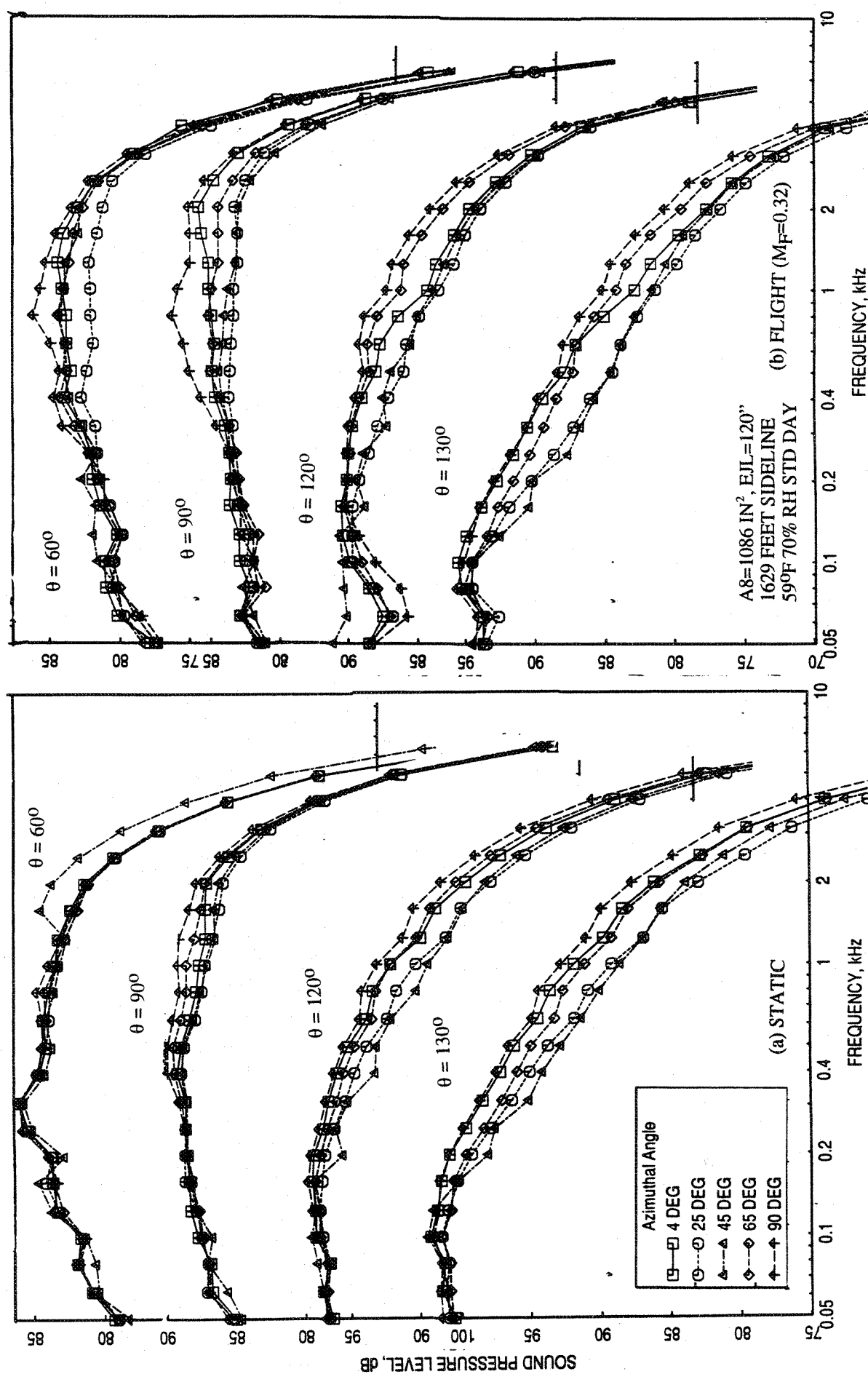
Figure 4.1-34. Azimuthal variation of SPL spectra at various polar angles (θ) for an aligned CD-chute mixer with treated long ejector; SAR=3.3, MAR=0.95, V_j = 2812 ft/sec, NPR = 4.5, T8 = 1860°R.

In general, the azimuthal variation of acoustic field is significant and is much higher at lower jet velocities. A variation of about 5 to 6 EPNdB is observed at jet velocities between 1147 ft/sec and 1600 ft/sec. Even at higher jet velocities the variation is of significance.

Results for the Mixer with SAR=2.8:

Some acoustic results for static and with flight simulation (M_F=0.32) conditions, showing the azimuthal variation for the aligned CD chute mixer of SAR=2.8 with long foam metal treated ejector (i.e., Configuration #21), are presented. Figures 4.1-35 shows the azimuthal variation of EPNL and PNLT at various polar angles (θ) as function of jet velocity (V_j) at a sideline distance of 1629'. Significant azimuthal variation is observed in these results. In general, the azimuthal variation is more at lower jet velocities. The variation diminishes with increasing jet velocity. The EPNL levels are higher at the community point with respect to the major axis. However, relatively smaller difference is observed between community and sideline points with respect to the minor axis for all the jet velocities. The levels are lowest at the sideline with respect to major axis (i.e., ϕ = 25°). The azimuthal variation of EPNL and peak PNLT is further studied by plotting these noise levels with respect to azimuthal angle for different L1M cycle conditions in Figures 4.1-36 and 4.1-37. Again, a minimum EPNL is observed at $\phi = 25^o$ for most cases.

At four different jet velocities the azimuthal variation of PNLT directivities are shown in Figure 4.1-38. The azimuthal variation is higher at lower velocities and is observed for all polar angles. Spectral comparisons at various polar angles (θ) for each of the four jet velocities are shown in Figures 4.1-39 through 4.1-42. Azimuthal variation of SPL is more dominant for lower jet velocities and at higher frequencies (see Figure 4.1-39). For higher jet velocities, the azimuthal variation of SPL is small and is insignificant at lower frequencies.

In general, the azimuthal variation of acoustic field is significant and is much higher at lower jet velocities. A variation of about 4 to 6 EPNdB is observed at jet velocities between 1147 ft/sec and 1600 ft/sec. Even at higher jet velocities the variation is of significance. The azimuthal variation of farfield noise for 2D nozzles is caused by the non-axisymmetric radiation pattern of internal noise and the externally generated mixing noise from non-axisymmetric jet. At lower velocities the internal noise is significant and the jet plume responsible for external component of the noise remains axially non-axisymmetric
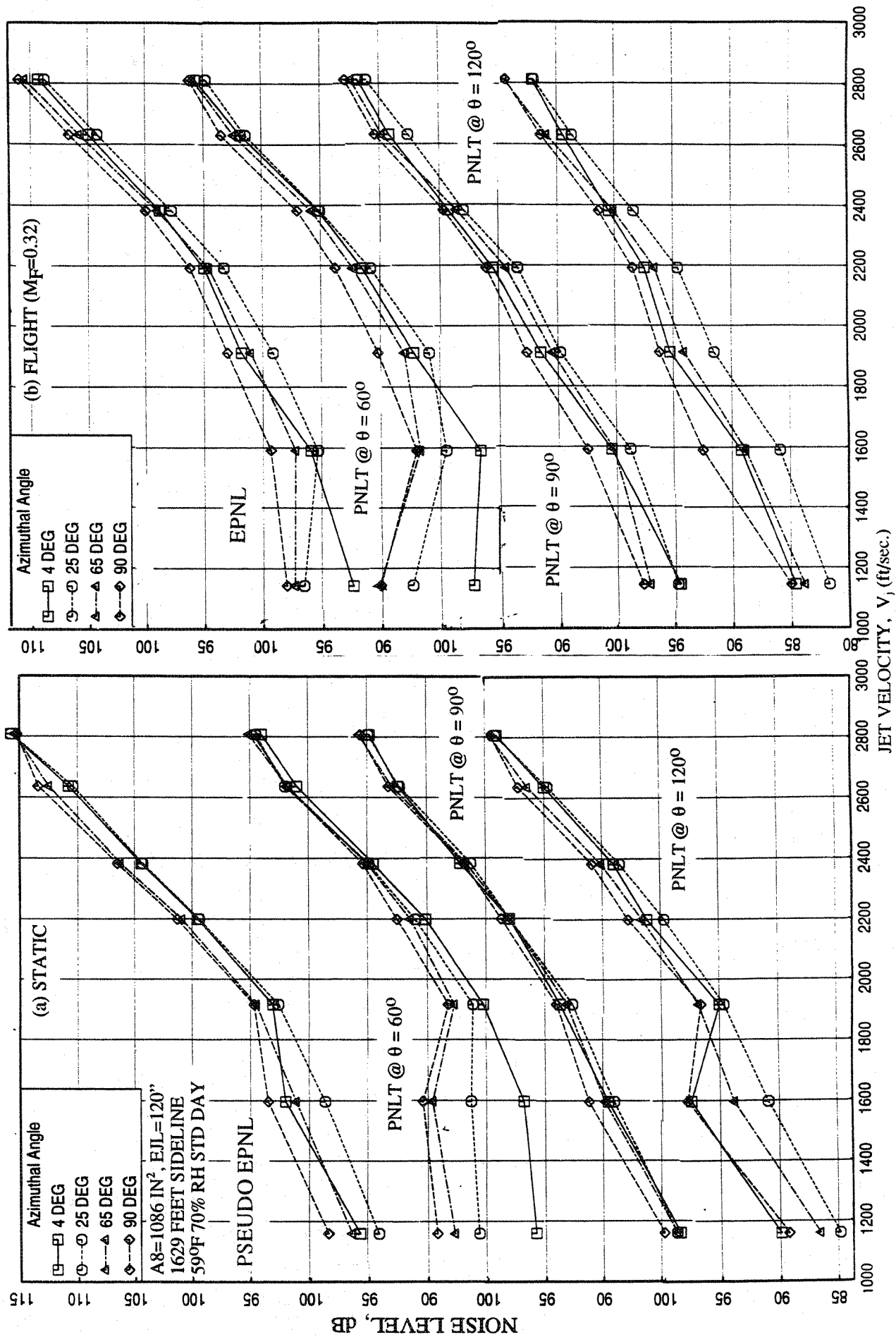
Figure 4.1-35. Azimuthal variation of EPNL and PNLT at various polar angles (θ) as function of jet velocity of L1M cycle conditions for an aligned CD-chute mixer with foam metal treated long ejector; SAR=2.8, MAR=0.95.
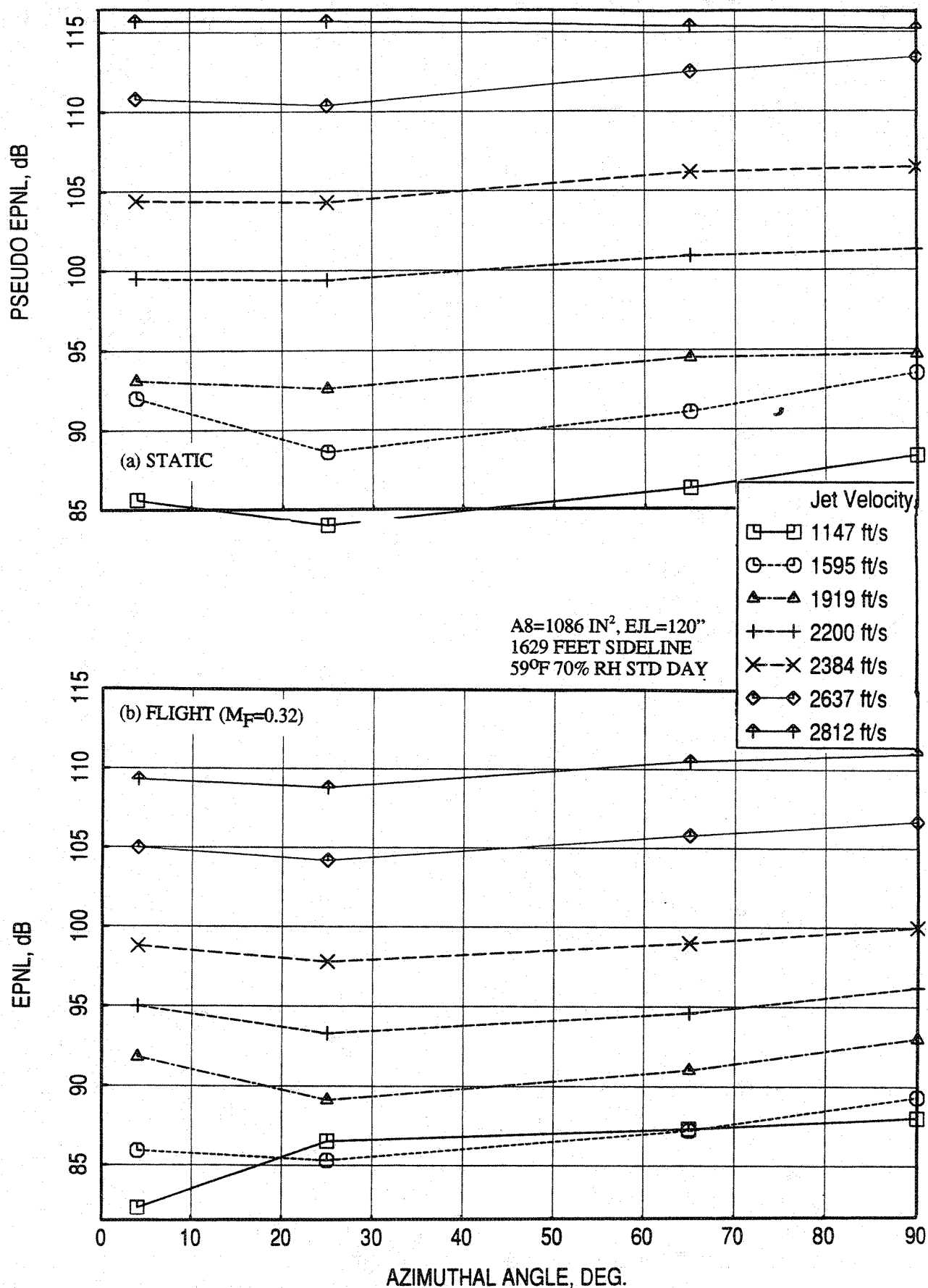
Figure 4.1-36. Variation of EPNL with respect to azimuthal angle (φ) at different L1M cycle conditions for an aligned CD-chute mixer with foam metal treated long ejector; SAR=2.8, MAR=0.95.
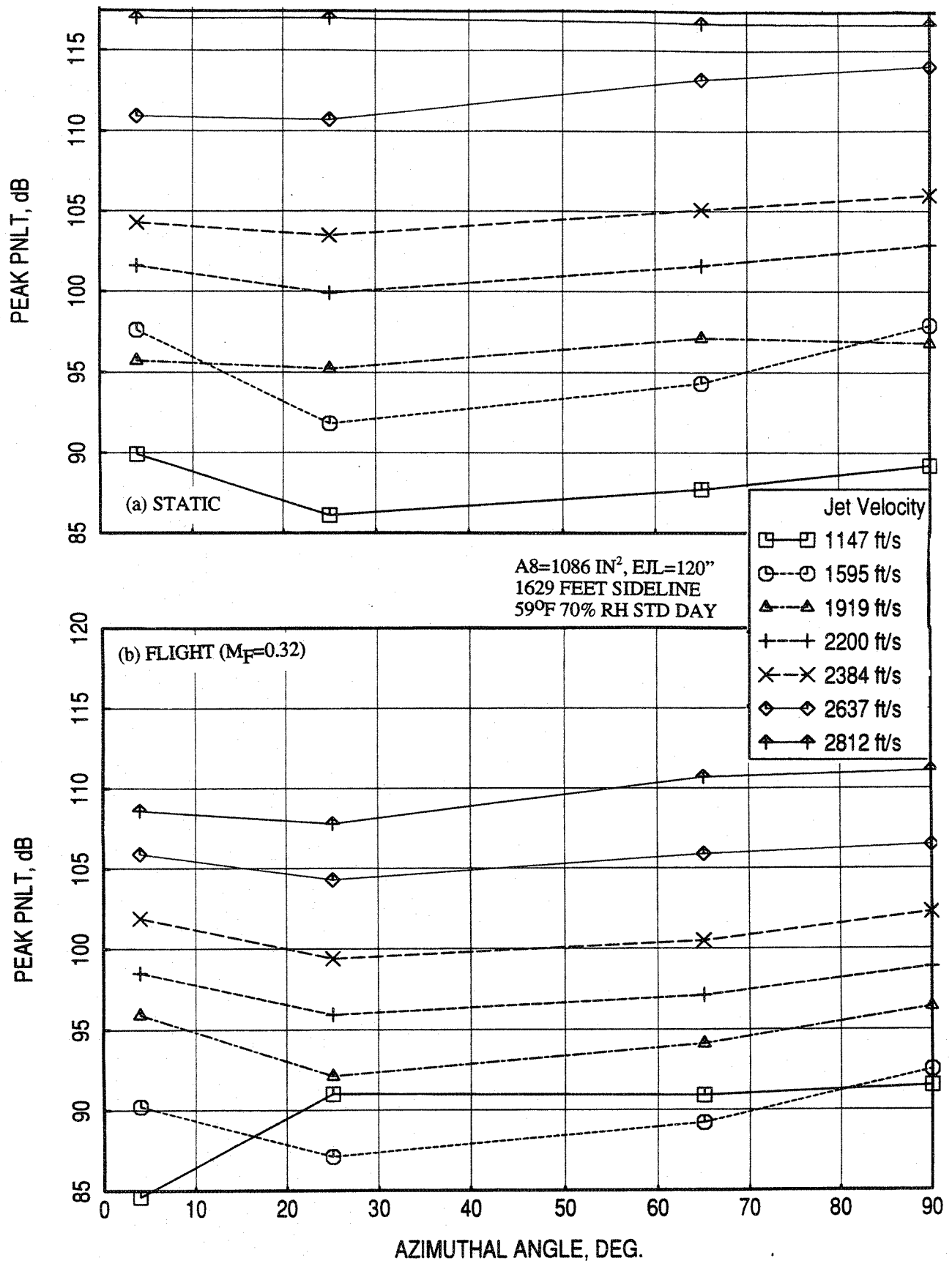
Figure 4.1-37. Variation of peak PNLT with respect to azimuthal angle (φ) at different L1M cycle conditions for an aligned CD-chute mixer with foam metal treated long ejector; SAR=2.8, MAR=0.95.
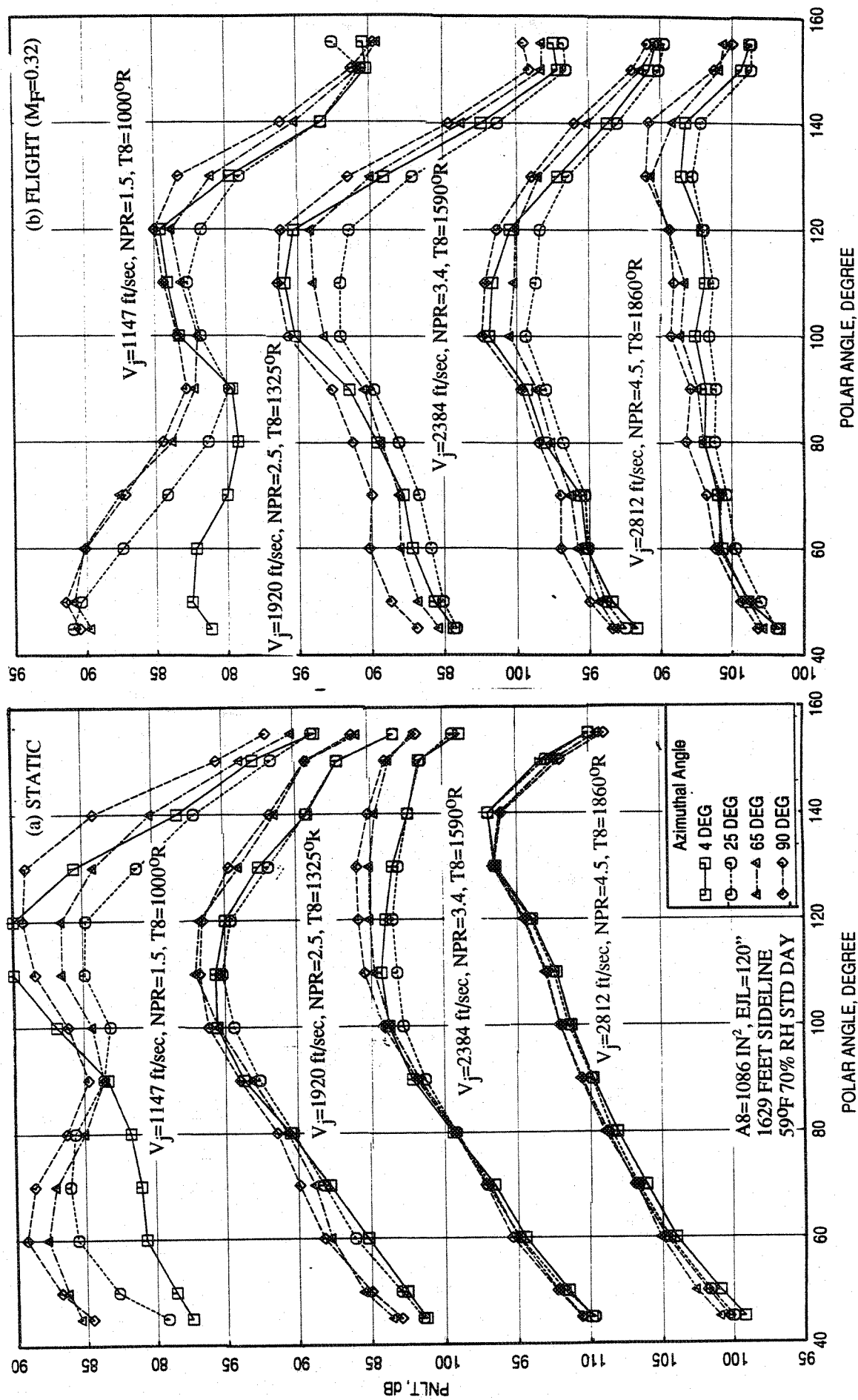
Figure 4.1-38. Azimuthal variation of PNLT directivities for different jet velocities (V_j) of L1M cycle conditions for an aligned CD-chute mixer with foam metal treated long ejector; SAR=2.8, MAR=0.95.
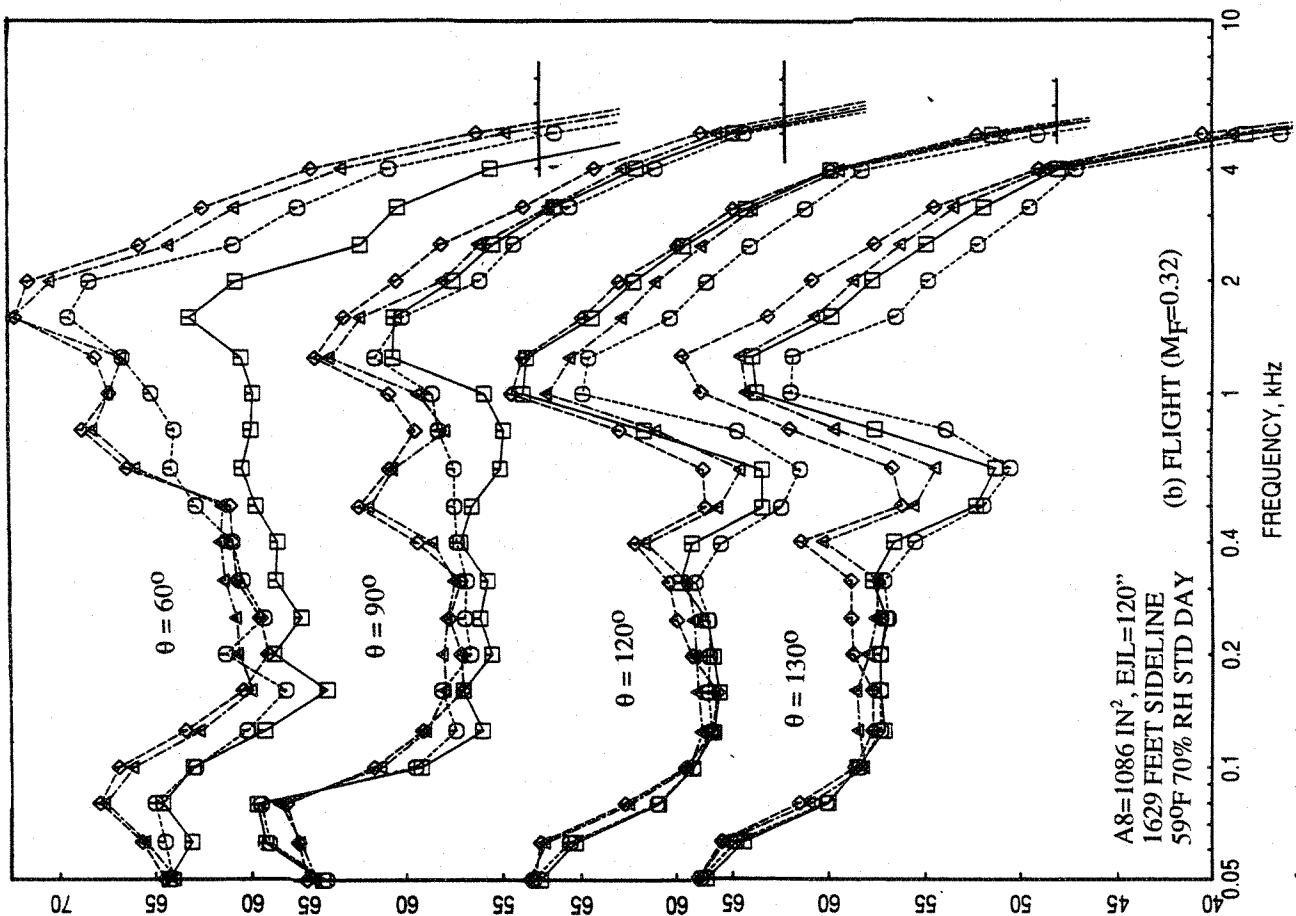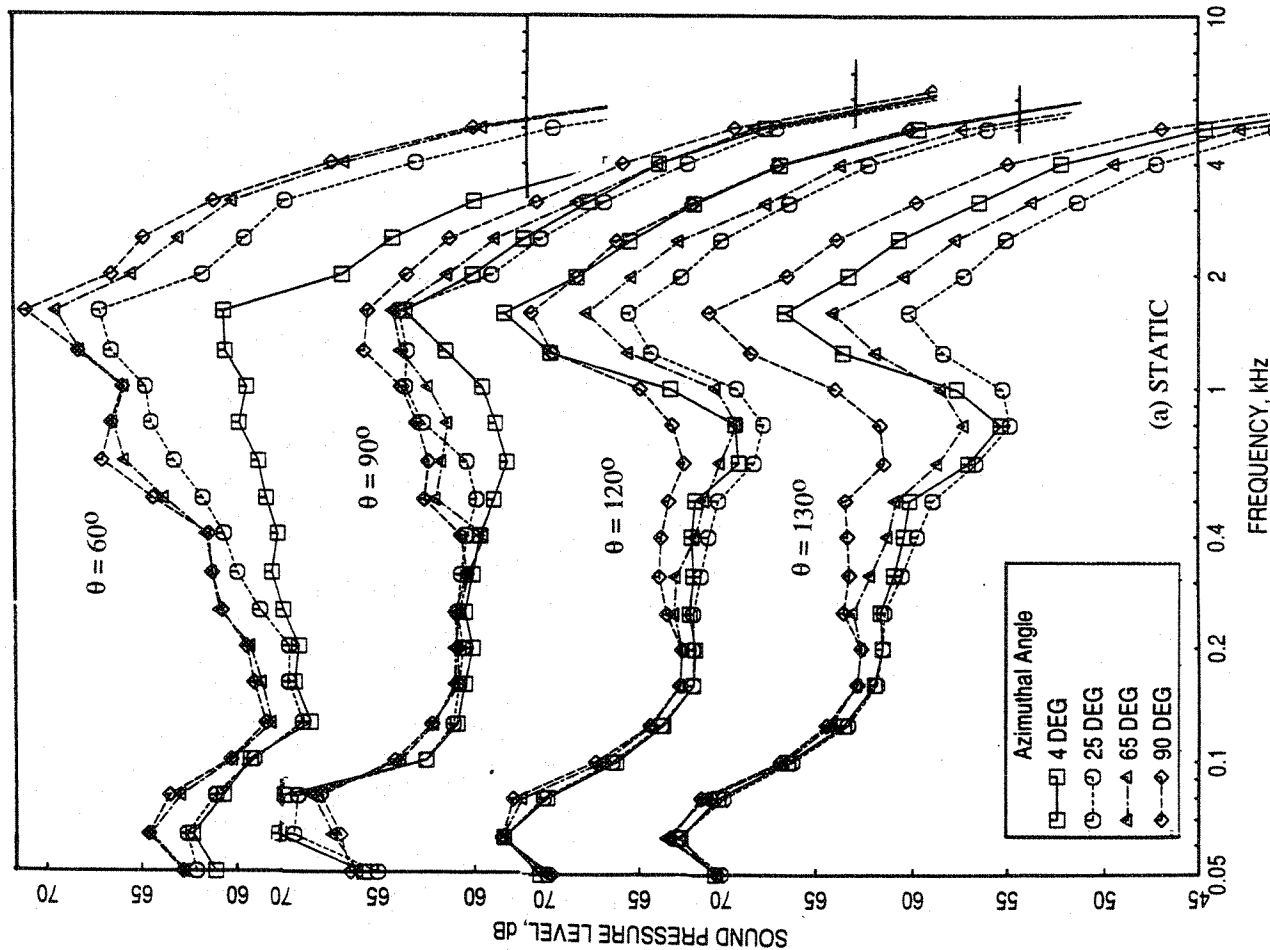
Figure 4.1-39. Azimuthal variation of SPL spectra at various polar angles (θ) for an aligned CD-chute mixer with foam metal treated long ejector; SAR=2.8, MAR=0.95, V_j = 1147 ft/sec, NPR = 1.5, T8 = 1000°R.
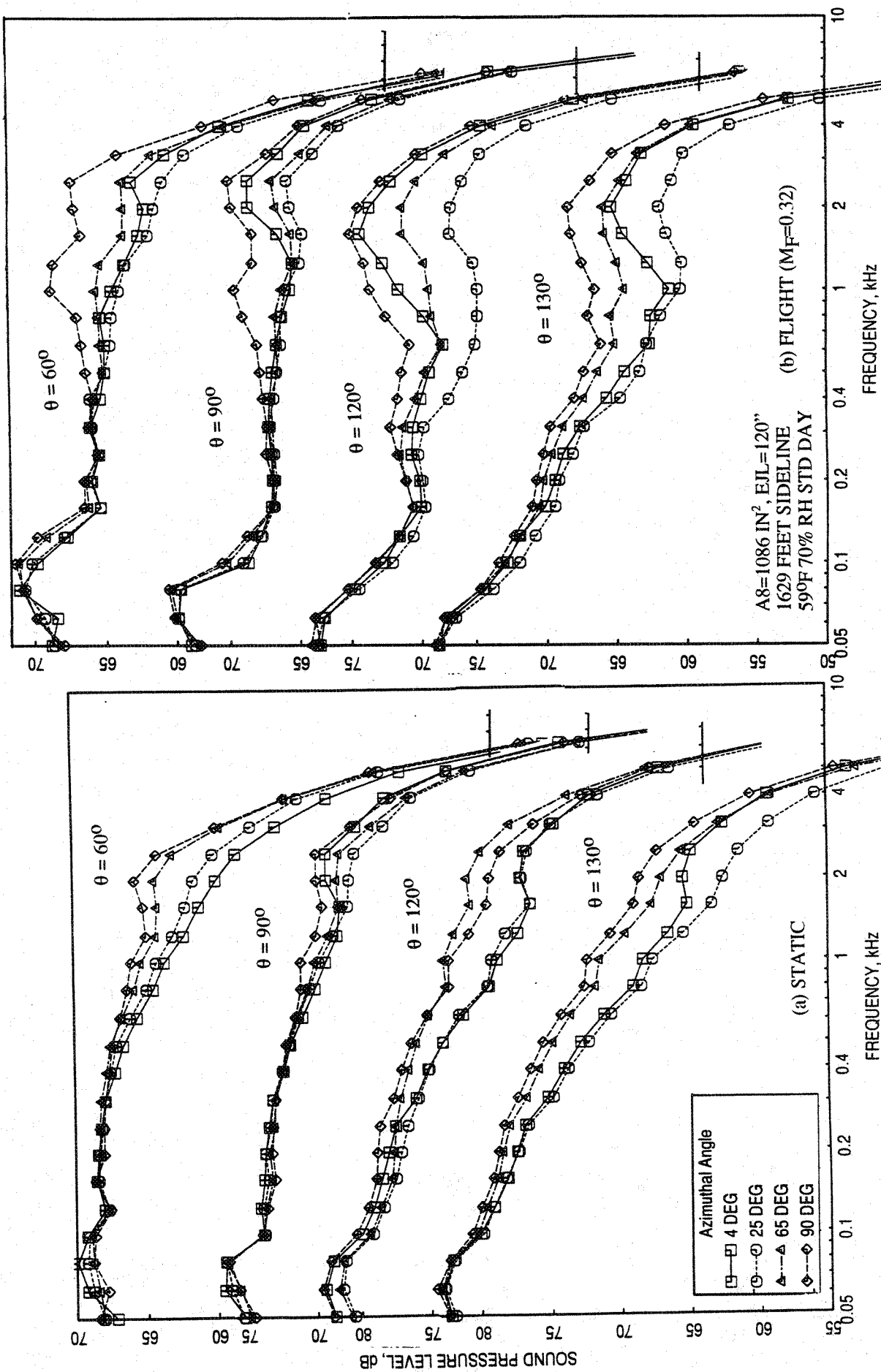
Figure 4.1-40. Azimuthal variation of SPL spectra at various polar angles (θ) for an aligned CD-chute mixer with foam metal treated long ejector; SAR=2.8, MAR=0.95, V_j = 1919 ft/sec, NPR = 2.5, T8 = 1325°R.
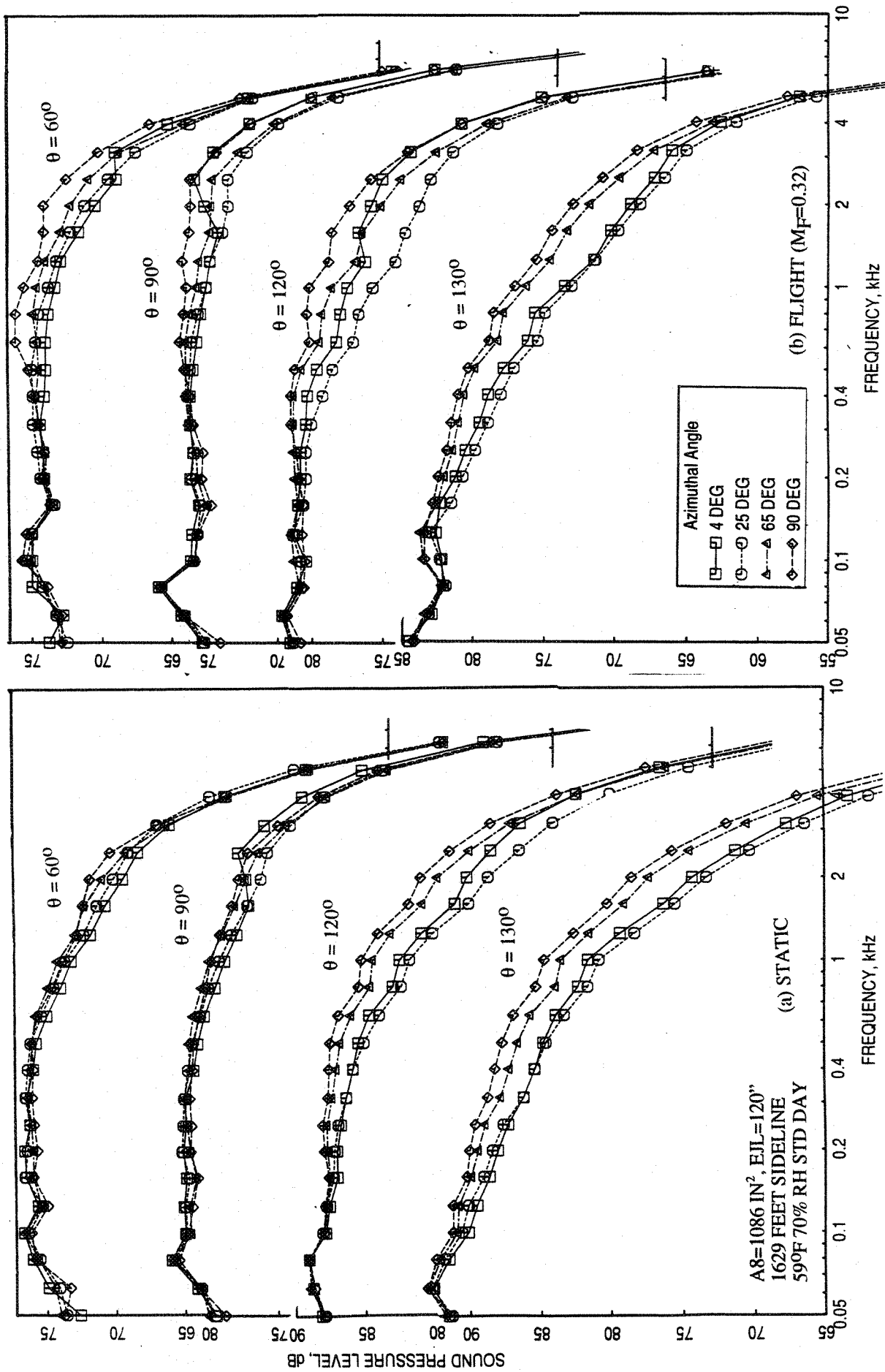
Figure 4.1-41. Azimuthal variation of SPL spectra at various polar angles (θ) for an aligned CD-chute mixer with foam metal treated long ejector; SAR=2.8, MAR=0.95, V_j = 2384 ft/sec, NPR = 3.4, T8 = 1590°R.
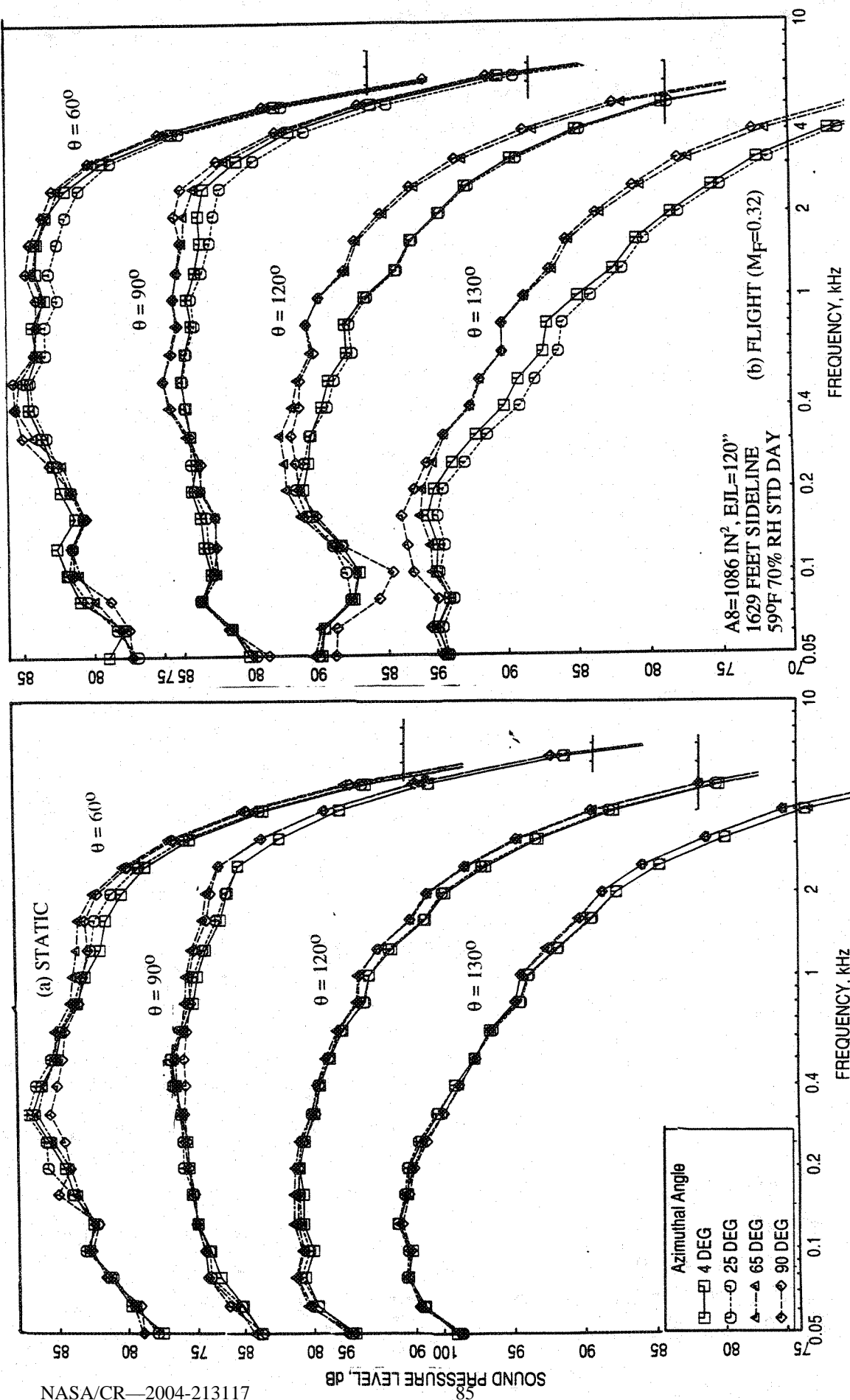
Figure 4.1-42. Azimuthal variation of SPL spectra at various polar angles (θ) for an aligned CD-chute mixer with foam metal treated long ejector; SAR=2.8, MAR=0.95, V_j = 2812 ft/sec, NPR = 4.5, T8 = 1860°R.

up to a larger distance. Thus, the azimuthal variation of farfield noise becomes significant. At higher jet velocities the internally radiated noise levels are relatively lower compared to jet mixing noise. In addition, the jet plume becomes very close to symmetric within a short axial distance. Thus, the azimuthal variation of farfield noise is small for higher jet velocity conditions.

4.1.4 Effect of Flight Simulation

Some acoustic and performance related results, showing the effect of flight simulation for the aligned CD chute mixer of SAR=2.8 and 3.3 with long treated ejector (i.e., Configurations #21 and #1, respectively), are presented. While the ejector for mixer of SAR=2.8 was treated with foam metal, the ejector treatment for mixer of SAR=3.3 was astroquartz. The effect of flight simulation on acoustic characteristics and the performance related parameters of the mixer-ejector configurations is obtained from the measurements made at four flight conditions of Mach 0.0, 0.12, 0.24, and 0.32.

Acoustic Results : Acoustic results showing the flight simulation effects at an azimuthal angle $\phi = 25^{\circ}$ (i.e., the sideline location with respect to major axis) are presented here. Figures 4.1-43 shows the effect of flight simulation on EPNL and PNLT as function of jet velocity (V_j) at a sideline distance of 1629'. EPNL levels decrease with increasing flight Mach numbers for all jet velocities. Significant reduction is observed between Mach 0.12 and 0.24. Except for forward arc angles the PNLT levels decrease with increasing flight Mach number at all jet velocities.

At four different jet velocities the effect of flight simulation on PNLT directivities are shown in Figure 4.1-44. The effect of flight simulation is to lower the PNLT levels at polar angles above 60° and the trend is reversed at lower angles. Significant PNLT reduction is observed at rear arc. Effect of flight on SPL spectra at various polar angles (θ) for each of the four jet velocities are shown in Figures 4.1-45 through 4.1-48. Significant SPL reduction is observed at higher polar angles for the entire frequency range. Major noise reduction took place between Mach 0 and 0.24.

Flow and Performance Related Results : Model pressure data measured for the aligned CD chute mixer-ejector of SAR=2.8 are analyzed and presented to show the effect of cycle conditions and simulated flight on various flow and performance related parameters. Axial static pressure distributions on the ramp and on the chute leading edge on secondary
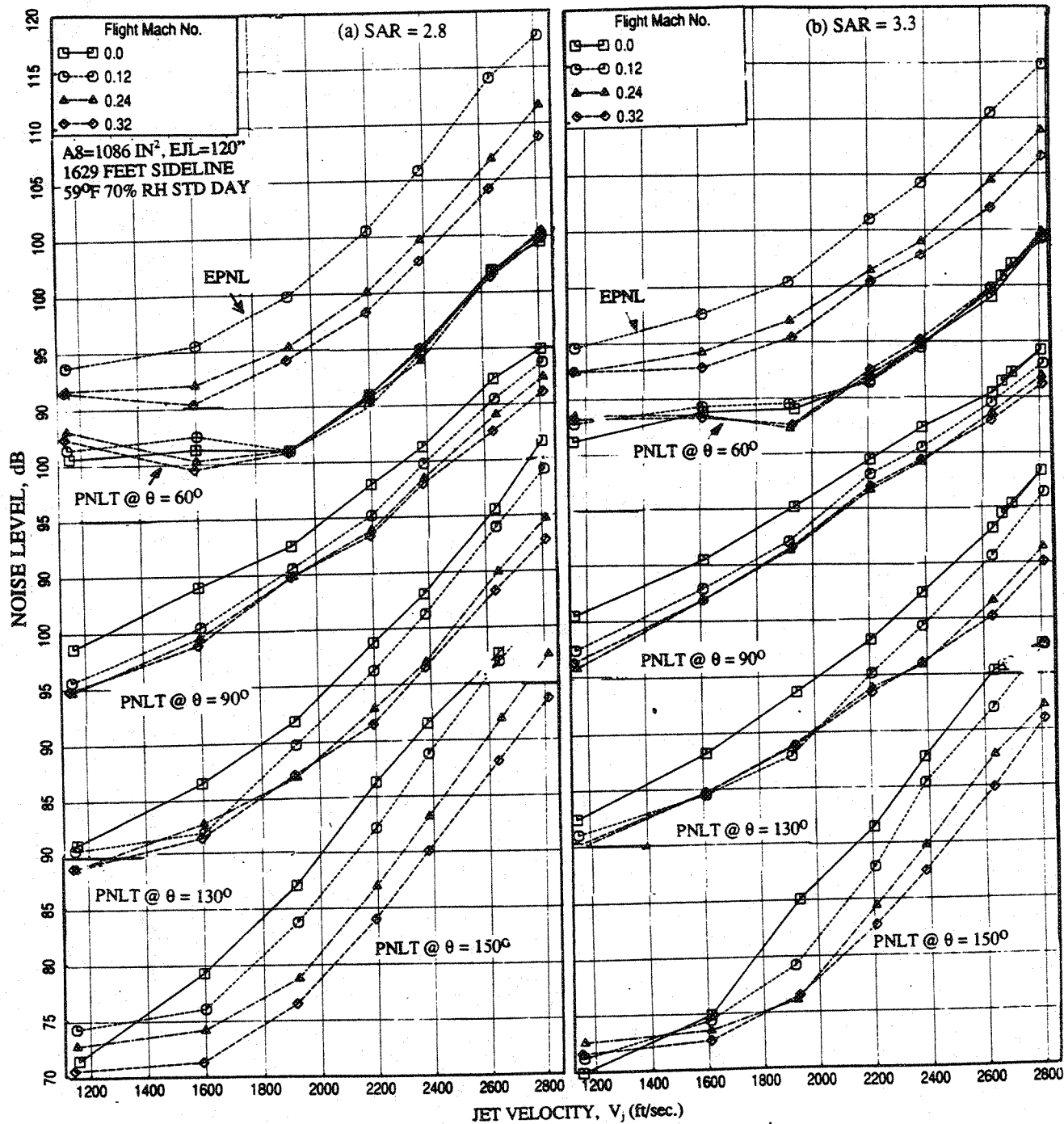
Figure 4.1-43. Effect of flight simulation on EPNL and PNLT at various polar angles (θ) as function of jet velocity for aligned CD-chute mixers with treated long ejector at an azimuthal angle φ=25°; MAR=0.95.

Figure 4.1-44. Effect of flight simulation on PNLT directivities for different jet velocities (V_j) for aligned CD-chute mixers with treated long ejector at an azimuthal angle $\phi=25°$; MAR=0.95.
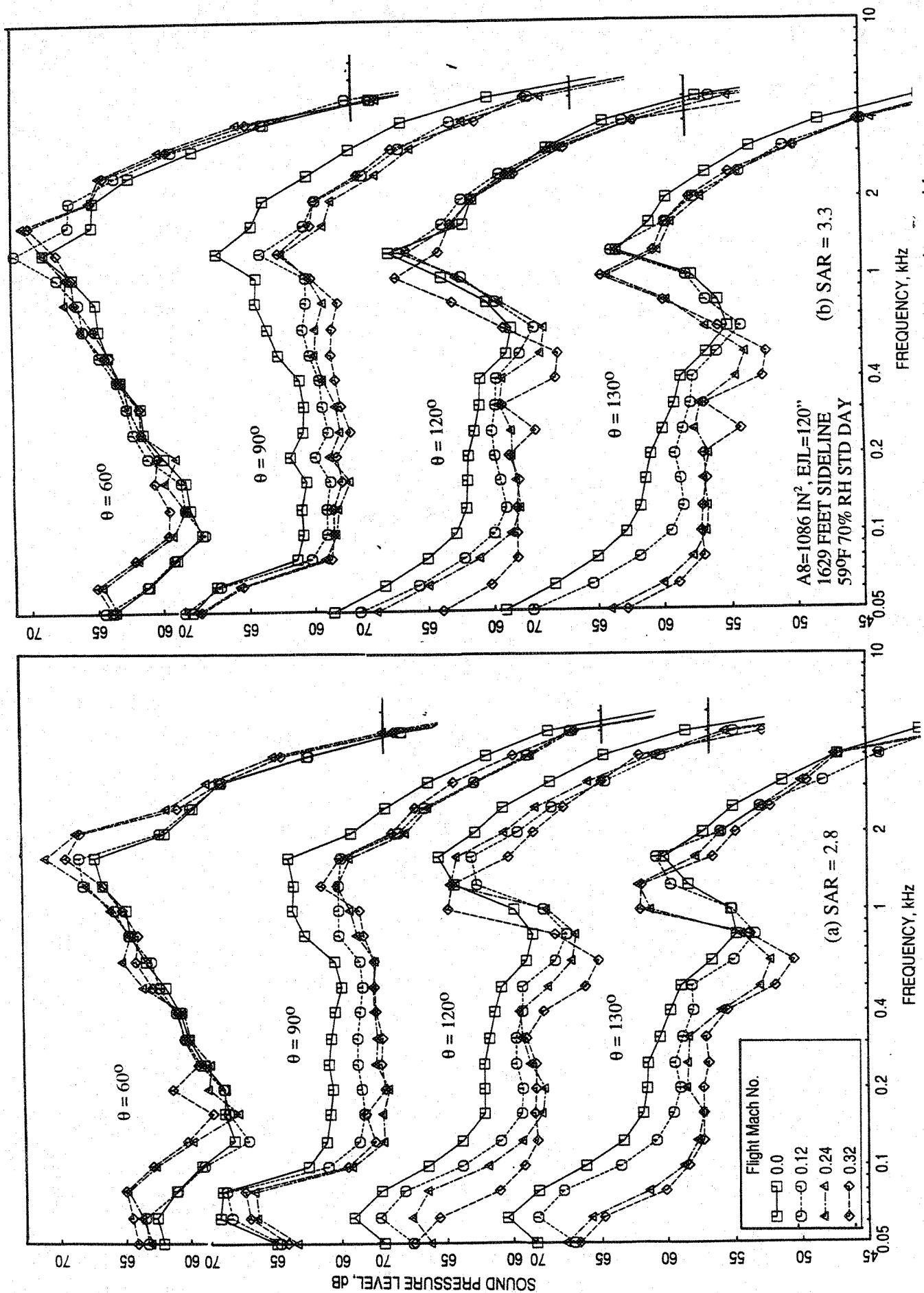
Figure 4.1-45. Effect of flight simulation on SPL spectra at various polar angles (θ) for aligned CD-chute mixers with treated long ejector at an azimuthal angle φ=25°; MAR=0.95; MAR=0.95, V_j = 1147 ft/sec, NPR = 1.5, T8 = 1000°R.
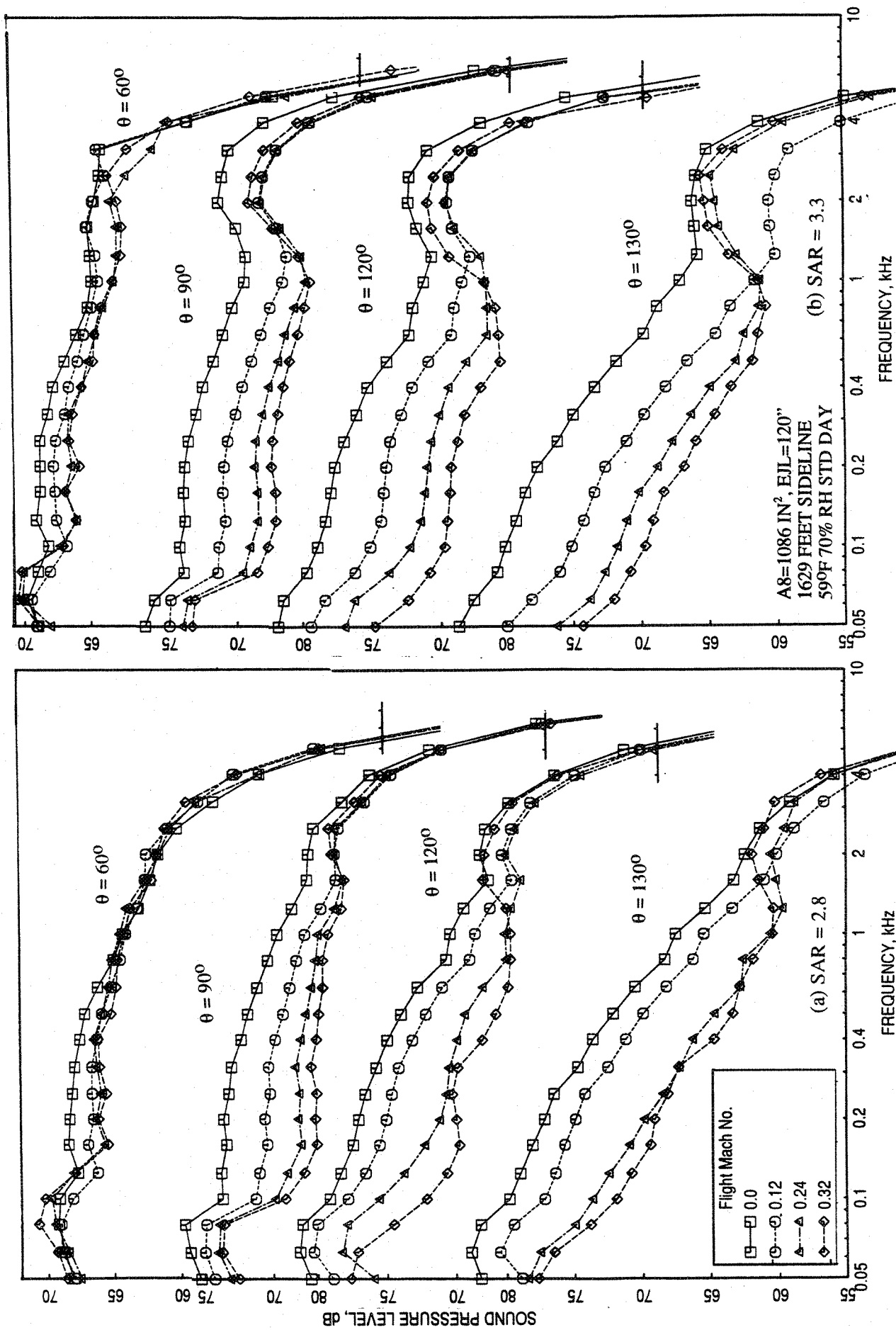
Figure 4.1-46. Effect of flight simulation on SPL spectra at various polar angles (θ) for aligned CD-chute mixers with treated long ejector at an azimuthal angle φ=25°; MAR=0.95, V_j = 1919 ft/sec, NPR = 2.5, T8 = 1325°R.
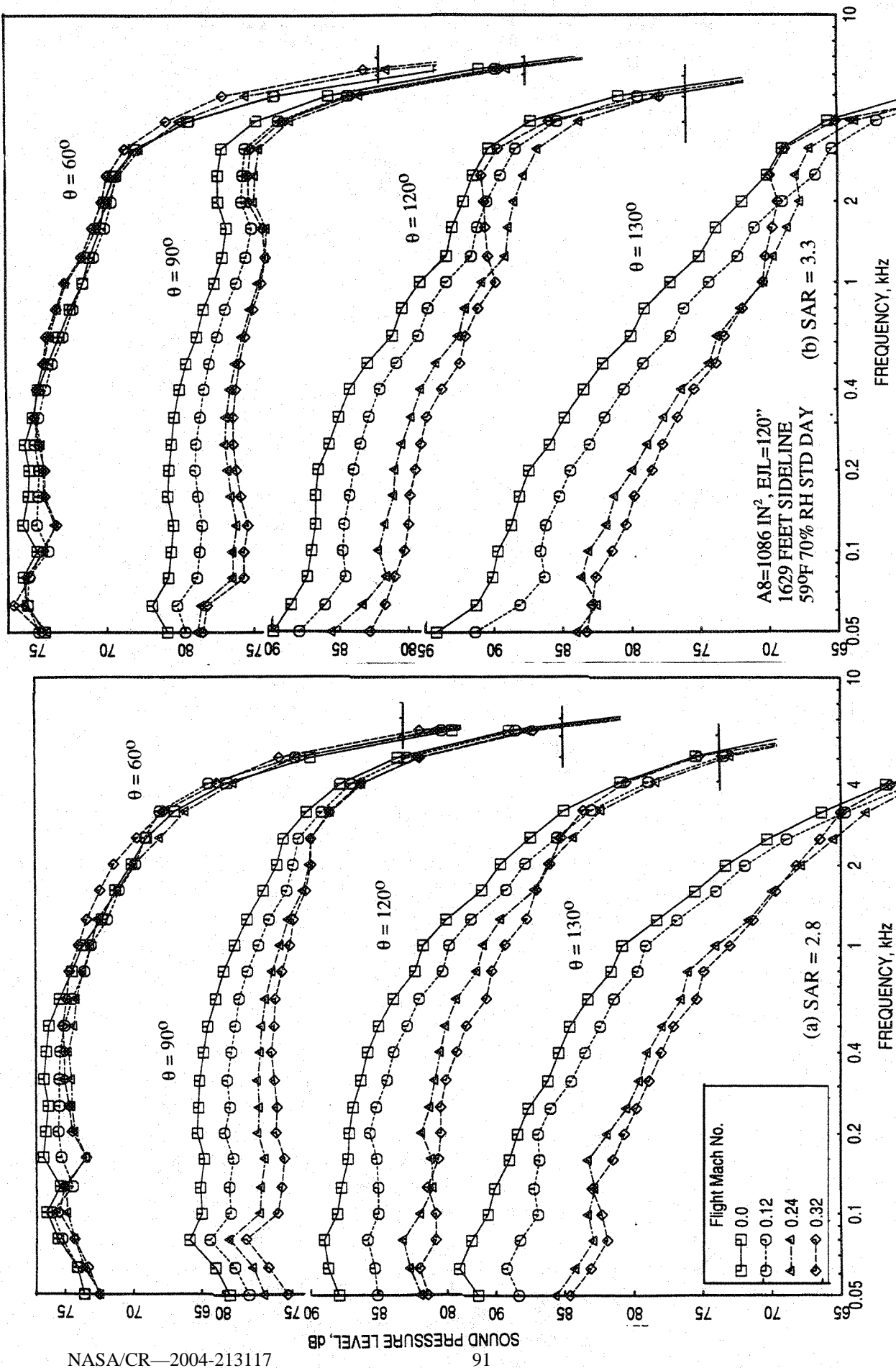
Figure 4.1-47. Effect of flight simulation on SPL spectra at various polar angles (θ) for aligned CD-chute mixers with treated long ejector at an azimuthal angle φ=25°; MAR=0.95, V_j = 2384 ft/sec, NPR = 3.4, T8 = 1590°R.
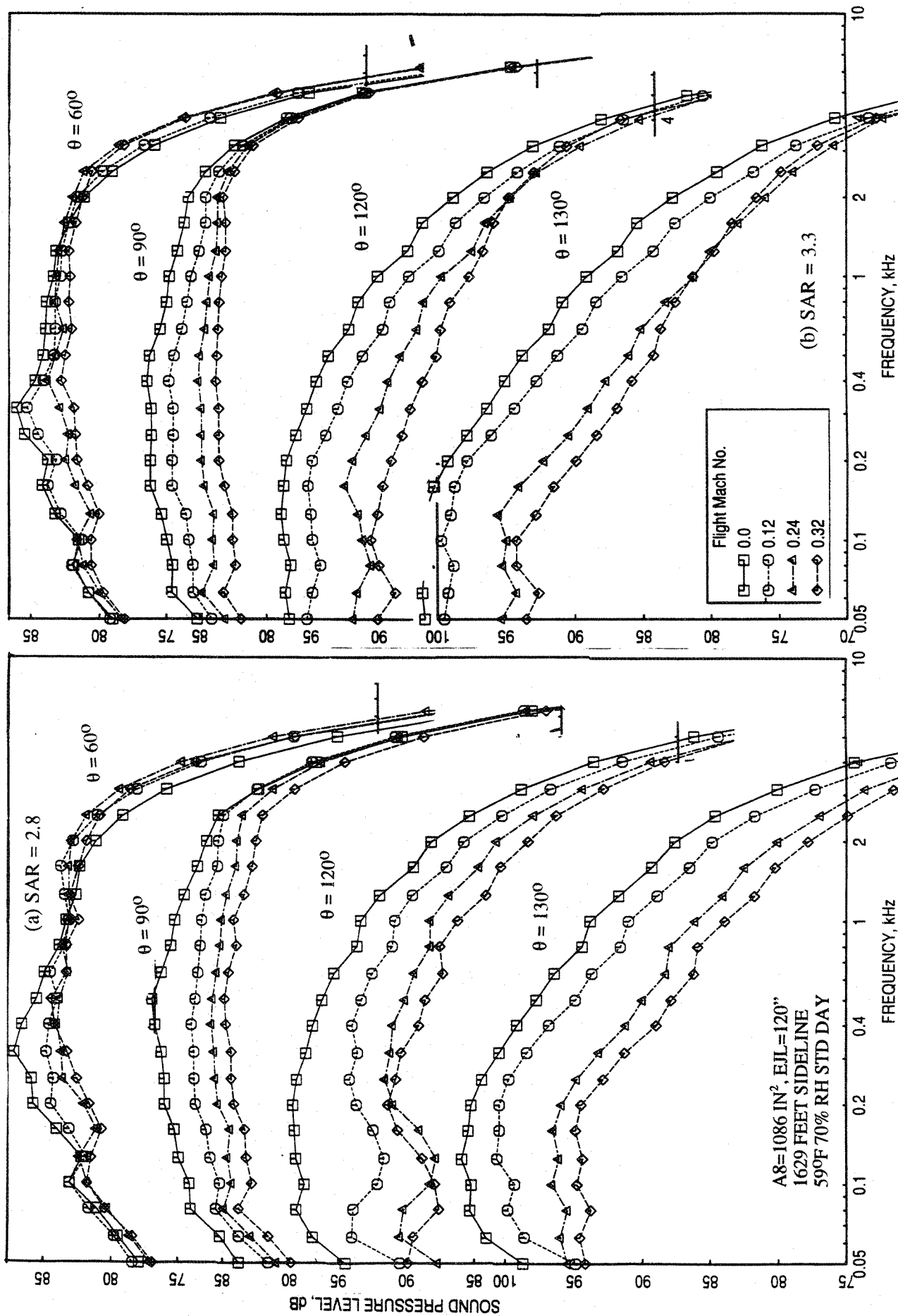
Figure 4.1-48. Effect of flight simulation on SPL spectra at various polar angles (θ) for aligned CD-chute mixers with treated long ejector at an azimuthal angle φ=25°; MAR=0.95, V_j = 2812 ft/sec, NPR = 4.5, T8 = 1860°R.

flow surface are shown in Figure 4.1-49 at a number of L1M cycle conditions. For static condition the ramp static pressure decreases slightly with increasing nozzle pressure ratio (NPR) due to suction at chute exit. However, with flight simulation the effect of NPR is reduced. On the chute surface, for static as well as with flight simulation, the pressure distribution first decreases and then increases with increasing NPR. The static pressure increase on the chute surface with increasing NPR after a certain NPR level is most likely due to choking of secondary flow. The effect of flight simulation on ramp and chute static pressure distributions are shown in Figure 4.1-50 for different L1M cycle conditions. For each case the static pressure increases with increasing flight Mach number, both on the ramp and chute surfaces due to freejet fan pressure rise, indicating lesser loading for the chutes. This is clearly observed in Figure 4.1-51, where chute loading coefficient due to chute static pressure distributions is plotted against NPR.

Average total pressure distributions across the inlet width for different L1M cycle conditions, obtained from total pressure rakes, are shown in Figure 4.1-52. At static condition very little pressure loss is observed from the vicinity of the ramp surface to almost 70% in to the inlet width. Closer to the inlet flow guide significant pressure drop is observed. Most likely the flow separates on the inlet flow guide leading edge at static condition due to suction and causes this pressure drop. Also, the boundary layer buildup on inlet ramp could cause total pressure drop. The inlet flow characteristics seem to be invariant above a certain NPR, indicating flattening out of secondary mass flow rate. However, with flight simulation, the trend is changed. Closer to ramp surface the total pressure is lower compared to those at the inlet, since the total pressure increases at the inlet due to flight. In true flight situation also, total pressure increases with increasing flight Mach number. The effect of flight on total pressure distributions across the inlet width is further demonstrated in Figure 4.1-53 at a number of L1M cycle conditions. The effect of flight on pumping and corrected pumping, computed from the total pressure distributions across the inlet width, is shown in Figure 4.1-54. With respect to NPR the pumping decreases. However, the pumping increases with increasing flight Mach number, since the total pressure at the inlet goes up. Even though, the pumping increases with flight, the effect is very small on the mixed jet velocity (see Figure 4.1-55).

The static pressure distribution on the inlet flow guide and on the flap along cold and hot chute flow centerlines are shown in Figure 4.1-56 at different L1M cycle conditions without flight simulation. A gradual transition from subsonic to supersonic mode with increasing NPR is clearly observed from this figure, both along hot and cold chute
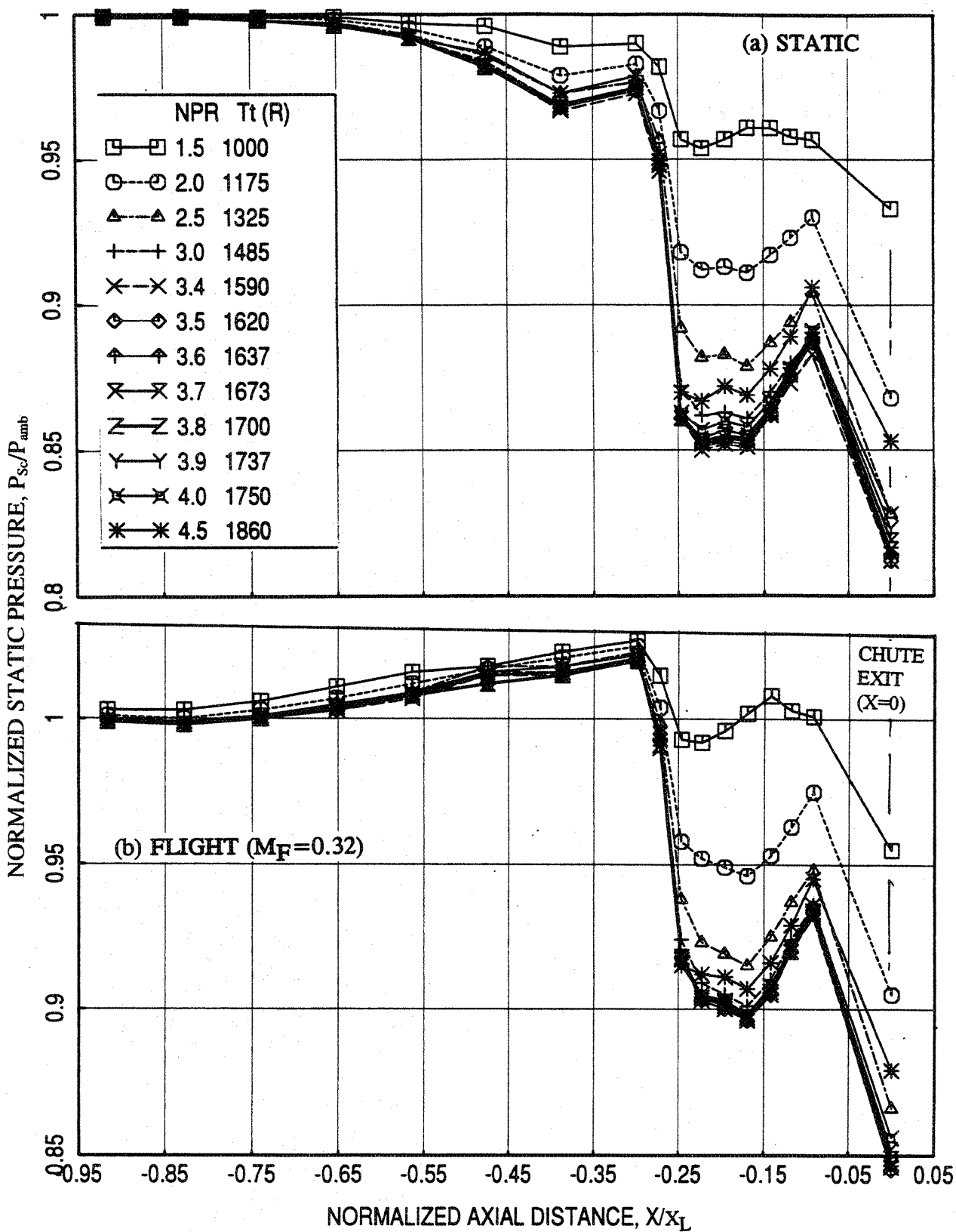
Figure 4.1-49. Axial static pressure distributions on the inlet ramp and on the secondary flow side of chute surface at different L1M cycle conditions for an aligned CD chute mixer with treated (by foam metal) long ejector, SAR = 2.8, MAR = 0.95.
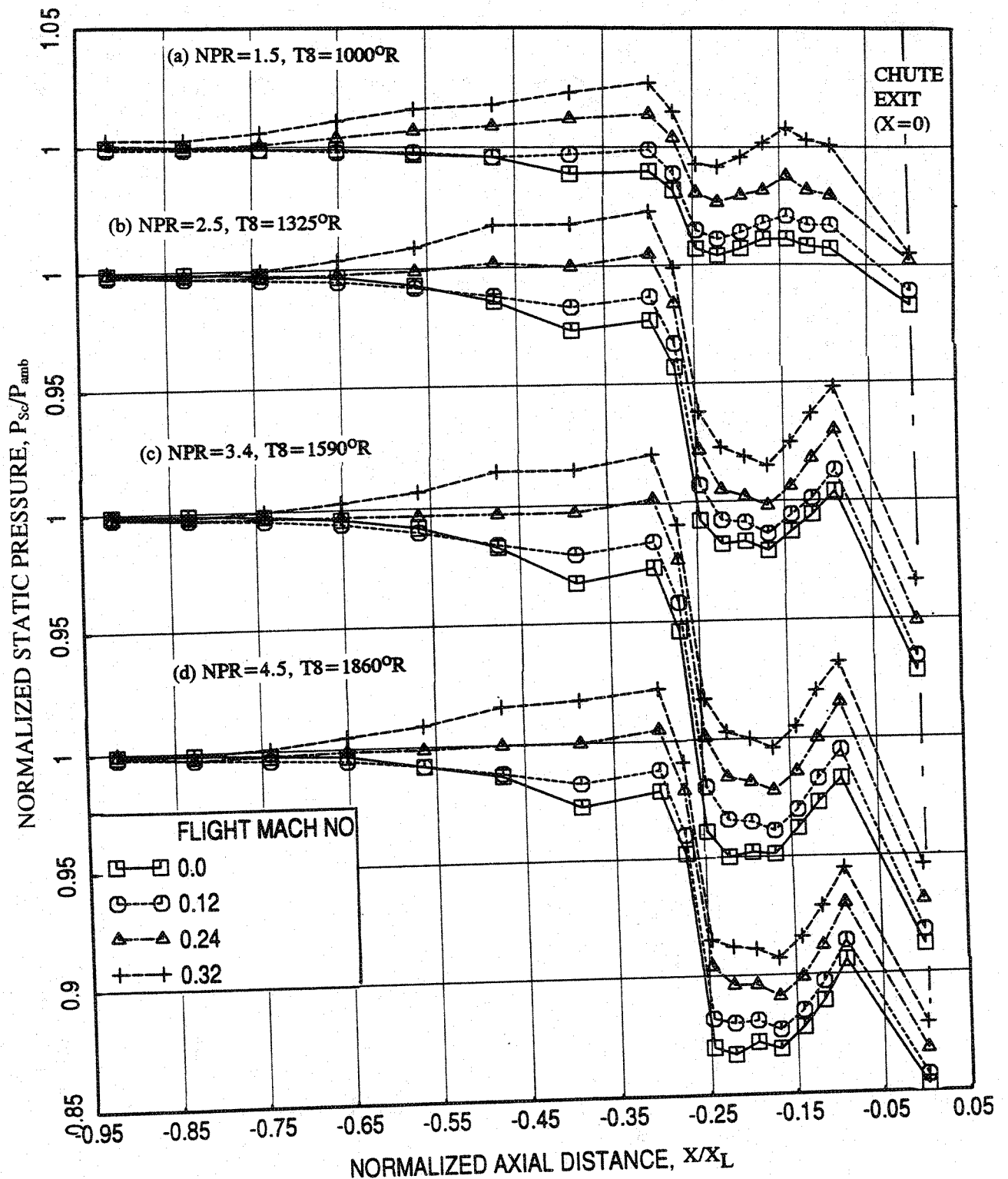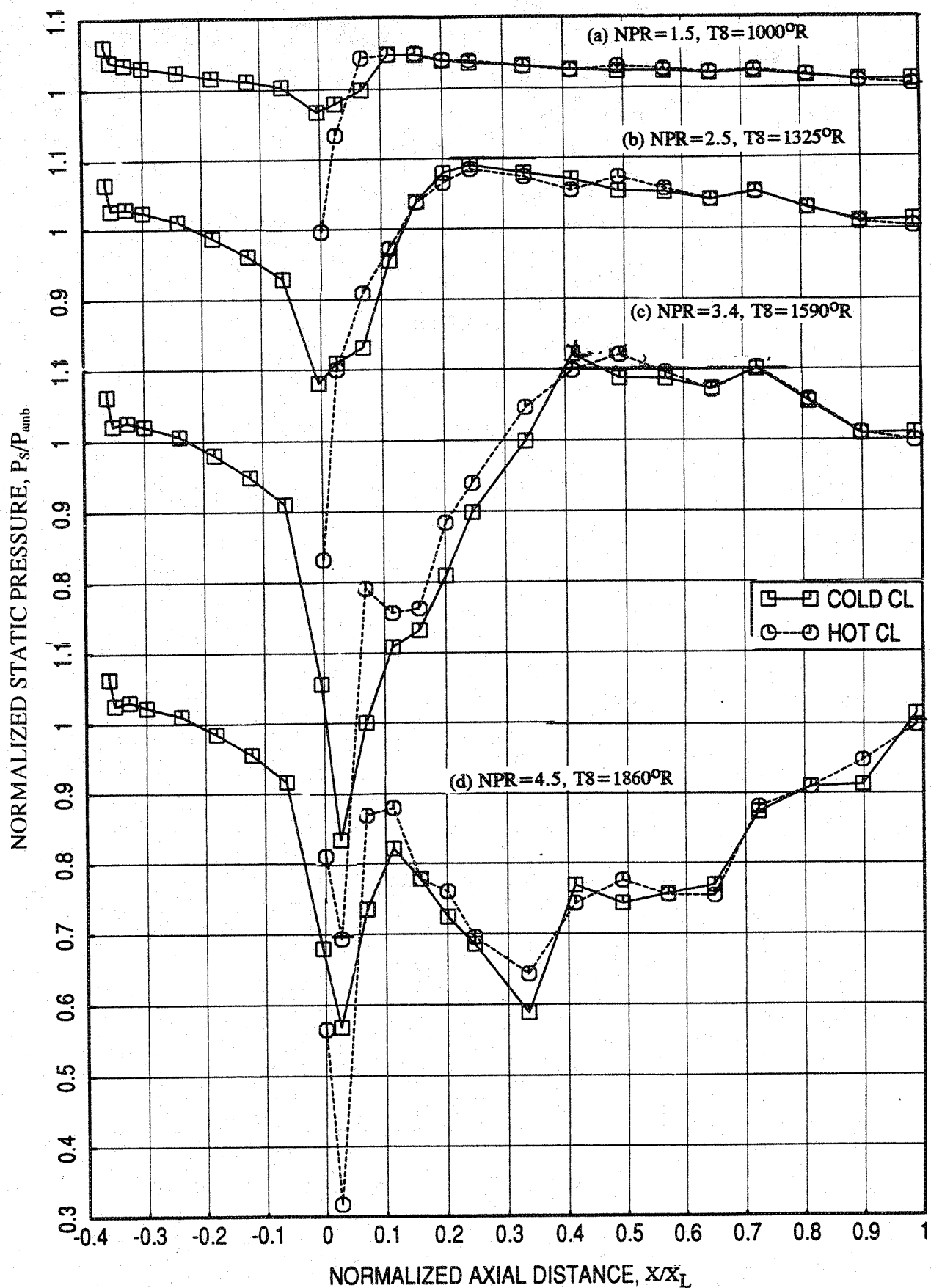
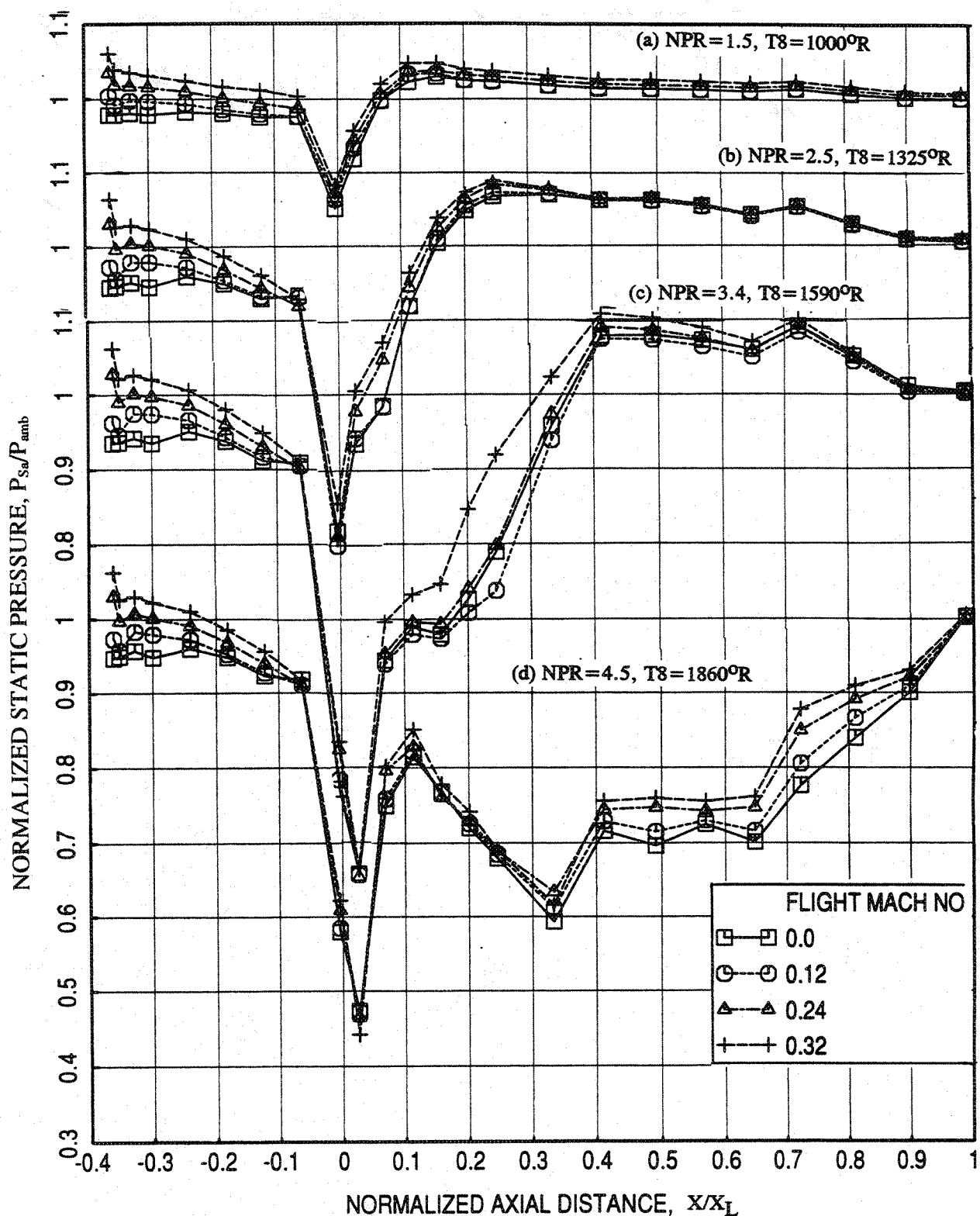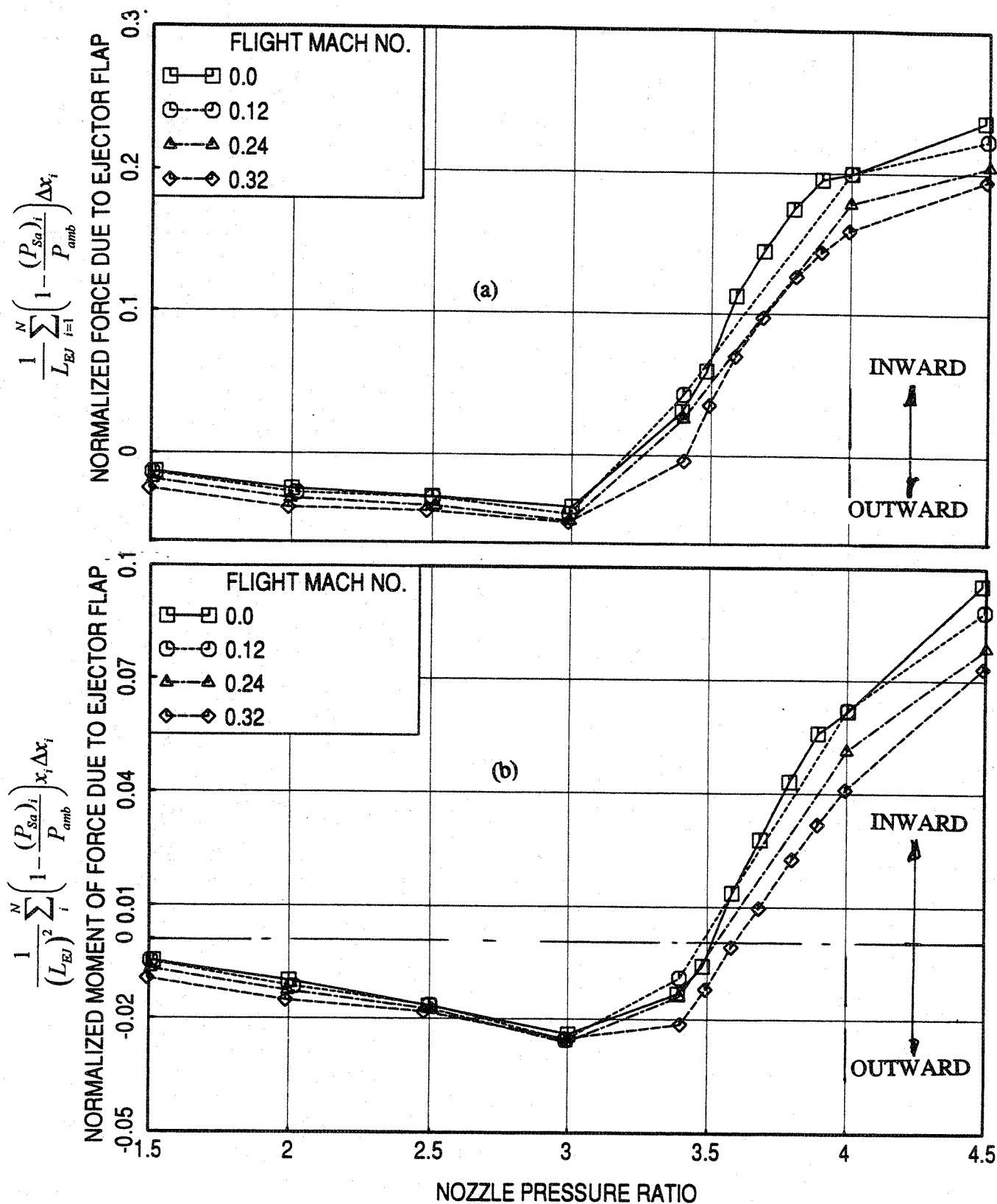Figure 4.1-50. Effect of flight simulation on the static pressure distributions on the inlet ramp and on the secondary flow side of chute surface at different L1M cycle conditions for an aligned CD chute mixer with treated (by foam metal) long ejector, SAR = 2.8, MAR = 0.95.
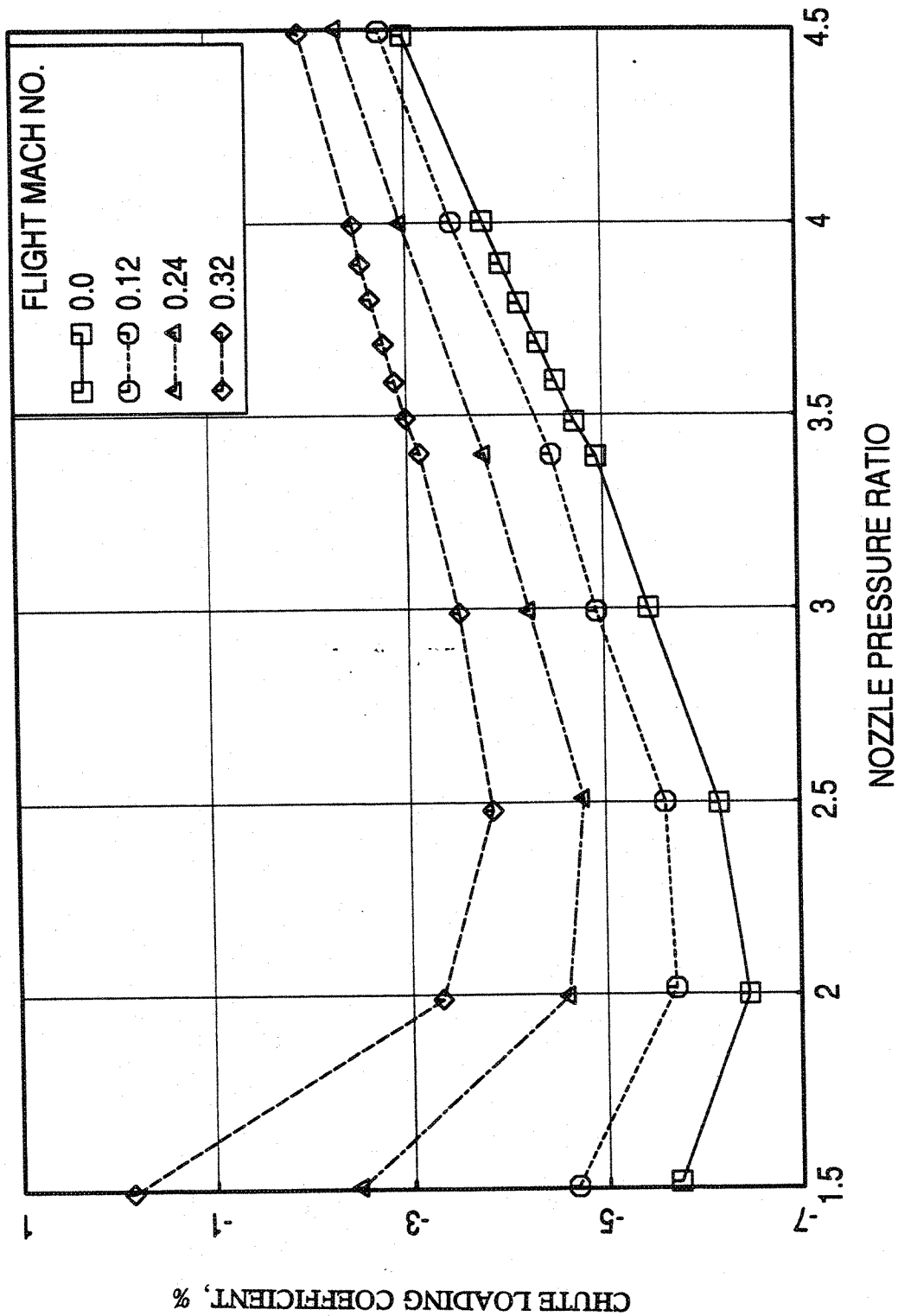
Figure 4.1-51.   Effect of flight simulation on chute loading coefficient, computed by measured static pressure distributions on secondary flow side chute leading edge, with respect to nozzle pressure ratios for an aligned CD chute mixer with treated (by foam metal) long ejector, SAR = 2.8, MAR = 0.95.
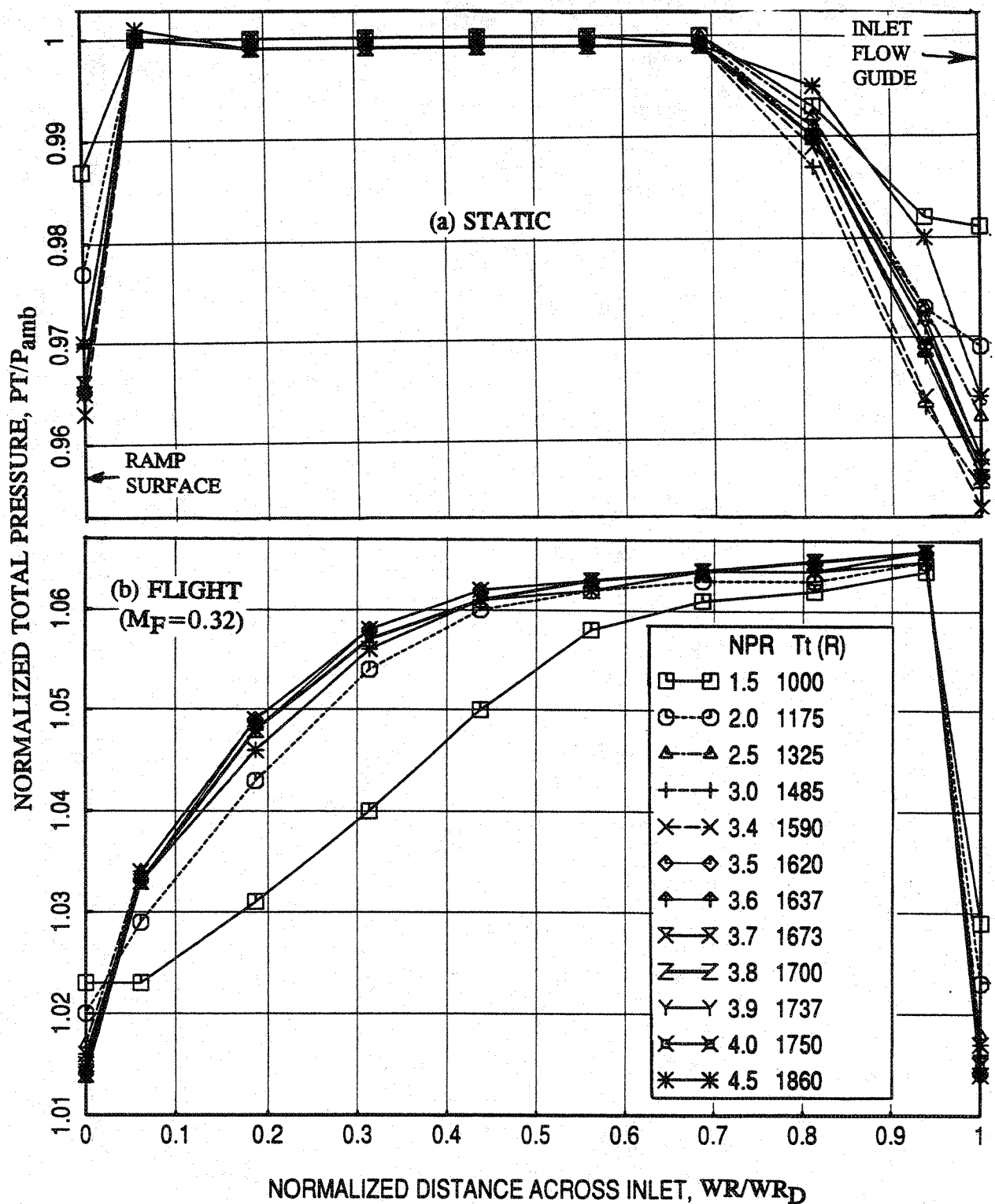
Figure 4.1-52. Total pressure distribution across the inlet at different L1M cycle conditions for an aligned CD chute mixer with treated (by foam metal) long ejector, SAR = 2.8, MAR = 0.95.
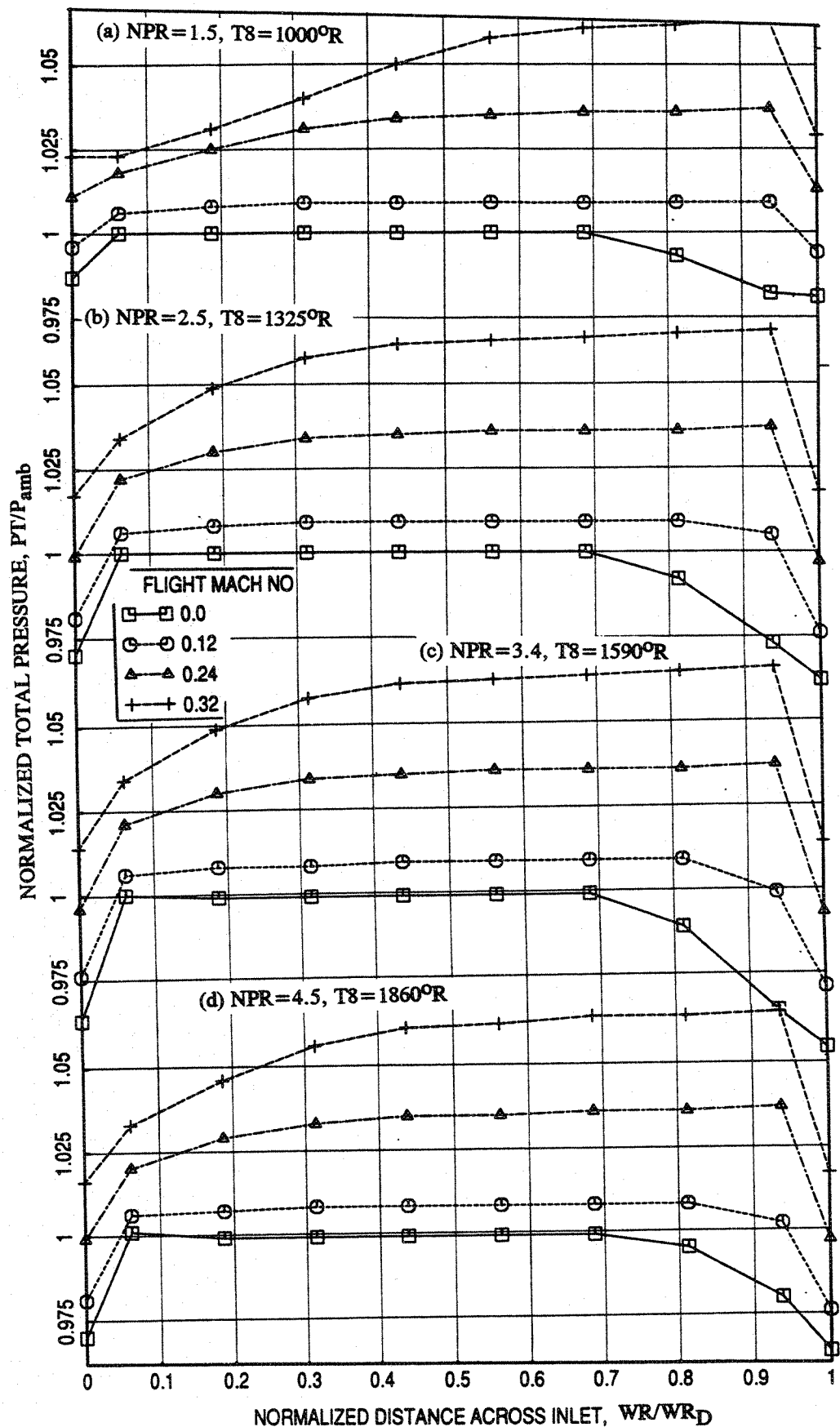
Figure 4.1-53. Effect of flight simulation on total pressure distribution across the inlet at different L1M cycle conditions for an aligned CD chute mixer with treated (by foam metal) long ejector, SAR = 2.8, MAR = 0.95.
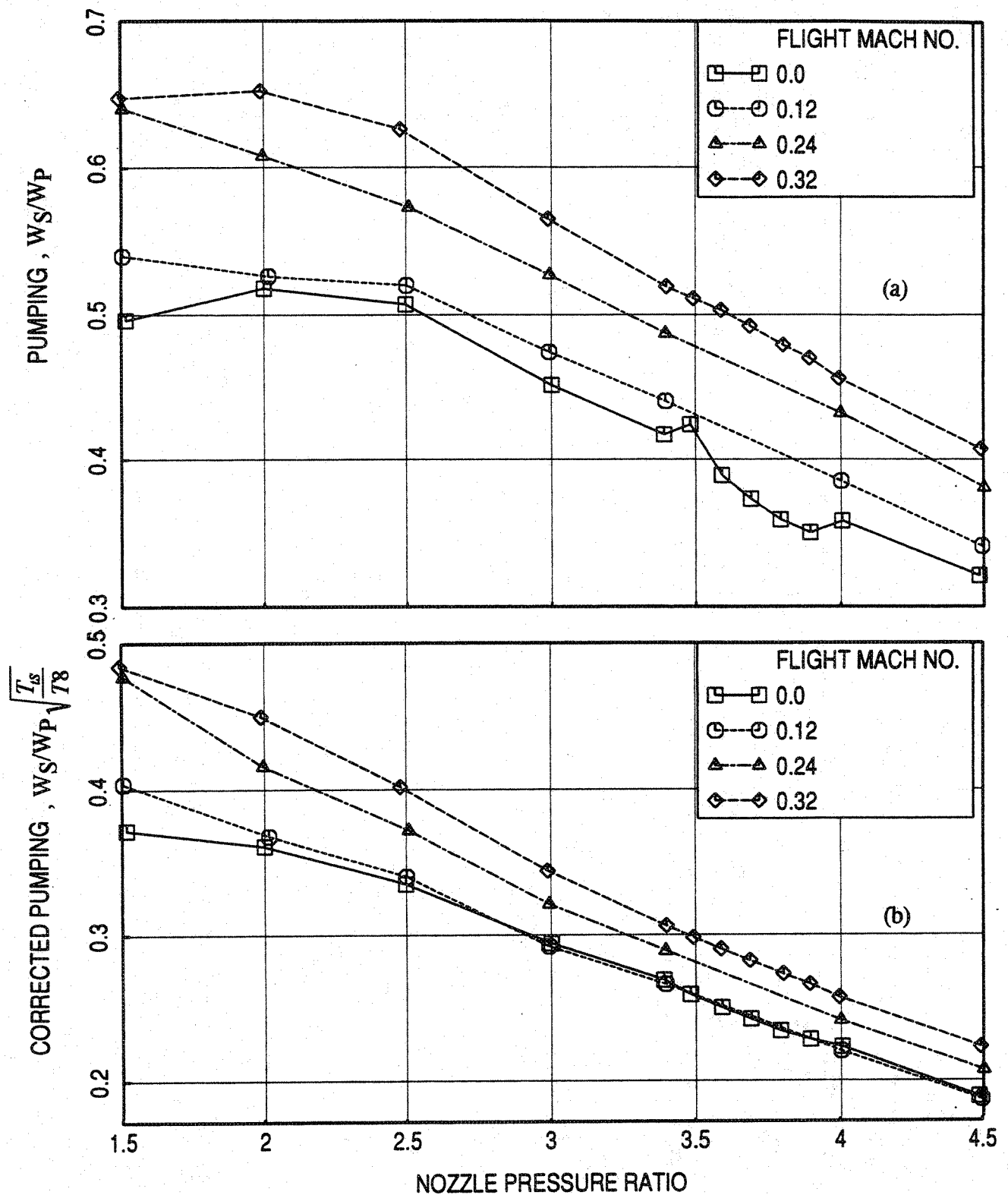
Figure 4.1-54. Effect of flight simulation on pumping, computed by measured rake total pressure distributions at the inlet, with respect to nozzle pressure ratios for an aligned CD chute mixer with treated (by foam metal) long ejector, SAR = 2.8, MAR = 0.95.
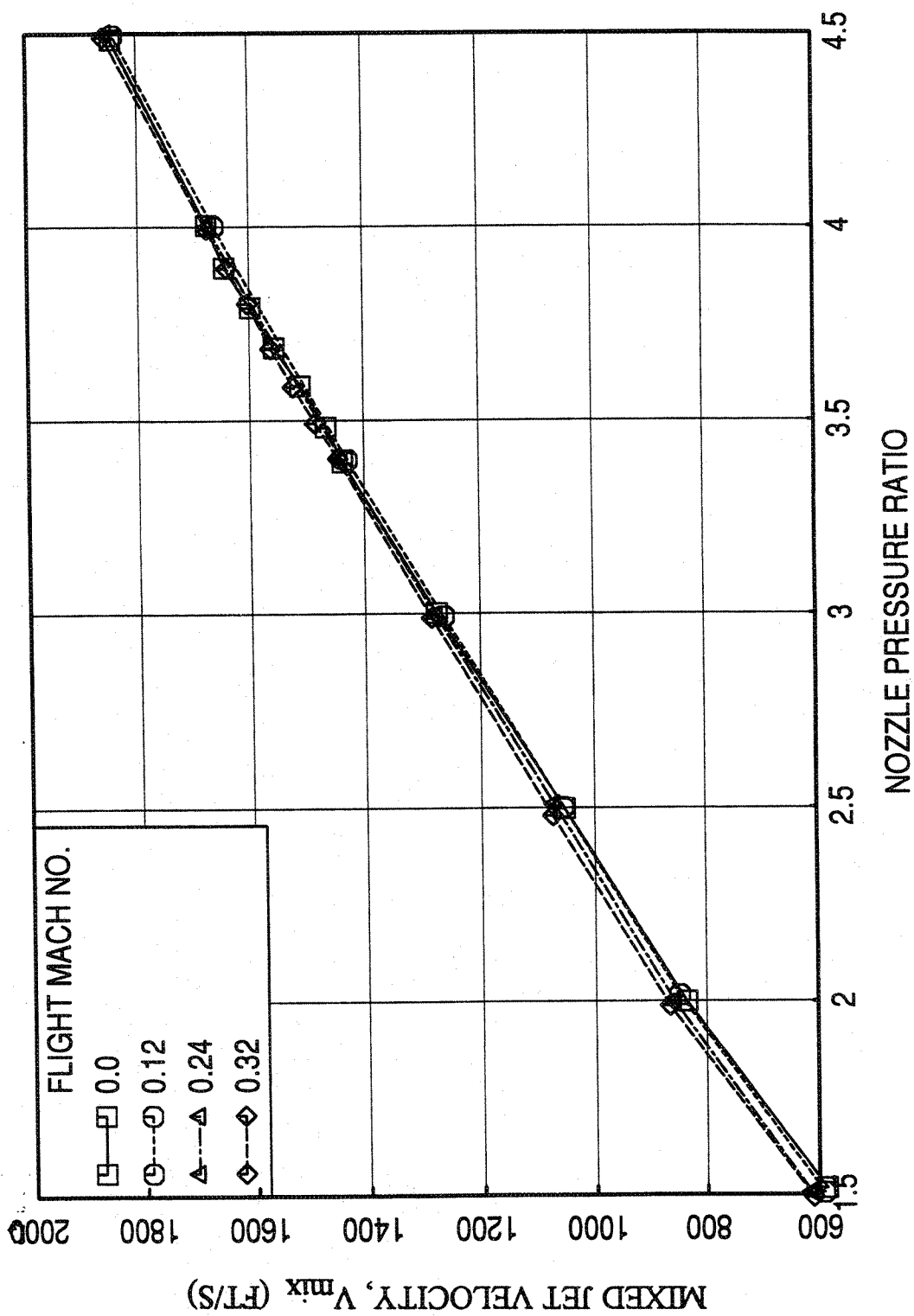
Figure 4.1-55. Effect of flight simulation on mixed jet velocity, computed by measured rake total pressure distributions at the inlet, with respect to nozzle pressure ratios for an aligned CD chute mixer with treated (by foam metal) long ejector, SAR = 2.8, MAR = 0.95.
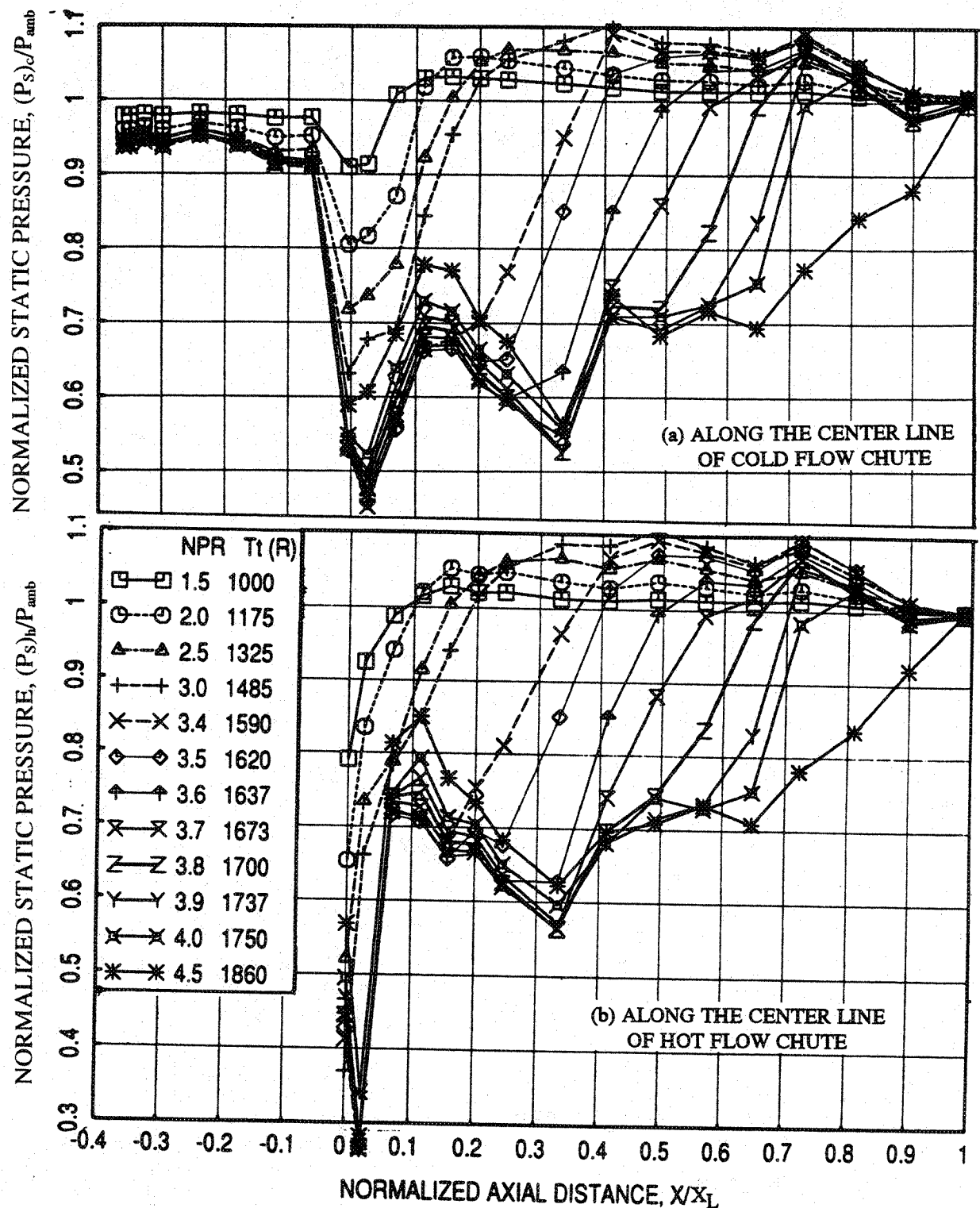
Figure 4.1-56. Axial static pressure distributions on the inlet and the flap surface at different L1M cycle conditions for an aligned CD chute mixer with treated (by foam metal) long ejector at static condition; (a) along centerline of cold flow chute and (b) along centerline of hot flow chute, SAR = 2.8, MAR = 0.95.

centerline data. Figure 4.1-57 shows similar characteristics with flight simulation of $M_F=0.32$.

Figures 4.1-58 and 4.1-59 illustrate the comparison of axial static pressure distributions on the flap between the hot flow row and cold flow row with and without flight simulation at a number of NPR. Except closer to mixer exit, there is no appreciable difference in flap static pressure distributions between hot and cold flow rows. Thus, static pressure equalization between primary and secondary streams takes place over a short but finite axial distance. As the flow exits from the mixer (hot flow stream), it accelerates, which results in lower pressure near the mixer exit, indicated by pressure taps along hot flow row. However, with increasing axial distance the pressure level along chute hot flow centerline increases due to flow deceleration caused by mixing. Mode transition related interpretations on the basis of flap pressure distributions are the same whether we consider pressure distributions along hot or cold chute flow directions or an arithmetic average of these two. Hence, an arithmetic average of these two measurements is computed and presented in Figure 4.1-60. Figure 4.1-61 shows the effect of flight on the average axial static pressure distributions at different L1M cycle conditions. Small amount of pressure increase due to increasing M_F is noted, especially at much higher NPR and in supersonic mode. The effect of flight on normalized force and normalized moment of force with respect to flap leading edge due to static pressure difference on flap surface are shown in Figure 4.1-62. Both the force and the moment seem to decrease slightly with increasing flight simulation due to increased static pressure. The transition from subsonic to supersonic mode seems to be slightly delayed with respect to NPR due to M_F. The effect of flight simulation on the flow and performance related results for the mixer of SAR=3.3 are qualitatively similar to the results presented here for the mixer of SAR=2.8 and hence not included here.

4.1.5 Effect of Suppressor Area Ratio (SAR)

The two aligned CD chute mixers with fully treated (by astroquartz) long ejector are of different suppressor area ratio (SAR) of 2.8 and 3.3. The influence of SAR, therefore, briefly described in this section for acoustic characteristics and performance related parameters.

Acoustic Results: Since the mixers with SAR of 2.8 and 3.3 have different throat areas of $22.16 \ in^2$ and $19.14 \ in^2$, the scaling process in the data analysis to convert model scale
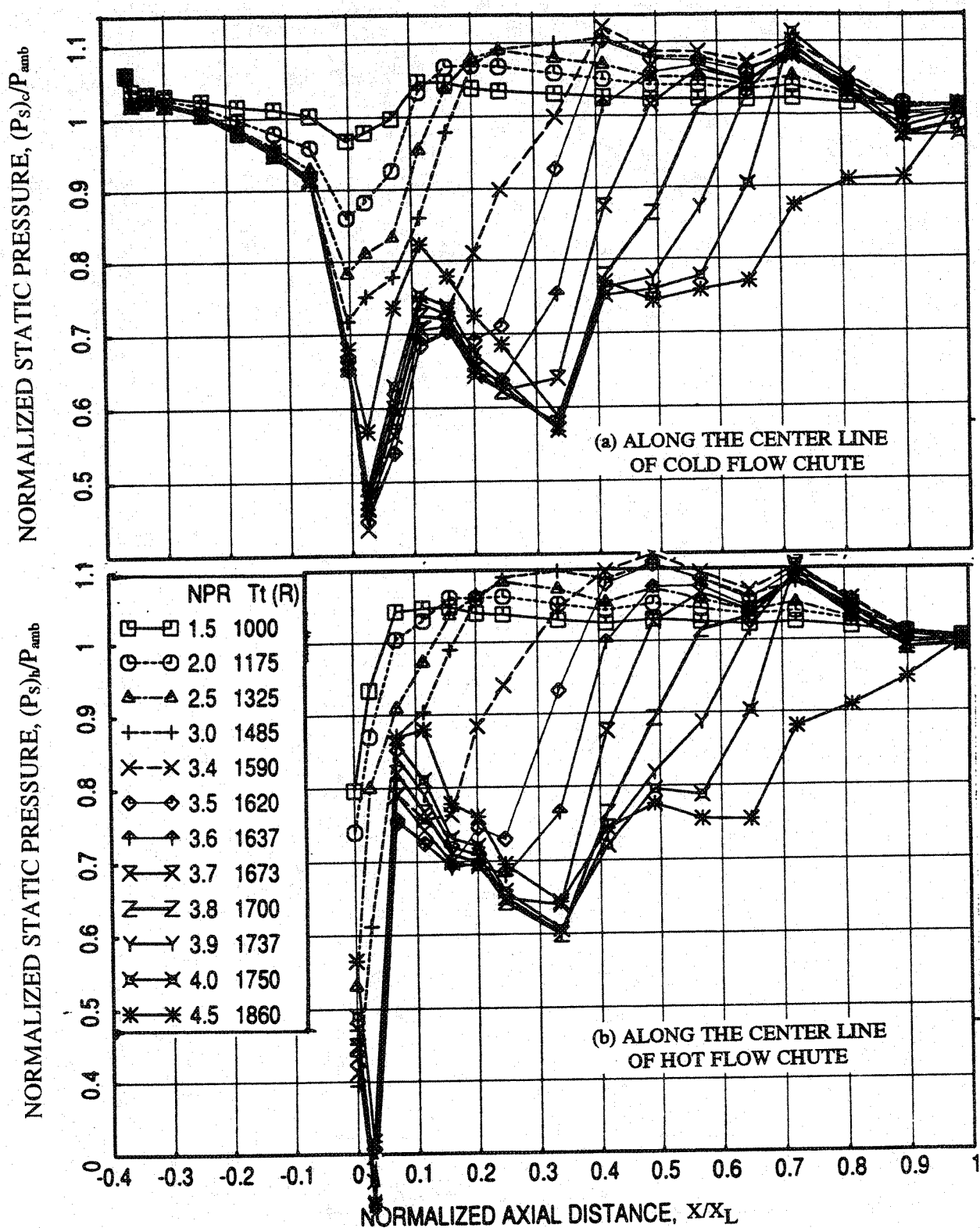
Figure 4.1-57. Axial static pressure distributions on the inlet and the flap surface at different L1M cycle conditions for an aligned CD chute mixer with treated (by foam metal) long ejector with flight simulation (M_F=0.32); (a) along centerline of cold flow chute and (b) along centerline of hot flow chute, SAR = 2.8, MAR = 0.95.
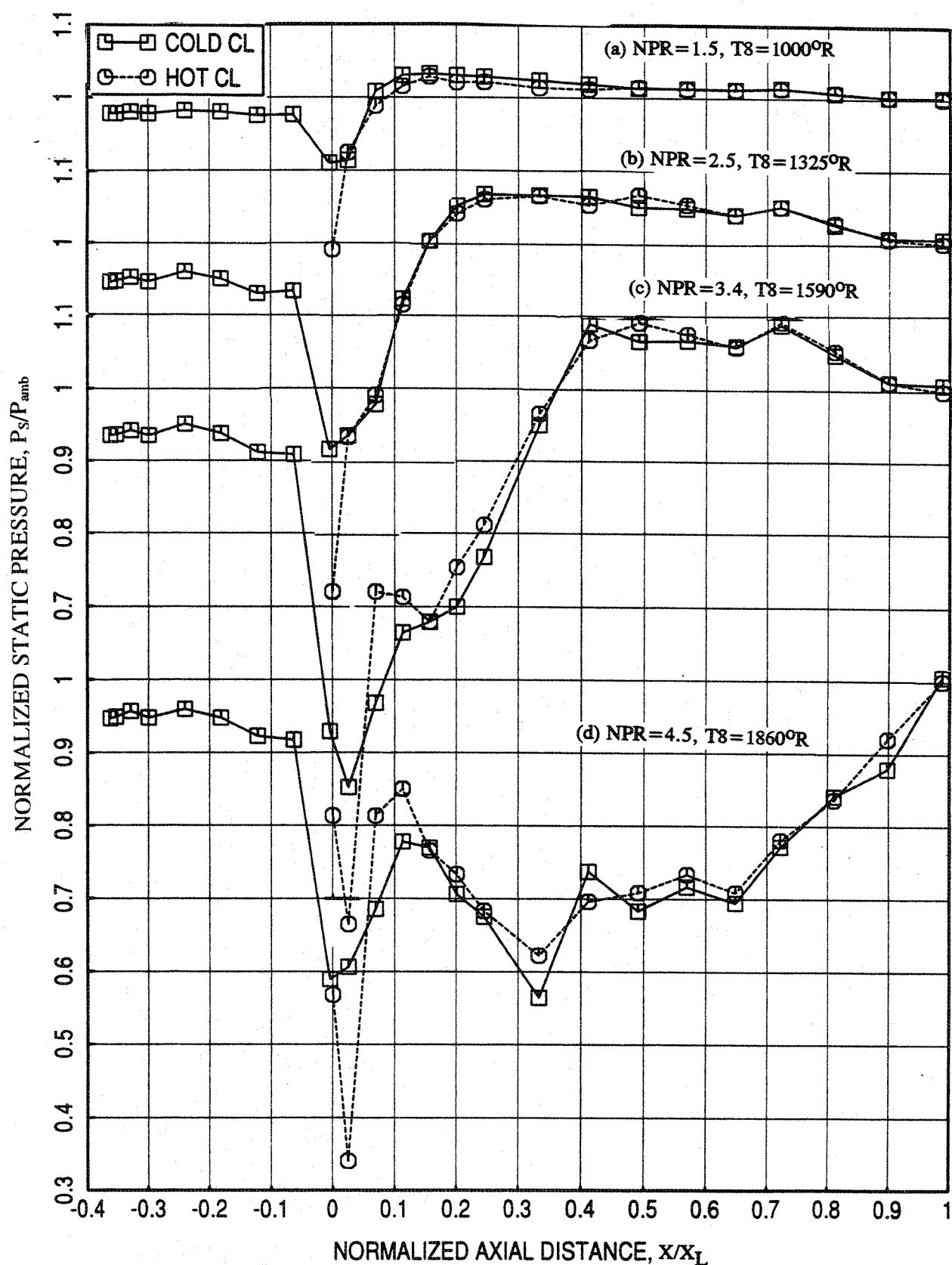
Figure 4.1-58. Comparison of axial static pressure distributions along centerline of cold flow chute with those along centerline of hot flow chute on the flap surface at different L1M cycle conditions for an aligned CD chute mixer with treated (by foam metal) long ejector at static condition, SAR = 2.8, MAR = 0.95.

Figure 4.1-59. Comparison of axial static pressure distributions along centerline of cold flow chute with those along centerline of hot flow chute on the flap surface at different L1M cycle conditions for an aligned CD chute mixer with treated (by foam metal) long ejector with flight simulation (M_F=0.32), SAR = 2.8, MAR = 0.95.
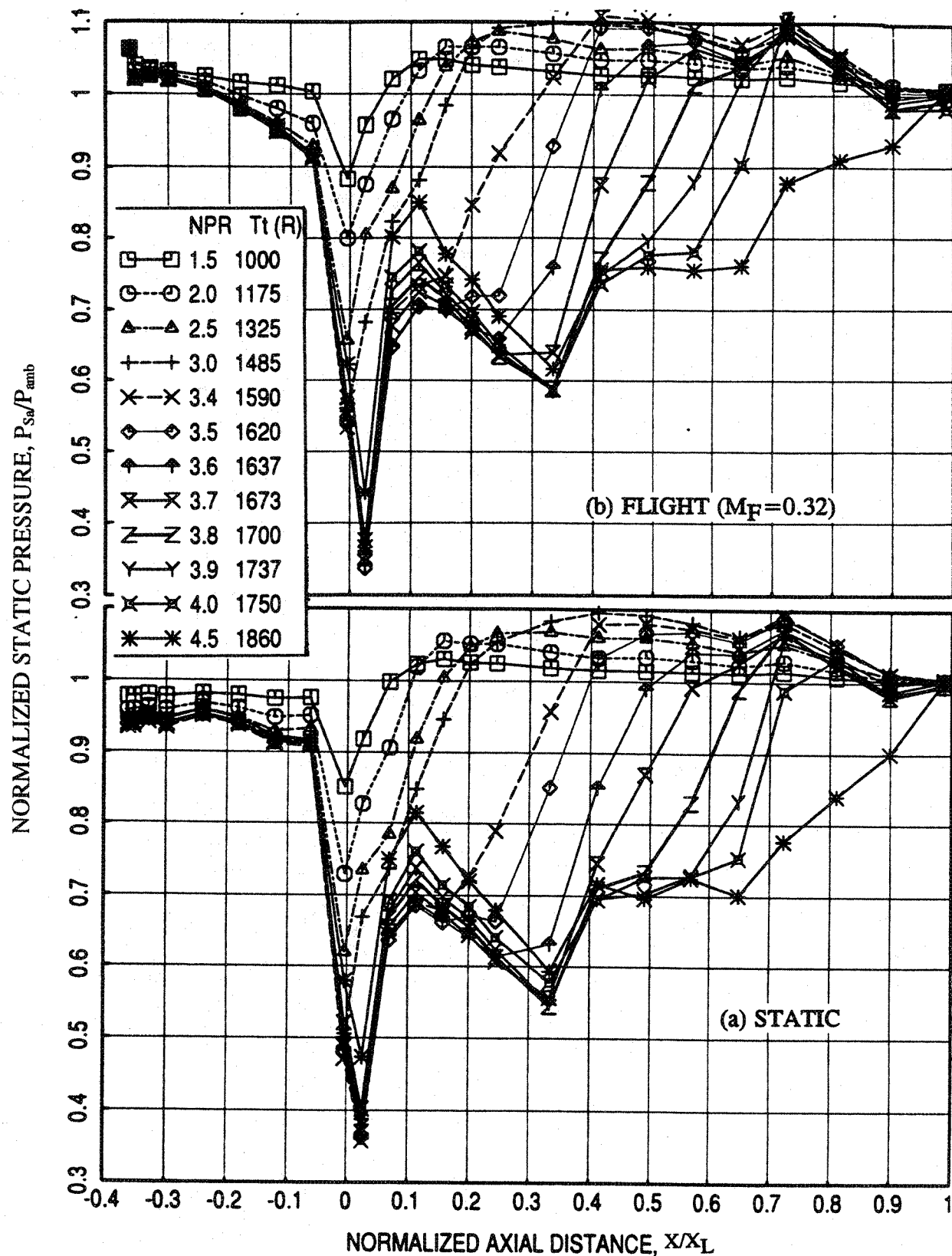
Figure 4.1-60. Axial distributions of average static pressure on the inlet and the flap surface at different L1M cycle conditions for an aligned CD chute mixer with treated (by foam metal) long ejector, SAR = 2.8, MAR = 0.95.

Figure 4.1-61. Effect of flight simulation on axial distribution of average static pressure on the inlet and the flap surface at different L1M cycle conditions for an aligned CD chute mixer with treated (by foam metal) long ejector, SAR = 2.8, MAR = 0.95.

Figure 4.1-62. Effect of flight simulation on normalized (a) force and (b) moment of force due to ejector flap with respect to nozzle pressure ratio for an aligned CD chute mixer with treated (by foam metal) long ejector, SAR = 2.8, MAR = 0.95.

acoustic data into full size nozzle utilized at GEAE might result in slightly inaccurate comparison. Therefore, before presenting the acoustic results to show the influence of SAR the possible inaccuracy inherent with the scaling process is outlined. The scaling process involves the noise level change and corresponding frequency shift. Results of two slightly different approaches of scaling the scale model acoustic data to full scale using 1/3-octave band data are compared to show the extent of variability in full scale projections between the two approaches. Both methods have some level of inaccuracy/imprecision in them.

Scaling Process : Strouhal scaling relationship is utilized in GEAE in scaling model scale 1/3-octave band data to full scale. If the throat areas of the model scale and the full size nozzles are A_m and A_f, respectively, then the noise data for the model scale nozzle in terms of sound pressure level is increased by $10 \log_{10}(A_f/A_m)$ dB for full size nozzle.

This correction is applied to the lossless acoustic data at measurement location or at a standard location (such as 40' arc). Then the noise levels after scaling are projected to needed farfield sideline/arc distance using the inverse square law. The corresponding scale model frequencies f_m are converted to the full scale size frequency f_f, utilizing the Strouhal scaling relationship and for the same jet velocity, which reduces to :

$$f_f = \frac{f_m}{\sqrt{A_f/A_m}}$$

The atmospheric absorption to the lossless SPL is then applied at the full scale size nozzle frequency f_f and appropriate farfield distance. The current scaling process utilizes 1/3-octave band data. In this process the full size nozzle frequency is obtained by shifting the 1/3-octave band frequencies by a factor $5 \log_{10}(A_f/A_m)$. This factor is rounded to the nearest integer. This could introduce some imprecision in full scale frequency. The amplitude levels accrue some imprecision due to its correspondence with the full integer number shifted frequency and the use of atmospheric absorption at the center frequency of 1/3-octave band for full scale data based on full integer 1/3-octave band number shift rather than the use of atmospheric absorption based on Strouhal scaling. In PNLT calculation another error due to inaccurate NOY based on inaccurate frequency and amplitude is also introduced.

The acoustic data for two full scale (throat area of 1086 square inches) CD chute aligned mixer nozzles of SAR 2.8 and 3.3 with fully treated (by astroquartz) ejectors at static and with a flight simulation of $M_F=0.32$, scaled from the model scale nozzles using the conventional GEAE scaling procedure, are shown in Figures 4.1-63 and 4.1-64. These figures show the effect of SAR on PNLT and EPNL as functions of jet velocity. The conic nozzle data, obtained under NRA program, is also plotted in these figures. The mixer with SAR=2.8 is quieter at lower velocities up to about 2350 ft/sec compared to the mixer with SAR=3.3. The trend is reversed at higher velocities.

The model scale throat areas for the mixers with SAR of 2.8 and 3.3 are 22.16 and 19.14 square inches, respectively. The linear scale factors for these mixers with respect to a full size area of 1086 square inches are 7.00 and 7.53, respectively. The 1/3-octave band shifts of 8.45 and 8.77 are required for the mixers of SAR 2.8 and 3.3, respectively to scale the frequency for a full size area of 1086 square inches. However, the number of 1/3-octave band shifts are rounded to the nearest integers of 8 and 9 for the mixers of SAR 2.8 and 3.3, respectively in the scaling process.

Next, full scale noise results are evaluated for the mixer with SAR=3.3 by shifting the 1/3-octave band frequency by 8, but the lossless SPL amplitude increase is maintained the same with respect to full scale size area of 1086 square inches in the scaling process to illustrate the effect of rounding the band shift on the noise. This is achieved by applying the scaling process to the model scale data for a full size area of 938 square inches, which allows a frequency band shift of 8 (and the exact shift of 8.45), same as that for the mixer with SAR=2.8 and applying an additional noise increase due to area change from 938 to 1086 (i.e., $10 \log_{10}(1086/938)$ dB). Various acoustic parameters derived for the mixer of SAR=3.3 with this approach (called as Approach 2) are compared with those derived using the full scale area of 1086 directly with a frequency band shift of 9 (called as Approach 1) in Figures 4.1-65 through 4.1-70. Results for mixer with SAR=2.8 are also plotted in these figures.

Figure 4.1-65 shows the comparison of PNLT at various polar angles and EPNL as functions of jet velocity between the two mixers, with two sets of results for SAR=3.3 based on approaches 1 and 2. The PNLT and EPNL are slightly lower when a frequency shift of 8 bands are applied (approach 2) compared to those with 9 band shift for the mixer with SAR=3.3 (approach 1). Comparisons in terms of PNLT directivities at four different velocity conditions are shown in Figure 4.1-66. The effect of reduced band shift is mostly
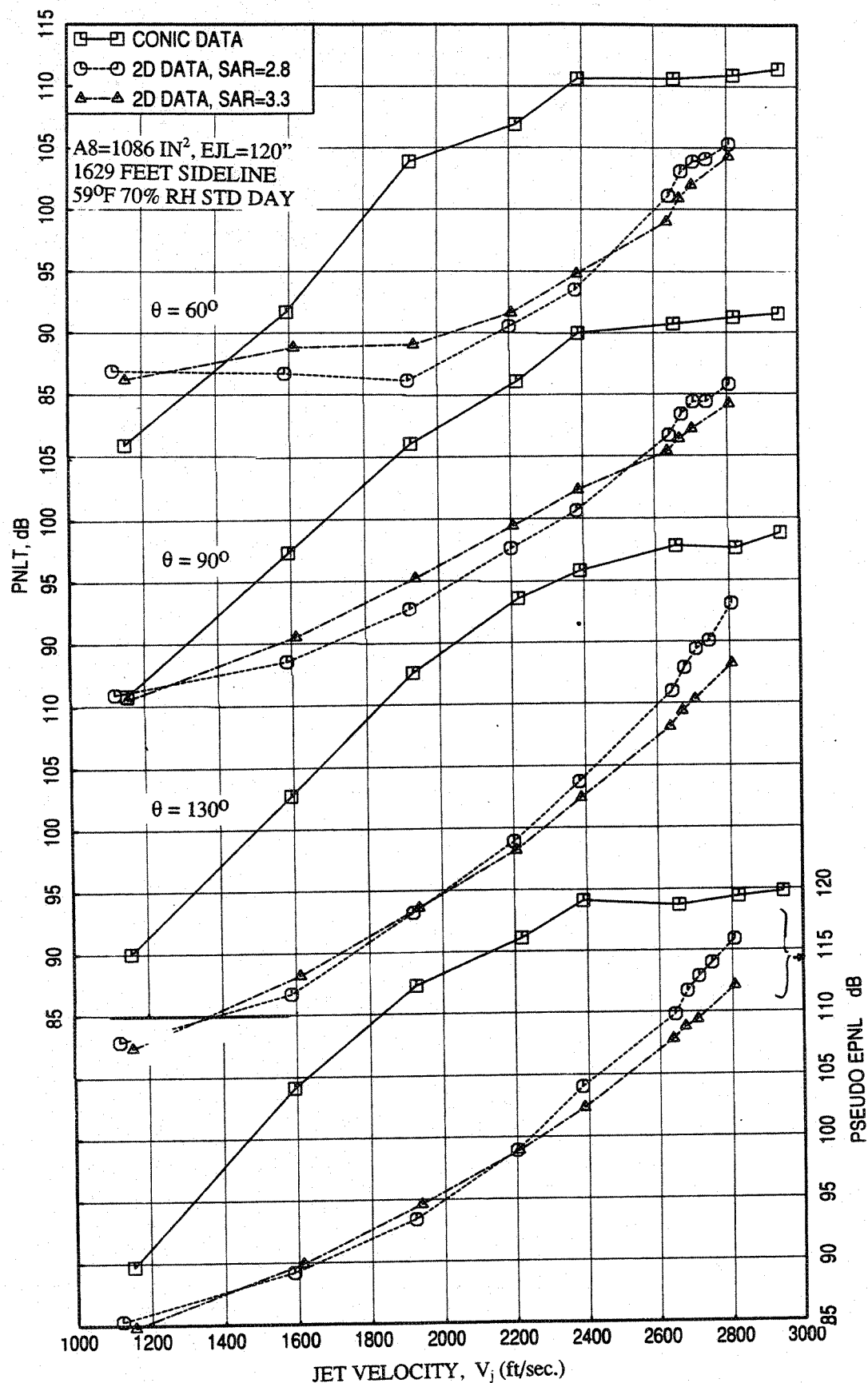
Figure 4.1-63. Effect of SAR on PNLT at various polar angles (θ) and EPNL as functions of jet velocity for aligned CD-chute mixer with fully treated (by Astroquartz) long ejector at static condition; MAR=0.95.
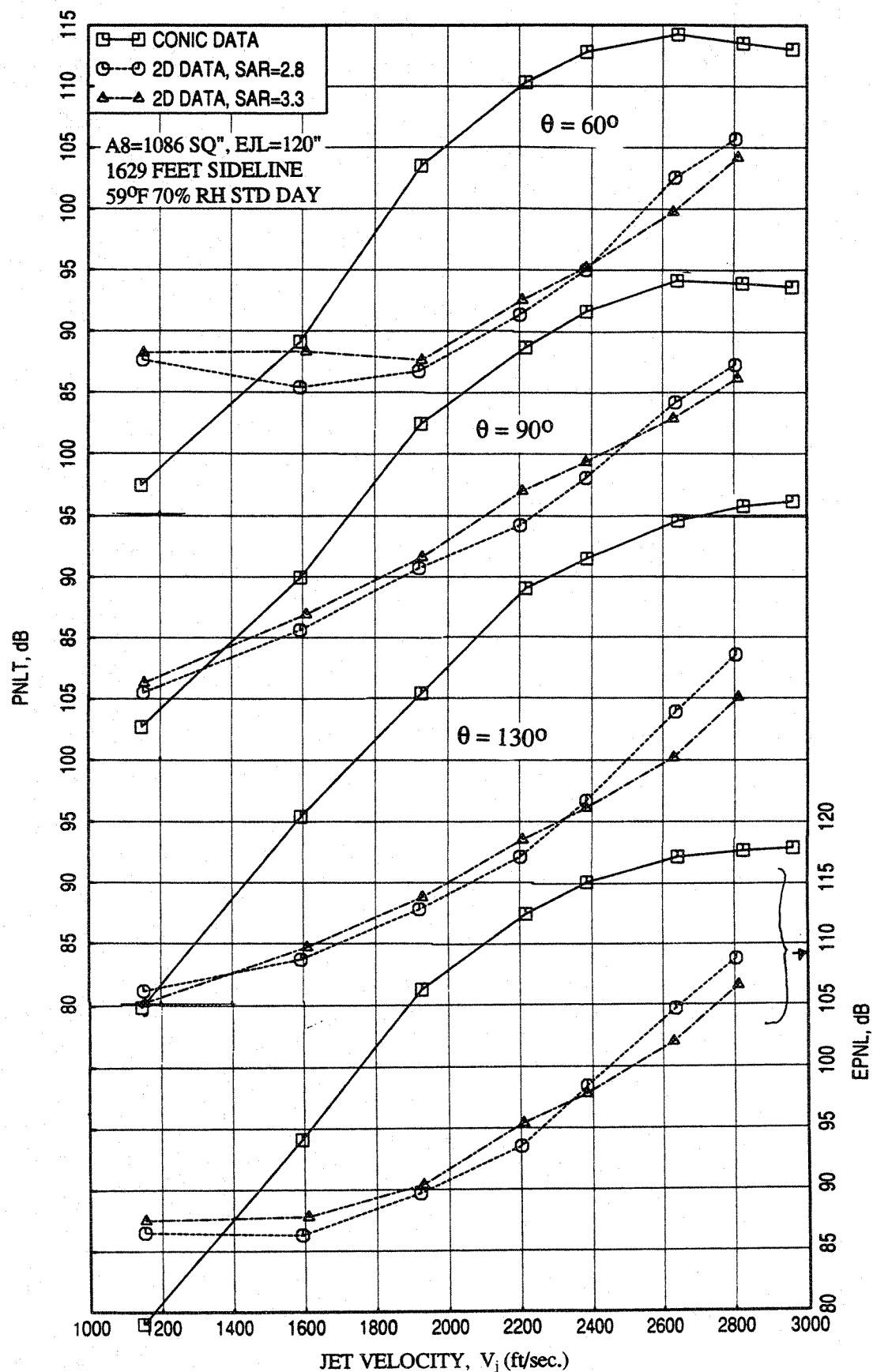
Figure 4.1-64. Effect of SAR on PNLT at various polar angles (θ) and EPNL as functions of jet velocity for aligned CD-chute mixer with fully treated (by Astroquartz) long ejector with flight simulation (M_F=0.32); MAR=0.95.

Figure 4.1-65. Effect of SAR on PNLT at various polar angles (θ) and EPNL as functions of jet velocity for aligned CD-chute mixer with fully treated (by Astroquartz) long ejector; MAR=0.95.

Figure 4.1-66. Effect of SAR on PNLT directivities for different jet velocities (V_j) for aligned CD-chute mixer with fully treated (by Astroquartz) long ejector; MAR=0.95.
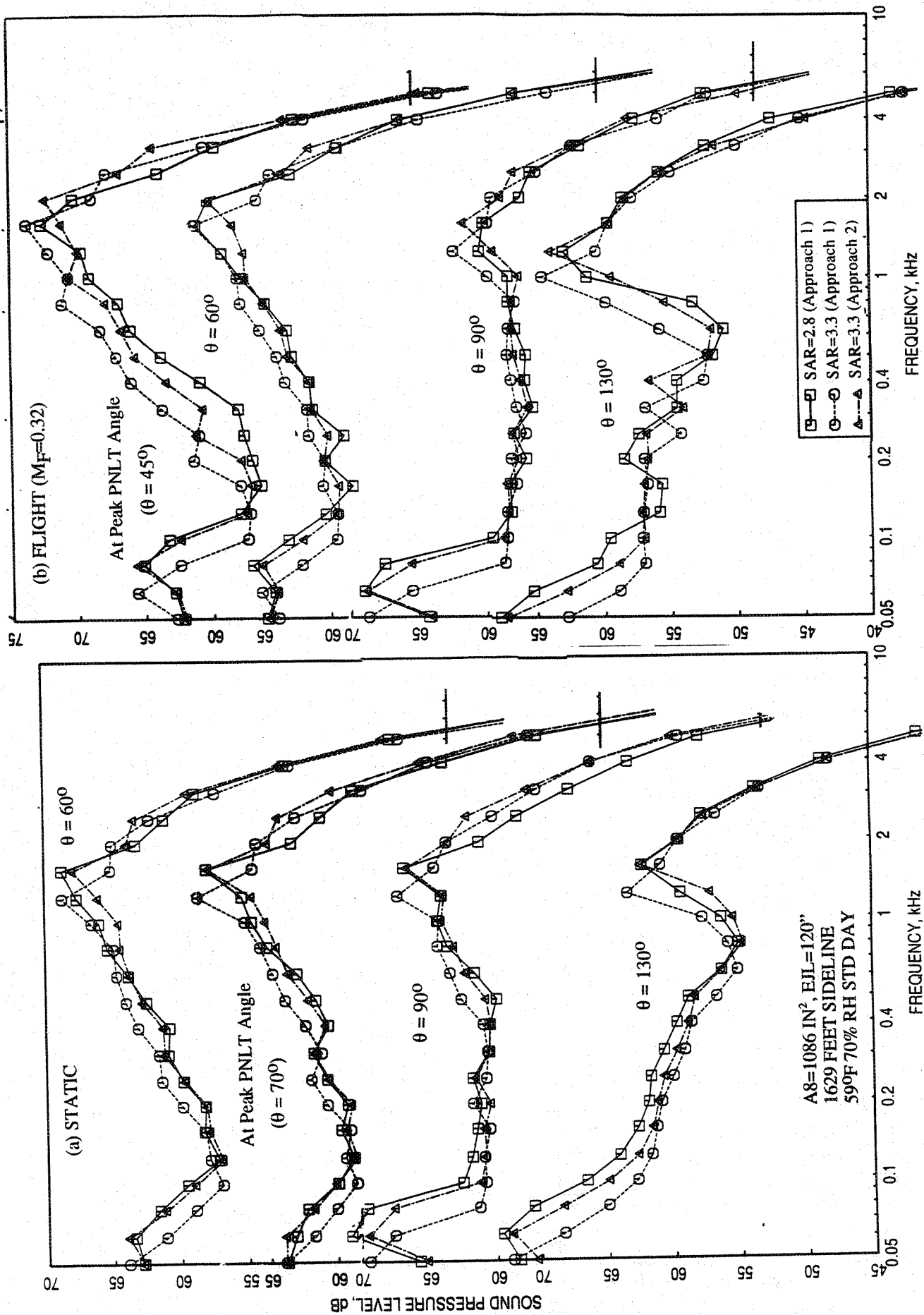
Figure 4.1-67. Effect of SAR on SPL spectra at various polar angles (θ) for aligned CD-chute mixer with fully treated (by Astroquartz) long ejector; MAR = 0.95, V_j = 1147 ft/sec, NPR = 1.5, T8 = 1000°R.
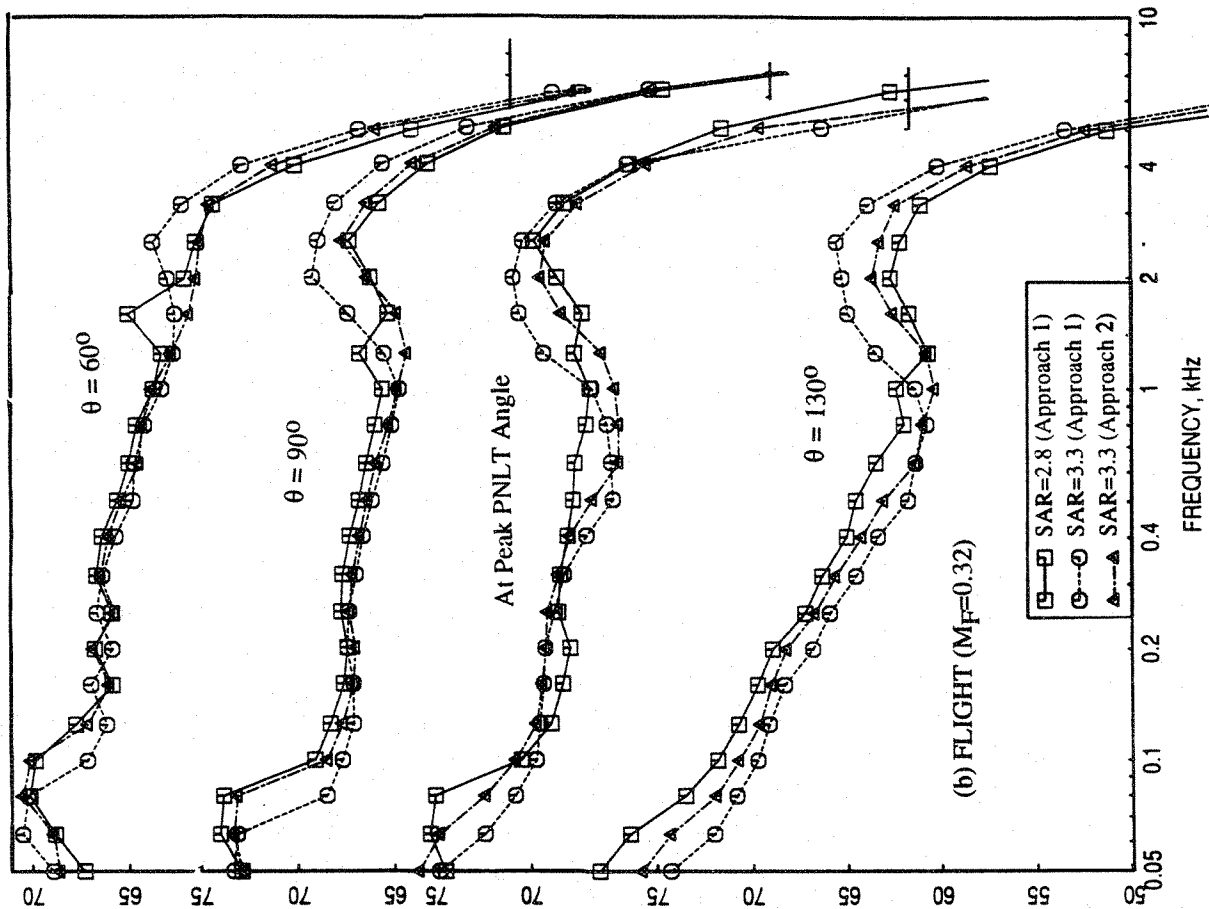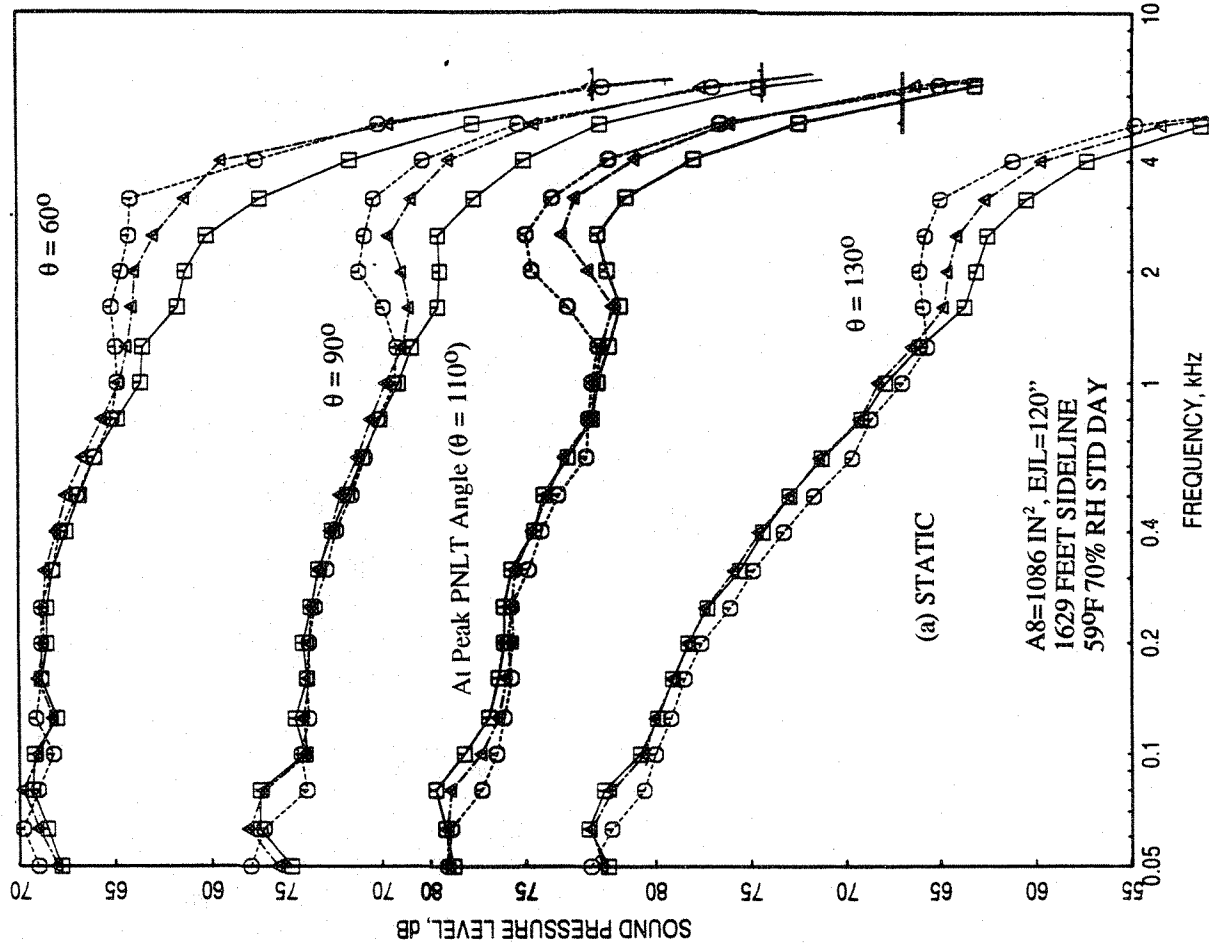
Figure 4.1-68.   Effect of SAR on SPL spectra at various polar angles (θ) for aligned CD-chute mixer with fully treated (by Astroquartz) long ejector; MAR = 0.95, V_j = 1919 ft/sec, NPR = 2.5, T8 = 1325°R.
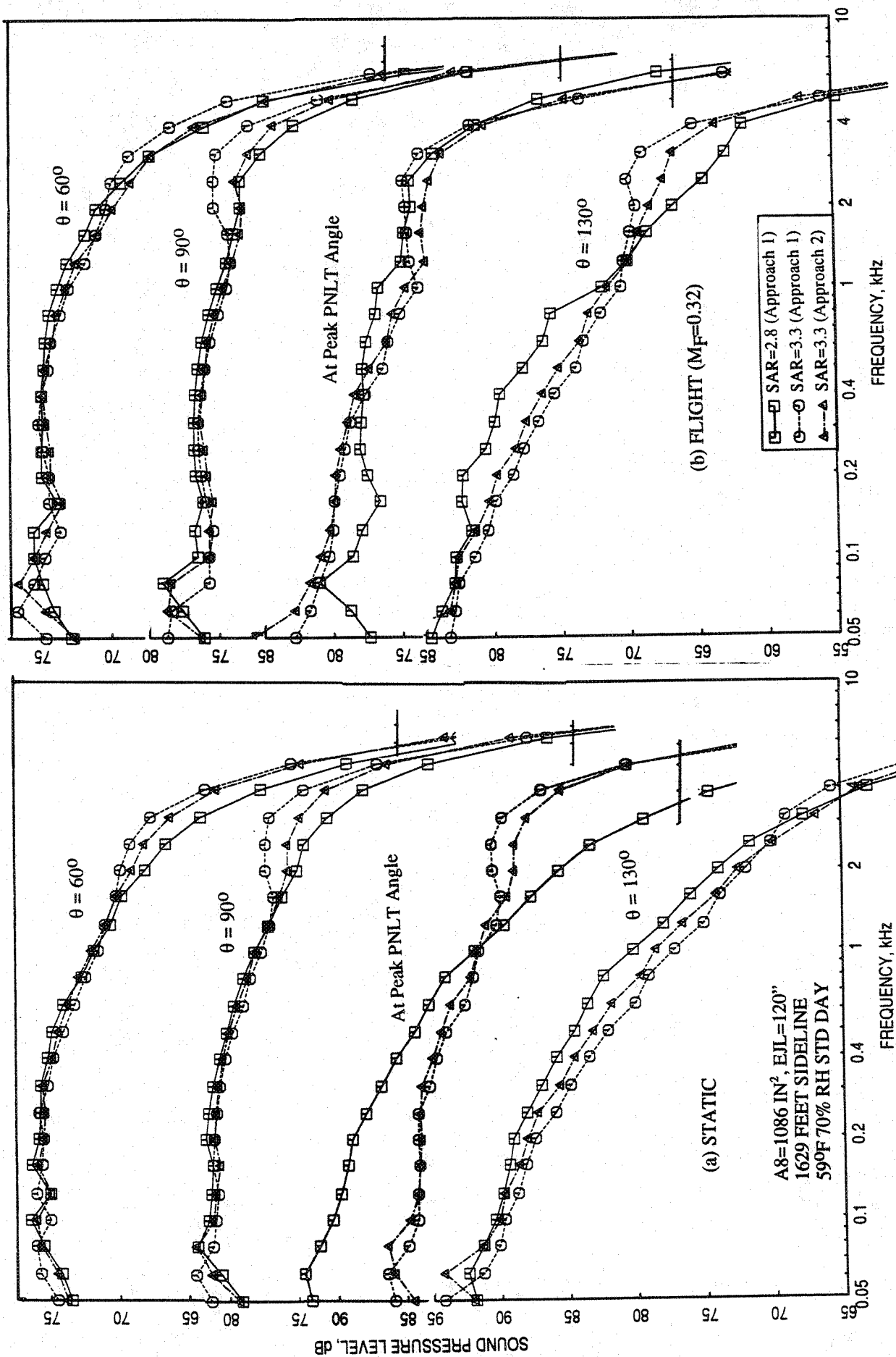
Figure 4.1-69. Effect of on SPL spectra at various polar angles (θ) for aligned CD-chute mixer with fully treated (by Astroquartz) long ejector; MAR = 0.95, V_j = 2384 ft/sec, NPR = 3.4, T8 = 1590°R.
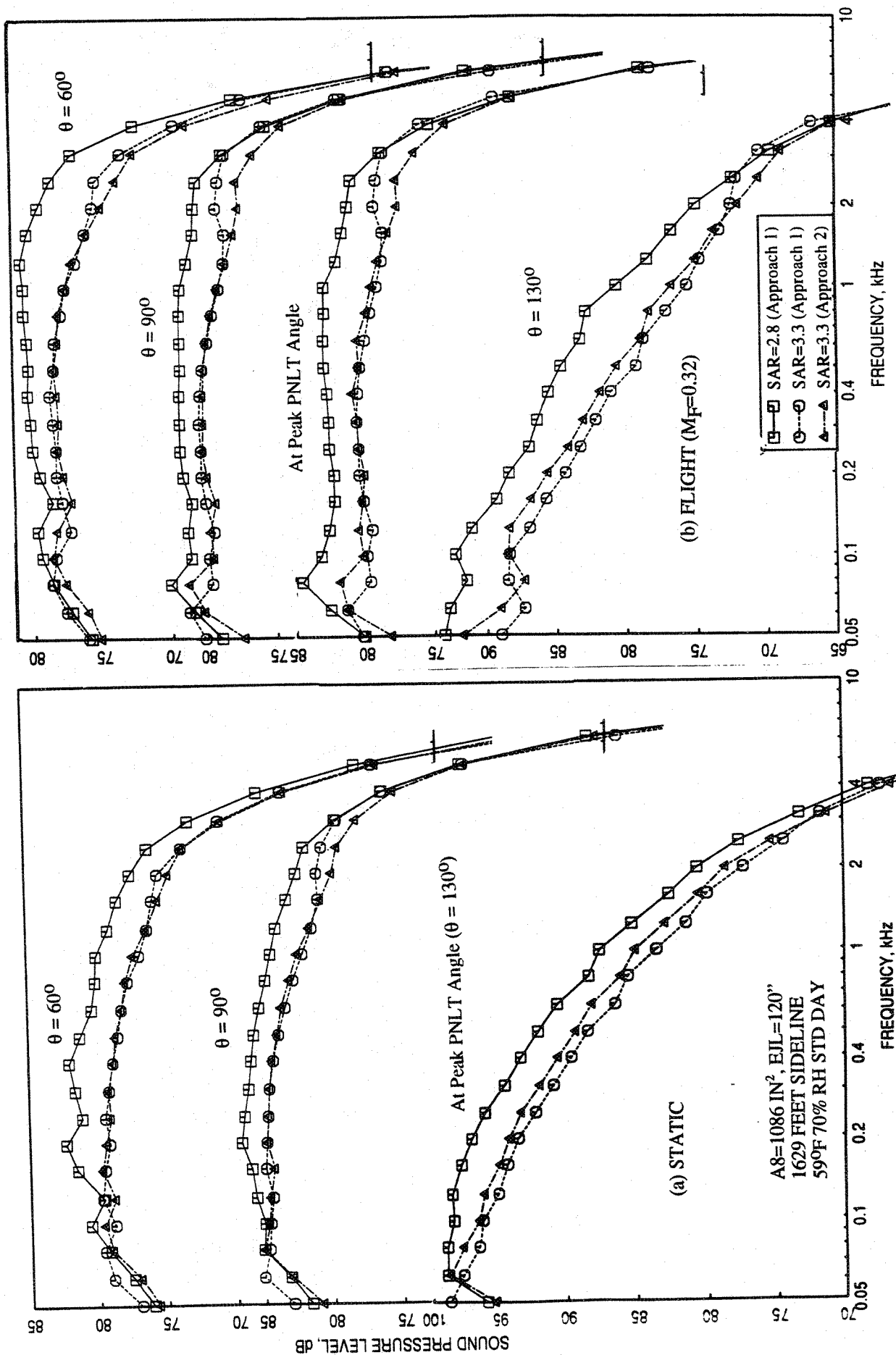
Figure 4.1-70. Effect of SAR on SPL spectra at various polar angles (θ) for aligned CD-chute mixer with fully treated (by Astroquartz) long ejector; MAR = 0.95, V_j = 2637 ft/sec, NPR = 4.0, T8 = 1750°R.

a reduction in PNLT, but the trend is reversed at shallow angles to jet axis. This behavior is based on the spectral content with respect to 1/3-octave band frequencies for each cases of band shifts and the changed NOY weightings for PNLT calculation. The spectral comparisons at each of the four velocity conditions are shown in Figures 4.1-67 through 4.1-70 at a number of polar angles. The effect of different band shift alters the SPL and is mostly lower with 8 frequency band shift situation. For flat SPL spectrum the frequency band shift does not influence the spectral distribution. However, high frequency peaks occur at one 1/3-octave band lower for approach 1 compared to approach 2 (see Figure 4.1-67 for θ=130°). This alters PNL and PNLT results.

In either approaches, the absolute noise levels and the corresponding center frequencies have some imprecision due to the simplification associated with utilizing the integer value band number shift for 1/3-octave band data. The above exercise, basically demonstrates the variability of noise levels due to two consecutive band shifts. The actual noise levels lie with in the limits shown in these figures between the two approaches and the amount of the maximum possible variations are small. Such imprecision can be reduced if one utilizes scale model narrowband data of a sufficiently small band width and scales such data using above scaling process for frequency and then constitutes 1/3-octave band on the basis of full scale frequencies. Alternately, fractional frequency shift due to scaling can be applied to lossless 1/3-octave spectral data and then an interpolation/extrapolation can be applied to construct the SPL at 1/3-octave center frequencies.

Based on the PNLT directivities of Figure 4.1-66, for velocities up to about 2400 ft/sec the PNLT for SAR=3.3 are slightly higher compared to those for SAR=2.8, when the results for SAR=3.3 mixer are derived using 9 frequency band shift (i.e., the conventional method or Approach 1). Insignificant difference between the two mixers is observed when Approach 2 is applied for mixer of SAR=3.3 in this velocity range. At higher velocities, the mixer with SAR=3.3 seems to be quieter compared to the mixer of SAR=2.8 irrespective of data analysis approaches. Spectral results, shown in Figures 4.1-67 through 4.1-70, show the similar characteristics with respect to jet velocity.

Flow and Performance Related Results: The measured static and total pressure data for the models are analyzed and the performance and flow related results with flight simulation (MF=0.32) to show the influence of SAR are presented in this section. the influence of SAR on ramp and chute static pressure distributions are shown in Figure 4.1-71 for different L1M cycle conditions. For each case the static pressure increases with
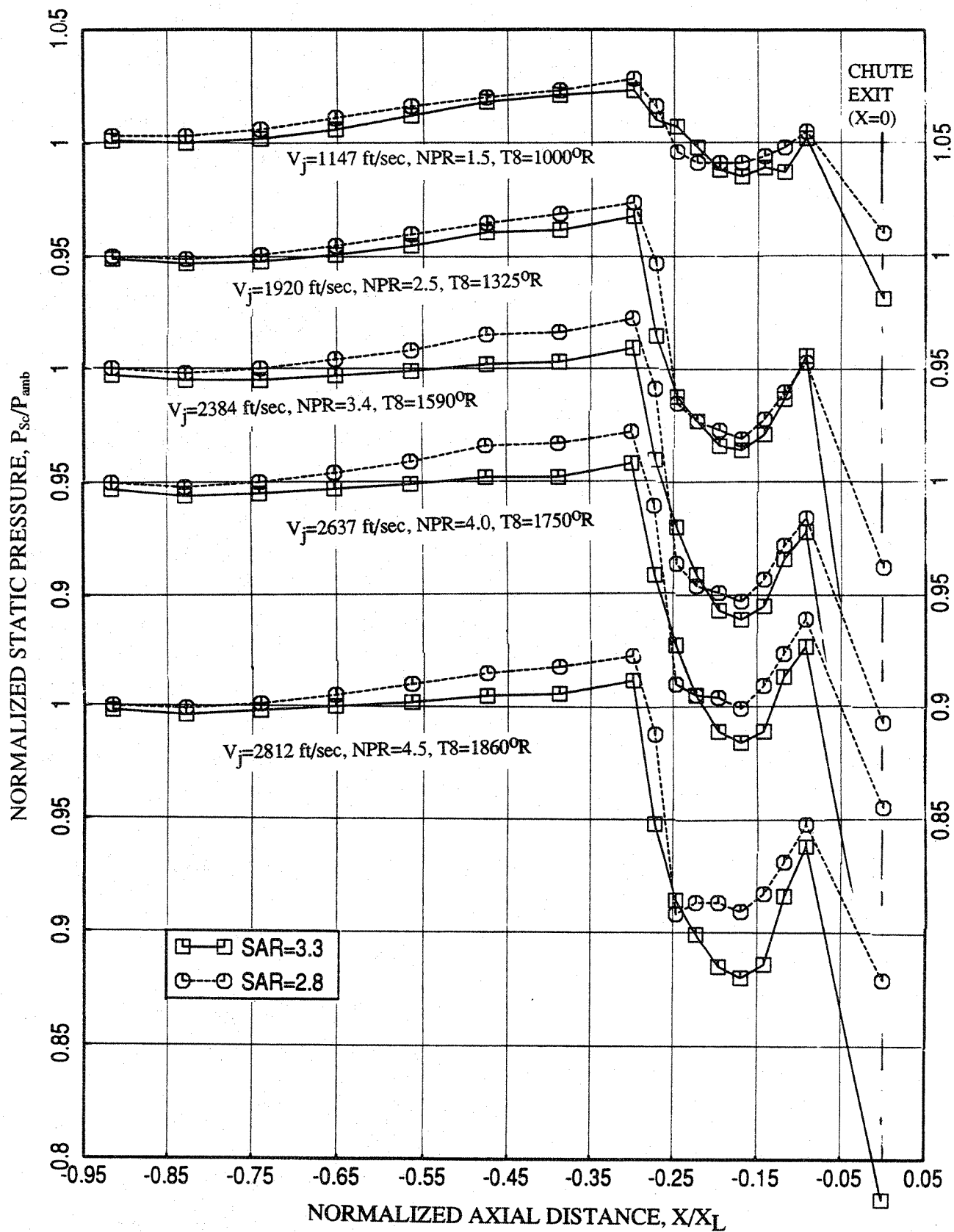
Figure 4.1-71. Effect of SAR on the static pressure distributions on the inlet ramp and on the secondary flow side of chute surface at different L1M cycle conditions for aligned CD chute mixer with treated (by Astroquartz) long ejector with flight simulation (M_F=0.32), MAR = 0.95.

decreasing SAR, both on the ramp and chute surfaces, indicating lesser loading for the chutes for higher SAR. This is clearly observed in Figure 4.1-72, where chute loading coefficient due to chute static pressure distributions is plotted against NPR.

Average total pressure distributions across the inlet width for mixers of different SAR for different L1M cycle conditions are shown in Figure 4.1-73. Slight total pressure drop is observed for lower SAR of 2.8 compared to SAR=3.3. The influence of SAR on pumping and corrected pumping is shown in Figure 4.1-74 The pumping as well as corrected pumping increases with increasing SAR and the mixed jet velocity decreases with increasing SAR (see Figure 4.1-75), which is a favorable behavior from noise consideration.

Figure 4.1-76 illustrates the influence of SAR on the axial static pressure distributions on the flap for different L1M cycle conditions. At lower NPR very little change on flap static pressure distribution is observed due to SAR. However, the transition from subsonic to supersonic mode occurs at a lower NPR for SAR=2.8 compared to SAR=3.3. In the supersonic mode (i.e., at a much higher NPR) the static pressure on the flap is higher for SAR=3.3 compared to SAR=2.8. The influence of SAR on normalized force and normalized moment of force with respect to flap leading edge due to static pressure difference on flap surface are shown in Figure 4.1-77. The transition from subsonic to supersonic mode is delayed with respect to NPR due to increasing SAR.
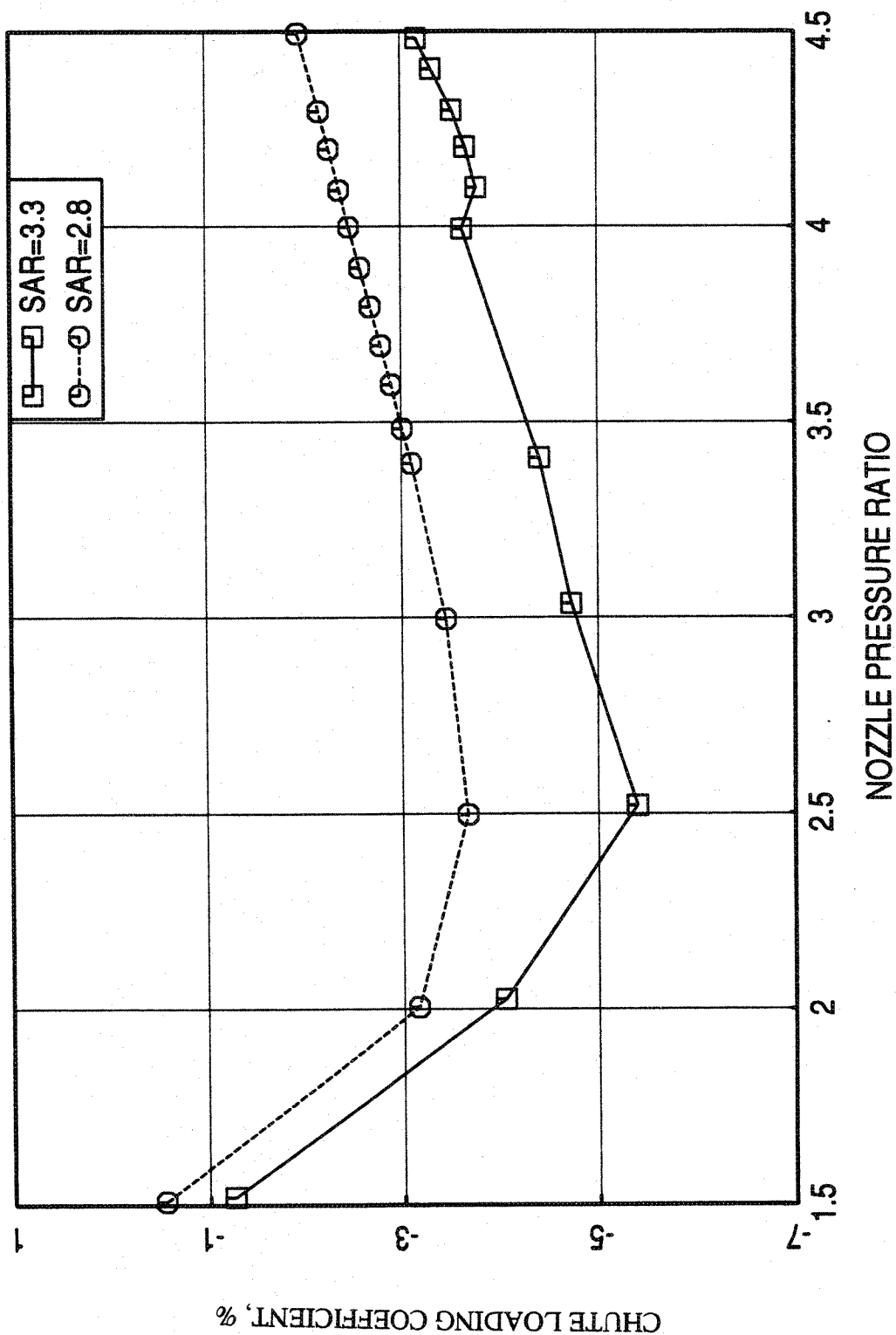
Figure 4.1-72. Effect of SAR on chute loading coefficient, computed by measured static pressure distributions on secondary flow side chute leading edge, with respect to nozzle pressure ratios for aligned CD chute mixer with treated (by Astroquartz) long ejector with flight simulation (M_F=0.32), MAR = 0.95.
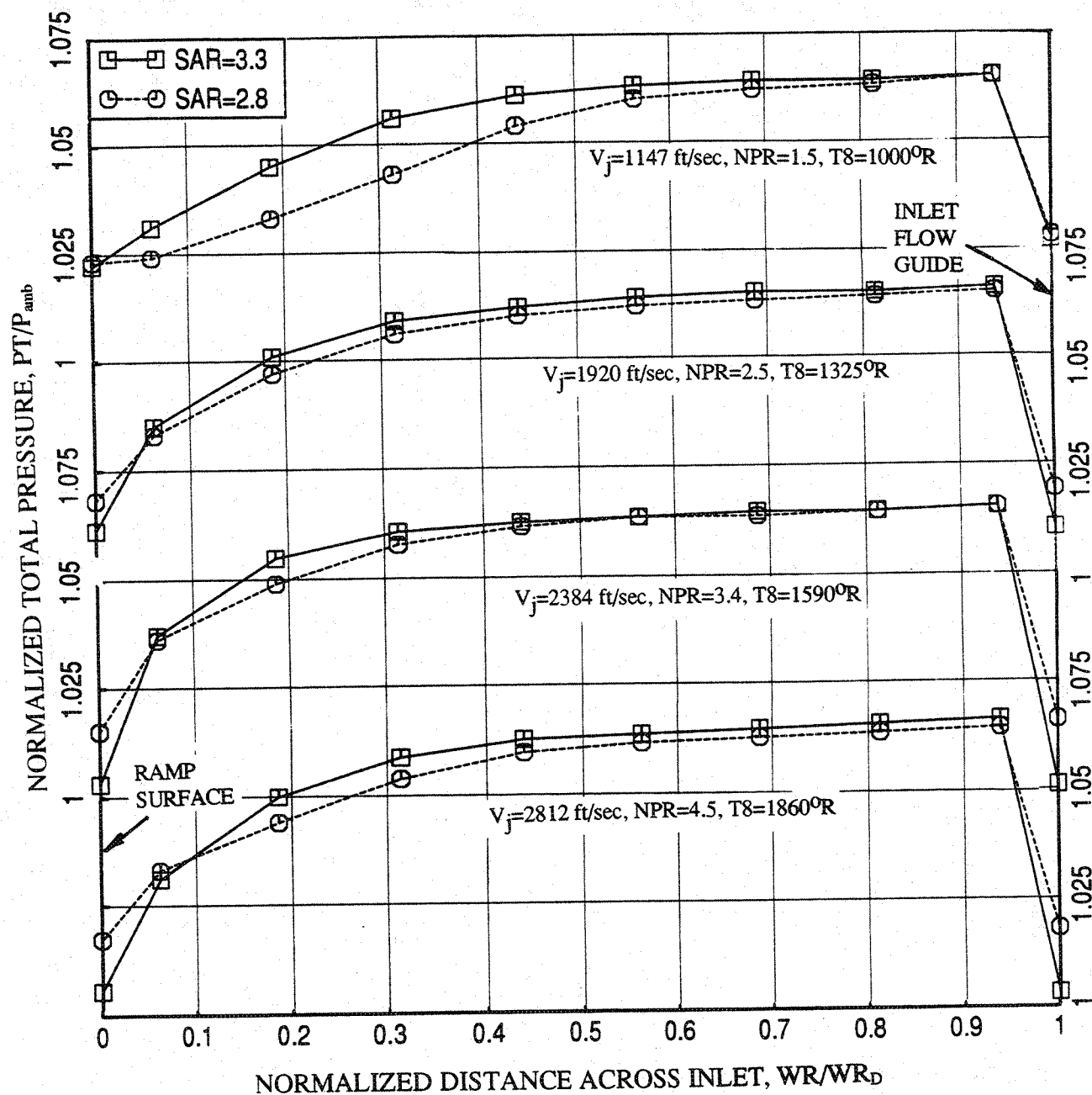
Figure 4.1-73. Effect of SAR on total pressure distribution across the inlet at different L1M cycle conditions for aligned CD chute mixer with treated (by Astroquartz) long ejector with flight simulation (M_F=0.32), MAR = 0.95.
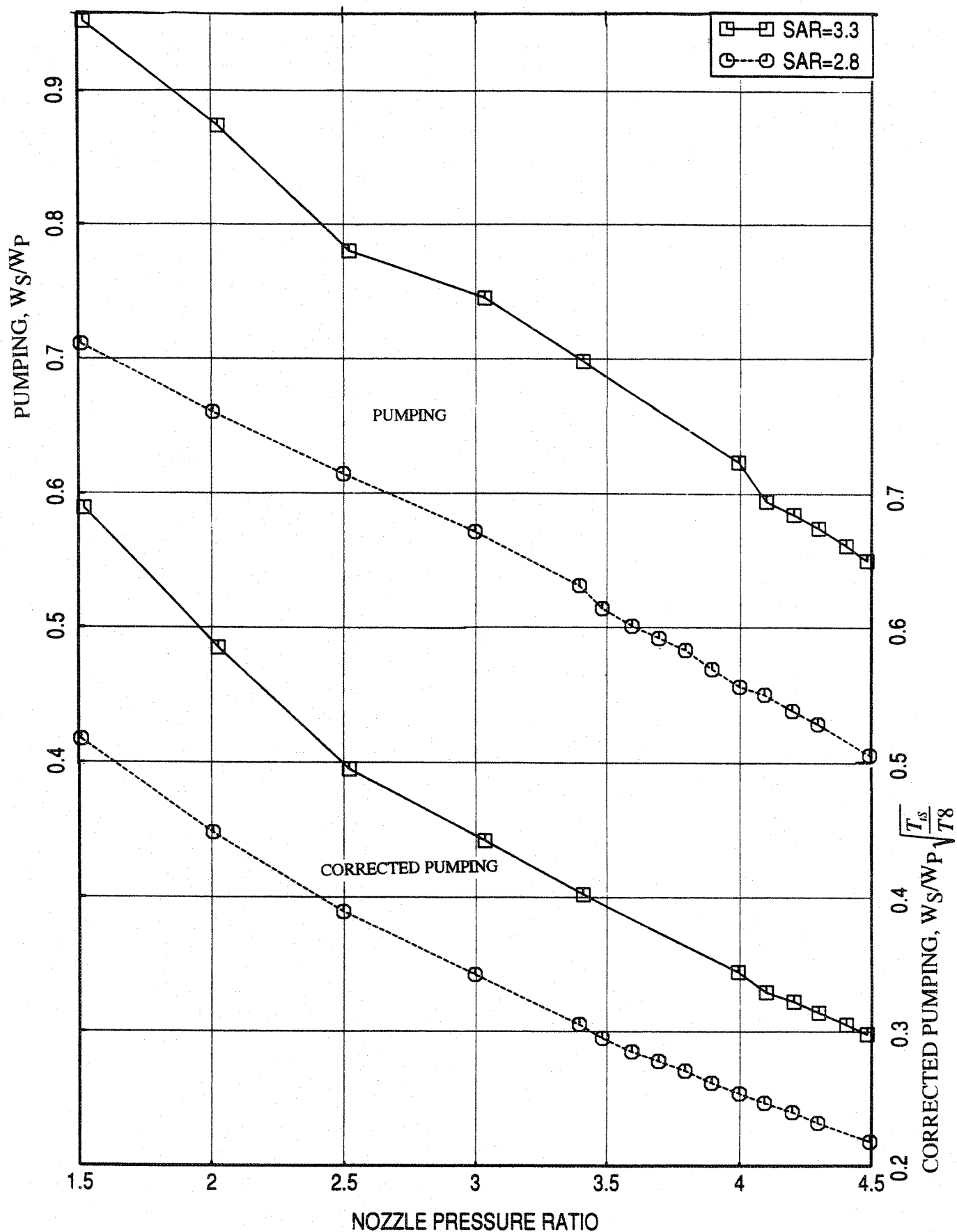
Figure 4.1-74. Effect of SAR on pumping, computed by measured rake total pressure distributions at the inlet, with respect to nozzle pressure ratios for aligned CD chute mixer with treated (by Astroquartz) long ejector with flight simulation (M_F=0.32), MAR = 0.95.
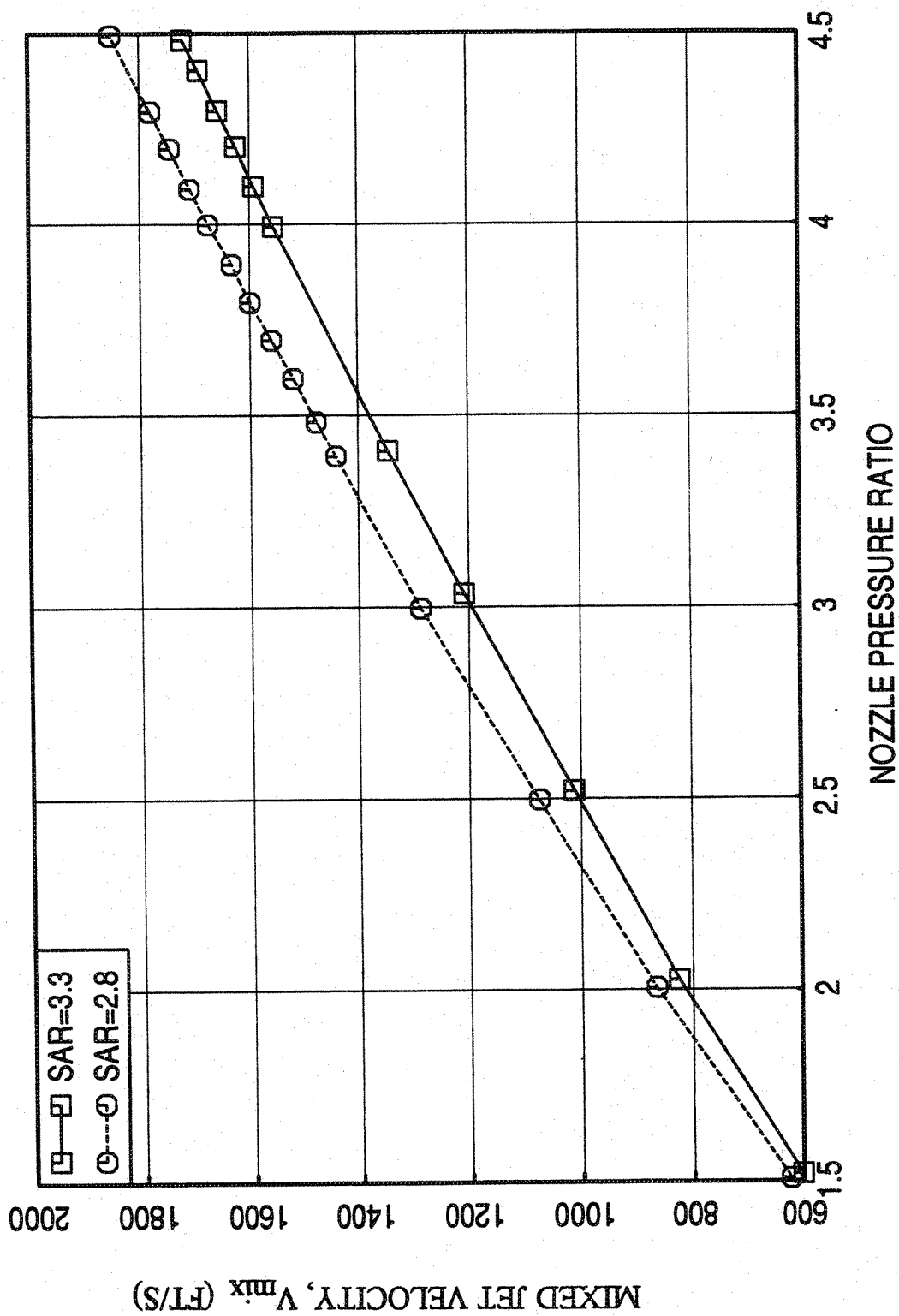
Figure 4.1-75.   Effect of SAR on mixed jet velocity, computed by measured rake total pressure distributions at the inlet, with respect to nozzle pressure ratios for aligned CD chute mixer with treated (by Astroquartz) long ejector with flight simulation (M_F=0.32), MAR = 0.95.
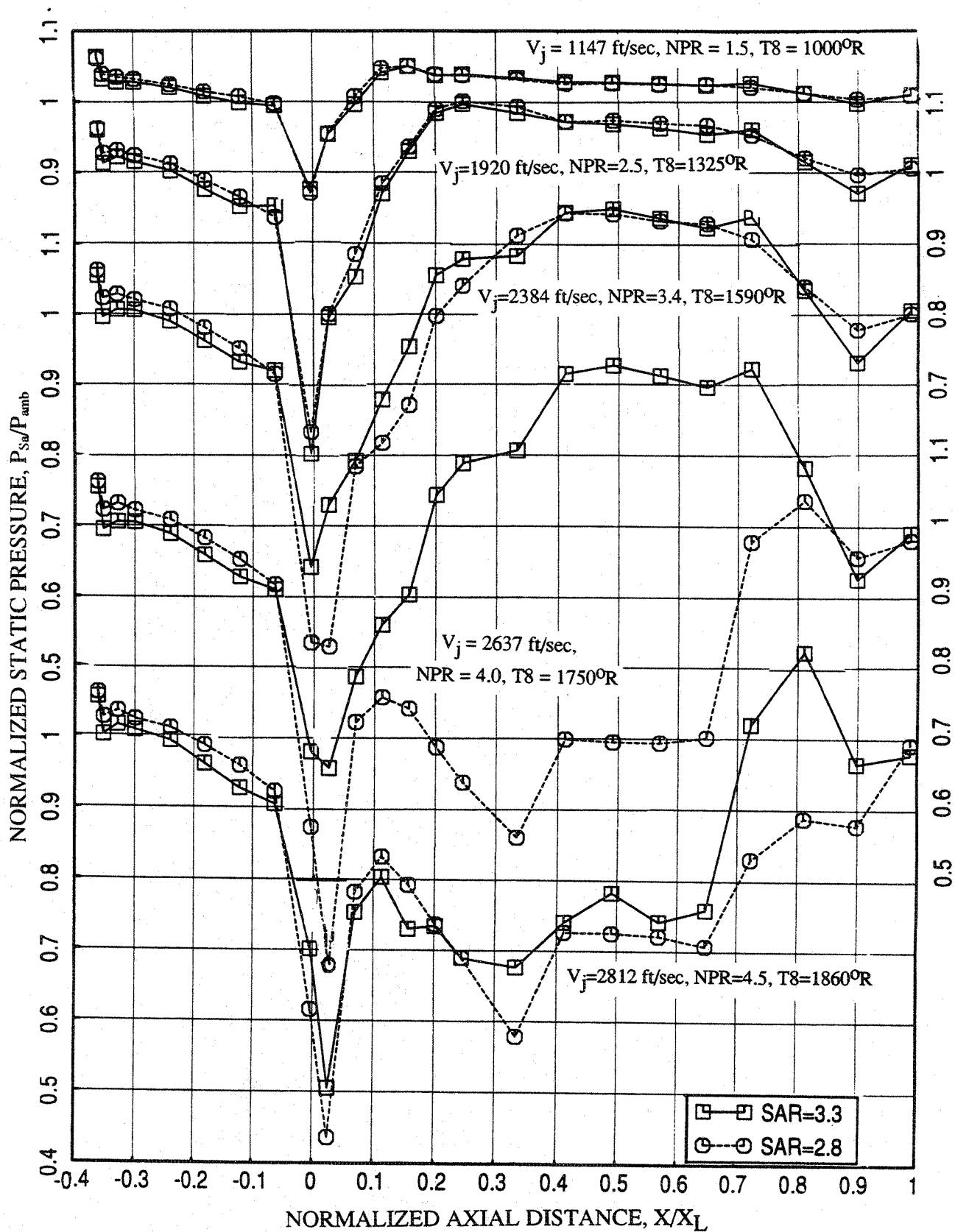
Figure 4.1-76. Effect of SAR on axial distribution of average static pressure on the inlet and the flap surface at different L1M cycle conditions for aligned CD chute mixer with treated (by Astroquartz) long ejector with flight simulation (M_F=0.32), MAR = 0.95.
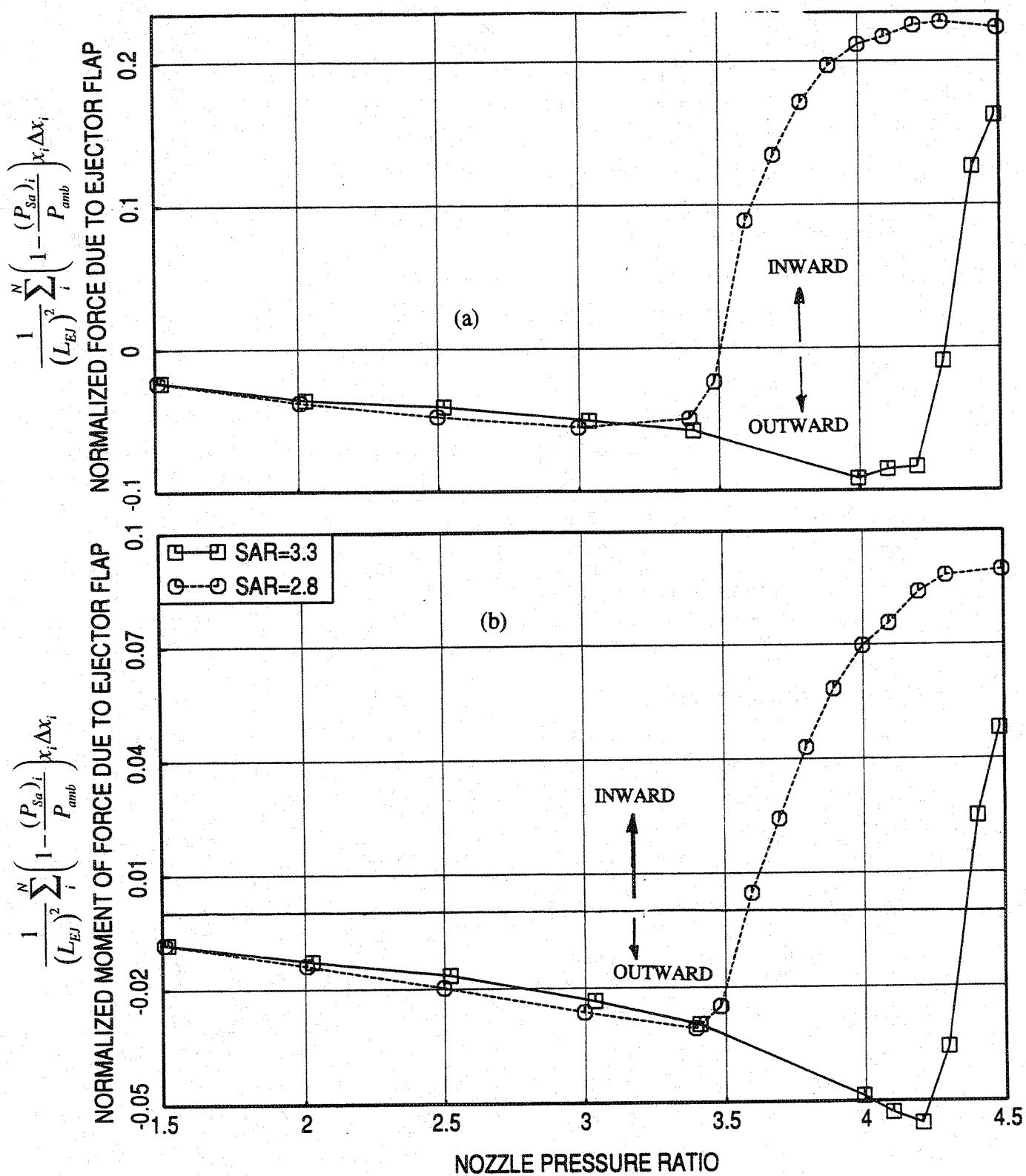
Figure 4.1-77. Effect of SAR on normalized (a) force and (b) moment of force due to ejector flap with respect to nozzle pressure ratio for aligned CD chute mixer with treated (by Astroquartz) long ejector with flight simulation (M_F=0.32, MAR = 0.95.

4.2 ALIGNED CONVERGENT-CHUTE MIXER CONFIGURATIONS:

The acoustic, the flow related, and performance related results for 2D aligned convergent-chute mixer-ejector configurations of SAR=2.8 with long and short flaps and with and without acoustic treatment are described in this section. These results include the effect of flap length, acoustic treatment, and simulated flight of M_F=0.32. The long and short ejectors with flap lengths of 16.055" and 10.935", respectively, with MAR=0.95 were used for the current configurations. For treated configurations the flaps and sidewalls were fully treated with nickel based metal foam with a 37% porous facesheet.

The side view of the mixer-ejector configuration with convergent chute is shown in Figure 4.2-1. The ramp, the inlet, and the upper portion of the primary flow sections are identical to those for the aligned CD chute mixer configuration described in section 4.1. However, the exit plane for the convergent chute mixer is terminated upstream at the throat plane compared to the CD chute mixer. For appropriate comparison of the results the origin is maintained at the same axial location as that of the aligned CD chute mixers (i.e., 0.58" downstream of the convergent-chute mixer exit plane). Hence, the origin for the convergent chute mixer does not lie at the mixer exit plane. The plan view of the inlet and the upper chute rack with 10 convergent chutes is shown in Figures 4.2-2, which indicates the static pressure tap locations on the ramp, inlet flow guide, and chute surfaces and total pressure element locations in the secondary flow passage. The instrumentation is identical to that for the aligned CD chute configuration, except that an additional static pressure tap (PS138) is placed along the chute hot flow region between the mixer exit plane and the static pressure tap PS26. The instrumentation on the lower inlet and lower chute rack for convergent mixer is identical to that of the aligned CD chute case (see Figure 4.1-6).

The instrumentation upstream of the mixer exit is the same for both the long and short flap configurations. The flap instrumentation is different for short flap configuration. The side view of the mixer-ejector configuration with convergent chute with short flaps is shown in Figure 4.2-3. Figure 4.2-4 shows the plan and side views of a short ejector with static pressure tap locations. A line of 10 static pressure taps, PS60 through PS65 and PS70 through PS73, are placed on the flap in line with the centerline of a cold flow chute. Similarly, another 10 static pressure taps, PS74 through PS79 and PS84 through PS87, are placed on the flap in line with the centerline of a hot flow chute (see Figures 4.2-4).
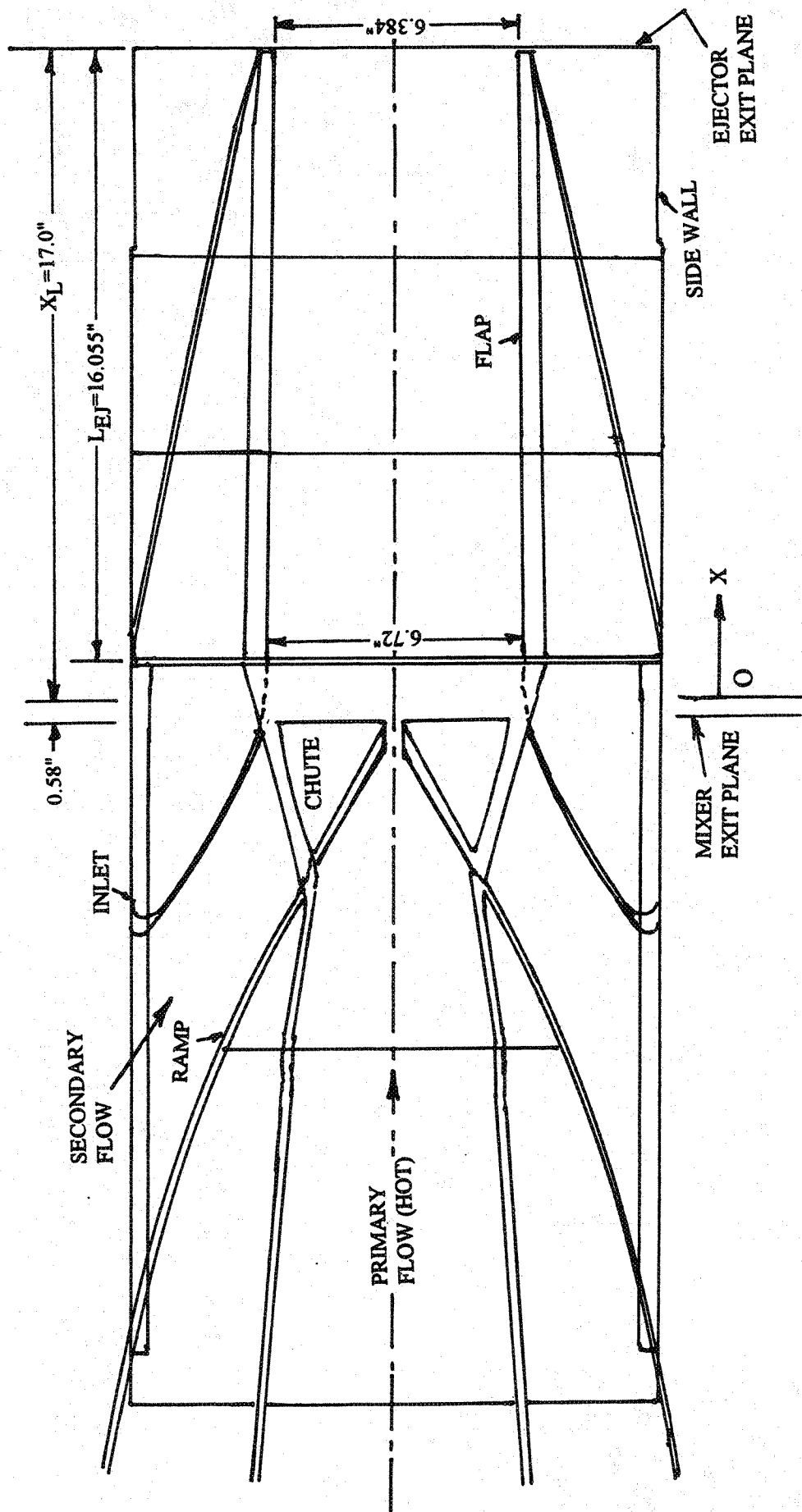
Figure 4.2-1. Side view of a 2D mixer-ejector nozzle with convergent chutes and with 16.055" (120" full scale) ejector; SAR=2.8, MAR=0.95.
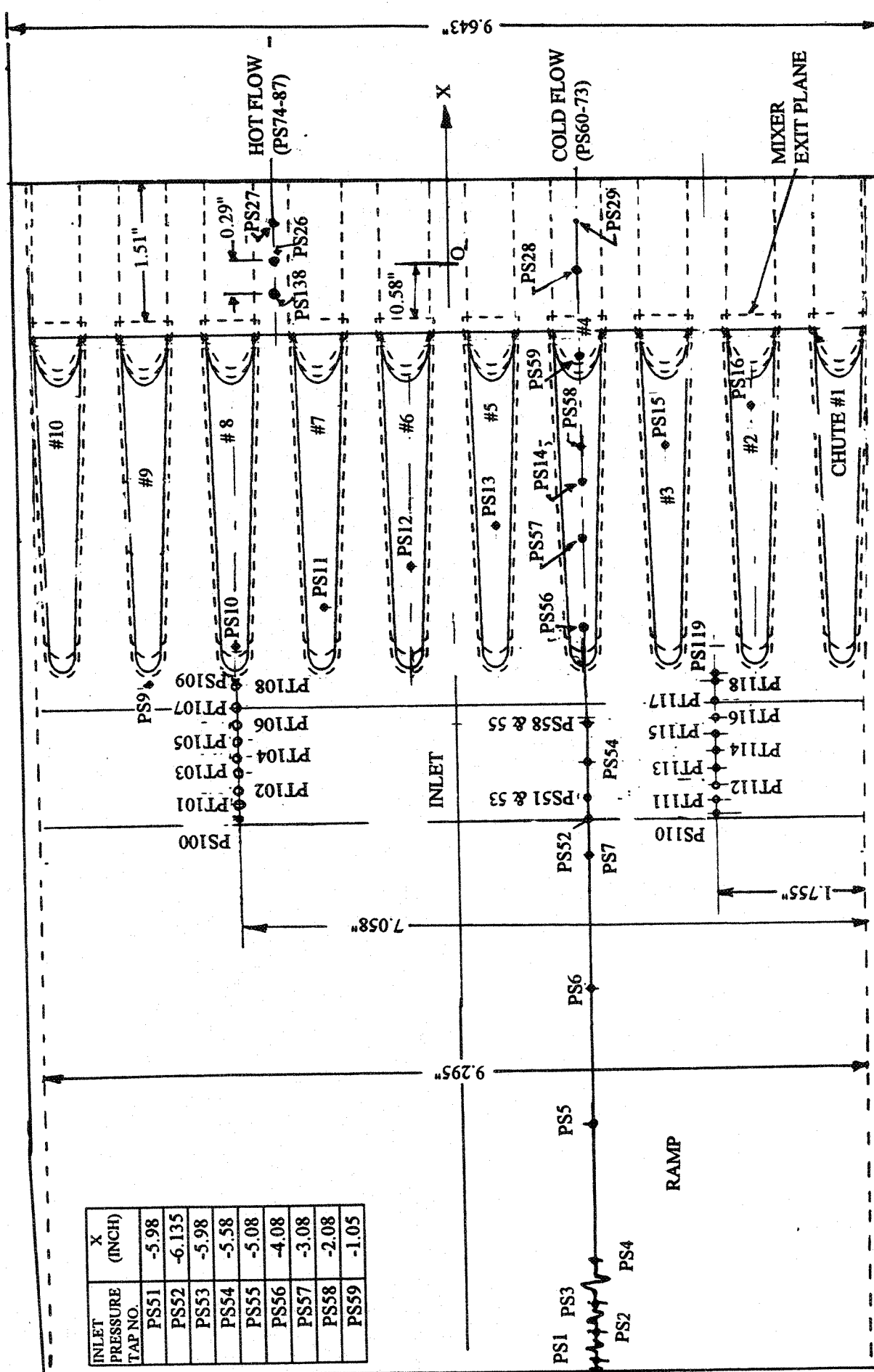
Figure 4.2-2. Plan view of the inlet and the upper chute rack with 10 convergent chutes for a 2D mixer-ejector nozzle showing the static pressure tap locations on the ramp, inlet flow guide, and chute surfaces and total pressure element locations in the secondary flow passage.
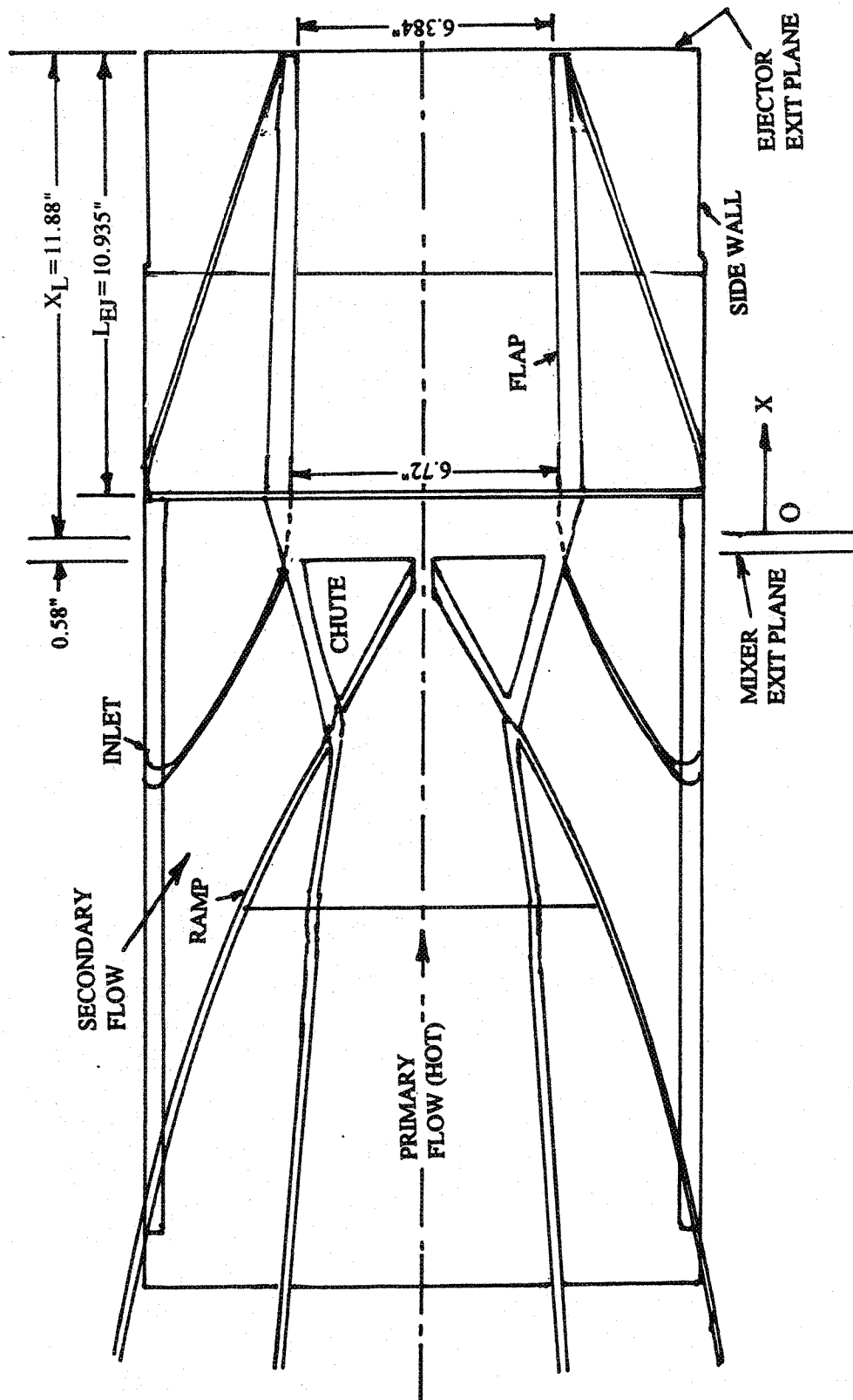
Figure 4.2-3. Side view of a 2D mixer-ejector nozzle with 20 convergent aligned chutes and with short flap of 10.935" long (80" full scale); SAR=2.8, MAR=0.95.

CHUTE COLD CENTERLINE	PS28	PS29	PS60	PS61	PS62	PS63	PS64	PS65	PS70	PS71	PS72	PS73
CHUTE HOT CENTERLINE	PS26	PS27	PS74	PS75	PS76	PS77	PS78	PS79	PS84	PS85	PS86	PS87
X (INCH)	-0.08	0.42	1.17	1.92	2.67	3.42	4.17	5.67	7.17	8.67	10.17	11.67

Figure 4.2-4. (a) Plan and (b) side views of a short ejector of a 2D aligned convergent-chute mixer-ejector nozzle showing the static pressure tap locations.
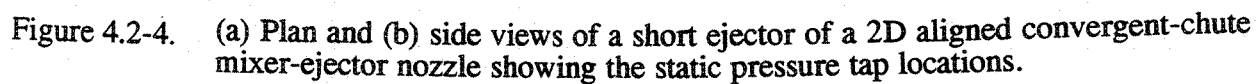
4.2.1 Effect of Acoustic Treatment and Flap Length:

All the results in this section show the simultaneous comparisons between treated and hard wall configurations and between short and long flaps for static and with flight simulation condition of $M_F=0.32$. While the long flap results are presented by open symbols, the same filled symbols show the results for short flap configurations.

Figure 4.2-5 shows the effect of treatment and flap length on PNLT and EPNL as function of jet velocity (V_j) at an azimuthal angle $\phi=25^\circ$. Noise reductions in terms of EPNdB and PNLTdB are observed both due to treatment and increased flap length. However, the effect is reduced with increasing jet velocity. Noise reduction due to acoustic treatment is higher for the long flap configuration compared to the short flap case. Acoustic benefit of about 3 EPNdB due to treatment is observed for the long flap configuration with flight simulation at velocities between 1600 and 2200 ft/sec. At higher velocities the treatment benefit is not significant due to dominant externally (i.e., external to the ejector) generated noise. At lower velocities the EPNdB reduction due to treatment as well as due to flap length is significant at static case compared to flight condition. This is due to the PNLT increase in the forward angles with flight simulation, since the jet noise increase due to dynamic amplification is much higher compared to source strength reduction due to flight simulation. Noise benefit due to increased flap length is the result of better mixing within the ejector compared to a shorter ejector case.

At four different jet velocities the effect of treatment and flap length on PNLT directivities is shown in Figure 4.2-6. Noise suppressions due to treatment and due to flap length are more significant at lower jet velocities and at lower polar angles. The effect of flight at a lower jet velocity, as described above, can be seen in this figure for $V_j=1147$ ft/sec. Effect of treatment and flap length on SPL spectra at various polar angles (θ) for each of the four jet velocities is shown in Figures 4.2-7 through 4.2-10. Significant SPL reduction is observed at higher polar angles for higher frequency range above 700 to 800 Hz. The acoustic benefit in terms of SPL diminishes with increasing jet velocity. At NPR=3.4 condition the SPL results indicate the possible presence of strong shock in the ejector for short flap configurations. Shock-associated noise in terms of SPL is dominantly observed at 60° and in moderate amount at 90° for the short flap configurations.

The static pressure tap locations on the flap surface downstream of the origin (i.e., for positive X) are normalized with respect to the ejector length associated with the test
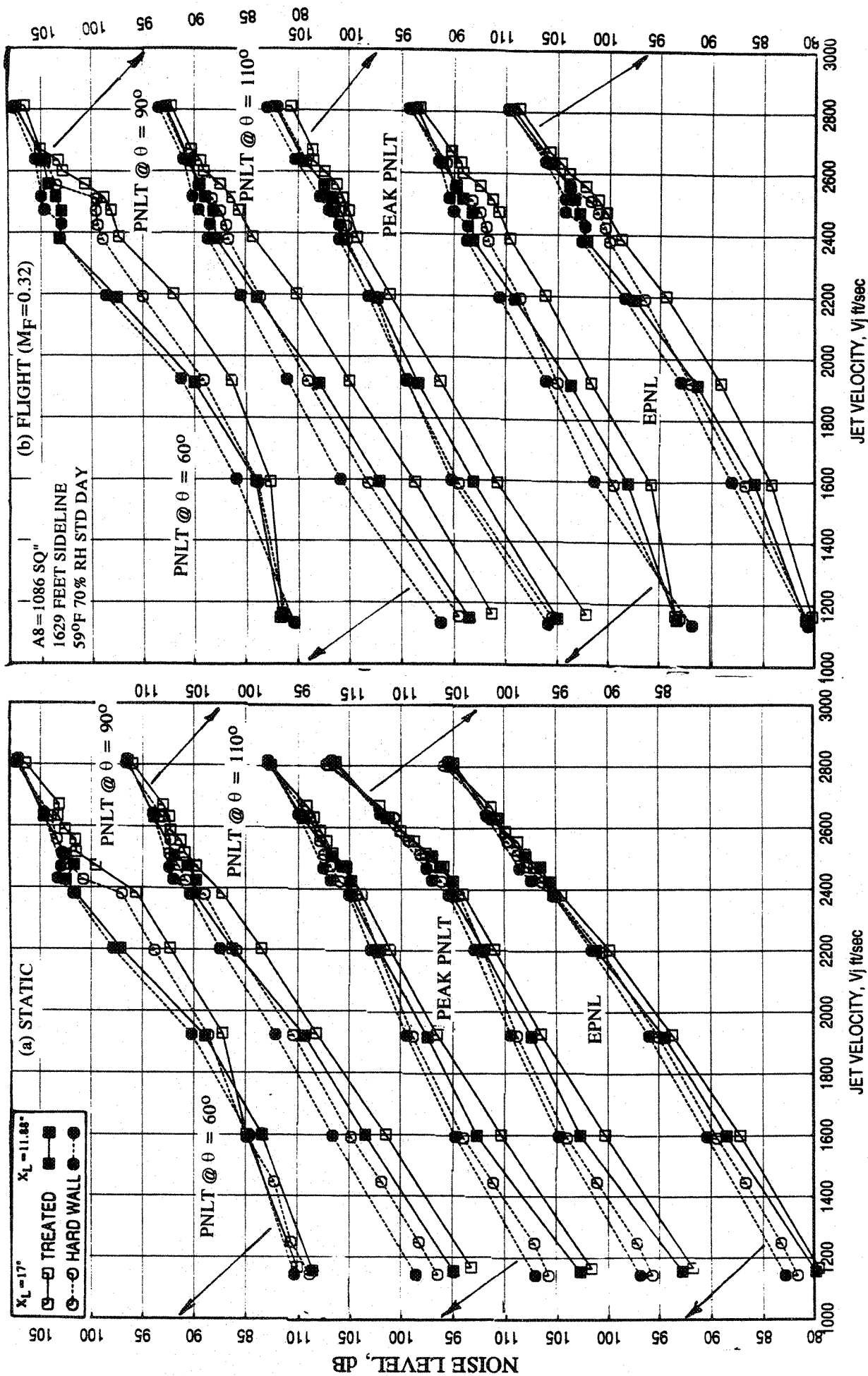
Figure 4.2-5. Effect of acoustic treatment and flap length on EPNL and PNLT at various polar angles (θ) as function of jet velocity of L1M cycle conditions for an aligned convergent-chute mixer-ejector at an azimuthal angle φ=250°; SAR=2.8, MAR=0.95.
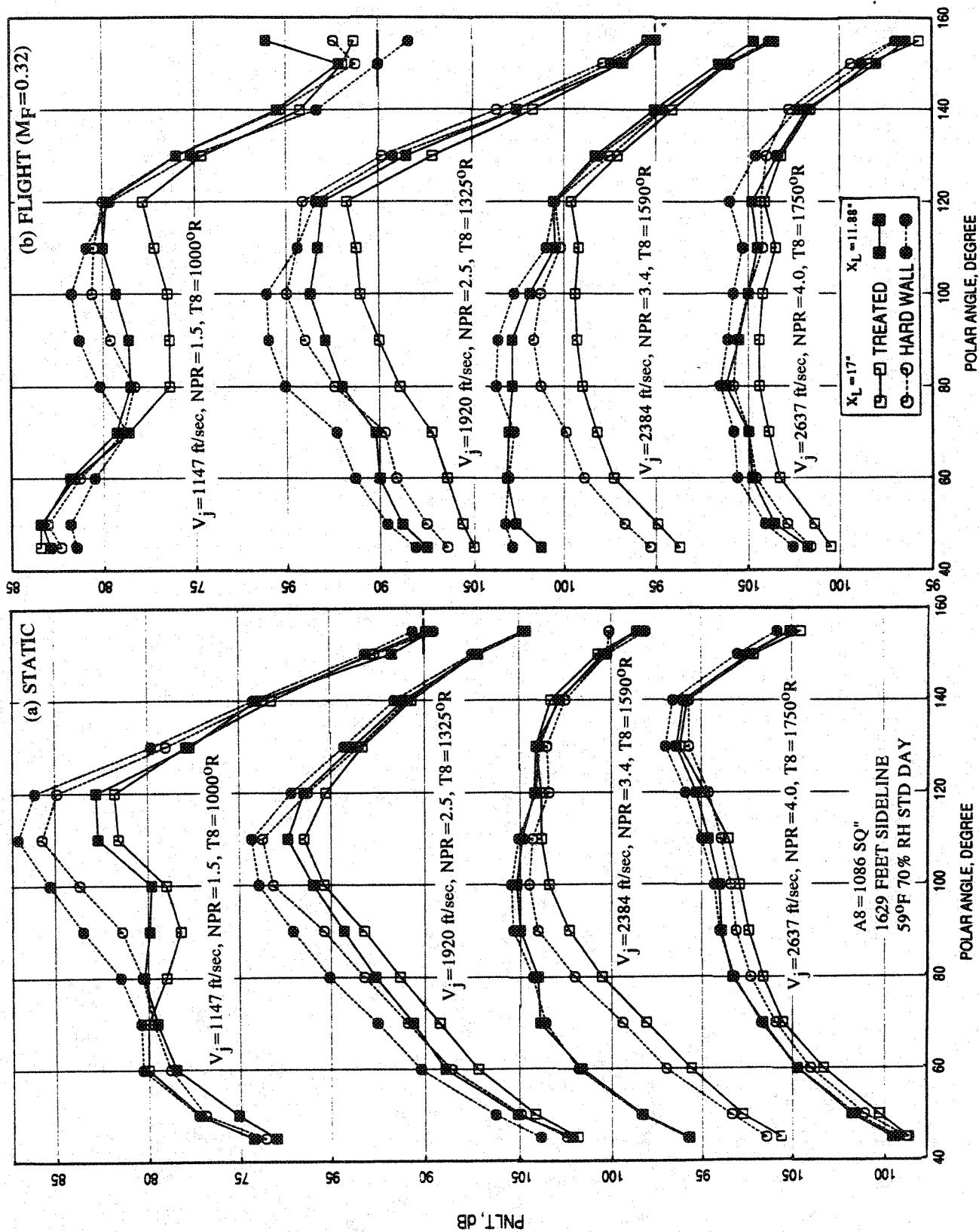
Figure 4.2-6. Effect of acoustic treatment and flap length on PNLT directivities at different L1M cycle conditions for an aligned convergent-chute mixer-ejector at an azimuthal angle $\phi = 25°$; SAR = 2.8, MAR = 0.95.
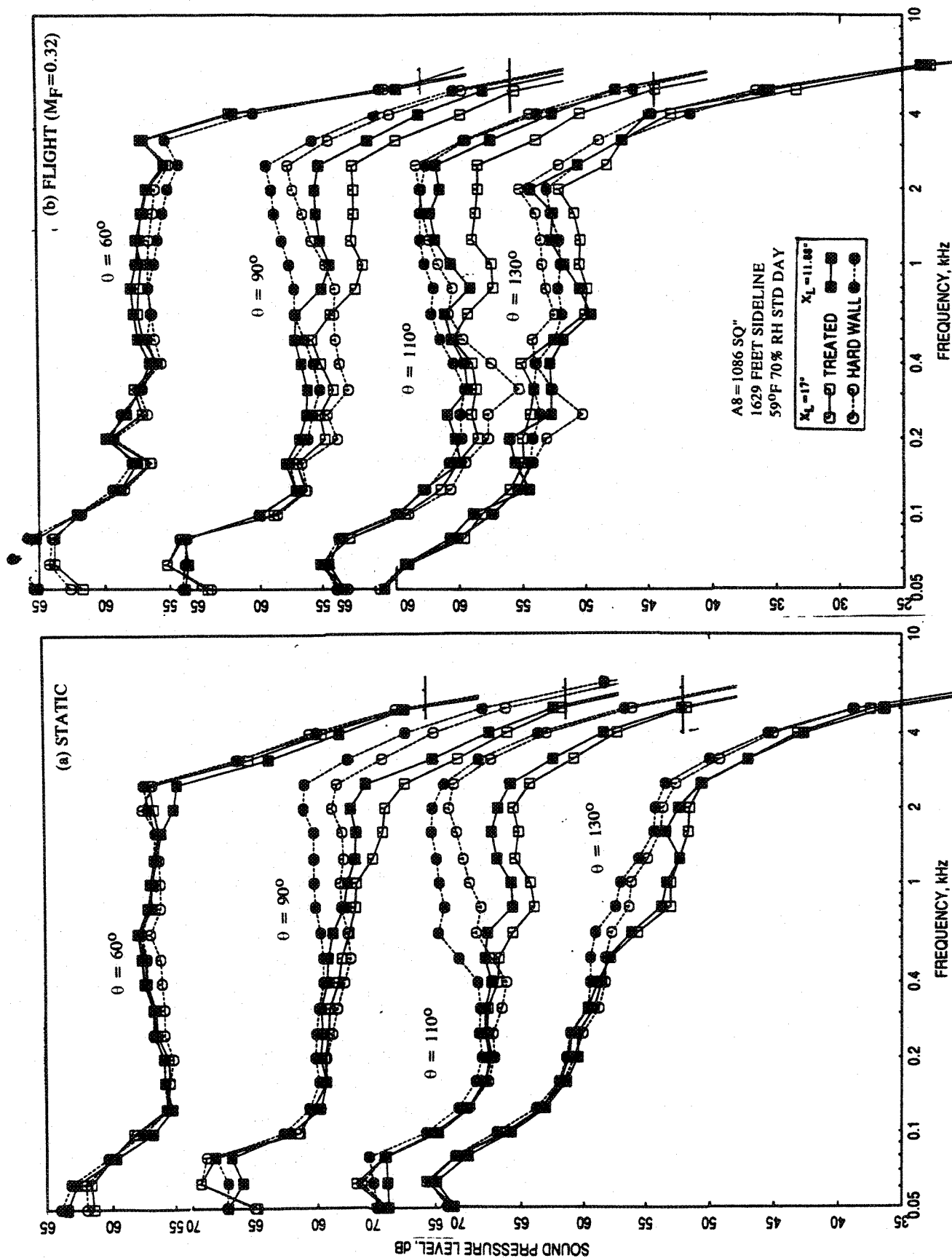
Figure 4.2-7. Effect of acoustic treatment and flap length on SPL spectra at various polar angles (θ) for an aligned convergent-chute mixer-ejector at an azimuthal angle φ=25°, SAR=2.8, MAR=0.95, V$_j$ = 1147 ft/sec, NPR = 1.5, T8 = 1000°R.
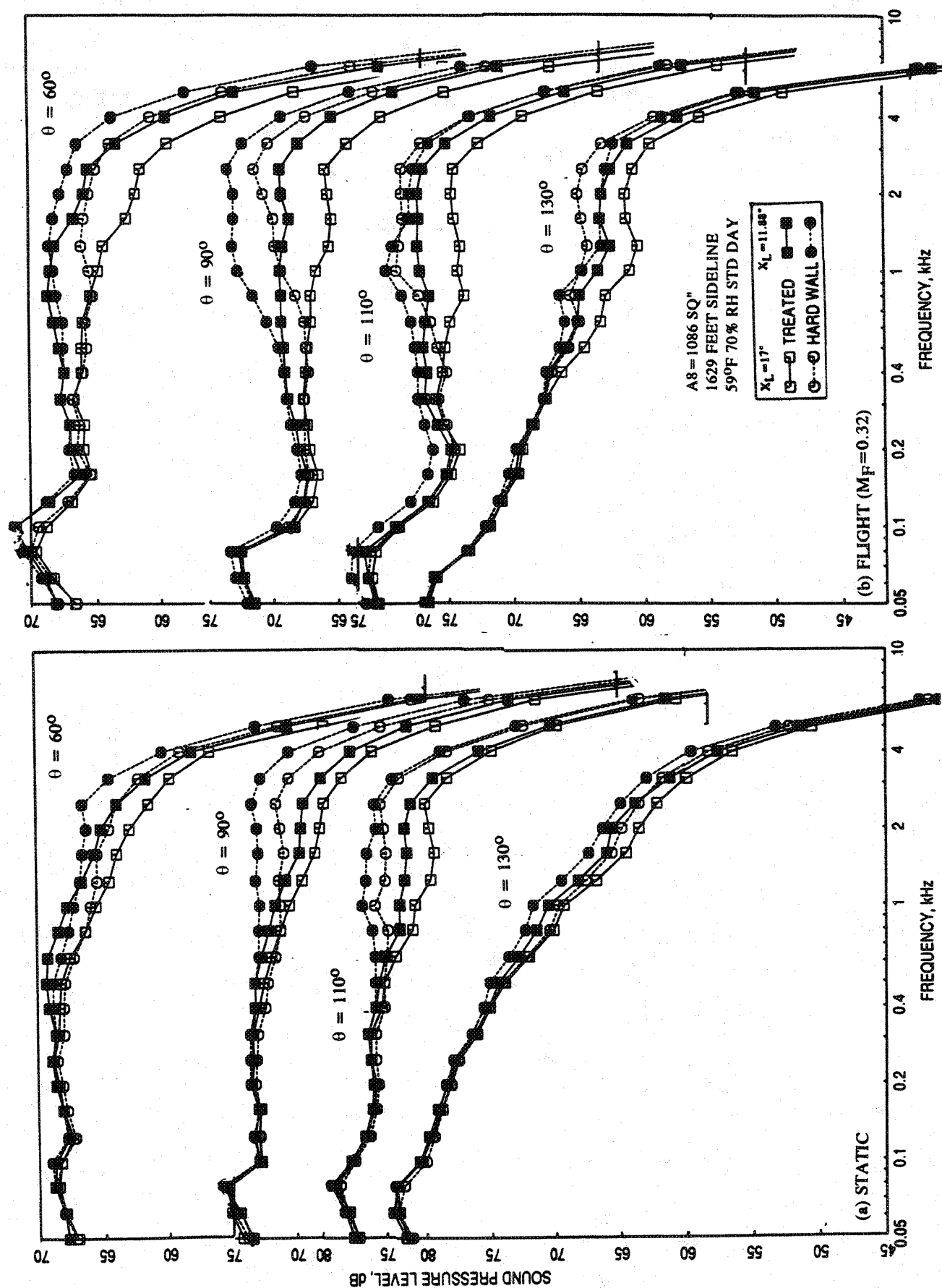
Figure 4.2-8. Effect of acoustic treatment and flap length on SPL spectra at various polar angles (θ) for an aligned convergent-chute mixer-ejector at an azimuthal angle φ=25°; SAR=2.8, MAR=0.95, V_j = 1920 ft/sec, NPR = 2.5, T8 = 1325°R.
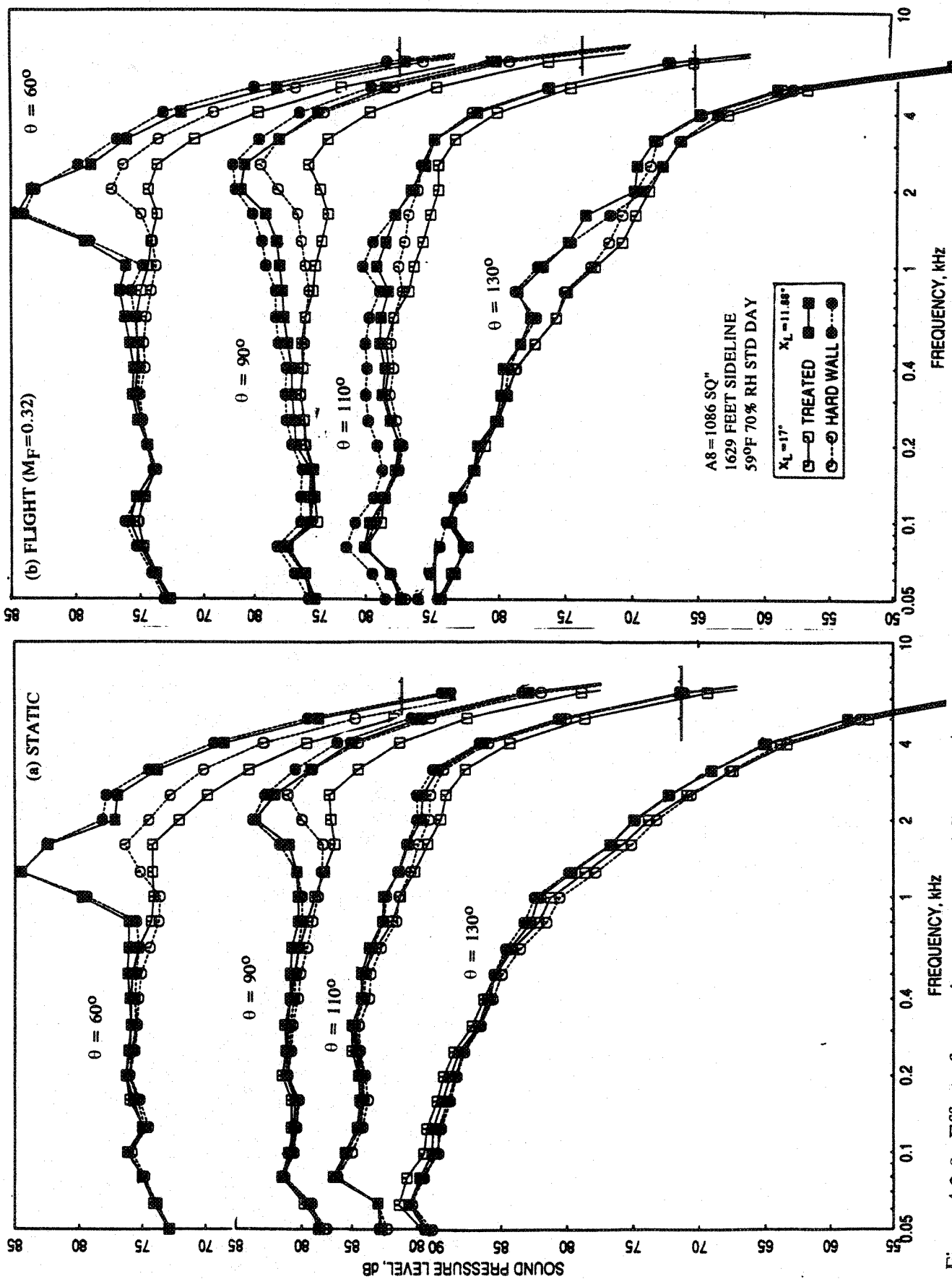
Figure 4.2-9. Effect of acoustic treatment and flap length on SPL spectra at various polar angles (θ) for an aligned convergent-chute mixer-ejector at an azimuthal angle φ=25°. SAR=2.8, MAR=0.95, V_j = 2384 ft/sec, NPR = 3.4, T8 = 1590°R.
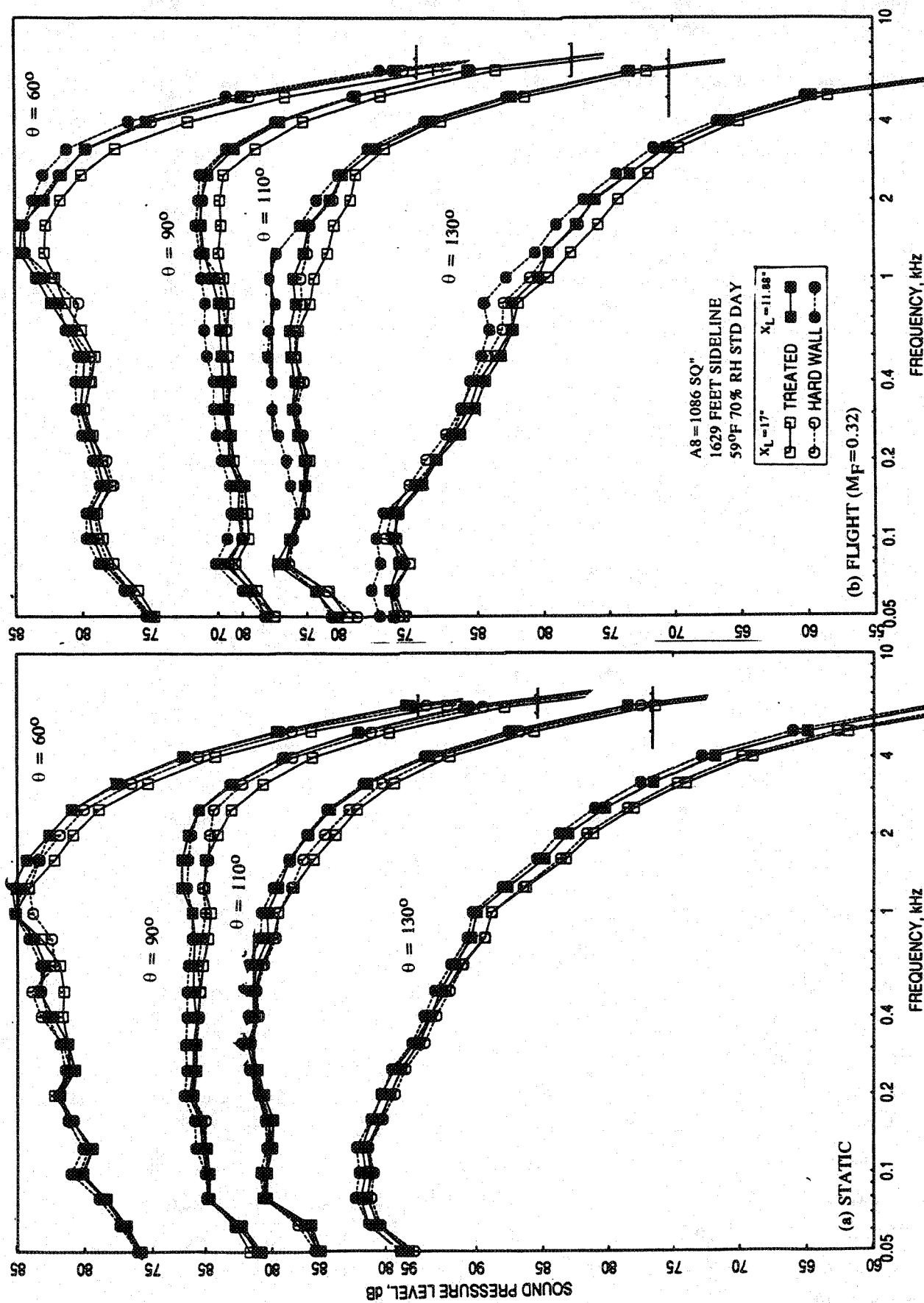
Figure 4.2-10. Effect of acoustic treatment and flap length on SPL spectra at various polar angles (θ) for an aligned convergent-chute mixer-ejector at an azimuthal angle φ=25°; SAR=2.8, MAR=0.95, V$_j$ = 2637 ft/sec, NPR = 4.0, T8 = 1750°R.

configuration for axial static pressure distribution results. However, the static pressure tap locations upstream of the origin (i.e., for negative X) are normalized with respect to the longer ejector length (i.e., 17"), since these instrument locations are identical for both long and short ejector configurations.

The effect of treatment, flap length and flight simulation on ramp and chute static pressure distributions is shown in Figure 4.2-11 for different L1M cycle conditions. The effect of treatment and flap length is insignificant on the static pressure distributions on the ramp and chute surfaces. However, the static pressure increases due to flight simulation for each case, both on the ramp and chute surfaces due to freejet fan pressure rise, indicating lesser loading for the chutes. Figure 4.2-12 shows the effect of treatment and flap length on chute loading coefficient plotted against NPR. Again, the effects of treatment and f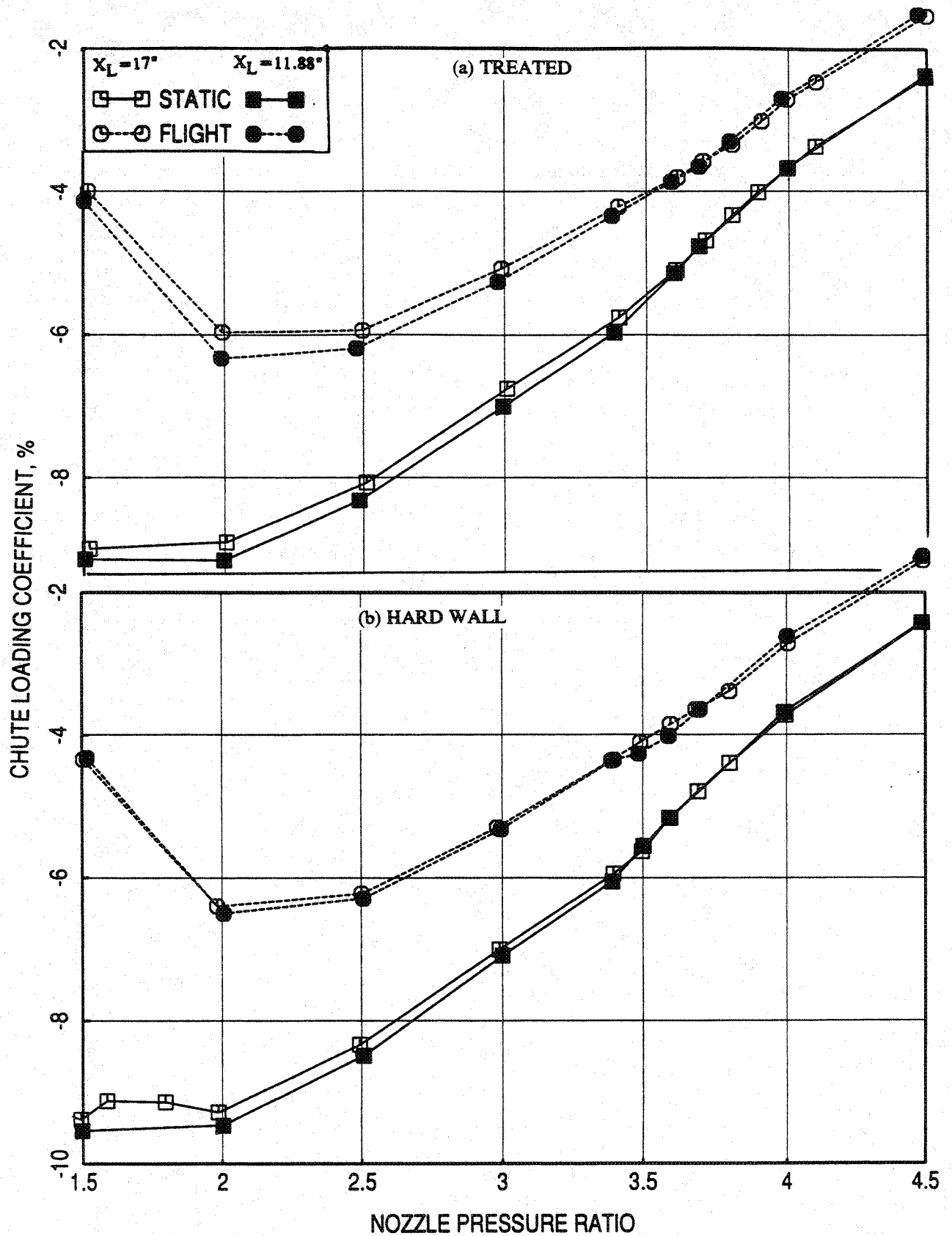lap length are very small on chute loading coefficient, especially at higher NPR. For lower NPR conditions the coefficient increases slightly with treatment as well as with increased flap length. The effect of treatment and flap length on pumping and corrected pumping is shown in Figures 4.2-13 and 4.2-14, respectively. The pumping is significantly lower for treated ejector compared to hard wall for short flap configuration at static case for lower NPRs. This difference is most probably due to the difference in static temperature between the two configurations and not the effect of treatment. The effect of flap length is very small. With flight simulation these effects are almost negligible on pumping. The effect of treatment as well as flap length is almost negligible for corrected pumping for entire NPR range for static and flight cases. The same is the case with the mixed jet velocity (see Figure 4.2-15).

Figure 4.2-16 shows the effect of treatment and flap length on the average axial static pressure distributions on the inlet and the flap surface at different L1M cycle conditions. Static pressure distributions on the inlet are not influenced by the treatment and by the ejector length. However, the ejector length influences the flap static pressure distribution for all conditions. The static pressure is higher on the flap surface for longer ejector compared to the shorter configuration. The effect of treatment is insignificant on flap static pressure distributions at lower NPR conditions. However, at higher NPRs, closer to the transition from subsonic to supersonic mode and above this condition, the flap static pressure is higher for the treated ejector compared to hard wall configuration. Acoustic treatment seems to soften shock/boundary-layer interaction which in turn seems to increase the critical NPR at which the ejector transitions from subsonic to supersonic mode. This is further illustrated in Figure 4.2-17 by plotting the normalized force on flap
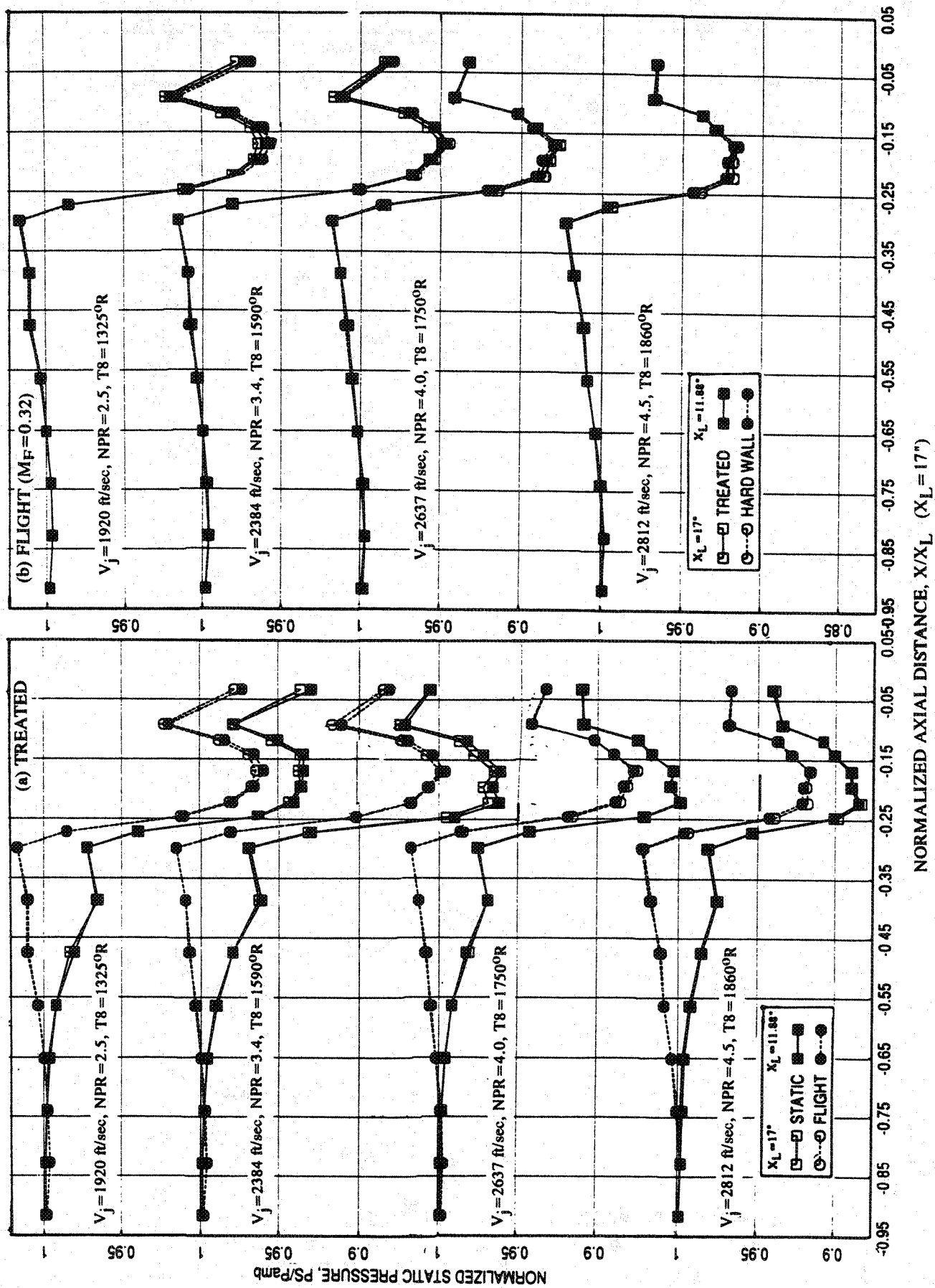
Figure 4.2-11. Effect of acoustic treatment, flap length and flight simulation on axial static pressure distributions on the inlet ramp and on the secondary flow side of chute surface at different L1M cycle conditions for an aligned convergent-chute mixer-ejector SAR=2.8, MAR=0.95.
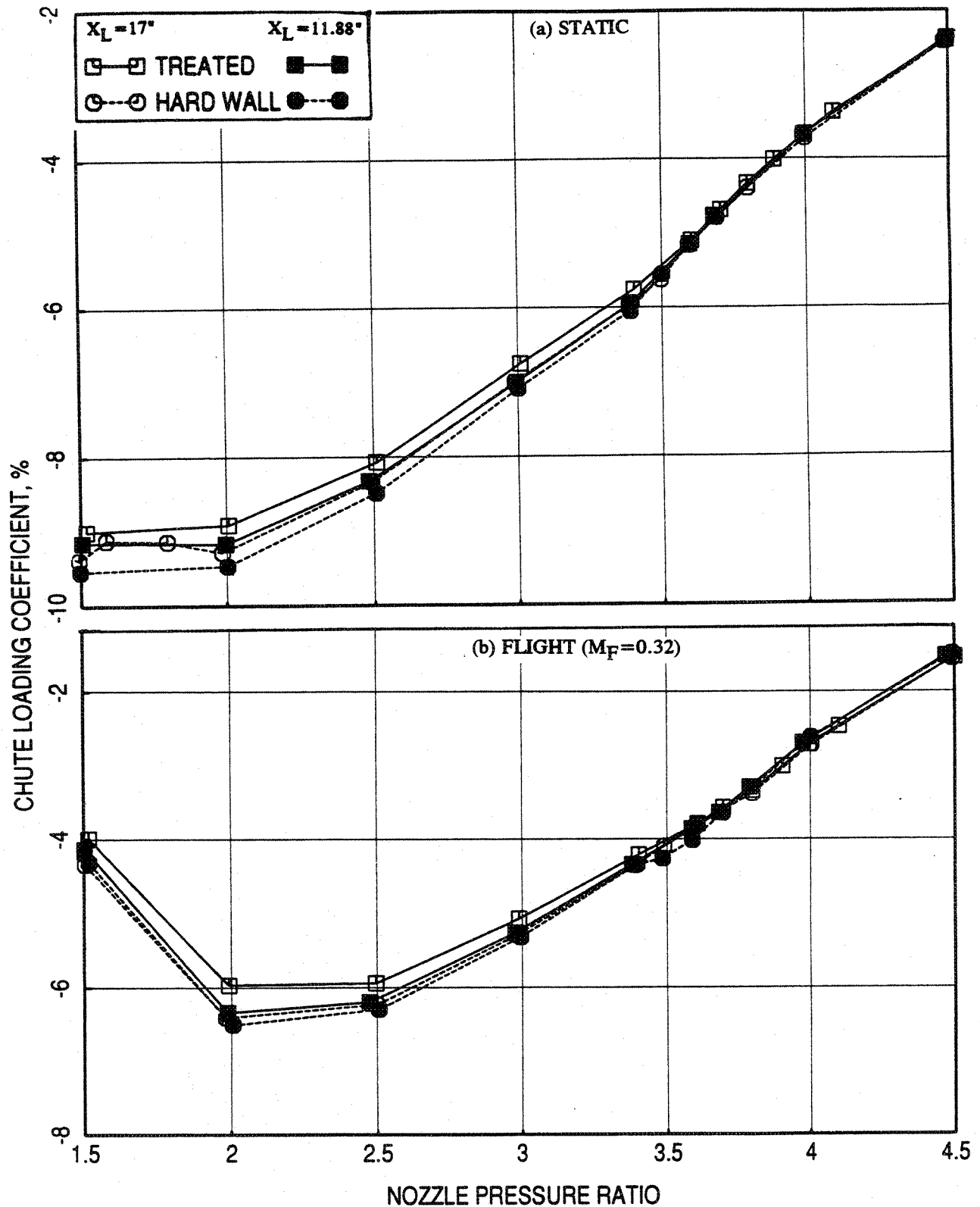
Figure 4.2-12. Effect of acoustic treatment and flap length on chute loading coefficient with respect to nozzle pressure ratio of L1M cycle conditions for an aligned convergent-chute mixer-ejector; SAR=2.8, MAR=0.95.
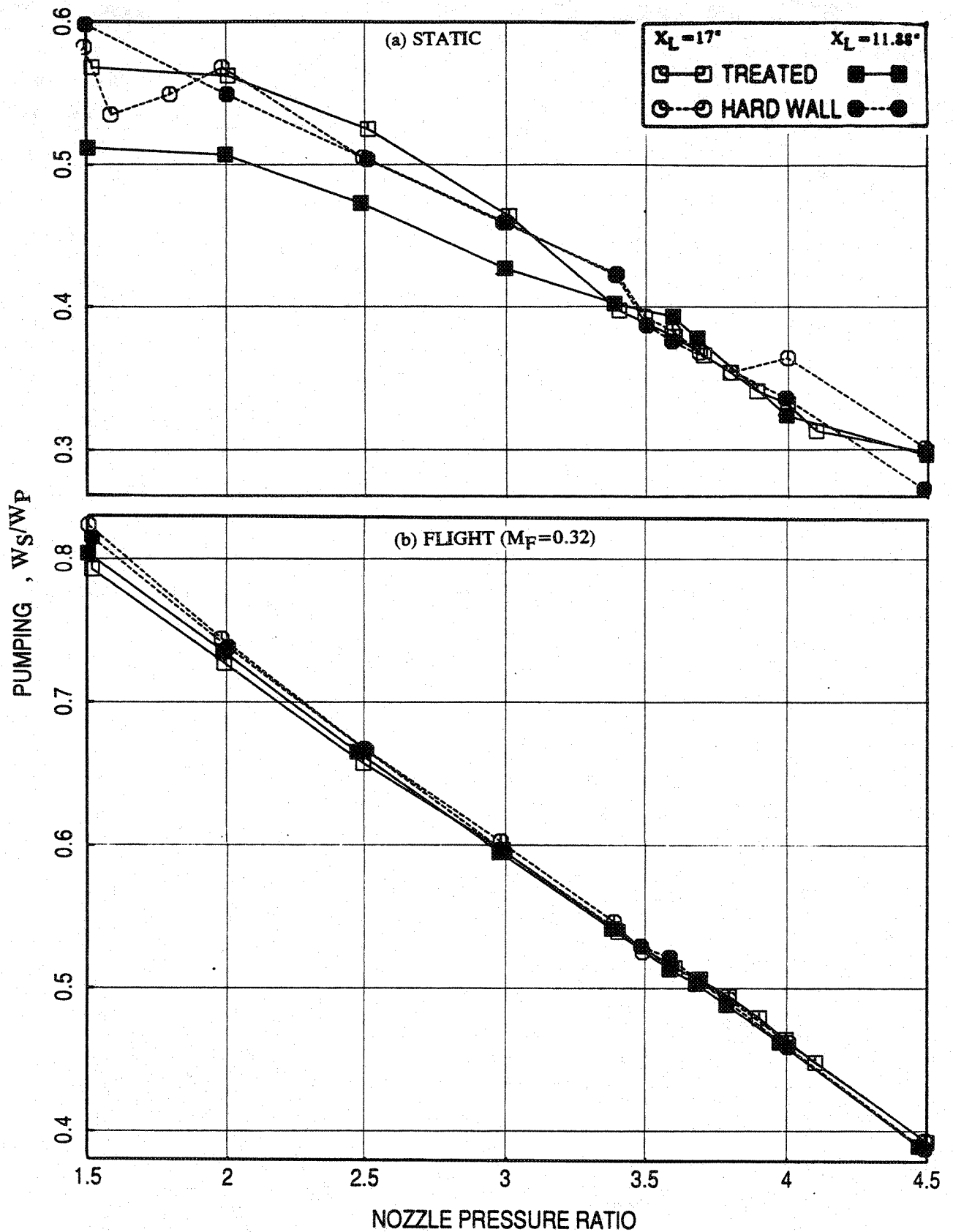
Figure 4.2-13. Effect of acoustic treatment and flap length on pumping with respect to nozzle pressure ratio of L1M cycle conditions for an aligned convergent-chute mixer-ejector; SAR=2.8, MAR=0.95.
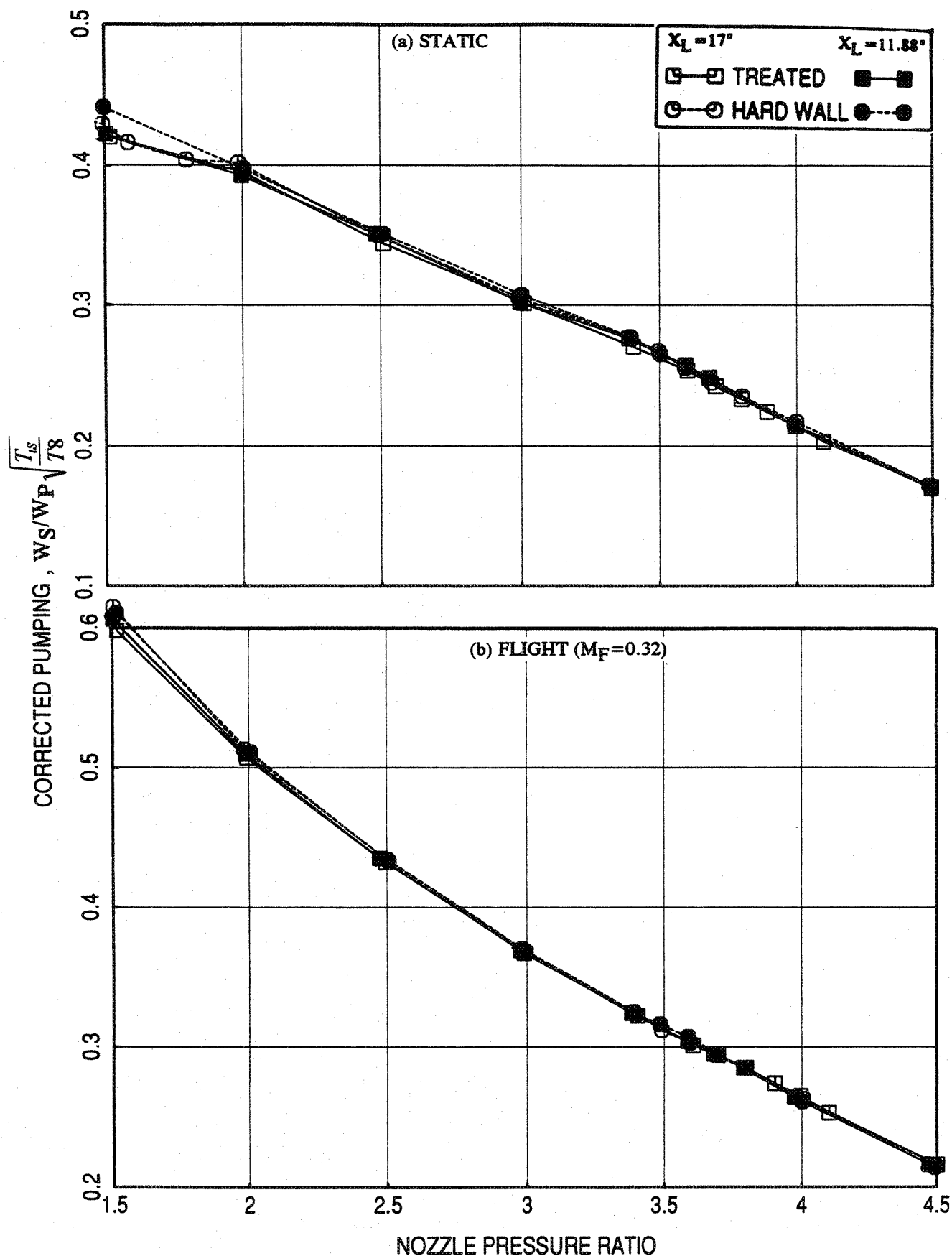
Figure 4.2-14. Effect of acoustic treatment and flap length on corrected pumping with respect to nozzle pressure ratio of L1M cycle conditions for an aligned convergent-chute mixer-ejector; SAR=2.8, MAR=0.95.
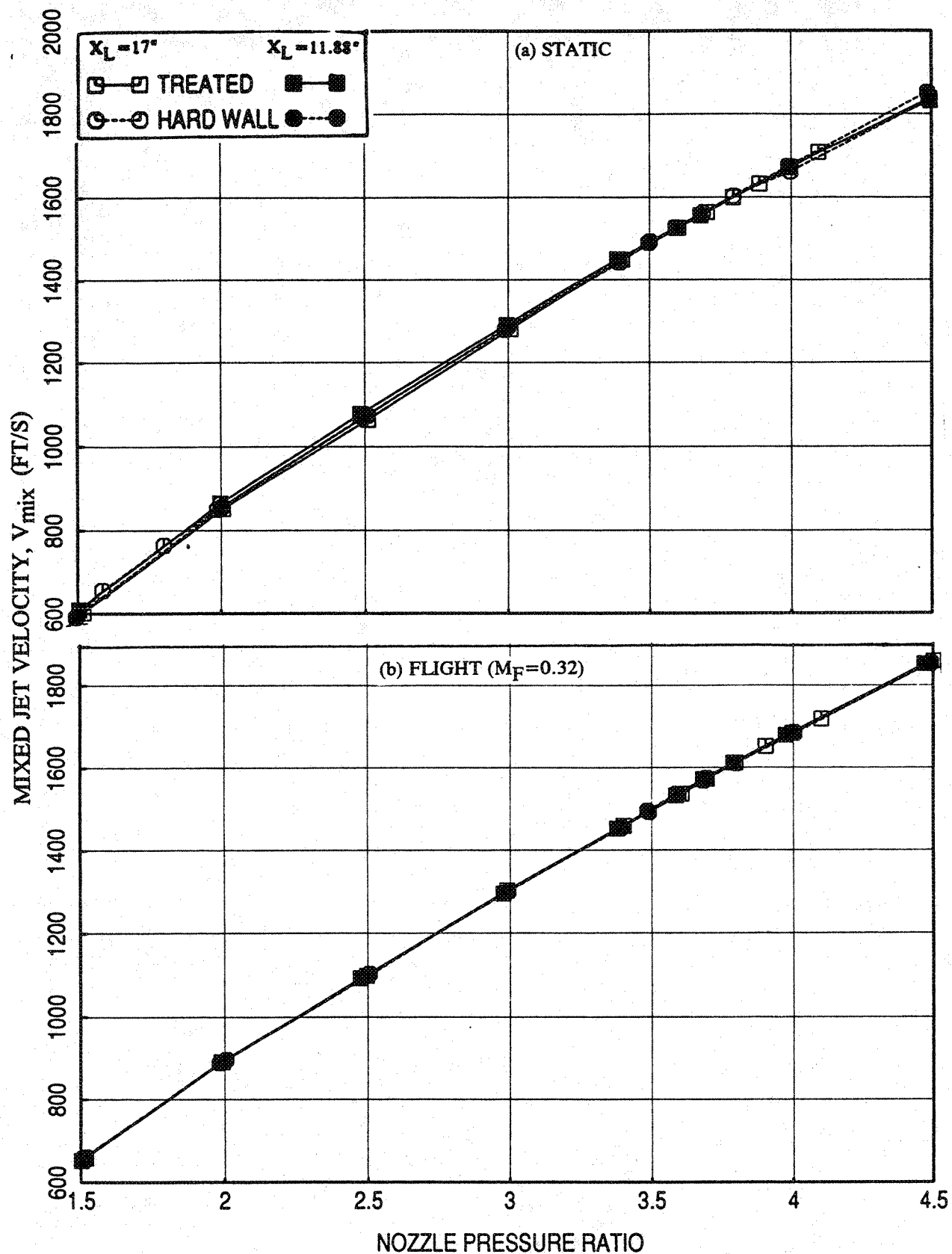
Figure 4.2-15. Effect of acoustic treatment and flap length on mixed jet velocity with respect to nozzle pressure ratio of L1M cycle conditions for an aligned convergent-chute mixer-ejector; SAR=2.8, MAR=0.95.
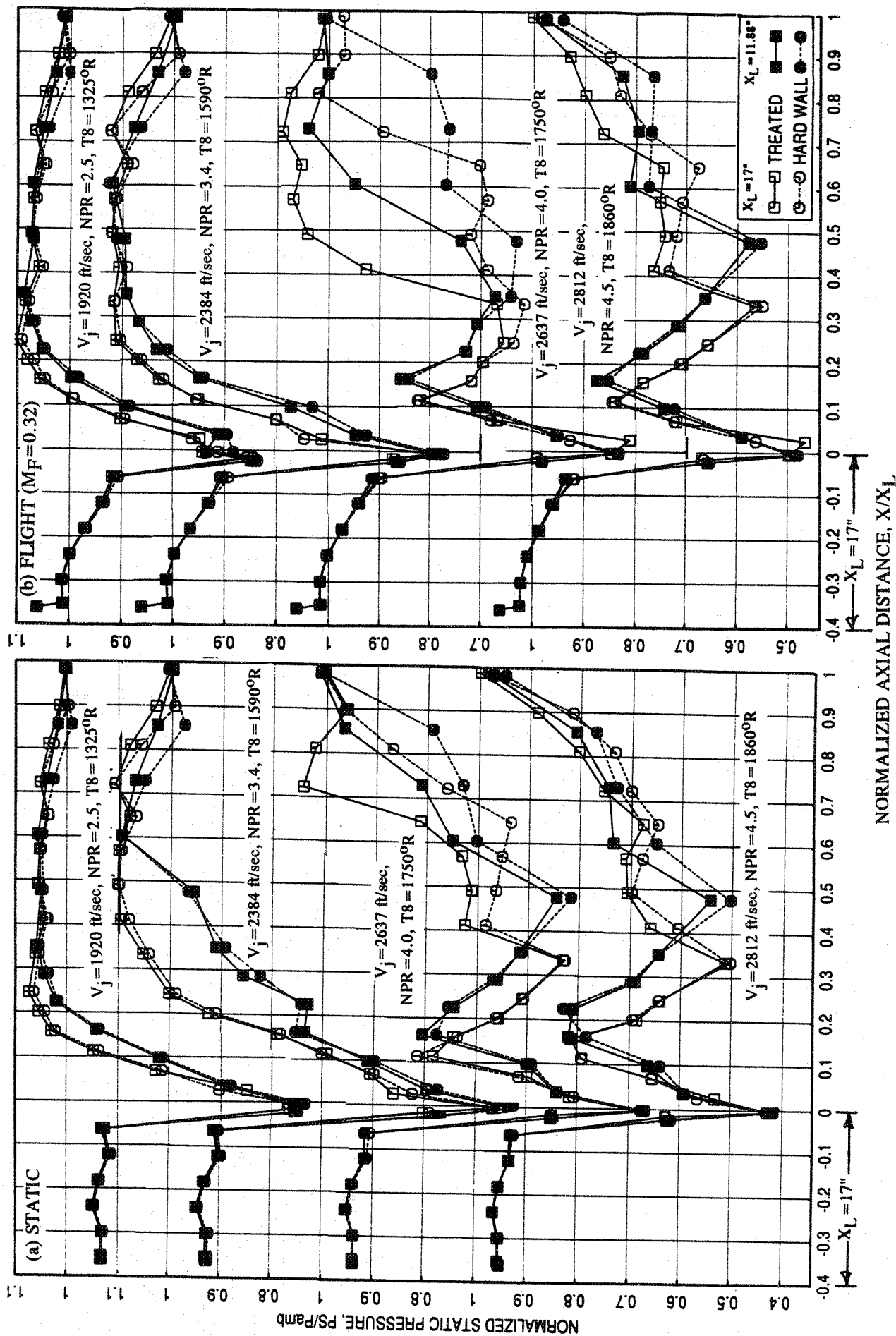
Figure 4.2-16. Effect of acoustic treatment and flap length on axial average static pressure distributions on the inlet and the flap surface at different L1M cycle conditions for an aligned convergent-chute mixer-ejector SAR=2.8, MAR=0.95.
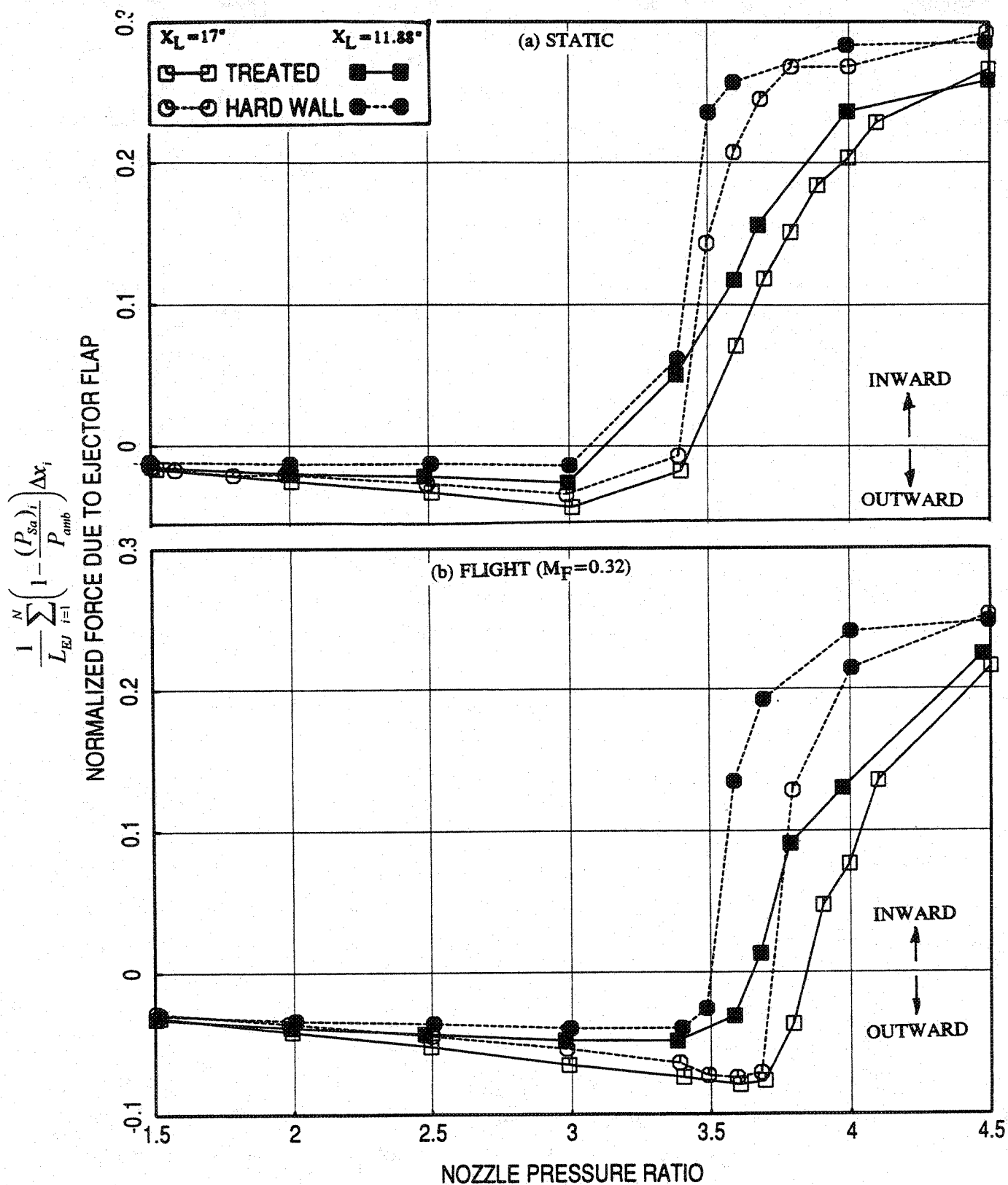
Figure 4.2-17. Effect of acoustic treatment and flap length on normalized force due to ejector flap with respect to nozzle pressure ratio of L1M cycle conditions for an aligned convergent-chute mixer-ejector SAR=2.8, MAR=0.95.

surface with respect to NPR, that the transition from subsonic to supersonic mode seems to be slightly delayed for treated ejector compared to hard wall configuration and for longer ejector compared to the shorter configuration.

4.2.2 Effect of Simulated Flight and Flap Length :

All the results in this section show the simultaneous comparisons between static and simulated flight of $M_F=0.32$ conditions and between short and long flap for treated and hard wall configurations. While the long flap results are presented by open symbols, the same filled symbols show the results for short flap configurations.

Figure 4.2-18 shows the effect of flight simulation and flap length on PNLT and EPNL as function of jet velocity (V_j) at an azimuthal angle $\phi=25^O$ for treated and hard wall configurations. EPNL decreases with flight simulation for all jet velocities for hard wall configuration and for treated case at velocities 1600 ft/sec and above. The EPNdB reduction due to flight simulation is higher for treated ejector compared to hard wall case, since the noise generated internal to the ejector is reduced due to treatment and thus the reduction of externally generated noise due to flight simulation dominates the observed noise. The EPNL is lower for longer ejector compared to the short flap case and the noise reduction is higher with flight simulation. Except for forward arc angles the PNLT decreases with flight simulation and is lower for longer ejector at all jet velocities.

At four different jet velocities the effect of flight simulation and flap length on PNLT directivities is shown in Figure 4.2-19. The effect of flight simulation is to lower the PNLT levels at polar angles above 60° due to source strength reductions and the trend is reversed at lower angles due to dynamic amplification of jet noise overcoming the source strength reduction effects. Significant PNLT reduction is observed at the rear arc. PNLT is lower for longer ejector at all angles and the impact is less realized in the rear arc angles. Effect of flight simulation and flap length on SPL spectra at various polar angles (θ) for each of the four jet velocities is shown in Figures 4.2-20 through 4.2-23. Significant SPL reduction is observed at higher polar angles for the entire frequency range due to flight simulation. The SPL levels are lower for long ejector compared to the shorter configuration, mostly at higher frequencies.

The effect of flight simulation and flap length on chute loading coefficient plotted against NPR is shown in Figure 4.2-24. While the effect of flap length on chute loading coefficient
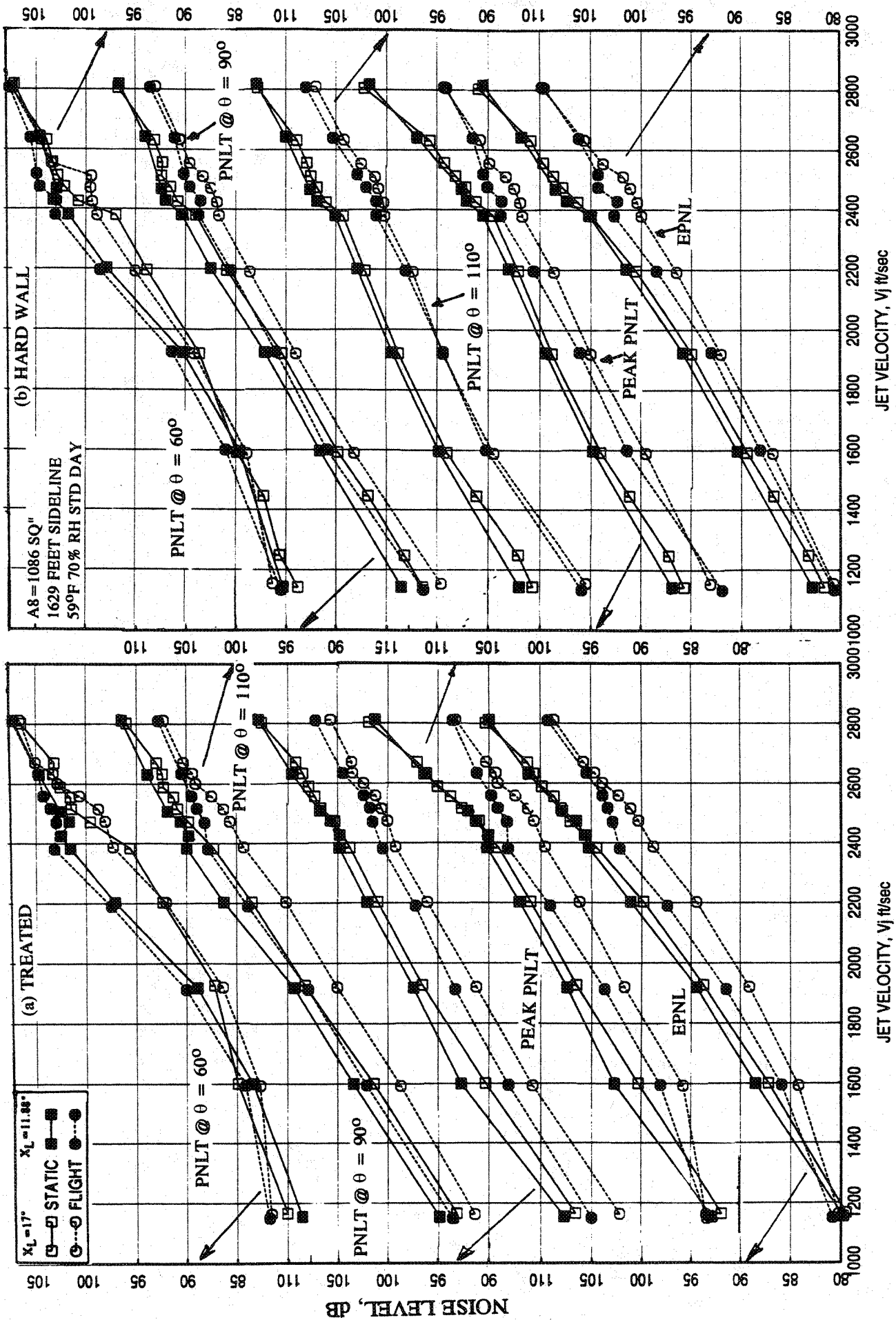
Figure 4.2-18. Effect of flight simulation and flap length on EPNL and PNLT at various polar angles (θ) as function of jet velocity of L1M cycle conditions for an aligned convergent-chute mixer-ejector at an azimuthal angle φ=25°; SAR=2.8, MAR=0.95.
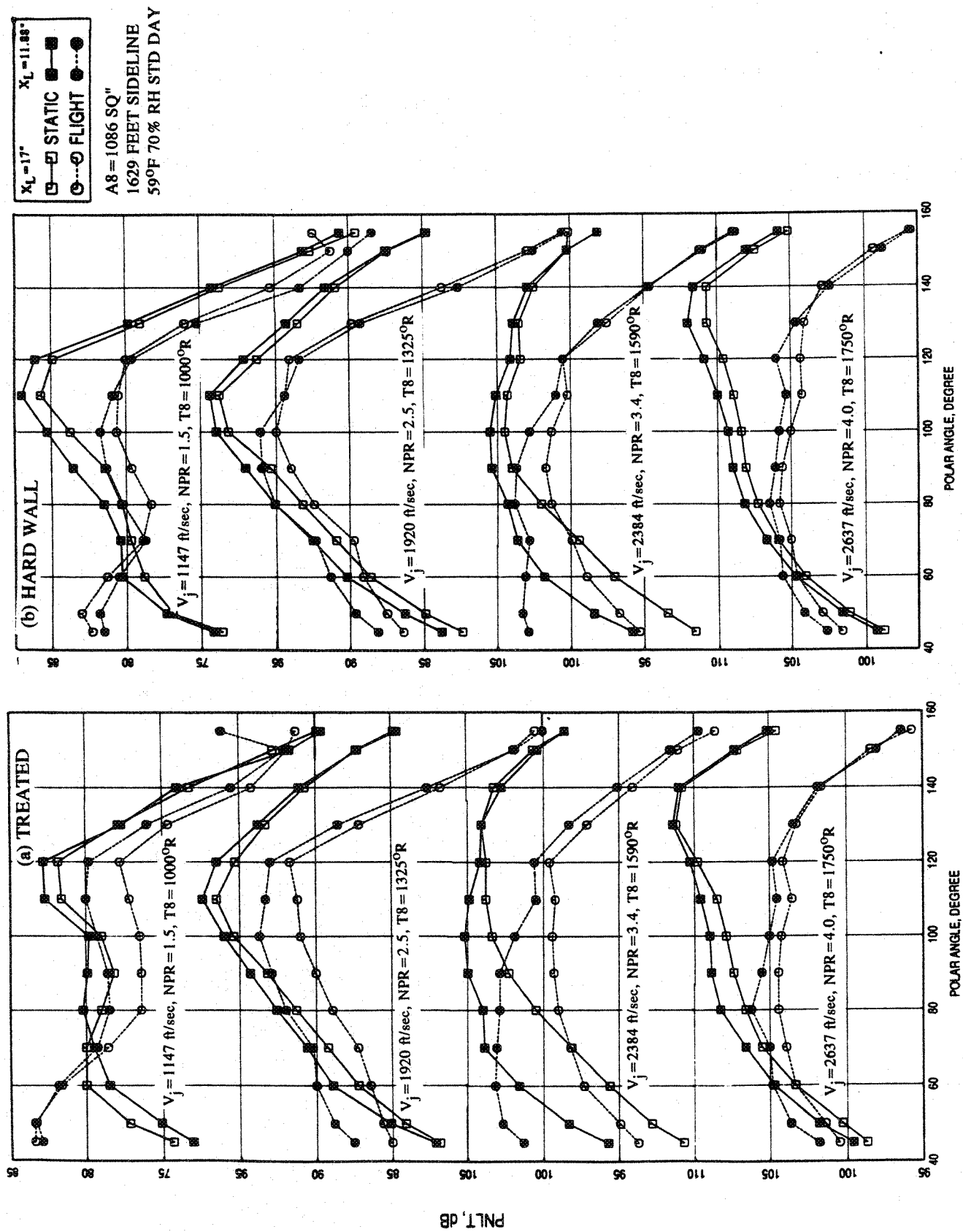
Figure 4.2-19. Effect of flight simulation and flap length on PNLT directivities at different L1M cycle conditions for an aligned convergent-chute mixer-ejector at an azimuthal angle $\phi = 25^\circ$; SAR = 2.8, MAR = 0.95.
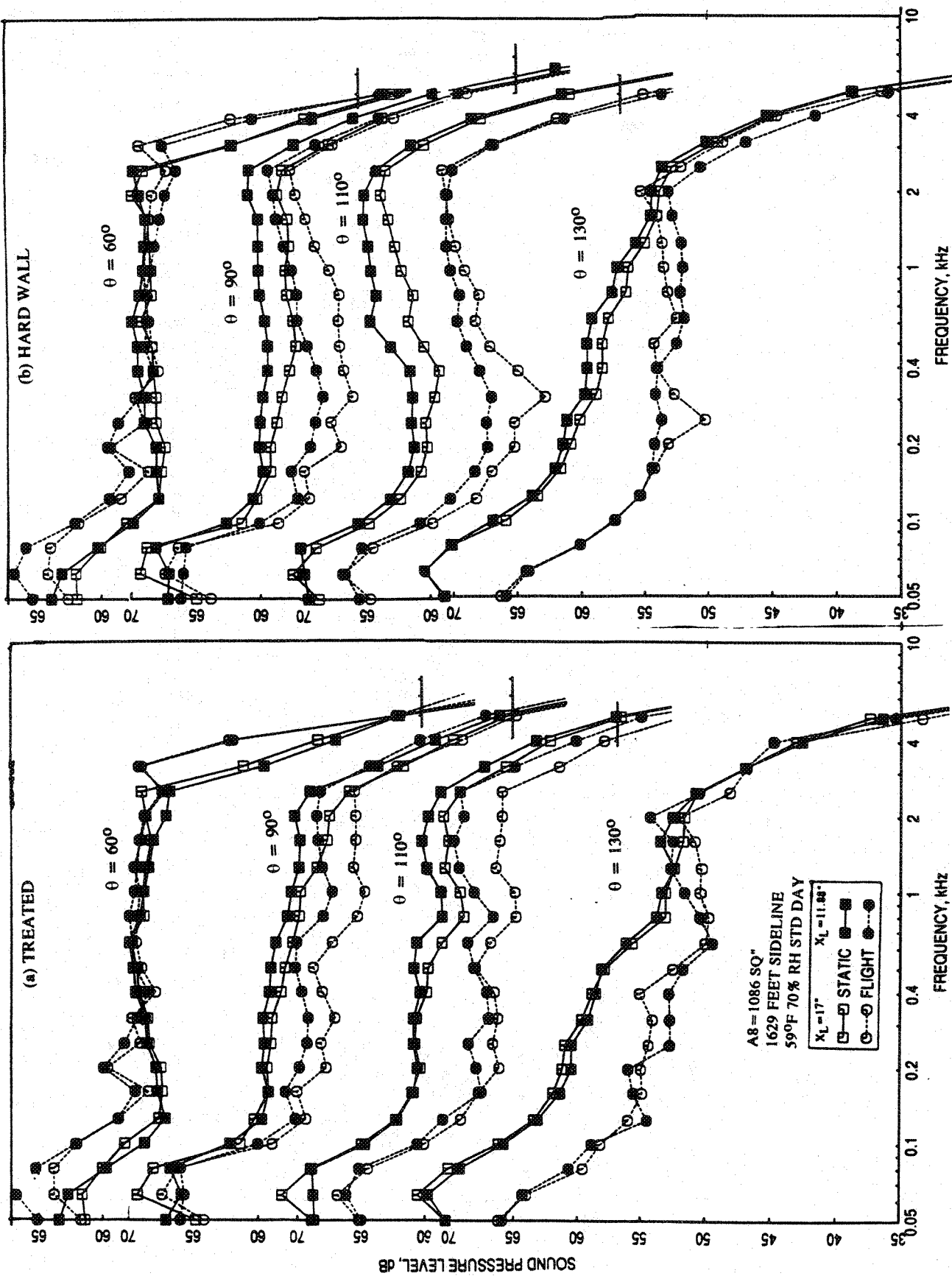
Figure 4.2-20. Effect of flight simulation and flap length on SPL spectra at various polar angles (θ) for an aligned convergent-chute mixer-ejector at an azimuthal angle φ=25°; SAR=2.8, MAR=0.95, V_j = 1147 ft/sec, NPR = 1.5, T8 = 1000°R.
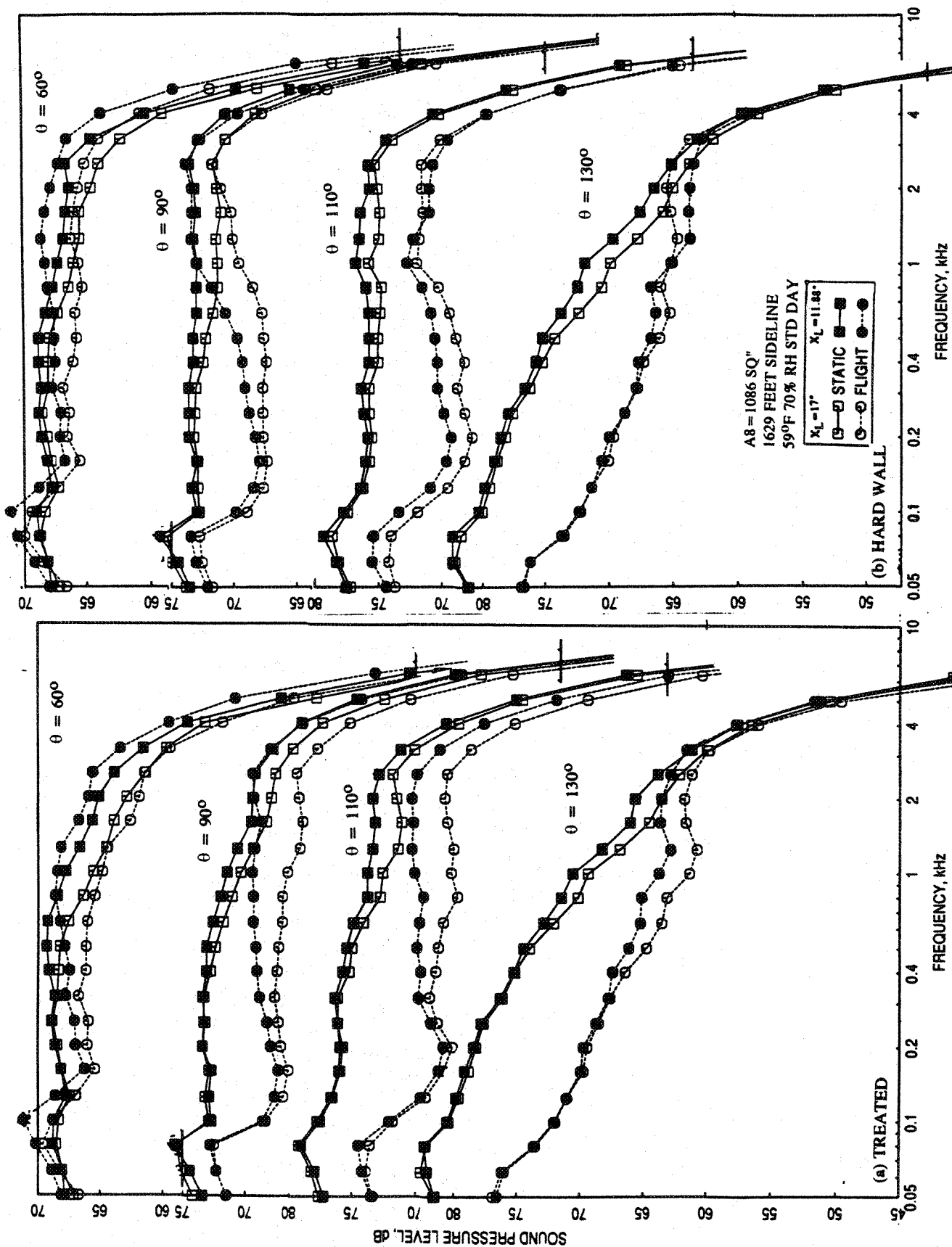
Figure 4.2-21. Effect of flight simulation and flap length on SPL spectra at various polar angles (θ) for an aligned convergent-chute mixer-ejector at an azimuthal angle φ=25°, SAR=2.8, MAR=0.95, V$_j$ = 1920 ft/sec, NPR = 2.5, T8 = 1325°R.
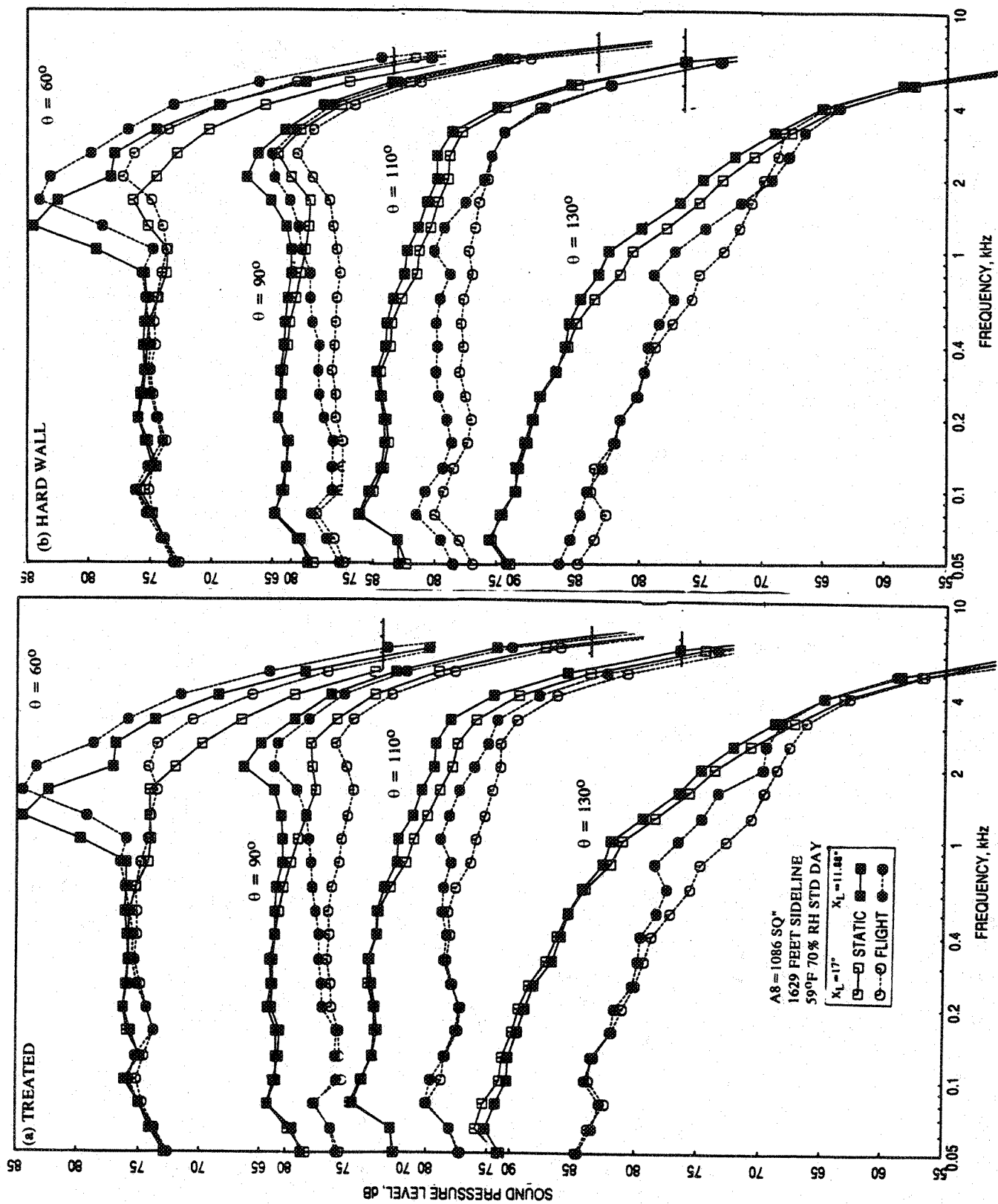
Figure 4.2-22. Effect of flight simulation and flap length on SPL spectra at various polar angles (θ) for an aligned convergent-chute mixer-ejector at an azimuthal angle φ=25°; SAR=2.8, MAR=0.95, V_j = 2384 ft/sec, NPR = 3.4, T8 = 1590°R.
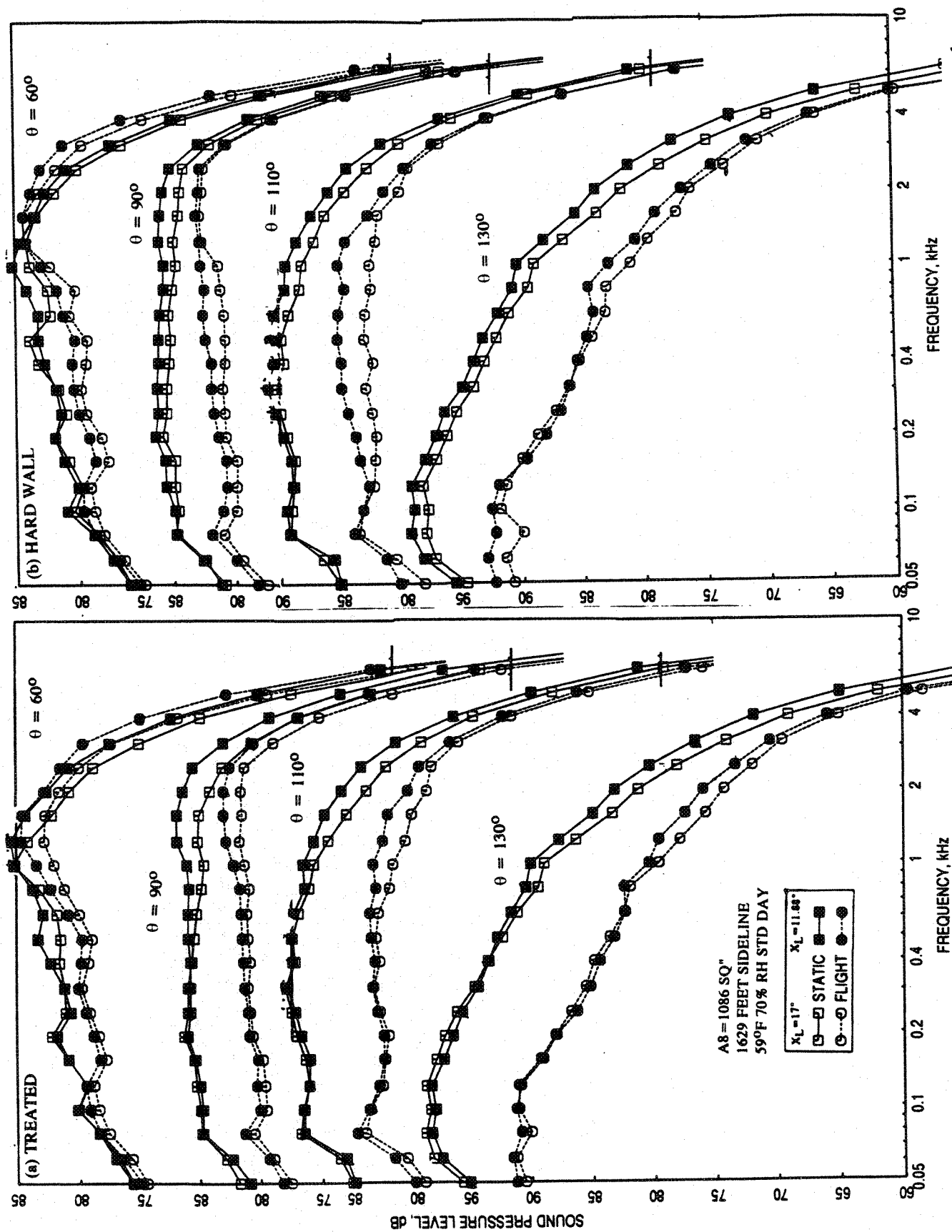
Figure 4.2-23. Effect of flight simulation and flap length on SPL spectra at various polar angles (θ) for an aligned convergent-chute mixer-ejector at an azimuthal angle φ=25°, SAR=2.8, MAR=0.95, V_j = 2637 ft/sec, NPR = 4.0, T8 = 1750°R.

Figure 4.2-24. Effect of flight simulation and flap length on chute loading coefficient with respect to nozzle pressure ratio of L1M cycle conditions for an aligned convergent-chute mixer-ejector; SAR=2.8, MAR=0.95.

is small, the levels increase significantly with flight simulation. The effect of flight and flap length on pumping and corrected pumping is shown in Figures 4.2-25 and 4.2-26, respectively. The pumping increases significantly with flight simulation, since the total pressure at the inlet goes up. Even though, the pumping increases with flight, the effect is relatively small on the mixed jet velocity (see Figure 4.2-27).

Figure 4.2-28 shows the effect of flight and flap length on the average axial static pressure distributions on the inlet and the flap surface at different L1M cycle conditions. Small amount of pressure increase on the inlet and the flap due to flight simulation is noted at lower NPR conditions. However, the effect of flight simulation is significant on the flap surface close to the transition from subsonic to supersonic mode and at supersonic mode conditions. The effect of flight and flap length on normalized force due to static pressure difference on flap surface is shown in Figure 4.2-29. The force decreases slightly with flight simulation due to increased static pressure on the flap surface. The transition from subsonic to supersonic mode seems to be slightly delayed with respect to NPR due to flight simulation. Similar is the effect due to the longer ejector compared to the shorter configuration.
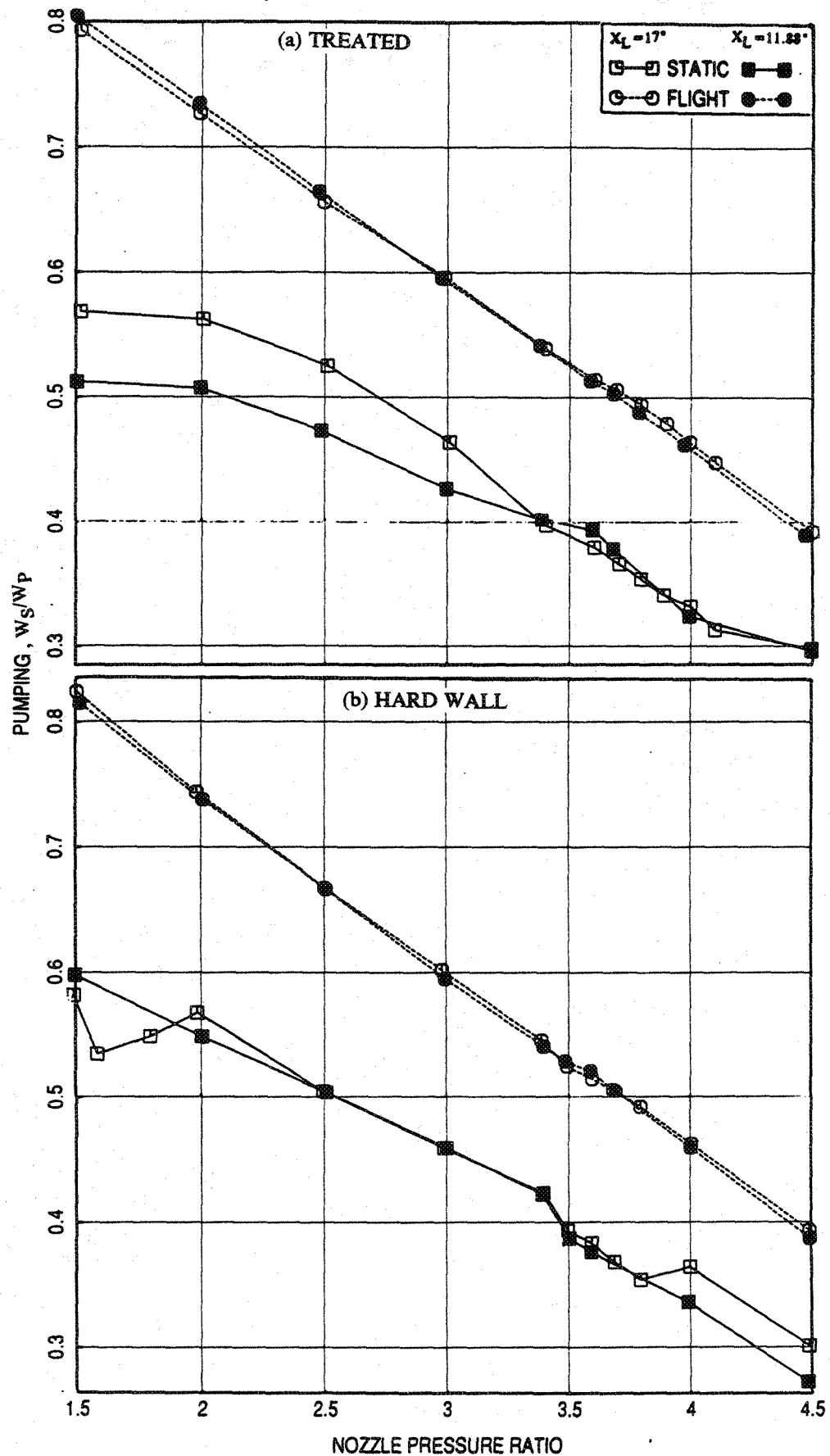
Figure 4.2-25. Effect of flight simulation and flap length on pumping with respect to nozzle pressure ratio of L1M cycle conditions for an aligned convergent-chute mixer-ejector; SAR=2.8, MAR=0.95.
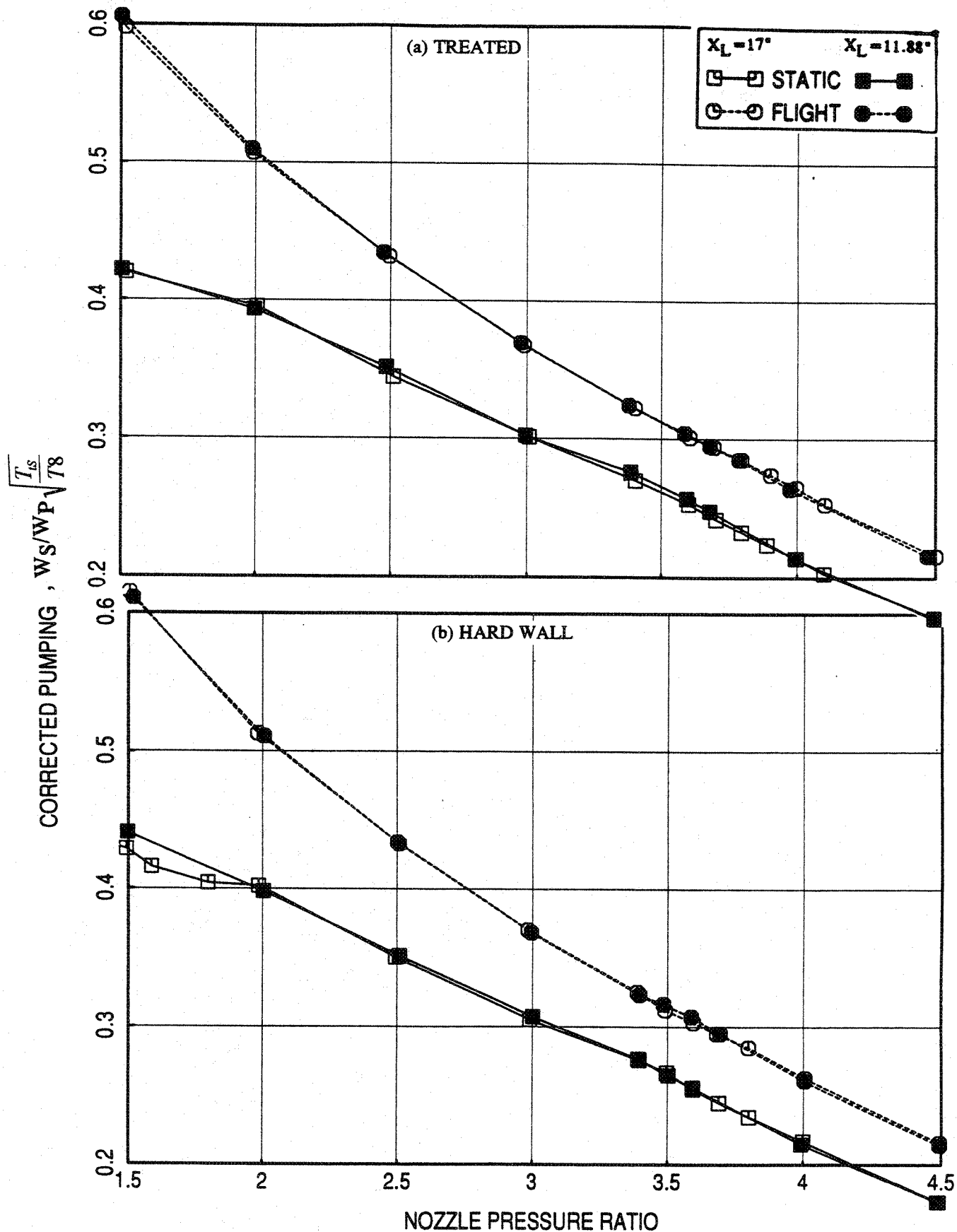
Figure 4.2-26. Effect of flight simulation and flap length on corrected pumping with respect to nozzle pressure ratio of L1M cycle conditions for an aligned convergent-chute mixer-ejector; SAR=2.8, MAR=0.95.
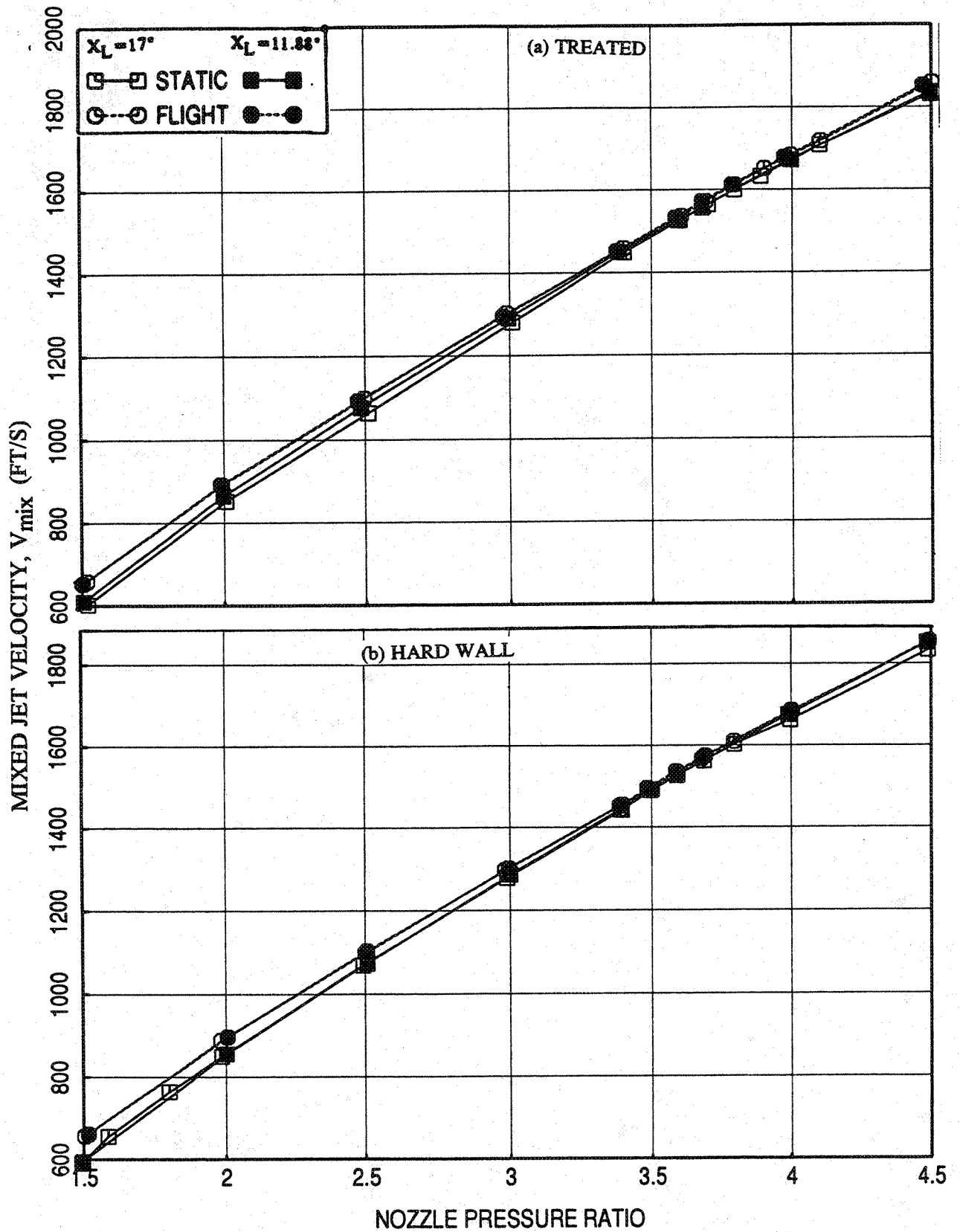
Figure 4.2-27. Effect of flight simulation and flap length on mixed jet velocity with respect to nozzle pressure ratio of L1M cycle conditions for an aligned convergent-chute mixer-ejector; SAR=2.8, MAR=0.95.
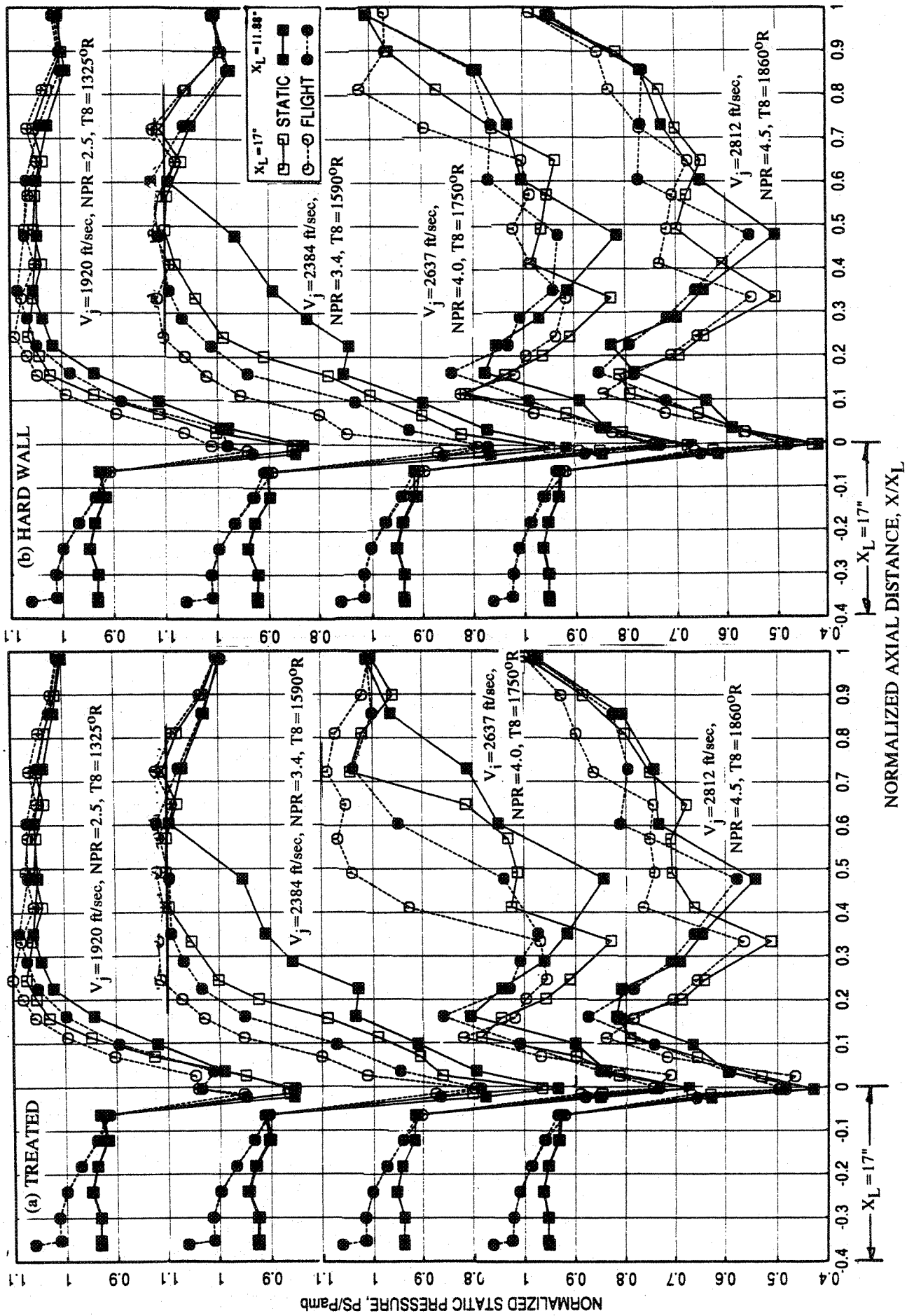
Figure 4.2-28. Effect of flight simulation and flap length on axial average static pressure distributions on the inlet and the flap surface at different L1M cycle conditions for an aligned convergent-chute mixer-ejector SAR=2.8, MAR=0.95.
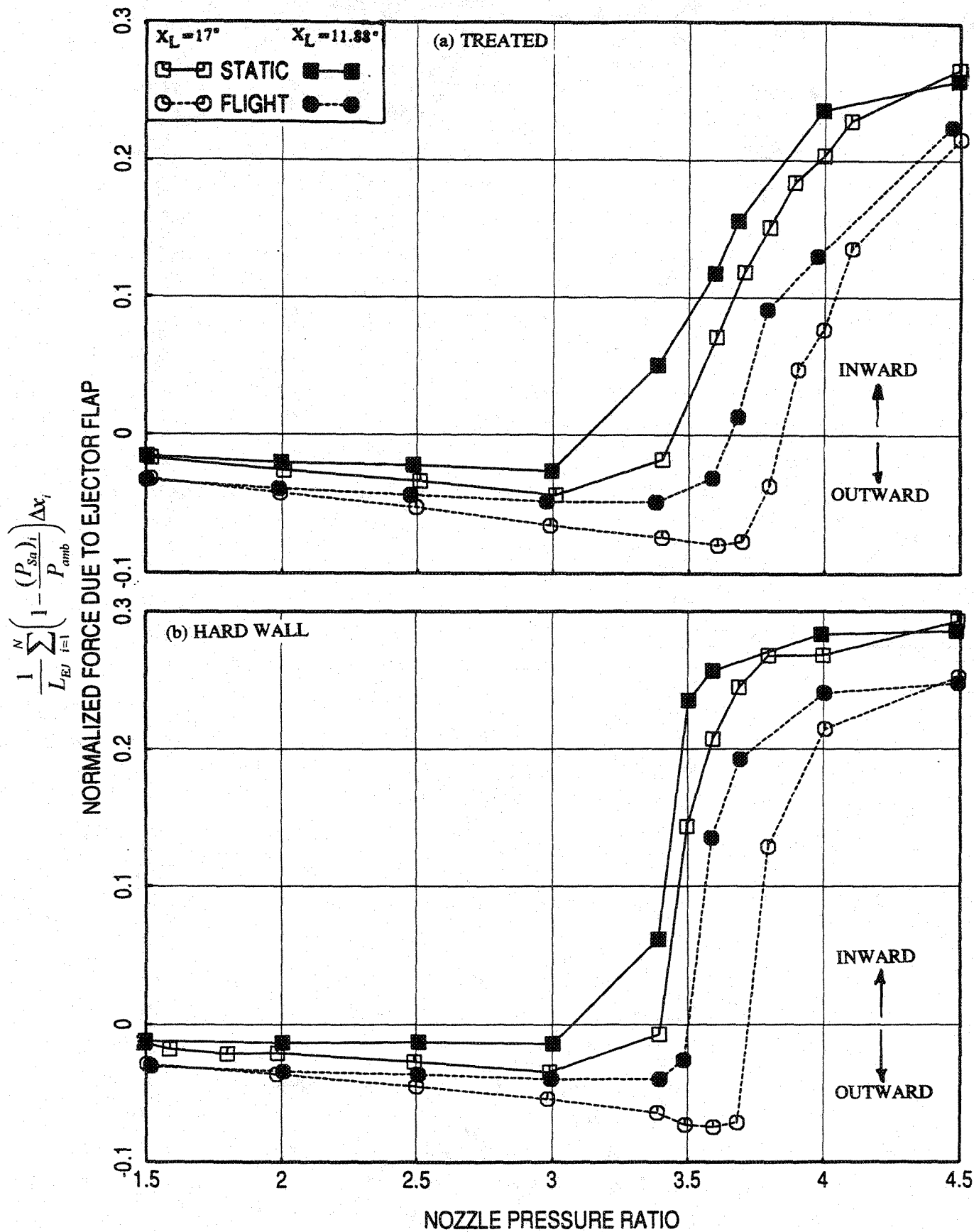
Figure 4.2-29. Effect of flight simulation and flap length on normalized force due to ejector flap with respect to nozzle pressure ratio of L1M cycle conditions for an aligned convergent-chute mixer-ejector SAR=2.8, MAR=0.95.

4.3 STAGGERED CONVERGENT-DIVERGENT-CHUTE MIXER CONFIGURATIONS:

Two staggered CD chute mixers with SAR of 2.8 were tested using new lower racks with the existing SAR 2.8 10 CD chute upper rack. One of the staggered lower chute rack configuration has 9 full cold chutes, as shown in Figure 4.3-1, which are slightly larger than the 10 CD chutes on the top in order to keep the hot and cold flow areas the same. These chutes are partially staggered top to bottom. The center bottom chute mid-plane is aligned with the hot core mid-plane on the top. However, moving away from the center toward the sidewall, the degree of stagger becomes smaller. All core widths are identical except for the two half core side widths on the top. The inlet and upper chute rack instrumentation for this configuration are the same as those for the aligned CD-chute mixer configuration (see Figure 4.1-5). The plan view with instrumentation locations on the inlet and lower chute rack for the staggered chute mixer is shown in Figure 4.3-2.

The second staggered lower chute rack configuration has 9 full cold CD chutes and two half cold CD chutes, as shown in Figure 4.3-3. The 9 full chutes are offset laterally by one-half chute-to-chute period, so that the center of the primary stream on the upper rack is aligned with the center of the secondary stream on the lower rack. A half chute is placed on each end of the lower rack. This geometry provides uniform stagger of the cold to hot flow elements while matching the hot and cold flow areas. The inlet and upper chute rack instrumentation for this configuration are the same as those for aligned CD-chute mixer configuration (see Figure 4.1-5). Figure 4.3-4 shows the plan view of the inlet and lower chute rack with 9 and two half CD chutes for the staggered mixer configuration indicating the locations of the static pressure taps on the chute surfaces and the total pressure rake in the secondary flow path.

The long ejector of 16.055" and the short ejector of 10.935" with MAR=0.95 were used for the current configurations. The instrumentation upstream of the mixer exit is the same for both the long and short flap configurations. The flap instrumentation is different for short flap configuration and is the same as those shown in Figure 4.2-4 for convergent chute mixer-ejector configurations with short flap. For the treated configurations, the flaps and sidewalls were fully treated with nickel based metal foam with a 37% porous facesheet. Tests were conducted for each of the staggered chute configurations along the L1M cycle line for static and simulated flight condition of Mach 0.32 and the acoustic data were measured at community and sideline planes with respect to the major axis only

TEN FULL CHUTE
UPPER RACK

NINE FULL CHUTE
LOWER RACK
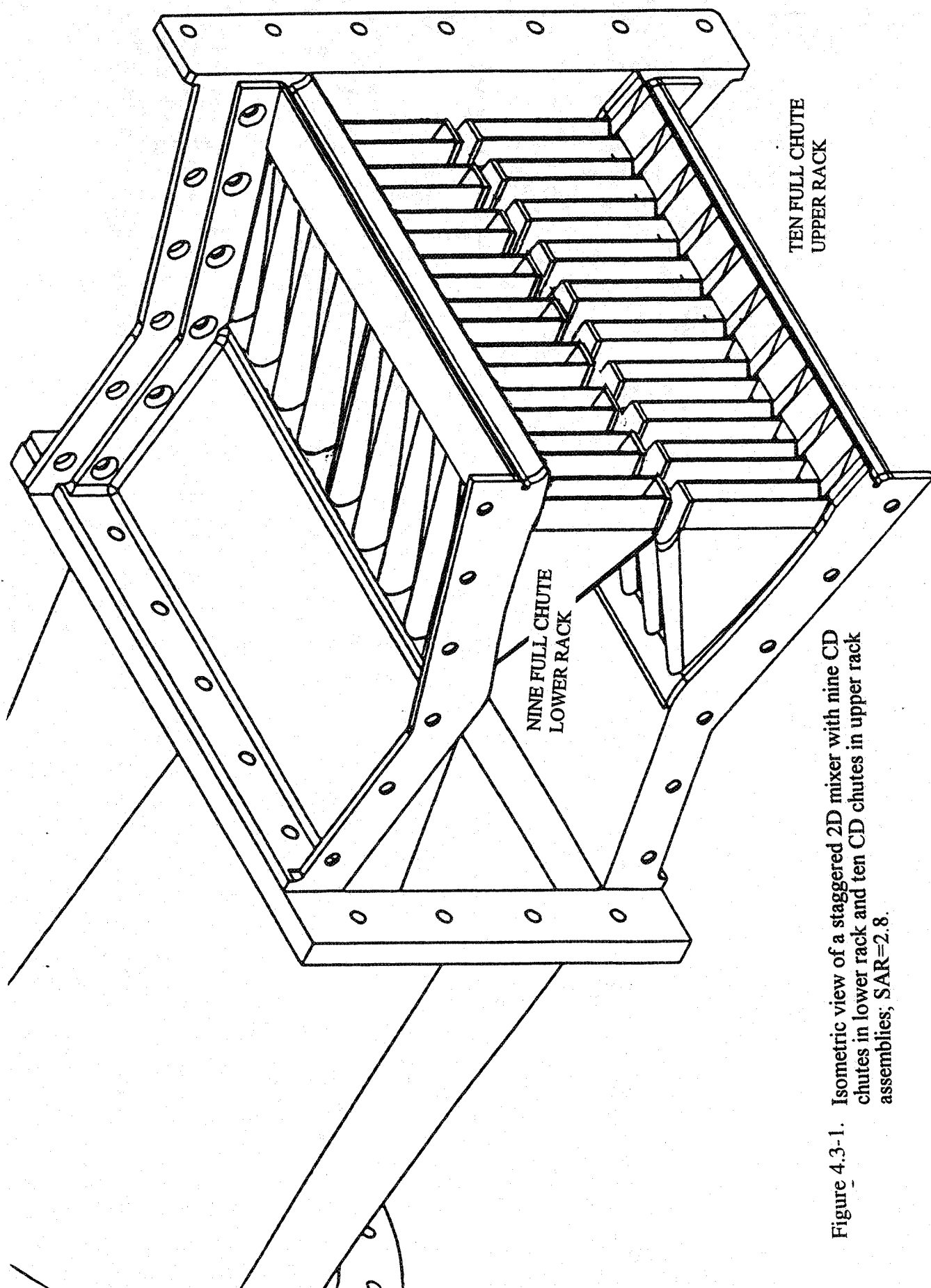
Figure 4.3-1. Isometric view of a staggered 2D mixer with nine CD chutes in lower rack and ten CD chutes in upper rack assemblies; SAR=2.8.
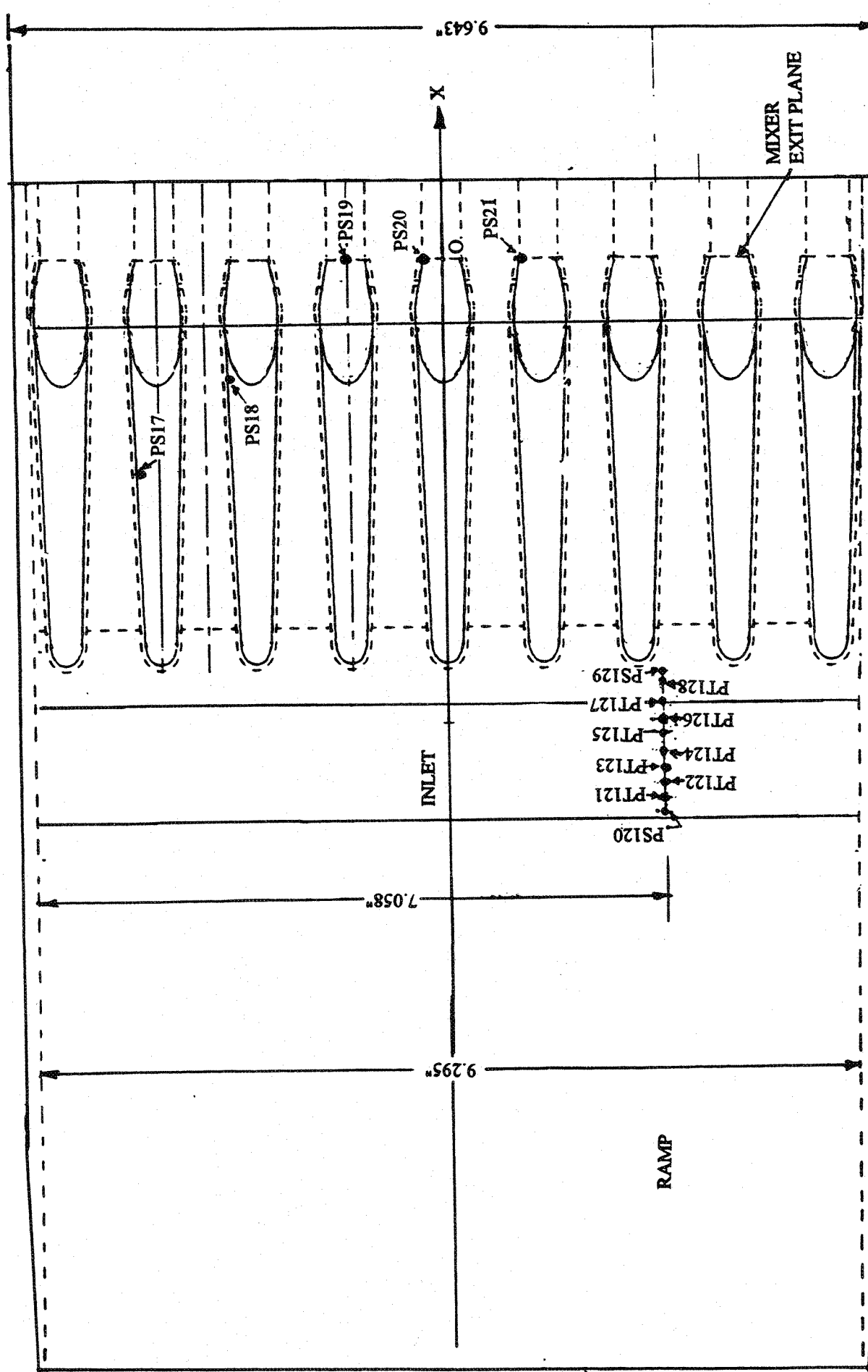
Figure 4.3-2. Plan view of the inlet and the lower chute rack with 9 CD chutes for a 2D mixer-ejector nozzle showing the static pressure tap locations on the chute surfaces and total pressure element locations in the secondary flow passage.

NINE & TWO HALH
CHUTE LOWER RACK

HALF CHUTE

TEN FULL CHUTE
UPPER RACK
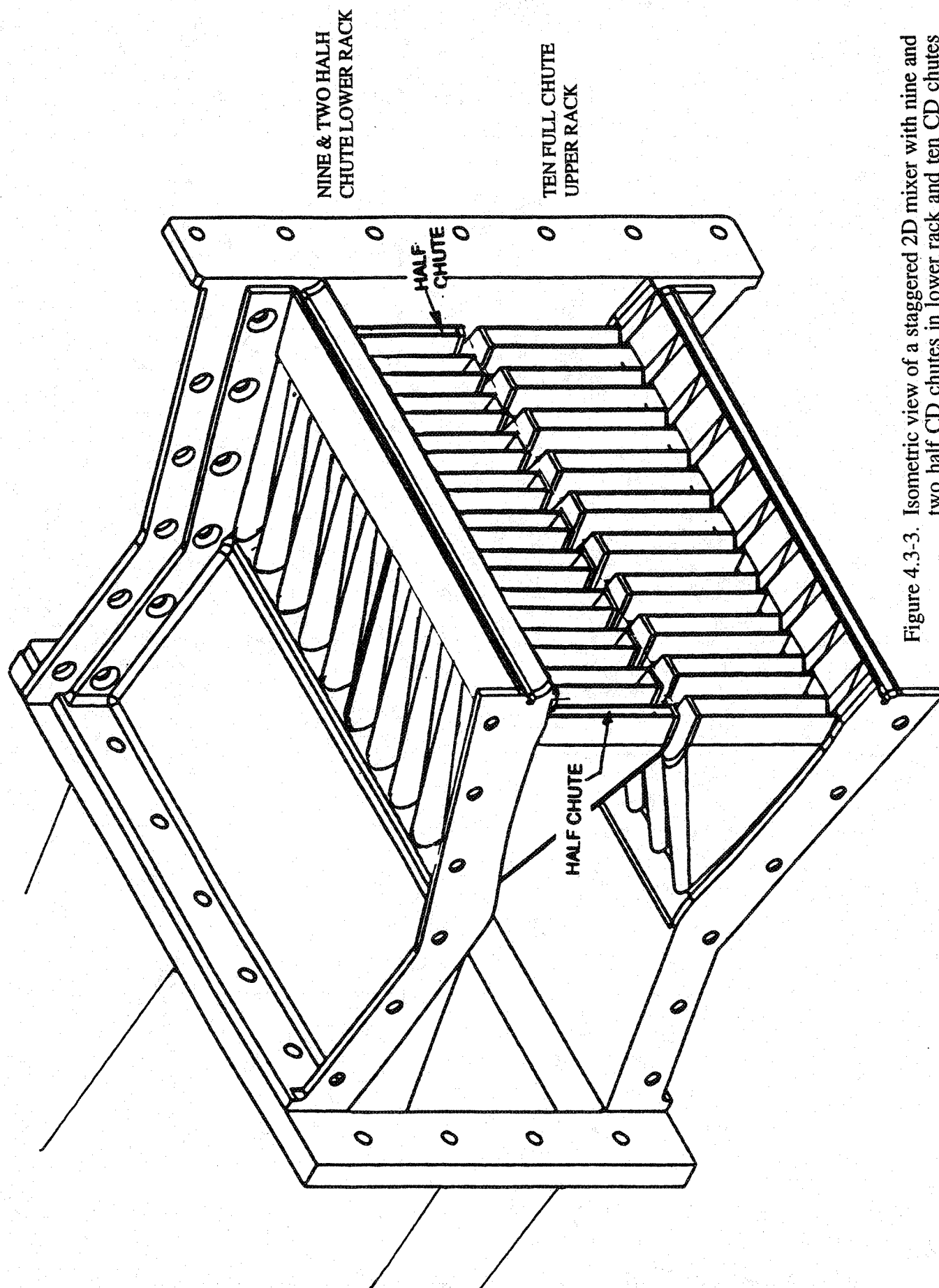
HALF CHUTE

Figure 4.3-3. Isometric view of a staggered 2D mixer with nine and two half CD chutes in lower rack and ten CD chutes in upper rack assemblies; SAR=2.8.
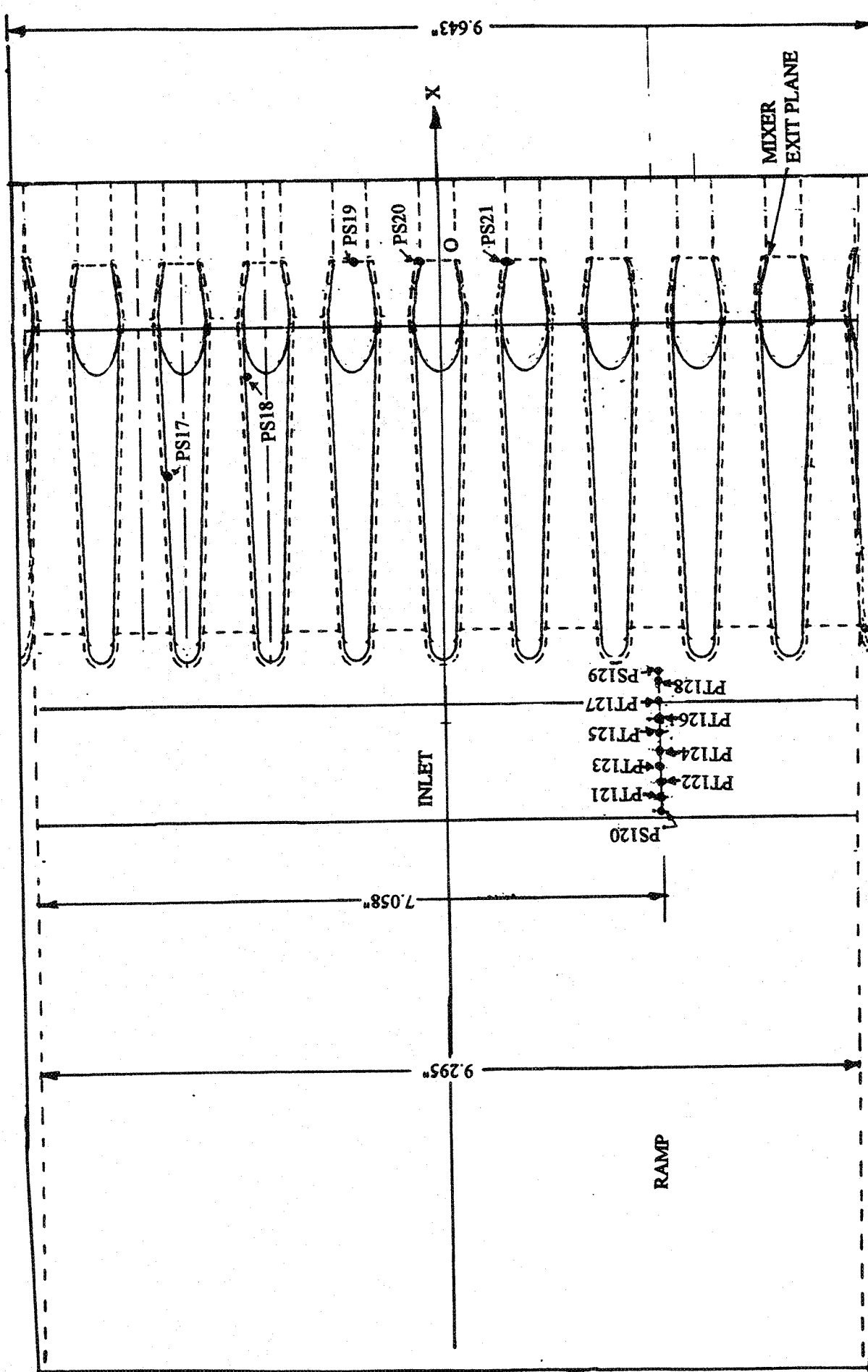
Figure 4.3-4. Plan view of the inlet and the lower chute rack with 9 full and 2 half CD chutes for a 2D mixer-ejector nozzle showing the static pressure tap locations on the chute surfaces and total pressure element locations in the secondary flow passage.

by positioning the microphone tower at 90° and 25°, respectively. Acoustic data was also measured at 45° azimuthal location using the fixed microphone array (see Figure 4.3-5). The model surface pressure data was measured for each aerothermodynamic condition.

4.3.1 Results for 10 and 9 Full CD-chute Staggered Mixer-Ejector Configurations:

Effect of Acoustic Treatment and Flap Length: All the results in this section show the simultaneous comparisons between treated and hard wall configurations and between short and long flaps for static and with flight simulation condition of M_F=0.32. While the long flap results are presented by open symbols, the same filled symbols show the results for short flap configurations.

Figure 4.3-6 shows the effect of treatment and flap length on PNLT and EPNL as function of jet velocity (V_j) at an azimuthal angle ϕ=25°. Noise reductions in terms of EPNdB and PNLTdB are observed both due to treatment and increased flap length. However, the effect is reduced with increasing jet velocity. Noise reduction due to acoustic treatment is higher for the long flap configuration compared to the short flap case. Acoustic benefit of about 2 to 3 EPNdB due to treatment is observed for long flap configuration with flight simulation at velocities between 1600 and 2200 ft/sec. At higher velocities the treatment benefit is not significant due to dominant externally (i.e., external to the ejector) generated noise. Noise benefit due to increased flap length is the result of better mixing within the ejector compared to a shorter ejector case.

At four different jet velocities of L1M cycle conditions the effect of treatment and flap length on PNLT directivities is shown in Figure 4.3-7. Noise suppressions due to treatment and due to flap length are more significant at lower jet velocities and at lower polar angles, except for V_j=1147 ft/sec. At this condition the effect of treatment as well as flap length are observed in the mid polar angles. At lower forward angles the effect is insignificant due to the probable dominant shock noise and noise from the inlet. Effect of treatment and flap length on SPL spectra at various polar angles (θ) for each of the four jet velocities is shown in Figures 4.3-8 through 4.3-11. Significant SPL reduction is observed at higher polar angles for higher frequency range. The acoustic benefit in terms of SPL diminishes with increasing jet velocity. At NPR=3.4 condition the SPL results indicate the possible presence of shock in the ejector for short flap configurations. Shock-associated noise in terms of SPL is dominantly observed at 60° and in moderate amount at 90° for the short flap configurations.

(a) Partially staggered, 9 full chutes on bottom

(b) Fully staggered, 9 full and 2 half chutes on bottom
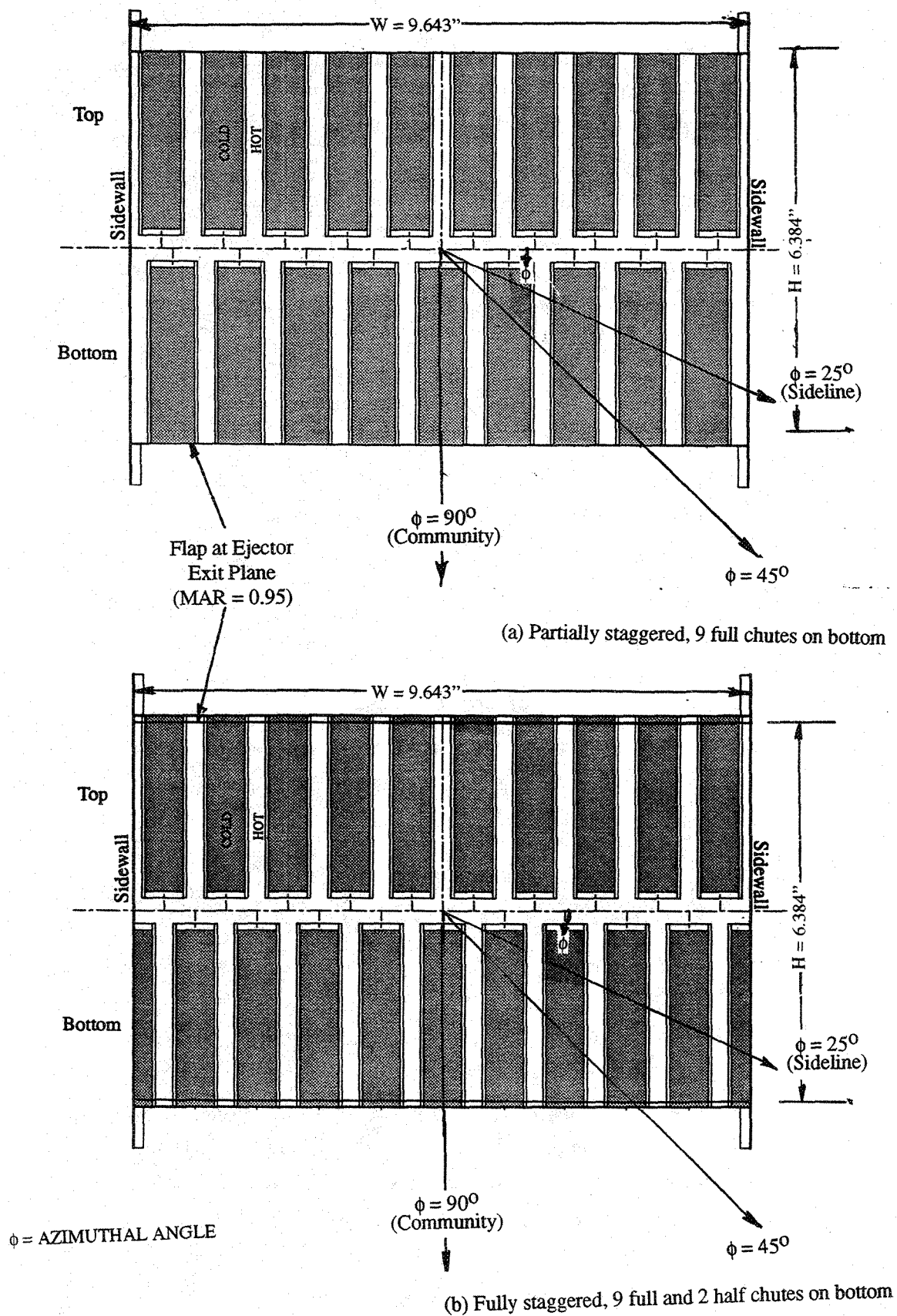
Figure 4.3-5. Azimuthal measurement locations indicated on the end views of two different staggered CD-chute mixer-ejectors; SAR=2.8, MAR=0.95.
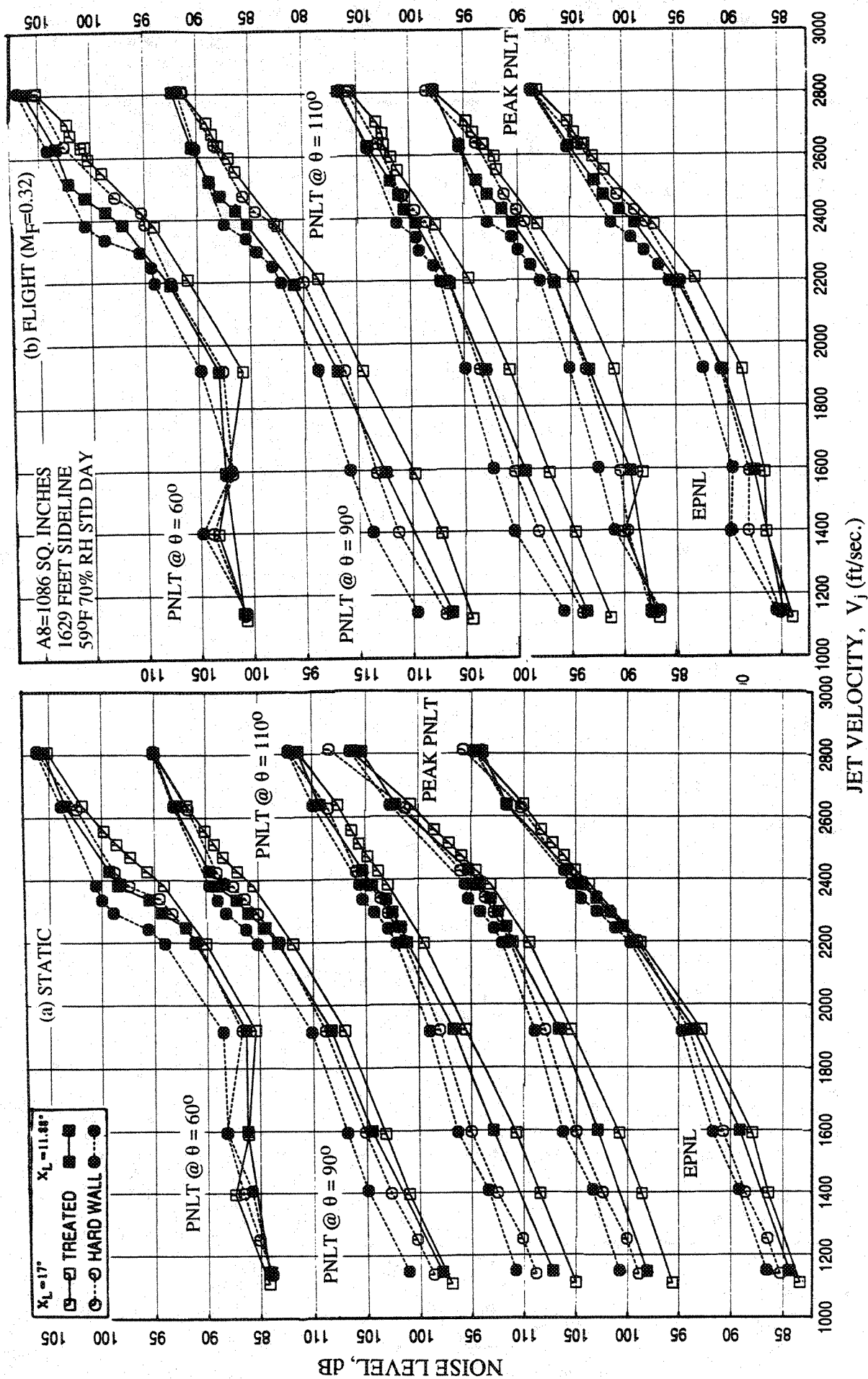
Figure 4.3-6. Effect of acoustic treatment and flap length on EPNL and PNLT at various polar angles (θ) as function of jet velocity of L1M cycle conditions for a 10 and 9 full staggered CD-chute mixer-ejector at an azimuthal angle φ=25°; SAR=2.8, MAR=0.95.
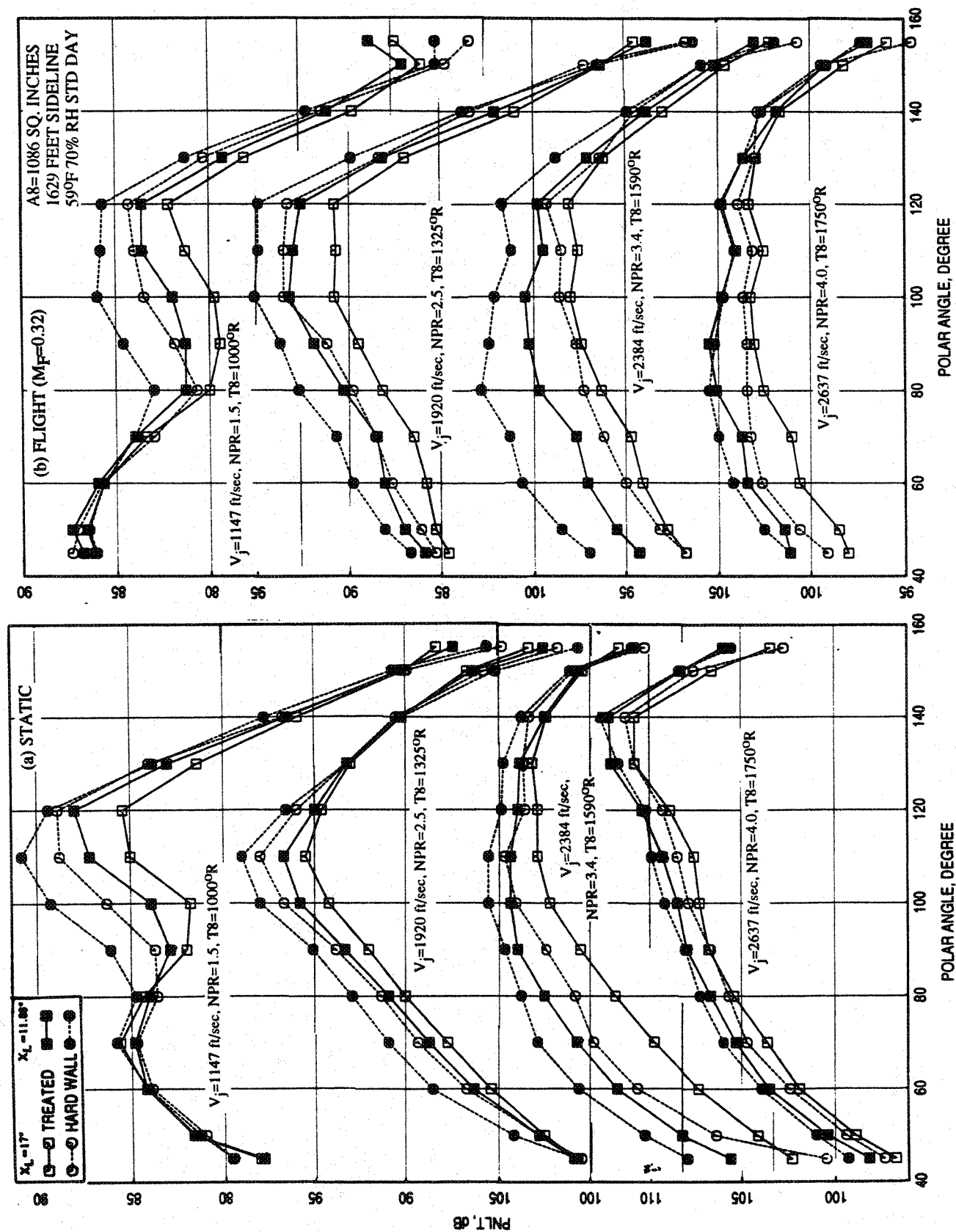
Figure 4.3-7. Effect of acoustic treatment and flap length on PNLT directivities at different L1M cycle conditions for a 10 and 9 full staggered CD-chute mixer-ejector at an azimuthal angle ϕ=250°; SAR=2.8, MAR=0.95.
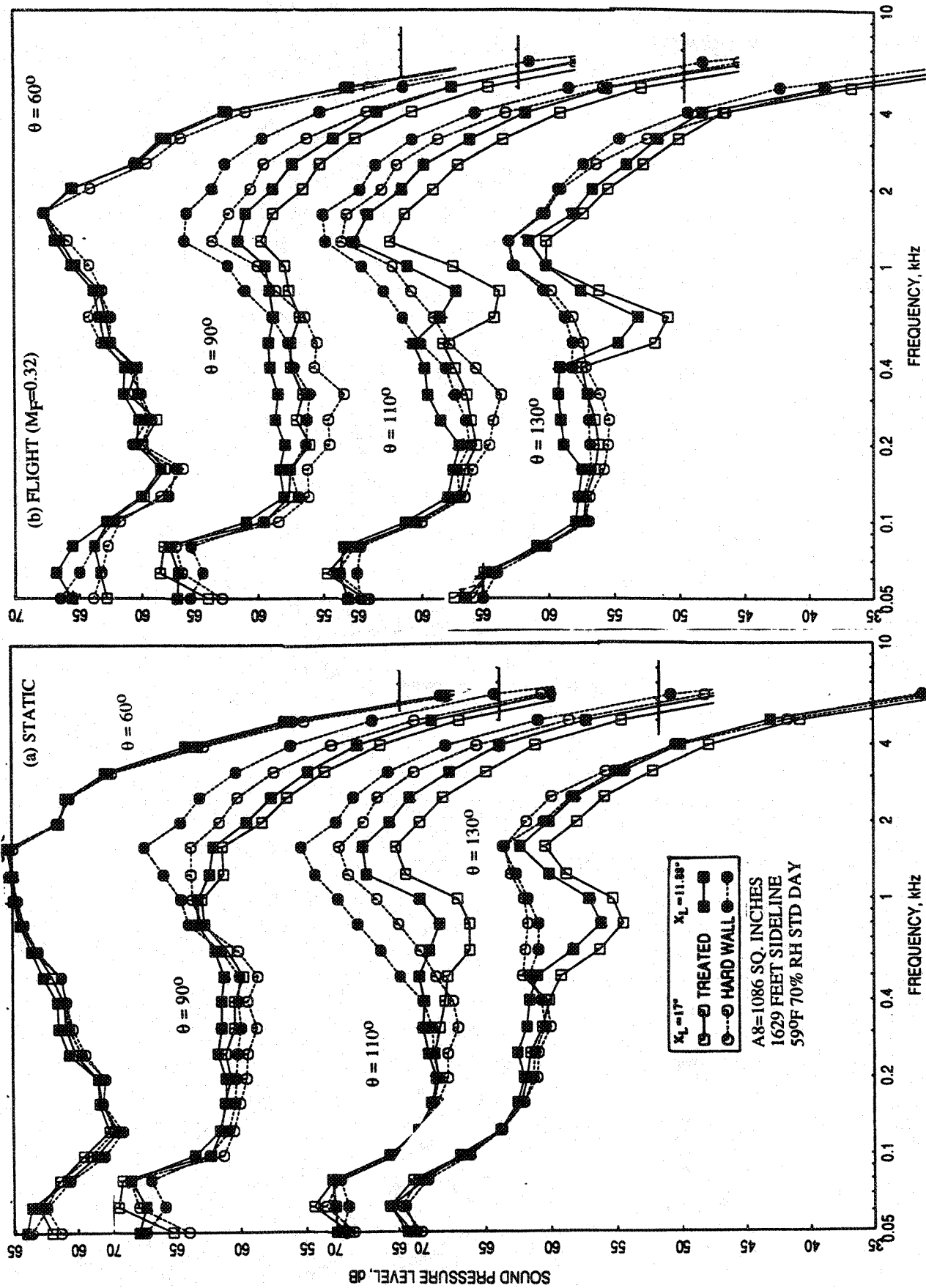
Figure 4.3-8. Effect of acoustic treatment and flap length on SPL spectra at various polar angles (θ) for a 10 and 9 full staggered CD-chute mixer-ejector at an azimuthal angle φ=25°; SAR=2.8, MAR=0.95, V_j = 1147 ft/sec, NPR = 1.5, T8 = 1000°R.
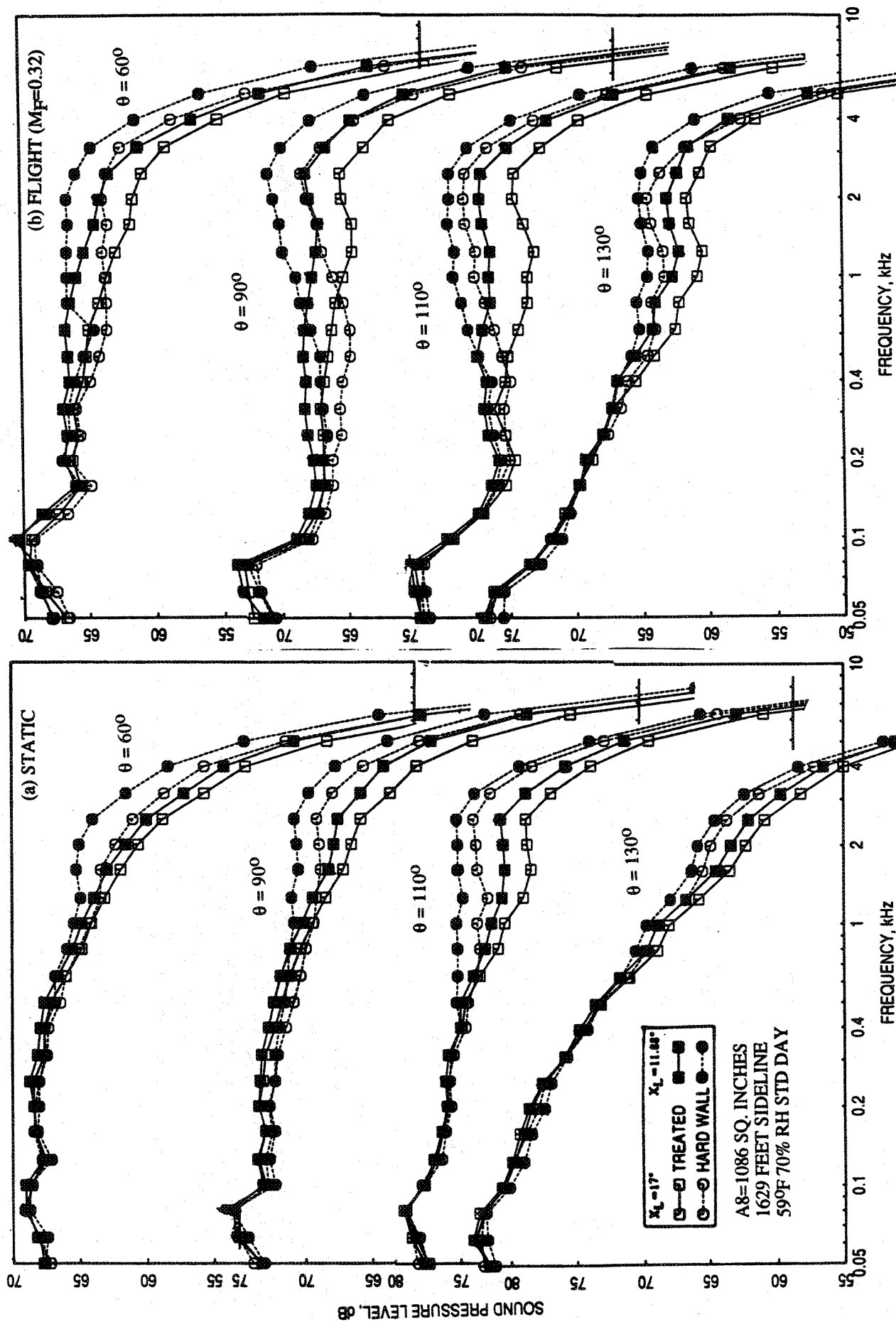
Figure 4.3-9. Effect of acoustic treatment and flap length on SPL spectra at various polar angles (θ) for a 10 and 9 full staggered CD-chute mixer-ejector at an azimuthal angle φ=25°, SAR=2.8, MAR=0.95, V$_j$ = 1920 ft/sec, NPR = 2.5, T8 = 1325°R.

172
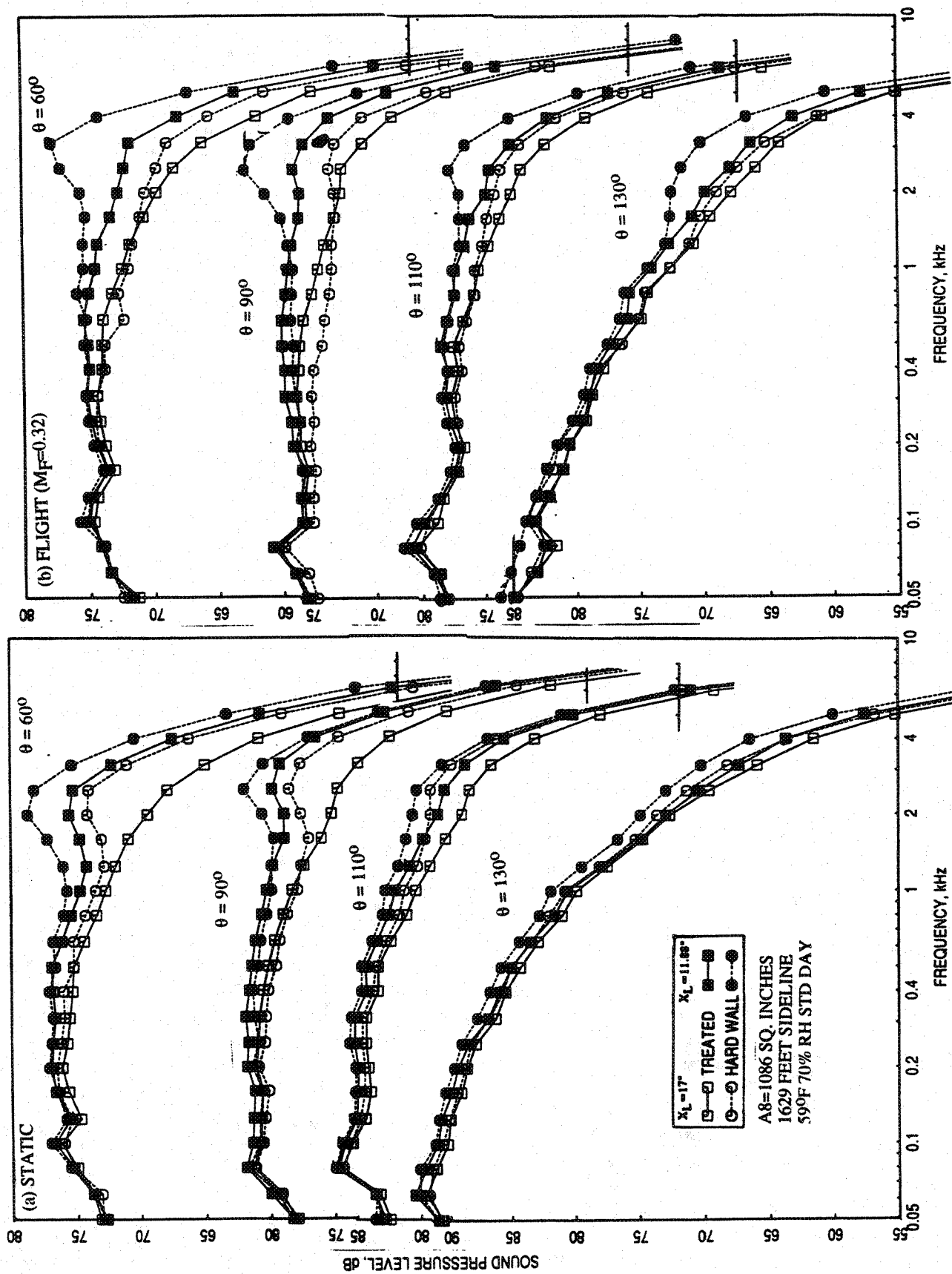
Figure 4.3-10. Effect of acoustic treatment and flap length on SPL spectra at various polar angles (θ) for a 10 and 9 full staggered CD-chute mixer-ejector at an azimuthal angle φ=25°; SAR=2.8, MAR=0.95, V_j = 2384 ft/sec, NPR = 3.4, T8 = 1590°R.
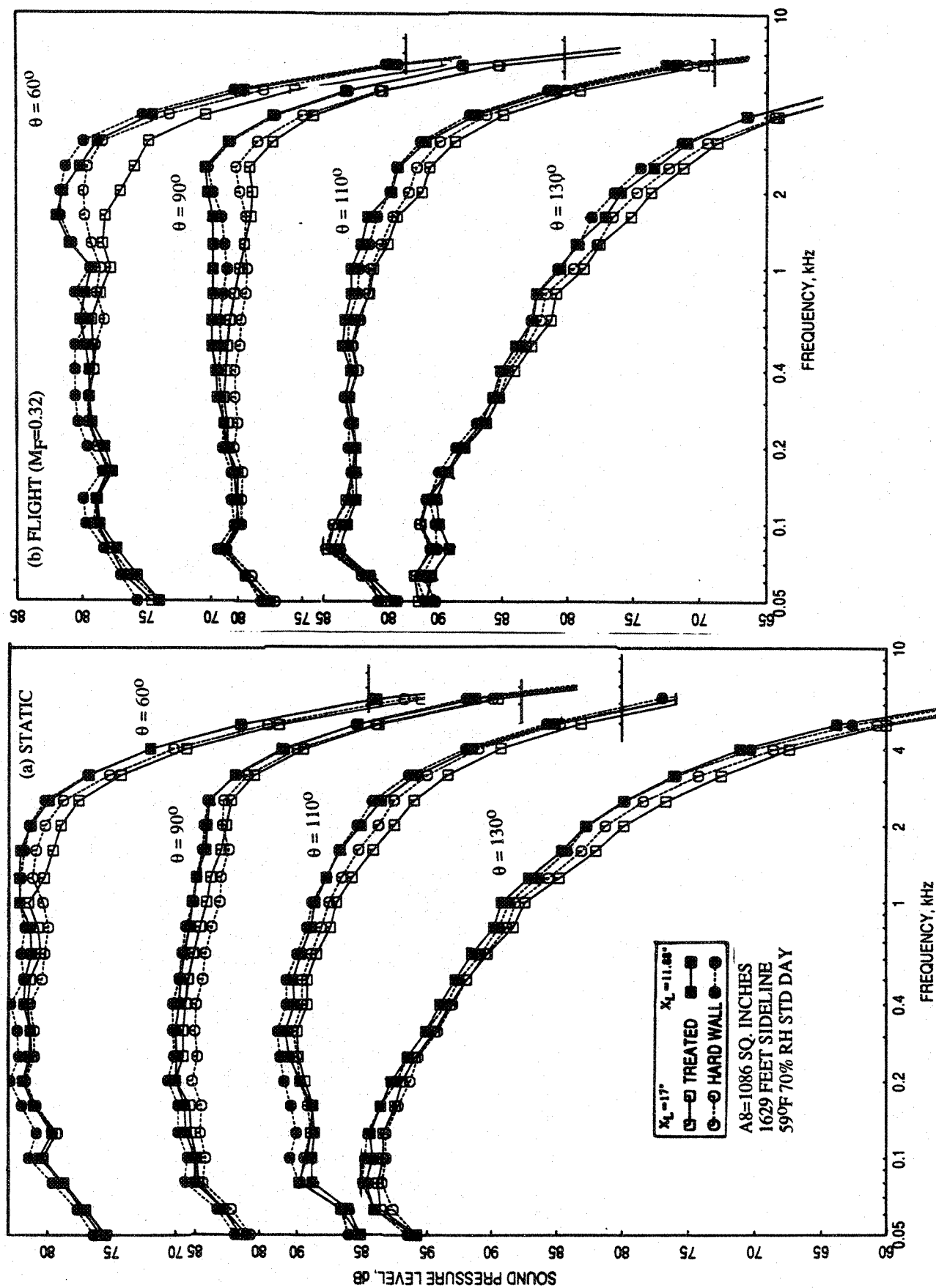
Figure 4.3-11. Effect of acoustic treatment and flap length on SPL spectra at various polar angles (θ) for for for a 10 and 9 full staggered CD-chute mixer-ejector at an azimuthal angle $\phi=25^\circ$, SAR=2.8, MAR=0.95, $V_j = 2637$ ft/sec, NPR = 4.0, T8 = 1750°R.

The static pressure tap locations on the flap surface downstream of the origin (i.e., for positive X) are normalized with respect to the ejector length associated with the test configuration for axial static pressure distribution results. However, the static pressure tap locations upstream of the origin (i.e., for negative X) are normalized with respect to the longer ejector length (i.e., 17"), since these instrument locations are identical for both long and short ejector configurations.

The effect of treatment, flap length, and flight simulation on ramp and chute static pressure distributions is shown in Figure 4.3-12 for different L1M cycle conditions. The effect of treatment and flap length is insignificant on the static pressure distributions on the ramp and chute surfaces. However, the static pressure increases due to flight simulation for each case, both on the ramp and on the chute surfaces due to freejet fan pressure rise, indicating lesser loading for the chutes. Figure 4.3-13 shows the effect of treatment and flap length on chute loading coefficient plotted against NPR. Again, the effects of treatment and flap length are very small on chute loading coefficient. The effect of treatment and flap length on pumping and corrected pumping is shown in Figure 4.3-14. The pumping is lower for treated ejector compared to hard wall for short flap configuration at static case for lower NPRs. This difference is most probably due to the difference in static temperature between the two configurations and not the effect of treatment. The effect of flap length is very small. With flight simulation these effects are almost negligible on pumping. The effect of treatment as well as flap length is almost negligible for corrected pumping for entire NPR range for static and flight cases. The same is the case with the mixed jet velocity (see Figure 4.3-15).

Figure 4.3-16 shows the effect of treatment and flap length on the average axial static pressure distributions on the inlet and the flap surface at different L1M cycle conditions. Static pressure distributions on the inlet are not influenced by the treatment and by the ejector length. However, the ejector length influences the flap static pressure distribution for all conditions. The static pressure is higher on the flap surface for longer ejector compared to the shorter configuration. The effect of treatment is insignificant on flap static pressure distributions at lower NPR conditions. However, at higher NPRs, closer to the transition from subsonic to supersonic mode and above this condition, the flap static pressure is higher for the treated ejector compared to hard wall configuration. Acoustic treatment seems to soften shock/boundary-layer interaction which in turn seems to increase the critical NPR at which the ejector transitions from subsonic to supersonic mode. This is further illustrated in Figure 4.3-17 by plotting the normalized force on flap
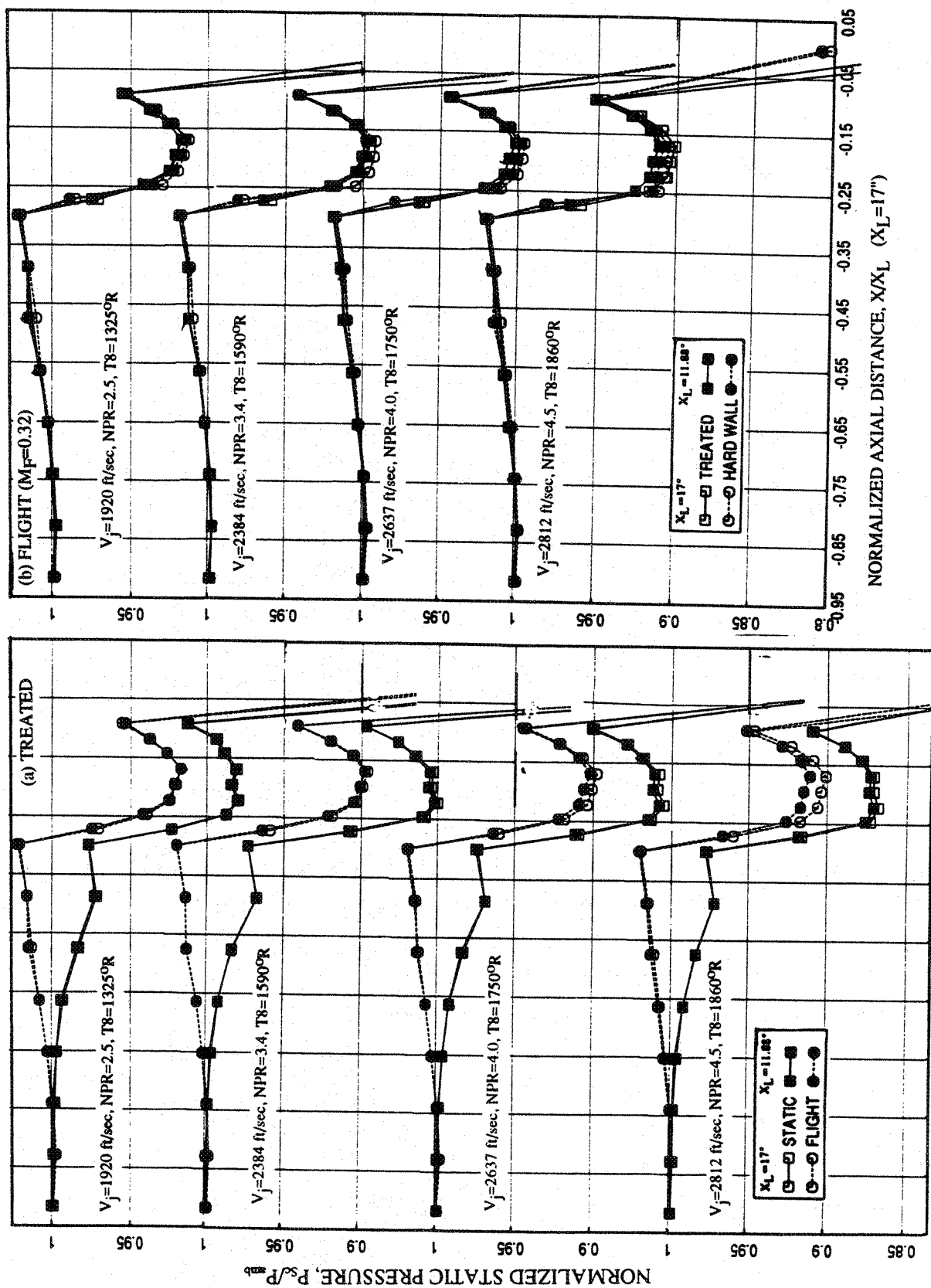
Figure 4.3-12. Effect of acoustic treatment, flap length and flight simulation on axial static pressure distributions on the inlet ramp and on the secondary flow side of chute surface at different L1M cycle conditions for a 10 and 9 full staggered CD-chute mixer-ejector SAR=2.8, MAR=0.95.
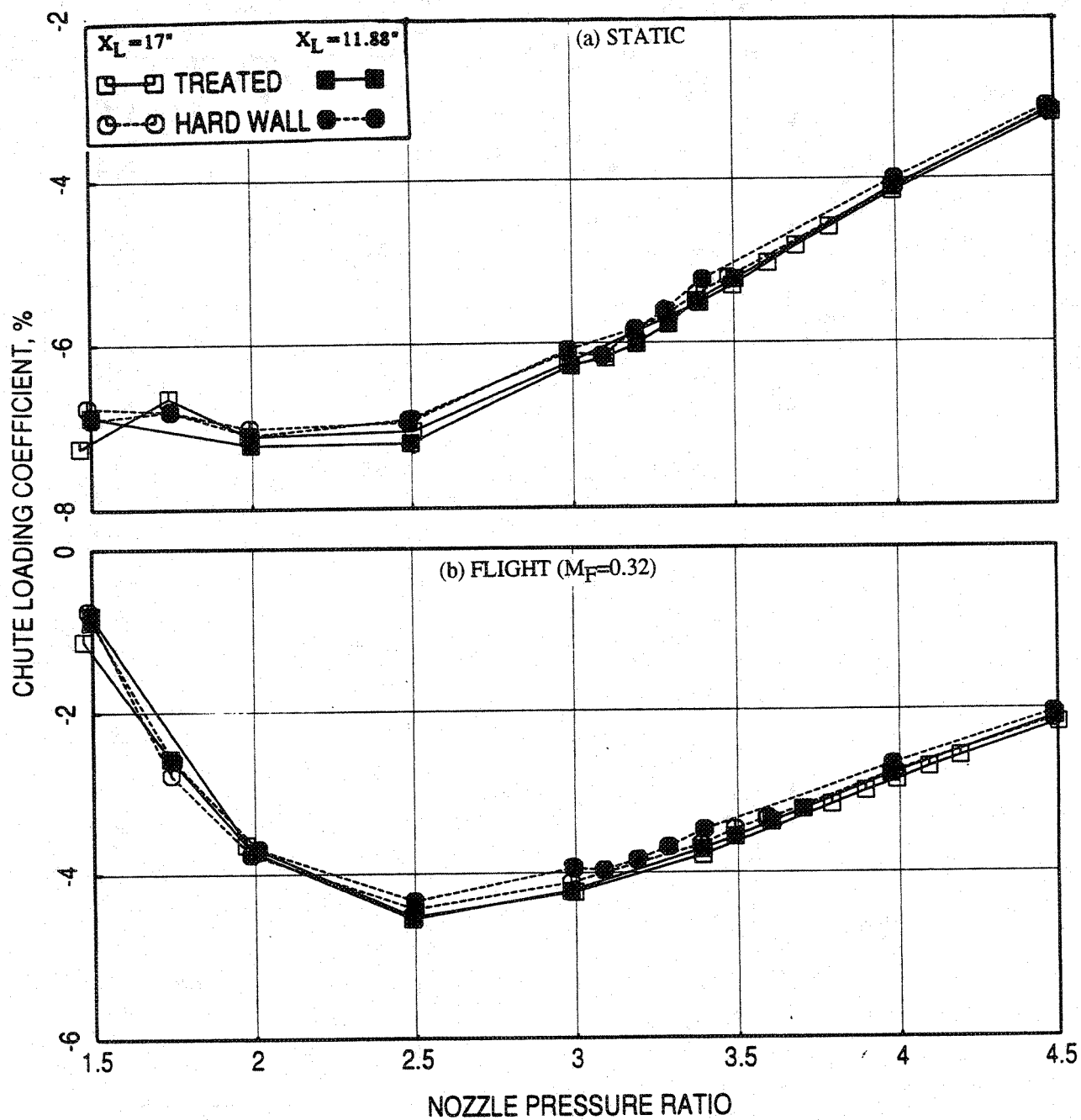
Figure 4.3-13. Effect of acoustic treatment and flap length on chute loading coefficient with respect to nozzle pressure ratio of L1M cycle conditions for a 10 and 9 full staggered CD-chute mixer-ejector; SAR=2.8, MAR=0.95.
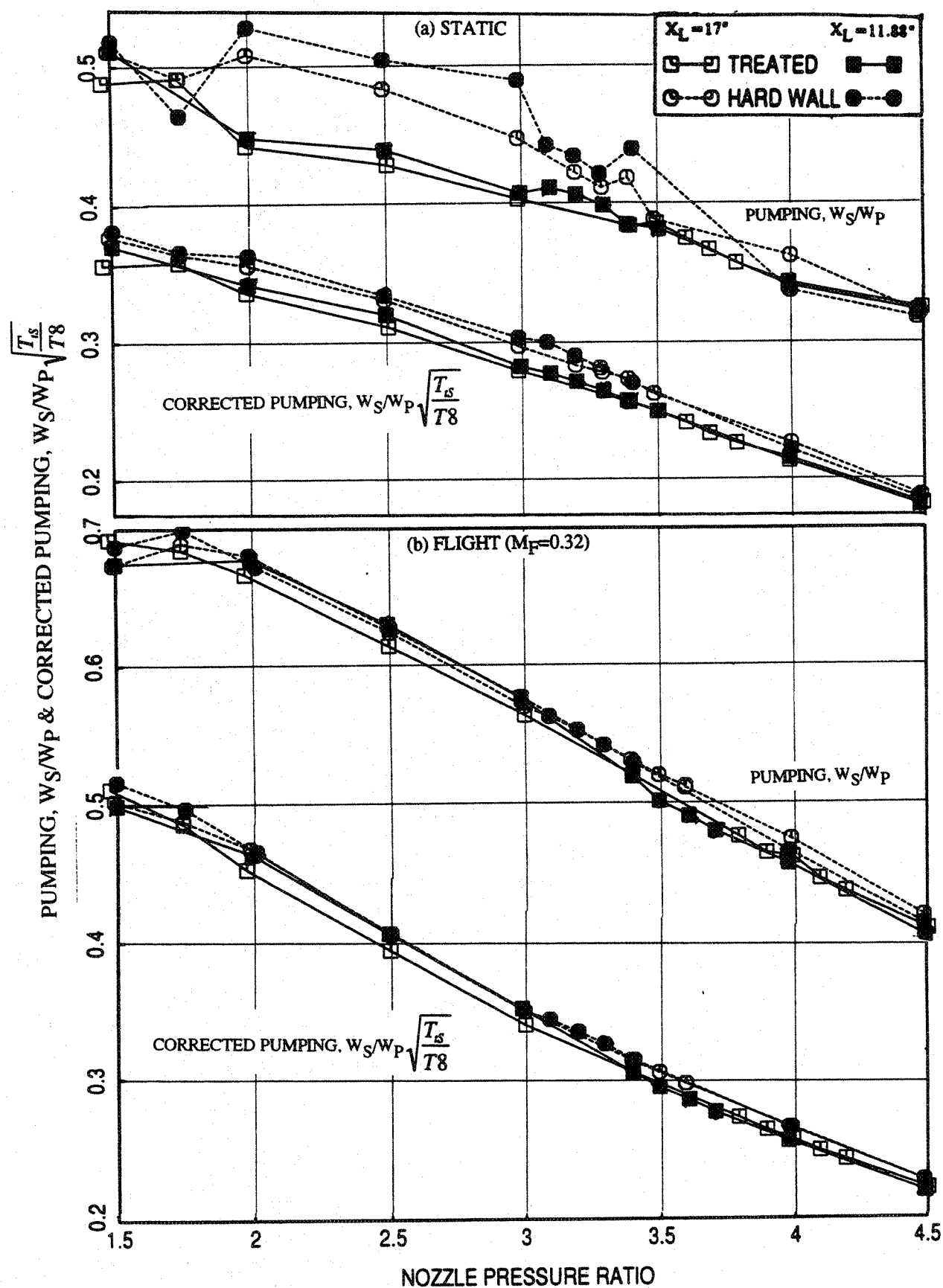
Figure 4.3-14. Effect of acoustic treatment and flap length on pumping and corrected pumping with respect to nozzle pressure ratio of L1M cycle conditions for a 10 and 9 full staggered CD-chute mixer-ejector; SAR=2.8, MAR=0.95.
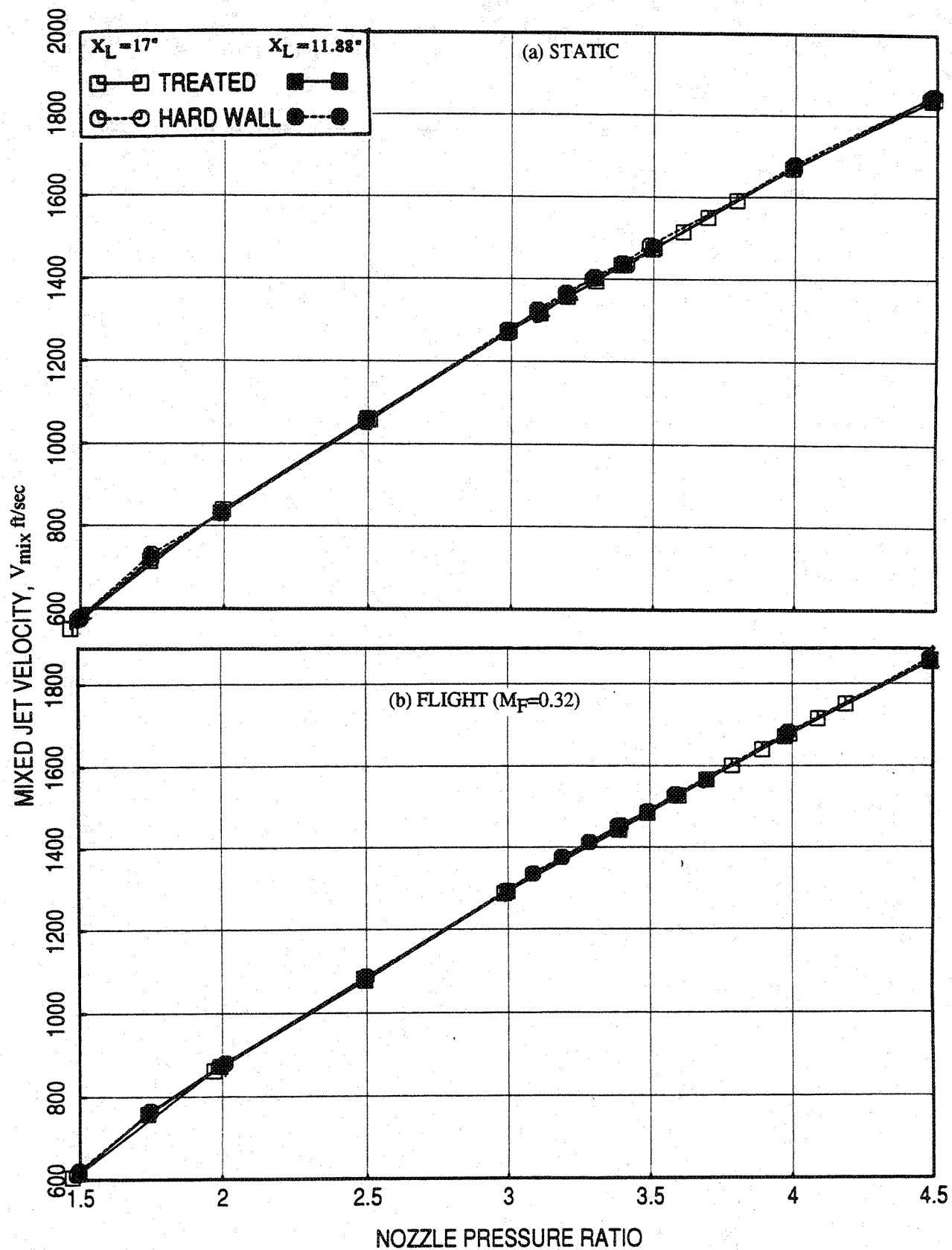
Figure 4.3-15. Effect of acoustic treatment and flap length on mixed jet velocity with respect to nozzle pressure ratio of L1M cycle conditions for a 10 and 9 full staggered CD-chute mixer-ejector; SAR=2.8, MAR=0.95.
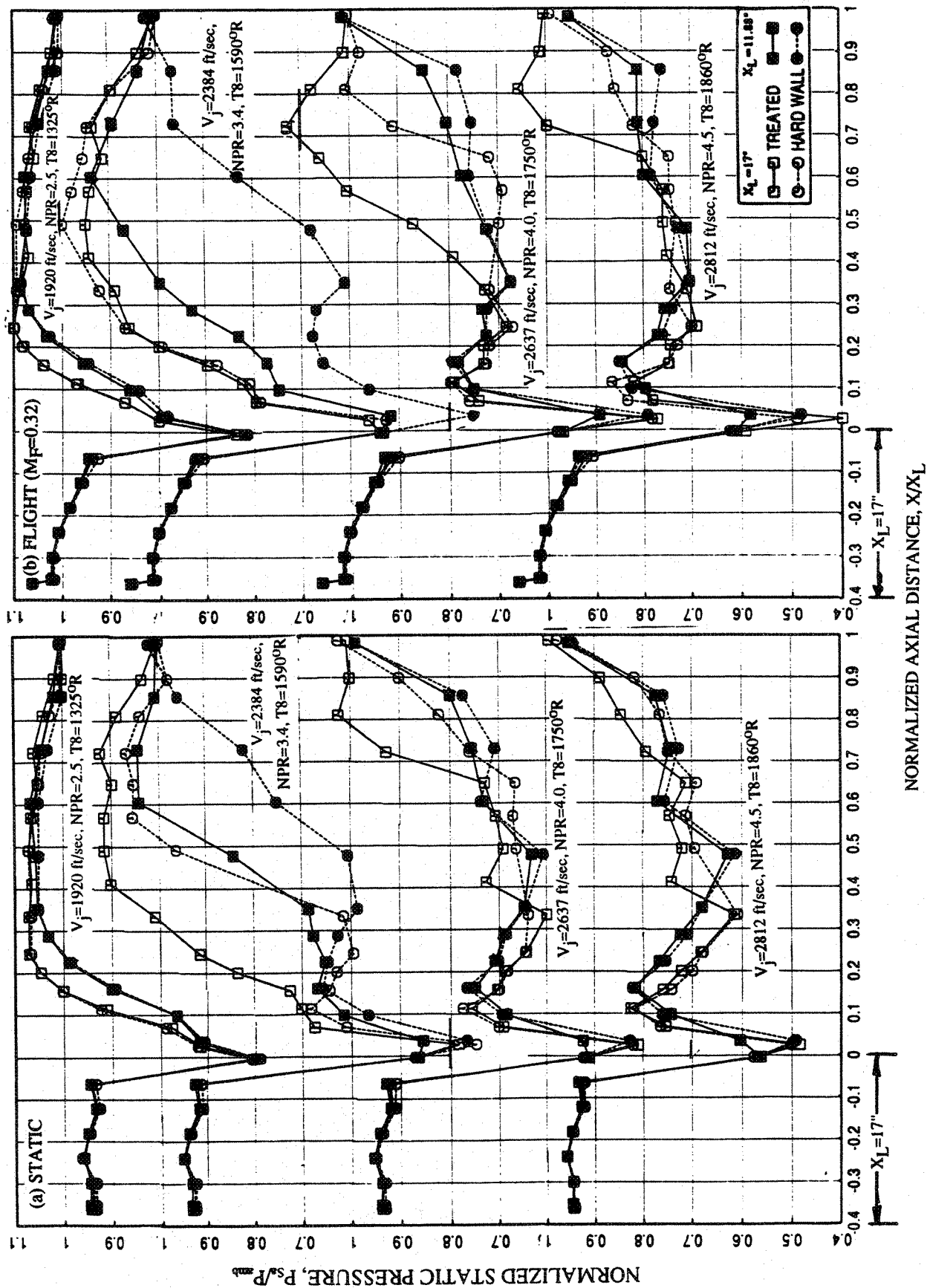
Figure 4.3-16. Effect of acoustic treatment and flap length on axial average static pressure distributions on the inlet and the flap surface at different L1M cycle conditions for a 10 and 9 full staggered CD-chute mixer-ejector SAR=2.8, MAR=0.95.
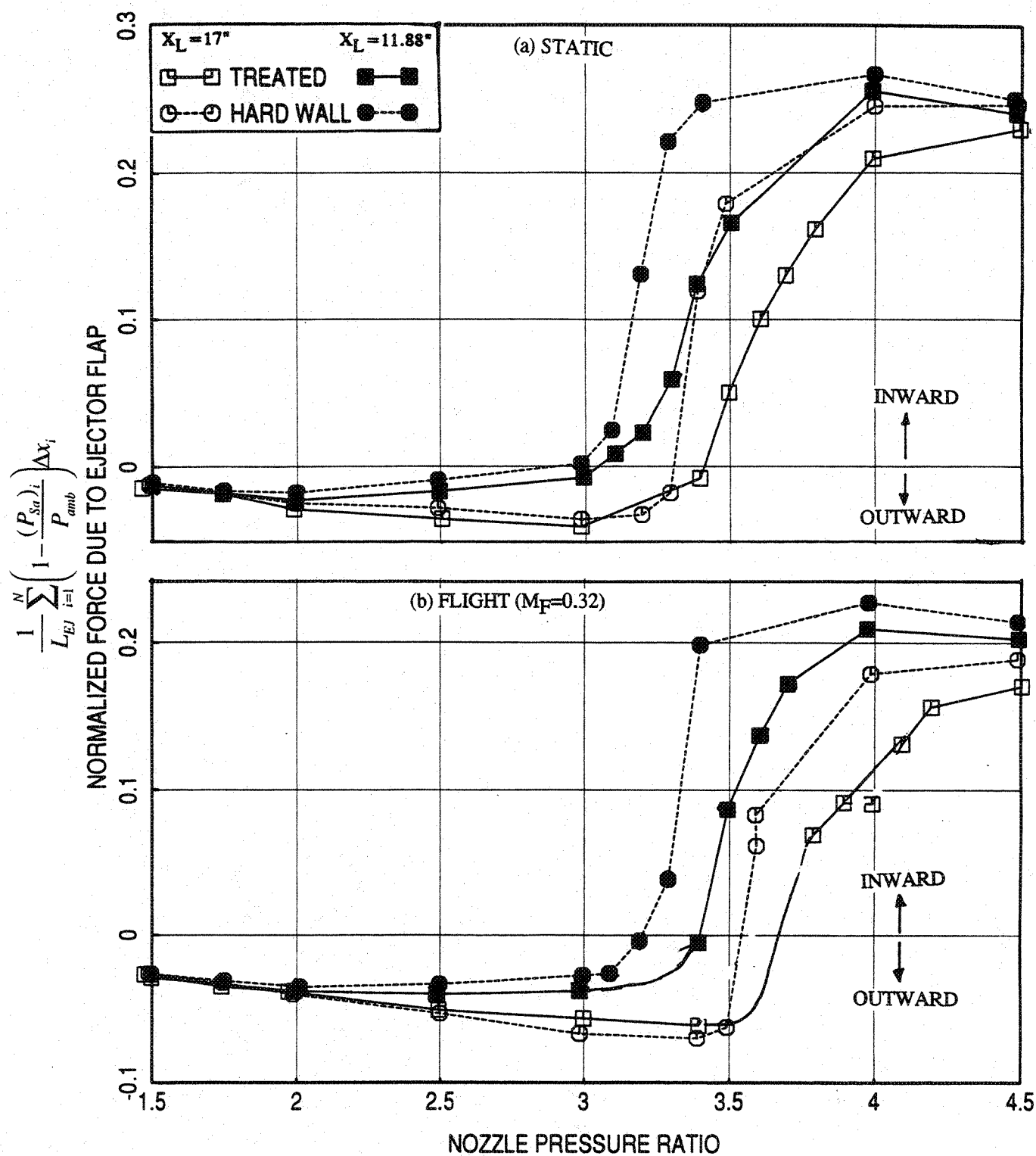
Figure 4.3-17. Effect of acoustic treatment and flap length on normalized force due to ejector flap with respect to nozzle pressure ratio of L1M cycle conditions for a 10 and 9 full staggered CD-chute mixer-ejector SAR=2.8, MAR=0.95.

surface with respect to NPR, that the transition from subsonic to supersonic mode seems to be slightly delayed for treated ejector compared to hard wall configuration and for longer ejector compared to the shorter configuration.

Effect of Simulated Flight and Flap Length : All the results in this section show the simultaneous comparisons between static and simulated flight of $M_F=0.32$ conditions and between short and long flap for treated and hard wall configurations. While the long flap results are presented by open symbols, the same filled symbols show the results for short flap configurations.

Figure 4.3-18 shows the effect of flight simulation and flap length on PNLT and EPNL as function of jet velocity (V_j) at an azimuthal angle $\phi=25^o$ for treated and hard wall configurations. EPNL decreases with flight simulation for all jet velocities for hard wall configuration and for treated case at velocities 1600 ft/sec and above. The EPNdB reduction due to flight simulation is slightly higher for treated ejector compared to hard wall case, since the noise generated internal to the ejector is reduced due to treatment and thus the reduction of externally generated noise due to flight simulation dominates the observed noise. The EPNL is lower for longer ejector compared to the short flap case and the noise reduction is higher with flight simulation. Except for forward arc angles the PNLT decreases with flight simulation and is lower for longer ejector at all jet velocities.

At four different jet velocity conditions the effect of flight simulation and flap length on PNLT directivities is shown in Figure 4.3-19. The effect of flight simulation is to lower the PNLT levels at polar angles above 60° due to source strength reductions and the trend is reversed at lower angles due to dynamic amplification of jet noise overcoming the source strength reduction effects. Significant PNLT reduction is observed at the rear arc. PNLT is lower for longer ejector at all angles and the impact is less realized in the rear arc angles. Effect of flight simulation and flap length on SPL spectra at various polar angles (θ) for each of the four jet velocities is shown in Figures 4.3-20 through 4.3-23. Significant SPL reduction is observed at higher polar angles for the entire frequency range due to flight simulation. The SPL levels are lower for long ejector compared to the shorter configuration, mostly at higher frequencies.

The effect of flight simulation and flap length on chute loading coefficient plotted against NPR is shown in Figure 4.3-24. While the effect of flap length on chute loading coefficient is small, the levels increase significantly with flight simulation. The effect of flight and flap
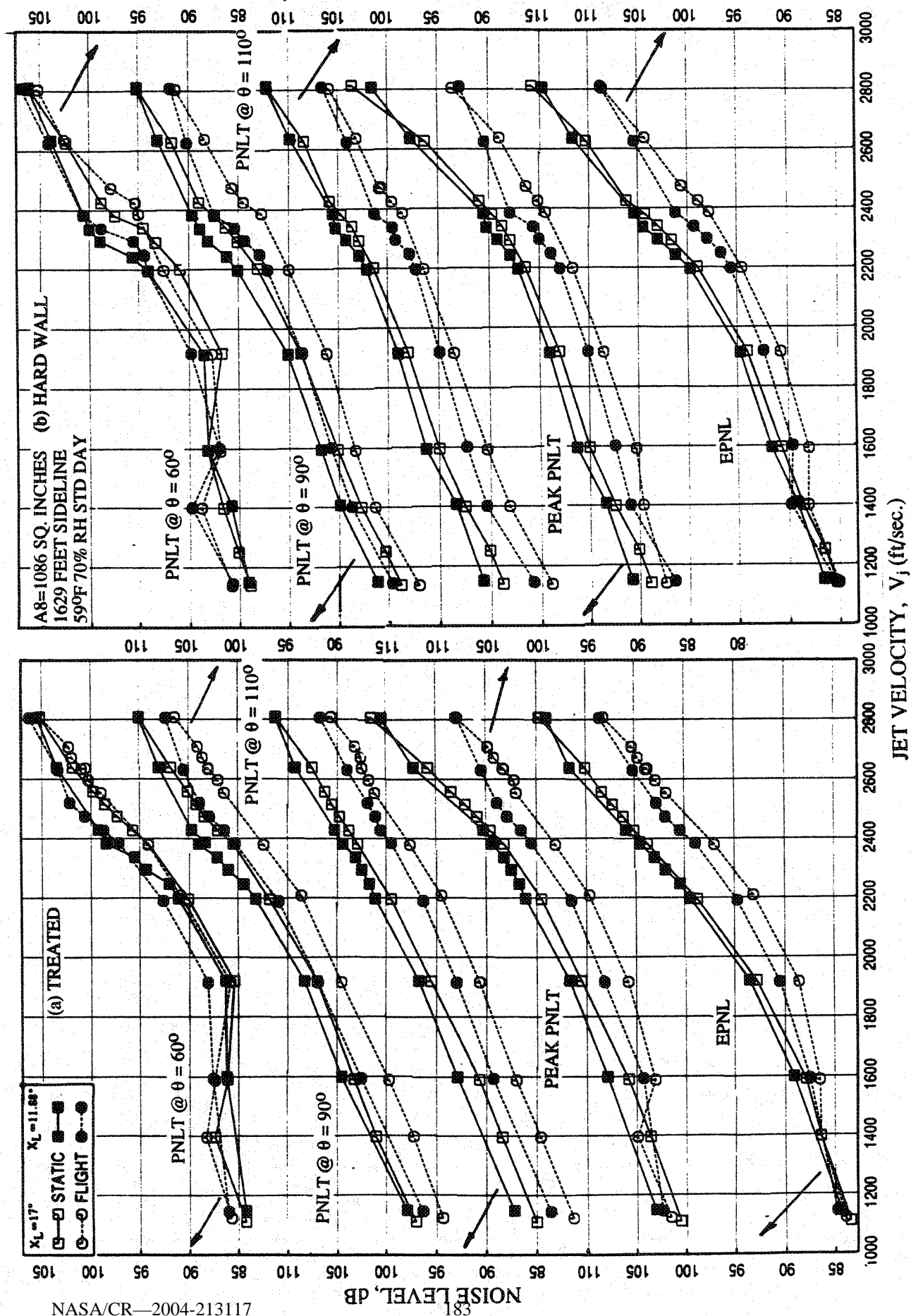
Figure 4.3-18. Effect of flight simulation and flap length on EPNL and PNLT at various polar angles (θ) as function of jet velocity of L1M cycle conditions for a 10 and 9 full staggered CD-chute mixer-ejector at an azimuthal angle φ=25°; SAR=2.8, MAR=0.95.
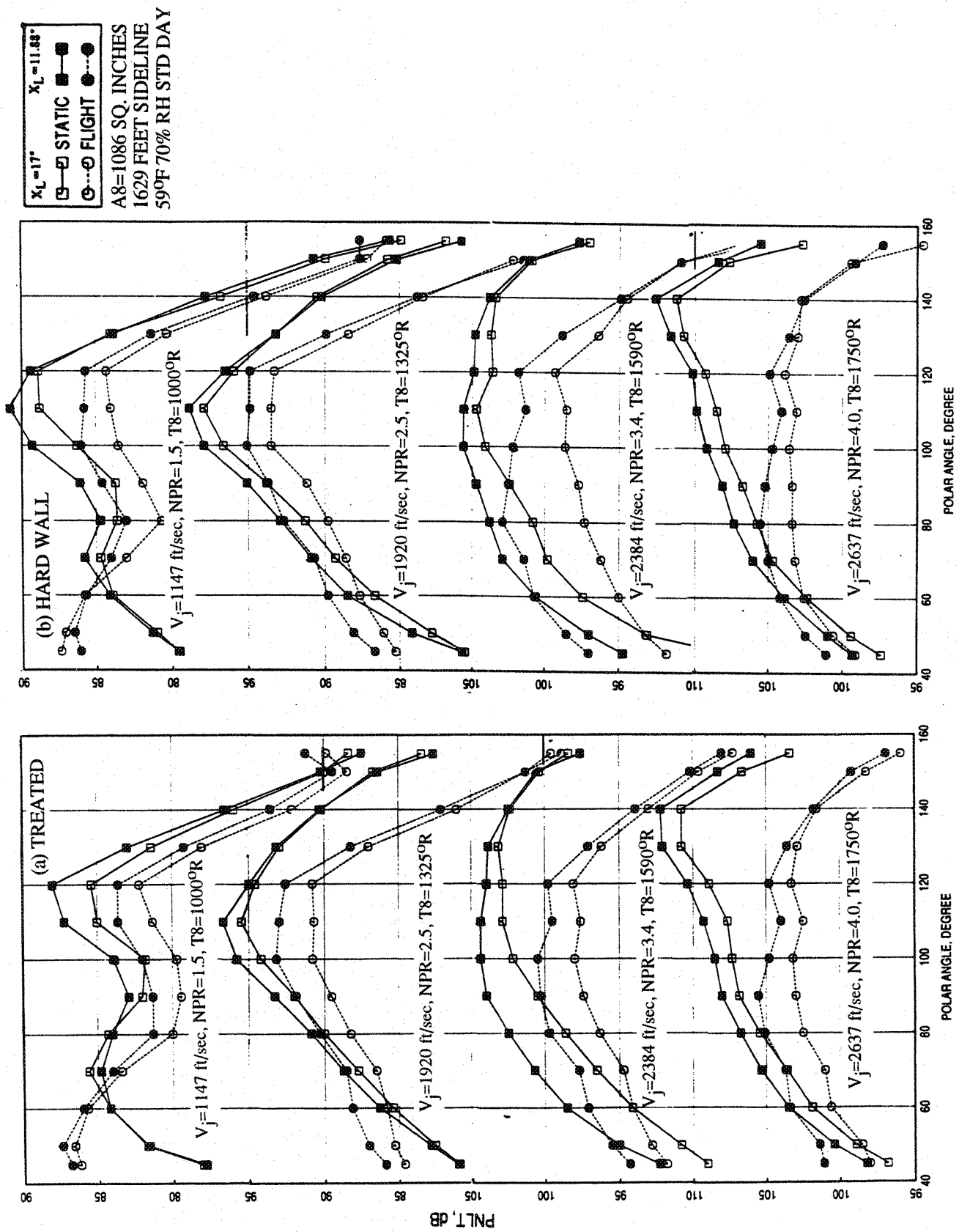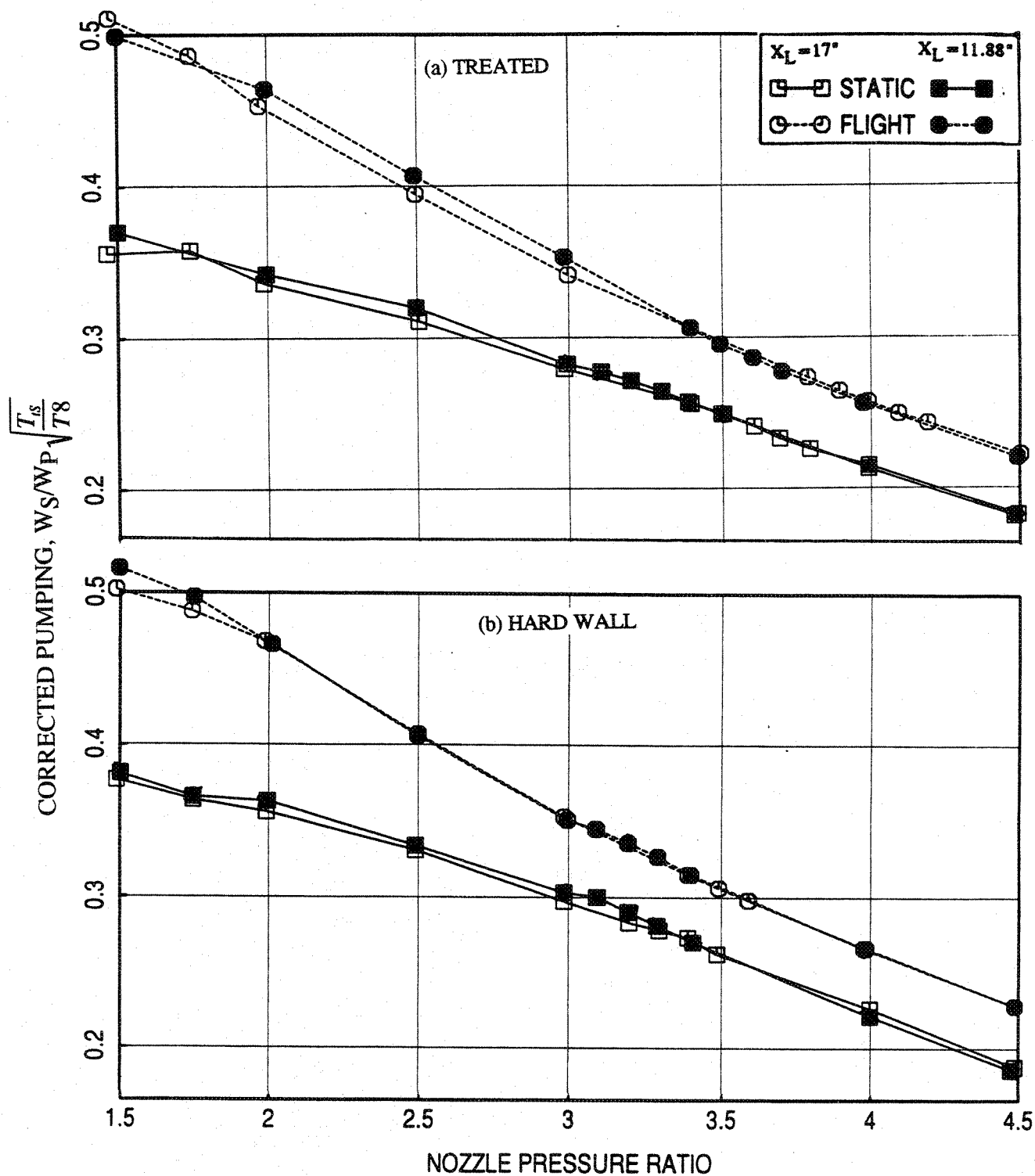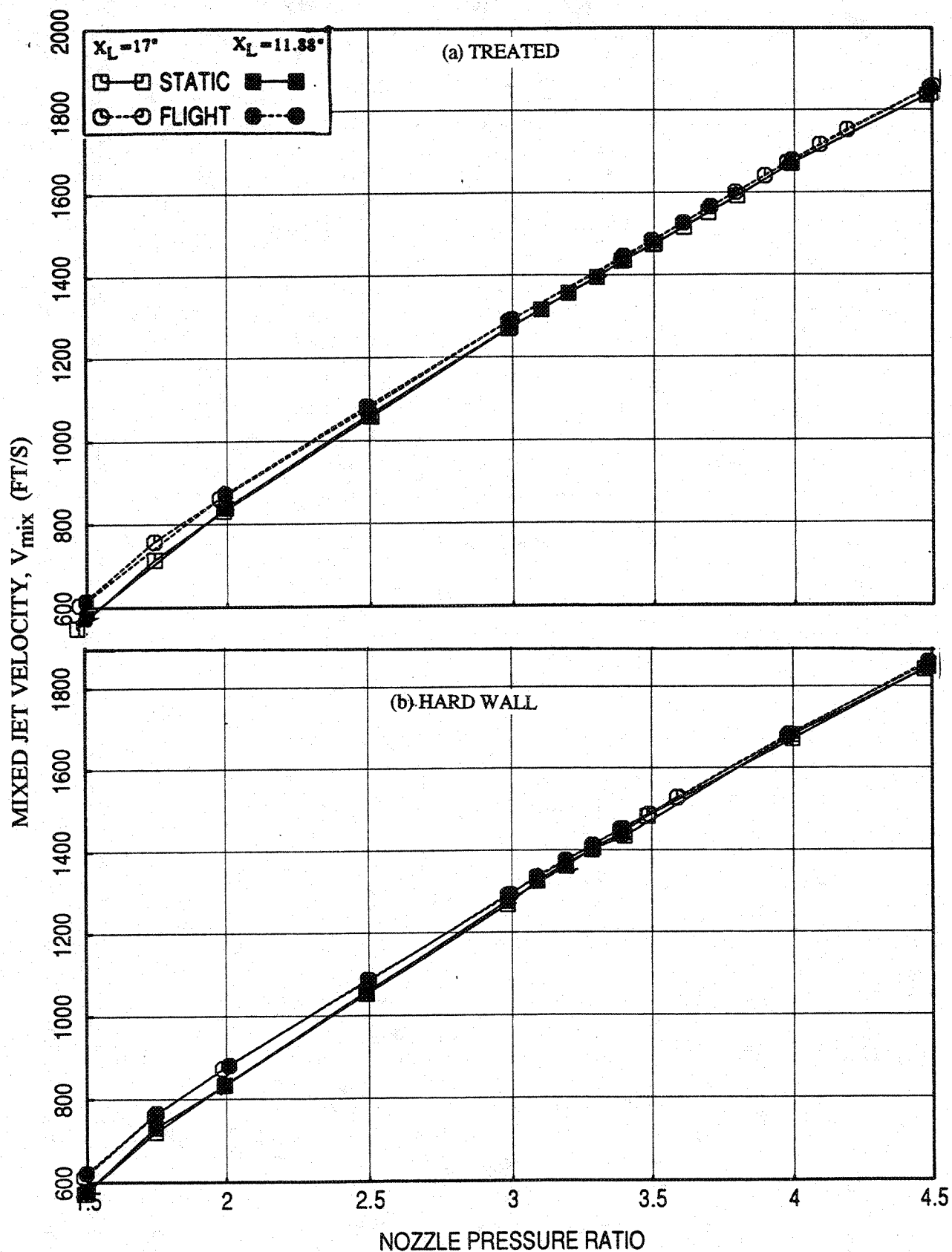
Figure 4.3-19. Effect of flight simulation and flap length on PNLT directivities at different L1M cycle conditions for a 10 and 9 full staggered CD-chute mixer-ejector at an azimuthal angle φ=25°, SAR=2.8, MAR=0.95.
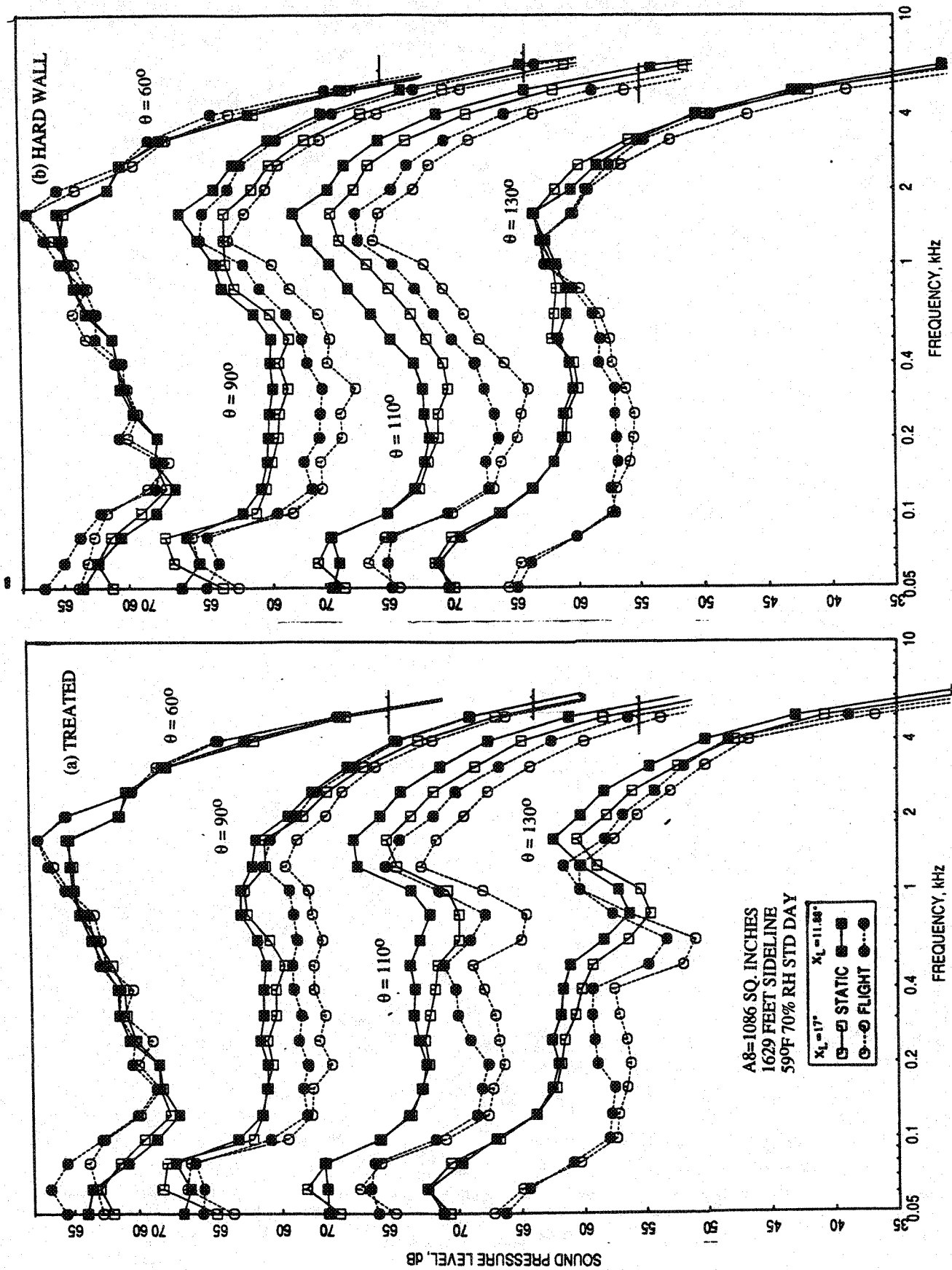
Figure 4.3-20. Effect of flight simulation and flap length on SPL spectra at various polar angles (θ) for a 10 and 9 full staggered CD-chute mixer-ejector at an azimuthal angle φ=25°. SAR=2.8, MAR=0.95, V_j = 1147 ft/sec, NPR = 1.5, T8 = 1000°R.
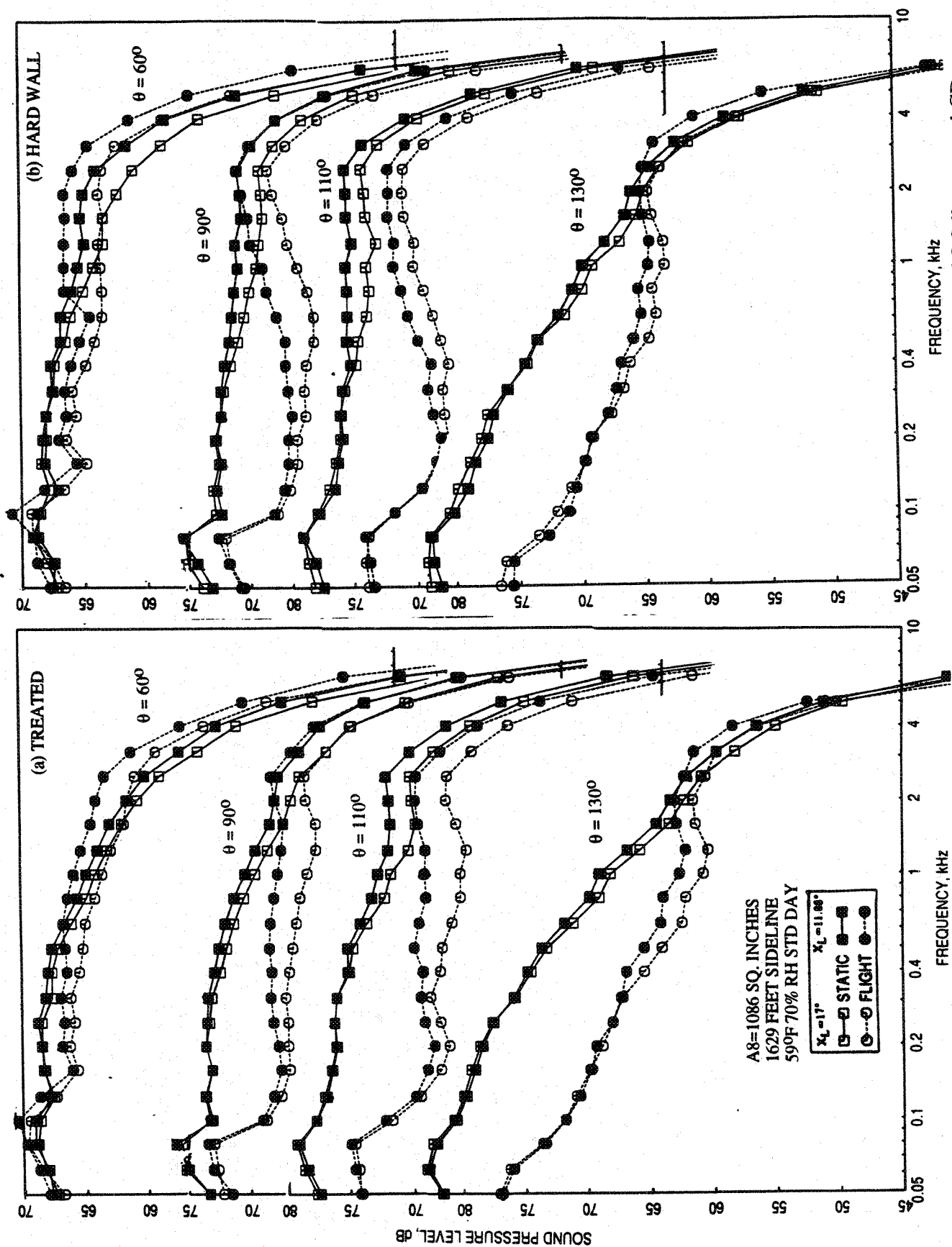
Figure 4.3-21. Effect of flight simulation and flap length on SPL spectra at various polar angles (θ) for a 10 and 9 full staggered CD-chute mixer-ejector at an azimuthal angle φ=25°; SAR=2.8, MAR=0.95, V_j = 1920 ft/sec, NPR = 2.5, T8 = 1325°R.
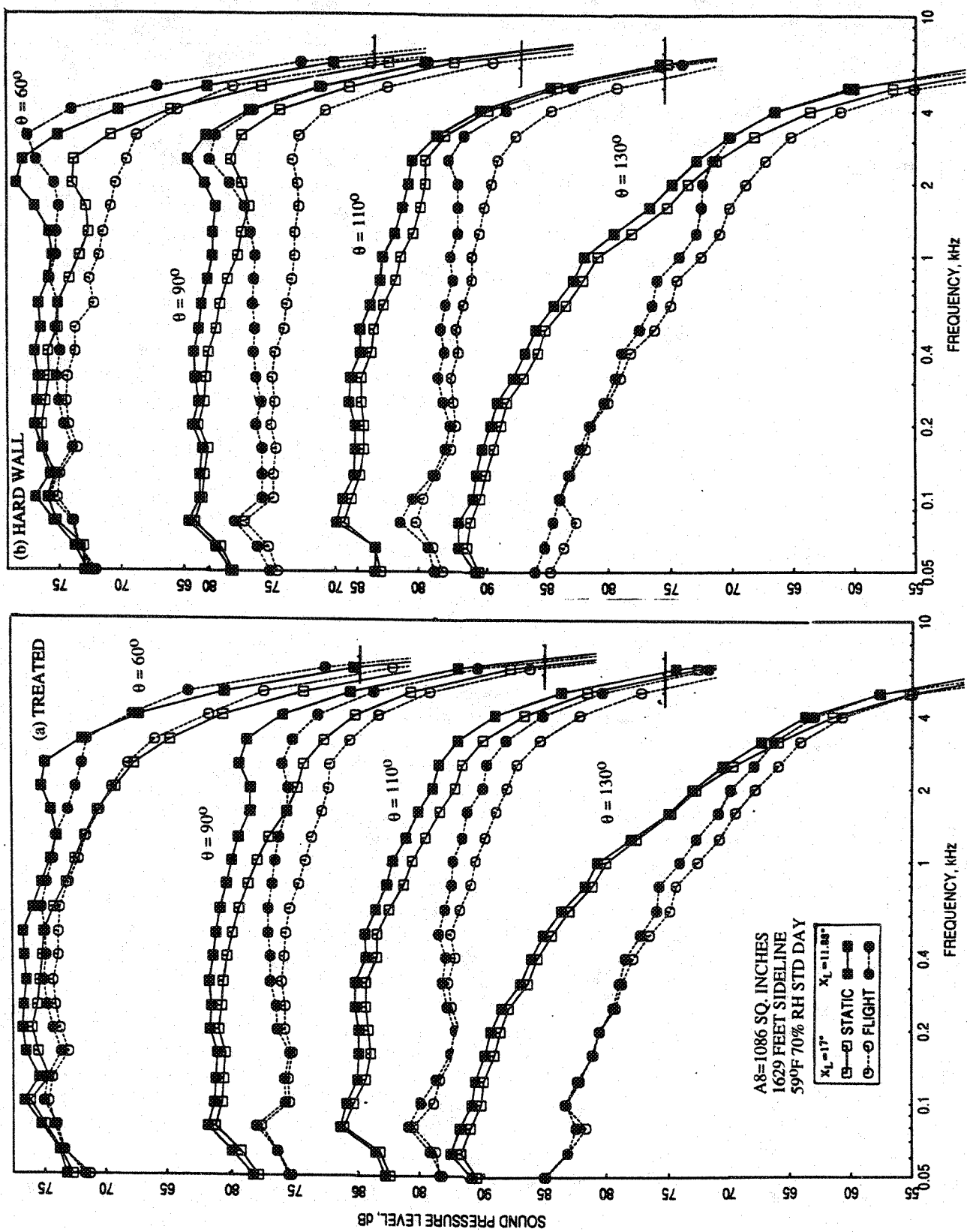
Figure 4.3-22. Effect of flight simulation and flap length on SPL spectra at various polar angles (θ) for a 10 and 9 full staggered CD-chute mixer-ejector at an azimuthal angle φ=25°; SAR=2.8, MAR=0.95, V_j = 2384 ft/sec, NPR = 3.4, T8 = 1590°R.
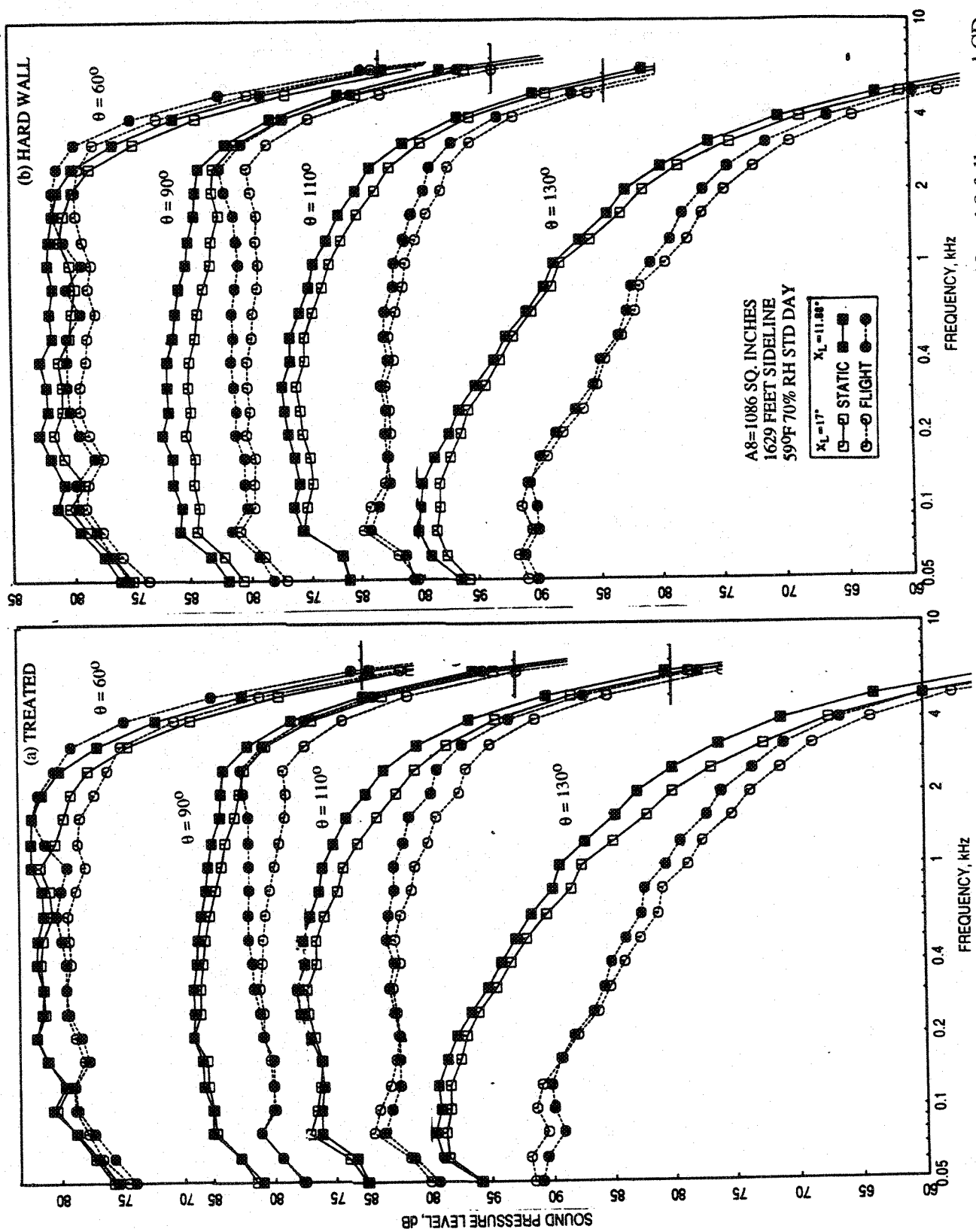
Figure 4.3-23. Effect of flight simulation and flap length on SPL spectra at various polar angles (θ) for a 10 and 9 full staggered CD-chute mixer-ejector at an azimuthal angle φ=25°. SAR=2.8, MAR=0.95, V_j = 2637 ft/sec, NPR = 4.0, T8 = 1750°R.
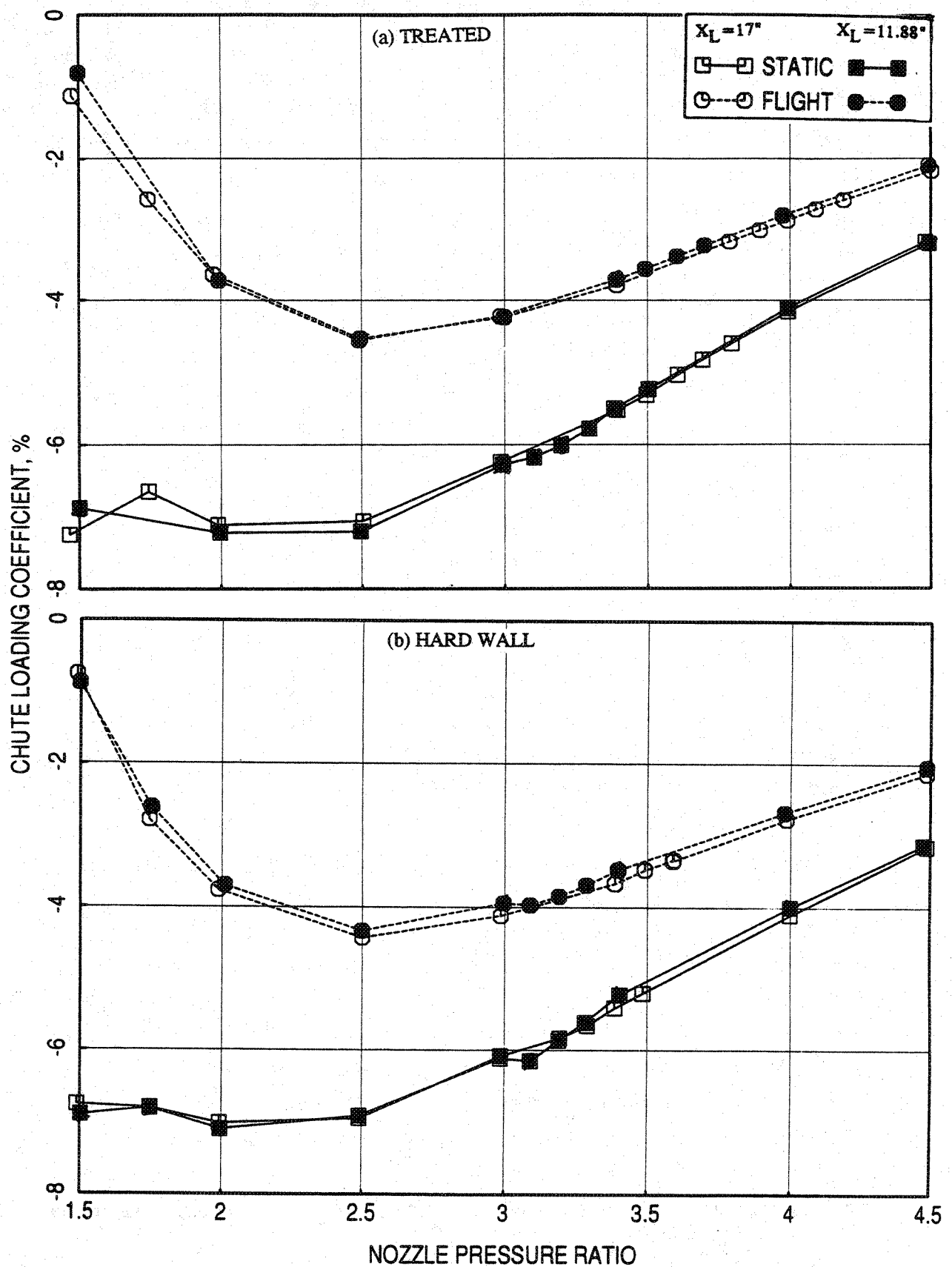
Figure 4.3-24. Effect of flight simulation and flap length on chute loading coefficient with respect to nozzle pressure ratio of L1M cycle conditions for a 10 and 9 full staggered CD-chute mixer-ejector; SAR=2.8, MAR=0.95.

length on pumping and corrected pumping is shown in Figures 4.3-25 and 4.3-26, respectively. The pumping increases significantly with flight simulation, since the total pressure at the inlet goes up. Even though, the pumping increases with flight, the effect is relatively small on the mixed jet velocity (see Figure 4.3-27).

Figure 4.3-28 shows the effect of flight and flap length on the average axial static pressure distributions on the inlet and the flap surface at different L1M cycle conditions. Small amount of pressure increase on the inlet and the flap due to flight simulation is noted at lower NPR conditions. However, the effect of flight simulation is significant on the flap surface close to the transition from subsonic to supersonic mode and at supersonic mode conditions. The effect of flight and flap length on normalized force due to static pressure difference on flap surface is shown in Figure 4.3-29. The force decreases slightly with flight simulation due to increased static pressure on the flap surface. The transition from subsonic to supersonic mode seems to be slightly delayed with respect to NPR due to flight simulation. Similar is the effect due to the longer ejector compared to the shorter configuration.

4.3.2. Azimuthal Variation of Farfield Noise

Acoustic data was acquired at sideline ($\phi=25^\circ$) and community ($\phi=90^\circ$) locations with respect to the ejector major axis using traversing microphone array and at an in-between location of $\phi=45^\circ$ using the fixed microphone array of Cell 41 facility (see Figure 4.3-5). Acoustic results are compared between these three locations to examine the azimuthal characteristics of farfield noise for the four CD 9-chute staggered mixer-ejector configurations, namely, hardwalled and treated ejectors with short and long flaps.

Figures 4.3-30 and 4.3-31 show the variation of EPNL and peak PNLT for different ejector configurations with respect to the L1M cycle points at three azimuthal locations. For all conditions the noise level in terms of EPNL and peak PNLT is higher at the community point compared to the sideline for all four configurations. The difference of noise levels between these two locations generally increases with decreasing jet velocity. Most cases the noise levels, in terms of EPNL and peak PNLT, at $\phi=45^\circ$ lie between the sideline and the community point levels, and are very close to the sideline levels. Based on the $\phi=45^\circ$ location on the mixer-ejector cross section (see Figure 4.3-5), the azimuthal variation of EPNL and peak PNLT are more dominant on the flap side, closer to the community location. Figures 4.3-32 and 4.3-33 show the variation of PNLT at polar angles of $\theta=60^\circ$ and $\theta=90^\circ$, respectively for different ejector configurations with respect to the L1M cycle
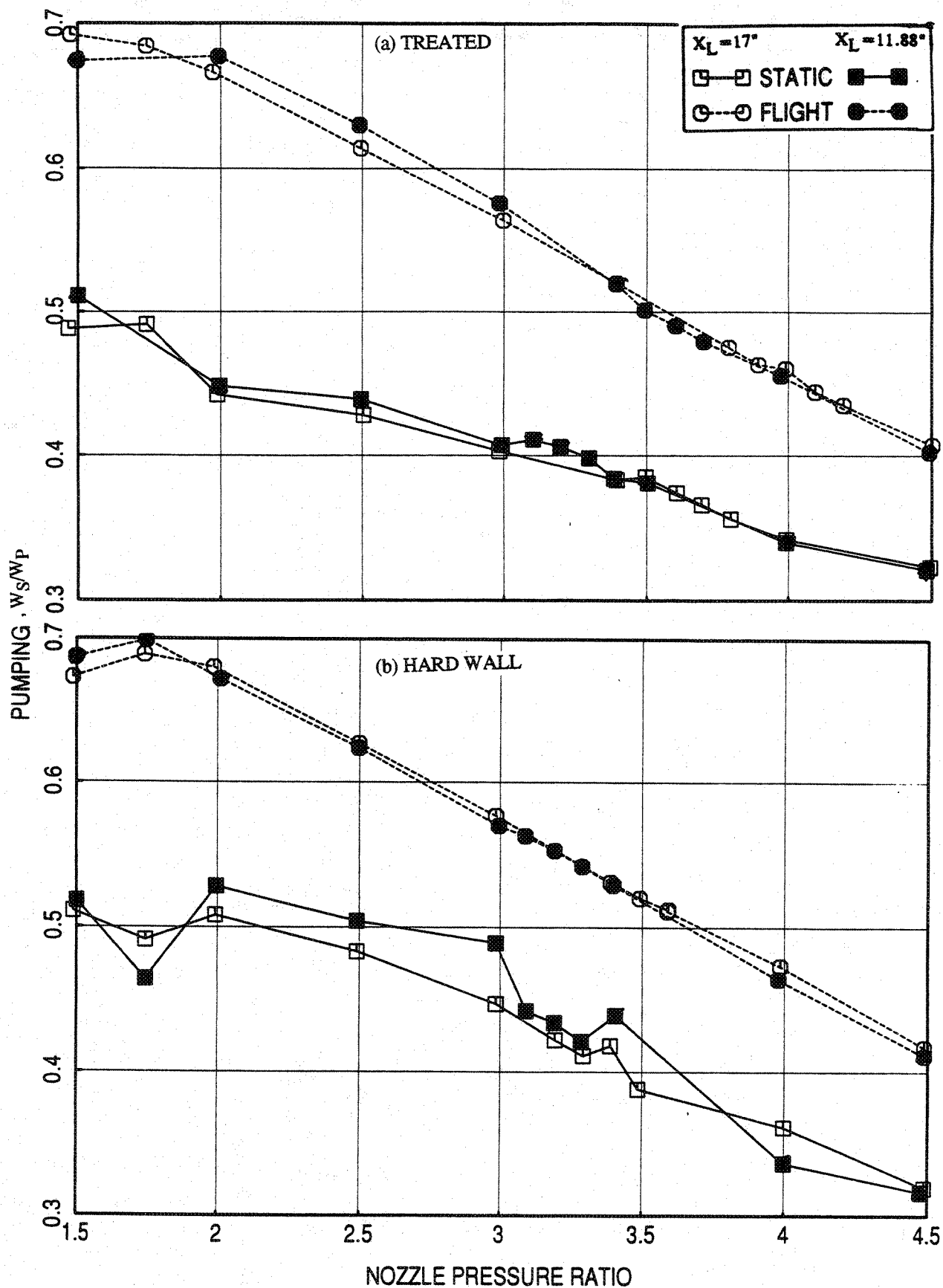
Figure 4.3-25. Effect of flight simulation and flap length on pumping with respect to nozzle pressure ratio of L1M cycle conditions for a 10 and 9 full staggered CD-chute mixer-ejector; SAR=2.8, MAR=0.95.

Figure 4.3-26. Effect of flight simulation and flap length on corrected pumping with respect to nozzle pressure ratio of L1M cycle conditions for a 10 and 9 full staggered CD-chute mixer-ejector; SAR=2.8, MAR=0.95.

Figure 4.3-27. Effect of flight simulation and flap length on mixed jet velocity with respect to nozzle pressure ratio of L1M cycle conditions for a 10 and 9 full staggered CD-chute mixer-ejector; SAR=2.8, MAR=0.95.
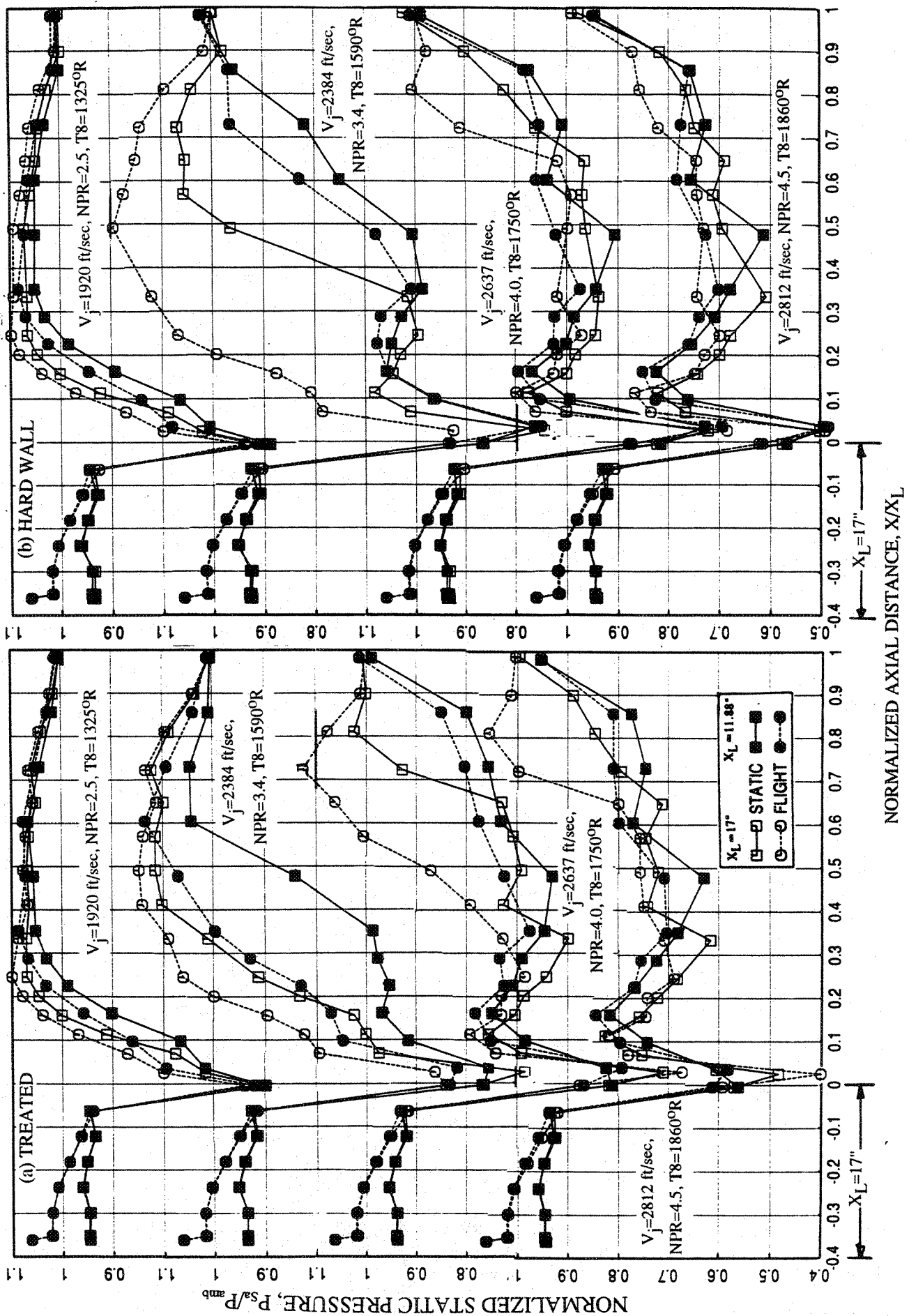
Figure 4.3-28. Effect of flight simulation and flap length on axial average static pressure distributions on the inlet and the flap surface at different L1M cycle conditions for a 10 and 9 full staggered CD-chute mixer-ejector SAR=2.8, MAR=0.95.
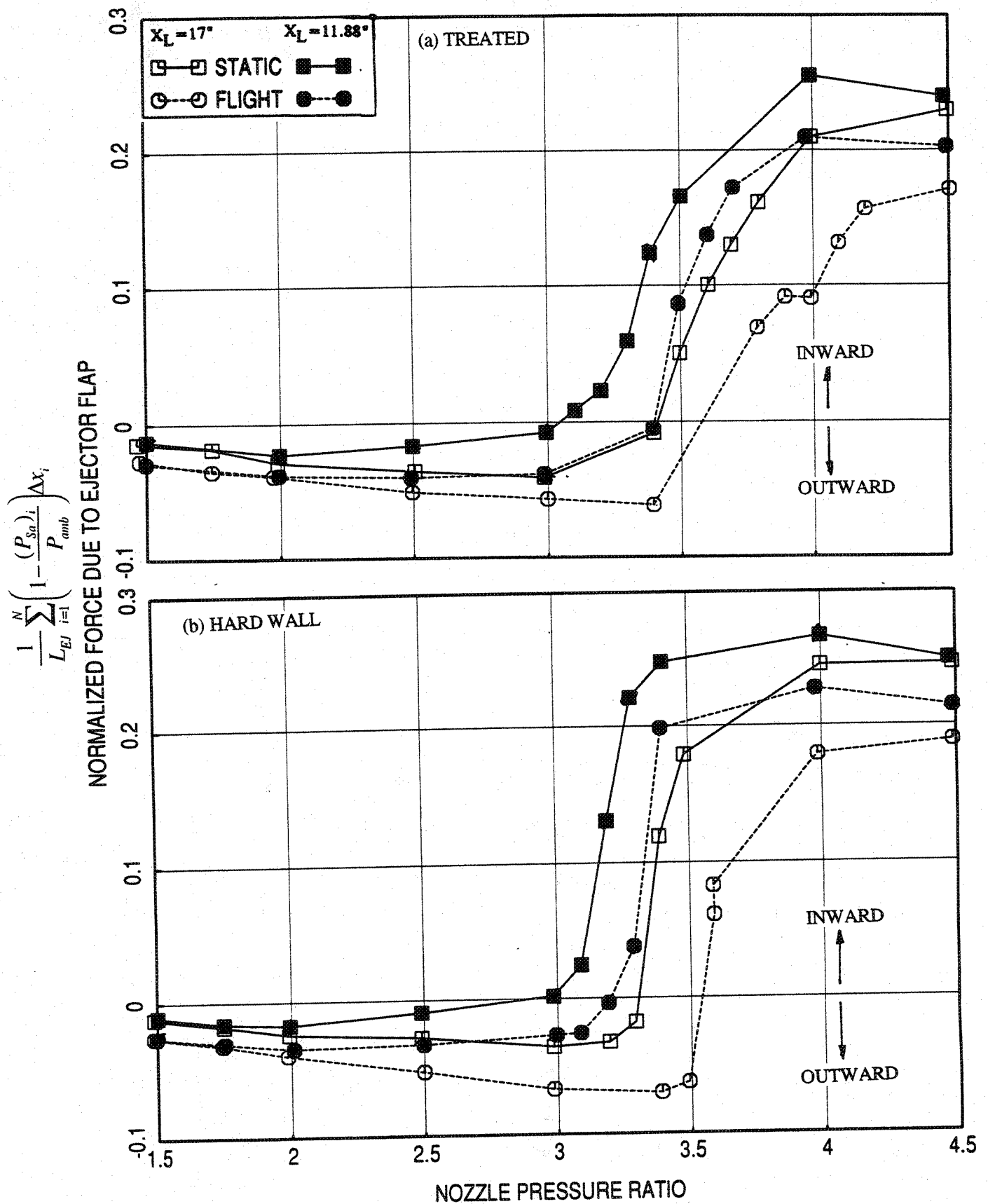
Figure 4.3-29. Effect of flight simulation and flap length on normalized force due to ejector flap with respect to nozzle pressure ratio of L1M cycle conditions for a 10 and 9 full staggered CD-chute mixer-ejector SAR=2.8, MAR=0.95.
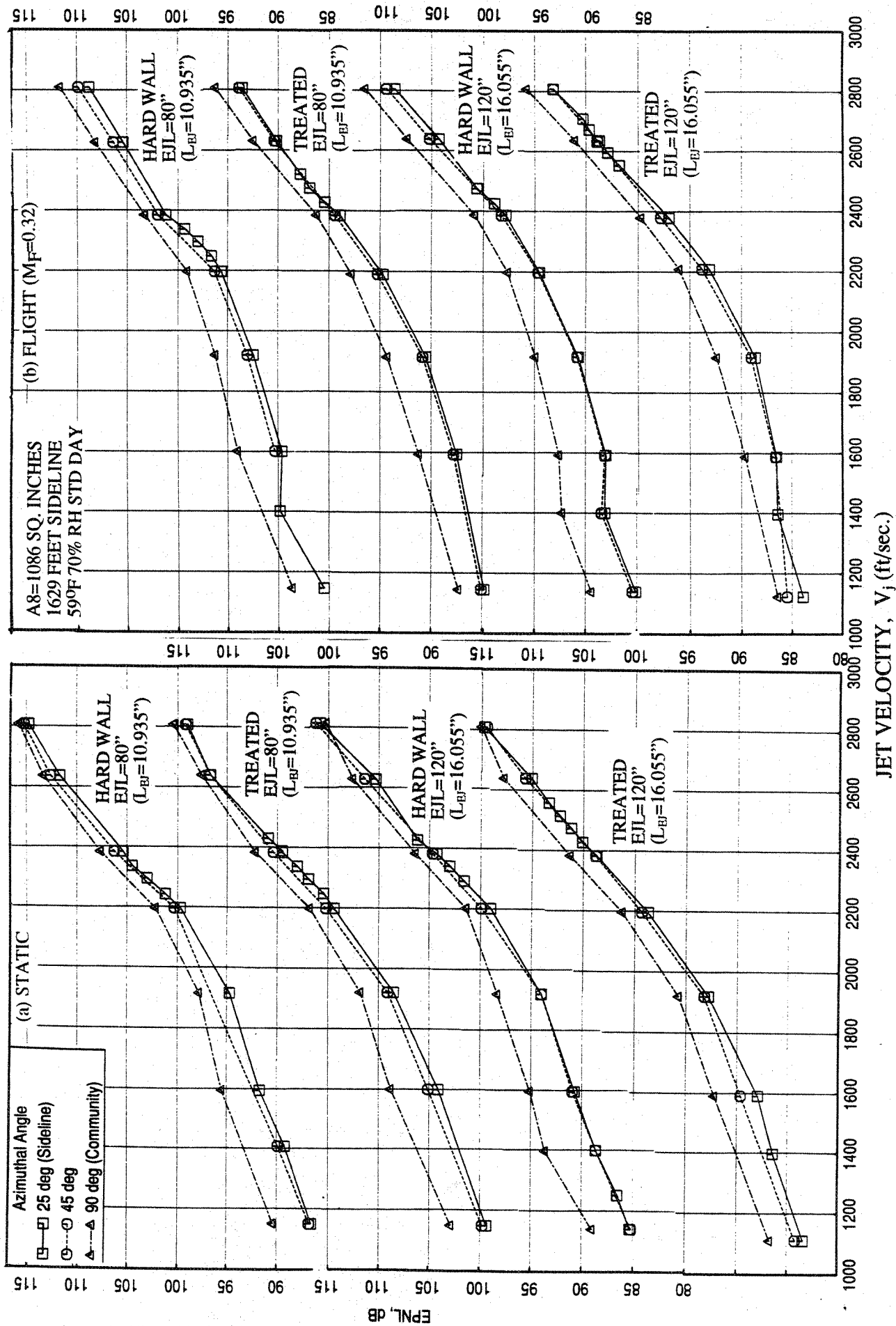
Figure 4.3-30. Effect of flap length and ejector treatment on azimuthal variation of EPNL with respect to the L1M cycle points for a 10 and 9 full staggered CD-chute mixer-ejector, SAR=2.8, MAR=0.95.
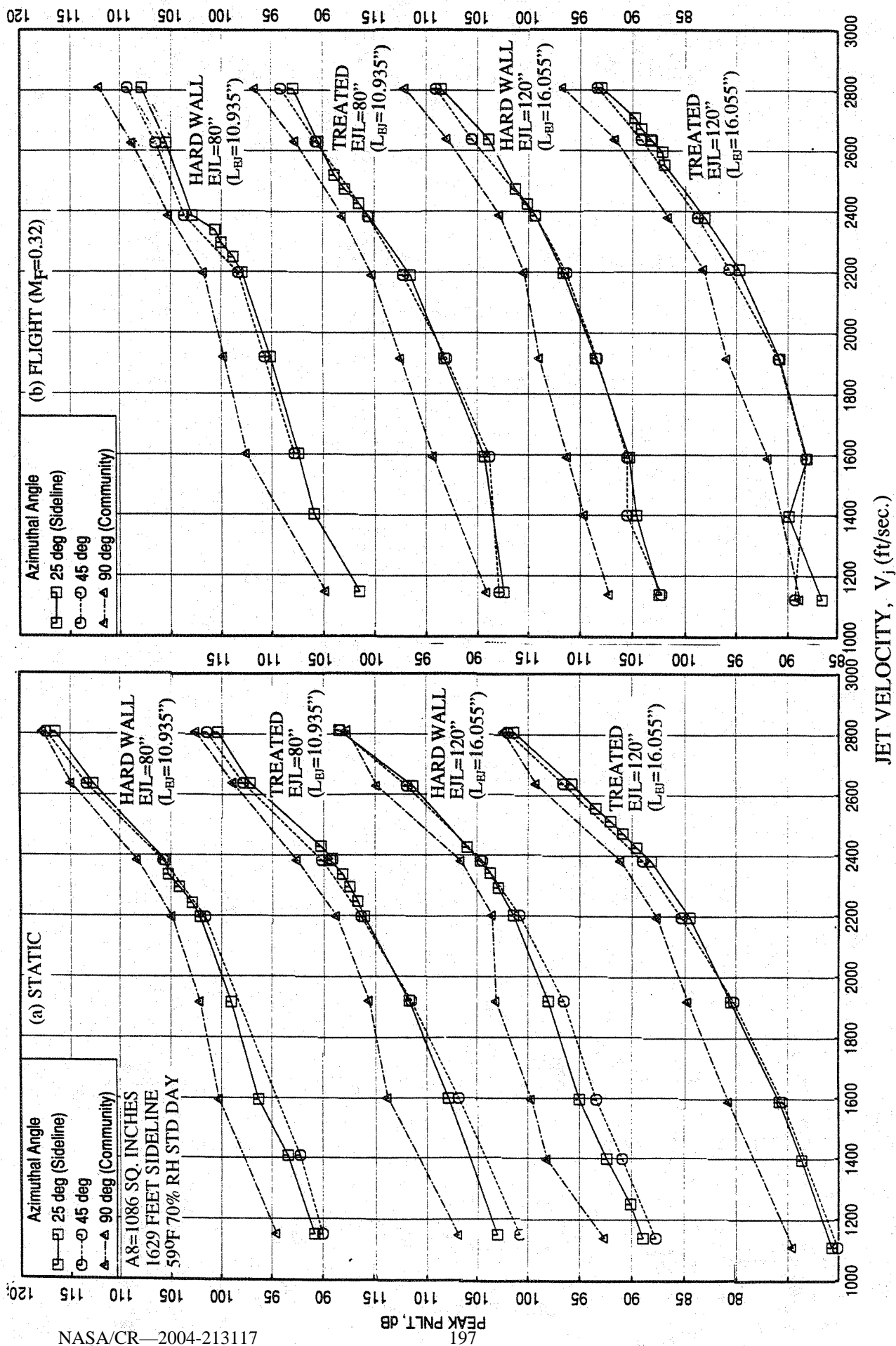
Figure 4.3-31. Effect of flap length and ejector treatment on azimuthal variation of peak PNLT with respect to the L1M cycle points for a 10 and 9 full staggered CD-chute mixer-ejector, SAR=2.8, MAR=0.95.
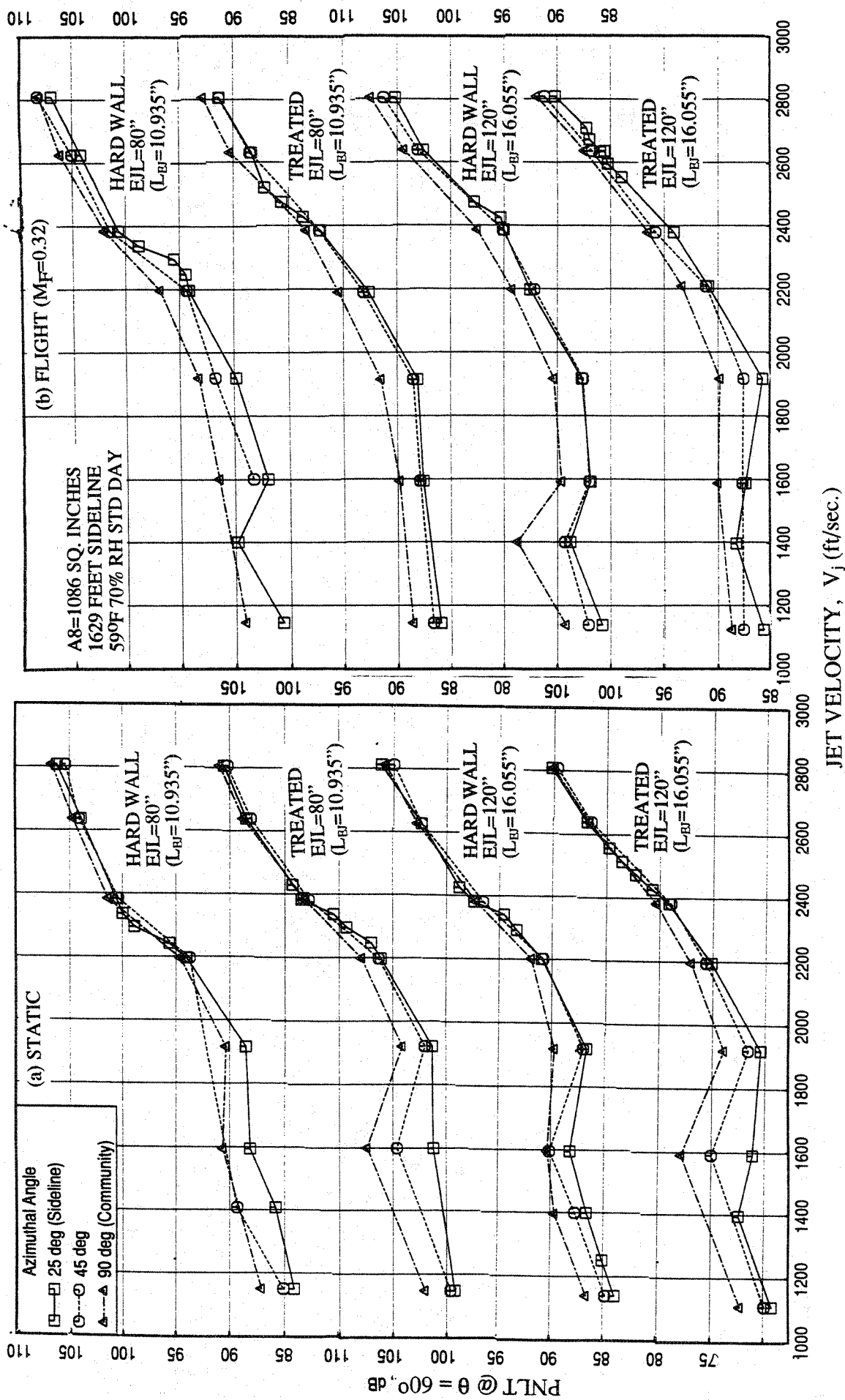
Figure 4.3-32. Effect of flap length and ejector treatment on azimuthal variation of PNLT at θ=60° with respect to the L1M cycle points for a 10 and 9 full staggered CD-chute mixer-ejector, SAR=2.8, MAR=0.95.
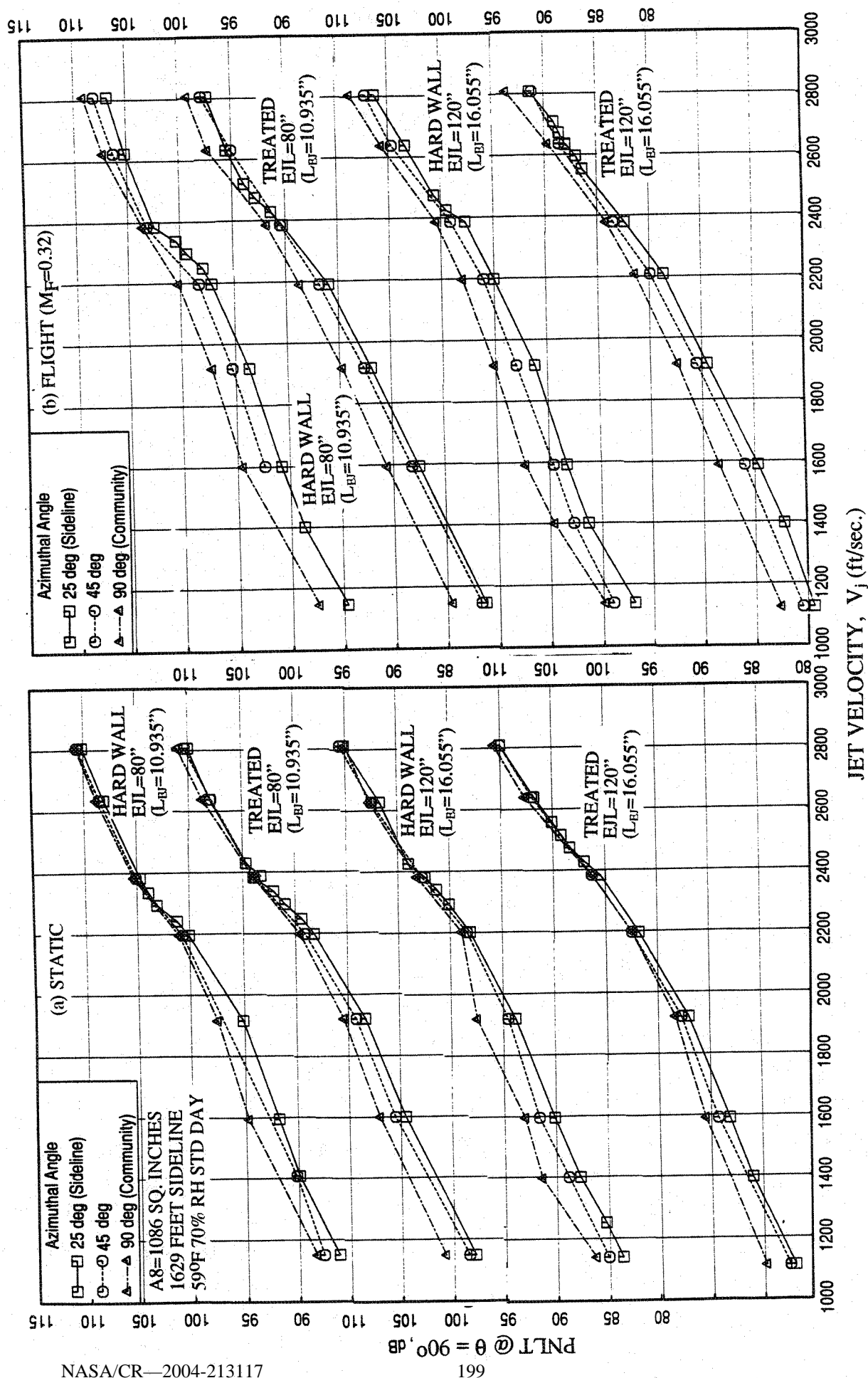
Figure 4.3-33. Effect of flap length and ejector treatment on azimuthal variation of PNLT at θ=90° with respect to the L1M cycle points for a 10 and 9 full staggered CD-chute mixer-ejector, SAR=2.8, MAR=0.95.

points at three azimuthal locations. For all conditions the noise level in terms PNLT is higher at the community point compared to the sideline. The difference of noise levels between these two locations generally increases with decreasing jet velocity. Most cases the noise levels, in terms PNLT, at $\phi=45^\circ$ lie between the sideline and the community point levels, and are relatively closer to sideline levels. Noise level difference between community and sideline locations in terms of EPNL and PNLT is higher with flight simulation. In addition, compared to treated configurations the noise level difference is higher for hardwalled configurations.

Azimuthal variation of PNLT directivities for different ejector configurations are plotted in Figures 4.3-34 through 4.3-37 for four different L1M cycle conditions. For all configurations the PNLT levels are higher at the community point compared to the sideline at most polar angles. The difference of PNLT between the sideline and community, in general, decreases with increasing jet velocity. At higher velocities the azimuthal variation of PNLT is small in the forward arc at static condition. However, with flight simulation the azimuthal variation of PNLT is equally significant at all polar angles. Similar results for SPL spectra for three L1M cycle conditions are plotted for three polar angles in Figures 4.3-38 through 4.3-46. The azimuthal variation of SPL is more dominant in the high frequency range, above 400 Hz (corresponding model scale frequency being 3000 Hz). The SPL levels are higher at the community compared to the sideline location. The difference decreases with increasing jet velocity. With respect to polar angle, the SPL difference between sideline and community is higher in the rear arc. The impact of treatment is to reduce the azimuthal noise variation. Similarly, the azimuthal variation in terms of SPL is lower for long flap compared to short flap. With flight simulation the azimuthal variation of SPL increases.

One of the reasons for azimuthal variation of noise is the aspect ratio effect of the rectangular ejector. It is well known that the azimuthal variation of jet mixing noise increases with increasing aspect ratio. For the mixer-ejector under consideration the aspect ratio of the ejector is about 1.51, which is significant to introduce azimuthal variation of jet mixing noise. However, the farfield noise for mixer-ejector type nozzles is not entirely due to the jet mixing or externally generated noise. Some contribution is due to the radiation of internally generated noise. This is evident from the fact that the azimuthal variation is higher for hardwalled ejector, for which most internally generated noise is radiated out. In addition, the azimuthal variation is higher for flight simulation case, for which jet-mixing noise is reduced due to dynamic effects, resulting in more dominant internally radiated noise.
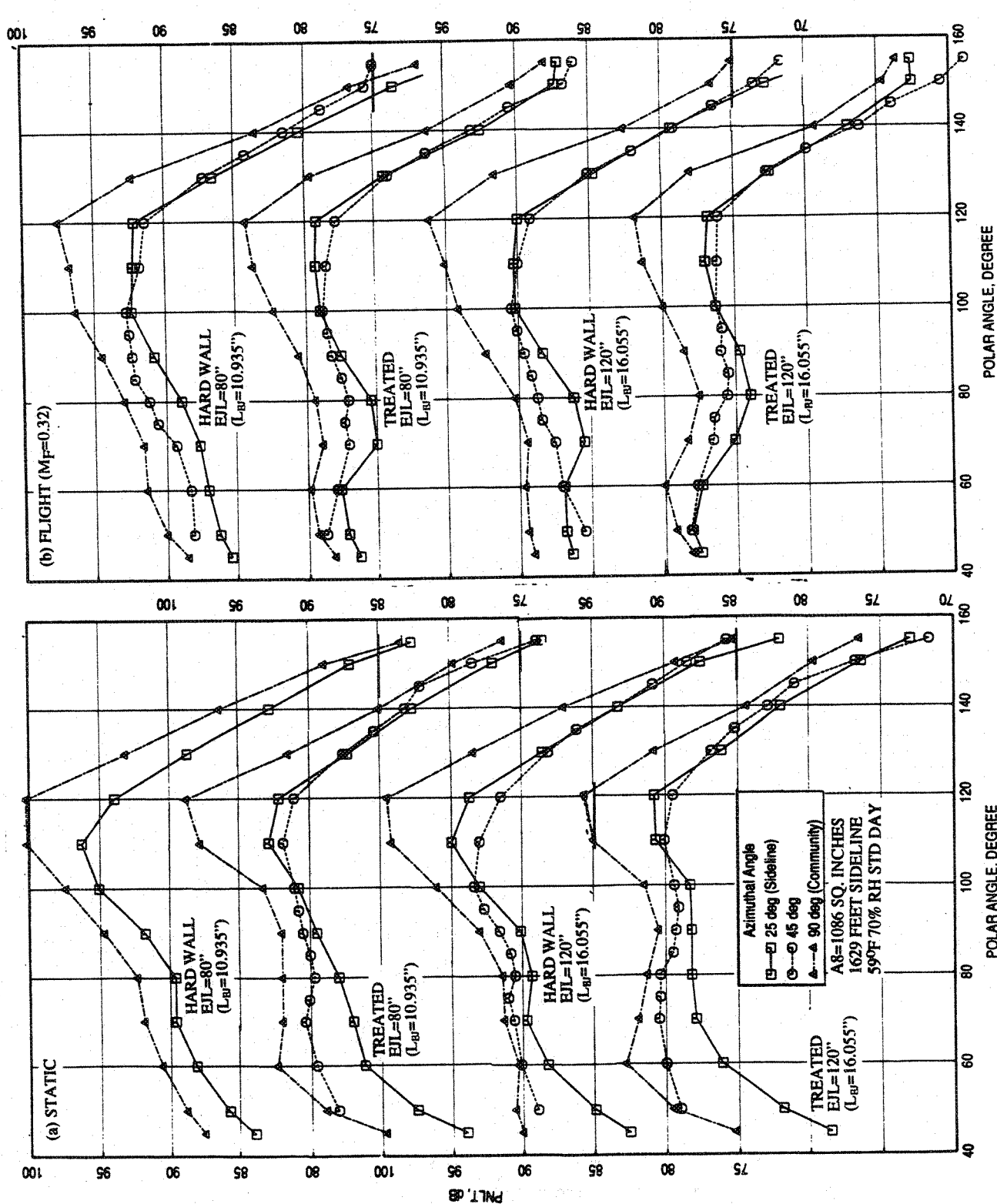
Figure 4.3-34. Effect of flap length and ejector treatment on azimuthal variation of PNLT directivity for a 10 and 9 full staggered CD-chute mixer-ejector, SAR=2.8, MAR=0.95", V$_j$ = 1595 ft/sec, NPR = 2.0, T8 = 1175°R.
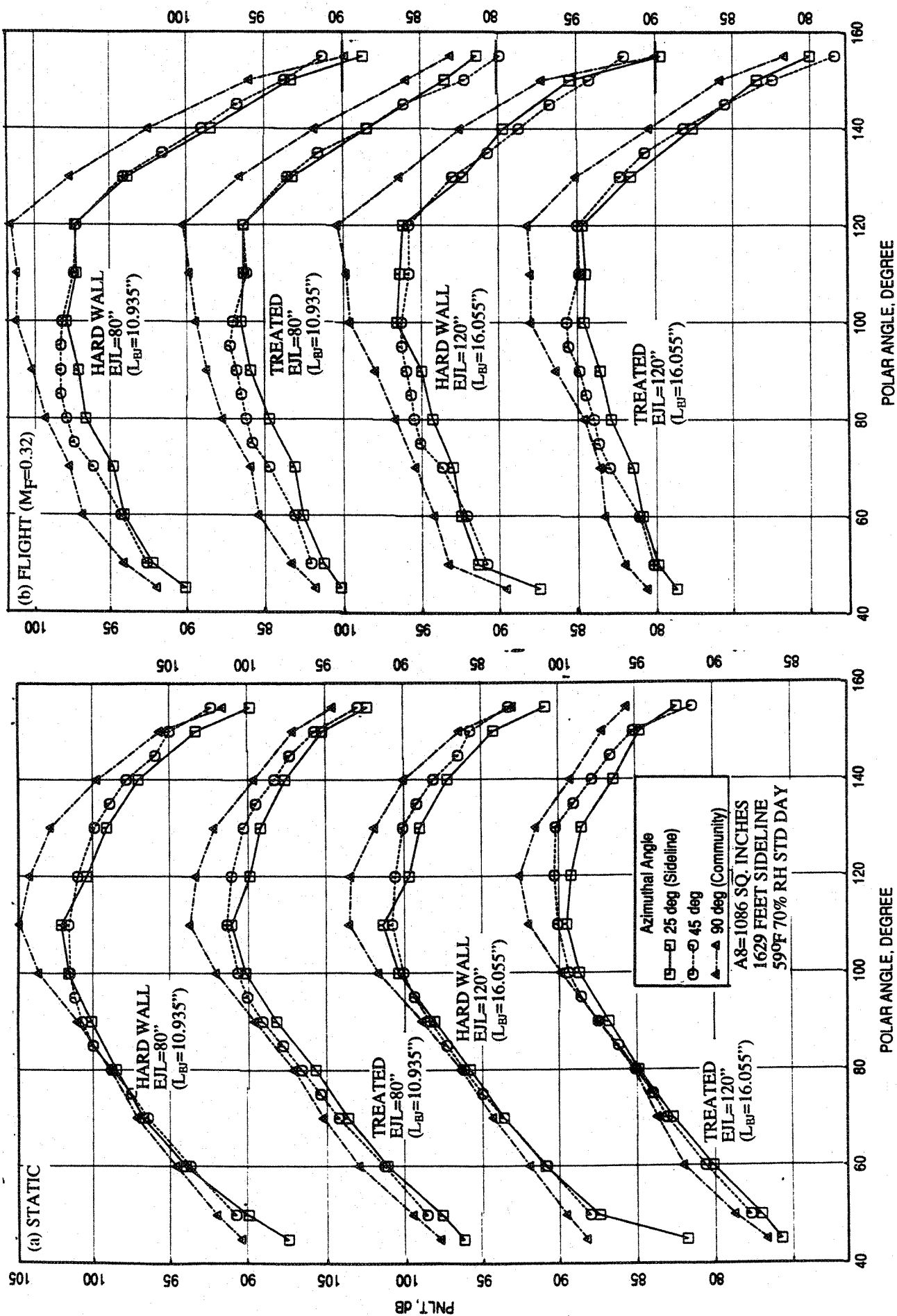
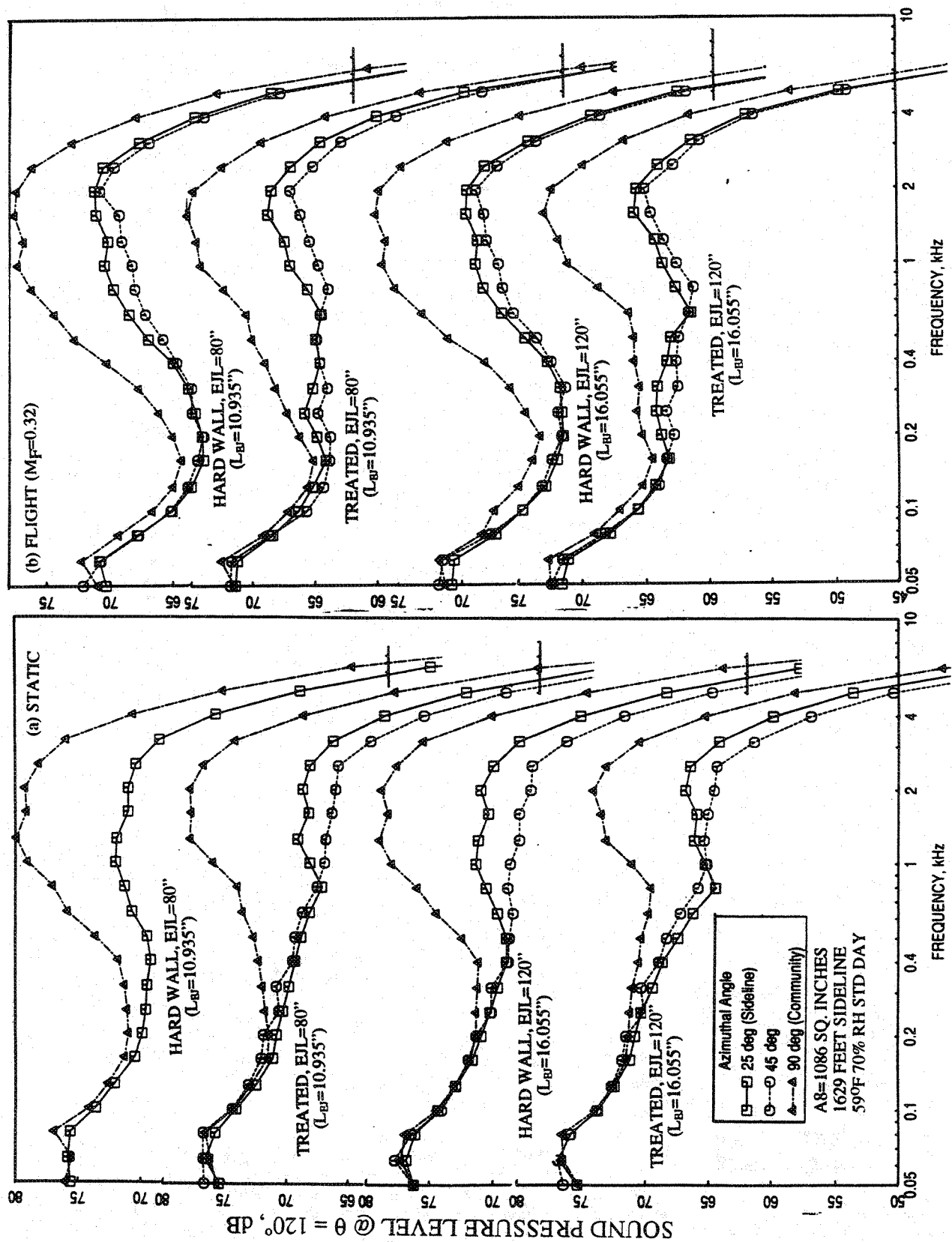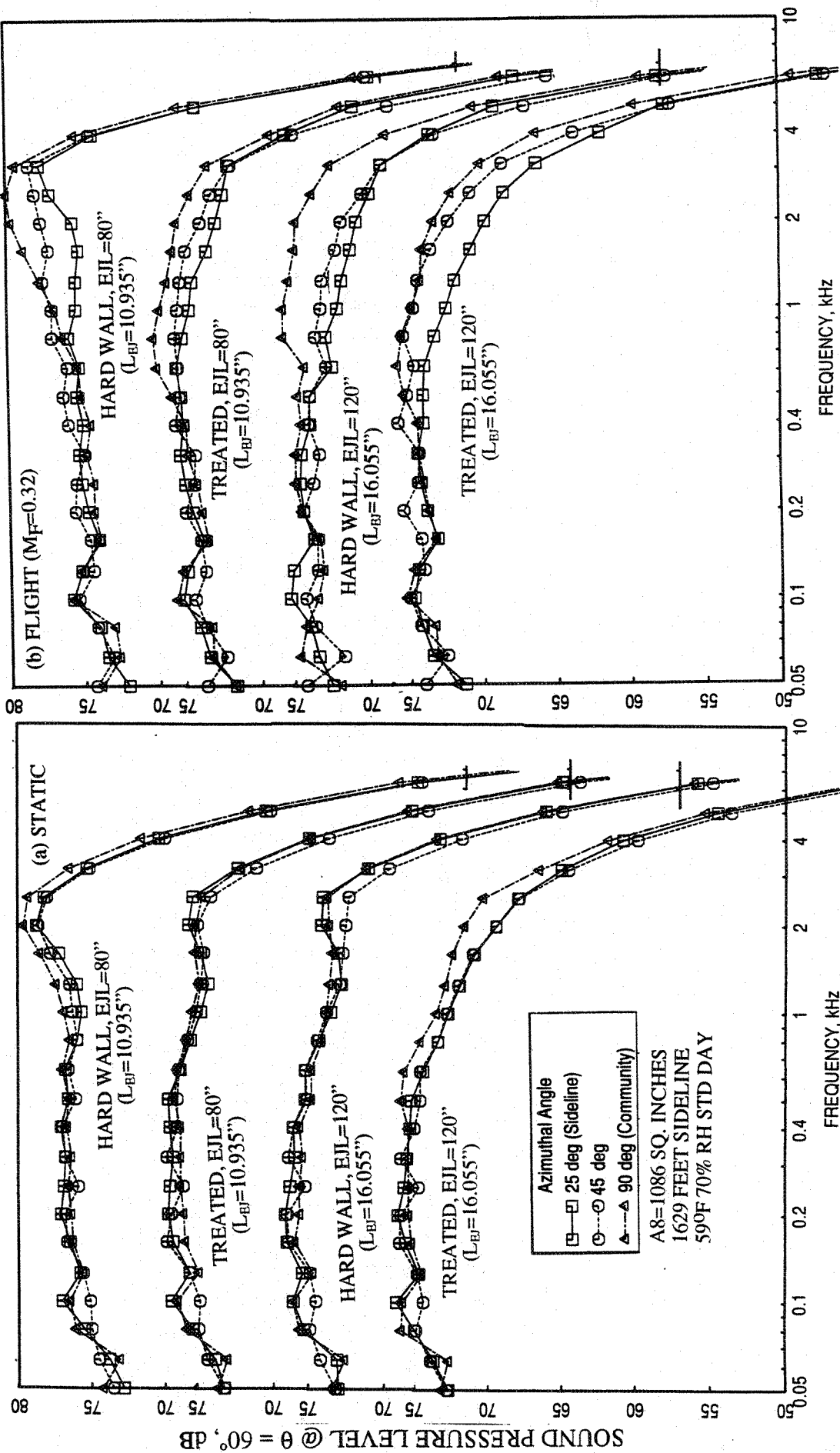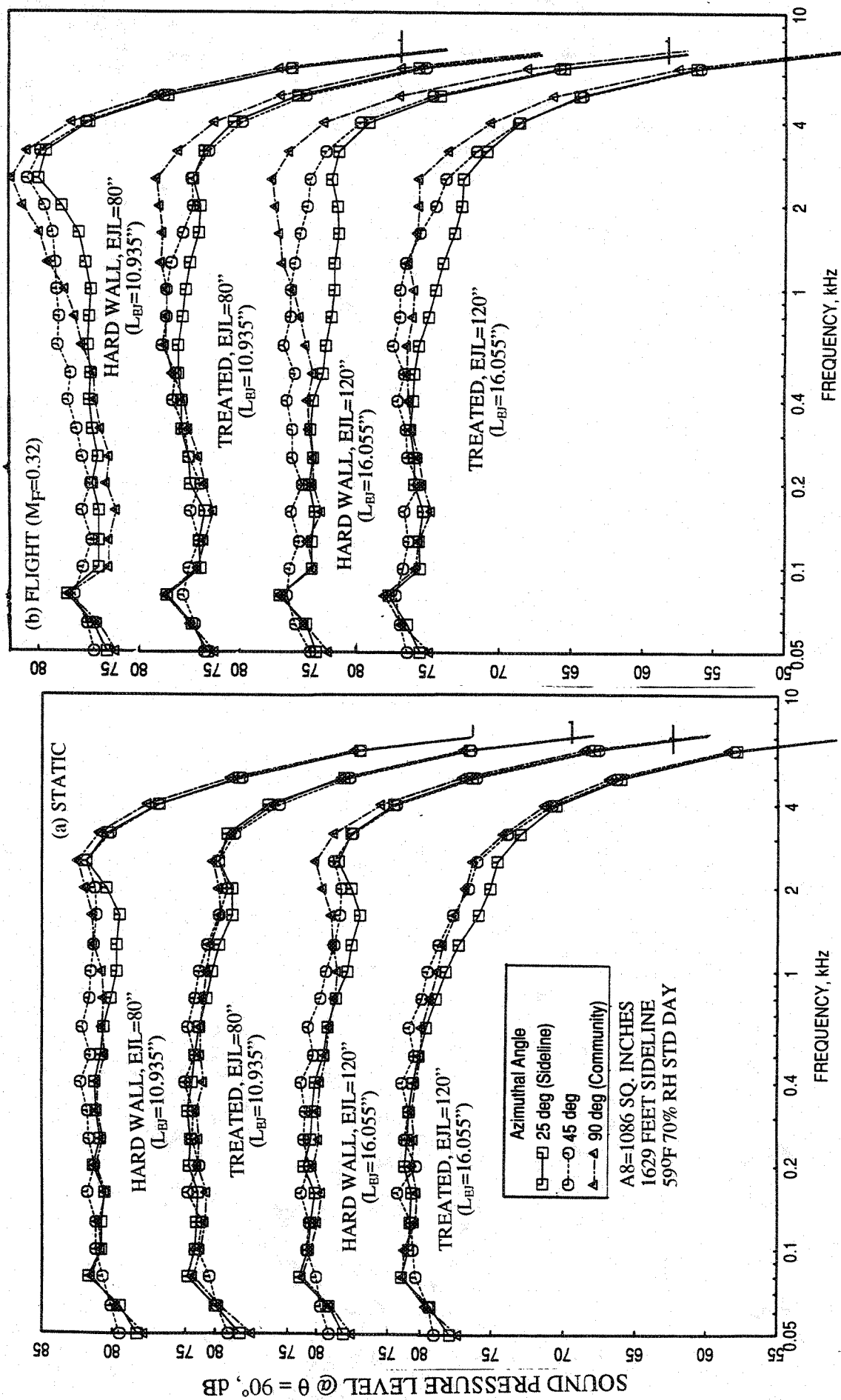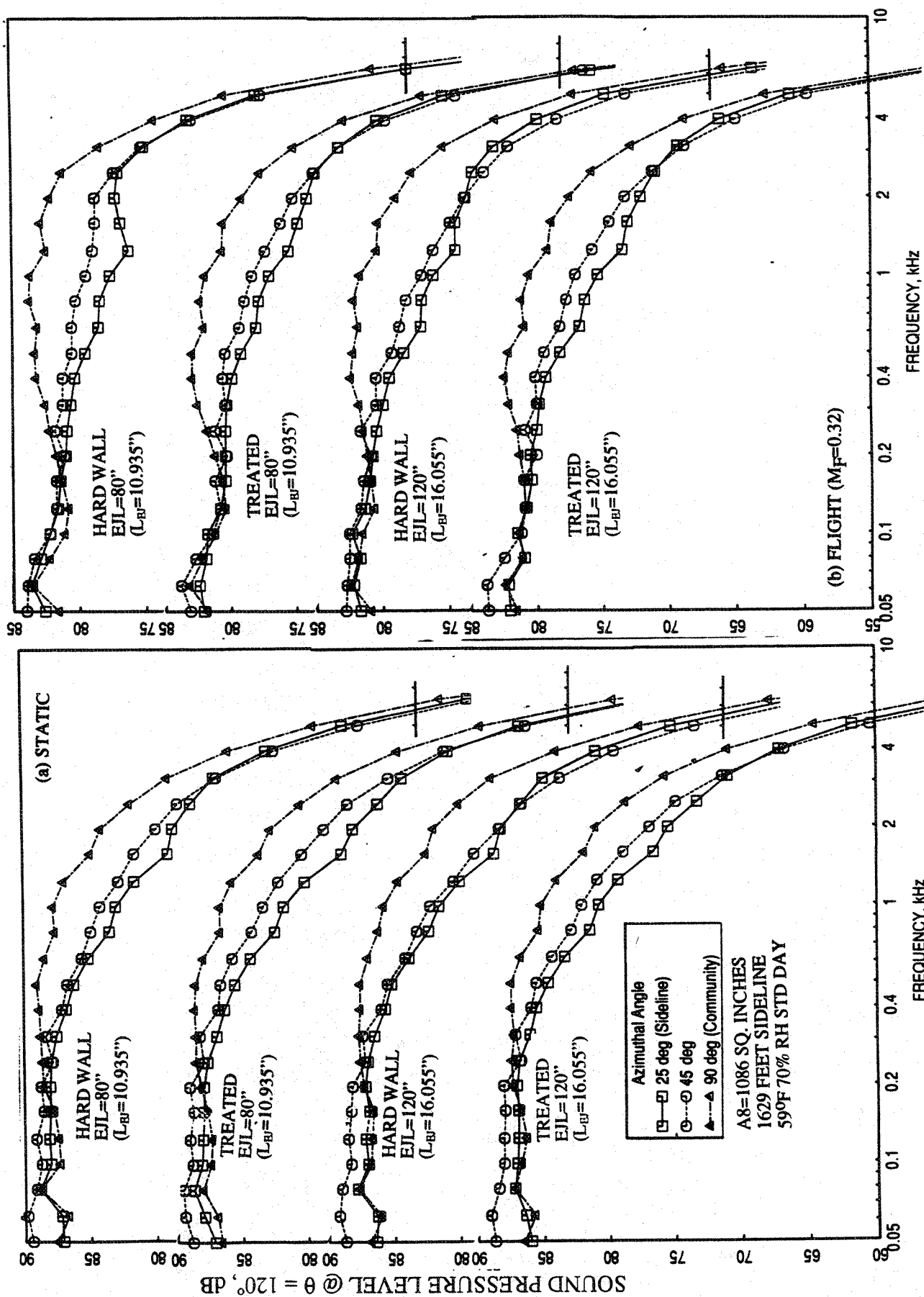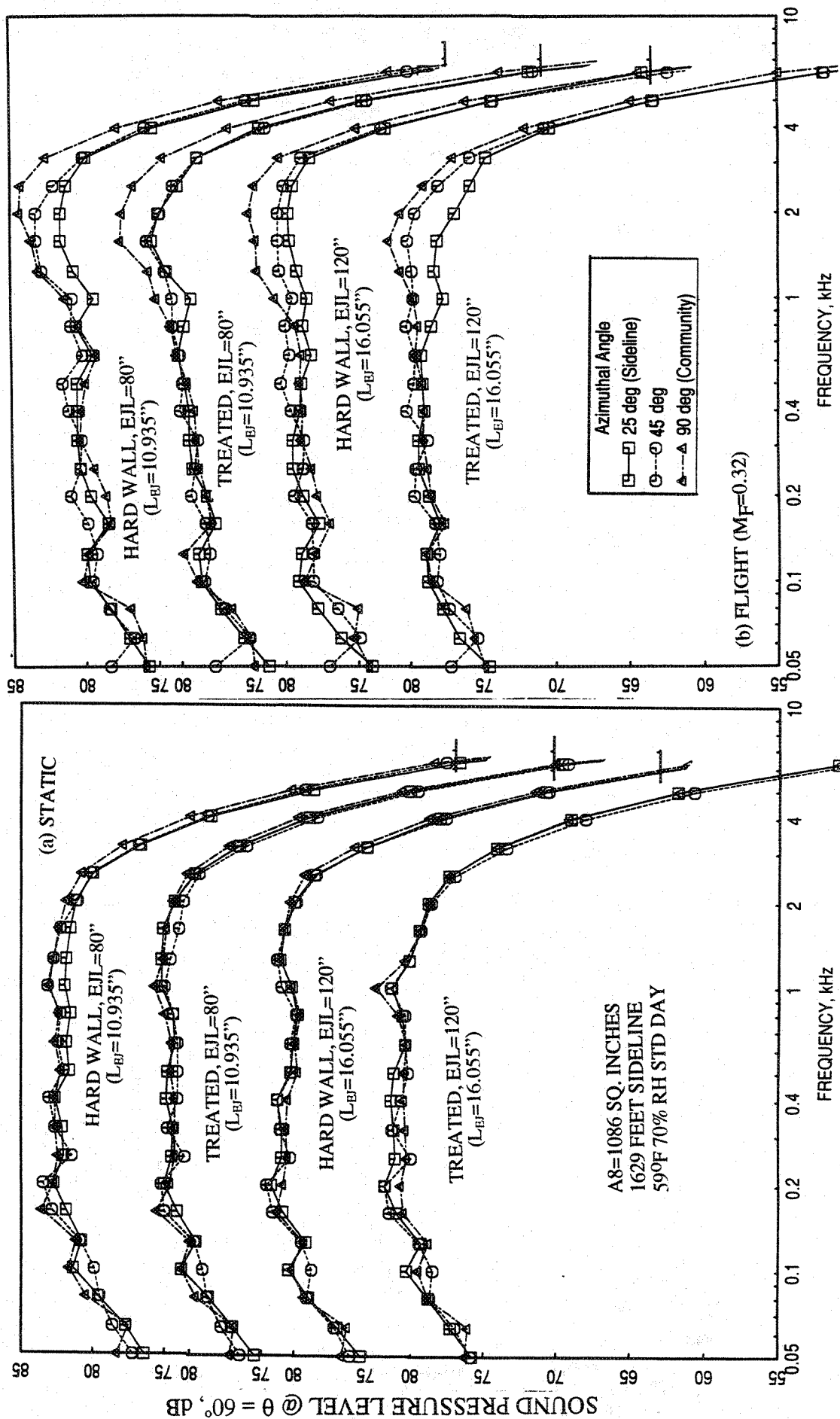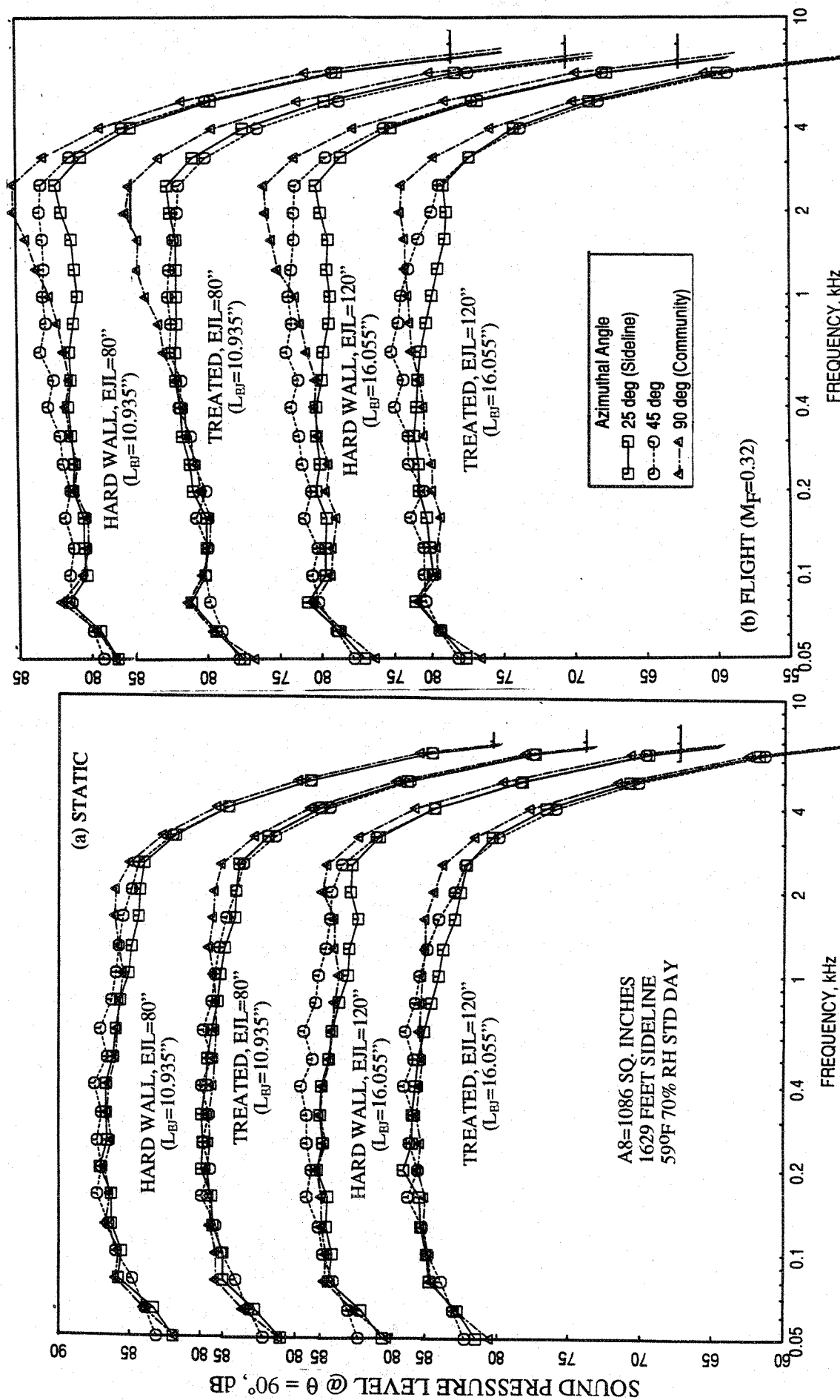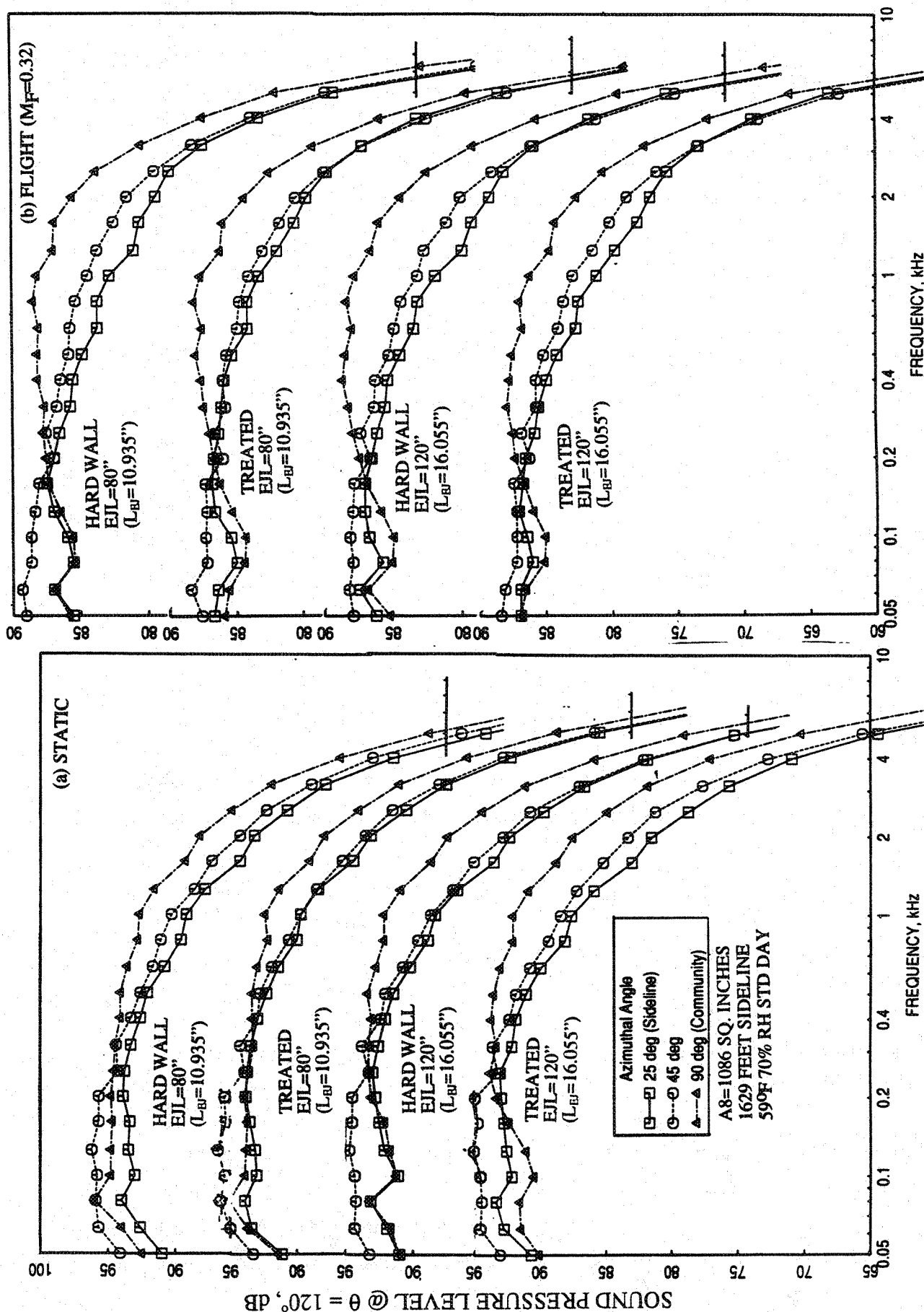Figure 4.3-35. Effect of flap length and ejector treatment on azimuthal variation of PNLT directivity for a 10 and 9 full staggered CD-chute mixer-ejector, SAR=2.8, MAR=0.95", V_j = 2200 ft/sec, NPR = 3.0, T8 = 1485°R.
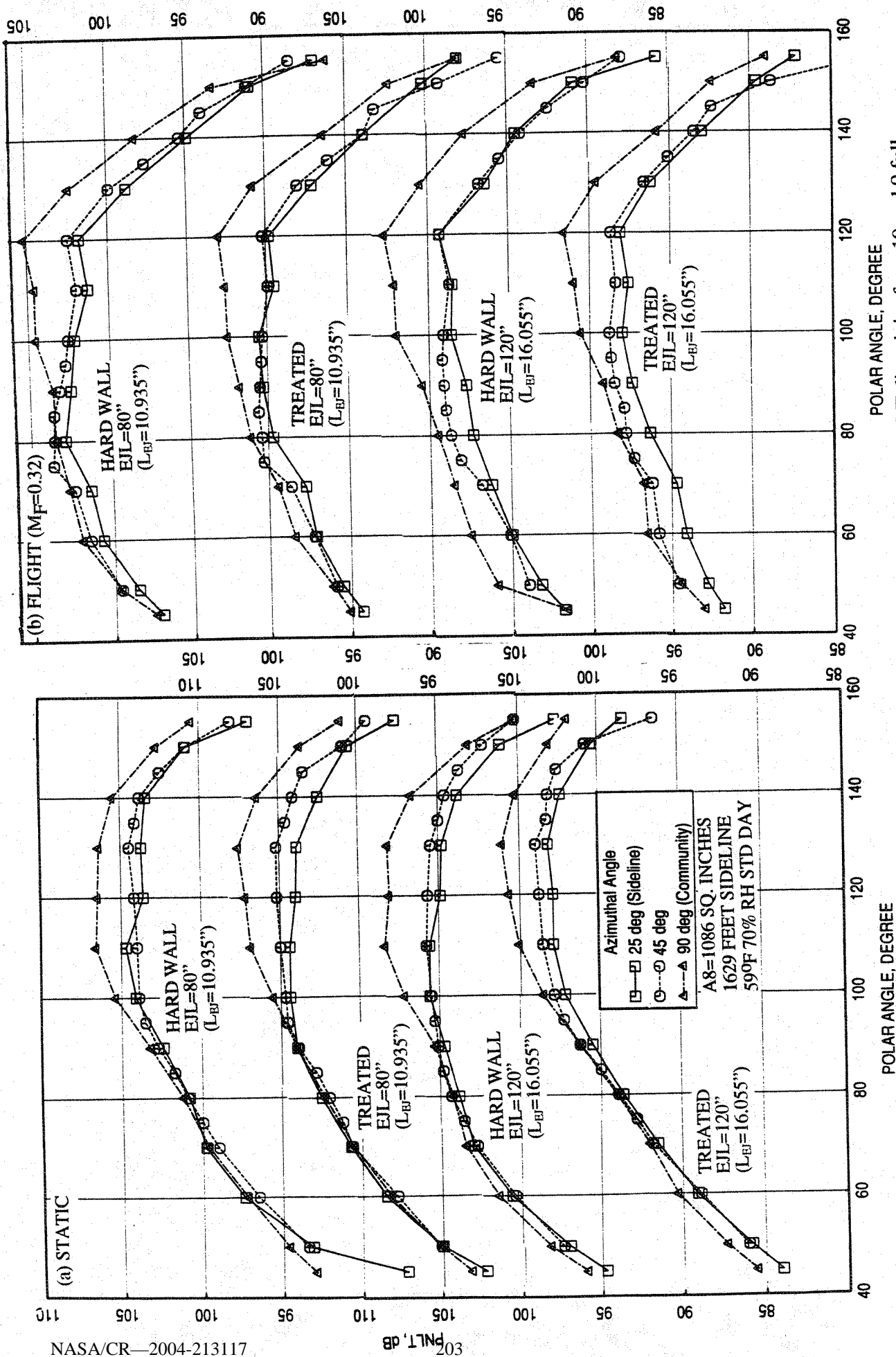
Figure 4.3-36. Effect of flap length and ejector treatment on azimuthal variation of PNLT directivity for a 10 and 9 full staggered CD-chute mixer-ejector, SAR=2.8, MAR=0.95", V_j = 2384 ft/sec, NPR = 3.4, T8 = 1590°R.
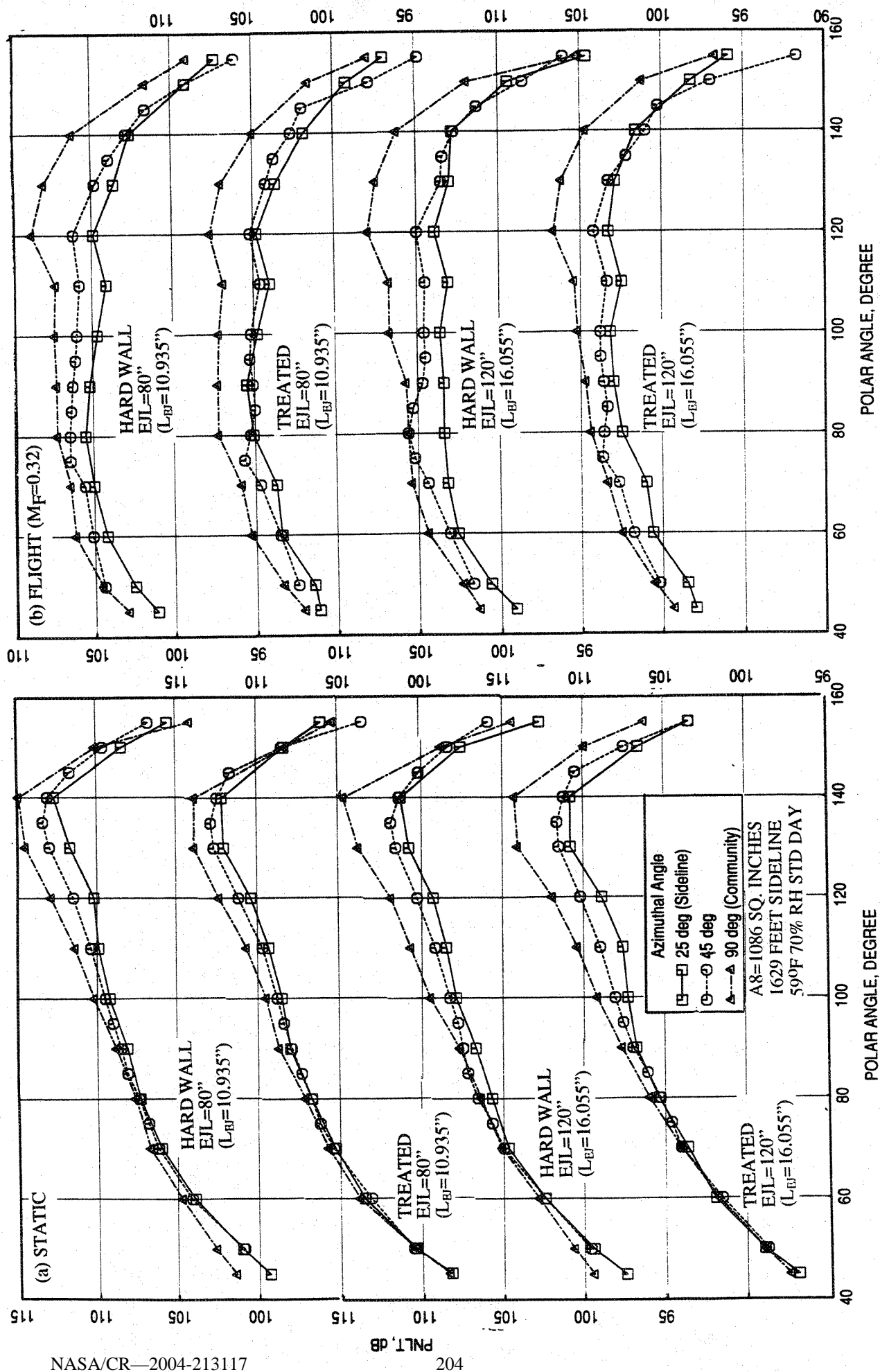
Figure 4.3-37. Effect of flap length and ejector treatment on azimuthal variation of PNLT directivity for a 10 and 9 full staggered CD-chute mixer-ejector, SAR=2.8, MAR=0.95", V_j = 2637 ft/sec, NPR = 4.0, T8 = 1750°R.
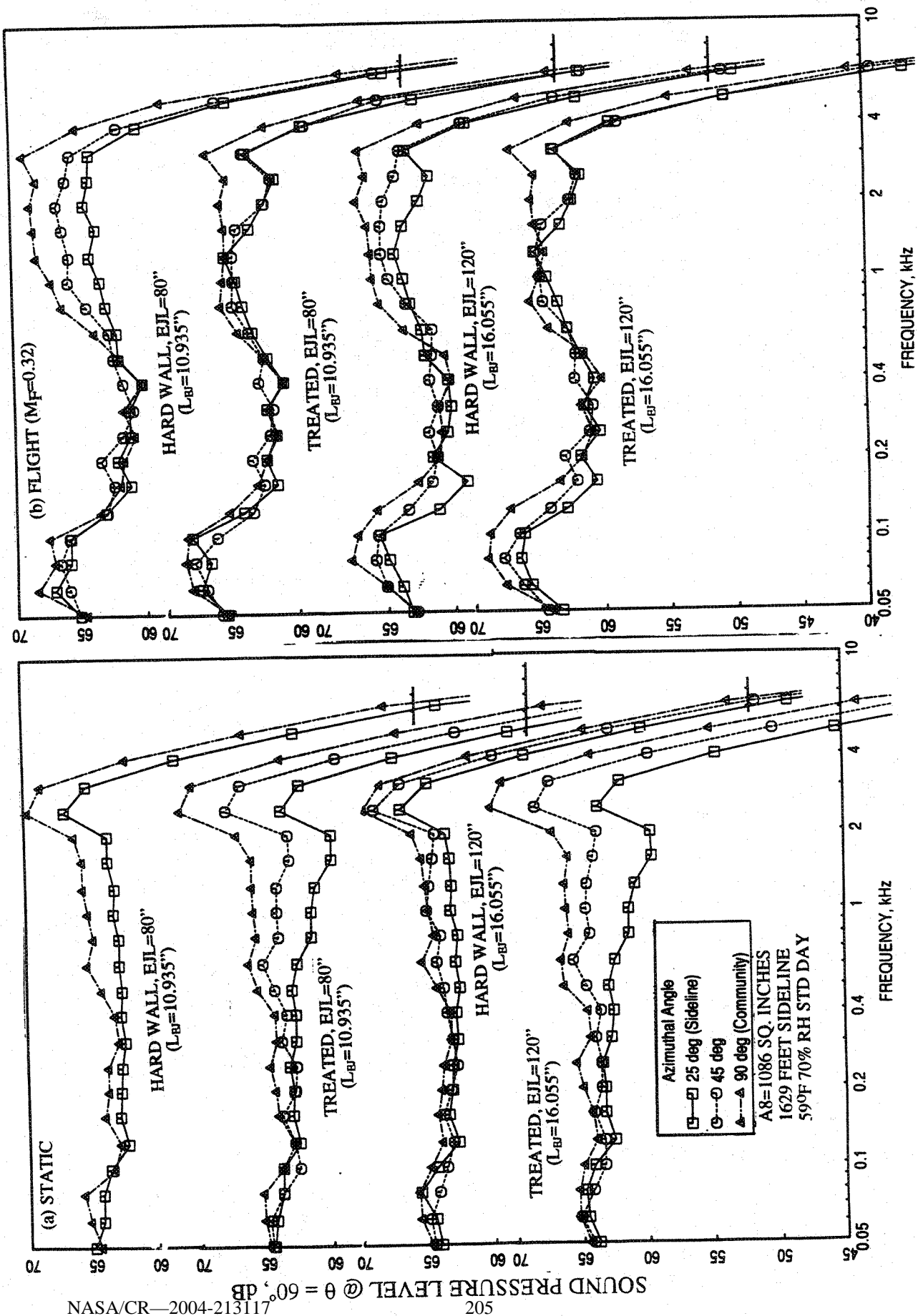
Figure 4.3-38. Effect of flap length and ejector treatment on azimuthal variation of SPL spectrum at θ=60° for a 10 and 9 full staggered CD-chute mixer-ejector, SAR=2.8, MAR=0.95", Vj = 1595 ft/sec, NPR = 2.0, T8 = 1175°R.
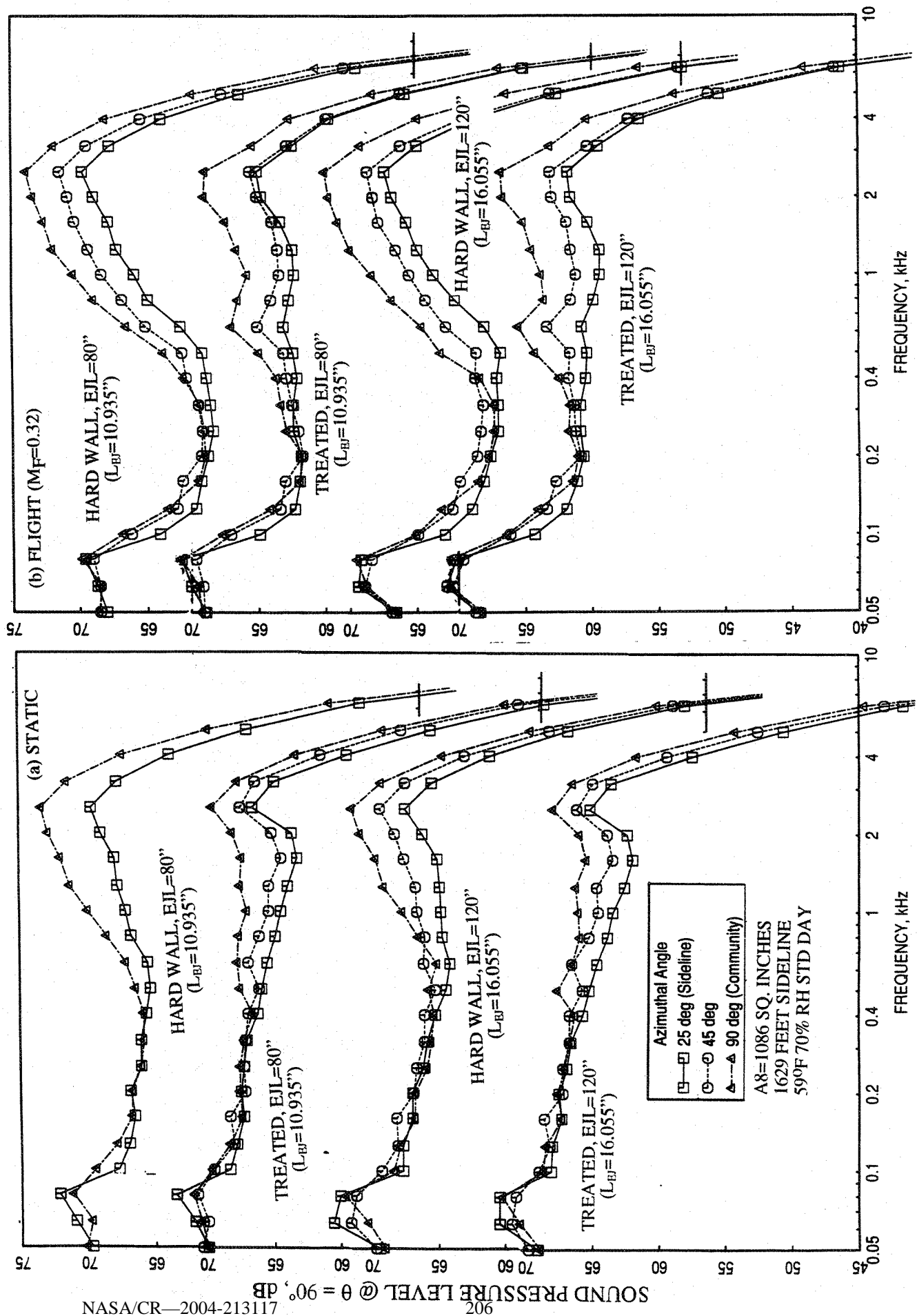
Figure 4.3-39. Effect of flap length and ejector treatment on azimuthal variation of SPL spectrum at θ=90° for a 10 and 9 full staggered CD-chute mixer-ejector, SAR=2.8, MAR=0.95", V_j = 1595 ft/sec, NPR = 2.0, T8 = 1175°R.

Figure 4.3-40. Effect of flap length and ejector treatment on azimuthal variation of SPL spectrum at θ=120° for a 10 and 9 full staggered CD-chute mixer-ejector, SAR=2.8, MAR=0.95", Vj = 1595 ft/sec, NPR = 2.0, T8 = 1175°R.

Figure 4.3-41. Effect of flap length and ejector treatment on azimuthal variation of SPL spectrum at θ=60° for a 10 and 9 full staggered CD-chute mixer-ejector, SAR=2.8, MAR=0.95", V_j = 2384 ft/sec, NPR = 3.4, T8 = 1590°R.

Figure 4.3-42. Effect of flap length and ejector treatment on azimuthal variation of SPL spectrum at θ=90° for a 10 and 9 full staggered CD-chute mixer-ejector, SAR=2.8, MAR=0.95", V_j = 2384 ft/sec, NPR = 3.4, T8 = 1590°R.

Figure 4.3-43. Effect of flap length and ejector treatment on azimuthal variation of SPL spectrum at θ=120° for a 10 and 9 full staggered CD-chute mixer-ejector, SAR=2.8, MAR=0.95", V_j = 2384 ft/sec, NPR = 3.4, T8 = 1590°R.

Figure 4.3-44. Effect of flap length and ejector treatment on azimuthal variation of SPL spectrum at θ=60° for a 10 and 9 full staggered CD-chute mixer-ejector, SAR=2.8, MAR=0.95", V_j = 2637 ft/sec, NPR = 4.0, T8 = 1750°R.

Figure 4.3-45. Effect of flap length and ejector treatment on azimuthal variation of SPL spectrum at θ=90° for a 10 and 9 full staggered CD-chute mixer-ejector, SAR=2.8, MAR=0.95", V_j = 2637 ft/sec, NPR = 4.0, T8 = 1750°R.

Figure 4.3-46. Effect of flap length and ejector treatment on azimuthal variation of SPL spectrum at θ=120° for a 10 and 9 full staggered CD-chute mixer-ejector, SAR=2.8, MAR=0.95'', V$_j$ = 2637 ft/sec, NPR = 4.0, T8 = 1750°R.

4.3.3 Results for 10 Full & 9 Full and Two Half CD-chute Staggered Mixer-Ejector Configurations:

Effect of treatment, flap length, and flight simulation on the performance related results for staggered chute configurations with 10 full and 9 and 2 half CD-chute mixer is almost identical to those observed for the staggered chute configurations with 9 full CD-chute lower rack mixer. For acoustic results the effect of treatment, flap length, and flight simulation for 9 and 2 half CD-chute mixer are not identical, but qualitatively similar, to those observed for the staggered chute configurations with 9 full CD-chute lower rack mixer. Hence, for brevity, a few typical acoustic results for the 9 and 2 half CD-chute staggered mixer are included in this section.

Effect of Acoustic Treatment and Flap Length: All the results in this section show the simultaneous comparisons between treated and hard wall configurations and between short and long flaps for static and with flight simulation condition of $M_F=0.32$. While the long flap results are presented by open symbols, the same filled symbols show the results for short flap configurations.

Figure 4.3-47 shows the effect of treatment and flap length on PNLT and EPNL as function of jet velocity (V_j) at an azimuthal angle $\phi=25^\circ$. Noise reductions in terms of EPNdB and PNLTdB are observed both due to treatment and increased flap length. However, the effect is reduced with increasing jet velocity. Noise reduction due to acoustic treatment is higher for the long flap configuration compared to short flap case. Acoustic benefit of about 2 to 3 EPNdB due to treatment is observed for long flap configuration with flight simulation at velocities between 1600 and 2200 ft/sec. At higher velocities the treatment benefit is not significant due to dominant externally (i.e., external to the ejector) generated noise. Noise benefit due to increased flap length is the result of better mixing within the ejector compared to a shorter ejector case.

At four different jet velocities of L1M cycle conditions the effect of treatment and flap length on PNLT directivities is shown in Figure 4.3-48. Noise suppressions due to treatment and due to flap length are more significant at lower jet velocities and at lower polar angles, except for $V_j=1147$ ft/sec. At this condition the effect of treatment as well as flap length are observed in the mid polar angles. At lower forward angles the effect is insignificant due to the probable dominant shock noise and noise from the inlet. Effect of treatment and flap length on SPL spectra at various polar angles (θ) for two jet velocities
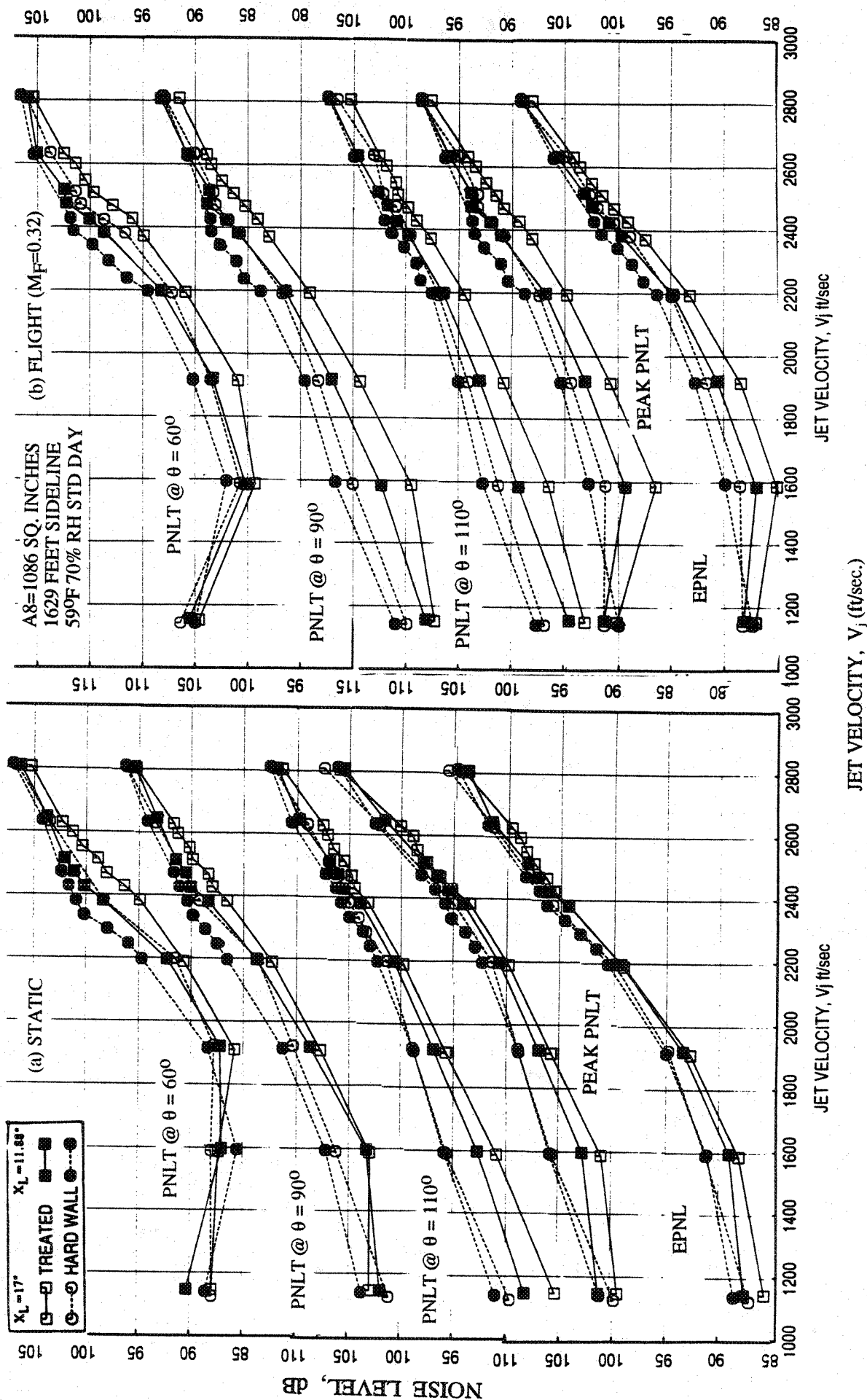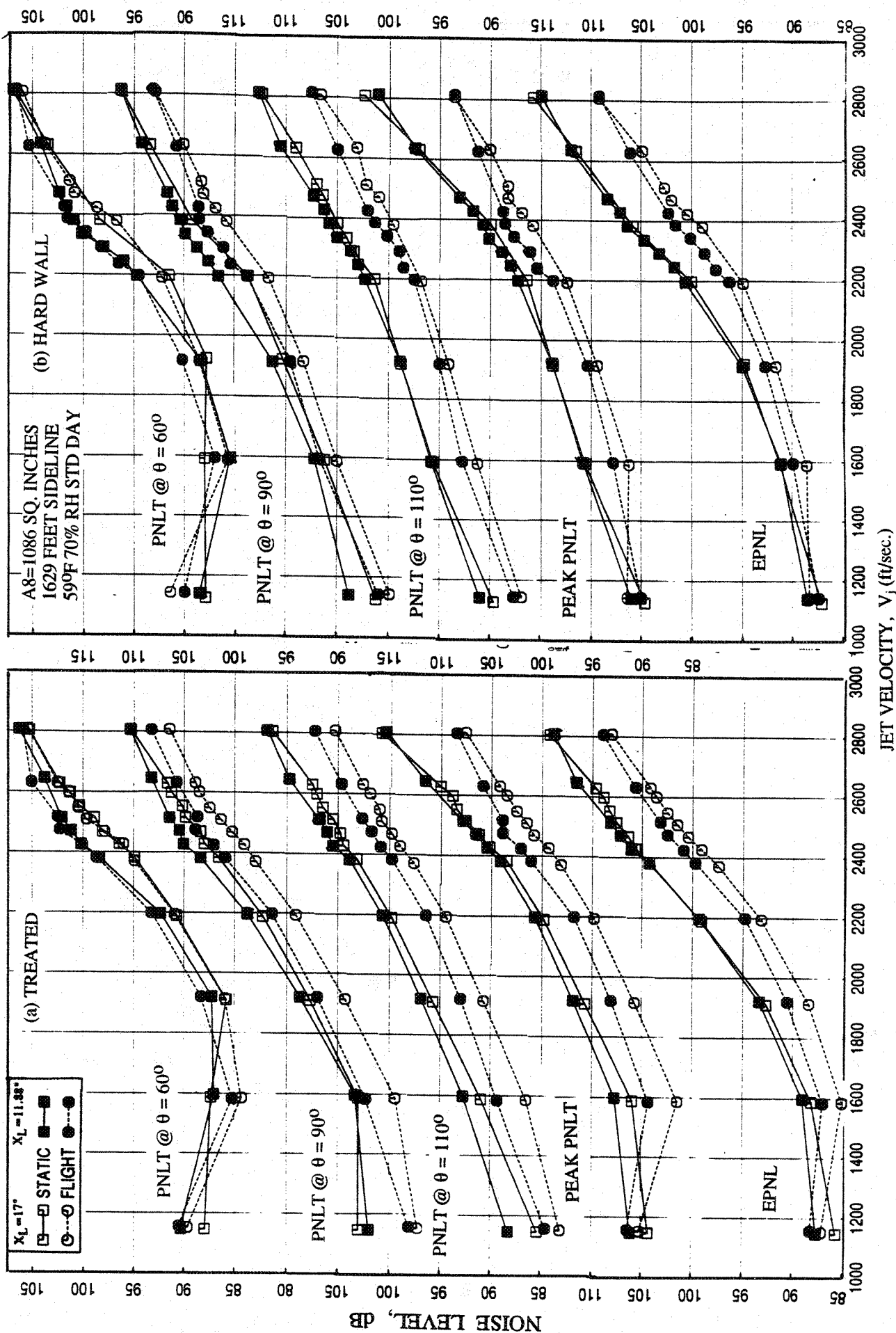
Figure 4.3-47. Effect of acoustic treatment and flap length on EPNL and PNLT at various polar angles (θ) as function of jet velocity of L1M cycle conditions for a 10 and 9 full & two half staggered CD-chute mixer-ejector at an azimuthal angle φ=25°; SAR=2.8, MAR=0.95.
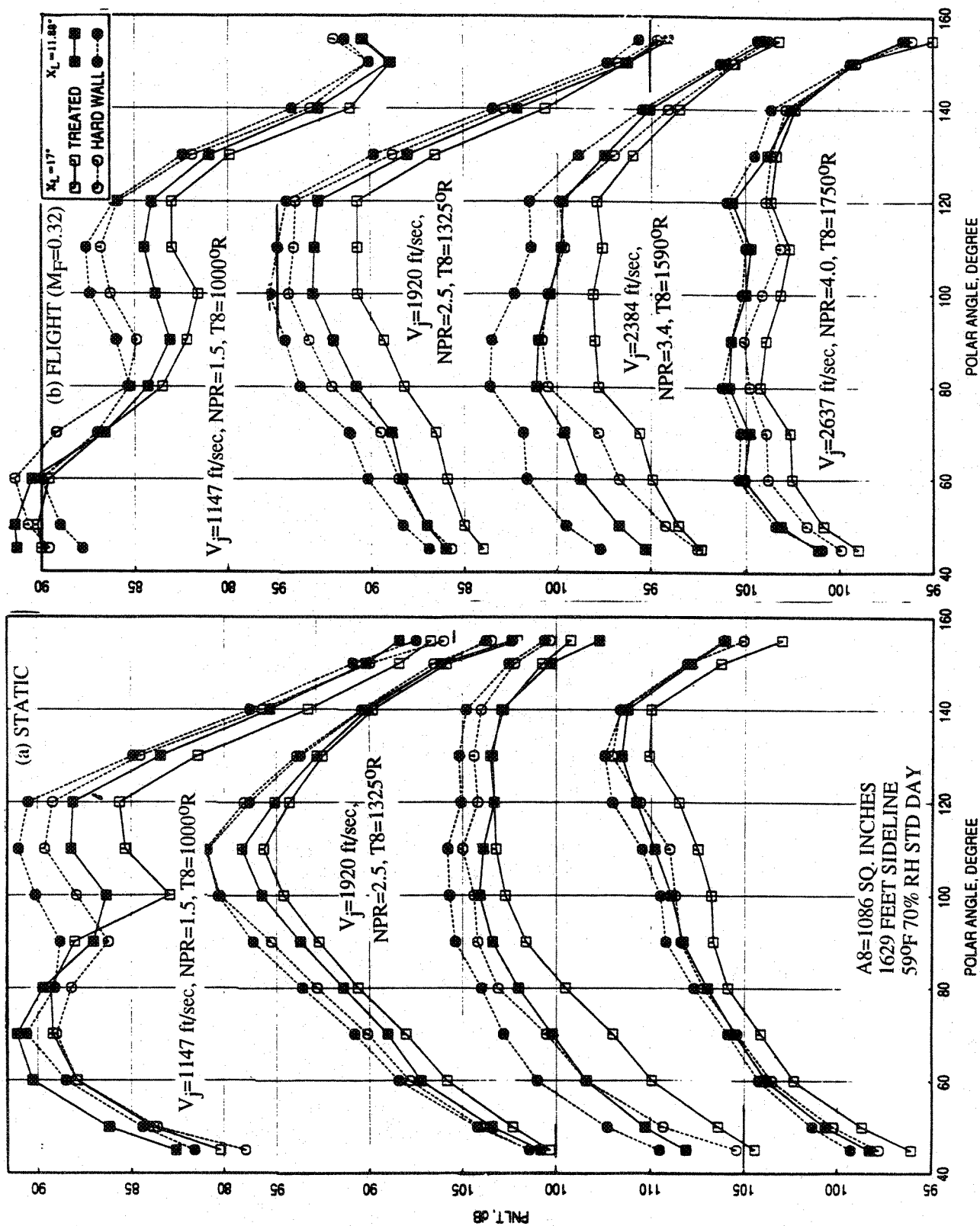
Figure 4.3-48. Effect of acoustic treatment and flap length on PNLT directivities at different L1M cycle conditions for a 10 and 9 full & two half staggered CD-chute mixer-ejector at an azimuthal angle φ=25°; SAR=2.8, MAR=0.95.

is shown in Figures 4.3-49 and 4.3-50. Significant SPL reduction is observed at higher polar angles for higher frequency range. The acoustic benefit in terms of SPL diminishes with increasing jet velocity. At NPR=3.4 condition the SPL results indicate the possible presence of shock in the ejector for short flap configurations. Shock-associated noise in terms of SPL is dominantly observed at 60° and in moderate amount at 90° for the short flap configurations.

Effect of Simulated Flight and Flap Length : All the results in this section show the simultaneous comparisons between static and simulated flight of $M_F=0.32$ conditions and between short and long flap for treated and hard wall configurations. While the long flap results are presented by open symbols, the same filled symbols show the results for short flap configurations.

Figure 4.3-51 shows the effect of flight simulation and flap length on PNLT and EPNL as function of jet velocity (V_j) at an azimuthal angle $\phi=25^{\circ}$ for treated and hard wall configurations. EPNL decreases with flight simulation for all the jet velocities for hard wall configuration and for treated case at velocities 1600 ft/sec and above. The EPNdB reduction due to flight simulation is slightly higher for treated ejector compared to hard wall case, since the noise generated internal to the ejector is reduced due to treatment and thus the reduction of externally generated noise due to flight simulation dominates the observed noise. The EPNL is lower for longer ejector compared to the short flap case and the noise reduction is higher with flight simulation. Except for forward arc angles the PNLT decreases with flight simulation and is lower for longer ejector at all jet velocities.

At four different jet velocity conditions the effect of flight simulation and flap length on PNLT directivities is shown in Figure 4.3-52. The effect of flight simulation is to lower the PNLT levels at polar angles above 60° due to source strength reductions and the trend is reversed at lower angles due to dynamic amplification of jet noise overcoming the source strength reduction effects. Significant PNLT reduction is observed at the rear arc. PNLT is lower for longer ejector at all angles and the impact is less realized in the rear arc angles. Effect of flight simulation and flap length on SPL spectra at various polar angles (θ) for two jet velocities is shown in Figures 4.3-53 and 4.3-54. Significant SPL reduction is observed at higher polar angles for the entire frequency range due to flight simulation. The SPL levels are lower for long ejector compared to the shorter configuration, mostly at higher frequencies.
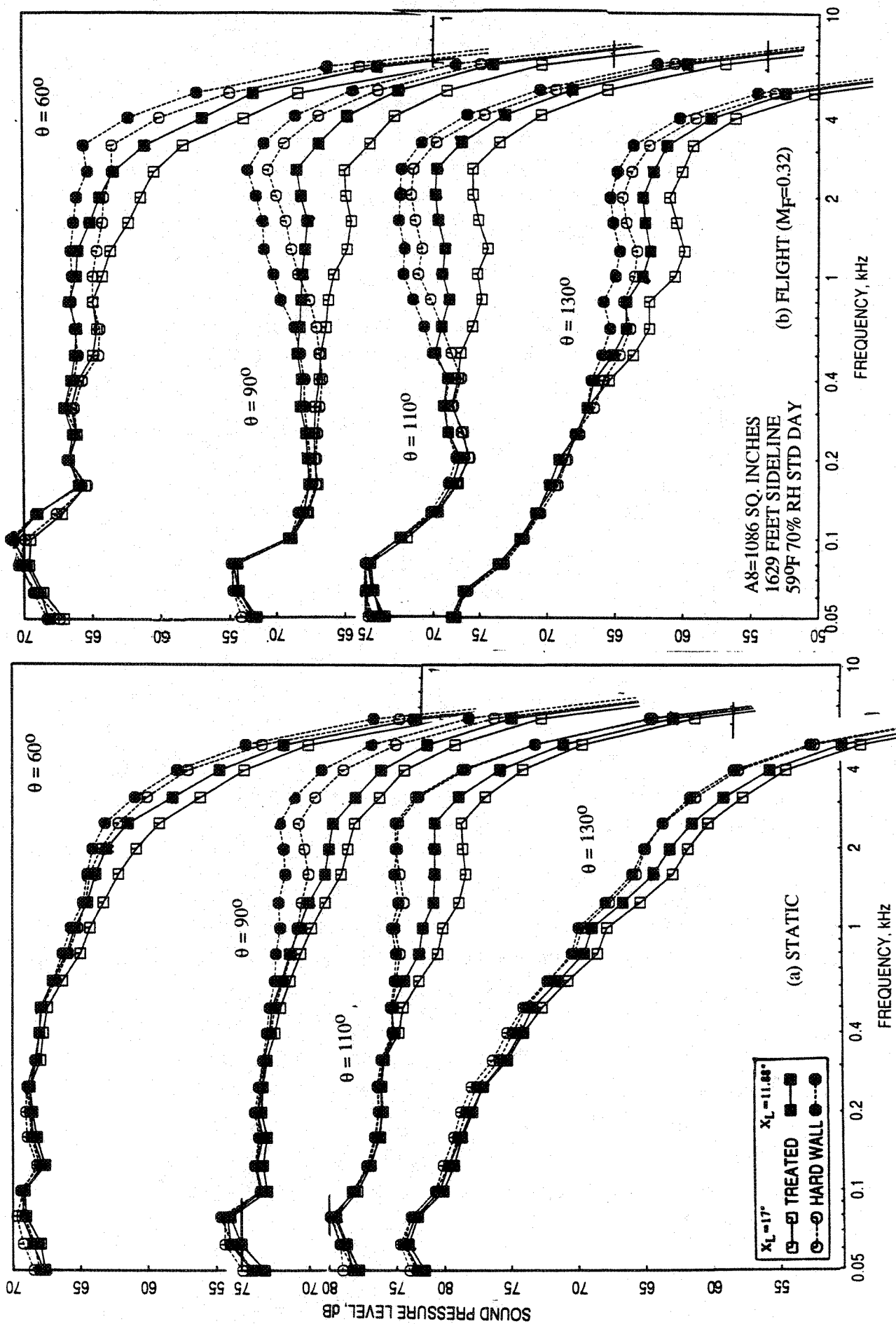
Figure 4.3-49. Effect of acoustic treatment and flap length on SPL spectra at various polar angles (θ) for a 10 and 9 full & two half staggered CD-chute mixer-ejector at an azimuthal angle φ=25°, SAR=2.8, MAR=0.95, V_j = 1920 ft/sec, NPR = 2.5, T8 = 1325°R.
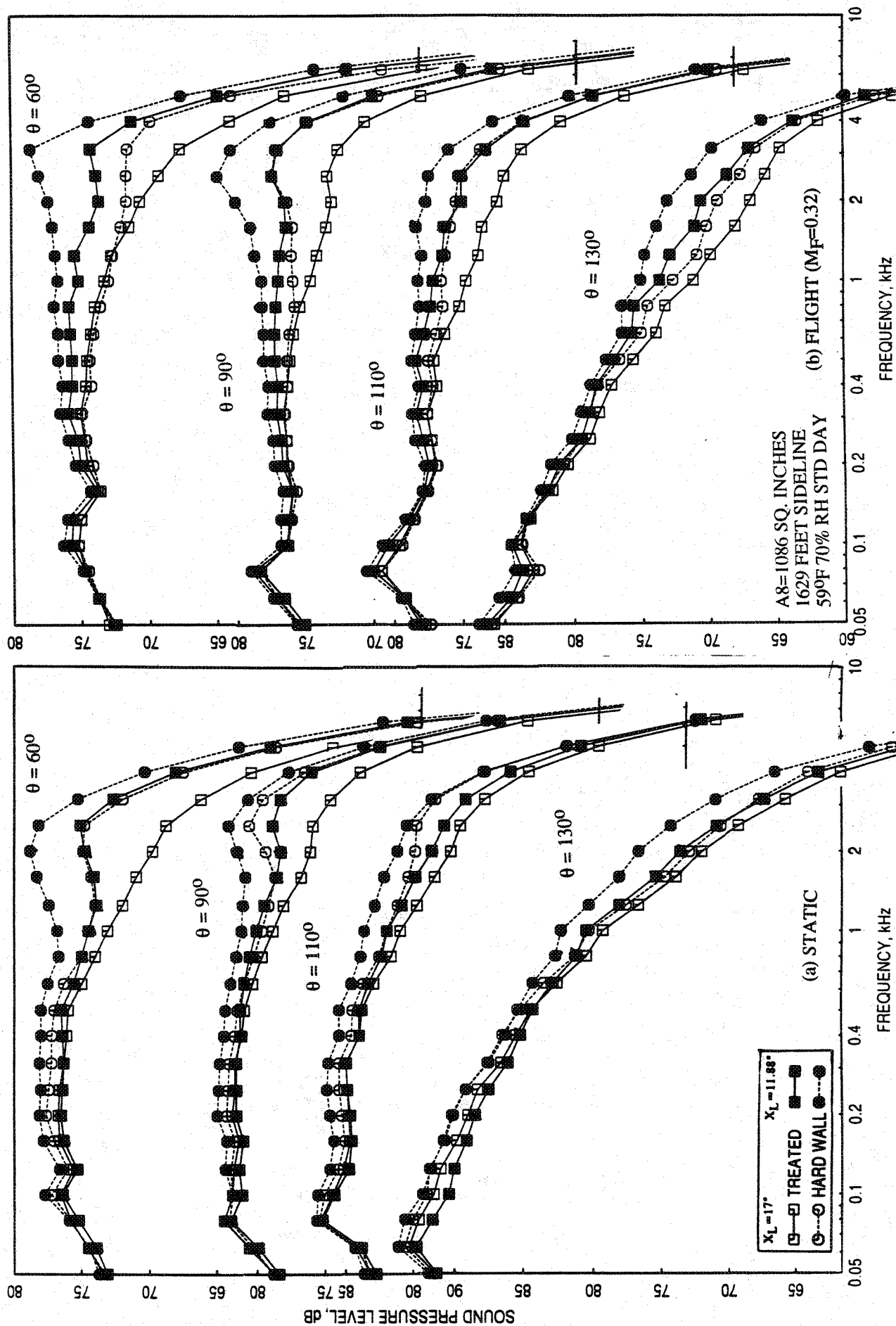
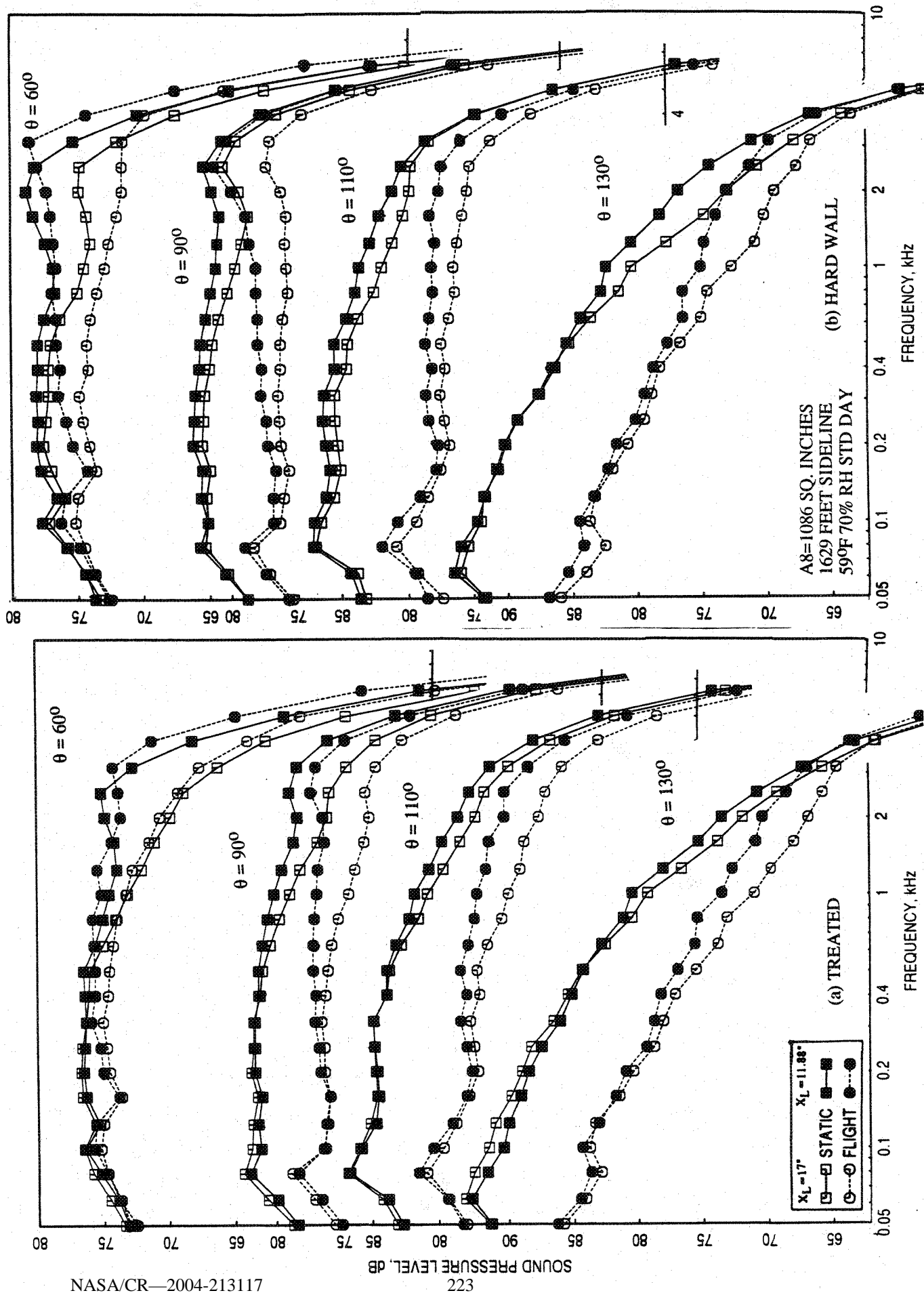Figure 4.3-50. Effect of acoustic treatment and flap length on SPL spectra at various polar angles (θ) for a 10 and 9 full & two half staggered CD-chute mixer-ejector at an azimuthal angle φ=250° SAR=2.8, MAR=0.95, V_j = 2384 ft/sec, NPR = 3.4, T8 = 1590°R.

Figure 4.3-51. Effect of flight simulation and flap length on EPNL and PNLT at various polar angles (θ) as function of jet velocity of L1M cycle conditions for a 10 and 9 full & two half staggered CD-chute mixer-ejector at an azimuthal angle ϕ=25°; SAR=2.8, MAR=0.95.
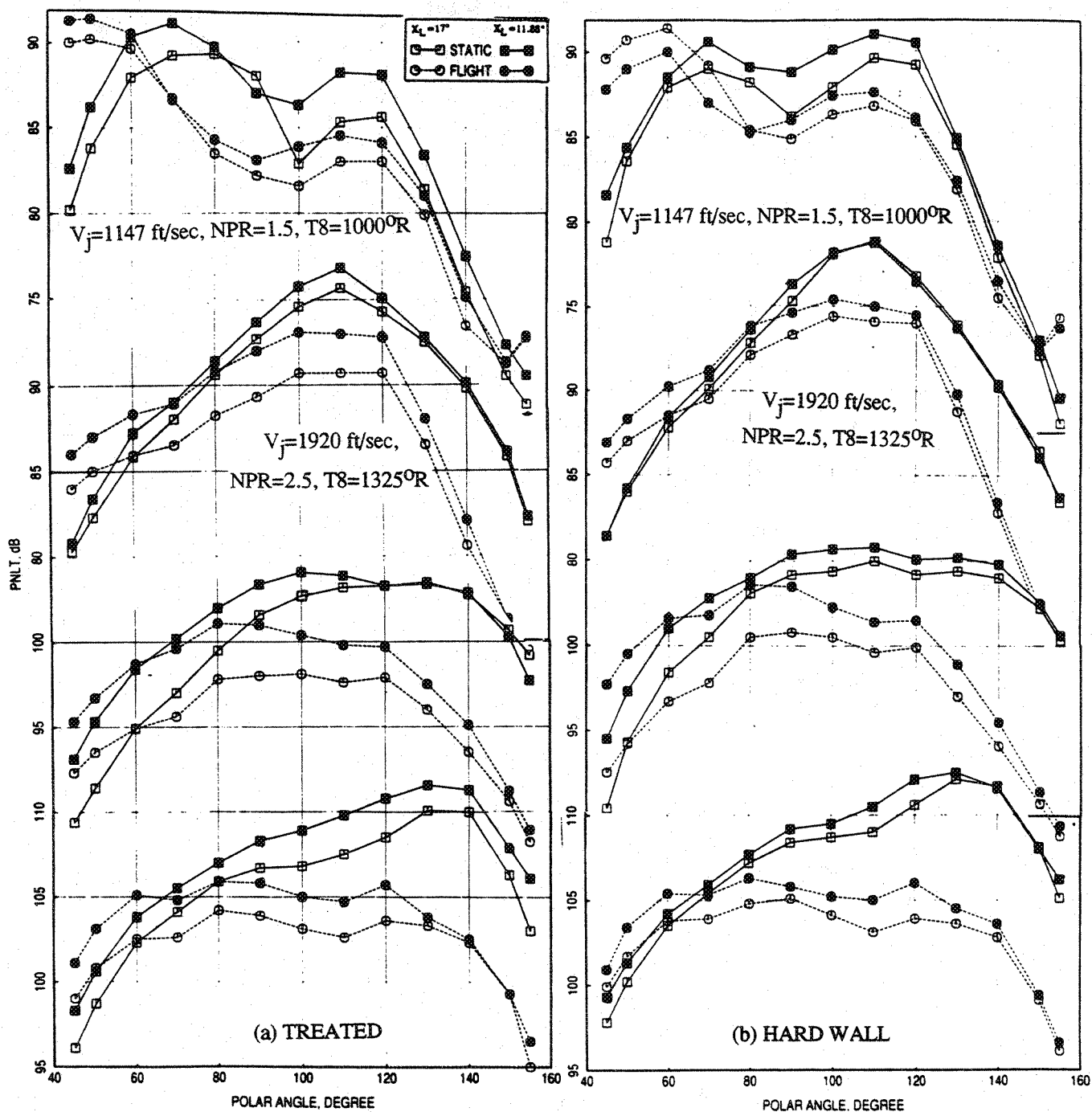
Figure 4.3-52. Effect of flight simulation and flap length on PNLT directivities at different L1M cycle conditions for a 10 and 9 full & two half staggered CD-chute mixer-ejector at an azimuthal angle φ=25°; SAR=2.8, MAR=0.95.
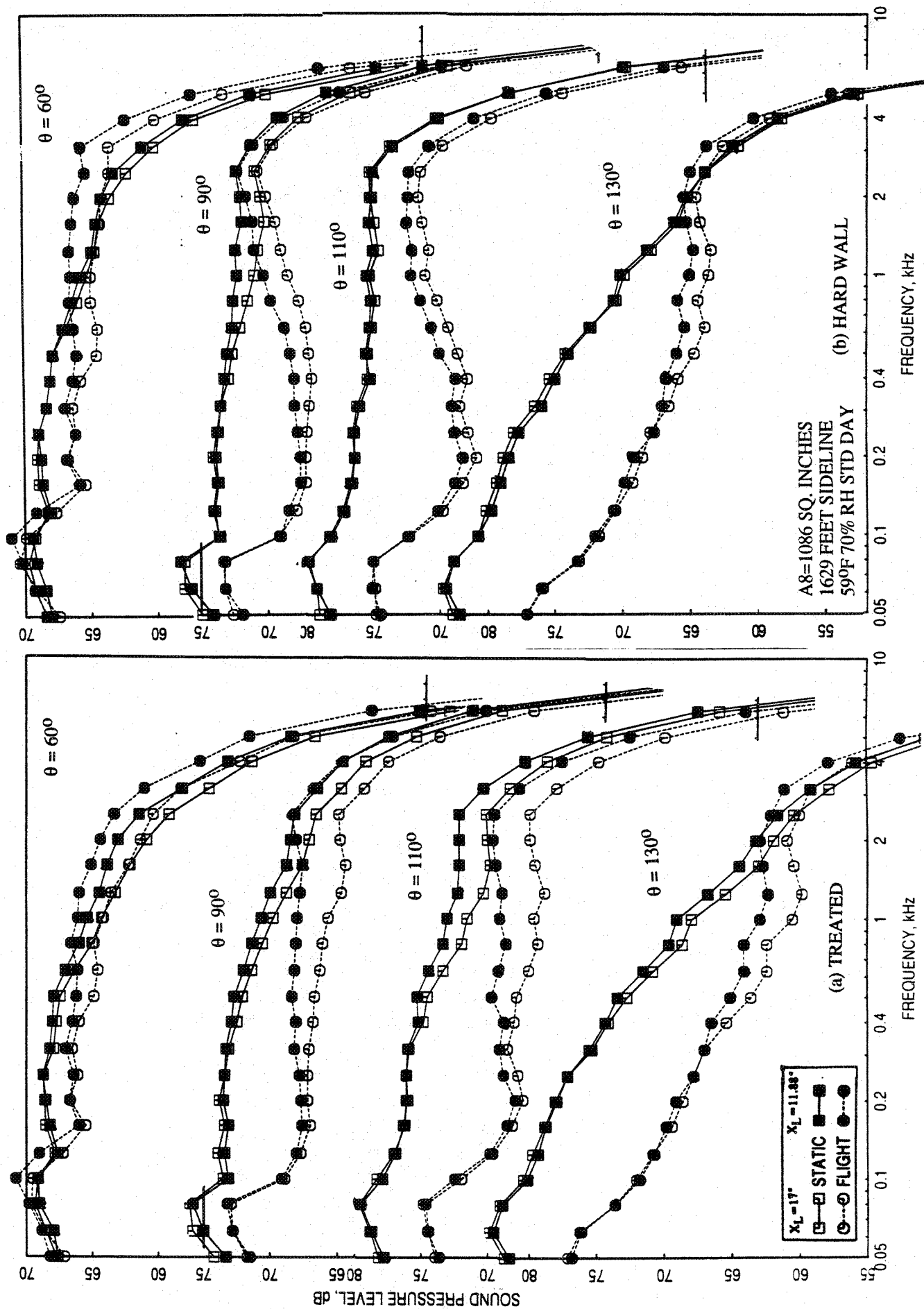
Figure 4.3-53. Effect of flight simulation and flap length on SPL spectra at various polar angles (θ) for a 10 and 9 full & two half staggered CD-chute mixer-ejector at an azimuthal angle φ=25°. SAR=2.8, MAR=0.95, V_j = 1920 ft/sec, NPR = 2.5, T8 = 1325°R.

Figure 4.3-54. Effect of flight simulation and flap length on SPL spectra at various polar angles (θ) for a 10 and 9 full & two half staggered CD-chute mixer-ejector at an azimuthal angle φ=25°; SAR=2.8, MAR=0.95, V_j = 2384 ft/sec, NPR = 3.4, T8 = 1590°R.

4.4 IMPACT OF MIXER DESIGN:

Acoustic, flow related, and performance related results for the treated long ejector configurations comparing between the four mixer designs, namely, aligned CD chute, staggered 9 and 2 half CD chute, staggered 9 full CD chute, and aligned convergent chute, are presented in this section.

4.4.1 Acoustic Results at Static Condition:

Figure 4.4-1 shows the comparison of pseudo EPNL, peak PNLT, and PNLT at various polar angles (θ) as functions of jet velocity (V_j) at a slant distance of 1629', and at sideline ($\phi=25°$) and community ($\phi=90°$) azimuthal locations relative to major axis at static condition for the above mentioned four mixer configurations with treated long ejector. The pseudo EPNL levels are with in a spread of about 1 EPNdB to one another for these configurations at velocities above 1600 ft/sec. In this velocity range, the staggered 9 full CD chute configuration seems to be performing acoustically best among these configurations. At lower velocities (i.e., below 1900 ft/sec) the aligned convergent chute configuration generates the lowest EPNL level. EPNL for this configuration is about 4 dB lower at 1147 ft/sec compared to the staggered 9 full CD chute configuration. Similar behavior is also observed with respect to peak PNLT and PNLT at other polar angles. This behavior of convergent chute compared to CD chute is discussed later in this section.

PNLT directivities at jet velocities of 1147, 1920, 2384, and 2637 ft/sec are compared for the four mixer configurations in Figure 4.4-2. At 1147 ft/sec (i.e., for NPR=1.5) the 9 and two half chute configuration is the noisiest and the convergent chute configuration is the quietest at all angles. The same trend is observed at 1595 ft/sec case (NPR=2.0), except the PNLT levels for all these configurations are much closer to each other (not shown here). The trend changes at higher velocities, as observed in Figure 4.4-2, for 1920, 2384, and 2637 ft/sec conditions. At these conditions, the convergent chute configuration is the noisiest and 9 full chute staggered configuration is the quietest at all angles. Spectral comparisons at various polar angles (θ) for each of the four jet velocities are shown in Figures 4.4-3 through 4.4-6. At 1147 ft/sec the three CD chute configurations generate SPL humps peaking around 2 kHz, which is possibly due to shock associated noise. Although NPR=1.5 is a subcritical pressure ratio, locally supersonic flows can exist inside the CD chutes due to overexpansion. Thus, shock noise is possibly generated across the
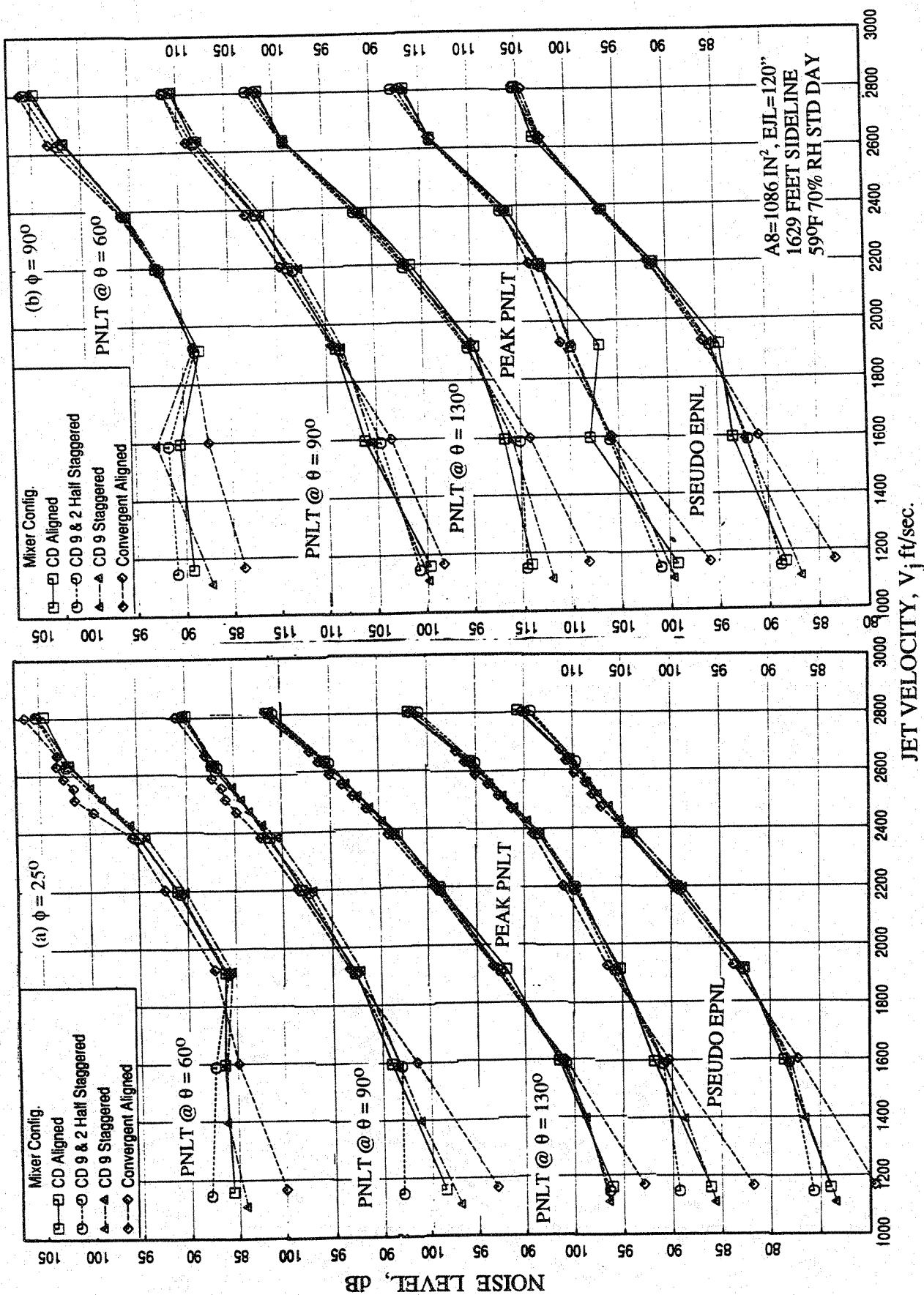
Figure 4.4-1. Comparison of pseudo EPNL, peak PNLT, and PNLT at various polar angles (θ) as functions of jet velocity of L1M cycle conditions between four mixer designs for 2D nozzle configurations with long treated ejector at static condition; SAR=2.8, MAR = 0.95.
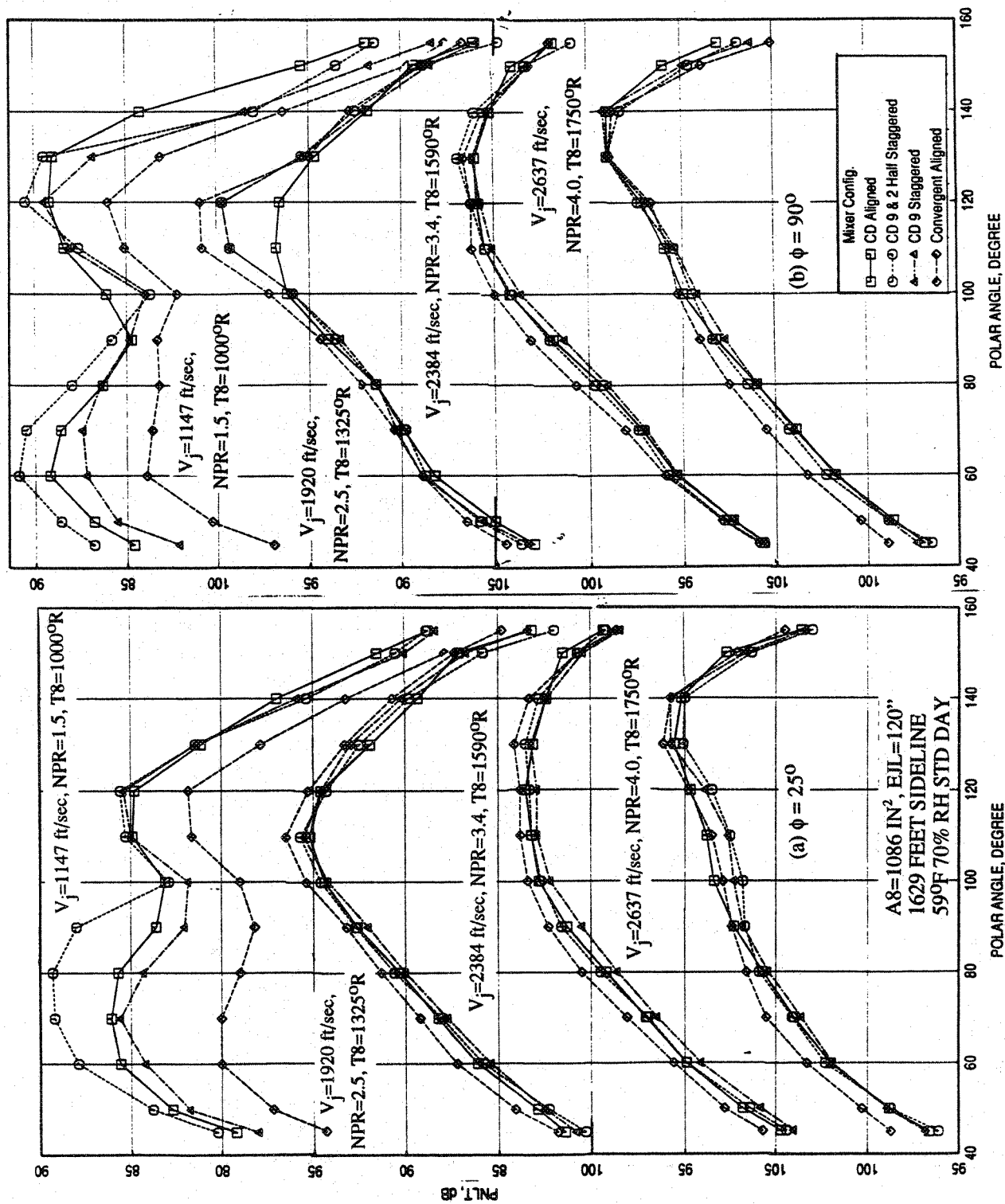
Figure 4.4-2. Comparison of PNLT directivities for different jet velocities (V$_j$) of L1M cycle conditions between four mixer designs for 2D nozzle configurations with long treated ejector at static condition; SAR=2.8, MAR = 0.95.
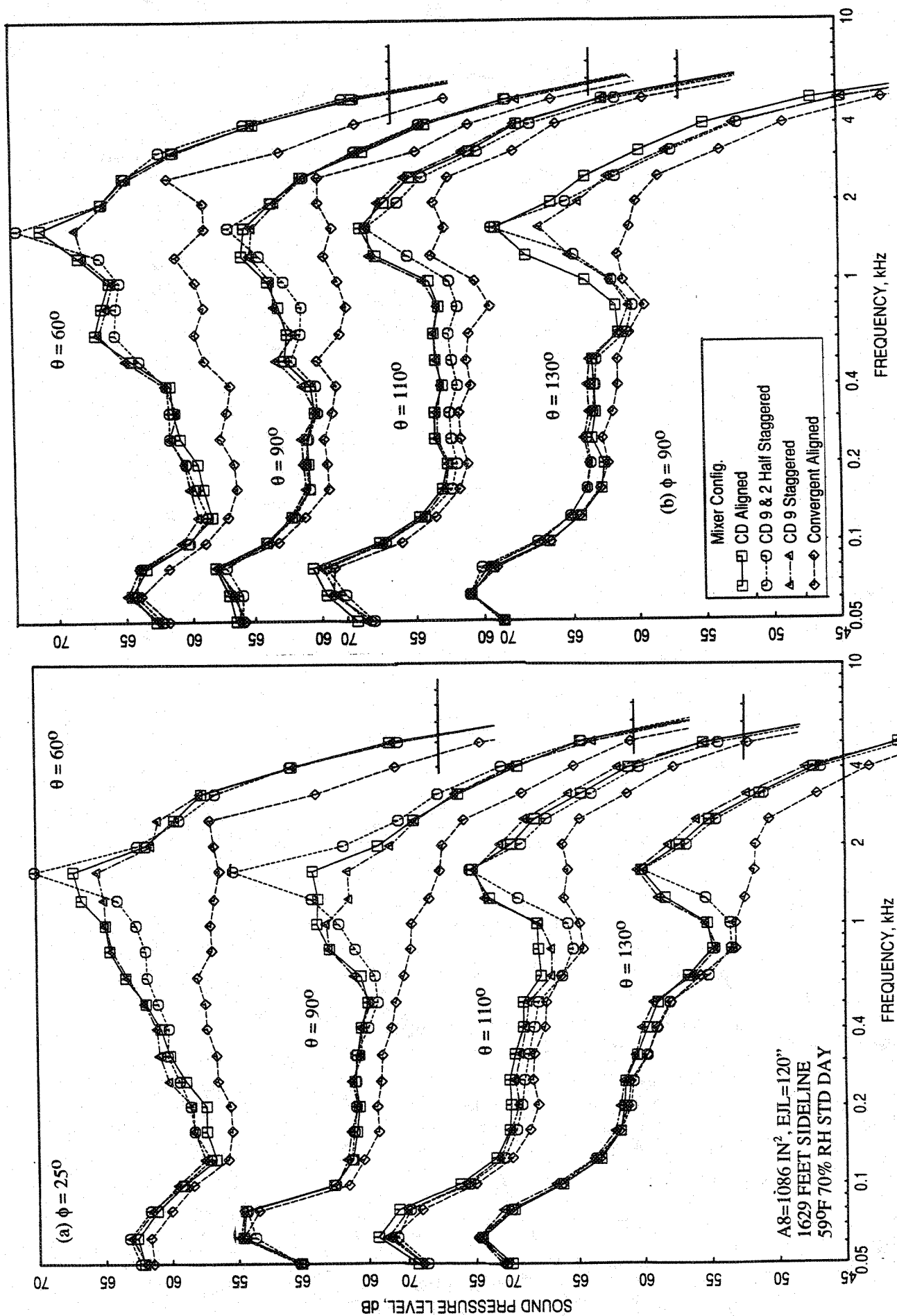
Figure 4.4-3. Comparison of SPL spectra at various polar angles (θ) between four mixer designs for 2D nozzle configurations with long treated ejector at static condition; SAR=2.8, MAR = 0.95, V_j = 1147 ft/sec, NPR = 1.5, T8 = 1000°R.
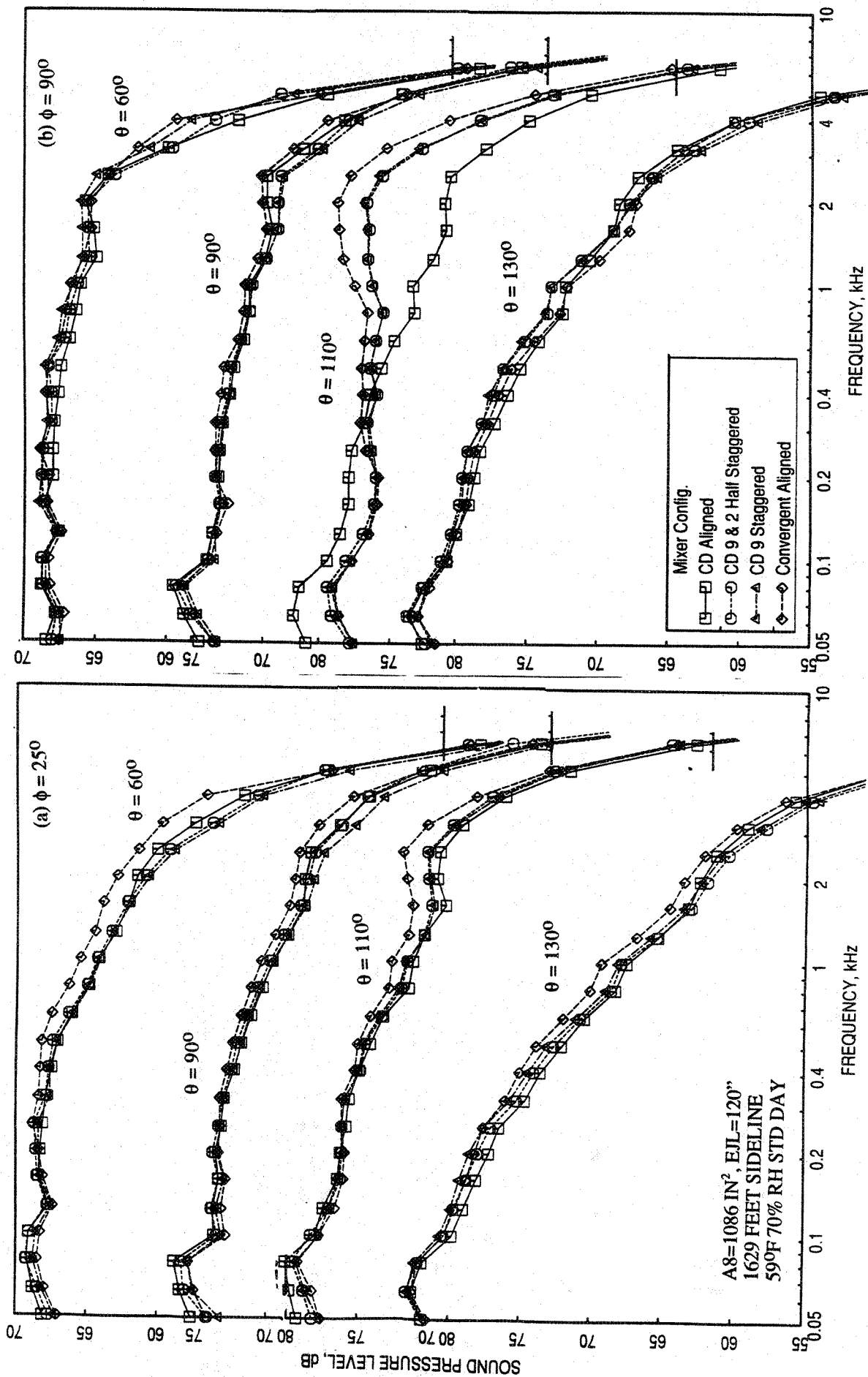
Figure 4.4.4. Comparison of SPL spectra at various polar angles (θ) between four mixer designs for 2D nozzle configurations with long treated ejector at static condition; SAR=2.8, MAR = 0.95, V_j = 1920 ft/sec, NPR = 2.5, T8 = 1325°R.
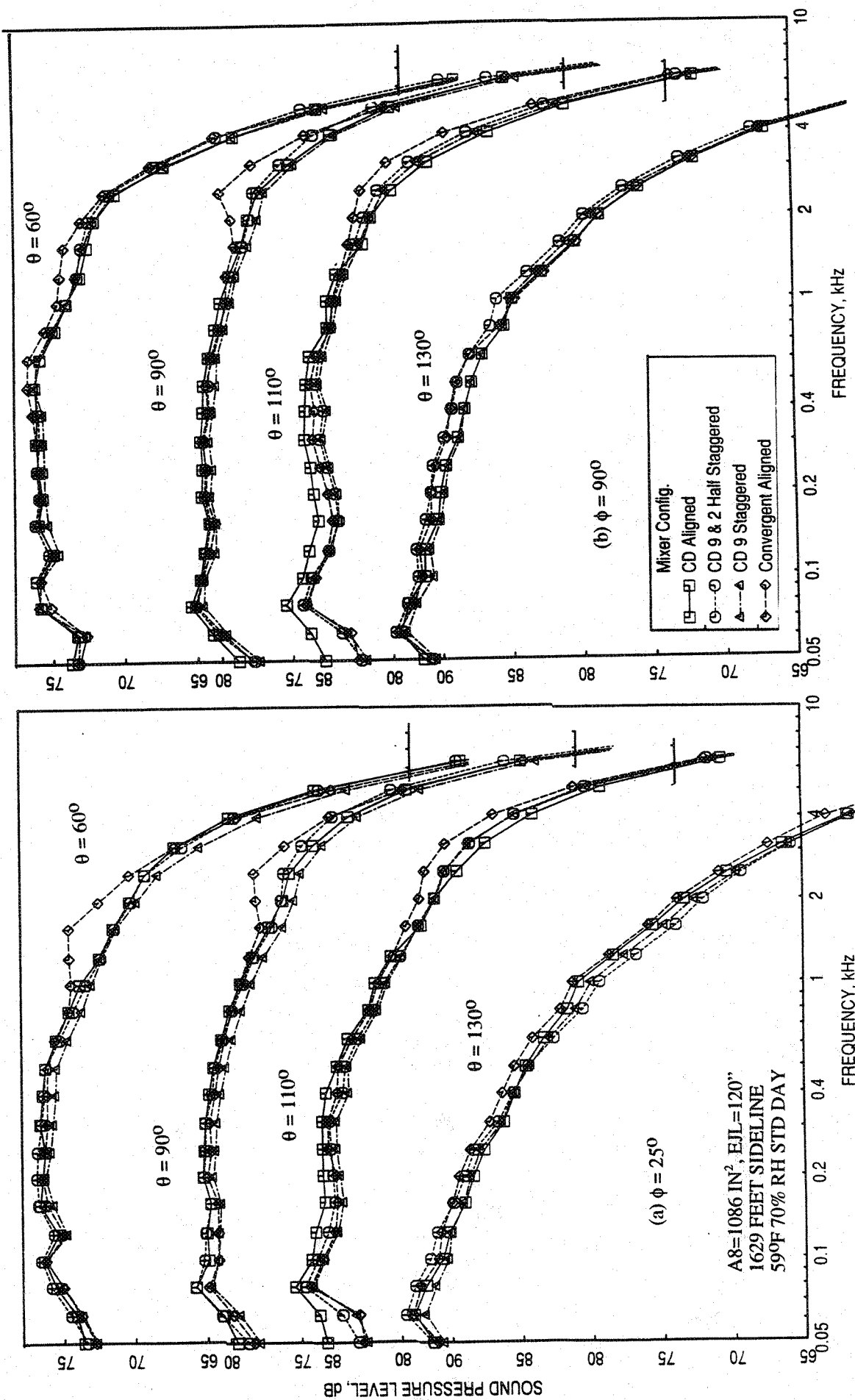
Figure 4.4-5. Comparison of SPL spectra at various polar angles (θ) between four mixer designs for 2D nozzle configurations with long treated ejector at static condition; SAR=2.8, MAR = 0.95, V_j = 2384 ft/sec, NPR = 3.4, T8 = 1590°R.
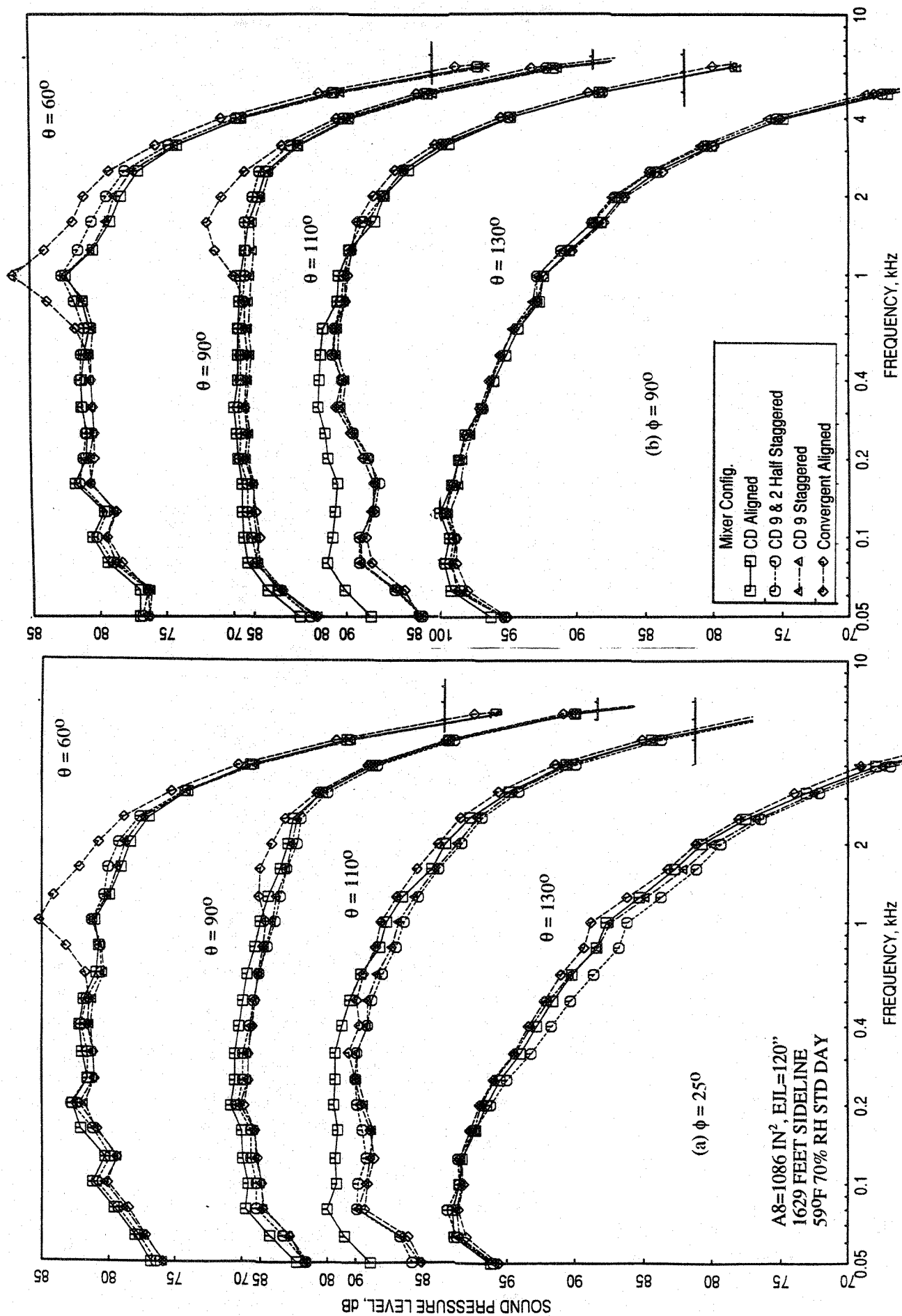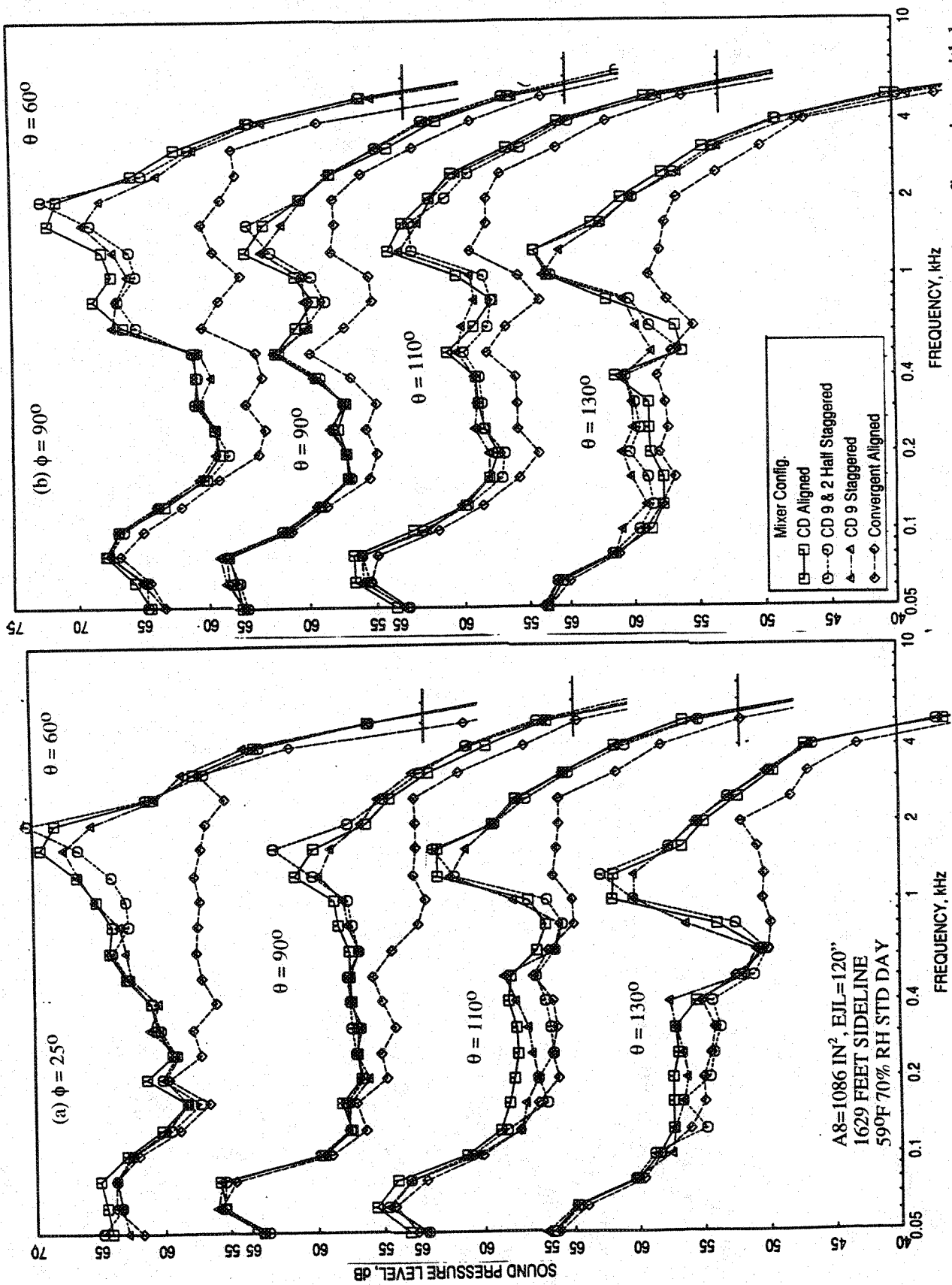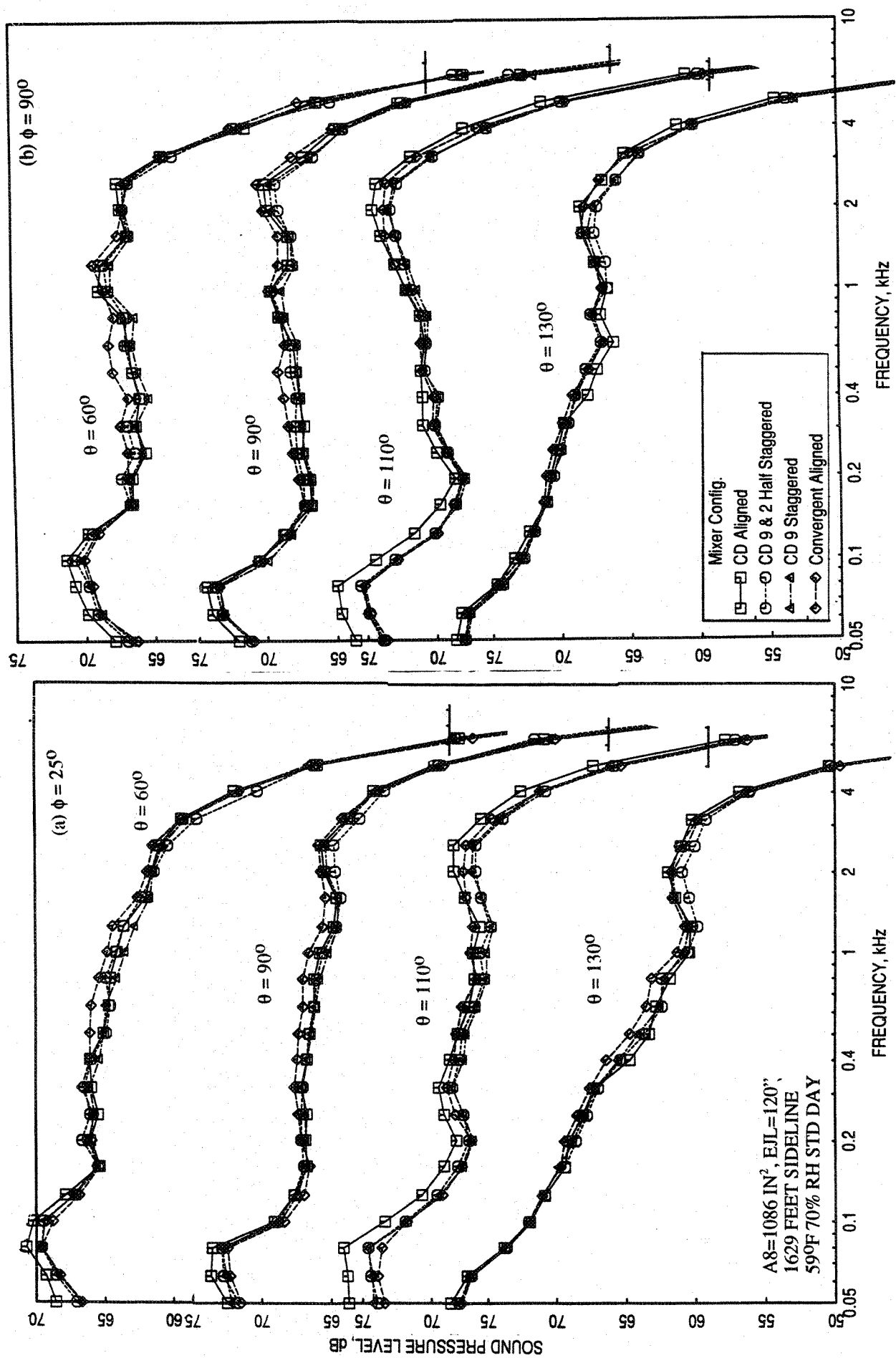
Figure 4.4-6. Comparison of SPL spectra at various polar angles (θ) between four mixer designs for 2D nozzle configurations with long treated ejector at static condition; SAR=2.8, MAR = 0.95, V_j = 2637 ft/sec, NPR = 4.0, T8 = 1750°R.

shocks for pressure equalization in side the divergent portion of the chutes. Acoustic data at this NPR confirms this behavior indicating higher shock-associated noise for CD chute configurations compared to convergent chute case. Static pressure distributions on the flap and on the mixer walls will be examined to assess the relative shock strengths between CD and convergent chute configurations in the ejector. In this frequency range the convergent chute configuration exhibits noise levels without any significant hump indicating minimal shock structures within the confines of the ejector flaps for the convergent chute case. For 1595 ft/sec the spectral distributions for all four configurations are closer to each other. However, the high frequency humps for CD-chute configurations are still observed (not shown here). For higher velocity conditions (see Figures 4.4-4 through 4.4- 6) the spectral levels for all the configurations are closer to each other for frequencies up to about 2 kHz. At higher frequency a hump is observed for convergent chute configuration in the forward arc indicating potentially larger contribution of shock-associated noise by aligned convergent chute design for this underexpanded case. As NPR increases, CD chutes tend to operate closer to the design case of shock-free situation compared to convergent chutes and hence lower forward quadrant high frequency noise levels.

4.4.2 Acoustic Results with Flight Simulation (M_F=0.32):

Figure 4.4-7 shows the comparison of EPNL, peak PNLT, and PNLT at various polar angles (θ) as functions of jet velocity (V_j) at a distance of 1629' at sideline and community locations with respect to major axis with a simulated flight Mach number of 0.32 between the four mixer configurations with treated long ejector. The EPNL levels are with in a spread of 2 to 3 EPNdB to one another for these configurations at velocities above 1600 ft/sec. In this velocity range, the staggered 9 full CD chute configuration seems to be performing acoustically best among these configurations. At lower velocities (i.e., below 1900 ft/sec) the aligned convergent chute configuration generates the lowest EPNL level. EPNL for this configuration is about 4 dB lower at 1147 ft/sec compared to the staggered 9 full CD chute configuration. Similar behavior is also observed with respect to peak PNLT and PNLT at other polar angles.

PNLT directivities at jet velocities of 1147, 1920, 2384, and 2637 ft/sec are compared between the four configurations in Figure 4.4-8. At 1147 ft/sec (i.e., for NPR=1.5) the 9 and two half chute configuration is the noisiest and the convergent chute configuration is
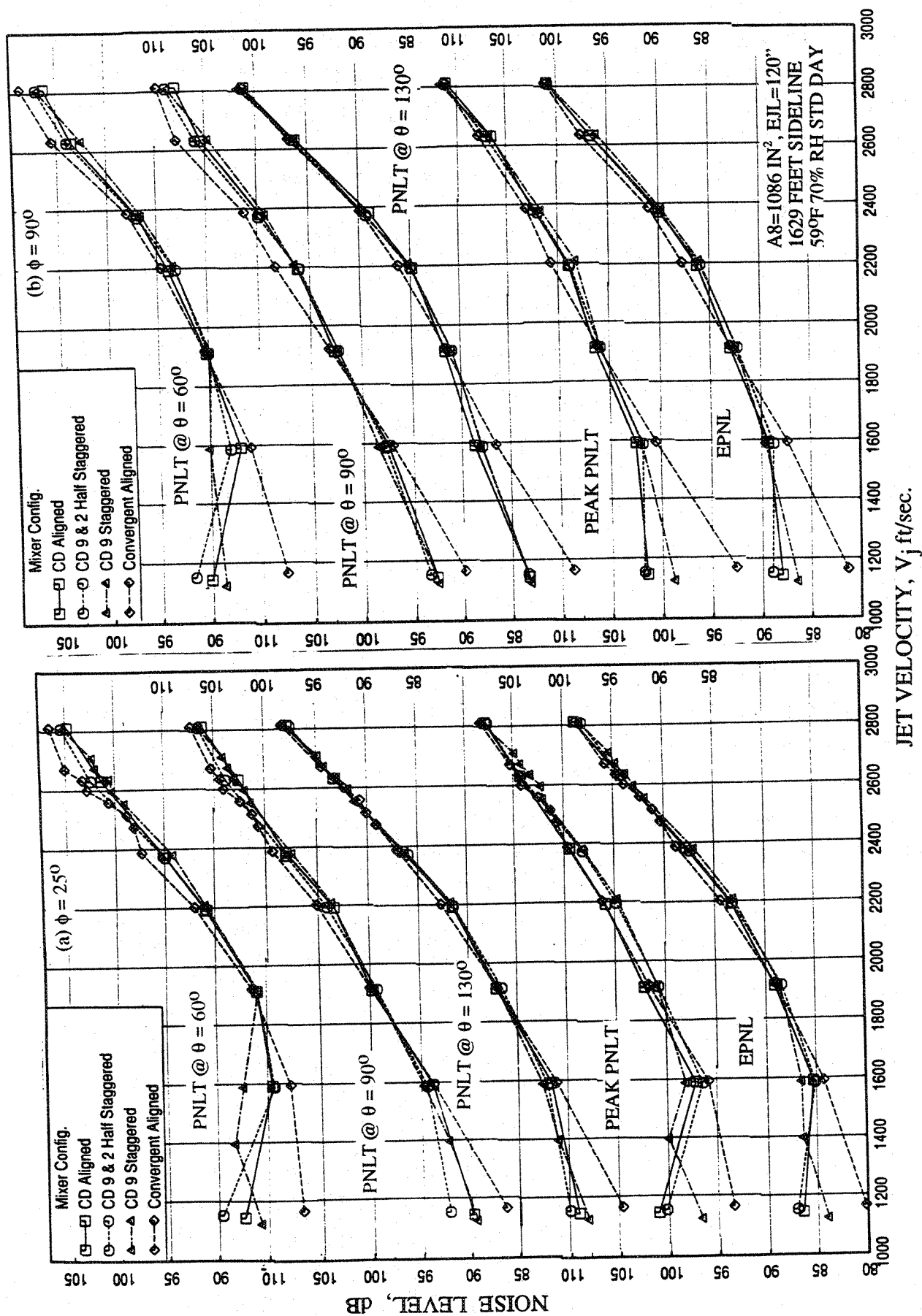
Figure 4.4-7. Comparison of EPNL, peak PNLT, and PNLT at various polar angles (θ) as functions of jet velocity of L1M cycle conditions between four mixer designs for 2D nozzle configurations with long treated ejector with flight simulation ($M_F=0.32$); SAR=2.8, MAR = 0.95.
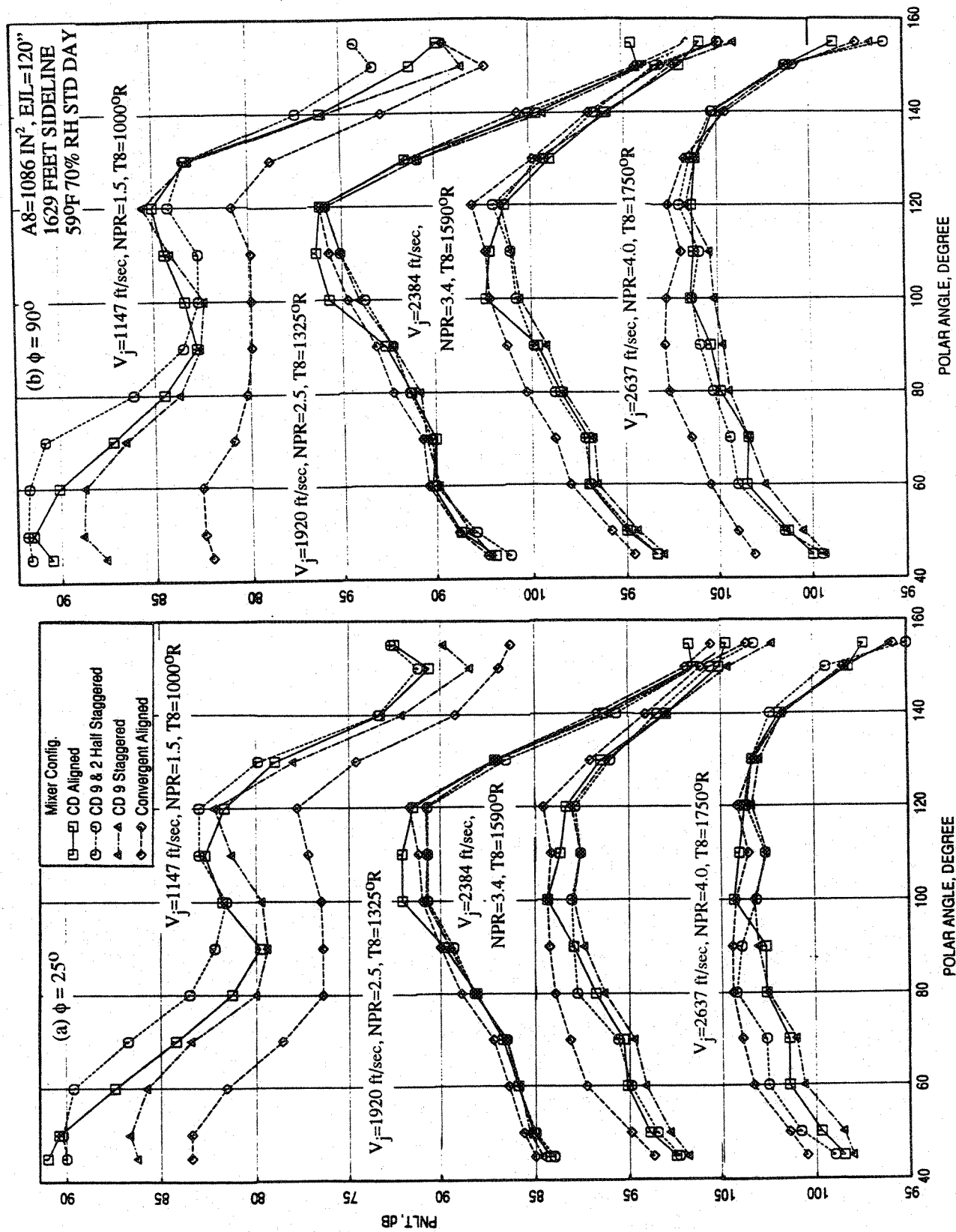
Figure 4.4-8. Comparison of PNLT directivities for different jet velocities (Vj) of L1M cycle conditions between four mixer designs for 2D nozzle configurations with long treated ejector with flight simulation (MF=0.32); SAR=2.8, MAR = 0.95.

the quietest at all angles. The same trend is observed at 1595 ft/sec case, except the PNLT levels for all these configurations are much closer to each other (not shown here). The trend changes at higher velocities. In these conditions, the convergent chute configuration becomes the noisiest and 9 full chute staggered configuration becomes the quietest at all angles. Spectral comparisons at various polar angles (θ) for each of these four jet velocities are shown in Figures 4.4-9 through 4.4-12. At 1147 ft/sec the three CD chute configurations generate SPL humps peaking around 2 kHz, which is possibly due to shock associated noise. In this frequency range the convergent chute configuration exhibits noise levels without any significant hump indicating minimal shock structures within the confines of the ejector flaps for the convergent chute case. For 1595 ft/sec the spectral distributions for all four configurations are closer to each other (not shown here). However, the high frequency humps for CD chute configurations are still observed . For 2384 ft/sec the spectral levels for all the configurations are closer to each other for frequencies up to about 2 kHz. At higher frequency a hump is observed for convergent chute configuration indicating potentially larger contribution due to shock-associated noise by aligned convergent chute design for this underexpanded case.

In general, the 9 full chute staggered chute configuration seems to be acoustically the optimum design among the four cases studied in this section for higher velocities. However, the convergent chute configuration performs better acoustically at lower velocities.

4.4.3 Flow and Performance Related Results:

The 2D mixer-ejector models are instrumented for static and total pressure measurements at various locations to evaluate a number of flow and performance related parameters. The model instrumentation and the related results for 2D mixer-ejector nozzles with SAR=2.8 are compared between different mixer configurations, namely, aligned CD chute, staggered CD chute, and aligned convergent chute mixers, and are described in this section. Tests for all the four mixer-ejector configurations were conducted along the L1M cycle line for static and simulated flight conditions of Mach 0.32. Model pressure data measured in these tests are analyzed to show the effect of cycle conditions and the mixer geometry on various flow and performance related parameters.

The effect of mixer geometry on ramp and chute static pressure distributions are shown in Figures 4.4-13 and 4.4-14 for different L1M cycle conditions, at static condition and with
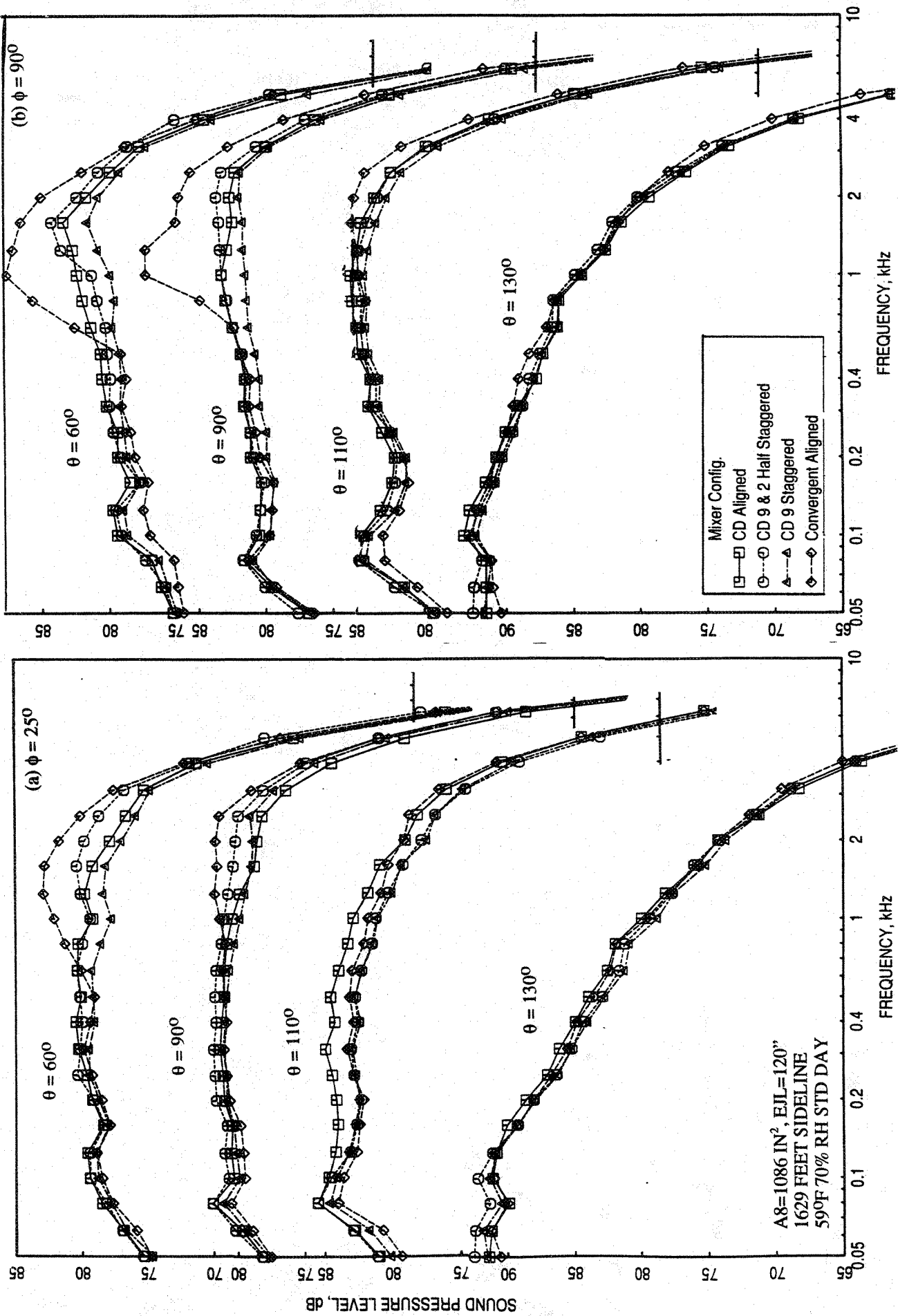
Figure 4.4-9. Comparison of SPL spectra at various polar angles (θ) between four mixer designs for 2D nozzle configurations with long treated ejector with flight simulation ($M_F=0.32$; SAR=2.8, MAR = 0.95, $V_j = 1147$ ft/sec, NPR = 1.5, T8 = 1000°R.

Figure 4.4-10. Comparison of SPL spectra at various polar angles (θ) between four mixer designs for 2D nozzle configurations with long treated ejector with flight simulation (M_F=0.32); SAR=2.8, MAR = 0.95, V_j =1920 ft/sec, NPR = 2.5, T8 = 1325°R.
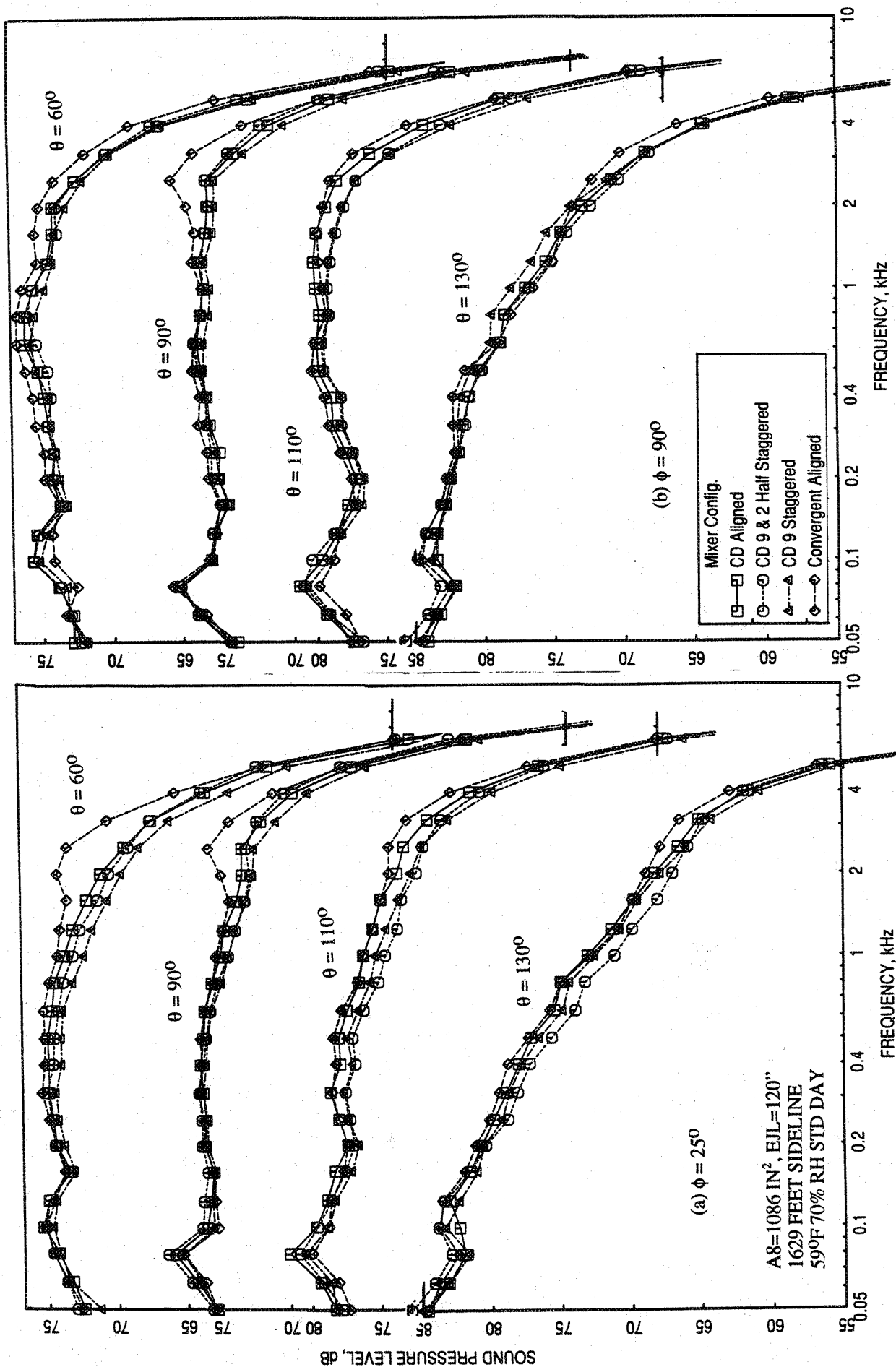
Figure 4.4-11. Comparison of SPL spectra at various polar angles (θ) between four mixer designs for 2D nozzle configurations with long treated ejector with flight simulation (M_F=0.32); SAR=2.8, MAR = 0.95, V_j = 2384 ft/sec, NPR = 3.4, T8 = 1590°R.

Figure 4.4-12. Comparison of SPL spectra at various polar angles (θ) between four mixer designs for 2D nozzle configurations with long treated ejector with flight simulation (M_F=0.32); SAR=2.8, MAR = 0.95, V_j = 2637 ft/sec, NPR = 4.0, T8 = 17500°R.
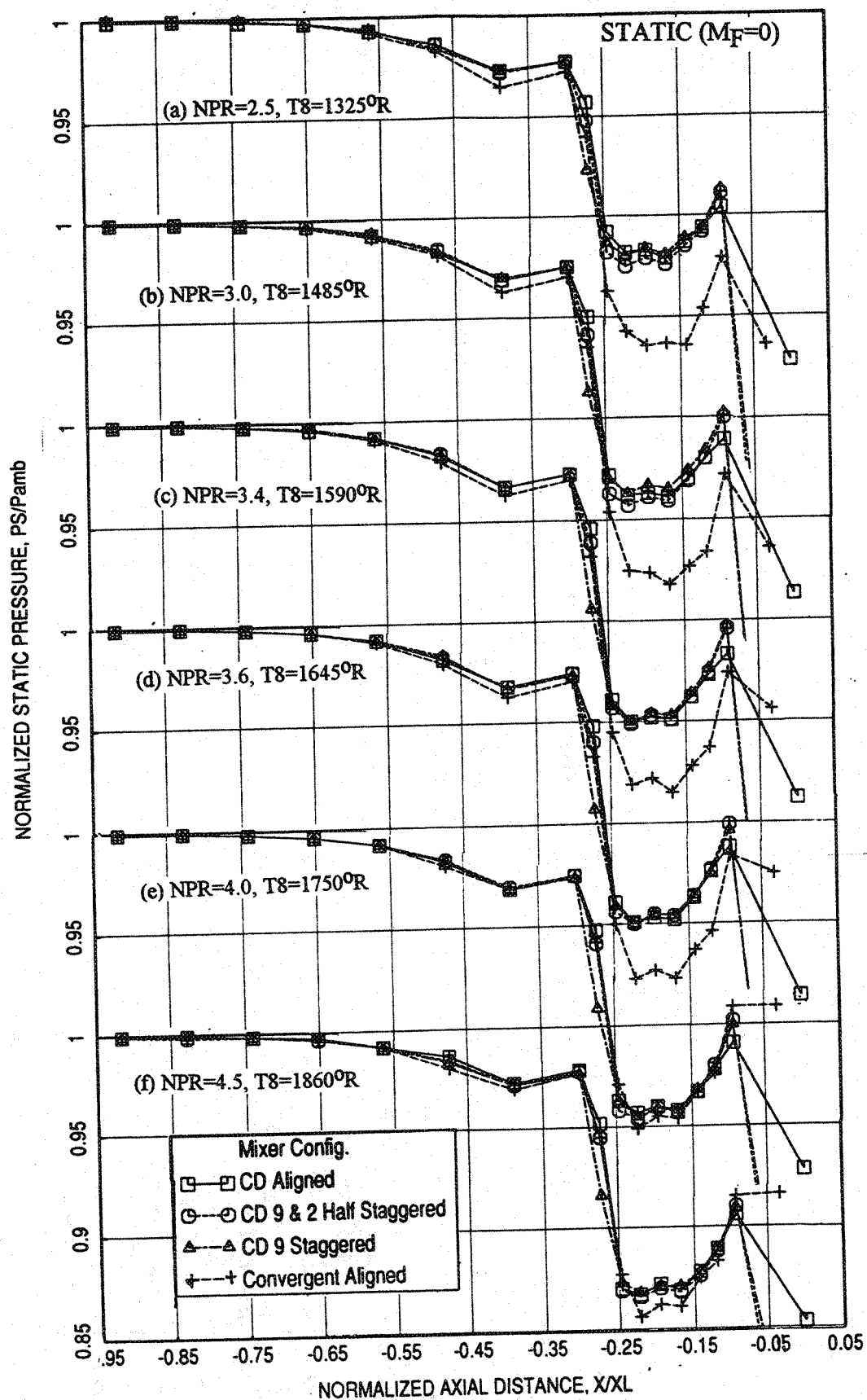
Figure 4.4-13. Effect of mixer geometry on the static pressure distributions on the inlet ramp and on the secondary flow side of chute surface at different L1M cycle conditions for 2D long treated mixer-ejector nozzle at static condition.
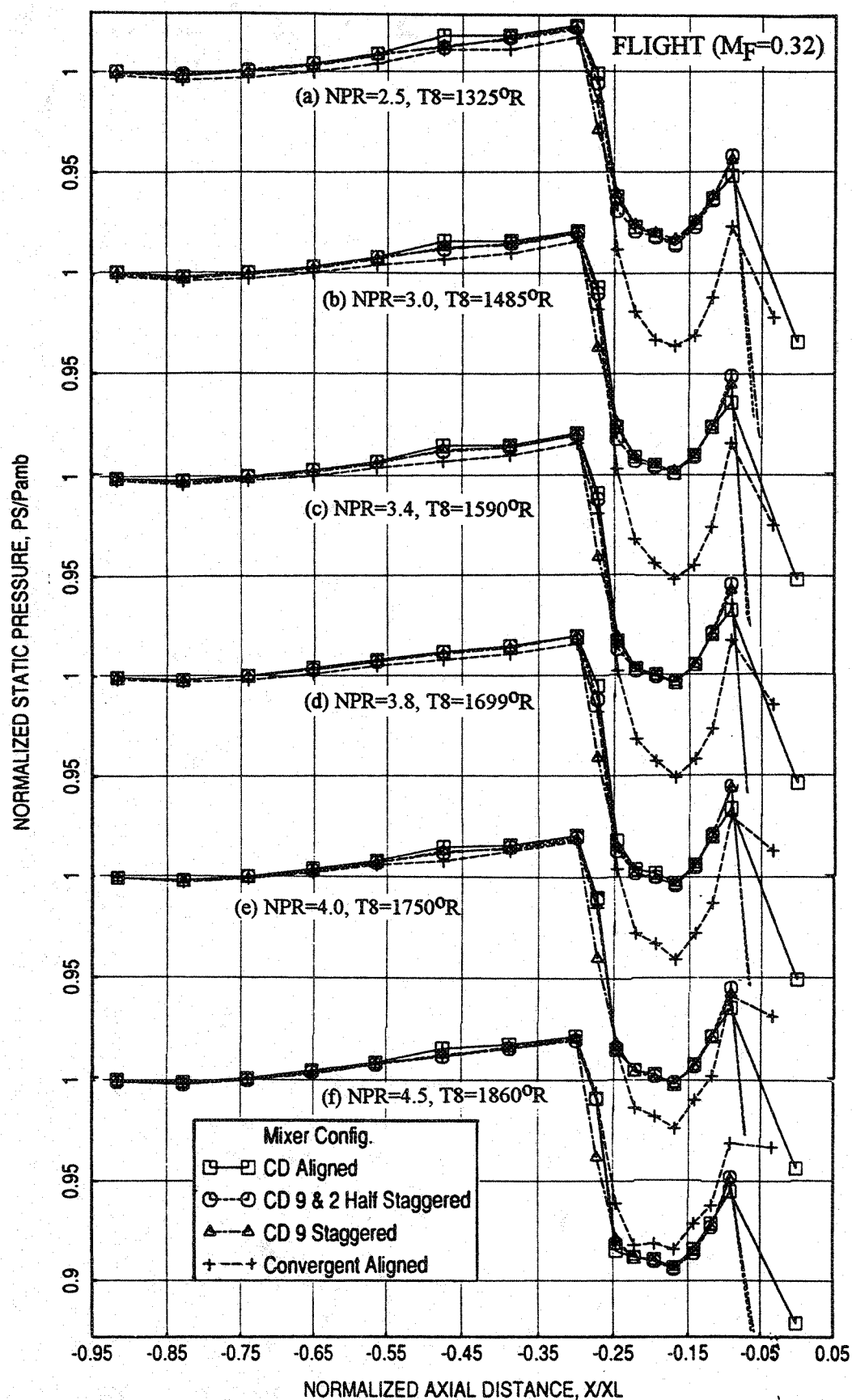
Figure 4.4-14. Effect of mixer geometry on the static pressure distributions on the inlet ramp and on the secondary flow side of chute surface at different L1M cycle conditions for 2D long treated mixer-ejector nozzle with flight simulation (M_F=0.32).

flight simulation, respectively. For each case the effect of mixer geometry on ramp static pressure distributions is insignificant. The static pressure distributions on the chute surface is more or less the same for the three CD chute mixers. However, it is significantly different for convergent chute mixer, especially at lower NPRs. The static pressure levels for convergent chute are much lower compared to those for CD chute configurations. The location of mixing plane of secondary and primary streams for convergent chutes is upstream compared to the CD chutes. This may be contributing to a more rapid acceleration of secondary flow (reduced static pressure) for convergent chutes. The secondary flow paths for CD chute mixers get narrower due to divergent primary stream flowpath imposes relatively higher back pressure for CD chutes. This would allow higher acceleration for convergent chutes compared to CD chutes. Again, for the same reason, the deceleration process is also higher for CD chutes compared to convergent ones closer to the exit plane. At higher NPR the chute static pressure distributions between CD and convergent chutes are almost the same, most likely, due to the higher back pressure at the throat plane for both chute configurations.

The chute loading coefficients due to chute static pressure distributions showing the effect of mixer geometry are plotted against NPR in Figure 4.4-15. For static as well as flight cases the convergent chutes exhibit lower chute loading force at lower NPR. Between the CD chute mixer configurations the aligned chutes exhibit higher loading due to chute static pressure distribution..

The effect of mixer geometry on pumping and corrected pumping is shown in Figures 4.4-16 and 4.4-17 for static and flight cases, respectively. With respect to NPR the pumping decreases. However, the pumping is higher for convergent chute mixer compared to CD chute mixers at static and at flight conditions. There is very little pumping difference between CD chute mixers with flight. At static condition, the aligned CD chute mixer seems to have higher pumping compared to staggered ones. It should be noted that the location of the total pressure rack on lower inlet with respect to the aligned CD chutes is some what different for staggered configurations. Hence, the pumping estimations for staggered configurations may be inconsistent with respect to aligned cases. Even though, the pumping is higher for convergent chute mixer, the mixer geometry effect is very small on the mixed jet velocity, computed on the basis of 1-D ejector flow (see Figure 4.4-18).

Figure 4.4-19 illustrates the comparison of axial static pressure distributions on the flap between various mixer configurations at static condition at different L1M cycle conditions. Insignificant difference in pressure distributions between mixer configurations is observed
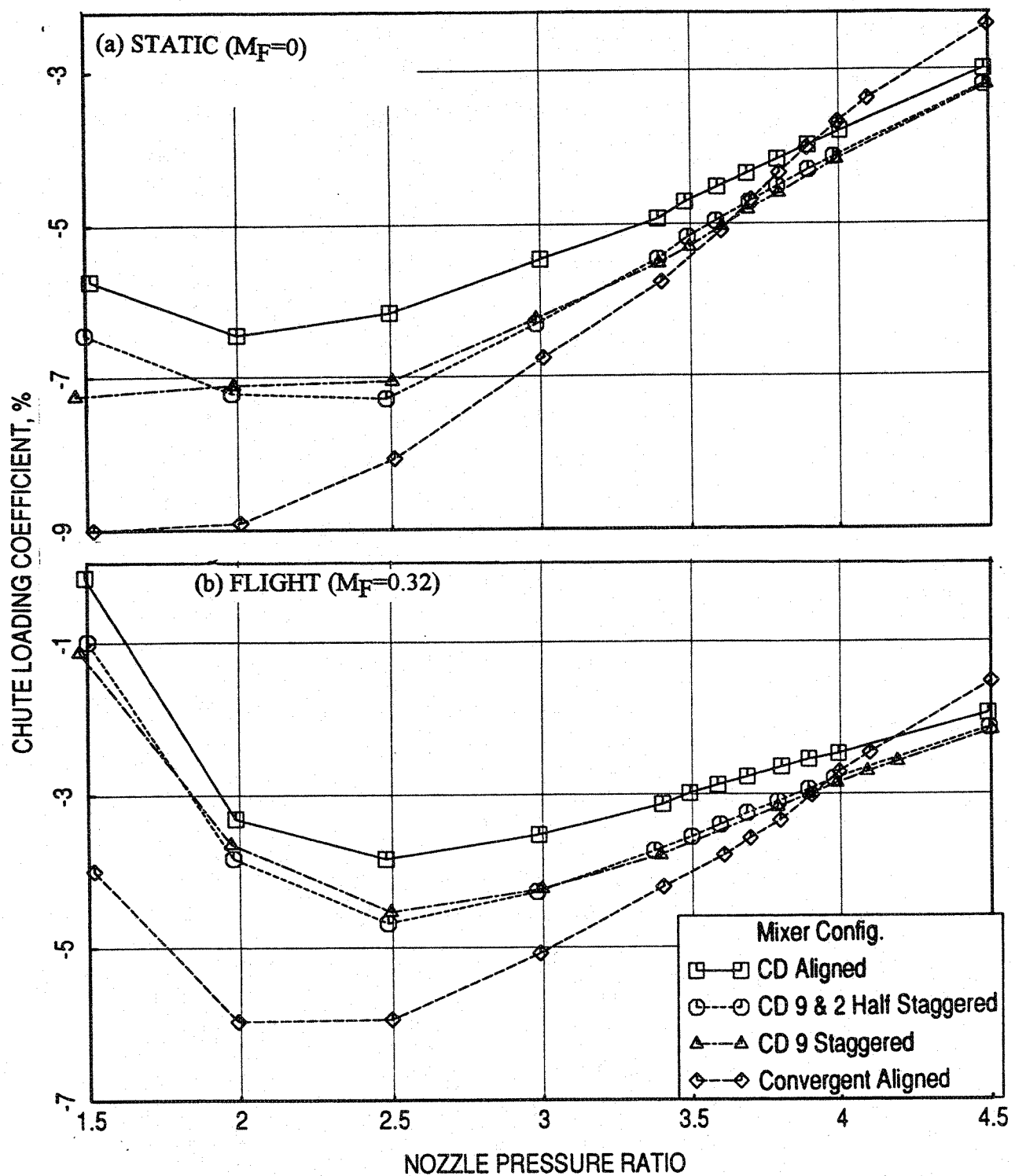
Figure 4.4-15. Effect of mixer geometry on chute loading coefficient, computed by measured static pressure distributions on secondary flow side chute leading edge, with respect to nozzle pressure ratios of L1M cycle conditions for 2D long treated mixer-ejector nozzle, (a) at static condition and (b) with flight simulation (M_F=0.32).
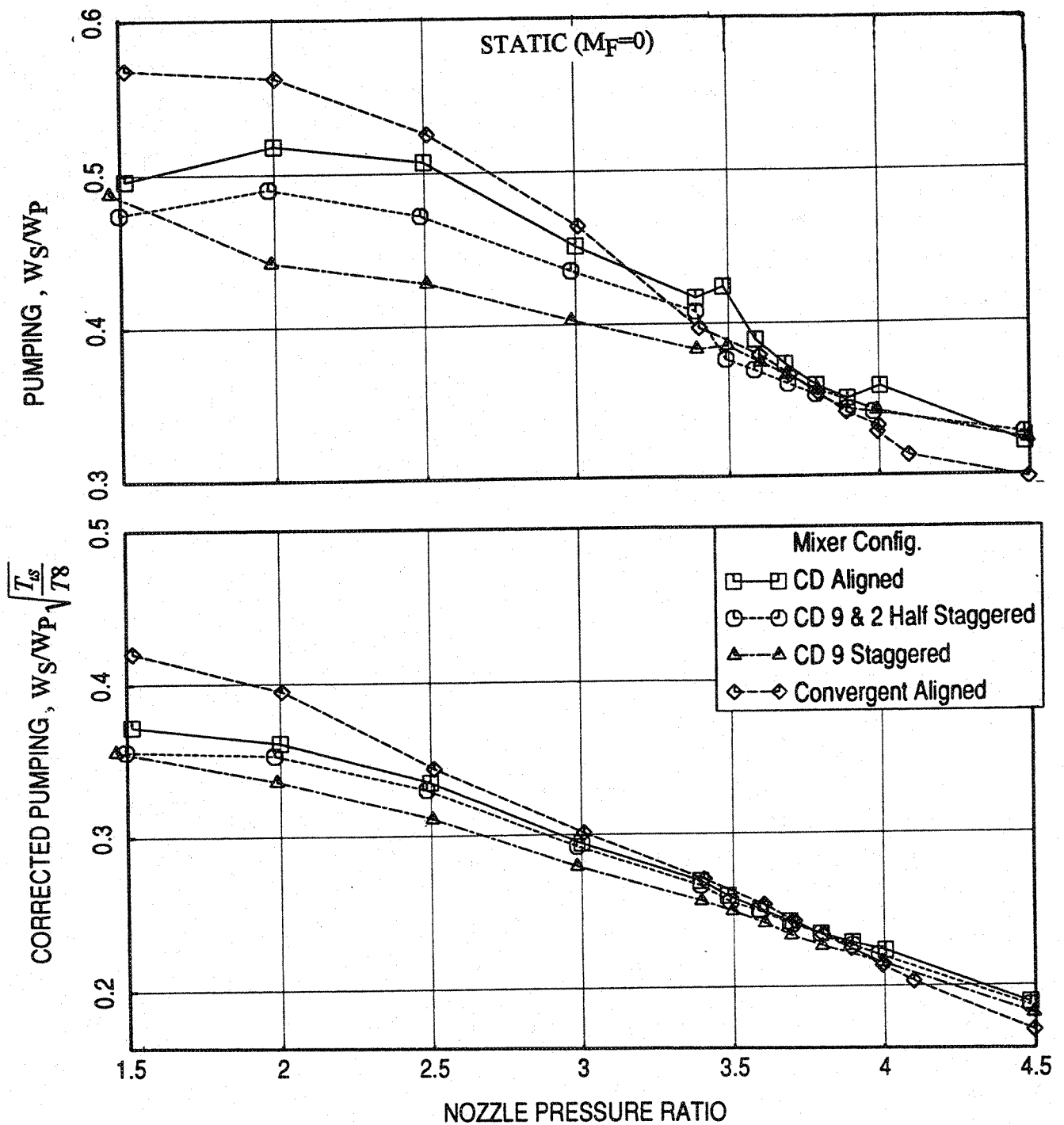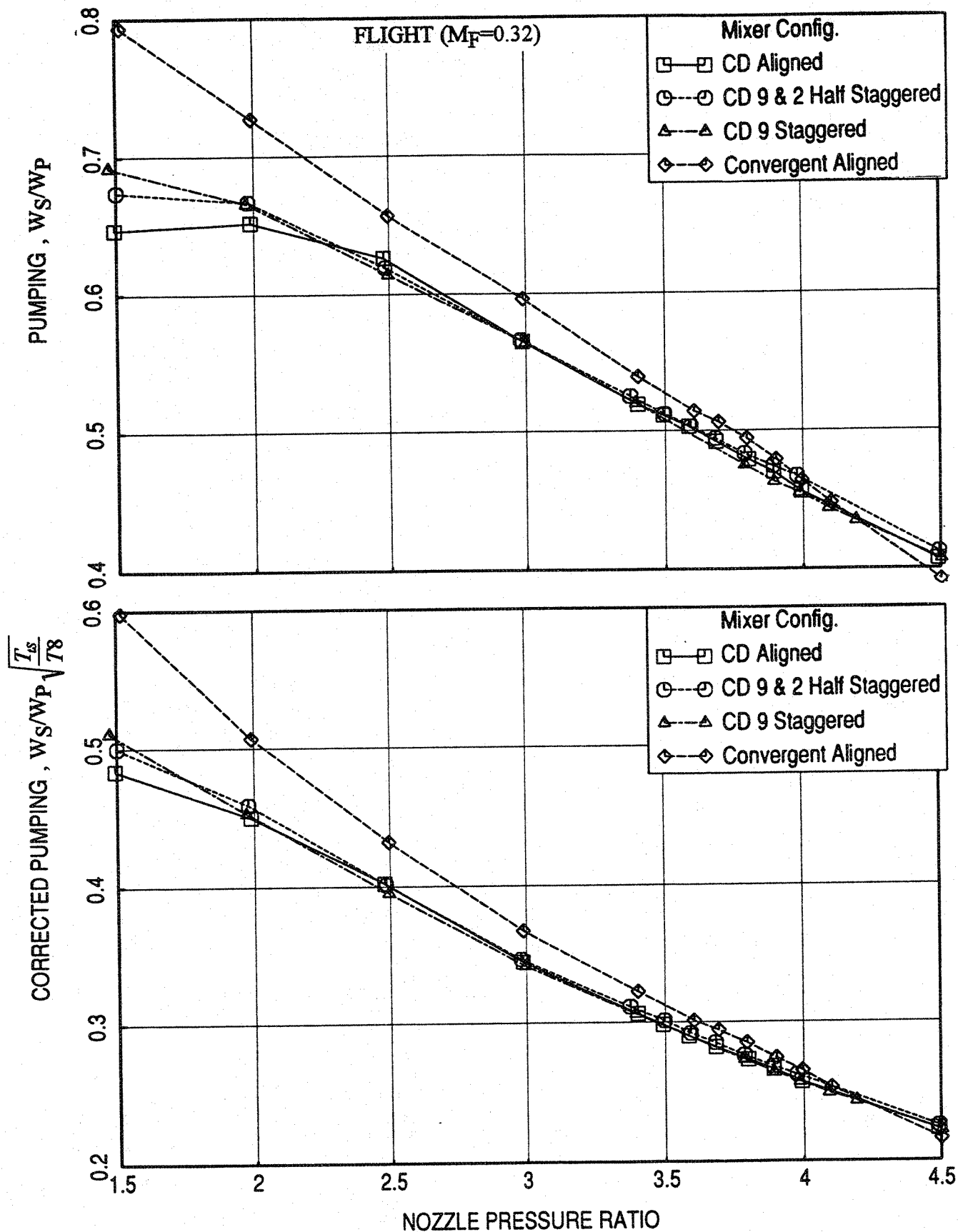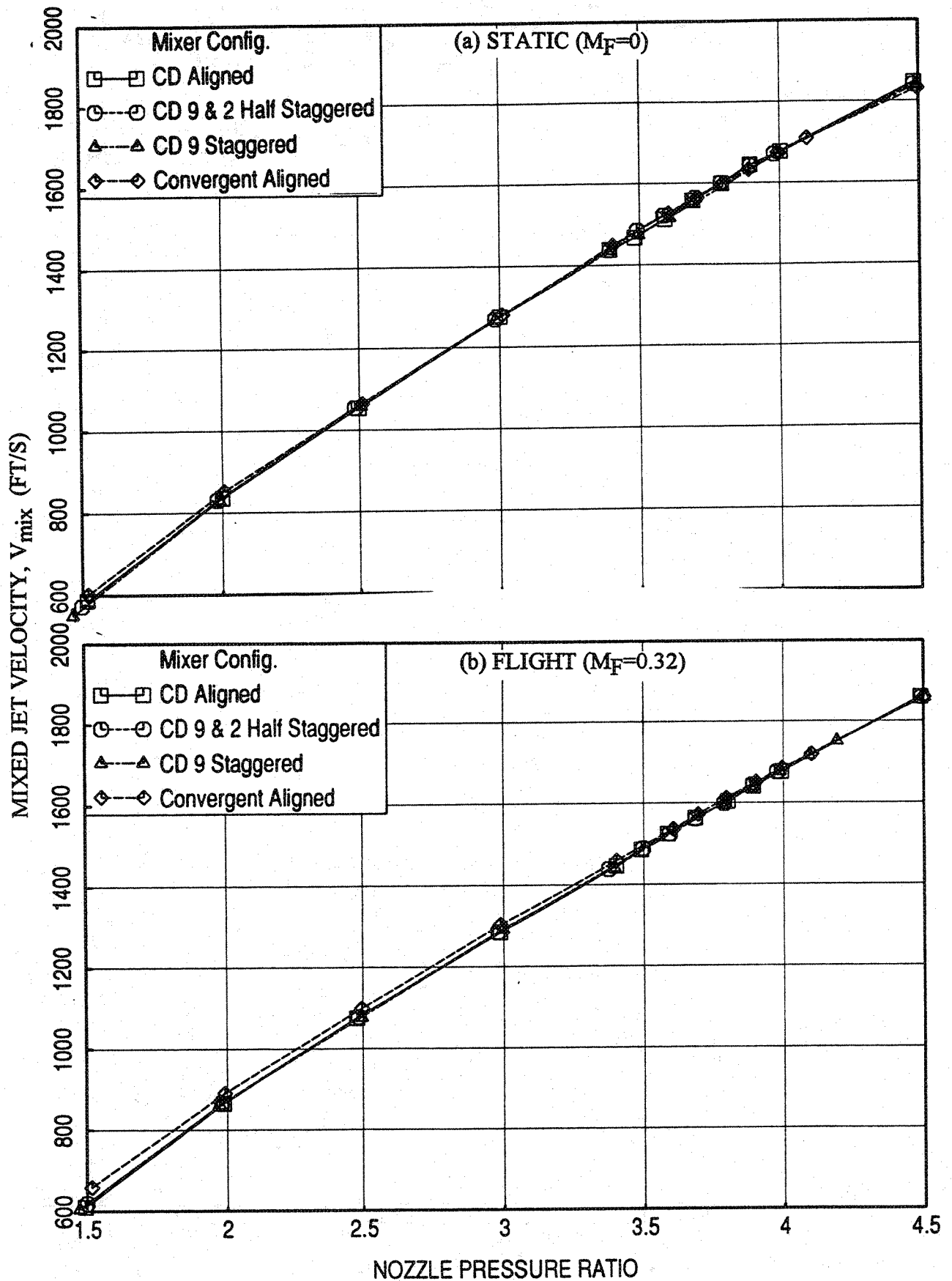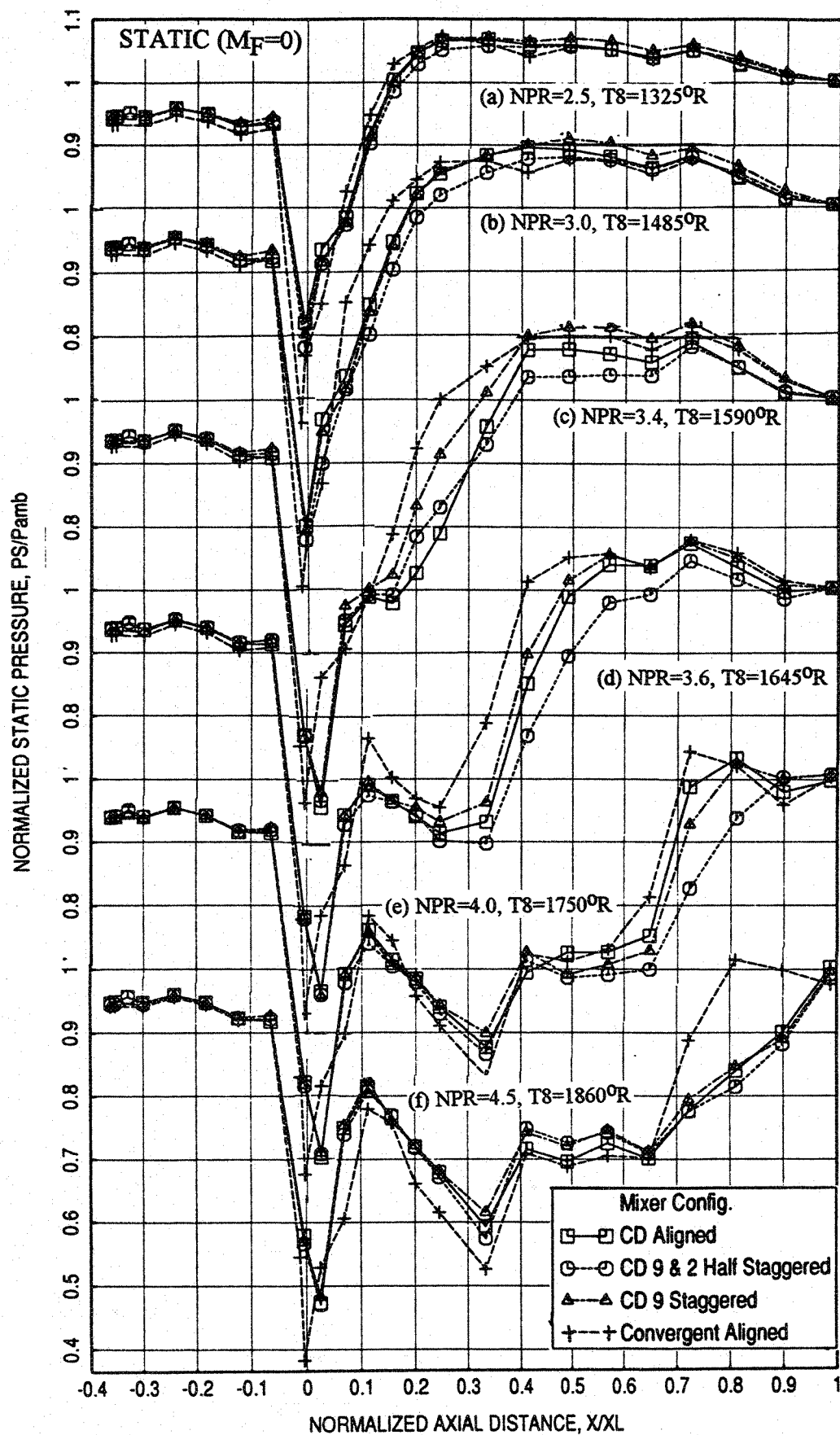
Figure 4.4-16. Effect of mixer geometry on pumping, computed by measured rake total pressure distributions at the inlet, with respect to nozzle pressure ratios of L1M cycle conditions for 2D long treated mixer-ejector nozzle at static condition.

Figure 4.4-17. Effect of mixer geometry on pumping, computed by measured rake total pressure distributions at the inlet, with respect to nozzle pressure ratios of L1M cycle conditions for 2D long treated mixer-ejector nozzle with flight simulation (M_F=0.32).

Figure 4.4-18. Effect of mixer geometry on mixed jet velocity, computed by measured rake total pressure distributions at the inlet, with respect to nozzle pressure ratios of L1M cycle conditions for 2D long treated mixer-ejector nozzle, (a) at static condition and (b) with flight simulation (M_F=0.32).
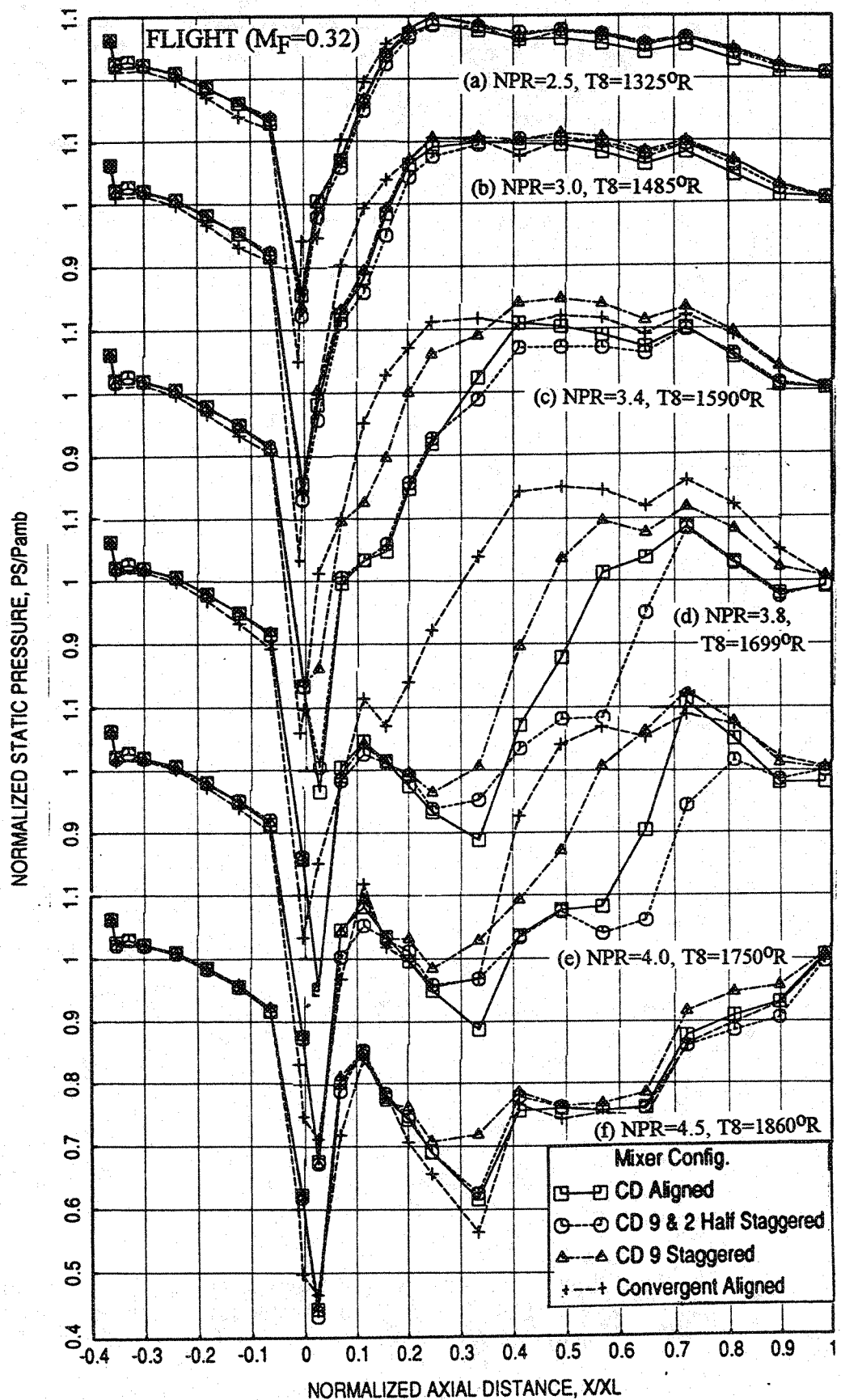
Figure 4.4-19. Effect of mixer geometry on axial distribution of average static pressure on the inlet and the flap surface at different L1M cycle conditions for 2D long treated mixer-ejector nozzle at static condition.

at lower NPRs. At higher NPR the static pressure distribution on the flap is higher for convergent chute mixer in subsonic flow mode. The 9 and two half staggered chute configuration exhibits lowest static pressure distribution on the flap. In supersonic mode the trend is reversed at the initial portion of the flap. Figure 4.4-20 shows the effect of mixer geometry on force and moment of force with respect to flap leading edge due to static pressure difference on flap surface as a function of nozzle pressure ratio. Both the force and the moment are slightly lower for convergent chute mixer and the levels are higher for the 9 and 2 half CD chute mixer configuration. The transition from subsonic to supersonic mode seems to be slightly delayed with respect to NPR for convergent chute mixer.

Similar results with flight simulation are plotted in Figures 4.4-21 and 4.4-22. The static pressure distributions between the mixer configurations clearly indicate that the mode switch is delayed for convergent chute mixer and is relatively early for 9 and 2 half staggered chute configuration. Similar conclusions are deduced from the force and moment of the force results, as shown in Figure 4.4-22.

4.4.4 Effect of Chute Design at Lower Jet Velocity Conditions:

The impact of chute designs, namely, convergent compared to convergent-divergent (CD), on acoustic characteristics of mixer-ejector nozzles are examined for lower velocity conditions (i.e., velocities between 700 and 1900 ft/sec). In this study, the convergent aligned and 9 CD-chute staggered mixers with long hardwalled ejector configurations were tested statically at lower NPR and nozzle total temperature conditions by extrapolating the L1M cycle line. The nozzle pressure ratio (NPR) is varied between 1.2 and 2.5. The corresponding nozzle total temperature is varied between 880°R to 1325°R.

Figure 4.4-23 shows the OASPL directivity comparisons between the above mentioned mixer configurations at seven different jet velocity conditions. The corresponding PNLT results are shown in Figure 4.4-24. The OASPL and PNLT levels are significantly higher for the CD-chute mixer compared to convergent chute at lower velocity conditions. The difference in these noise levels are much higher in the forward arc indicating strong shock associated noise for CD chute mixer. The noise levels become comparable with increasing velocity conditions and the trend begins to reverse at about 1600 ft/sec condition (i.e., NPR=2.0 and T8=1175°R). The SPL comparisons between these two mixers at four polar angles, namely, 60°, 90°, 110°, and 130°, for the corresponding seven velocity conditions are shown in Figures 4.4-25 through 4.4-28, respectively.
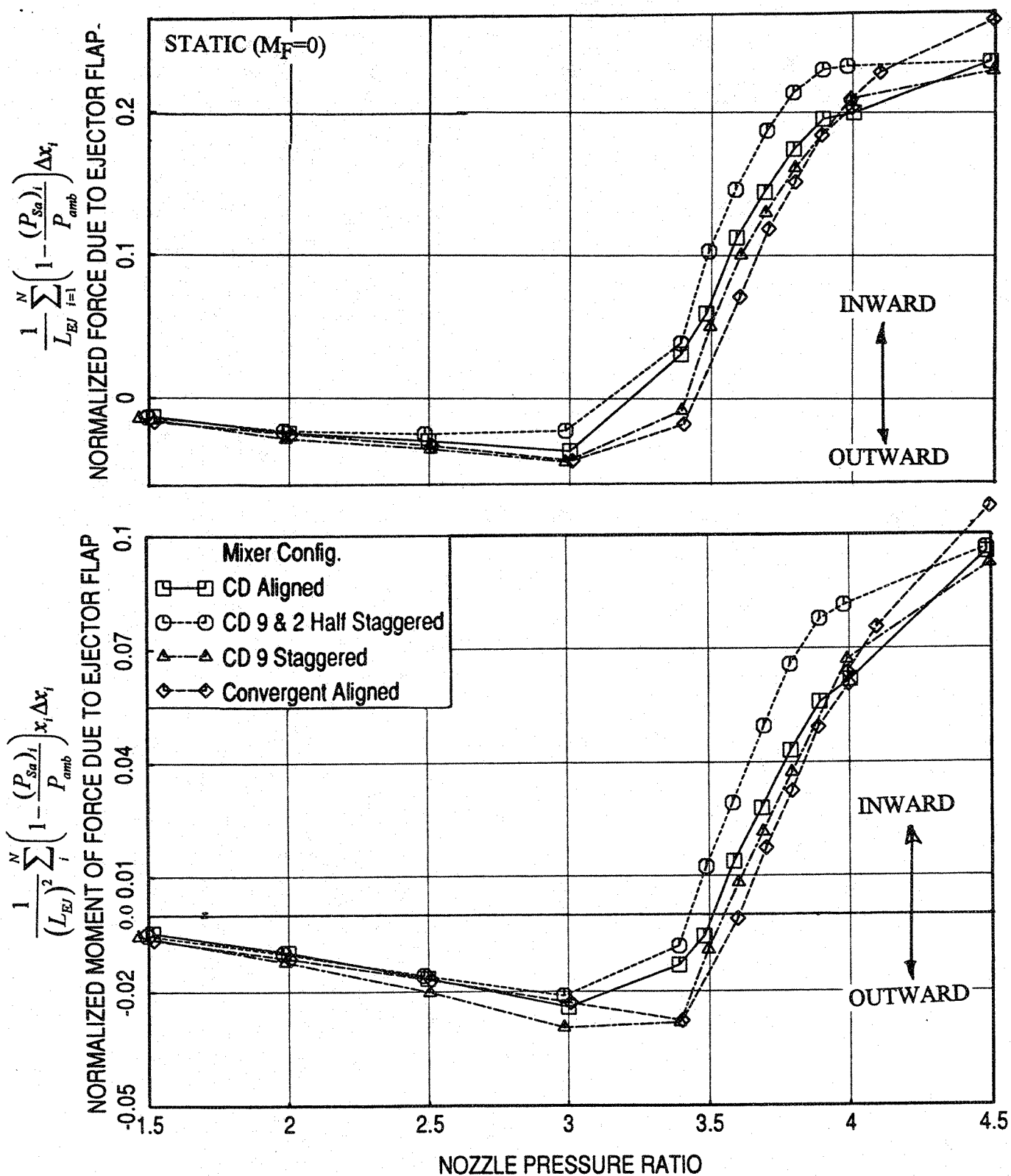
Figure 4.4-20. Effect of mixer geometry on normalized (a) force and (b) moment of force due to ejector flap with respect to nozzle pressure ratio of L1M cycle conditions for 2D long treated mixer-ejector nozzle at static condition.

Figure 4.4-21. Effect of mixer geometry on axial distribution of average static pressure on the inlet and the flap surface at different L1M cycle conditions for 2D long treated mixer-ejector nozzle with flight simulation (M_F=0.32).
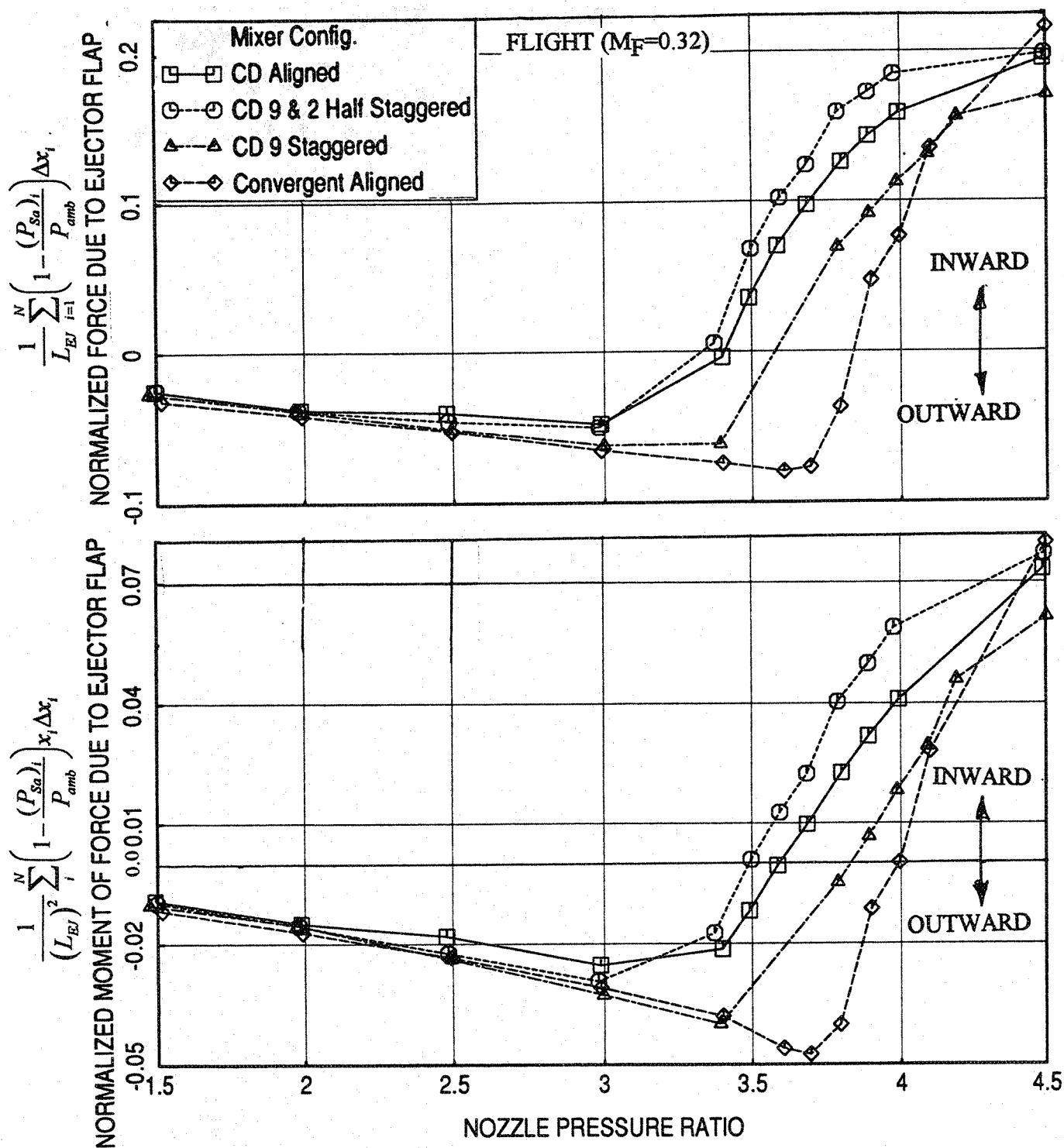
Figure 4.4-22. Effect of mixer geometry on normalized (a) force and (b) moment of force due to ejector flap with respect to nozzle pressure ratio of L1M cycle conditions for 2D long treated mixer-ejector nozzle with flight simulation (M_F=0.32).
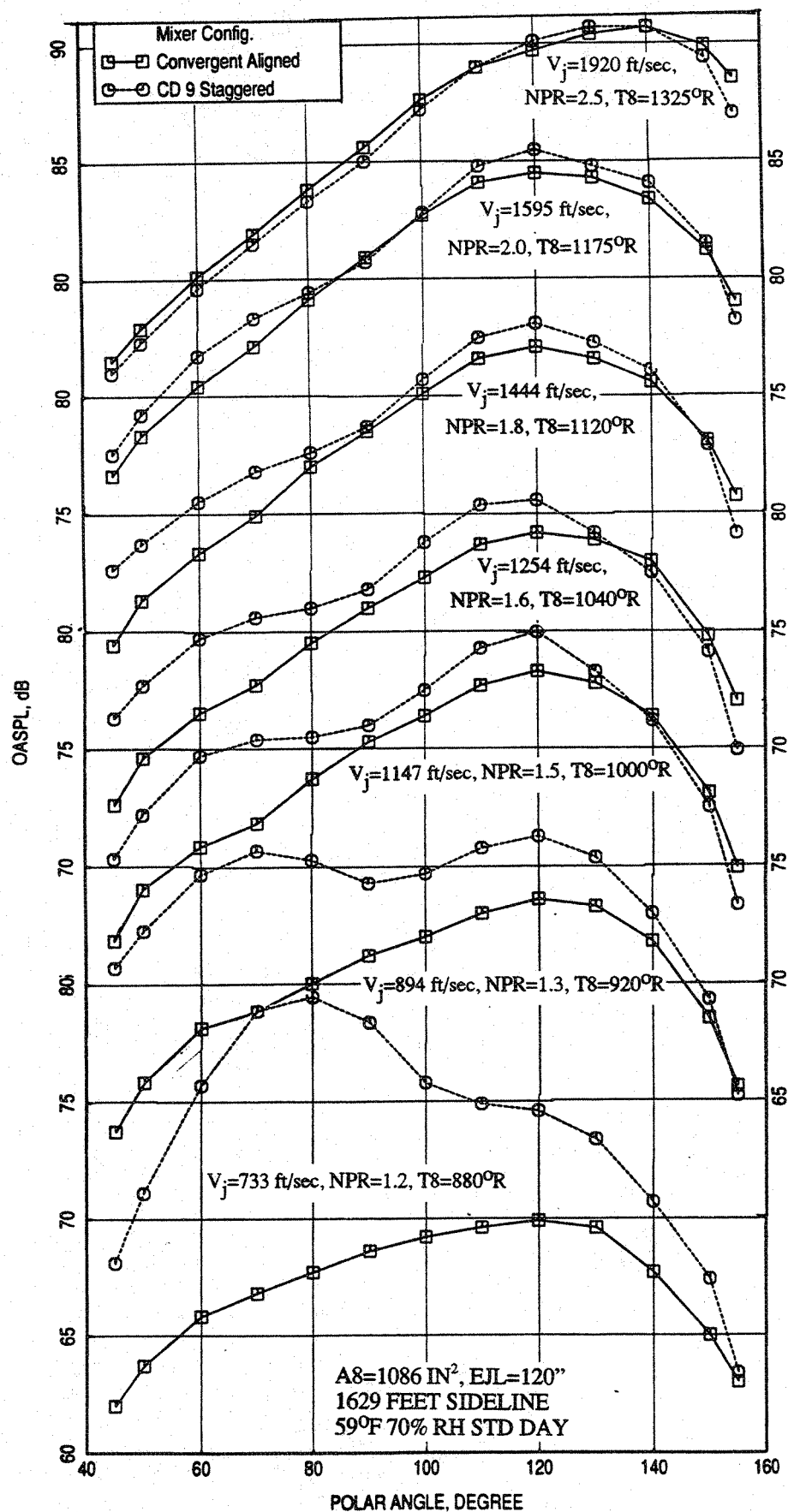
Figure 4.4-23. Comparison of OASPL directivities for different low nozzle pressure ratio jet velocities (V_j) between convergent chute aligned and CD 9-chute staggered mixers with long hardwalled ejector at static condition; SAR=2.8, MAR = 0.95, ϕ=25°.
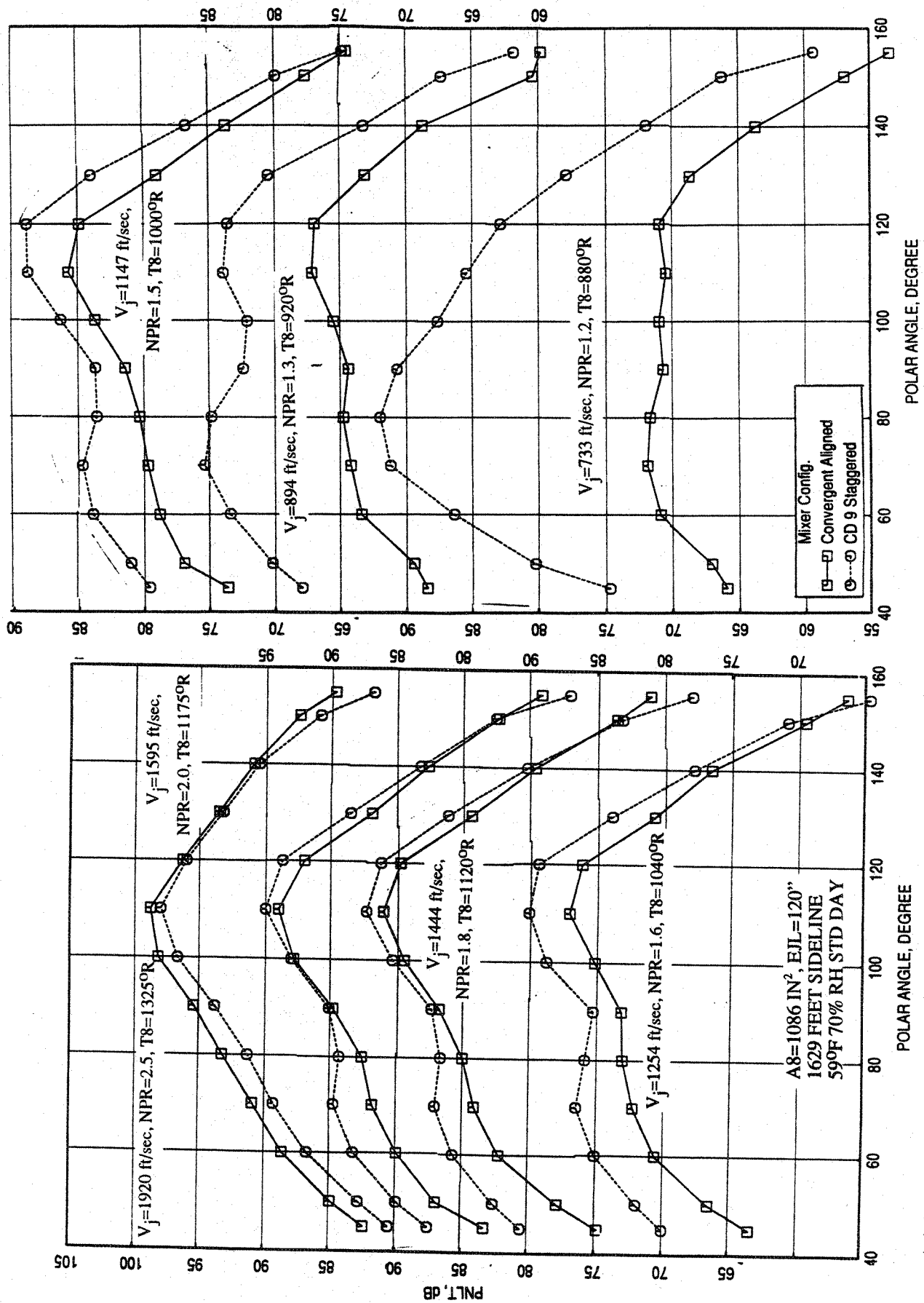
Figure 4.4-24. Comparison of PNLT directivities for different low nozzle pressure ratio jet velocities (V_j) between convergent chute aligned and CD 9-chute staggered mixers with long hardwalled ejector at static condition; SAR=2.8, MAR = 0.95, ϕ=25°.
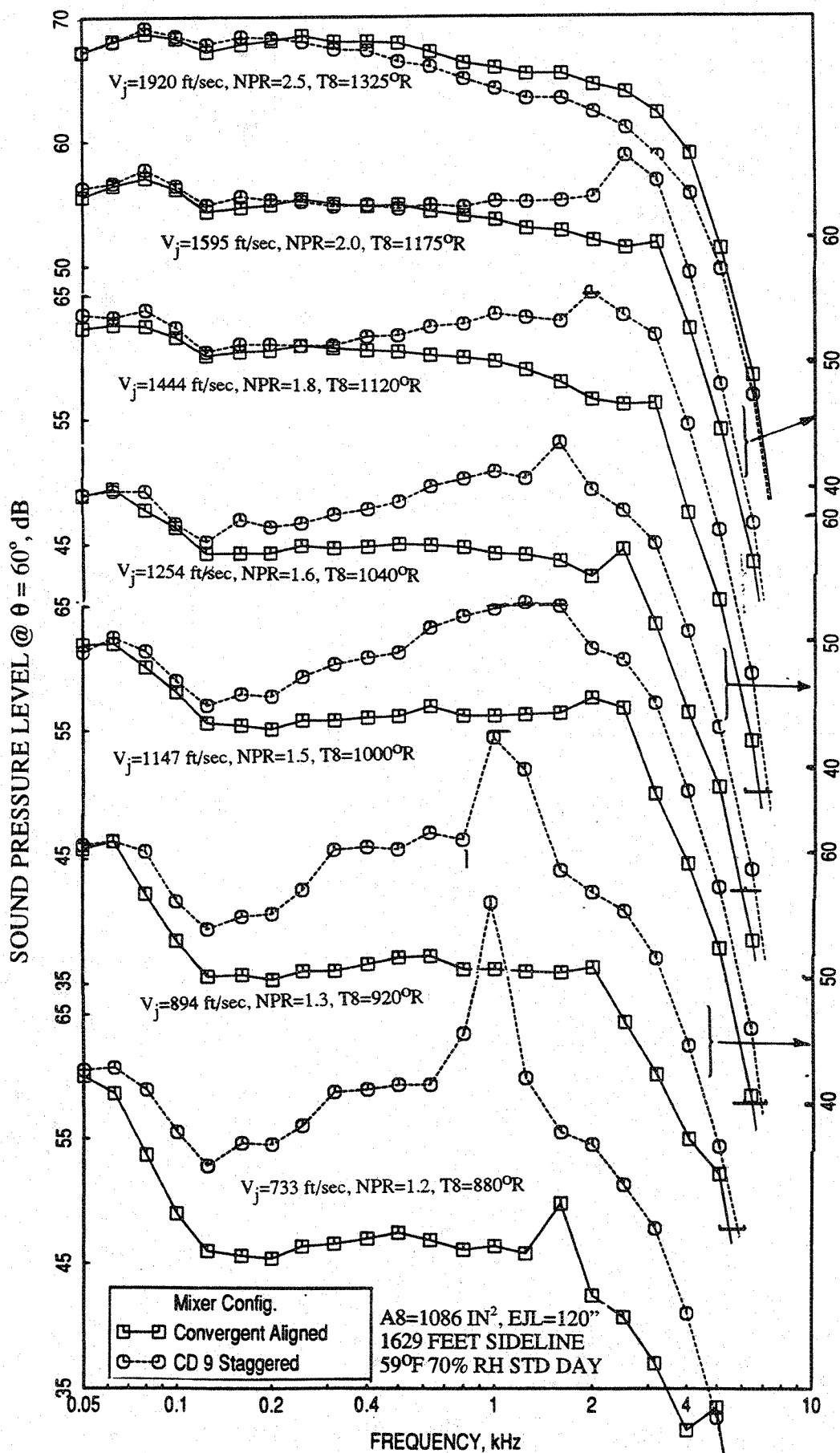
Figure 4.4-25. Comparison of SPL spectra at a polar angle (θ) of 60° for different low nozzle pressure ratio jet velocities (V_j) between convergent chute aligned and CD 9-chute staggered mixers with long hardwalled ejector at static condition; SAR=2.8, MAR = 0.95, φ=25°.
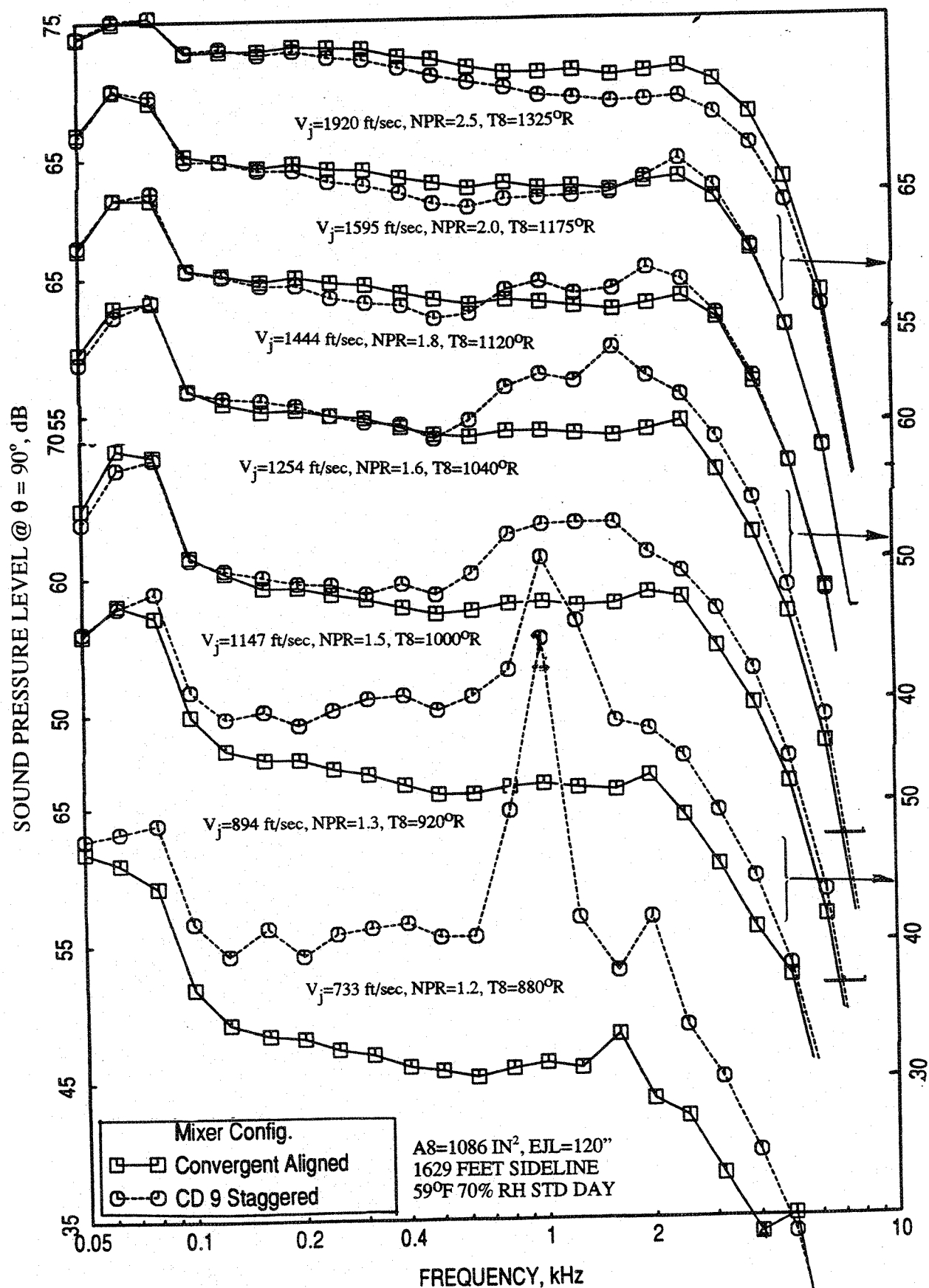
Figure 4.4-26. Comparison of SPL spectra at a polar angle (θ) of 90° for different low nozzle pressure ratio jet velocities (V_j) between convergent chute aligned and CD 9-chute staggered mixers with long hardwalled ejector at static condition; SAR=2.8, MAR = 0.95, ϕ=25°.
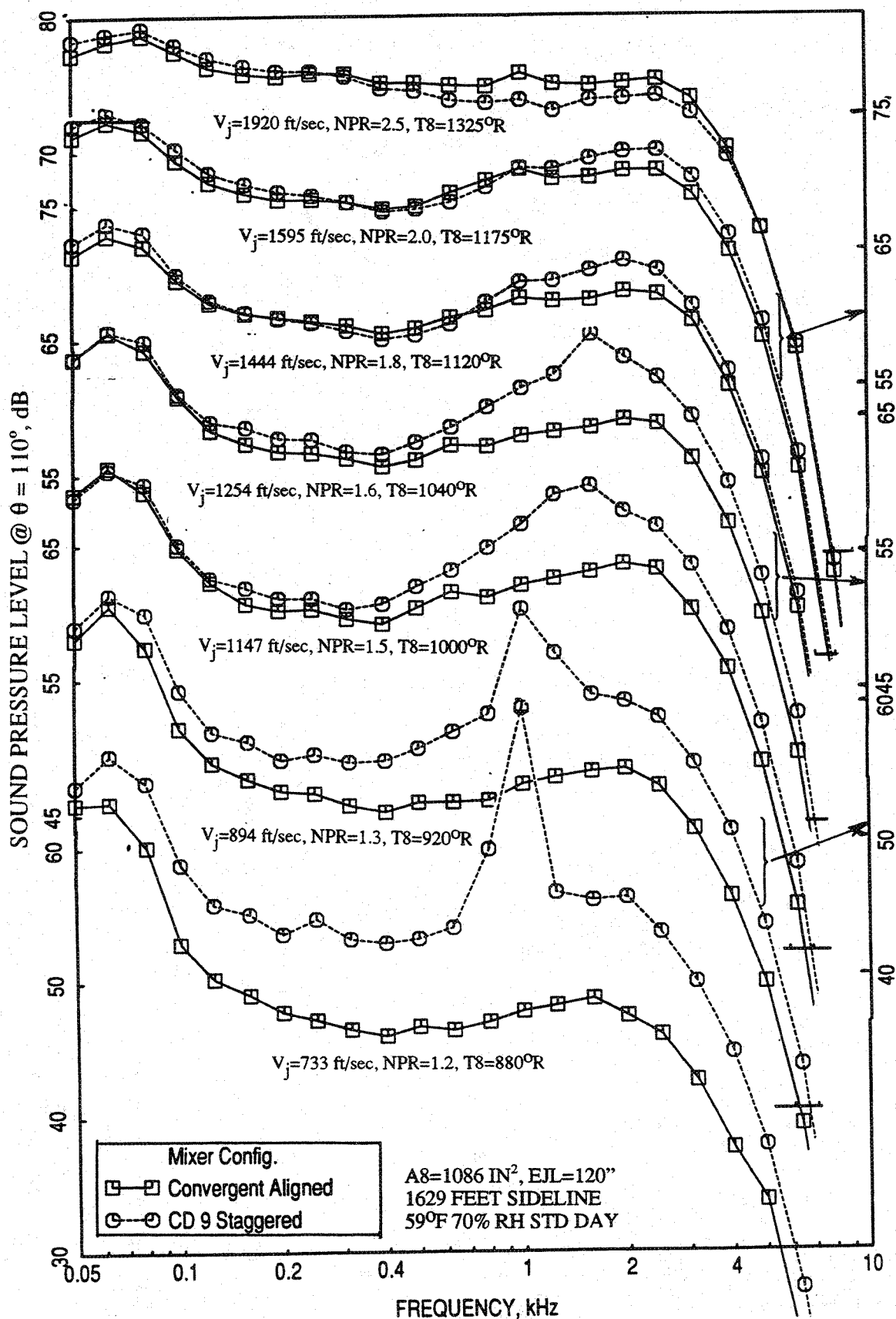
Figure 4.4-27. Comparison of SPL spectra at a polar angle (θ) of 110° for different low nozzle pressure ratio jet velocities (V$_j$) between convergent chute aligned and CD 9-chute staggered mixers with long hardwalled ejector at static condition; SAR=2.8, MAR = 0.95, φ=25°.
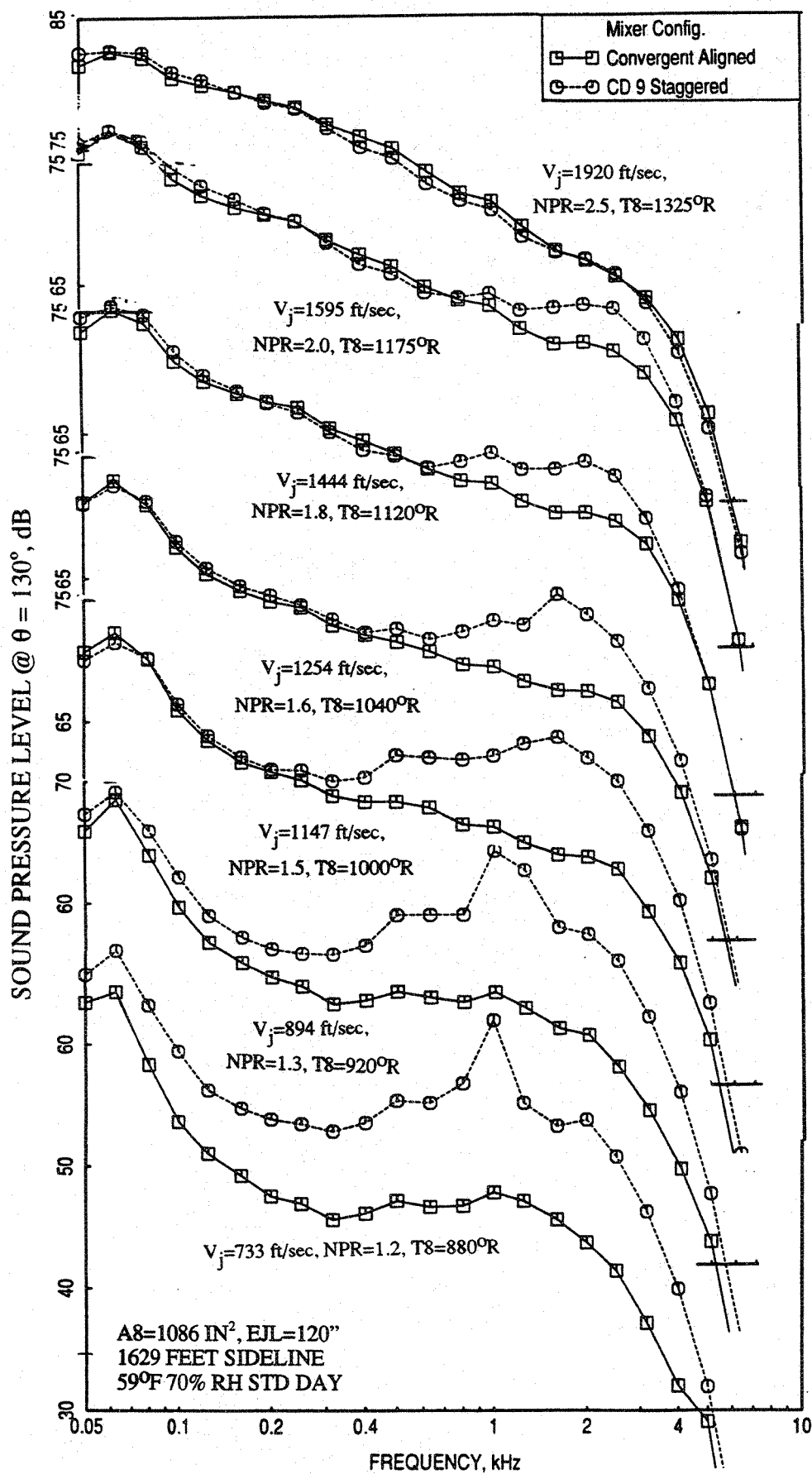
Figure 4.4-28. Comparison of SPL spectra at a polar angle (θ) of 130° for different low nozzle pressure ratio jet velocities (Vⱼ) between convergent chute aligned and CD 9-chute staggered mixers with long hardwalled ejector at static condition; SAR=2.8, MAR = 0.95, φ=25°.

Indication of a strong shock (or screech) is observed for the CD-chute mixer at lower NPR conditions. The frequency of the noise peak increases with increasing NPR. However, the frequency change with respect to polar angle is not apparent from these results, since the band width is relatively higher on 1/3-octave band basis. Peak frequency shift with respect to polar angle would have positively identified whether the peak is due to shock or screech. However, the probability of strong shock generation in the CD chute is much higher at lower NPR. The static pressure distribution on chute surface, as shown in Figure 4.4-29, indicates lower static pressure at the CD chute exit compared to convergent mixer. This behavior increases the local NPR by certain amount. Based on the pressure and temperature conditions the flow in the CD chutes does not attain critical level for lower NPR cases. However, the flow overexpands in the divergent portion of the chute and creates strong shocks, across which static pressure increases. There is a region of supersonic flow ahead of the shock with choked throat. Behind the shock, the flow is subsonic, hence the Mach number decreases towards the exit and the static pressure increases to the exit static pressure.

This is further illustrated in Figure 4.4-30 by plotting the static pressure distributions inside the CD chute at different flow conditions. As shown in Figure 4.1-4, static pressure taps are placed within a chute in the hot core flow segment from the throat to the exit plane, at mid-span height. Static pressures were measured at these taps for some flow conditions, which are plotted in Figure 4.4-30. Static pressures for flow conditions not measured are shown in Figure 4.4-30 by interpolation of the measured data in a qualitative manner and calculating the static pressures at the throat for choked condition. It should be noted that the minimum area (i.e., actual throat) is apparently formed slightly upstream of the physical throat due to boundary layer formation. Therefore, the measured (as well as the interpolated) static pressures at the throat are slightly lower than the pressures corresponding to choked conditions. From this figure it is clear that a normal shock was formed in the divergent portion of the chute at NPRs of 1.2 and higher. The location of the shock moves towards the exit and the shock strength diminishes with increasing NPR. The flow remains subsonic in the CD chute with acceleration in convergent section and deceleration in the divergent section at NPR=1.08 without any shock formation.

The higher noise level and the noise peak observed at lower NPR conditions are most likely the contribution of strong shock associated noise in the CD chutes. For convergent chutes the flow remains subsonic up to the chute exit for local subcritical NPR conditions. At higher NPR condition the flow becomes sonic at the convergent chute exit and generates some amount of shock associated noise in the confinement of the ejector by creating diamond type shock structures.
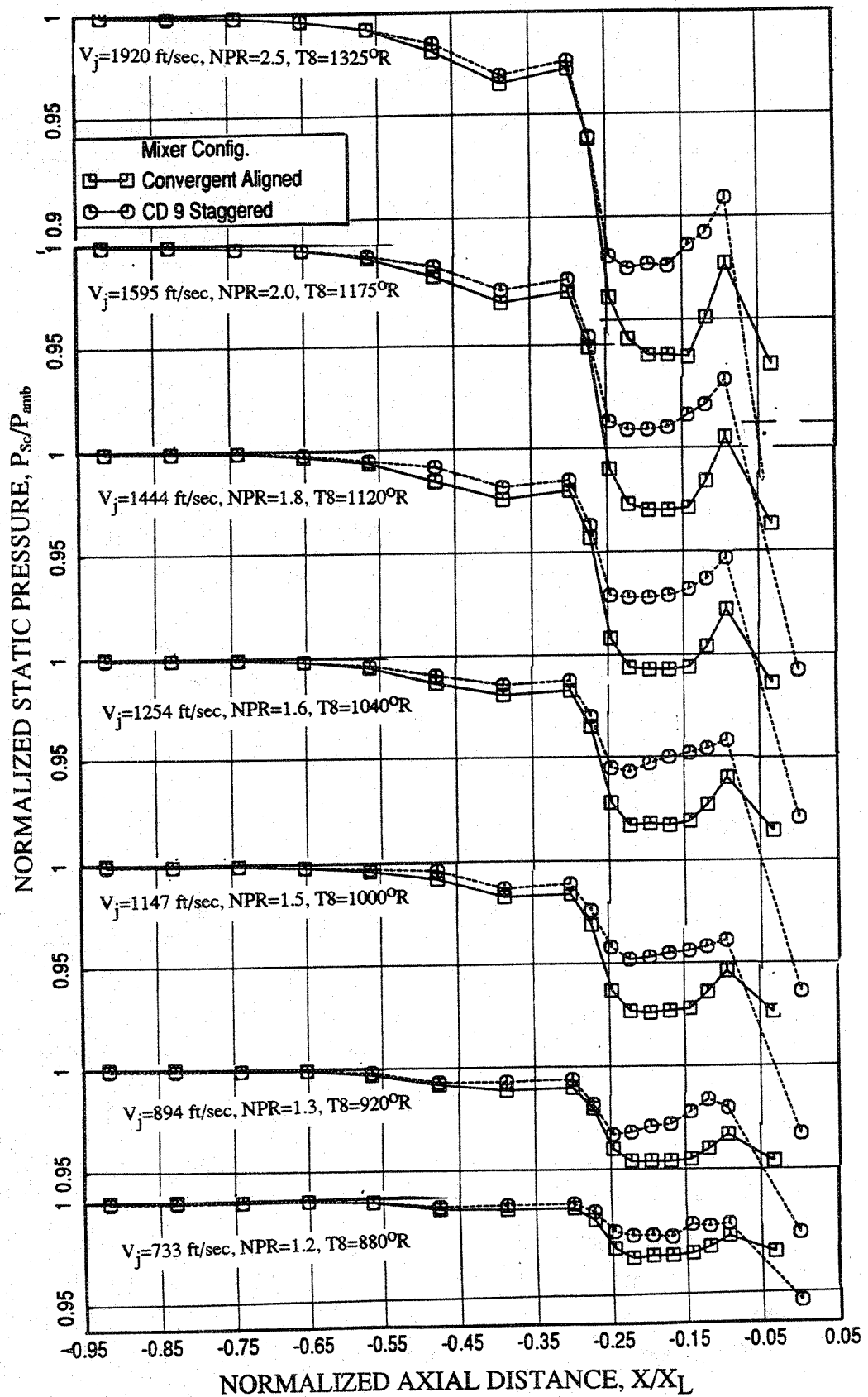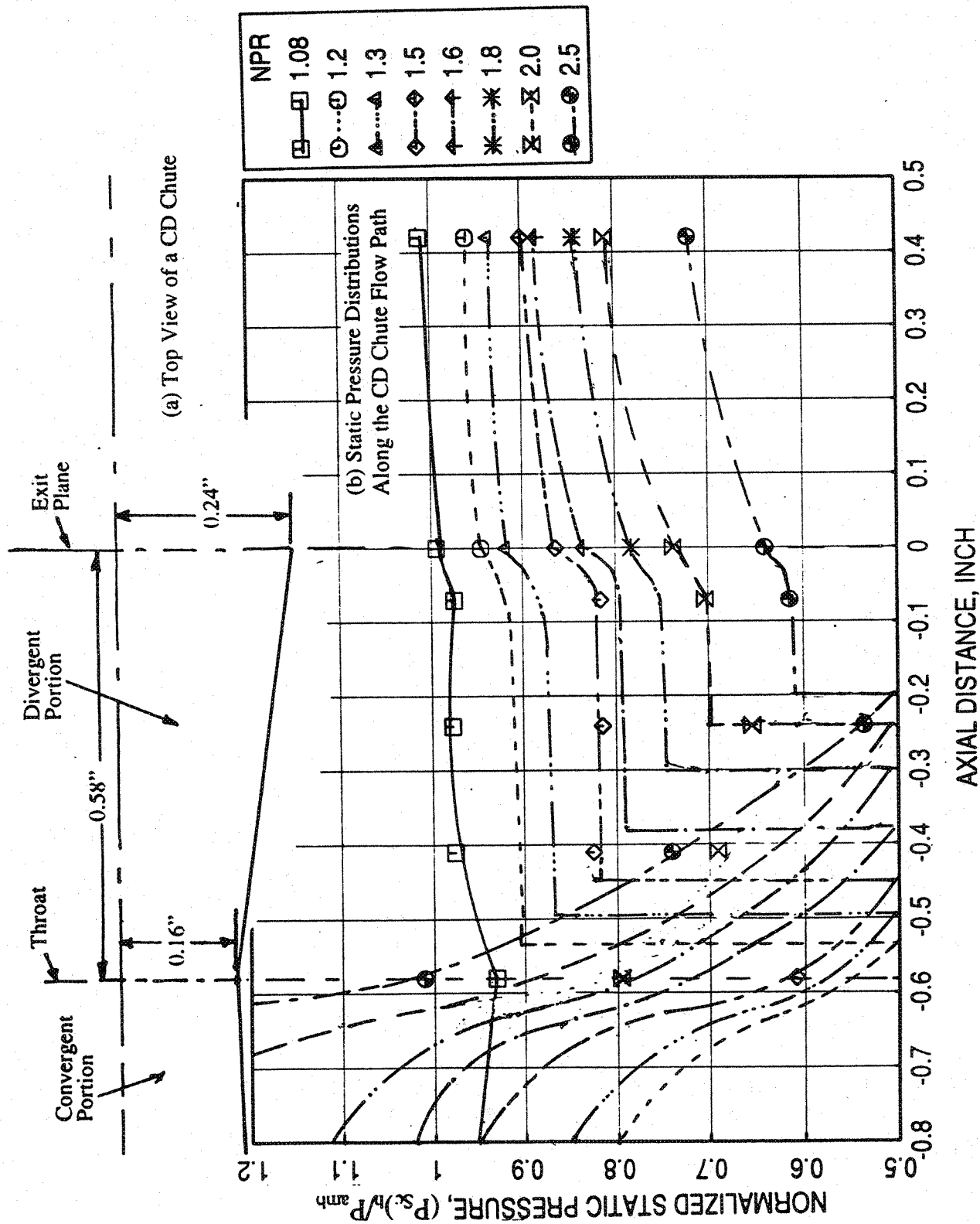
Figure 4.4-29. Comparison of static pressure distributions on the inlet ramp and on the secondary flow side of chute surface for different low nozzle pressure ratio jet velocities (V_j) between convergent chute aligned and CD 9-chute staggered mixers with long hardwalled ejector at static condition; SAR=2.8, MAR = 0.95, $\phi=25^O$.

Figure 4.4-30. Static pressure distributions inside the hot core flow segment of a CD chute from convergent section, upstream of the throat, to the exit plane at different flow conditions.

260

5.0 INFLUENCE OF OFF-CYCLE AEROTHERMODYNAMIC CONDITIONS ON ACOUSTIC AND PERFORMANCE RELATED RESULTS FOR 10 AND 9 FULL CD-CHUTE STAGGERED MIXER-EJECTOR CONFIGURATIONS

The acoustic, the flow related, and performance related results at L1M cycle conditions for various 2D mixer-ejector configurations are examined in the previous section to determine acoustically best performing mixer geometry. The staggered chute mixer-ejector with 10 full CD chutes in upper rack and 9 full CD chutes in lower rack with SAR=2.8 seems to be the quietest among all the mixers tested under this program. It is important to optimize the acoustic performance of the mixer with respect to the aerothermodynamic conditions at takeoff and cutback. It is also important to determine the relative strength of noise generated internal to the ejector compared to the jet mixing noise, generated in the freefield, at least, in a qualitative manner. This knowledge would help in further noise optimization process, including the design of acoustic liners for the ejector.

Additional tests were conducted to achieve these objectives for two 2D staggered chute mixer-ejector configurations with 10 full CD chutes in upper rack and 9 full CD chutes in lower rack, one with fully treated (with nickel based metal foam with a 37% porous facesheet) long ejector and the second with hardwalled short ejector. These tests include (1) flight simulation tests for L1M cycle conditions at flight Mach numbers of 0.24 and 0.36, (2) tests at fixed jet velocities by varying the nozzle pressure ratio and total temperature at static and simulated flight Mach numbers of 0.24, 0.32, and 0.36, and (3) tests at fixed nozzle pressure ratios by varying the total temperature at static and simulated flight Mach numbers of 0.24, 0.32, and 0.36. The higher flight Mach number of 0.36 is selected for these tests to obtain the maximum flight effect on noise to qualitatively evaluate the internal and external noise components.

5.1 EFFECT OF SIMULATED FLIGHT :

Figure 5-1 shows the effect of flight simulation on PNLT and EPNL as function of jet velocity (V_j) for the fully treated long ejector configuration at an azimuthal angle $\phi=25^o$. EPNL decreases with increasing flight Mach number for all jet velocities. Except for forward arc angles the PNLT also decreases with increasing flight Mach Number at all jet velocities. Similar results for the hardwalled short ejector configuration are plotted in Figure 5-2. The influence of flight on these results are qualitatively similar to those for the
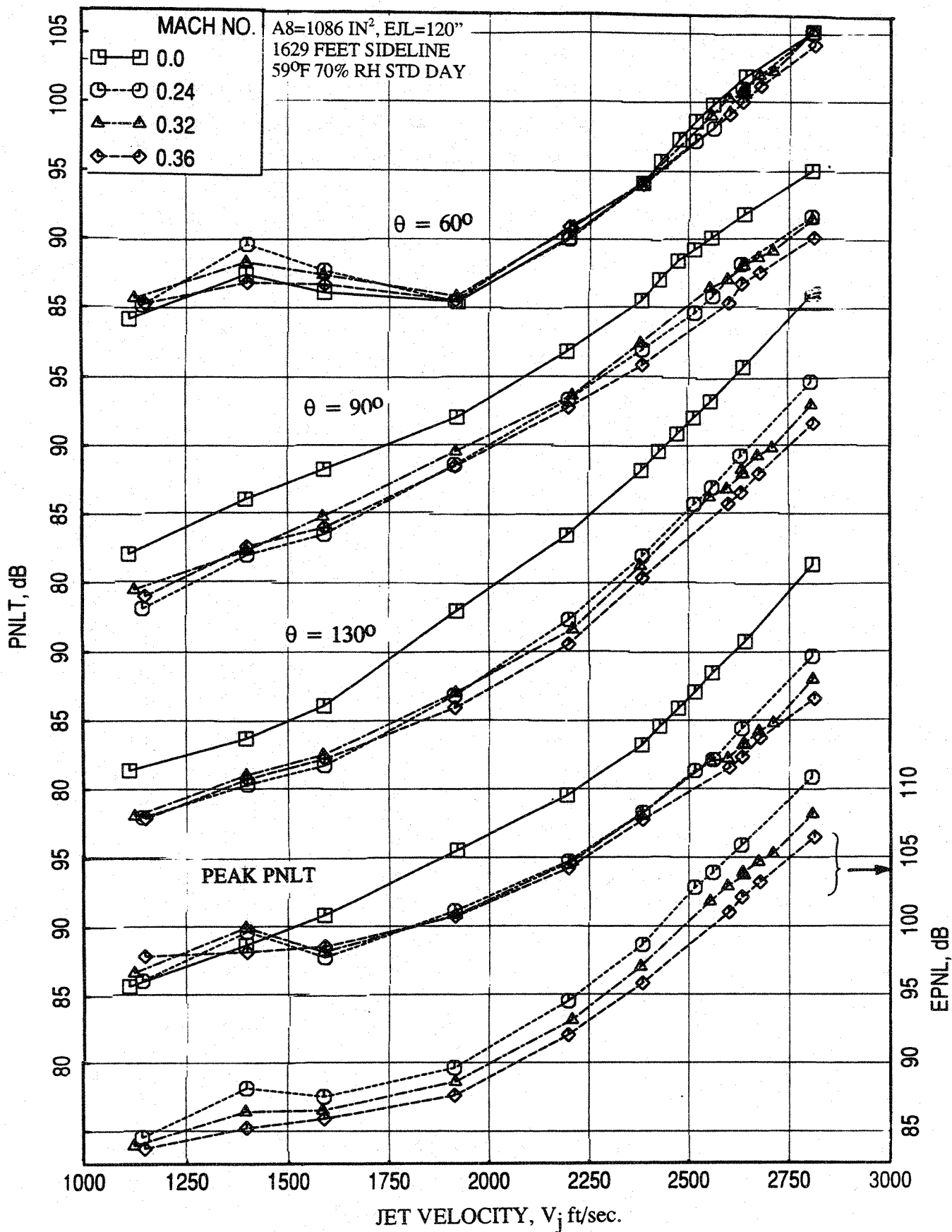
Figure 5-1. Effect of flight simulation on EPNL and PNLT at various polar angles (θ) as function of jet velocity of L1M cycle conditions for a 10 and 9 full staggered CD-chute mixer with fully treated long ejector at an azimuthal angle φ=25°; SAR=2.8, MAR=0.95.
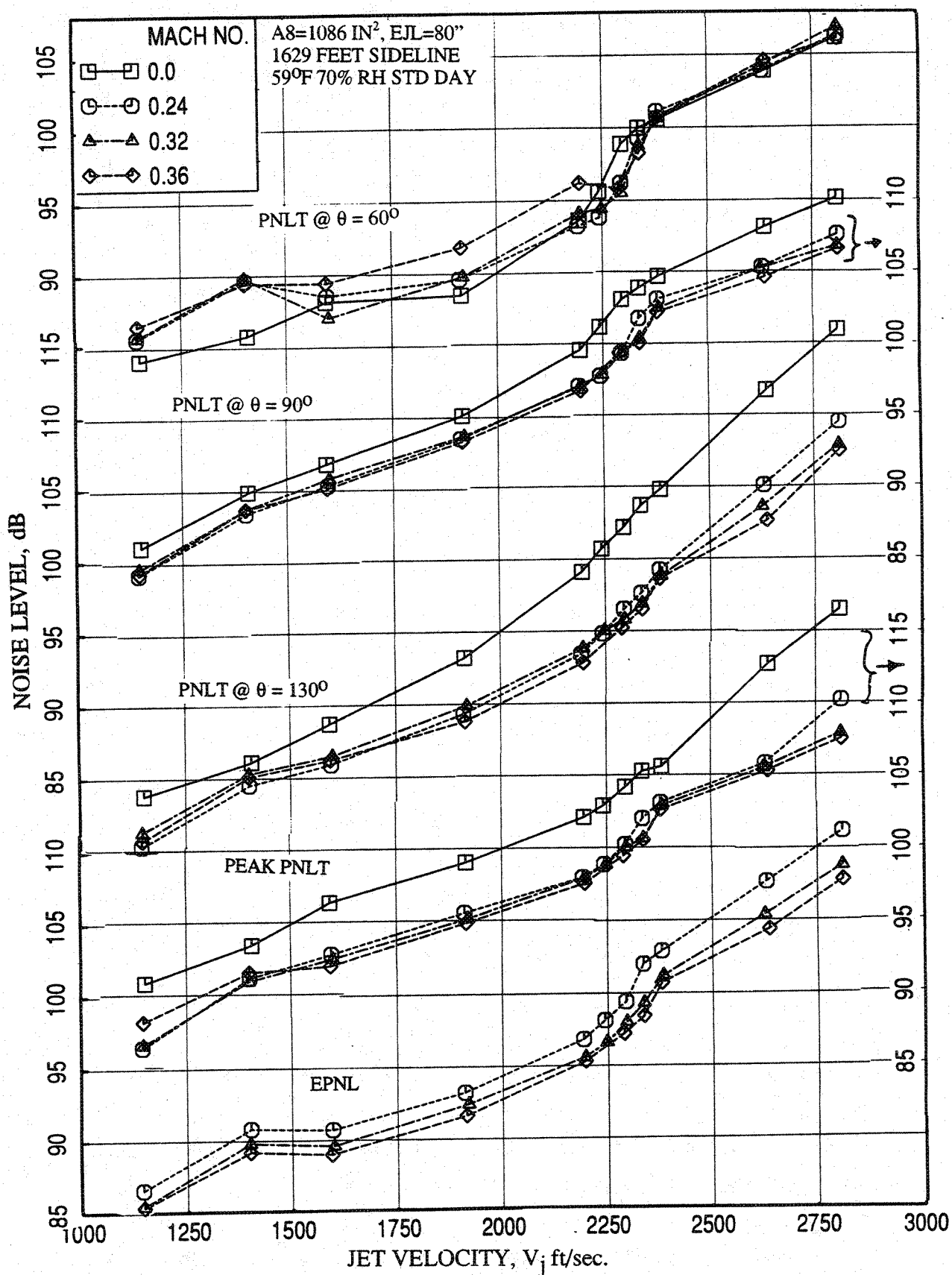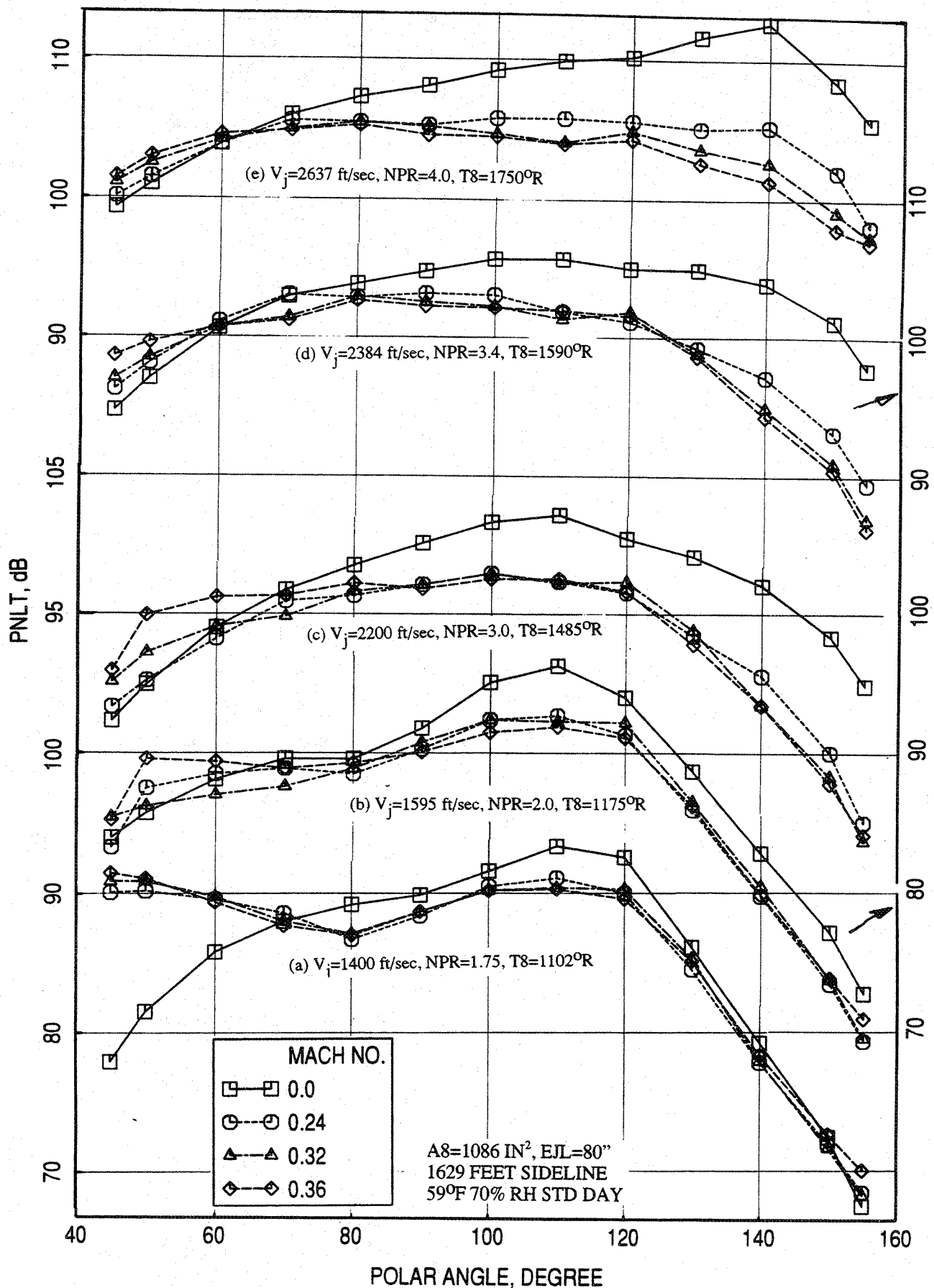
Figure 5-2. Effect of flight simulation on EPNL and PNLT at various polar angles (θ) as function of jet velocity of L1M cycle conditions for a 10 and 9 full staggered CD-chute mixer with hardwalled short ejector at an azimuthal angle ϕ=25°; SAR=2.8, MAR=0.95.

long treated ejector. The Noise reduction due to flight between static and at $M_F=0.24$ is somewhat the same for both configurations. However, with further increase in flight Mach number, the noise reduction for hardwalled short ejector configuration is much lower compared to the long treated ejector configuration. This indicates that the internally generated noise for the hardwalled configuration is higher and that the impact of this noise is dominant at and above $M_F=0.24$, so that the further increase in flight is ineffective in reducing the farfield noise. It should be noted that a sudden noise increase is observed at a jet velocity of about 2350 ft/sec for the hardwalled configuration, especially with flight simulation. This is due to transition of ejector flow from subsonic to supersonic mode, at which additional internal noise is being generated. While the impact of mode switch related noise is observed in the farfield for hardwalled configuration, its impact is minimal for treated long ejector. This is another indication of dominant internally generated noise for hardwalled short ejector compared to treated long ejector configuration.

At five different jet velocities the effect of flight simulation on PNLT directivities for long treated ejector are shown in Figure 5-3. The effect of flight simulation is to lower the PNLT levels at polar angles above 60° and the trend is reversed at lower angles. The levels increase at forward angles ($<60^O$) due to dynamic amplification of jet noise after overcoming source strength reduction due to flight effect. Significant PNLT reduction is observed at the rear arc. The PNLT directivities at lower NPR values, namely at 1.75 and 2.0, exhibit two humps. The first hump in the forward arc could be the result of dominant internal noise (i.e., at lower NPR jet mixing noise level is relatively lower) radiated to farfield, noise radiated from the secondary inlet for unchoked secondary flow at lower NPR conditions, and the shock-associated noise in the forward arc angles. Similar results for the hardwalled short ejector are presented in Figure 5-4.

Effect of flight simulation on SPL spectra at various polar angles (θ) for both configurations at four different jet velocities are shown in Figures 5-5 through 5-8. Significant SPL reduction is observed at higher polar angles for the entire frequency range with increasing flight Mach number. Major noise reduction took place between Mach 0 and 0.24. Noise reduction due to further flight Mach number increase is relatively higher for long treated configuration, especially at higher jet velocities.

The effect of flight simulation on ramp and chute static pressure distributions for the long treated ejector configuration are shown in Figure 5-9 for different L1M cycle conditions. For each case the static pressure increases with increasing flight Mach number, both on
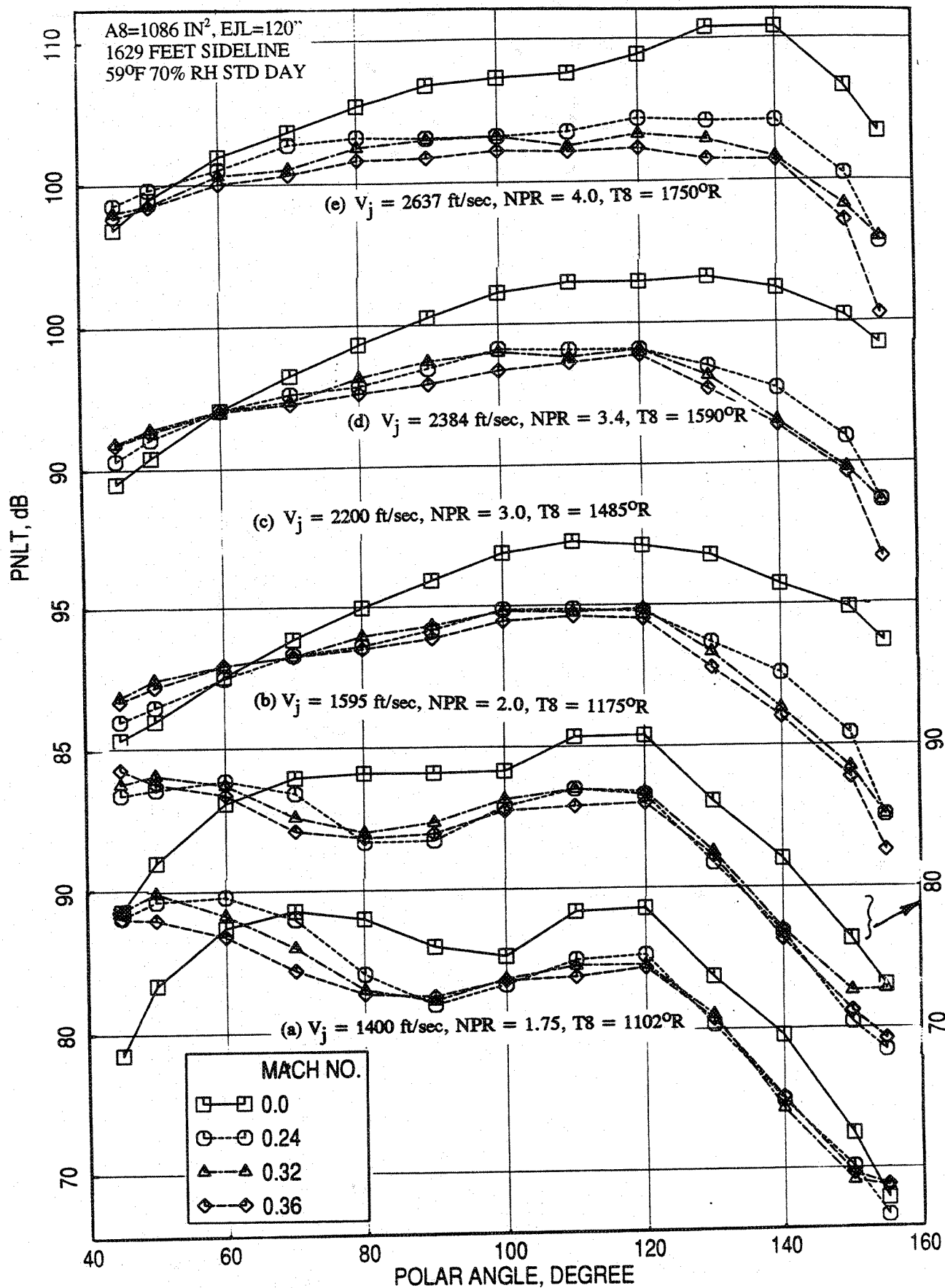
Figure 5-3. Effect of flight simulation on PNLT directivities at different L1M cycle conditions for a 10 and 9 full staggered CD-chute mixer with fully treated long ejector at an azimuthal angle φ=25°; SAR=2.8, MAR=0.95.

Figure 5-4. Effect of flight simulation on PNLT directivities at different L1M cycle conditions for a 10 and 9 full staggered CD-chute mixer with hardwalled short ejector at an azimuthal angle φ=25°; SAR=2.8, MAR=0.95.
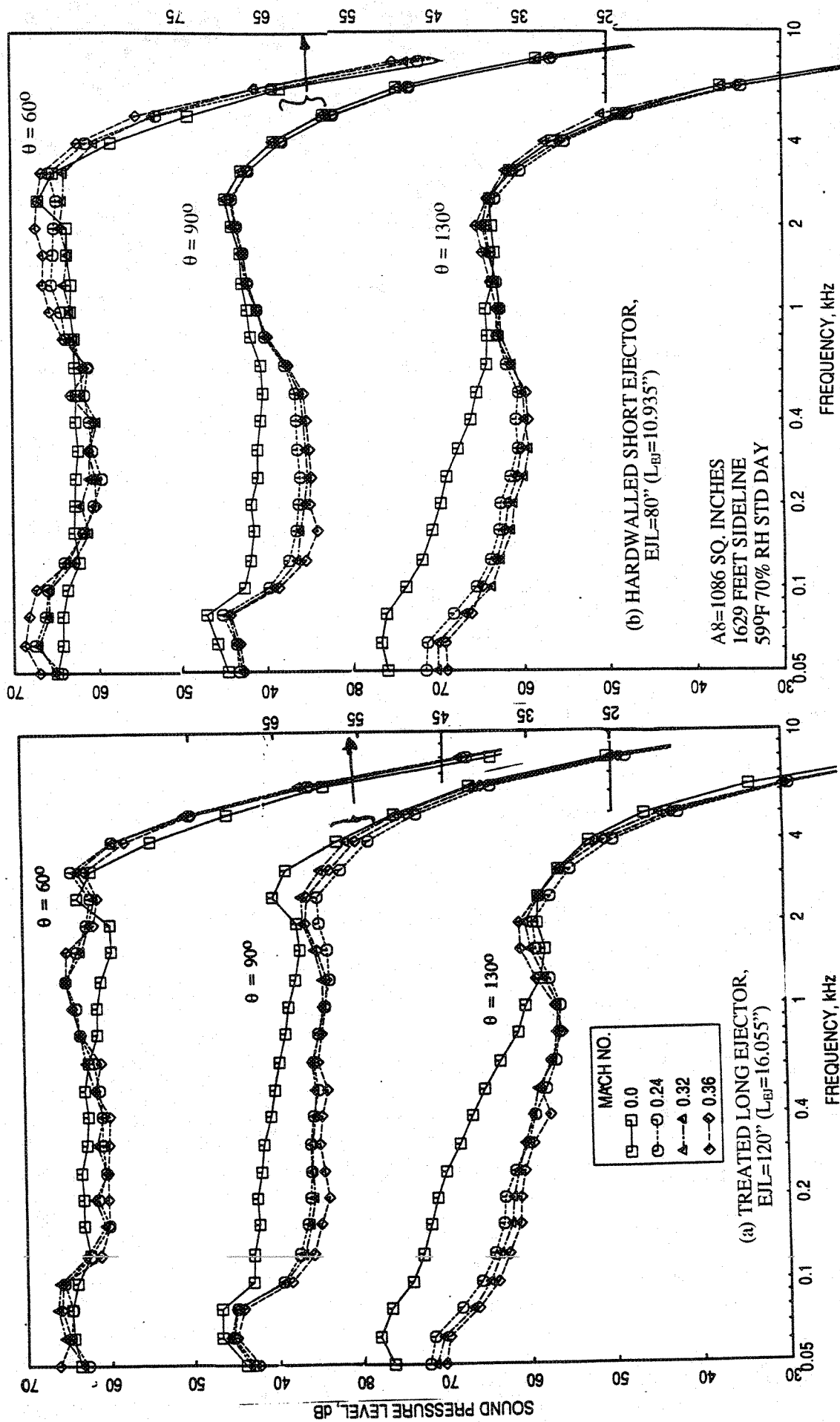
Figure 5-5. Effect of flight simulation on SPL spectra at various polar angles (θ) for 10 and 9 full staggered CD-chute mixer-ejector configurations at an azimuthal angle φ=25°; SAR=2.8, MAR=0.95, V_j = 1595 ft/sec, NPR = 2.0, T8 = 1175°R.
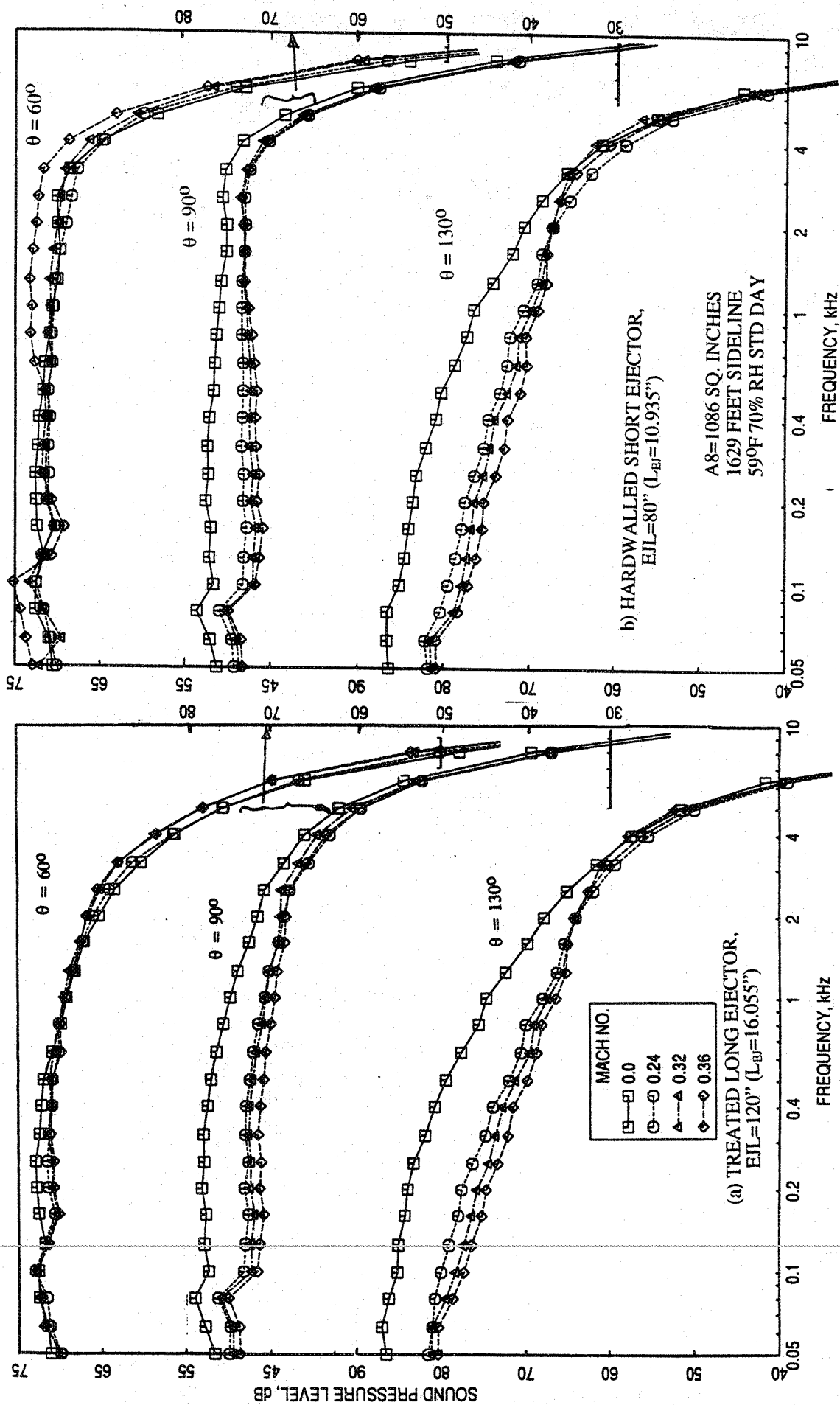
Figure 5-6. Effect of flight simulation on SPL spectra at various polar angles (θ) for 10 and 9 full staggered CD-chute mixer-ejector configurations at an azimuthal angle φ=25°, SAR=2.8, MAR=0.95, V_j = 2200 ft/sec, NPR = 3.0, T8 = 1485°R.
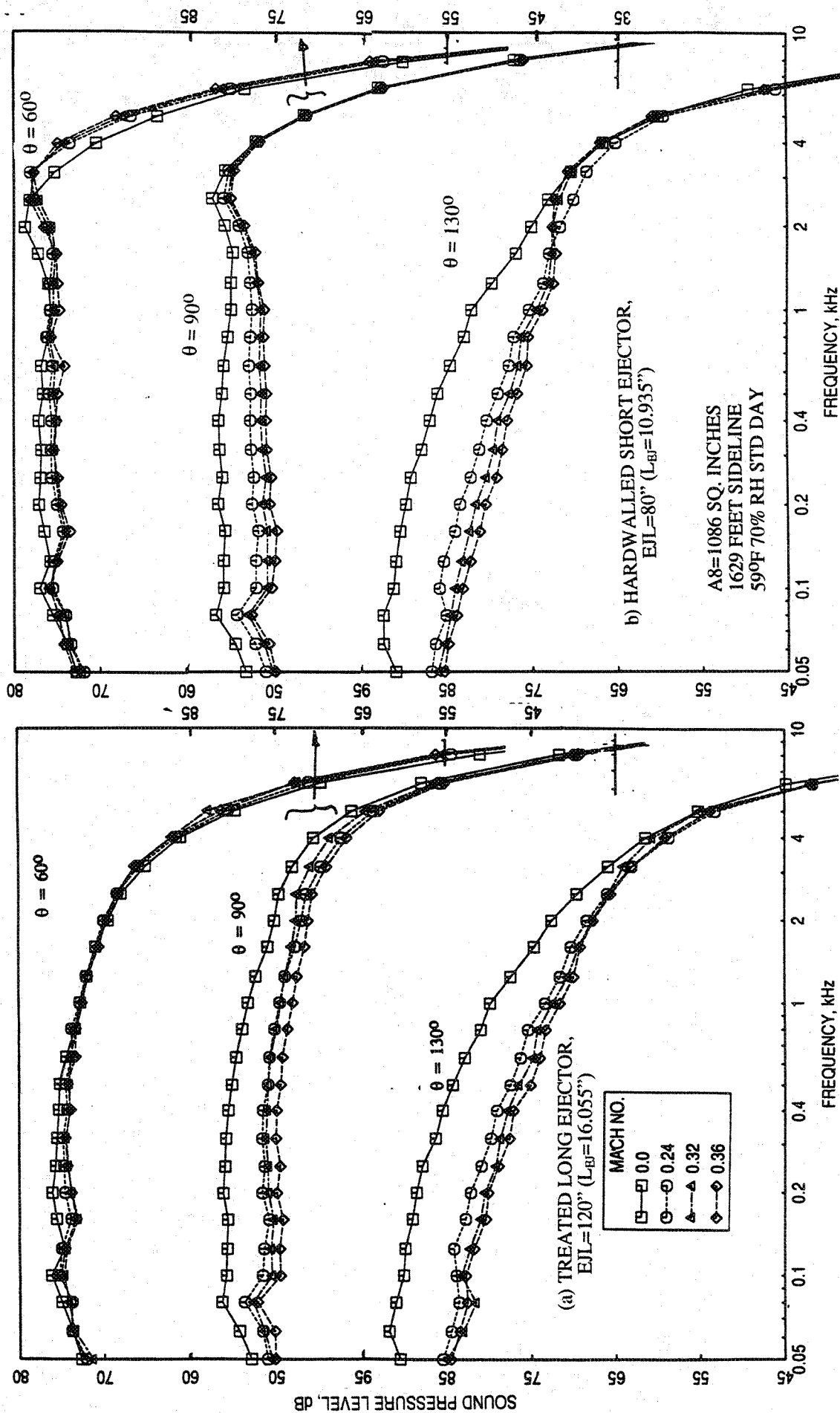
Figure 5-7. Effect of flight simulation on SPL spectra at various polar angles (θ) for 10 and 9 full staggered CD-chute mixer-ejector configurations at an azimuthal angle φ=25°; SAR=2.8, MAR=0.95, Vj = 2384 ft/sec, NPR = 3.4, T8 = 1590°R.
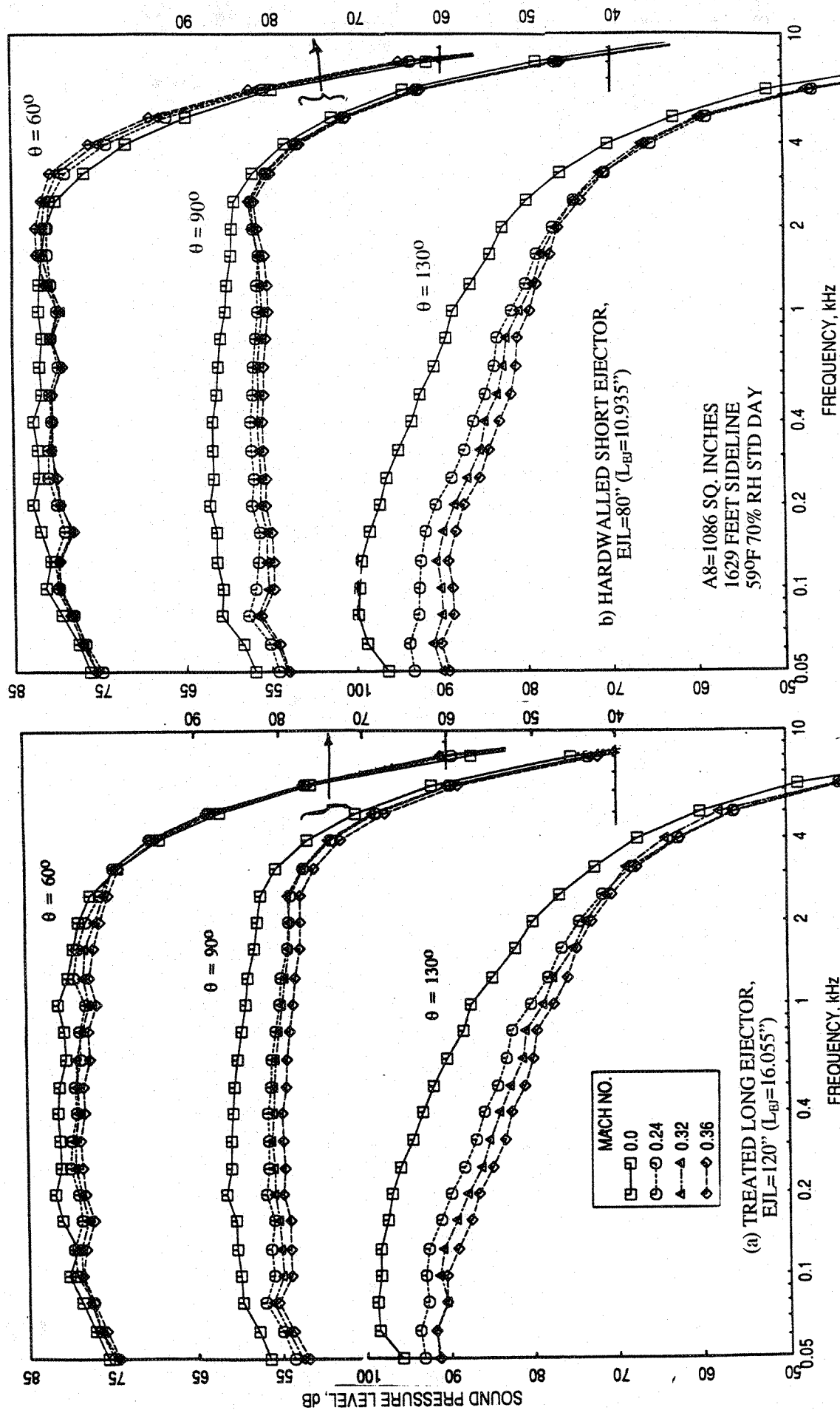
Figure 5-8. Effect of flight simulation on SPL spectra at various polar angles (θ) for 10 and 9 full staggered CD-chute mixer-ejector configurations at an azimuthal angle φ=25°; SAR=2.8, MAR=0.95, V_j = 2637 ft/sec, NPR = 4.0, T8 = 1750°R.
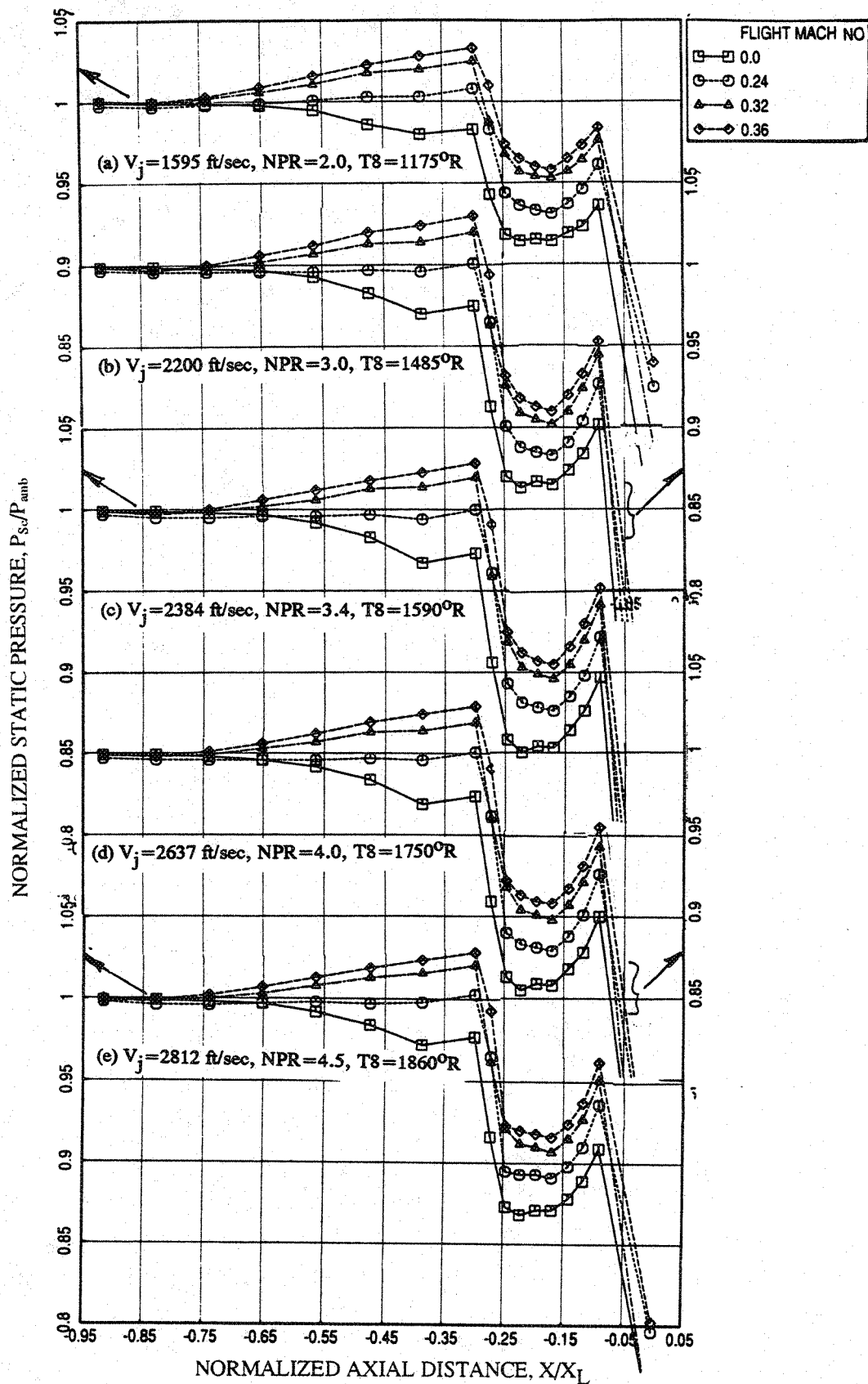
Figure 5-9. Effect of flight simulation on axial static pressure distributions on the inlet ramp and on the secondary flow side of chute surface at different L1M cycle conditions for a 10 and 9 full staggered CD-chute mixer with fully treated long ejector; SAR=2.8, MAR=0.95, X_L=17".

the ramp and chute surfaces due to freejet fan pressure rise, indicating lesser loading for the chutes. This is clearly observed in Figure 5-10, where the chute loading coefficient due to chute static pressure distributions is plotted against NPR. The effect of flight on pumping and corrected pumping for this configuration is shown in Figure 5-11. The pumping increases with increasing flight Mach number, since the total pressure at the inlet goes up. Even though, the pumping increases with flight, the effect is relatively small on the computed mixed jet velocity (see Figure 5-12). Similar results for the short hardwalled ejector are almost identical to those for treated long ejector, indicating insignificant influence of the ejector configuration on upstream flow related parameters.

Figure 5-13 shows the effect of flight on the average axial static pressure distributions on the inlet and the flap surface at different L1M cycle conditions for the treated long ejector. Small amount of pressure increase due to increasing M_F is noted at lower nozzle pressure ratio conditions. However, the effect is significant at higher NPRs (particularly closer to mode switch NPR) and in supersonic mode. The effect of flight on normalized force and normalized moment of force with respect to flap leading edge due to static pressure difference on flap surface are shown in Figure 5-14. Both the force and the moment seem to decrease slightly with increasing flight simulation due to increased static pressure. The transition from subsonic to supersonic mode seems to be slightly delayed with respect to NPR due to M_F. Similar results for the short hardwalled ejector are shown in Figures 5-15 and 5-16. The transition from subsonic to supersonic mode for this configuration is relatively abrupt compared to the long treated ejector.

5.2 EFFECT OF NOZZLE PRESSURE RATIO (NPR) AND TOTAL TEMPERATURE AT FIXED V_J:

Tests were conducted at fixed jet velocities by varying the nozzle pressure ratio and total temperature at static and simulated flight Mach numbers of 0.24, 0.32, and 0.36. Results presented in this section include the data for static and for flight simulation Mach number of 0.36 only. The acoustic results are normalized with respect to a reference ideal thrust of 60,000 lb to illustrate the effect of aerothermodynamic conditions at fixed jet velocity for the same ideal thrust.
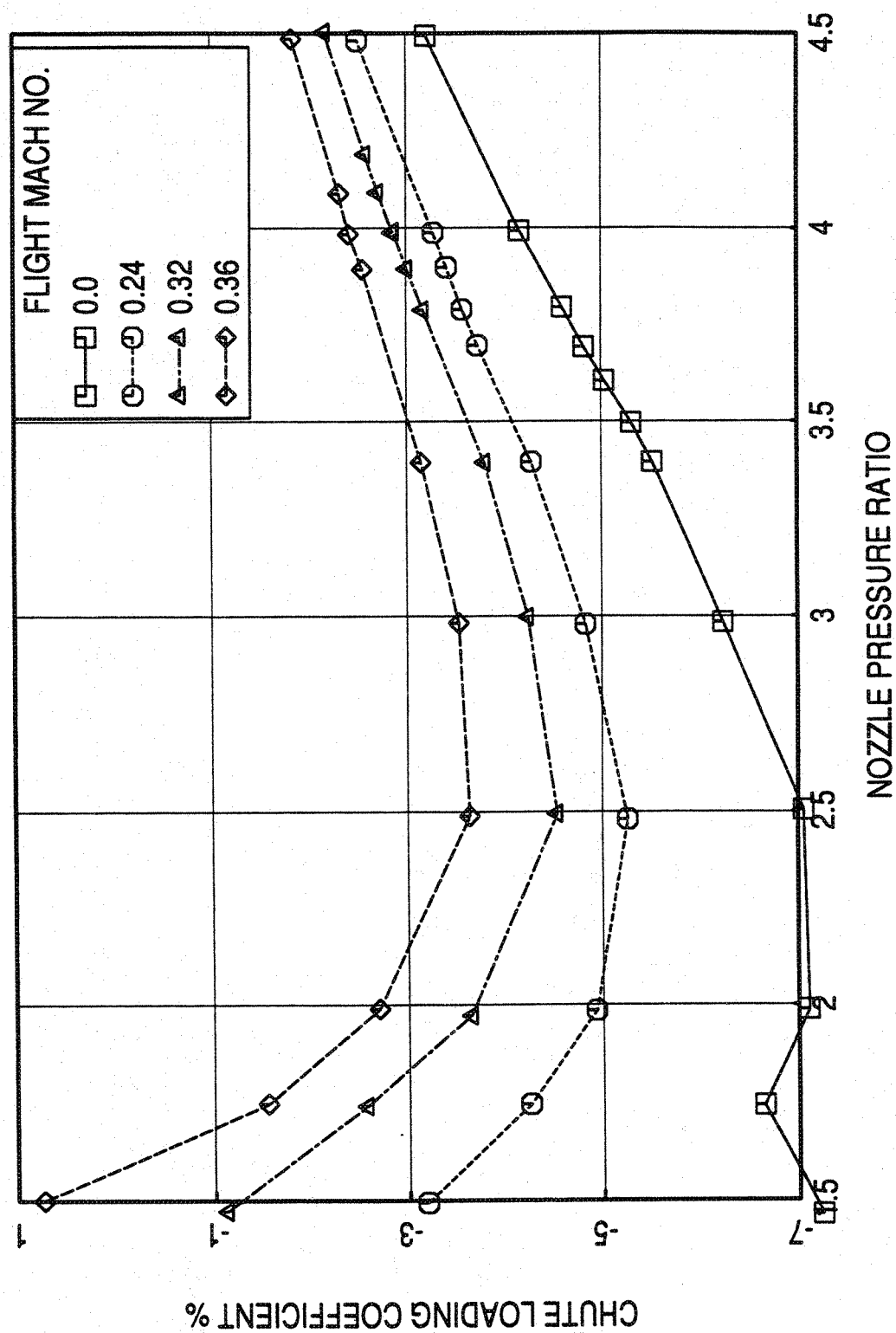
Figure 5-10. Effect of flight simulation on chute loading coefficient with respect to nozzle pressure ratio of L1M cycle conditions for a 10 and 9 full staggered CD-chute mixer with fully treated long ejector; SAR=2.8, MAR=0.95.
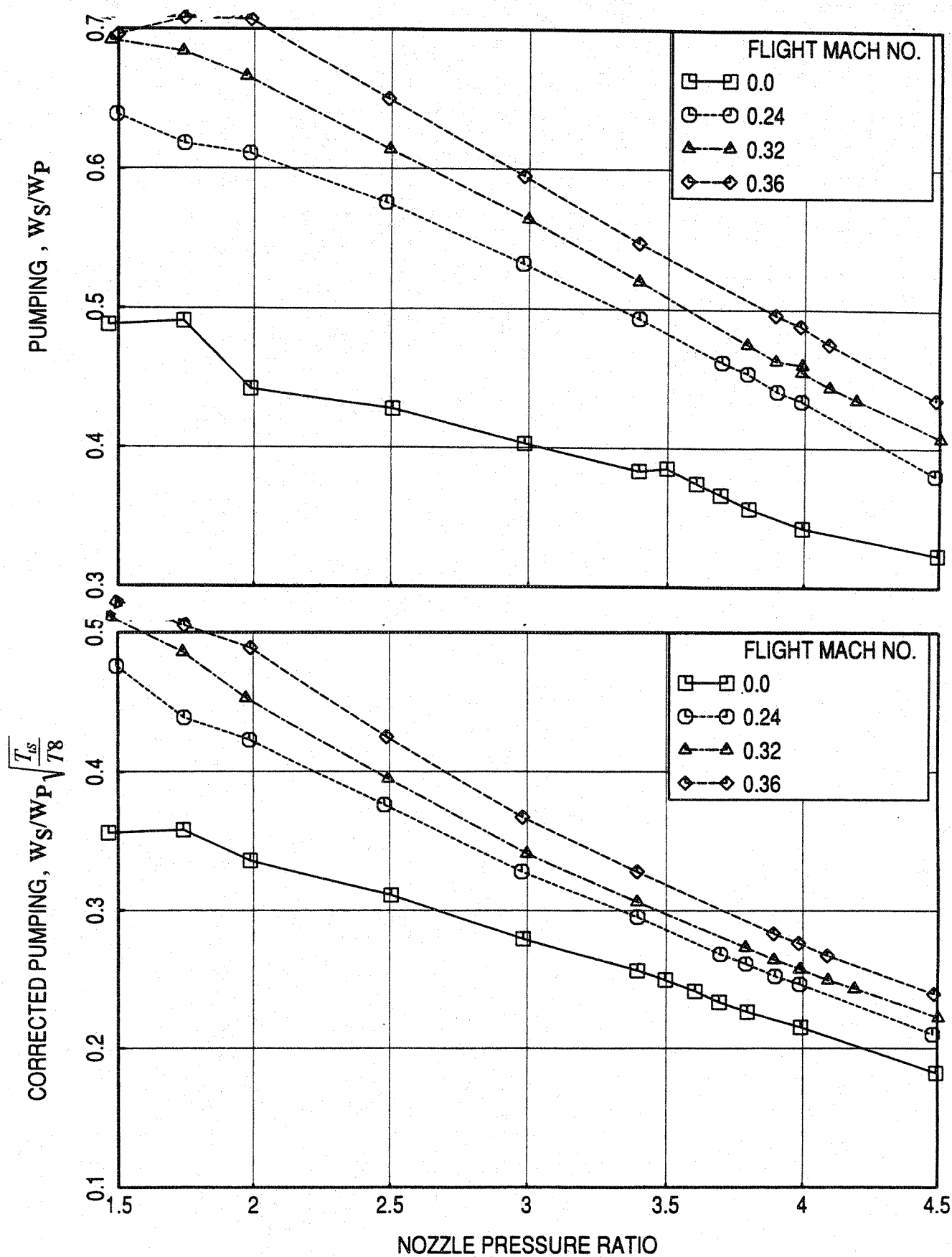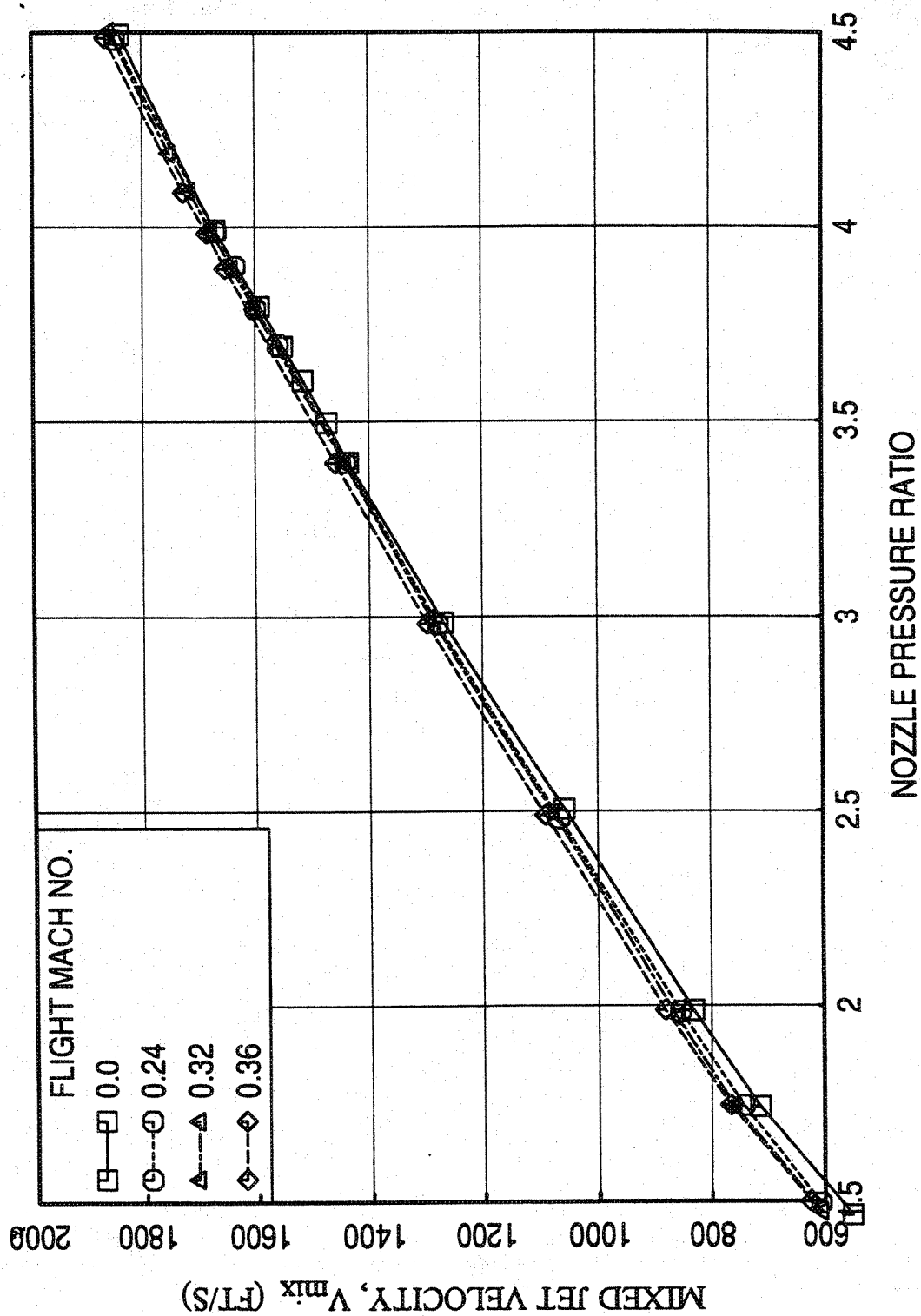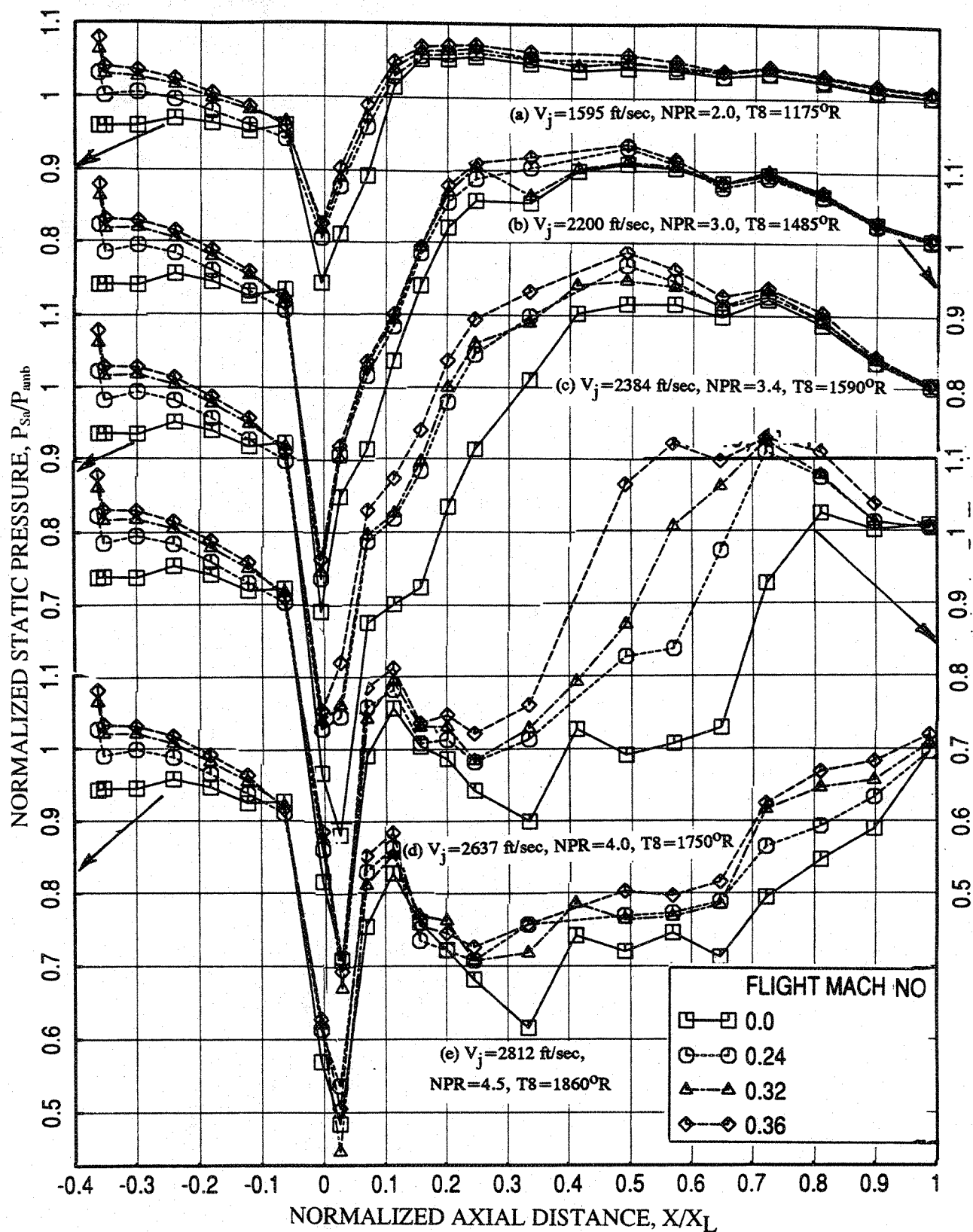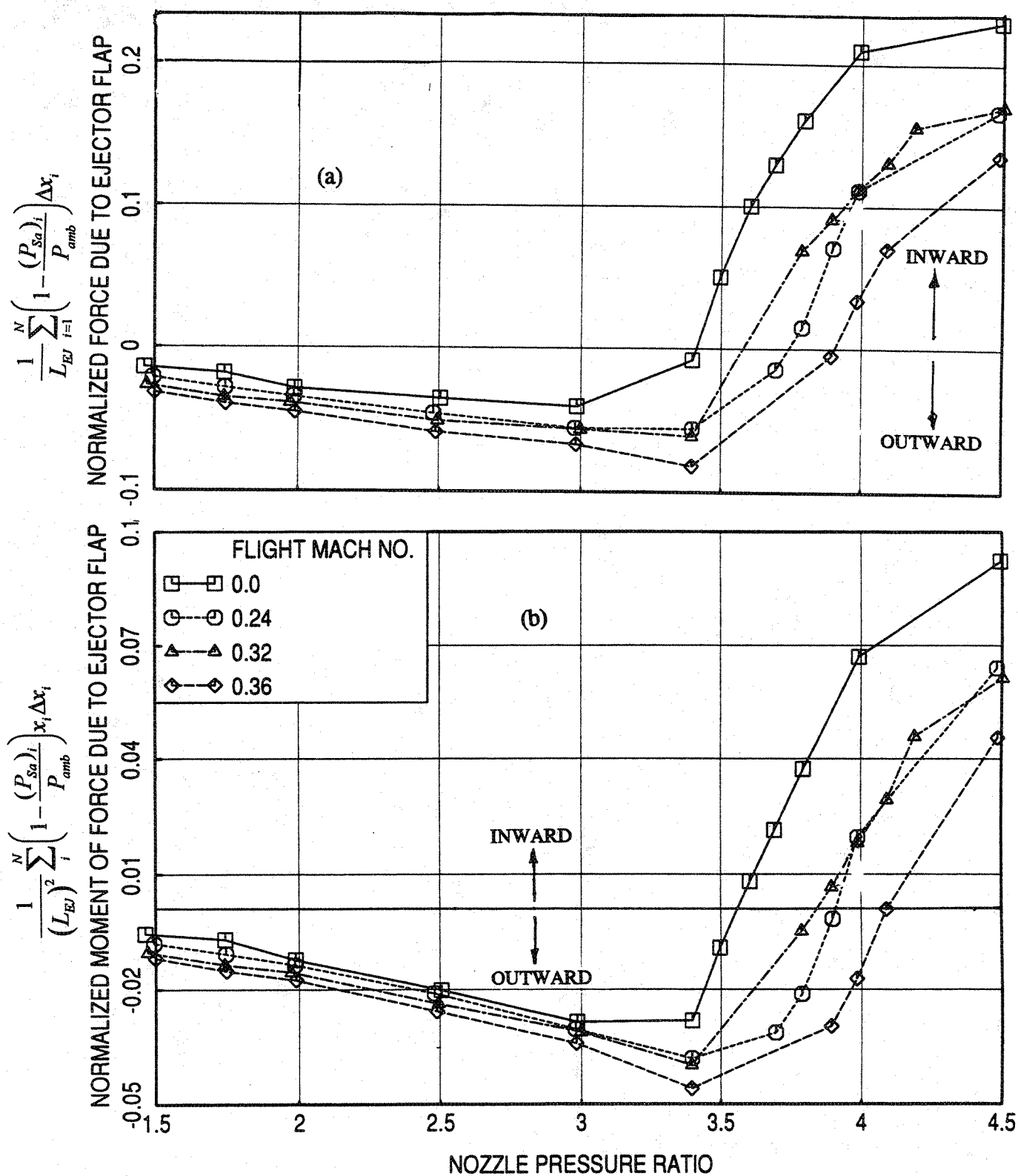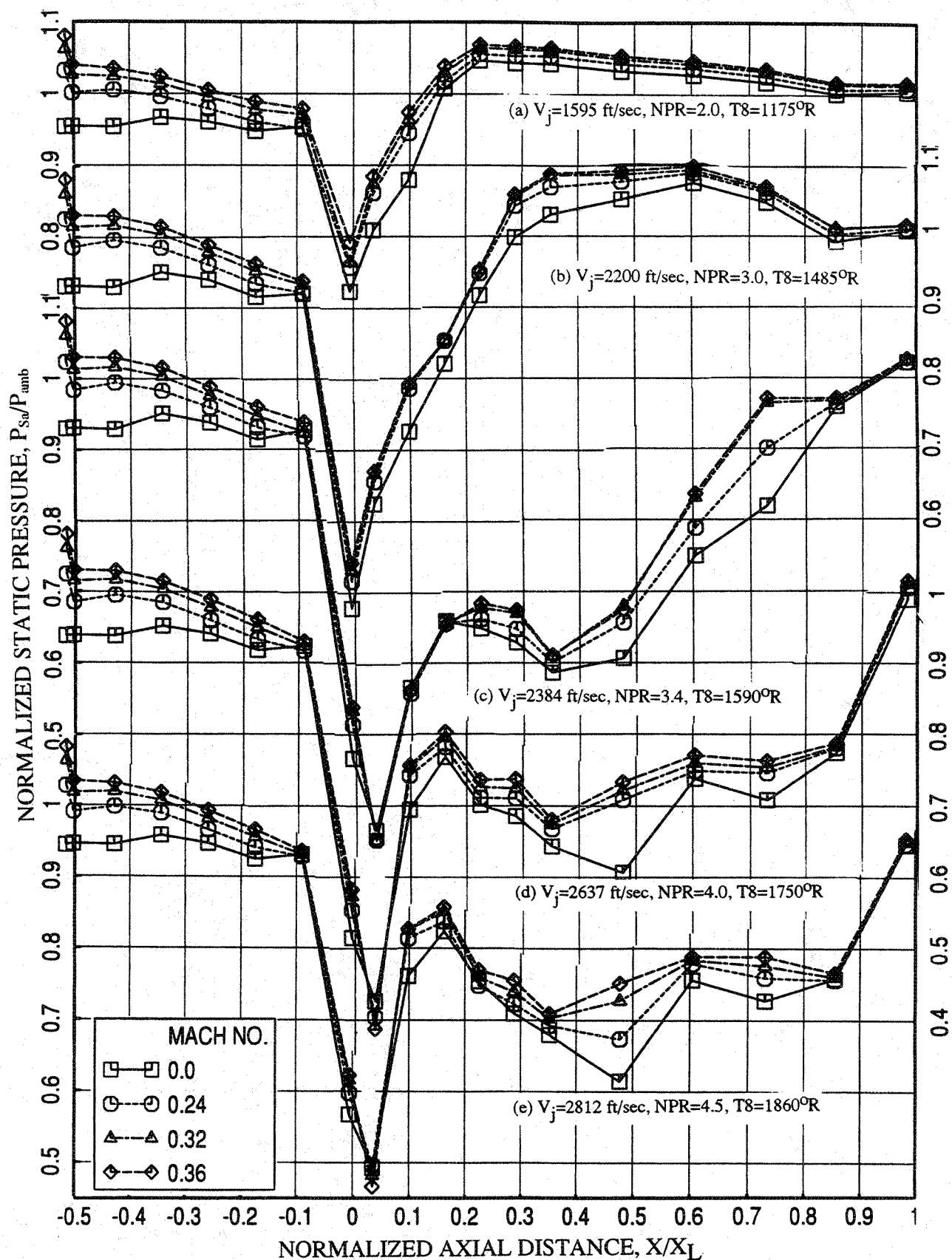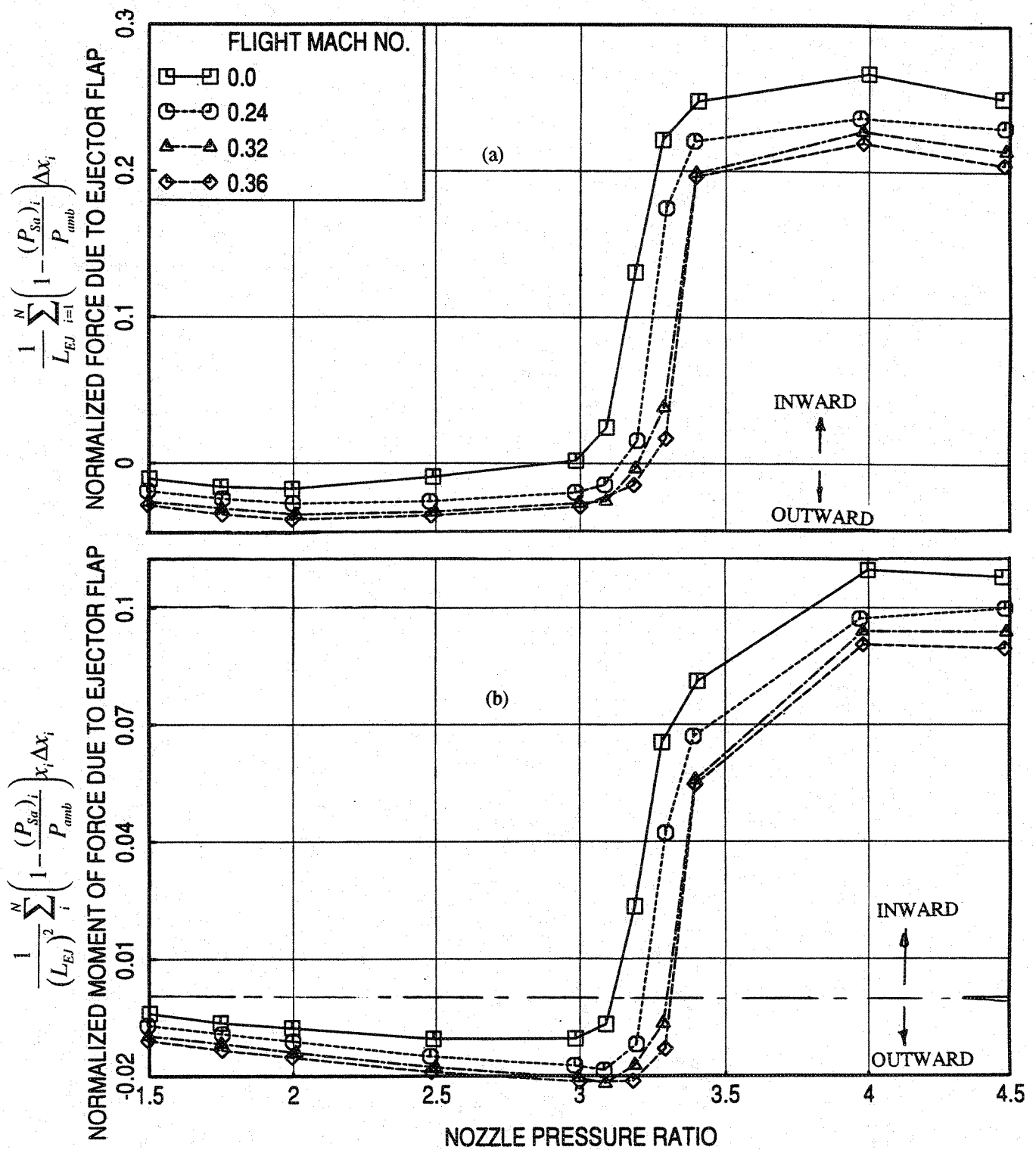
Figure 5-11. Effect of flight simulation on pumping and corrected pumping with respect to nozzle pressure ratio of L1M cycle conditions for a 10 and 9 full staggered CD-chute mixer with fully treated long ejector; SAR=2.8, MAR=0.95.

Figure 5-12. Effect of flight simulation on mixed jet velocity with respect to nozzle pressure ratio of L1M cycle conditions for a 10 and 9 full staggered CD-chute mixer with fully treated long ejector; SAR=2.8, MAR=0.95.

Figure 5-13. Effect of flight simulation on axial distribution of average static pressure on the inlet and the flap surface at different L1M cycle conditions for a 10 and 9 full staggered CD-chute mixer with fully treated long ejector; SAR=2.8, MAR=0.95, X_L=17".

Figure 5-14. Effect of flight simulation on normalized (a) force and (b) moment of force due to ejector flap with respect to nozzle pressure ratio of L1M cycle conditions for a 10 and 9 full staggered CD-chute mixer with fully treated long ejector; SAR=2.8, MAR=0.95.

Figure 5-15. Effect of flight simulation on axial distribution of average static pressure on the inlet and the flap surface at different L1M cycle conditions for a 10 and 9 full staggered CD-chute mixer with hardwalled short ejector; SAR=2.8, MAR=0.95, X_L=11.88".

Figure 5-16. Effect of flight simulation on normalized (a) force and (b) moment of force due to ejector flap with respect to nozzle pressure ratio of L1M cycle conditions for a 10 and 9 full staggered CD-chute mixer with hardwalled short ejector; SAR=2.8, MAR=0.95.

5.2.1 For Long Treated Ejector Configuration:

Figure 5-17 shows the variation of EPNL with respect to NPR and nozzle total temperature at five jet velocities. The EPNL increases with increasing jet velocity. With respect to aerothermodynamic conditions the EPNL increases with increasing NPR and with decreasing nozzle total temperature. The trend is reversed at lower jet velocities, especially, with flight simulation. The EPNL levels are significantly lowered due to flight simulation of Mach 0.36. These results are presented in a form of fixed EPNL contours between NPR and nozzle total temperature in Figure 5-18. In general EPNL increases with increasing NPR and nozzle total temperature. However, it is interesting to note that the fixed EPNL can be achieved by lowering the NPR and nozzle total temperature together at a lower NPR conditions, as observed in Figure 5-18 (b) for flight simulated case.

Normalized PNLT directivities at fixed jet velocities are plotted in Figure 5-19 for static condition as well as for flight simulation case with Mach 0.36. At lower jet velocities (i.e., at 1400 and 1590 ft/sec) and at lower NPR values (i.e., at 1.5 and 1.75) the PNLT increases in the forward arc and decreases in the mid arc. However, the levels decrease in the forward arc and increase in the rear arc by increasing NPR above 1.75, as observed for V_j=1590 ft/sec. The ejector internal noise is most likely dominant at lower jet velocity conditions. Hence, the influence of varying NPR and nozzle total temperature on internal noise and its radiation pattern to the freefield may be the reason for the type of PNLT variation observed at lower jet velocities, since the externally generated jet mixing noise is relatively lower due to near complete mixing in the long ejector, resulting in a lower uniform exit velocity. In addition, sound radiated from the unchoked secondary inlet may be the reason for such forward arc noise increase. At higher jet velocities the normalized PNLT levels monotonically increase with increasing NPR associated with decreasing nozzle total temperature for all polar angles. At higher velocities, the externally generated jet mixing noise is most likely the dominant component to influence the PNLT directivity. Since, the mixed jet velocity (shown later in Figure 5-31) increases with increasing NPR for fixed jet velocities, the PNLT (normalized for thrust) should increase with NPR, as observed in Figure 5-19 at V_j of 1920, 2200, and 2384 ft/sec. The SPL spectra at various polar angles for fixed jet velocities of 1400, 1590, 1920, 2200, and 2384 ft/sec conditions are shown in Figures 5-20 through 24, respectively. Similar conclusions can be drawn from these results.
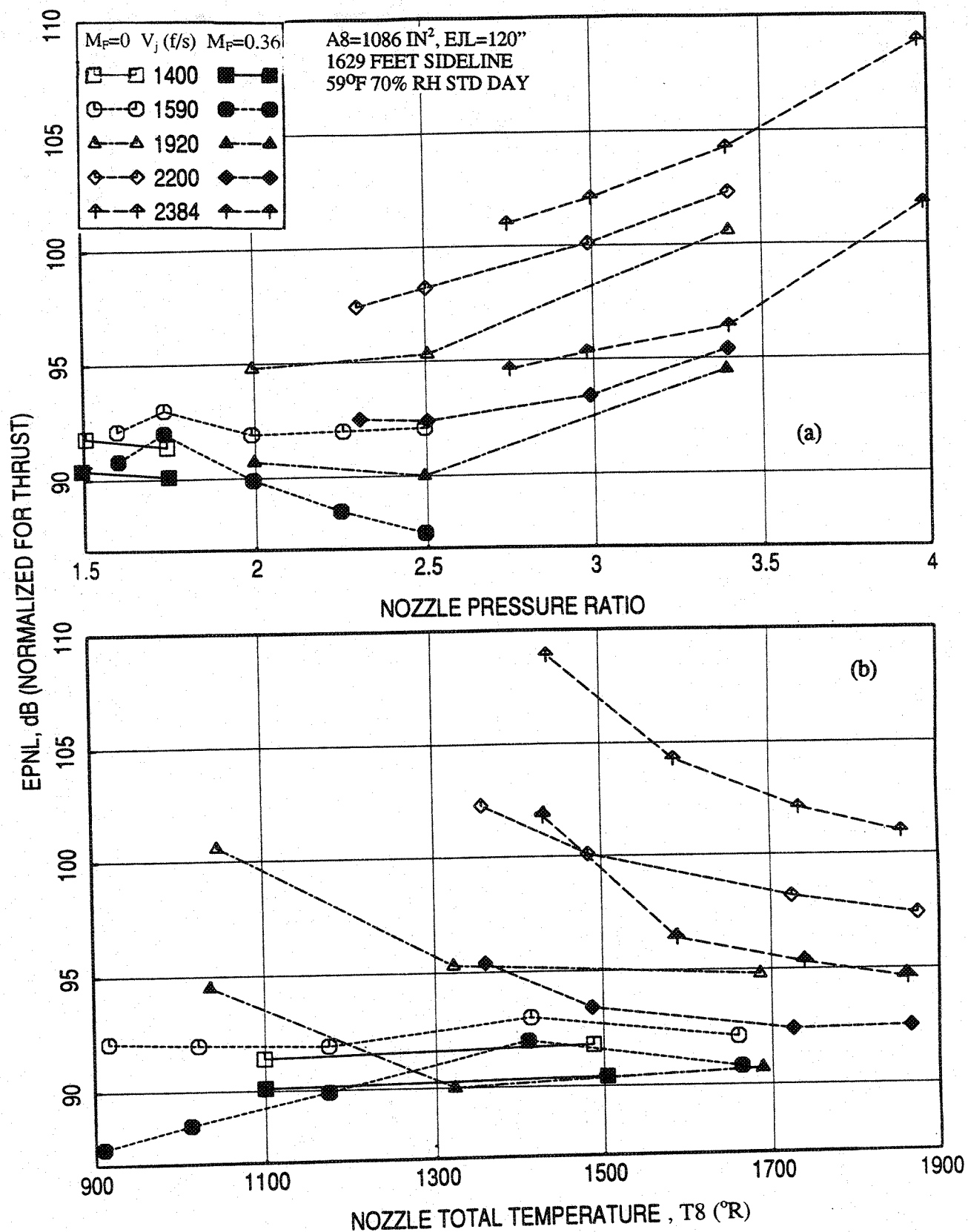
Figure 5-17. Effect of nozzle pressure ratio and total temperature on normalized EPNL at fixed jet velocities (V_j) for a 10 and 9 full staggered CD-chute mixer with fully treated long ejector at an azimuthal angle $\phi=25^\circ$; SAR=2.8, MAR=0.95.
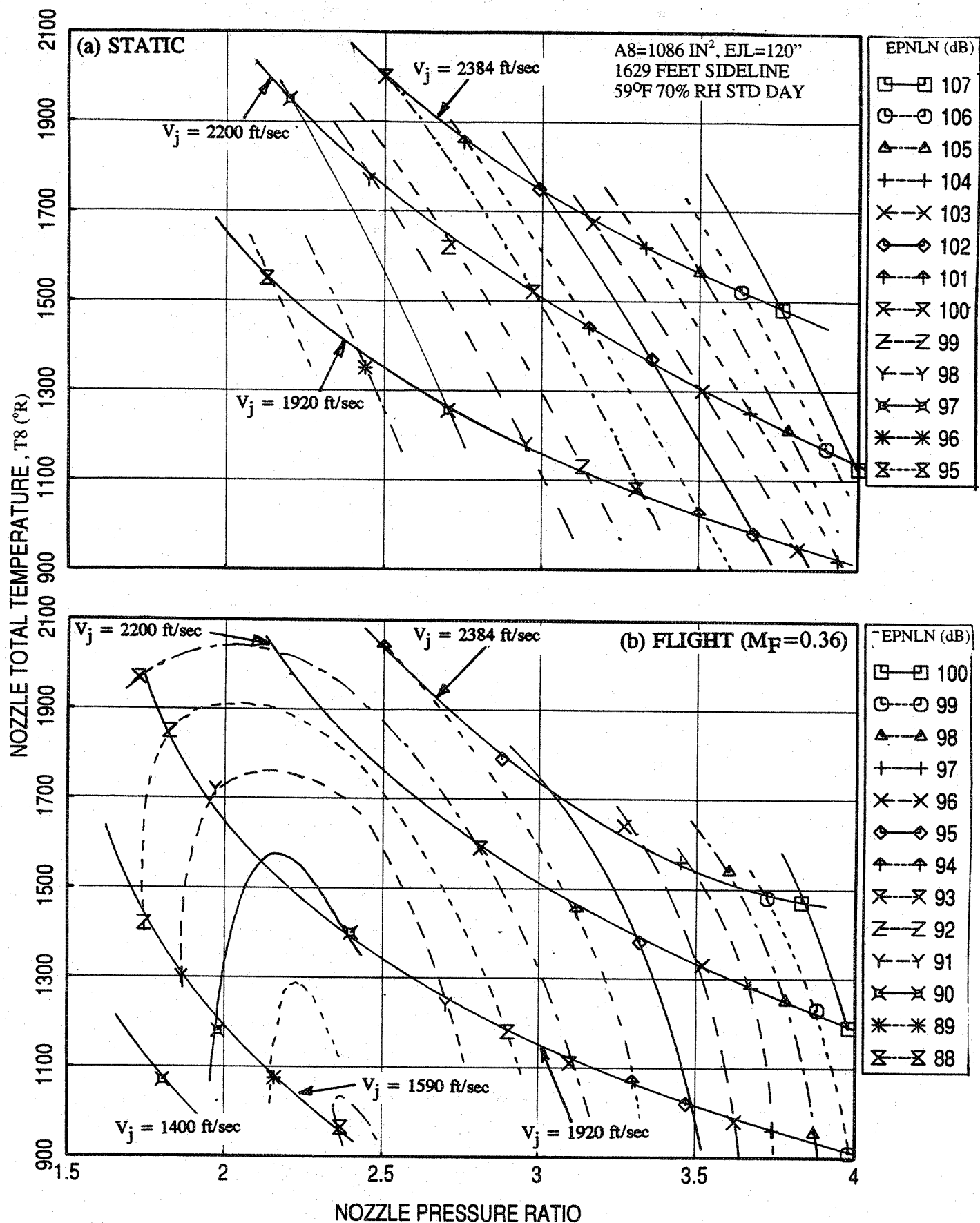
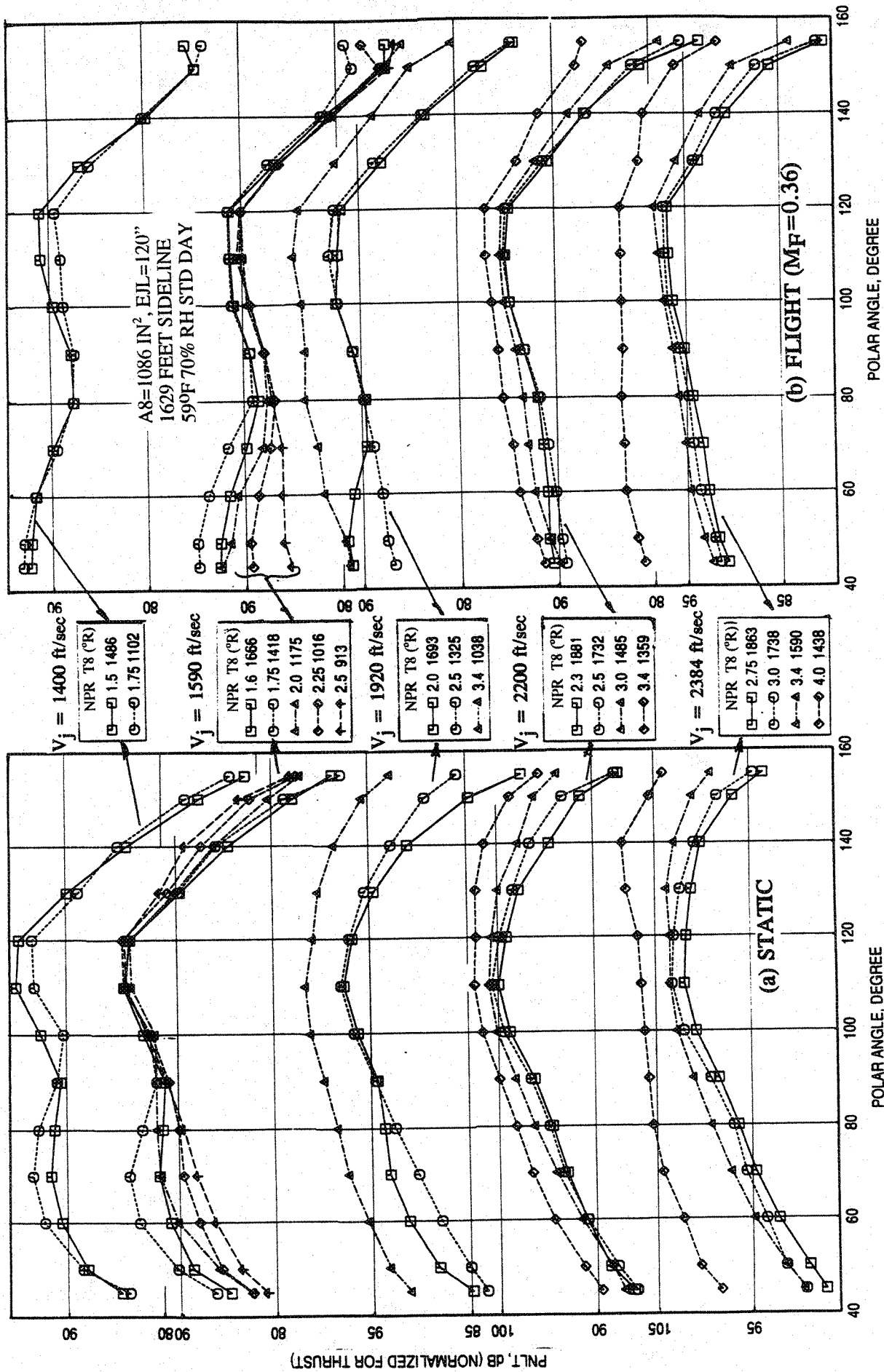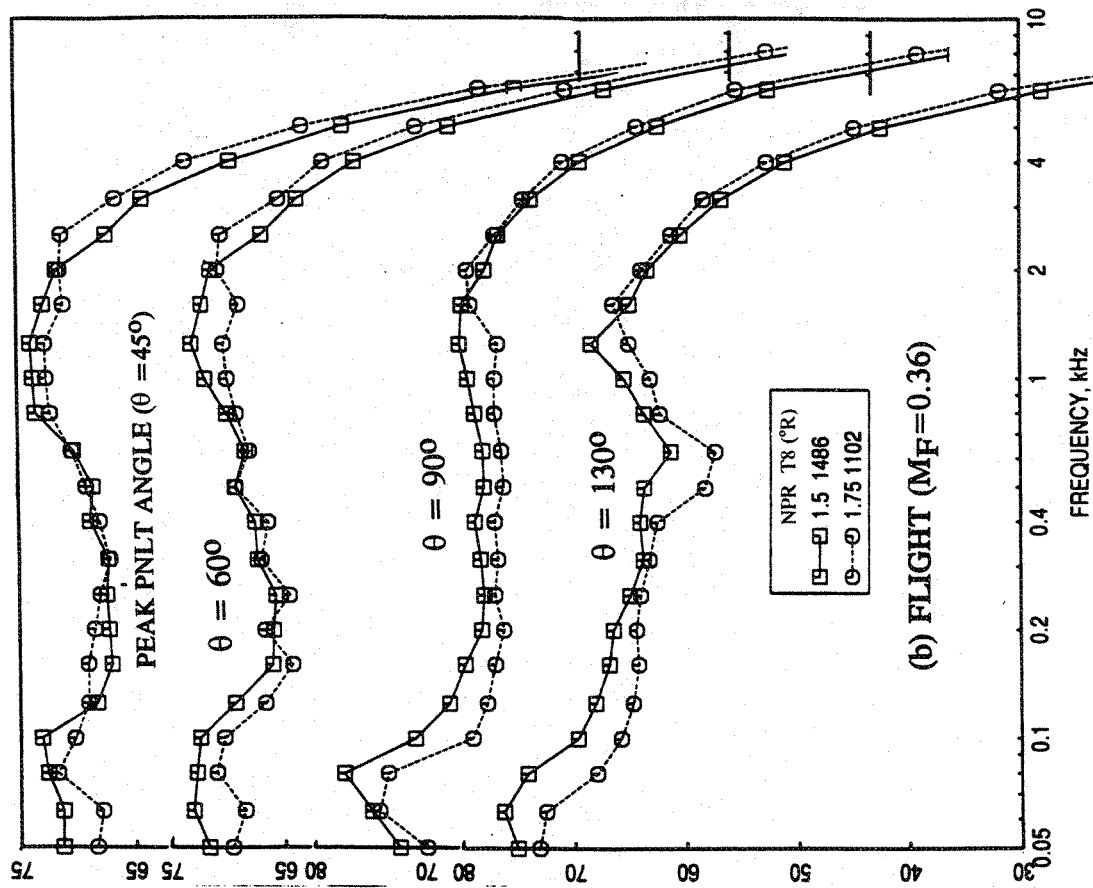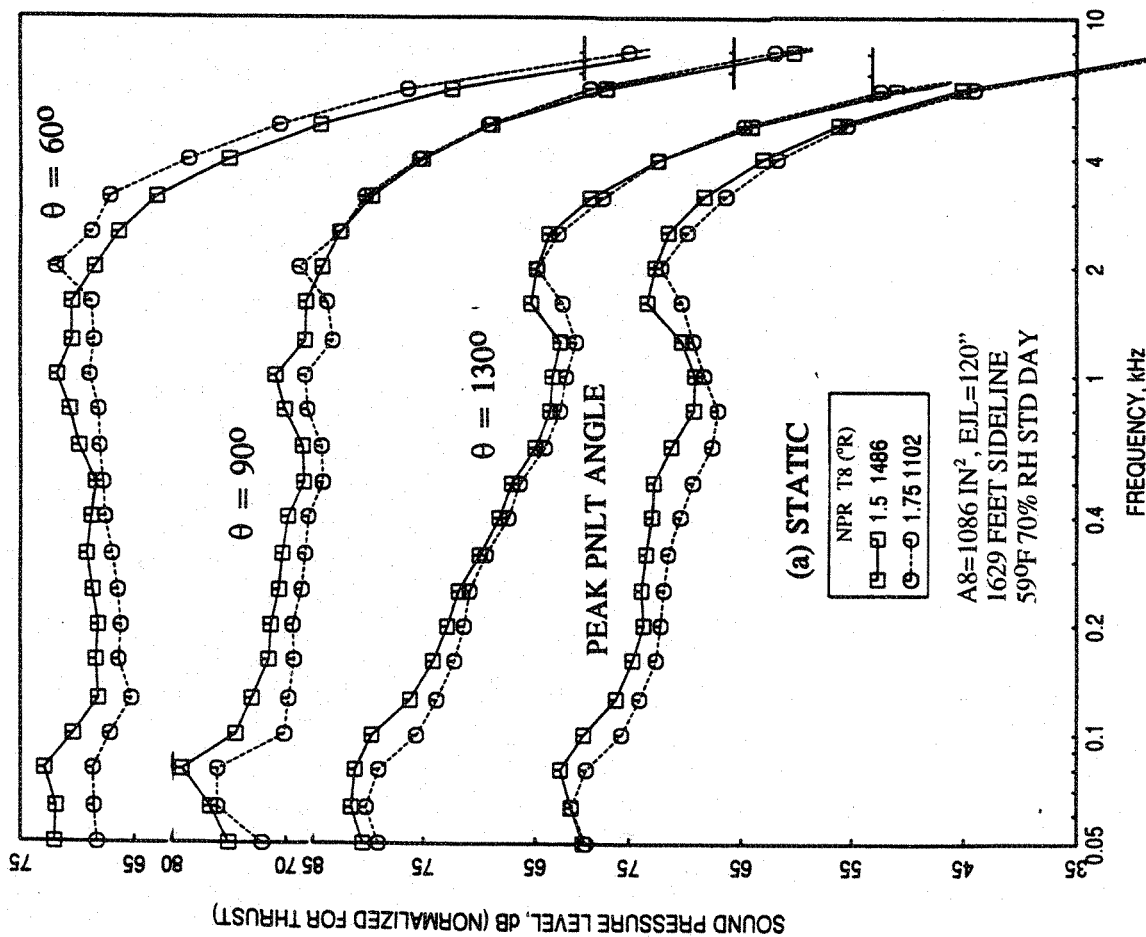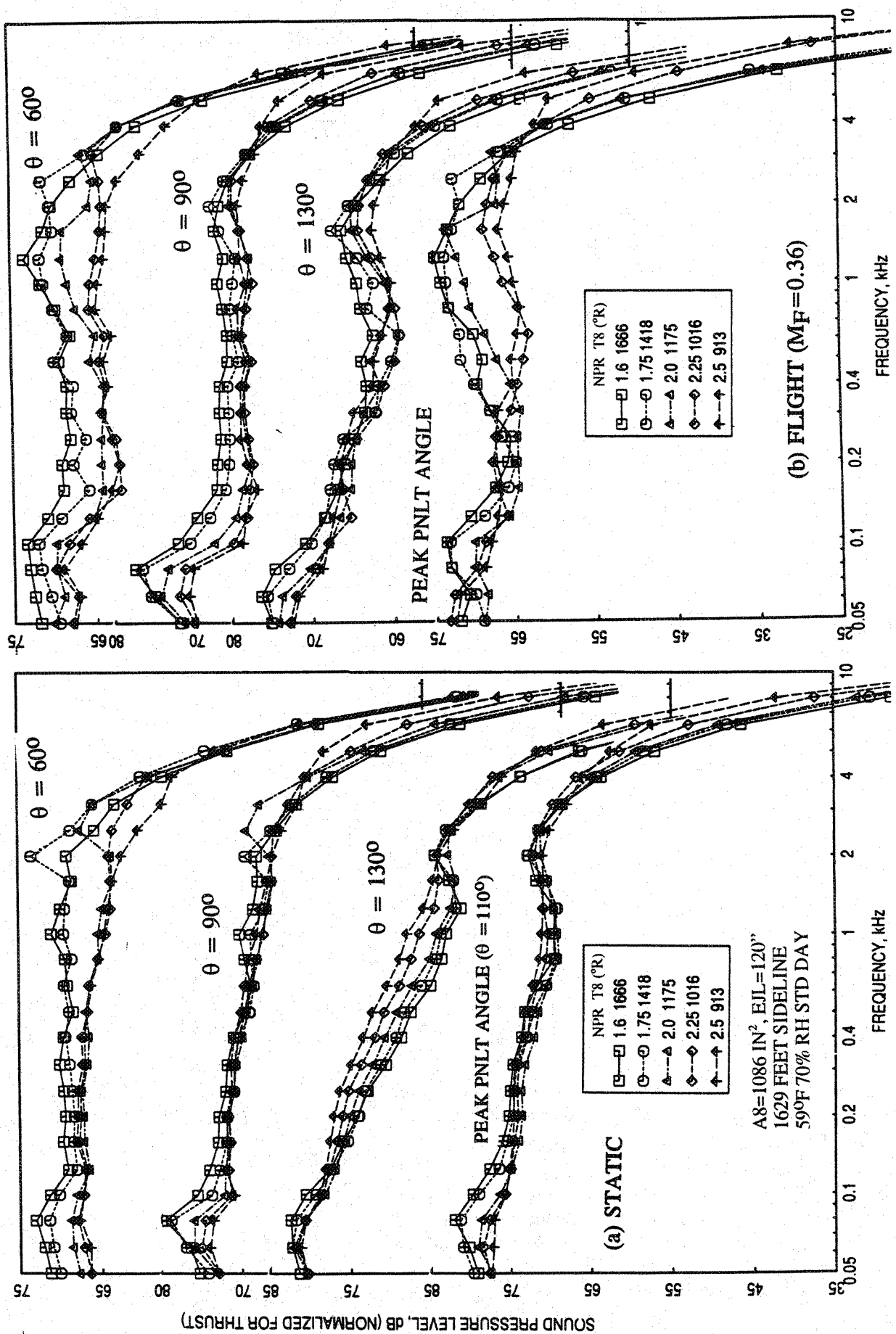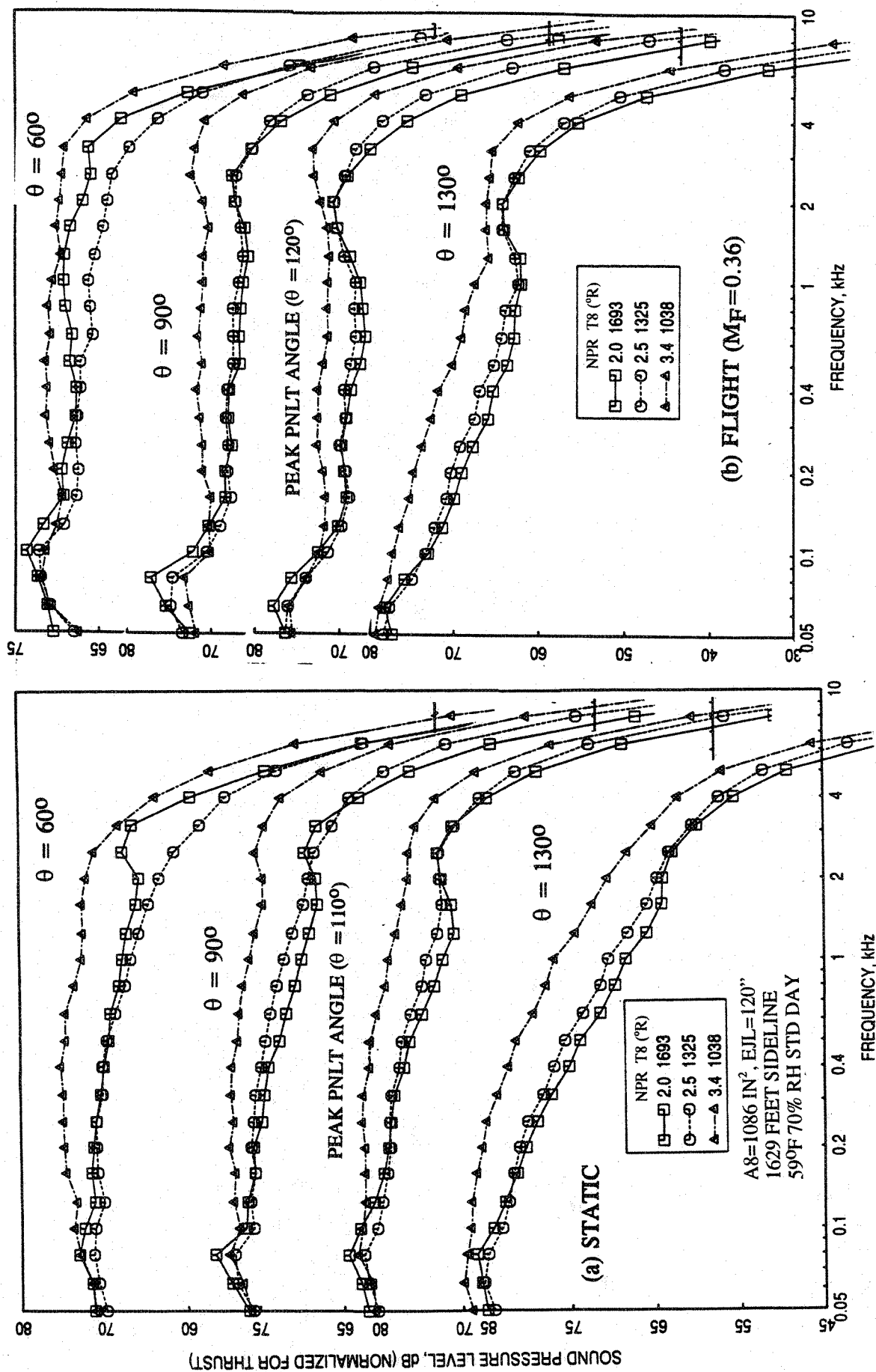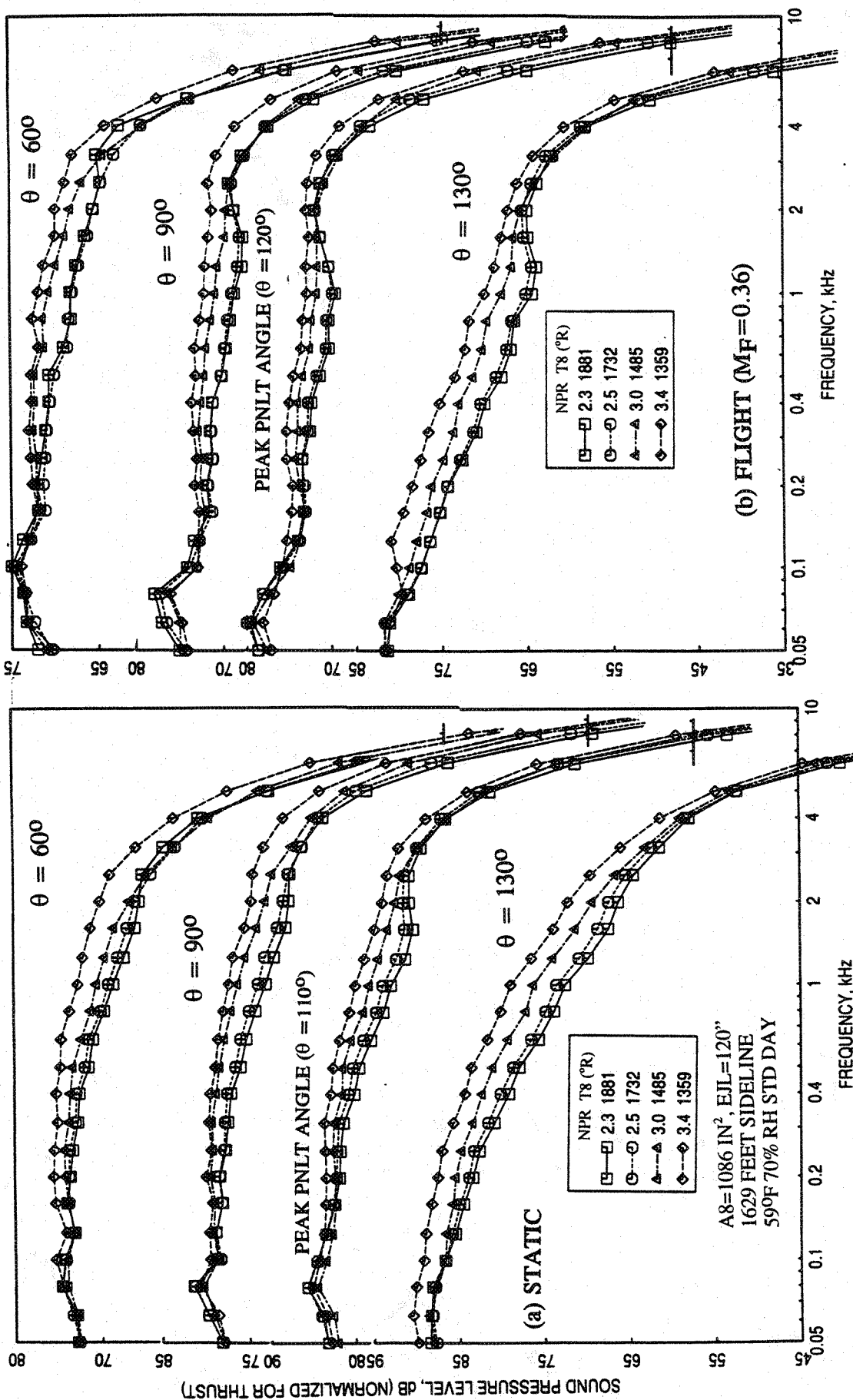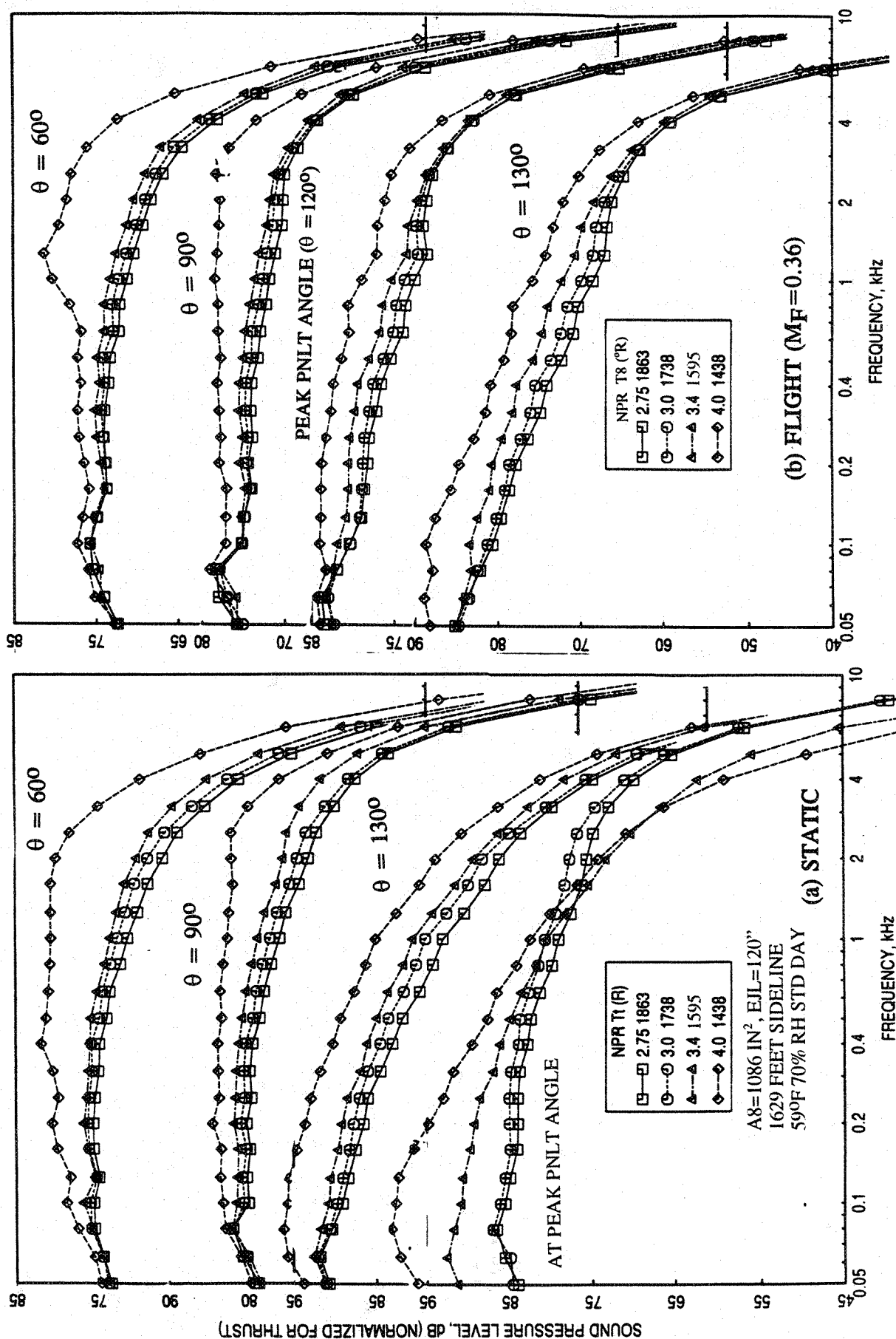Figure 5-18. Normalized EPNL contours with respect to nozzle pressure ratio and total temperature at (a) static and (b) M_F=0.36 for a 10 and 9 full staggered CD-chute mixer with fully treated long ejector at an azimuthal angle ϕ=25°; SAR=2.8, MAR=0.95.

Figure 5-19. Effect of nozzle pressure ratio and total temperature on normalized PNLT directivities for different jet velocities (Vⱼ) for a 10 and 9 full staggered CD-chute mixer with fully treated long ejector at an azimuthal angle φ=25°; SAR=2.8, MAR=0.95.

Figure 5-20. Effect of nozzle pressure ratio and total temperature on normalized SPL spectra at various polar angles (θ) for a 10 and 9 full staggered CD-chute mixer with fully treated long ejector at an azimuthal angle φ=25°, SAR=2.8, MAR=0.95, V_j=1400 ft/sec.

Figure 5-21. Effect of nozzle pressure ratio and total temperature on normalized SPL spectra at various polar angles (θ) for a 10 and 9 full staggered CD-chute mixer with fully treated long ejector at an azimuthal angle ϕ=25°; SAR=2.8, MAR=0.95, V_j=1590 ft/sec.

Figure 5-22.   Effect of nozzle pressure ratio and total temperature on normalized SPL spectra at various polar angles (θ) for a 10 and 9 full staggered CD-chute mixer with fully treated long ejector at an azimuthal angle φ=250°; SAR=2.8, MAR=0.95, V_j=1920 ft/sec.

Figure 5-23. Effect of nozzle pressure ratio and total temperature on normalized SPL spectra at various polar angles (θ) for a 10 and 9 full staggered CD-chute mixer with fully treated long ejector at an azimuthal angle φ=25°; SAR=2.8, MAR=0.95, Vⱼ=2200 ft/sec.

Figure 5-24. Effect of nozzle pressure ratio and total temperature on normalized SPL spectra at various polar angles (θ) for a 10 and 9 full staggered CD-chute mixer with fully treated long ejector at an azimuthal angle φ=250°, SAR=2.8, MAR=0.95, V_J=2384 ft/sec.

The chute static pressure distributions are predominately the functions of NPR. The effect of increasing NPR with decreasing nozzle total temperature at fixed V_j on ramp and chute static pressure distributions are shown in Figure 5-25 for M_F=0.0 and 0.36 cases. For each V_j the static pressure decreases with increasing NPR, both on the ramp and chute surfaces. However, at higher NPR the trend on chute static pressure distribution is reversed. The chute loading coefficient decreases and then increases with increasing NPR with decreasing nozzle total temperature as shown in Figure 5-26. The fixed chute loading coefficient contours are plotted with respect to NPR and nozzle temperature in Figure 5-27. Fixed jet velocity lines are superimposed on these plots. An optimum NPR and temperature combination seems to be possible for a desired chute loading coefficient.

The effect of increasing NPR with decreasing nozzle total temperature at fixed V_j on pumping and corrected pumping is shown in Figures 5-28 and 5-29, respectively. With respect to increasing NPR and with decreasing total temperature the pumping decreases. The fixed pumping contours plotted in Figure 5-30 also indicates the similar behavior. Since, the pumping decreases with increasing NPR (i.e., with decreasing nozzle temperature), the computed mixed jet velocity increases (see Figure 5-31). It should be noted that the computed mixed jet velocity is higher with the flight simulation of Mach 0.36.

Figure 5-32 shows the effect of increasing NPR with decreasing nozzle total temperature at fixed V_j on the average axial static pressure distributions on the inlet and the flap surface. Significant amount of pressure drop on the inlet and the flap surface closer to mixer exit is observed with increasing NPR with decreasing nozzle total temperature. Small amount of pressure increase due to increasing NPR with decreasing temperature is noted on the flap towards the ejector exit. For V_j =2384 ft/sec the transition between subsonic to supersonic mode occurs when NPR increases from 3.4 to 4.0 with decreasing nozzle temperature from 1590 to 1438°R. The effect of increasing NPR with decreasing nozzle total temperature at fixed V_j on normalized force due to static pressure difference on flap surface are shown in Figure 5-33. The force on the flap decreases first and then increases with increasing NPR along with decreasing nozzle total temperature.

5.2.2 For Short Hardwalled Ejector Configuration:

Figure 5-34 shows the variation of EPNL with respect to NPR and nozzle total temperature at five jet velocities. The EPNL increases slightly with increasing jet velocity
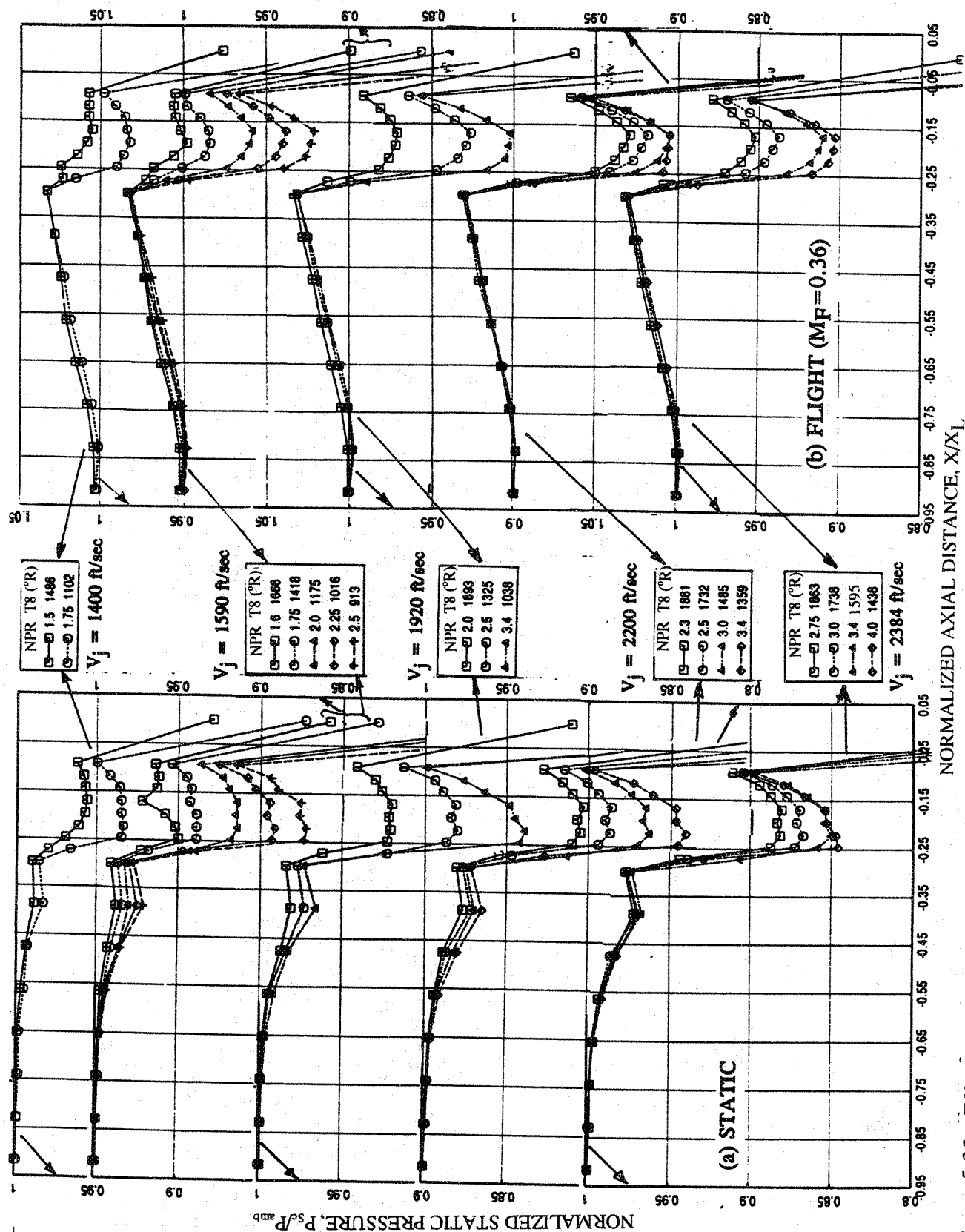
Figure 5-25. Effect of nozzle pressure ratio and total temperature on axial static pressure distributions on the inlet ramp and on the secondary flow side of chute surface at different jet velocities (V_j) for a 10 and 9 full staggered CD-chute mixer with fully treated long ejector; SAR=2.8, MAR=0.95, X_L=17".
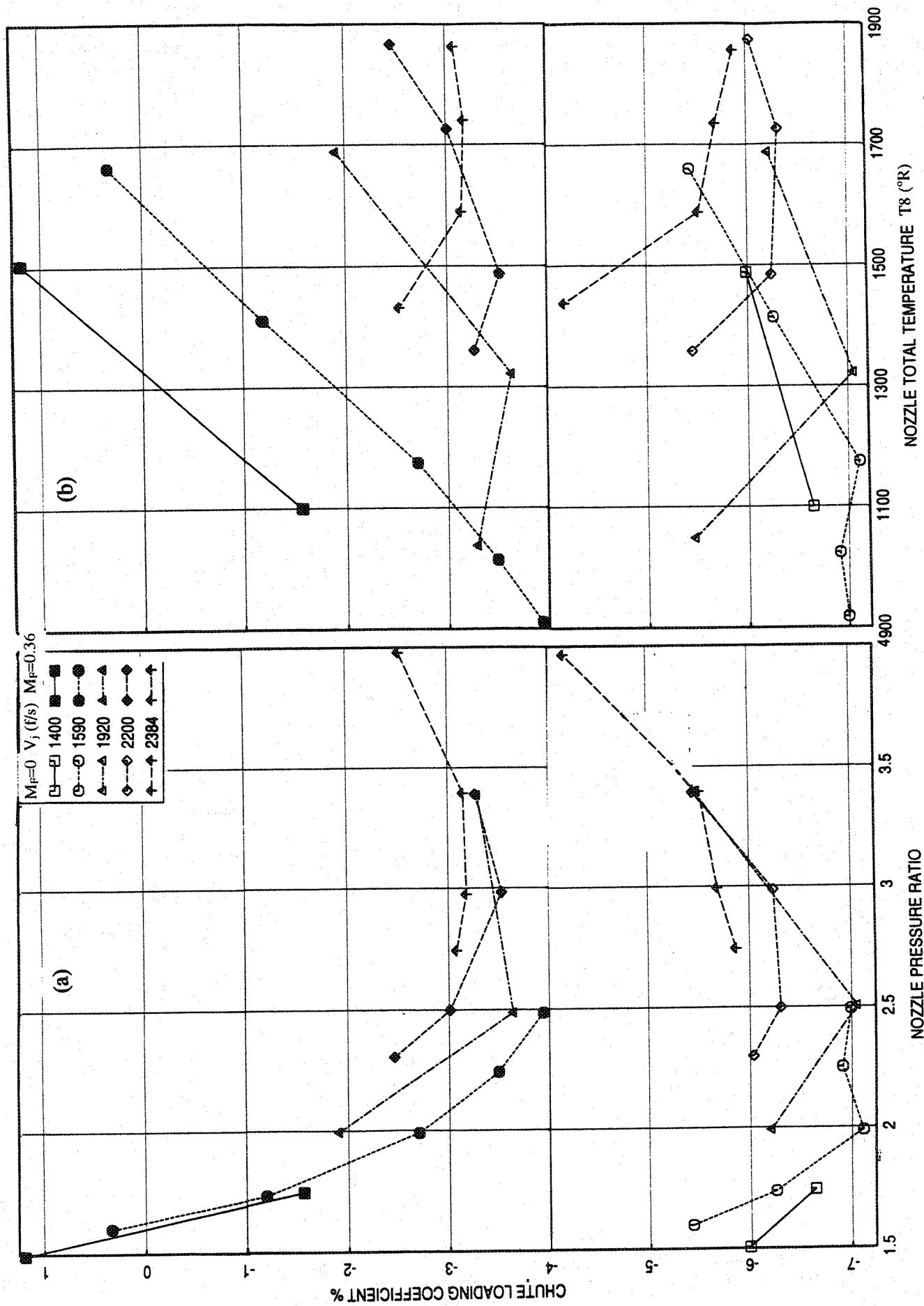
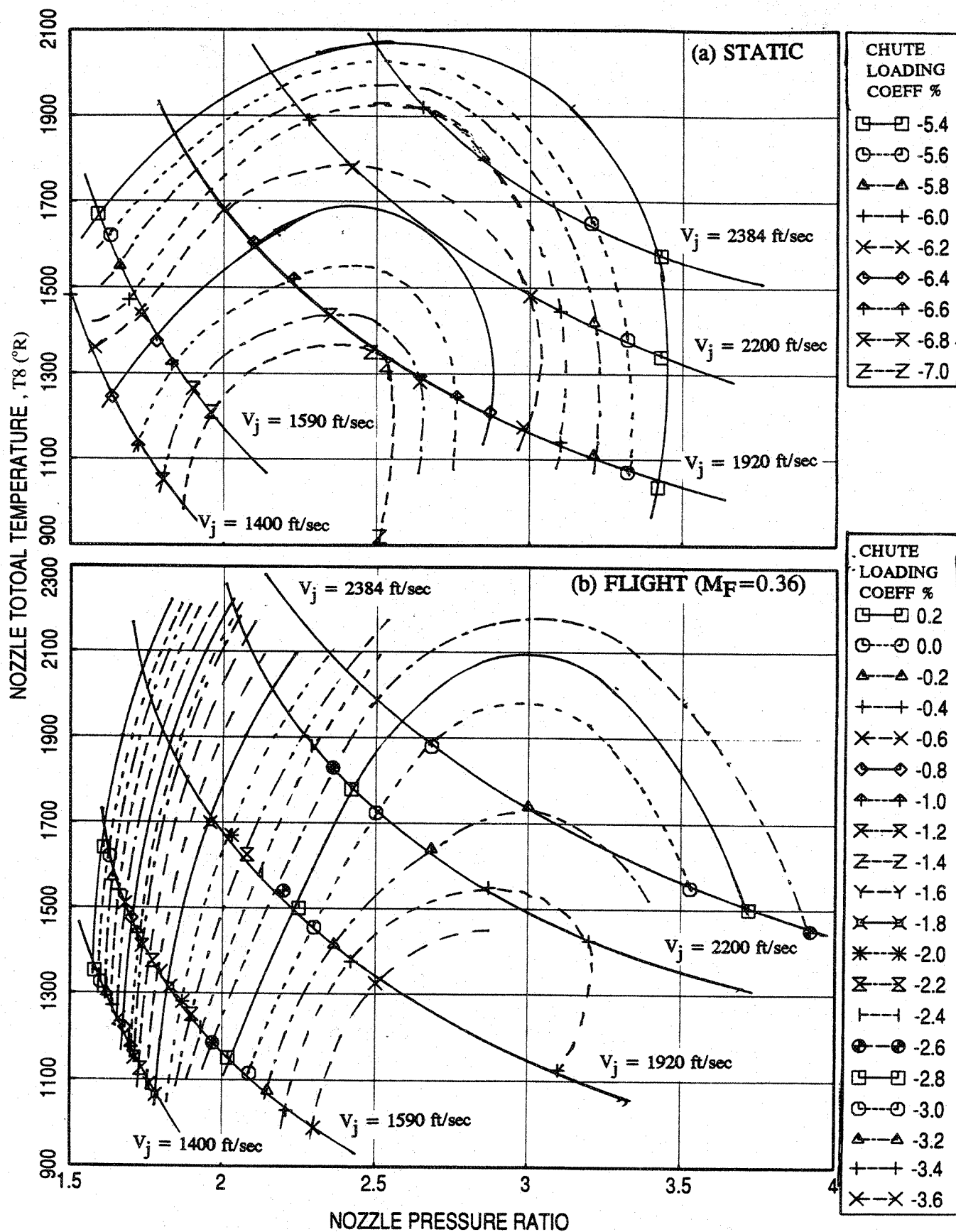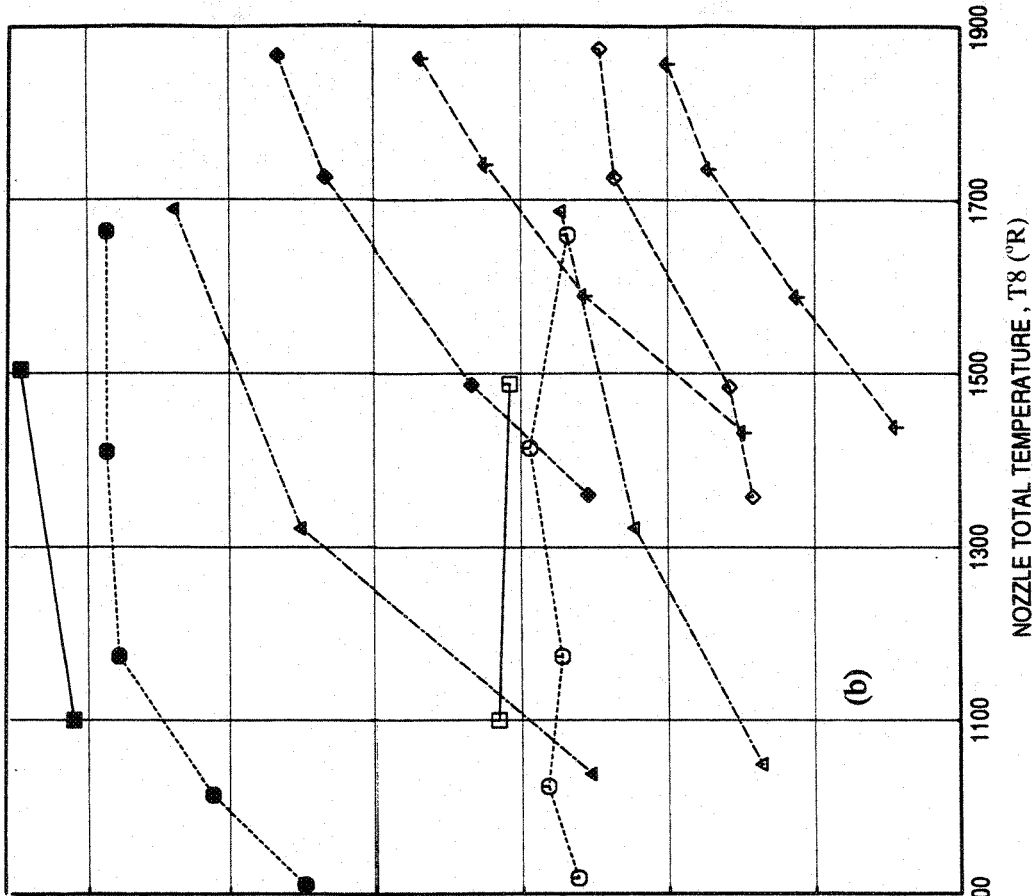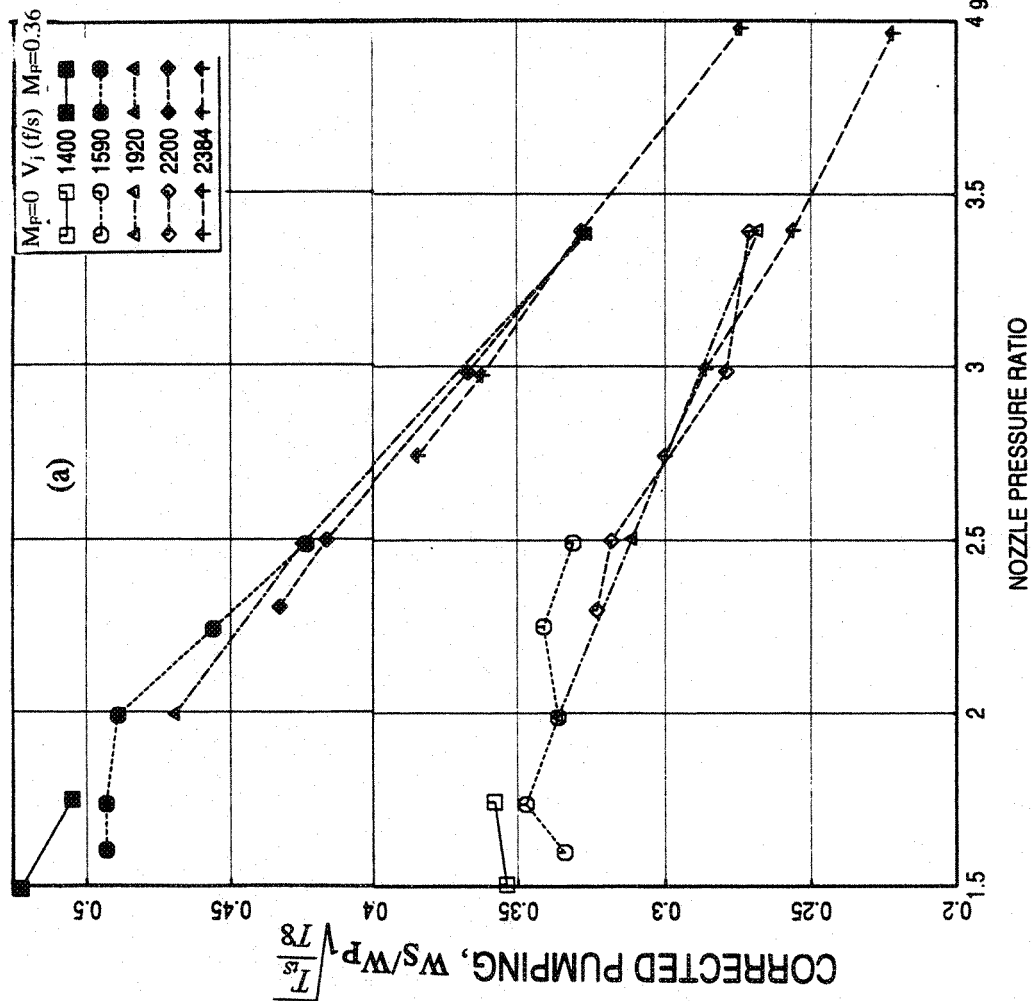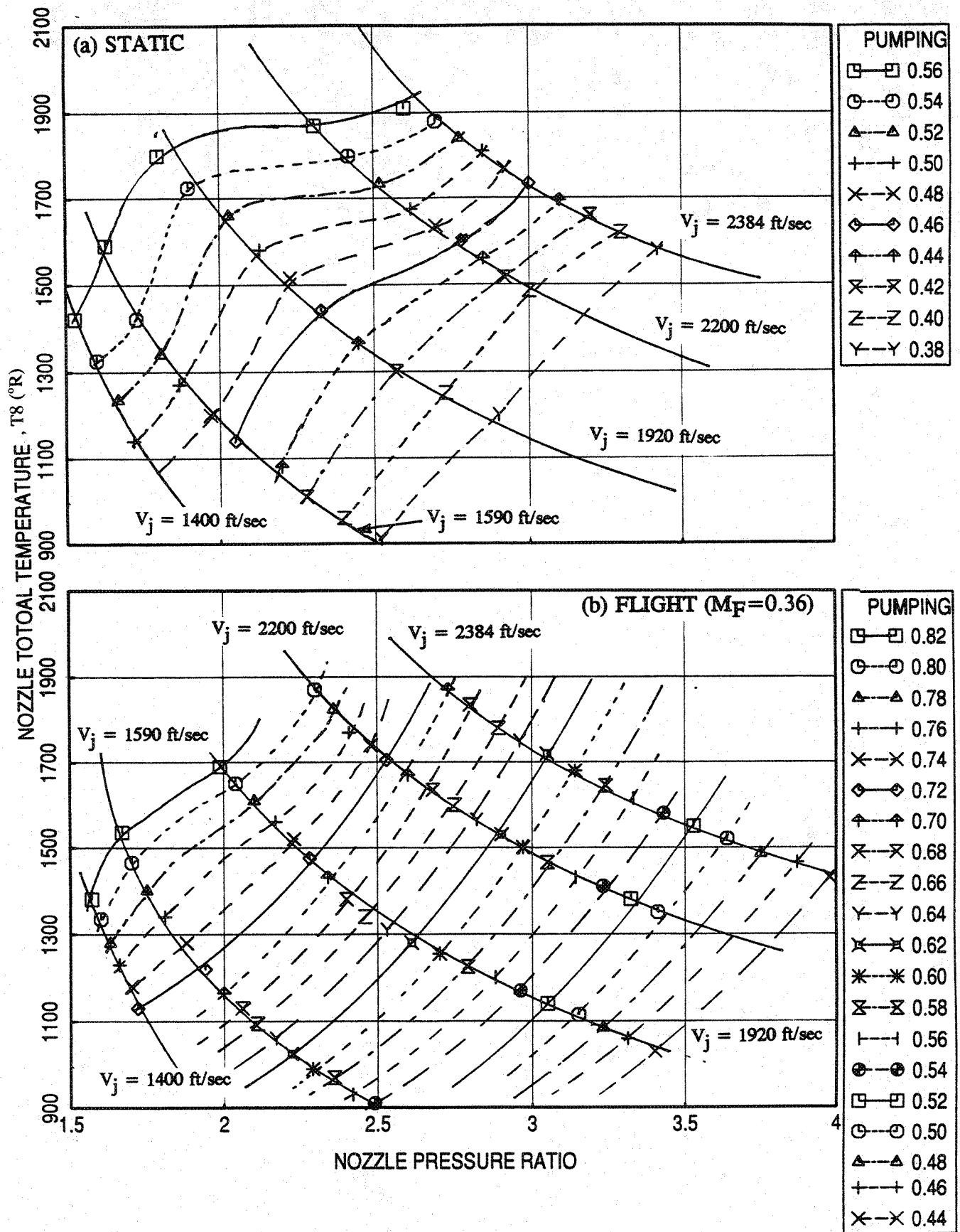Figure 5-26. Effect of nozzle pressure ratio and total temperature on chute loading coefficient at different jet velocities (Vj) for a 10 and 9 full staggered CD-chute mixer with fully treated long ejector; SAR=2.8, MAR=0.95.

Figure 5-27. Chute loading coefficient contours with respect to nozzle pressure ratio and total temperature at (a) static and (b) at M_F=0.36 for a 10 and 9 full staggered CD-chute mixer with fully treated long ejector; SAR=2.8, MAR=0.95.
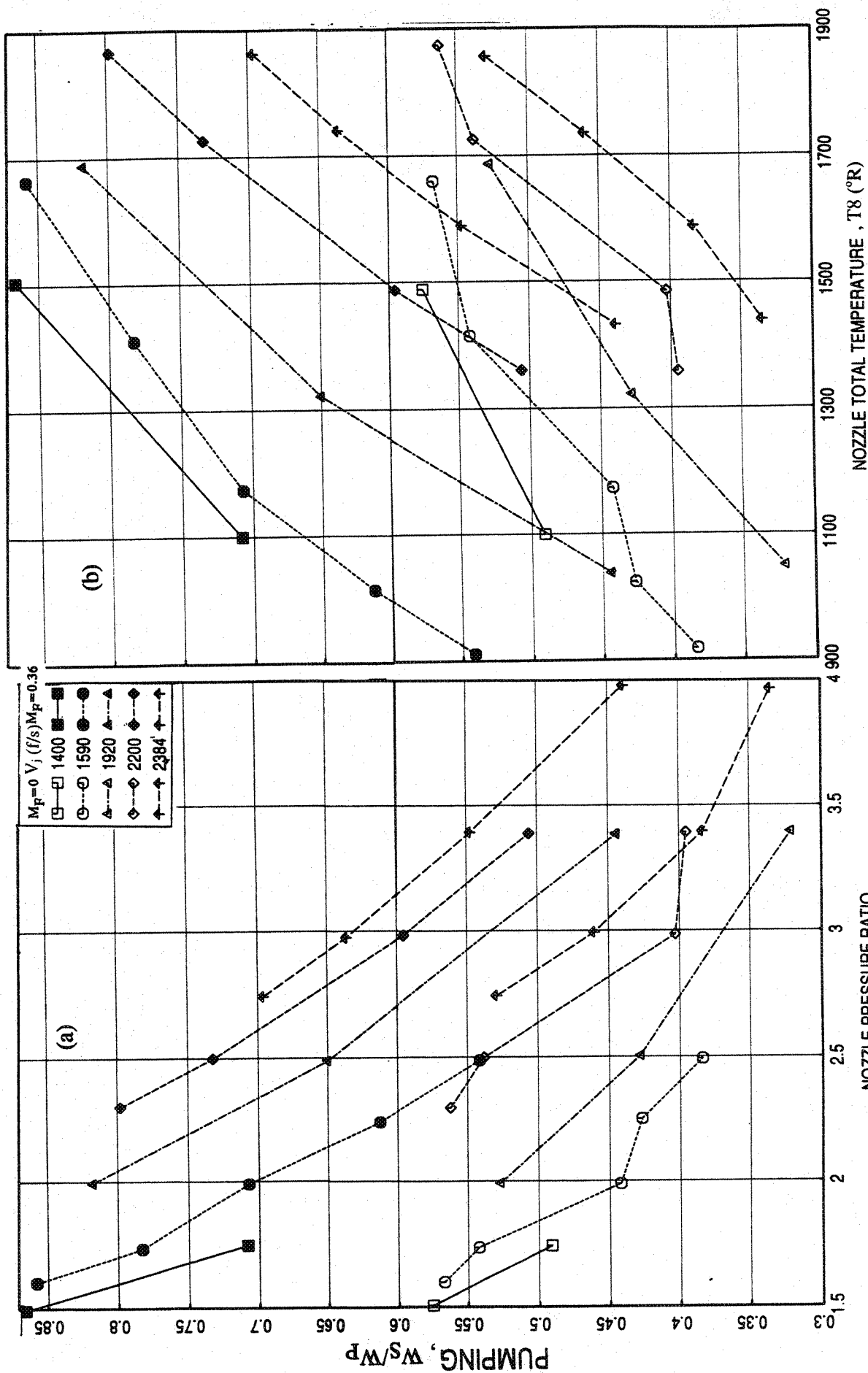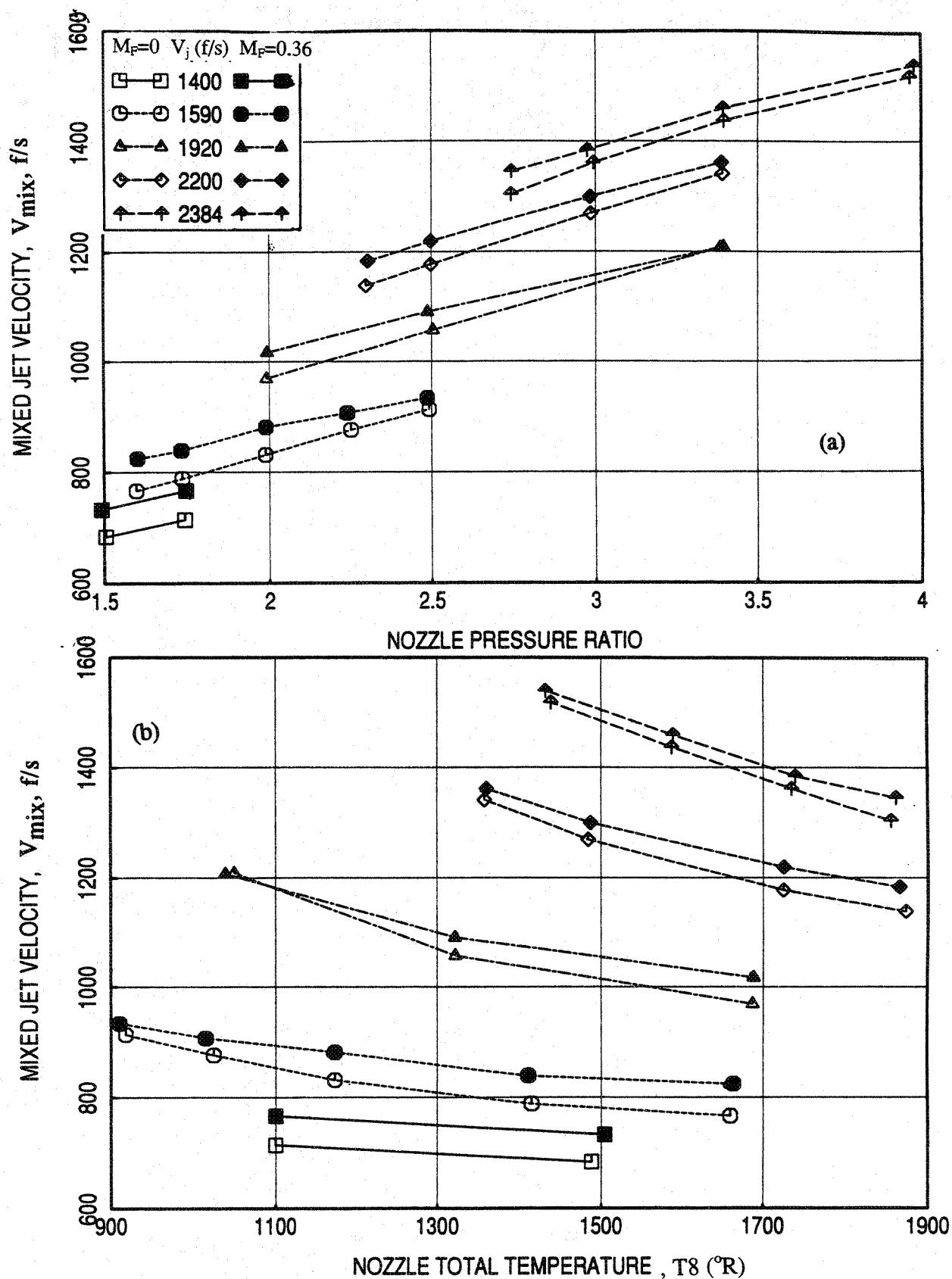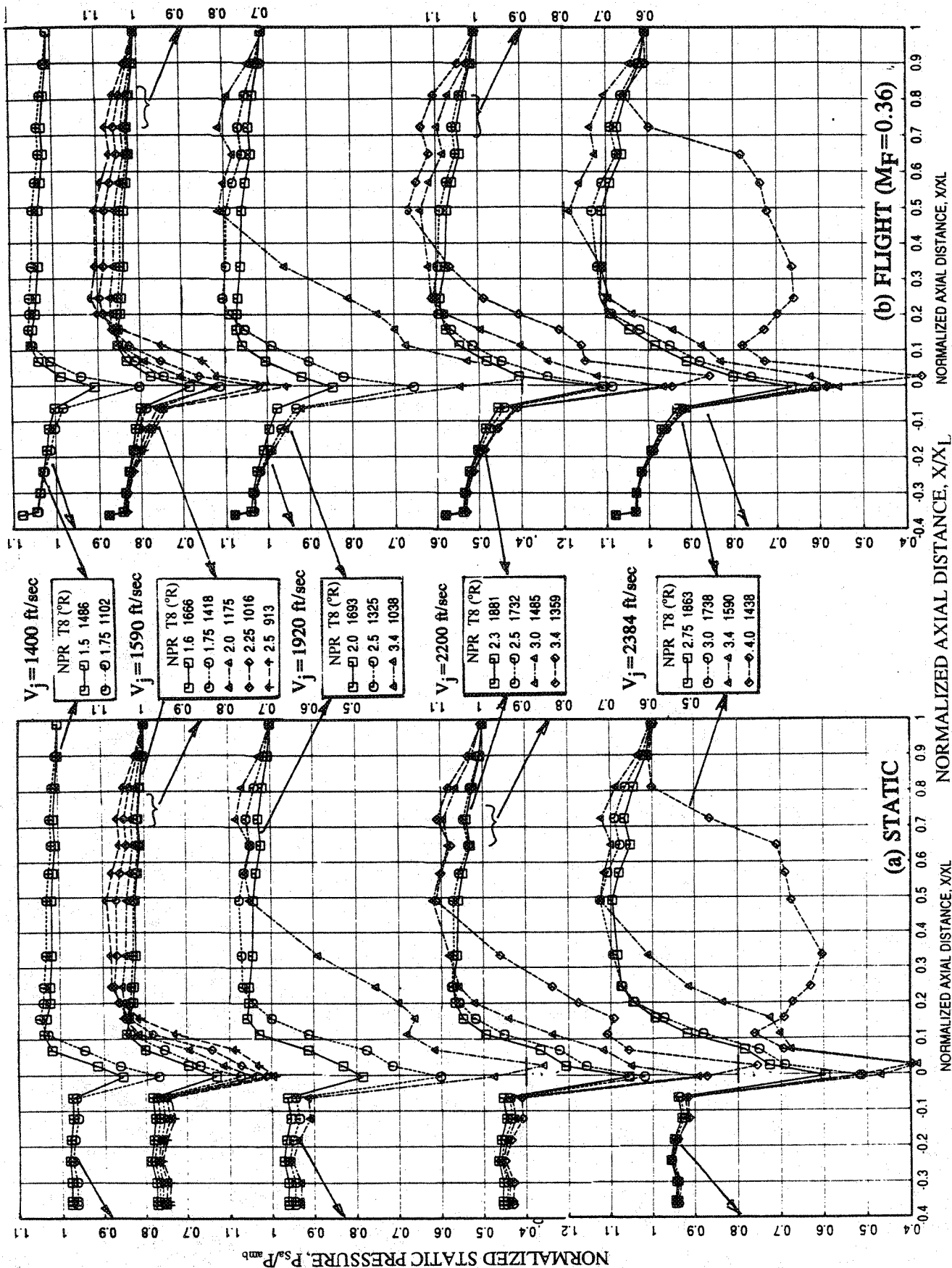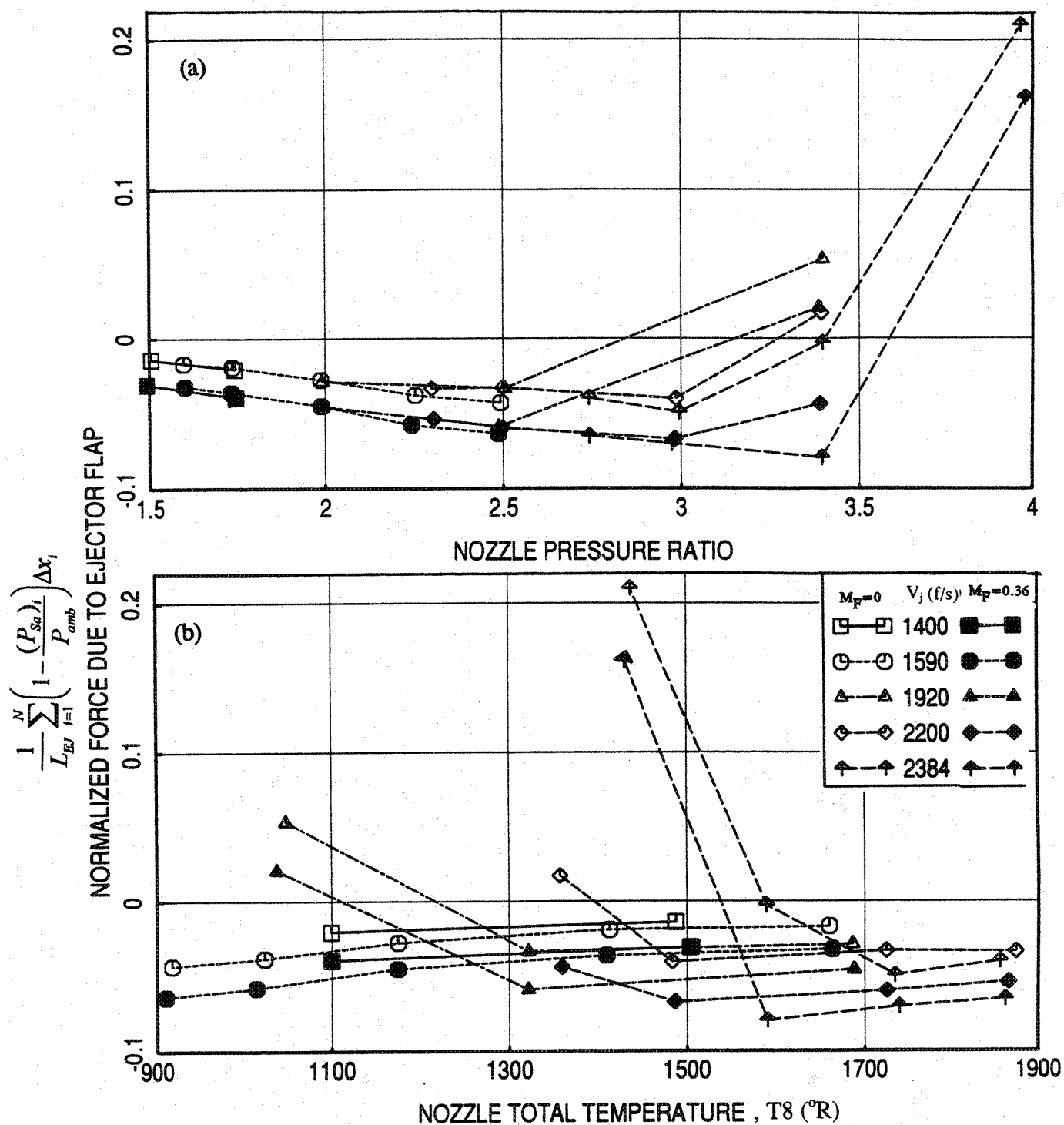
Figure 5-28. Effect of nozzle pressure ratio and total temperature on pumping at different jet velocities (V_j) for a 10 and 9 full staggered CD-chute mixer with fully treated long ejector; SAR=2.8, MAR=0.95.

Figure 5-29. Effect of nozzle pressure ratio and total temperature on corrected pumping at different jet velocities (V_j) for a 10 and 9 full staggered CD-chute mixer with fully treated long ejector; SAR=2.8, MAR=0.95.

Figure 5-30. Contours of pumping with respect to nozzle pressure ratio and total temperature at (a) static and (b) at M_F=0.36 for a 10 and 9 full staggered CD-chute mixer with fully treated long ejector; SAR=2.8, MAR=0.95.

Figure 5-31. Effect of nozzle pressure ratio and total temperature on mixed jet velocity at different jet velocities (V_j) for a 10 and 9 full staggered CD-chute mixer with fully treated long ejector; SAR=2.8, MAR=0.95.

Figure 5-32. Effect of nozzle pressure ratio and total temperature on axial distribution of average static pressure on the inlet and the flap surface at different jet velocities (V_j) for a 10 and 9 full staggered CD-chute mixer with fully treated long ejector; SAR=2.8, MAR=0.95, X_L=17"

Figure 5-33. Effect of nozzle pressure ratio and total temperature on normalized force on ejector flap surface at different jet velocities (V_j) for a 10 and 9 full staggered CD-chute mixer with fully treated long ejector; SAR=2.8, MAR=0.95.
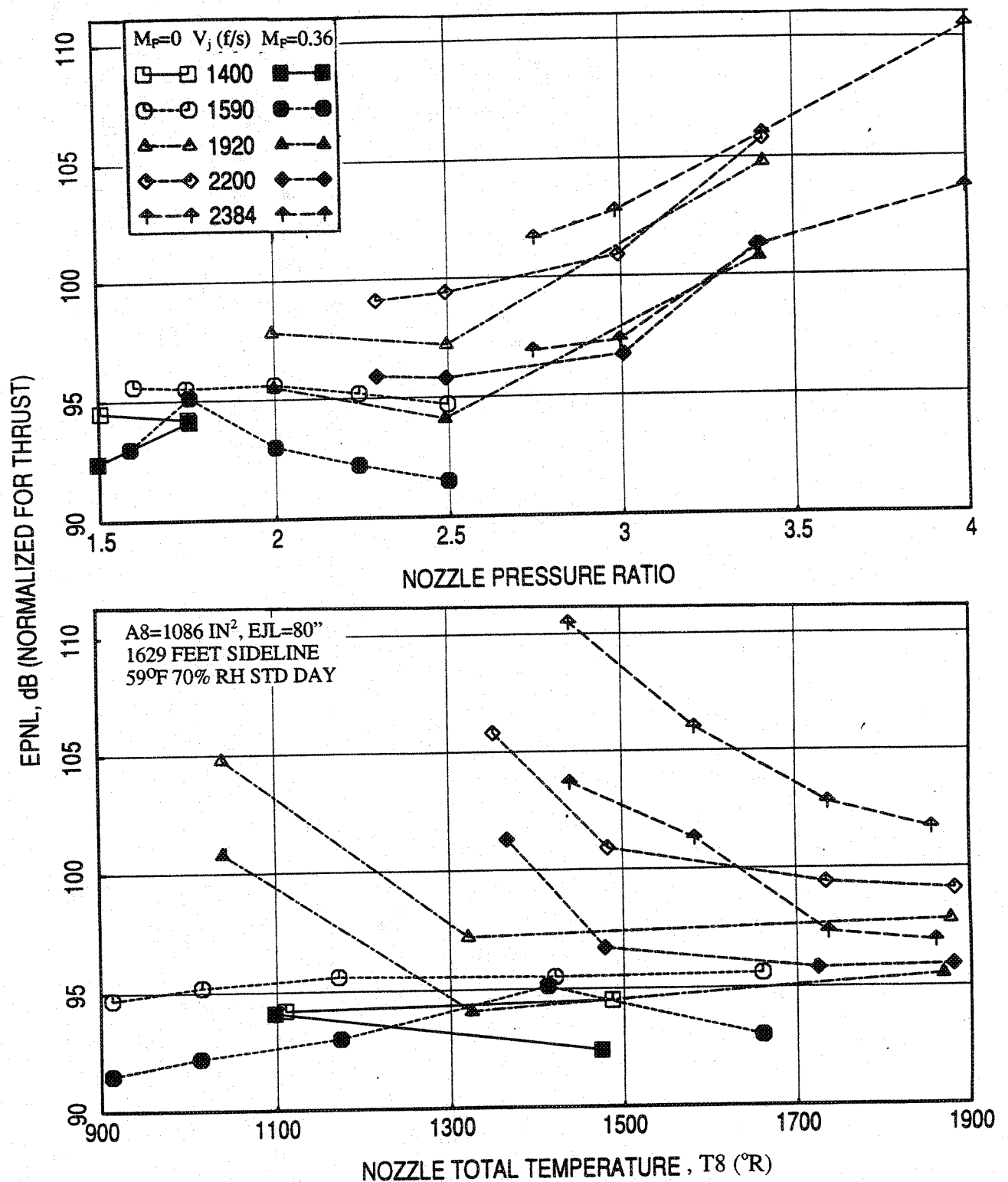
Figure 5-34. Effect of nozzle pressure ratio and total temperature on normalized EPNL at fixed jet velocities (V_j) for a 10 and 9 full staggered CD-chute mixer with hardwalled short ejector at an azimuthal angle φ=25°; SAR=2.8, MAR=0.95.

at static condition and is much less with flight simulation. This is in contrast to the behavior observed for long treated ejector, for which, the EPNL increases significantly with increasing velocity (see Figure 5-17). With respect to aerothermodynamic conditions the EPNL increases with increasing NPR and with decreasing nozzle total temperature. The trend is reversed at lower jet velocities, especially, with flight simulation. The EPNL levels are lowered due to flight simulation of Mach 0.36, but not as much as observed for long treated ejector (see Figure 5-17). These results are presented in a form of fixed EPNL contours between NPR and nozzle total temperature in Figure 5-35. In general EPNL increases with increasing NPR and nozzle total temperature. However, it is interesting to note that the fixed EPNL can be achieved by lowering the NPR and nozzle total temperature together at a lower NPR conditions, as observed in Figure 5-35 (b) for flight simulated case. EPNL with respect to NPR and T8 is relatively higher for this configuration compared to treated long ejector (see Figure 5-18).

Normalized PNLT directivities at fixed jet velocities are plotted in Figure 5-36 for static condition as well as for flight simulation case with Mach 0.36. Unlike the long treated ejector the PNLT does not increase significantly in the forward arc at lower jet velocities (i.e., at 1400 and 1590 ft/sec) and at lower NPR values (i.e., at 1.5 and 1.75). The ejector internal noise is most likely dominant at lower jet velocity conditions and is not significantly effected by NPR and T8. At the same time, the jet mixing noise is also higher due to lack of mixing in the short ejector and is increased due increasing NPR. Thus, the resultant PNLT levels in the farfield are relatively less effected by NPR and T8. At higher jet velocities the normalized PNLT levels monotonically increase with increasing NPR associated with decreasing nozzle total temperature for all polar angles, similar to long treated ejector (see Figure 5-19). At higher velocities, the externally generated jet mixing noise is most likely the dominant component to influence the PNLT directivity. Since, the mixed jet velocity increases with increasing NPR for fixed jet velocities, the PNLT (normalized for thrust) should increase with NPR, as observed in Figure 5-36 at V_j of 1920, 2200, and 2384 ft/sec. The SPL spectra at various polar angles for fixed jet velocities of 1400, 1590, 1920, 2200, and 2384 ft/sec conditions are shown in Figures 5-37 through 5-41, respectively. At higher velocities of 1920 and 2200 ft/sec, significant increase of SPL in the forward arc, resulting in humps, are observed when the nozzle pressure ratio exceeds 3. Strong shocks inside the ejector are most likely the cause for such SPL hump.
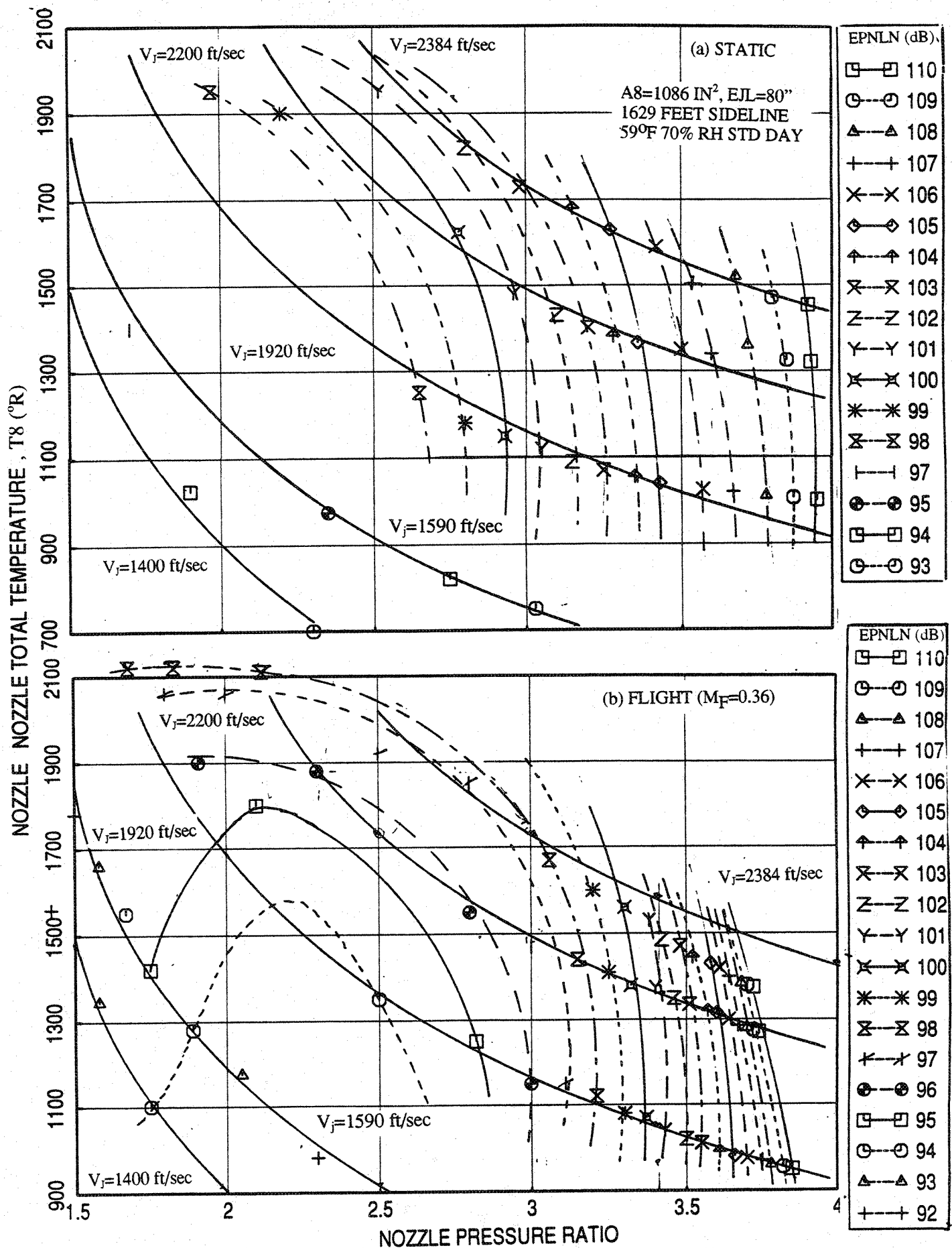
Figure 5-35. Normalized EPNL contours with respect to nozzle pressure ratio and total temperature at (a) static and (b) M_F=0.36 for a 10 and 9 full staggered CD-chute mixer with hardwalled short ejector at an azimuthal angle φ=25°; SAR=2.8, MAR=0.95.
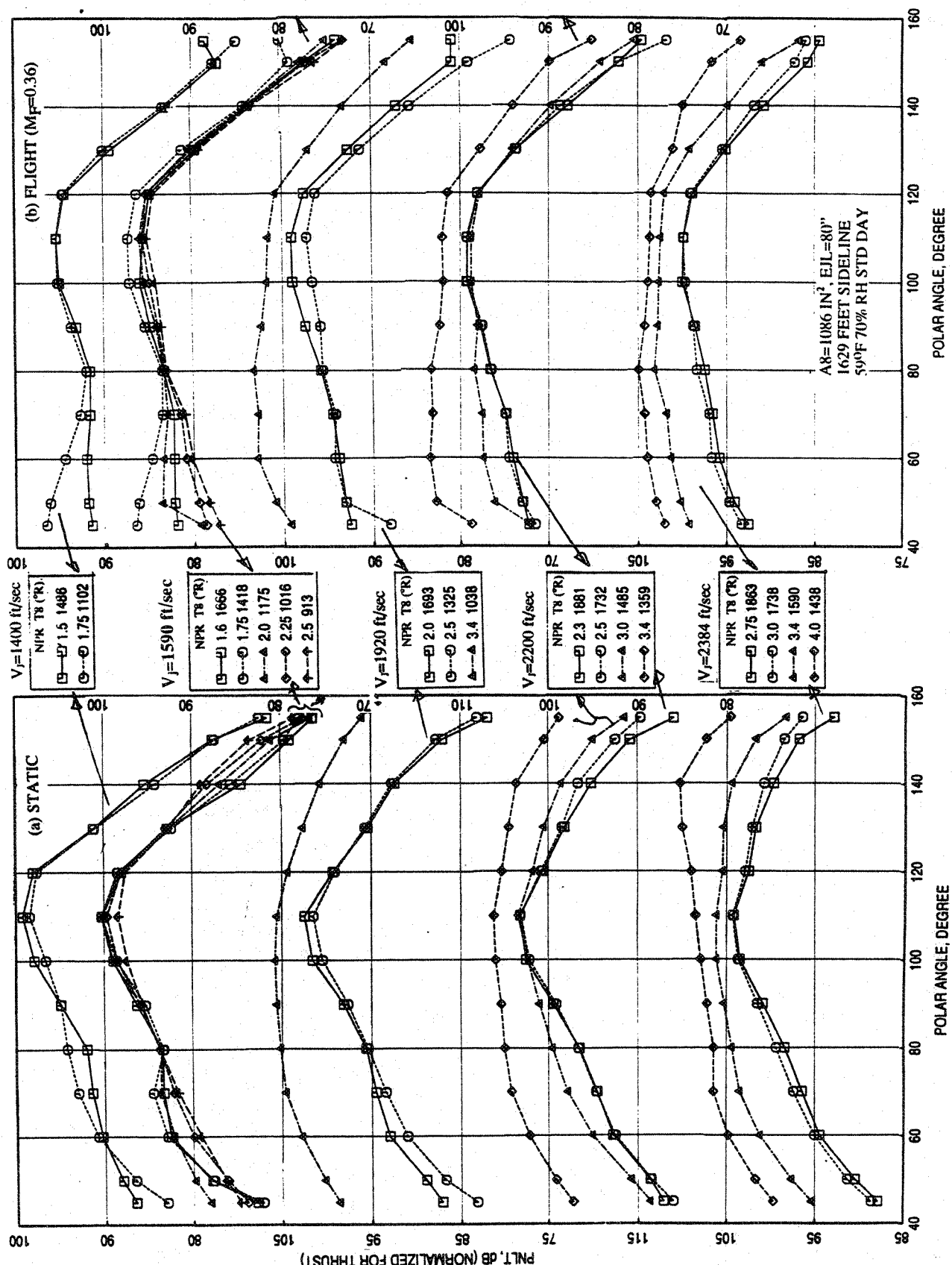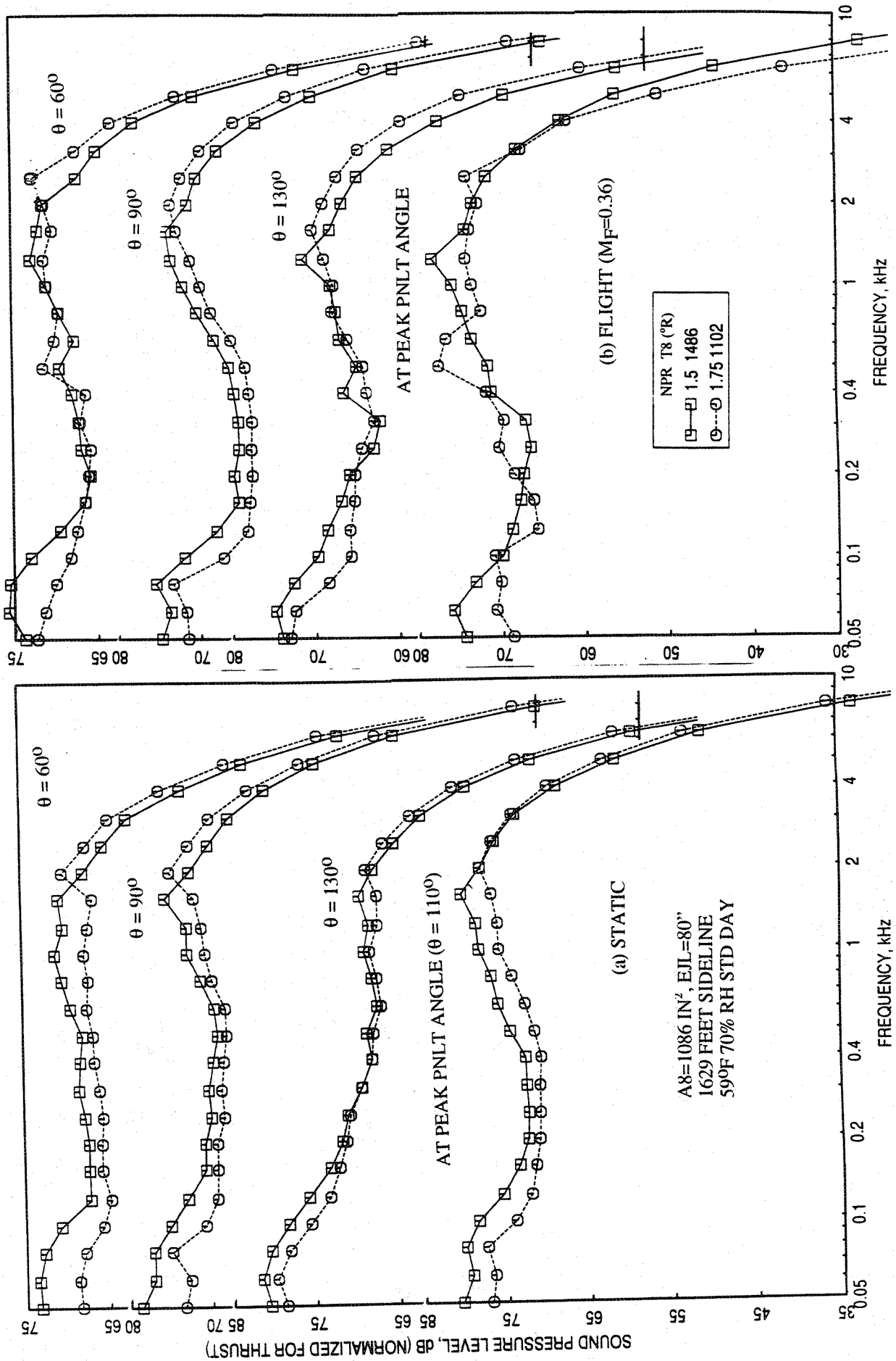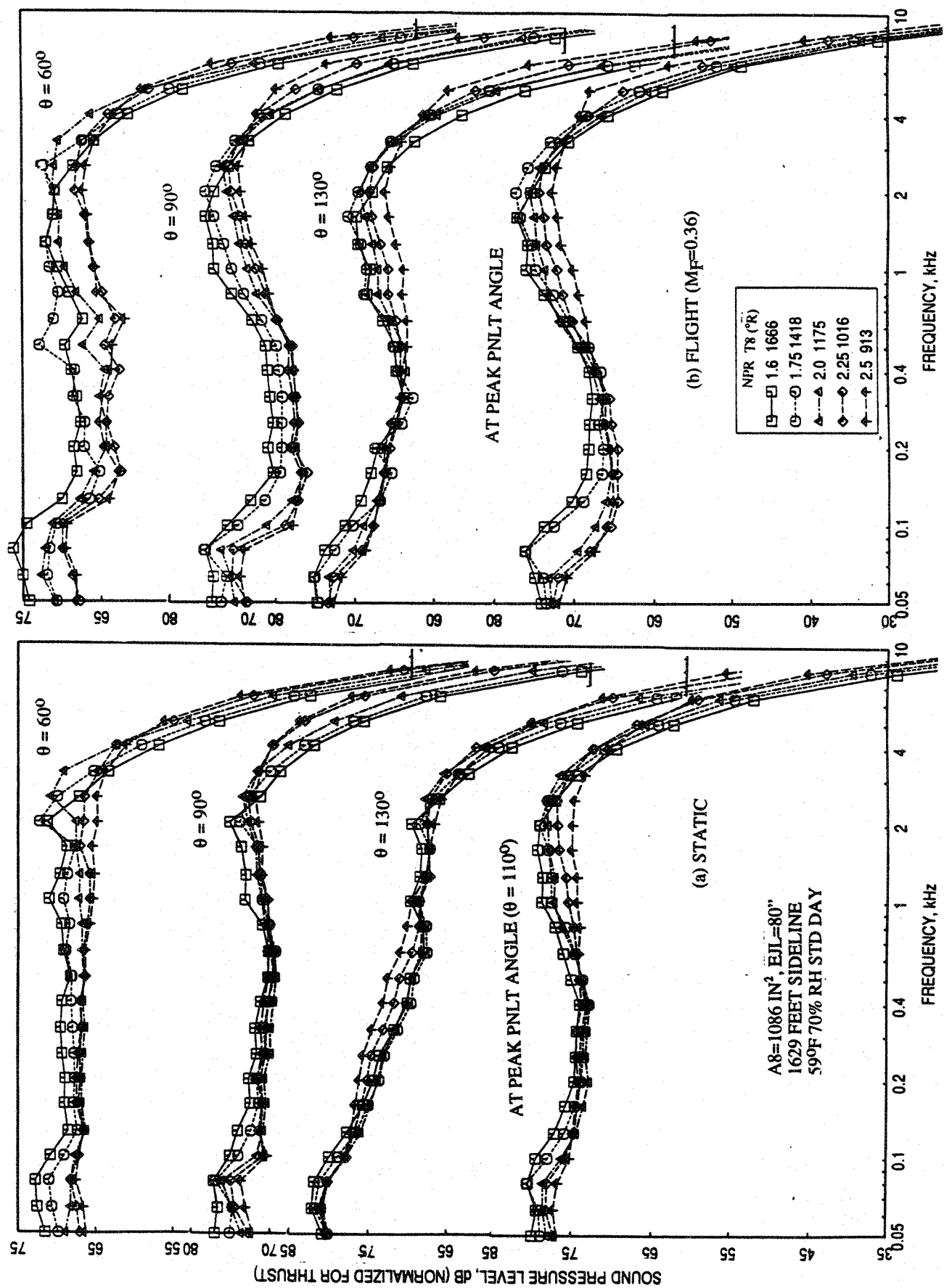
Figure 5-36. Effect of nozzle pressure ratio and total temperature on normalized PNLT directivities for different jet velocities (V_j) for a 10 and 9 full staggered CD-chute mixer with hardwalled short ejector at an azimuthal angle φ=25°; SAR=2.8, MAR=0.95.
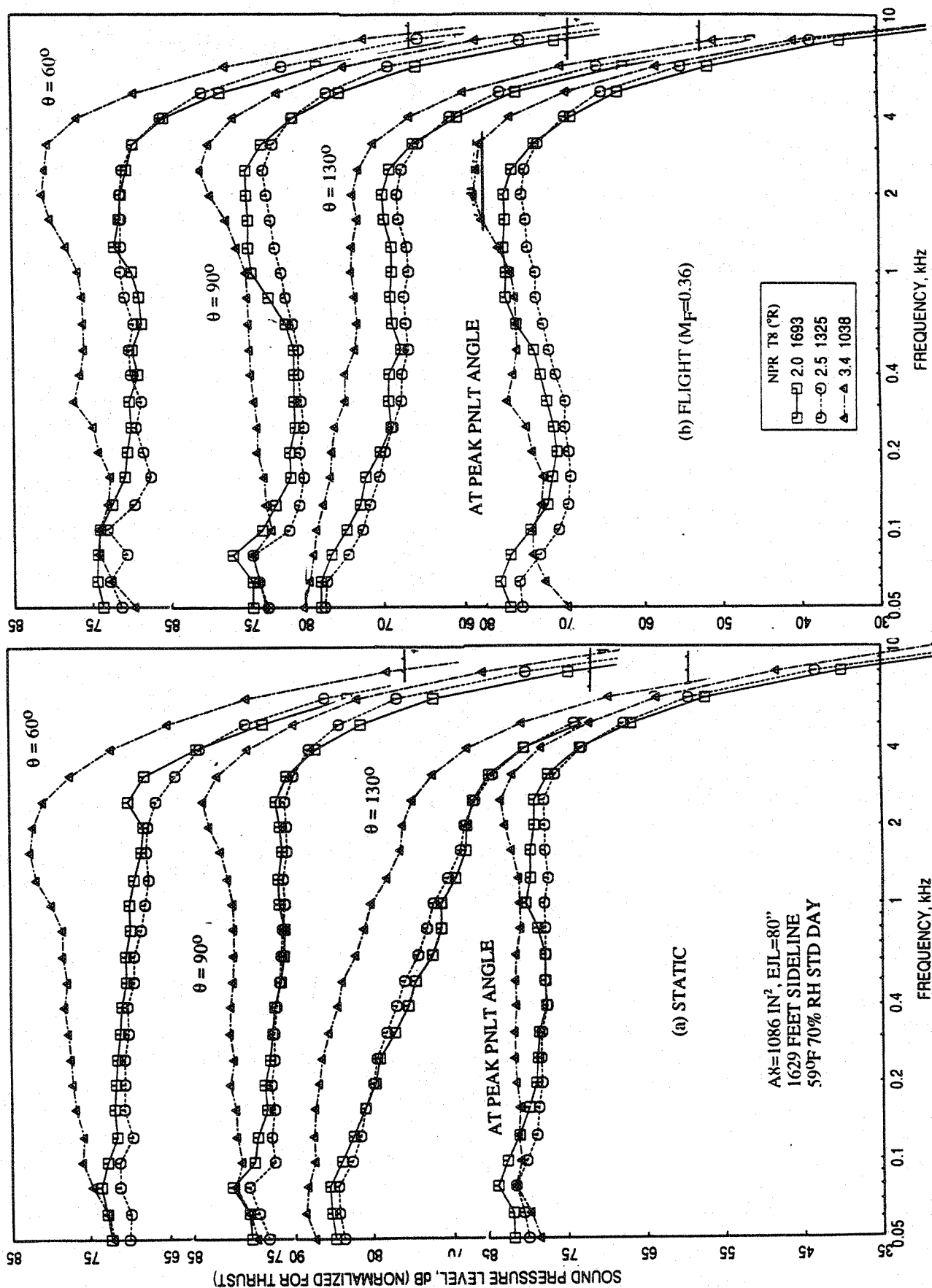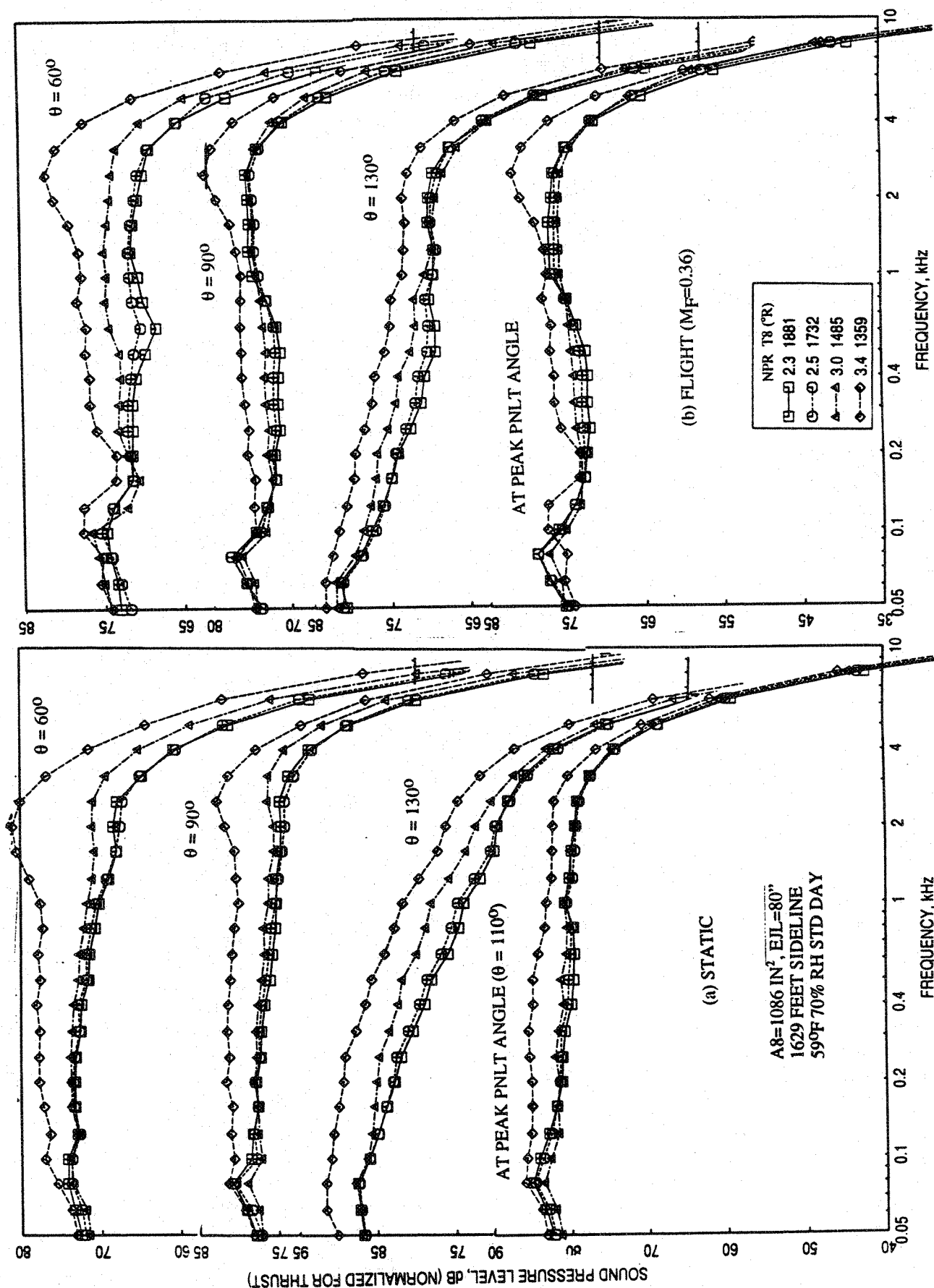
Figure 5-37. Effect of nozzle pressure ratio and total temperature on normalized SPL spectra at various polar angles (θ) for a 10 and 9 full staggered CD-chute mixer with hardwalled short ejector at an azimuthal angle φ=25°; SAR=2.8, MAR=0.95, V_j=1400 ft/sec.
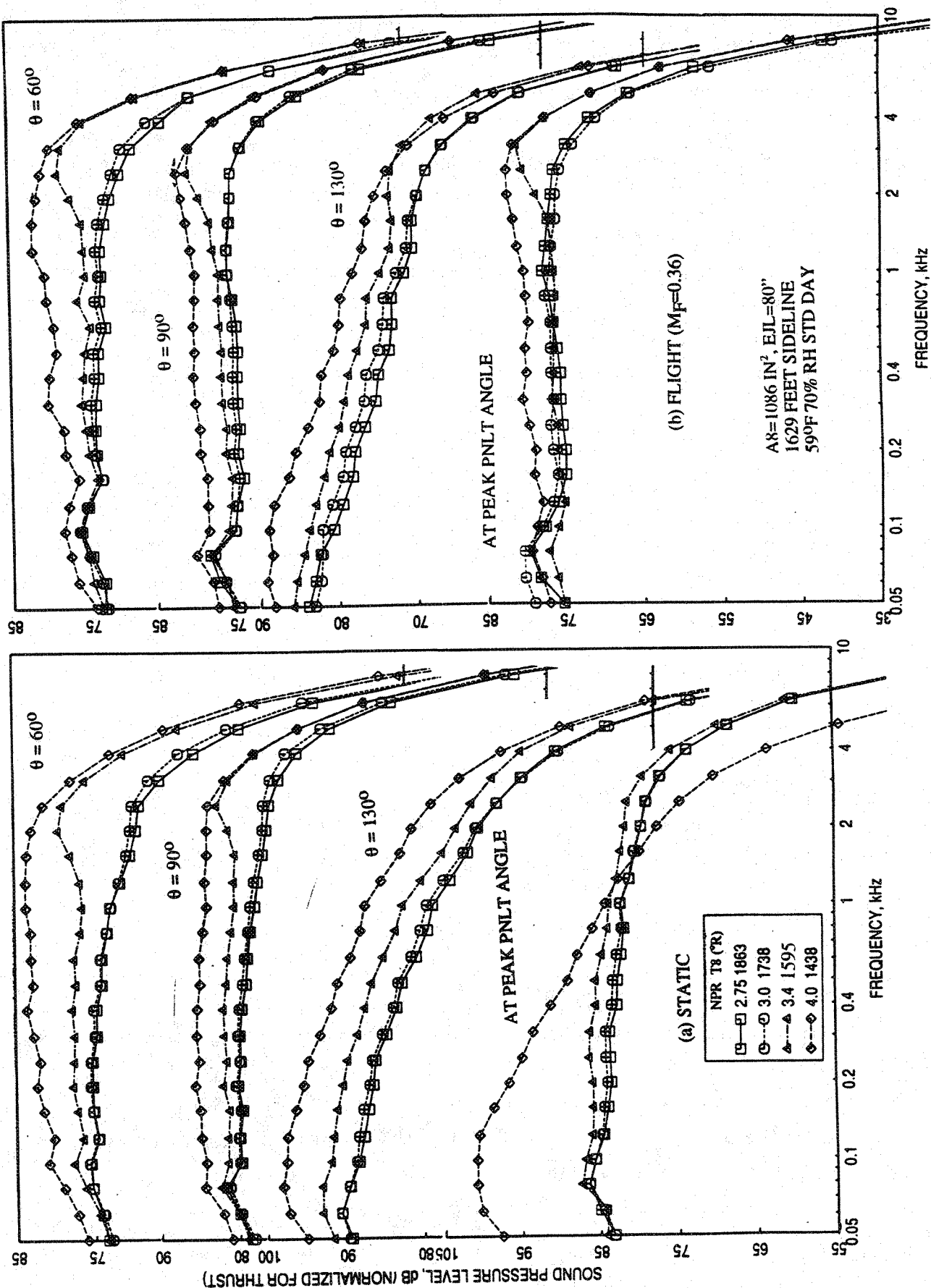
Figure 5-38. Effect of nozzle pressure ratio and total temperature on normalized SPL spectra at various polar angles (θ) for a 10 and 9 full staggered CD-chute mixer with hardwalled short ejector at an azimuthal angle φ=250°; SAR=2.8, MAR=0.95, Vⱼ=1590 ft/sec.

Figure 5-39. Effect of nozzle pressure ratio and total temperature on normalized SPL spectra at various polar angles (θ) for a 10 and 9 full staggered CD-chute mixer with hardwalled short ejector at an azimuthal angle φ=250°; SAR=2.8, MAR=0.95, V$_j$=1920 ft/sec.

Figure 5-40. Effect of nozzle pressure ratio and total temperature on normalized SPL spectra at various polar angles (θ) for a 10 and 9 full staggered CD-chute mixer with hardwalled short ejector at an azimuthal angle φ=25°; SAR=2.8, MAR=0.95, V_j=2200 ft/sec.

Figure 5-41. Effect of nozzle pressure ratio and total temperature on normalized SPL spectra at various polar angles (θ) for a 10 and 9 full staggered CD-chute mixer with hardwalled short ejector at an azimuthal angle φ=25°; SAR=2.8, MAR=0.95, V_j=2384 ft/sec.

The flow and performance related results, derived from the measurements made upstream of the mixer exit plane, are almost identical to those for the long treated ejector. Hence, those results are not included for the short hardwalled ejector configuration.

Figure 5-42 shows the effect of increasing NPR with decreasing nozzle total temperature at fixed V_j on the average axial static pressure distributions on the inlet and the flap surface. Significant amount of pressure drop on the inlet and the flap surface closer to mixer exit is observed with increasing NPR with decreasing nozzle total temperature. Small amount of pressure increase due to increasing NPR with decreasing temperature is noted on the flap towards the ejector exit. For V_j =1920 ft/sec the transition between subsonic to supersonic mode occurs when NPR increases from 2.5 to 3.4 with decreasing nozzle temperature from 1325 to 1038°R. Similar transitions between NPR 0f 3.0 and 3.4 are observed for V_j =2200 and 2384 ft/sec. The transition seems to be earlier with respect to NPR for this configuration compared to long treated ejector (see Figure 5-32).

Although it seems beneficial to go for higher temperature from noise consideration on a constant thrust basis, higher T8 will require a larger A8, which has large implications on nozzle envelope and weight.

5.3 EFFECT OF NOZZLE TOTAL TEMPERATURE AT FIXED NPR :

To evaluate the effect of nozzle total temperature on acoustic and flow related results the test data for fixed NPR conditions are examined. The acoustic results are normalized with respect to a reference ideal thrust of 60,000 lb to illustrate the effect of aerothermodynamic conditions at fixed nozzle pressure ratio for the same ideal thrust.

5.3.1 For Long Treated Ejector Configuration:

Figure 5-43 shows the normalized PNLT directivities at a number of fixed NPR conditions with different nozzle total temperatures for static and for a flight case of Mach of 0.36. Except for the lowest NPR of 1.5 the PNLT level increases at all angles for all NPR conditions with increasing nozzle total temperature. At NPR=1.5 the PNLT level is lower in the forward arc due to increasing temperature. This could be the result of dominant internally generated noise at lower jet velocity conditions, where, the radiation directivity of the internal noise could have caused the observed directivity at NPR=1.5.
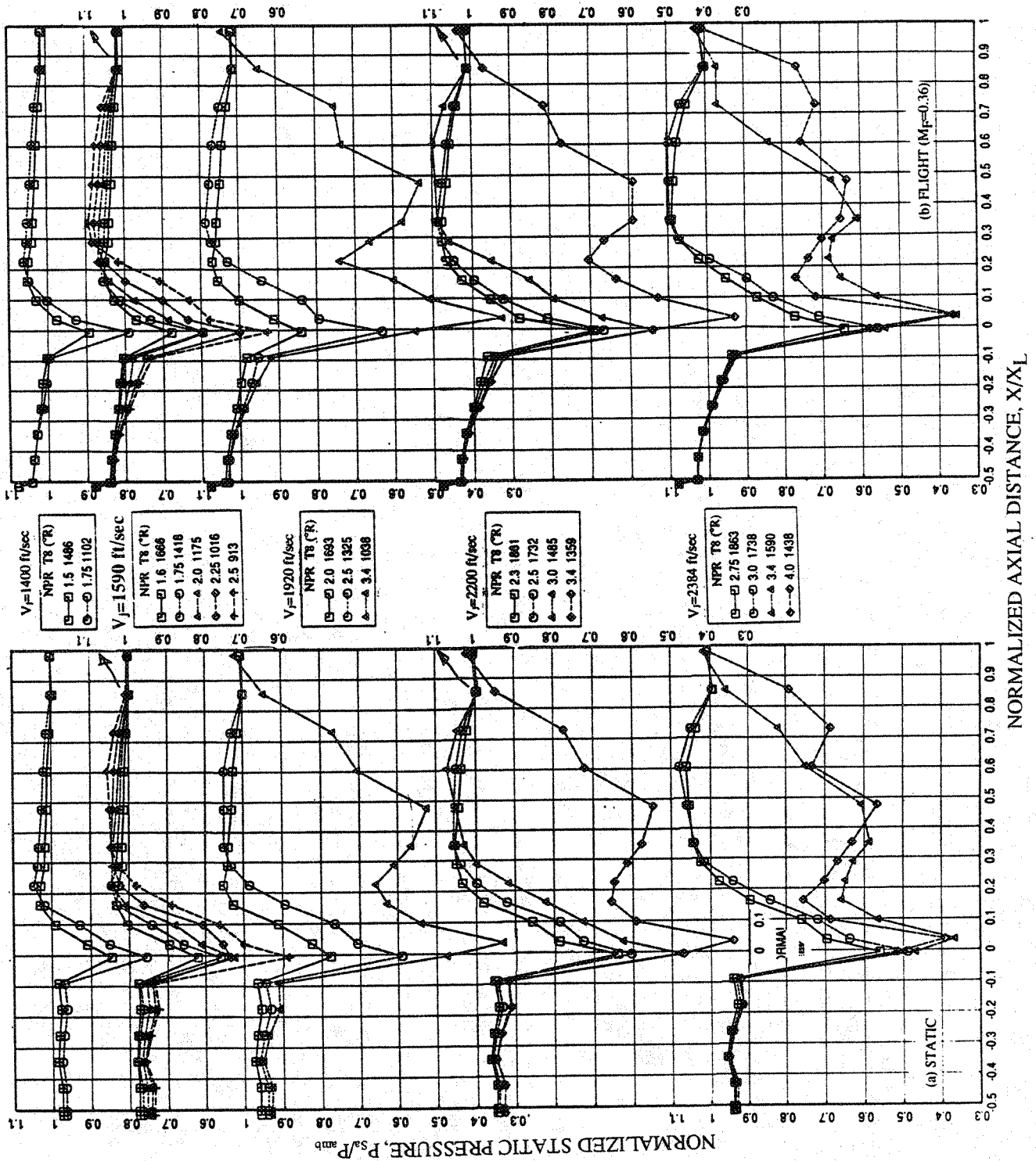
Figure 5-42. Effect of nozzle pressure ratio and total temperature on axial distribution of average static pressure on the inlet and the flap surface at different jet velocities (V_j) for a 10 and 9 full staggered CD-chute mixer with hardwalled short ejector; SAR=2.8, MAR=0.95, X_L= 11.88''.
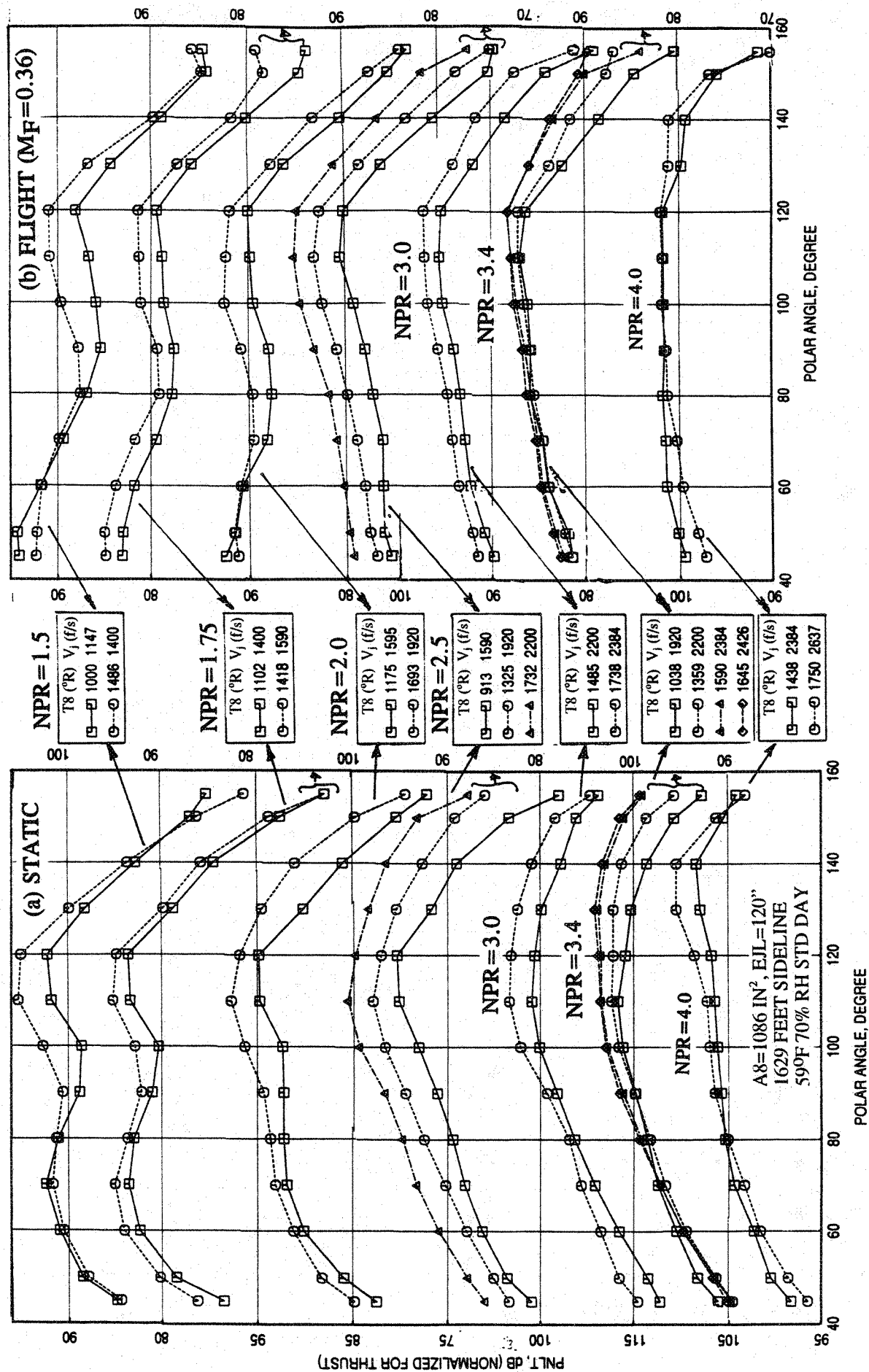
Figure 5-43. Effect of nozzle total temperature on normalized PNLT directivities for fixed NPRs for a 10 and 9 full staggered CD-chute mixer with fully treated long ejector at an azimuthal angle φ=25°; SAR=2.8, MAR=0.95.

The effect of nozzle total temperature on SPL spectra for three fixed NPR conditions of 1.5, 2.5, and 3.4 is shown in Figures 5-44 through 5-46. In general, the normalized SPL increases with increasing temperature for the entire frequency range and at all polar angles for static case, except for the lowest NPR of 1.5. At this case the SPL is lower at some frequencies with increasing nozzle temperature. The variation of normalized SPL with nozzle total temperature at M_F=0.36 is similar to those of static case for lower and mid frequency ranges. At higher frequencies the normalized SPL decreases with increasing nozzle total temperature.

The effect of increasing nozzle total temperature at fixed NPR on ramp and chute static pressure distributions are shown in Figure 5-47 for M_F=0.0 and 0.36 cases. For each NPR the static pressure remains unaffected on the ramp and increases on the chute surfaces with increasing nozzle total temperature. Figure 5-48 shows the effect of increasing nozzle total temperature at fixed NPR on the average axial static pressure distributions on the inlet and the flap surface. There is no effect on inlet static pressure distribution due to nozzle temperature variation. However, significant amount of pressure drop on the flap surface is observed with increasing nozzle total temperature for higher NPR conditions.

5.3.2 For Short Hardwalled Ejector Configuration:

Figure 5-49 shows the normalized PNLT directivities at a number of fixed NPR conditions with different nozzle total temperatures for static and for a flight case of Mach of 0.36. Except for the lowest NPR of 1.5 the PNLT level increases at all angles for all NPR conditions with increasing nozzle total temperature. This could be the result of dominant internally generated noise at lower jet velocity conditions, where, the radiation directivity of the internal noise could have caused the observed directivity at NPR=1.5.

The effect of nozzle total temperature on SPL spectra for three fixed NPR conditions of 1.5, 2.5, and 3.4 is shown in Figures 5-50 through 5-52. In general, the normalized SPL increases with increasing temperature for the entire frequency range and at all polar angles for static case, except for the lowest NPR of 1.5. At this case the SPL is lower at some frequencies with increasing nozzle temperature. The variation of normalized SPL with nozzle total temperature at M_F=0.36 is similar to those of static case for lower and mid frequency ranges. At higher frequencies the normalized SPL decreases with increasing nozzle total temperature.
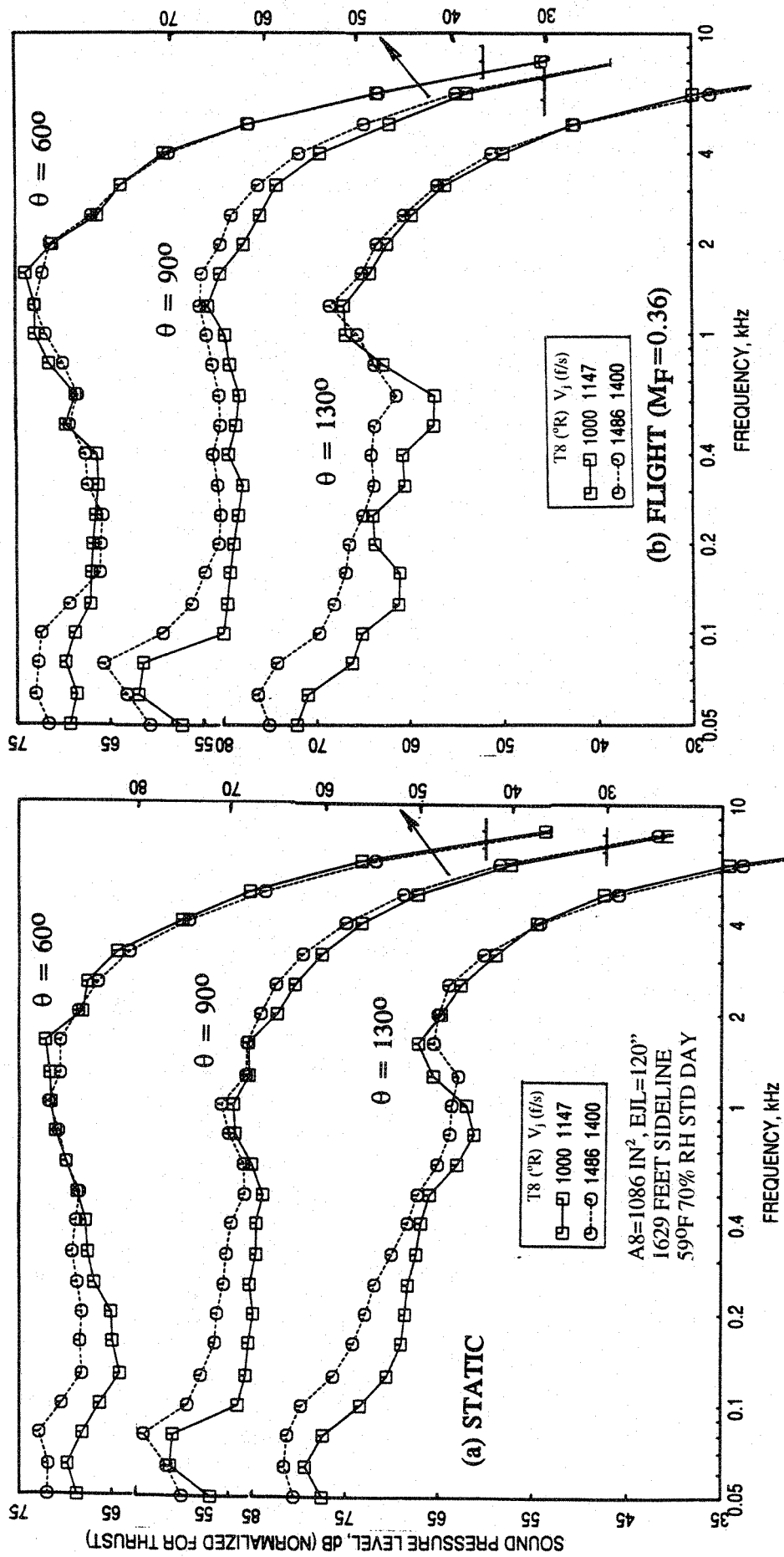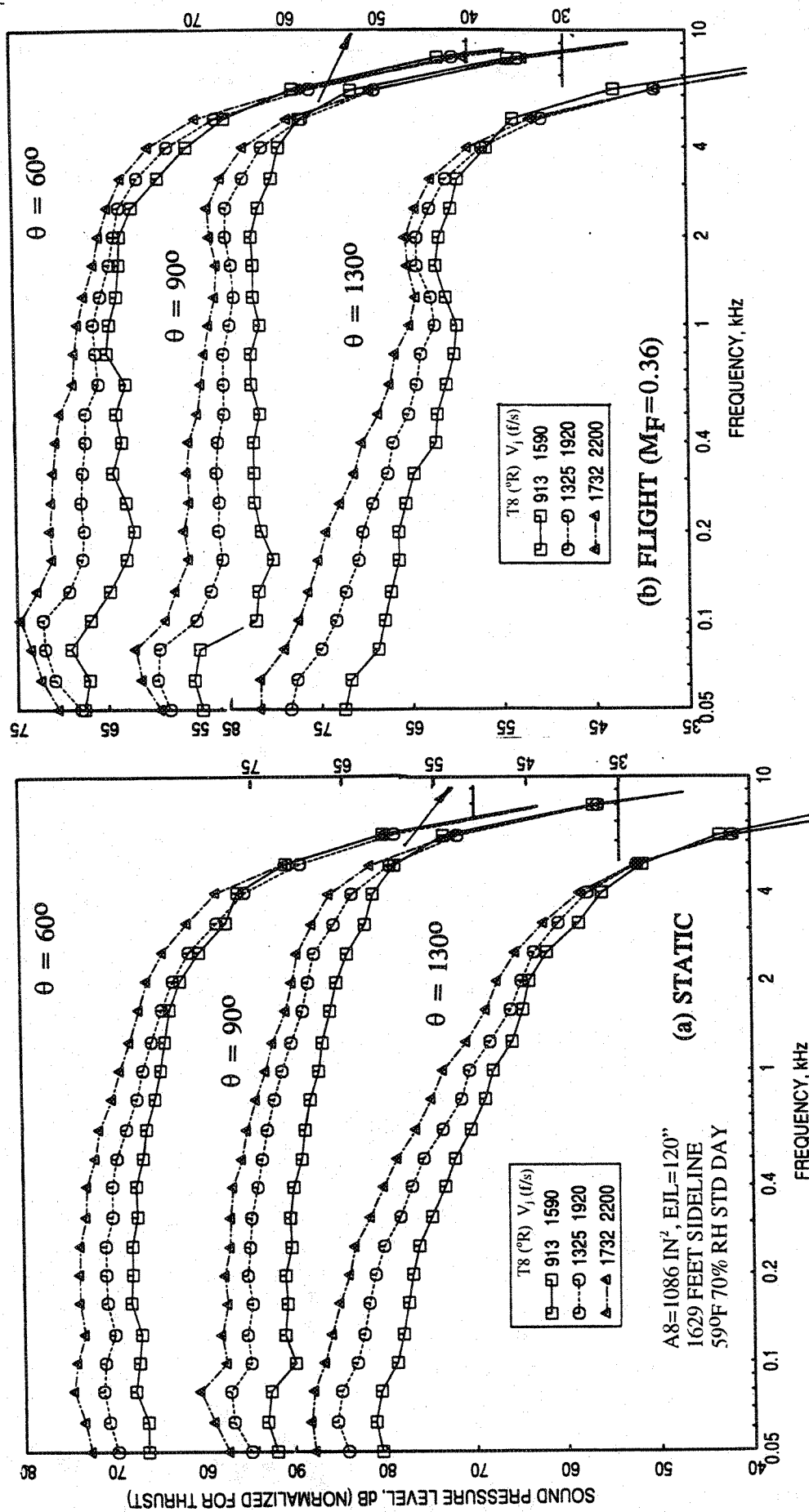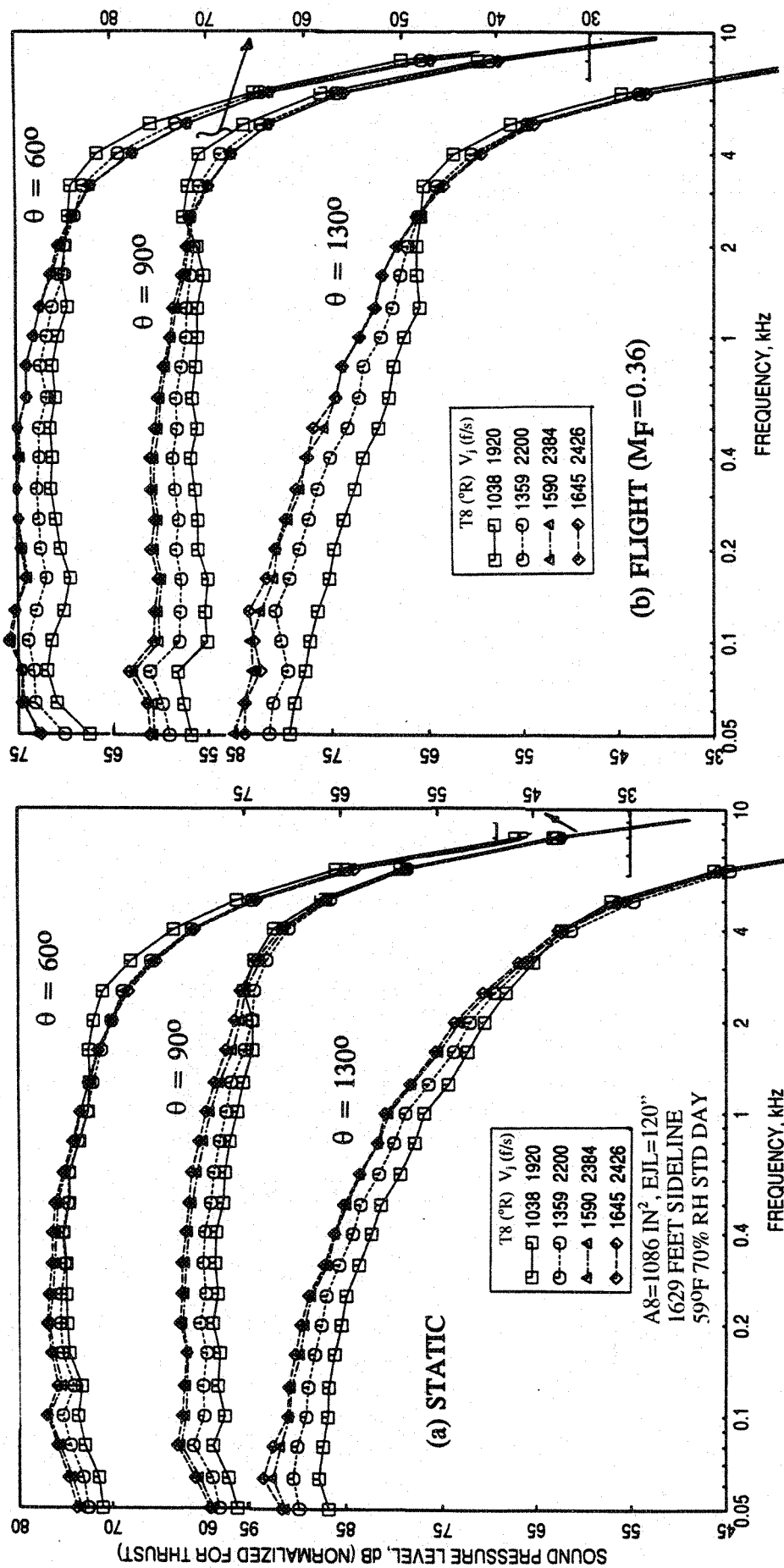
Figure 5-44. Effect of nozzle total temperature on normalized SPL spectra at various polar angles (θ) at a fixed NPR of 1.5 for a 10 and 9 full staggered CD-chute mixer with fully treated long ejector at an azimuthal angle φ=25°; SAR=2.8, MAR=0.95.
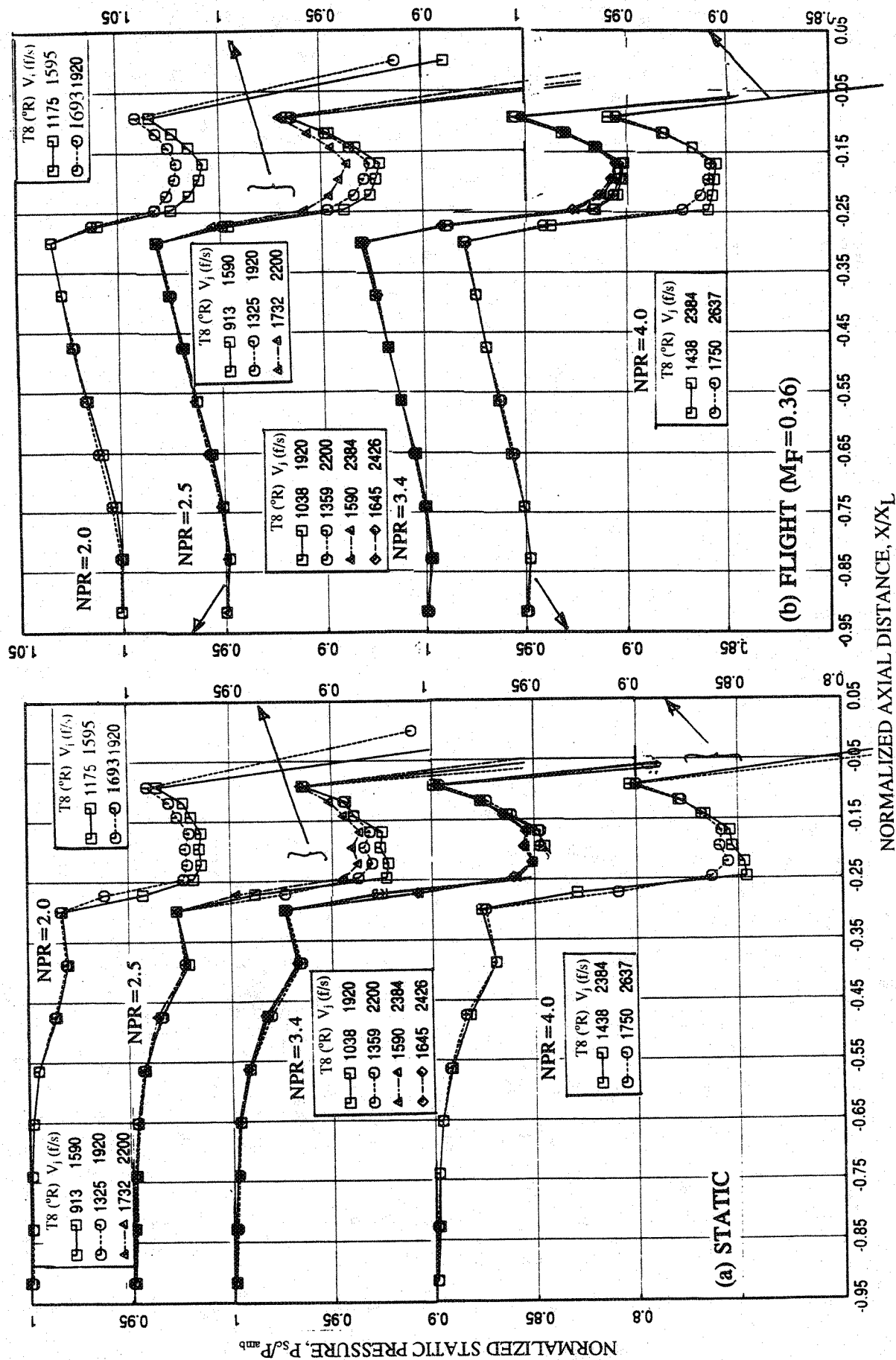
Figure 5-45. Effect of nozzle total temperature on normalized SPL spectra at various polar angles (θ) at a fixed NPR of 2.5 for a 10 and 9 full staggered CD-chute mixer with fully treated long ejector at an azimuthal angle φ=25°; SAR=2.8, MAR=0.95.

Figure 5-46. Effect of nozzle total temperature on normalized SPL spectra at various polar angles (θ) at a fixed NPR of 3.4 for a 10 and 9 full staggered CD-chute mixer with fully treated long ejector at an azimuthal angle φ=250°; SAR=2.8; MAR=0.95.

Figure 5-47. Effect of nozzle total temperature on axial static pressure distributions on the inlet ramp and on the secondary flow side of chute surface for a 10 and 9 full staggered CD-chute mixer with fully treated long ejector; SAR=2.8, MAR=0.95, X_L=17".
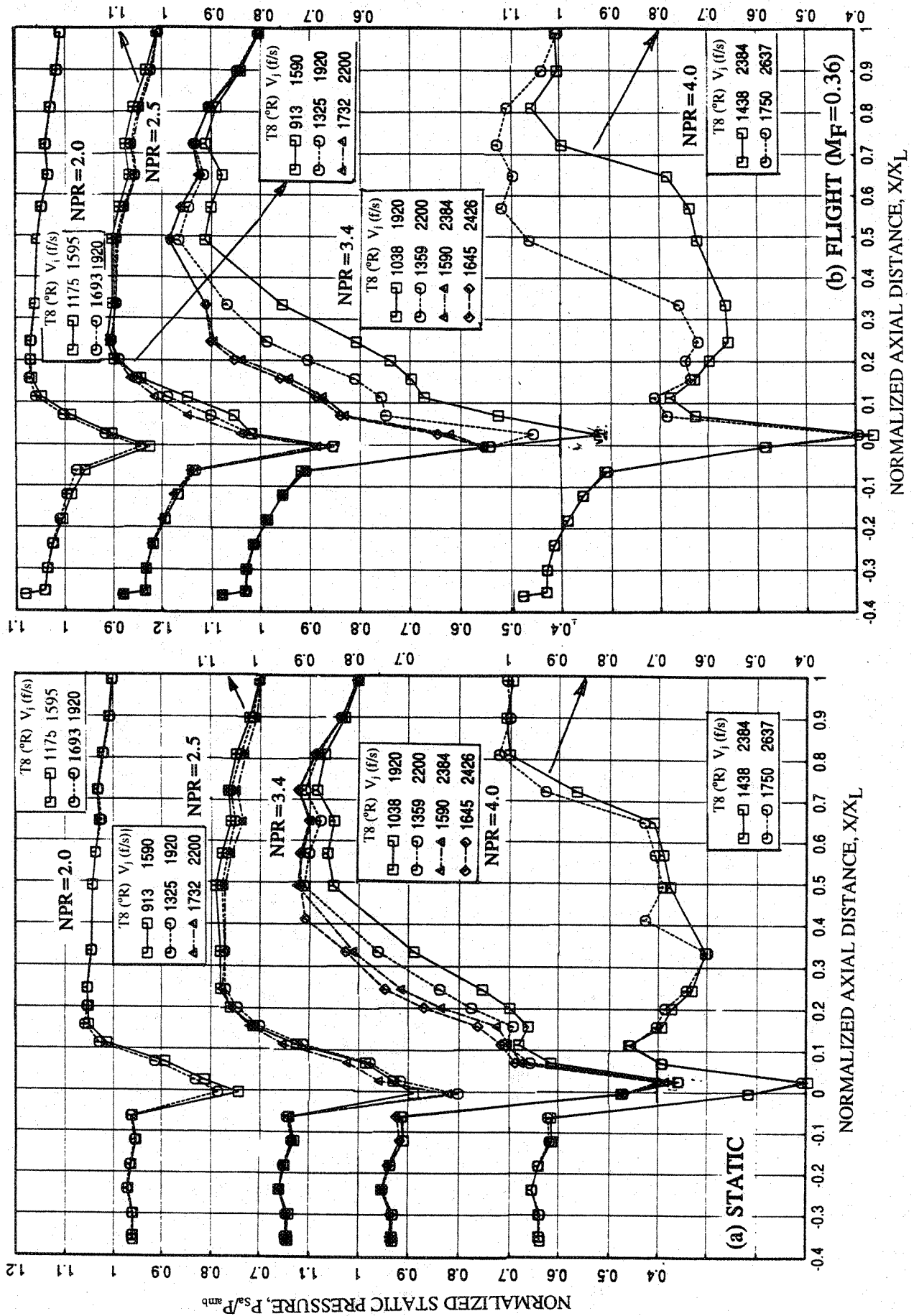
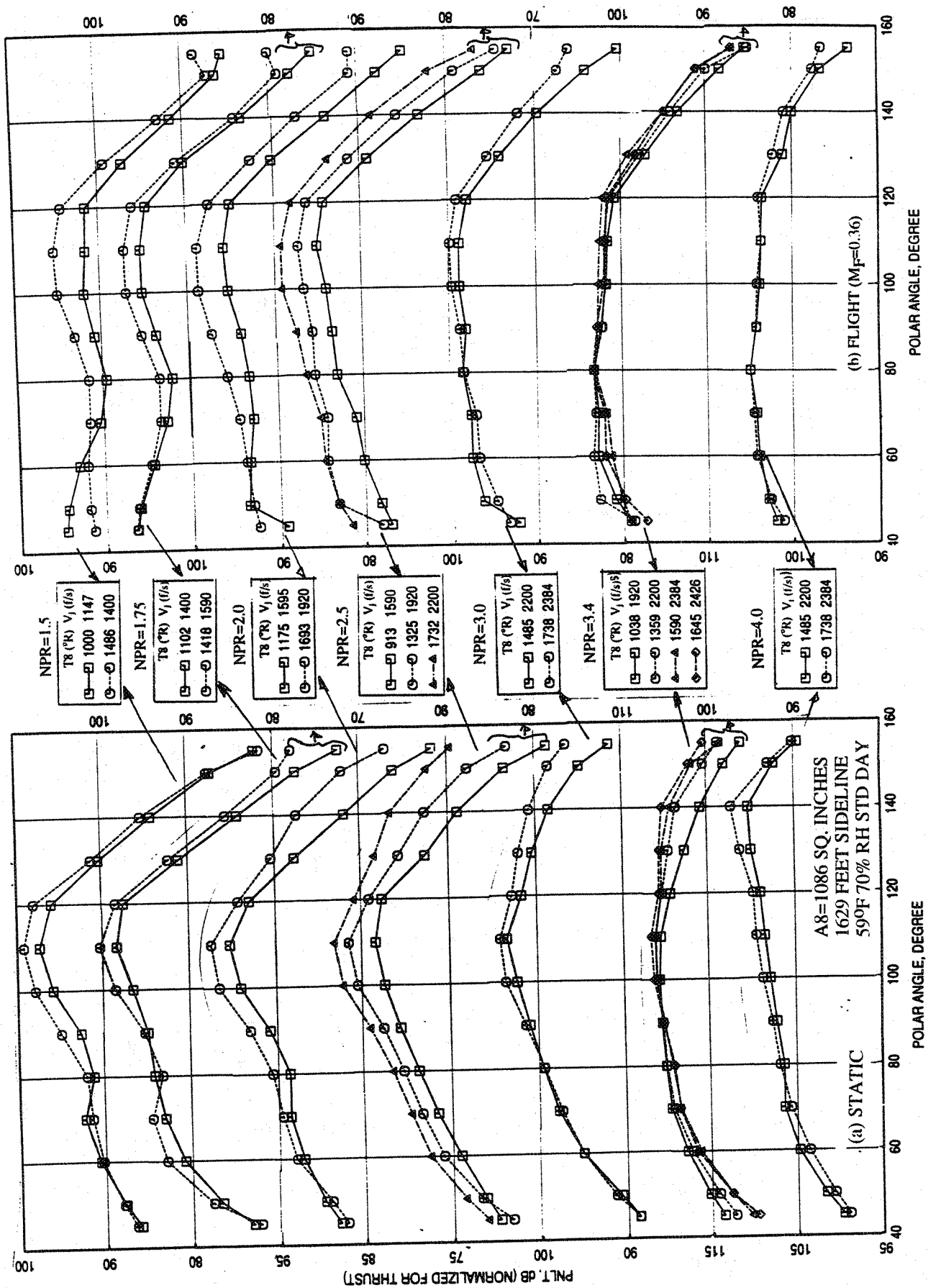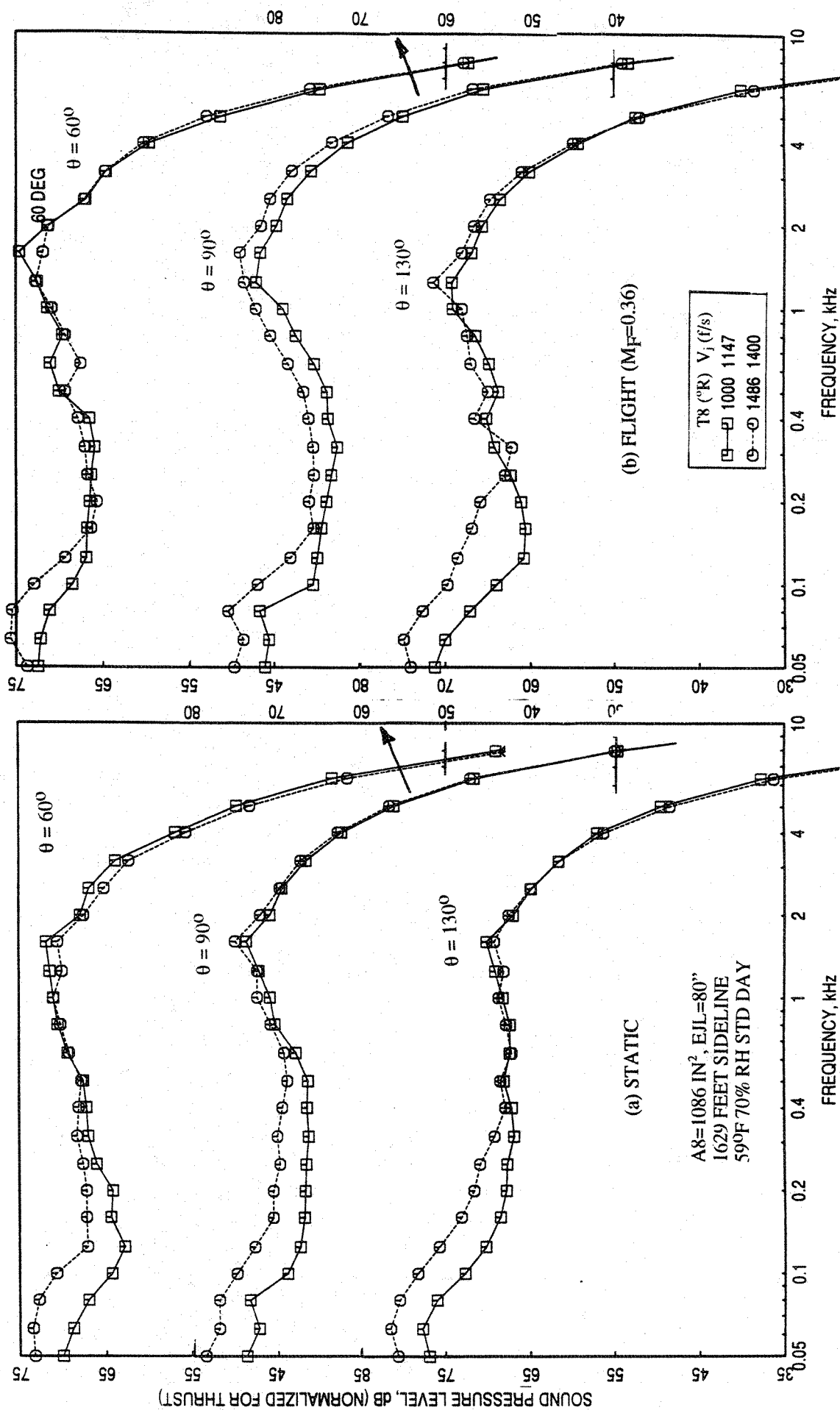Figure 5-48. Effect of nozzle total temperature on axial distribution of average static pressure on the inlet and the flap surface at fixed NPRs for a 10 and 9 full staggered CD-chute mixer with fully treated long ejector; SAR=2.8, MAR=0.95, X_L=17".

Figure 5-49. Effect of nozzle total temperature on normalized PNLT directivities for fixed NPRs for a 10 and 9 full staggered CD-chute mixer with hardwalled short ejector at an azimuthal angle φ=250; SAR=2.8, MAR=0.95.
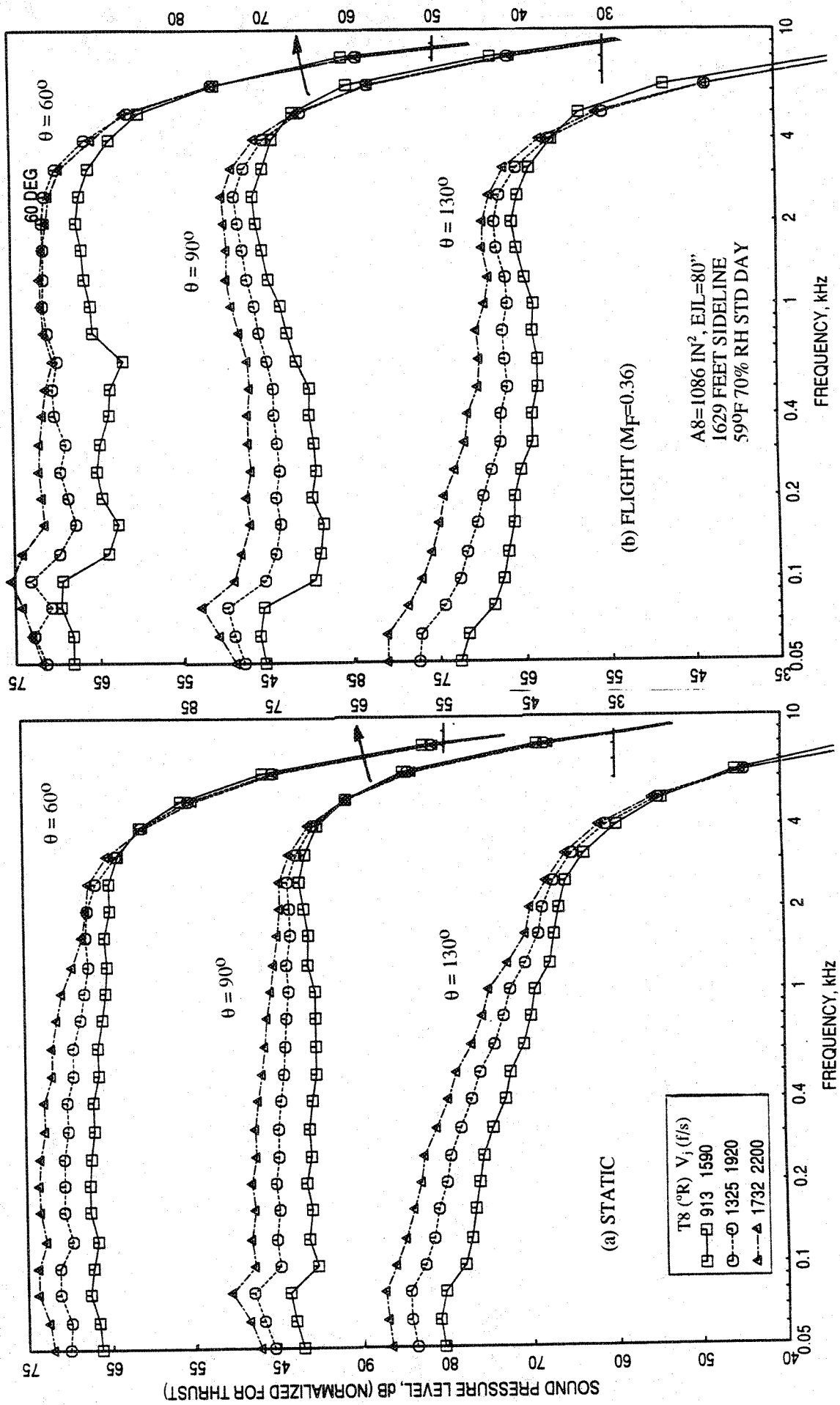
Figure 5-50. Effect of nozzle total temperature on normalized SPL spectra at various polar angles (θ) at a fixed NPR of 1.5 for a 10 and 9 full staggered CD-chute mixer with hardwalled short ejector at an azimuthal angle φ=25°; SAR=2.8, MAR=0.95.
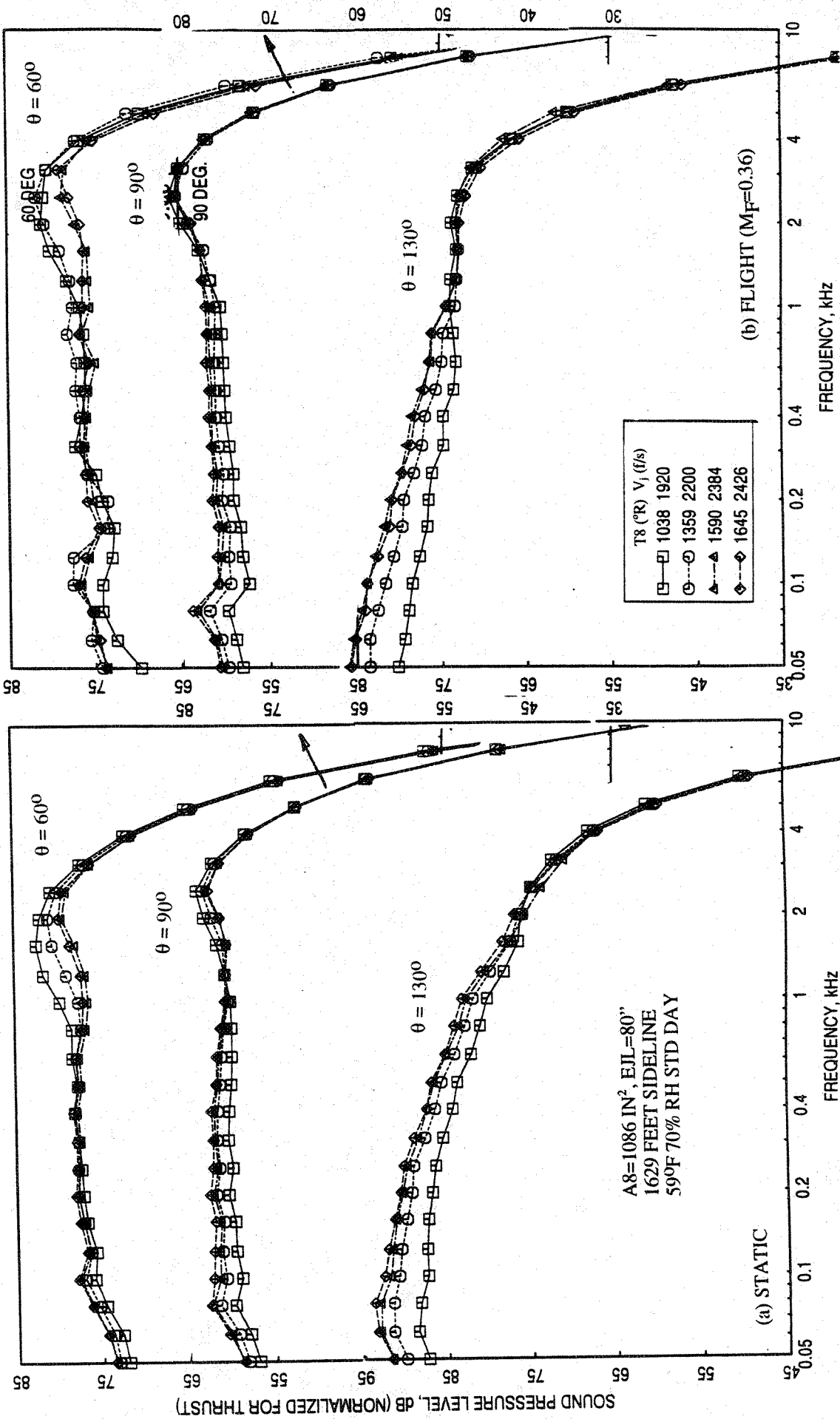
Figure 5-51.   Effect of nozzle total temperature on normalized SPL spectra at various polar angles (θ) at a fixed NPR of 2.5 for a 10 and 9 full staggered CD-chute mixer with hardwalled short ejector at an azimuthal angle φ=25°; SAR=2.8, MAR=0.95.

Figure 5-52. Effect of nozzle total temperature on normalized SPL spectra at various polar angles (θ) at a fixed NPR of 3.4 for a 10 and 9 full staggered CD-chute mixer with hardwalled short ejector at an azimuthal angle φ=25°; SAR=2.8, MAR=0.95.

Figure 5-53 shows the effect of increasing nozzle total temperature at fixed NPR on the average axial static pressure distributions on the inlet and the flap surface. There is no effect on inlet static pressure distribution due to nozzle temperature variation. However, significant amount of pressure drop on the flap surface is observed with increasing nozzle total temperature for higher NPR conditions closer to and above the transition NPR.
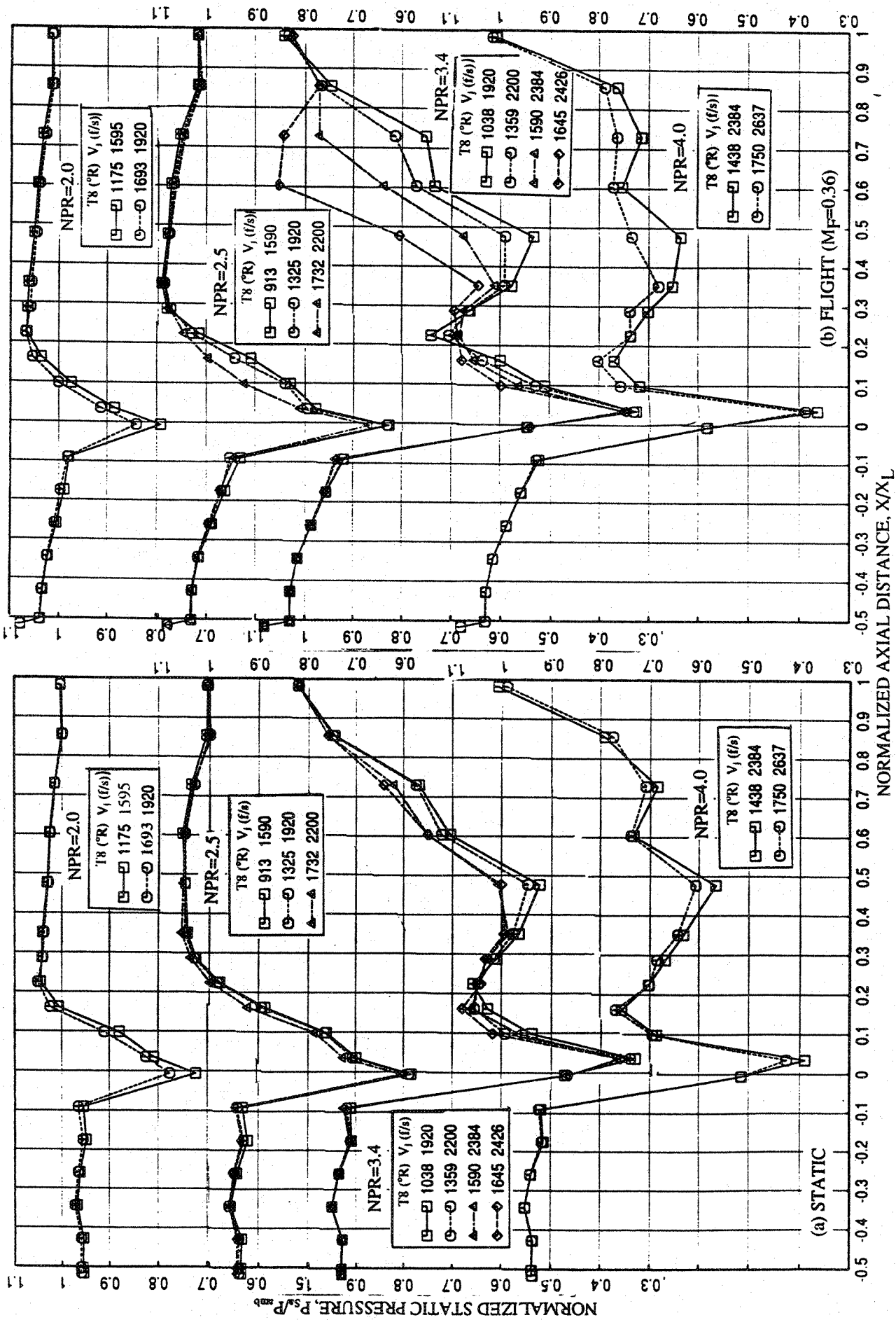
Figure 5-53. Effect of nozzle total temperature on axial distribution of average static pressure on the inlet and the flap surface at fixed NPRs for a 10 and 9 full staggered CD-chute mixer with hardwalled short ejector; SAR=2.8, MAR=0.95, X_L=11.88".

6.0 EJECTOR INTERNAL DYNAMIC PRESSURE MEASUREMENT

It is important to measure the dynamic pressure field inside the ejector for the 2D mixer-ejector nozzles to assess internal noise component, to develop internal noise source models, and to design acoustic treatment panels for the ejector. However, it is difficult to measure internal pressure fluctuation due to the high temperature environment, where the conventional probes can not be used. Recently, fiber optic microphone technique is being developed at a few research organizations, including the NASA Langley Research Center. A few prototype fiber optic microphones were built at NASA Langley, which could be used at higher temperature environment, up to a temperature of 1000°F, to measure dynamic pressure. A few of such microphones were loaned to GE at no cost and were used to measure the dynamic pressures inside an ejector, with and without acoustic treatment, of a scale model 2D 9 vs 10 staggered CD-chute mixer-ejector exhaust nozzle. Relevant results for the configurations, for which the internal dynamic pressure measurements were made, are presented in this section.

6.1 HIGH TEMPERATURE FIBER OPTIC MICROPHONE :

Figure 6-1 shows a fiber optic microphone with optoelectronic amplifier. The optoelectronic amplifier transmits light to a mirror on the underside of the microphone membrane, receives the reflected light in a photodiode, and provides an output voltage proportional to the membrane motion. The optical fiber, protected by nichrome coil spring, connects the microphone to the amplifier. The optical fiber looses its transmission capability when bent sharply (i.e., the bending radius must not be less than 2"). The diameter of the active membrane for the microphone is 0.072" and can withstand temperature up to 1000°F. The dynamic range and the frequency response of this microphone are 130 to 190 dB and 20 Hz to 50 kHz, respectively. Figure 6-2 shows the frequency response of the fiber optic microphone at room temperature and at 1000°F. The frequency response is reasonably flat up to about 40 kHz. All internal dynamic measurements were made up to 40 kHz, since the microphone diaphragm seems to resonate slightly above this frequency.

6.2 DATA ACQUISITION AND ANALYSIS:

The fiber optic microphone was used to measure the dynamic pressures inside the ejector of a model scale 2D mixer-ejector nozzle with staggered CD chute racks of nine and ten
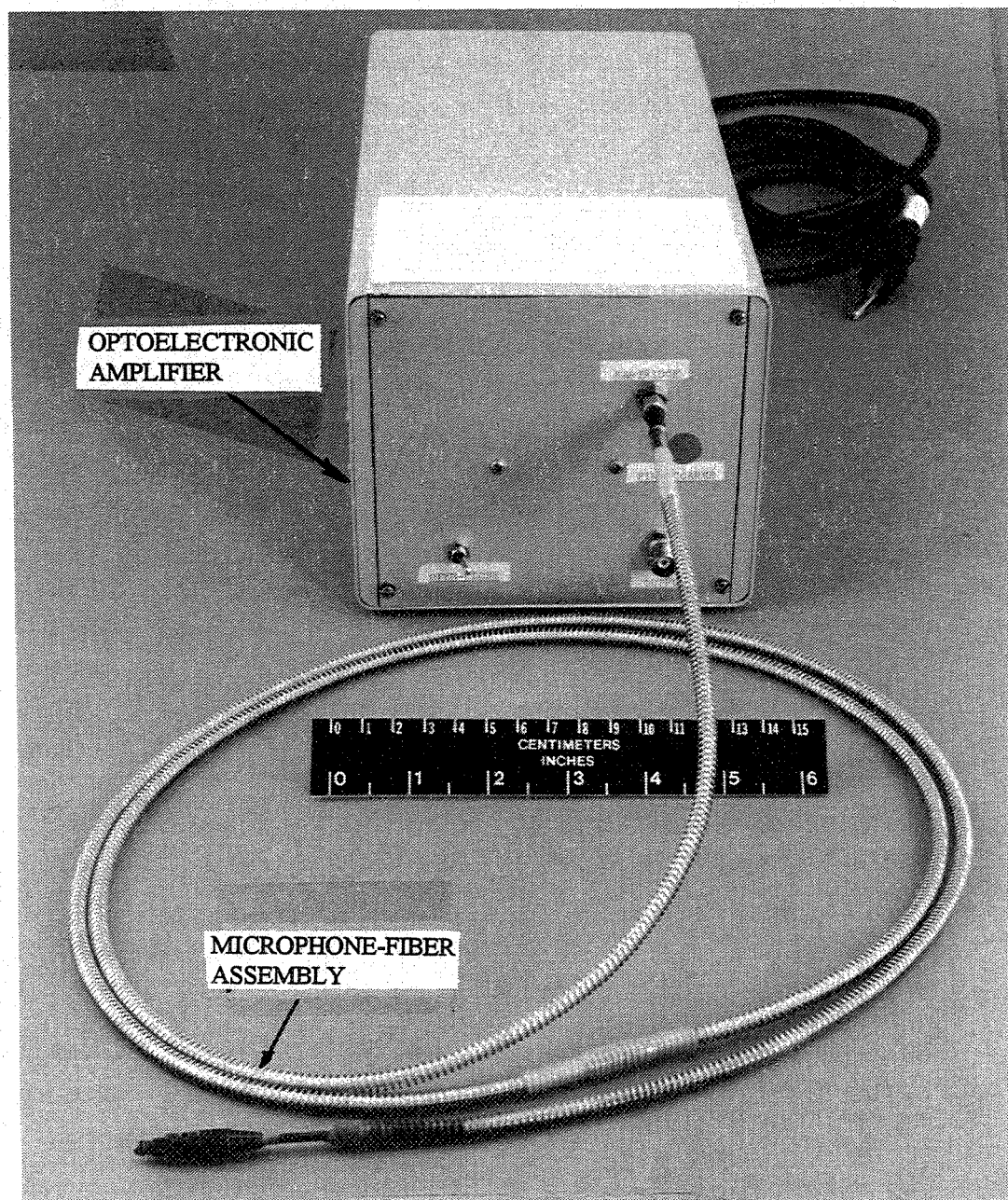
Figure 6-1. Fiber optic microphone with optoelectronic amplifier for dynamic pressure measurement at high temperature conditions up to 1000°F (Loaned from NASA Langley Research Center - Model H Fiber Optic Lever Microphone [FOLM]).
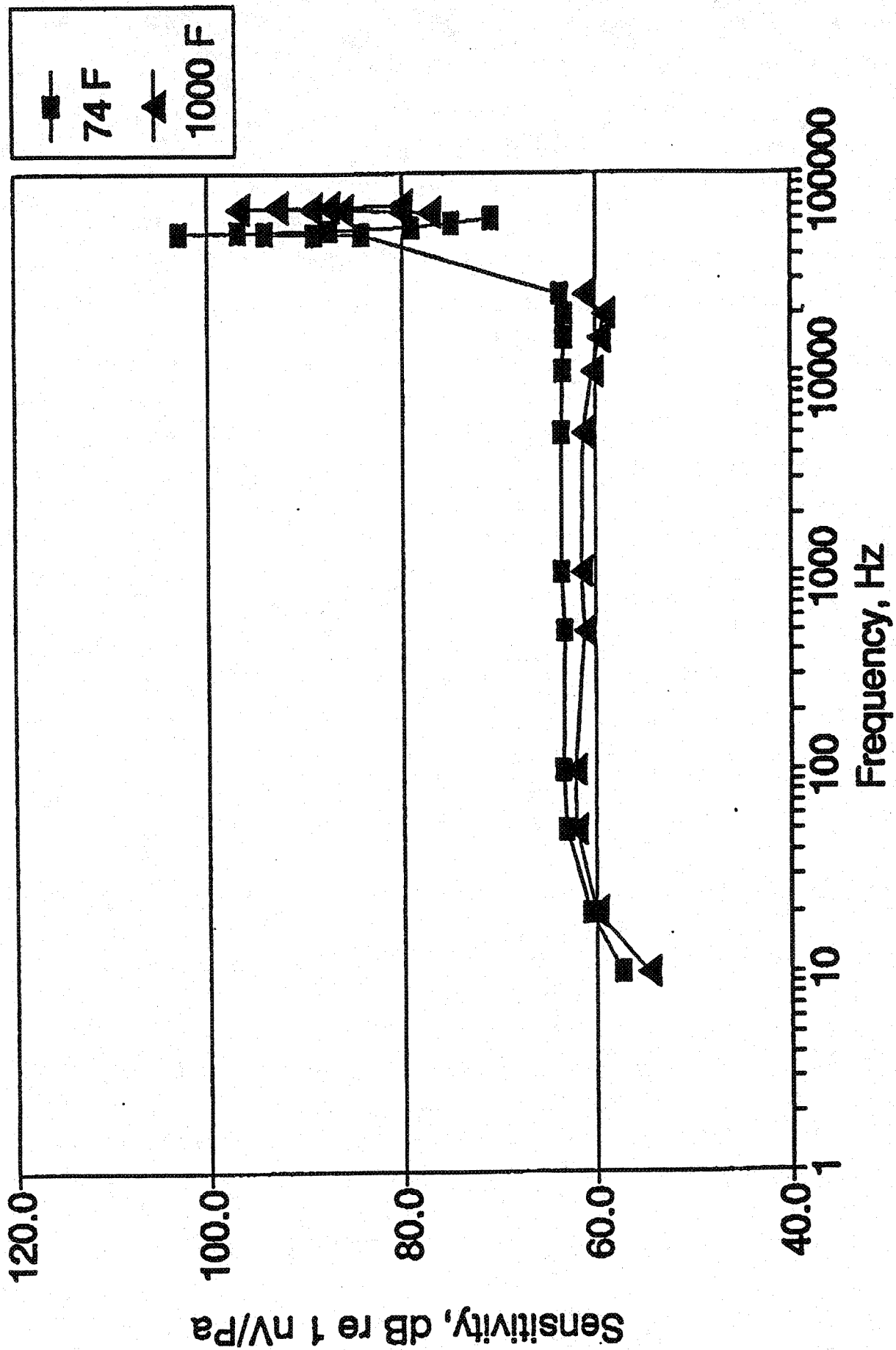
Figure 6-2.   Frequency response of the fiber optic microphone at room temperature and at 1000°F (Courtesy of NASA Langley Research Center - Microphone H18 Cal III).

full chutes. The nine full chute rack provides non-uniform chute stagger in the span wise direction. The side view of the mixer-ejector is shown in Figure 6-3. The suppressor area ratio (SAR) for the staggered mixer is 2.8 and has a throat area of 22.16 square inches (A8). The long ejector of 16.055" with MAR=0.95 is used for the current configurations. For the treated configurations, the flaps and sidewalls were fully treated with nickel based metal foam with a 37% porous facesheet.

Internal dynamic pressures were measured at two flap locations, as shown in Figure 6-3, one closer to the mixer exit plane and the other closer to the ejector exit plane. These measurements were made for hard wall as well as for fully treated configurations. Figure 6-4 shows the fiber optic microphone mounted on the flap surface at the ejector exit plane for the treated 2D Mixer-ejector nozzle in Cell 41. All the results presented in this section were acquired at a fixed primary stream total temperature of 900°F (i.e., 1360°R) without any flight simulation. Flight simulation was not possible due to the short length of the optical fiber connecting the microphone and the amplifier (about 1 meter), and also the amplifier was located across the tertiary flight simulation stream. Internal dynamic pressure is acquired up to a frequency of 40 kHz (i.e., bandwidth of 100 Hz) at a number of nozzle pressure ratios ranging from 1.4 to 4.7.

The farfield noise was measured at community and sideline azimuthal locations by positioning the microphone tower at 90° and 25°, respectively. However, farfield acoustic results only at the sideline position (i.e., tower at 25°) are presented in this section. Spectral results for internal dynamic pressure and farfield acoustic pressure are presented in narrowband frequency scale. Farfield spectral results are presented up to 40 kHz, to be consistent with the internal dynamic pressure data, even though, the farfield data was acquired up to 100 kHz (i.e., bandwidth of 250 Hz). Overall sound pressure levels (OASPL) and overall sound power levels (OAPWL) in the farfield are evaluated using the data up to 100 kHz. Since, this is a unique set of results acquired at fixed temperature condition (unlike the L1M cycle simulation, where the nozzle pressure ratio and total temperature are varied along a typical throttle line), the aerodynamic results based on static and total pressure data on the model are also included in this section.

6.3 Results Based on Model Static and Total Pressure Data :

Axial static pressure distributions on inlet ramp, secondary side of chute surface, and on the inlet and flap surfaces are presented at various primary stream nozzle pressure ratios
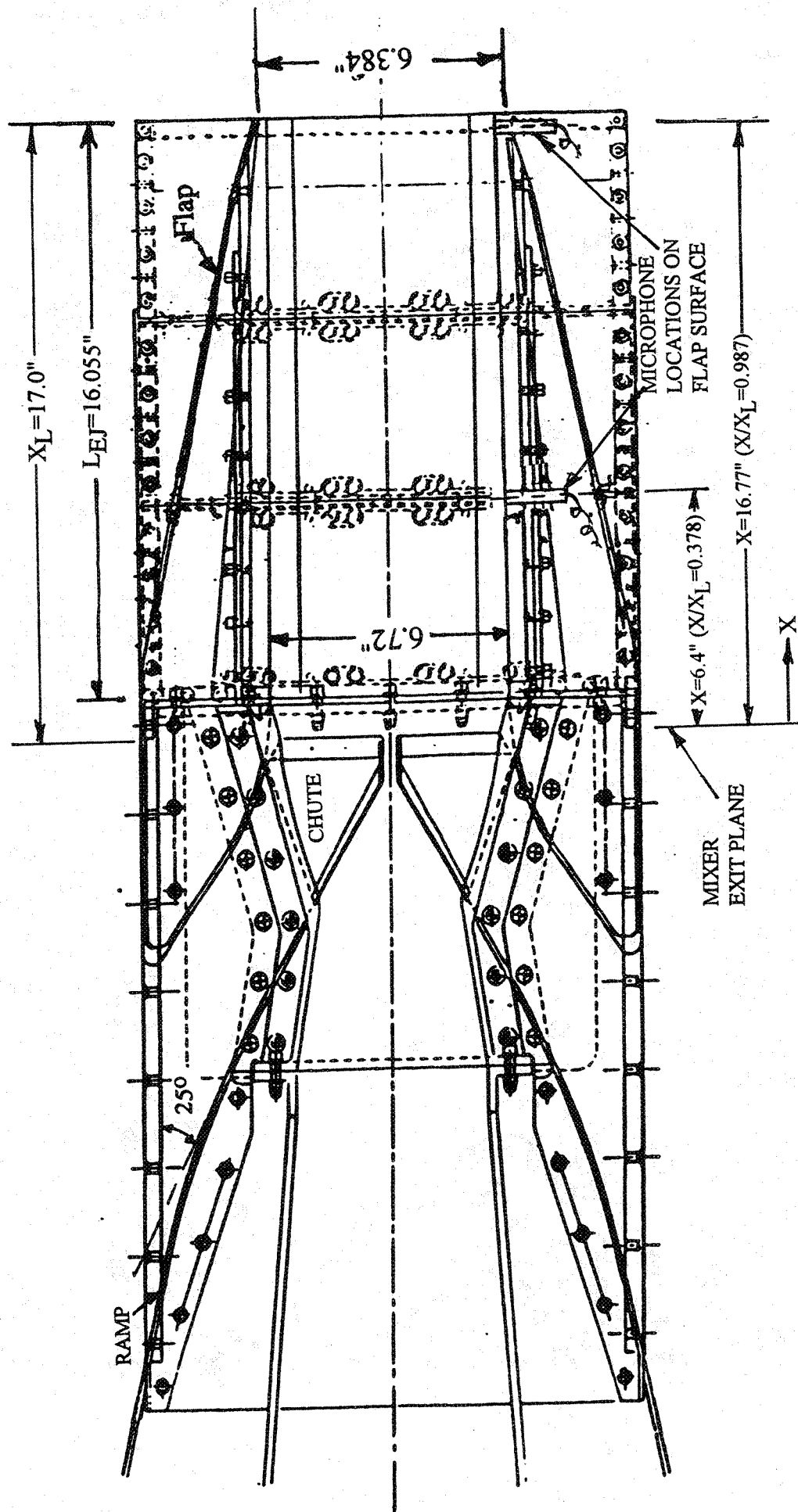
Figure 6-3. Side view of a 10 and 9 full staggered CD-chute mixer with long ejector showing the fiber optic microphone locations for dynamic pressure measurement internal to the ejector; SAR=2.8, MAR = 0.95.
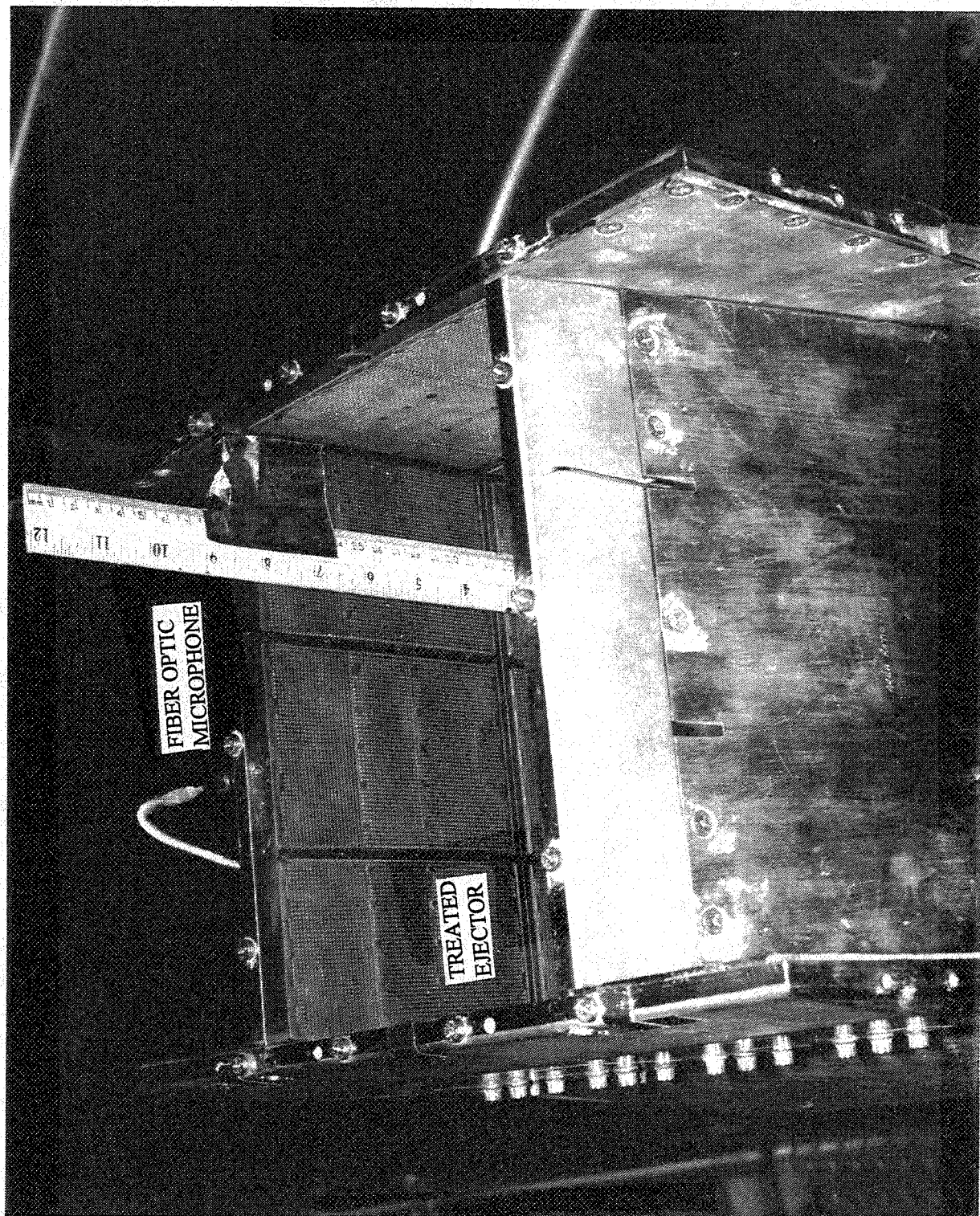
Figure 6-4. Fiber optic microphone mounted at the exit plane of treated ejector for a model scale 2D mixer-ejector nozzle in Cell 41.

(NPR) in terms of normalized pressure and distance. The pressure is normalized with respect to ambient pressure and the axial distance is normalized with respect to the length between the mixer exit plane and the ejector exit plane (X_L). This length is about an inch longer than the actual flap length (see Figure 6-3). Figure 6-5 shows the axial static pressure distributions on inlet ramp and secondary side of chute surface for hard wall and treated ejector configurations. The effect of treatment is insignificant in these distributions. The static pressure decreases with increasing NPR up to an NPR (i.e., 3.4 in this case), at which the transition from subsonic to supersonic mode begins. With further increase of NPR, the static pressure increases slightly. The flow accelerates down the inlet ramp and then decelerates in the secondary flow passage through the chutes due to axial turning of the secondary flow. An integrated coefficient, called chute loading coefficient, is computed using the static pressure distributions on the chute leading edge of secondary flow side. Effect of treatment on chute loading coefficient is shown in Figure 6-6 with respect to NPR. This parameter decreases first and then increases with NPR, indicating better performance at higher nozzle pressure ratio. The effect of treatment on chute loading coefficient is insignificant at higher NPR but improves the thrust performance slightly at lower nozzle pressure ratios. The presence of treatment on the ejector modifies the boundary layer growth and hence alters the effective MAR slightly. Hence, at lower NPR (i.e., for subsonic flow in the ejector) the pumping gets effected until the ejector flow transitions to supersonic mode.

The secondary mass flow rate is estimated from the total and static pressure distributions across the inlet, which were measured by a set of 3 total pressure rakes. The pumping is thus evaluated as the ratio of secondary to primary mass flow rates. The corrected pumping is calculated by multiplying the square root of the secondary to primary absolute total temperature ratio with the mass flow rate ratio (i.e. pumping). Figure 6-7 shows the effect of treatment on pumping with respect to NPR. Pumping decreases with increasing NPR and is further reduced due to treatment. The probable cause of this effect is the effective MAR change caused by boundary layer growth for the treated ejector, which is likely to be different compared to hard wall configuration.

Figures 6-8 and 6-9 show the axial static pressure distributions on the inlet and the flap surfaces for hard wall and treated configurations, respectively. In each case the axial pressure distributions along the centerlines of cold and hot flow chutes are evaluated and shown. Some differences between the hot and cold flow rows are observed at the vicinity of the mixer exit as static pressure equalization between primary and secondary streams
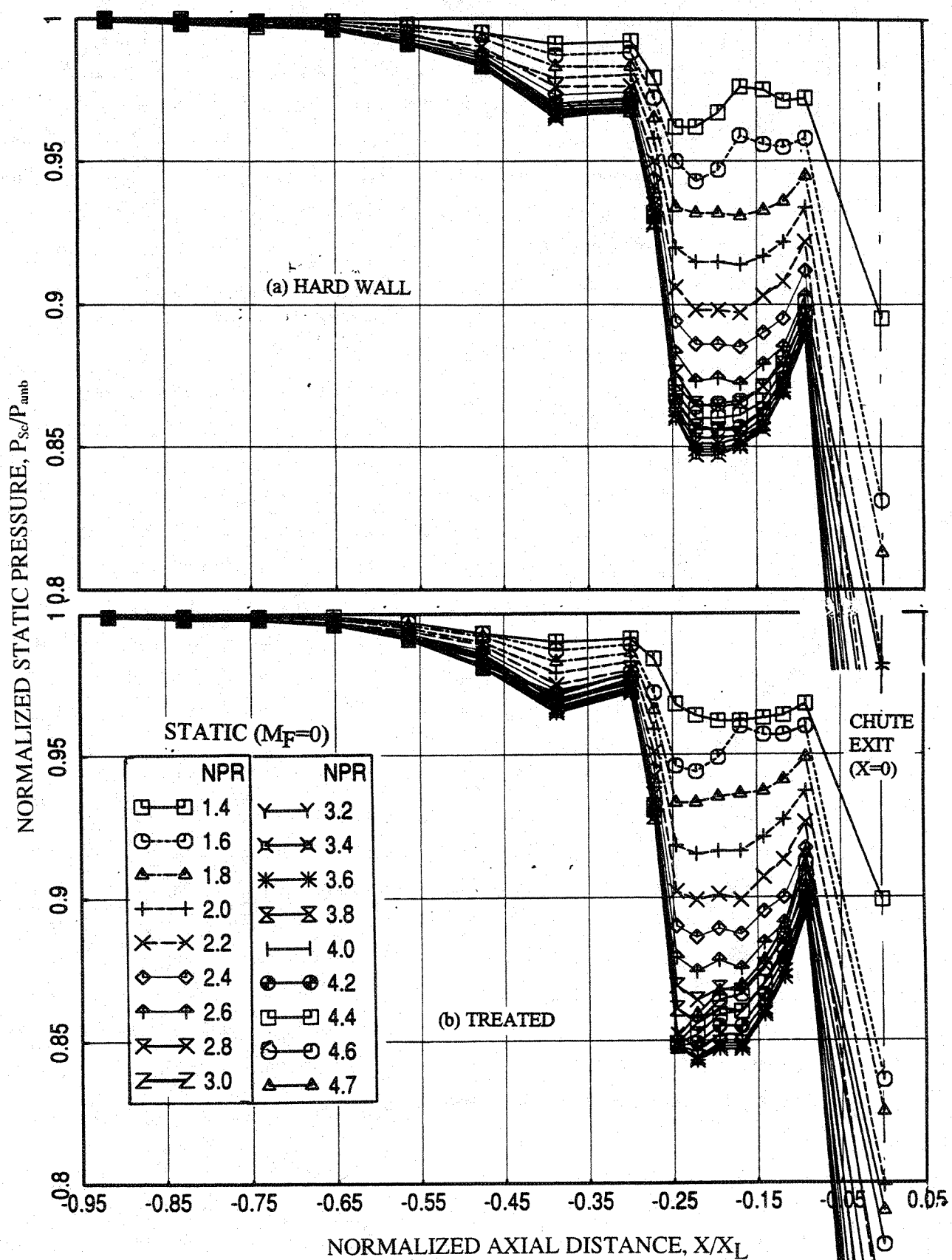
Figure 6-5. Axial static pressure distributions on the inlet ramp and on the secondary flow side of chute surface at different nozzle pressure ratios for 2D mixer-ejector nozzle configurations with staggered CD chutes, T8=1360°R.
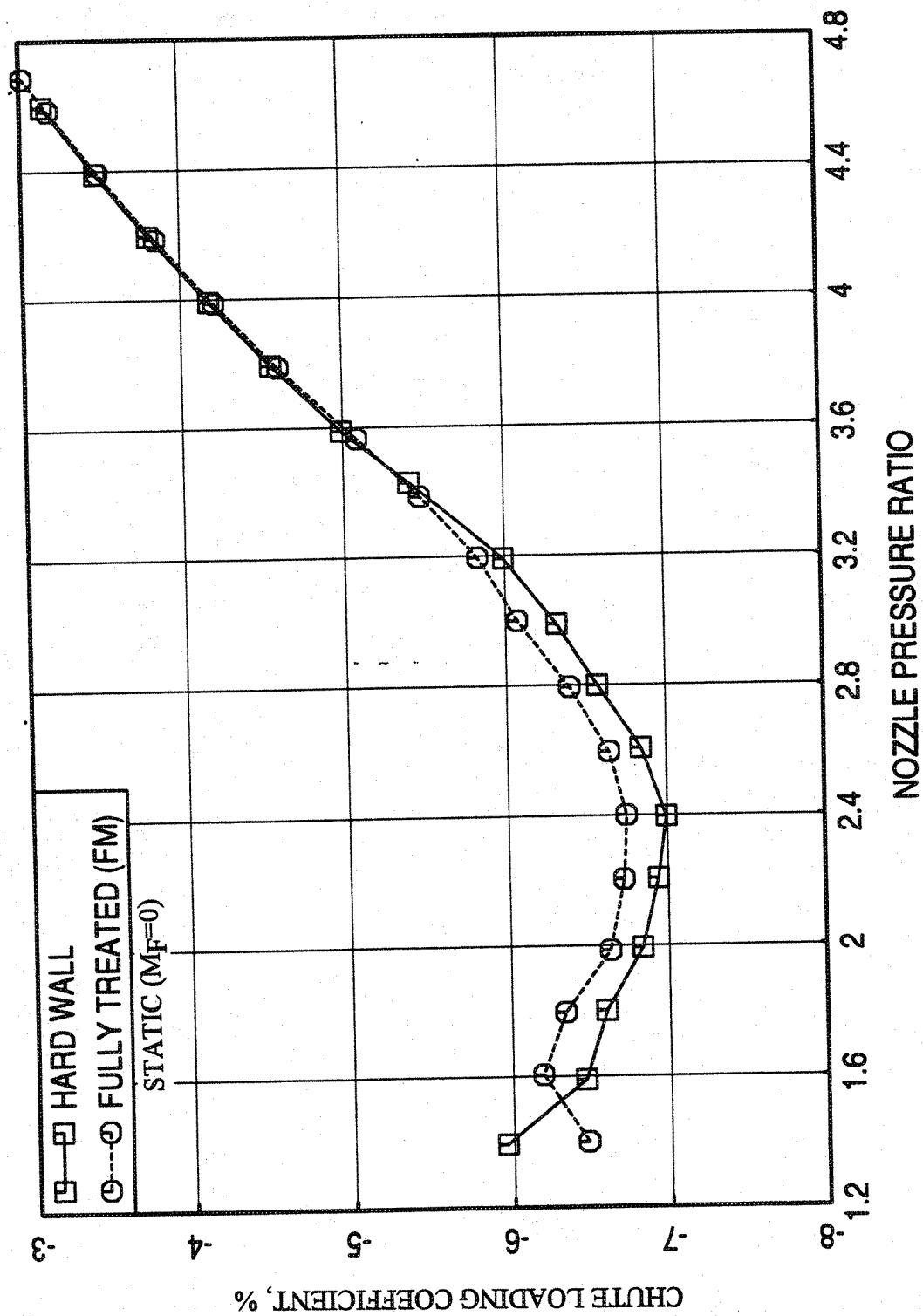
Figure 6-6. Effect of ejector treatment on chute loading coefficient, computed by measured static pressure distributions on secondary flow side chute leading edge, with respect to nozzle pressure ratios for 2D mixer-ejector nozzle configurations with staggered CD chutes, T8=1360°R.
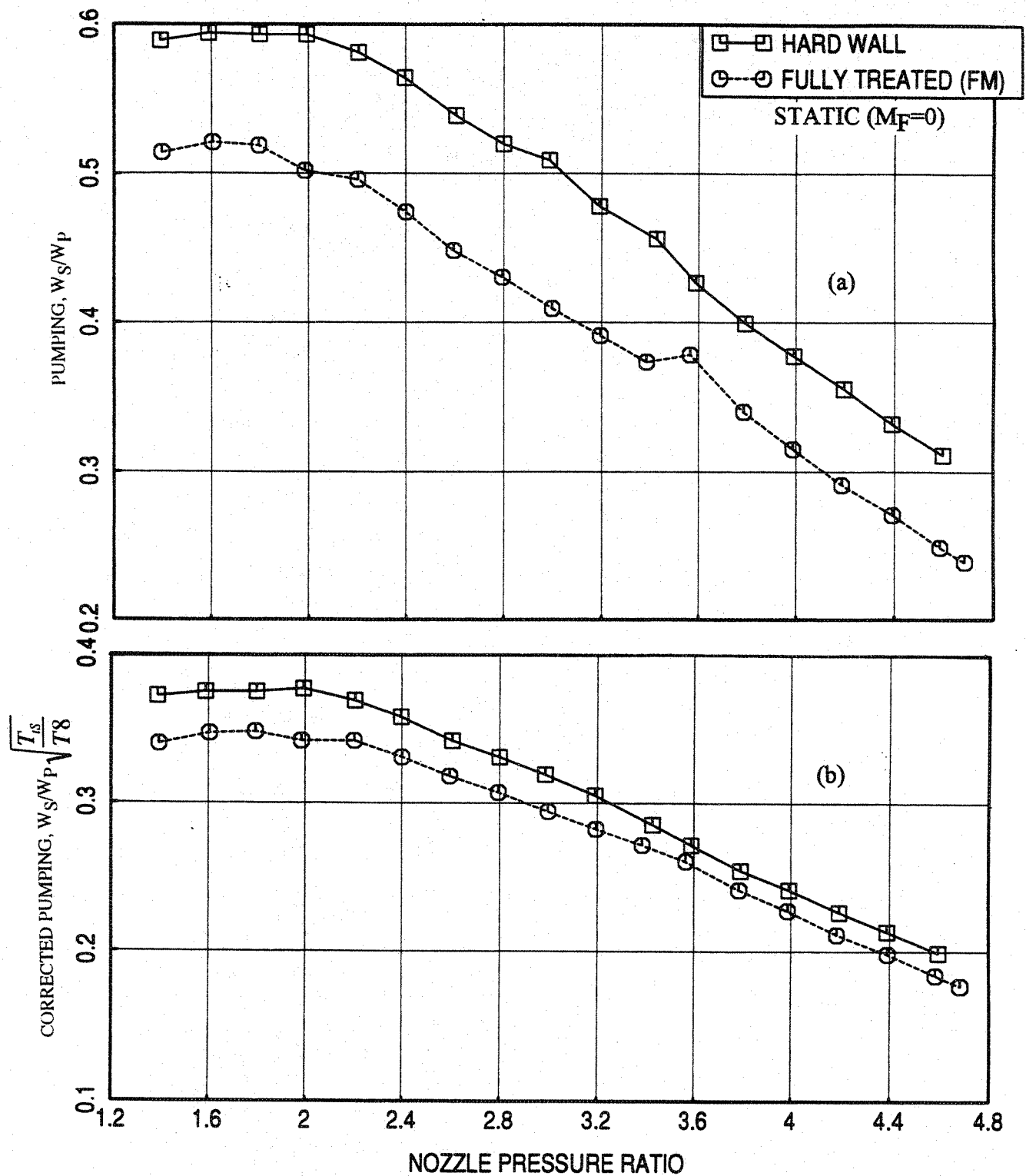
Figure 6-7. Effect of ejector treatment on pumping, computed by measured rake total pressure distributions at the inlet, with respect to nozzle pressure ratios for 2D mixer-ejector nozzle configurations with staggered CD chutes, T8=1360°R.
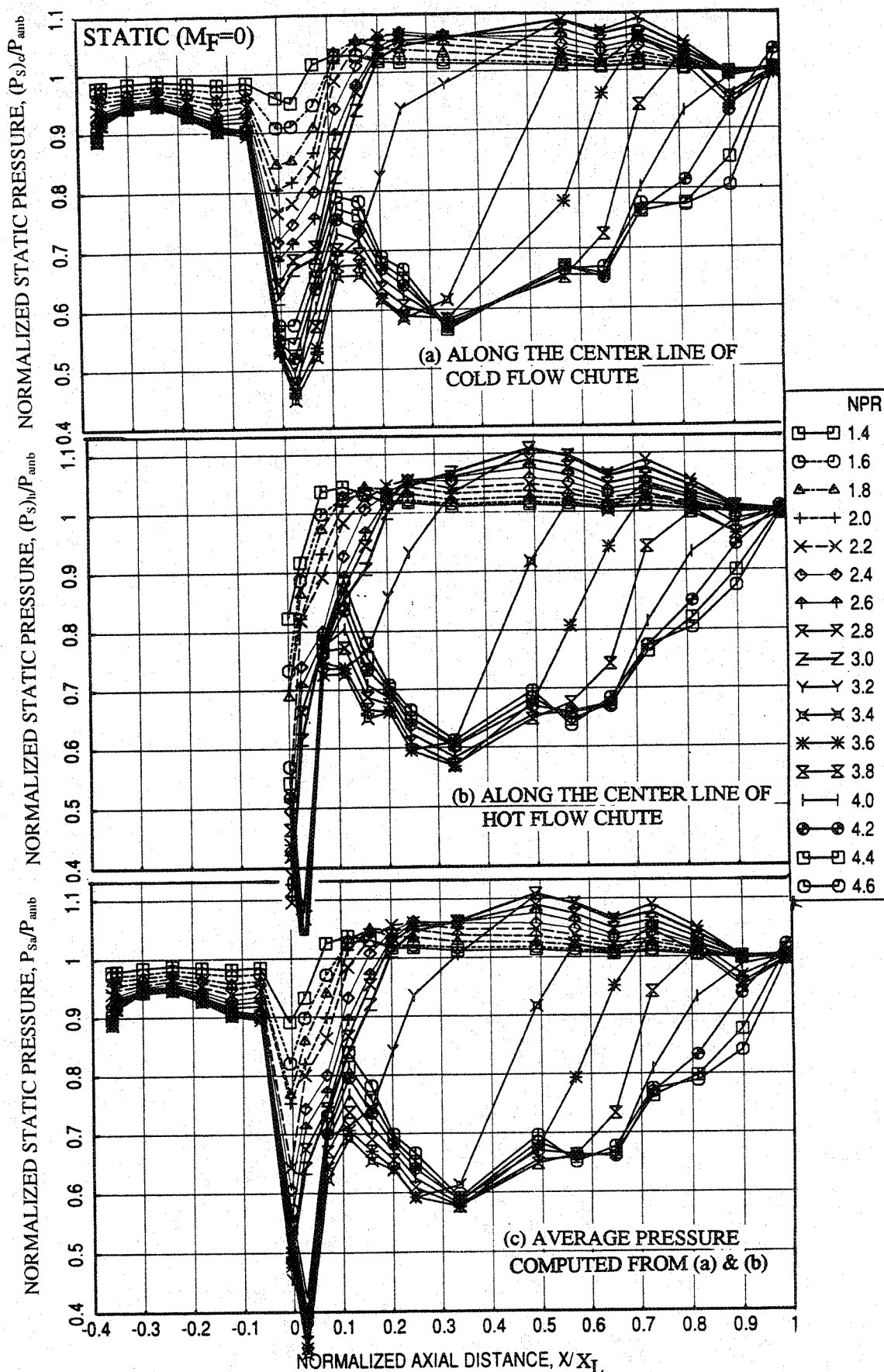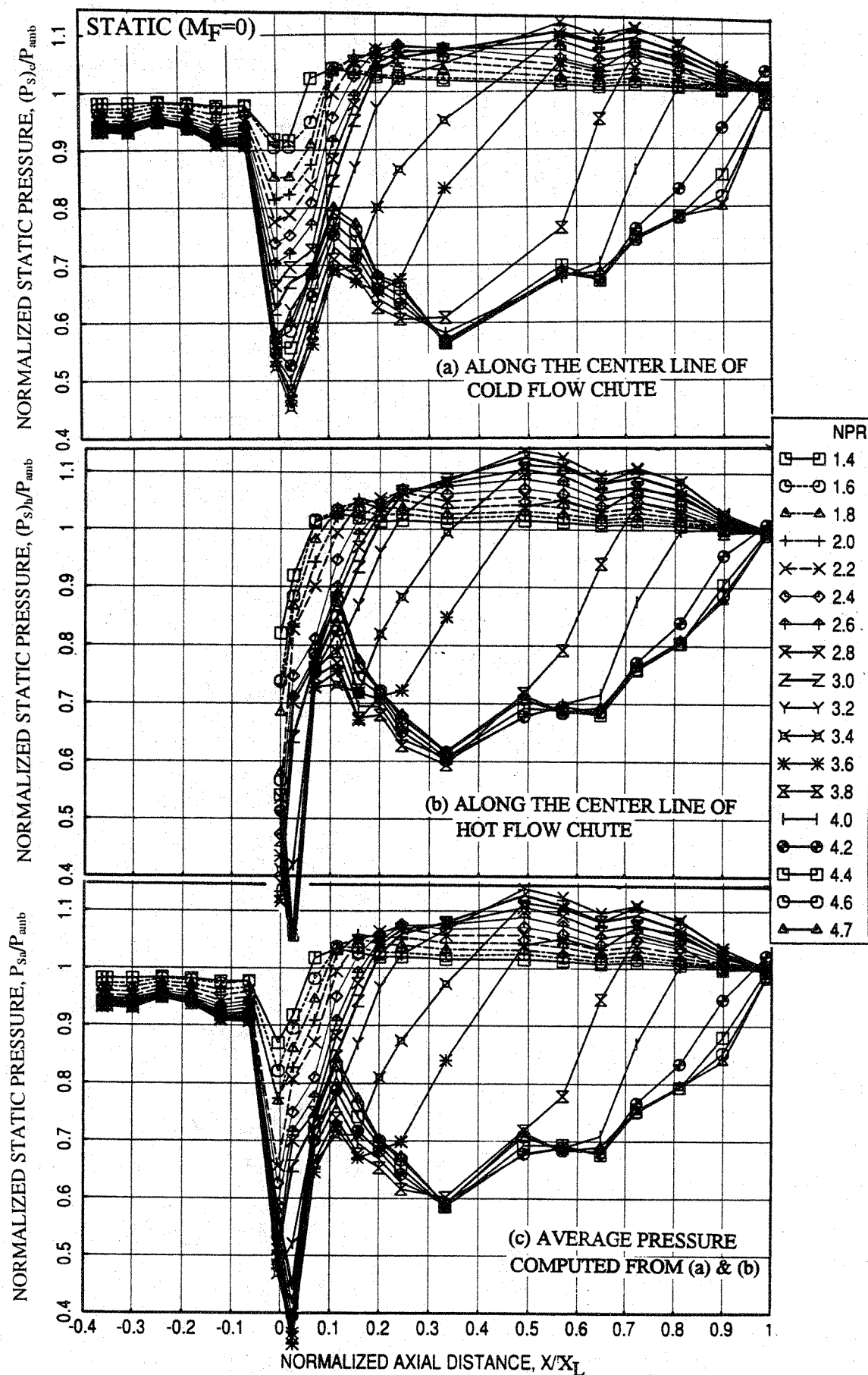
Figure 6-8. Axial static pressure distributions on the inlet and the flap surface at different nozzle pressure ratios for a 2D mixer-ejector nozzle of hard wall configuration with staggered CD chutes, T8=1360°R; (a) along centerline of cold flow chute, (b) along centerline of hot flow chute, (c) average pressure.

Figure 6-9. Axial static pressure distributions on the inlet and the flap surface at different nozzle pressure ratios for a 2D mixer-ejector nozzle with fully treated ejector and with staggered CD chutes, T8=1360°R; (a) along centerline of cold flow chute, (b) along centerline of hot flow chute, (c) average pressure.

takes place over a finite axial distance. Once this happens, very little difference exists further downstream, which is the portion experiences the transition of mode from subsonic to supersonic. Mode transition related interpretations on the basis of flap pressure distributions are the same whether we consider pressure distributions along hot or cold chute flow directions or the arithmetic average of these two. Hence, an arithmetic average of these two measurements is computed and presented in Figures 6-8 and 6-9. In both the cases we see gradual transition of flow from subsonic to supersonic mode with increasing NPR. However, Figure 6-10 shows the effect of treatment on axial static pressure distributions at a number of NPR. At lower NPR the axial pressure distributions between hard wall and treated configurations are identical. For higher NPR values treated configuration seems to be delaying the mode transition with respect to NPR compared to hard wall case until the mode transition is completed. Thus at very high NPR again the axial pressure distributions between treated and hard wall configurations are identical.

To identify the impact of mode switch the force and the moment about the flap leading edge (i.e., X=0.945") of the force due to the ejector flap are evaluated by utilizing the static pressure distributions on the flap. Figure 6-11 shows the effect of treatment on these parameters with respect to NPR. Force as well as the moment with respect to NPR indicate slightly delayed initiation of mode switch for the treated configuration. During the transition period the force and the moment, both increase rapidly with NPR and change directions. In general, the mode transition is gradual with respect to NPR and not abrupt as noted in cold flow model tests at NASA Langley. This indicates the effect of temperature on mode transition. In addition, treatment seems to delay the mode transition by increasing the critical NPR.

6.4 DYNAMIC PRESSURE FIELD INSIDE THE EJECTOR :

The internal dynamic pressure field results presented in this section were acquired by using two different fiber optic microphones. One of these microphone was generating strong tones at a number of frequencies and also generating very high level noise at lower frequencies, up to about 2 kHz, as shown in Figure 6-12. A numerical smoothing is applied to the measured spectra to eliminate these tones and to smooth out the small pressure fluctuations caused by limited sample averaging, as shown in Figure 6-12. Internal dynamic pressure field consists of acoustic as well as hydrodynamic pressure fluctuations. It is difficult to separate these components to identify only the acoustic portion of the fluctuation to correlate with the farfield noise in a quantitative manner. Two
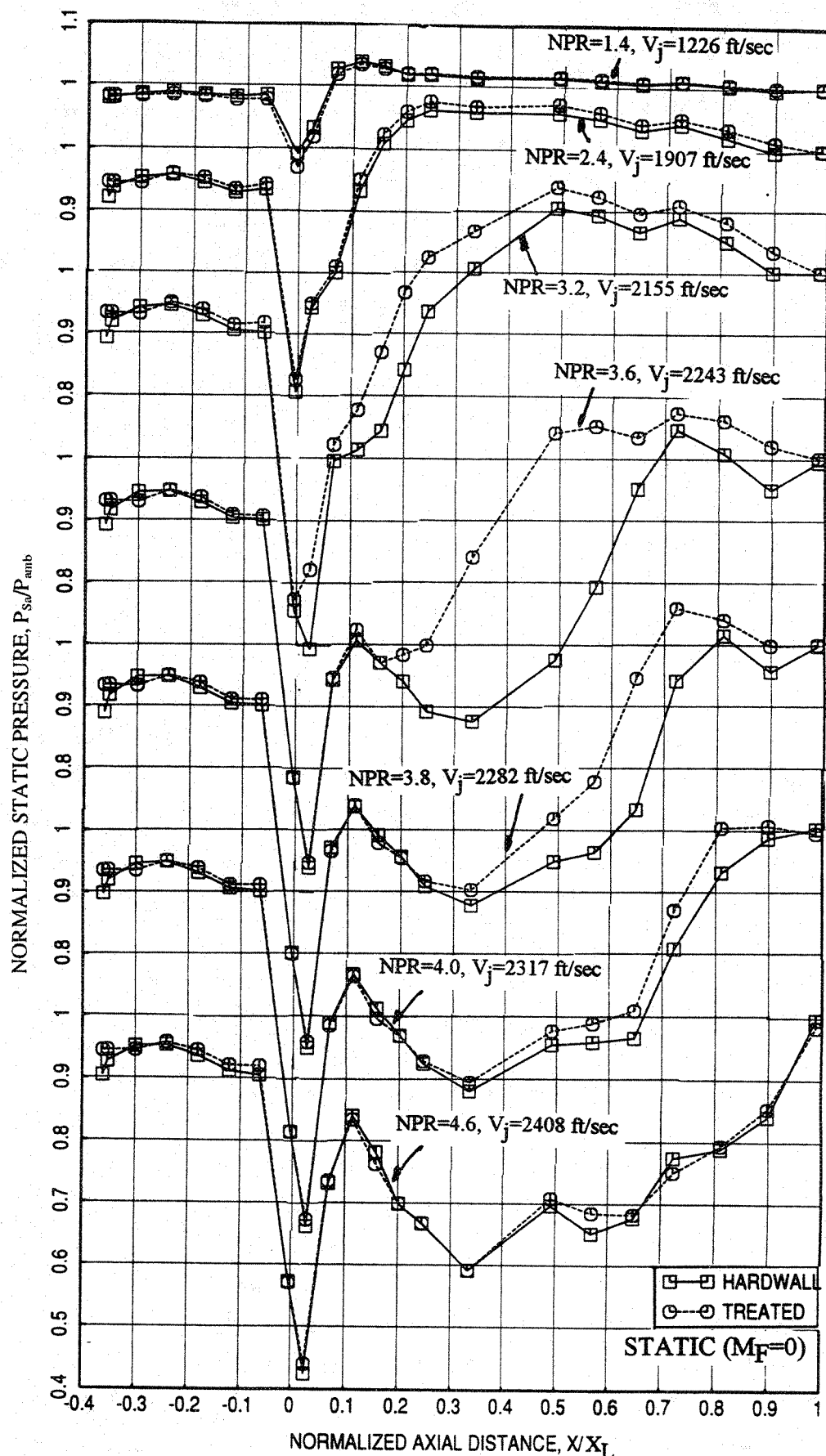
Figure 6-10. Effect of treatment on average axial static pressure distributions on the inlet and the flap surface at different nozzle pressure ratios for a 2D mixer-ejector nozzle configuration with staggered CD chutes, T8=1360°R.
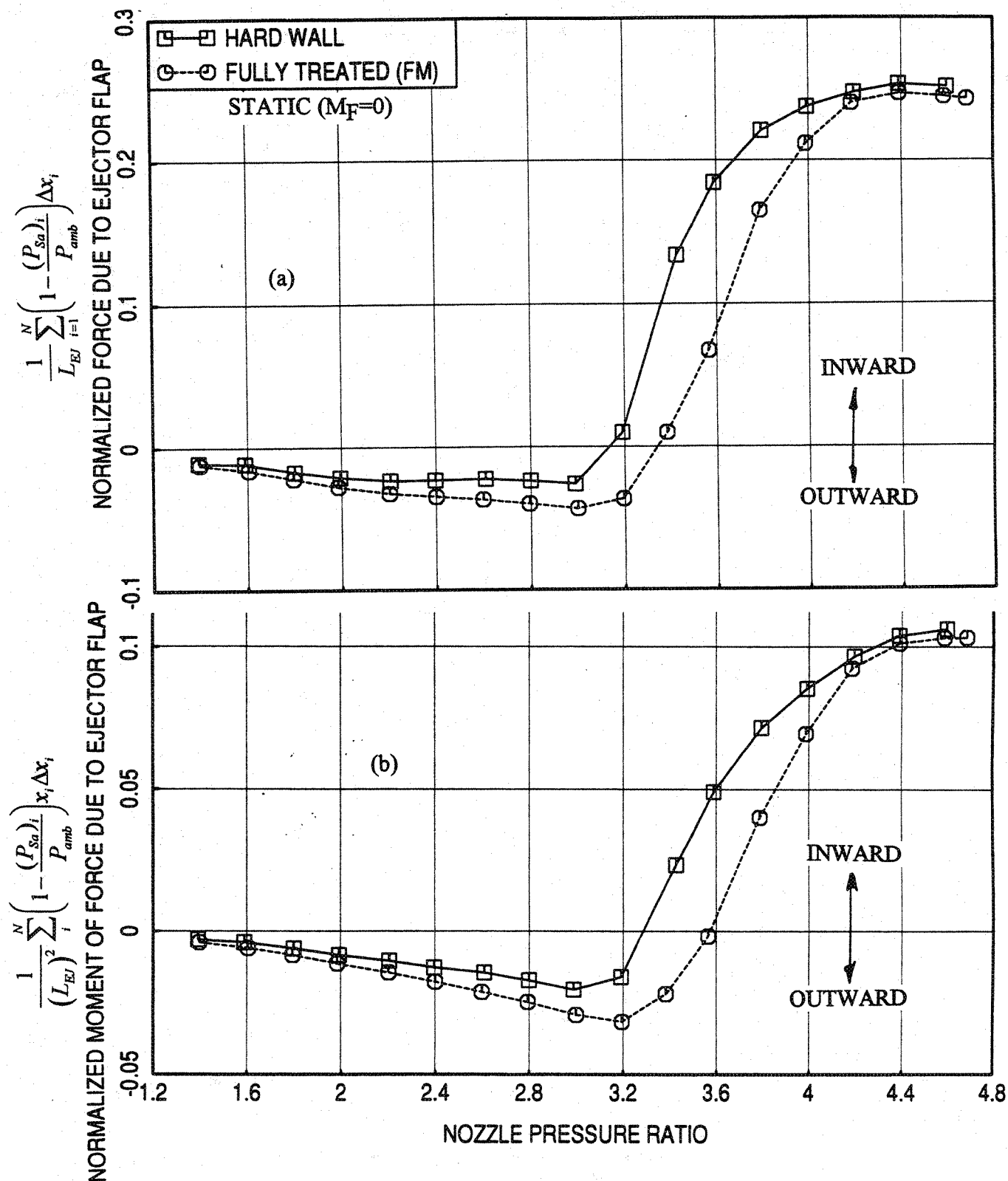
Figure 6-11. Effect of treatment on normalized (a) force and (b) moment of force due to ejector flap with respect to nozzle pressure ratio for a 2D mixer-ejector nozzle configuration with staggered CD chutes, T8=1360°R.
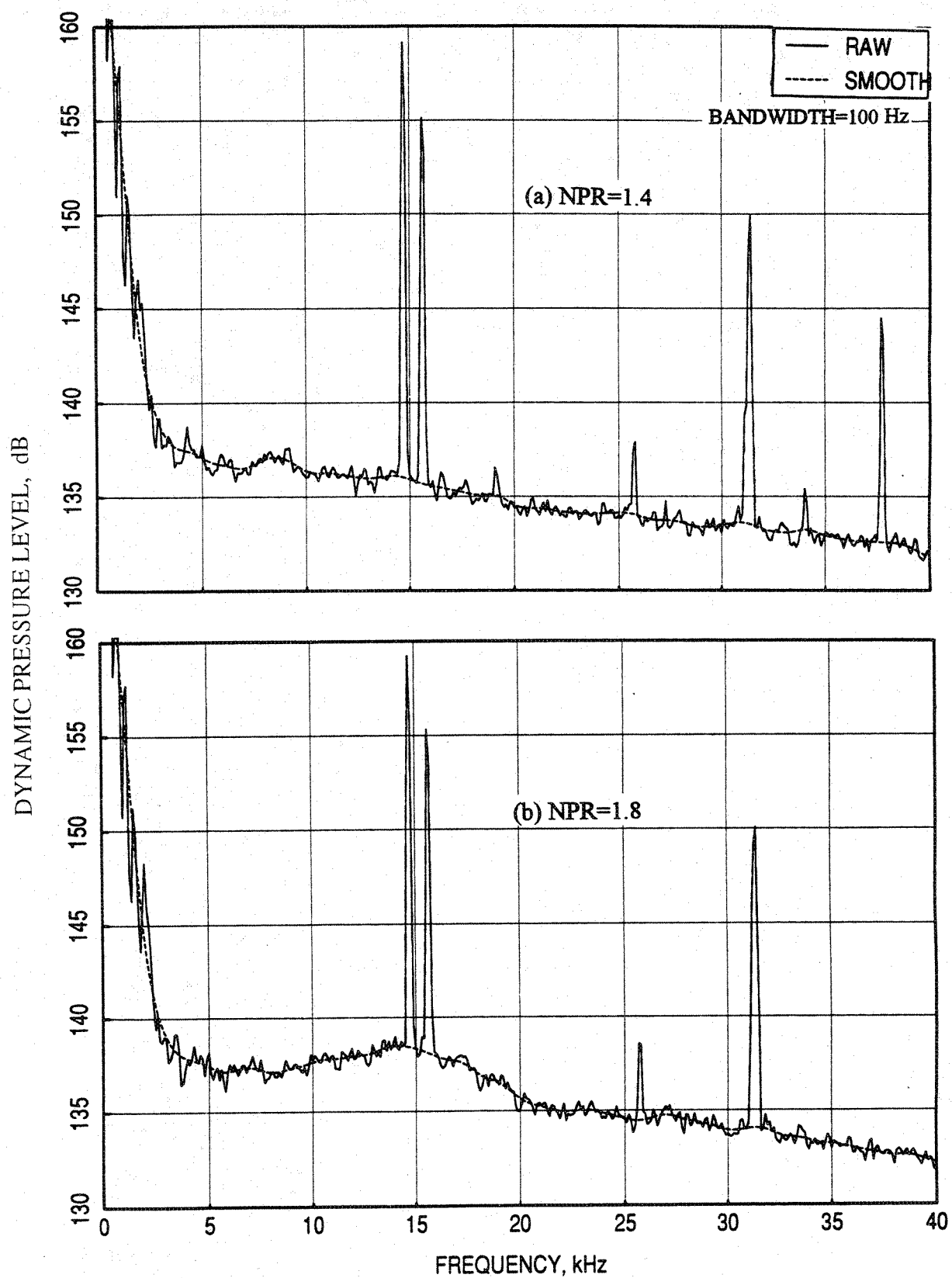
Figure 6-12. Ejector interior dynamic pressure level spectra, as measured and with numerical smoothing, at X/X_L =0.987 for a 2D mixer-ejector nozzle with hard wall, T8=1360°R.

point cross-correlation (of two closely spaced points) technique can be utilized to separate hydrodynamic and acoustic pressures, provided the speed of sound and flow velocity are distinctly different. Such techniques are not utilized here. However, qualitative understanding of internal noise field can still be achieved from the measured dynamic pressures. It should be noted that the noise levels were measured at isolated locations and hence the variation of pressure fluctuations along span and vertical directions are not accounted for.

6.4.1 Hardwalled Ejector Configuration :

Figure 6-13 shows the effect of NPR on the dynamic pressure spectrum close to the ejector exit plane. The dynamic pressure levels increase gradually with increasing NPR. For this location, the microphone stays in the subsonic flow region for all pressure ratios (for supersonic mode, this microphone is downstream of the strong shock). Figure 6-14 shows the similar results at a location, X/X_L=0.378, closer to the mixer exit. In this location, the microphone experiences a mode transition from subsonic to supersonic at an NPR between 3.4 and 3.6 (see Figure 6-8). In the subsonic mode and across the shock (i.e., transition between subsonic to supersonic mode) the dynamic pressure levels increase with NPR (i.e., up to NPR=3.6). With further NPR increase the shock moves downstream of the microphone (i.e., downstream of X/X_L=0.378). For such cases, the dynamic pressure levels at X/X_L=0.378 varied slightly without clear trend with increasing NPR. At higher frequencies, the levels decreased with NPR and no clear trend is noted at other frequencies. This type of unsteady pressure spectral behavior upstream of a shock is measured by GEAE in previous investigation of shock boundary layer interaction using rectangular nozzles at room temperature.

The major components responsible for the acoustic field inside an ejector for a mixer-ejector nozzle, in a very simplistic way, are the noise generation due to shear layer growth or turbulent mixing as the primary jet elements mix with entrained secondary flows and the convection of noise sources. The noise sources evolve within the ejector are characterized by different length scales along the axial distance of the ejector. At the mixer exit the length scale associated with the noise generation mechanism is very small and hence, more high frequency noise is generated in this region. The length scale increases along the ejector length and gradually the source frequency reduces. In addition, noise is convected by the mean flow in the downstream direction. In subsonic mean flows, noise could still propagate upstream. The mixing process between the two flows begins at the mixer exit,
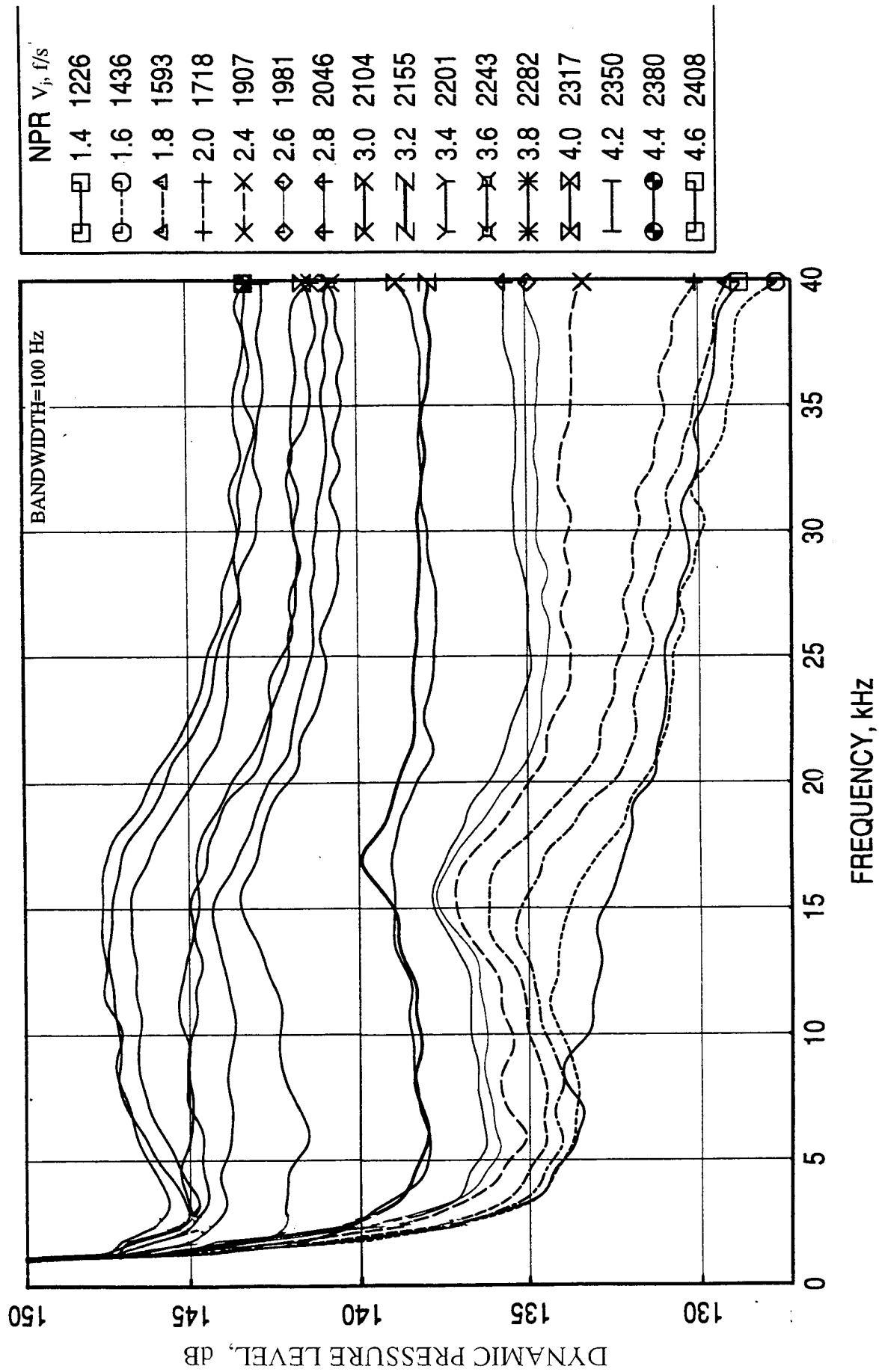
Figure 6-13. Dynamic pressure level spectra internal to the ejector on the flap at $X/X_L=0.987$ for different nozzle pressure ratio for a 2D mixer-ejector nozzle with hard wall and with staggered CD chutes, T8=1360ºR.
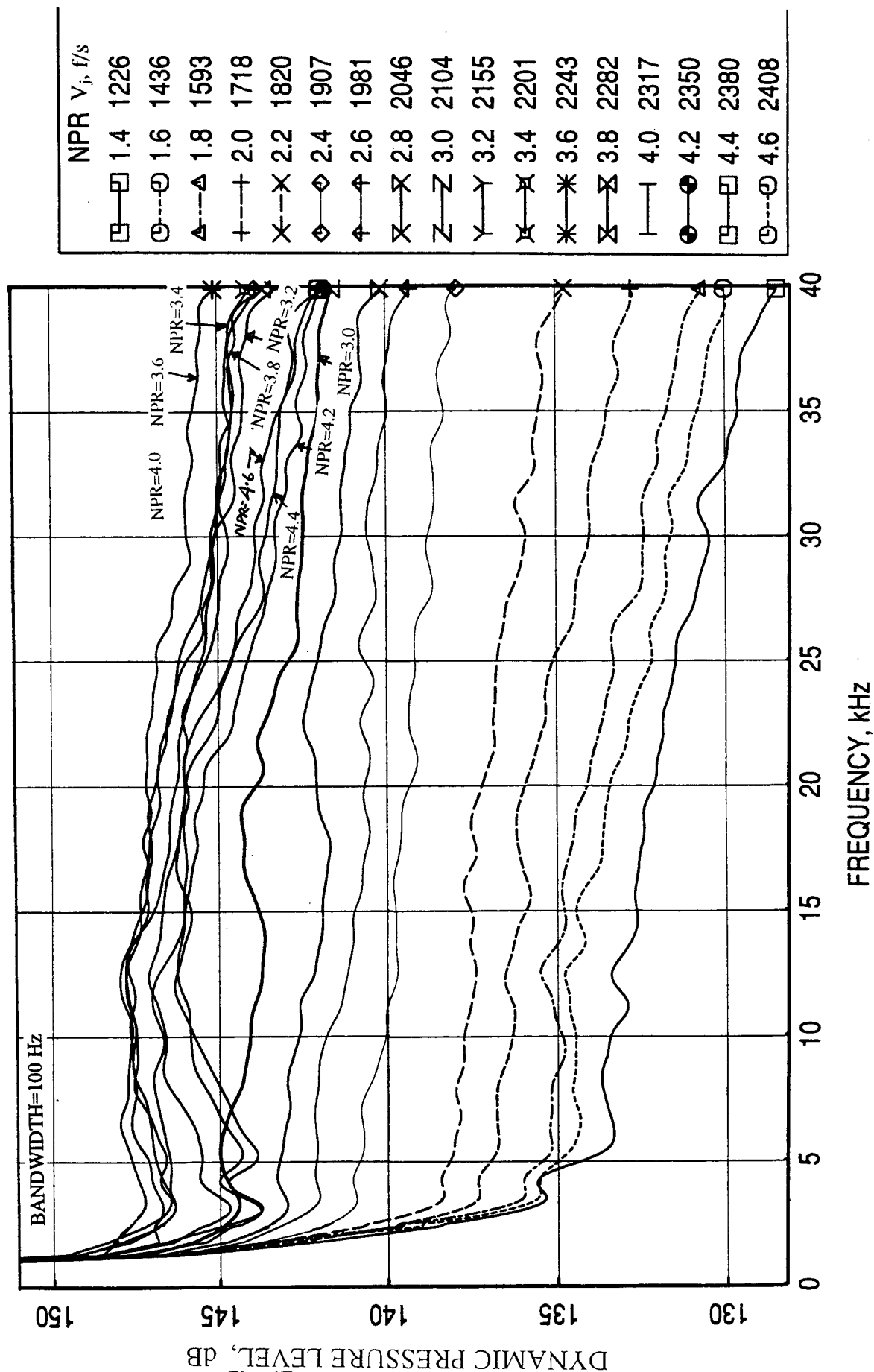
Figure 6-14. Dynamic pressure spectra level internal to the ejector on the flap at $X/X_L=0.378$ for different nozzle pressure ratio for a 2D mixer-ejector nozzle with hard wall and with staggered CD chutes, T8=1360°R.

NPR	V_j, f/s
1.4	1226
1.6	1436
1.8	1593
2.0	1718
2.2	1820
2.4	1907
2.6	1981
2.8	2046
3.0	2104
3.2	2155
3.4	2201
3.6	2243
3.8	2282
4.0	2317
4.2	2350
4.4	2380
4.6	2408

which reduces noise by lowering the mixed velocity. While the mean flow parameters, like velocity, temperature, etc., become uniform relatively faster along the ejector length, the first and second order moments which contribute to the shear stress tensor and hence to noise generally take more distance to damp out. It is expected that for very low NPR the mixing and noise generating processes reach completion within a shorter distance from the mixer exit, while for very high NPR these processes continue even outside the ejector. With the help of this plausible physical mechanism we will try to explain the dynamic pressure data measured inside the ejector.

Dynamic pressure level spectra measured at fixed NPR are compared between the two axial locations in Figure 6-15. At NPR=4.6 dynamic pressure is higher at the exit plane compared to X/X_L=0.378 for lower frequencies and a very moderate reduction at higher frequencies. With decreasing NPR the dynamic pressure levels are lowered at ejector exit plane compared to those at X/X_L=0.378. With further lowering of NPR the difference of dynamic pressure levels between these two locations gradually diminished and finally showed no difference. At lower NPR the mixing process between primary and secondary streams and thereby, the internal noise generation continues for a shorter distance from the mixer exit due to lower flow velocity. For higher NPR (i.e., with higher flow velocity) the noise generation continues for a longer distance in the ejector. In addition, mixing process between primary and secondary flows, which reduces the internal noise level, follows the same trend, that the mixing becomes complete in a shorter distance for lower NPR and for very high NPR only partial mixing is possible inside the ejector. It should be noted that the noise measured by the microphone at the ejector exit plane includes the noise source convection effects by the mean flow. Thus, the noise generation term utilized here includes turbulent mixing and source convection effects. On this basis the noise generation and mixing, both must have been completed before X/X_L=0.378 for NPR=1.4 and hence there is no significant change in dynamic pressure levels axially further downstream. For a slightly higher NPR (like 2.4) the dominant noise generation might have been complete before X/X_L=0.378, but the mixing process to reduce noise levels continues further downstream. Thus gives a reasonably lower dynamic pressure level spectrum at the ejector exit compared to X/X_L=0.378. At an intermediate NPR (like 3.2) the noise generation and mixing processes possibly continue even after X/X_L=0.378, so that the microphone at this location measures relatively lower dynamic pressure levels compared to the levels further downstream. Most of the noise reduction due to mixing at this condition must have taken place between X/X_L=0.378 and the ejector exit plane to give maximum noise reduction. Hence, the dynamic pressure difference between these two locations is very high. With
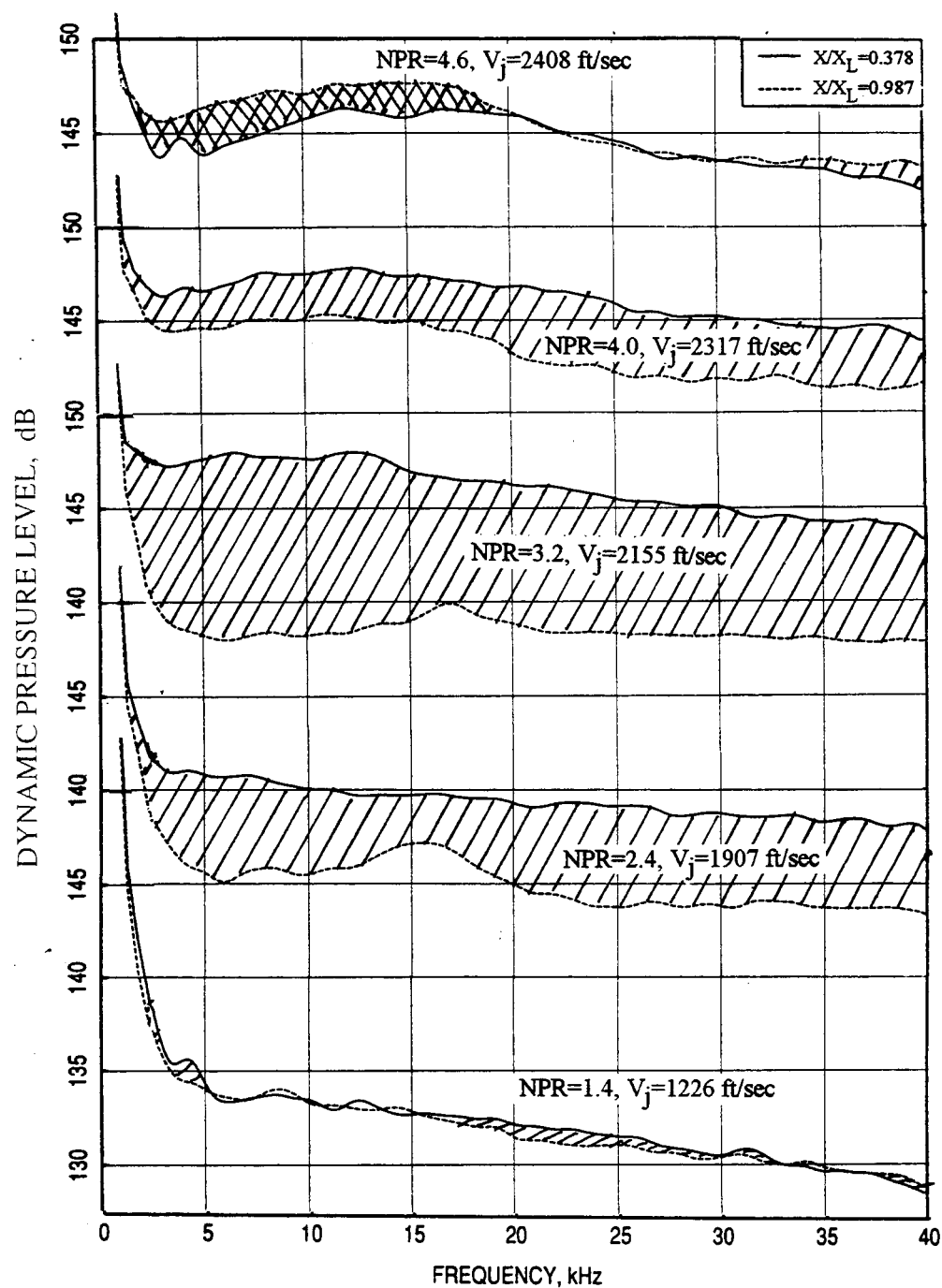
Figure 6-15. Effect of flap measurement location on dynamic pressure level spectra for different nozzle pressure ratio for a 2D mixer-ejector nozzle with hard wall and with staggered CD chutes, T8=1360°R.

further increase in NPR (i.e., at 4.0), the microphone at X/X_L=0.378 measures lower dynamic pressure levels due to incomplete noise generation process. The noise generation and mixing processes continue downstream of this location. At the ejector exit plane the noise reduction due to mixing might have been slightly higher than the noise generated between X/X_L=0.378 and the exit plane. Hence, the microphone at the ejector exit plane sees slightly lower dynamic pressure level compared to X/X_L=0.378 location. For very high NPR (i.e., 4.6 in this case) the noise generation and mixing processes are most likely be incomplete within the ejector. Hence the relative contributions of noise generation and reduction at these two locations are such that the dynamic pressure levels seem to be higher at the ejector exit plane compared to X/X_L=0.378.

Overall sound pressure levels are computed using the dynamic pressure levels for frequencies between 2.4 kHz and 40 kHz. Since one of the fiber optic microphone was generating low frequency noise, the data for frequencies lower than 2.4 kHz are not included in OASPL calculation The results are plotted with respect to jet velocity and NPR in Figure 6-16. The comparison of OASPL between the two axial locations follows the trend as explained above.

6.4.2 Fully Treated Ejector Configuration :

Figures 6-17 and 6-18 show the dynamic pressure level spectra for the fully treated ejector at X/X_L=0.987 and X/X_L=0.378, respectively, at different nozzle pressure ratios. While the absolute levels for these spectra are different from those for hard wall configuration (see Figures 6-13 and 6-14) the trends with respect to NPR are similar and can be explained in the same manner as explained earlier.

Dynamic pressure level spectra measured at fixed NPR are compared between the two axial locations in Figure 6-19. Compared to hard wall configuration (see Figure 6-15) dynamic pressure level differences between X/X_L=0.378 and ejector exit plane are relatively higher. The dynamic pressure level reduction at ejector exit plane compared to that at X/X_L=0.378 is higher compared to hard wall case due to the additional attenuation of dynamic pressure by acoustic treatment between these two locations. At NPR=1.4 most attenuation might have been achieved by X/X_L=0.378. Hence we note small amount of benefit due the treatment downstream of this location. However, the treatment effectiveness between these two locations increases with increasing NPR due to lesser noise interaction with the treatment closer to mixer exit and relatively higher noise levels.
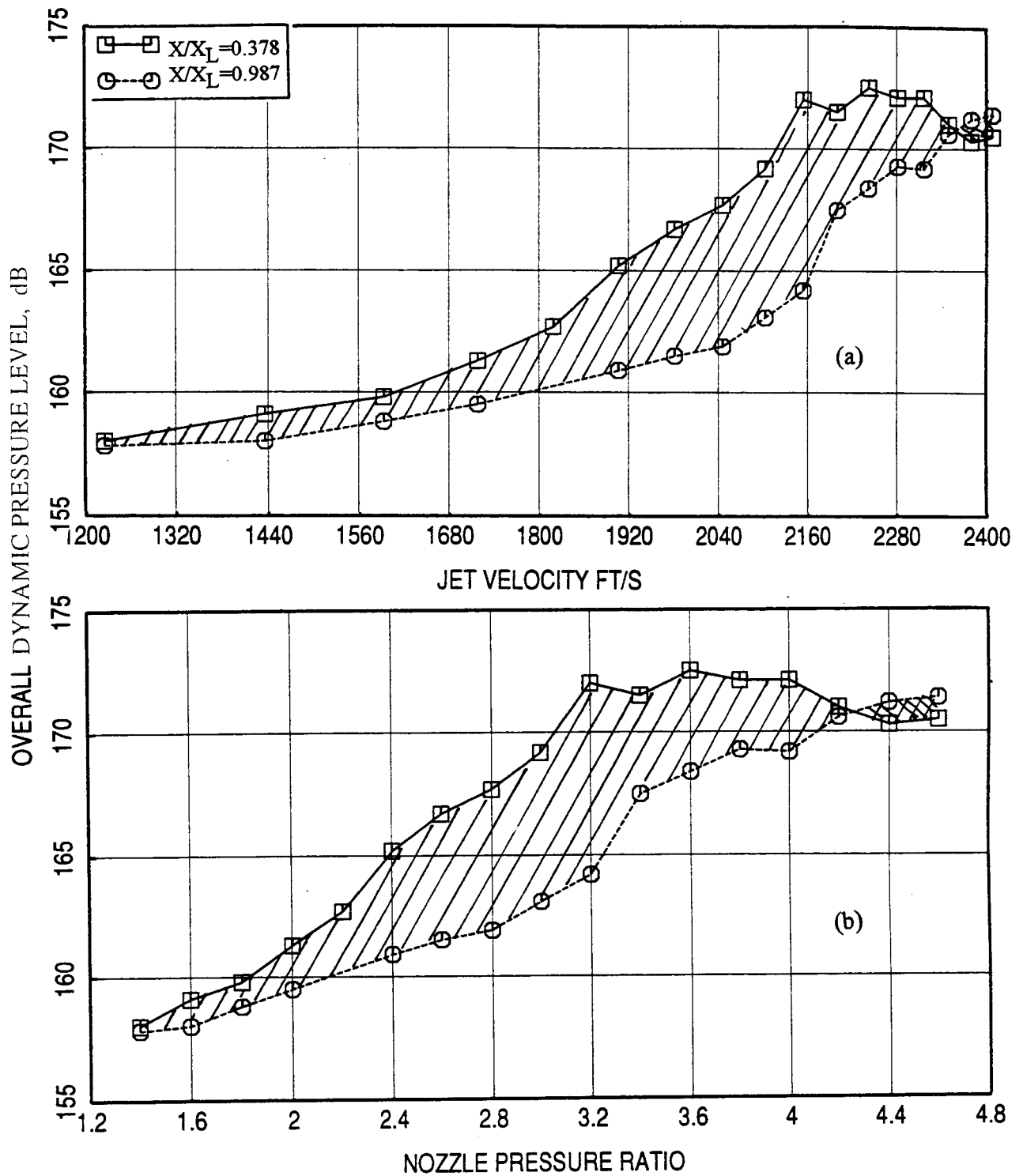
Figure 6-16. Effect of flap measurement location on overall dynamic pressure level with respect to (a) jet velocity and (b) nozzle pressure ratio for a 2D mixer-ejector nozzle with hard wall and with staggered CD chutes, T8=1360°R.
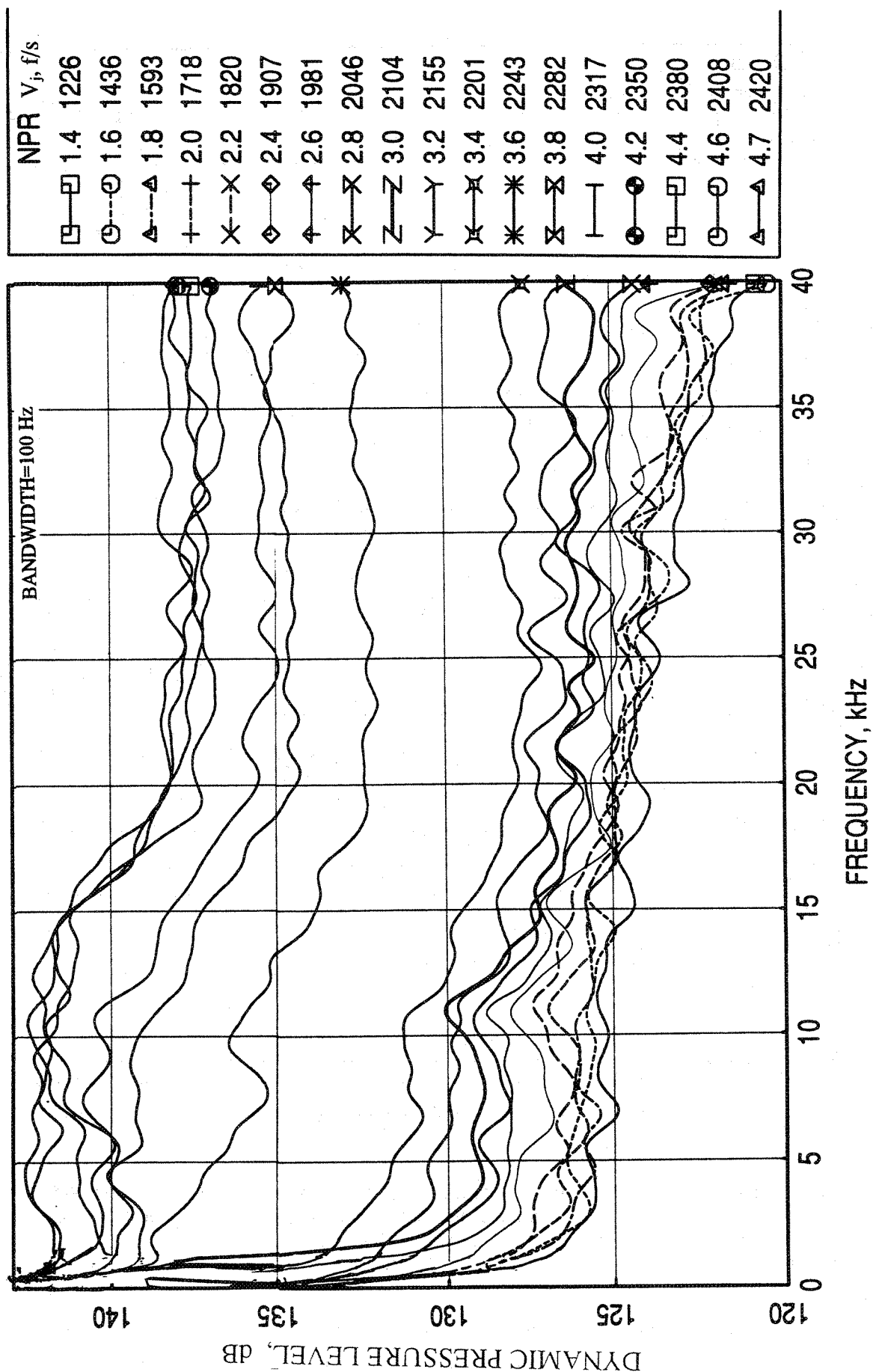
Figure 6-17. Dynamic pressure level spectra internal to the ejector on the flap at $X/X_L=0.987$ for different nozzle pressure ratio for a 2D mixer-ejector nozzle with fully treated ejector and with staggered CD chutes, T8=1360°R.
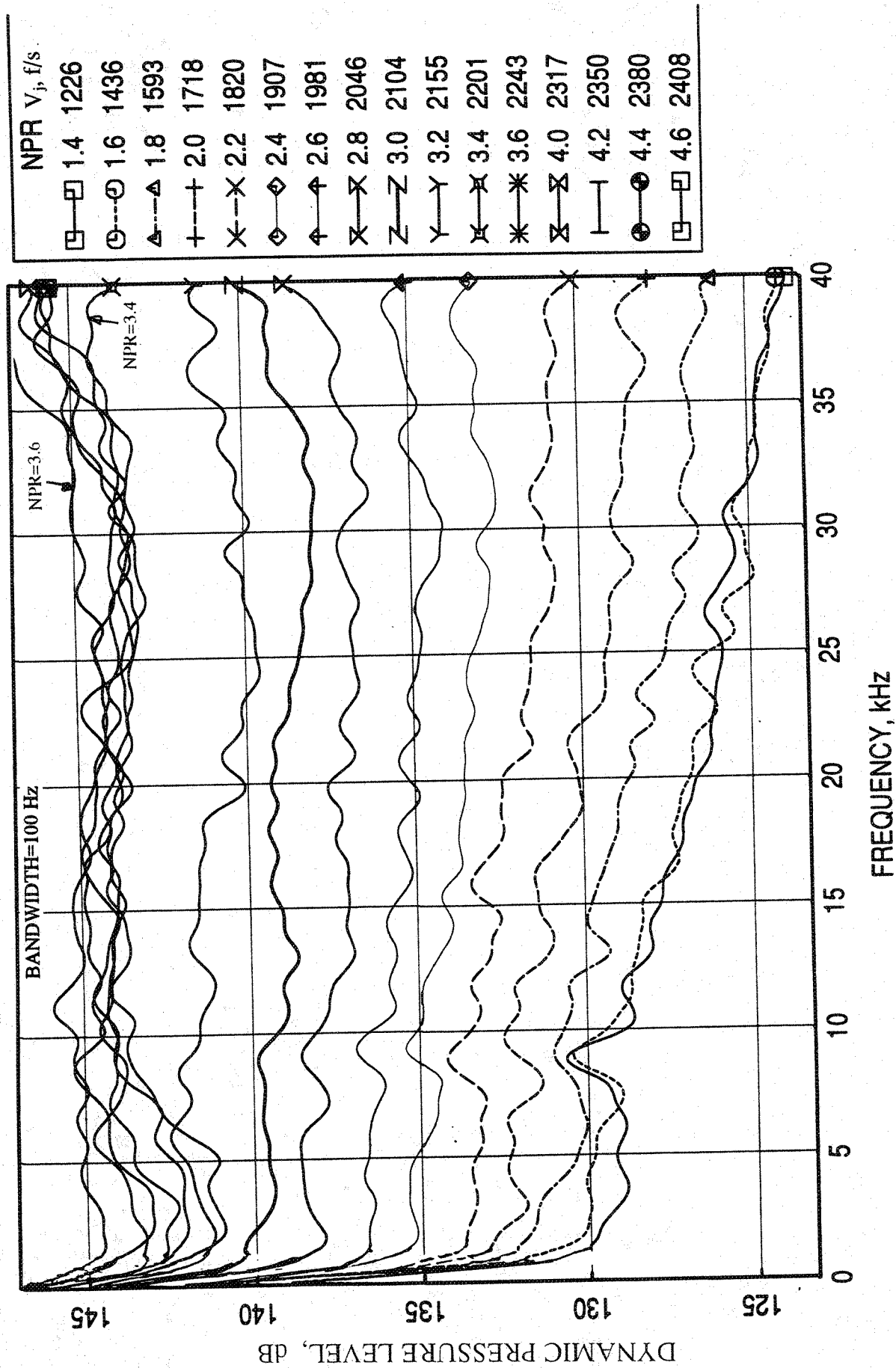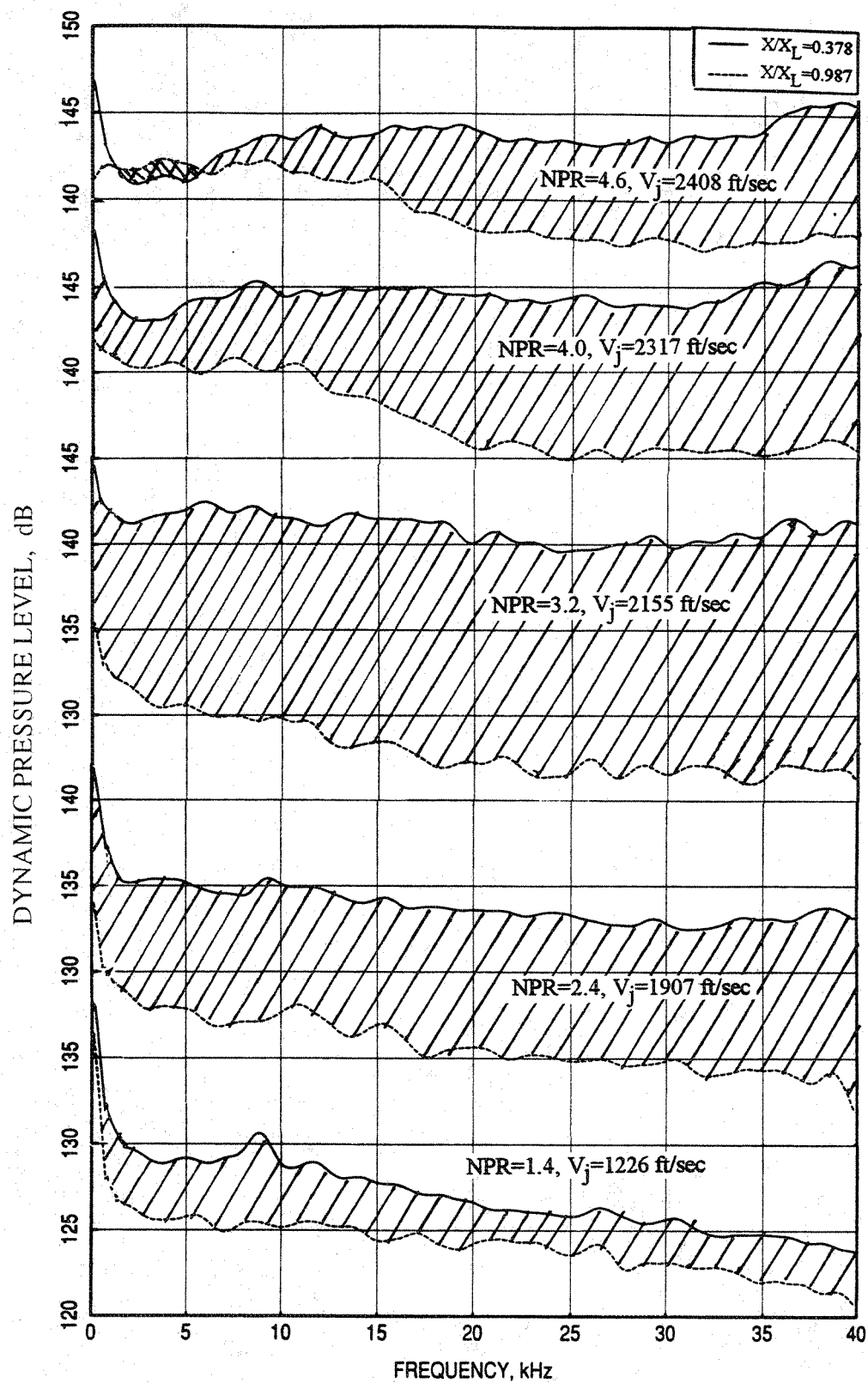
Figure 6-18. Dynamic pressure level spectra internal to the ejector on the flap at $X/X_L = 0.378$ for different nozzle pressure ratio for a 2D mixer-ejector nozzle with fully treated ejector and with staggered CD chutes, $T8 = 1360^oR$.

Figure 6-19. Effect of flap measurement location on dynamic pressure level spectra for different nozzle pressure ratio for a 2D mixer-ejector nozzle with fully treated ejector and with staggered CD chutes, T8=1360°R.

For very high NPR the effectiveness of treatment is less since the noise propagates at much higher speed and get less interaction duration with the treatment. In addition, at higher NPRs the convected noise interacts with small area of the treatment closer to the ejector exit if any. Thus the attenuation due to treatment first increases and then decreases with increasing NPR. Noise difference between the two locations shown in Figure 6-19 is the sum of the differences due to mixing process (see Figure 6-15) and the attenuation due to treatment. Maximum attenuation seems to be attained at NPR=3.2. This is further demonstrated in Figure 6-20 by plotting the OASPL with respect to jet velocity and NPR.

6.4.3 Impact of Ejector Treatment :

Figure 6-21 shows the comparison of dynamic pressure level spectra at X/X_L=0.987 between hard wall and fully treated configurations. The amount of dynamic pressure attenuation due to treatment first increases slightly at higher frequencies and then decreases for entire frequency range with increasing NPR. For lower NPR the interaction between the dynamic pressure and the treatment surface begins closer to the mixer exit and hence substantial dynamic pressure attenuation is achieved. It should be noted that for very low NPR the maximum possible suppression is most likely achieved and since the noise level is relatively lower at higher frequencies for lower NPR the attenuated levels might have fallen below the instruments lower dynamic measurement limits. This may explain why the high frequency attenuation increases with NPR at the beginning. For very high NPR the noise interacts only with the downstream portion of the treatment and hence a small amount of dynamic pressure attenuation is achieved. This is further shown in Figure 6-22 in terms of OASPL with respect to jet velocity and NPR. It should be noted that the acoustic attenuation due to treatment is a function of its acoustic impedance, which varies with the grazing flow (i.e., with NPR). Hence, some of the attenuation variation with respect to NPR could be due to acoustic impedance variation of the treatment.

The above explanation is further confirmed by comparing the dynamic pressure level spectra at different NPR and OASPL with respect to jet velocity and NPR at X/X_L=0.378 between hard wall and fully treated configurations in Figures 6-23 and 6-24, respectively. The amount of dynamic pressure attenuation due to treatment at X/X_L=0.378 is lower compared to what was observed at the ejector exit plane. This is due to the lesser treatment area responsible for the attenuation measured at X/X_L=0.378 location
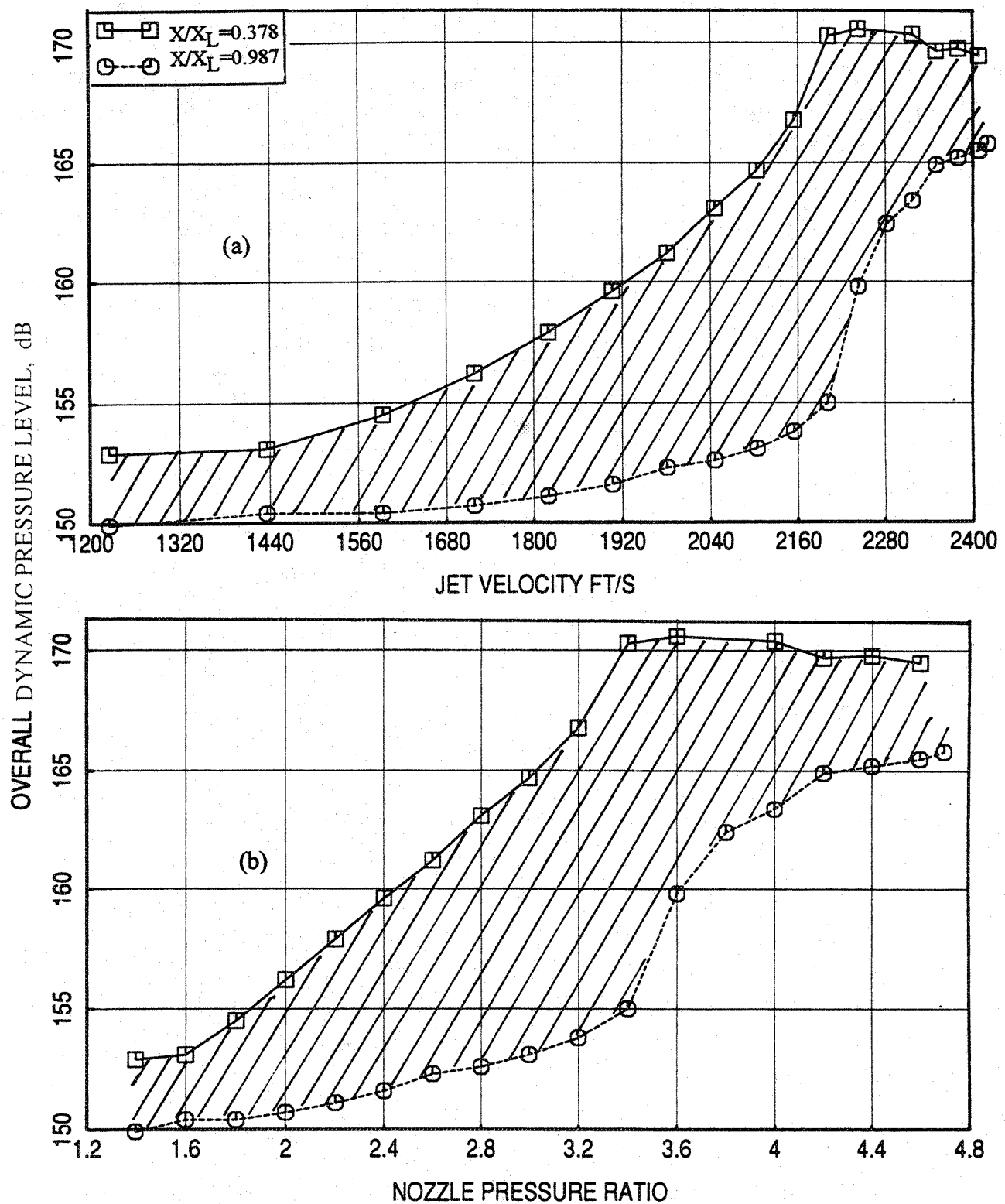
Figure 6-20. Effect of flap measurement location on overall dynamic pressure level with respect to
(a) jet velocity and (b) nozzle pressure ratio for a 2D mixer-ejector nozzle with fully
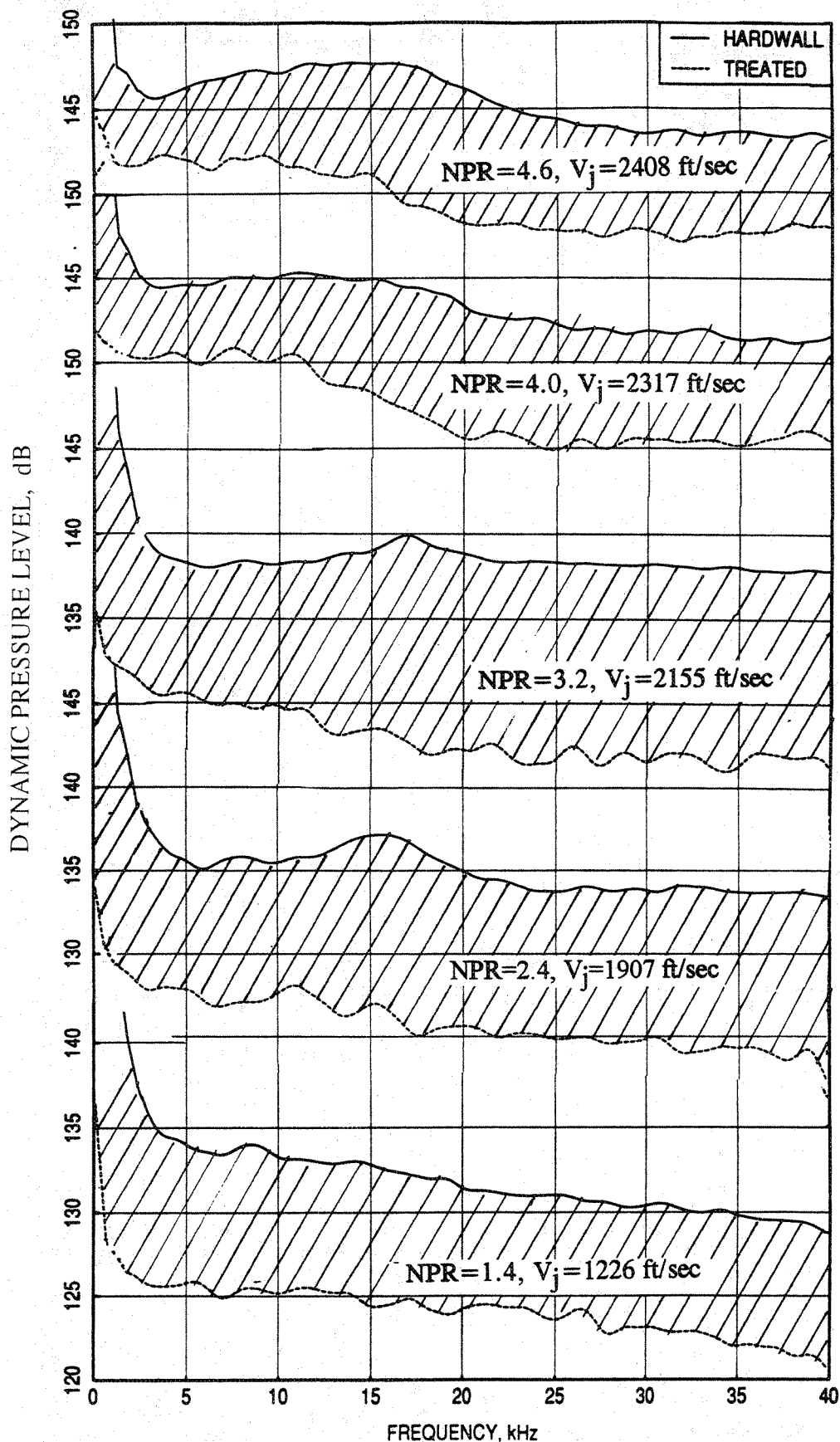treated ejector and with staggered CD chutes, T8=1360°R.

Figure 6-21. Effect of treatment on dynamic pressure level spectra internal to the ejector on the flap at X/X_L=0.987 for different nozzle pressure ratio for a 2D mixer-ejector nozzle with staggered CD chutes, T8=1360°R.
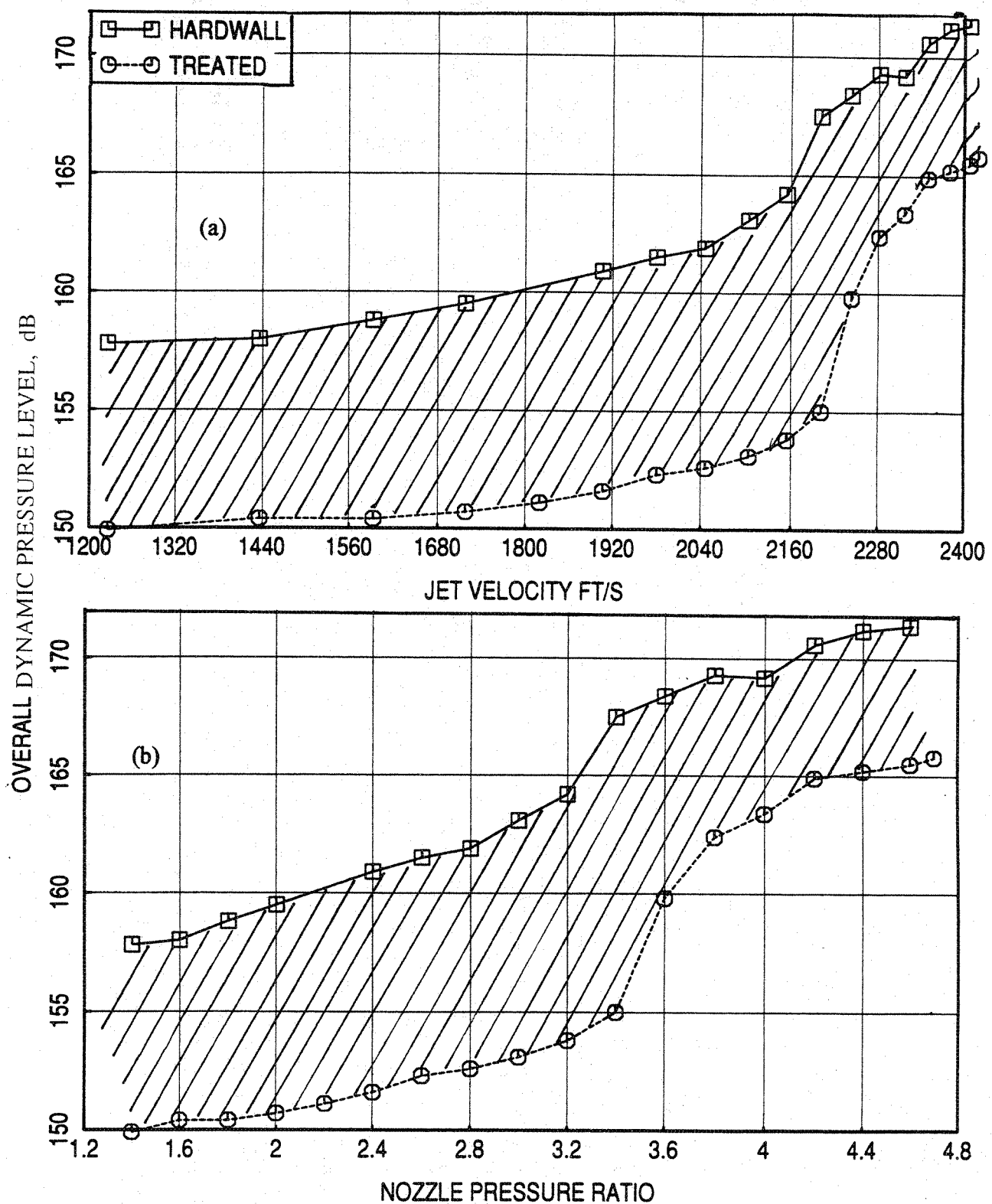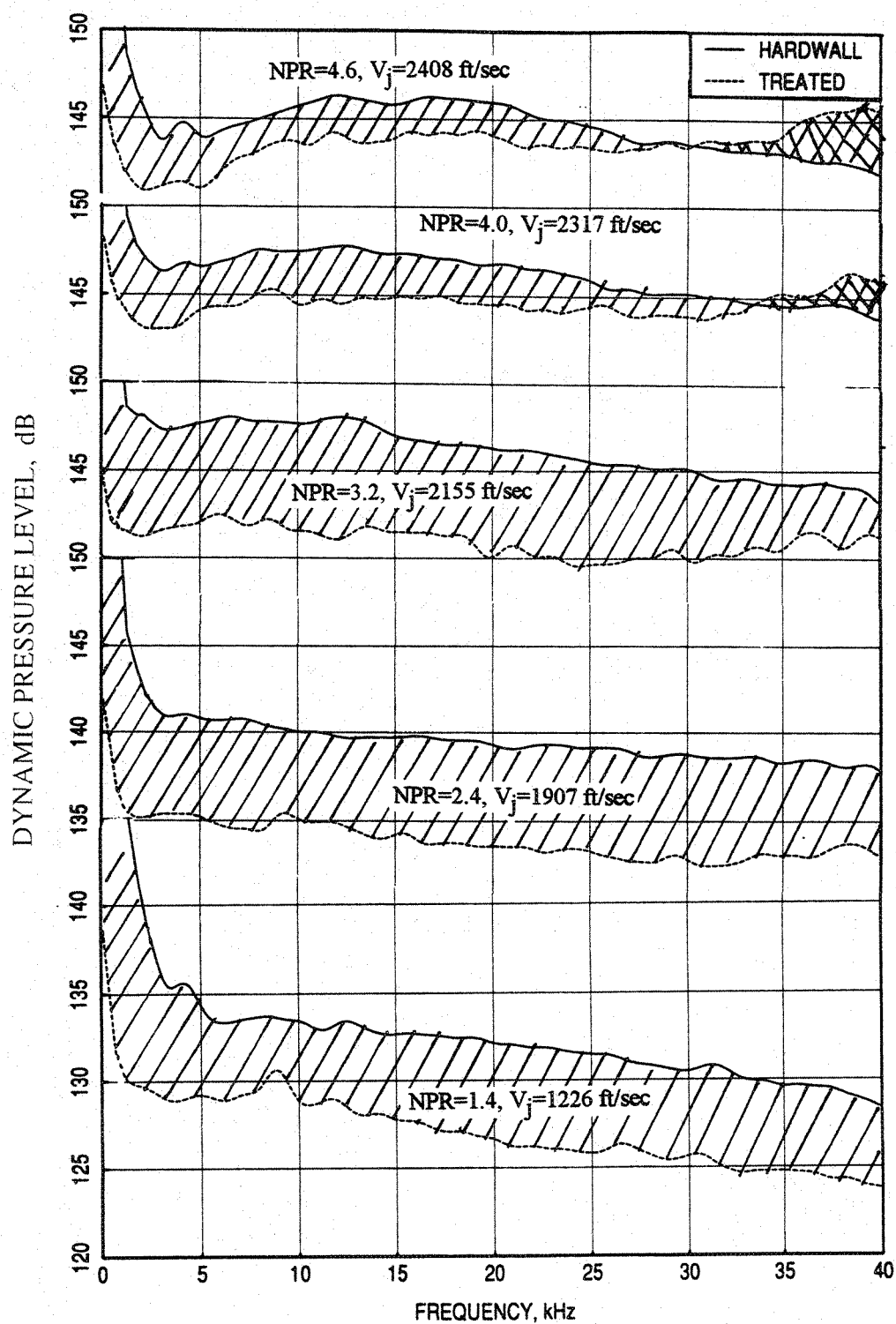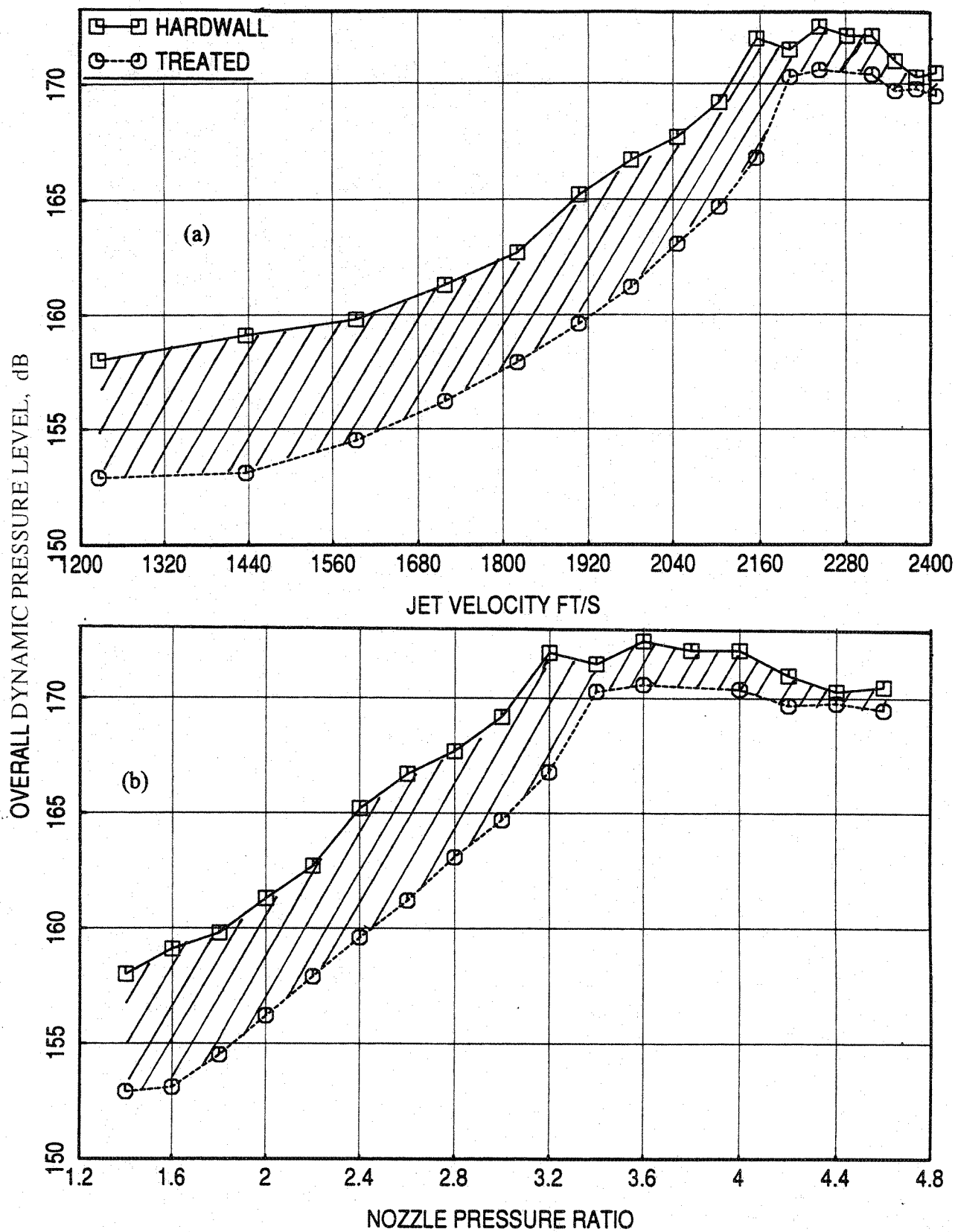
Figure 6-22. Effect of treatment on overall dynamic pressure level internal to the ejector on the flap at X/X_L=0.987 with respect to (a) jet velocity and (b) nozzle pressure ratio for a 2D mixer-ejector nozzle with staggered CD chutes, T8=1360°R.

Figure 6-23. Effect of treatment on dynamic pressure level spectra internal to the ejector on the flap at X/X_L=0.378 for different nozzle pressure ratio for a 2D mixer-ejector nozzle with staggered CD chutes, T8=1360°R.

Figure 6-24. Effect of treatment on overall dynamic pressure level internal to the ejector on the flap at X/X_L =0.378 with respect to (a) jet velocity and (b) nozzle pressure ratio for a 2D mixer-ejector nozzle with staggered CD chutes, T8=1360°R.

compared to the exit plane location. However, the treatment upstream of $X/X_L=0.378$ does attenuate dynamic pressure noticeably at all NPR but less effective at higher NPR.

6.5 FARFIELD NOISE :

Narrowband farfield noise for the model scale mixer ejector nozzle at 40 feet arc location at standard day conditions are presented in this section. Figure 6-25 shows the pseudo sound power level (PWL) spectra at different NPR for hard wall and treated ejector configurations. These results are termed pseudo PWL, since they are evaluated by assuming azimuthal symmetry. However, the trends are of interest. The summations are performed accounting their polar variations. For both the configurations the PWL increases with increasing NPR. The levels are constant at higher frequencies above 15 kHz.

The effect of ejector treatment is examined by comparing SPL spectra between hard wall and treated configurations at different NPR for various polar angles in Figures 6-26 through 6-28. At each angle the SPL suppression first increases and then decreases with increasing NPR. With respect to polar direction, higher SPL suppression is observed at polar angles between 80° and 120°. Very little SPL suppression is noted for higher NPR. At $\theta=150^o$ the SPL seems to be higher for treated configuration compared to hard wall ejector for NPR=4.6. Spectral comparisons of PWL between hard wall and treated ejector configurations at different NPR are shown in Figure 6-29. Again, the PWL suppression increases first and then decreases with increasing NPR. At NPR=4.6 treated case yields slightly higher PWL than hard wall configuration. A possible explanation for this behavior is given below.

Farfield noise is the sum of the noise radiated out of the ejector and the noise generated outside the ejector. The radiation directivities for both the noise components influence the farfield noise characteristics. One of the important factors which influences the effect of ejector treatment in the farfield is the relative contribution of internal and external noise components. If the internal noise component is higher than the externally generated noise at a measurement location, then any modification of the internal noise component will influence the farfield noise. In this situation the noise suppression due to ejector treatment will reduce the farfield noise compared to hard wall configuration. Again, this will be noted until the internal noise component is sufficiently lower compared to the external component. Further reduction of internal noise component will have limited effect on the
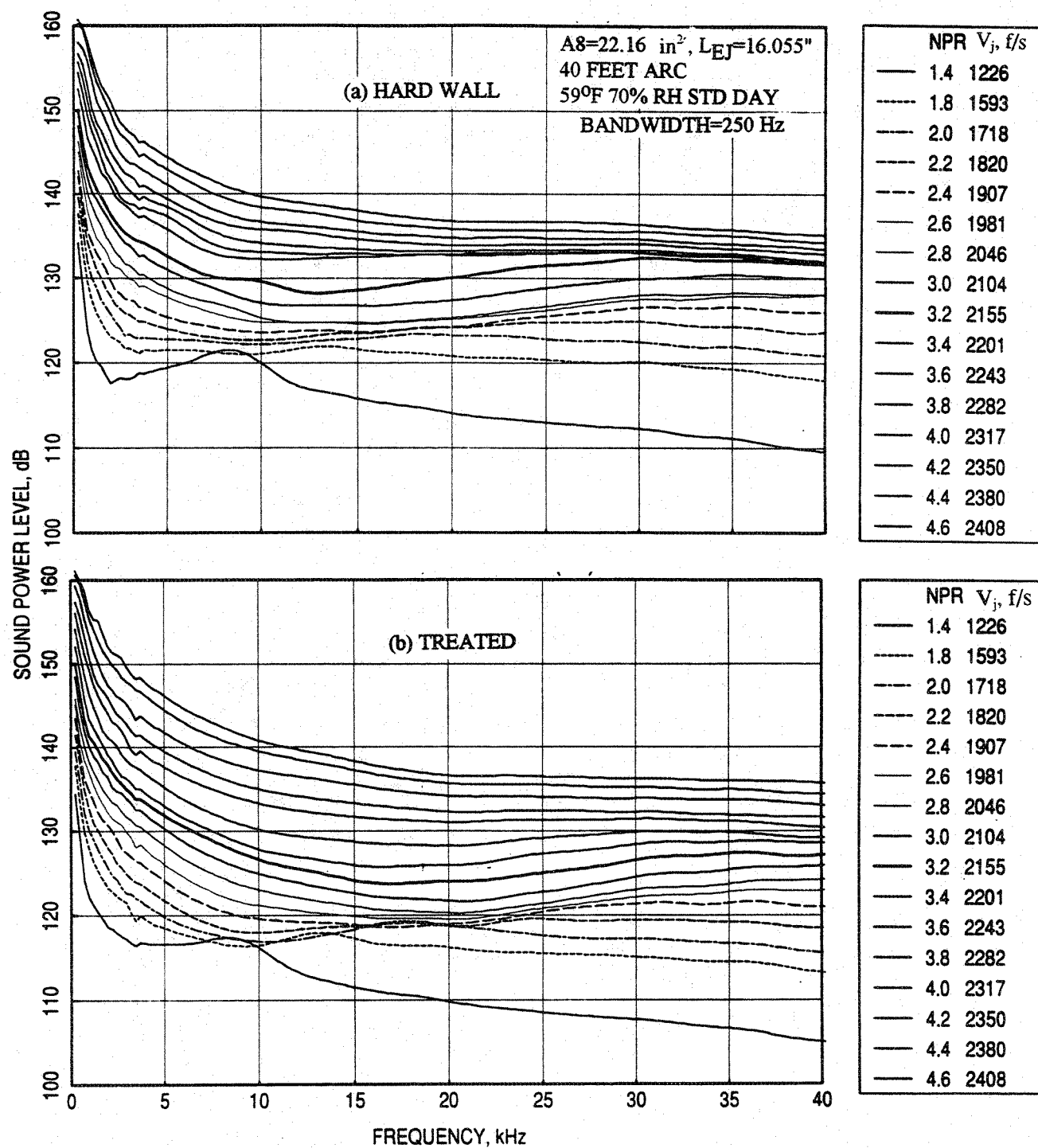
Figure 6-25. Sound power level spectra in the farfield for different nozzle pressure ratio for a 2D mixer-ejector nozzle with staggered CD chutes for (a) hard wall and (b) fully treated ejector configurations, T8=1360°R.
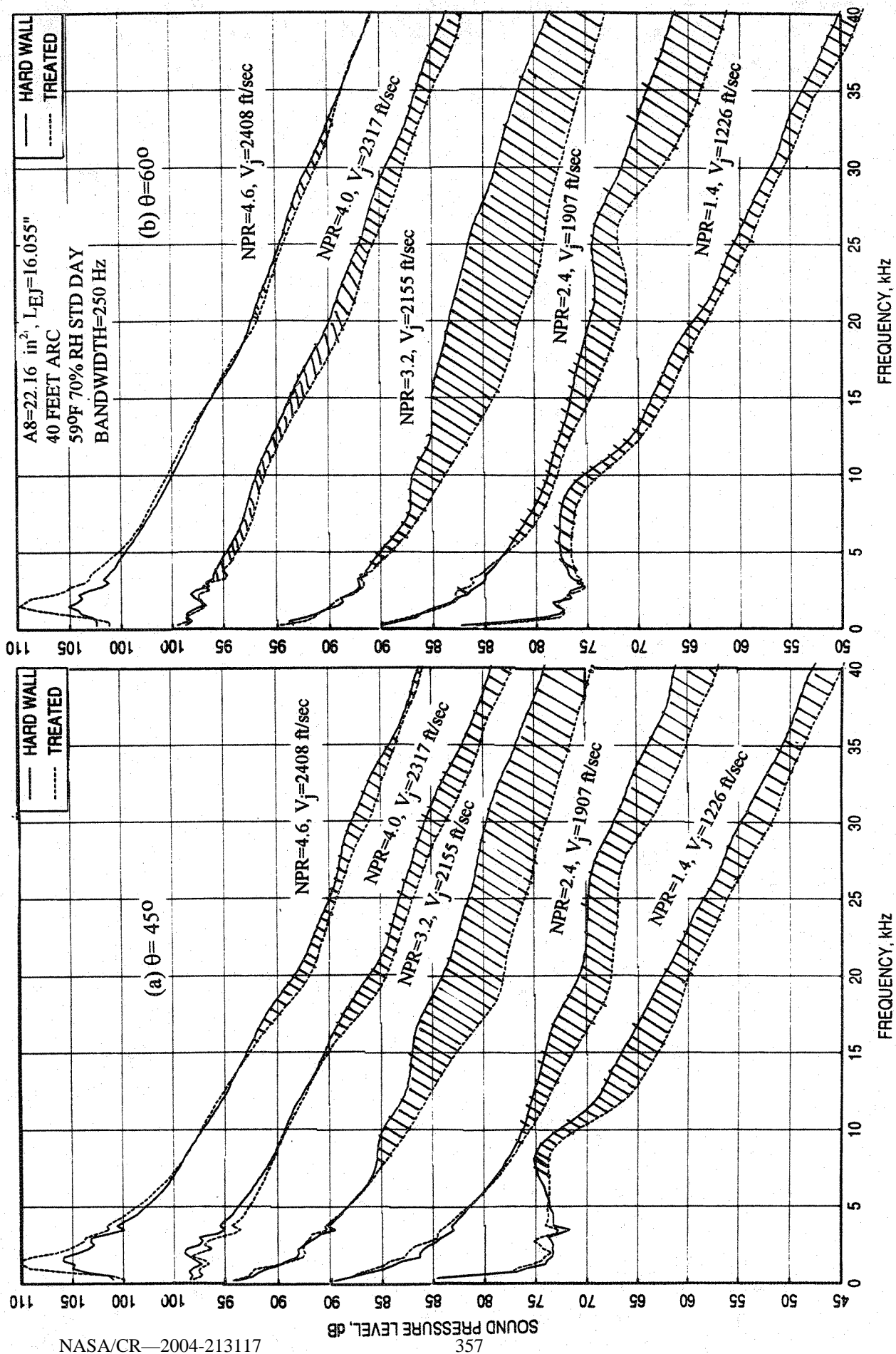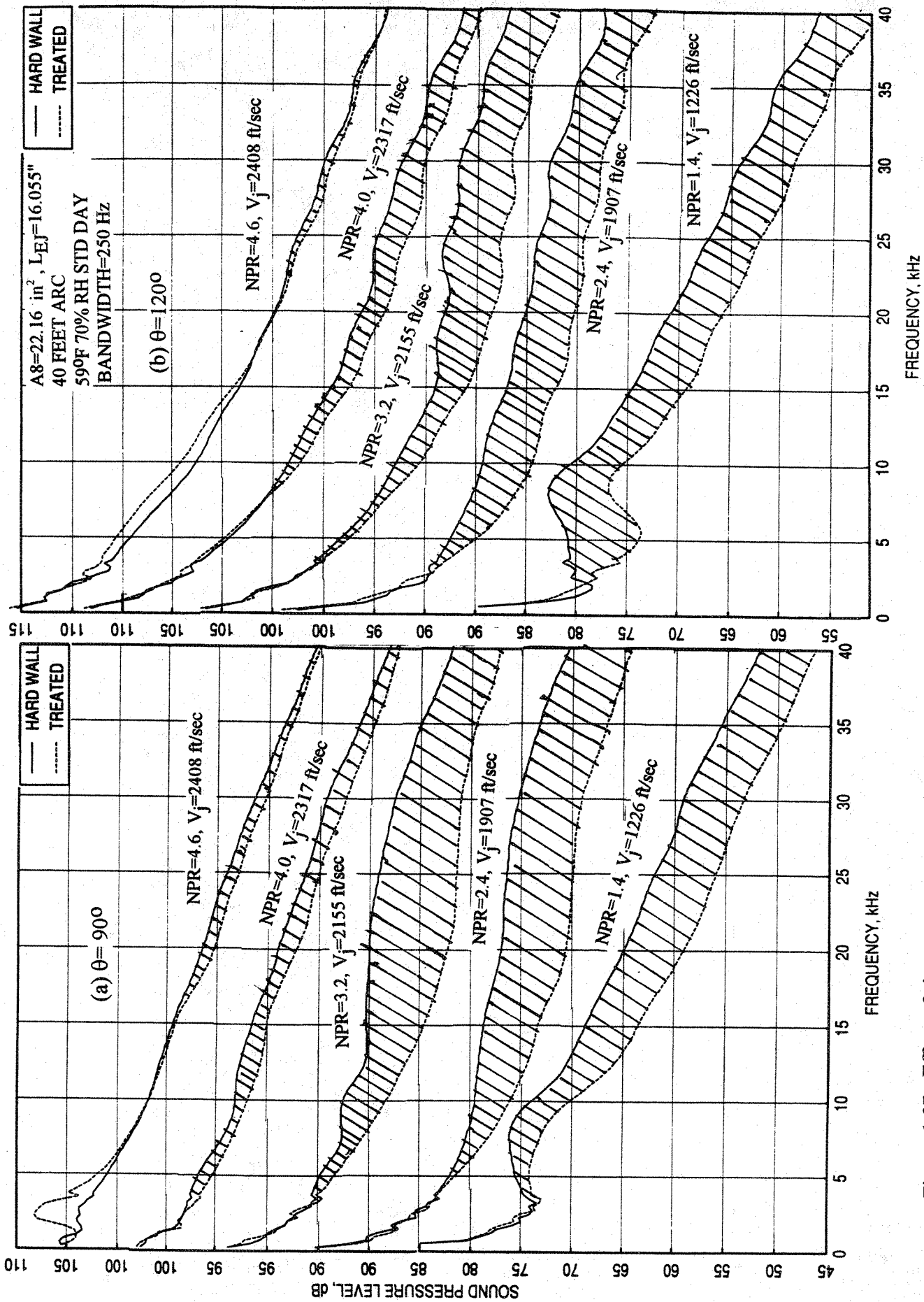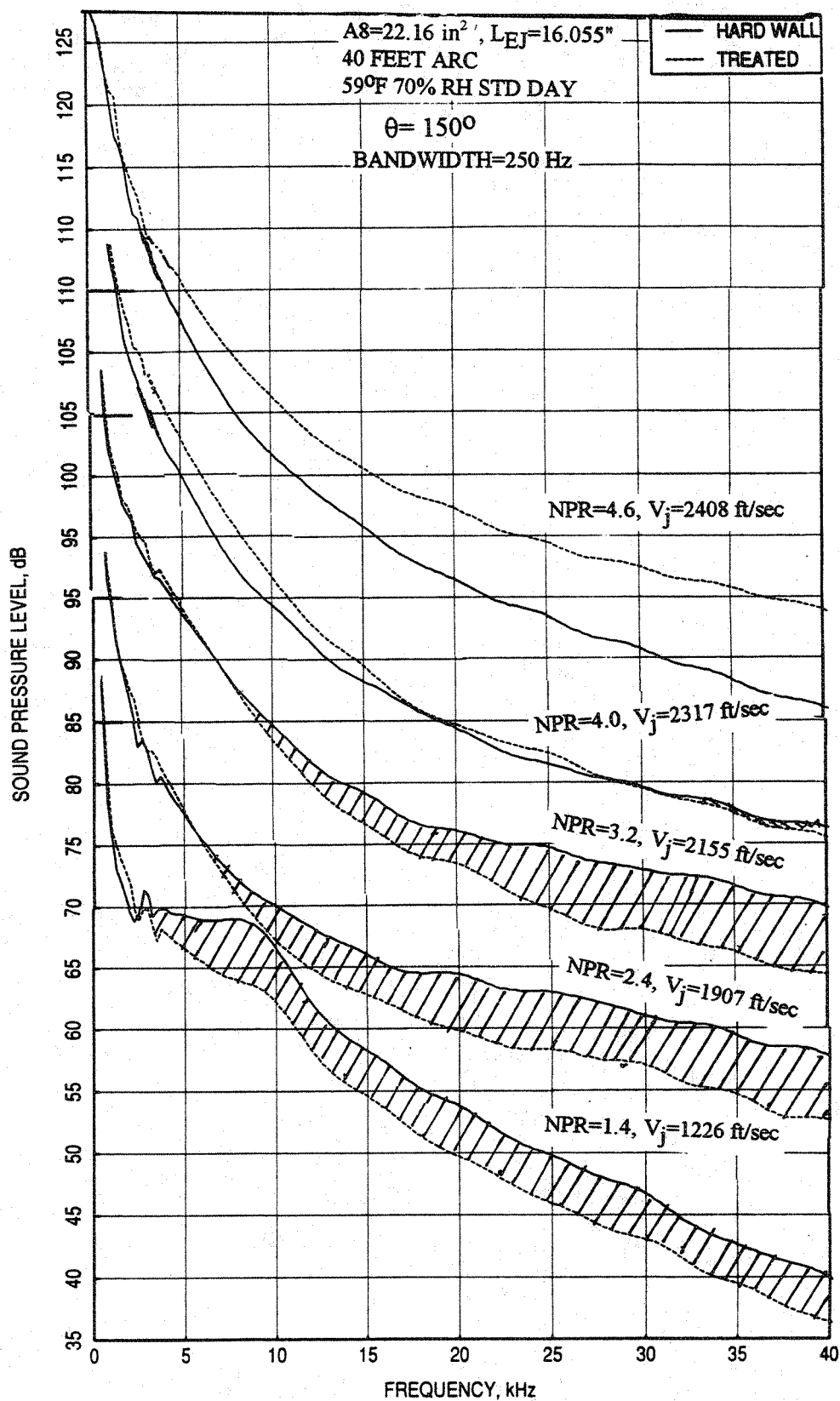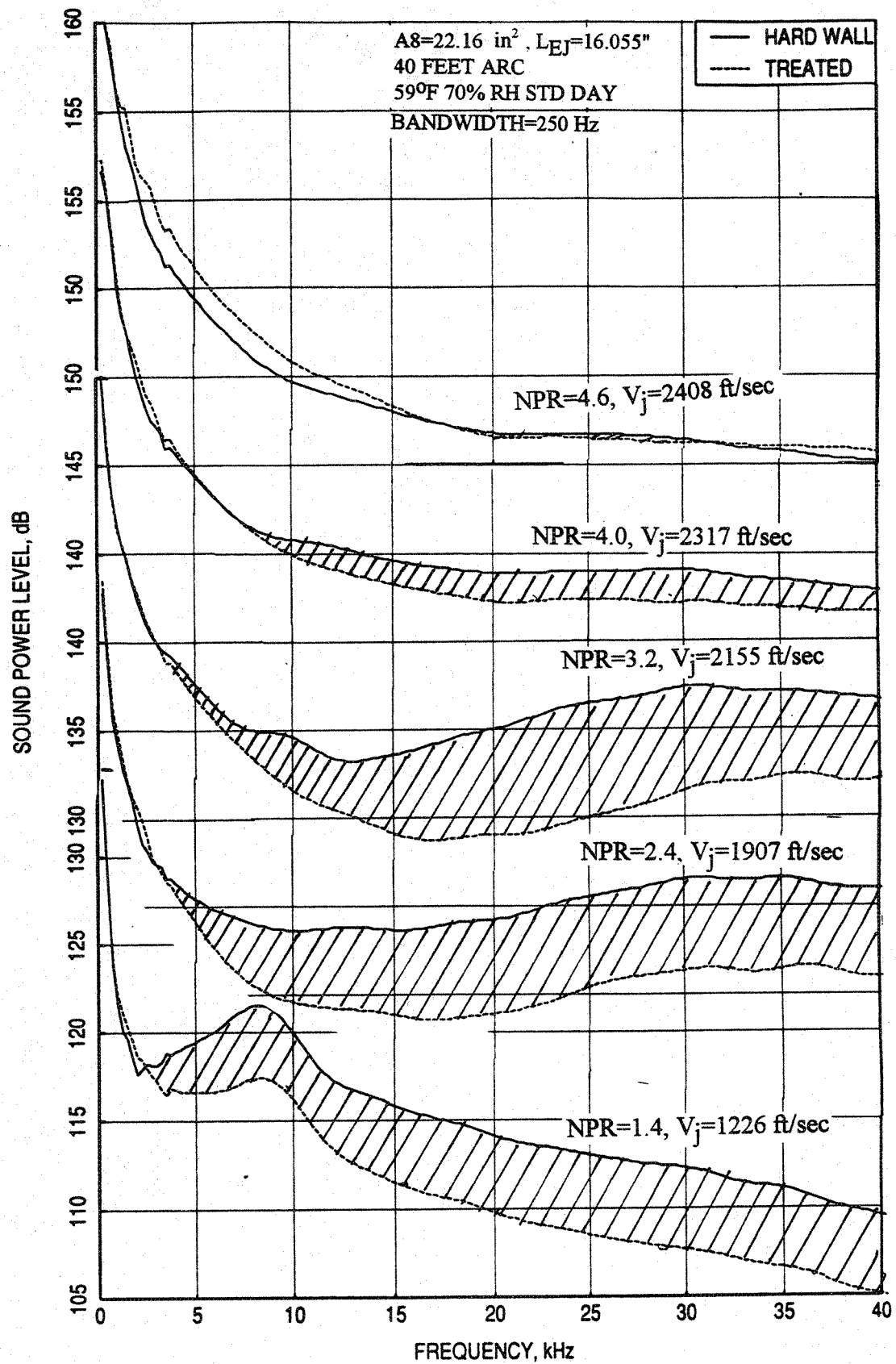
Figure 6-26. Effect of ejector treatment on sound pressure level spectra in the farfield for different nozzle pressure ratio for a 2D mixer-ejector nozzle with staggered CD chutes at (a) θ= 45° and (b) θ=60°, θ=60°, T8=1360°R.

Figure 6-27. Effect of ejector treatment on sound pressure level spectra in the farfield for different nozzle pressure ratio for a 2D mixer-ejector nozzle with staggered CD chutes at (a) θ= 90º and (b) θ=120º, T8=1360ºR.

Figure 6-28. Effect of ejector treatment on sound pressure level spectra in the farfield for different nozzle pressure ratio for a 2D mixer-ejector nozzle with staggered CD chutes at θ= 150°, T8=1360°R.

Figure 6-29. Effect of ejector treatment on sound power level spectra in the farfield for different nozzle pressure ratio for a 2D mixer-ejector nozzle with staggered CD chutes, T8=1360°R.

farfield noise. Hence, the benefit of treatment would depend on the relative magnitudes of noise components and their directivity patterns.

A small increase in farfield noise is noted for treated case at higher NPRs (above 4.0) compared to hard wall configuration. A plausible physical mechanism for this could be the reduction of turbulent level due to treatment in the ejector which slows down the mixing process outside the ejector and hence the external noise levels become higher for treated case compared to hard wall. Another mechanism could be the increased boundary layer thickness for treated ejector compared to hard wall case, which would increase the mixed jet velocity at the exit. This will increase the external noise. For lower NPRs the internal noise component is comparable to external noise and hence the internal noise attenuation due to treatment overcomes any small external noise increase. However, for very high NPR the external noise seems to be much higher than internal noise component and its attenuation due to treatment does not influence the total farfield noise. On the other hand, any increase in external noise due to turbulence reduction and increased mixed jet velocity due to increased boundary layer thickness, caused by ejector treatment, are likely to increase the total farfield noise level. This may be the reason, why we see higher noise levels for treated configuration at NPR above 4 compared to hard wall case.

Farfield results shown in Figures 6-26 through 6-29 can be interpreted with the above explanation. At lower NPR the internal noise component is most likely dominant compared to external noise, since the mixed velocity of the jet at the ejector exit is low. At this situation any internal noise reduction due to treatment will most likely influence the farfield noise level. At higher NPR both the noise components are increased and most likely the external noise component becomes dominant due to reduced mixing within the ejector. In addition, at higher NPR the internal noise attenuation due to treatment is relatively smaller, as observed in the internal dynamic pressure data due to high grazing flow Mach numbers. At this situation the effect of treatment is not likely to be noticed in the farfield noise. This is clearly observed in the SPL and PWL spectra (see Figures 6-26 through 6-29).

Figure 6-30 shows the OASPL directivities at different NPR for hard wall and treated ejector configurations. For both configurations the OASPL increases with increasing NPR at all polar angles. However, comparison of these directivities between hard wall and fully treated configurations, as shown in Figure 6-31 for a number of NPRs, indicate noise suppression at lower NPR values, predominantly in the forward arc. At higher NPR, as
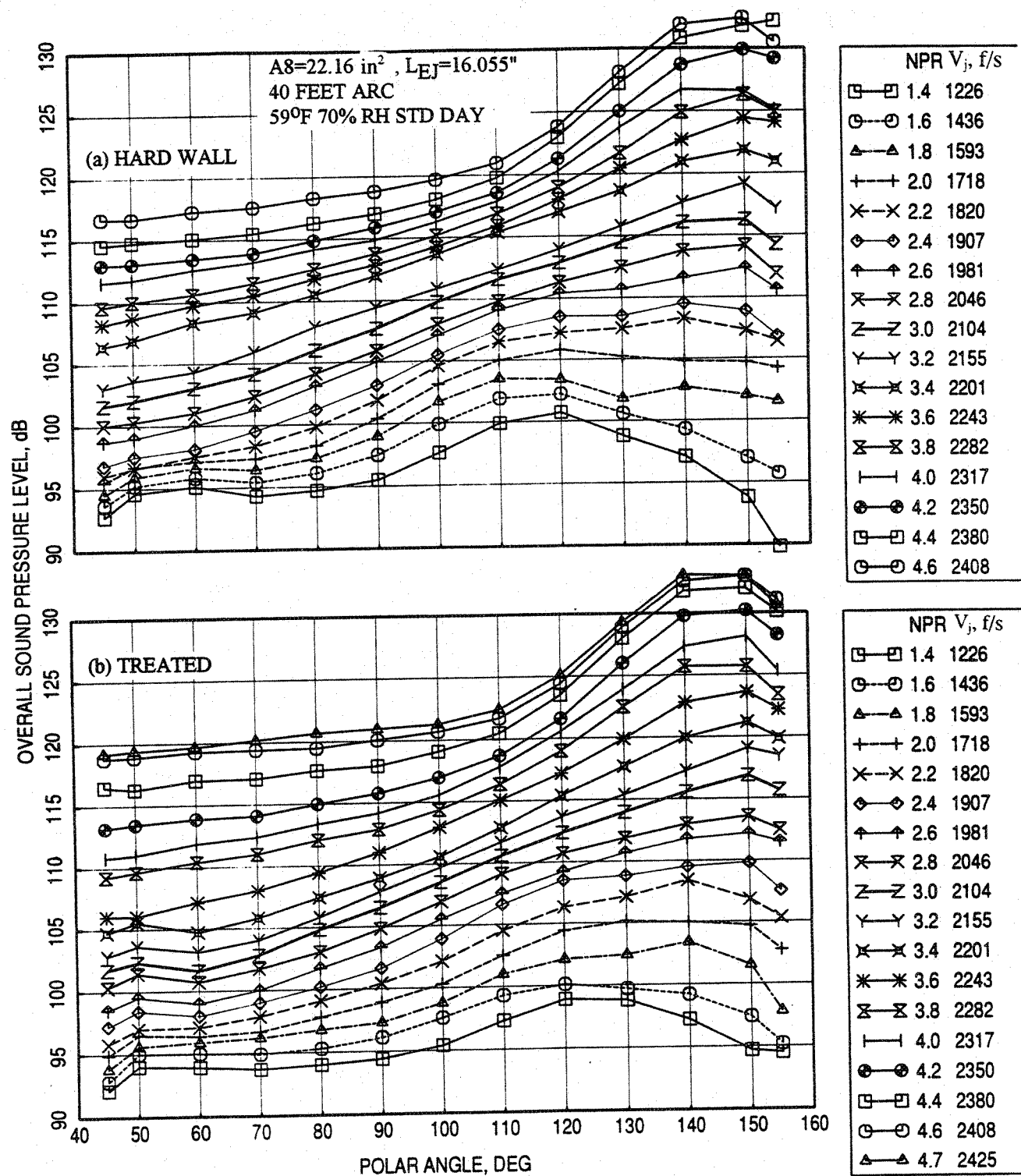
Figure 6-30. Overall sound pressure level directivities in the farfield for different nozzle pressure ratio for a 2D mixer-ejector nozzle with staggered CD chutes for (a) hard wall and (b) fully treated ejector configurations, T8=1360°R.
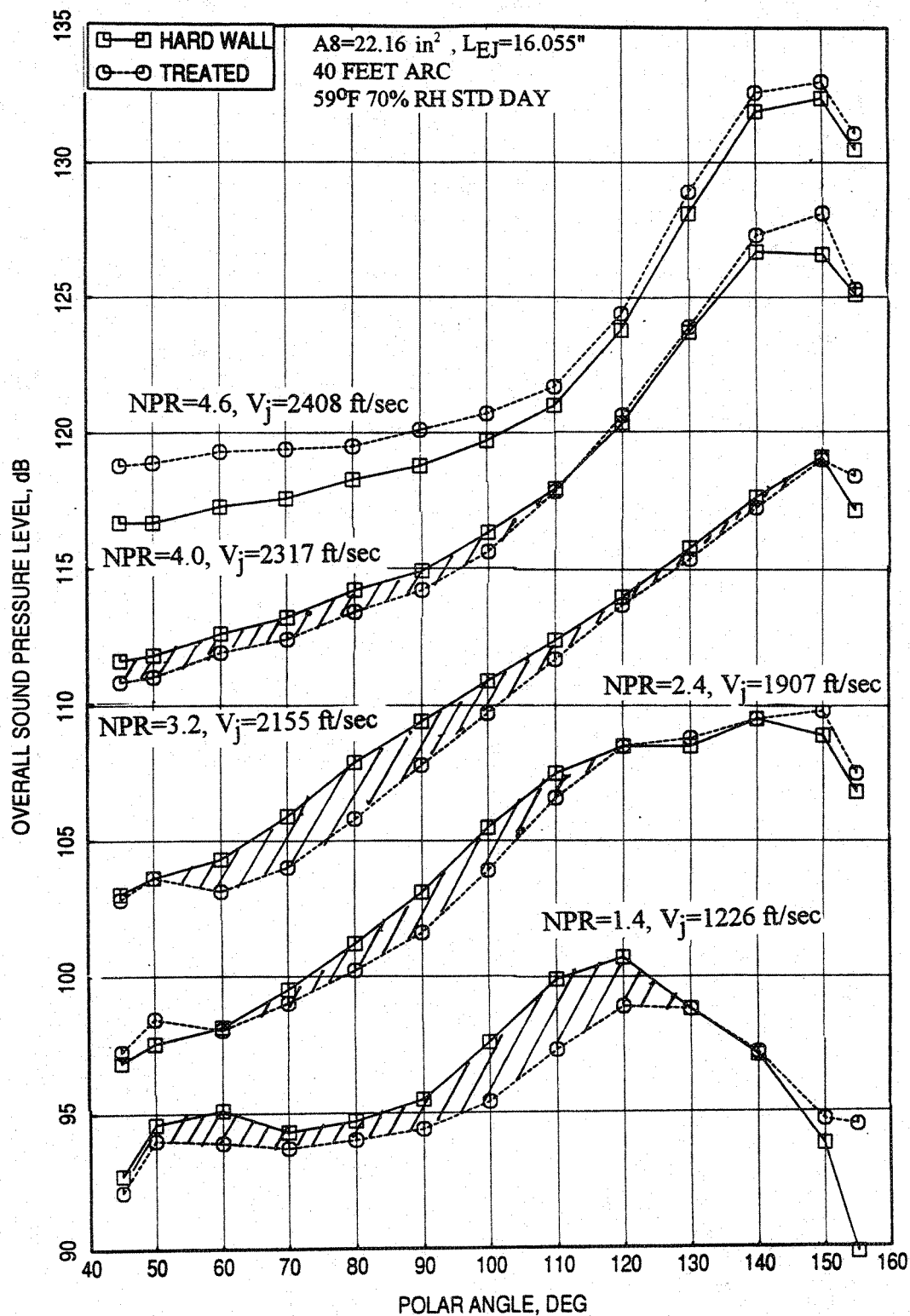
Figure 6-31. Effect of ejector treatment on overall sound pressure level directivities in the farfield for different nozzle pressure ratio for a 2D mixer-ejector nozzle with staggered CD chutes, T8=1360°R.

explained above, there is very little noise suppression due to treatment in the farfield. For NPR=4.6, the OASPL directivity with treatment is higher compared to the hard wall configuration. The possible reasons for this behavior is given above. The effect of ejector treatment is summarized in Figures 6-32 and 6-33 by plotting OASPL with respect to jet velocity at different polar angles and overall sound power level (OAPWL) with respect to jet velocity and NPR, respectively. Again, these results indicate the noise benefit of treatment, which is more at lower NPR and at forward angles.

Conclusions : The ejector treatment attenuates internal noise and is more effective at lower NPR (or jet velocity). Treatment closer to the mixer exit is also effective in flap dynamic pressure attenuation, but relatively less compared to a similar treatment area closer to ejector exit, especially for very high NPR. Ejector treatment is important, especially on entire surface, when the externally generated noise component is lower or of the same magnitude compared to the internal noise component.
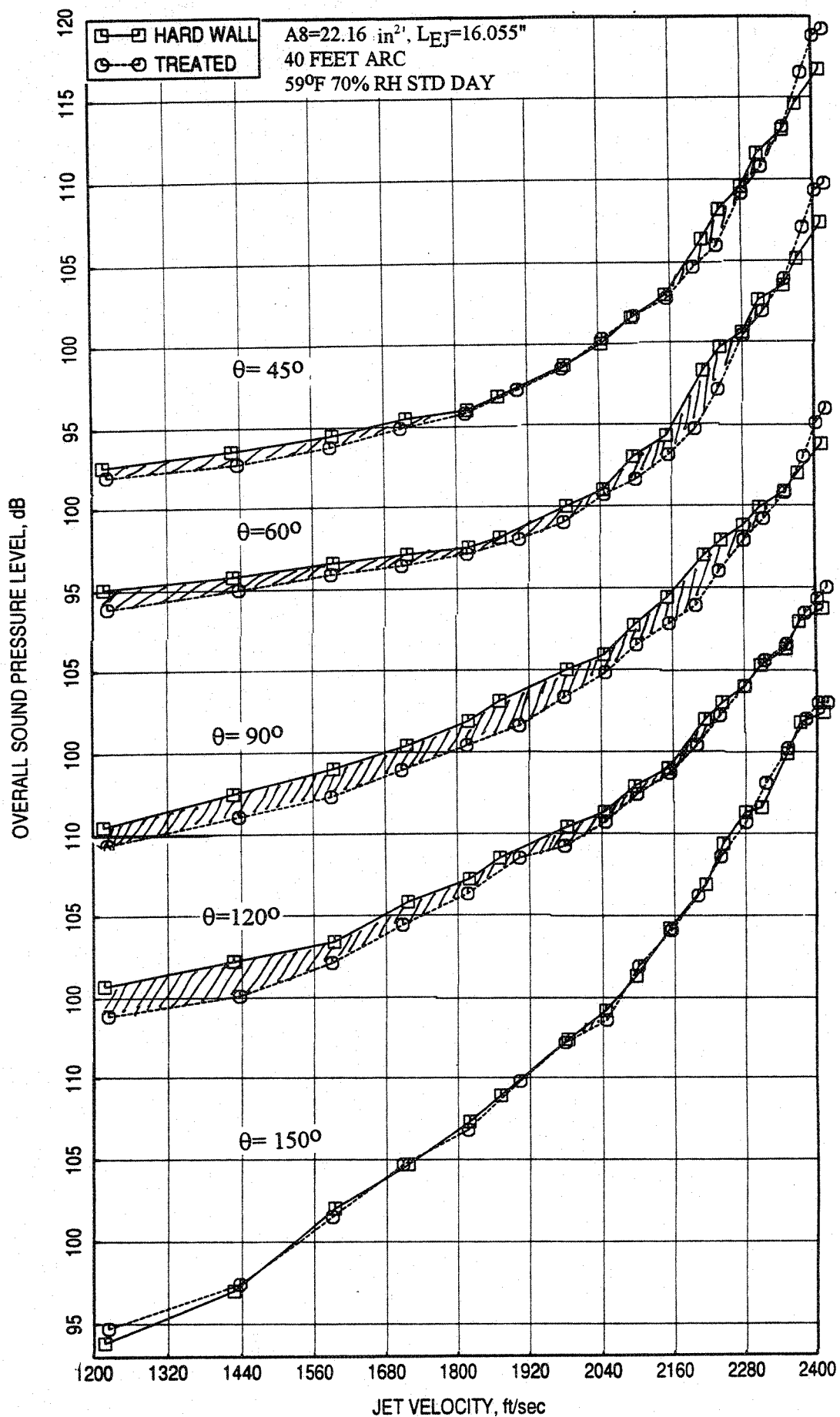
Figure 6-32. Effect of ejector treatment on overall sound pressure level in the farfield with respect to jet velocity for a 2D mixer-ejector nozzle with staggered CD chutes, T8=1360°R.
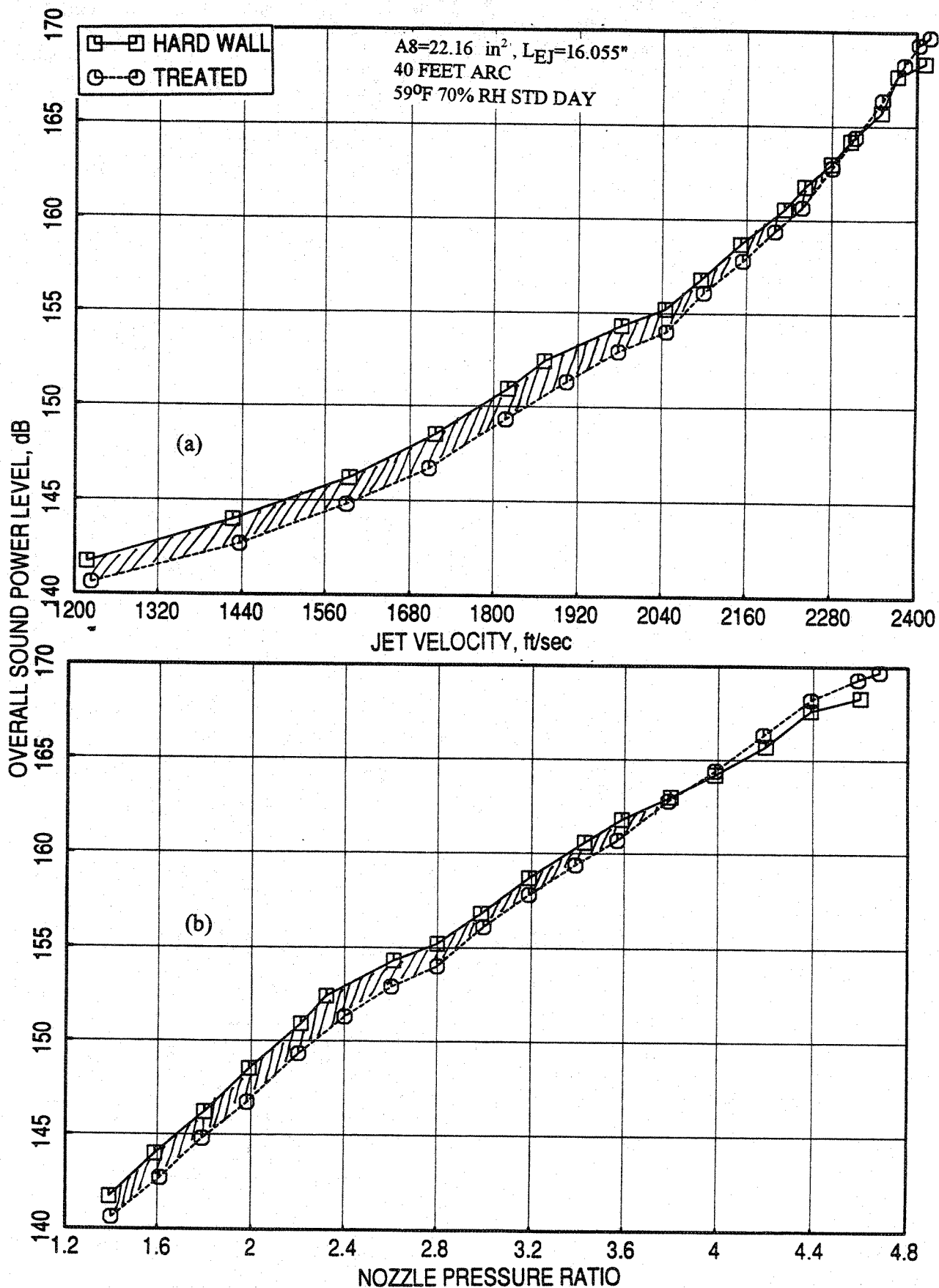
Figure 6-33. Effect of ejector treatment on overall sound power level in the farfield with respect to (a) jet velocity and (b) nozzle pressure ratio for a 2D mixer-ejector nozzle with staggered CD chutes, T8=1360°R.

7.0 ACOUSTIC TREATMENT STUDY

Based on the study on mixer geometry, it has been established that the 10 and 9 full staggered CD-chute mixer with long ejector performs acoustically the best. Any additional acoustic benefit could be obtained by suppressing noise internal to the ejector by treating the ejector appropriately with proper acoustic treatment. While such an elaborate study to optimize the treatment effectiveness is out of scope for this program, a few selected parametric variation of ejector treatment were conducted. Acoustic treatment study includes the effect of (1) ejector treatment area, (2) treatment thickness, (3) treatment location on the ejector, (4) flaps only treated configuration compared to full ejector treatment, and (5) the bulk material type used in the ejector treatment on the farfield noise characteristics and on the flow and performance related parameters. For these studies the tests were conducted for the 9 and 10 full CD-chute mixer with the long ejector configuration.

7.1 EFFECT OF EJECTOR TREATMENT AREA

For this study the treatment area on the ejector is varied and the acoustic, flow related, and performance related parameters are evaluated from experimental data. Results, showing the effect of ejector treatment area, include four configurations, one without any treatment (i.e., configuration #12) and three treated configurations. For the treated configurations (i.e., #11, 23, and 16), the flaps and sidewalls are fully treated, realistically treated on the basis of boat tail limitation (which covers approximately 7/9th of fully treated area), and partially treated (which covers approximately 4/9th of fully treated area), respectively, with 0.5"-thick nickel based metal foam with a 37% porous facesheet (designated as FM). Figures 7-1 through 7-3 show the exact location of the treatment and the exact area covered by the treatment for these three configurations. The treatment areas are shaded in these figures. The acoustic treatment areas for the three treated configurations are listed in the following table:

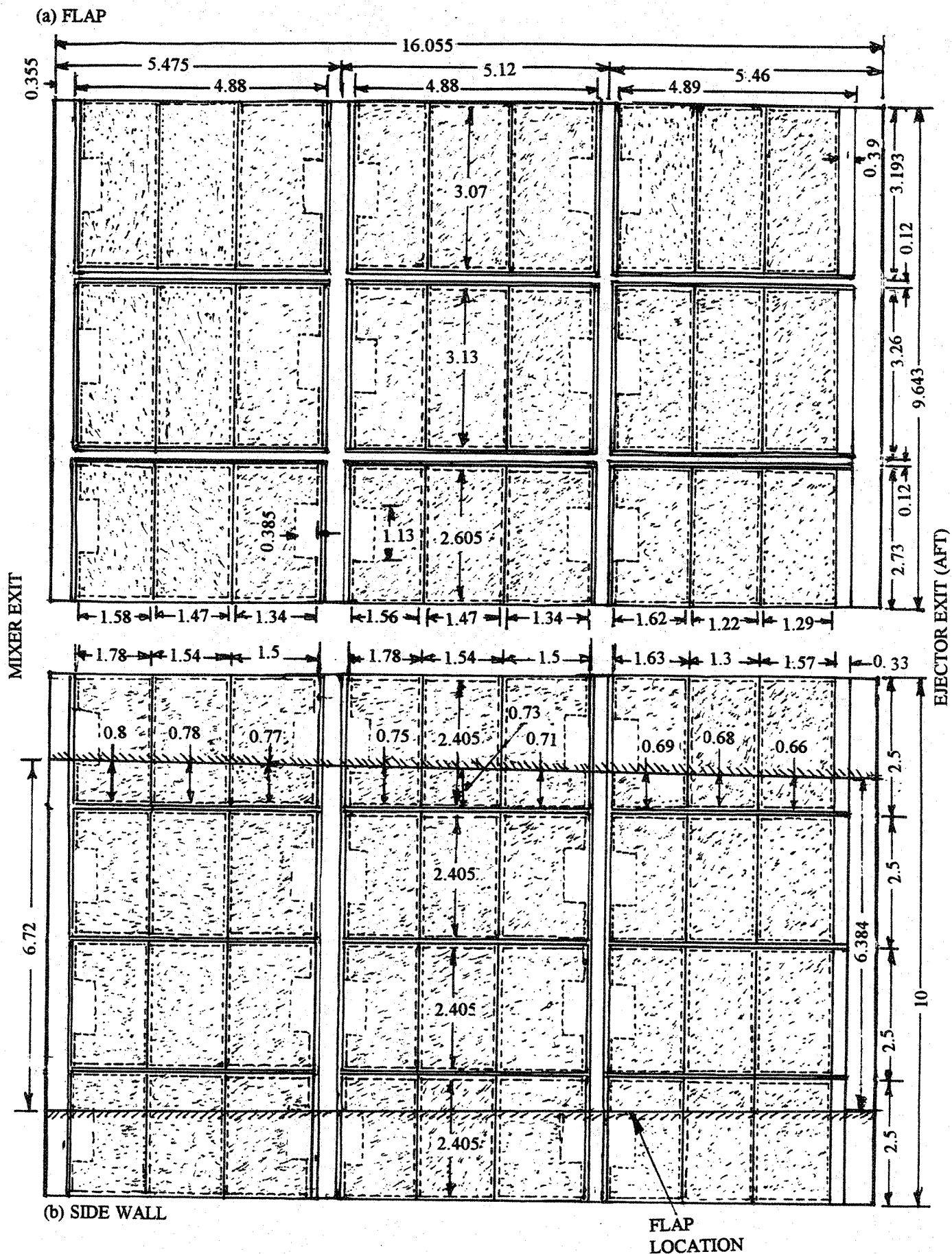| Configuration Definition	Ejector Area (in^2)	Treatment Area (in^2)	% wrt Ejector Area	% wrt Full treatment
Hard wall Configuration	529.65	0	100	144.3
Fully Treated	529.65	366.985	69.3	100
7/9th Treated	529.65	269.670	50.9	73.5
4/9th Treated	529.65	145.980	27.6	39.6

Figure 7-1. Fully treated flap and side wall surfaces for a long ejector, MAR=0.95 (all dimensions are in inches).
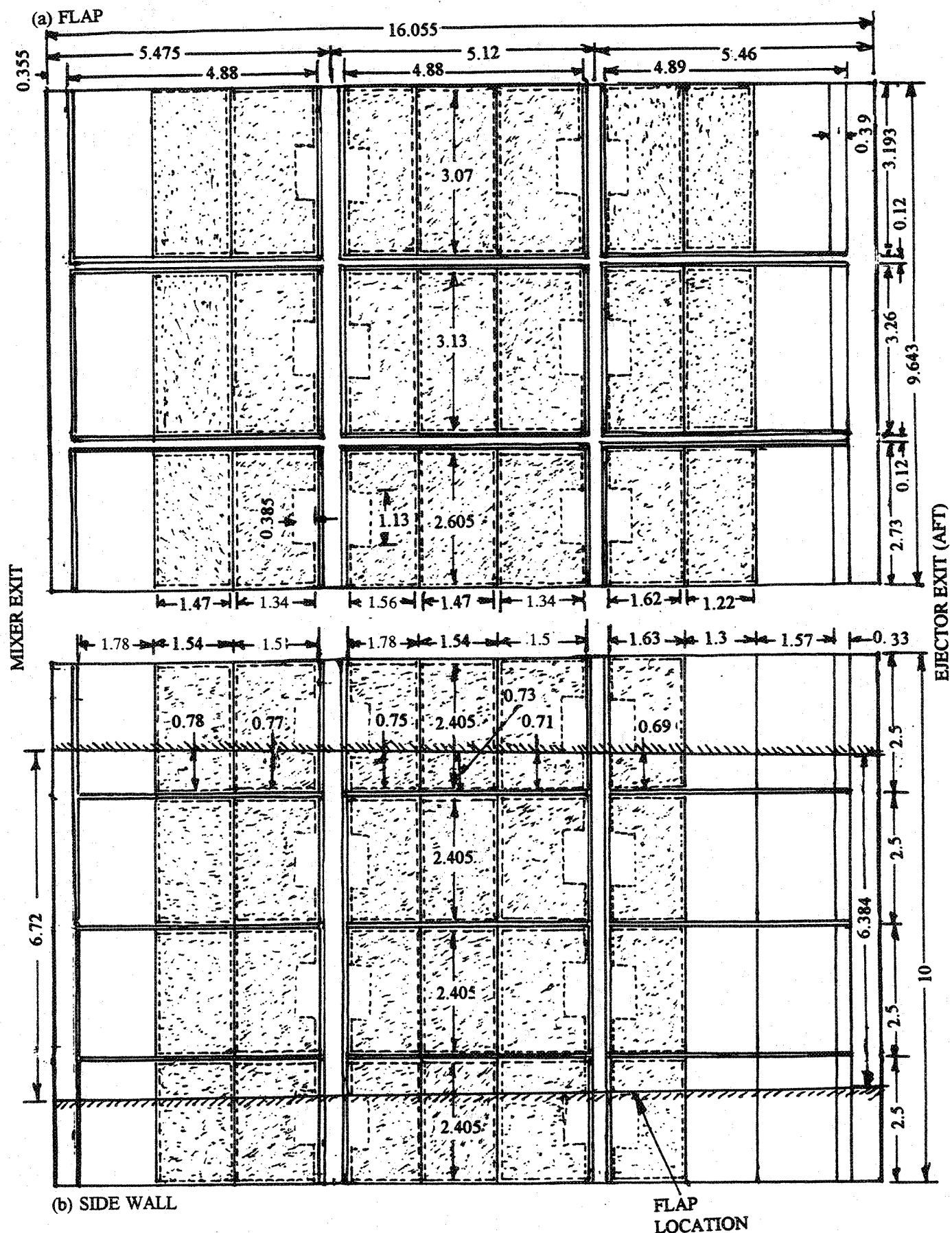
Figure 7-2. Boat tail limited (i.e., approximately 7/9th of full treatment) treated flap and side wall surfaces for a long ejector, MAR=0.95 (all dimensions are in inches).
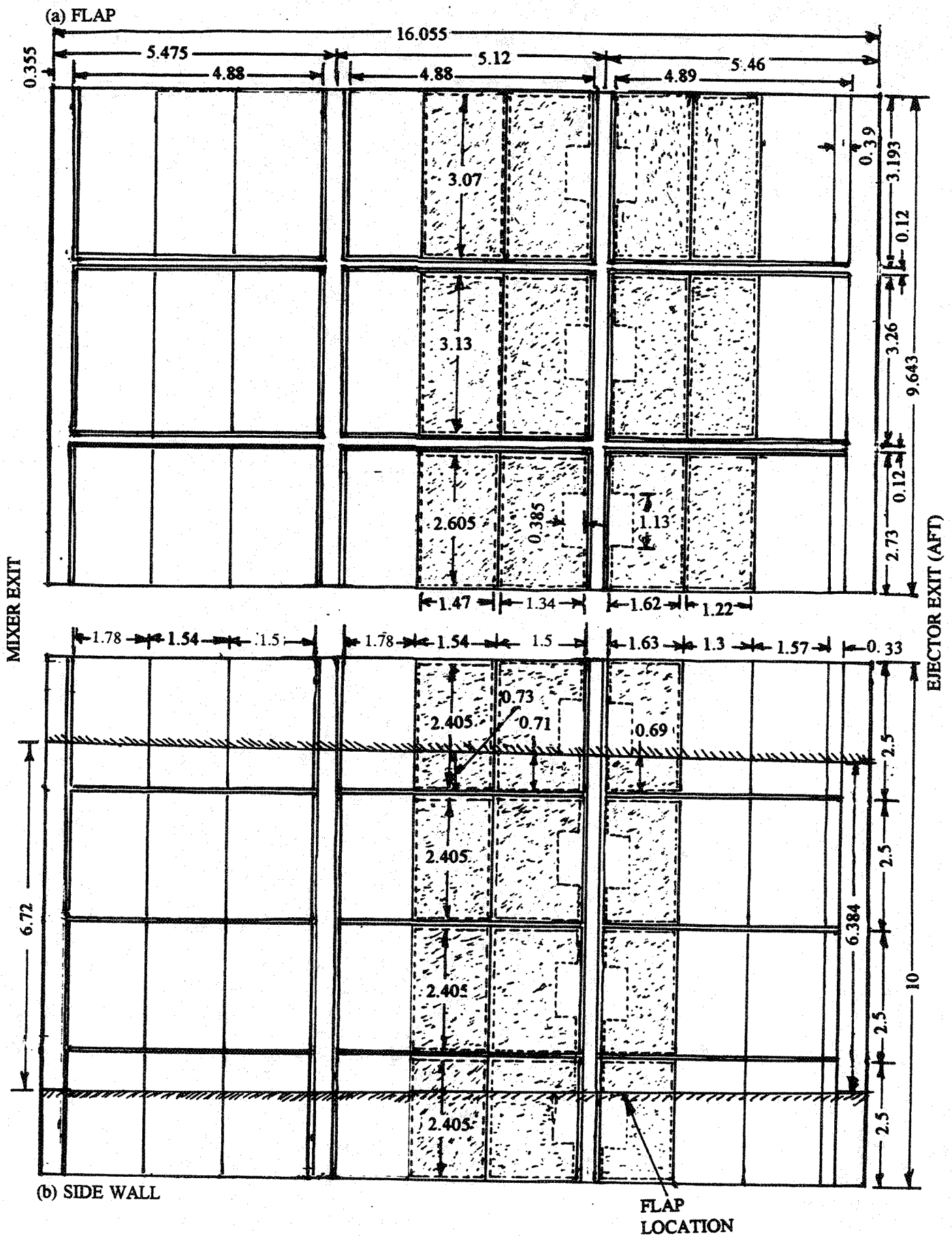
Figure 7-3. Partially (i.e., approximately 4/9th of full treatment) treated flap and side wall surfaces for a long ejector, MAR=0.95 (all dimensions are in inches).

Since the % of actual treatment for the partially treated configurations with respect to fully treated case are 73.5% and 39.6%, which are close to 7/9 and 4/9, these configurations are identified as 7/9 treatment and 4/9 treatment.

7.1.1 Acoustic Results:

The farfield acoustic results for the sideline azimuthal location relative to major axis (i.e., at $\phi=25°$), at a slant distance of 1629', at static and with flight simulation ($M_F=0.32$) are presented in this section. Figure 7-4 shows the effect of ejector treatment area on EPNL, peak PNLT, and PNLT at various polar angles (θ) as functions of jet velocity (V_j). At jet velocities at and below 2400 ft/sec the EPNL levels are lower for treated configurations compared to the hard wall configuration. The effect of treatment area is observed more distinctly at lower velocities, especially below 1900 ft/sec, that the EPNL levels decrease with increasing treatment area. Similar trends are observed with respect to PNLT.

Effect of ejector treatment area on PNLT directivities at jet velocities of 1147, 1400, 1920, 2384, and 2637 ft/sec are shown in Figure 7-5. The PNLT levels decrease with increasing treatment area at most polar angles and at all the velocities. However, the effect is more significant at lower velocities and at mid polar angles. Effect of ejector treatment area on SPL spectra at various polar angles (θ) for each of the above mentioned five jet velocities are shown in Figures 7-6 through 7-10. Noise suppression due to acoustic treatment in terms of SPL is observed at higher frequencies for most polar angles and the suppression level increases with increasing treatment area. The effect of treatment area on SPL seems to be less significant at higher velocities (see Figures 7-9 and 7-10).

In general, the noise suppression, as measured in the farfield, due to acoustic treatment on the ejector increases with increasing treatment area. However, the effect is insignificant at higher velocities above 2400 ft/sec. The noise measured in the farfield is the sum total of noise propagated out of the ejector (i.e., internal noise) and the noise generated exterior to the ejector (i.e., external noise). If the external noise level is much higher compared to internal noise propagating out of the ejector, then the total noise measured in the farfield will be less influenced by changes in the internal noise. The results shown here are indicative of the fact that the internal noise is higher or comparable to the external noise at lower velocities. Hence, the increasing internal noise suppression due to increasing
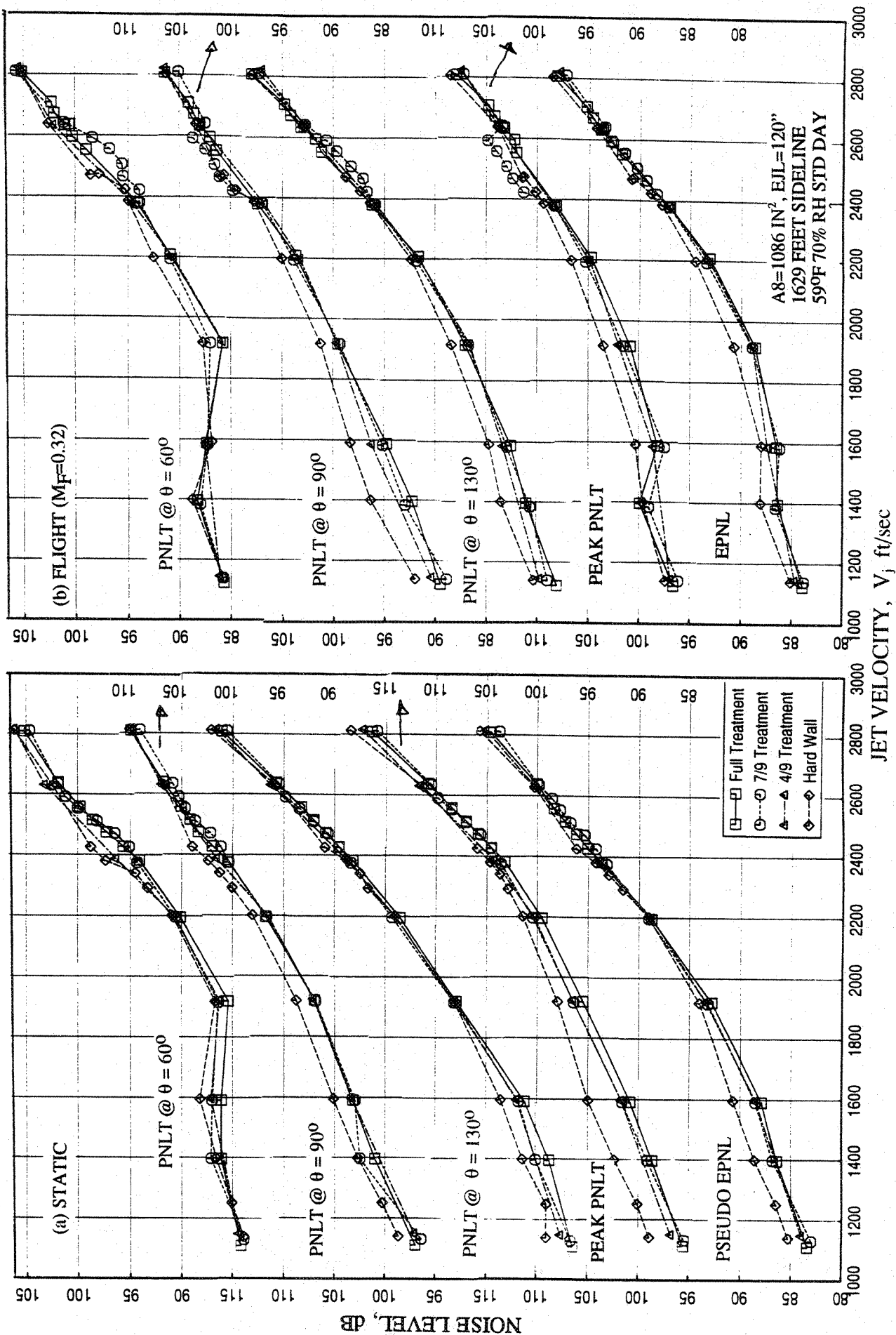
Figure 7-4. Effect of treatment area on EPNL, peak PNLT, and PNLT at various polar angles (θ) as functions of jet velocity for a 10 and 9 full staggered CD-chute mixer with long ejector; SAR=2.8, MAR = 0.95.
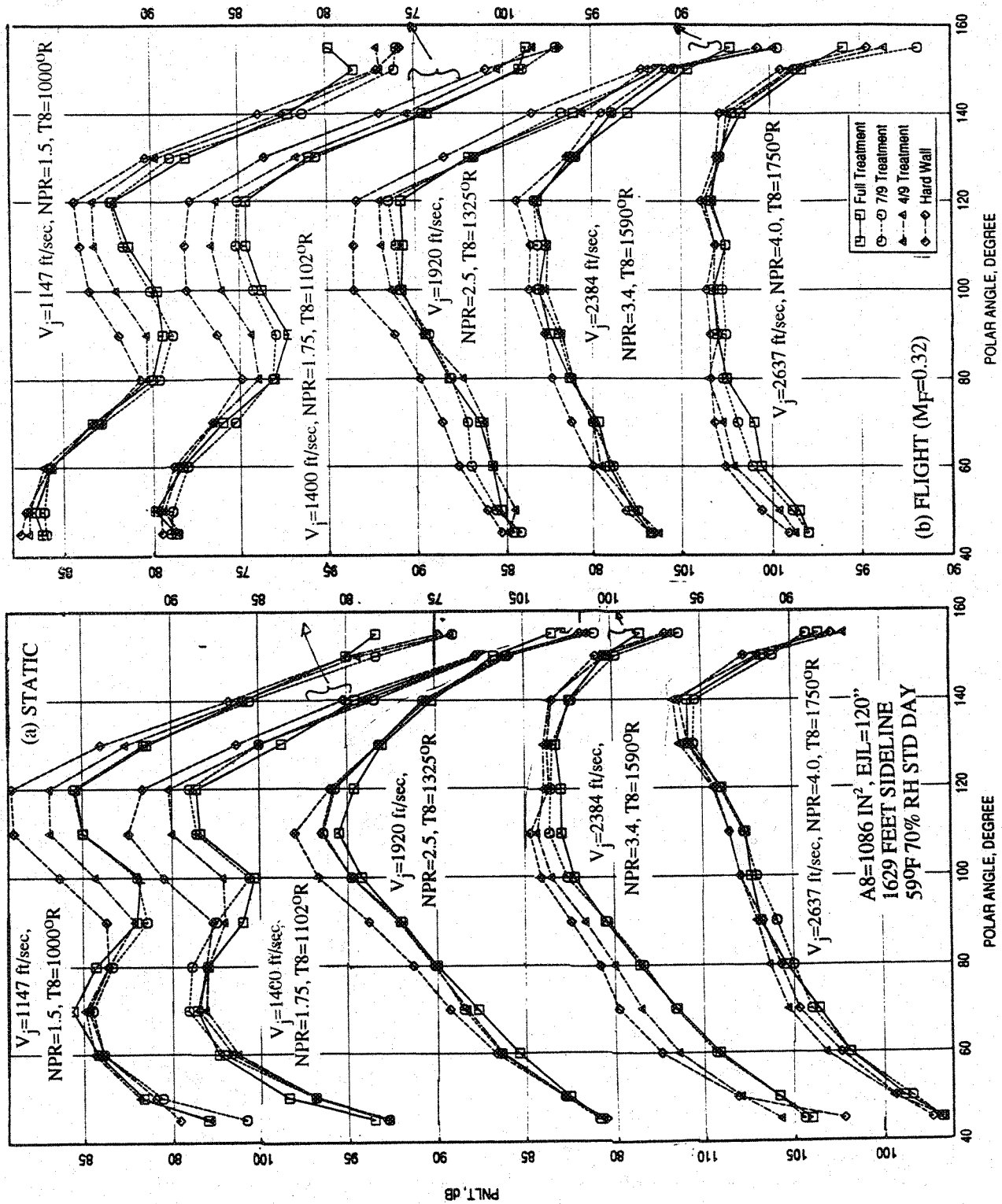
Figure 7-5. Effect of treatment area on PNLT directivities for different jet velocities (V_j) for a 10 and 9 full staggered CD-chute mixer with long ejector; SAR=2.8, MAR = 0.95.
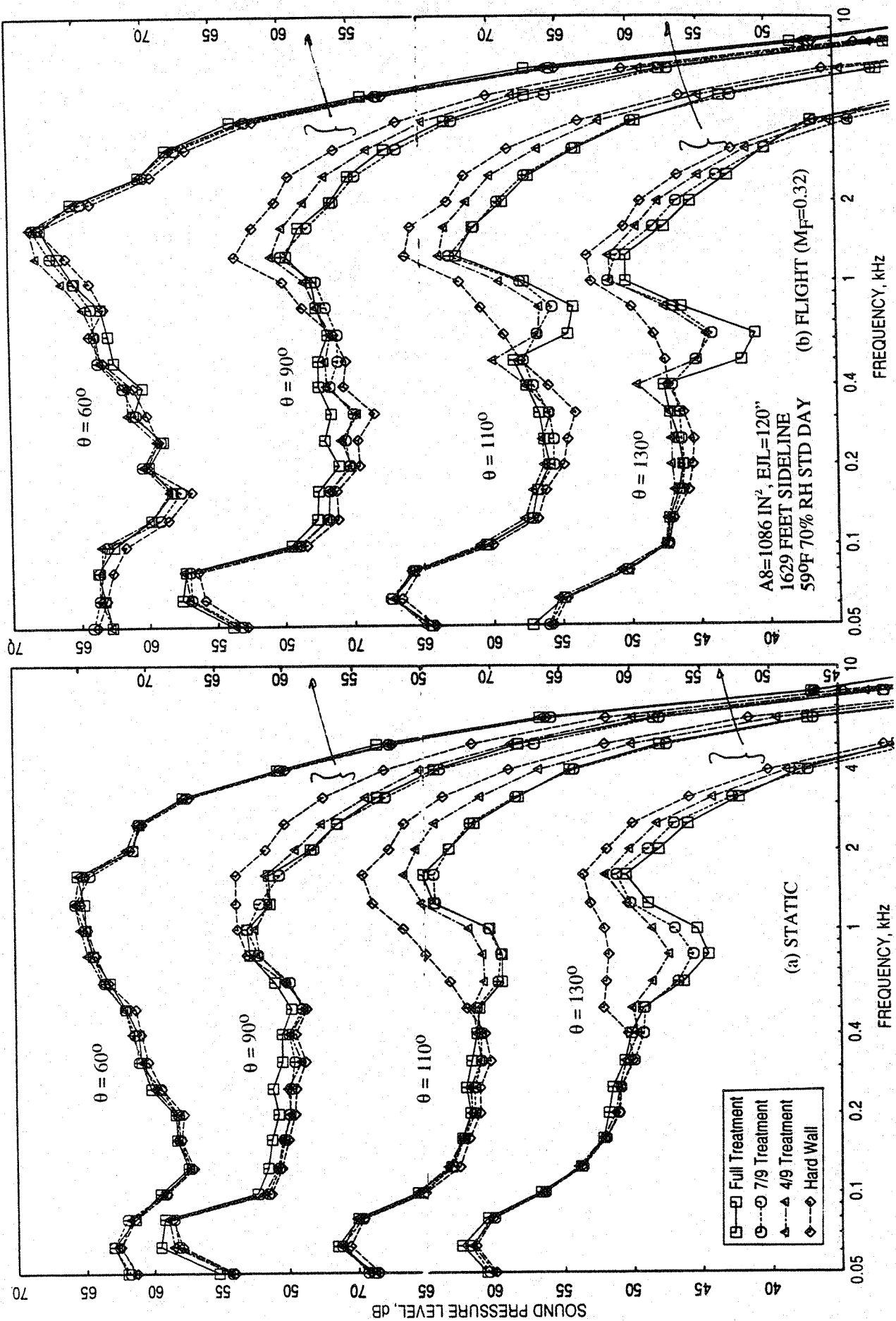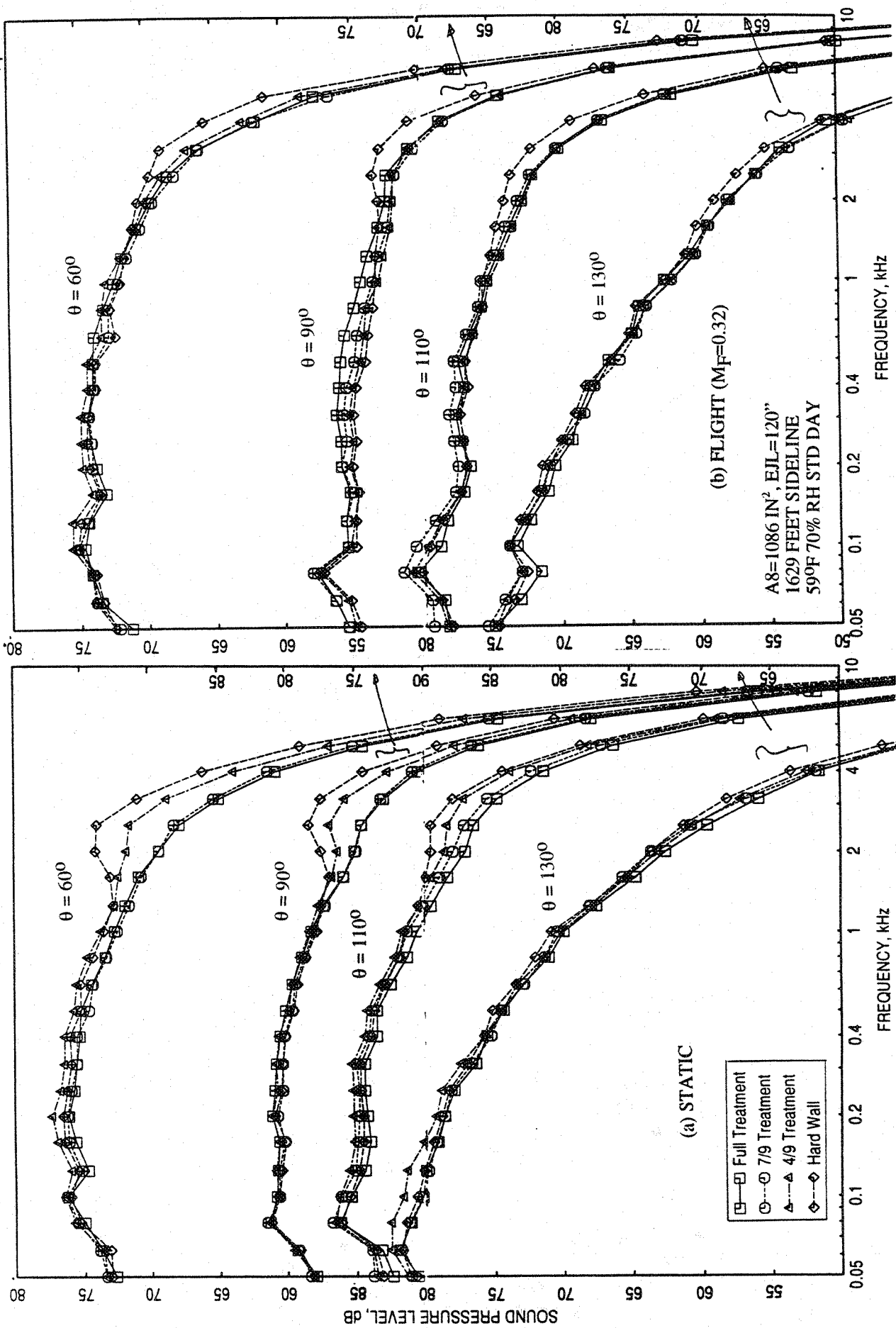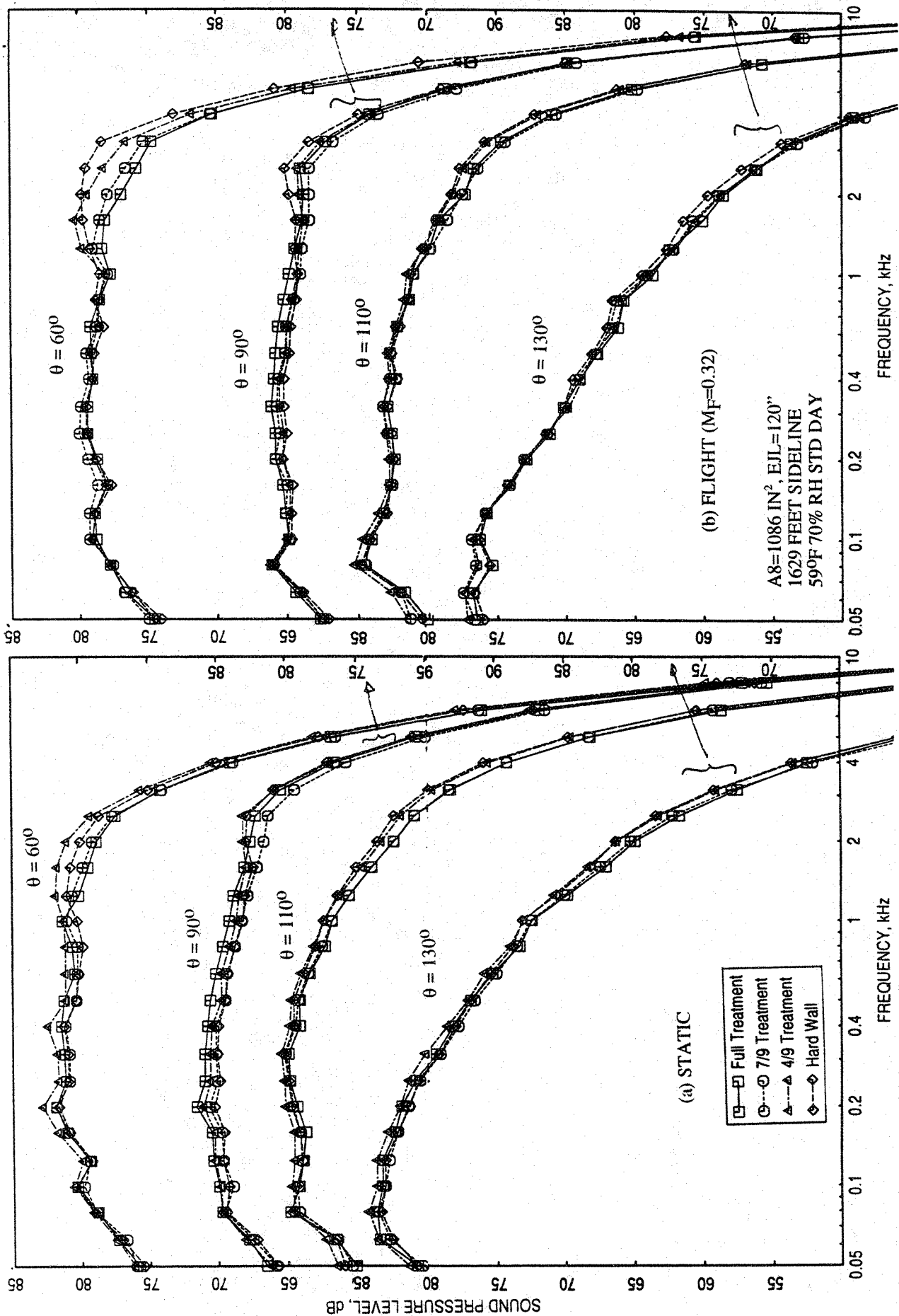
Figure 7-6. Effect of treatment area on SPL spectra at various polar angles (θ) for a 10 and 9 full staggered CD-chute mixer with long ejector; SAR=2.8, MAR = 0.95, V_j = 1147 ft/sec, NPR = 1.5, T8 = 1000°R.
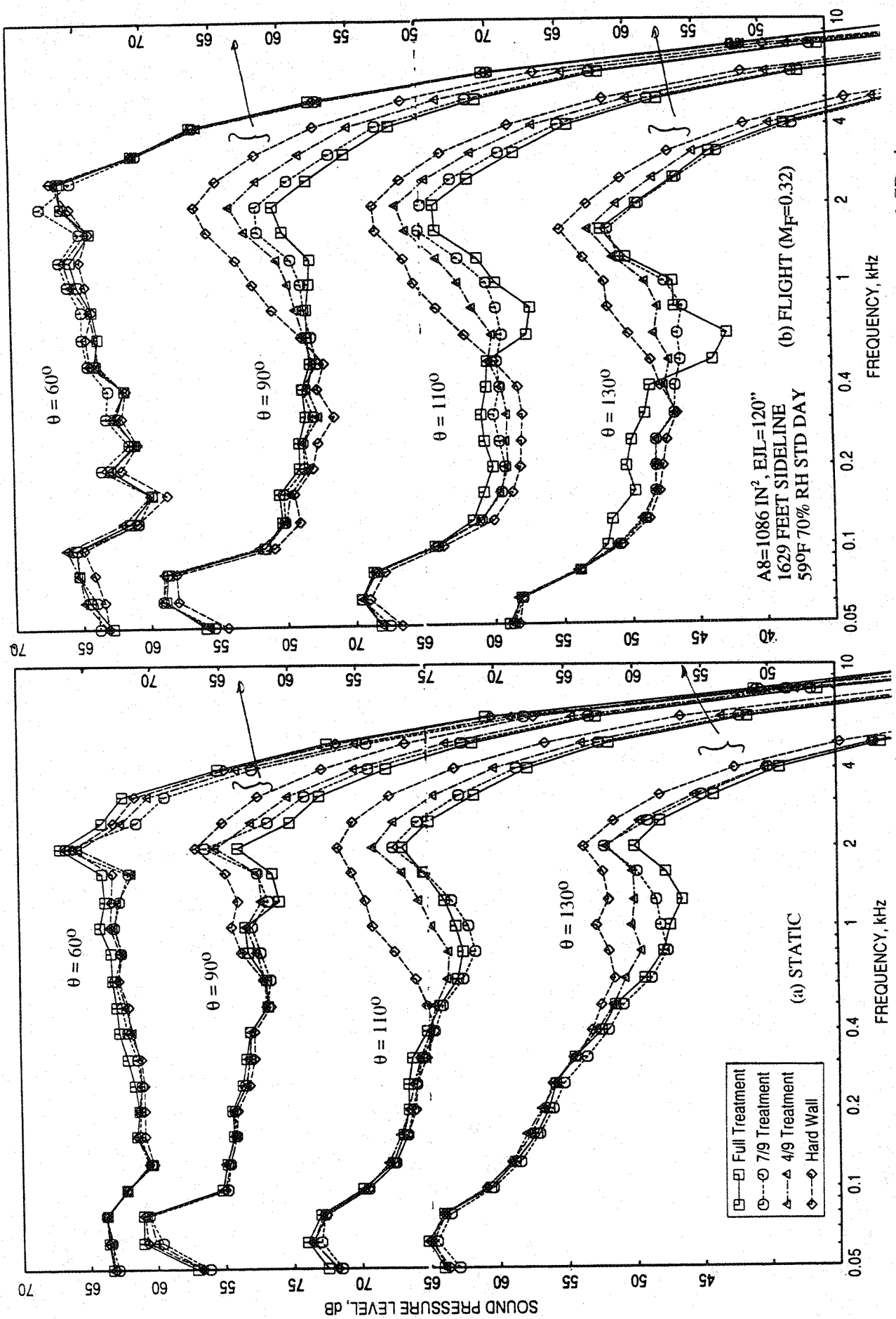
Figure 7-7.   Effect of treatment area on SPL spectra at various polar angles (θ) for a 10 and 9 full staggered CD-chute mixer with long ejector; SAR=2.8, MAR = 0.95, V_j = 1400 ft/sec, NPR = 1.75, T8 = 1120°R.
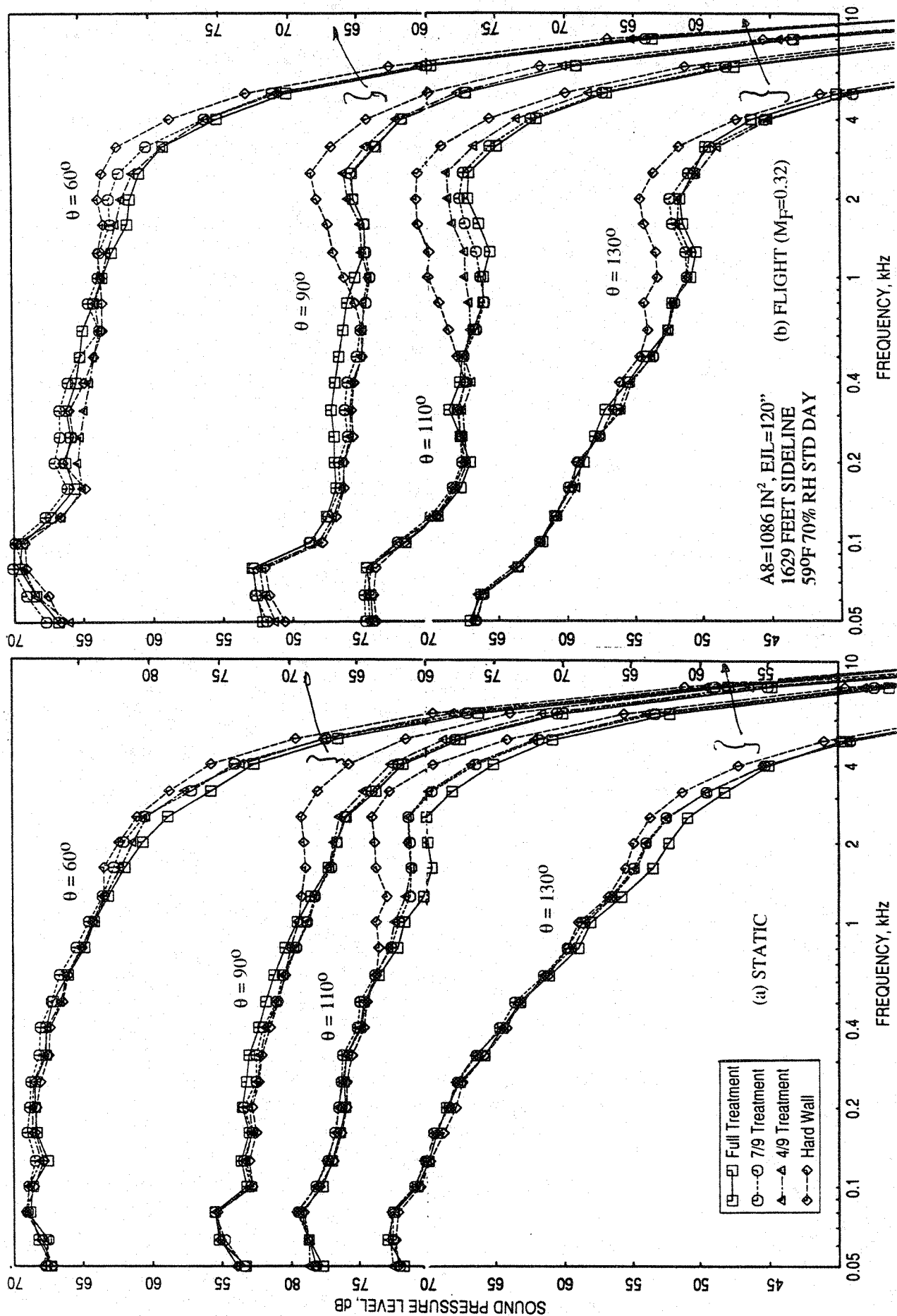
Figure 7-8. Effect of treatment area on SPL spectra at various polar angles (θ) for a 10 and 9 full staggered CD-chute mixer with long ejector; SAR=2.8, MAR = 0.95, V_j = 1919 ft/sec, NPR = 2.5, T8 = 1325°R.

Figure 7-9. Effect of treatment area on SPL spectra at various polar angles (θ) for a 10 and 9 full staggered CD-chute mixer with long ejector; SAR=2.8, MAR = 0.95, $M_F = 0.32$, $V_j = 2384$ ft/sec, NPR = 3.4, T8 = 1590°R.

Figure 7-10. Effect of treatment area on SPL spectra at various polar angles (θ) for a 10 and 9 full staggered CD-chute mixer with long ejector; SAR=2.8, MAR = 0.95, Vⱼ = 2637 ft/sec, NPR = 4.0, T8 = 1750ºR.

treatment area is observed from the farfield results for lower jet velocities. However, at higher velocities, the external noise seems to be higher compared to internal noise, and hence the influence of treatment area is insignificant in the farfield results.

7.1.2 Flow and Performance Related Parameters:

The effect of ejector treatment area on ramp and chute static pressure distributions are insignificant for static as well as with flight simulation. The chute loading coefficients due to chute static pressure distributions showing the effect of ejector treatment area are plotted against NPR in Figure 7-11. Again the effect is insignificant. The effect of ejector treatment area on pumping and corrected pumping is shown in Figures 7-12 and 7-13 for static and flight cases, respectively. With respect to increasing NPR the pumping decreases. However, the pumping increases slightly with reduced treatment area.

Figure 7-14 illustrates the effect of ejector treatment area on axial static pressure distributions on the flap at static condition at different L1M cycle conditions. Insignificant difference in pressure distributions with respect to treatment area is observed at lower NPRs. At higher NPRs the static pressure distribution on the flap indicates delayed mode switch with increasing treatment area. Figure 7-15 shows the effect of ejector treatment area on force and moment of force with respect to flap leading edge due to static pressure difference on flap surface as a function of nozzle pressure ratio. Both the force and the moment are lower for fully and 7/9th treated ejector at higher NPRs. The transition from subsonic to supersonic mode seems to be slightly delayed with respect to increasing treatment area. Similar results with flight simulation are plotted in Figures 7-16 and 7-17. The static pressure distributions between the mixer configurations clearly indicate that the mode switch is delayed for 7/9th treated ejector configuration. Similar conclusions are deduced from the force and moment of the force results, as shown in Figure 7-17.

7.2 EFFECT OF TREATMENT THICKNESS:

Results, showing the effect of ejector treatment thickness, include four configurations, one without any treatment (i.e., configuration #12) and three treated configurations. For the treated configurations (i.e., #23, 18, and 20), the flaps and sidewalls were realistically treated on the basis of boat tail limitation (which covers approximately 7/9th of fully treated area) with nickel based metal foam of thickness 0.5" (i.e., 100% thick), 0.3" (i.e.,
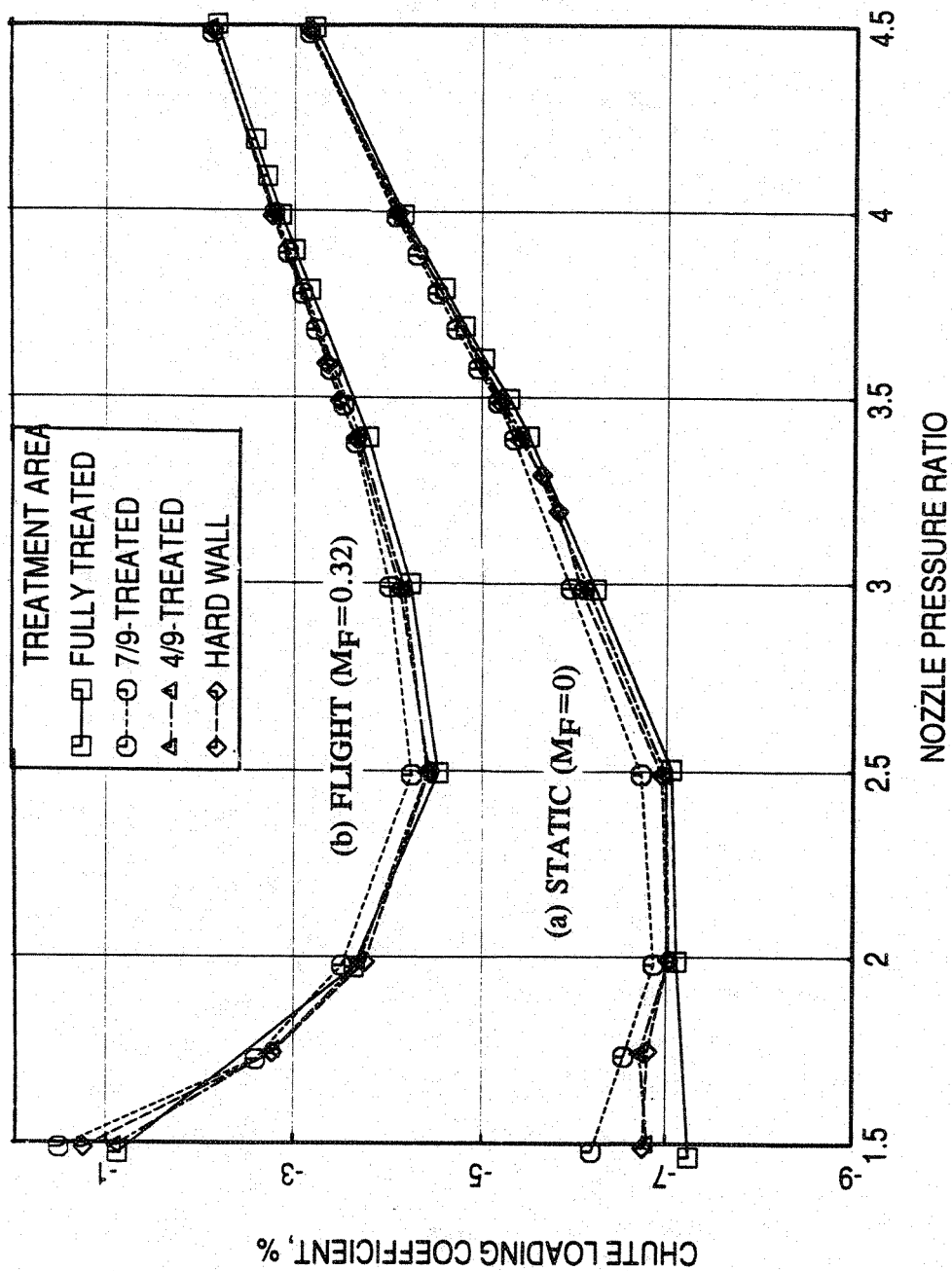
Figure 7-11. Effect of treatment area on chute loading coefficient with respect to nozzle pressure ratio for a 10 and 9 full staggered CD-chute mixer long ejector for L1M cycle conditions (a) at static condition and (b) with flight simulation (M_F=0.32).
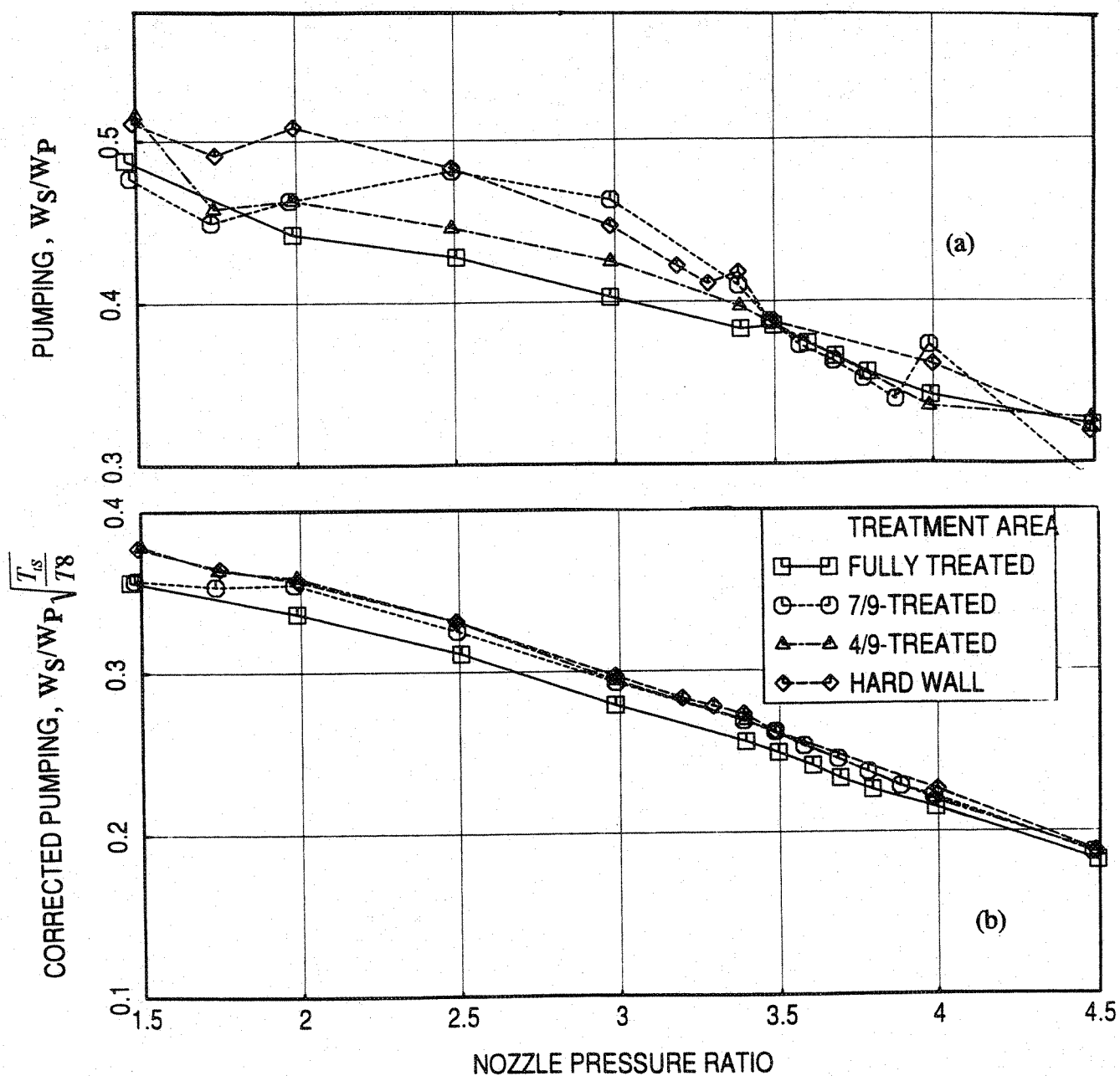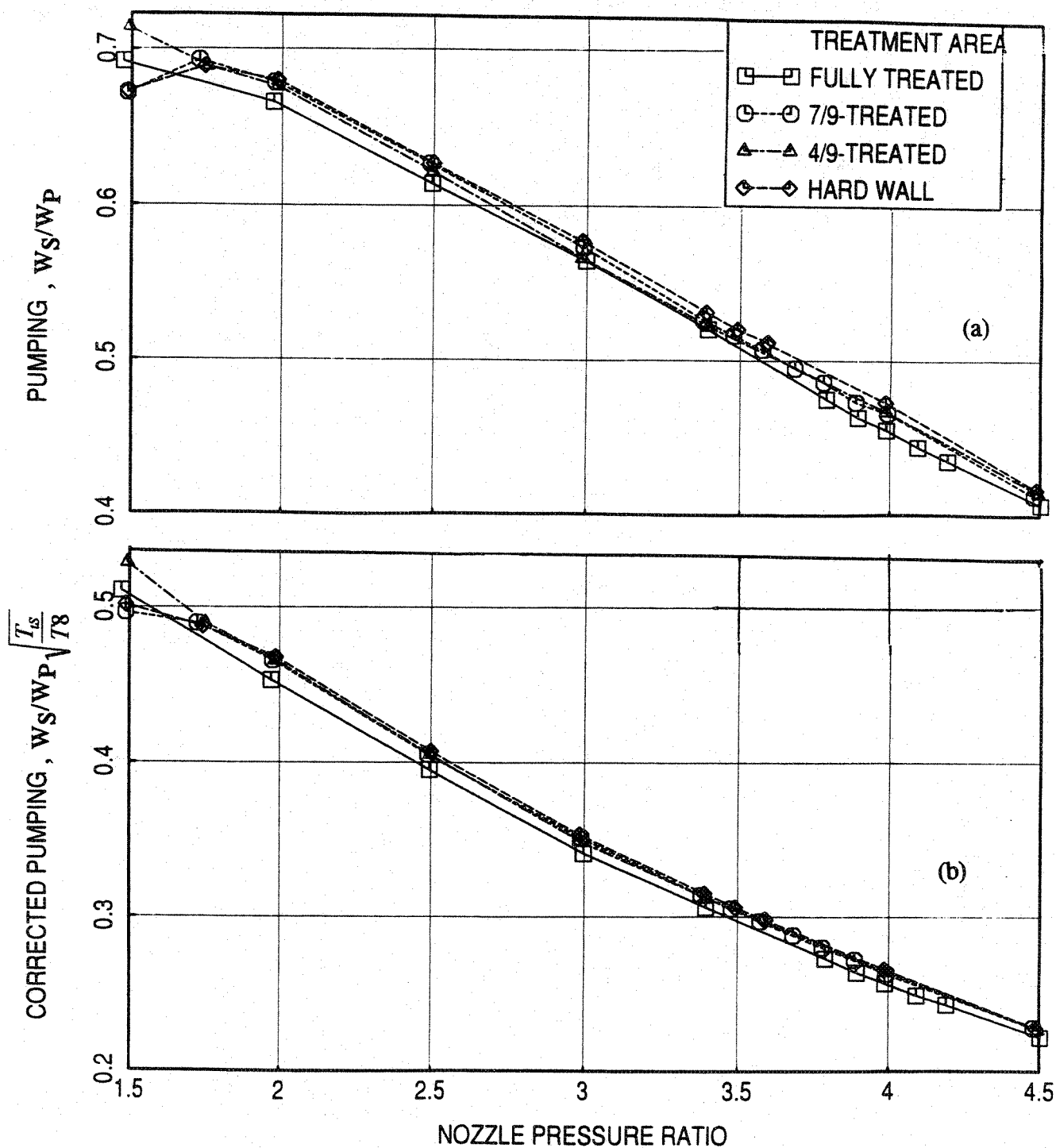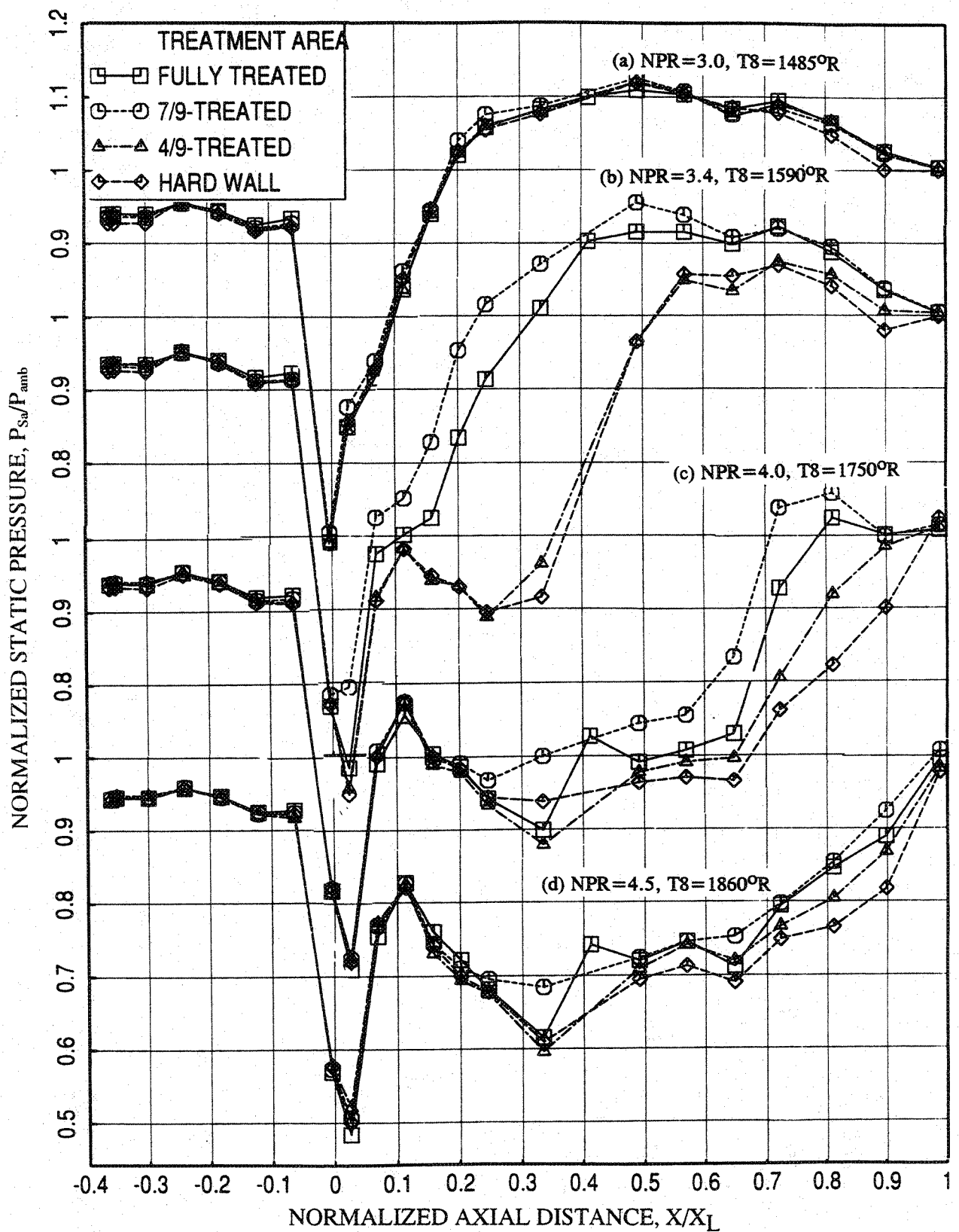
Figure 7-12. Effect of treatment area on pumping with respect to nozzle pressure ratio for a 10 and 9 full staggered CD-chute mixer with long ejector for L1M cycle conditions at static condition.

Figure 7-13. Effect of treatment area on pumping with respect to nozzle pressure ratio for a 10 and 9 full staggered CD-chute mixer with long ejector for L1M cycle conditions with flight simulation (M_F=0.32).
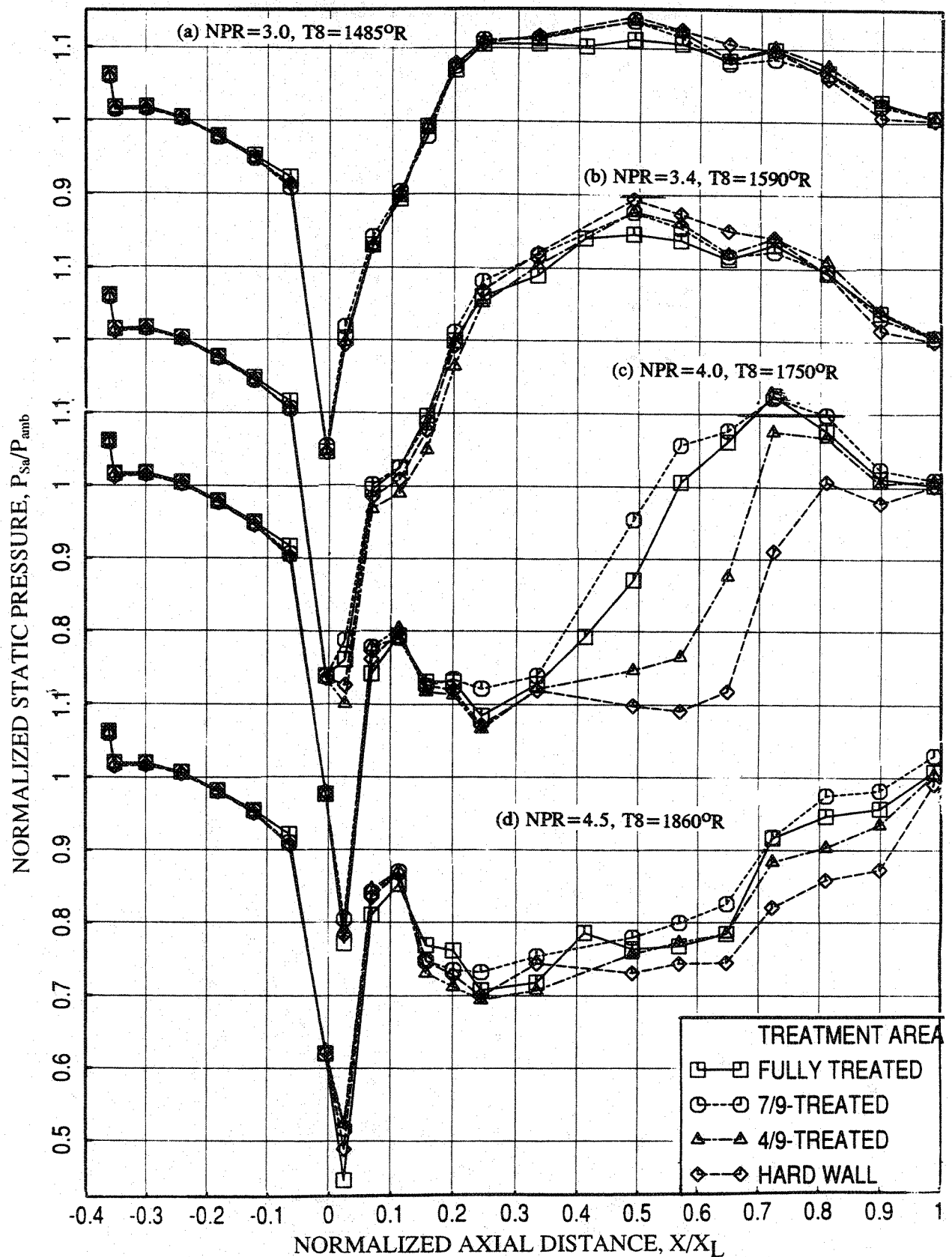
Figure 7-14. Effect of treatment area on axial distribution of average static pressure on the inlet and the flap surface at different L1M cycle conditions for a 10 and 9 full staggered CD-chute mixer with long ejector at static condition.
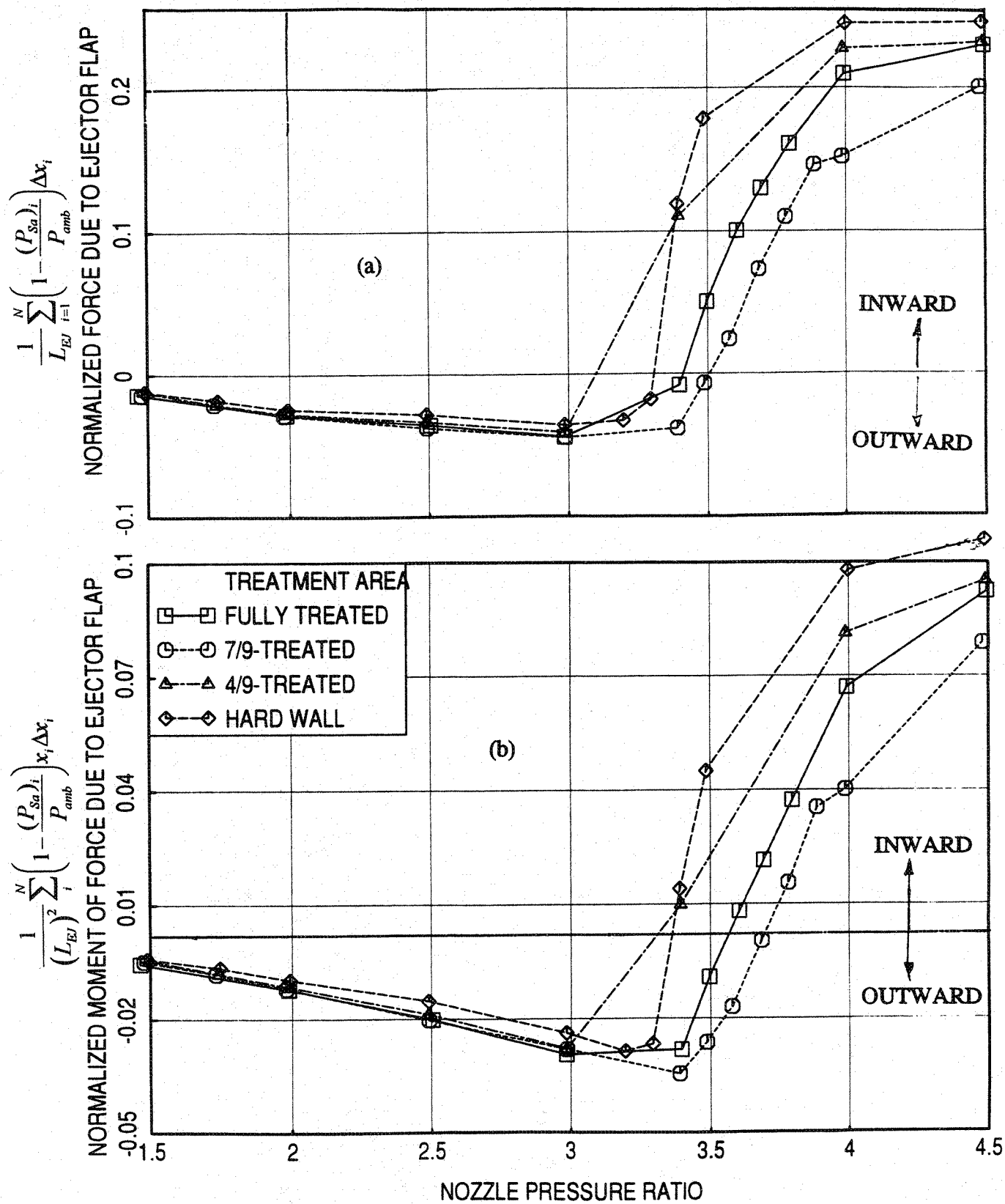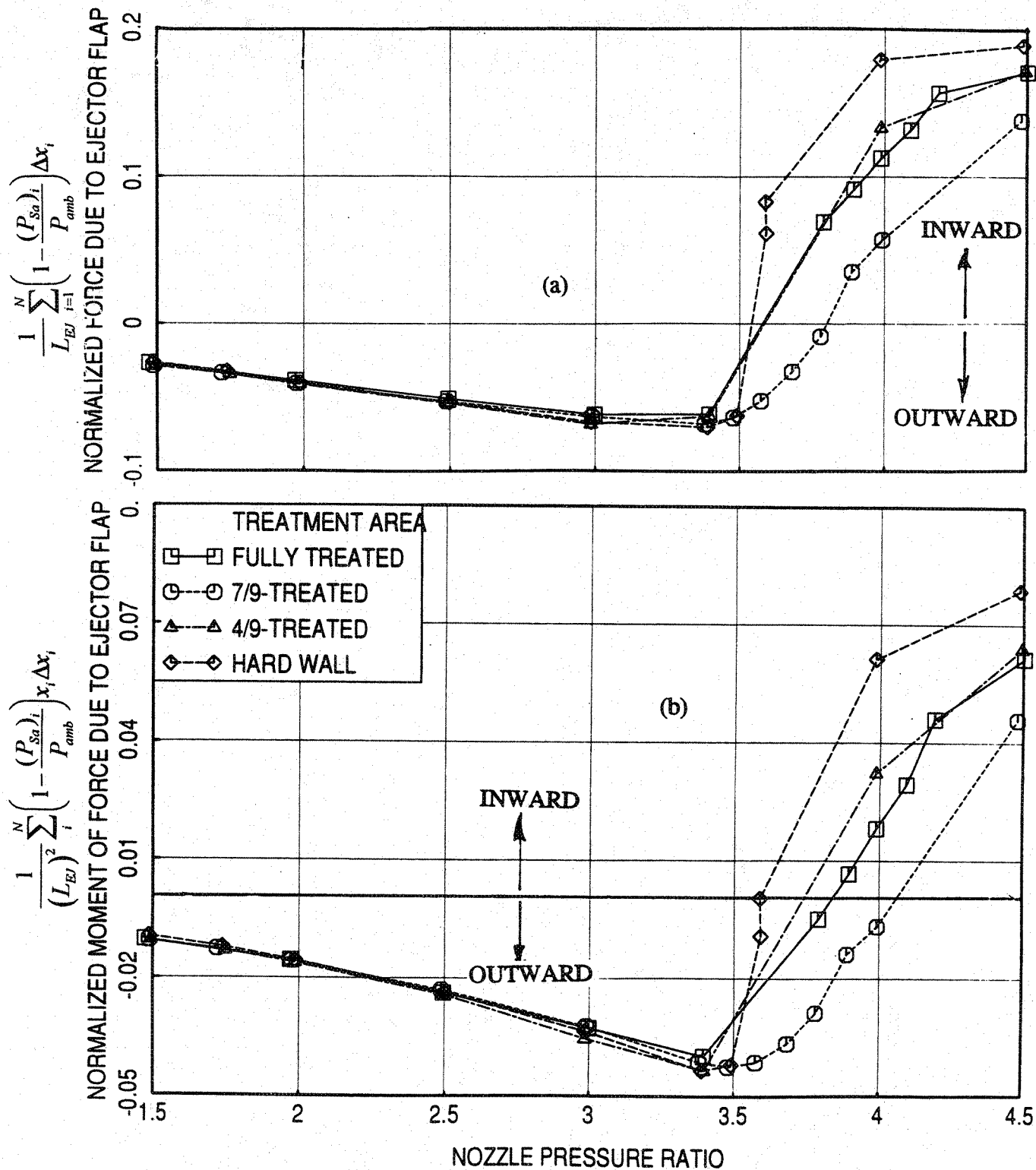
Figure 7-15. Effect of treatment area on normalized (a) force and (b) moment of force due to ejector flap with respect to nozzle pressure ratio for a 10 and 9 full staggered CD-chute mixer with long ejector for L1M cycle conditions at static condition.

Figure 7-16. Effect of treatment area on axial distribution of average static pressure on the inlet and the flap surface at different L1M cycle conditions for a 10 and 9 full staggered CD-chute mixer with long ejector with flight simulation (M_F=0.32).

Figure 7-17. Effect of treatment area on normalized (a) force and (b) moment of force due to ejector flap with respect to nozzle pressure ratio for a 10 and 9 full staggered CD-chute mixer with long ejector for L1M cycle conditions with flight simulation (M_F=0.32).

60% thick), and 0.2" (i.e., 40% thick), respectively, with a 37% porous facesheet (facesheet thickness=0.025" and hole diameter=0.045"). The original foam metal of 0.5" thick was cut into two, with thickness of 0.3" and 0.2". A stainless steel sheet metal was used between these two parts of the foam metal treatment while mounted on the ejector surfaces. Based on the foam metal piece exposed to the ejector flow acoustic data was obtained for 0.3" and 0.2" thick treatments.

7.2.1 Acoustic Results:

The normal impedance spectra for the nickel based foam metal of different thicknesses (with 37% porous facesheet) were measured at room temperature by using 0.6" diameter samples and are compared in Figure 7-18. The actual levels of resistance and reactance would be different at the operating condition of the ejector. In general, the specific resistance is likely to increase and the reactance is slightly to decrease due to grazing flow. At the same time, some decrease in resistance is expected due to temperature increase. However, the impedance results of Figure 7-18 is a relative comparison between the same treatment with different thickness at the same condition. At low frequencies, below 5 kHz the resistance decreases with bulk thickness. The reactance increases with increasing bulk thickness up to about 10 kHz. Beyond this frequency 0.5"-thick treatment shows a sudden decrease of reactance. Also, the resistance for 0.5" treatment increases with frequency up to about 10 kHz and then decreases with a peak at about 11 kHz. This is due to the anti-resonant frequency of the 0.5" deep cavity at room temperature. For 0.3" treatment the anti-resonance occurs at about 18 kHz, at which a resistance peak is observed. Based on the reactance variation with the frequency the thicker treatment attains the desired level of zero at a lower frequency. For thinner bulk samples, the zero reactance is attained at a much higher frequency. A resistance level of about 1.5 to 2.0 with a reactance level between -0.5 and 0 is the optimum condition for better acoustic suppression. Based on the normal impedance results, the 0.5"-thick foam metal was expected to perform better for lower (i.e., 3 to 6 kHz) and at higher (i.e., 9 to 17 kHz) frequency ranges due to its near optimum reactance levels. In the same manner, the 0.3" and 0.2" treatments were expected to perform better at frequency ranges of 7 to 10 and 8 to 12 kHz, respectively.

It should be noted that the scale model frequency is plotted in Figure 7-18, whereas, the full scale frequencies to be compatible with the acoustic results, will be 1/7-times of these
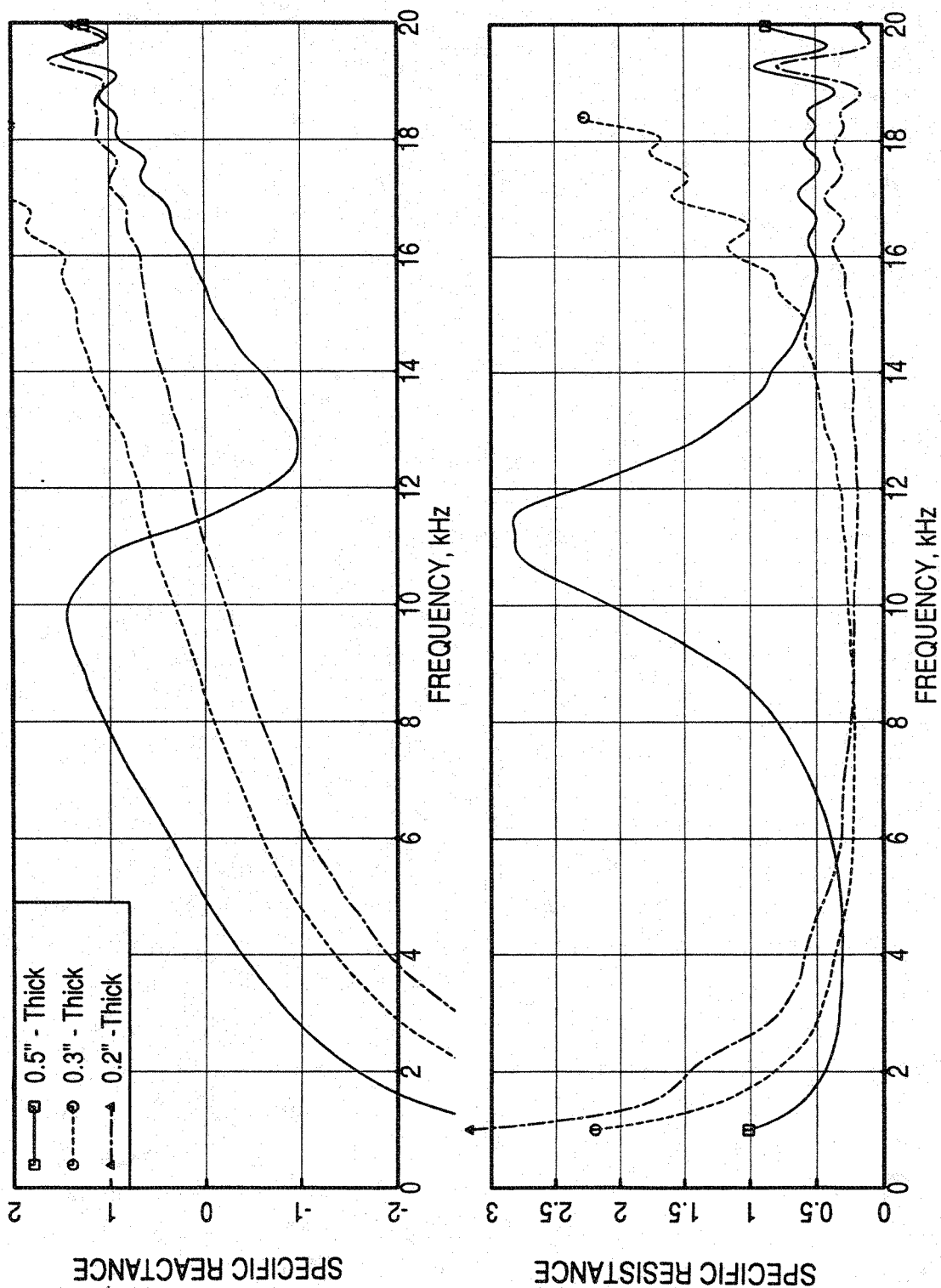
Figure 7-18. Effect of Nickel Foam (bulk material) depth on the normal acoustic impedance of the ejector treatment (with the 37% open perforated facesheet, thickness=0.025", hole diameter=0.045") at room temperature, excitation OASPL = 150 dB.

values. The farfield noise level is relatively higher and crucial in terms of EPNL in the frequency range of 2 to 3.5 kHz. To achieve a better acoustic suppression at this frequency range the 1/7-scale treatment should be effective at a frequency range of 14 to 24 kHz. Based on the impedance results of Figure 7-18, 0.5" treatment is expected to perform slightly better than the other two in the farfield noise suppression in terms of EPNdB.

The farfield acoustic results for the sideline azimuthal location relative to major axis (i.e., at $\phi=25°$), at a slant distance of 1629',) at static and with flight simulation ($M_F=0.32$) are presented in this section. Figure 7-19 shows the effect of ejector treatment thickness on EPNL and PNLT at various polar angles (θ)as functions of jet velocity (V_j). The effect of treatment thickness is distinctly observed at lower velocities, especially below 2400 ft/sec, that the EPNL levels decrease with increasing treatment thickness. For higher jet velocities the effect of treatment is not apparent, since the farfield noise is dominated by external noise (i.e., jet mixing noise). Similar trends are observed with respect to PNLT levels also.

Effect of ejector treatment thickness on PNLT directivities at jet velocities of 1147, 1920, 2384, and 2637 ft/sec are shown in Figure 7-20. The PNLT levels decrease with increasing treatment thickness at most polar angles for lower jet velocities. Effect of ejector treatment thickness on SPL spectra at various polar angles (θ) for each of the above mentioned four jet velocities are shown in Figures 7-21 through 7-24. Noise suppression due to acoustic treatment in terms of SPL is observed at higher frequencies for most polar angles, especially, for lower jet velocities and the suppression level increases with increasing treatment thickness.

In general, the noise suppression, as measured in the farfield, due to acoustic treatment on the ejector increases with increasing treatment thickness. However, the effect is insignificant at higher velocities above 2400 ft/sec. The noise measured in the farfield is the sum total of noise propagated out of the ejector (i.e., internal noise) and the noise generated exterior to the ejector (i.e., external noise). If the external noise level is much higher compared to internal noise propagating out of the ejector, then the total noise measured in the farfield will be less influenced by changes in the internal noise. The results shown here are indicative of the fact that the internal noise is higher or comparable to the external noise at lower velocities. Hence, the increasing internal noise suppression due to increasing treatment thickness is observed from the farfield results for lower jet velocities.
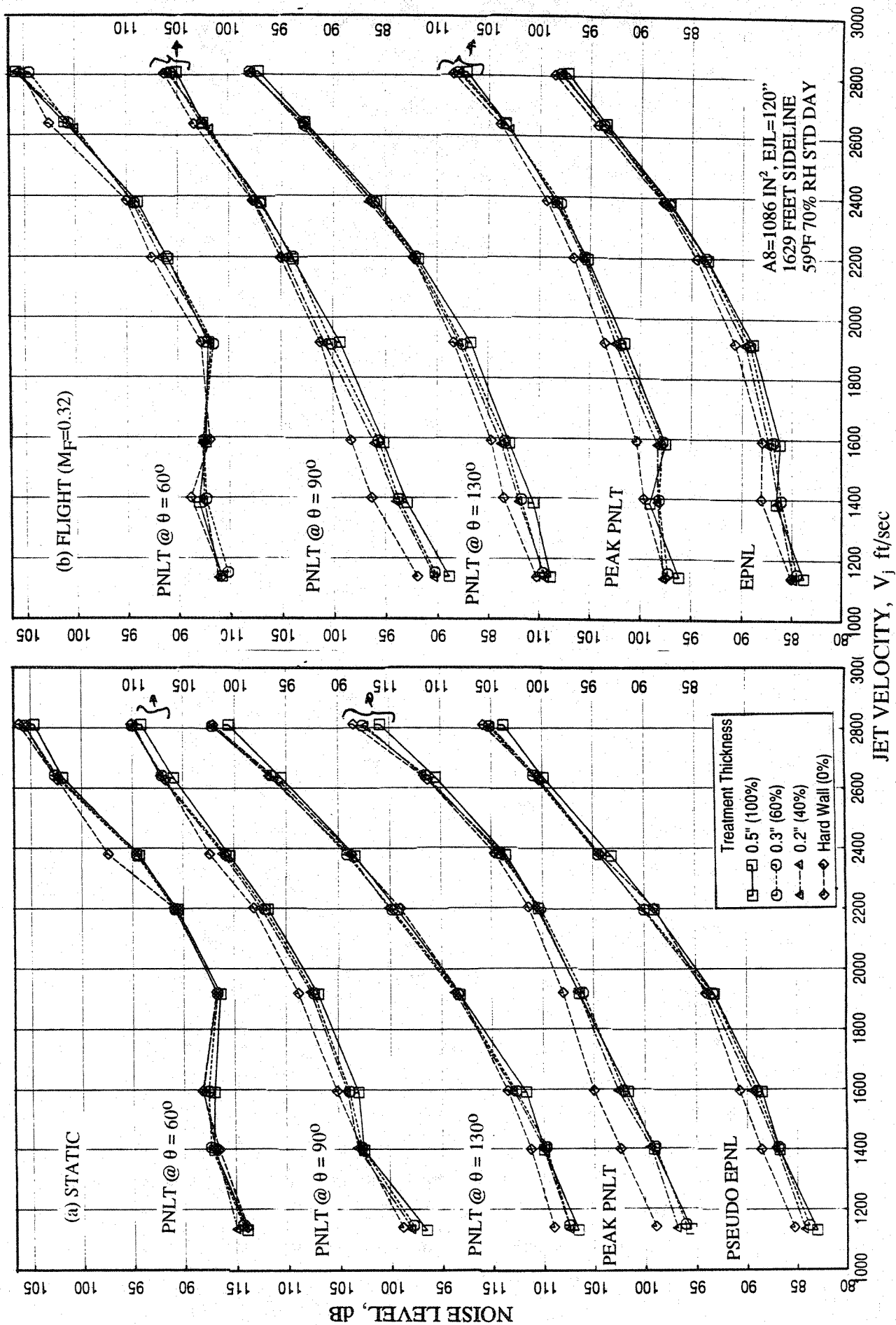
Figure 7-19. Effect of treatment thickness on EPNL, peak PNLT, and PNLT at various polar angles (θ) as functions of jet velocity for a 10 and 9 full staggered CD-chute mixer with long ejector; SAR=2.8, MAR = 0.95.
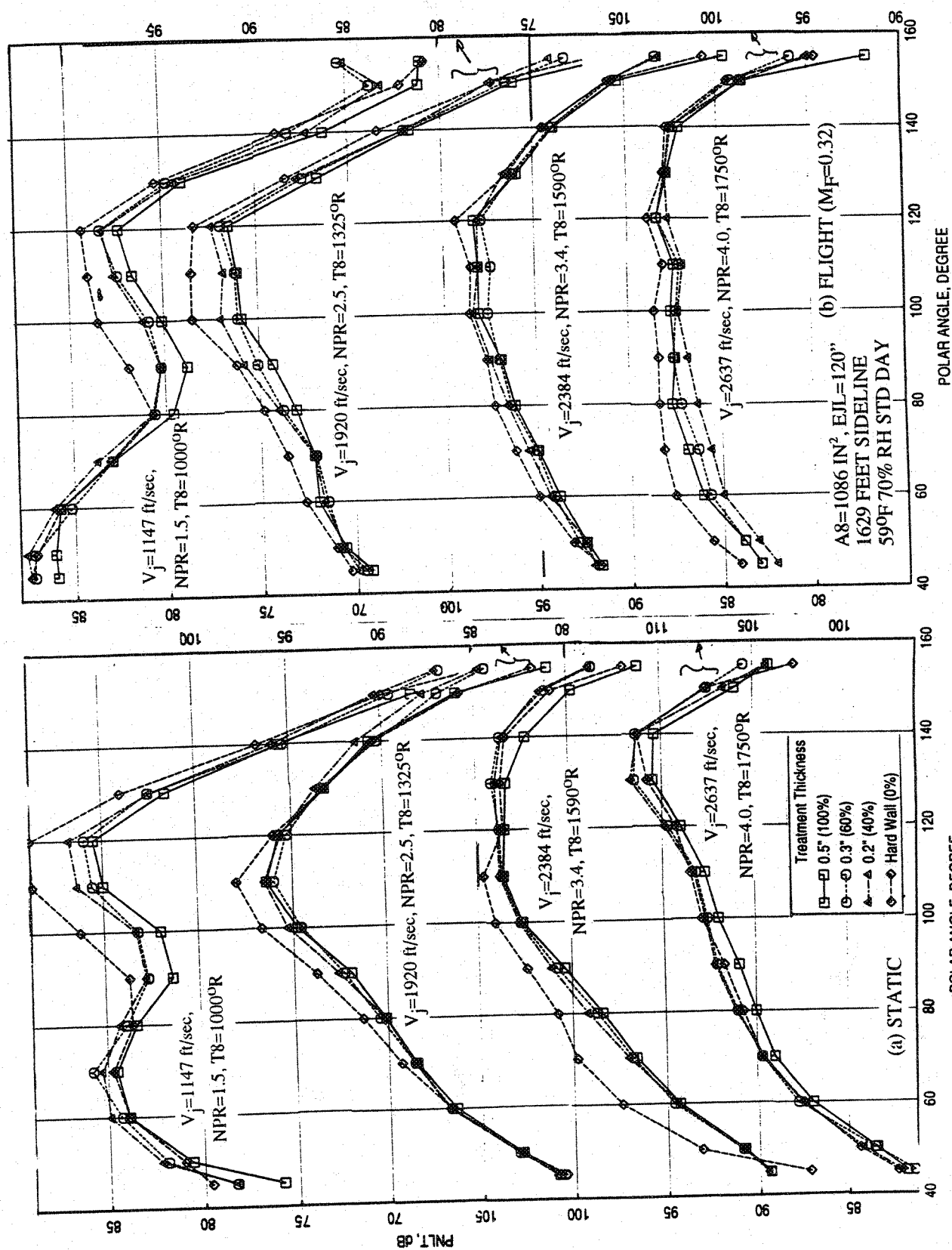
Figure 7-20. Effect of treatment thickness on PNLT directivities for different jet velocities (V_j) for a 10 and 9 full staggered CD-chute mixer with long ejector; SAR=2.8, MAR = 0.95.
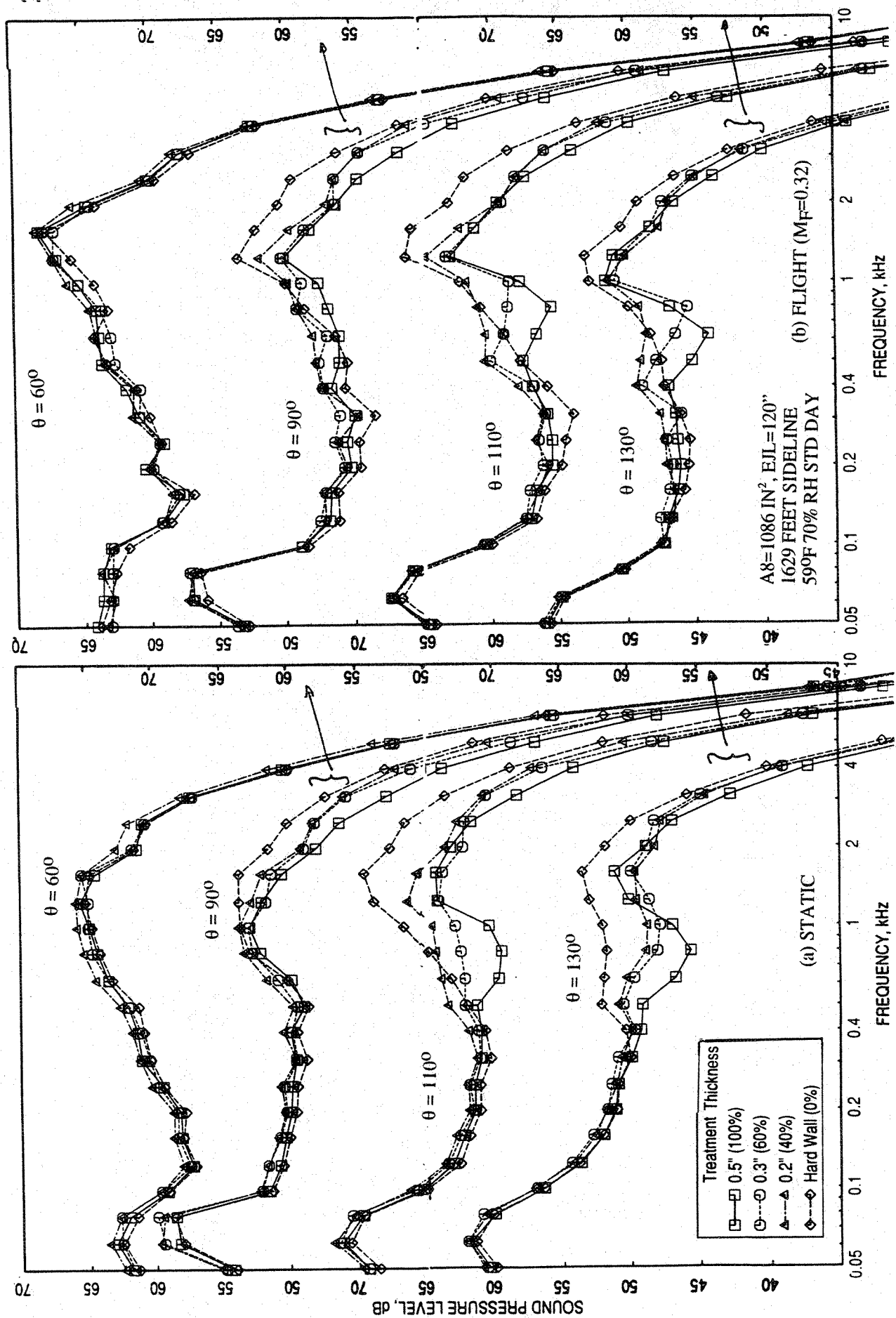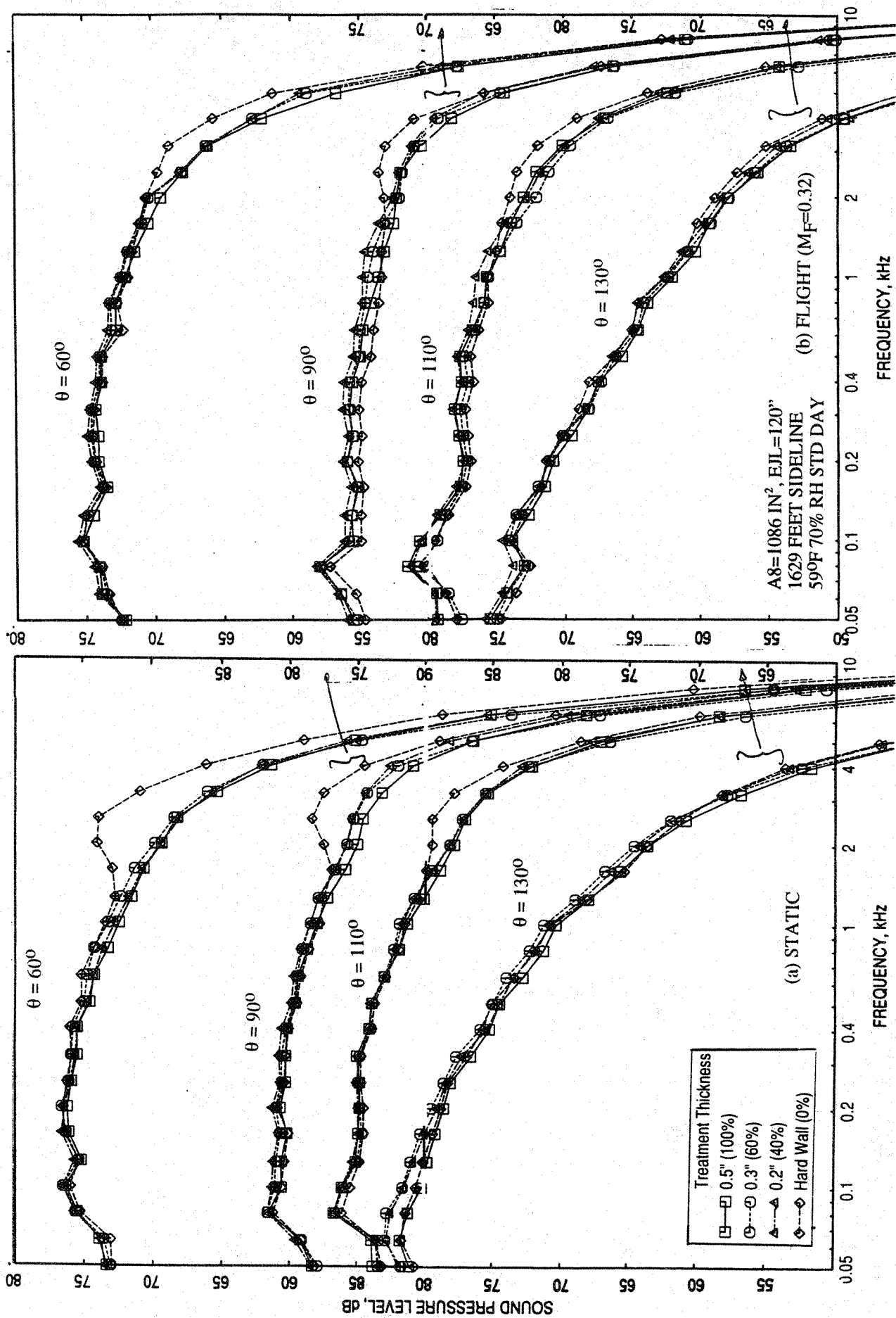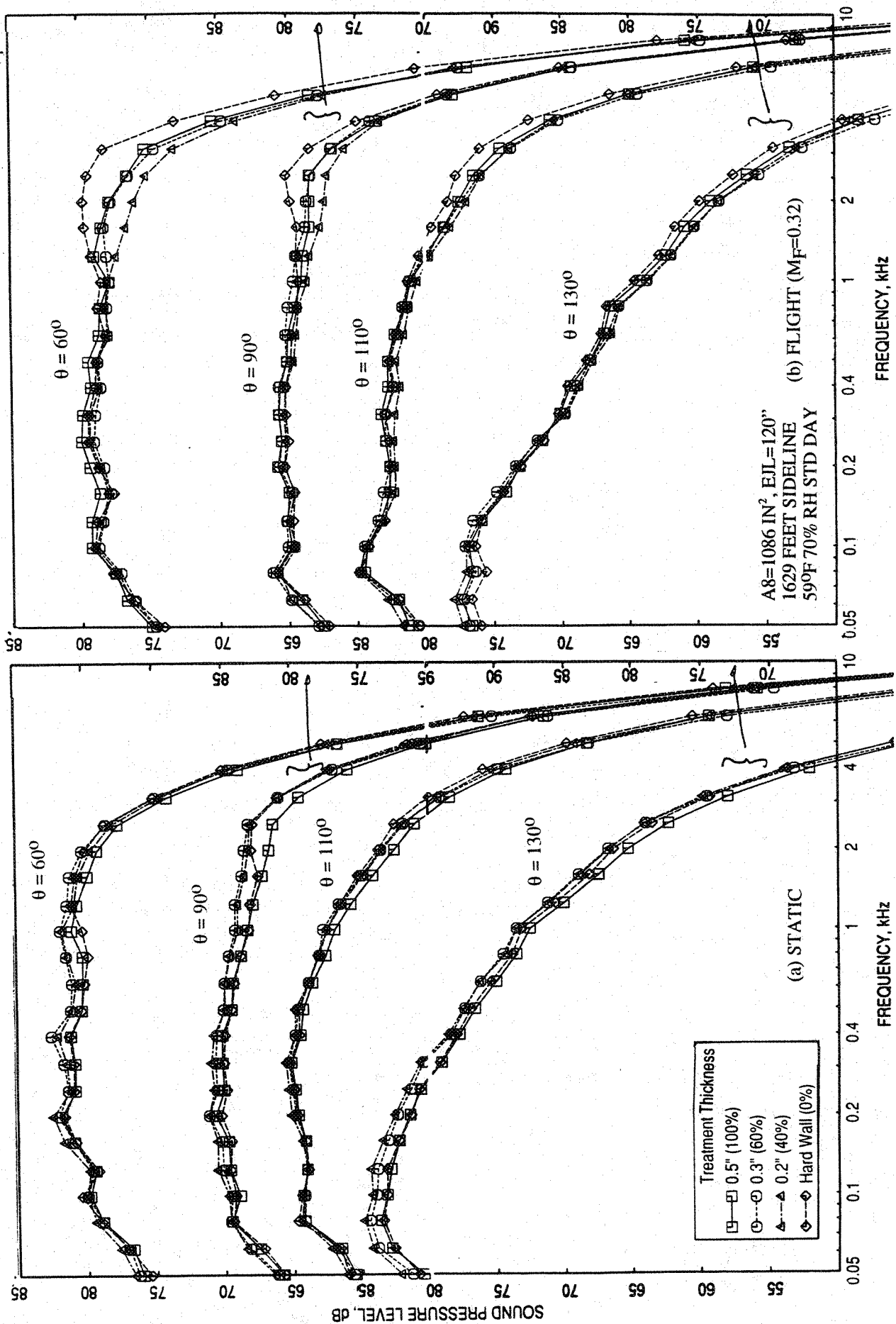
Figure 7-21. Effect of treatment thickness on SPL spectra at various polar angles (θ) for a 10 and 9 full staggered CD-chute mixer with long ejector; SAR=2.8, MAR = 0.95, V_j = 1147 ft/sec, NPR = 1.5, T8 = 1000°R.
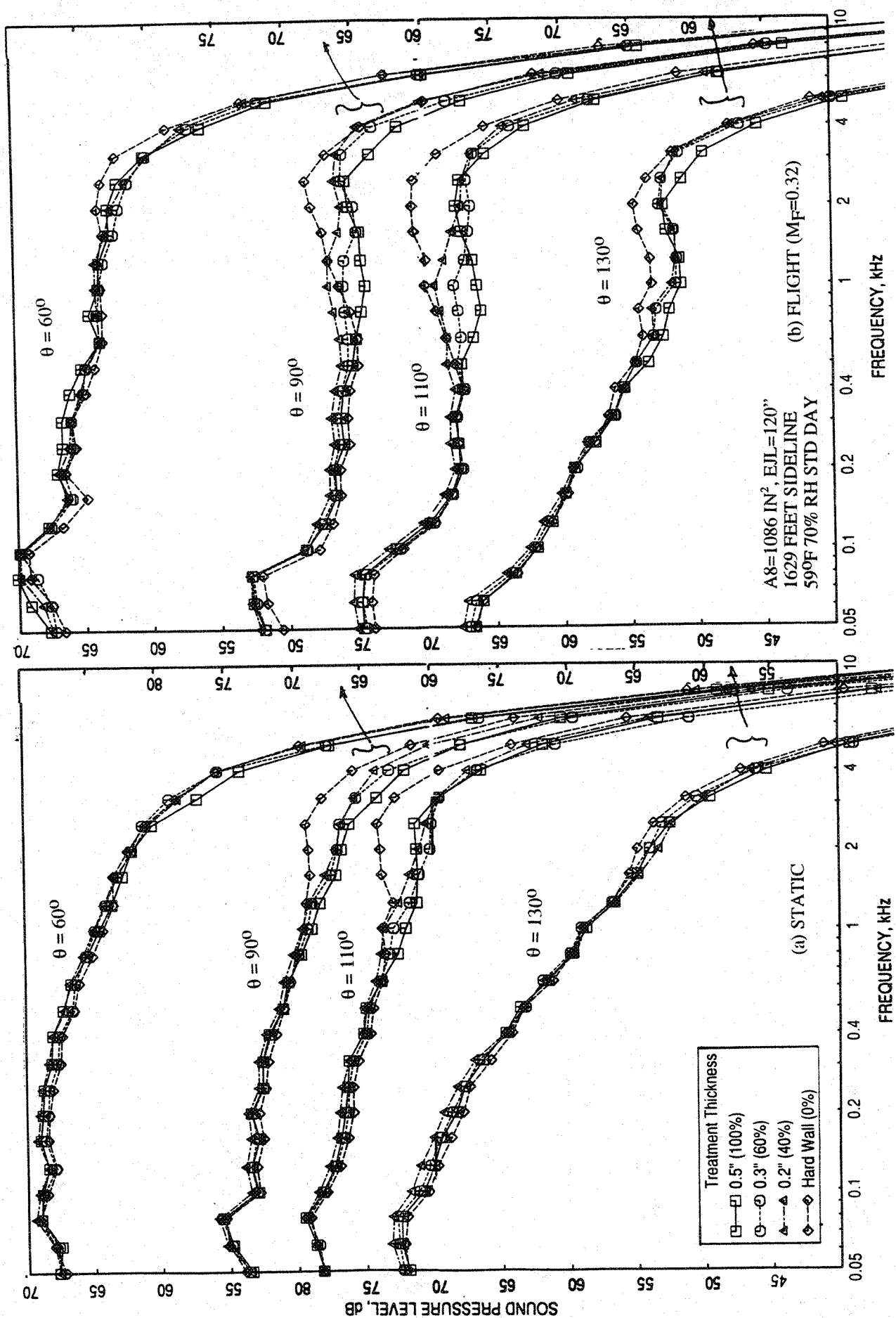
Figure 7-22. Effect of treatment thickness on SPL spectra at various polar angles (θ) for a 10 and 9 full staggered CD-chute mixer with long ejector; SAR=2.8, MAR = 0.95, V_j = 1919 ft/sec, NPR = 2.5, T8 = 1325°R.

Figure 7-23. Effect of treatment thickness on SPL spectra at various polar angles (θ) for a 10 and 9 full staggered CD-chute mixer with long ejector; SAR=2.8, MAR = 0.95, V_j = 2384 ft/sec, NPR = 3.4, T8 = 1590°R.

Figure 7-24. Effect of treatment thickness on SPL spectra at various polar angles (θ) for a 10 and 9 full staggered CD-chute mixer with long ejector; SAR=2.8, MAR = 0.95, V$_j$ = 2637 ft/sec, NPR = 4.0, T8 = 1750°R.

However, at higher velocities, the external noise seems to be higher compared to internal noise, and hence the influence of treatment thickness is insignificant in the farfield results.

7.2.2 Flow and Performance Related Parameters:

The effect of ejector treatment thickness on ramp and chute static pressure distributions is insignificant for static as well as with flight simulation. The chute loading coefficients due to chute static pressure distributions showing the effect of ejector treatment thickness are plotted against NPR in Figure 7-25. For static as well as flight cases the hardwalled configuration exhibits slightly lower loading force at lower NPR.

The effect of ejector treatment thickness on pumping and corrected pumping is shown in Figures 7-26 and 7-27 for static and flight cases, respectively. The pumping shows some variation with respect to treatment thickness at static condition. However, the corrected pumping at static condition and the pumping and corrected pumping with flight simulation are unaffected due to treatment thickness.

Figure 7-28 illustrates the effect of ejector treatment thickness on axial static pressure distributions on the flap at static condition at different L1M cycle conditions. Insignificant difference in pressure distributions with respect to treatment thickness is observed at lower NPRs. At higher NPRs the static pressure distribution on the flap indicates delayed mode switch with increasing treatment thickness. Figure 7-29 shows the effect of ejector treatment thickness on force and moment of force with respect to flap leading edge due to static pressure difference on flap surface as a function of nozzle pressure ratio. Both the force and the moment are lower for 0.5"-thick treatment. The transition from subsonic to supersonic mode seems to be slightly delayed with respect to increasing treatment thickness. Similar results with flight simulation are plotted in Figures 7-30 and 7-31. The static pressure distributions between the treatment configurations clearly indicate that the mode switch is delayed with increasing treatment thickness. Similar conclusion is deduced from the force and moment of the force results, as shown in Figure 7-31.

7.3 EFFECT OF TREATMENT LOCATION

Results, showing the effect of treatment location on the ejector, include two configurations, one with treatment closer to ejector exit plane or aft location (i.e.,
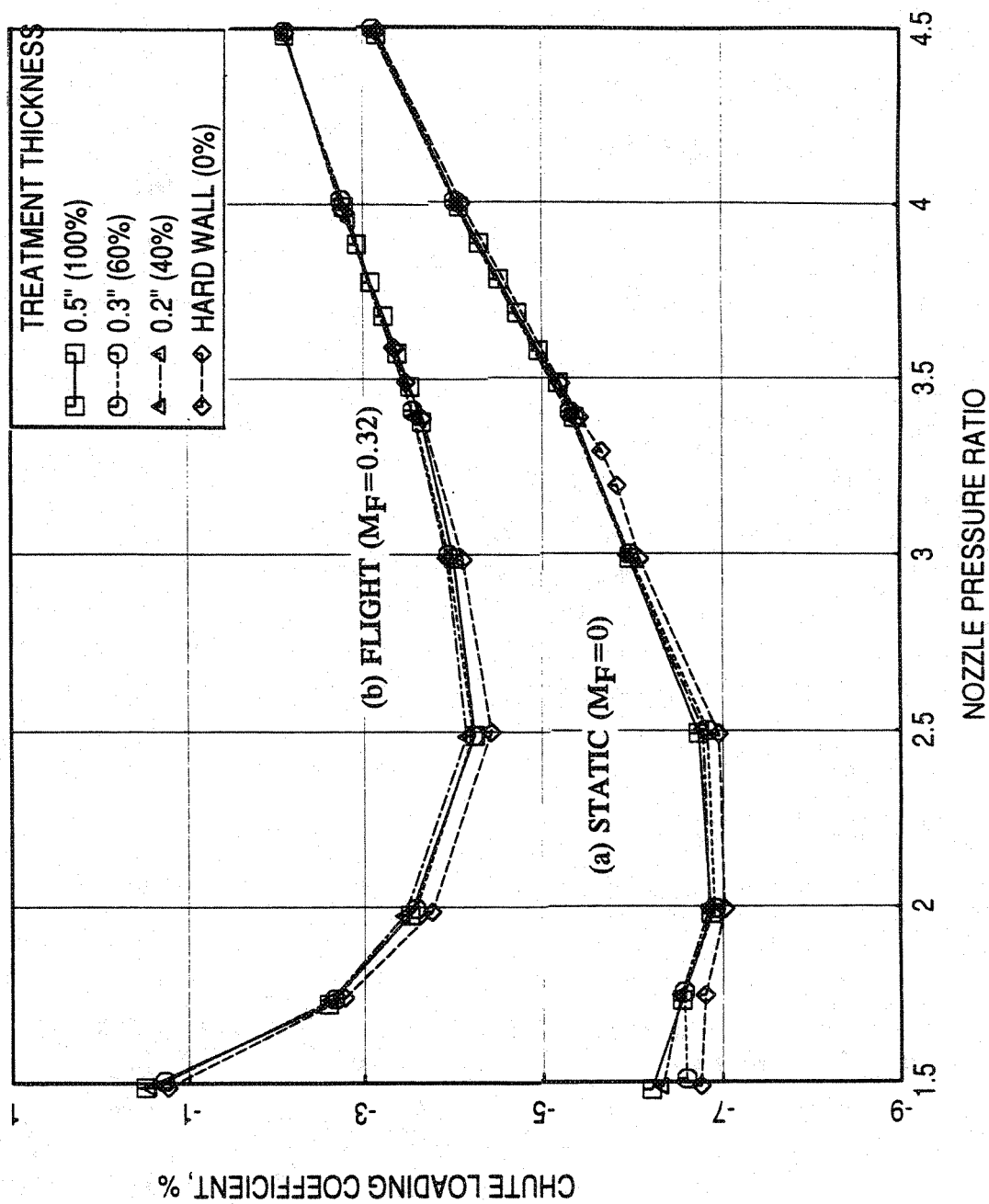
Figure 7-25. Effect of treatment thickness on chute loading coefficient with respect to nozzle pressure ratio for a 10 and 9 full staggered CD-chute mixer with long ejector for L1M cycle conditions (a) at static condition and (b) with flight simulation (M_F=0.32).
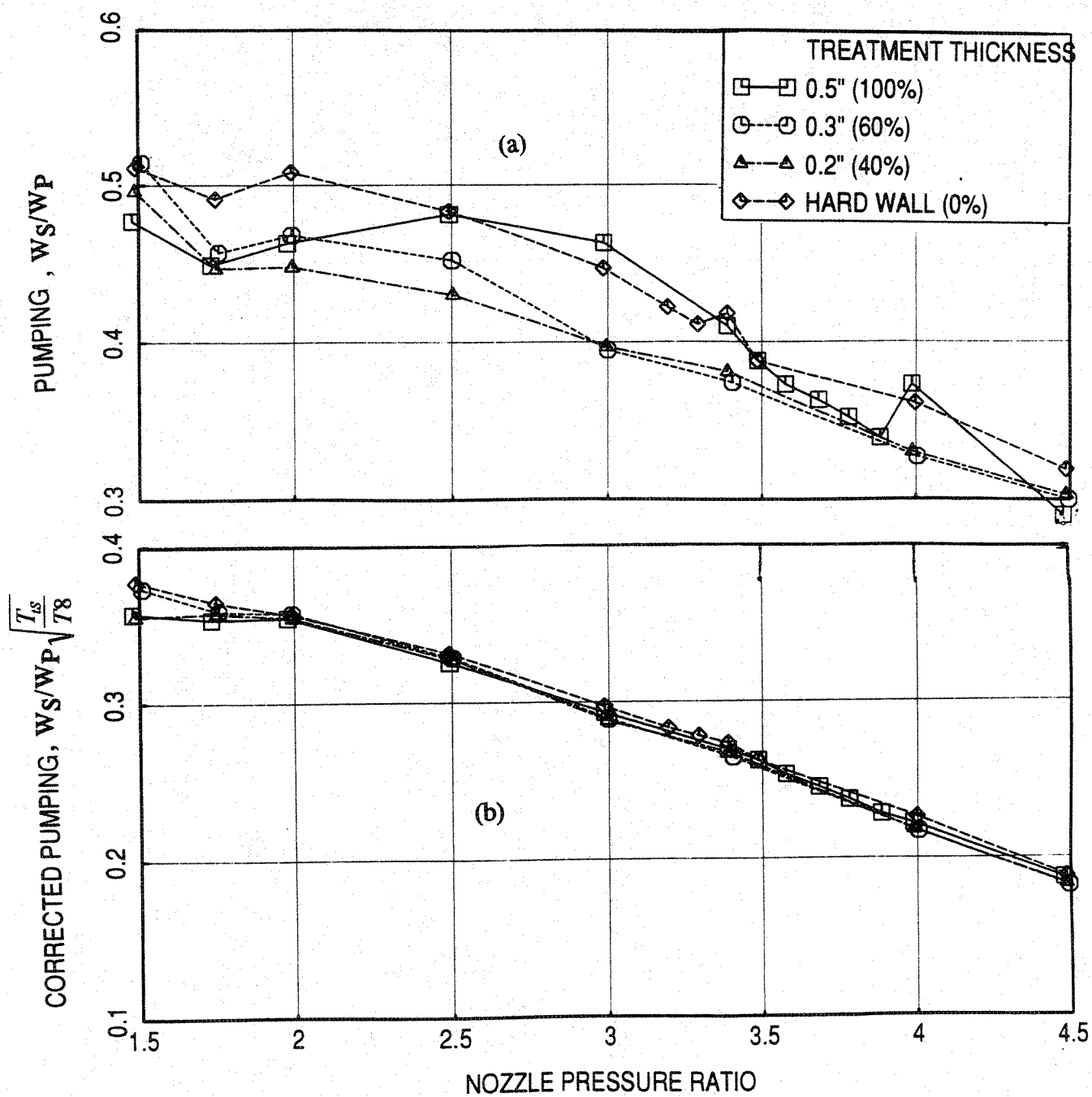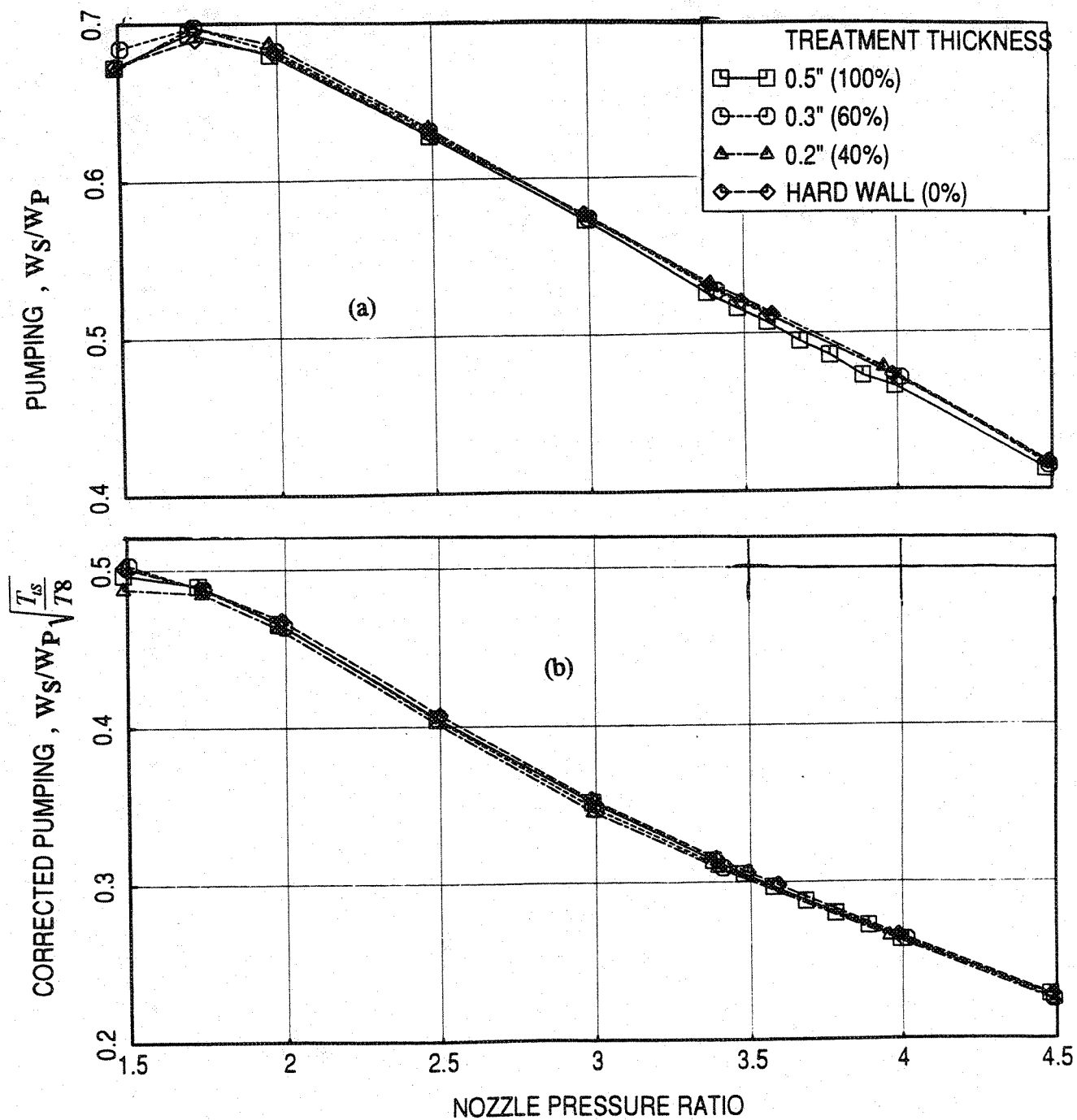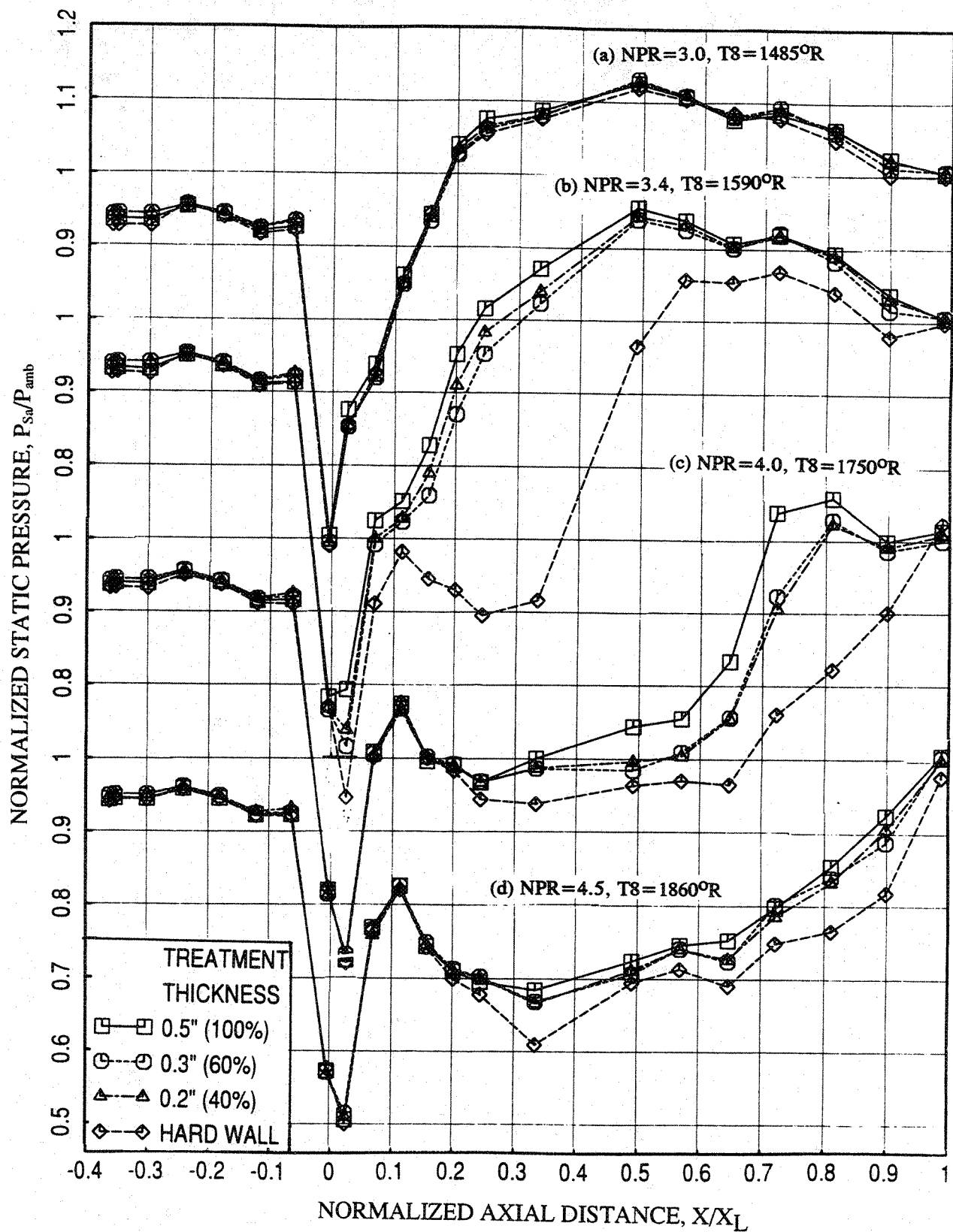
Figure 7-26. Effect of treatment thickness on pumping with respect to nozzle pressure ratio for a 10 and 9 full staggered CD-chute mixer with long ejector for L1M cycle conditions at static condition.

Figure 7-27. Effect of treatment thickness on pumping with respect to nozzle pressure ratio for a 10 and 9 full staggered CD-chute mixer with long ejector for L1M cycle conditions with flight simulation (M_F=0.32).

Figure 7-28. Effect of treatment thickness on axial distribution of average static pressure on the inlet and the flap surface at different L1M cycle conditions for a .10 and 9 full staggered CD-chute mixer with long ejector at static condition.
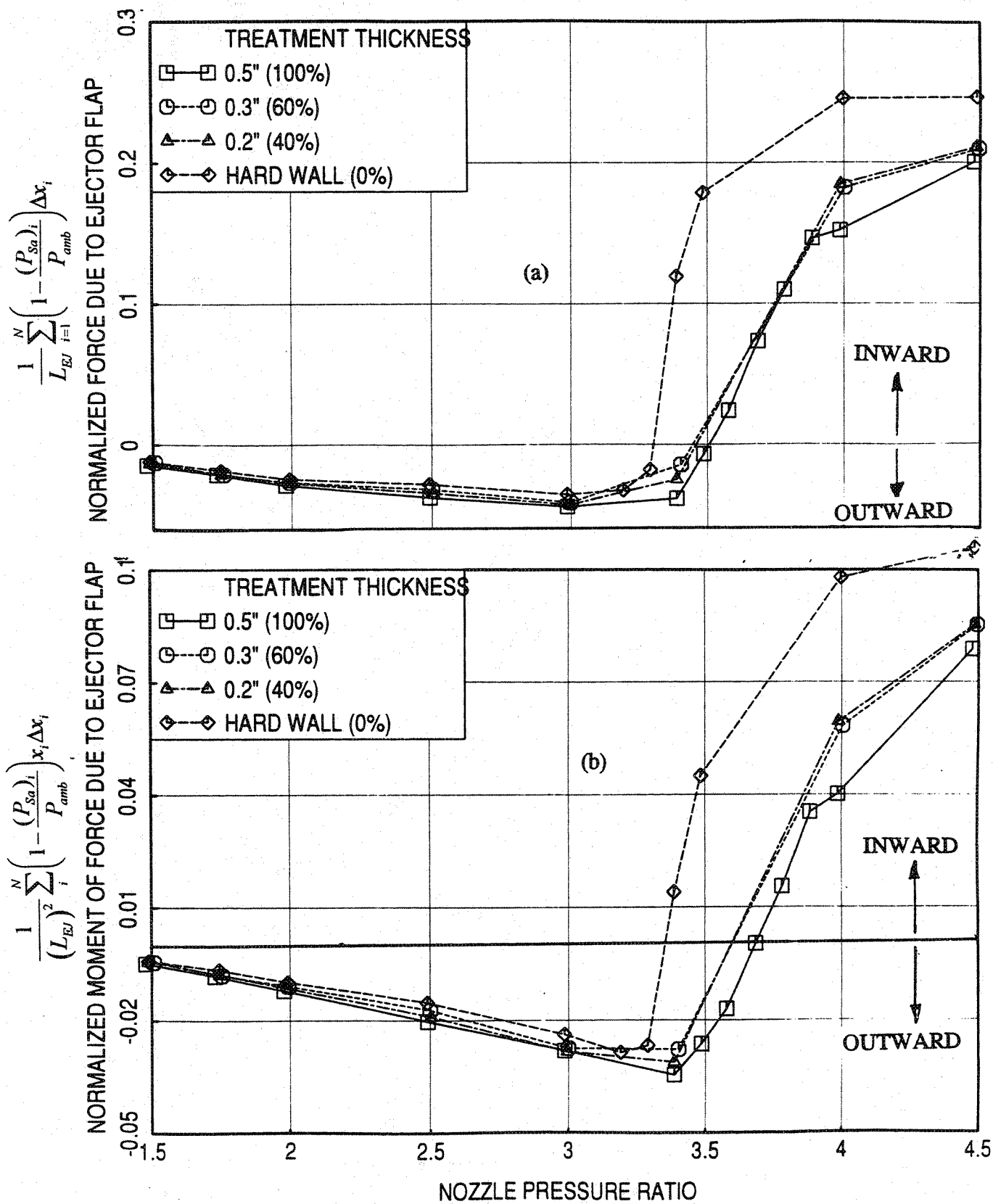
Figure 7-29. Effect of treatment thickness on normalized (a) force and (b) moment of force due to ejector flap with respect to nozzle pressure ratio for a 10 and 9 full staggered CD-chute mixer with long ejector for L1M cycle conditions at static condition.
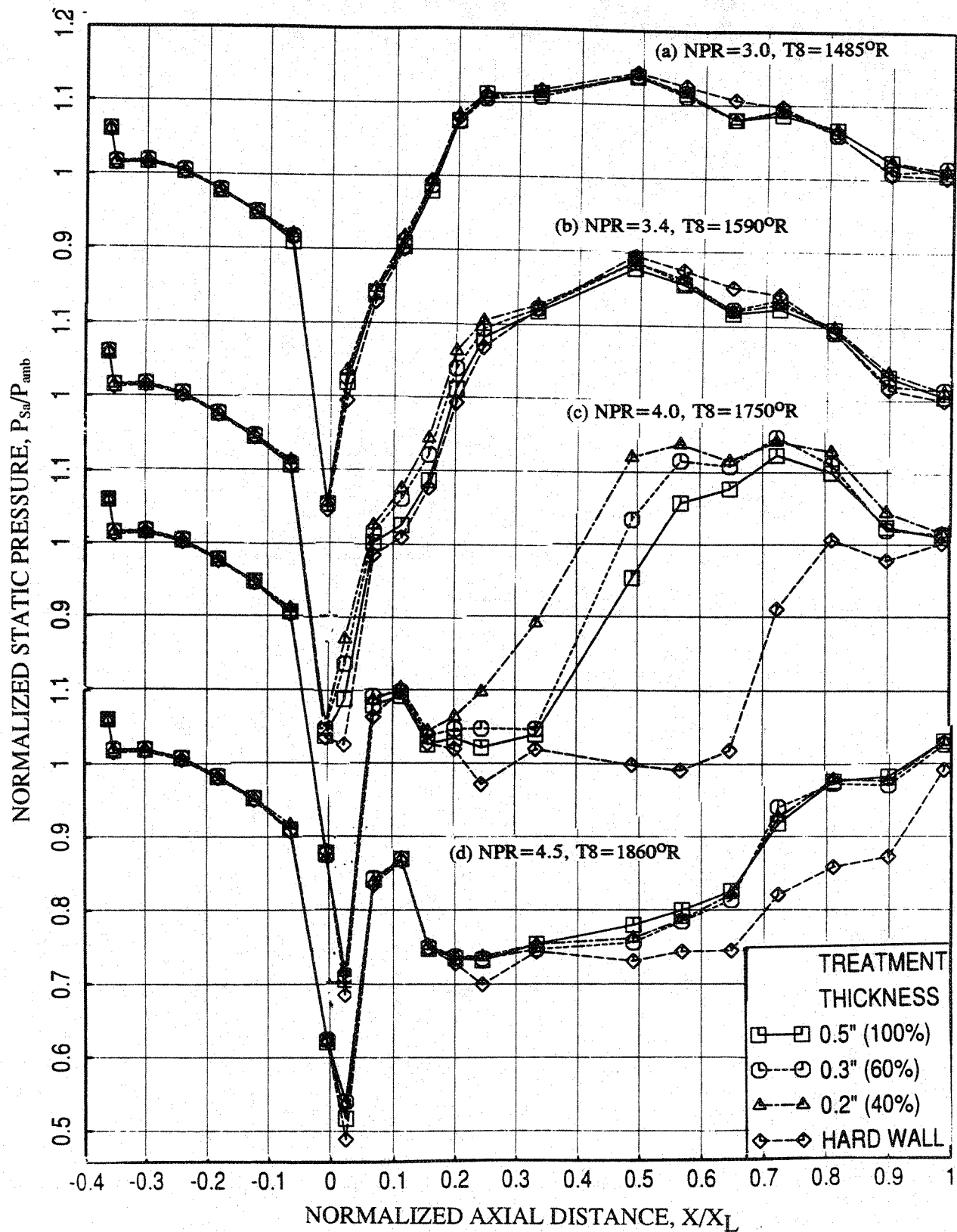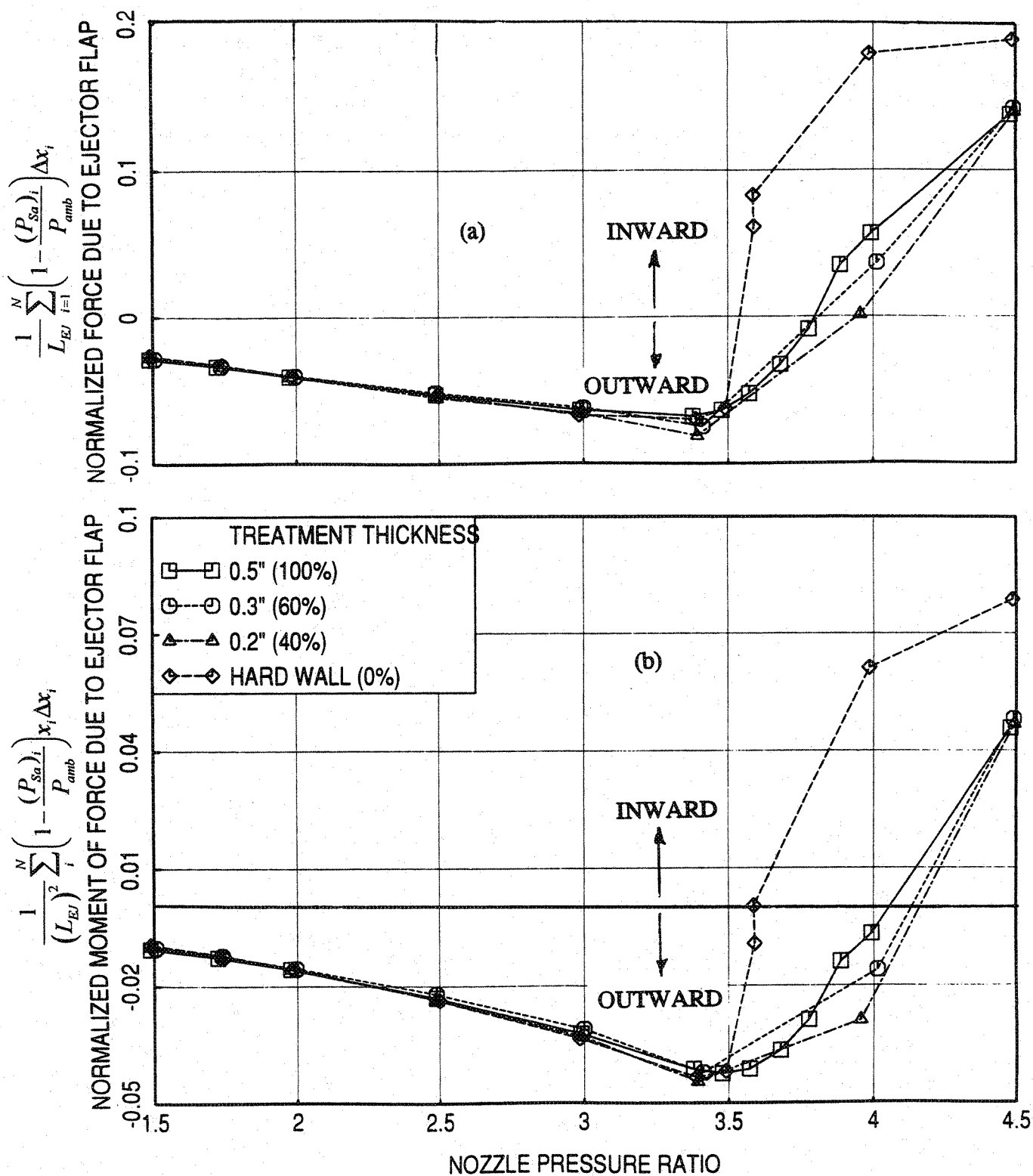
Figure 7-30. Effect of treatment thickness on axial distribution of average static pressure on the inlet and the flap surface at different L1M cycle conditions for a 10 and 9 full staggered CD-chute with long ejector mixer with flight simulation (M_F=0.32).

Figure 7-31. Effect of treatment thickness on normalized (a) force and (b) moment of force due to ejector flap with respect to nozzle pressure ratio for a 10 and 9 full staggered CD-chute mixer with long ejector for L1M cycle conditions with flight simulation (M_F=0.32).

configuration #16) and the other with treatment at the ejector middle (i.e., configuration #17). The treatment area for both cases is about 146 square inches (i.e., about 40% of total treated area or about 28% of total ejector area (which is approximately 4/9th of fully treated area). Nickel based metal foam of 0.5"-thick with a 37% porous facesheet (designated as FM) is used as the acoustic treatment. Figures 7-3 and 7-32 show the exact location of the treatment and the exact area covered by the treatment for these configurations. The treatment areas are shaded in these figures.

7.3.1 Acoustic Results:

The farfield acoustic results for the sideline azimuthal location relative to major axis (i.e., at $\phi=25°$), at a slant distance of 1629',) at static and with flight simulation ($M_F=0.32$) are presented in this section. Figure 7-33 shows the effect of ejector treatment location on EPNL, peak PNLT, and PNLT at various polar angles (θ) as functions of jet velocity (V_j). At jet velocities at and below 2400 ft/sec and above 1400 ft/sec the EPNL levels are lower for aft treated configuration compared to the middle treated configuration. The effect of treatment location is significant at velocities, between 1600 and 2200 ft/sec. Effect of treatment location at very low and high velocities is negligible. Similar trends are also observed with respect to PNLT.

Effect of ejector treatment location on PNLT directivities at jet velocities of 1147, 1920, 2384, and 2637 ft/sec are shown in Figure 7-34. The PNLT levels are lower for aft treated configuration compared to the middle treated configuration for mid velocities, namely between 1400 and 2384 ft/sec at most polar angles. Effect of ejector treatment location on SPL spectra at various polar angles (θ) for each of the above mentioned four jet velocities are shown in Figures 7-35 through 7-38. Noise suppression due to aft location of acoustic treatment in terms of SPL is observed at higher frequencies. Again the effect of treatment location on SPL seems to be less significant at lower, as well as, higher velocities (see Figures 7-35 and 7-38).

For the mixer-ejector configurations, the internal noise generation process continues inside the ejector with respect to its length until a reasonably mixed condition is reached. Most of the noise is generated in the initial portion of the ejector. The acoustic treatment on the ejector after this location is expected to be more effective in noise suppression. This length
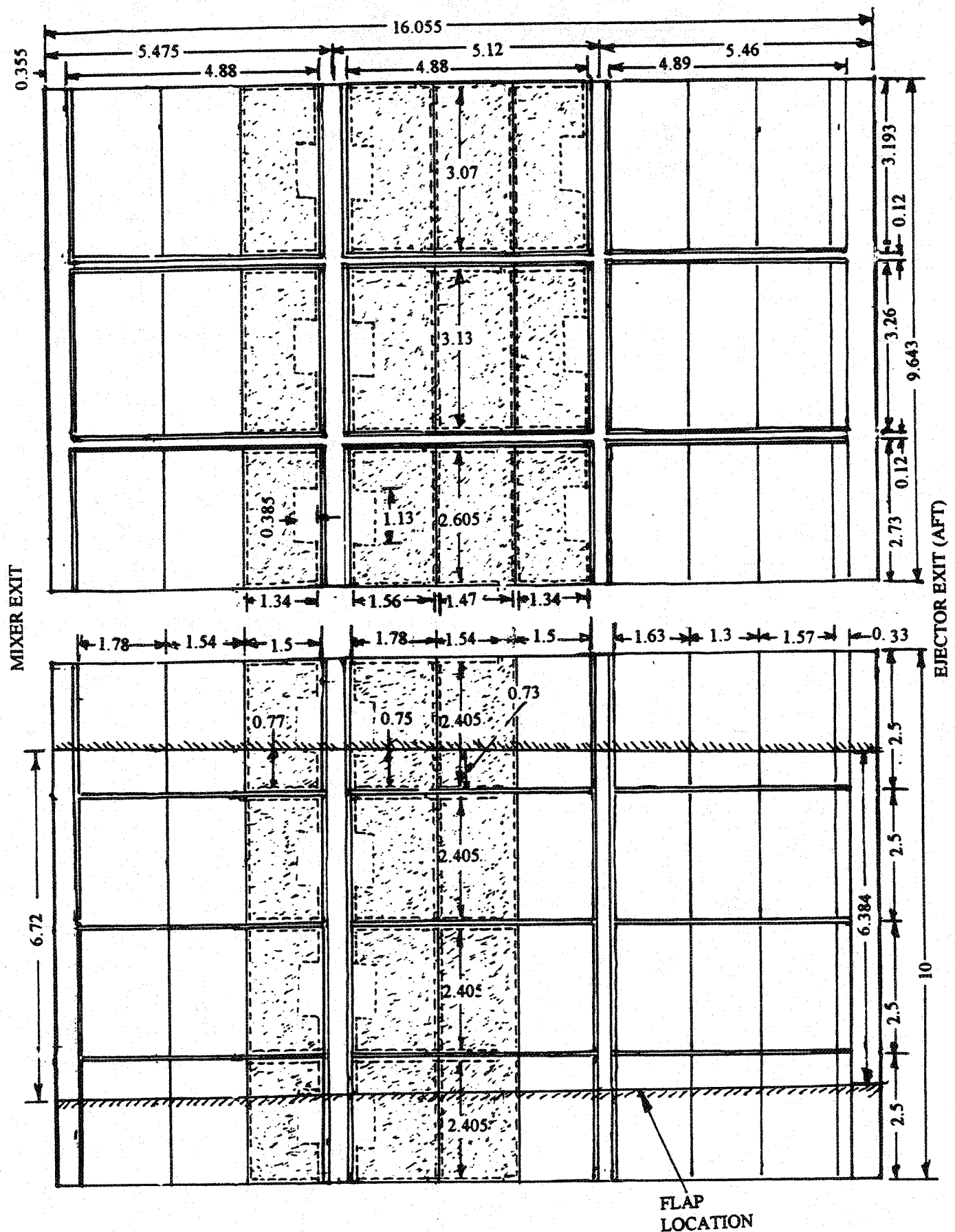
Figure 7-32. Partially (i.e., approximately 4/9th of full treatment) treated flap and side wall surfaces at ejector middle location (all dimensions are in inches).
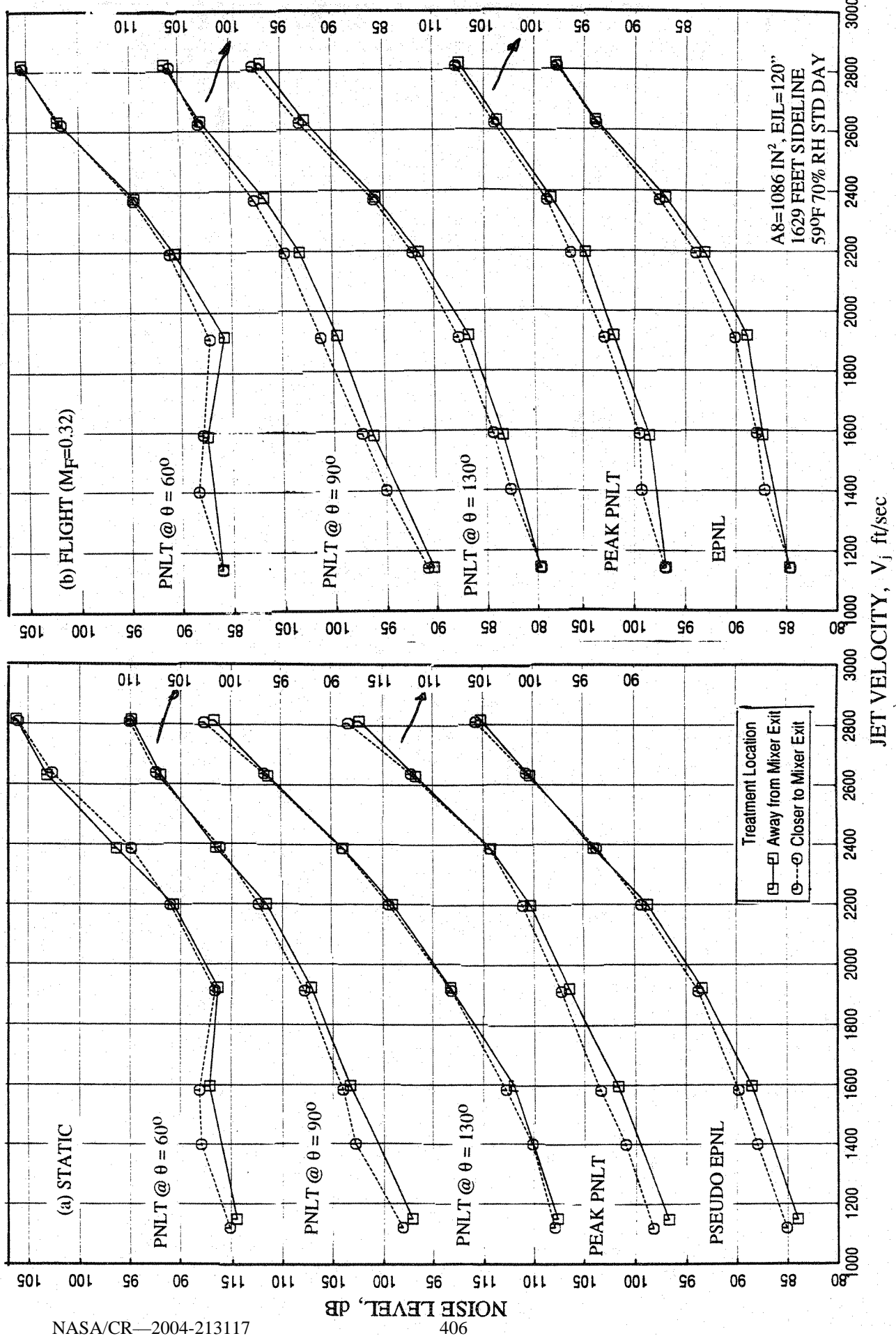
Figure 7-33. Effect of treatment location on EPNL, peak PNLT, and PNLT at various polar angles (θ) as functions of jet velocity for a 10 and 9 full staggered CD-chute mixer with 4/9-treated long ejector; SAR=2.8, MAR = 0.95.
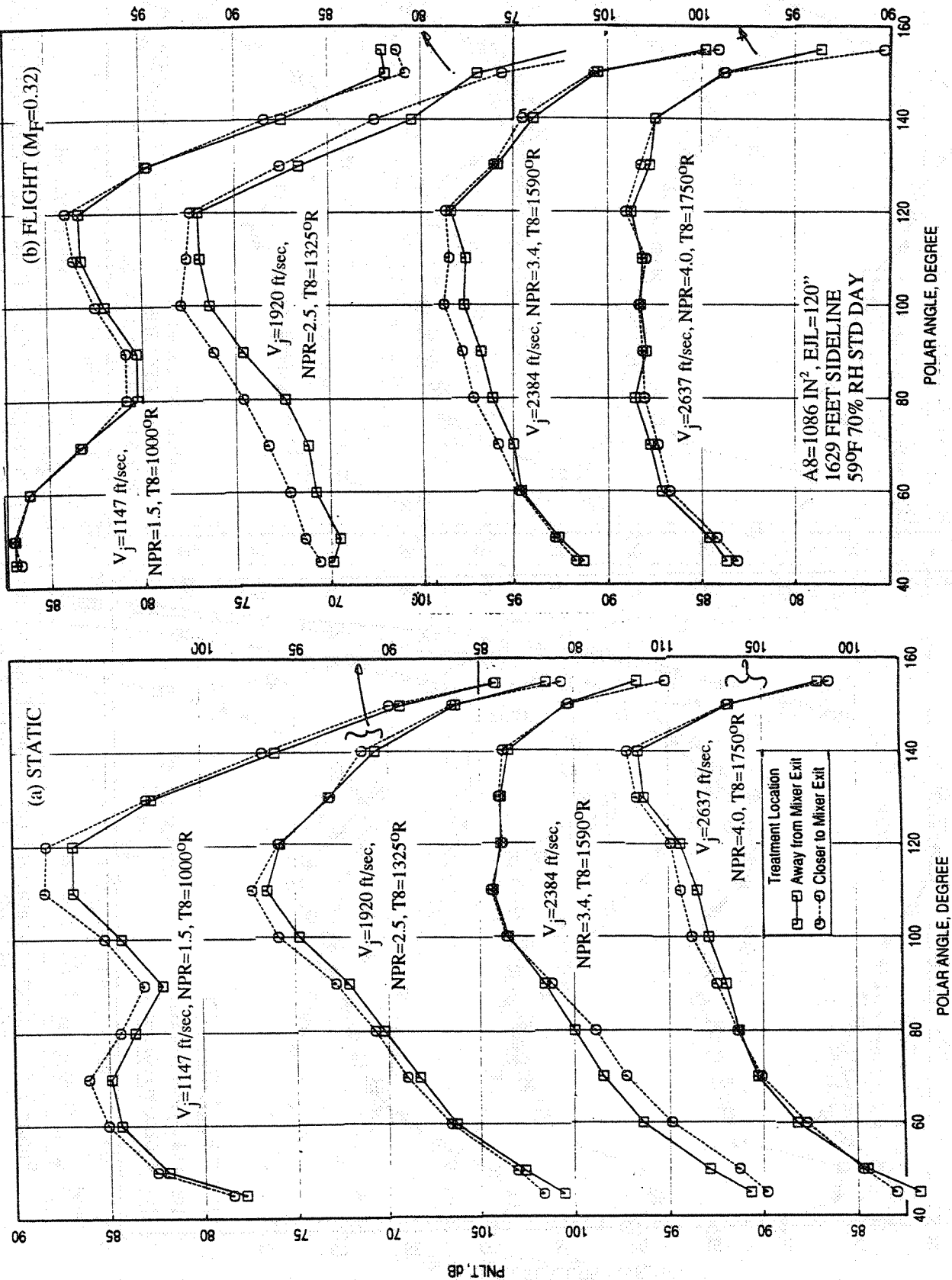
Figure 7-34. Effect of treatment location on PNLT directivities for different jet velocities (V_j) for a 10 and 9 full staggered CD-chute mixer with 4/9-treated long ejector; SAR=2.8, MAR = 0.95.
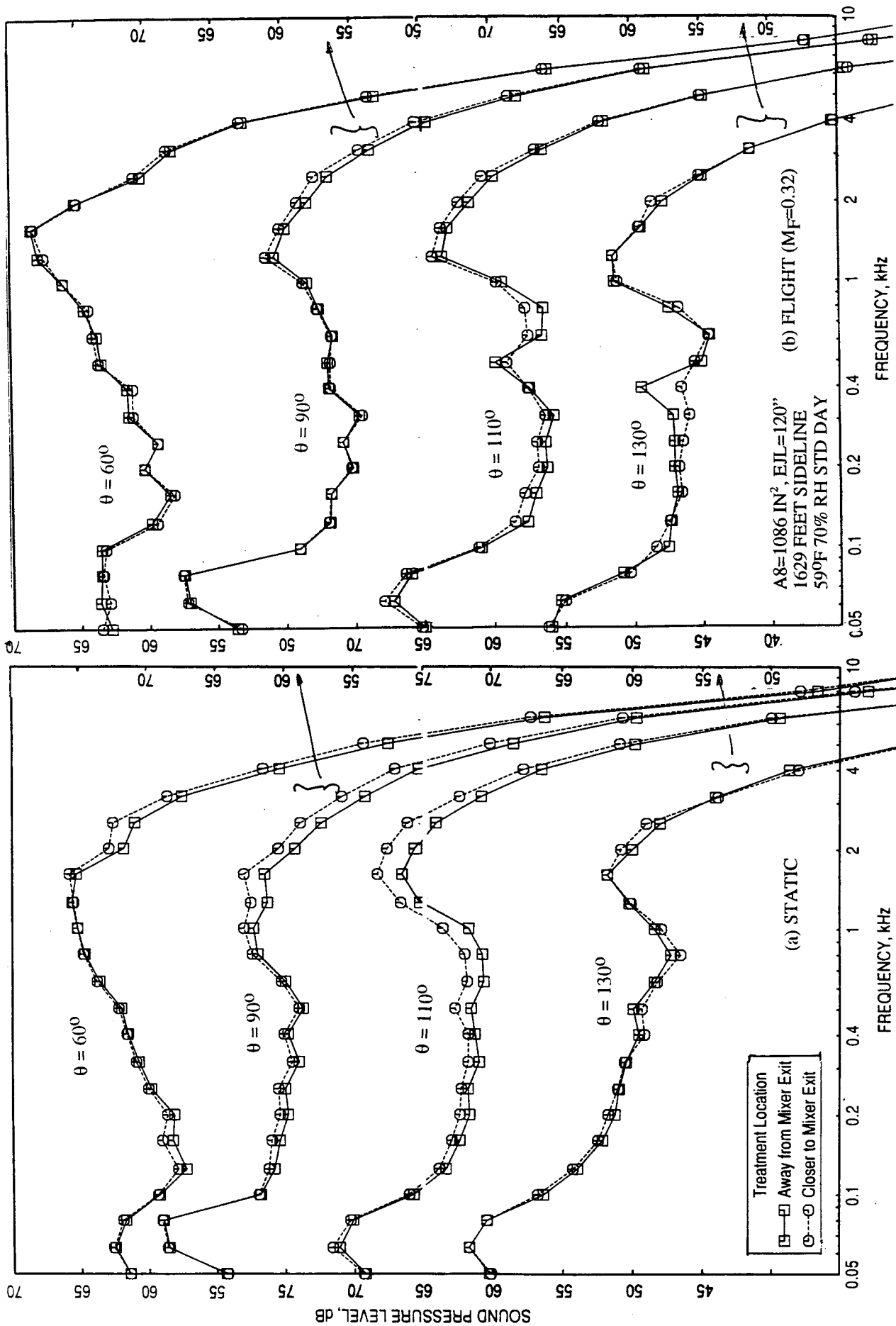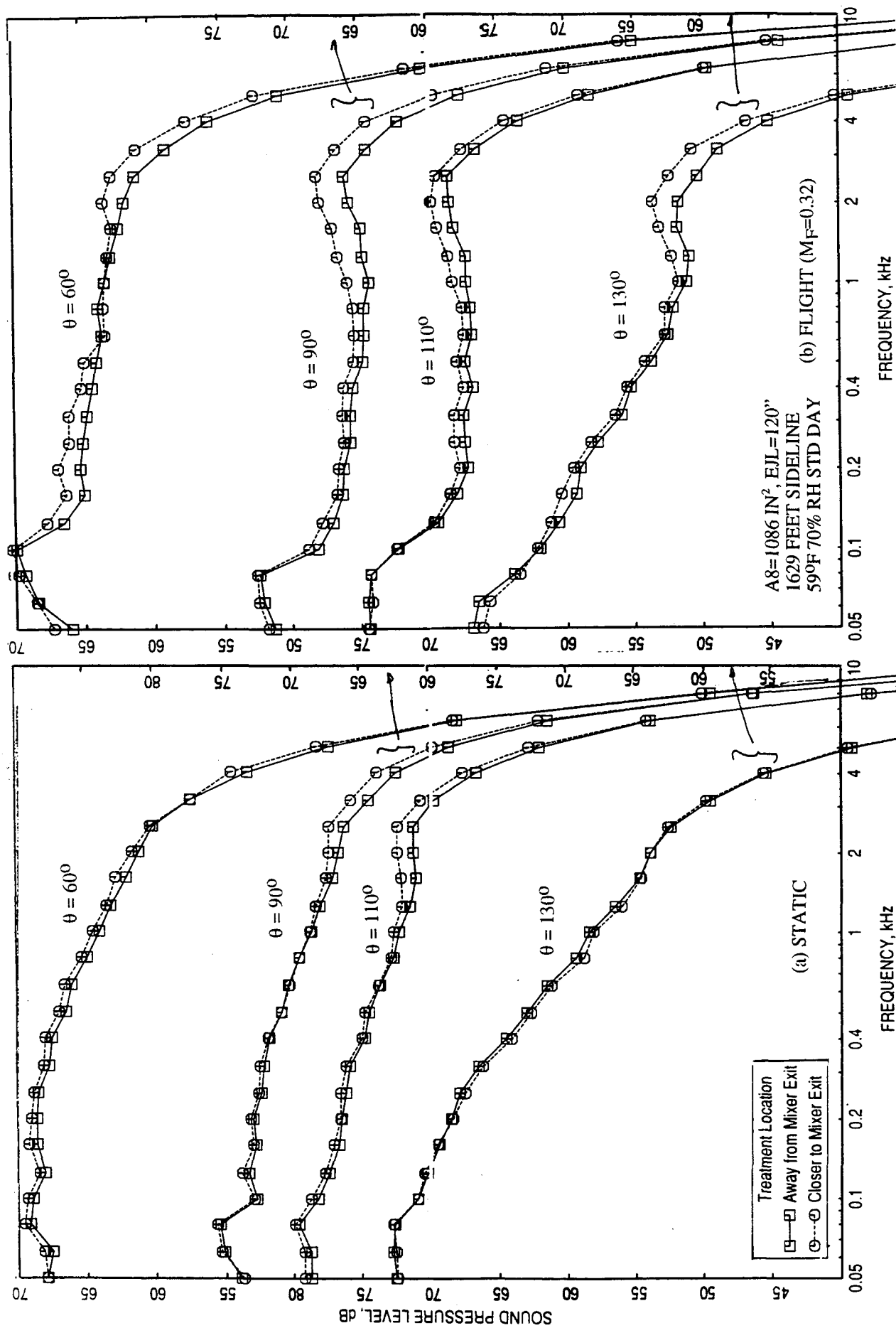
Figure 7-35. Effect of treatment location on SPL spectra at various polar angles (θ) for a 10 and 9 full staggered CD-chute mixer with 4/9-treated long ejector; SAR=2.8, MAR = 0.95, V_j = 1147 ft/sec, NPR = 1.5, T8 = 1000°R.

Figure 7-36. Effect of treatment location on SPL spectra at various polar angles (θ) for a 10 and 9 full staggered CD-chute mixer with 4/9-treated long ejector; SAR=2.8, MAR = 0.95, V_j = 1919 ft/sec, NPR = 2.5, T8 = 1325°R.
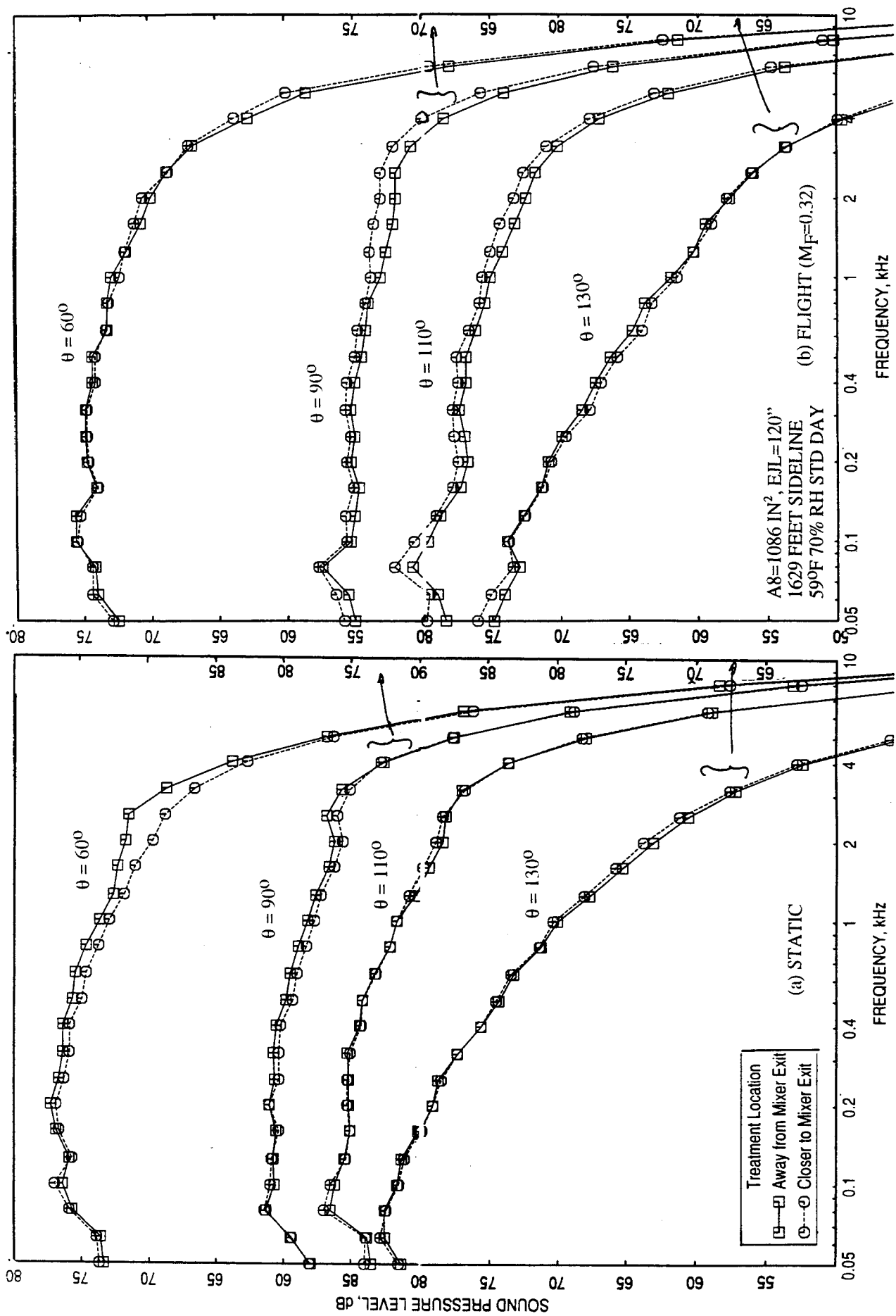
Figure 7-37. Effect of treatment location on SPL spectra at various polar angles (θ) for a 10 and 9 full staggered CD-chute mixer with 4/9-treated long ejector; SAR=2.8, MAR = 0.95, V_j = 2384 ft/sec, NPR = 3.4, T8 = 1590°R.
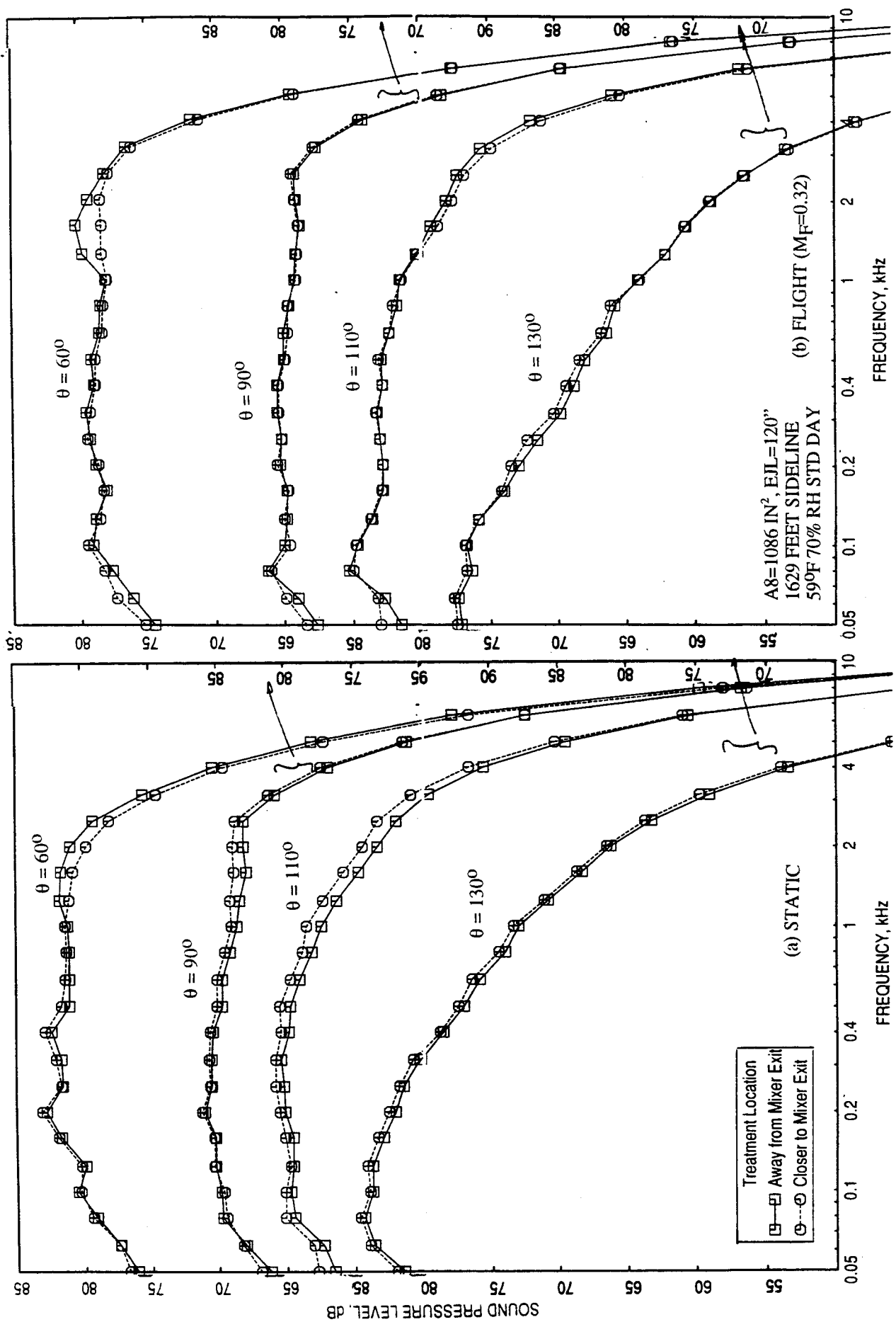
Figure 7-38. Effect of treatment location on SPL spectra at various polar angles (θ) for a 10 and 9 full staggered CD-chute mixer with 4/9-treated long ejector; SAR=2.8, MAR = 0.95, V_j = 2637 ft/sec, NPR = 4.0, T8 = 1750°R.

of the ejector, after which the acoustic treatment becomes effective, increases with increasing jet velocity. In addition, the internal noise level also increases with jet velocity. For lower jet velocity conditions, the interaction of noise with ejector surface occurs much closer to the mixer exit and is shifted downstream with increasing jet velocity. Hence, a fixed amount (i.e., area) of acoustic treatment on the ejector, not covering the entire surface, will be more effective for higher velocities if located at the aft of the ejector. However, the noise suppression with respect to the liner location will be less sensitive for lower velocities.

In general, the noise suppression, as measured in the farfield, is higher for aft located treatment compared to middle location. However, the effect is insignificant at higher velocities above 2400 ft/sec and at lower velocities below 1600 ft/sec. The lower and mid velocity results can be justified with the above explanation. For higher velocities, the insensitiveness of treatment location on noise suppression can be explained as follows:

The noise measured in the farfield is the sum total of noise propagated out of the ejector (i.e., internal noise) and the noise generated exterior to the ejector (i.e., external noise). If the external noise level is much higher compared to internal noise propagating out of the ejector, then the total noise measured in the farfield will be less influenced by changes in the internal noise. The higher jet velocity results shown here are indicative of the fact that the external noise is higher compared to internal noise, and in spite of more noise suppression due to aft located treatment the influence of treatment location is insignificant in the farfield results.

7.3.2 Flow and Performance Related Parameters:

The effect of ejector treatment location on ramp and chute static pressure distributions are insignificant for static as well as with flight simulation. The chute loading coefficients due to chute static pressure distributions showing the effect of ejector treatment location are plotted against NPR in Figure 7-39. The chute loading coefficients are slightly higher for the treatment closer to the mixer exit.

The effect of ejector treatment location on pumping and corrected pumping is shown in Figures 7-40 and 7-41 for static and flight cases, respectively. Pumping is slightly higher
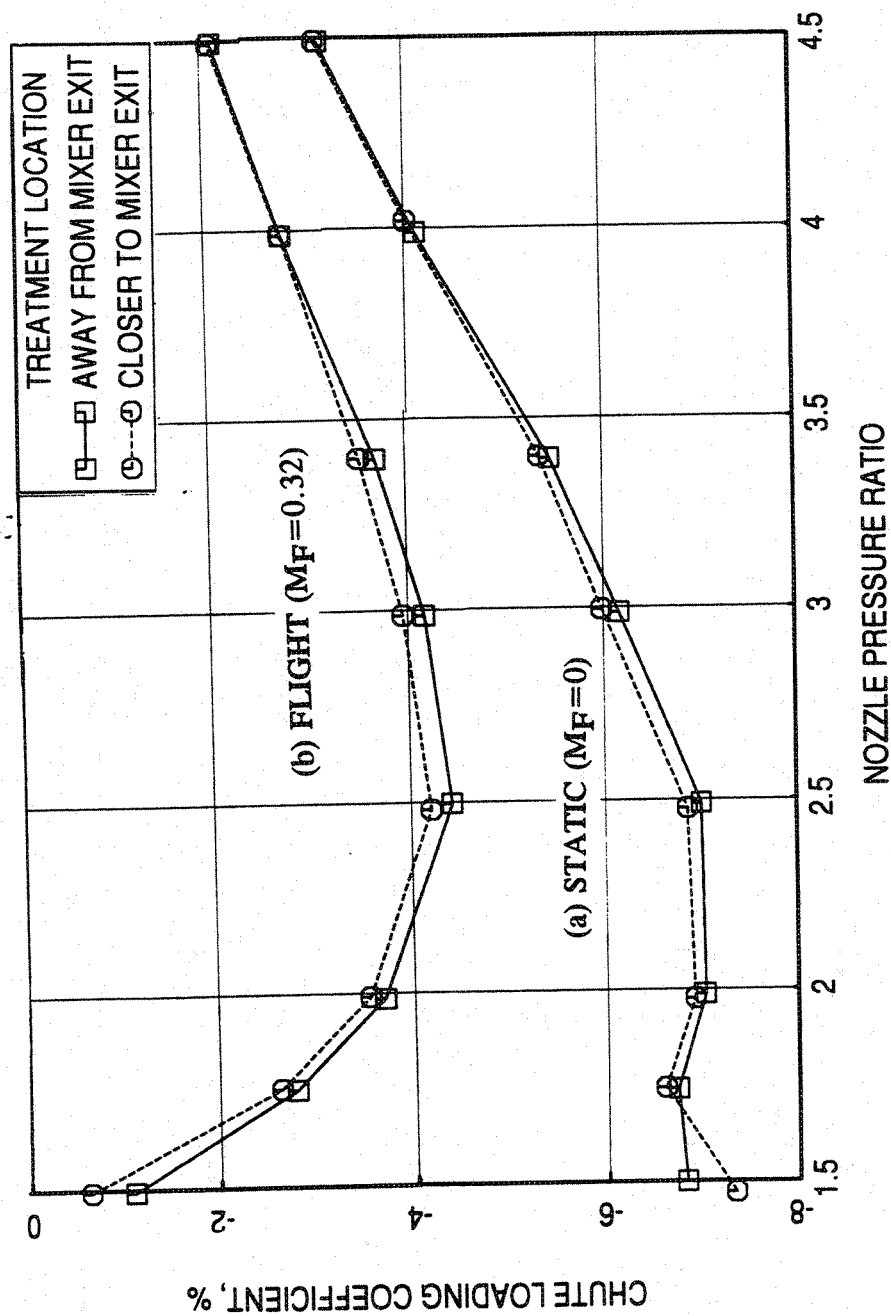
Figure 7-39. Effect of treatment location on chute loading coefficient with respect to nozzle pressure ratio for a 10 and 9 full staggered CD-chute mixer with 4/9-treated long ejector for L1M cycle conditions (a) at static condition and (b) with flight simulation (M_F=0.32).
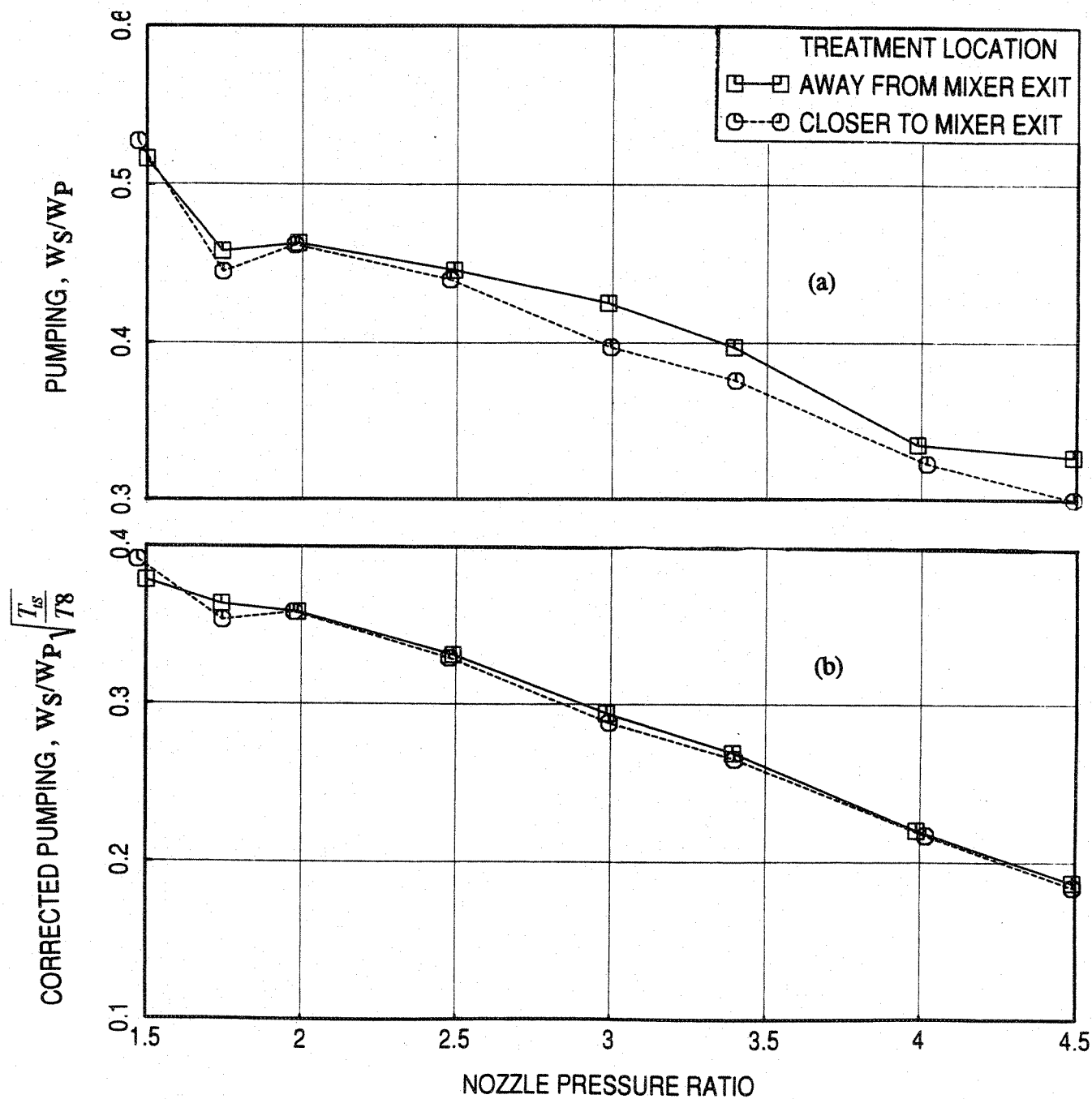
Figure 7-40. Effect of treatment location on pumping with respect to nozzle pressure ratio for a 10 and 9 full staggered CD-chute mixer with 4/9-treated long ejector for L1M cycle conditions at static condition.
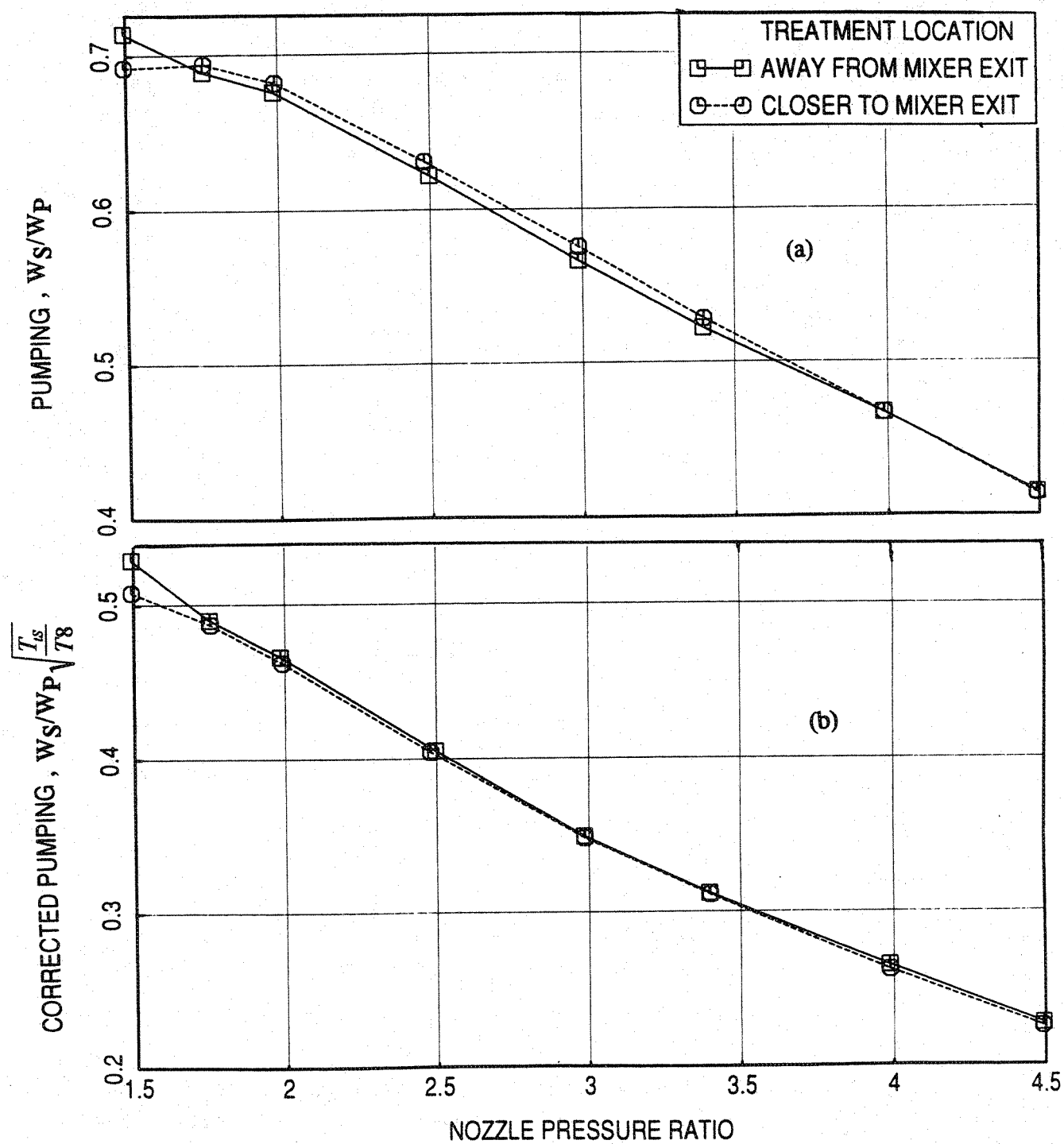
Figure 7-41. Effect of treatment location on pumping with respect to nozzle pressure ratio for a 10 and 9 full staggered CD-chute mixer with 4/9-treated long ejector for L1M cycle conditions with flight simulation (M_F=0.32).

for the ejector with treatment away from the mixer exit at static condition. There is very little effect due to treatment location on the pumping with flight simulation.

Figure 7-42 illustrates the effect of ejector treatment location on axial static pressure distributions on the flap at static condition at different L1M cycle conditions. Insignificant difference in pressure distributions with respect to treatment location is observed at lower NPRs. At higher NPRs the static pressure distribution on the flap indicates delayed mode switch for ejector treatment closer to the mixer exit, which is also observed from the force and moment of force with respect to flap leading edge due to static pressure difference on flap surface as a function of nozzle pressure ratio shown in Figure 7-43. Similar results with flight simulation are plotted in Figures 7-44 and 7-45. The static pressure distributions between the mixer configurations clearly indicate that the mode switch is delayed for ejector treatment closer to the mixer exit. Similar conclusion is deduced from the force and moment of the force results, as shown in Figure 7-45.

7.4 FULLY TREATED EJECTOR VERSUS FLAPS ONLY TREATED EJECTOR:

The results showing the comparison between fully treated and flaps only treated ejectors include two configurations with 0.5"-thick nickel based foam metal treatment with a 37% porous facesheet (i.e., configurations #11 and 19).

7.4.1 Acoustic Results:

For the flap only treated configuration the azimuthal asymmetry of internally generated noise radiated to the farfield is likely to be more compared to the fully treated and hardwalled configurations. Thus the farfield acoustic results for the sideline as well as community azimuthal locations relative to the major axis (i.e., at $\phi=25°$ and $90°$, respectively), at a slant distance of 1629', at static and with flight simulation ($M_F=0.32$) are examined in this section. Results for hard wall ejector configuration are also included in these plots.

Results at Sideline Location ($\phi=25°$): Figure 7-46 shows the comparison of EPNL, peak PNLT, and PNLT at various polar angles (θ) as functions of jet velocity (V_j) between fully treated and flaps only treated ejector configurations. Fully treated ejector configuration exhibits lower noise levels in terms of EPNL as well as PNLT for entire
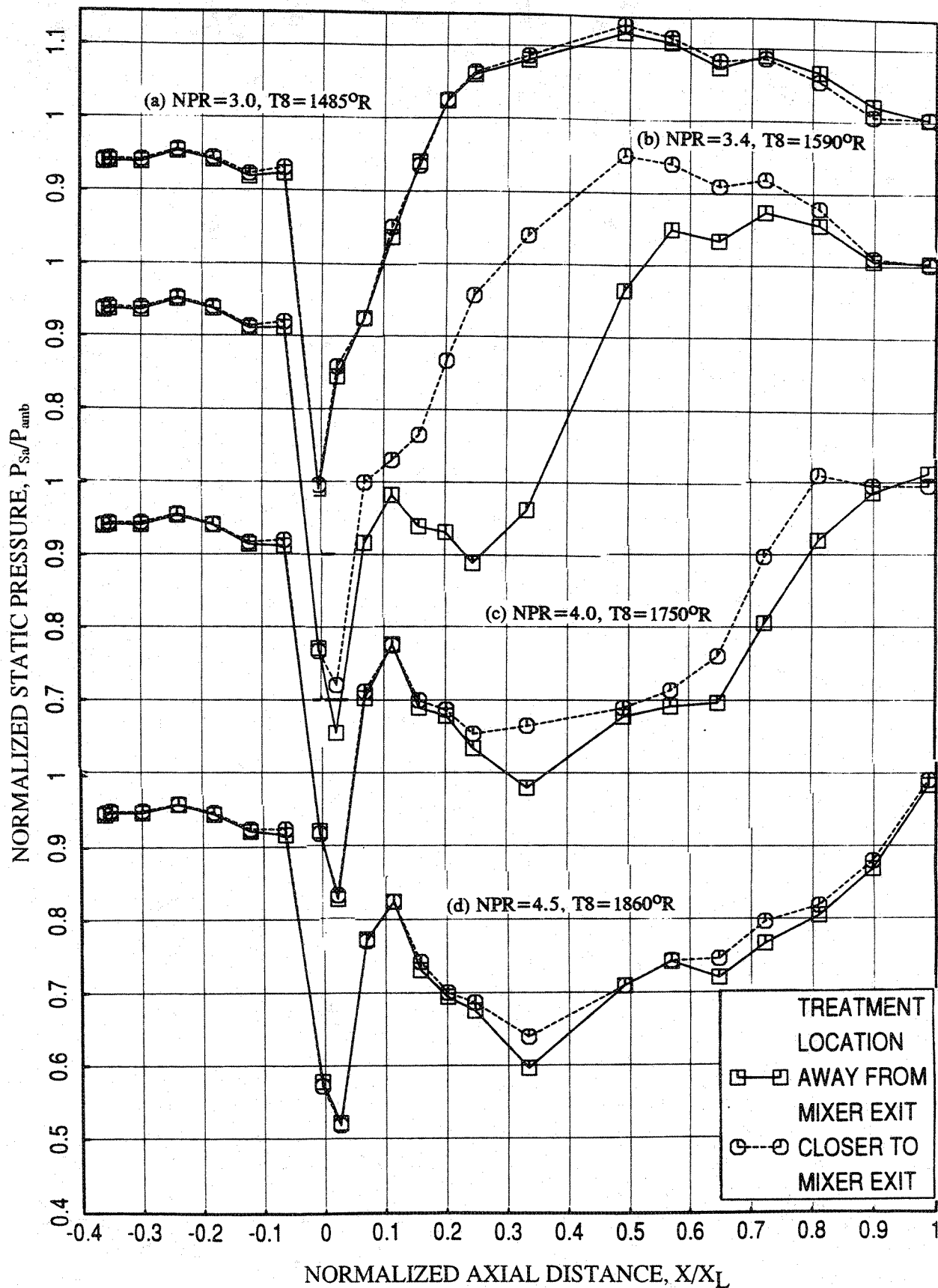
Figure 7-42. Effect of treatment location on axial distribution of average static pressure on the inlet and the flap surface at different L1M cycle conditions for a 10 and 9 full staggered CD-chute mixer with 4/9-treated long ejector at static condition.
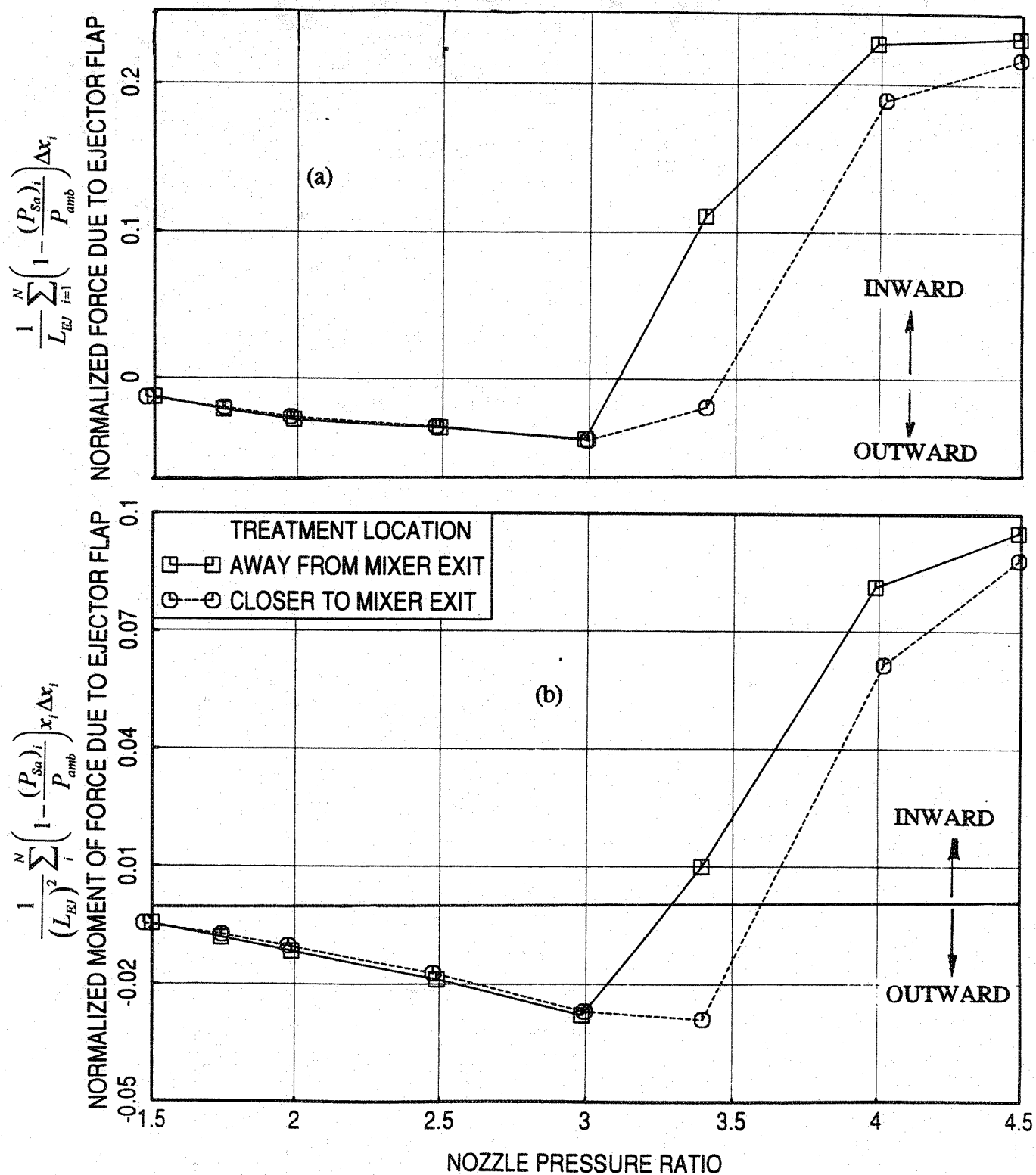
Figure 7-43. Effect of treatment location on normalized (a) force and (b) moment of force due to ejector flap with respect to nozzle pressure ratio for a 10 and 9 full staggered CD-chute mixer with 4/9-treated long ejector for L1M cycle conditions at static condition.
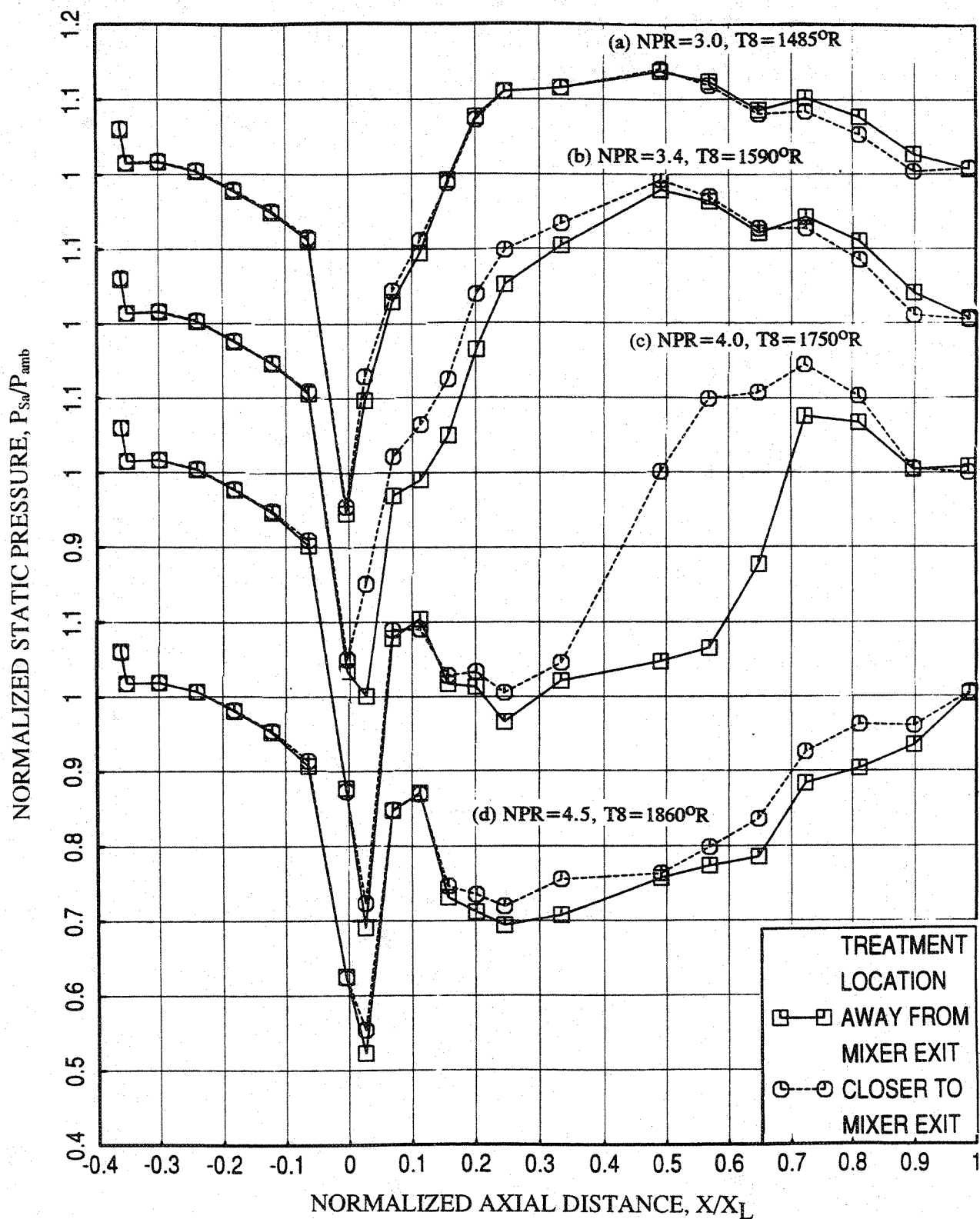
Figure 7-44. Effect of treatment location on axial distribution of average static pressure on the inlet and the flap surface at different L1M cycle conditions for a 10 and 9 full staggered CD-chute with 4/9-treated long ejector mixer with flight simulation (M_F=0.32).
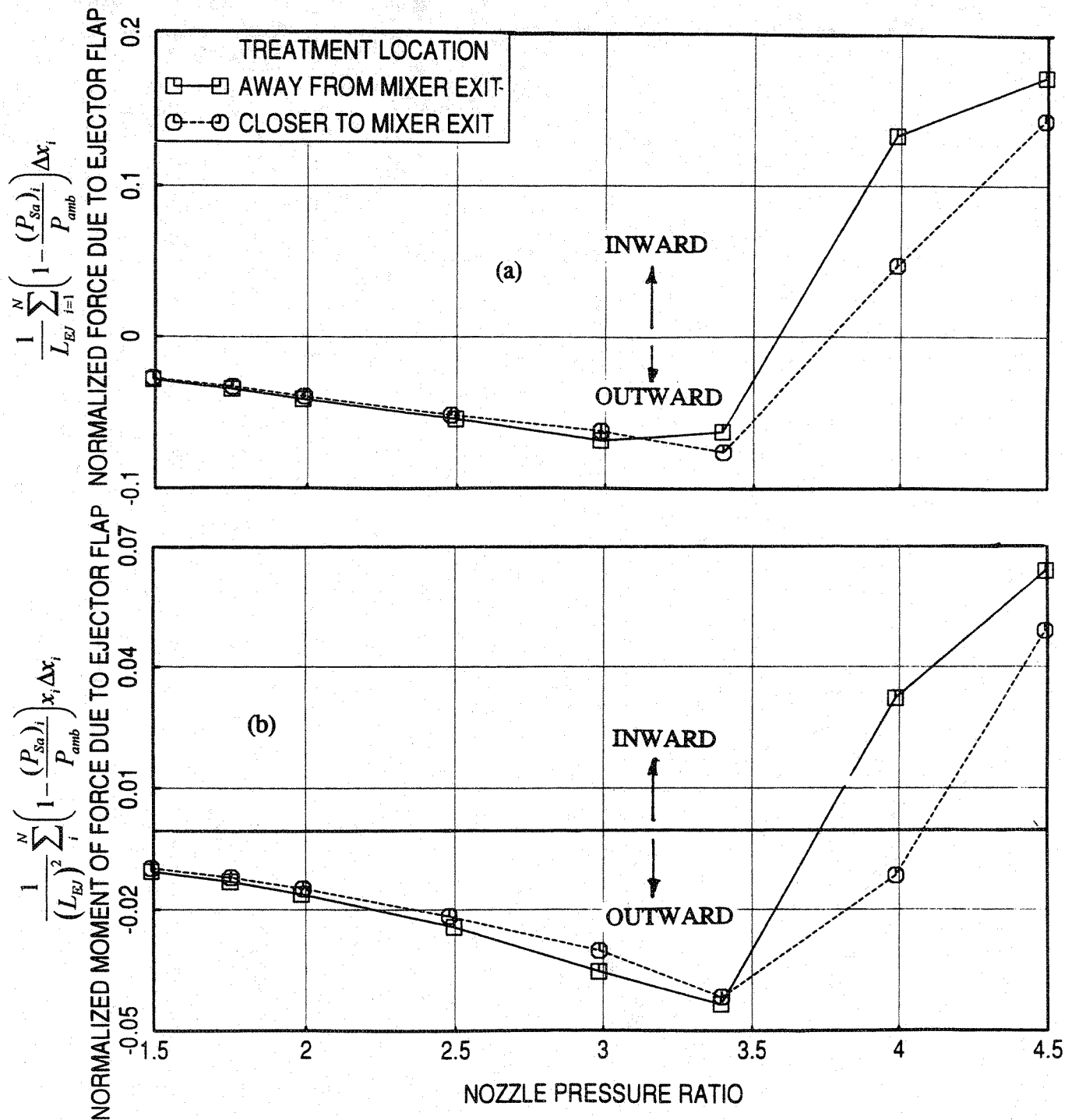
Figure 7-45. Effect of treatment location on normalized (a) force and (b) moment of force due to ejector flap with respect to nozzle pressure ratio for a 10 and 9 full staggered CD-chute mixer with 4/9-treated long ejector for L1M cycle conditions with flight simulation (M_F=0.32).
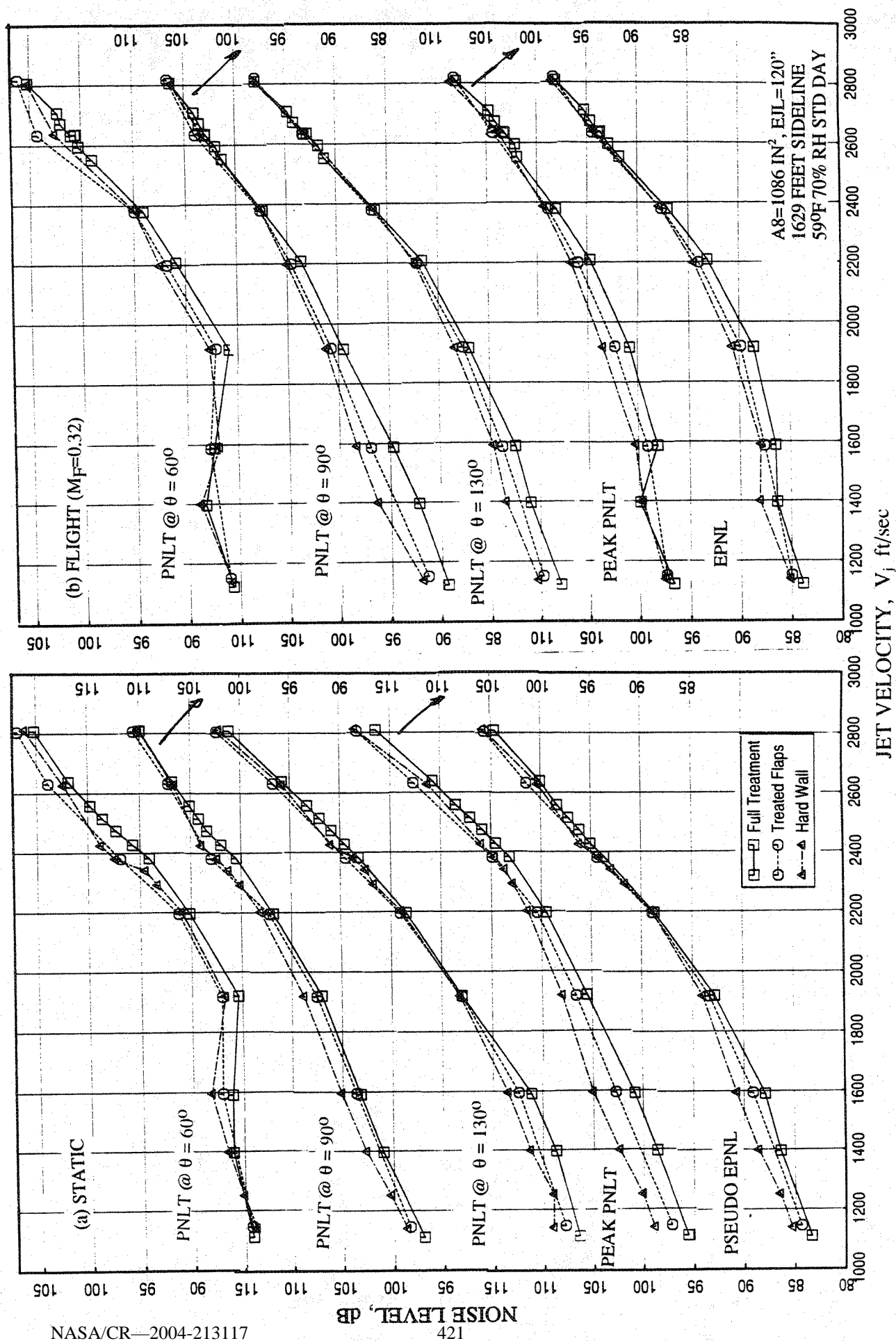
Figure 7-46. Comparison of EPNL, peak PNLT, and PNLT at various polar angles (θ) as functions of jet velocity between fully treated and flaps only treated long ejectors for a 10 and 9 full staggered CD-chute mixer; SAR=2.8, MAR = 0.95, ϕ=25°.

velocity range. However, the effect is more dominant at jet velocities below 2400 ft/sec. Compared to fully treated configuration, the acoustic suppression due to flap treatment is almost half in terms of EPNL and peak PNLT.

Comparison of PNLT directivities at jet velocities of 1147, 1920, 2384, and 2637 ft/sec between fully treated and flaps only treated ejector configurations are shown in Figure 7-47. The acoustic suppression in terms of PNLT due to flaps only treated ejector is lower compared to fully treated case. At most angles, especially for lower velocities, the acoustic suppression due to flaps is almost half of the total amount. Comparison of SPL spectra at various polar angles (θ) for each of the above mentioned four jet velocities between fully treated and flaps only treated ejector configurations are shown in Figures 7-48 through 7-51. Noise suppression due flap treatment in terms of SPL is significant at higher frequencies, especially for lower velocity conditions, compared to fully treated ejector. For higher velocity conditions the flaps only treated configuration contributes even higher SPL compared to hard wall ejector at lower frequencies. At V_j=2637 ft/sec the SPL levels are much higher for flaps only treated ejector compared to hard wall case in the forward arc, indicating the presence of stronger shock in the ejector (see Figure 7-51).

Results at Sideline Location (ϕ=90°): Comparison of PNLT directivities at jet velocities of 1147, 1920, 2384, and 2637 ft/sec between fully treated and flaps only treated ejector configurations are shown in Figure 7-52. The acoustic suppression in terms of PNLT due to flaps only treated ejector is lower compared to fully treated case. At most angles, especially for lower velocities, the acoustic suppression due to flaps is almost half of the total amount. The PNLT directivity patterns for flaps only treated ejector are distinctly different compared to those at ϕ=25°. Comparison of SPL spectra at various polar angles (θ) for each of the above mentioned four jet velocities between fully treated and flaps only treated ejector configurations are shown in Figures 7-53 through 7-56. Noise suppression due flap treatment in terms of SPL is significant at higher frequencies, especially for lower velocity conditions, compared to fully treated ejector, but is not of the same amount as of ϕ=25°. For higher velocity conditions the flaps only treated configuration contributes even higher SPL compared to hard wall ejector at lower frequencies. At V_j=2637 ft/sec the SPL levels are slightly higher, not as much at ϕ=25°, for flaps only treated ejector compared to the hard wall case in the forward arc (see Figure 7-56).
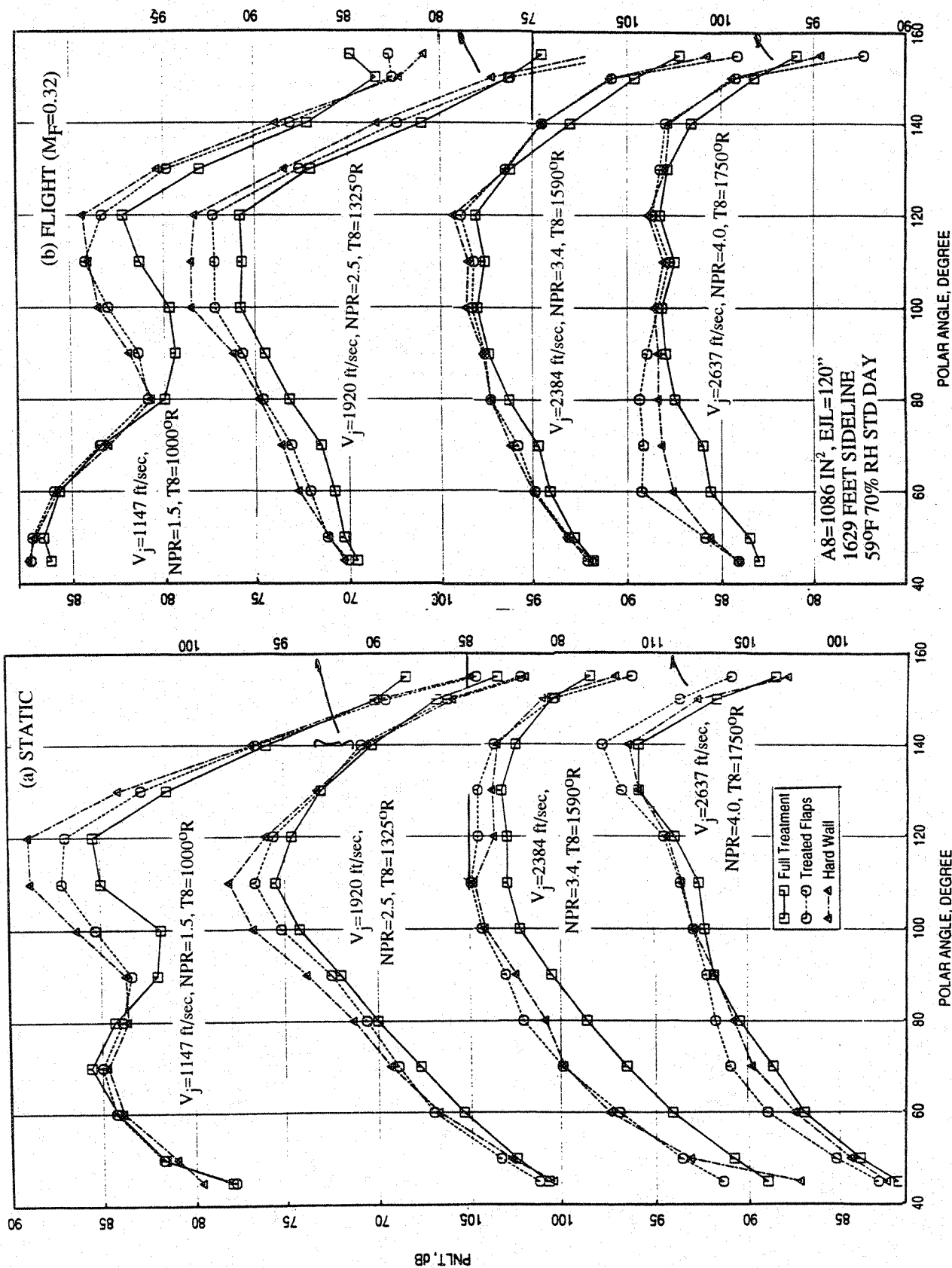
Figure 7-47. Comparison of PNLT directivities for different jet velocities (V_j) between fully treated and flaps only treated long ejectors for a 10 and 9 full staggered CD-chute mixer; SAR=2.8, MAR = 0.95, ϕ=25°.
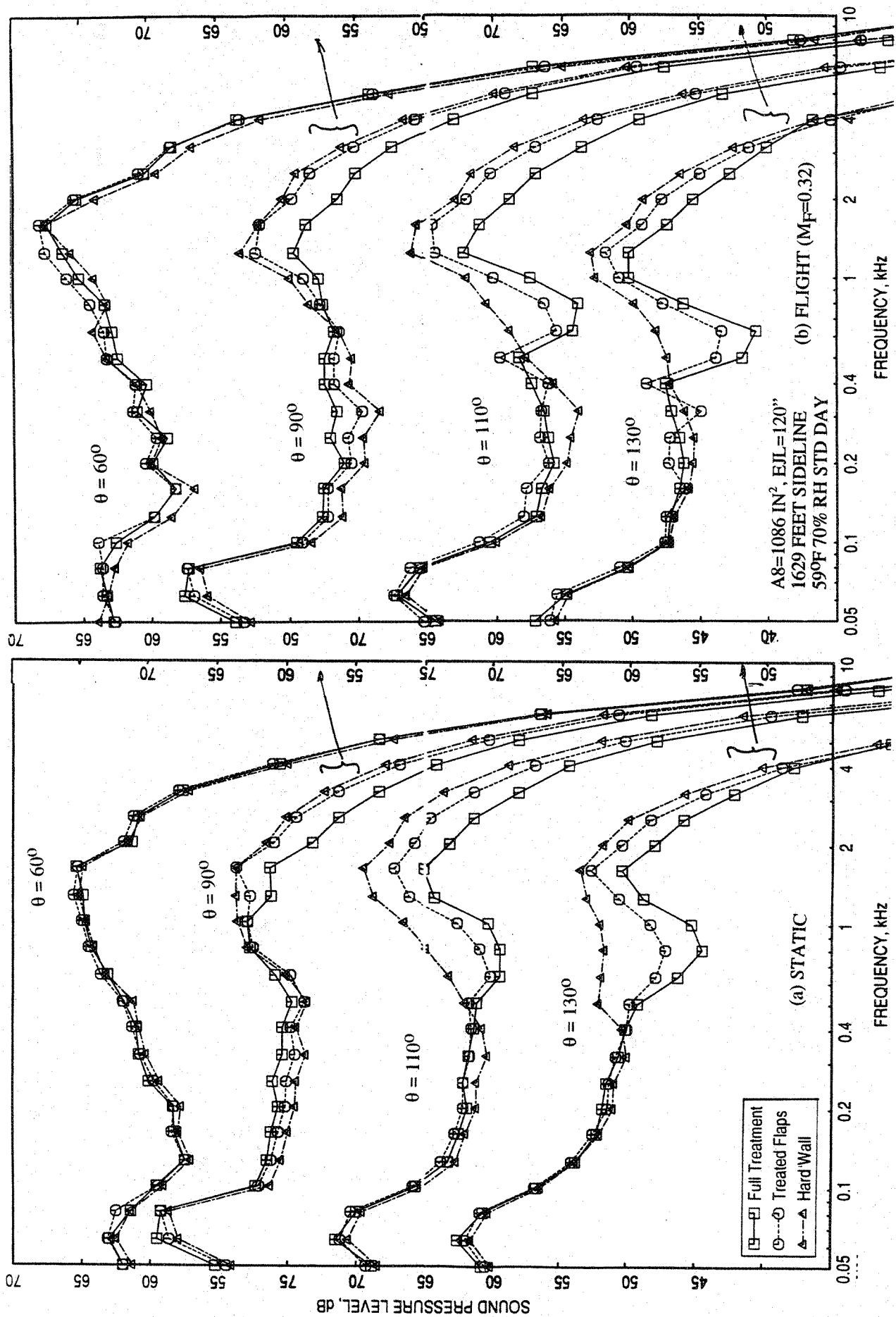
Figure 7-48. Comparison of SPL spectra at various polar angles (θ) between fully treated and flaps only treated long ejectors for a 10 and 9 full staggered CD-chute mixer; SAR=2.8, MAR = 0.95, V_j = 1147 ft/sec, NPR = 1.5, T8 = 1000°R, φ=25°.
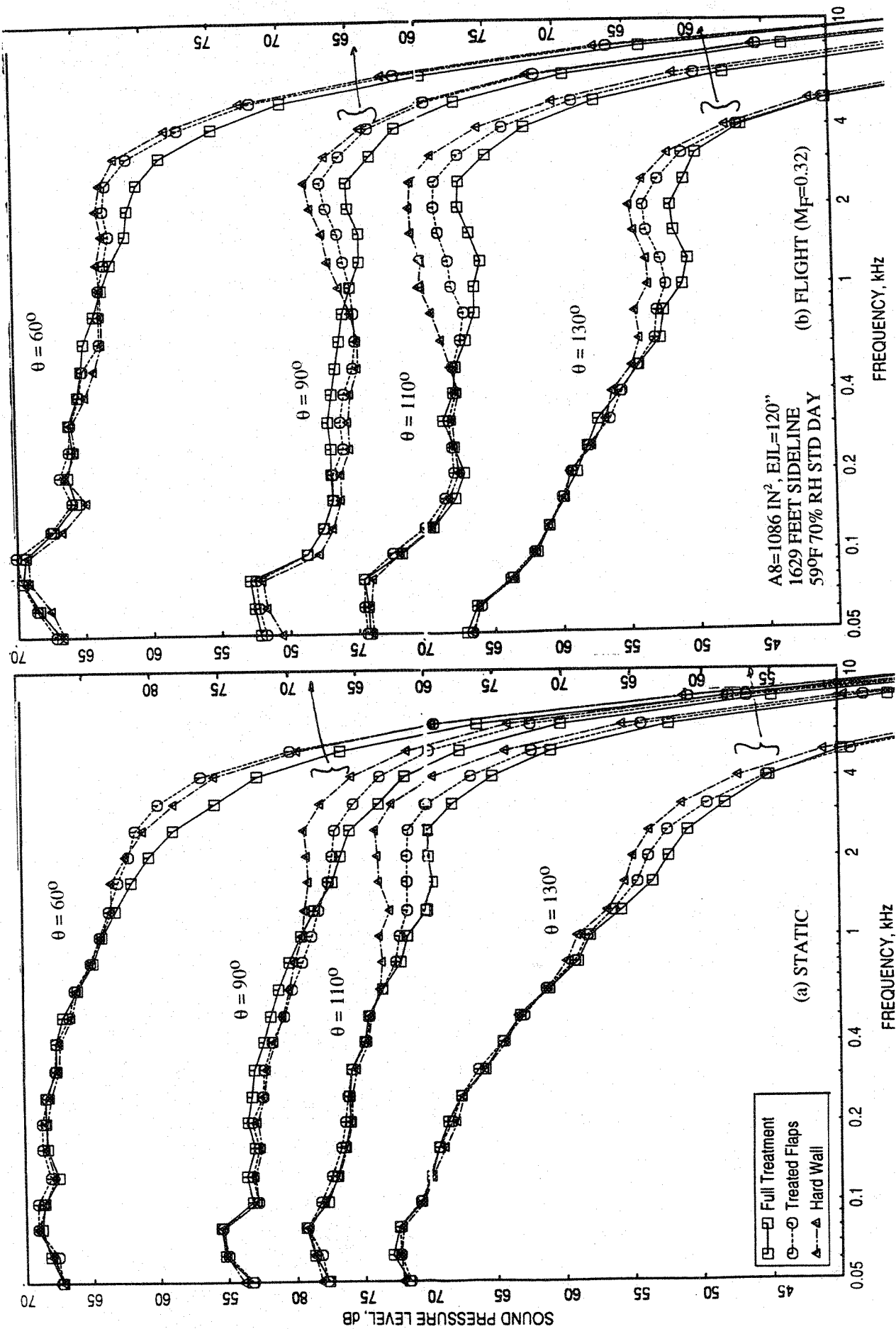
Figure 7-49. Comparison of SPL spectra at various polar angles (θ) between fully treated and flaps only treated long ejectors for a 10 and 9 full staggered CD-chute mixer; SAR=2.8, MAR = 0.95, V$_j$ = 1919 ft/sec, NPR = 2.5, T8 = 1325ºR, φ=25°.
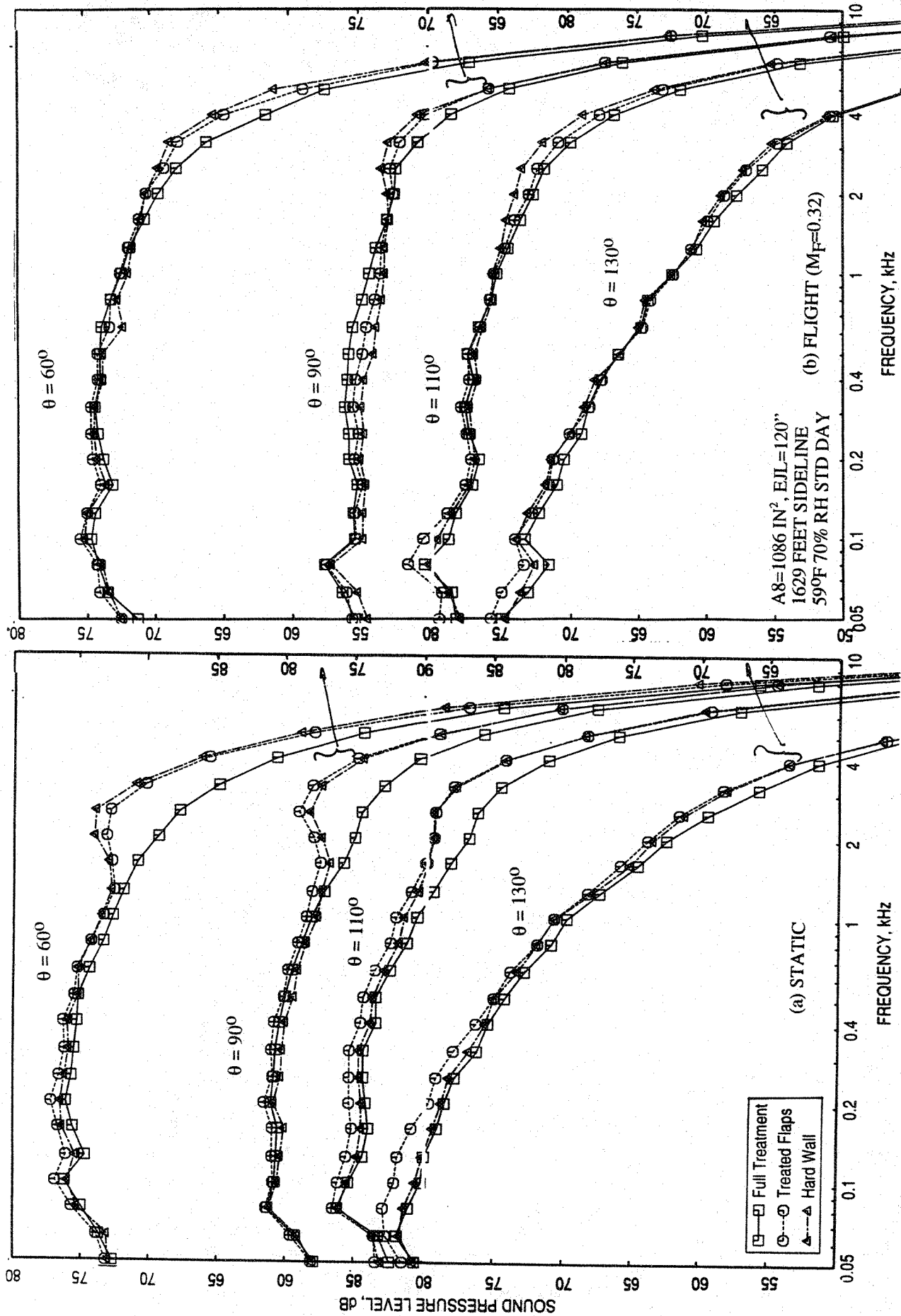
Figure 7-50. Comparison of SPL spectra at various polar angles (θ) between fully treated and flaps only treated long ejectors for a 10 and 9 full staggered CD-chute mixer; SAR=2.8, MAR = 0.95, V_j = 2384 ft/sec, NPR = 3.4, T8 = 1590°R, φ=25°.
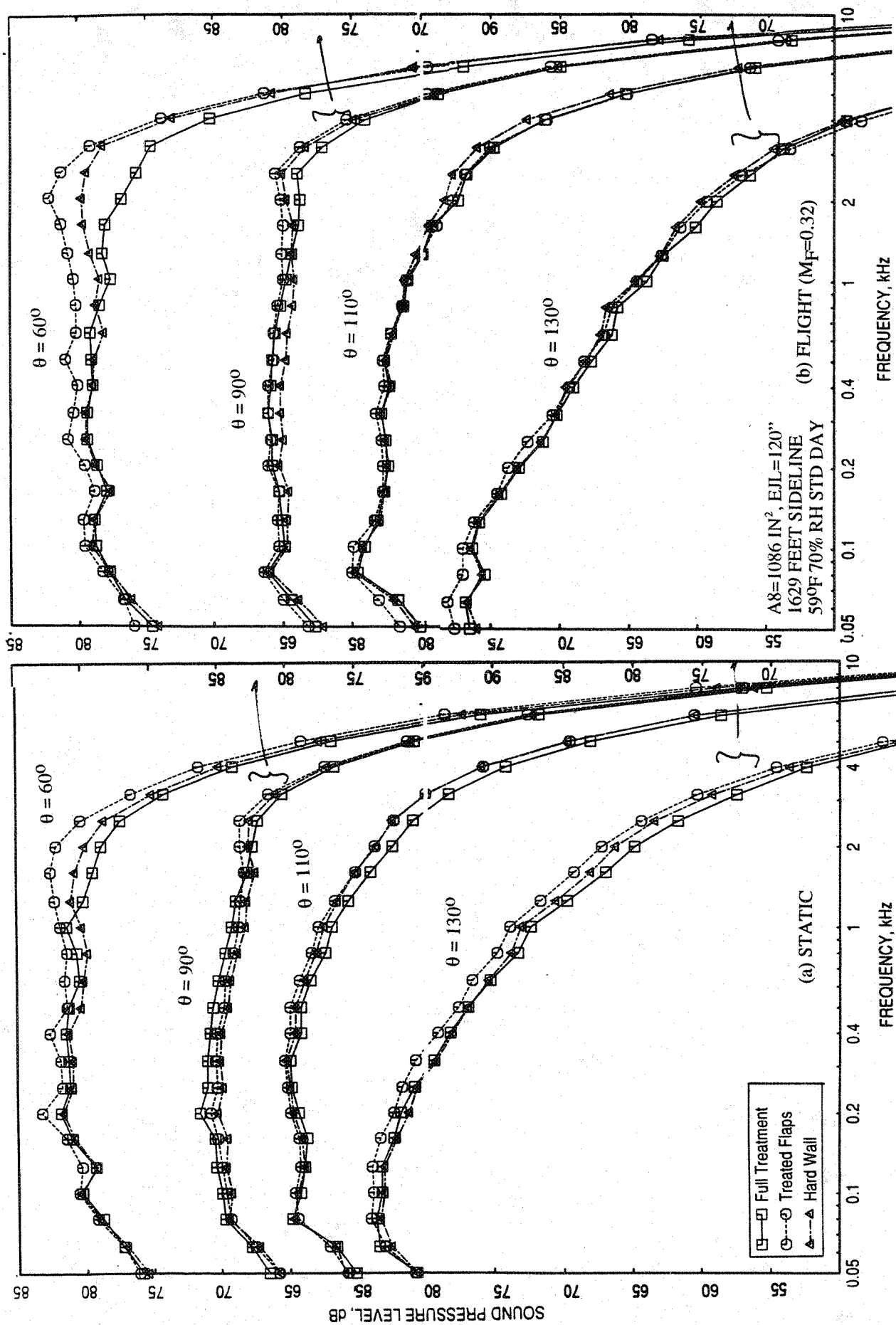
Figure 7-51. Comparison of SPL spectra at various polar angles (θ) between fully treated and flaps only treated long ejectors for a 10 and 9 full staggered CD-chute mixer; SAR=2.8, MAR = 0.95, V_j = 2637 ft/sec, NPR = 4.0, T8 = 1750°R, φ=25°.
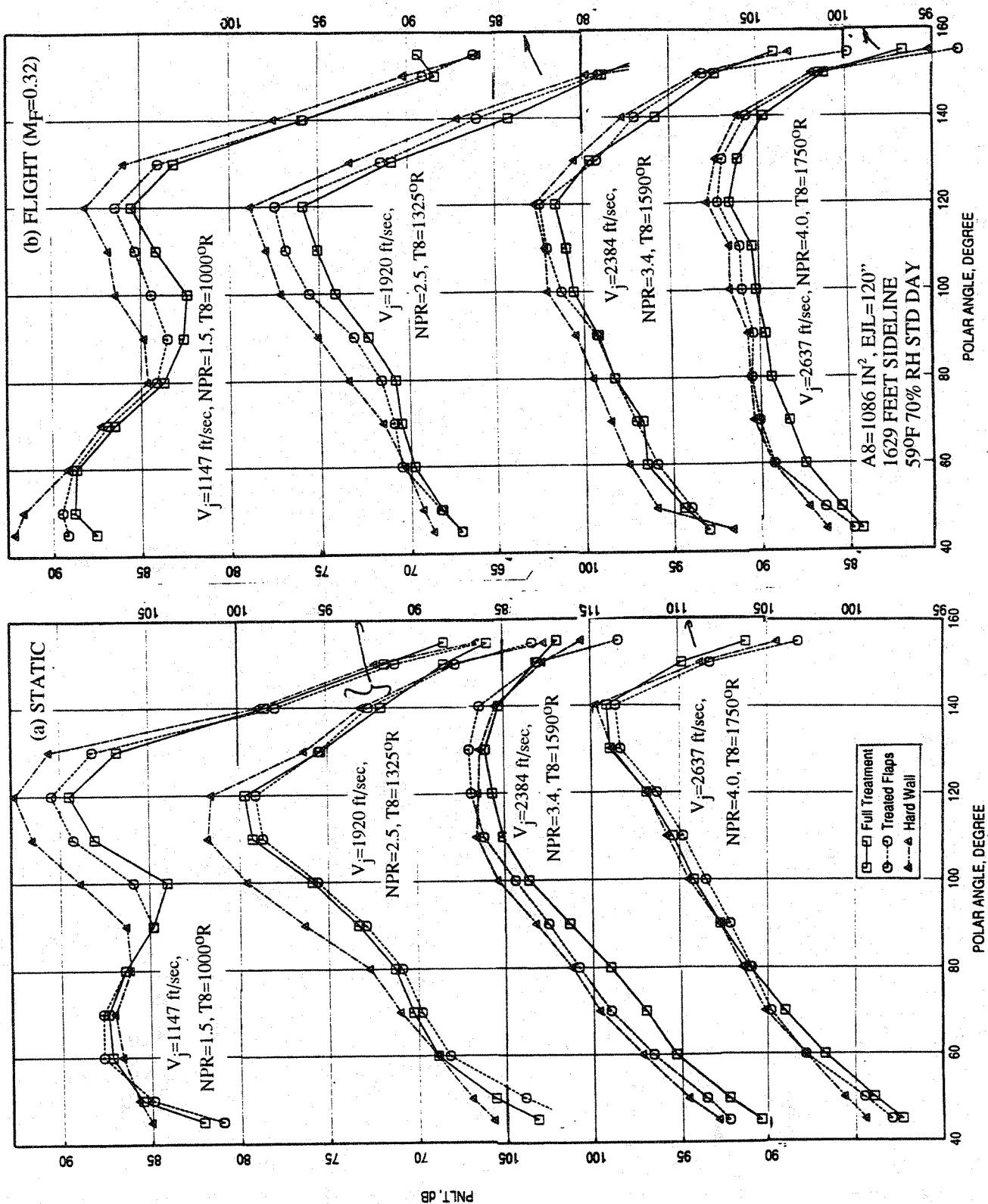
Figure 7-52. Comparison of PNLT directivities for different jet velocities (Vj between fully treated and flaps only treated long ejectors for a 10 and 9 full staggered CD-chute mixer; SAR=2.8, MAR = 0.95, φ=90°.

Figure 7-53. Comparison of SPL spectra at various polar angles (θ) between fully treated and flaps only treated long ejectors for a 10 and 9 full staggered CD-chute mixer; SAR=2.8, MAR = 0.95, V_j = 1147 ft/sec, NPR = 1.5, T8 = 1000°R, φ=90°.

Figure 7-54. Comparison of SPL spectra at various polar angles (θ) between fully treated and flaps only treated long ejectors for a 10 and 9 full staggered CD-chute mixer; SAR=2.8, MAR = 0.95, V_j = 1919 ft/sec, NPR = 2.5, T8 = 1325°R, φ=90°.
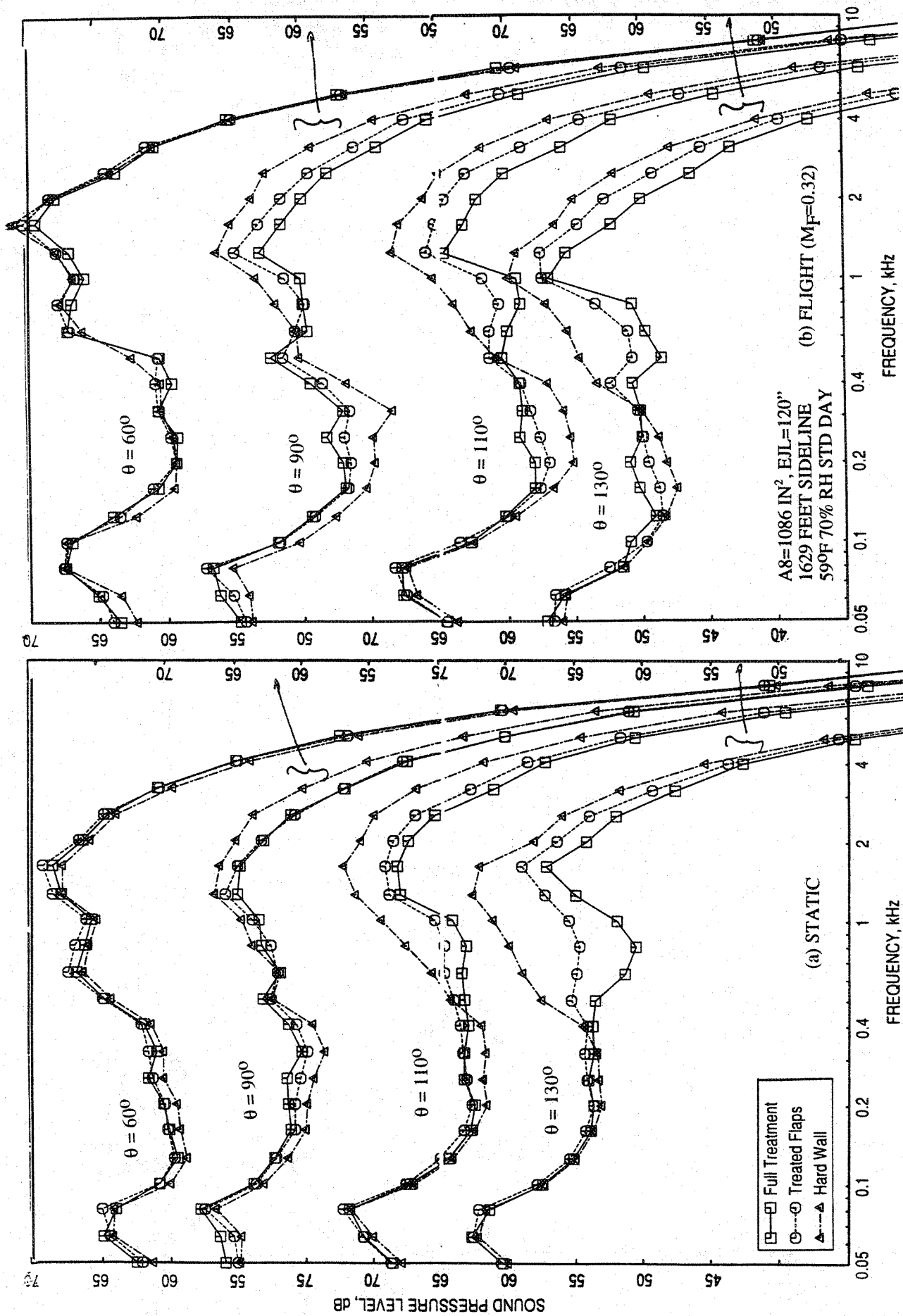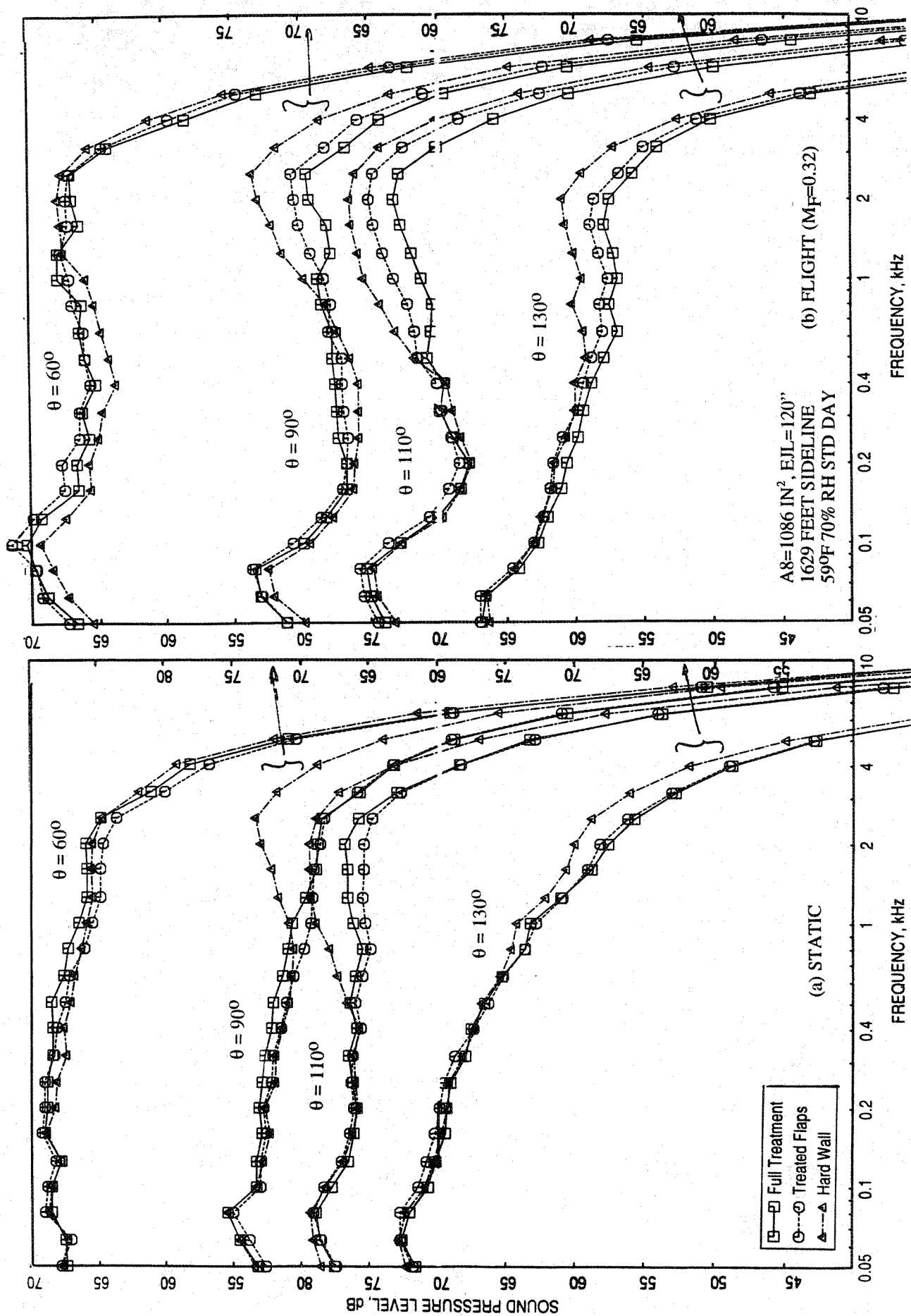
Figure 7-55. Comparison of SPL spectra at various polar angles (θ) between fully treated and flaps only treated long ejectors for a 10 and 9 full staggered CD-chute mixer; SAR=2.8, MAR = 0.95, V_j = 2384 ft/sec, NPR = 3.4, T8 = 1590ºR, ϕ=90º.
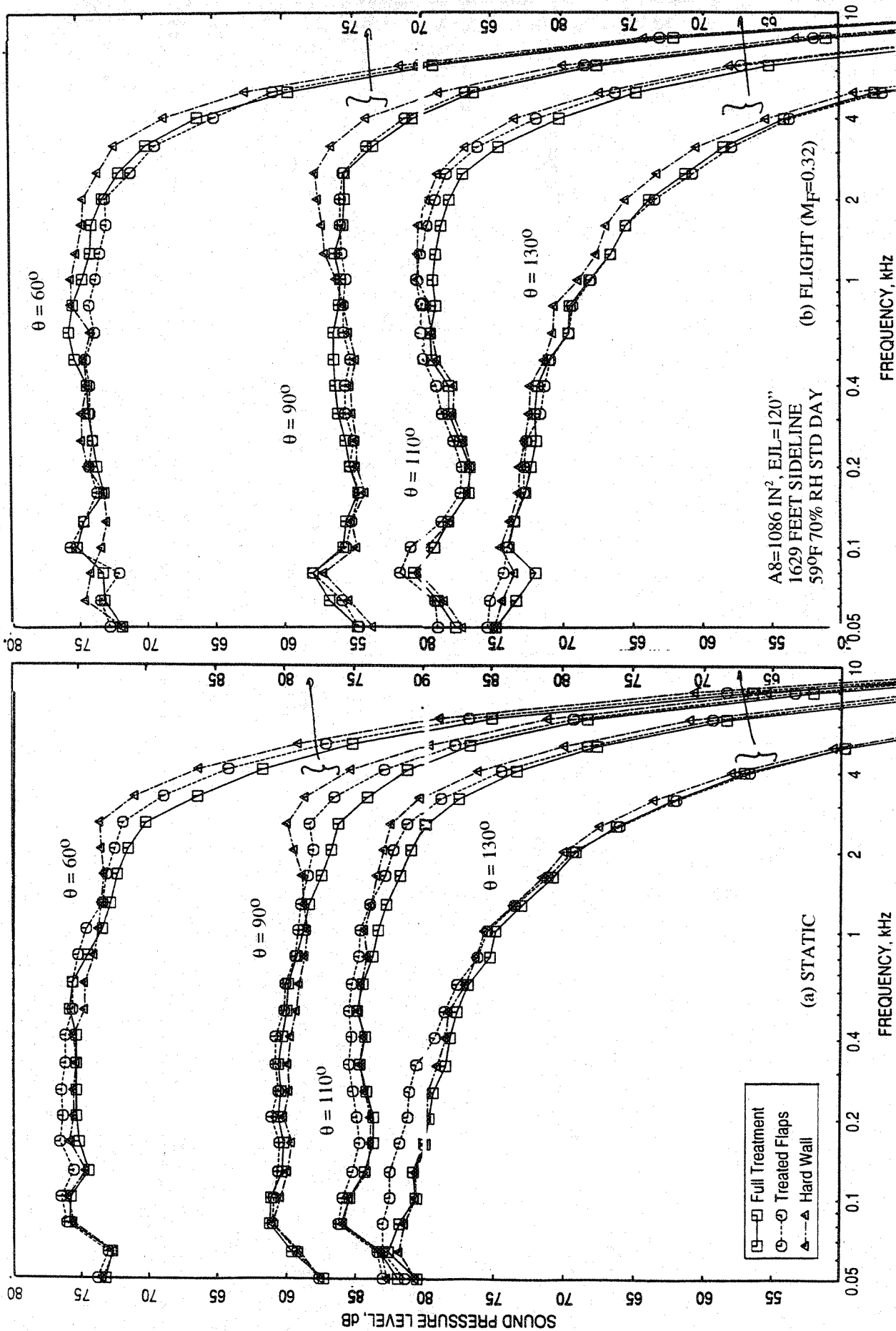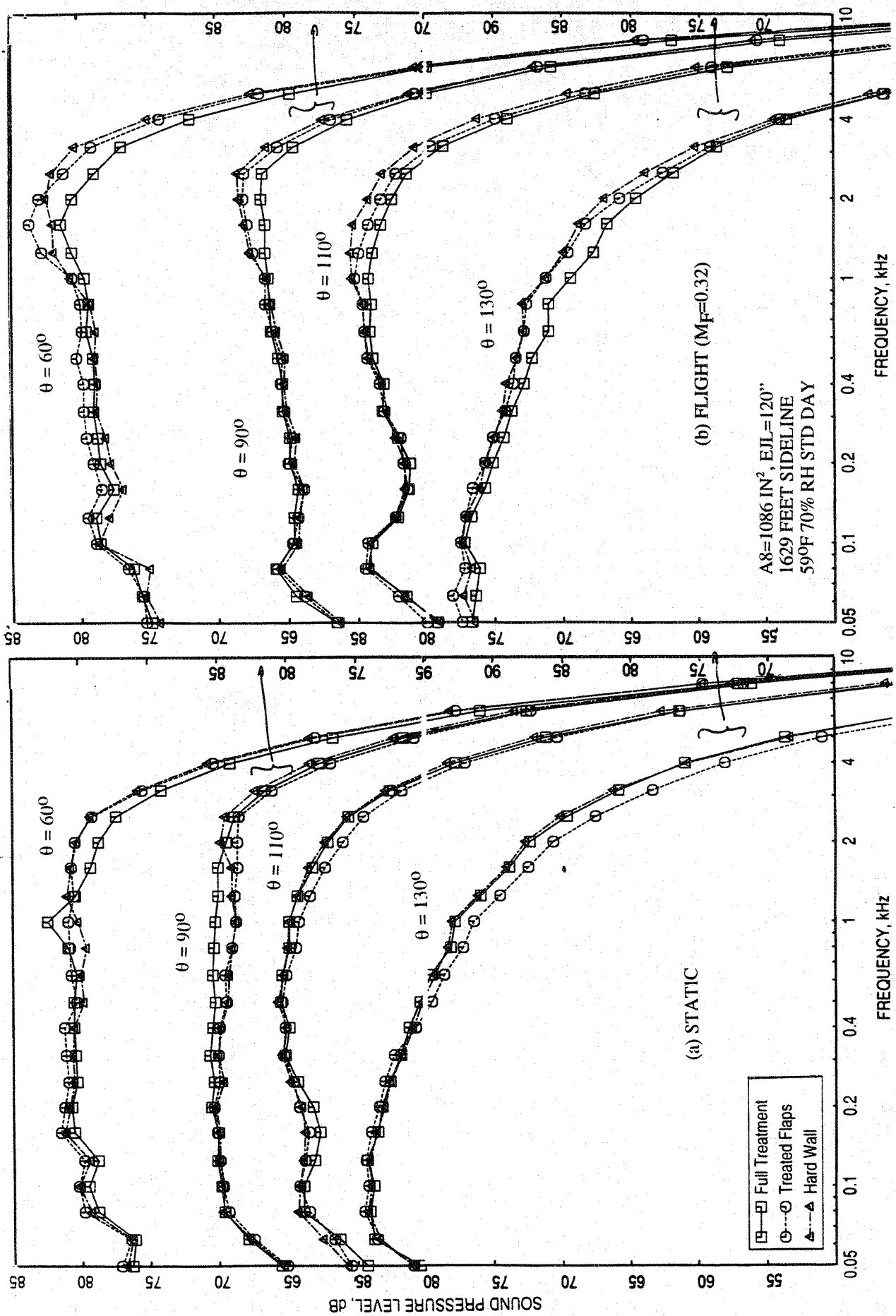
Figure 7-56. Comparison of SPL spectra at various polar angles (θ) between fully treated and flaps only treated long ejectors for a 10 and 9 full staggered CD-chute mixer; SAR=2.8, MAR = 0.95, V_j = 2637 ft/sec, NPR = 4.0, T8 = 1750°R, ϕ=90°.

The impact of full treatment to partial treatment (i.e., flaps only case) in terms of noise suppression is more distinct at lower velocities for the same reason that the externally generated mixing noise is lower at these velocities. At higher velocity conditions the externally generated noise dominates in the farfield and thus blankets out the actual impact of ejector treatment variation.

7.4.2 Flow and Performance Related Parameters:

The influence of fully treated ejector compared to flaps only treated ejector on ramp and chute static pressure distributions is insignificant for static as well as with flight simulation. The chute loading coefficients due to chute static pressure distributions showing the effect of fully treated ejector compared to flaps only treated ejector are plotted against NPR in Figure 7-57. The chute loading coefficients for flaps only treated configuration are slightly higher compared to those for fully treated case.

Comparison of pumping and corrected pumping between fully treated and flaps only treated ejectors is shown in Figures 7-58 and 7-59 for static and flight cases, respectively. Pumping is slightly higher for flaps only treated configuration. For flaps only treated configuration the ejector cross-sectional area is higher compared to the fully treated configuration. This may be the reason for higher pumping for flaps only treated configuration.

Figure 7-60 shows the comparison of axial static pressure distributions on the flap at static condition at different L1M cycle conditions between fully treated and flaps only treated configurations. Very little difference in pressure distributions is observed between these configurations at lower NPRs. At higher NPRs the static pressure distribution on the flap indicates delayed mode switch for fully treated ejector compared to flaps only treated configuration. Figure 7-61 shows the comparison of force and moment of force with respect to flap leading edge due to static pressure difference on flap surface as a function of nozzle pressure ratio between fully treated and flaps only treated configurations. The transition from subsonic to supersonic mode seems to be slightly delayed for fully treated ejector configuration. Similar results with flight simulation are plotted in Figures 7-62 and 7-63. The static pressure distributions and the force and moment of the force results between these configurations clearly indicate that the mode switch is delayed for fully treated ejector configuration compared to flaps only treated case with flight simulation.
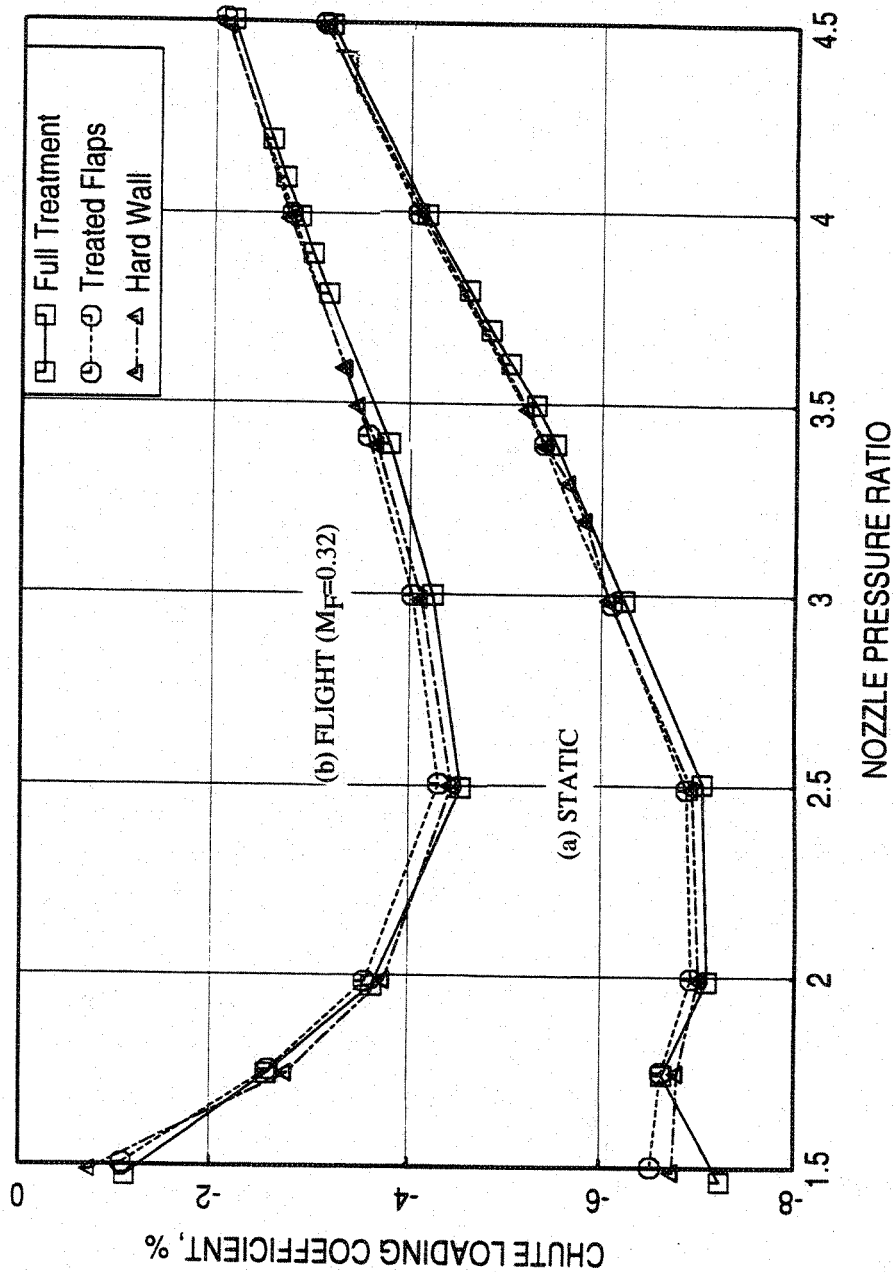
Figure 7-57. Comparison of chute loading coefficient with respect to nozzle pressure ratio between fully treated and flaps only treated long ejectors for a 10 and 9 full staggered CD-chute mixer; SAR=2.8, MAR = 0.95 for L1M cycle conditions (a) at static condition and (b) with flight simulation (M_F=0.32).

Figure 7-58. Comparison of pumping with respect to nozzle pressure ratio between fully treated and flaps only treated long ejectors for a 10 and 9 full staggered CD-chute mixer; SAR=2.8, MAR = 0.95 for L1M cycle conditions at static condition.
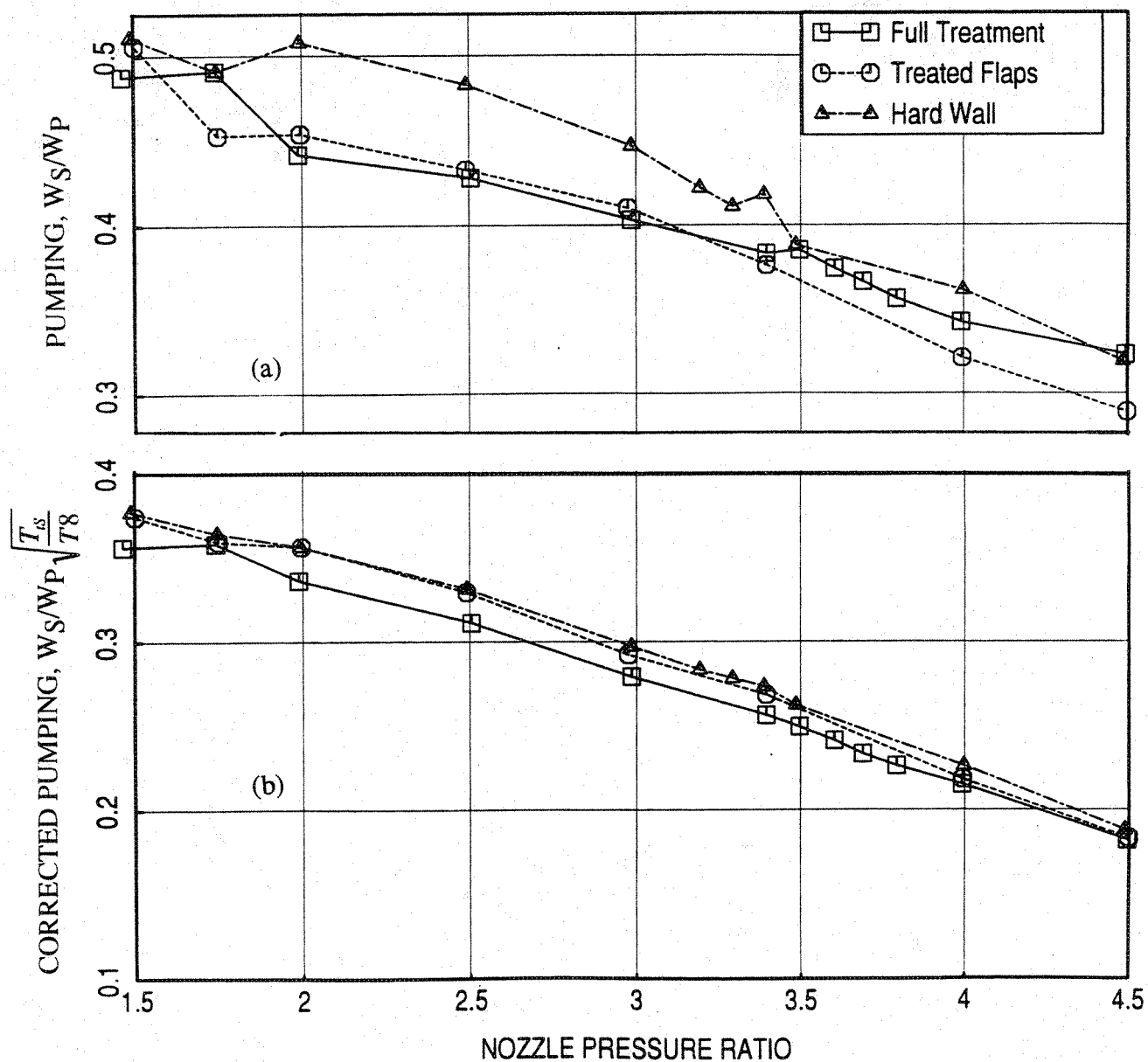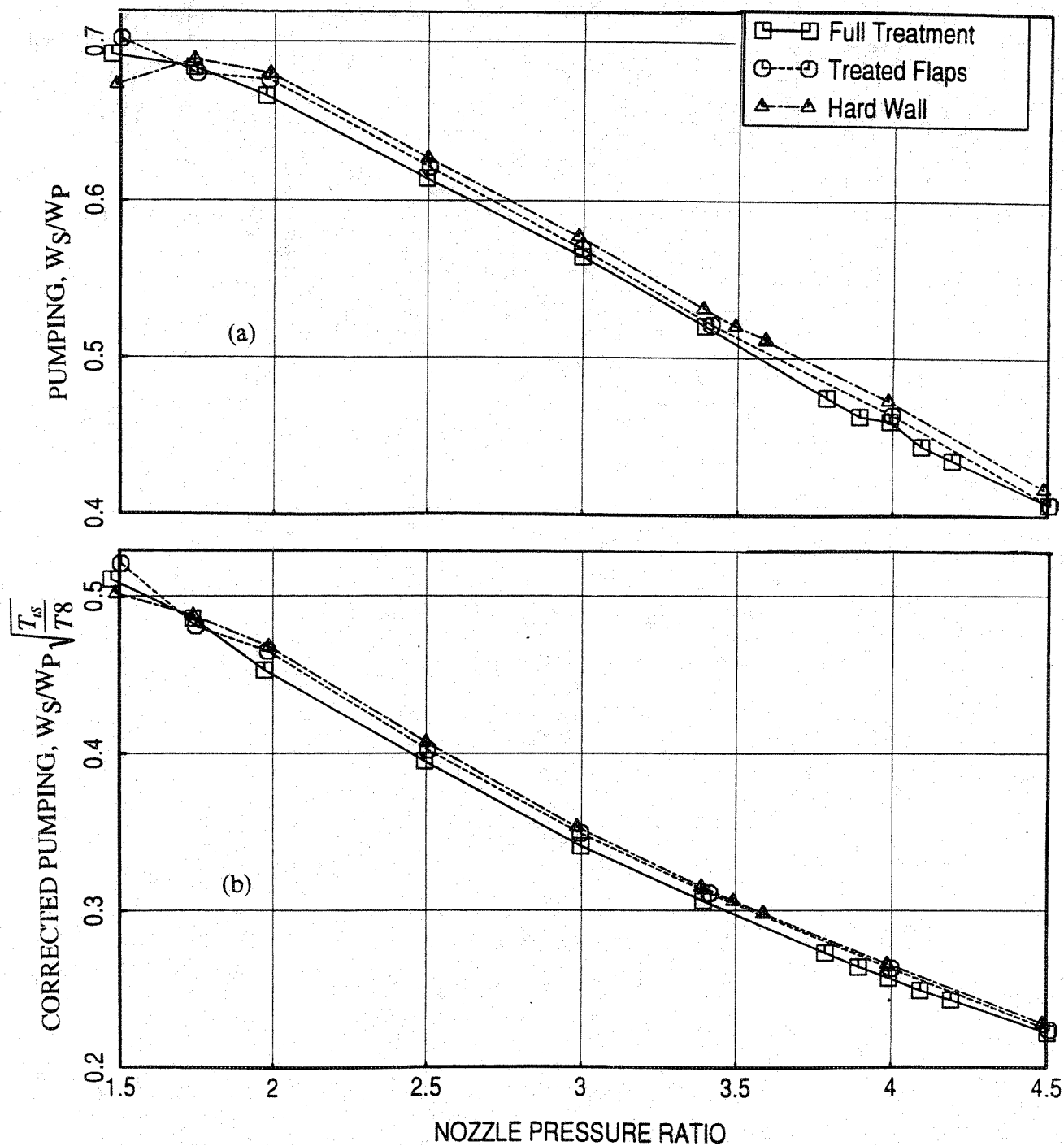
Figure 7-59. Comparison of pumping with respect to nozzle pressure ratio between fully treated and flaps only treated long ejectors for a 10 and 9 full staggered CD-chute mixer; SAR=2.8, MAR = 0.95 for L1M cycle conditions with flight simulation (M_F=0.32).

Figure 7-60. Comparison of axial distribution of average static pressure on the inlet and the flap surface between fully treated and flaps only treated ejectors at different L1M cycle conditions for a 10 and 9 full staggered CD-chute mixer; SAR=2.8, MAR = 0.95 at static condition.

Figure 7-61. Comparison of normalized (a) force and (b) moment of force due to ejector flap between fully treated and flaps only treated ejectors with respect to nozzle pressure ratio for a 10 and 9 full staggered CD-chute mixer; SAR=2.8, MAR = 0.95 at static condition.
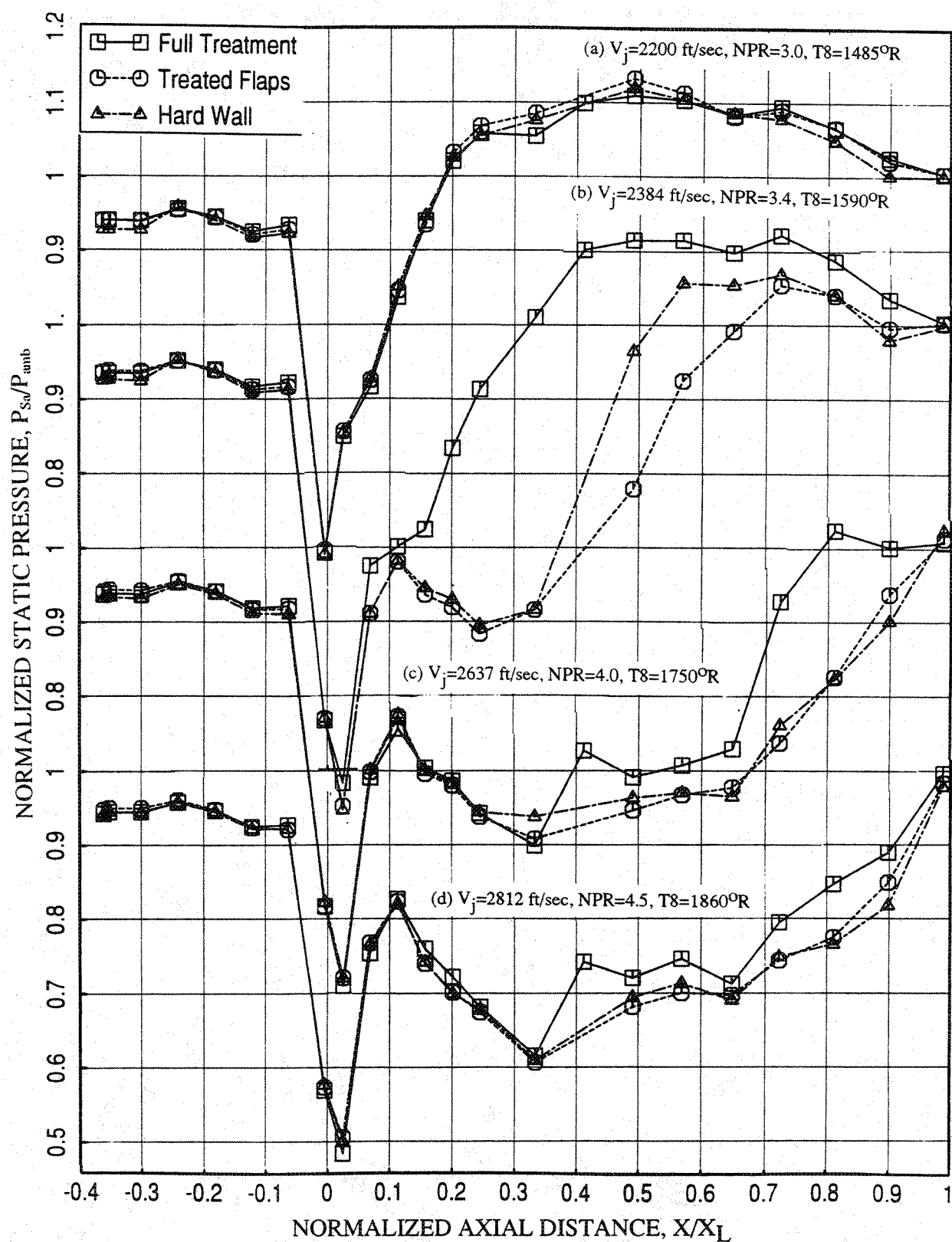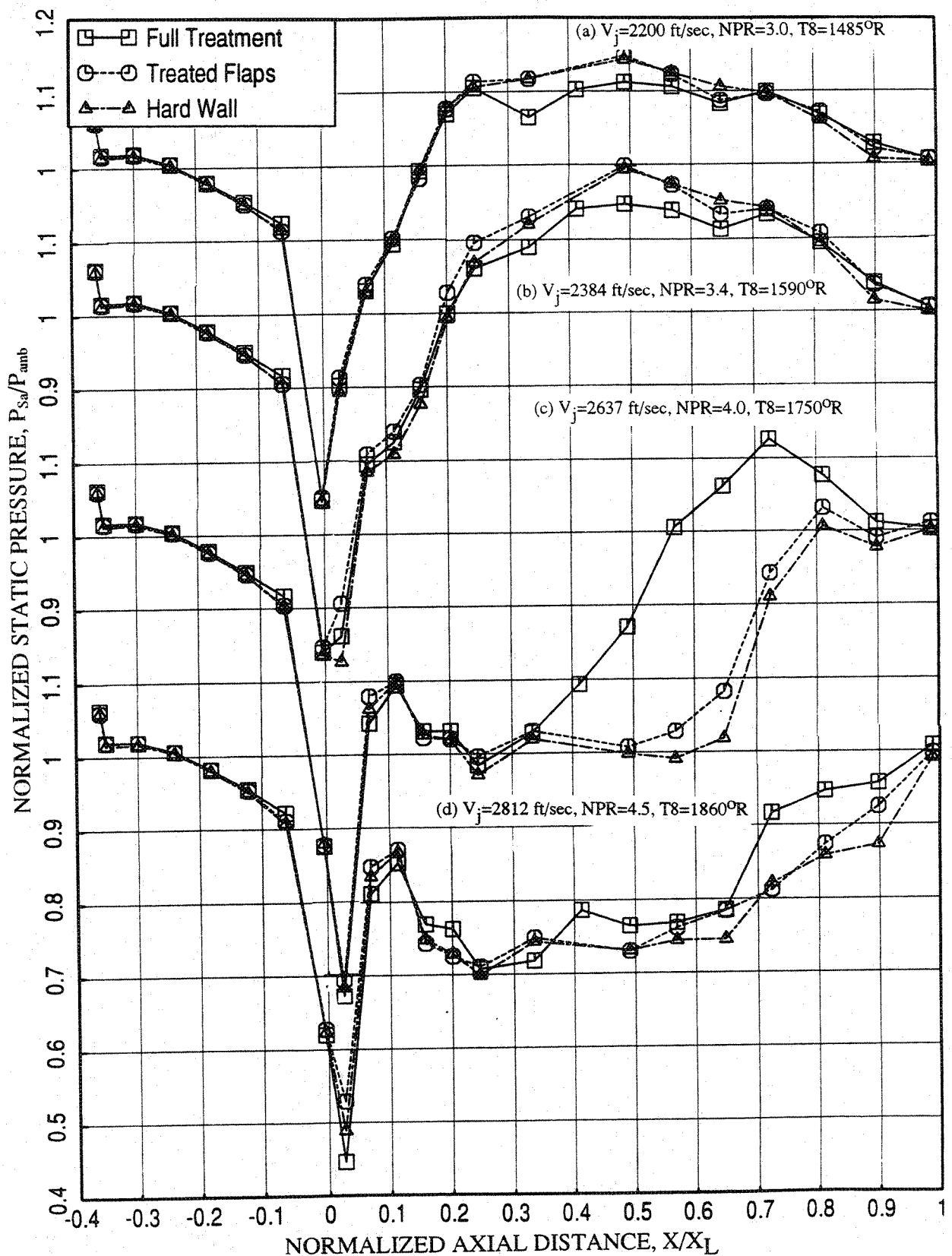
Figure 7-62. Comparison of axial distribution of average static pressure on the inlet and the flap surface between fully treated and flaps only treated ejectors at different L1M cycle conditions for a 10 and 9 full staggered CD-chute mixer; SAR=2.8, MAR = 0.95 with flight simulation (M_F=0.32).
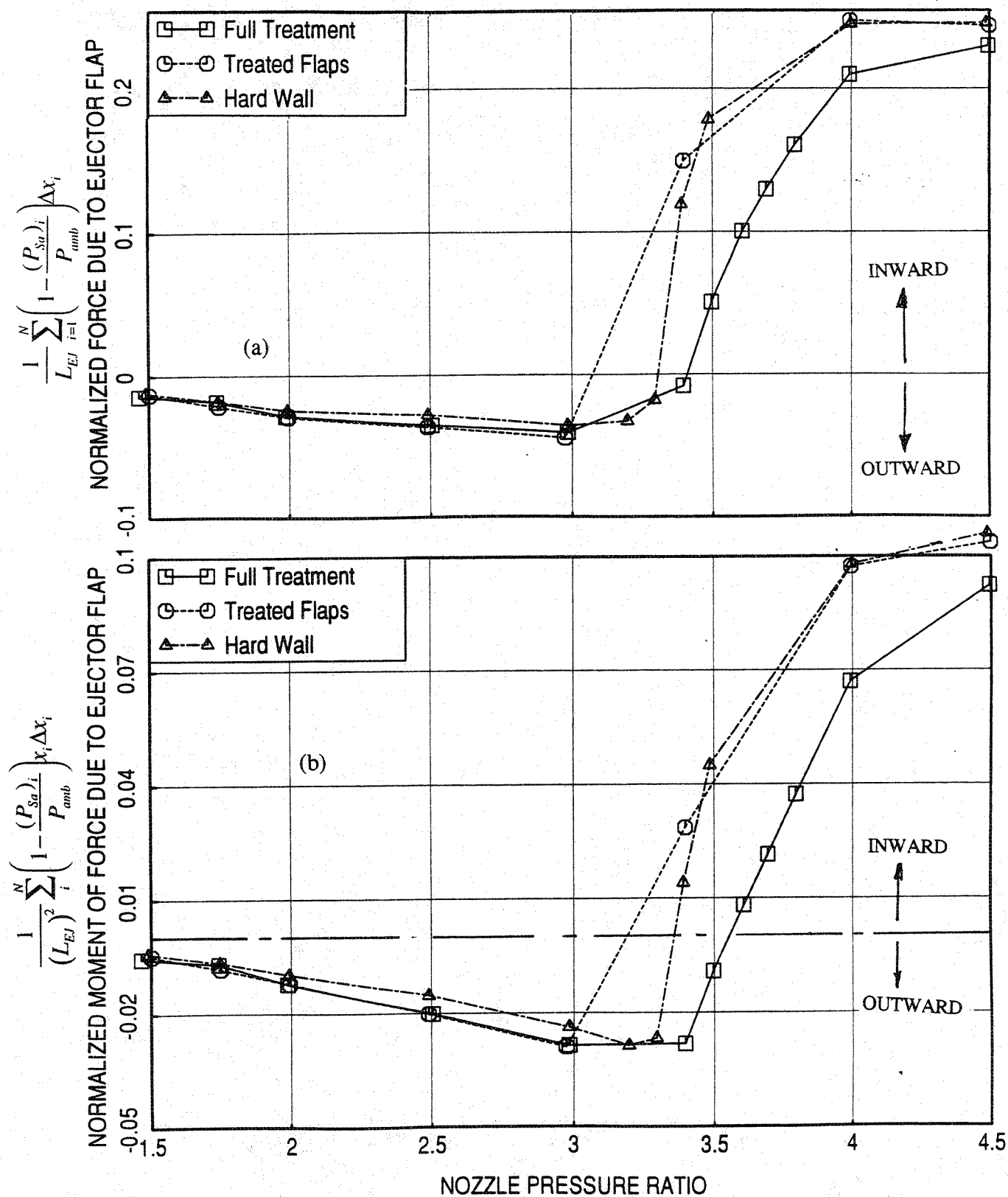
Figure 7-63. Comparison of normalized (a) force and (b) moment of force due to ejector flap between fully treated and flaps only treated ejectors with respect to nozzle pressure ratio for a 10 and 9 full staggered CD-chute mixer; SAR=2.8, MAR = 0.95 with flight simulation (M_F=0.32).
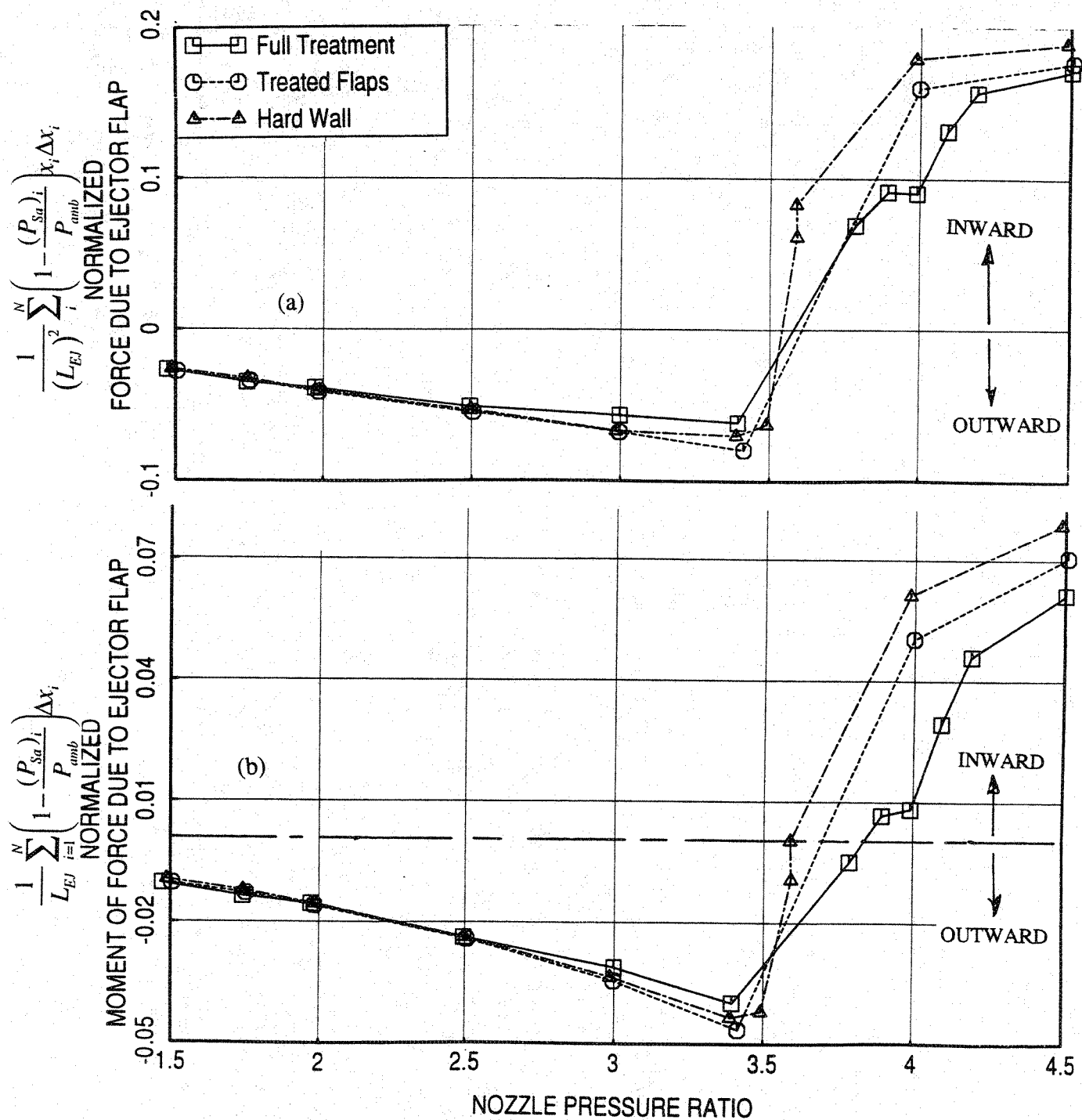
7.5 INFLUENCE OF BULK MATERIAL USED FOR EJECTOR TREATMENT:

The nickel based bulk absorber used in most configurations has relatively higher density and thus it is unlikely to be a candidate for HSCT application. Therefore, another bulk material, namely, silicon carbide with about 100 pores per inch is tested as the ejector treatment material. The 10 and 9 full staggered CD-chute mixer-ejector nozzle configurations with fully treated ejector (i.e., Configurations #11 and 22) were tested in Cell 41 with two different bulk absorber treatments, namely, a Nickel based foam metal (FM) and a Silicon Carbide foam with the same 37% open perforated facesheet. The farfield acoustic results for these two configurations are compared in this section to evaluate the relative suppression capability of these two absorbers.

The normal impedance for these two treatments (i.e., bulk with perforated facesheet) was measured at room temperature by using 0.6" diameter samples and compared in Figure 7-64. The actual levels of resistance and reactance would be different at the operating condition of the ejector. In general, the specific resistance is likely to increase and the reactance is slightly to decrease due to grazing flow. At the same time, some decrease in resistance is expected due to temperature increase. However, the impedance result of Figure 7-64 is a relative comparison between the two different treatments at the same condition. Optimum specific resistance and reactance for better acoustic suppression are established to be between 1.5 to 2.0 and -0.5 to 0, respectively. At frequencies between 7 and 12 kHz, the resistance as well as the reactance levels for silicon carbide are lower compared to nickel foam. Also, at higher frequencies above 14 kHz the reactance levels for Silicon Carbide treatment remains lower (closer to 0 level) compared to nickel foam. In general, the resistance and reactance levels remain near optimum goals for larger frequency ranges for Silicon Carbide treatment compared to nickel foam. Thus, the silicon carbide treatment is expected to perform better compared to nickel foam. It should be noted that the scale model frequency is plotted in Figure 7-64, whereas, the full scale frequencies to be compatible with the acoustic results, will be 1/7-times of these values.

The acoustic results presented in this section are the comparisons of test data between the same mixer-ejector with foam metal (FM) and silicon carbide foam acoustic treatments at the sideline point at a distance of 1629' with respect to major axis with respect to the major axis (i.e., $\phi = 25°$). Figure 7-65 shows the comparison of EPNL, peak PNLT, and
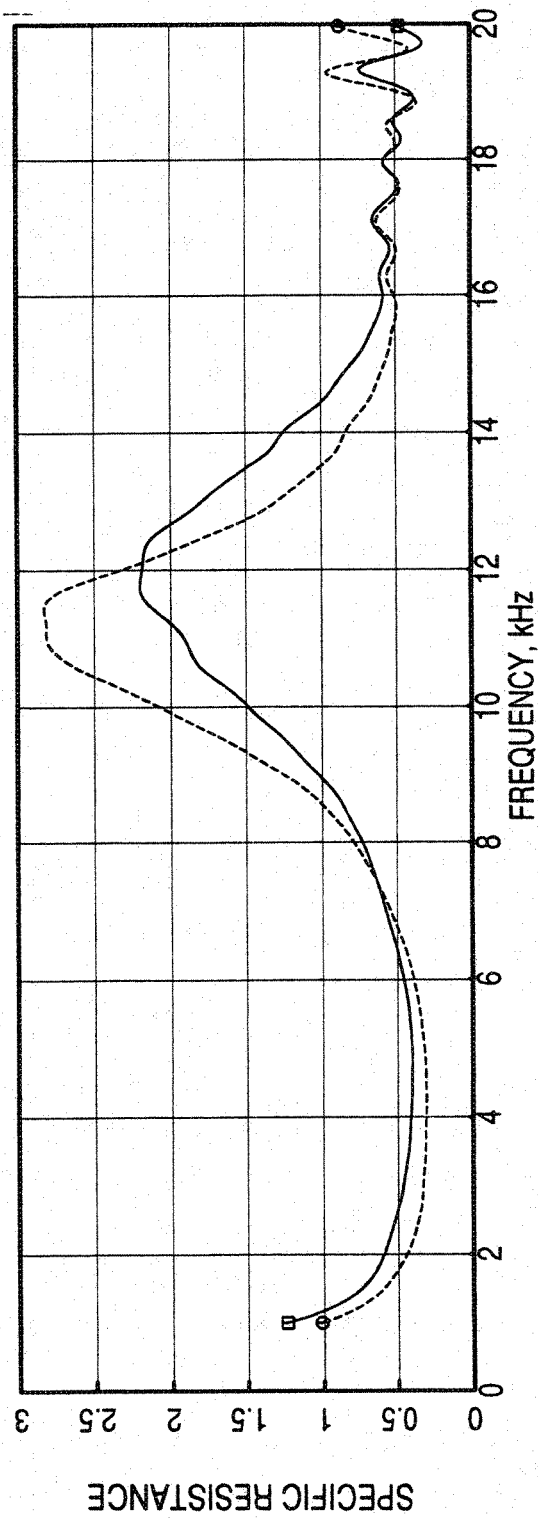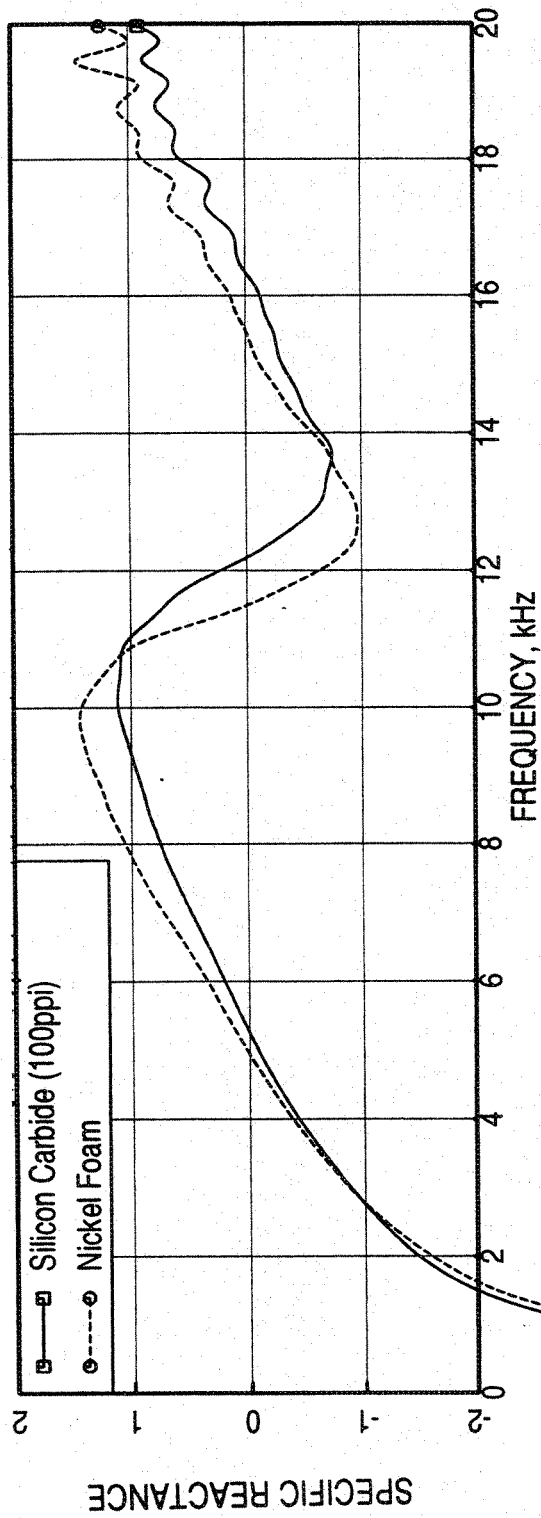
Figure 7-64. Effect of bulk material on the normal acoustic impedance of the ejector treatment (with the 37% open perforated facesheet, thickness=0.025", hole diameter=0.045") at room temperature temperature, excitation OASPL = 150 dB.
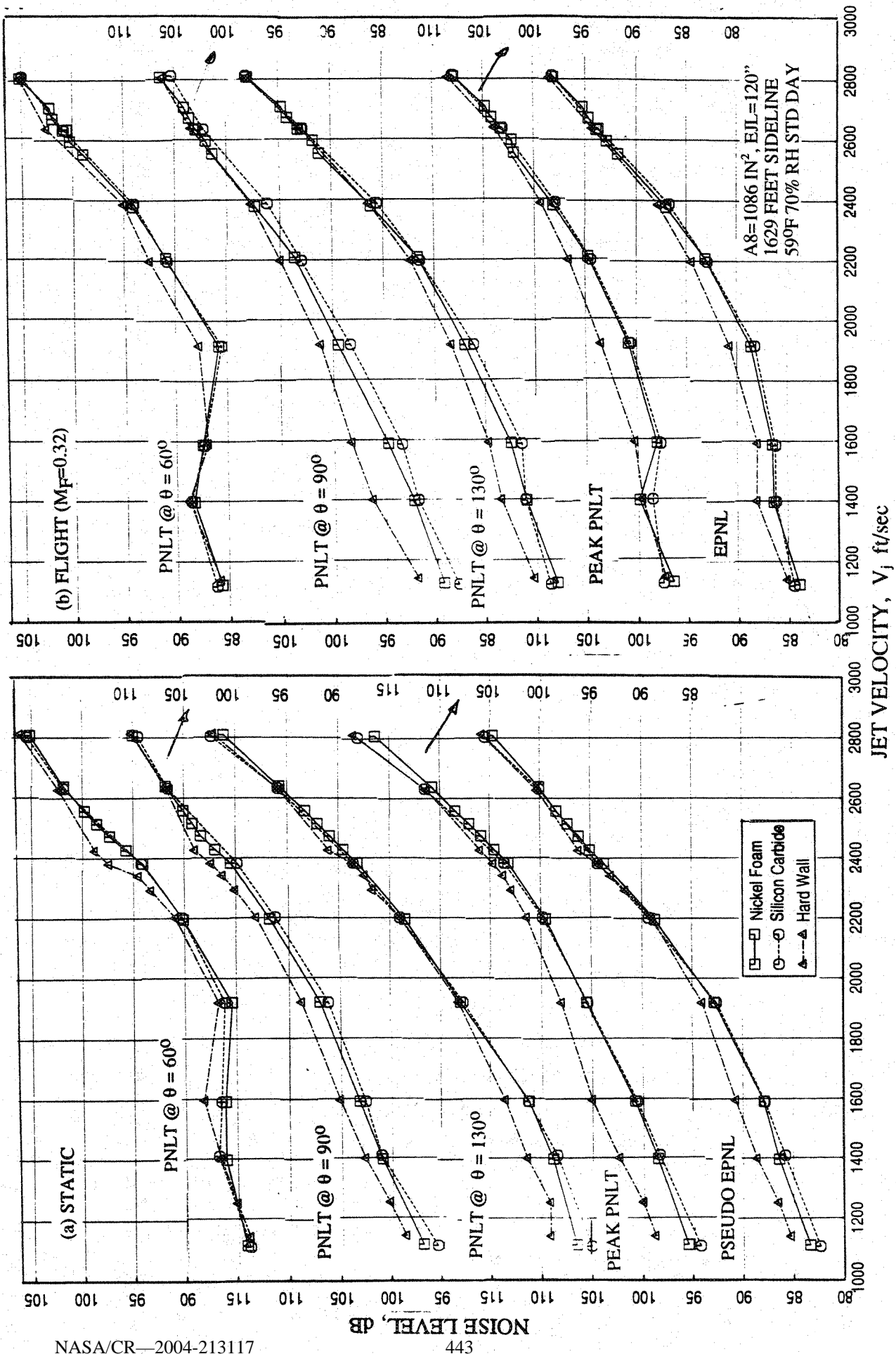
Figure 7-65. Effect of treatment material on EPNL, peak PNLT, and PNLT at various polar angles (θ) as functions of jet velocity for a 10 and 9 full staggered CD-chute mixer with fully treated long ejector; SAR=2.8, MAR = 0.95.

PNLT at various polar angles (θ) as functions of jet velocity (V_j) between ejectors with foam metal and silicon carbide treatments. Results for hardwalled configuration are also plotted in these figures. The EPNL levels for silicon carbide treatment are almost the same as those for foam metal configuration at higher velocity conditions. At lower jet velocities the acoustic suppression in terms of EPNdB is slightly higher for silicon carbide treatment compared to foam metal. Similar trends are observed with respect to PNdB.

PNLT directivities at jet velocities of 1147, 1595, 1920, and 2384 ft/sec are compared between foam metal and silicon carbide treated configurations in Figure 7-66. The PNLT levels with silicon carbide treatment are lower at most polar angles, except at lower angles in the forward arc, compared to foam metal configuration. Spectral comparisons at various polar angles (θ) for each of the four jet velocities are shown in Figures 7-67 through 7-70. Again, the sound pressure levels for silicon carbide treated configuration are lower compared to foam metal treatment, especially, at higher frequencies with lower jet velocity conditions. In general, the silicon carbide seems to be performing as well as and, in most cases, slightly better than the foam metal treatment. The performance and flow related results are very little influenced by the type of bulk used in the ejector treatment. Hence these results are not included in this section.

Conclusions: For the treatment study, the acoustically performing best mixer-ejector configuration (i.e., the 10 and 9 full staggered CD-chute mixer with long ejector) is used to identify any additional acoustic benefit. The mixer-ejector configurations used under current programs generate dominant jet mixing noise compared to internally generated noise in the farfield, especially at higher jet velocity conditions. Thus, the influence of various parameters altered in ejector treatment on the farfield noise is small at higher velocities. However, significant impact is noticed on farfield noise due to treatment variation at lower jet velocities. It is believed that the influence of all these treatment parameters on internally generated noise is similar, even though, not experienced in the farfield for higher jet velocity conditions. If the jet-mixing noise is reduced by better mixer design or suitably applying other innovative means the impact of internal noise will be realized even at higher jet velocity conditions and the treatment study would be beneficial. Following are the major observations due to treatment study:

(1) The fully treated ejector performs the best. However, 7/9 treatment is close to the full treatment configuration, especially at higher velocities. (2) The 0.5"-thick treatment is

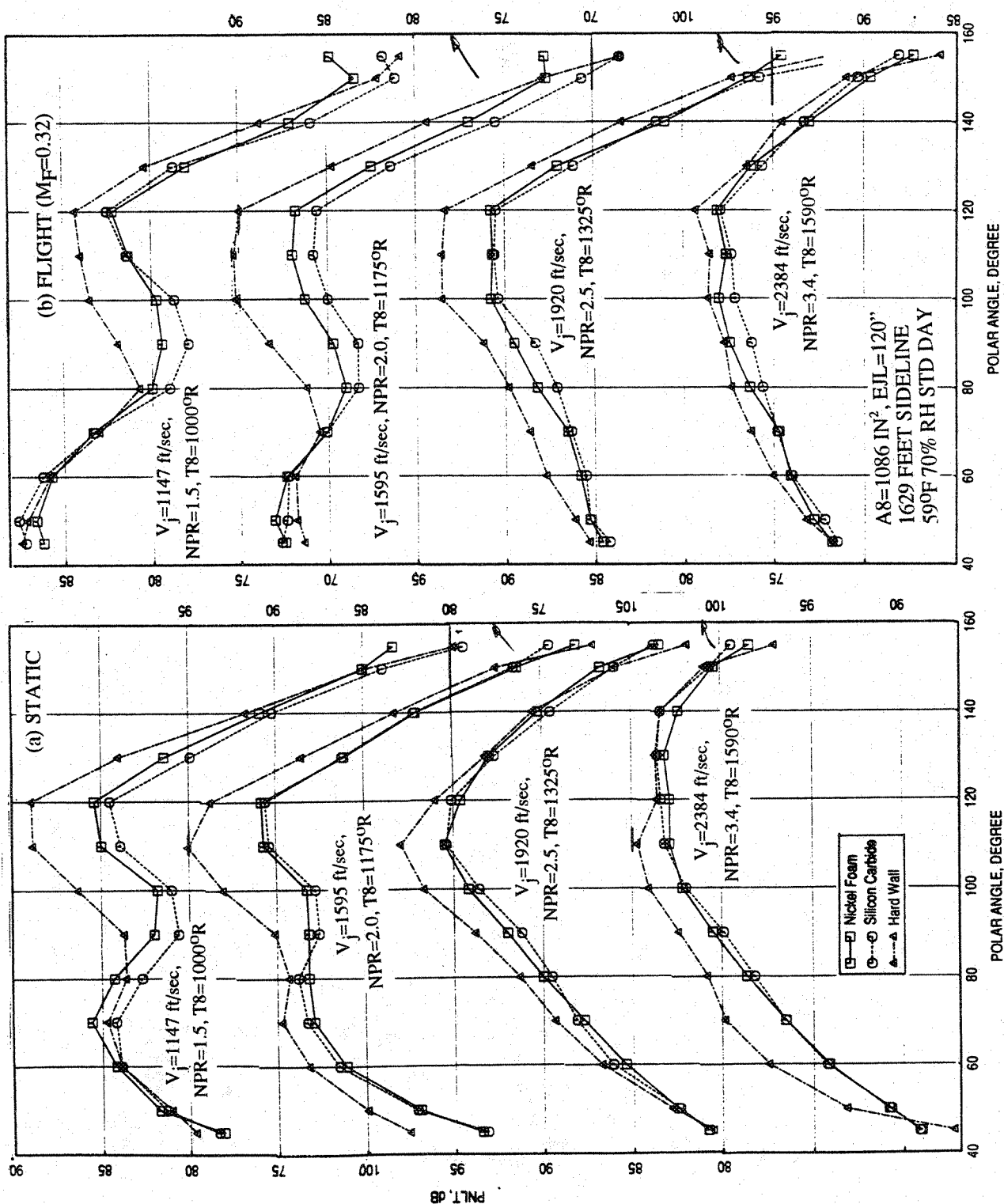Figure 7-66. Effect of treatment material on PNLT directivities for different jet velocities (V_j) for a 10 and 9 full staggered CD-chute mixer with fully treated long ejector; SAR=2.8, MAR = 0.95.

Figure 7-67. Effect of treatment material on SPL spectra at various polar angles (θ) for a 10 and 9 full staggered CD-chute mixer with fully treated long ejector; SAR=2.8, MAR = 0.95, V_j = 1147 ft/sec, NPR = 1.5, T8 = 1000°R.

Figure 7-68. Effect of treatment material on SPL spectra at various polar angles (θ) for a 10 and 9 full staggered CD-chute mixer with fully treated long ejector; SAR=2.8, MAR = 0.95, V_j = 1595 ft/sec, NPR = 2.0, T8 = 1175°R.
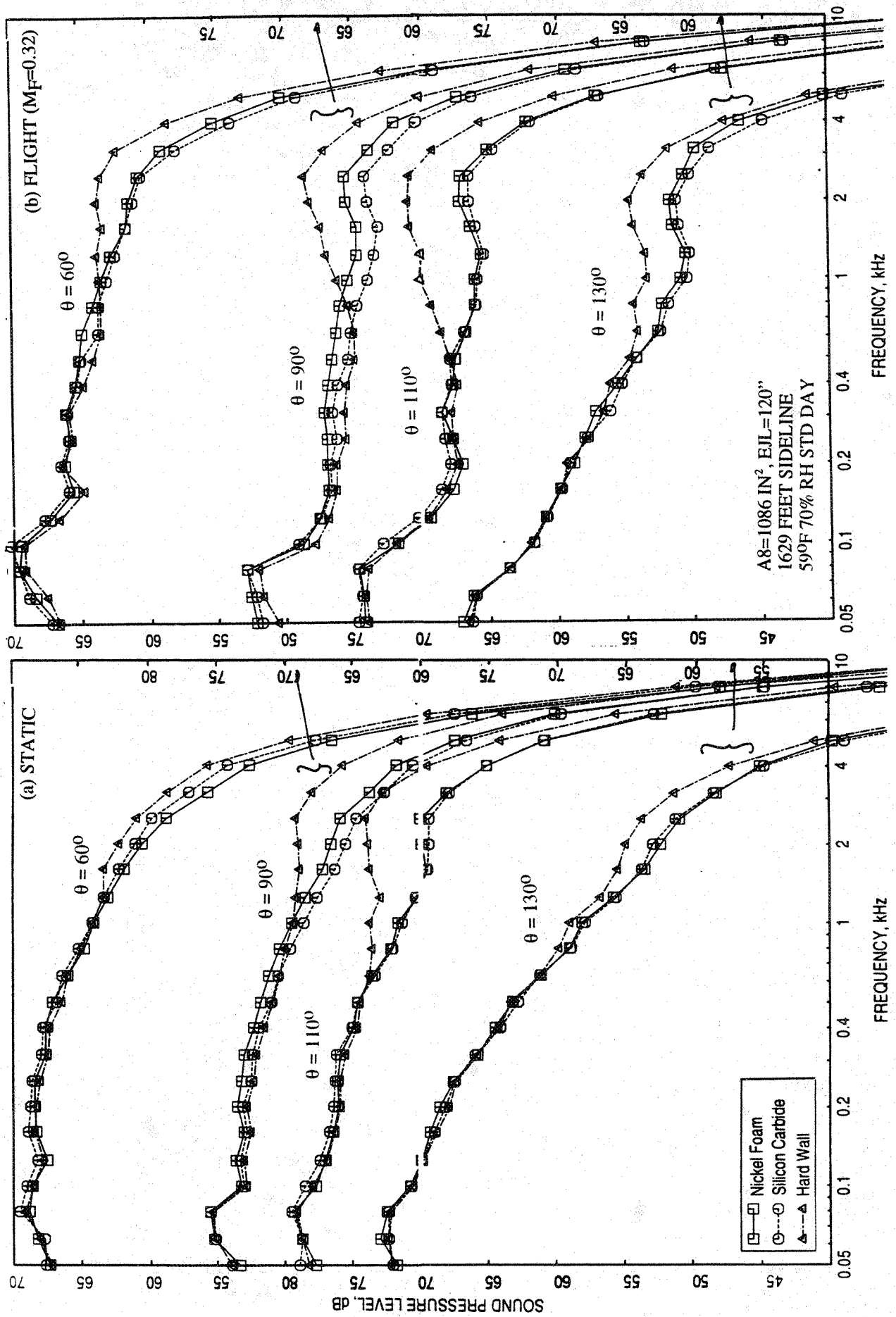
Figure 7-69. Effect of treatment material on SPL spectra at various polar angles (θ) for a 10 and 9 full staggered CD-chute mixer with fully treated long ejector; SAR=2.8, MAR = 0.95, V_j = 1919 ft/sec, NPR = 2.5, T8 = 1325°R.
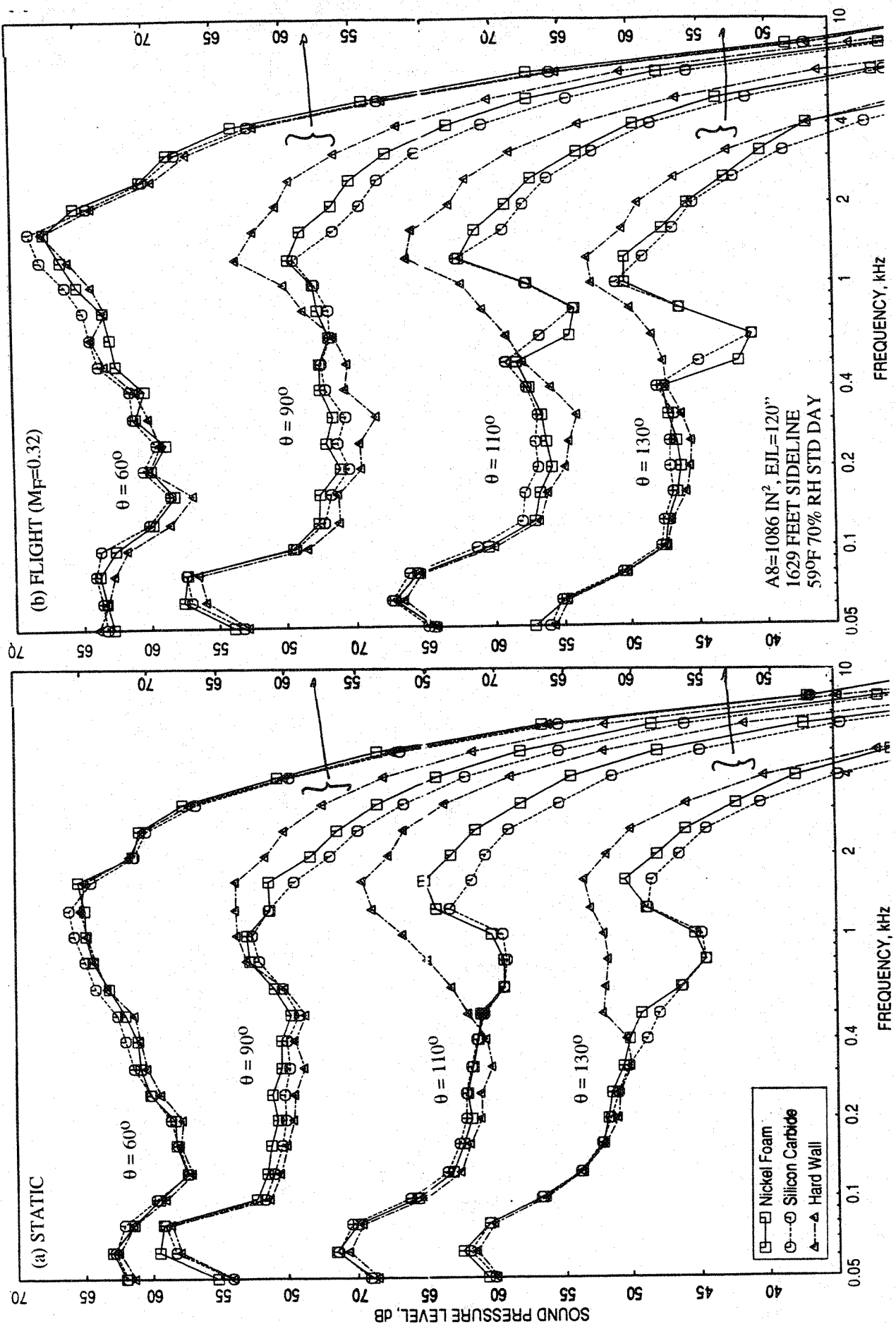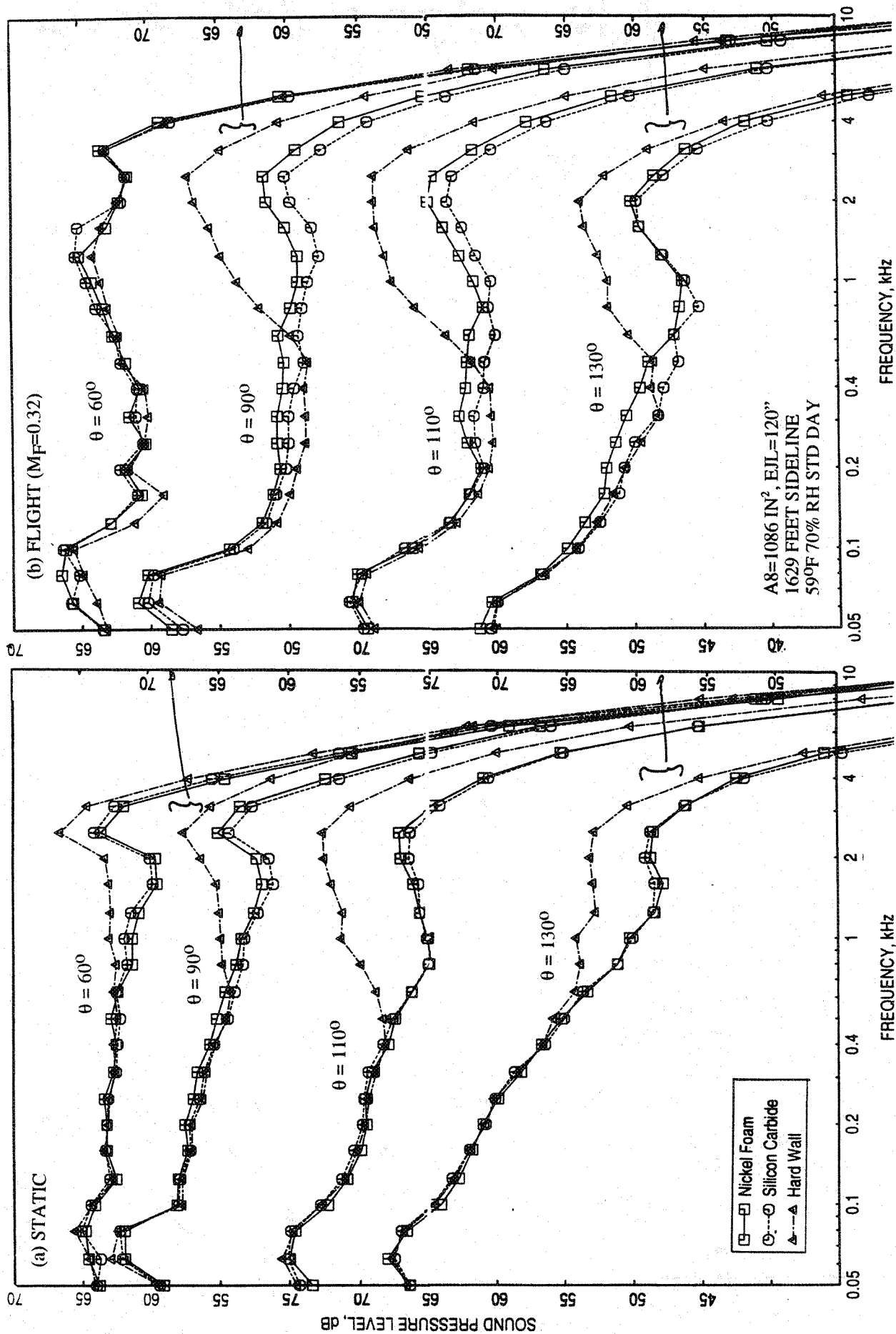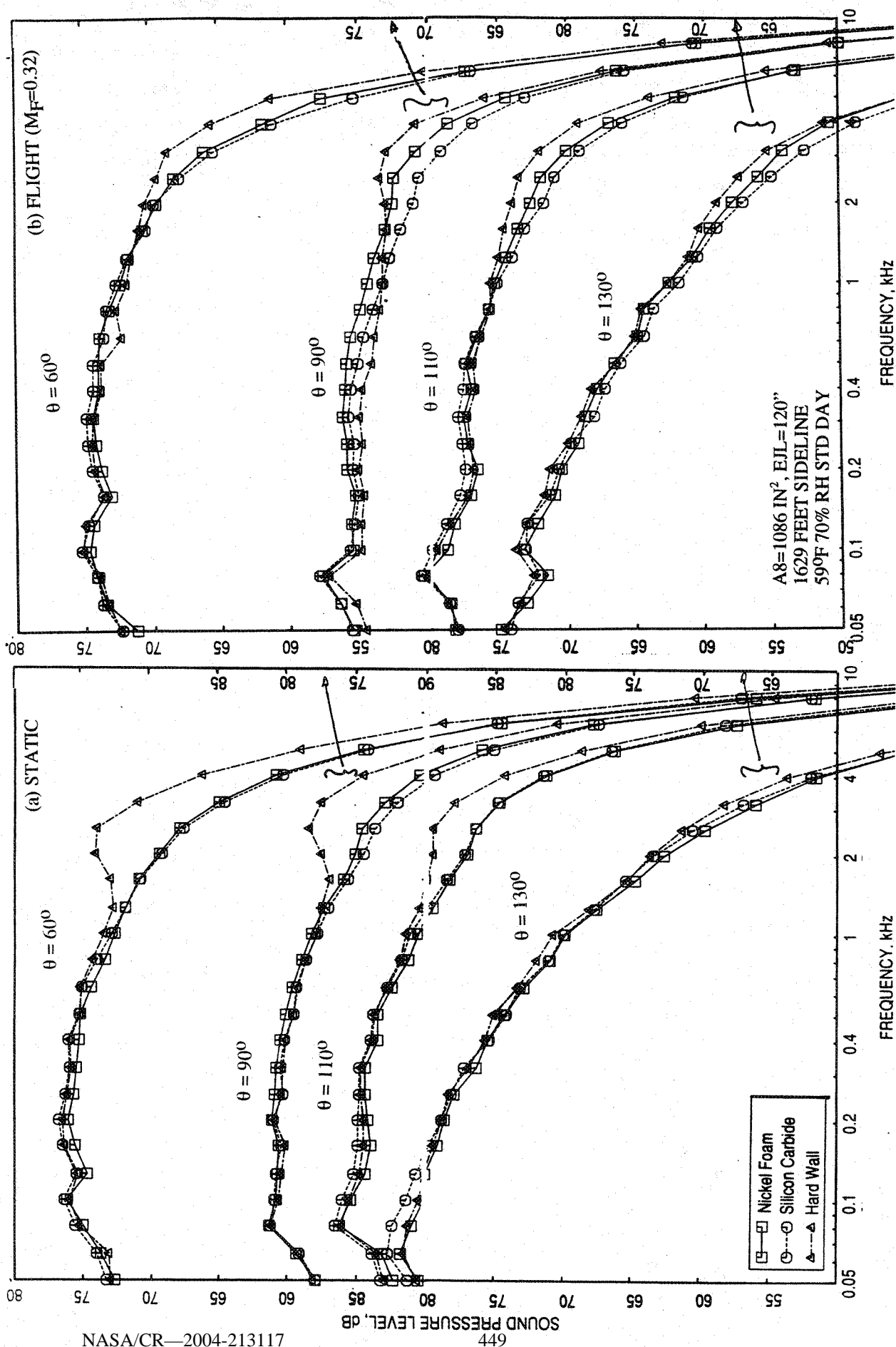
Figure 7-70. Effect of treatment material on SPL spectra at various polar angles (θ) for a 10 and 9 full staggered CD-chute mixer with fully treated long ejector; SAR=2.8, MAR = 0.95, V_j = 2384 ft/sec, NPR = 3.4, T8 = 1590°R.

better in suppressing acoustic energy. (3) Treatment location closer to ejector exit suppresses more acoustic energy. (4) Fully treated ejector is acoustically better that the flaps only treated configuration. (5) Silicon carbide bulk material seems to have more potential in suppressing internal noise.

8.0 EFFECT OF SECONDARY INLET GEOMETRY

The secondary inlet for the scale model mixer-ejector configurations is not designed on the basis of a realistic engine. The inlet ramp is designed with a gradual gradient to avoid any possible flow separation, which may not be possible for a realistic engine due to length and weight constraints. In addition, there is no blockage across the secondary inlet for the model mixer-ejector configurations, which may not be the case for an installed realistic engine. To study the impact of such geometric configurations of the secondary inlet on farfield acoustic characteristics and on flow and performance related parameters a few simplistic modifications are applied to a staggered mixer-ejector configuration with 10 and 9 full CD-chute racks with long treated ejector. The flaps and sidewalls for these configurations are realistically treated (which covers approximately 7/9th of fully treated area, as shown in Figure 7-2) with nickel based metal foam with a 37% porous facesheet. All the acoustic data presented in this section are at a slant distance of 1629', and sideline azimuthal location relative to major axis (i.e., $\phi = 25°$).

8.1 EFFECT OF A FIN ACROSS THE SECONDARY INLET:

Fin Design : According to conceptual studies by Boeing a fin structure across the ejector inlet of the mixer-ejector may be required to support the mixer-ejector nozzles, particularly in the out-board locations due to reduced thickness of wing spar. The full scale dimensions of this structure would be about 30" high and 8" wide, per Boeing's preliminary estimates. Figure 8-1 shows the isometric views of the fin geometry provided by Boeing. To get a preliminary assessment of the effect of the fin on the farfield noise and the flow entrainment a 7th scale model fin is designed to fit the existing 2D mixer-ejector nozzle hardware, fabricated and tested in Cell 41. Note that in Cell 41, cross-flow simulation is not present. Hence, this test is to be viewed as a very preliminary assessment of blockage effect of the fin on farfield acoustics. A more realistic assessment is investigated in the integrated HEAT test conducted at NASA Ames in 1995. Figure 8-2 shows the side view of the fin, which is about 4" deep and 1" wide and is contoured to the shape of the existing hardware. Figures 8-3 and 8-4 show the detail design of the fin. The fin was attached to the existing hardware by three bolts (h_1, h_2, and h_3), one of them (i.e., h_3) was bolted through a slotted hole to accommodate the expansion of the fin due to
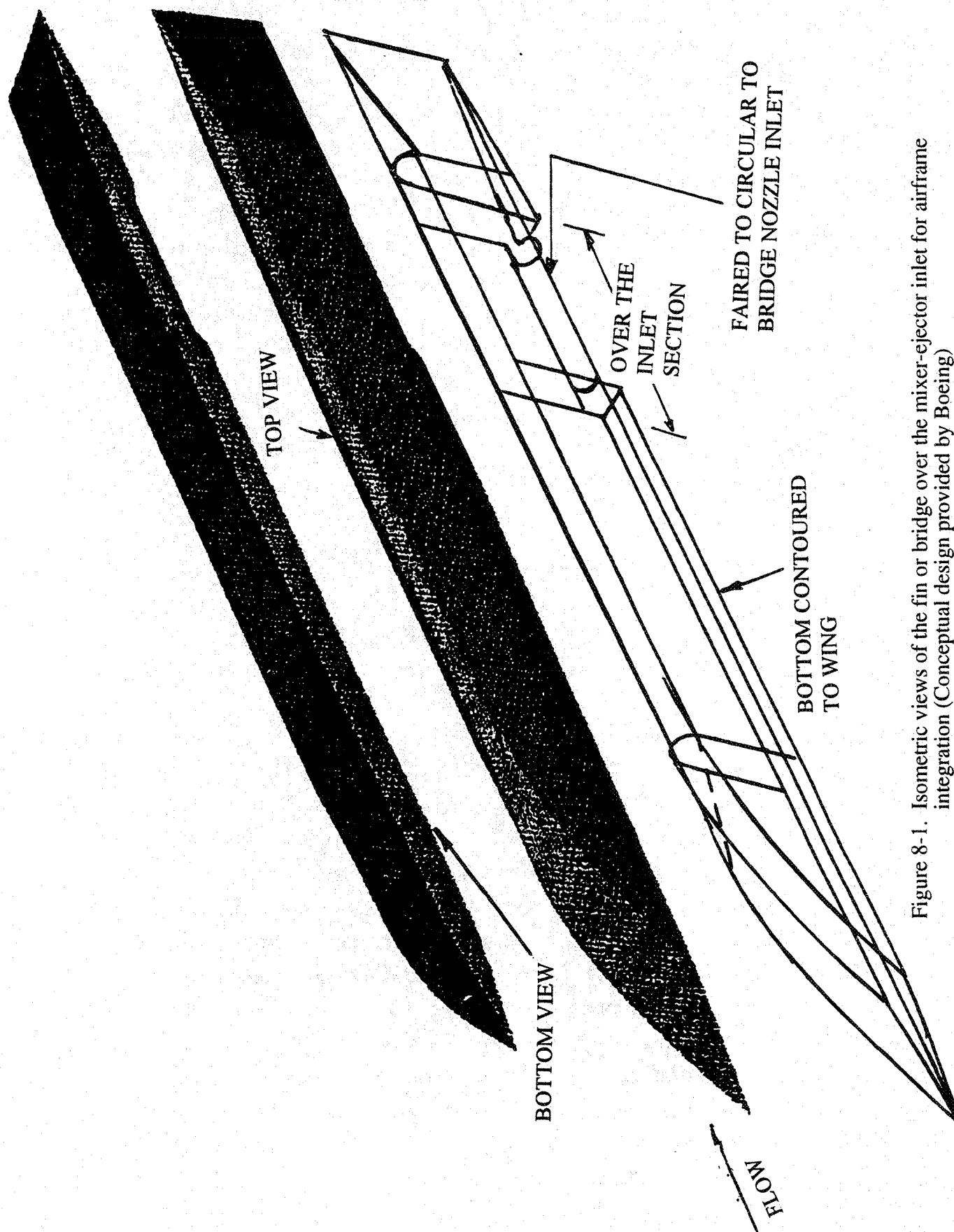
Figure 8-1. Isometric views of the fin or bridge over the mixer-ejector inlet for airframe integration (Conceptual design provided by Boeing)
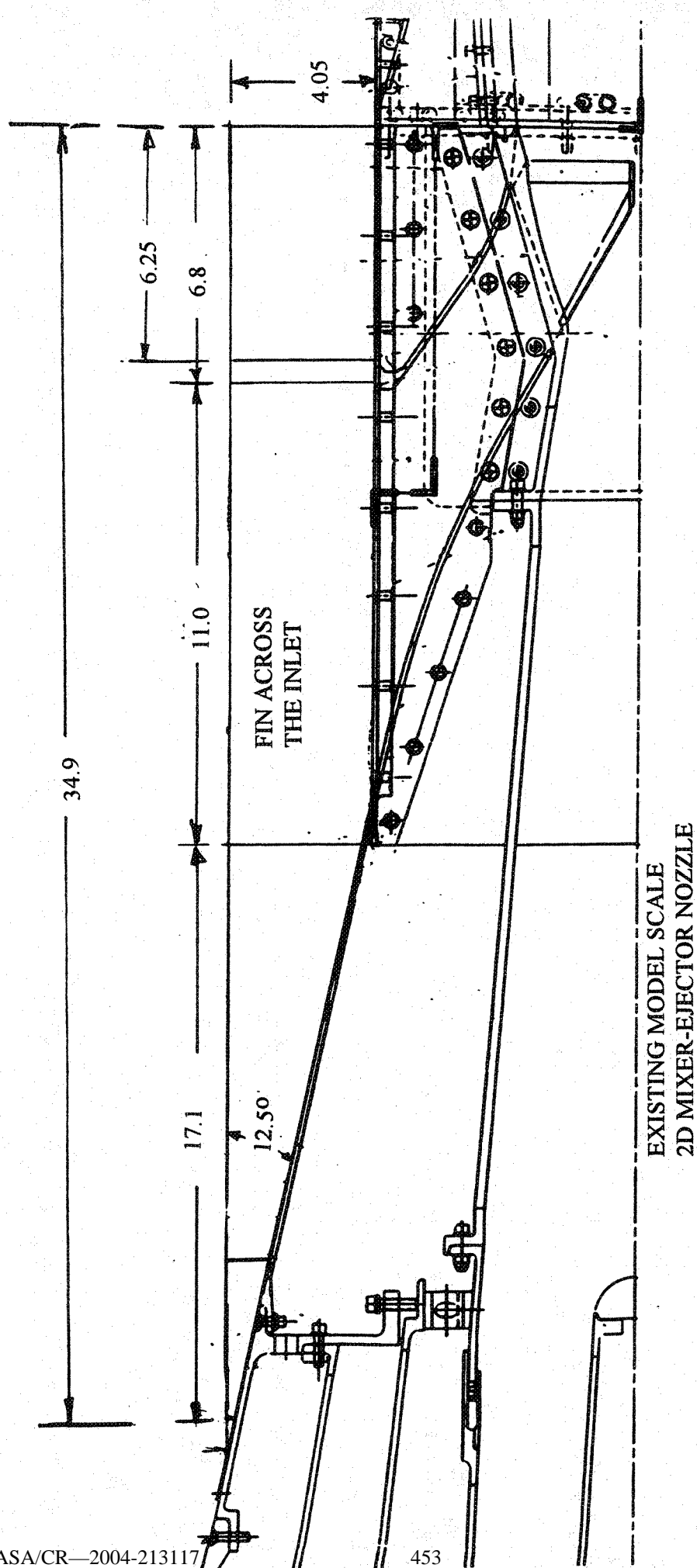
Figure 8-2. Side view of the fin, contoured to fit the 1/7-th scale model 2D mixer-ejector nozzle, for Cell 41 tests.

Figure 8-3. Dimensions of the fin, designed for the existing 1/7-th scale model 2D mixer-ejector nozzle, for Cell 41 tests; h_1, h_2, and h_3 being the holes for bolts to fasten the fin on the nozzle, shown in detail in the next figure (all length dimensions are in inches).
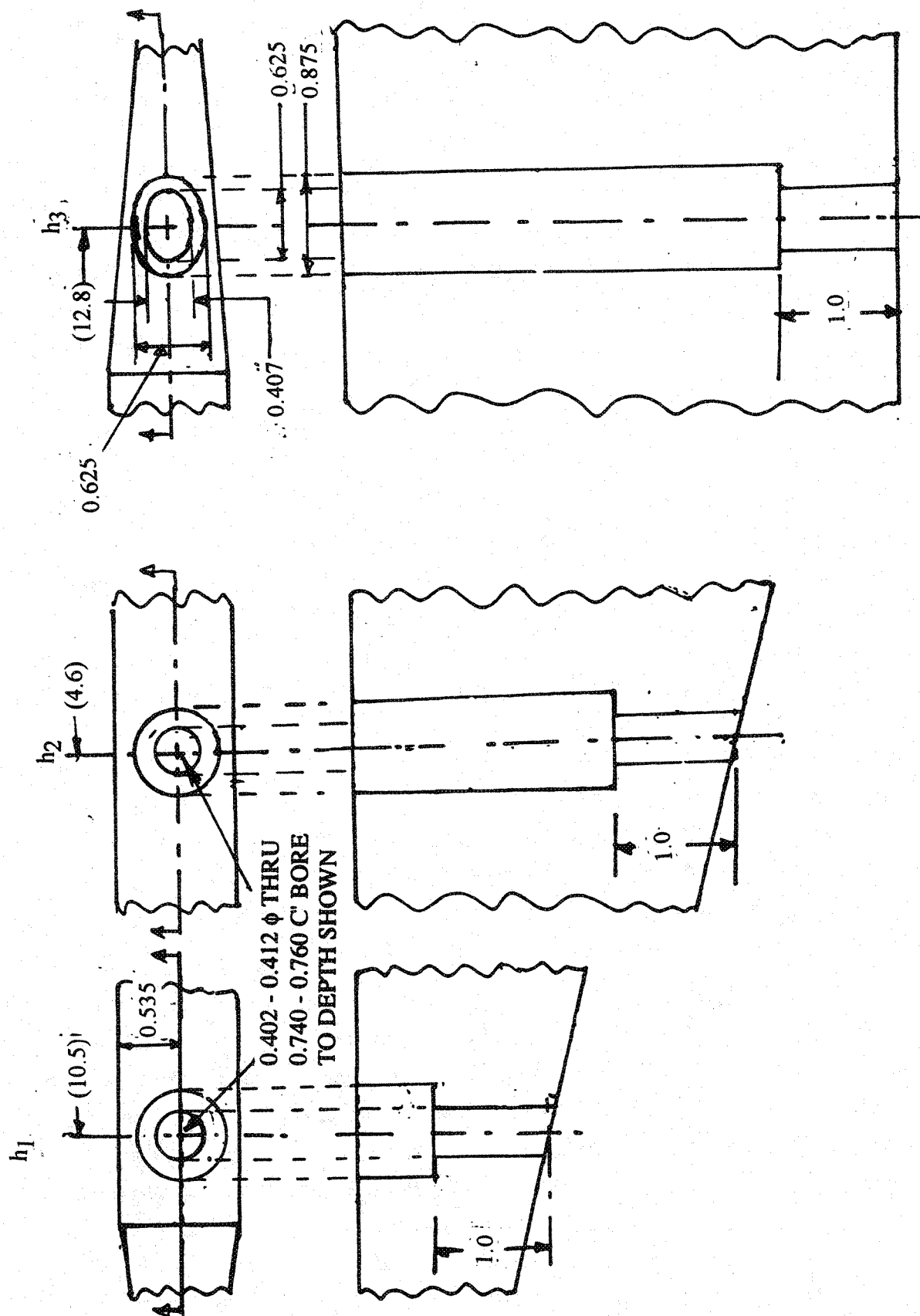
Figure 8-4. Detail design of the holes on the fin to fasten it on the existing 2D scale model nozzle in Cell 41(all length dimensions are in inches).

heating. The fin was made out of Aluminum. Figures 3-10 and 8-5 are the photographs of the mixer-ejector configuration with the fin in Cell 41.

8.1.1 Acoustic Results:

Figure 8-6 shows the effect of the fin across the inlet on EPNL and PNLT at various polar angles (θ) as functions of jet velocity (V_j). At lower and higher jet velocities the EPNL is hardly influenced due to the presence of the fin. However, at mid velocities the EPNL levels are slightly lower for the configuration with fin compared to that without the fin. Similar trends are observed with respect to PNLT levels.

Effect of fin across the secondary flow inlet on PNLT directivities at jet velocities of 1147, 1400, 1919, 2384, and 2637 ft/sec are shown in Figure 8-7. At 1400 ft/sec (i.e., for NPR=1.75) the PNLT levels increase slightly due to the fin in the forward arc, whereas, the trend is reversed at higher velocities for simulated flight case. Statically, the PNLT is higher due to the presence of the fin in the forward arc at higher velocity conditions. At higher polar angles the influence of fin on PNLT seems to be insignificant. Effect of fin on SPL spectra at various polar angles (θ) for each of the above mentioned five jet velocities are shown in Figures 8-8 through 8-12. At lower velocities of 1147 and 1400 ft/sec the SPL levels are slightly higher due to the fin for most frequencies compared to no fin configuration. There is almost no effect on SPL levels due to the presence of the fin for jet velocities of 1919 and 2384 ft/sec. At higher velocity of 2637 ft/sec the SPL levels are lower due to the fin compared to no fin configuration with flight simulation and the trend is opposite at static condition.

One may reason that the secondary flow through the inlet might be reduced due to the blockage provided by the fin. As will be shown later that the pumping is lower due to the presence of the fin at static condition. However, there is no blockage effect experience with flight simulation. The acoustic results indicate that the effect of the fin is minimal on the farfield noise. Small noise increase is observed at lower velocities and the trend is reversed at higher velocities. The wake and vortices shed at the trailing edge of the fin along with modified secondary flow entrainment is probably responsible for the effects observed with the noise field. While the vortex created by the fin is helping the mixing process inside the ejector, it also increases the turbulence level. At lower velocities, the
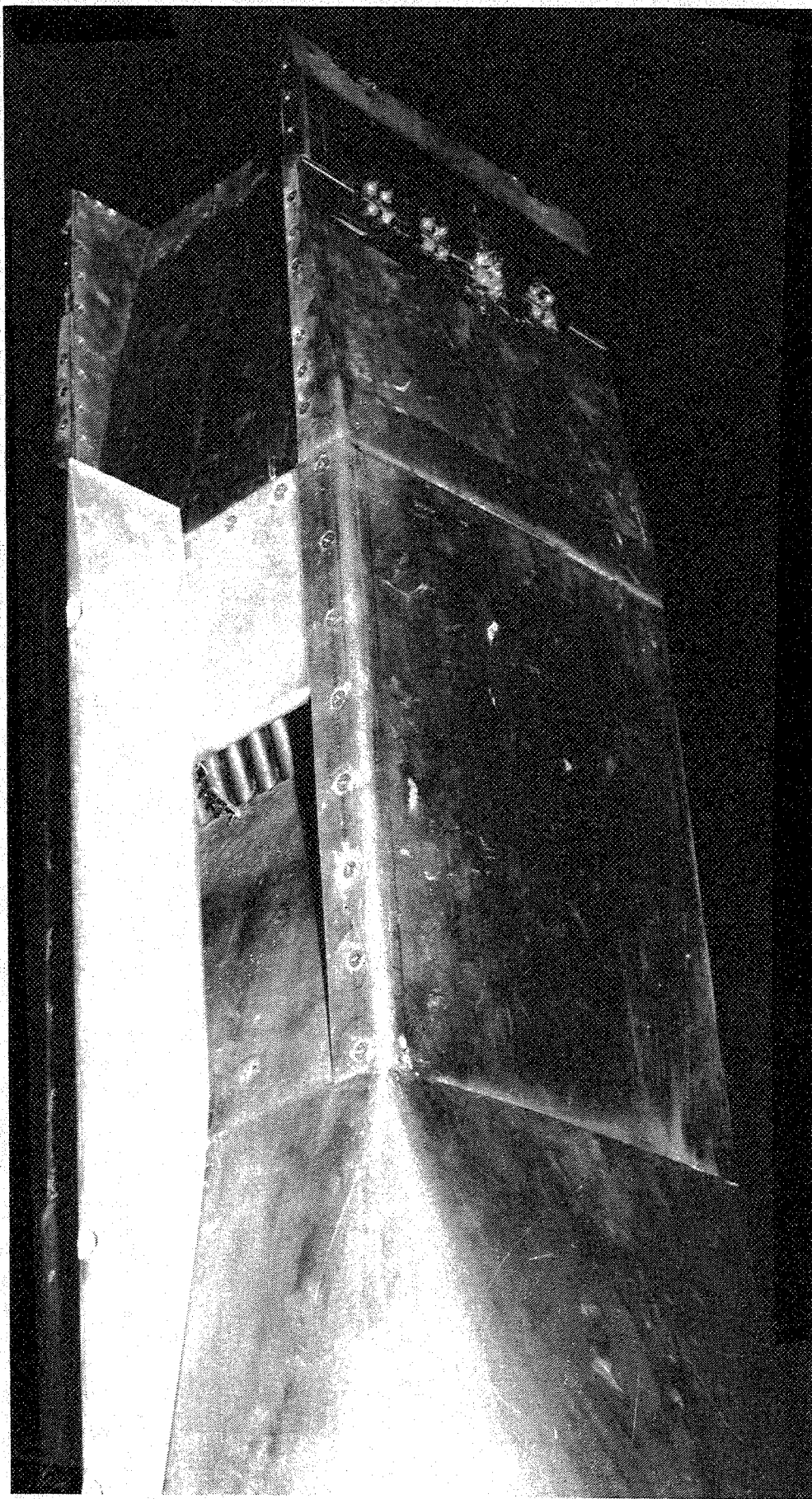
Figure 8-5. Side view of the fin mounted across the 2D mixer-ejector nozzle inlet.
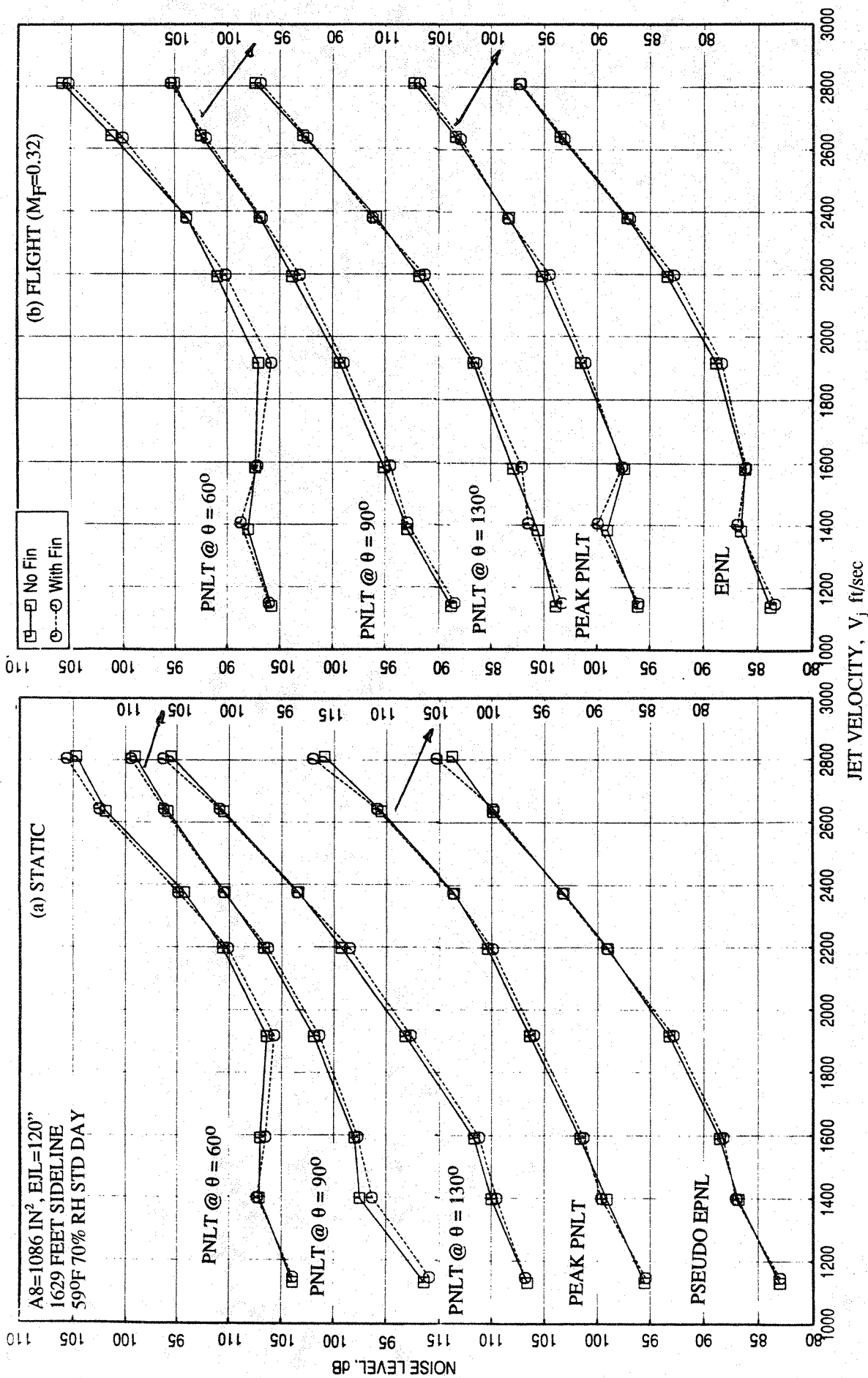
Figure 8-6. Effect of the fin across the inlet on PNLT at various polar angles (θ), peak PNLT, and EPNL as functions of jet velocity for a 10 and 9 full staggered CD-chute mixer with long 7/9-treated ejector; SAR=2.8, MAR = 0.95.
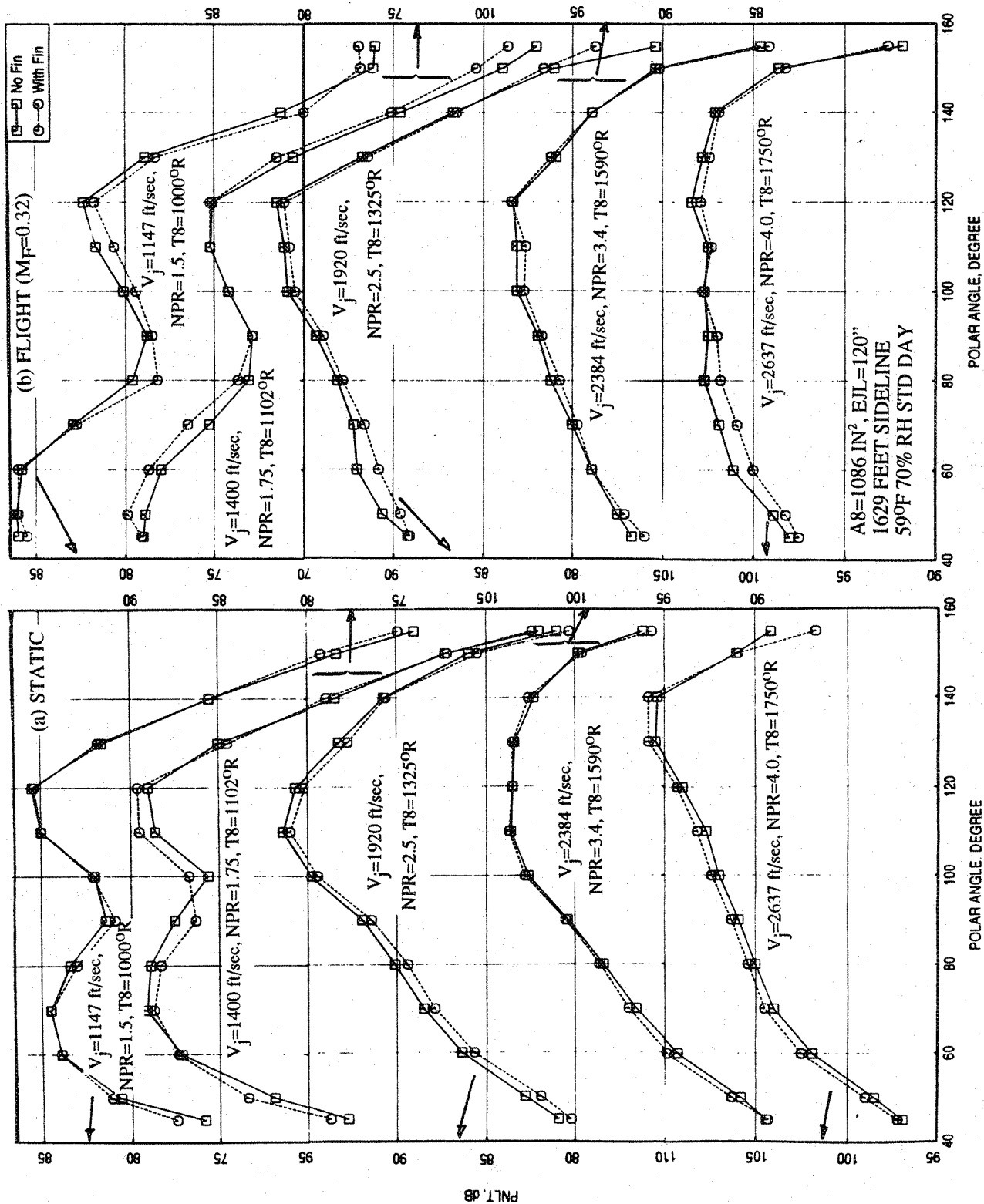
Figure 8-7. Effect of the fin across the inlet on PNLT directivities for different jet velocities (V_j) for a 10 and 9 full staggered CD-chute mixer with long 7/9-treated ejector; SAR=2.8, MAR = 0.95.

Figure 8-8. Effect of fin across the inlet on SPL spectra at various polar angles (θ) for a 10 and 9 full staggered CD-chute mixer with long 7/9-treated ejector; SAR=2.8, MAR = 0.95, V_j = 1147 ft/sec, NPR = 1.5, T8 = 1000°R.

Figure 8-9. Effect of fin across the inlet on SPL spectra at various polar angles (θ) for a 10 and 9 full staggered CD-chute mixer with long 7/9-treated ejector; SAR=2.8, MAR = 0.95, Vj = 1400 ft/sec, NPR = 1.75, T8 = 1102°R.

Figure 8-10. Effect of fin across the inlet on SPL spectra at various polar angles (θ) for a 10 and 9 full staggered CD-chute mixer with long 7/9-treated ejector; SAR=2.8, MAR = 0.95, V_j = 1919 ft/sec, NPR = 2.5, T8 = 1325ºR.

Figure 8-11. Effect of fin across the inlet on SPL spectra at various polar angles (θ) for a 10 and 9 full staggered CD-chute mixer with long 7/9-treated ejector; SAR=2.8, MAR = 0.95, V_j = 2384 ft/sec, NPR = 3.4, T8 = 1590°R.
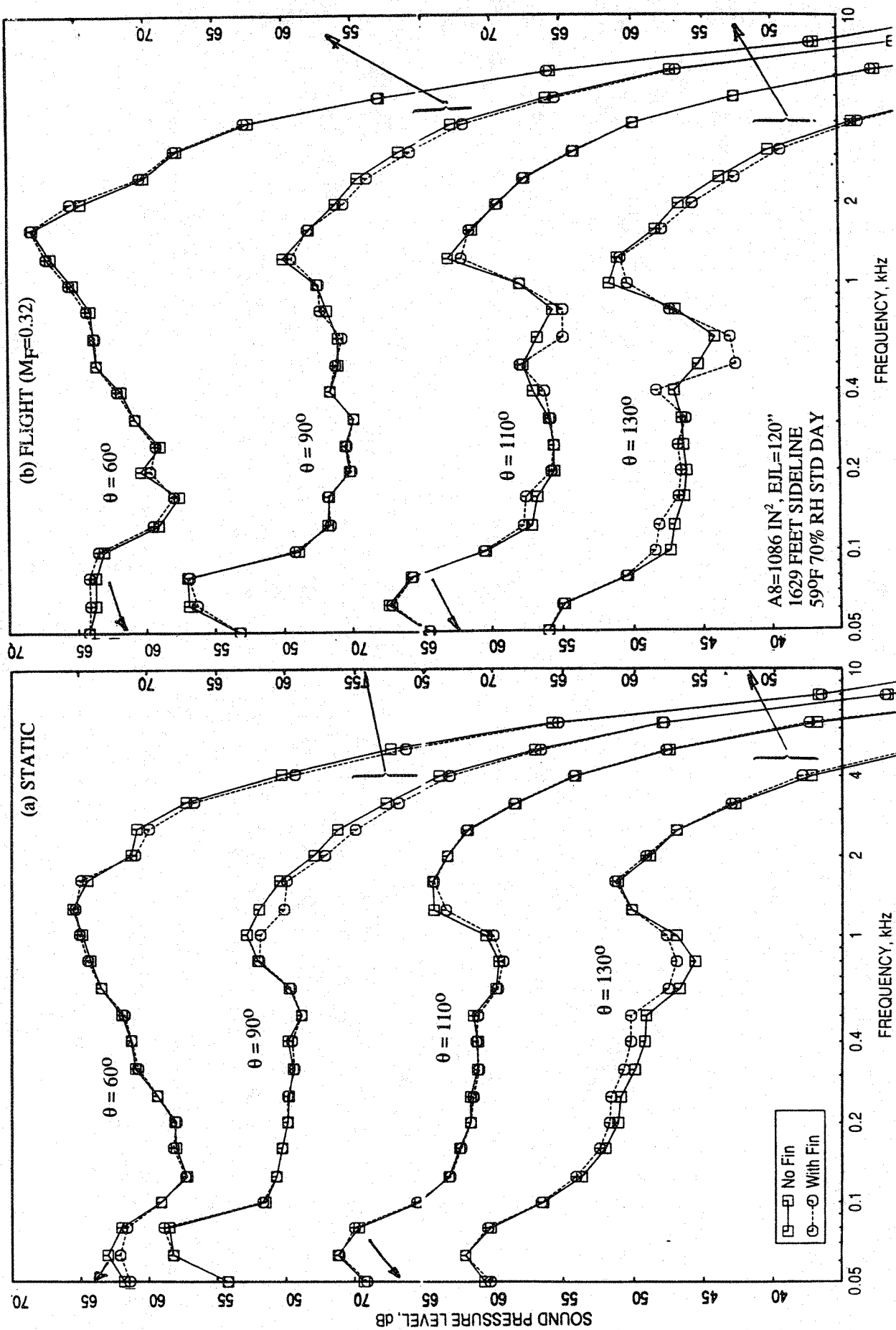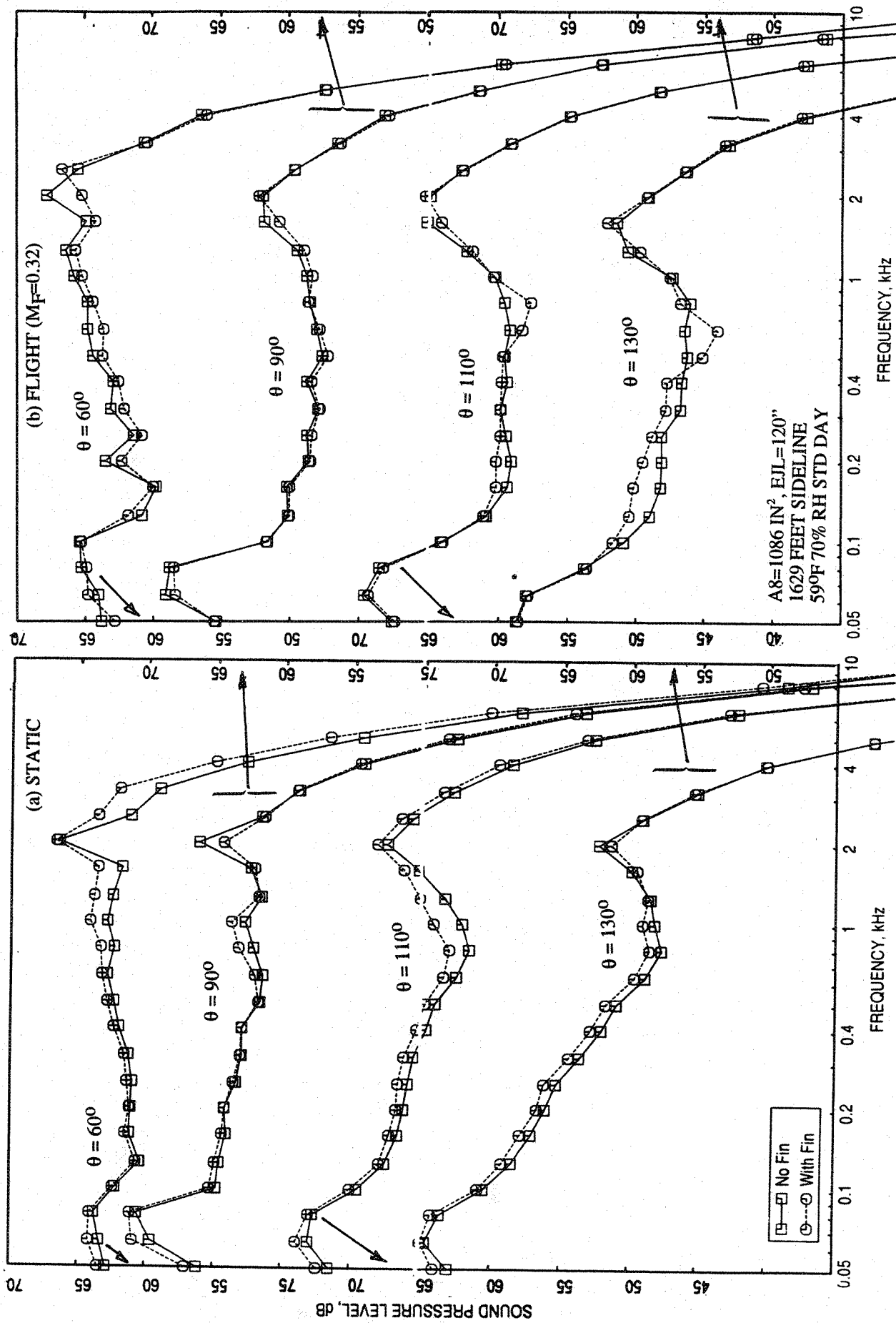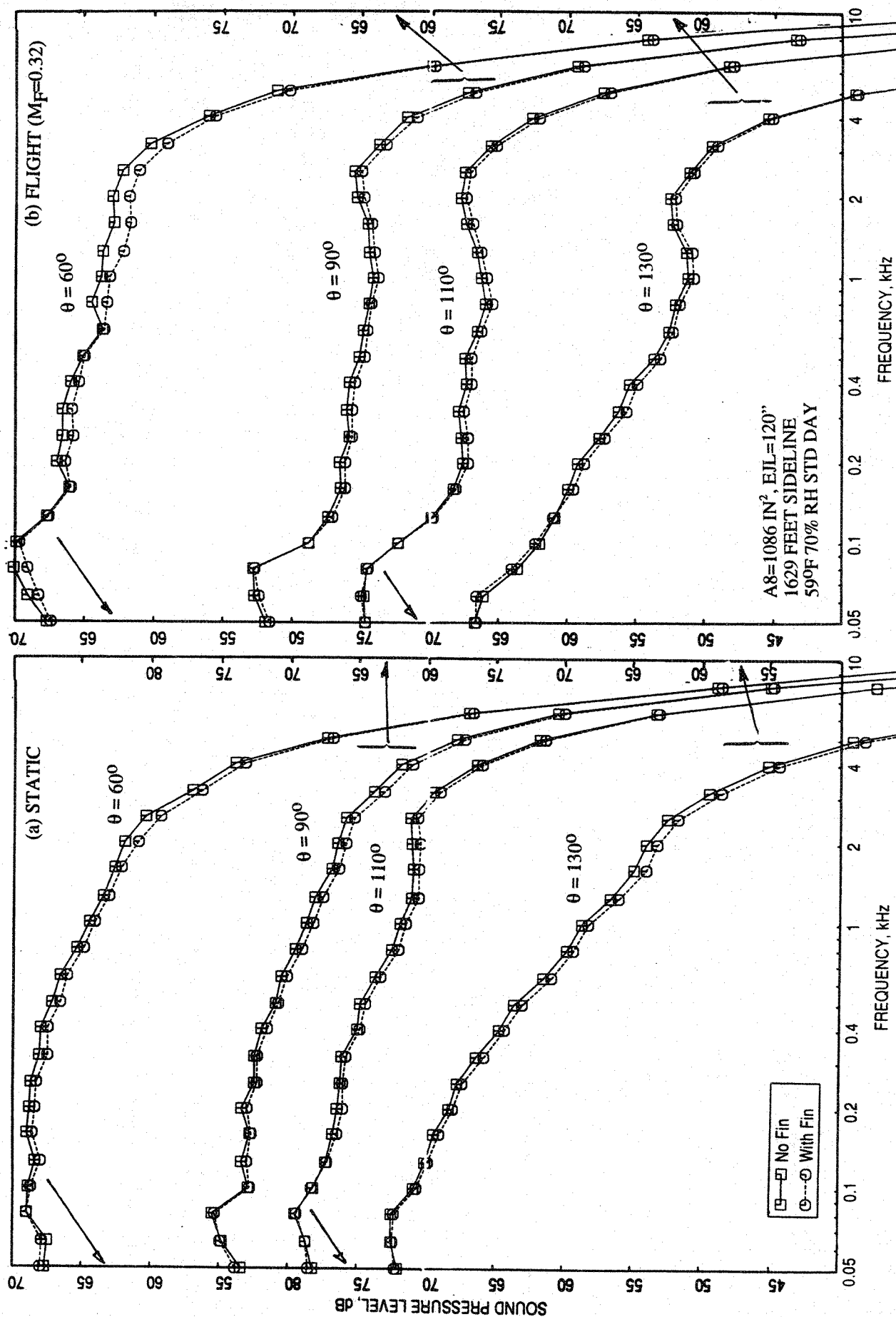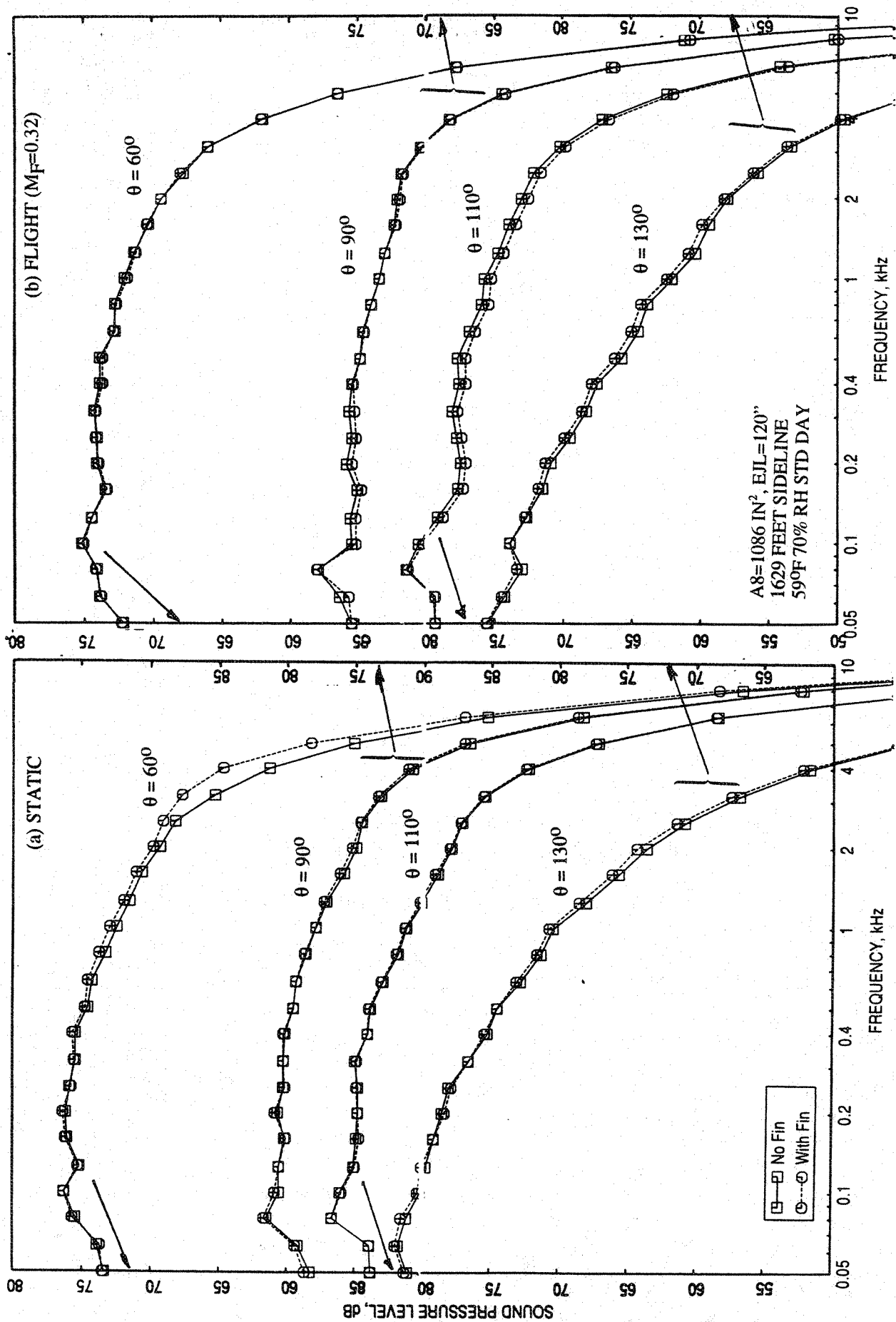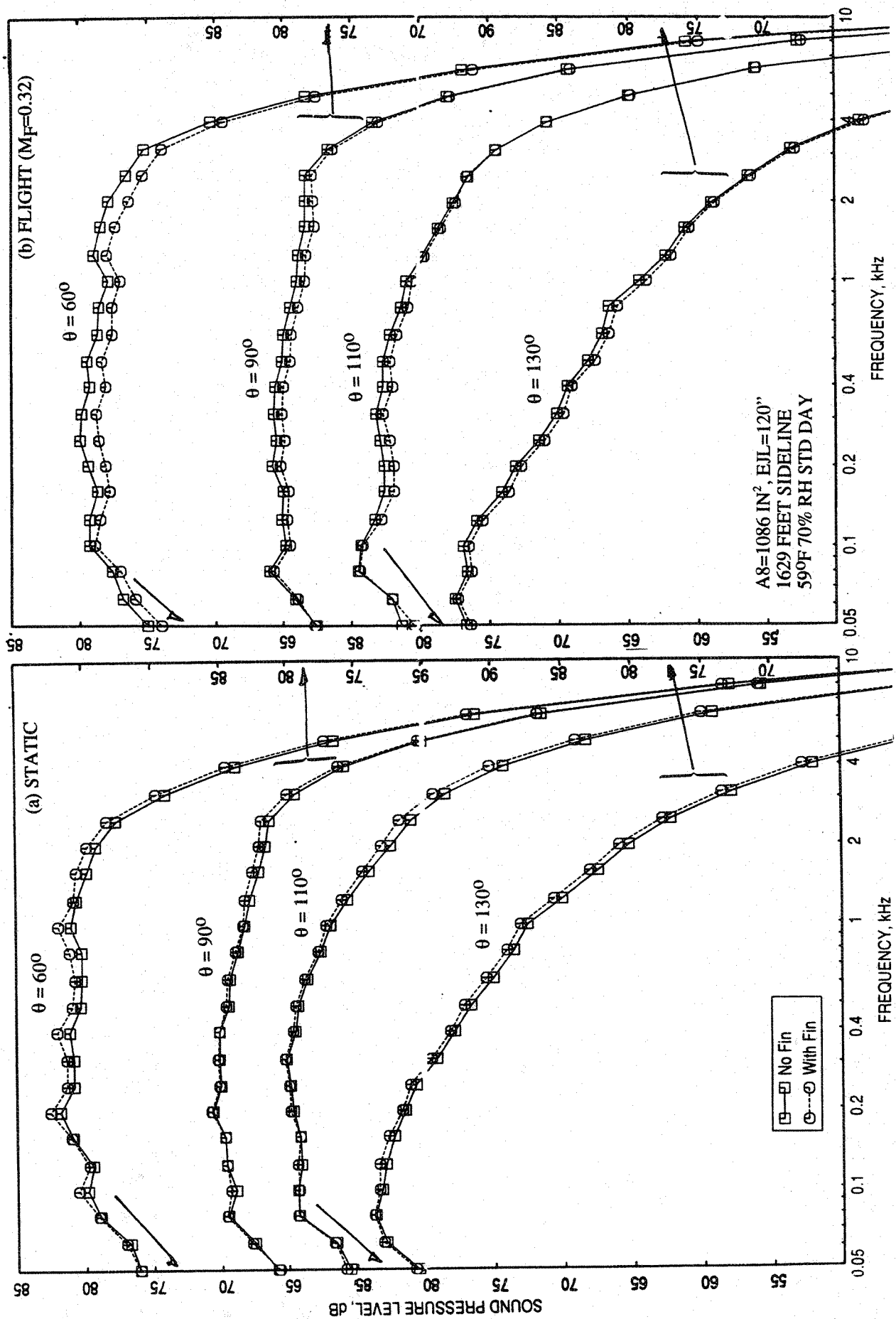
Figure 8-12. Effect of fin across the inlet on SPL spectra at various polar angles (θ) for a 10 and 9 full staggered CD-chute mixer with long 7/9-treated ejector; SAR=2.8, MAR = 0.95, M_F = 0.95, V_j = 2637 ft/sec, NPR = 4.0, T8 = 1750°R.

increased turbulence might be the cause of increased internal noise. At higher velocities, the enhanced mixing due to the fin generated vortex might be the reason for noise reduction.

8.1.2 Flow and Performance Related Parameters:

The effect of the fin on the ramp and the chute static pressure distributions are shown in Figures 8-13 and 8-14 for different L1M cycle conditions, at static condition and with flight simulation, respectively. For each case, the effect of the fin on the ramp and on the chute surface static pressure distributions is insignificant. Figure 8-15 shows the effect of the fin on the chute loading coefficients, due to chute static pressure distributions, plotted against NPR. For the static case the chute loading coefficients are slightly lower due to the presence of the fin. However, the effect of fin is insignificant with flight simulation. The effect of the fin on corrected pumping is shown in Figure 8-16. The pumping is slightly lower due to the presence of the fin at static condition. With flight simulation, the pumping is not affected.

Figures 8-17 and 8-18 illustrate the effect of the fin on axial static pressure distributions on the ejector flap at static and flight simulation conditions, respectively, at different L1M cycle conditions. The effect of the fin on flap static pressure distributions is insignificant at lower NPRs. At higher NPR, the static pressure distribution on the flap is lower due to the fin at static condition. The trend is reversed with flight simulation. This is further illustrated in terms of the force due to static pressure difference on flap surface as a function of nozzle pressure ratio in Figure 8-19. The transition from subsonic to supersonic mode seems to be slightly delayed with respect to NPR due to the fin with flight simulation.

8.2 EFFECT OF A MODIFIED SCAB-ON SECONDARY INLET :

Modified Scab-on Inlet Design : The basic inlet configuration of the 2D model scale mixer nozzle is based on the preliminary design of a full-scale 2D mixer-ejector nozzle (NRA design) with chute stowability for a variable cycle engine for M2.4 HSCT (Gen. 1) as shown in Figure 8-20. The inlet for secondary flow has a relatively smaller angle of about 27°. The 1/7th scale model, shown in Figure 4.1-1, is designed and fabricated with non-movable chutes. The model does not simulate chute stowability. The inlet is extended
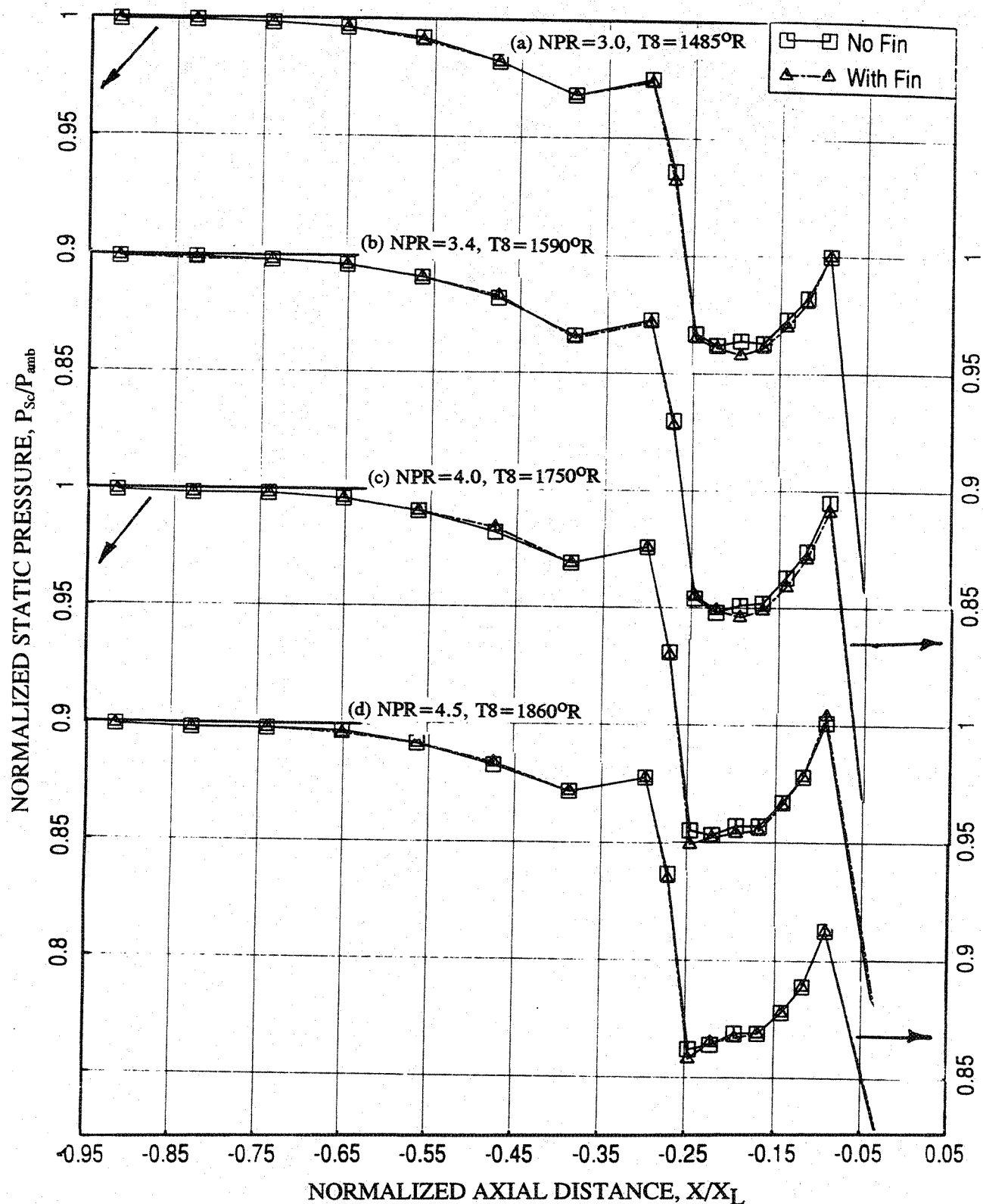
Figure 8-13. Effect of the fin across the inlet on the static pressure distributions on the inlet ramp and on the secondary flow side of chute surface at different L1M cycle conditions for a 10 and 9 full staggered CD-chute mixer with long 7/9-treated ejector at static condition; SAR=2.8, MAR = 0.95.

Figure 8-14. Effect of the fin across the inlet on the static pressure distributions on the inlet ramp and on the secondary flow side of chute surface at different L1M cycle conditions for a 10 and 9 full staggered CD-chute mixer with long 7/9-treated ejector with flight simulation (M_F=0.32) ; SAR=2.8, MAR = 0.95.

Figure 8-15. Effect of the fin across the inlet on chute loading coefficient, computed by measured static pressure distributions on secondary flow side chute leading edge, with respect to nozzle pressure ratios for a 10 and 9 full staggered CD-chute mixer with long 7/9-treated ejector; SAR=2.8, MAR = 0.95.
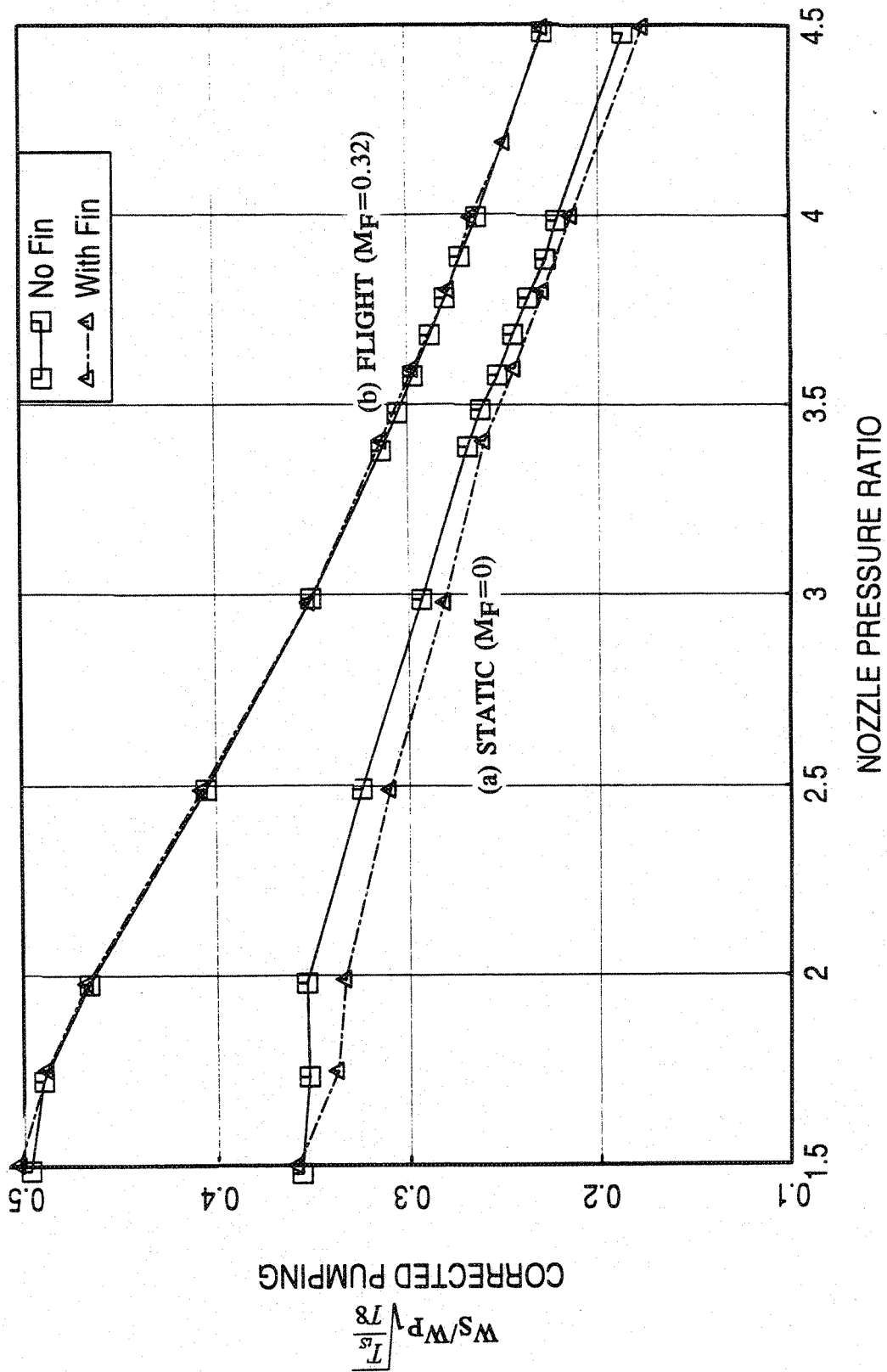
Figure 8-16. Effect of the fin across the inlet on pumping, computed by measured rake total pressure distributions at the inlet, with respect to nozzle pressure ratios for a 10 and 9 full staggered CD-chute mixer with long 7/9-treated ejector; SAR=2.8, MAR = 0.95.
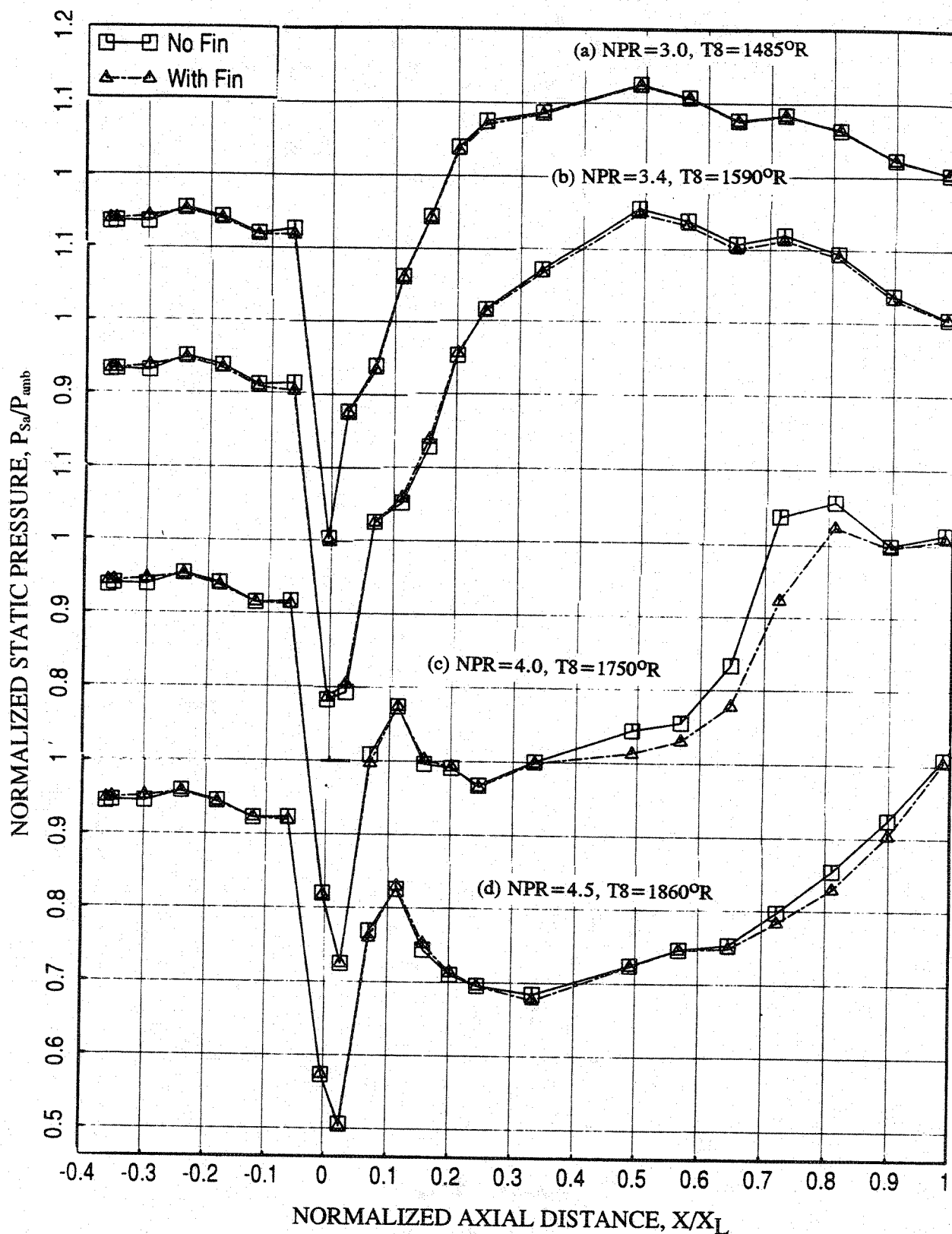
Figure 8-17. Effect of the fin across the inlet on axial distribution of average static pressure on the inlet and the flap surface at different L1M cycle conditions for a 10 and 9 full staggered CD-chute mixer with long 7/9-treated ejector at static condition; SAR=2.8, MAR = 0.95.
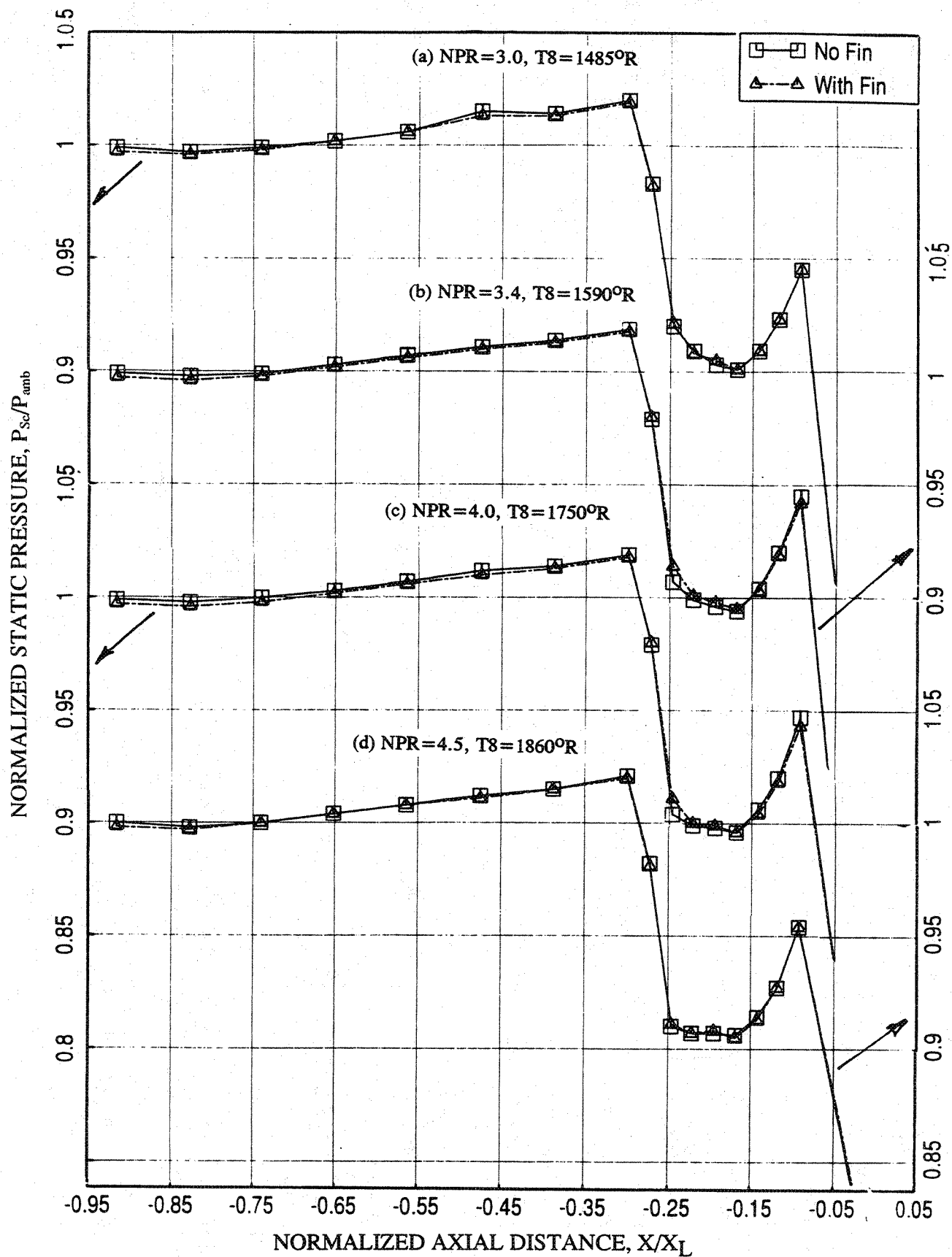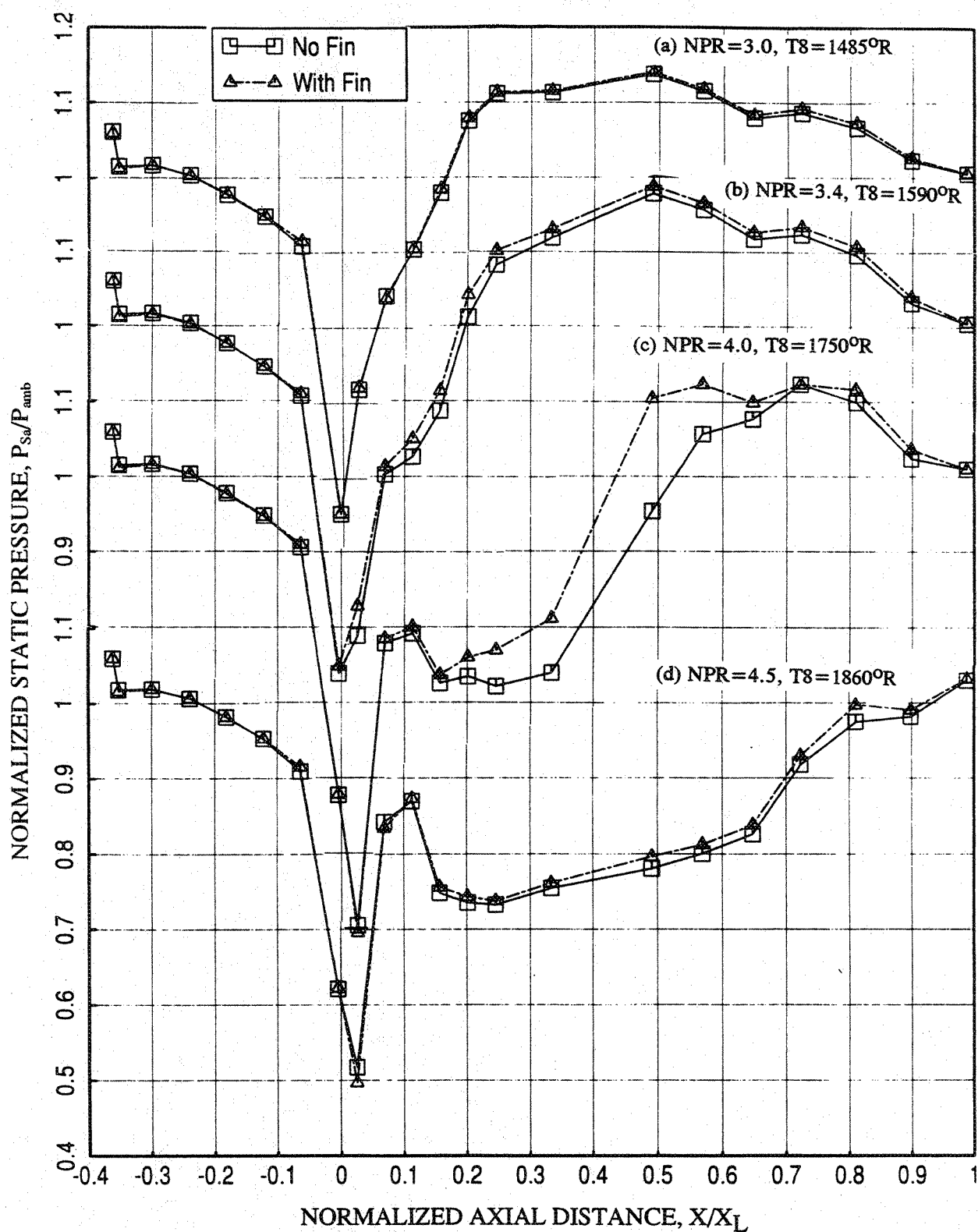
Figure 8-18. Effect of the fin across the inlet on axial distribution of average static pressure on the inlet and the flap surface at different L1M cycle conditions for a 10 and 9 full staggered CD-chute mixer with long 7/9-treated ejector with flight simulation (M_F=0.32) ; SAR=2.8, MAR = 0.95.
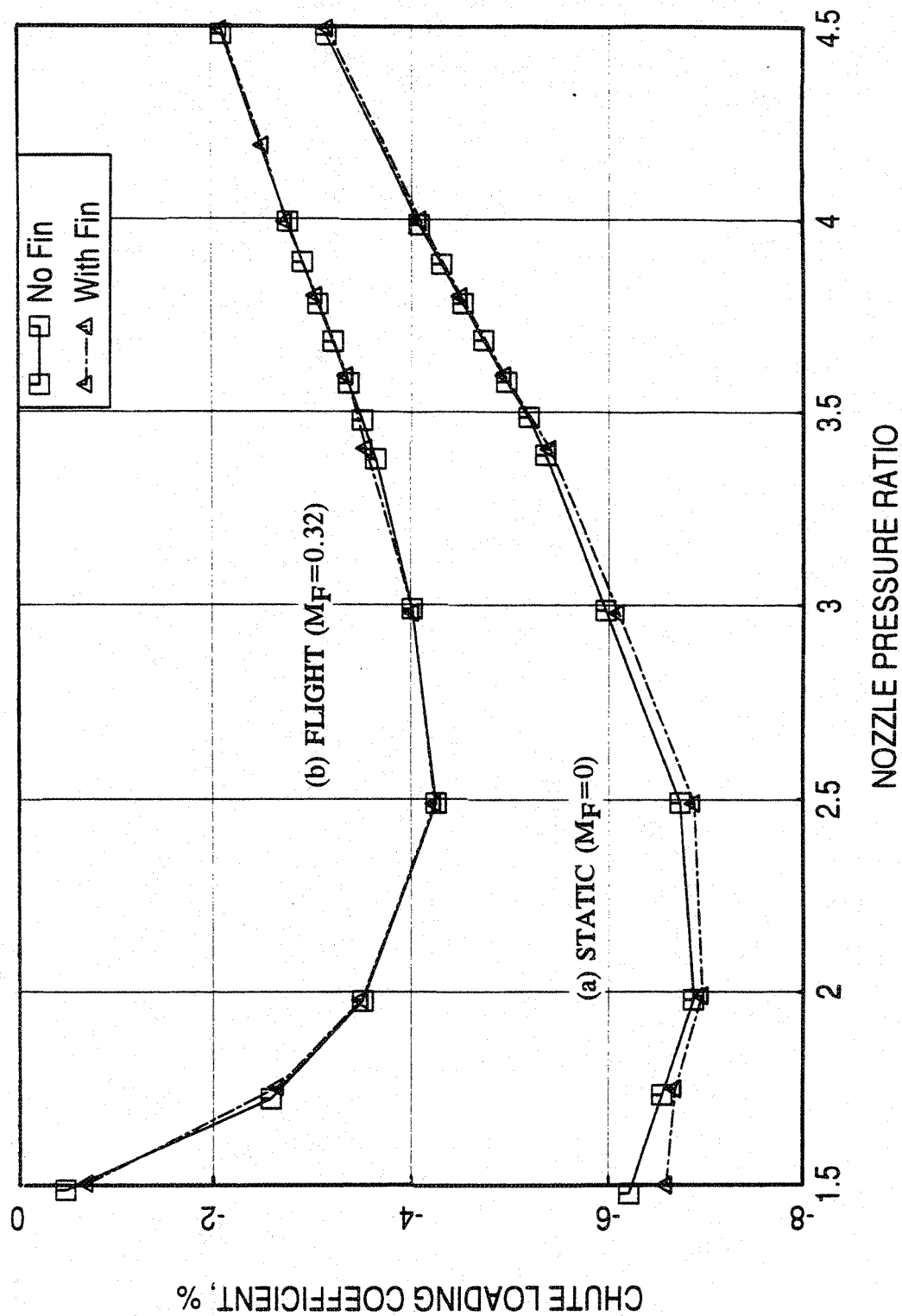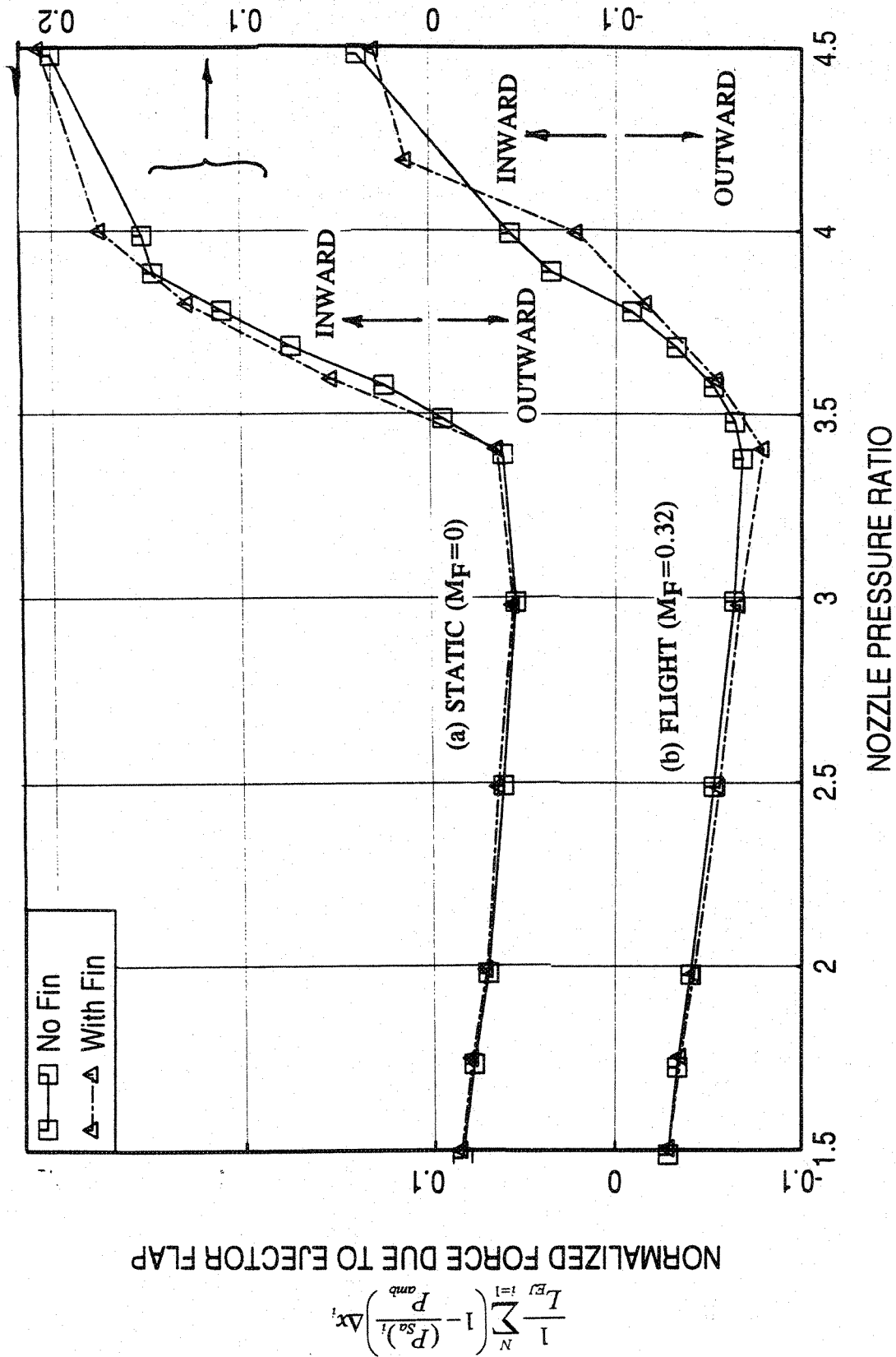
Figure 8-19. Effect of the fin across the inlet on normalized force due to ejector flap with respect to nozzle pressure ratio for a 10 and 9 full staggered CD-chute mixer with long 7/9-treated ejector; SAR=2.8, MAR = 0.95.

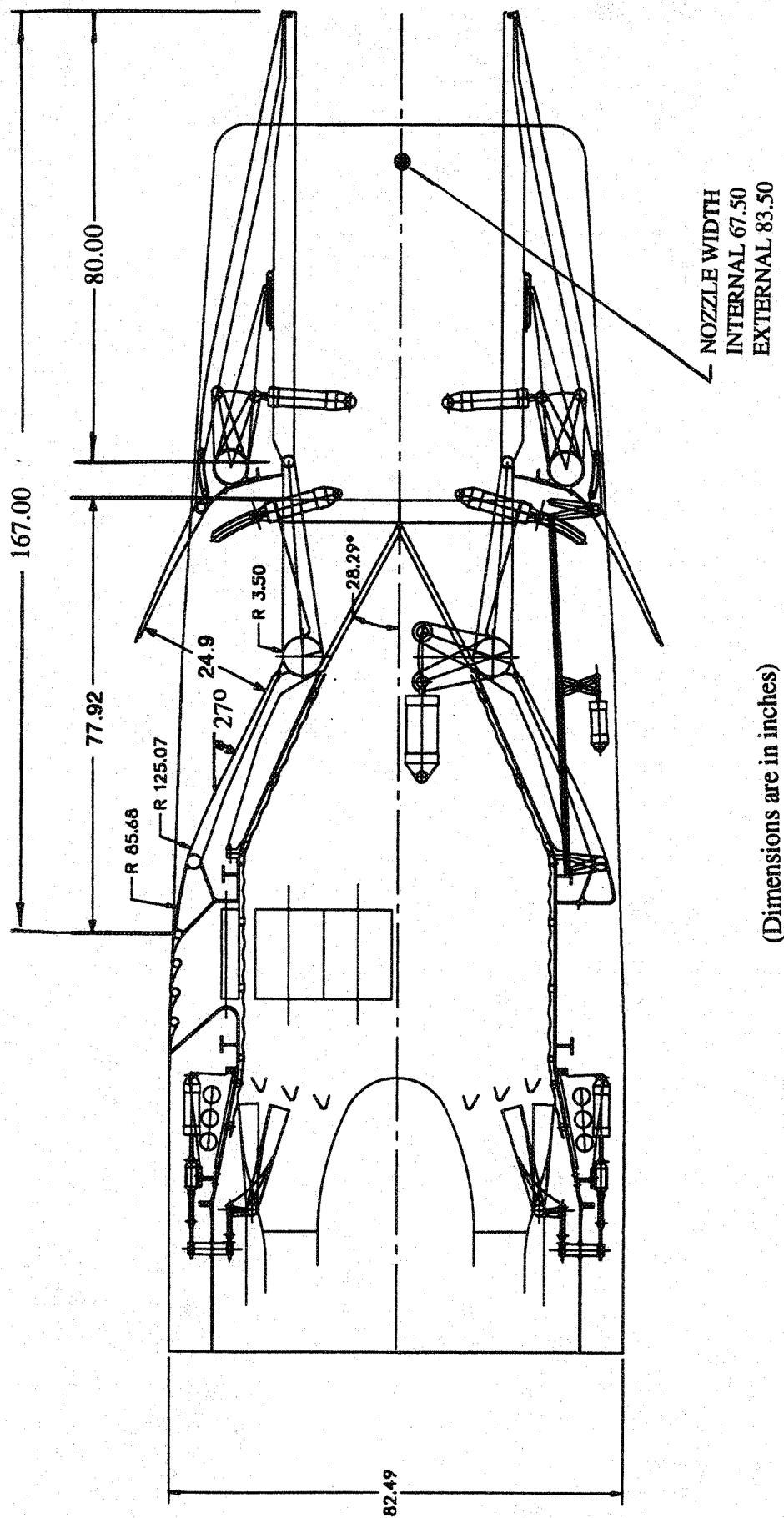Figure 8-20.   Preliminary design of a full-scale 2D mixer-ejector nozzle with chute stowability for a variable cycle engine for M2.4 HSCT (Gen 1, NAS3 - 25415).

NOZZLE WIDTH
INTERNAL 67.50
EXTERNAL 83.50

(Dimensions are in inches)

further upstream with a slightly smaller angle of about 25° to mate with facility adaptations, whereas the chute angles of 28-29° is maintained in the scale model design. It should be noted that the full-scale preliminary design (NRA) of Figure 8-20 has 80" long flaps, whereas, the scale model nozzle shown in Figure 4.1-1 has 16.055" long flaps, corresponding to 120" long full-scale flaps.

The current 2D fixed chute nozzle preliminary design employs fixed (non-retracting) chute mixer for a mixed flow turbo fan for M2.4 HSCT (see Figure 8-21) and has a much smaller inlet length resulting in an ejector inlet angle of about 35° , which is relatively steeper compared to Gen 1 design. Aerodynamically, such a steep inlet might cause flow separation and could influence the noise and the performance of the nozzle. Before finalizing the Gen 2 design it is essential to assess the impact of the new inlet design. To facilitate this objective an add-on adapter is designed with 35° inclination, which could be installed on the existing inlet of Gen 1 scale model nozzle configuration (see Figure 3-11). Two adapters are designed and fabricated, which are 8" long and 9.25" wide (see Figure 8-22). The width of these components are exactly the same as the existing inlet width. One of the adapter is instrumented with 5 static pressure taps, as shown in Figure 8-22, at locations corresponding to those of the existing inlet. These adapters are attached to the existing inlets with screws and the modified inlets exhibits a 35° slope. The modified inlets are named as scab-on inlets. Figure 8-23 shows the top views of the original and the scab-on inlets for the 1/7th scale 2D mixer-ejector model in Cell 41. The blockage effect due to the fin across the inlet is also studied with the modified scab-on inlet. Figure 8-24 shows the side view of the fin attached to the existing hardware with scab-on inlet. Figure 8-25 shows the scab-on inlet mixer-ejector configuration with the fin in Cell 41.

8.2.1 Acoustic Results:

Figure 8-26 shows the effect of the scab-on inlet and the fin across the scab-on inlet on EPNL and PNLT at various polar angles (θ) as functions of jet velocity (V_j). The influence of the scab-on inlet on EPNL is practically negligible for the entire velocity range. However, the fin seems to be influencing EPNL by a small amount. At lower jet velocities the EPNL level increases slightly due to the influence of the fin. However, at higher velocities, at and above 1600 ft/sec, the EPNL levels are slightly lower or the same for the configuration with fin compared to that without the fin. Similar trends are observed with respect to PNLT levels.
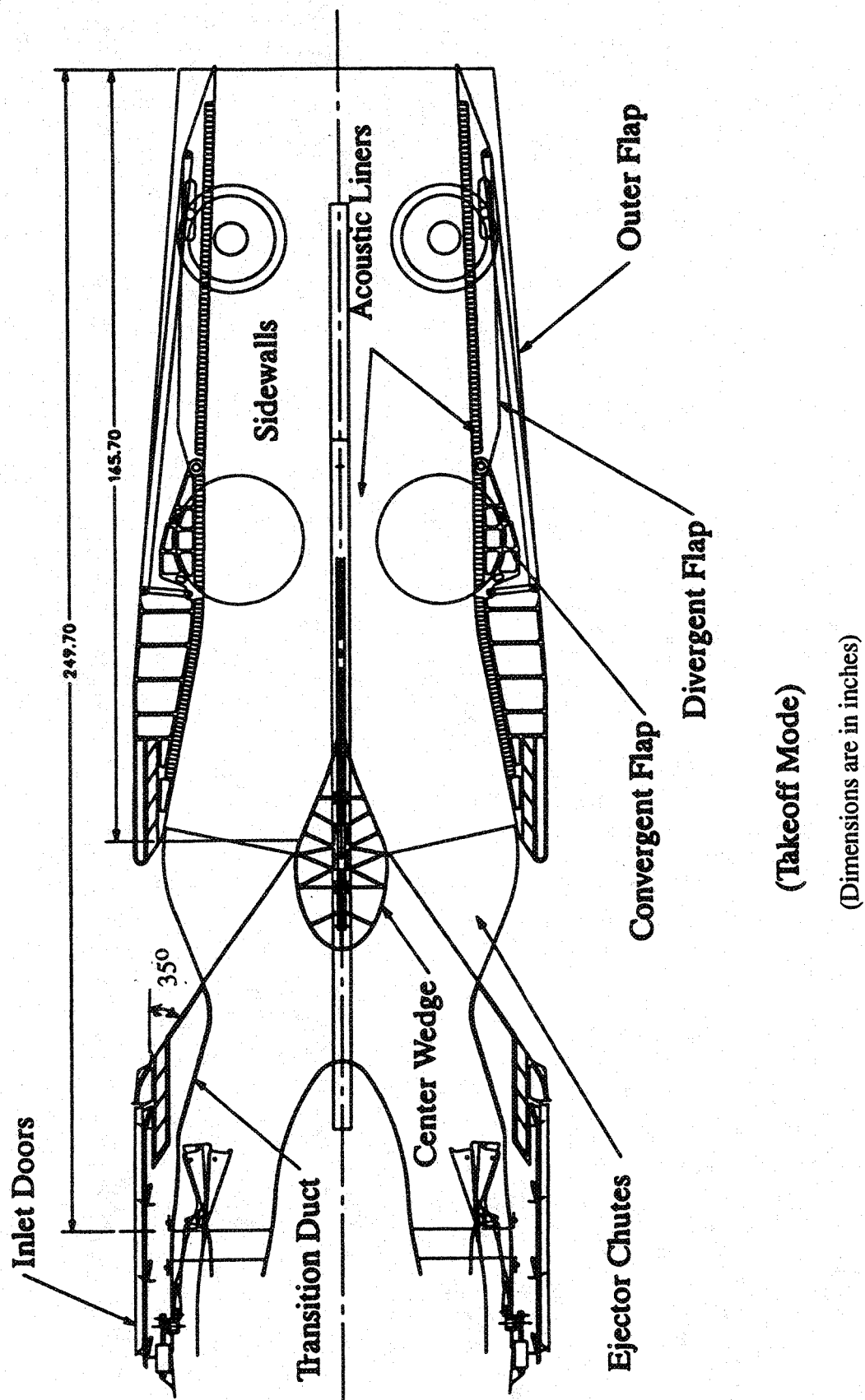
Figure 8-21. Preliminary design of a full-scale 2D mixer-ejector nozzle with fixed chute for a mixed flow turbo fan for M2.4 HSCT (Gen 2, NAS3 - 26617).
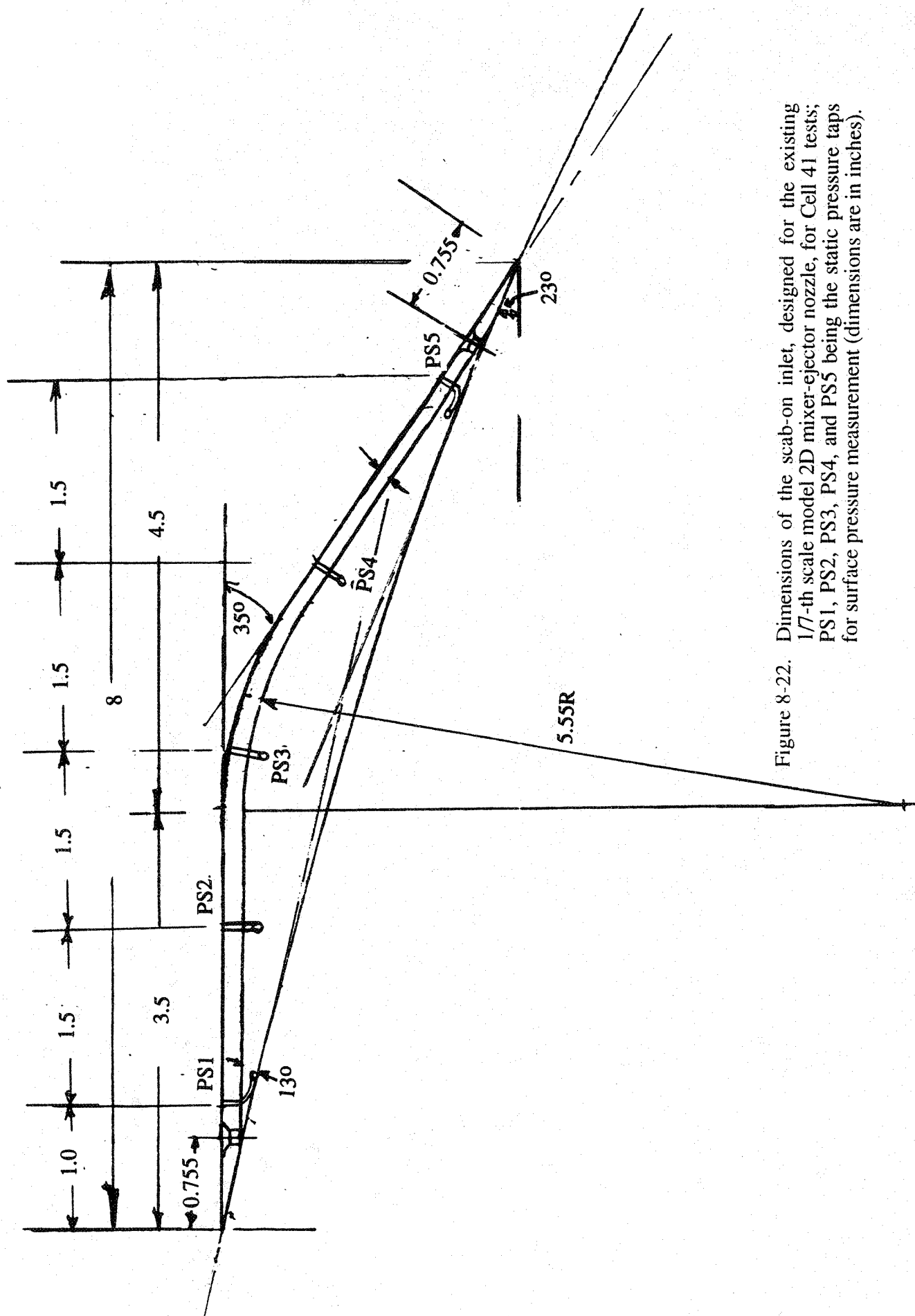
Figure 8-22. Dimensions of the scab-on inlet, designed for the existing 1/7-th scale model 2D mixer-ejector nozzle, for Cell 41 tests; PS1, PS2, PS3, PS4, and PS5 being the static pressure taps for surface pressure measurement (dimensions are in inches).
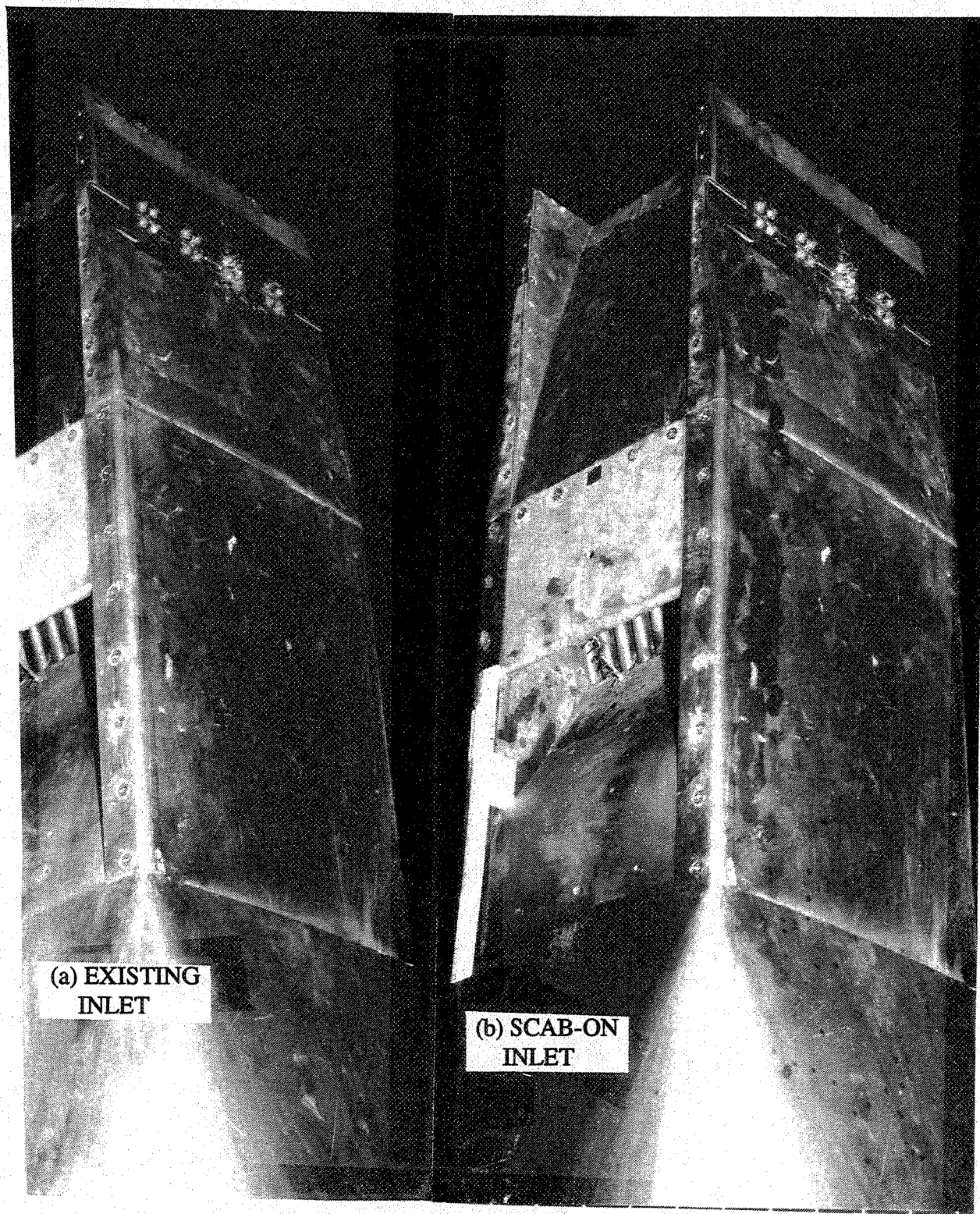
Figure 8-23. Top views of the (a) existing and (b) the scab-on inlets for the existing 1/7-th scale model 2D mixer-ejector nozzle
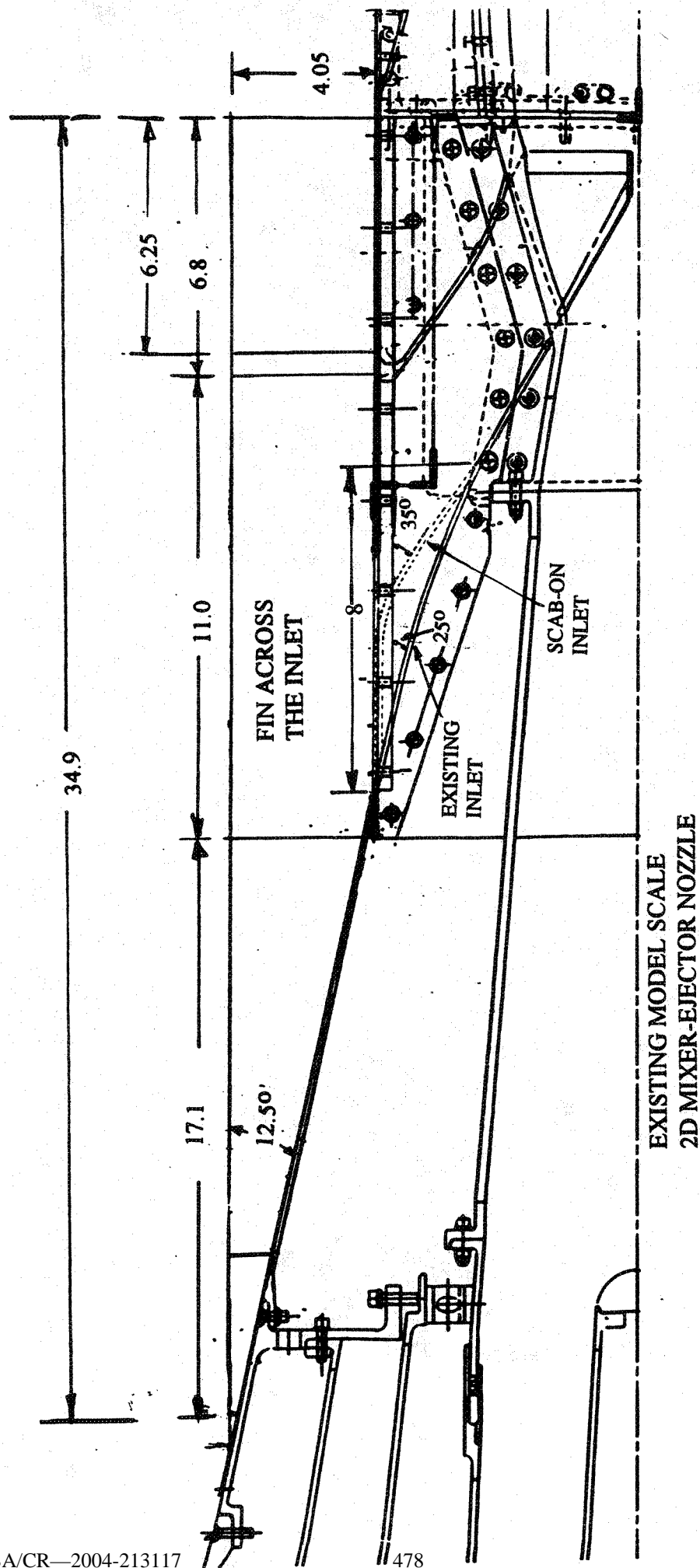
Figure 8-24. Side view of the fin, contoured to fit the 1/7-th scale model 2D mixer-ejector nozzle with scab-on inlet, for Cell 41 tests.
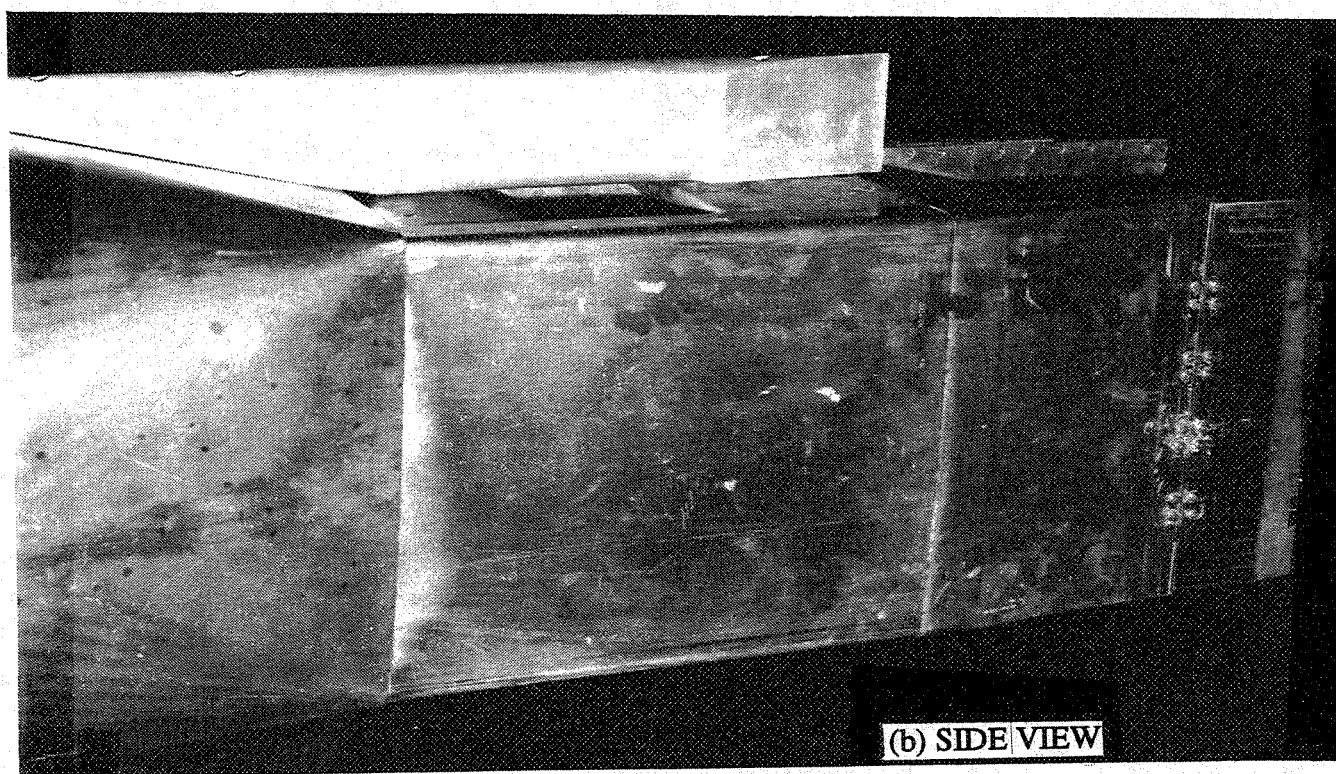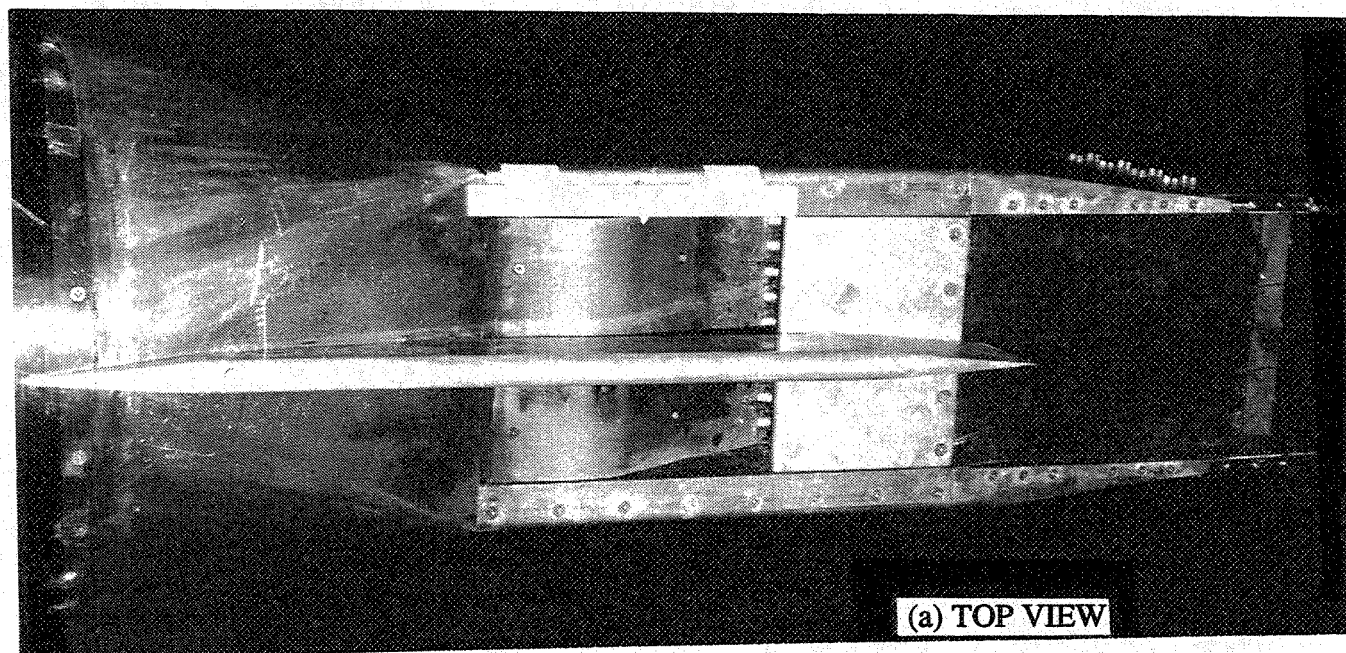
Figure 8-25. Top and side views of the fin mounted across the scab-on inlet of the 2D mixer-ejector nozzle.
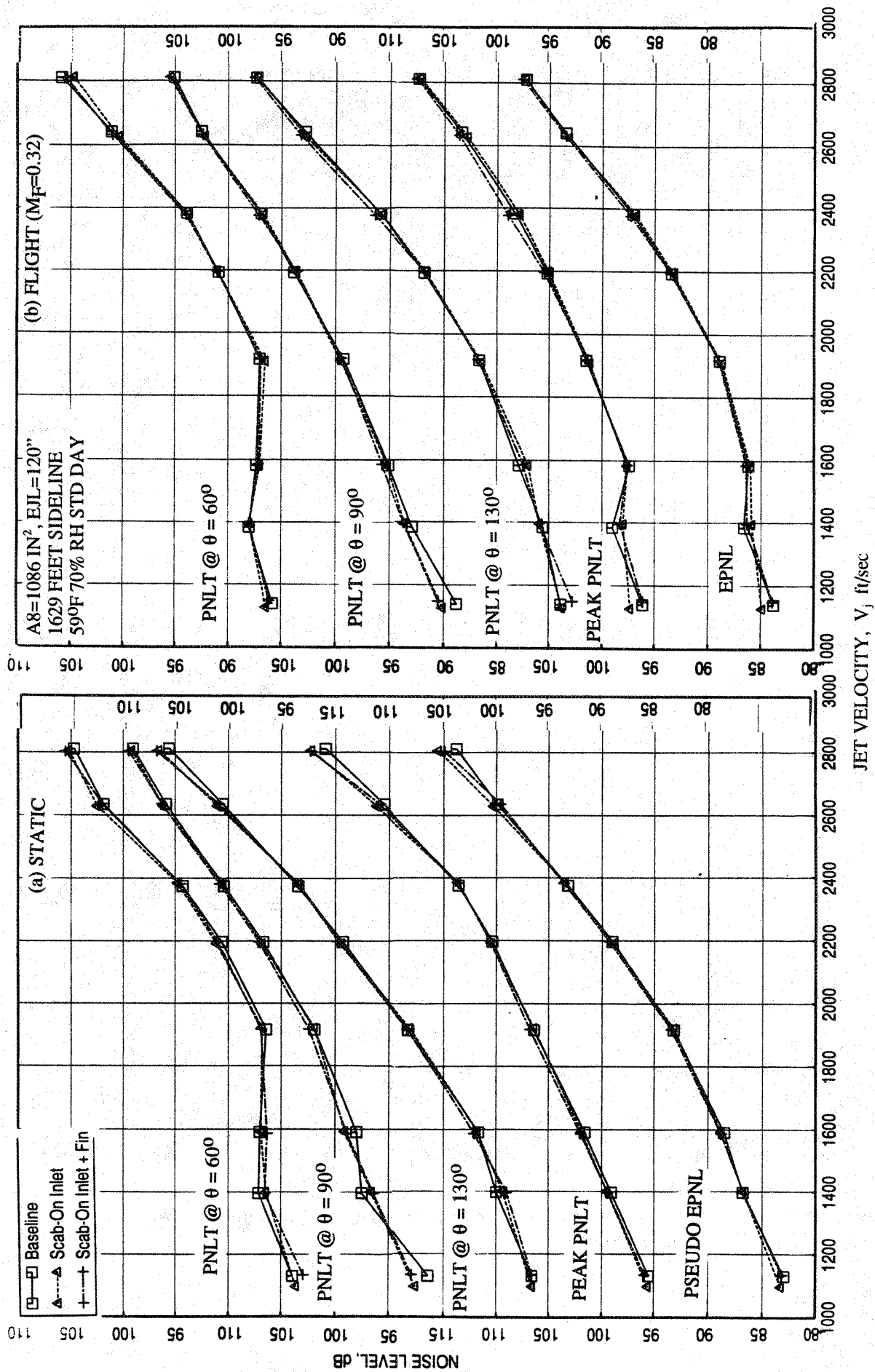
Figure 8-26. Effect of the scab-on inlet and the fin across the scab-on inlet on PNLT at various polar angles (θ), peak PNLT, and EPNL as functions of jet velocity for a 10 and 9 full staggered CD-chute mixer with long 7/9-treated ejector; SAR=2.8, MAR = 0.95.

Effect of the scab-on inlet and the fin across the scab-on inlet on PNLT directivities at jet velocities of 1147, 1400, 1919, 2384, and 2637 ft/sec are shown in Figure 8-27. At 1147 ft/sec (i.e., NPR=1.5) and 1400 ft/sec (i.e., for NPR=1.75) the PNLT levels are higher for the scab-on inlet compared to the baseline configuration at forward angles. For higher jet velocity conditions the influence of the scab-on inlet is insignificant. At 1147 and 1400 ft/sec the PNLT levels increase slightly due to the fin at polar angles between 70° and 100°, whereas, very little effect is observed at higher velocities. Effect of the scab-on inlet and the fin across the scab-on inlet on SPL spectra at various polar angles (θ) for each of the above mentioned five jet velocities are shown in Figures 8-28 through 8-32. Again, the influence of scab-on inlet on SPL is insignificant for all the jet velocity conditions. At lower velocities of 1147 and 1400 ft/sec the SPL levels are slightly higher due to the fin for most frequencies compared to no fin configuration in the forward arc. Very little effect on SPL levels is observed due to the presence of the fin for higher jet velocities.

8.2.2 Flow and Performance Related Parameters:

Figure 8-33 shows the scab-on inlet applied over the existing ramp for the 2D mixer-ejector nozzle. Static pressure taps are also shown in this figure. The effect of the scab-on inlet, with and without the fin, on the ramp and on the chute static pressure distributions is shown in Figures 8-34 and 8-35 for different L1M cycle conditions, at static condition and with flight simulation, respectively. For the static case, the effect of the fin on the ramp and on the chute surface static pressure distributions is insignificant. However, with flight simulation, the static pressure on the scab-on inlet drops in the vicinity of the sharp bend at PS3 (see Figure 8-33) and then gradually increases along the ramp due to the modified inlet shape. The effect of the fin on this inlet is again very small. The apparent gradual decrease of pressure (i.e., acceleration of flow over the ramp) between PS1 and PS3, as indicated in Figure 8-35, may not be realistic, since the modified ramp remains horizontal in this section. This is caused by insufficient static pressure taps in this area. (Note that PS2 was not operating for this case). A sharp pressure drop (or flow acceleration) is expected at or near PS3 due to the sharp 35° bending of the modified ramp. The chute loading coefficients, due to the chute static pressure distributions, as effected by the scab-on inlet, are plotted against NPR in Figure 8-36. For static case, the effect of the scab-on inlet, with and without the fin, on chute loading coefficient is insignificant. However, the chute loading coefficients are slightly lower due to the scab-on inlet with flight simulation.
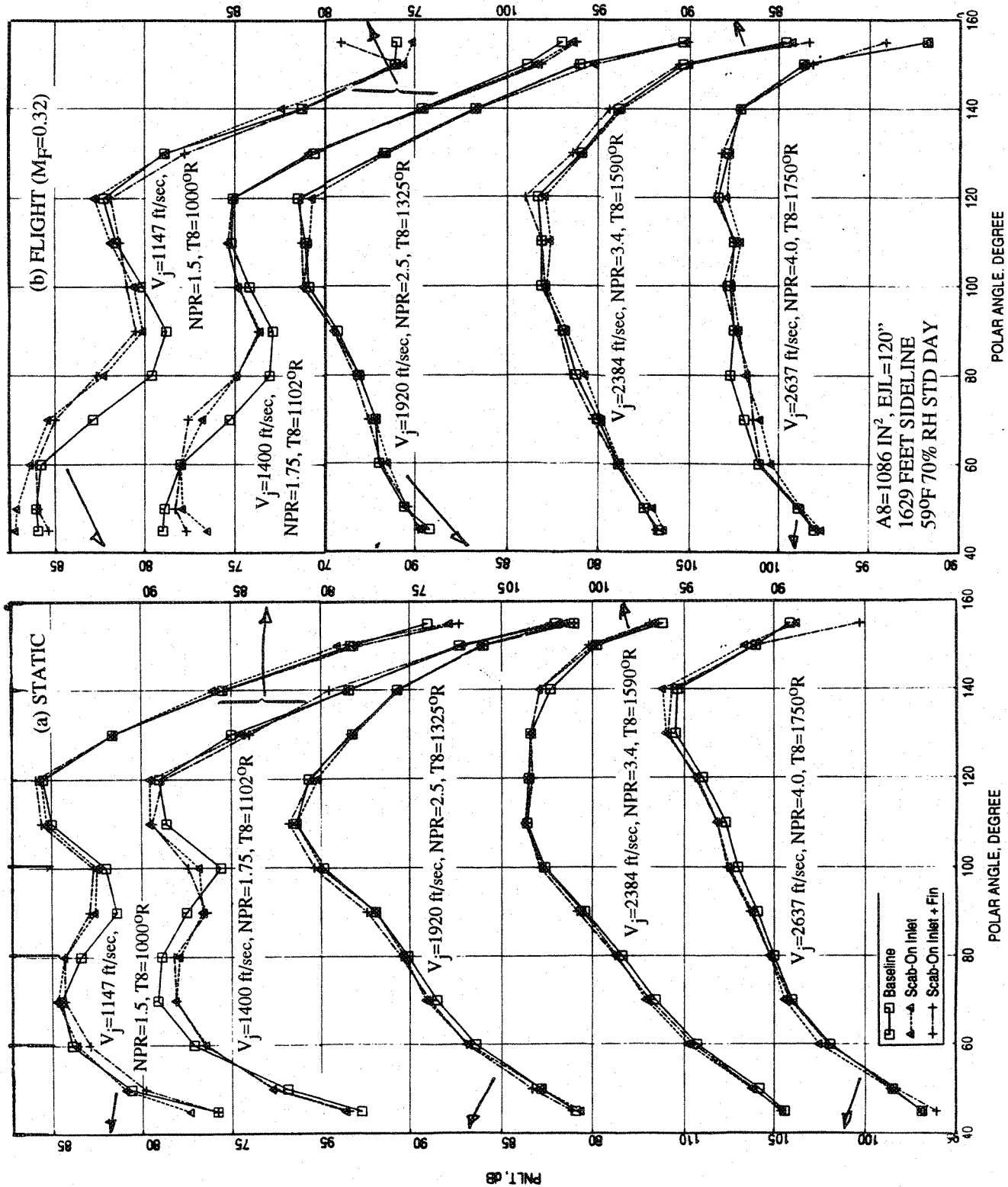
Figure 8-27. Effect of the scab-on inlet and the fin across the scab-on inlet on PNLT directivities for different jet velocities (V_j) for a 10 and 9 full staggered CD-chute mixer with long 7/9-treated ejector; SAR=2.8, MAR = 0.95.
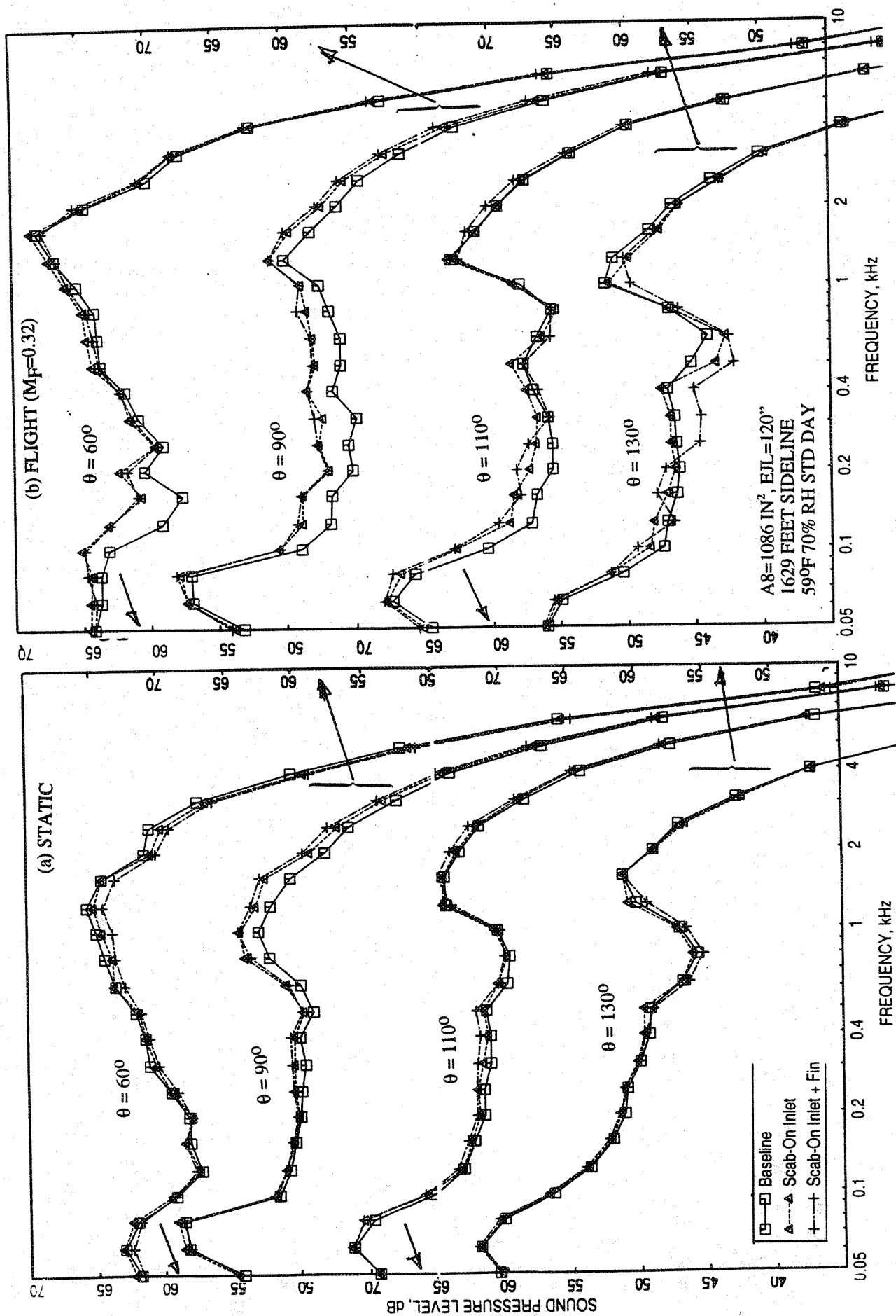
Figure 8-28. Effect of the scab-on inlet and the fin across the scab-on inlet on SPL spectra at various polar angles (θ) for a 10 and 9 full staggered CD-chute mixer with long 7/9-treated ejector; SAR=2.8, MAR = 0.95, V_j = 1147 ft/sec, NPR = 1.5, T8 = 1000°R.
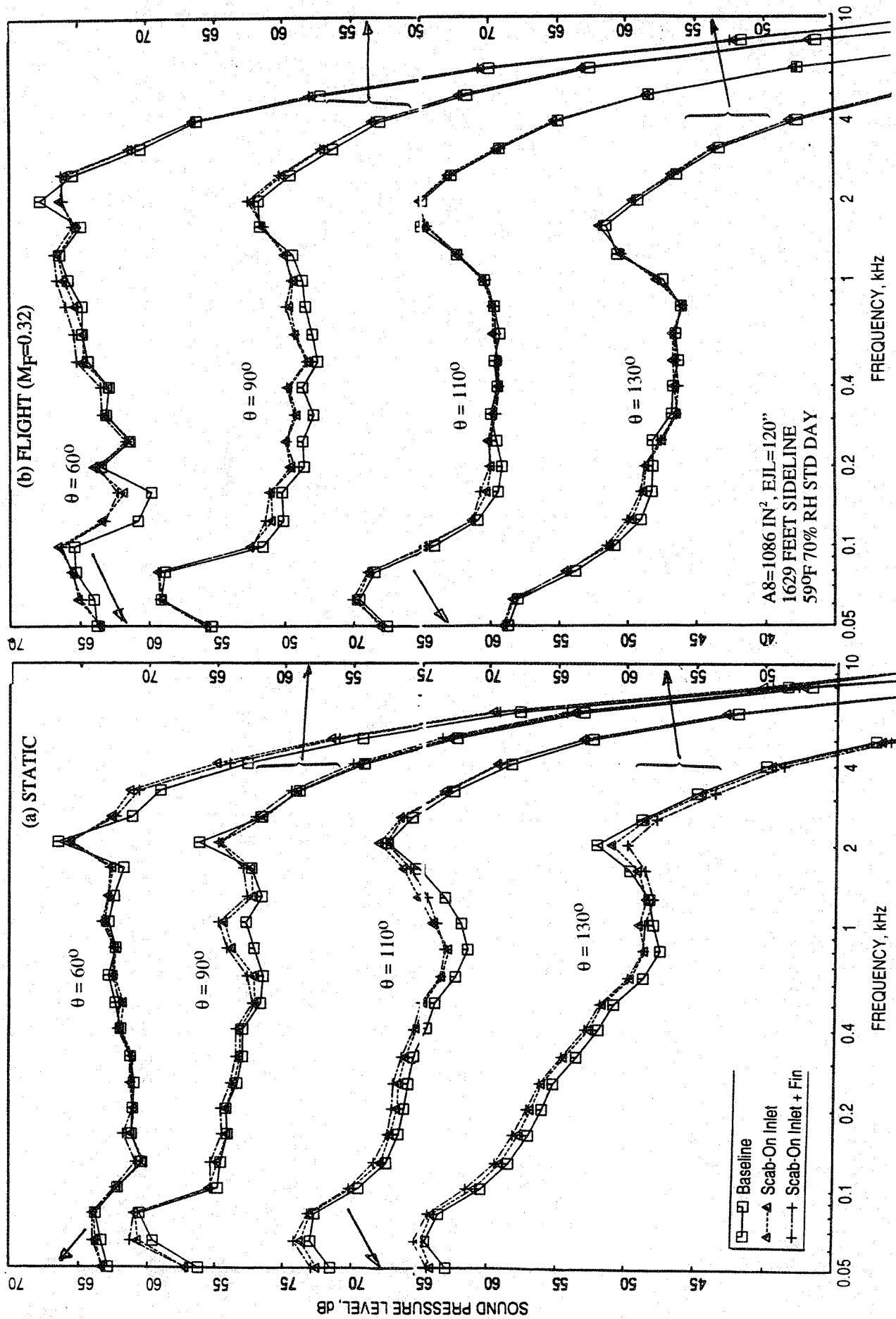
Figure 8-29. Effect of the scab-on inlet and the fin across the scab-on inlet on SPL spectra at various polar angles (θ) for a 10 and 9 full staggered CD-chute mixer with long 7/9-treated ejector; SAR=2.8, MAR = 0.95, V_j = 1400 ft/sec, NPR = 1.75, T8 = 1102°R.
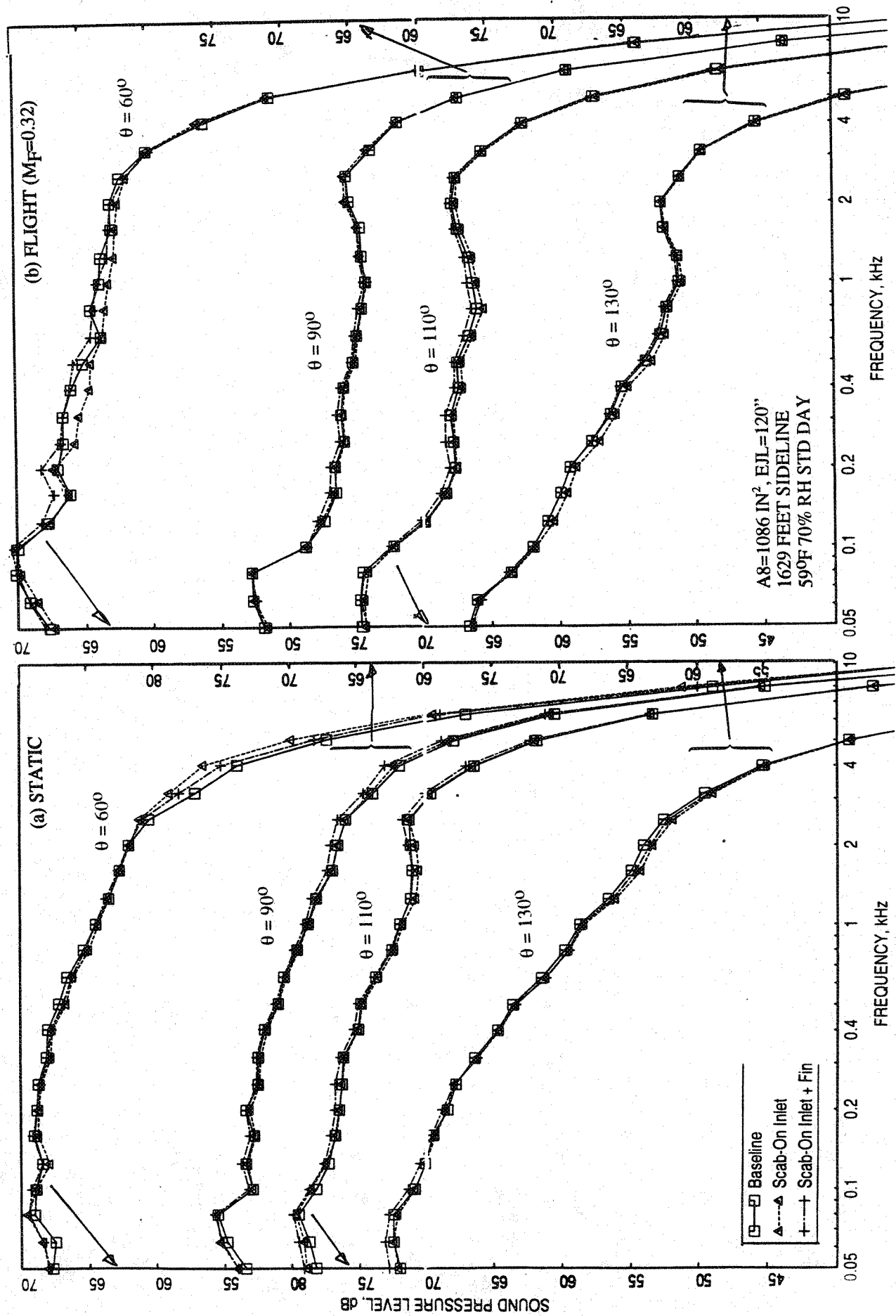
Figure 8-30. Effect of the scab-on inlet and the fin across the scab-on inlet on SPL spectra at various polar angles (θ) for a 10 and 9 full staggered CD-chute mixer with long 7/9-treated ejector; SAR=2.8, MAR = 0.95, V_j = 1919 ft/sec, NPR = 2.5, T8 = 1325°R.
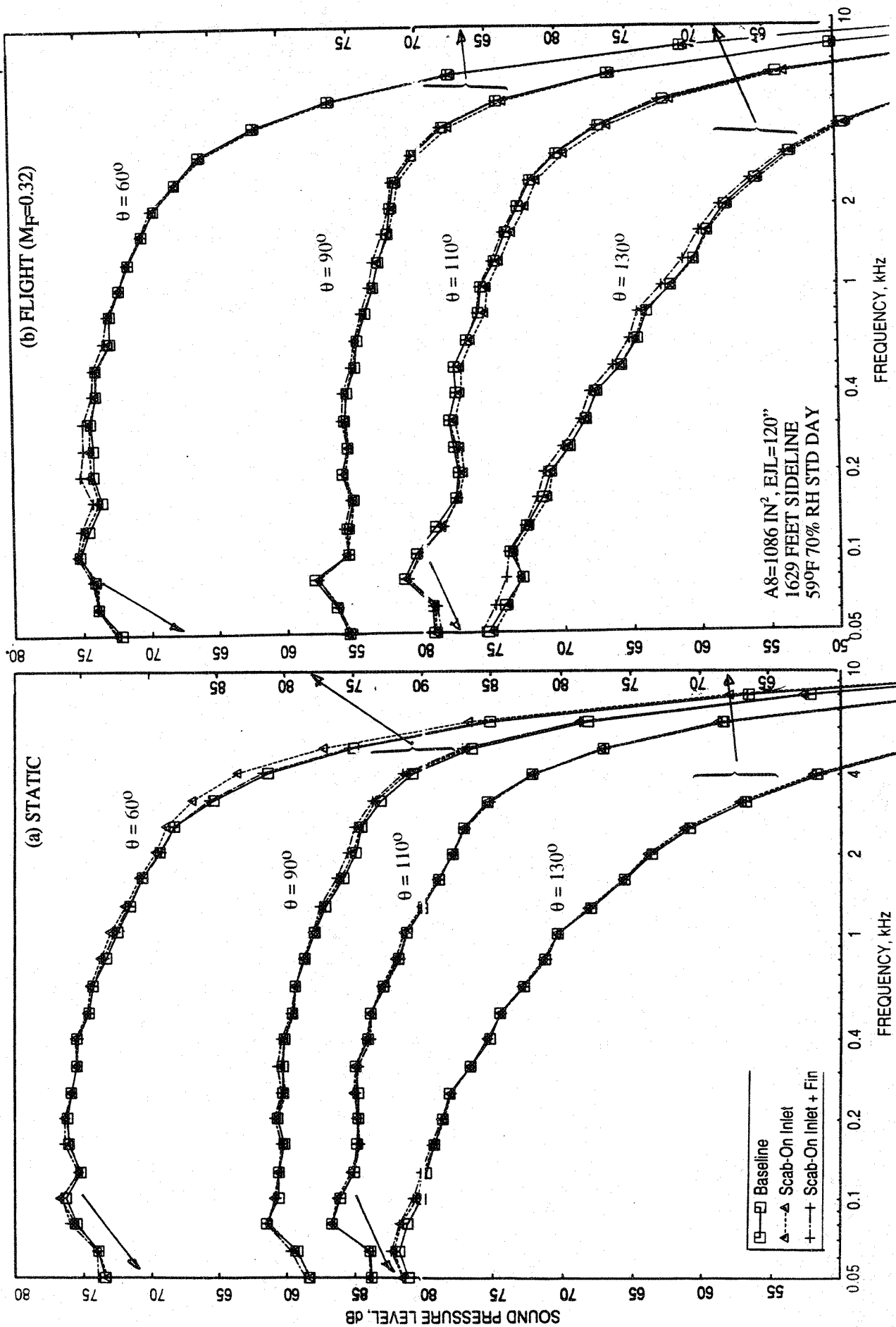
Figure 8-31. Effect of the scab-on inlet and the fin across the scab-on inlet on SPL spectra at various polar angles (θ) for a 10 and 9 full staggered CD-chute mixer with long 7/9-treated ejector; SAR=2.8, MAR = 0.95, V_j = 2384 ft/sec, NPR = 3.4, T8 = 1590°R.
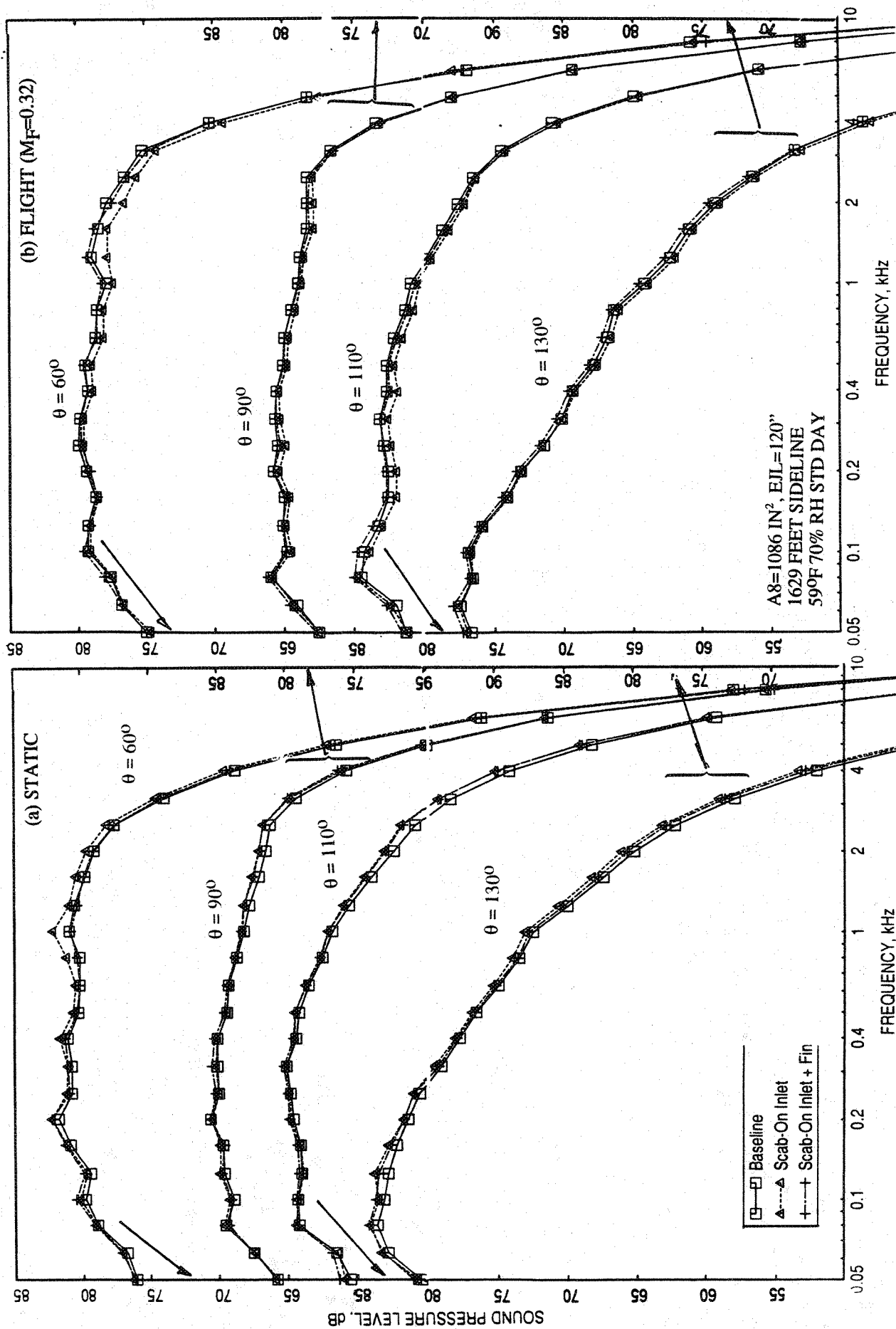
Figure 8-32. Effect of the scab-on inlet and the fin across the scab-on inlet on SPL spectra at various polar angles (θ) for a 10 and 9 full staggered CD-chute mixer with long 7/9-treated ejector; SAR=2.8, MAR = 0.95, Vⱼ = 2637 ft/sec, NPR = 4.0, T8 = 1750°R.
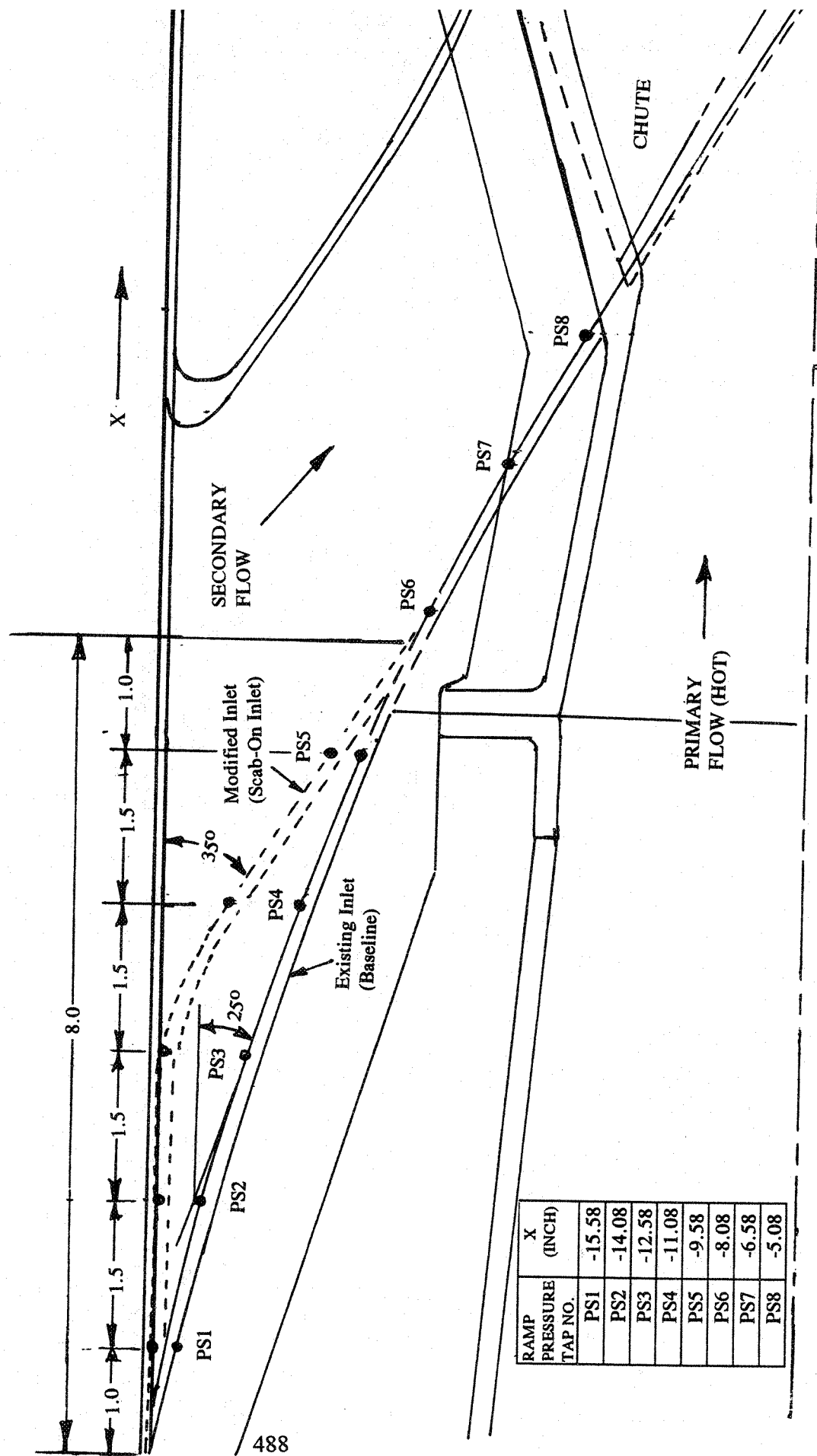
Figure 8-33. A modified inlet (or scab-on inlet) simulating the Gen 2 design used on the existing 2D model scale mixer-ejector nozzle (dimensions are in inches).

RAMP PRESSURE TAP NO.	X (INCH)
PS1	-15.58
PS2	-14.08
PS3	-12.58
PS4	-11.08
PS5	-9.58
PS6	-8.08
PS7	-6.58
PS8	-5.08
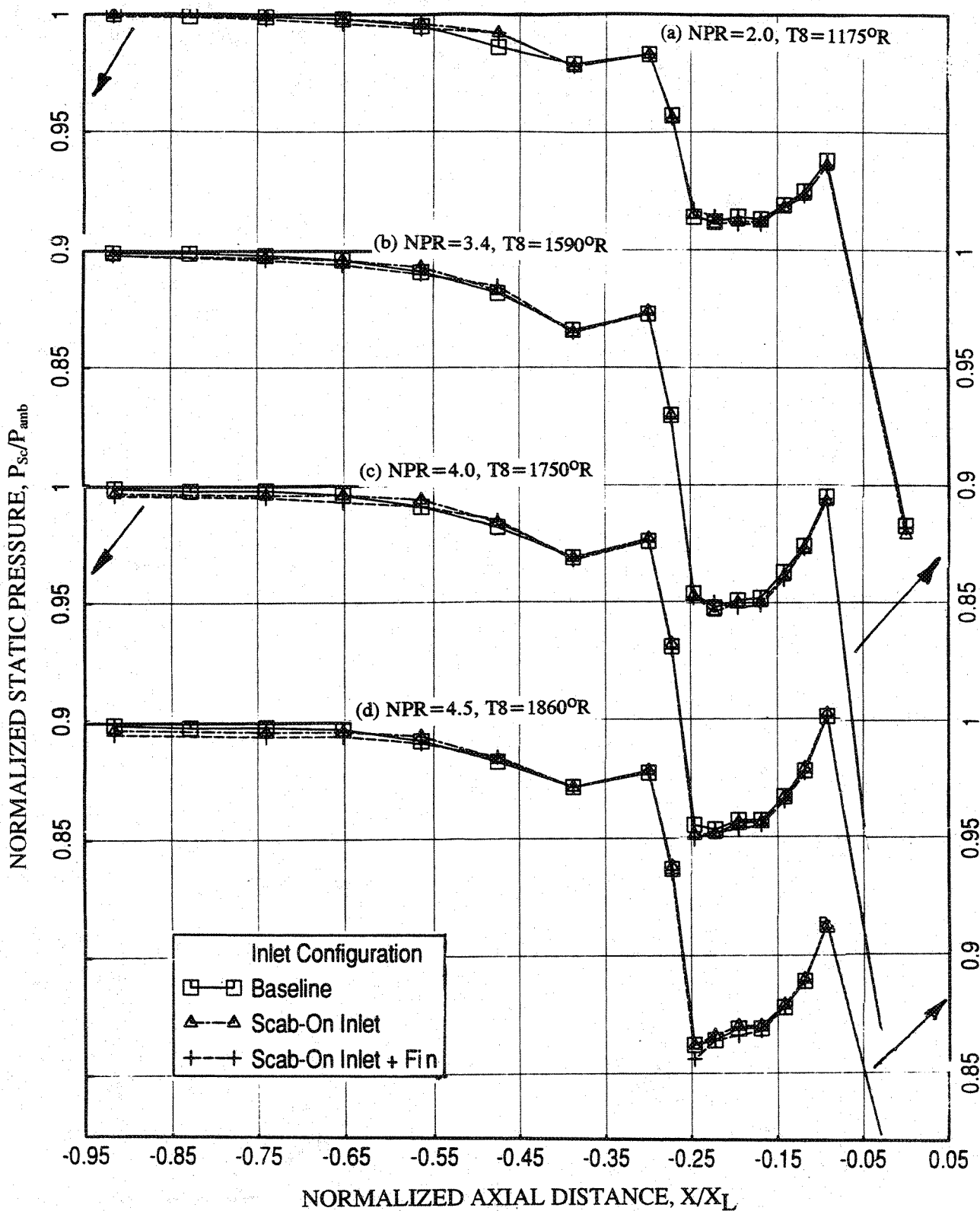
Figure 8-34. Effect of the scab-on inlet and the fin across the scab-on inlet on the static pressure distributions on the inlet ramp and on the secondary flow side of chute surface at different L1M cycle conditions for a 10 and 9 full staggered CD-chute mixer with long 7/9-treated ejector at static condition; SAR=2.8, MAR = 0.95.
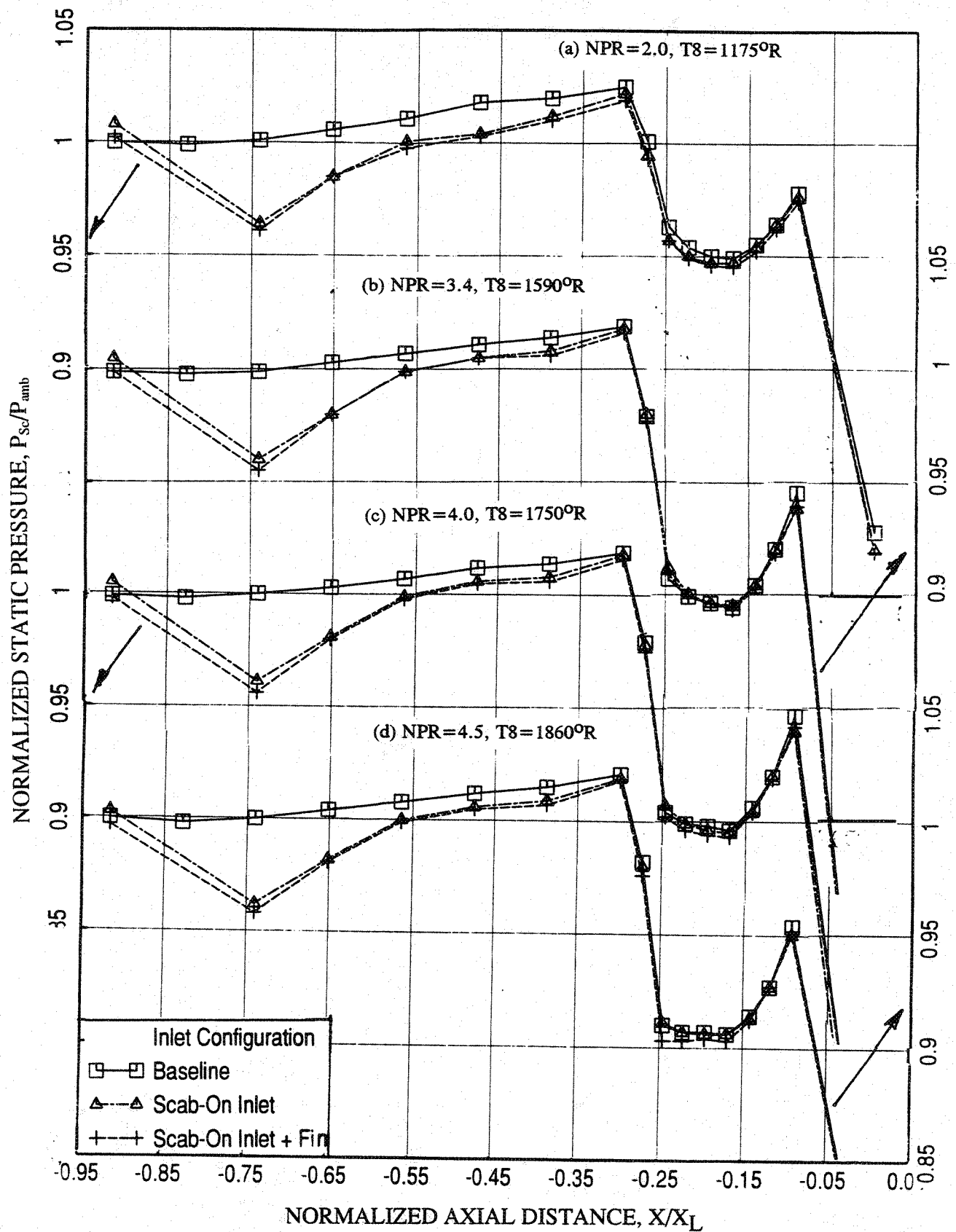
Figure 8-35. Effect of the scab-on inlet and the fin across the scab-on inlet on the static pressure distributions on the inlet ramp and on the secondary flow side of chute surface at different L1M cycle conditions for a 10 and 9 full staggered CD-chute mixer with long 7/9-treated ejector with flight simulation (M_F=0.32) ; SAR=2.8, MAR = 0.95.

Figure 8-36. Effect of the scab-on inlet and the fin across the scab-on inlet on chute loading coefficient, computed by measured static pressure distributions on secondary flow side chute leading edge, with respect to nozzle pressure ratios for a 10 and 9 full staggered CD-chute mixer with long 7/9-treated ejector; SAR=2.8, MAR = 0.95

The effect of the scab-on inlet with and without the fin on corrected pumping is shown in Figure 18-37. The pumping is slightly higher due to the scab-on inlet (without the fin) at static condition. With flight simulation the pumping is significantly higher due to the scab-on inlet, with and without the fin. Basically, the pumping is increased due to scab-on inlet. For static case, since the pumping is lowered due to fin (see Figure 8-16), the pumping increase due to scab-on inlet with fin is compensated. With flight simulation, since the presence of fin has no influence on pumping (see Figure 8-16), the influence of scab-on inlet to increase pumping is clearly observed with and without the fin (see Figure 8-37).

Figures 8-38 and 8-39 illustrate the effect of the scab-on inlet, with and without the fin, on axial static pressure distributions on the ejector flap at static and flight simulation conditions, respectively, at different L1M cycle conditions. The effect is insignificant at lower NPRs for static as well as flight simulation cases. At higher NPR, the static pressure distribution on the flap is lower due to the scab-on inlet at static condition. The effect slightly diminishes with the presence of the fin. The trend is reversed with flight simulation. This is further illustrated in terms of the force due to static pressure difference on flap surface as a function of nozzle pressure ratio in Figure 8-40. The transition from subsonic to supersonic mode seems to be slightly delayed, with respect to NPR, due to the scab-on inlet with flight simulation.

In general, the influence of scab-on inlet as a high gradient inlet ramp and the fin as a blockage to the secondary flow is relatively small on farfield acoustic characteristics as well as on the flow and performance related parameters.
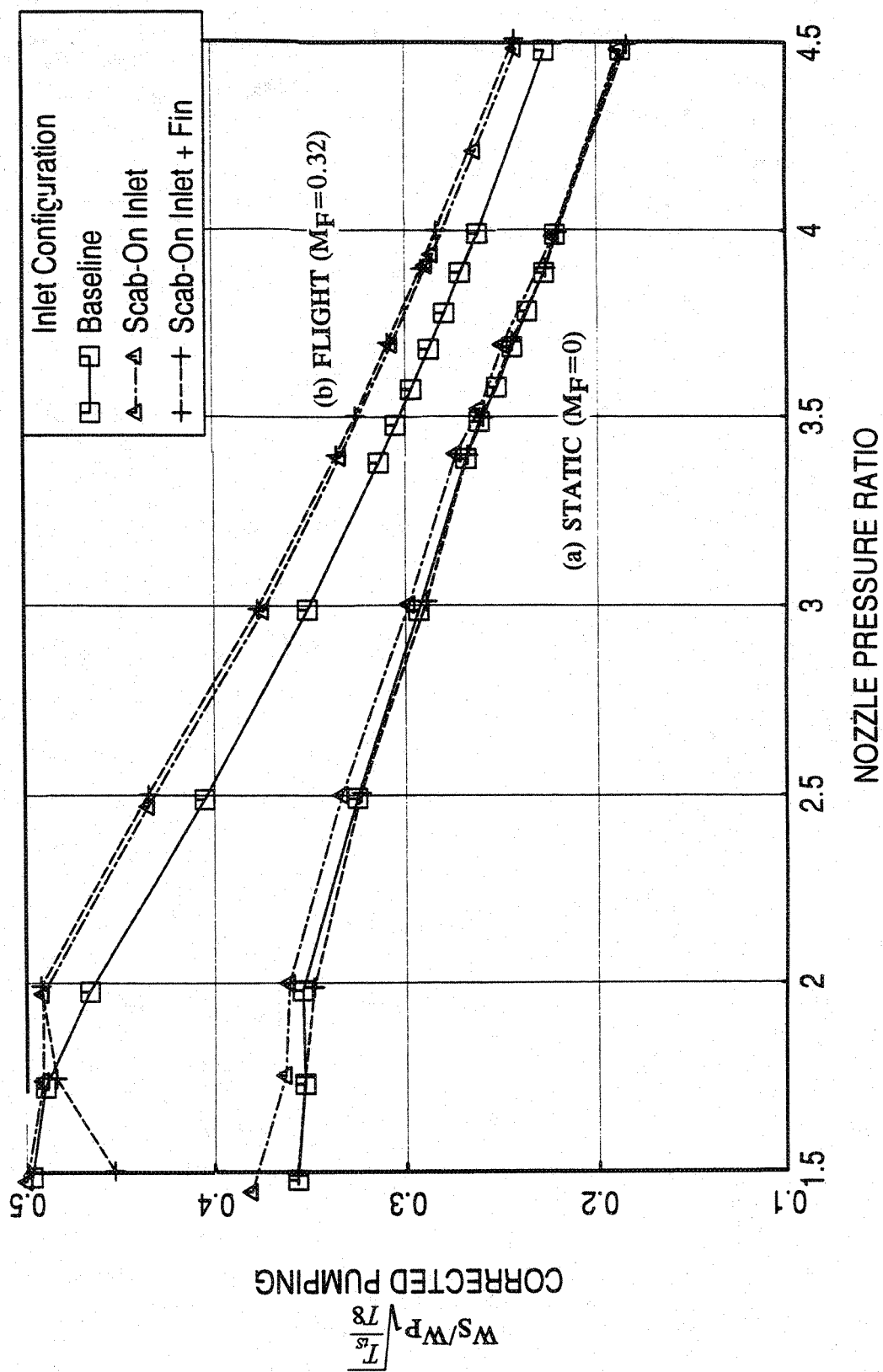
Figure 8-37. Effect of the scab-on inlet and the fin across the scab-on inlet on pumping, computed by measured rake total pressure distributions at the inlet, with respect to nozzle pressure ratios for a 10 and 9 full staggered CD-chute mixer with long 7/9-treated ejector; SAR=2.8, MAR = 0.95.
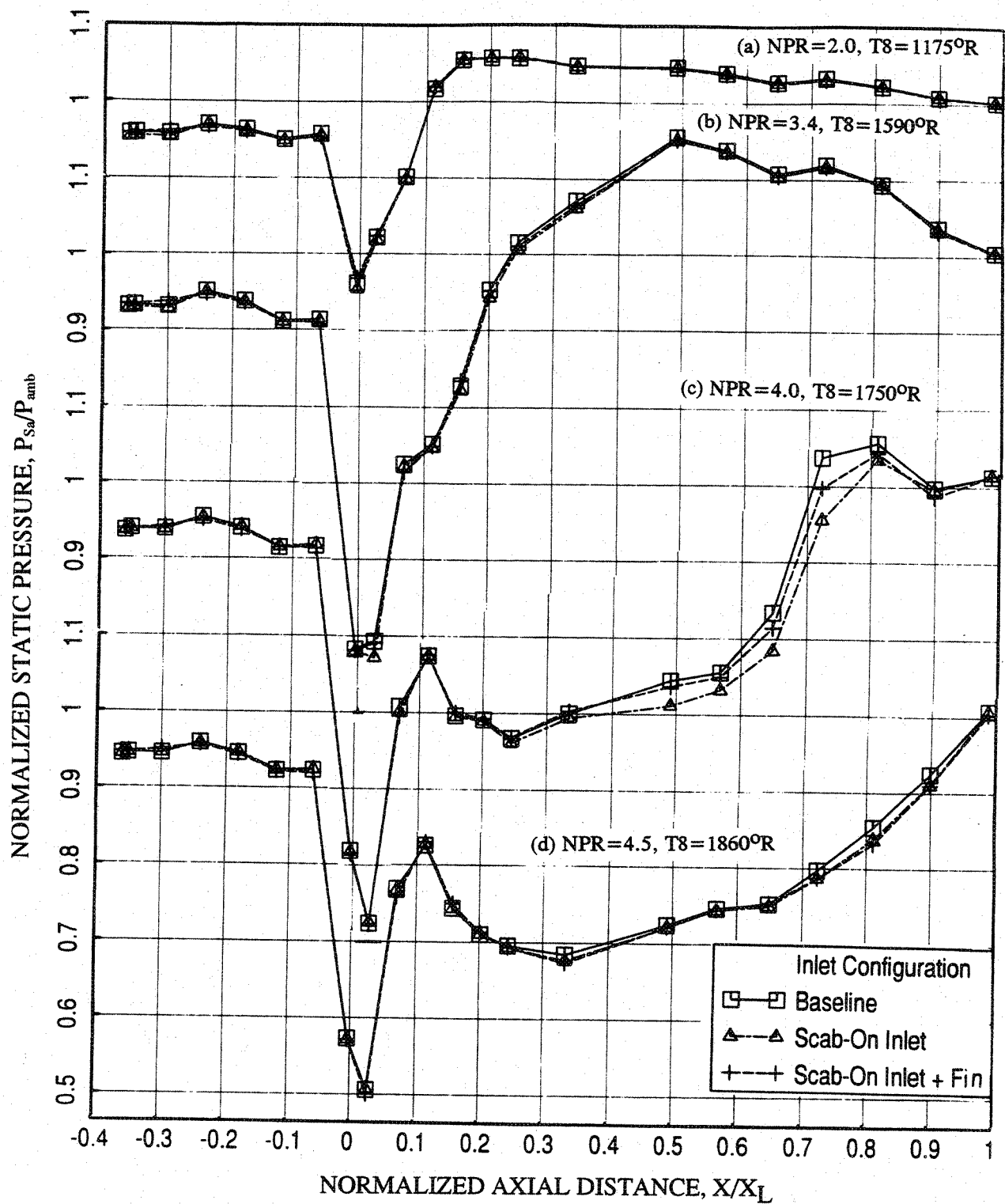
Figure 8-38. Effect of the scab-on inlet and the fin across the scab-on inlet on axial distribution of average static pressure on the inlet and the flap surface at different L1M cycle conditions for a 10 and 9 full staggered CD-chute mixer with long 7/9-treated ejector at static condition; SAR=2.8, MAR = 0.95.
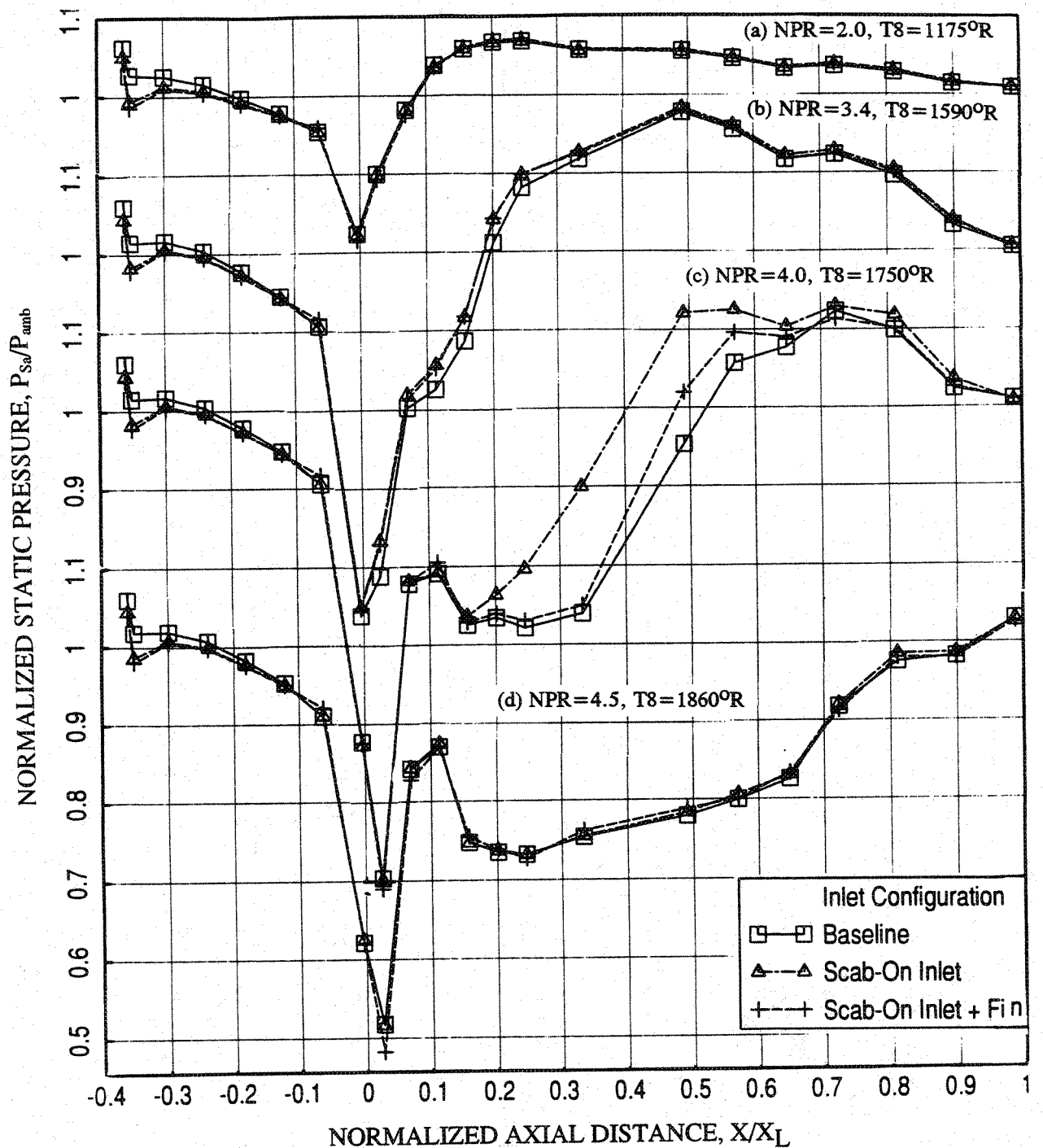
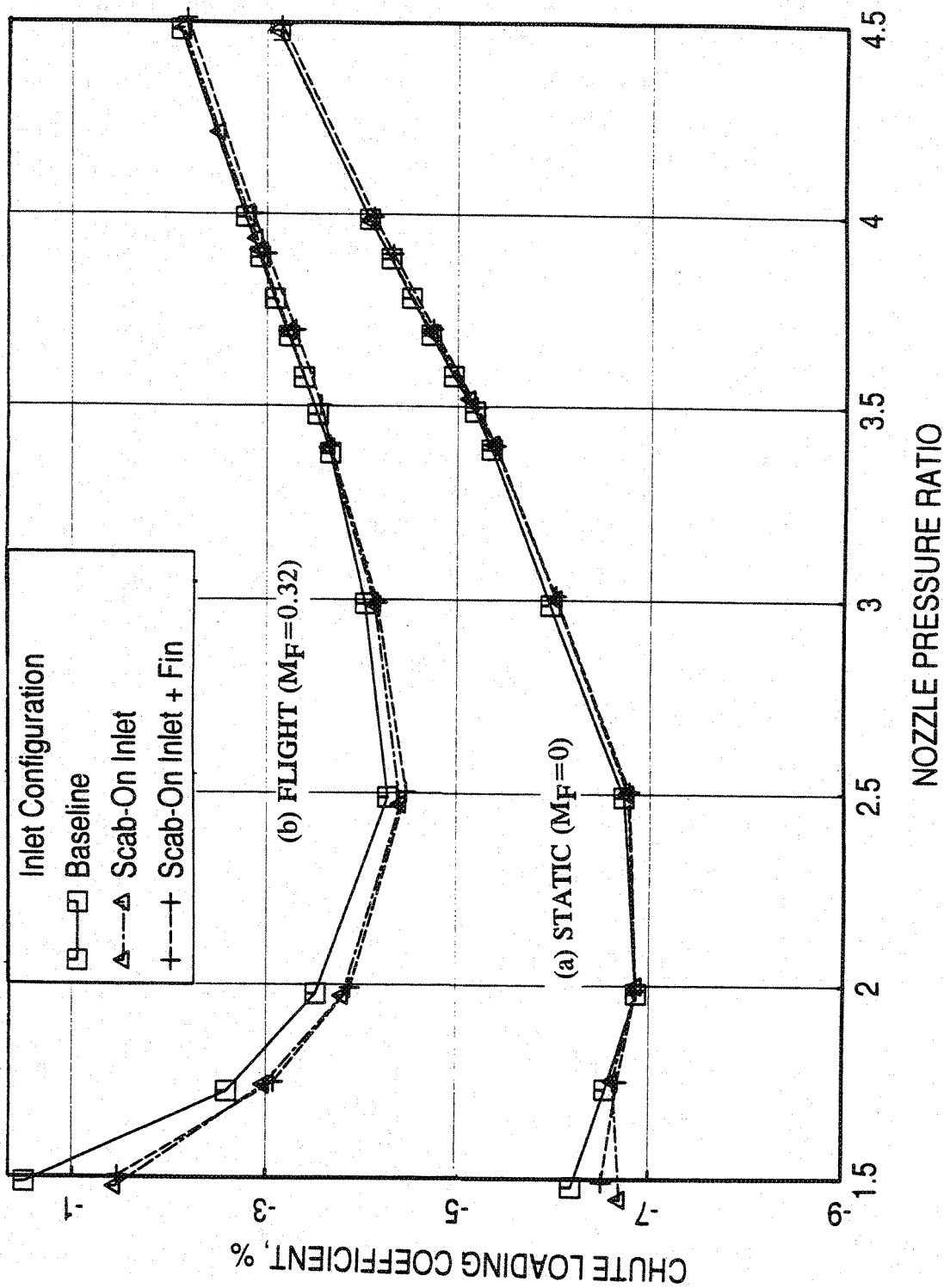Figure 8-39. Effect of the scab-on inlet and the fin across the scab-on inlet on axial distribution of average static pressure on the inlet and the flap surface at different L1M cycle conditions for a 10 and 9 full staggered CD-chute mixer with long 7/9-treated ejector with flight simulation (M_F=0.32) ; SAR=2.8, MAR = 0.95.

Figure 8-40. Effect of the scab-on inlet and the fin across the scab-on inlet on normalized force due to ejector flap with respect to nozzle pressure ratio for a 10 and 9 full staggered CD-chute mixer with long 7/9-treated ejector; SAR=2.8, MAR = 0.95.

9.0 CONCLUSIONS

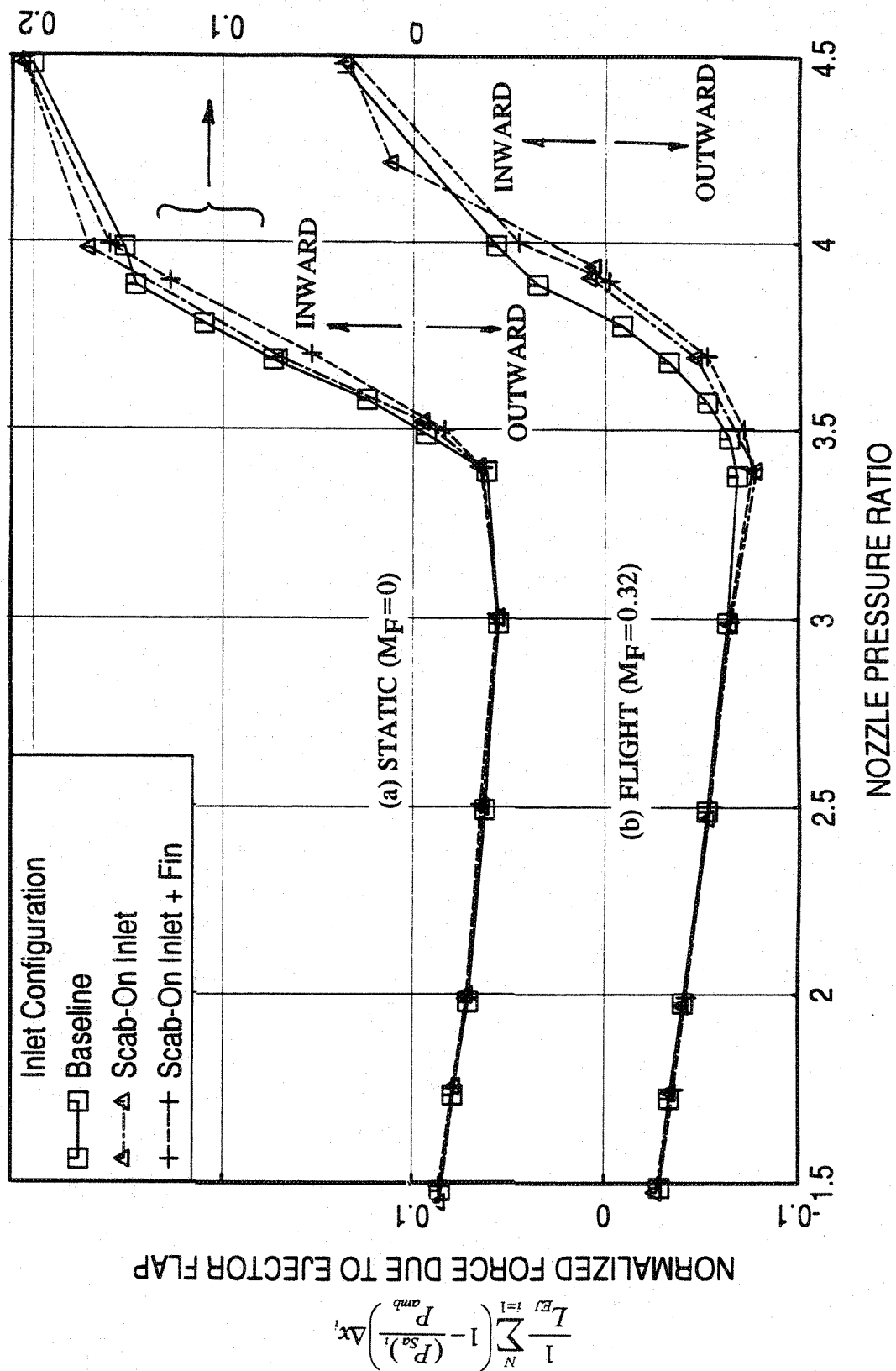The principle objectives of the current program are to experimentally investigate the repeatability of acoustic and aerodynamic characteristics of 2D mixer-ejector nozzles and the effects on the acoustic and aerodynamic characteristics of 2D mixer-ejectors due to (1) the configurational variations, which include mixers with aligned CD chutes, aligned convergent chutes, and staggered CD chutes and aerodynamic cycle variables, (2) treatment variations by using different treatment materials, treating the ejector with varying area, location, and treatment thickness for a mixer-ejector configuration, and (3) secondary inlet shape (i.e., a more realistic inlet) and the blockage across the inlet (a possible fin-like structure needed for installation purpose) by modifying one of the inlet of a mixer-ejector configuration. In addition, internal dynamic pressures for a few selected configuration were measured to examine the internal noise characteristics.

Acoustic testing in General Electric's Jet Noise Test Facility, Cell 41 was conducted for five basic mixer configurations, namely, two aligned CD chute mixers of SAR (Suppressor Area Ratio) 2.8 and 3.3, an aligned convergent chute mixer with SAR= 2.8, and two staggered CD chute mixers with SAR=2.8. With the variation of treatment type, treatment area, treatment thickness, ejector length, modifications at the secondary inlet, and the above listed five mixer geometry, 25 different configurations, were tested.

The major observations made from the analysis of the measured acoustic and model static and total pressure are as follows:

1.   Tests were conducted for two aligned CD-chute mixers of SAR 3.3 and 2.8 with long fully treated ejector to establish the repeatability of measurement by comparing the current results with previously obtained data. In general, the repeatability of test results for both the mixer-ejector configurations is very good. Small differences observed in the data shown here could be due to uncertainty of exact duplication of ejector treatment, flight Mach number and aerothermodynamic conditions.

2.   The azimuthal variation of acoustic field for the aligned CD-chute mixers with long ejector is significant and is much higher at lower jet velocities. A variation of about

4 to 6 EPNdB is observed at jet velocities between 1147 ft/sec and 1600 ft/sec. Even at higher jet velocities the variation is of significance.

3.   Significant noise reduction is observed due to flight simulation for the aligned CD-chute mixers with long ejector. Significant SPL reduction is observed at higher polar angles for the entire frequency range. Major noise reduction took place between Mach 0 and 0.24. The static pressure increases with increasing flight Mach number, both on the ramp and chute surfaces due to freejet fan pressure rise, indicating lesser loading for the chutes. The pumping increases with increasing flight Mach number, since the total pressure at the inlet goes up. The transition from subsonic to supersonic mode seems to be slightly delayed with respect to NPR due to flight simulation.

4.   A nickel based brick-like foam metal was used as the bulk absorber, instead of astroquartz, for an aligned CD-chute mixers of SAR 2.8 with long ejector to determine its effectiveness in noise suppression. The foam metal seems to be performing as well as and, in most cases, slightly better than the astroquartz treatment. This is a very encouraging result, since maintaining proper astroquartz treatment is more laborious and time consuming. Since the foam metal is solid in structure and did not show any deterioration during testing, this treatment is being used in all the subsequent treated configurations, instead of astroquartz.

5.   Acoustically the staggered 10 and 9 full CD-chute mixer performs best compared to other configurations at velocities above 1600 ft/sec. At lower velocities the aligned convergent chute mixer performs much superior to other mixer designs acoustically. The effect of mixer geometry on ramp static pressure distributions is insignificant. The static pressure distributions on the chute surface is more or less the same for the three CD chute mixers. However, it is significantly different for convergent chute mixer, especially at lower NPRs. The static pressure levels for convergent chute are much lower compared to those for CD chute configurations. The static pressure distributions between the mixer configurations clearly indicate that the mode switch is delayed for convergent chute mixer and is relatively early for 9 and 2 half staggered chute configuration.

6.   Tests were conducted for 10 and 9 full CD-chute staggered mixer with fully treated long ejector and with short hardwalled ejector to study the acoustic, flow related,

and performance related characteristics at fixed jet velocities by varying the nozzle pressure ratio and total temperature. The EPNL increases with increasing jet velocity. With respect to aerothermodynamic conditions the EPNL increases with increasing NPR and with decreasing nozzle total temperature. The trend is reversed at lower jet velocities, especially, with flight simulation. Based on the fixed EPNL contours, the EPNL increases with increasing NPR and nozzle total temperature. However, it is interesting to note that the fixed EPNL can be achieved by lowering the NPR and nozzle total temperature together at a lower NPR conditions. Static pressure decreases with increasing NPR, both on the ramp and chute surfaces. However, at higher NPR the trend on chute static pressure distribution is reversed. The chute loading coefficient decreases and then increases with increasing NPR with decreasing nozzle total temperature. An optimum NPR and temperature combination seems to be possible for a desired chute loading coefficient as indicated from the fixed chute loading coefficient contours. With respect to increasing NPR and with decreasing total temperature the pumping decreases.

7.   Based on the dynamic pressure measurements made inside the ejector the following observations are made; The ejector treatment attenuates internal noise and is more effective at lower NPR (or jet velocity). Treatment closer to the mixer exit is also effective in flap dynamic pressure attenuation, but relatively less compared to a similar treatment area closer to ejector exit, especially for very high NPR. Ejector treatment is important, especially on entire surface, when the externally generated noise component is lower or of the same magnitude compared to the internal noise component.

8.   For the treatment study, the acoustically performing best mixer-ejector configuration (i.e., the 10 and 9 full staggered CD-chute mixer with long ejector) was used to identify any additional acoustic benefit. The mixer-ejector configurations used under current programs generate dominant jet mixing noise compared to internally generated noise in the farfield, especially at higher jet velocity conditions. Thus, the influence of various parameters altered in ejector treatment on the farfield noise is small at higher velocities. However, significant impact is noticed on farfield noise due to treatment variation at lower jet velocities. It is believed that the influence of all these treatment parameters on internally generated noise is similar, even though, not experienced in the farfield for higher jet velocity conditions. If the jet-mixing noise is reduced by better mixer design or suitably applying other innovative means the impact of internal noise will be

realized even at higher jet velocity conditions and the treatment study would be beneficial. Following are the major observations due to treatment study:

(i) The fully treated ejector performs the best. However, 7/9 treatment is close to the full treatment configuration, especially at higher velocities. (ii) The 0.5"-thick treatment is better in suppressing acoustic energy. (iii) Treatment location closer to ejector exit suppresses more acoustic energy. (iv) Fully treated ejector is acoustically better that the flaps only treated configuration. (v) Silicon carbide bulk material seems to have more potential in suppressing internal noise.

9.   Based on the tests conducted to evaluate the impact of secondary inlet geometry the following observation is made; In general, the influence of scab-on inlet as a high gradient inlet ramp and the fin as a blockage to the secondary flow is relatively small on farfield acoustic characteristics as well as on the flow and performance related parameters.

APPENDIX - LIST OF SYMBOLS

A_i = Elemental projected area in axial direction for the static pressure $(P_{sc})_i$ in sq. inch

A_{exit} = Mixer Exit Area, in^2

A_{SEC} = Total ambient (secondary) flow area, in^2

A_{MIX} = A8 + A_{SEC} , in^2

A8 = Primary stream throat area, in^2

CD = Convergent Divergent

CER = Core Expansion Ratio = A_{exit} /A8

$D8_{eq}$ = Equivalent diameter for A8, in

EJL = Full Scale Ejector Length, in

EPNL = Effective Tone corrected Perceived Noise Level based on PNLT, dB

EPNLN = Normalized Effective Tone corrected Perceived Noise Level based on PNLT, dB

$(FG)_i$ = Ideal gross thrust in lbs

f = Frequency, Hz

F_{ref} = Reference Gross Thrust, 60000 lbs

GEAE = General Electric Aircraft Engines

HEAT = High-lift Engine Aeroacoustic Test

HSCT = High Speed Civil Transport

L_{EJ} = Model Scale Flap Length, in

MAR = Mixing Area Ratio

M_F = Simulated flight Mach number

n = Jet velocity exponent

NASA = National Aeronautics and Space Administration

NF = Total normalization factor with respect to thrust and density

$\quad$ {-10 Log $((FG)_i/F_{ref})$ $(r/r_0)^{\omega-1}$, dB}

NF_{th} = Normalization factor with respect to thrust {-10 Log $((FG)_i/F_{ref})$, dB}

NPR = Nozzle Pressure Ratio

NRA = 2D Mixer-ejector nozzle designed under NASA Research Announcement
$\quad$ (Contact NAS3 25415)

OAPWL = Overall Sound Power Level, dB

OAPWLN = Normalized Overall Sound Power Level, dB

OASPL = Overall Sound Pressure Level, dB

OASPLN = Normalized Overall Sound Pressure Level, dB

P_{amb} = Ambient pressure

PNL = Perceived Noise Level, dB

PNLN = Normalized Perceived Noise Level, dB

PNLT = Tone corrected Perceived Noise Level, dB

PNLTN = Normalized Tone corrected Perceived Noise Level, dB

Pseudo EPNL = EPNL for static case assuming a hypothetical flight velocity.

Pseudo PWL = PWL assuming azimuthal symmetry for azimuthally varying sound field.

P_{sa}= Static pressure on ejector flap surface

$(P_{sa})_i$ = Static pressure measured by the ith tap on ejector flap surface

$(P_s)_c$ = Static pressure on ejector flap surface along the cold flow line

$(P_s)_h$ = Static pressure on ejector flap surface along the hot flow line

P_{sc} = Static pressure on ramp and chute surface

$(P_{sc})_i$ = Static pressure measured by the ith tap on chute surface

PWL = Sound Power Level, dB

PWLN = Normalized Sound Power Level, dB

RH = Relative Humidity, %

SAR = Suppressor Area Ratio = A_{MIX} / A8

SPL = Sound Pressure Level, dB

SPLN = Normalized Sound Pressure Level, dB

TOGW = Takeoff Gross Weight

T_{tS} = Secondary Stream Total Temperature, °R

T8 = Nozzle Total Temperature, °R

V_j = Ideal Jet velocity, ft/sec

V_{mix} = Mass averaged mixed velocity, ft/sec

W_p = Mass Flow Rate for primary stream, lbs/sec

W_s = Mass Flow Rate for secondary stream, lbs/sec

X = Axial distance measured downstream of the CD -chute mixer exit plane, in

X_L = Model Scale Ejector Length, in

ω = Density exponent, 2 for high velocities

γ = Specific Heat Ratio

θ = Angle to Inlet or Polar Angle, degree

ϕ = Azimuthal angle for traversing microphone array in Cell 41, degree

ρ = Jet density

ρ_0 = Ambient Density of Air

ΔC_{fg} = Correction factor to the gross thrust coefficient in % due to the drag or thrust
contributions by the relative pressure distributions chute surfaces

REPORT DOCUMENTATION PAGE

Public reporting burden for this collection of information is estimated to average 1 hour per response, including the time for reviewing instructions, searching existing data sources, gathering and maintaining the data needed, and completing and reviewing the collection of information. Send comments regarding this burden estimate or any other aspect of this collection of information, including suggestions for reducing this burden, to Washington Headquarters Services, Directorate for Information Operations and Reports, 1215 Jefferson Davis Highway, Suite 1204, Arlington, VA 22202-4302, and to the Office of Management and Budget, Paperwork Reduction Project (0704-0188), Washington, DC 20503.

1. AGENCY USE ONLY (Leave blank)	2. REPORT DATE July 2004	3. REPORT TYPE AND DATES COVERED Final Contractor Report

4. TITLE AND SUBTITLE

Acoustic, Flow Related, and Performance Related Experimental Results for Generation 1.5 High Speed Civil Transport (HSCT) 2-Dimensional Exhaust Nozzles

6. AUTHOR(S)

M. Salikuddin, S. Wisler, and R. Majjigi

5. FUNDING NUMBERS

WBS–22–714–09–46
NAS3–26617

7. PERFORMING ORGANIZATION NAME(S) AND ADDRESS(ES)

General Electric Aircraft Engines
One Neumann Way, MD B–5
Cincinnati, Ohio 45125

8. PERFORMING ORGANIZATION REPORT NUMBER

E–14611

9. SPONSORING/MONITORING AGENCY NAME(S) AND ADDRESS(ES)

National Aeronautics and Space Administration
Washington, DC 20546–0001

10. SPONSORING/MONITORING AGENCY REPORT NUMBER

NASA CR—2004-213117

11. SUPPLEMENTARY NOTES

This research was originally published internally as HSR046 in December 1996. Project Manager, Doug Harrington (retired). Responsible person, Diane Chapman, organization code 2100, 216–433–2309.

12a. DISTRIBUTION/AVAILABILITY STATEMENT

Unclassified - Unlimited
Subject Categories: 01 and 07   Distribution: Nonstandard

Available electronically at http://gltrs.grc.nasa.gov

This publication is available from the NASA Center for AeroSpace Information, 301–621–0390.

12b. DISTRIBUTION CODE

13. ABSTRACT (Maximum 200 words)

The principle objectives of the current program were to experimentally investigate the repeatability of acoustic and aerodynamic characteristics of 2D–CD mixer-ejector nozzles and the effects on the acoustic and aerodynamic characteristics of 2D mixer-ejectors due to (1) the configurational variations, which include mixers with aligned CD chutes, aligned convergent chutes, and staggered CD chutes and aerodynamic cycle variables, (2) treatment variations by using different treatment materials, treating the ejector with varying area, location, and treatment thickness for a mixer-ejector configuration, and (3) secondary inlet shape (i.e., a more realistic inlet) and the blockage across the inlet (a possible fin-like structure needed for installation purpose) by modifying one of the inlet of a mixer-ejector configuration. The objectives also included the measurement dynamic pressures internal to the ejector for a few selected configuration to examine the internal noise characteristics.

14. SUBJECT TERMS

2D–CD mixer-ejector nozzles; Gen 1.5 HSCT exhaust nozzles; Aligned CD chutes; Staggered CD chutes

15. NUMBER OF PAGES
515

16. PRICE CODE

17. SECURITY CLASSIFICATION OF REPORT	18. SECURITY CLASSIFICATION OF THIS PAGE	19. SECURITY CLASSIFICATION OF ABSTRACT	20. LIMITATION OF ABSTRACT
Unclassified	Unclassified	Unclassified	